Voice and Audio Compression for Wireless Communications

Second Edition

Lajos Hanzo
University of Southampton, UK

F. Clare Somerville
picoChip Designs Ltd, UK

Jason Woodard
CSR plc, UK

IEEE
IEEE PRESS
IEEE Communications Society, Sponsor

1807 WILEY 2007

John Wiley & Sons, Ltd

Voice and Audio Compression for Wireless Communications

Voice and Audio Compression for Wireless Communications

Second Edition

Lajos Hanzo
University of Southampton, UK

F. Clare Somerville
picoChip Designs Ltd, UK

Jason Woodard
CSR plc, UK

IEEE PRESS
IEEE Communications Society, Sponsor

BICENTENNIAL 1807 WILEY 2007 BICENTENNIAL

John Wiley & Sons, Ltd

Telephone (+44) 1243 779777

Email (for orders and customer service enquiries): cs-books@wiley.co.uk
Visit our Home Page on www.wiley.com

Other Wiley Editorial Offices

John Wiley & Sons Inc., 111 River Street, Hoboken, NJ 07030, USA

Jossey-Bass, 989 Market Street, San Francisco, CA 94103-1741, USA

Wiley-VCH Verlag GmbH, Boschstr. 12, D-69469 Weinheim, Germany

John Wiley & Sons Australia Ltd, 42 McDougall Street, Milton, Queensland 4064, Australia

John Wiley & Sons (Asia) Pte Ltd, 2 Clementi Loop #02-01, Jin Xing Distripark, Singapore 129809

John Wiley & Sons Canada Ltd, 22 Worcester Road, Etobicoke, Ontario, Canada M9W 1L1

Wiley also publishes its books in a variety of electronic formats. Some content that appears in print may not be available in electronic books.

IEEE Communications Society, Sponsor
COMMS-S Liaison to IEEE Press, Mostafa Hashem Sherif

Library of Congress Cataloging-in-Publication Data

Hanzo, Lajos, 1952-
Voice and Audio Compression for Wireless Communications / L. Hanzo,
F.C.A. Somerville and J.P. Woodard – 2nd ed.
p. cm.
Rev. ed. of: Voice and Audio Compression for Wireless Communications. c2001
Includes bibliographical references and index.
ISBN 978-0-470-51581-5 (cloth : alk. paper)
1. Compressed speech. 2. Speech processing systems. 3. Telecommunication systems.
I. Somerville, F. Clare A. II. Woodard, Jason P. III. Hanzo, Lajos,
1952- Voice compression and communications. IV. Title.
TK7882.S65H35 2007
621.384–dc22

2007011025

British Library Cataloguing in Publication Data

A catalogue record for this book is available from the British Library

ISBN 978-0-470- 51581-5 (HB)

Typeset by the authors using LaTeX software.
Printed and bound in Great Britain by Antony Rowe Ltd, Chippenham, England.
This book is printed on acid-free paper responsibly manufactured from sustainable forestry in which at least two trees are planted for each one used for paper production.

Contents

About the Authors

Lajos Hanzo FREng, FIEEE, FIET, DSc received his degree in electronics in 1976 and his doctorate in 1983. During his 30 year career in telecommunications he has held various research and academic posts in Hungary, Germany and the UK. Since 1986 he has been with the School of Electronics and Computer Science, University of Southampton, UK, where he holds the chair in telecommunications. He has co-authored 14 books on mobile radio communications totalling in excess of 10 000 pages, published about 700 research papers, acted as TPC Chair of IEEE conferences, presented keynote lectures and been awarded a number of distinctions. Currently he is directing an academic research team, working on a range of research projects in the field of wireless multimedia communications sponsored by industry, the Engineering and Physical Sciences Research Council (EPSRC) UK, the European IST Programme and the Mobile Virtual Centre of Excellence (VCE), UK. He is an enthusiastic supporter of industrial and academic liaison and he offers a range of industrial courses. He is also an IEEE Distinguished Lecturer of both the Communications Society and the Vehicular Technology Society (VTS). Since 2005 he has been a Governor of the VTS. For further information on research in progress and associated publications please refer to http://www-mobile.ecs.soton.ac.uk.

Clare Somerville (nee Brooks) received the M.Eng in Information Engineering, in 1995, from the University of Southampton, UK. From 1995 to 1998 she performed research into low-bitrate speech coders for wireless communications leading to a PhD in 1999, also from the University of Southampton. From 1998 to 2001 she was with the Global Wireless Systems Research department, Bell Laboratories, Swindon, UK where she undertook research into real-time services over GPRS networks. Since 2001 she has been a Principal Systems Engineer at picoChip Designs Ltd, Bath UK. working on protocol layer aspects in both UMTS and WiMAX wireless systems. Her current interests lie within the picoChip WiMAX product range where she is lead architect for the MAC. She is a member of the 802.16 standards forum and is a registered mentor for Women in SET (Science, Engineering and Technology).

Jason Woodard was born in Northern Ireland in 1969. He received a BA degree in Physics from Oxford University in 1991, and an MSc with distinction in Electronics from the University of Southampton in 1992. In 1995 he completed a PhD in speech coding, also at the University of Southampton, and then held a three year postdoctoral fellowship, researching turbo-coding techniques for the FIRST project within the European ACTS programme. In 1998 he joined the PA Consulting Group in Cambridge, UK and in 1999 he was a founding member of UbiNetics, a supplier of mobile communications test and IP solutions. Currently he is working on the research and development of advanced wireless technologies for CSR, a leading supplier of single-chip wireless devices. Dr Woodard has published widely in wireless communications, including co-authoring two books.

Other Wiley and IEEE Press Books on Related Topics[1]

- R. Steele, L. Hanzo (Ed): *Mobile Radio Communications: Second and Third Generation Cellular and WATM Systems*, John Wiley & Sons, Ltd and IEEE Press, 2nd edition, 1999, ISBN 07 273-1406-8, 1064 pages
- L. Hanzo, F.C.A. Somerville, J.P. Woodard: *Voice Compression and Communications: Principles and Applications for Fixed and Wireless Channels*, IEEE Press and John Wiley & Sons, Ltd, 2001, 642 pages
- L. Hanzo, P. Cherriman, J. Streit: *Wireless Video Communications: Second to Third Generation and Beyond*, IEEE Press and John Wiley & Sons, Ltd, 2001, 1093 pages
- L. Hanzo, T.H. Liew, B.L. Yeap: *Turbo Coding, Turbo Equalisation and Space–time Coding*, John Wiley & Sons, Ltd and IEEE Press, 2002, 751 pages
- J.S. Blogh, L. Hanzo: *Third-Generation Systems and Intelligent Wireless Networking: Smart Antennas and Adaptive Modulation*, John Wiley & Sons, Ltd and IEEE Press, 2002, 408 pages
- L. Hanzo, C.H. Wong, M.S. Yee: *Adaptive Wireless Transceivers: Turbo-Coded, Turbo-Equalised and Space–time Coded TDMA, CDMA and OFDM Systems*, John Wiley & Sons, Ltd and IEEE Press, 2002, 737 pages
- L. Hanzo, L.-L. Yang, E.-L. Kuan, K. Yen: *Single- and Multi-Carrier CDMA: Multi-User Detection, Space–time Spreading, Synchronisation, Networking and Standards*, John Wiley & Sons, Ltd and IEEE Press, June 2003, 1060 pages
- L. Hanzo, M. Münster, T. Keller, B.-J. Choi: *OFDM and MC-CDMA for Broadband Multi-User Communications, WLANs and Broadcasting*, John-Wiley & Sons, Ltd and IEEE Press, 2003, 978 pages
- L. Hanzo, S.-X. Ng, T. Keller and W.T. Webb: *Quadrature Amplitude Modulation: From Basics to Adaptive Trellis-Coded, Turbo-Equalised and Space–time Coded OFDM, CDMA and MC-CDMA Systems*, John Wiley & Sons, Ltd and IEEE Press, 2004, 1105 pages

[1] For detailed contents and sample chapters please refer to http://www-mobile.ecs.soton.ac.uk.

- L. Hanzo, T. Keller: *An OFDM and MC-CDMA Primer*, John Wiley & Sons, Ltd and IEEE Press, 2006, 430 pages
- L. Hanzo, F.C.A. Somerville, J.P. Woodard: *Voice and Audio Compression for Wireless Communications*, John Wiley & Sons, Ltd and IEEE Press, 2007, 858 pages
- L. Hanzo, P.J. Cherriman, J. Streit: *Video Compression and Communications: H.261, H.263, H.264, MPEG4 and HSDPA-Style Adaptive Turbo-Transceivers*, John Wiley & Sons, Ltd and IEEE Press, 2007, 680 pages
- L. Hanzo, J.S. Blogh, S. Ni: 3G Systems and HSDPA-Style FDD Versus TDD Networking: Smart Antennas and Adaptive Modulation, John Wiley & Sons, Ltd and IEEE Press, 2007

Preface and Motivation

The Speech Coding Scene

Despite the emergence of sophisticated high-rate multimedia services, voice communications remain the predominant means of human communications, although the compressed voice signals may be delivered via the Internet. The large-scale, pervasive introduction of wireless Internet services is likely to promote the unified transmission of both voice and data signals using the Voice over Internet Protocol (VoIP) even in the third-generation (3G) wireless systems, despite wasting much of the valuable frequency resources for the transmission of packet headers. Even when the predicted surge of wireless data and Internet services becomes a reality, voice remains the most natural means of human communications, although this may be delivered via the Internet.

This book is dedicated to audio and voice compression issues, although the aspects of error resilience, coding delay, implementational complexity and bitrate are also at the centre of our discussions, characterising many different speech codecs incorporated in source-sensitivity matched wireless transceivers. A unique feature of this book is that it also provides cutting-edge turbo-transceiver-aided research-oriented design examples and a chapter on the VoIP protocol.

Here we attempt a rudimentary comparison of some of the codec schemes treated in the book in terms of their speech quality and bitrate, in order to provide a road map for the reader with reference to Cox's work [1,2]. The formally evaluated mean opinion score (MOS) values of the various codecs portrayed in this book are shown in Figure 1.

Observe in the figure that over the years a range of speech codecs have emerged, which attained the quality of the 64 kbps G.711 pulse-code modulation (PCM) speech codec, although at the cost of significantly increased coding delay and implementational complexity. The 8 kbps G.729 codec is the most recent addition to this range of the International Telecommunications Union's (ITU) standard schemes, which significantly outperforms all previous standard ITU codecs in robustness terms. The performance target of the 4 kbps ITU codec (ITU4) is also to maintain this impressive set of specifications. The family of codecs designed for various mobile radio systems – such as the 13 kbps regular pulse excited (RPE) scheme of the Global System of Mobile communications known as GSM, the 7.95 kbps IS-54, and the IS-95 Pan-American schemes, the 6.7 kbps Japanese digital cellular (JDC) and 3.45 kbps half-rate JDC arrangement (JDC/2) – exhibits slightly lower MOS values than the ITU codecs. Let us now consider the subjective quality of these schemes in a little more depth.

The 2.4 kbps US Department of Defence Federal Standard codec known as FS-1015 is the only vocoder in this group and it has a rather synthetic speech quality, associated with the lowest subjective assessment in the figure. The 64 kbps G.711 PCM codec and

the G.726/G.727 adaptive differential PCM (ADPCM) schemes are waveform codecs. They exhibit a low implementational complexity associated with a modest bitrate economy. The remaining codecs belong to the so-called hybrid coding family and achieve significant bitrate economies at the cost of increased complexity and delay.

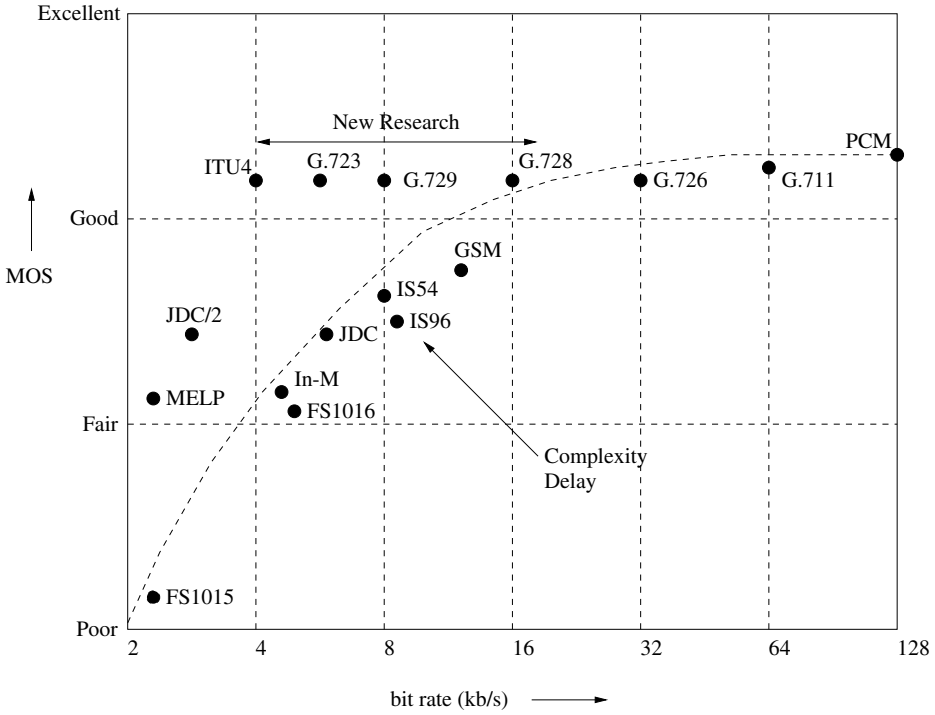

Figure 1: Subjective speech quality of various codecs [1] © IEEE, 1996.

Specifically, the 16 kbps G.728 backward-adaptive scheme maintains a similar speech quality to the 32 and 64 kbps waveform codecs, while also maintaining an impressively low, 2 ms delay. This scheme was standardised during the early 1990s. The similar quality, but significantly more robust 8 kbps G.729 codec was approved in March 1996 by the ITU. Its standardisation overlapped with the G.723.1 codec developments. The G.723.1 codec's 6.4 kbps mode maintains a speech quality similar to the G.711, G.726, G.727, G.728 and G.728 codecs, while its 5.3 kbps mode exhibits a speech quality similar to the cellular speech codecs of the late 1980s. The standardisation of a 4 kbps ITU scheme, which we refer to here as ITU4, is also a desirable design goal at the time of writing.

In parallel to the ITU's standardisation activities a range of speech coding standards have been proposed for regional cellular mobile systems. The standardisation of the 13 kbps RPE-long-term prediction (LTP) full-rate GSM (GSM-FR) codec dates back to the second half of the 1980s, representing the first standard hybrid codec. Its complexity is significantly lower than that of the more recent code excited linear predictive (CELP) based codecs. Observe in the figure that there is also a similar-rate enhanced full-rate GSM codec (GSM-EFR), which matches the speech quality of the G.729 and G.728 schemes. The original GSM-FR codec's

development was followed a little later by the release of the 7.95 kbps vector sum excited linear predictive (VSELP) IS-54 American cellular standard. Due to advances in the field the 7.95 kbps IS-54 codec achieved a similar subjective speech quality to the 13 kbps GSM-FR scheme. The definition of the 6.7 kbps Japanese JDC VSELP codec was almost coincident with that of the IS-54 arrangement. This codec development was also followed by a half-rate standardisation process, leading to the 3.2 kbps pitch-synchroneous innovation CELP (PSI-CELP) scheme.

The IS-95 Pan-American code division multiple access (CDMA) system also has its own standardised CELP-based speech codec, which is a variable-rate scheme, supporting bitrates between 1.2 and 14.4 kbps, depending on the prevalent voice activity. The perceived speech quality of these cellular speech codecs contrived mainly during the late 1980s was found subjectively similar to each other under the perfect channel conditions of Figure 1. Lastly, the 5.6 kbps half-rate GSM codec (GSM-HR) also met its specification in terms of achieving a similar speech quality to the 13 kbps original GSM-FR arrangements, although at the cost of quadruple complexity and higher latency.

Recently, the advantages of intelligent multimode speech terminals (IMT), which can reconfigure themselves in a number of different bitrates, quality and robustness modes, attracted substantial research attention in the community, which led to the standardisation of the high-speed downlink packet access (HSDPA) mode of the 3G wireless systems. The HSDPA-style transceivers employ both adaptive modulation and adaptive channel coding, which result in a channel-quality dependent bitrate fluctuation, hence requiring reconfigurable multimode voice and audio codecs, such as the advanced multirate codec, referred to as the AMR scheme. Following the standardisation of the narrowband AMR codec, the wideband AMR scheme, referred to as the AMR-WB arrangement and encoding the 0–7 kHz band, was also developed, which will also be characterised in this book. Finally, the most recent AMR codec, namely the so-called AMR-WB+ scheme, will also be the subject of our discussions.

Recent research on sub-2.4 kbps speech codecs is also covered extensively in this book, where the aspects of auditory masking become more dominant. Finally, since the classic G.722 sub-band-adaptive differential pulse code modulation (ADPCM) based wideband codec has become obsolete in the light of exciting new developments in compression, the most recent trend is to consider wideband speech and audio codecs, providing substantially enhanced speech quality. Motivated by early seminal work on transform-domain or frequency-domain based compression by Noll and his colleagues, in this field the wideband G.721.1 codec – which can be programmed to operate between 10 kbps and 32 kbps and hence lends itself to employment in HSDPA-style near-instantaneously adaptive wireless communicators – is the most attractive candidate. This codec is portrayed in the context of a sophisticated burst-by-burst adaptive wideband turbo-coded orthogonal frequency division multiplex (OFDM) IMT in this book. This scheme is also capable of transmitting high-quality audio signals, behaving essentially as a high-quality waveform codec.

Milestones in Speech Coding History

Over the years a range of excellent monographs and text books have been published, characterising the state-of-the-art at its various stages of development and constituting significant milestones. The first major development in the history of speech compression

can be considered to be the invention of the vocoder, dating back to as early as 1939. Delta modulation was contrived in 1952 and later it became well established following Steele's monograph on the topic in 1975 [3]. PCM was first documented in detail in Cattermole's classic contribution in 1969 [4]. However, it was realised in 1967 that predictive coding provides advantages over memoryless coding techniques, such as PCM. Predictive techniques were analysed in depth by Markel and Gray in their 1976 classic treatise [5]. This was shortly followed by the often cited reference [6] by Rabiner and Schafer. Also, Lindblom and Ohman contributed a book in 1979 on speech communication research [7].

The foundations of auditory theory were laid down as early as 1970 by Tobias [8], but these principles were not exploited to their full potential until the invention of the analysis-by-synthesis (AbS) codecs, which were heralded by Atal's multi-pulse excited codec in the early 1980s [9]. The waveform coding of speech and video signals has been comprehensively documented by Jayant and Noll in their 1984 monograph [10]. During the 1980s the speech codec developments were fuelled by the emergence of mobile radio systems, where spectrum was a scarce resource, potentially doubling the number of subscribers and hence the revenue, if the bitrate could be halved.

The RPE principle – as a relatively low-complexity AbS technique – was proposed by Kroon, Deprettere and Sluyter in 1986 [11], which was followed by further research conducted by Vary [12, 13] and his colleagues at PKI in Germany and IBM in France, leading to the 13 kbps Pan-European GSM codec. This was the first standardised AbS speech codec, which also employed LTP, recognising the important role the pitch determination plays in efficient speech compression [14, 15]. It was in this era, when Atal and Schroeder invented the code excited linear predictive (CELP) principle [16], leading to perhaps the most productive period in the history of speech coding during the 1980s. Some of these developments were also summarised, for example, by O'Shaughnessy [17], Papamichalis [18] and Deller, Proakis and Hansen [19].

It was during this era that the importance of speech perception and acoustic phonetics was duly recognised, for example, in the monograph by Lieberman and Blumstein [20]. A range of associated speech quality measures were summarised by Quackenbush, Barnwell III and Clements [21]. Nearly concomitantly Furui also published a book related to speech processing [22]. This period witnessed the appearance of many of the speech codecs seen in Figure 1, which found applications in the emerging global mobile radio systems, such as IS-54, JDC, etc. These codecs were typically associated with source-sensitivity matched error protection, where, for example, Steele, Sundberg and Wong [23–26] have provided early insights on the topic. Further sophisticated solutions were suggested, for example, by Hagenauer [27].

Both the narrowband and wideband AMR, as well as the AMR-WB+ codecs [28, 29] are capable of adaptively adjusting their bitrate. This also allows the user to adjust the ratio between the speech bitrate and the channel coding bitrate constituting the error protection oriented redundancy according to the prevalent near-instantaneous channel conditions in HSDPA-style transceivers. When the channel quality is inferior, the speech encoder operates at low bitrates, thus accommodating more powerful forward error control within the total bitrate budget. By contrast, under high-quality channel conditions the speech encoder may benefit from using the total bitrate budget, yielding high speech quality, since in this high-rate case low redundancy error protection is sufficient. Thus, the AMR concept allows the system to operate in an error-resilient mode under poor channel conditions, while benefitting

from a better speech quality under good channel conditions. Hence, the source coding scheme must be designed for seamless switching between rates available without annoying artifacts.

Overview of MPEG-4 Audio

The definition of the MPEG-4 audio standard was the culmination of the 60-year research conducted by the global research community, as portrayed in Figure 3, which will be detailed throughout out discussions in the book. The Moving Picture Experts Group (MPEG) was first established by the International Standard Organisation (ISO) in 1988 with the aim of developing a full audio-visual coding standard referred to as MPEG-1 [30–32]. The audio-related section MPEG-1 was designed to encode digital stereo sound at a total bitrate of 1.4 to 1.5 Mbps – depending on the sampling frequency, which was 44.1 kHz or 48 kHz – down to a few hundred kilobits per second [33]. The MPEG-1 standard is structured in layers, from Layer I to III. The higher layers achieve a higher compression ratio, albeit at an increased complexity. Layer I achieves perceptual transparency, i.e. subjective equivalence with the uncompressed original audio signal at 384 kbps, while Layer II and III achieve a similar subjective quality at 256 kbps and 192 kbps, respectively [34–38].

MPEG-1 was approved in November 1992 and its Layer I and II versions were immediately employed in practical systems. However, the MPEG Audio Layer III, MP3 for short only became a practical reality a few years later, when multimedia PCs were introduced having improved processing capabilities and the emerging Internet sparked off a proliferation of MP3 compressed teletraffic. This changed the face of the music world and the distribution of music. The MPEG-2 backward compatible audio standard was approved in 1994 [39], providing an improved technology that would allow those who had already launched MPEG-1 stereo audio services to upgrade their system to multichannel mode, optionally also supporting a higher number of channels at a higher compression ratio. Potential applications of the multichannel mode are in the field of quadraphonic music distribution or cinemas. Furthermore, lower sampling frequencies were also incorporated, which include 16, 22.05, 24, 32, 44.1 and 48 kHz [39]. Concurrently, MPEG commenced research into even higher-compression schemes, relinquishing the backward compatibility requirement, which resulted in the MPEG-2 advanced audio coding standard (AAC) standard in 1997 [40]. This provides those who are not constrained by legacy systems to benefit from an improved multichannel coding scheme. In conjunction with AAC, it is possible to achieve perceptual transparent stereo quality at 128 kbps and transparent multichannel quality at 320 kbps; for example in cinema-type applications.

The MPEG-4 audio recommendation is the latest standard completed in 1999 [41–45], which offers, in addition to compression, further unique features that will allow users to interact with the information content at a significant higher level of sophistication than is possible today. In terms of compression, MPEG-4 supports the encoding of speech signals at bitrates from 2 kbps up to 24 kbps. For coding of general audio, ranging from very low bitrates up to high quality, a wide range of bitrates and bandwidths are supported, ranging from a bitrate of 8 kbps and a bandwidth below 4 kHz to broadcast quality audio, including monaural representations up to multichannel configuration.

The MPEG-4 audio codec includes coding tools from several different encoding families, covering parametric speech coding, CELP-based speech coding and time/frequency (T/F)

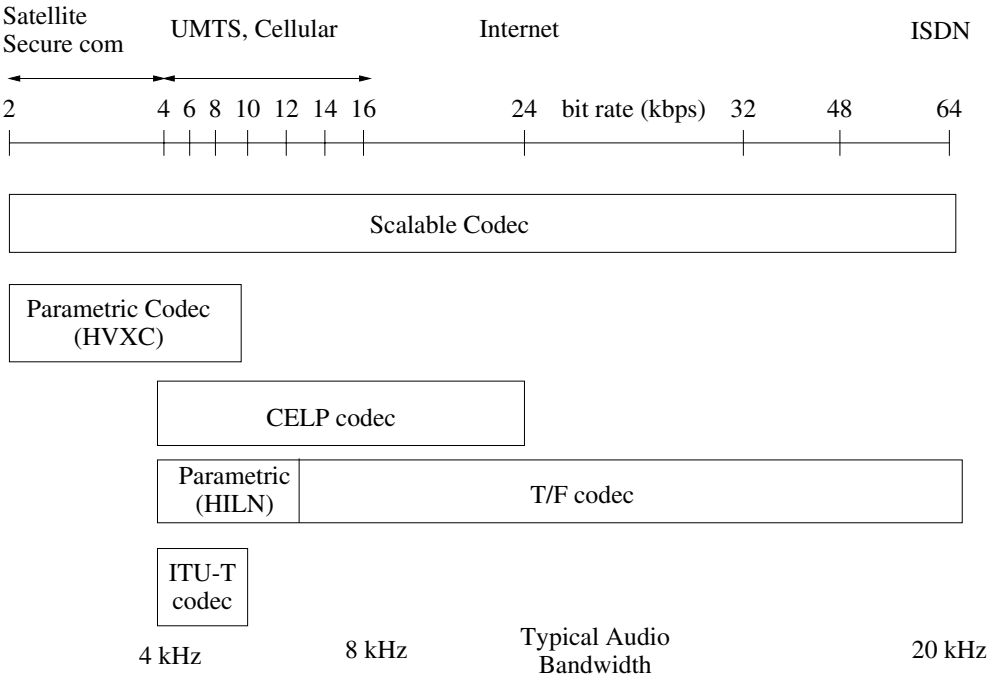

Figure 2: MPEG-4 framework [41].

audio coding, which are characterised in Figure 2. It can be observed that a parametric coding scheme, namely Harmonic Vector eXcitation Coding (HVXC) was selected for covering the bitrate range from 2 to 4 kbps. For bitrates between 4 and 24 kbps, a CELP-coding scheme was chosen for encoding narrowband and wideband speech signals. For encoding general audio signals at bitrates between 8 and 64 kbps, a T/F coding scheme based on the MPEG-2 AAC standard [40] endowed with additional tools is used. Here, a combination of different techniques was established, because it was found that maintaining the required performance for representing speech and music signals at all desired bitrates cannot be achieved by selecting a single coding architecture. A major objective of the MPEG-4 audio encoder is to reduce the bitrate, while maintaining a sufficiently high flexibility in terms of bitrate selection. The MPEG-4 codec also offers other new functionalities, which include bitrate scalability, object-based of a specific audio passage for example, where a distinct 'object' may be defined as a passage played by a certain instrument coding, as well as an increased robustness against transmission errors and supporting special audio effects.

MPEG-4 consists of Versions 1 and 2. Version 1 [41] contains the main body of the standard, while Version 2 [46] provides further enhancement tools and functionalities, that includes the issues of increasing the robustness against transmission errors and error protection, low-delay audio coding, finely grained bitrate scalability using the Bit-Sliced Arithmetic Coding (BSAC) tool, the employment of parametric audio coding, using the CELP-based silence compression tool and the 4 kbps extended variable bitrate mode of the HVXC tool. Due to the vast amount of information contained in the MPEG-4 standard, we

will only consider some of its audio compression components, which include the coding of natural speech and audio signals. Readers who are specifically interested in text-to-speech synthesis or synthetic audio issues are referred to the MPEG-4 standard [41] and to the contributions by Scheirer *et al.* [47, 48] for further information. Most of the material in Chapter 10 will be based on an amalgam of [34–38, 40, 41, 43, 44, 46, 49]. In this chapter, the operations of each component of the MPEG-4 audio component will be highlighted in greater detail. As an application example, we will employ the transform-domain weighted interleaved vector quantisation (TWINVQ) coding tool, which is one of the MPEG-4 audio codecs in the context of a wireless audio transceiver in conjunction with space–time coding [50] and various quadrature amplitude modulation (QAM) schemes [51]. The audio transceiver is introduced in Section 10.5 and its performance is discussed in Section 10.5.6.

Motivation and Outline of this Book

During the early 1990s, Atal, Cuperman and Gersho [52] edited prestigious contributions on speech compression. Also, Ince [53] contributed a book in 1992 related to the topic. Anderson and Mohan co-authored a monograph on source and channel coding in 1993 [54]. Research-oriented developments were then consolidated in Kondoz' excellent monograph in 1994 [55] and in the multi-authored contribution edited by Kleijn and Paliwal [56] in 1995. The most recent addition to the above range of contributions is the second edition of O'Shaughnessy well-referenced book cited above. However, at the time of writing no book spans the entire history of speech and audio compression, which is the goal of this volume.

Against this backcloth, this book endeavours to review the recent history of speech compression and communications in the era of wireless turbo-transceivers and joint source/channel coding. We attempt to provide the reader with a historical perspective, commencing with a rudimentary introduction to communications aspects, since throughout this book we illustrate the expected performance of the various speech codecs studied also in the context of jointly optimised wireless transceivers.

This book contains four parts. Parts I and II cover classic background material on speech signals, predictive waveform codecs and analysis-by-synthesis codecs as well as the entire speech and audio coding standardisation scene. The bulk of the book is contained in the research-oriented Parts III and IV, covering both standardised and proprietary speech codecs – including the most recent AMR-WB+ and the MPEG-4 audio codecs, as well as cutting-edge wireless turbo transceivers.

Specifically, Chapters 1 and 2 of Part I provide a rudimentary introduction to speech signals, classic waveform coding as well as predictive coding, respectively, quantifying the overall performance of the various speech codecs, in order to render our treatment of the topics as self-contained and all-encompassing as possible.

Part II of this book is centred around AbS based coding, reviewing the classic principles in Chapter 3 as well as both narrow and wideband spectral envelope quantisation in Chapter 4. RPE and CELP coding are the topic of Chapters 5 and 6, which are followed by a detailed chapter on the entire plethora of existing forward-adaptive standardised CELP codecs in Chapter 7 and on their associated source-sensitivity matched channel coding schemes. The subject of Chapter 8 is both proprietary and standard backward-adaptive CELP codecs,

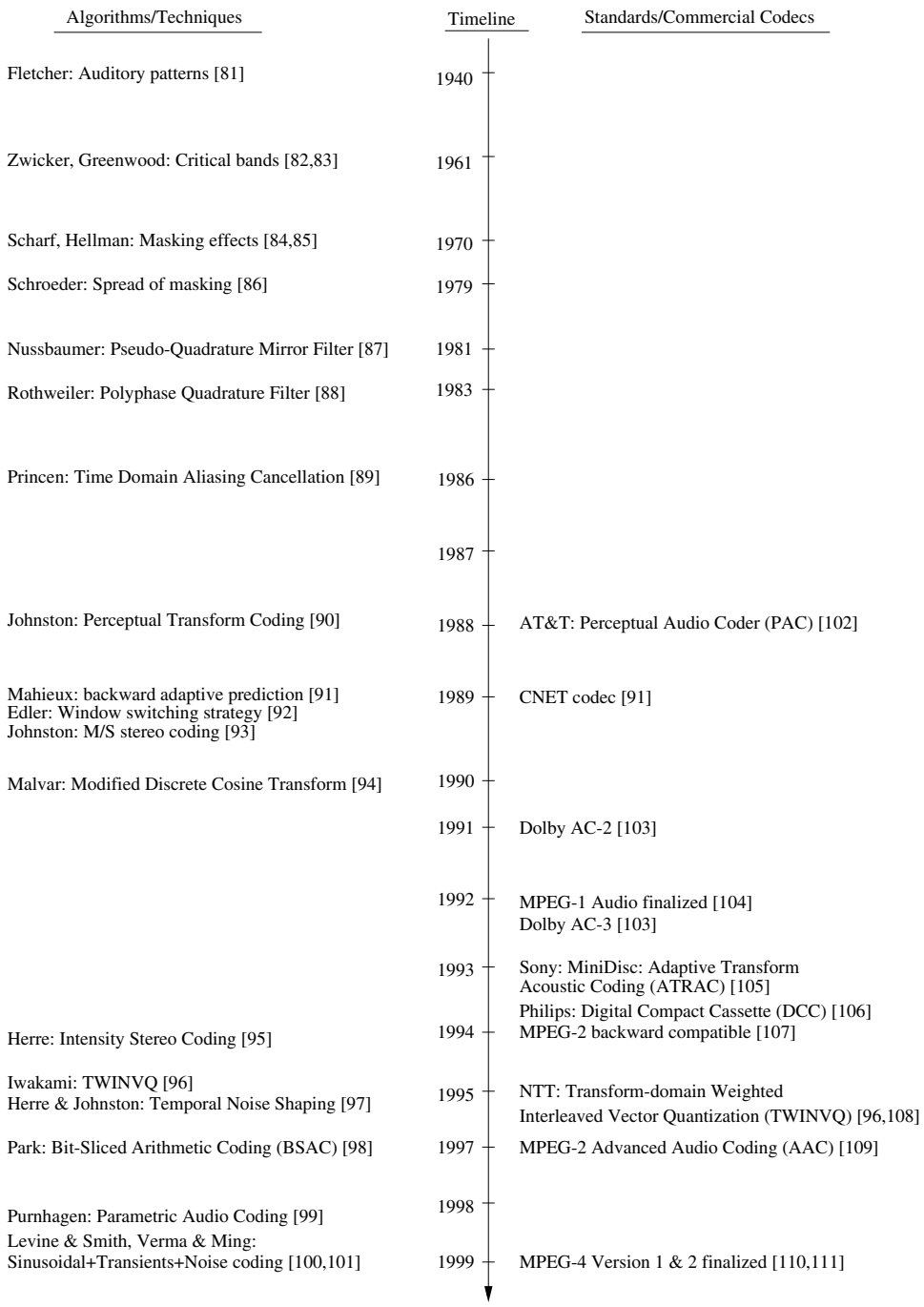

Figure 3: Important milestones in the development of perceptual audio coding.

which is concluded with a system design example based on a low-delay, multimode wireless transceiver.

The research-oriented Part III of this book is dedicated to a range of standard and proprietary wideband coding techniques and wireless systems. As an introduction to the wideband coding scene, in Chapter 9 the classic sub-band-based G.722 wideband codec is reviewed first, leading to the discussion of numerous low-rate wideband voice and audio codecs. Chapter 9 also contains diverse sophisticated wireless voice- and audio-system design examples, including a turbo-coded OFDM wideband audio system design study. This is followed by a wideband voice transceiver application example using the AMR-WB codec, a source-sensitivity matched Irregular Convolutional Code (IRCC) and extrinsic information transfer (EXIT) charts for achieving a near-capacity system performance. Chapter 9 is concluded with the portrayal of the AMR-WB+ codec. In Chapter 10 of Part III we detail the principles behind the MPEG-4 codec and comparatively studied the performance of the MPEG-4 and AMR-WB audio/speech codecs combined with various sophisticated wireless transceivers. Amongst others, a jointly optimised source-coding, outer unequal protection non-systematic convolutional (NSC) channel-coding, inner trellis coded modulation (TCM) and spatial diversity aided space–time trellis coded (STTC) turbo transceiver investigated. The employment of TCM provided further error protection without expanding the bandwidth of the system and by utilising STTC spatial diversity was attained, which rendered the error statistics experienced pseudo-random, as required by the TCM scheme, since it was designed for Gaussian channels inflicting randomly dispersed channel errors. Finally, the performance of the STTC-TCM-2NSC scheme was enhanced with the advent of an efficient iterative joint decoding structure.

Chapters 11–17 of Part IV are all dedicated to sub-4 kbps codecs and their wireless transceivers, while Chapter 18 is devoted to speech quality evaluation techniques as well as to a rudimentary comparison of various speech codecs and transceivers. The last chapter of the book is on VoIP.

This book is naturally limited in terms of its coverage of these aspects, simply owing to space limitations. We endeavoured, however, to provide the reader with a broad range of application examples, which are pertinent to a range of typical wireless transmission scenarios.

Our hope is that this book offers you – the reader – a range of interesting topics, portraying the current state-of-the-art in the associated enabling technologies. In simple terms, finding a specific solution to a voice communications problem has to be based on a compromise in terms of the inherently contradictory constraints of speech quality, bitrate, delay, robustness against channel errors, and the associated implementational complexity. Analysing these trade-offs and proposing a range of attractive solutions to various voice communications problems is the basic aim of this book.

Again, it is our hope that this book underlines the range of contradictory system design trade-offs in an unbiased fashion and that you will be able to glean information from it, in order to solve your own particular wireless voice communications problem, but most of all that you will find it an enjoyable and relatively effortless reading, providing you – the reader – with intellectual stimulation.

Lajos Hanzo
Clare Somerville
Jason Woodard

Acknowledgements

The book has been conceived in the Electronics and Computer Science Department at the University of Southampton, although Dr Somerville and Dr Woodard have moved on in the mean-time. We are indebted to our many colleagues who have enhanced our understanding of the subject, in particular to Professor Emeritus Raymond Steele. These colleagues and valued friends, too numerous all to be mentioned, have influenced our views concerning various aspects of wireless multimedia communications and we thank them for the enlightenment gained from our collaborations on various projects, papers and books. We are grateful to Jan Brecht, Jon Blogh, Marco Breiling, Marco del Buono, Sheng Chen, Stanley Chia, Byoung Jo Choi, Joseph Cheung, Peter Fortune, Sheyam Domeya, Lim Dongmin, Dirk Didascalou, Stephan Ernst, Eddie Green, David Greenwood, Hee Thong How, Thomas Keller, Ee-Lin Kuan, Joerg Kliewer, W.H. Lam, C.C. Lee, M.A. Nofal, Xiao Lin, Chee Siong Lee, Tong-Hooi Liew, Soon-Xin Ng, Matthias Muenster, Noor Othman, Vincent Roger-Marchart, Redwan Salami, David Stewart, Jeff Torrance, Spiros Vlahoyiannatos, Jin Wang, William Webb, John Williams, Jason Woodard, Choong Hin Wong, Henry Wong, James Wong, Lie-Liang Yang, Bee-Leong Yeap, Mong-Suan Yee, Kai Yen, Andy Yuen and many others with whom we enjoyed an association.

We also acknowledge our valuable associations with the Virtual Centre of Excellence in Mobile Communications, in particular with its Chief Executives, Dr Tony Warwick and Dr Walter Tuttlebee, Dr Keith Baughan and other members of its Executive Committee, Professors Hamid Aghvami, Mark Beach, John Dunlop, Barry Evans, Joe McGeehan, Steve MacLaughlin and Rahim Tafazolli. Our sincere thanks are also due to John Hand and Nafeesa Simjee, the EPSRC, UK; Dr Joao Da Silva, Dr Jorge Pereira, Bartholome Arroyo, Bernard Barani, Demosthenes Ikonomou and other colleagues from the Commission of the European Communities, Brussels, Belgium; Andy Wilton, Luis Lopes and Paul Crichton from Motorola ECID, Swindon, UK for sponsoring some of our recent research.

We feel particularly indebted to Hee Thong How for his invaluable contributions to the book by co-authoring some of the chapters and to Rita Hanzo as well as Denise Harvey for their skillful assistance in typesetting the manuscript in LaTeX. Similarly, our sincere thanks are due to Mark Hammond, Jennifer Beal, Sarah Hinton and a number of other staff from John Wiley & Sons for their kind assistance throughout the preparation of the camera-ready manuscript. Finally, our sincere gratitude is due to the numerous authors listed in the Author Index – as well as to those, whose work was not cited due to space limitations – for their contributions to the state-of-the-art, without whom this book would not have materialised.

Lajos Hanzo
Clare Somerville
Jason Woodard

Part I

Speech Signals and Waveform Coding

Chapter 1

Speech Signals and an Introduction to Speech Coding

1.1 Motivation of Speech Compression

According to the lessons of information theory, the minimum bitrate at which the condition of distortionless transmission of any source signal is possible is determined by the entropy of the speech source message. Note, however, that in practical terms the source rate corresponding to the entropy is only asymptotically achievable as the encoding memory length or delay tends to infinity. Any further compression is associated with information loss or coding distortion. Many practical source compression techniques employ so-called 'lossy' coding, which typically guarantees further bitrate economy at the cost of nearly imperceptible speech, audio, video, etc, source representation degradation.

Note that the optimum Shannonian source encoder generates a perfectly uncorrelated source coded stream, where all the source redundancy has been removed, therefore the encoded source symbols – which are in most practical cases constituted by binary bits – are independent and each one has the same significance. Having the same significance implies that the corruption of any of the source encoded symbols results in identical source signal distortion over imperfect channels.

Under these conditions, according to Shannon's fundamental work [57–59], best protection against transmission errors is achieved, if source and channel coding are treated as separate entities. When using a block code of length N channel coded symbols in order to encode K source symbols with a coding rate of $R = K/N$, the symbol error rate can be rendered arbitrarily low if N tends to infinity and hence the coding rate to zero. This condition also implies an infinite coding delay. Based on the above considerations and on the assumption of additive white Gaussian noise (AWGN), channel source and channel coding have historically been separately optimised.

In designing a telecommunications system one of the most salient parameters is the number of subscribers that can be accommodated by the transmission media utilised. Whether it is a time division multiplex (TDM) or a frequency division multiplex (FDM) system,

Voice and Audio Compression for Wireless Communications Second Edition
L. Hanzo, F. C. A. Somerville and J. P. Woodard

whether it is analog or digital, the number of subscribers is limited by the channel capacity needed for one speech channel. If the channel capacity demand of the speech channels is halved, the total number of subscribers can be doubled. This gain becomes particularly important in applications like power- and band-limited satellite or mobile radio channels, where the urging demand for free channels overshadows the inevitable cost constraints imposed by a more complex low bitrate speech codec. In the framework of the basic limitations of state-of-the-art very large scale integrated (VLSI) technology the design of a speech codec is based on an optimum trade-off between lowest bitrate and highest quality, at the price of lowest complexity, cost and system delay. The analysis of these contradictory factors pervades all our forthcoming discussions.

1.2 Basic Characterisation of Speech Signals

In contrast to the so-called deterministic signals – random signals, such as speech, music, video, etc – information signals cannot be described with the help of analytical formulae. They are typically characterised with the help of a variety of statistical characteristics. The so-called power spectral density (PSD), auto-correlation function (ACF), cumulative distribution function (CDF) and probability density function (PDF) are some of the most frequent ones invoked, which will be exemplified during our further discourse.

Transmitting speech information is one of the fundamental aims of telecommunications and in this book we mainly concentrate on the efficient encoding of speech signals. The human vocal apparatus has been portrayed in many books dealing with human anatomy and has also been treated in references dealing with speech processing [5, 17, 22]. Hence, here we dispense with its portrayal and simply note that human speech is generated by emitting sound pressure waves, radiated primarily from the lips, although significant energy emanates in the case of some sounds also from the nostrils, throat, etc.

The air compressed by the lungs excites the vocal cords in two typical modes. Namely, when generating *voiced sounds*, the vocal cords vibrate and generate a high-energy quasi-periodic speech wave form, while in the case of lower energy *unvoiced sounds* the vocal cords do not participate in the voice production and the source behaves similar to a noise generator. In a somewhat simplistic approach the excitation signal denoted by $E(z)$ is then filtered through the vocal apparatus, which behaves like a spectral shaping filter with a transfer function of $H(z) = 1/A(z)$ that is constituted by the spectral shaping action of the glottis, which is defined as the opening between the vocal folds. Further spectral shaping is carried out by the vocal tract, lip radiation characteristics, etc. This simplified speech production model is shown in Figure 1.1.

Typical voiced and unvoiced speech waveform segments are shown in Figures 1.2 and 1.3, respectively, along with their corresponding power densities. Clearly, the unvoiced segment appears to have a significantly lower magnitude, which is also reflected by its PSD. Observe in Figure 1.3 that the low-energy, noise-like unvoiced signal has a rather flat PSD, which is similar to that of white noise. In general, the more flat the signal's spectrum, the more unpredictable it becomes and hence it is not amenable to signal compression or redundancy removal.

In contrast, the voiced segment shown in Figure 1.2 is quasi-periodic in the time-domain and it has an approximately 80-sample periodicity, identified by the positions of the

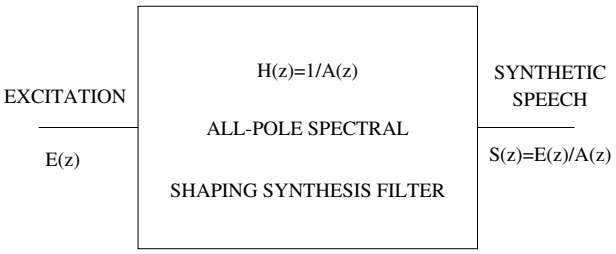

Figure 1.1: Linearly separable speech source model.

largest time-domain signal peaks, which corresponds to $80 \times 125\ \mu\text{s} = 10\,\text{ms}$. This interval is referred to as the *pitch period* and it is also often expressed in terms of the *pitch frequency* p, which is in this example $p = 1/10\ \text{ms} = 100\,\text{Hz}$. In the case of male speakers the typical pitch frequency range is between 40 and 120 Hz, while for females it can be as high as 300–400 Hz. Observe, furthermore, that within each pitch period there is a gradually decaying oscillation, which is associated with the excitation and gradually decaying vibration of the vocal cords.

A perfectly periodic time-domain signal would have a line spectrum, but since the voiced speech signal is quasi-periodic with a frequency of p – rather than being perfectly periodic – its spectrum in Figure 1.2 exhibits somewhat widened but distinctive spectral needles at frequencies of $n \times p$, rather than being perfectly periodic. As a second phenomenon, we can also observe three, sometimes four spectral envelope peaks. In our voiced spectrum of Figure 1.2 these so-called *formant frequencies* are observable around 500, 1500 and 2700 Hz and they are the manifestation of the resonances of the vocal tract at these frequencies. In contrast, the unvoiced segment of Figure 1.3 does not have a formant structure, it rather has a more dominant high-pass nature, exhibiting a peak around 2500 Hz. Observe, furthermore, that its energy is much lower than that of the voiced segment of Figure 1.2.

It is equally instructive to study the ACF of voiced and unvoiced segments, which are portrayed on an expanded scale in Figures 1.4 and 1.5, respectively. The voiced ACF shows a set of periodic peaks at displacements of about 20 samples, corresponding to $20 \times 125\ \mu\text{s} = 2.5\,\text{ms}$, which coincides with the positive quasi-periodic time-domain segments. Following four monotonously decaying peaks, there is a more dominant one around a displacement of 80 samples, which indicates the pitch periodicity. The periodic nature of the ACF can therefore be, for example, exploited to detect and measure the pitch periodicity in a range of applications, such as speech codecs, voice activity detectors, etc. Observe, however, that the first peak at a displacement of 20 samples is about as high as the one near 80 and hence a reliable pitch detector has to attempt to identify and rank all these peaks in order of prominence, exploiting also the *a priori* knowledge as to the expected range of pitch frequencies. Recall, furthermore, that, according to the Wiener–Khintshin Theorem, the ACF is the Fourier transform pair of the PSD of Figure 1.2.

By contrast, the unvoiced segment of Figure 1.5 has a much more rapidly decaying ACF, indicating no inherent correlation between adjacent samples and no long-term periodicity. Clearly, its sinc-function-like ACF is akin to that of band-limited white noise. The wider ACF of the voiced segment suggests predictability over a time-interval of some 3–400 μs.

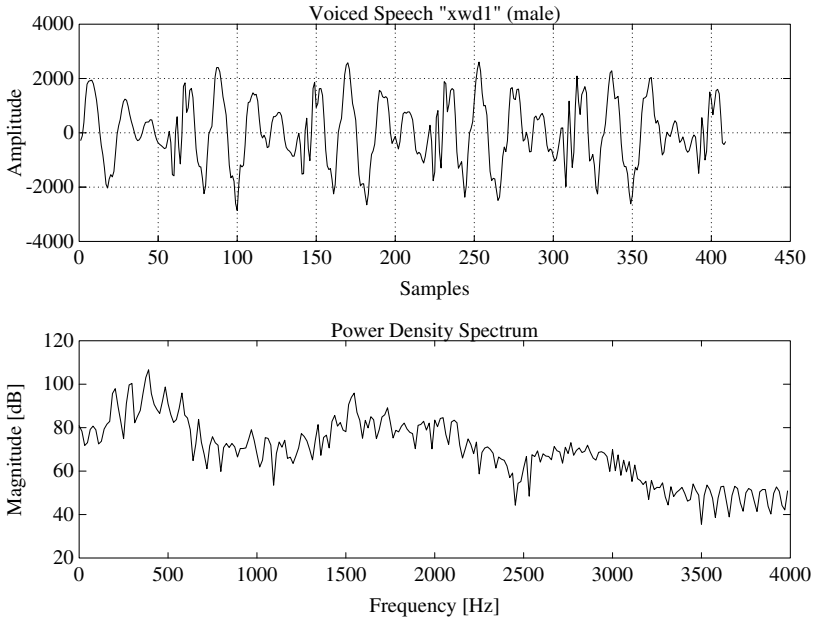

Figure 1.2: Typical voiced speech segment and its PSD for a male speaker.

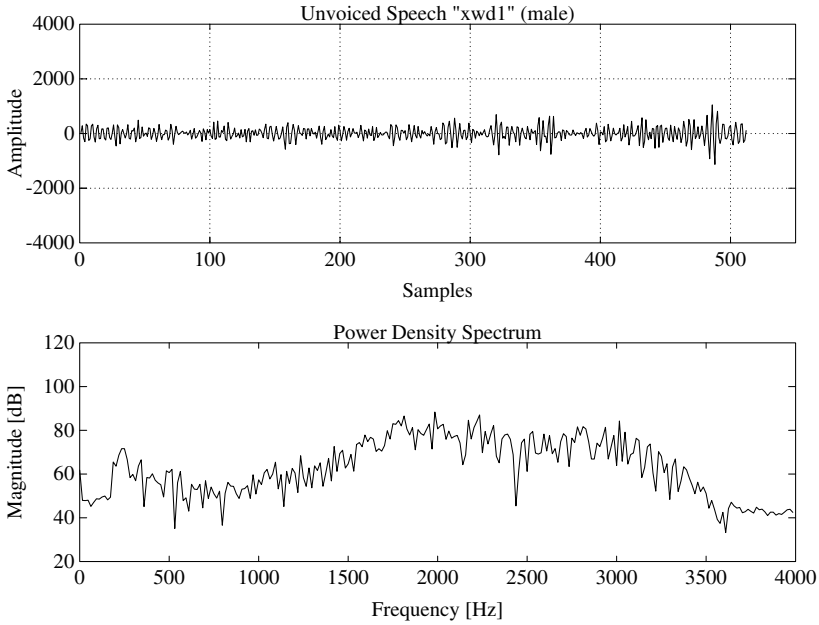

Figure 1.3: Typical unvoiced speech segment and its PSD for a male speaker.

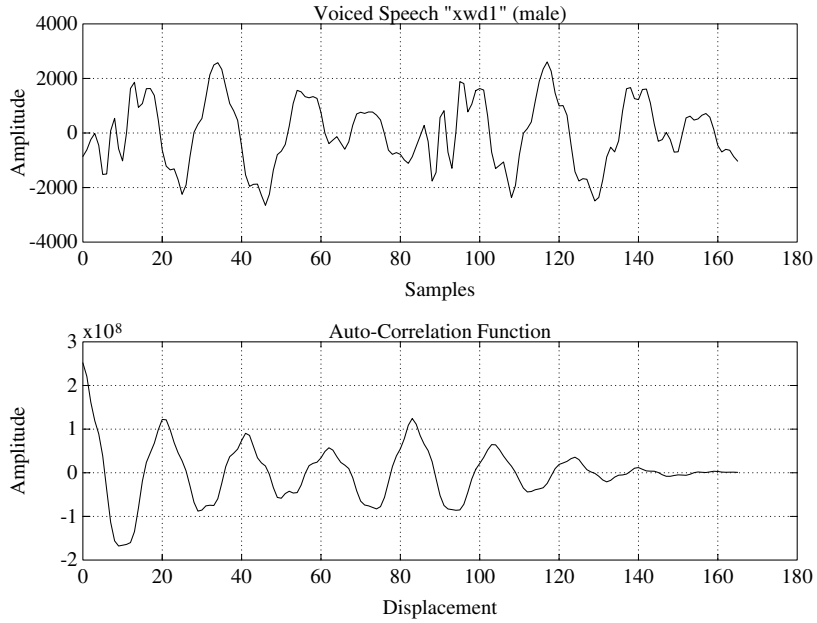

Figure 1.4: Typical voiced speech segment and its ACF for a male speaker.

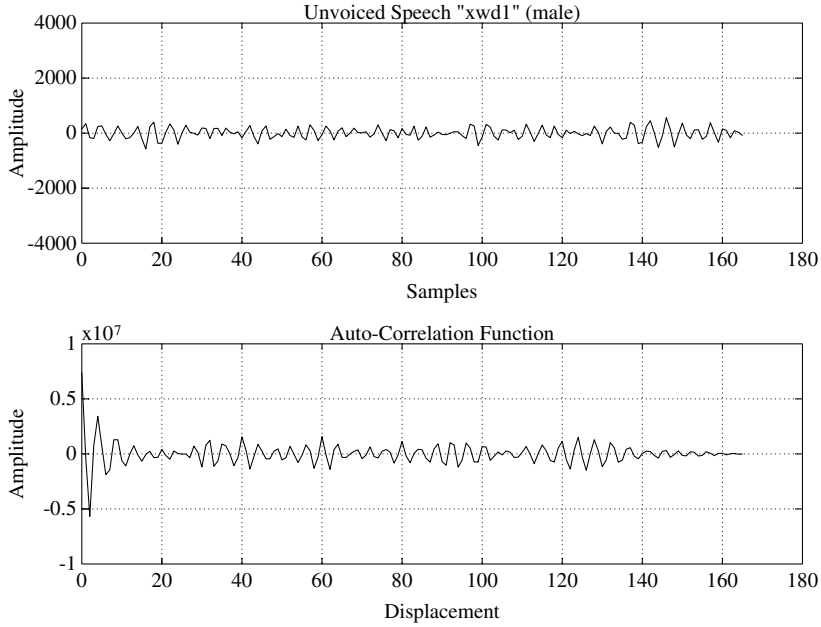

Figure 1.5: Typical unvoiced speech segment and its ACF for a male speaker.

Since human speech is voiced for about 2/3 of the time, redundancy can be removed from it using predictive techniques in order to reduce the bitrate required for its transmission.

Having characterised the basic features of speech signals, let us now focus our attention on their digital encoding. Intuitively it can be expected that the higher the encoder/decoder (codec) complexity, the lower the achievable bitrate and the higher the encoding delay. This is because more redundancy can be removed by considering longer speech segments and employing more sophisticated signal processing techniques.

1.3 Classification of Speech Codecs

Speech coding methods can be broadly categorised as *waveform coding, vocoding* and *hybrid coding*. The principle of these codecs will be considered later in this chapter, while the most prominent subclass of hybrid codecs referred to as analysis-by-synthesis schemes will be revisited in detail in Chapter 3 and will feature throughout this book. Their basic differences become explicit in Figure 1.6, where the speech quality versus bitrate performance of these codec families is portrayed in qualitative terms. The bitrate is plotted on a logarithmic axis and the speech quality classes 'poor to excellent' broadly correspond to the so-called five-point MOS scale values of 2–5 defined by the International Telegraph and Telephone Consultative Committee (CCITT), which was recently renamed as the International Telecommunications Union (ITU). We will refer to this diagram and to these codec families during our further discourse in order to allocate various codecs on this plane. Hence, here only a rudimentary interpretation is offered.

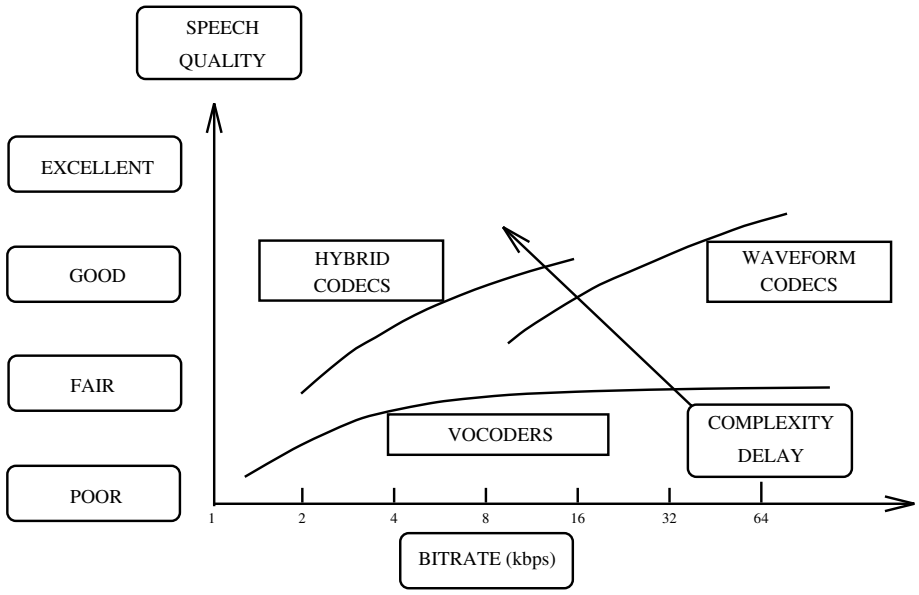

Figure 1.6: Speech quality versus bitrate classification of speech codecs.

1.3.1 Waveform Coding [10]

Waveform codecs have been comprehensively characterised by Jayant and Noll [10] and hence the spirit of virtually all treatises on the subject follows their approach. Our discourse in this section is no exception.

In general, waveform codecs are designed to be signal independent. They are designed to map the input waveform of the encoder into a facsimile-like replica of it at the output of the decoder. Due to this advantageous property they can also encode secondary types of information such as signalling tones, voice band data, or even music. Naturally, because of this signal 'transparency', their coding efficiency is usually quite modest. The coding efficiency can be improved by exploiting some statistical signal properties, if the codec parameters are optimised for the most likely categories of input signals, while still maintaining good quality for other types of signals as well. The waveform codecs can be further subdivided into time-domain waveform codecs and frequency-domain waveform codecs.

1.3.1.1 Time-domain Waveform Coding

The most well-known representative of signal independent time-domain waveform coding is the so-called A-law companded pulse code modulation (PCM) scheme, which has been standardised by the CCITT – now known as the International Telecommunications Union (ITU) – at 64 kbps, using nonlinear companding characteristics to result in near-constant signal-to-noise ratio (SNR) over the total input dynamic range. More explicitly, the nonlinear companding compresses large input samples and expands small ones. Upon quantising this companded signal, large input samples will tolerate higher quantisation noise than small samples.

Also well-known is the 32 kbps adaptive differential PCM (ADPCM) scheme standardised in ITU Recommendation G.721 – which will be the topic of Section 2.7 – and the so-called adaptive delta modulation (ADM) arrangement, where usually the most recent signal sample or a linear combination of the last few samples is used to form an estimate of the current one. Then their difference signal, the so-called prediction residual, is computed and encoded usually with a reduced number of bits, since it has a lower variance than the incoming signal. This estimation process is actually linear prediction with fixed coefficients. However, owing to the non-stationary statistics of speech, a fixed predictor cannot consistently characterise the changing spectral envelope of speech signals. Adaptive predictive coding (APC) schemes utilise, in general, two different time-varying predictors to describe speech signals more accurately. Namely, a so-called short-term predictor (STP) and a long-term predictor (LTP). During our further discourse we will show that the STP is utilised to model the speech spectral envelope, while the LTP is employed in order to model the line-spectrum-like fine-structure representing the voicing information due to quasi-periodic voiced speech.

All in all, time-domain waveform codecs treat the speech signal to be encoded as a full-band signal and attempt to map it into as close a replica of the input as possible. The difference amongst various coding schemes is in their degree and way of using prediction to reduce the variance of the signal to be encoded, so as to reduce the number of bits necessary to represent it.

1.3.1.2 Frequency-domain Waveform Coding

In frequency-domain waveform codecs the input signal undergoes a more or less accurate short-time spectral analysis. Clearly, the signal is split into a number of sub-bands, and the individual sub-band signals are then encoded by using different numbers of bits, to obey rate-distortion theory on the basis of their prominence. The various methods differ in their accuracies of spectral resolution and in the bit-allocation principle (fixed, adaptive, semi-adaptive). Two well-known representatives of this class are sub-band coding (SBC) and adaptive transform coding (ATC).

1.3.2 Vocoders

The philosophy of vocoders is based on our *a priori* knowledge about the way the speech signal to be encoded was generated at the signal source by a speaker, which was portrayed in Figure 1.1. The air compressed by the lungs excites the vocal cords in two typical modes. Namely, when generating voiced sounds they vibrate and generate a quasi-periodic speech wave form, while in the case of lower-energy unvoiced sounds they do not participate in the voice production and the source behaves similar to a noise generator. The excitation signal denoted by $E(z)$ in the z-domain is then filtered through the vocal apparatus, which behaves like a spectral shaping filter with a transfer function of $H(z) = 1/A(z)$ that is constituted by the spectral shaping action of the glotti, vocal tract, lip radiation characteristics, etc.

Accordingly, instead of attempting to produce a close replica of the input signal at output of the decoder, the appropriate set of source parameters is found, in order to characterise the input signal sufficiently closely for a given duration of time. First a decision must be made as to whether the current speech segment to be encoded is voiced or unvoiced. Then the corresponding source parameters must be specified. In the case of voiced sounds the source parameter is the time between periodic vocal tract excitation pulses, which is often referred to as the pitch p. In the case of unvoiced sounds the variance or power of the noise-like excitation must be determined. These parameters are quantised and transmitted to the decoder in order to synthesise a replica of the original signal.

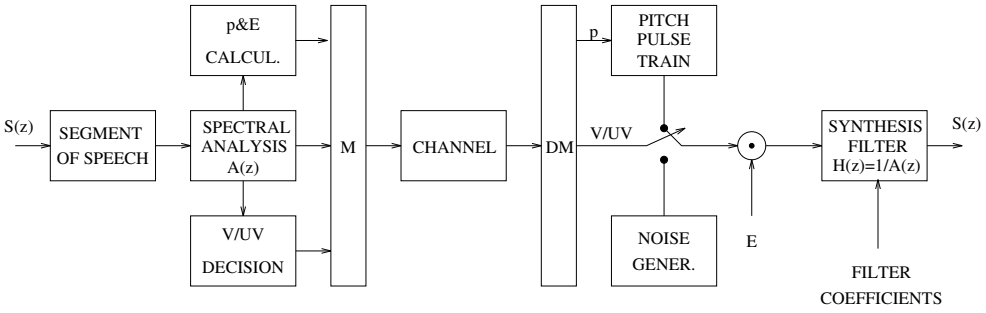

Figure 1.7: Vocoder schematic.

The simplest source codec arising from the above speech production model is depicted in Figure 1.7. The encoder is a simple speech analyser, determining the current source parameters. After initial speech segmentation it computes the linear predictive filter

coefficients a_i, $i = 1, \ldots, p$, which characterise the spectral shaping transfer function $H(z)$. A voiced/unvoiced decision is carried out and the corresponding pitch frequency and noise energy parameters are determined. These are then quantised, multiplexed and transmitted to the speech decoder, which is a speech synthesiser.

It is plausible that the associated speech quality of this type of system is predetermined by the adequacy of the source model, rather than by the accuracy of the quantisation of these parameters. This means that the speech quality of source codecs cannot simply be enhanced by increasing the accuracy of the quantisation, that is the bitrate, which is evidenced by the saturating MOS curve of Figure 1.6. Their speech quality is fundamentally limited by the fidelity of the model used. The main advantage of the above vocoding techniques is their low bitrate, with the penalty of relatively low, synthetic speech quality. A well-known representative of this class of vocoders is the 2400 bps American Military Standard LPC-10 codec.

In linear predictive coding (LPC) more complex excitation models are often used to describe the voice generating source. Once the vocal apparatus has been described with the help of its spectral domain transfer function $H(z)$, the central problem of coding is how to find the simplest adequate excitation for high-quality parametric speech representation. Strictly speaking this separable model represents a gross simplification of the vocal apparatus, but it provides the only practical approach to the problem. Vocoding techniques can also be categorised into frequency-domain and time domain sub-classes. However, frequency-domain vocoders are usually more effective than their time-domain counterparts.

1.3.3 Hybrid Coding

Hybrid coding methods constitute an attractive trade-off between waveform coding and source coding, both in terms of speech quality and transmission bitrate, although usually at the price of higher complexity. Every speech coding method, combining waveform and source coding methods in order to improve the speech quality and reduce the bitrate, falls into this broad category. However, adaptive predictive time-domain techniques used to describe the human spectral shaping tract combined with an accurate model of the excitation signal play the most prominent role in this category. The most important family of hybrid codecs, often referred to as *analysis-by-synthesis* (AbS) codecs, are ubiquitous at the time of writing and hence they will be treated in depth in a number of chapters after considering the conceptually more simple category of waveform codecs.

1.4 Waveform Coding [10]

1.4.1 Digitisation of Speech

The waveform coding of speech and video signals was comprehensively – in fact exhaustively – documented by Jayant and Noll in their classic monograph [10] and hence any treatise on the topic invariably follows a similar approach. Hence this section endeavours to provide a rudimentary overview of waveform coding following the spirit of Jayant and Noll [10]. In general, waveform codecs are designed to be signal independent. They are designed to map the input waveform of the encoder into a facsimile-like replica of it at the output of the decoder. Due to this advantageous property they can also encode secondary types of

information such as signalling tones, voice band data, or even music. Naturally, because of this transparency, their coding efficiency is usually quite modest. The coding efficiency can be improved by exploiting some statistical signal properties, if the codec parameters are optimised for the most likely categories of input signals, while still maintaining good quality for other types of signals.

The waveform codecs can be further subdivided into time-domain waveform codecs and frequency-domain waveform codecs. Let us initially consider the first category. The digitisation of analogue source signals, such as speech for example, requires the following steps, which are portrayed in Figure 1.8, while the corresponding waveforms are shown in Figure 1.9.

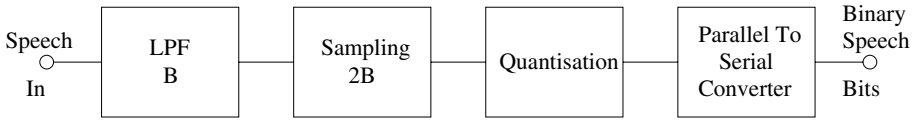

Figure 1.8: Digitisation of analogue speech signals.

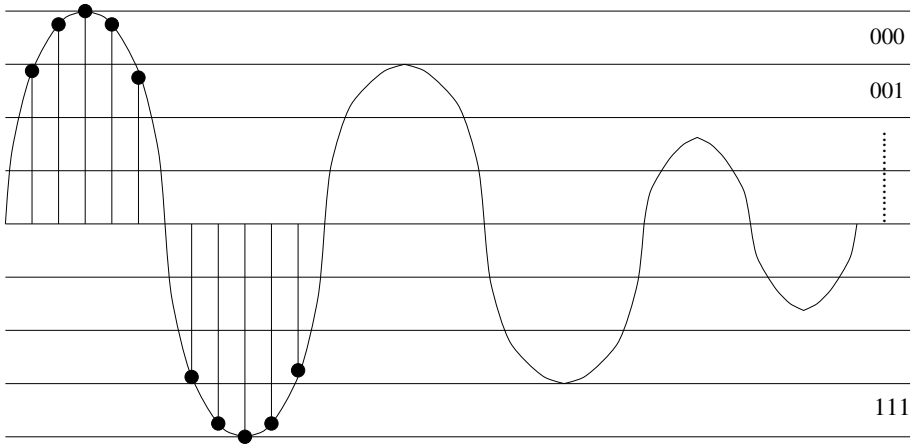

Figure 1.9: Sampled and quantised analogue speech signal.

- Anti-aliasing low-pass filtering (LPF) is necessary in order to bandlimit the signal to a bandwidth of B before sampling. In the case of speech signals about 1% of the energy resides above 4 kHz and only a negligible proportion above 7 kHz. Hence, so-called commentatory quality speech links, which are also often referred to as wideband speech systems, typically bandlimit the speech signal to 7–8 kHz. Conventional telephone systems usually employ a bandwidth limitation of 0.3–3.4 kHz, which results only in a minor speech degradation, hardly perceivable for the untrained listener.

- The bandlimited speech is sampled according to the Nyquist theorem, as seen in Figure 1.8, which requires a minimum sampling frequency of $f_{\text{Nyquist}} = 2 \cdot B$.

This process introduces time-discrete samples. Due to sampling, the original speech spectrum is replicated at multiples of the sampling frequency. This is why the previous bandlimitation was necessary, in order to prevent aliasing or frequency-domain overlapping of the spectral lobes. If this condition is met, the original analogue speech signal can be restored from its samples by passing the samples through a LPF having a bandwidth of B. In conventional speech systems, typically a sampling frequency of 8 kHz corresponding to a sampling interval of 125 μs is used.

- Lastly, amplitude discretisation or quantisation must be invoked, according to Figure 1.8, which requires an analogue-to-digital (A/D) converter. The out bits of the quantiser can be converted to a serial bitstream for transmission over digital links.

1.4.2 Quantisation Characteristics

It is clear from Figure 1.9 that the original speech signal is contaminated during the quantisation process by quantisation noise, which will be the subject of this section. The severity of contamination is a function of the signal's distribution, the quantiser's resolution and its transfer characteristic.

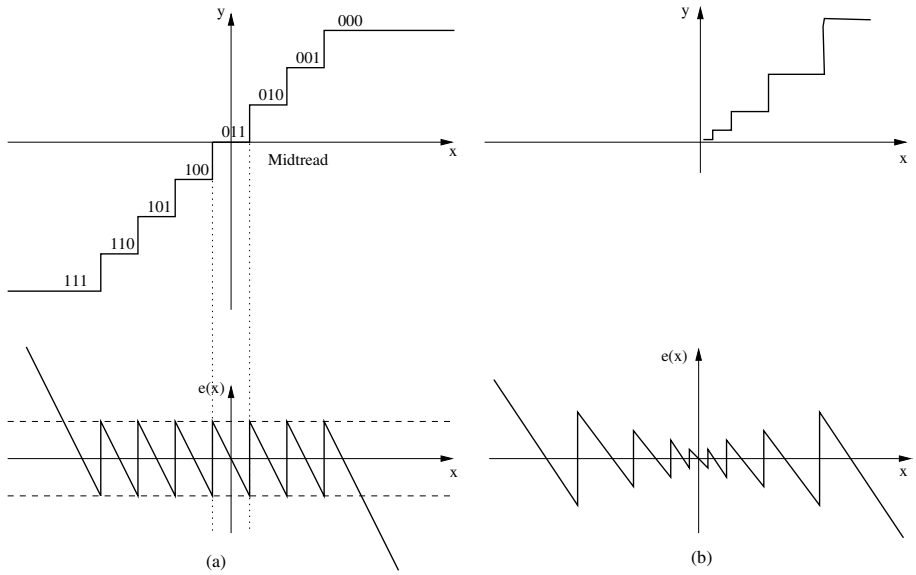

Figure 1.10: Linear quantisers and their quantisation errors: (a) midtread, (b) non-uniform.

The family of *linear quantisers* exhibits a linear transfer function within its dynamic range and saturation above that. They divide the input signal's dynamic range into a number of uniformly or non-uniformly spaced quantisation intervals, as seen in Figure 1.10, and assign an R-bit word to each so-called *reconstruction level*, which represent the legitimate output values. In Figure 1.10 according to $R = 3$ there are $2^3 = 8$ reconstruction levels which are labelled as 000, 001, -111 and a so-called *mid-tread quantiser* is featured, where the

quantiser's output is zero, if the input signal is zero. In the case of the so-called *mid-riser quantiser* the transfer function exhibits a level change at the abscissa value of zero. Note that the quantisation error characteristic of the quantisers is also shown in Figure 1.10. As expected, when the quantiser characteristic saturates at its maximum output level, the quantisation error increases without limit.

The difference between the *uniform* and *non-uniform quantiser* characteristics in Figure 1.10 is that the uniform quantiser maintains a constant maximum error across its total dynamic range, whereas the non-uniform quantiser employs unequal quantisation intervals (quantiles), in order to allow larger granular error, where the input signal is larger. Hence the non-uniform quantiser exhibits a near-constant SNR across its dynamic range. This may allow us to reduce the number of quantisation bits and the required transmission rate, while maintaining perceptually unimpaired speech quality.

In summary, linear quantisers are conceptually and implementationally simple and impose no restrictions on the analogue input signal's statistical characteristics, such as the PDF, etc. Clearly, they do not require *a priori* knowledge concerning the input signal. Note, however, that other PDF-dependent quantisers perform better in terms of overall quantisation noise power or SNR. These issues will be made more explicit during our further discourse.

1.4.3 Quantisation Noise and Rate-distortion Theory

Observe in Figure 1.10 that the instantaneous *quantisation error* $e(x)$ is dependent on the instantaneous input signal level. In other words, $e(x)$ is non-uniform across the quantiser's dynamic range and some amplitudes are represented without quantisation error, if they happen to be on a reconstruction level, while others are associated with larger errors. If the input signal's dynamic range exceeds the quantiser's linear range, the quantiser's output voltage saturates at its maximum level and the quantisation error may become arbitrarily high. Hence the knowledge of the input signal's statistical distribution is important for minimising the overall *granular* and *overload distortion*. The quantised version $\hat{x}(t)$ of the input signal $x(t)$ can be computed as

$$\hat{x}(t) = x(t) + e(t), \tag{1.1}$$

where $e(t)$ is the quantisation error.

It is plausible that if no amplitude discretisation is used for a source signal, a sampled analogue source has formally an infinite entropy, requiring an infinite transmission rate, which is underpinned by the formal application of Equation (1.2). If the analogue speech samples are quantised to R-bit accuracy, there are $q = 2^R$ different legitimate samples, each of which has a probability of occurrence $p_i, i = 1, 2, \ldots, q$. It is known from information theory that the above mentioned R bit/symbol channel capacity requirement can be further reduced using so-called entropy coding to the value of the source's entropy given by

$$H(x) = -\sum_{i=1}^{q} p_i \cdot \log_2 p_i, \tag{1.2}$$

without inflicting any further coding impairment, if an infinite delay entropy-coding scheme is acceptable. Since this is not the case in interactive speech conversations, we are more interested in quantifying the coding distortion, when using R bits per speech sample.

An important general result of information theory is the so-called *rate-distortion theorem*, which quantifies the minimum required average bitrate R_D in terms of [bpsample] in order to represent a random variable (rv) with less than D distortion. Explicitly, for a rv x with variance of σ_x^2 and quantised value $\hat{x}$ the distortion is defined as the mean squared error (MSE) expression given by

$$D = E\{(x - \hat{x})^2\} = E\{e^2(t)\}, \tag{1.3}$$

where E represents the expected value.

Observe that if $R_D = 0$ bits are used to quantise the quantity x, then the distortion is given by the signal's variance $D = \sigma_x^2$. If, however, more than zero bits are used, i.e. $R_D > 0$, then intuitively one additional bit is needed every time we want to halve the root mean squared (RMS) value of 'D', or quadruple the signal-to-noise ratio of $\mathrm{SNR} = \sigma_x^2/D$, which suggests a logarithmic relation between R_D and D. After Shannon and Gallager we can write

$$R_D = \frac{1}{2} \log_2 \frac{\sigma_x^2}{D} \quad \text{if } D \leq \sigma_x^2. \tag{1.4}$$

Upon combining $R_D = 0$ and $R_D > 0$ into one equation we arrive at

$$R_D = \begin{cases} \frac{1}{2} \log_2 \sigma_x^2/D & D < \sigma_x^2 \\ 0 & D \geq \sigma_x^2. \end{cases} \tag{1.5}$$

The qualitative or stylised relationship of D versus R_D inferred from Equation (1.5) is shown in Figure 1.11.

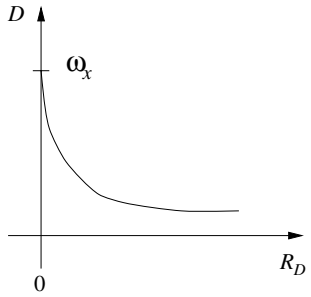

Figure 1.11: Stylised distortion (D) versus coding rate (R_D) curve.

In order to quantify the variance of the quantisation error it is reasonable to assume that if the quantisation interval q is small and no quantiser overload is incurred, then $e(t)$ is uniformly distributed in the interval $[-q/2, q/2]$. If the quantiser's linear dynamic range is limited to $[\pm V]$, then for a uniform quantiser the quantisation interval can be expressed with $q = 2V/2^{R_D}$, where R_D is the number of quantisation bits. The quantisation error variance can then be computed by squaring the instantaneous error magnitude e and weighting its contribution with its probability of occurrence expressed with the help of its PDF $p(e) = 1/q$

and finally integrating or averaging it over the range of $[-q/2, q/2]$ as follows:

$$\sigma_e^2 = \int_{-q/2}^{q/2} e^2 p(e)\,\mathrm{d}e = \int_{-q/2}^{q/2} e^2 \frac{1}{q}\,\mathrm{d}e$$
$$= \frac{1}{q}\left[\frac{e^3}{3}\right]_{-q/2}^{q/2} = \left(\frac{q^3}{8}\left(+\frac{q^3}{8}\right)\cdot 1/3q\right) = \frac{q^2}{12}, \tag{1.6}$$

which corresponds to an RMS quantiser noise of $q/\sqrt{12} \approx 0.3q$. In the case of uniform quantisers we can substitute $q = 2V/2^{R_D}$ into Equation (1.6) – where R_D is the number of bits used for encoding – giving the noise variance in the following form:

$$\sigma_q^2 = \frac{q^2}{12} = \frac{1}{12}\left(\frac{2V}{2_D^R}\right)^2 = \frac{1}{3}\frac{V^2}{2^{2R_D}}. \tag{1.7}$$

Similarly, assuming a *uniform signal PDF*, the signal's variance becomes

$$\sigma_x^2 = \int_{-\infty}^{\infty} x^2 p(x)\,\mathrm{d}x = \int_{-\infty}^{\infty} x^2 \frac{1}{2V}\,\mathrm{d}x = \frac{1}{2V}\left[\frac{x^3}{3}\right]_{-V}^{V} = \frac{1}{6E}\cdot 2V^3 = \frac{E^2}{3}. \tag{1.8}$$

Then the SNR can be computed as

$$\mathrm{SNR} = \frac{\sigma_x^2}{\sigma_q^2} = \frac{V^2}{3}\cdot\frac{2^{2R_D}}{V^2}\cdot 3 = 2^{2R_D}, \tag{1.9}$$

which can be expressed in terms of dB as

$$\mathrm{SNR}_{\mathrm{dB}} = 10\cdot\log_{10} 2^{2R} = 20R_D\cdot\log_{10} 2$$
$$\mathrm{SNR}_{\mathrm{dB}} \approx 6.02\cdot R_D\ [\mathrm{dB}]. \tag{1.10}$$

This simple result is useful for quick SNR estimates and it is also intuitively plausible, since every new bit used halves the quantisation error and hence doubles the SNR. In practice the speech PDF is highly non-uniform and hence the quantiser's dynamic range cannot be fully exploited in order to minimise the probability of quantiser characteristic overload error. Hence Equation (1.10) over-estimates the expected SNR.

1.4.4 Non-uniform Quantisation for a known PDF: Companding

If the input signal's PDF is known and can be considered stationary, higher SNR can be achieved by appropriately matched *non-uniform quantisation* (NUQ) than in the case of uniform quantisers. The input signal's dynamic range is partitioned into non-uniformly spaced segments as we have seen in Figure 1.10, where the quantisation intervals are more dense near the origin, in order to quantise the typically high-probability low-magnitude samples more accurately. In contrast, the lower-probability signal PDF tails are less accurately quantised. In contrast to uniform quantisation, where the maximum error was constant across

the quantiser's dynamic range, for non-uniform quantisers the SNR becomes more or less constant across the signal's dynamic range.

It is intuitively advantageous to render the width of the quantisation intervals or *quantiles* inversely proportional to the signal PDF, since a larger quantisation error is affordable in the case of infrequent signal samples and *vice versa*. Two different approaches have been proposed, for example, by Jayant and Noll [10] in order to minimise the total quantisation distortion in the case of non-uniform signal PDFs.

One of the possible system models is shown in Figure 1.12, where the input signal is first compressed using a so-called *nonlinear compander* characteristic and then uniformly quantised. The original signal can be recovered using an expander at the decoder, which exhibits an inverse characteristic with respect to that of the compander. This approach will be considered first, while the design of the minimum mean squared error (mmse) non-uniform quantiser using the so-called Lloyd–Max [60–62] algorithm will be portrayed during our further discussions.

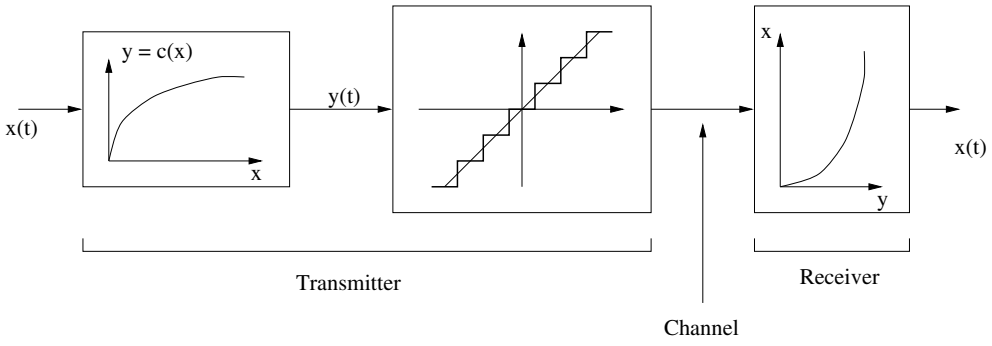

Figure 1.12: Stylised non-uniform quantiser model using companding, when the input signal's PDF is known.

The qualitative effect of nonlinear compression on the signal's PDF is portrayed in Figure 1.13, where it becomes explicit why the compressed PDF can be quantised by a uniform quantiser. Observe that the compander has a more gentle slope, where larger quantisation intervals are expected in the uncompressed signal's amplitude range and *vice versa*, implying that the compander's slope is proportional to the quantisation interval density and inversely proportional to the stepsize for any given input signal amplitude.

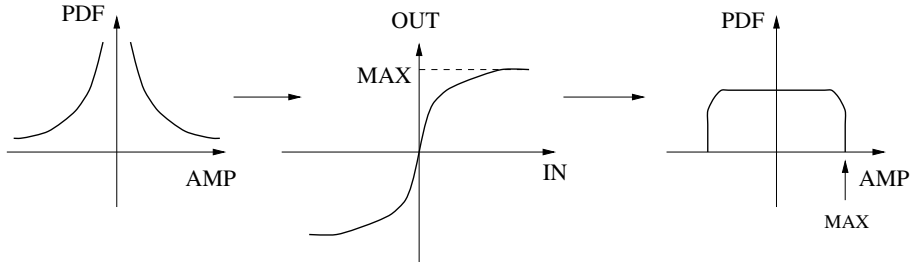

Figure 1.13: Qualitative effect of companding on a known input signal PDF shape.

Following Bennett's approach [63], Jayant and Noll [10] have shown that if the signal's PDF $p(x)$ is a smooth, known function and sufficiently fine quantisation is used – implying that $R \geq 6$ – then the quantisation error variance can be expressed as

$$\sigma_q^2 \approx \frac{q^2}{12} \int_{-x_{\max}}^{x_{\max}} \frac{p(x)}{|\dot{C}(x)|^2} \, \mathrm{d}x, \tag{1.11}$$

where $\dot{C}(x) = \mathrm{d}C(x)/\mathrm{d}x$ represents the slope of the compander's characteristic. It is instructive to note that where the input signal's PDF $p(x)$ is high, the σ_q^2 contributions are also high due to the high probability of occurrence of such signal amplitudes. This effect can be mitigated using a compander exhibiting a high gradient in this interval, since the factor $1/|\dot{C}(x)|^2$ de-weights the error contributions due to the highly peaked PDF near the origin. For an optimum compander characteristic $C(x)$ all quantiles give the same distortion contribution.

Jayant and Noll [10] have also shown that the minimum quantisation error variance is achieved by the compander characteristic given by

$$C(x) = x_{\max} \frac{\int_0^x \sqrt[3]{p(x)} \, \mathrm{d}x}{\int_0^{x_{\max}} \sqrt[3]{p(x)} \, \mathrm{d}x}, \tag{1.12}$$

where the denominator constitutes a normalising factor. Hence a simple practical compander design algorithm can be devised by evaluating the signal's histogram in order to estimate the PDF $p(x)$ and by graphically integrating $\sqrt[3]{p(x)}$ according to Equation (1.12) up to the abscissa value x, yielding the companding characteristic at the ordinate value $C(x)$, yielding the companding characteristic ordinate value $C(x)$.

Although this technique minimises the quantisation error variance or maximises the SNR in the case of a known signal PDF, if the input signal's PDF or variance is time-variant, the compander's performance degrades. In many practical scenarios this is the case and hence often it is advantageous to optimise the compander's characteristic to maximise the SNR independently of the shape of the PDF. Then no compander mismatch penalty is incurred. In order to achieve this, the quantisation error variance σ_e must be rendered proportional to the value of the input signal $x(t)$ across its dynamic range, implying that large signal samples will have larger quantisation error than small samples. This issue is the topic of the next section.

1.4.5 PDF-independent Quantisation using Logarithmic Compression

The input signal's variance is given in the case of an arbitrary PDF $p(x)$ as

$$\sigma_x^2 = \int_{-\infty}^{\infty} x^2 p(x) \, \mathrm{d}x. \tag{1.13}$$

Assuming zero saturation distortion, the SNR can be expressed from Equations (1.11) and (1.13) as

$$\mathrm{SNR} = \frac{\sigma_x^2}{\sigma_q^2} = \frac{\int_{-x_{\max}}^{x_{\max}} x^2 p(x) \, \mathrm{d}x}{\frac{q^2}{12} \int_{-x_{\max}}^{x_{\max}} (p(x)/|\dot{C}(x)|^2) \, \mathrm{d}x}. \tag{1.14}$$

In order to maintain an SNR value that is independent of the signal's PDF $p(x)$ the numerator of Equation (1.14) must be a constant times the denominator, which is equivalent to requiring that

$$|\dot{C}(x)|^2 \stackrel{!}{=} \left|\frac{K}{x}\right|^2, \tag{1.15}$$

or alternatively that

$$\dot{C}(x) = K/x \tag{1.16}$$

and hence

$$C(x) = \int_0^x \frac{K}{z}\,\mathrm{d}z = K \cdot \ln x + A. \tag{1.17}$$

This compander characteristic is shown in Figure 1.14(a) and it ensures a constant SNR across the signal's dynamic range, irrespective of the shape of the signal's PDF. Intuitively, large signals can have large errors, while small signal must maintain a low distortion, which gives a constant SNR for different input signal levels.

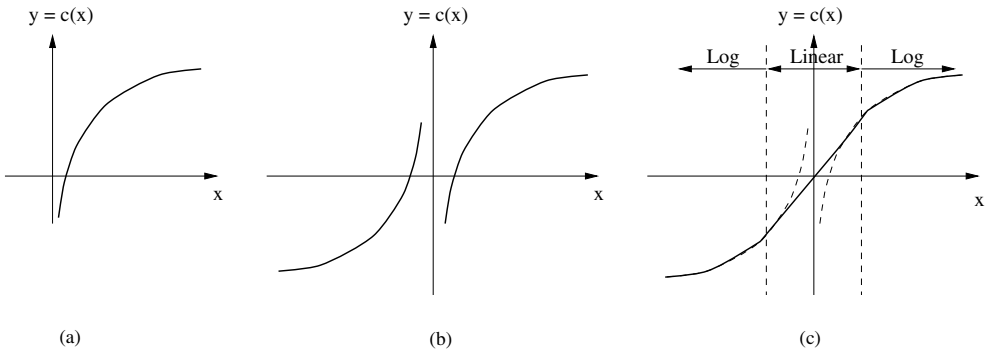

Figure 1.14: Stylised companding characteristic for a near-optimal quantiser.

Jayant and Noll also note that the constant A in Equation (1.17) allows for a vertical compander characteristic shift in order to satisfy the boundary condition of matching $x_{\max}$ and $y_{\max}$, yielding $y = y_{\max}$, when $x = x_{\max}$. Explicitly:

$$y_{\max} = C(x_{\max}) = K \cdot \ln x_{\max} + A. \tag{1.18}$$

Upon normalising Equation (1.17) to $y_{\max}$ we arrive at

$$\frac{y}{y_{\max}} = \frac{C(x)}{y_{\max}} = \frac{K \cdot \ln x + A}{K \cdot \ln x_{\max} + A}. \tag{1.19}$$

It is convenient to introduce an arbitrary constant B, in order to be able to express A as $A = K \cdot \ln B$, since then Equation (1.19) can be written as

$$\frac{y}{y_{\max}} = \frac{K \cdot \ln x + K \cdot \ln B}{K \cdot \ln x_{\max} + K \cdot \ln B} = \frac{\ln xB}{\ln x_{\max}B}. \tag{1.20}$$

Equation (1.20) can be further simplified upon rendering its denominator unity by stipulating $x_{\max} \cdot B = e^1$, which yields $B = e/x_{\max}$. Then Equation (1.20) simplifies to

$$\frac{y}{y_{\max}} = \frac{\ln xe/x_{\max}}{\ln e} = \ln\left(\frac{e \cdot x}{x_{\max}}\right), \tag{1.21}$$

which now gives $y = y_{\max}$, when $x = x_{\max}$. This logarithmic characteristic, which is shown in Figure 1.14(a), must be rendered symmetric with respect to the y-axis, which we achieve upon introducing the $\text{signum}(x) = \text{sgn}(x)$ function:

$$\frac{y}{y_{\max}} = \frac{C(x)}{y_{\max}} = \ln\left(\frac{e \cdot |x|}{x_{\max}}\right) \text{sgn}(x). \tag{1.22}$$

This symmetric function is displayed in Figure 1.14(b). However, a further problem is that the logarithmic function is non-continuous at zero. Hence around zero amplitude a linear section is introduced in order to ensure a seamless positive–negative transition in the compression characteristic.

Two practical logarithmic compander characteristics have emerged, which satisfy the above requirements. In the US the so-called μ-law compander was standardised [64–66], while in Europe the A-law compander was proposed [4]. The corresponding stylised logarithmic compander characteristic is depicted in Figure 1.14(c). Let us now consider the standard μ-law compander.

1.4.5.1 The μ-law Compander

This companding characteristic is given by

$$y = C(x) = y_{\max} \cdot \frac{\ln[1 + \mu \cdot (|x|/x_{\max})]}{\ln(1 + \mu)} \cdot \text{sgn}(x). \tag{1.23}$$

Upon inferring from the $\log(1 + z)$ function that

$$\log(1 + z) \approx z \text{ if } z \ll 1, \tag{1.24}$$

in the case of small and large signals, respectively, we have from Equation (1.23) that

$$y = C(x) = \begin{cases} y_{\max} \cdot \dfrac{\mu \cdot (|x|/x_{\max})}{\ln \mu} & \text{if } \mu \cdot \left(\dfrac{|x|}{x_{\max}}\right) \ll 1 \\ y_{\max} \cdot \dfrac{\ln[\mu \cdot (|x|/x_{\max})]}{\ln \mu} & \text{if } \mu \cdot \left(\dfrac{|x|}{x_{\max}}\right) \gg 1, \end{cases} \tag{1.25}$$

which is a linear function of the normalised input signal $x/x_{\max}$ for small signals and a logarithmic function for large signals. The $\mu \cdot |x|/x_{\max} = 1$ value can be considered to be the break-point between the small and large signal operation and the $|x| = x_{\max}/\mu$ is the corresponding abscissa value. In order to emphasise the logarithmic nature of the characteristic, μ must be large, which reduces the abscissa value of the beginning of the logarithmic section. It is plausible that the optimum value of μ is dependent on the quantiser

resolution R and for $R = 8$ the American standard so-called *pulse code modulation* (PCM) speech transmission system recommends $\mu = 255$.

Following the approach proposed by Jayant and Noll [10], the SNR of the μ-law compander can be derived upon substituting $y = C_\mu(x)$ from Equation (1.23) into the general SNR formula of Equation (1.14):

$$y = C_\mu(x) = y_{\max} \cdot \frac{\ln[1 + \mu(|x|/x_{\max})]}{\ln(1 + \mu)} \cdot \mathrm{sgn}(x) \tag{1.26}$$

$$\dot{C}_\mu(x) = \frac{y_{\max}}{\ln(1 + \mu)} \cdot \frac{1}{1 + \mu(|x|/x_{\max})} \cdot \mu \left(\frac{1}{x_{\max}}\right). \tag{1.27}$$

For large input signals we have $\mu(|x|/x_{\max}) \gg 1$, and hence

$$\dot{C}_\mu(x) \approx \frac{y_{\max}}{\ln \mu} \cdot \frac{1}{x}. \tag{1.28}$$

Upon substituting

$$\frac{1}{\dot{C}_\mu(x)} = \frac{\ln \mu}{y_{\max}} \cdot x \tag{1.29}$$

in Equation (1.14) we arrive at

$$\begin{aligned} \mathrm{SNR} &= \frac{\int_{-x_{\max}}^{x_{\max}} x^2 p(x)\, \mathrm{d}x}{(q^2/12) \int_{-x_{\max}}^{x_{\max}} (\ln \mu / y_{\max})^2 x^2 p(x)\, \mathrm{d}x} \\ &= \frac{1}{(q^2/12)(\ln \mu / y_{\max})^2} = 3 \left(\frac{2y_{\max}}{q}\right)^2 \cdot \left(\frac{1}{\ln \mu}\right)^2 \\ &= 3 \cdot 2^{2R} \cdot \left(\frac{1}{\ln \mu}\right)^2. \end{aligned} \tag{1.30}$$

Upon exploiting the fact that $2y_{\max}/q = 2^R$ represents the number of quantisation levels and expressing the above equation in terms of dB we get

$$\mathrm{SNR}_{\mathrm{dB}}^{\mu} = 6.02 \cdot R + 4.77 - 20 \log_{10}(\ln(1 + \mu)), \tag{1.31}$$

which gives an SNR of about 38 dB in the case of the American standard system using $R = 8$ and $\mu = 255$. Recall that under the assumption of no quantiser characteristic overload and a uniformly distributed input signal the corresponding SNR estimate would yield $6.02 \cdot 8 \approx 48$ dB. Note, however, that in practical terms this SNR is never achieved, since the input signal does not have a uniform distribution and saturation distortion is also often incurred.

1.4.5.2 The *A*-law Compander

Another practical logarithmic compander characteristic is the *A-Law Compander* [4] given below, which was standardised by the CCITT or ITU and which is used throughout Europe:

$$y = C(x) = \begin{cases} y_{\max} \cdot \dfrac{A(|x|/x_{\max})}{1+\ln A} \cdot \mathrm{sgn}(x) & 0 < \dfrac{|x|}{x_{\max}} < \dfrac{1}{A} \\ y_{\max} \cdot \dfrac{1+\ln[A(|x|/x_{\max})]}{1+\ln A} \cdot \mathrm{sgn}(x) & \dfrac{1}{A} < \dfrac{|x|}{x_{\max}} < 1, \end{cases} \tag{1.32}$$

where $A = 87.56$. Similar to the μ-law characteristic, it has a linear region near the origin and a logarithmic section above the break-point $|x| = x_{\max}/A$. Note, however, that in the case of $R = 8$ bits $A < \mu$, hence the A-law characteristic's linear–logarithmic break-point is at a higher input value than that of the μ-law characteristic.

Again, substituting

$$\frac{1}{\dot{C}_A(x)} = \frac{(1+\ln A)}{y_{\max}} \cdot x \tag{1.33}$$

into Equation (1.14) and exploiting the fact that $2y_{\max}/q = 2^R$ represents the number of quantisation levels, we have

$$\begin{aligned} \mathrm{SNR} &= \frac{\int_{-x_{\max}}^{x_{\max}} x^2 p(x)\,\mathrm{d}x}{(q^2/12)\int_{-x_{\max}}^{x_{\max}} ((1+\ln A)/y_{\max})^2 x^2 p(x)\,\mathrm{d}x} \\ &= \frac{1}{(q^2/12)((1+\ln A)/y_{\max})^2} = 3\left(\frac{2y_{\max}}{q}\right)^2 \cdot \left(\frac{1}{(1+\ln A)}\right)^2 \\ &= 3 \cdot 2^{2R} \cdot \left(\frac{1}{(1+\ln A)}\right)^2. \end{aligned} \tag{1.34}$$

Upon expressing the above equation in terms of dB we arrive at

$$\mathrm{SNR}_{\mathrm{dB}}^{A} = 6.02 \cdot R + 4.77 - 20\log_{10}(1+\ln A), \tag{1.35}$$

which, similar to the μ-law compander, gives an SNR of about 38 dB in the case of the European standard PCM speech transmission system using $R = 8$ and $A = 87.56$.

Further features of the European A-law standard system are that the characteristic given by Equation (1.32) is implemented in the form of a 16-segment piece-wise linear approximation, as seen in Figure 1.15. The segment retaining the lowest gradient of $1/4$ is at the top end of the input signal's dynamic range, which covers half of the positive dynamic range and it is divided into 16 uniformly spaced quantisation intervals. The second segment from the top covers a quarter of the positive dynamic range and doubles the top segment's steepness or gradient to $1/2$, etc. The bottom segment covers a 64th of the positive dynamic range, has the highest slope of 16 and the finest resolution. The first bit of each $R = 8$-bit PCM codeword represents the sign of the input signal, the next three bits specify which segment the input signal belongs to, while the last four bits divide a specific segment into 16 uniform-width quantisation intervals, as shown below:

$$\underbrace{b_7}_{\substack{\text{sign} \\ \text{(segment)}}} \quad \underbrace{b_6\ b_5\ b_4}_{\text{segments}} \quad \underbrace{b_3\ b_2\ b_1\ b_0}_{\substack{\text{uniform quant.} \\ \text{in each segment}}}$$

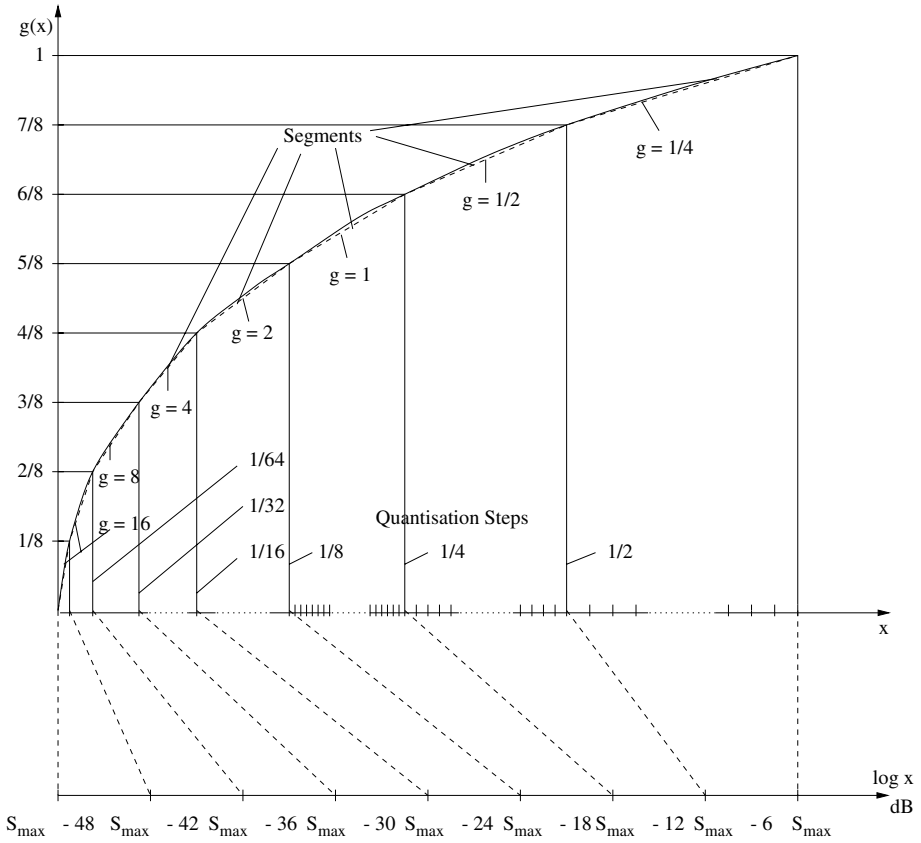

Figure 1.15: Stylised European A-law PCM standard characteristic.

This scheme was standardised by the *International Telegraph and Telephone Consultative Committee (CCITT)* as the G.711 Recommendation for the transmission of speech sampled at 8 kHz. Hence the transmission rate becomes $8 \times 8 = 64$ kbps (kbps). This results in perceptually unimpaired speech quality, which would require about 12 bits in the case of linear quantisation.

1.4.6 Optimum Non-uniform Quantisation

For non-uniform quantisers the quantisation error variance is given by

$$\sigma_q^2 = E\{|x - x_q|^2\} = \int_{-\infty}^{\infty} e^2(x) p(x)\, \mathrm{d}x, \tag{1.36}$$

which, again, corresponds to weighting and averaging the quantisation error energy over its magnitude range. Assuming an odd-symmetric quantiser transfer function and symmetric

PDF $p(x)$, the total quantisation distortion power σ_D^2 is

$$\sigma_D^2 = 2 \int_0^\infty e^2(x) p(x)\, \mathrm{d}x. \tag{1.37}$$

The total distortion can be expressed as the sum of the quantisation distortion in the quantiser's linear range, plus the saturation distortion in its nonlinear range

$$\sigma_D^2 = \underbrace{2 \int_0^V e^2(x) p(x)\, \mathrm{d}x}_{\sigma_q^2\text{: linear region}} + \underbrace{2 \int_V^\infty e^2(x) p(x)\, \mathrm{d}x}_{\sigma_s^2\text{: nonlinear region}} \tag{1.38}$$

or more simply as

$$\sigma_D^2 = \sigma_q^2 + \sigma_s^2. \tag{1.39}$$

In order to emphasise the fact that in the case of non-uniform quantisation each of the N quantisation intervals or so-called quantiles adds a different PDF-weighted contribution to the total quantisation distortion, we re-write the first term of Equation (1.38) as

$$\begin{aligned} \sigma_q^2 &= \sum_{n=1}^{N} \int_{x_n}^{x_{n+1}} e^2(x) p(x)\, \mathrm{d}x \\ &= \sum_{n=1}^{N} \int_{x_n}^{x_{n+1}} (x - x_q)^2 p(x)\, \mathrm{d}x \qquad (1.40) \\ &= \sum_{n=1}^{N} \int_{x_n}^{x_{n+1}} (x - r_n)^2 p(x)\, \mathrm{d}x, \qquad (1.41) \end{aligned}$$

where $x_q = r_n$ represents the so-called reconstruction levels.

Given a certain number of quantisation bits R and the PDF of the input signal, the optimum Lloyd–Max quantiser, which was independently invented by Lloyd [60, 61] and Max [62], determines the set of optimum quantiser decision levels and the corresponding set of quantisation levels.

Jayant and Noll [10] have provided a detailed discussion on two different methods of determining the mmse solution to the problem. One of the solutions is based on an iterative technique of rearranging the decision thresholds and reconstruction levels, while the other one is an approximate solution valid for fine quantisers using a high number of bits per sample. We first present the general approach to minimising the MSE by determining the set of optimum reconstruction levels r_n, $n = 1, \ldots, N$, and the corresponding decision threshold values t_n, $n = 1, \ldots, N$.

In general, it is a necessary but not sufficient condition for finding the global minimum of Equation (1.41) for its partial derivatives to become zero. However, if the PDF $p(s)$ is log-concave, that is the second derivative of its logarithm is negative, then the minimum found is a global one. For the frequently encountered uniform (U), Gaussian (G) and Laplacian (L) PDFs the log-concave condition is satisfied but, for example, for Gamma (Γ) PDFs is not.

Setting the partial derivatives of Equation (1.41) with respect to a specific r_n to zero, there is only one term in the sum which depends on the r_n value considered, hence we arrive at

$$\frac{\partial \sigma_q^2}{\partial r_n} = 2 \int_{t_n}^{t_{n+1}} (s - r_n) \cdot p(s)\, \mathrm{d}s = 0, \quad n = 1, \ldots, N, \tag{1.42}$$

which leads to

$$\int_{t_n^{\mathrm{opt}}}^{t_{n+1}^{\mathrm{opt}}} s \cdot p(s)\, \mathrm{d}s = r_n \int_{t_n^{\mathrm{opt}}}^{t_{n+1}^{\mathrm{opt}}} p(s)\, \mathrm{d}s, \tag{1.43}$$

yielding the optimum reconstruction level r_n^{opt} as

$$r_n^{\mathrm{opt}} = \frac{\int_{t_n^{\mathrm{opt}}}^{t_{n+1}^{\mathrm{opt}}} s \cdot p(s)\, \mathrm{d}s}{\int_{t_n^{\mathrm{opt}}}^{t_{n+1}^{\mathrm{opt}}} p(s)\, \mathrm{d}s}, \quad n = 1, \ldots, N. \tag{1.44}$$

Note that the above expression depends on the optimum quantisation interval thresholds t_n^{opt} and t_{n+1}^{opt}. Furthermore, for an arbitrary non-uniform PDF r_n^{opt} is given by the mean value or the 'centre of gravity' of s within the quantisation interval n, rather than by $(t_n^{\mathrm{opt}} + t_{n+1}^{\mathrm{opt}})/2$.

Similarly, when computing $\partial \sigma_q^2 / \partial t_n$, there are only two terms in Equation (1.41), which contain t_n, therefore we get

$$\frac{\partial \sigma_q^2}{\partial t_n} = (t_n - r_{n-1})^2 p(t_n) - (t_n - r_n)^2 p(t_n) = 0, \tag{1.45}$$

leading to

$$t_n^2 - 2t_n r_{n-1} + r_{n-1}^2 - t_n^2 + 2t_n r_n - r_n^2 = 0. \tag{1.46}$$

Hence the optimum decision threshold is given by

$$t_n^{\mathrm{opt}} = (r_n^{\mathrm{opt}} + r_{n-1}^{\mathrm{opt}})/2, \quad n = 2, \ldots, N,\ t_1^{\mathrm{opt}} = -\infty,\ t_N^{\mathrm{opt}} = \infty \tag{1.47}$$

which is half-way between the optimum reconstruction levels. Since these nonlinear equations are interdependent, they can only be solved by recursive iterations, starting from either a uniform quantiser or from a 'hand-crafted' initial non-uniform quantiser design.

Since most practical signals do not obey any analytically describable distribution, the signal's PDF typically has to be inferred from a sufficiently large and characteristic training set. Equations (1.44) and (1.47) will also have to be evaluated numerically for the training set. Below we provide a simple practical algorithm which can be easily implemented by the coding practitioner with the help of the flowchart of Figure 1.16.

Step 1: Input initial parameters such as the number of quantisation bits R, maximum number of iterations I, dynamic range minimum t_1 and maximum t_N.

Step 2: Generate the initial set of thresholds $t_1^0, \ldots, t_N^0$, where the superscript '0' represents the iteration index, either automatically creating a uniform quantiser between t_1 and t_N according to the required number of bits R, or by inputting a 'hand-crafted' initial design.

Step 3: While $t < T$, where T is the total number of training samples do:

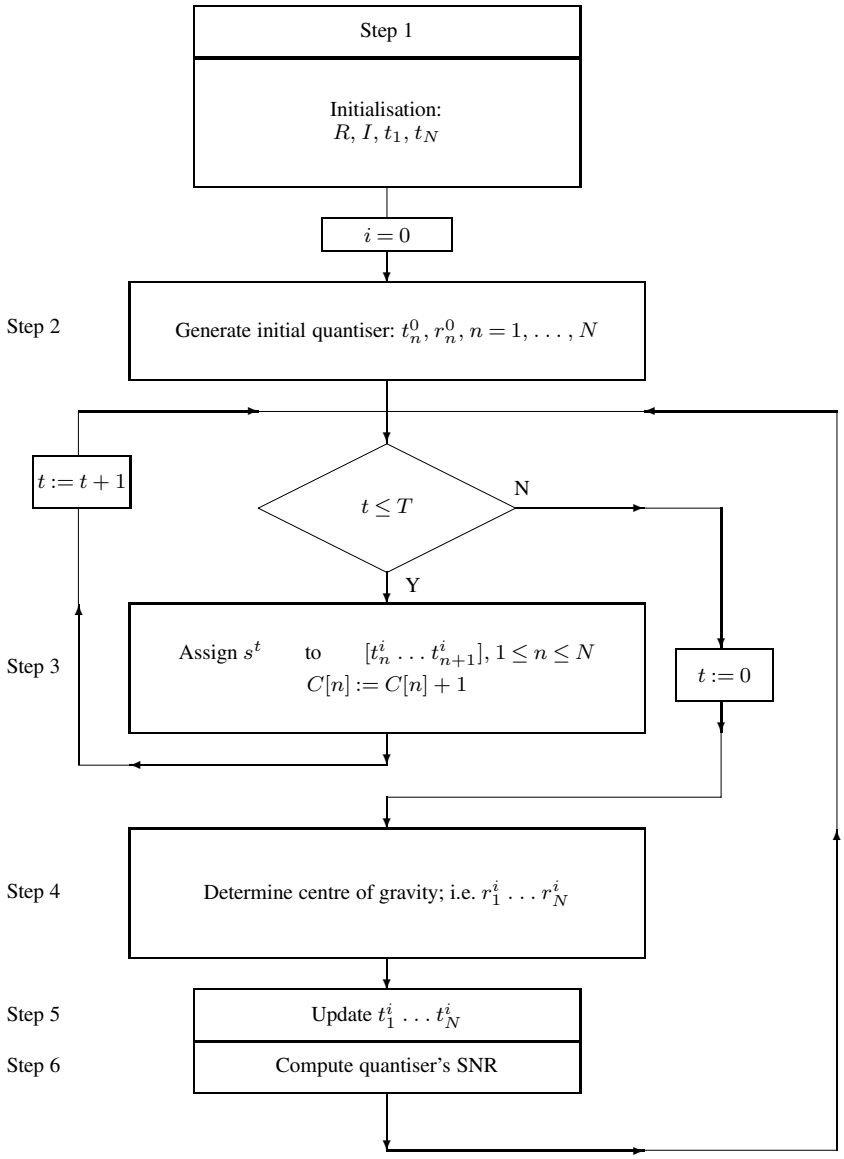

Figure 1.16: Lloyd–Max algorithm flowchart.

1. Assign the current training sample s^t, $t = 1, \ldots, T$ to the corresponding quantisation interval $[t_n^0 \ldots t_{n+1}^0]$ and increment the sample counter $C[n]$, $n = 1, \ldots, N$, holding the number of samples assigned to interval n. This corresponds to generating the histogram $p(s)$ of the training set.

2. Evaluate the MSE contribution due to assigning s^t to $\mathrm{bin}[n]$, that is $\mathrm{MSE}^t = (s^t - s_q^t)^2$ and the resultant total accumulated MSE, that is $\mathrm{MSE}^t = \mathrm{MSE}^{t-1} + \mathrm{MSE}^t$.

Step 4: Once all training samples have been assigned to their corresponding quantisation bins, that is the experimental PDF $p(s)$ is evaluated, the centre of gravity of each bin is computed by summing the training samples in each $\mathrm{bin}[n]$, $n = 1, \ldots, N$, and then dividing the sum by the number of training samples $C[n]$ in $\mathrm{bin}[n]$. This corresponds to the evaluation of Equation (1.44), yielding r_n.

Step 5: Rearrange the initial quantisation thresholds $t_1^0 \ldots t_N^0$ using Equation (1.47) by placing them half-way between the above computed initial reconstruction levels r_n^0, $n = 1, \ldots, N$, where again, the superscript '0' represents the iteration index. This step generates the updated set of quantisation thresholds $t_1^1 \ldots t_N^1$.

Step 6: Evaluate the performance of the current quantiser design in terms of

$$\mathrm{SNR} = 10 \log_{10} \left[\frac{\sum_{t=1}^{T} (s^t)^2}{\mathrm{MSE}^t} \right].$$

Recursion: Repeat Steps 3–6 by iteratively updating r_n^i, t_n^i for all bins $n = 1, \ldots, N$, until the iteration index i reaches its maximum I, while monitoring the quantiser SNR performance improvement given above.

Note that it is important to invoke the algorithm several times, while using a different initial quantiser, in order to ascertain its proper convergence to a global optimum. It is plausible from the inner workings of the algorithm that it will place the reconstruction levels and thresholds more sparsely, where the PDF $p(s)$ is low and *vice versa*. If the input signal's statistics obey a U, G, L or Γ distribution, the Lloyd–Max quantiser's SNR performance can be evaluated using Equations (1.44) and (1.47), and various authors have tabulated the achievable SNR values. Following Max [62], Noll and Zelinski [67] as well as Paez and Glisson [68], both Jayant and Noll [10] as well as Jain [69] collected these SNR values, which we have summarised in Table 1.1 for G and L distributions. Jayant and Noll [10] as well as Jain [69] also tabulated the corresponding t_n and r_n values for a variety of PDFs and R values.

Table 1.1: Maximum achievable SNR and MSE in the case of zero-mean, unit-variance input $[f(R)]$ for Gaussian (G) and Laplacian (L) PDFs for $R = 1, 2, \ldots, 7$. Copyright © Prentice Hall, Jayant-Noll [10] 1984, p. 135 and Jain [69] 1989, p. 104.

		$R=1$	$R=2$	$R=3$	$R=4$	$R=5$	$R=6$	$R=7$
G	SNR(dB)	4.40	9.30	14.62	20.22	26.01	31.89	37.81
	$f(R)$	0.3634	0.1175	0.0345	0.0095	0.0025	0.0006	0.0002
L	SNR(dB)	3.01	7.54	12.64	18.13	23.87	29.74	35.69
	$f(R)$	0.5	0.1762	0.0545	0.0154	0.0041	0.0011	0.0003

Note in Table 1.1 that apart from the achievable maximum SNR values the associated quantiser MSE $f(R)$ is also given as a function of the number of quantisation bits R. When designing a quantiser for an arbitrary non-unity input variance σ_s^2, the associated quantisation thresholds and reconstruction levels must be appropriately scaled by σ_s^2. It is plausible that in the case of a large input variance the reconstruction levels have to be sparsely spaced in

order to cater for the signal's expanded dynamic range. Hence the reconstruction MSE σ_q^2 must also be scaled by σ_s^2, giving

$$\sigma_q^2 = \sigma_s^2 \cdot f(R).$$

Here we curtail our discussion of *zero-memory quantisation* techniques, the interested reader is referred to the excellent in-depth reference [10] by Jayant and Noll for further details. Before we focus our attention on predictive coding techniques, the reader is reminded that in Section 1.2 we highlighted how redundancy is exhibited by both the time- and the frequency-domain features of the speech signal. In the next section we will endeavour to introduce a simple way of exploiting this redundancy in order to achieve better coding efficiency and reduce the required coding rate from 64 kbps to 32 kbps.

1.5 Chapter Summary

In this chapter we provided a rudimentary characterisation of voiced and unvoiced speech signals. It was shown that voice speech segments exhibit a quasi-periodic nature and convey significantly more energy than the more noise-like unvoiced segments. Due to their quasi-periodic nature voiced segments are more predictable, in other words they are more amenable to compression.

These discussions were followed by a brief introduction to the digitisation of speech and to basic waveform coding techniques. The basic principles of logarithmic compression were highlighted and the optimum non-uniform Lloyd–Max quantisation principle was introduced. In the next chapter we introduce the underlying principles of more efficient predictive speech coding techniques.

Chapter 2

Predictive Coding

2.1 Forward-Predictive Coding

In a simplistic but plausible approach one could argue that if the input signal is correlated, the previous sample can be used to predict the present one. If the signal is predictable, the so-called prediction error constituted by the difference of the current sample and the previous one is significantly smaller on average than the input signal. This reduces the region of uncertainty in which the signal to be quantised can reside, and whence allows us to use either a reduced number of quantisation bits or a better resolution in coding.

Clearly, redundancy reduction is achieved by subtracting the signal's predicted value from the current sample to be encoded and hence forming the so-called *prediction error*. We have shown in the previous section, how PCM employs a so-called *instantaneous* or *zero memory quantiser*. Differential pulse code modulation (DPCM) and other linear predictive codecs (LPC) exploit knowledge over the history of the signal and hence reduce its correlation, variance and, ultimately, the bitrate required for its quantisation. In a system context this will reduce the bandwidth required for a speech user and hence allow the system to support more users in a given bandwidth.

Recall that *redundancy* exhibits itself both in terms of the PSD and the ACF, as was demonstrated in Figures 1.2 and 1.4 in the case of voiced speech signals. The more flat the ACF, the more predictable the signal to be encoded and the more efficient its predictive encoding. This redundancy is also exhibited in terms of the non-flat PSD.

Let us now refine the above simple predictive approach based on the immediately preceding sample and consider the more general predictive coding schematic shown in Figure 2.1, where the predictor block generates a predicted sample $\tilde{x}(n)$ by some rule to be described at a later stage. This scheme is often referred to as a *forward-predictive* arrangement. If the input signal samples are represented by R-bit discrete values and an integer arithmetic is employed, where the quantiser is assumed to be simply a parallel to serial converter which does not introduce any quantisation impairment, then $s(n)$, $\tilde{s}(n)$ and $e(n) = e_q(n)$ are all represented by integer values. Since

$$e_q(n) = e(n) = s(n) - \tilde{s}(n), \tag{2.1}$$

Voice and Audio Compression for Wireless Communications Second Edition
L. Hanzo, F. C. A. Somerville and J. P. Woodard

we can generate the decoded speech $s_q(n) = s(n)$ with the help of the predictor at the decoder's end of the speech link by simply adding the quantised predicted value $\tilde{s}_q(n)$ to $e_q(n) = e(n)$ as follows:

$$s_q(n) = \tilde{s}_q(n) + e_q(n). \tag{2.2}$$

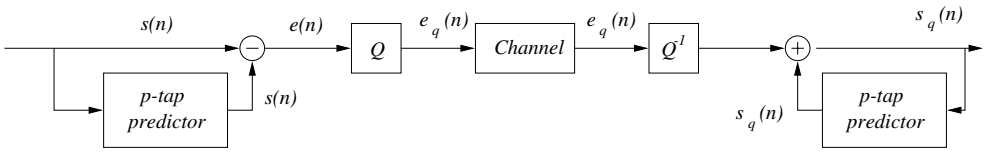

Figure 2.1: Block diagram of a forward-predictive codec using p-tap prediction.

2.2 DPCM Codec Schematic

Recall from the previous section that in our forward-predictive codec we assumed that no transmission errors occurred. It is plausible, however, that unfortunately the idealistic assumptions of Section 2.1 do not hold in the presence of transmission errors or if the quantiser introduces quantisation distortion, which is typically the case, if bitrate economy is an important factor. These problems can be circumvented by the *backward-predictive* scheme of Figure 2.2, where the input signal s_n is predicted on the basis of a backward oriented predictor. The operation of this arrangement will be the subject of our next section.

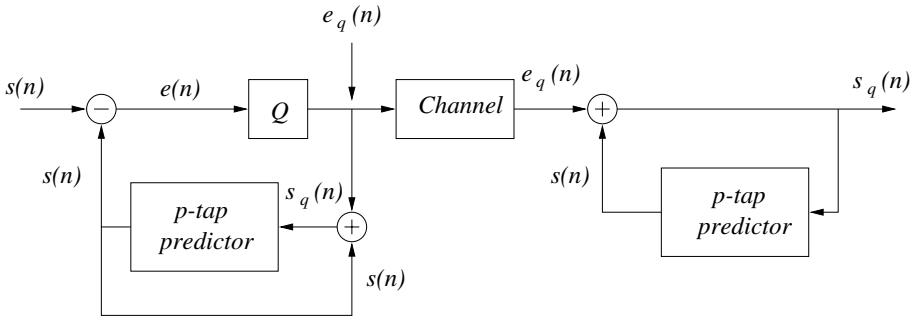

Figure 2.2: Block diagram of a DPCM codec using p-tap prediction.

Observe in Figure 2.2 that in contrast to the forward-predictive scheme of Figure 2.1 the input signal $s(n)$ is predicted not from the previous values of $s(n-k)$, $k = 1, \ldots, p$, but from

$$s_q(n) = \tilde{s}(n) + e_q(n). \tag{2.3}$$

Since the so-called locally re-constructed signal $s_q(n)$ is contaminated by the quantisation noise of $q(n) = e(n) - e_q(n)$ inherent in $e_q(n)$, one could argue that this prediction will be probably a less confident one than that based on $s(n-k),\ k = 1, \ldots, p$, which might affect the coding efficiency of the scheme. Observe, however, that the signal $s_q(n)$ is also available

at the decoder, irrespective of the accuracy of the quantiser's resolution. Although in the case of transmission errors this is not so, due to the codec's stabilising predictive feed-back loop the effect of transmission errors decays, while in the case of the forward-predictive scheme of Figure 2.1 the transmission errors persist. Observe in Figure 2.2 that the encoder's backward-oriented bottom section is identical to the decoder's schematic and therefore it is referred to as the *local decoder*. The local decoder is an important feature of most predictive codecs invoked, in order to be able to mitigate the effects of transmission errors. The output of the local decoder is the *locally re-constructed signal* $s_q(n)$.

The DPCM codec seen in Figure 2.2 is characterised by the following equations:

$$\begin{aligned} e(n) &= s(n) - \tilde{s}(n) \\ e_q(n) &= Q[e(n)] \\ s_q(n) &= \tilde{s}(n) + e_q(n). \end{aligned} \tag{2.4}$$

Since the variance of the prediction error $e(n)$ is typically lower than that of the signal $s(n)$, i.e. $\sigma_e < \sigma_s$, the bitrate required for the quantisation of $e(n)$ can be reduced, while maintaining an identical distortion or SNR value.

Following these rudimentary deliberations on redundancy removal using predictive coding, let us now focus our attention on the design of a general p-tap predictor.

2.3 Predictor Design

2.3.1 Problem Formulation

Due to the redundancy inherent in speech, any present sample can be predicted as a linear combination of p past speech samples as

$$\tilde{s}(n) = \sum_{k=1}^{p} a_k s(n-k), \tag{2.5}$$

where p is the predictor order, a_k represents the linear predictive filter coefficients and $\tilde{s}(n)$ the predicted speech samples. The prediction error, $e(n)$, is then given by

$$\begin{aligned} e(n) &= s(n) - \tilde{s}(n) \\ &= s(n) - \sum_{k=1}^{p} a_k s(n-k) \\ &= \sum_{k=0}^{p} a_k s(n-k) \quad \text{where } a_0 = 1. \end{aligned} \tag{2.6}$$

Upon taking the z-transform of Equation (2.6), we arrive at

$$E(z) = S(z) \cdot A(z), \tag{2.7}$$

which reflects the so-called *linearly separable speech generation model* of Figure 1.1 in Section 1.2. Observe that

$$A(z) = 1 - \sum_{k=1}^{p} a_k z^{-k} = \sum_{k=0}^{p} a_k z^{-k}, \quad a_0 = 1, \tag{2.8}$$

can be expressed as

$$\begin{aligned} A(z) &= 1 - a_1 \cdot z^{-1} - a_2 \cdot z^{-2} - \cdots - a_p \cdot z^{-p} \\ &= (z - z_i) \ldots (z - z_p), \end{aligned} \tag{2.9}$$

which explicitly shows that this polynomial has only zeros, but no poles and hence it is usually referred to as an *all-zero filter*. Expressing the speech signal $S(z)$ in terms of $E(z)$ and $A(z)$ gives

$$S(z) = \frac{E(z)}{A(z)} = E(z) \cdot H(z), \tag{2.10}$$

suggesting that any combination of $E(z)$ and $H(z) = 1/A(z)$ could adequately model the input signal $S(z)$. However, when the prediction residual $e(n)$ is quantised to $e_q(n)$ in order to achieve bitrate economy, this is not true. We will show that it is an attractive approach to determine the predictor coefficients a_k by minimising the expected value of the mean-squared prediction error of Equation (2.6).

Again, in accordance with our introductory observations in Figure 1.1 of Section 1.2, generating the synthesised speech using Equation (2.10) can also be portrayed as exciting the *all-pole synthesis filter* $H(z) = 1/A(z)$ with the excitation signal $E(z)$. If the predictor removes the redundancy from the speech signal by minimising the prediction residual, $e(n)$ becomes unpredictable, i.e. pseudo-random with an essentially flat spectrum, while $H(z) = 1/A(z)$ models the *spectral envelope of the speech*. Due to the relationship $A(z) = H^{-1}(z)$ the filter $A(z)$ is often referred to as the LPC *inverse filter*.

The expected value (E) of the mean-squared prediction error of Equation (2.6) can be written as

$$E[e^2(n)] = E\left[\left[s(n) - \sum_{k=1}^{p} a_k s(n-k)\right]^2\right]. \tag{2.11}$$

In order to arrive at the optimum LPC coefficients we compute the partial derivative of Equation (2.11) with respect to all LPC coefficients and set $\partial E/\partial a_i = 0$ for $i = 1, \ldots, p$, which yields a set of p equations for the p unknown LPC coefficients a_i as

$$\frac{\partial E[e^2(n)]}{\partial a_i} = -2 \cdot E\left\{\left[s(n) - \sum_{k=1}^{p} a_k s(n-k)\right] s(n-i)\right\} = 0, \tag{2.12}$$

yielding

$$E\{s(n)s(n-i)\} = E\left\{\sum_{k=1}^{p} a_k s(n-k)s(n-i)\right\}. \tag{2.13}$$

Upon exchanging the order of the summation and expected value computation at the right-hand side of Equation (2.13) we arrive at

$$E\{s(n)s(n-i)\} = \sum_{k=1}^{p} a_k E\{s(n-k)s(n-i)\}, \quad i = 1, \ldots, p. \tag{2.14}$$

Observe in the above equation that

$$C(i,k) = E\{s(n-i)s(n-k)\}, \tag{2.15}$$

represents the input signal's covariance coefficients, which allows us to rewrite the set of p Equations (2.14) in a more terse form as follows [70, 71]:

$$\sum_{k=1}^{p} a_k C(i,k) = C(i,0), \quad i = 1, \ldots, p. \tag{2.16}$$

2.3.2 Covariance Coefficient Computation

The above set of equations is often encountered in various signal processing problems, when minimising some error term as a function of a set of coefficients. Apart from linear predictive coding this set of equations is arrived at in optimising other adaptive filters, such as channel equalisers [72, 73] or in the auto-regressive filter representation of error correction block codes [74]. Ideally the covariance coefficients would have to be determined by evaluating the expected value term in Equation (2.15) over an infinite interval, but this is clearly impractical.

In low-complexity codecs or if the input signal can be considered to possess *stationary statistical properties*, implying that the signal's statistics are time-invariant, the covariance coefficients can be determined using a sufficiently long training sequence. Then the set of p Equations (2.16) can be solved, for example, by *Gauss–Jordan elimination* [75], or more efficiently by the iterative *Levinson–Durbin algorithm* [6, 71] which will be highlighted later in this chapter.

In more complex, low bitrate codecs the LPC coefficients are determined adaptively for shorter so-called *quasi-stationary* input signal segments in order to improve the efficiency of the predictor, that is to reduce the prediction error's variance and hence to improve the coding efficiency. These time-variant LPC coefficients must be quantised and transmitted to the decoder, in order to ensure that the encoder's and decoder's p-tap predictors are identical. This technique, which is often referred to as *forward-adaptive prediction*, implies that at the encoder the quantised coefficients must also be employed, although there the more accurate unquantised coefficients are also available. Another alternative is to invoke the principle of so-called *backward-adaptive prediction*, where the LPC coefficients are not transmitted to the decoder, instead they are recovered from previous segments of the decoded signal. Again, in order to ensure the identical operation of the local and distant decoders, the encoder also uses previous decoded signal segments, rather than unquantised input signal segments in order to determine the LPC coefficients. It is plausible that for the sake of efficient prediction the delay associated with backward-adaptive prediction must be as low as possible, while the decoded

signal quality has to be as high as possible. Hence this technique is not used in low bitrate applications, where the typically higher delay and higher coding distortion would reduce the predictor's efficiency. Here we will not analyse the specific advantages and disadvantages of the forward- and backward-adaptive schemes, but during our further discourse we will return to these codec classes and augment their main features by referring to practical standardised coding arrangements belonging to both families.

In spectrally efficient high quality forward-adaptive predictive codecs the covariance coefficients $C(i,k)$ of Equation (2.15) are typically computed for intervals, during which the signal's statistics can be considered quasi-stationary. A severe limitation is, however, that the quantised coefficients must be transmitted to the decoder and hence their frequent transmission may result in excessive bitrate contributions. In the case of backward adaptive arrangements this bitrate limitation does not exist, hence typically higher-order predictors can and must be used in order to achieve high prediction gains. The more stringent limiting factor becomes, however, the computational complexity associated with the frequent solution of the high-order set of Equations (2.16), since the low-delay spectral estimation requirement does not tolerate the too infrequent updating of the LPC coefficients, since the associated coefficients would become obsolete and inaccurate.

2.3.3 Predictor Coefficient Computation

A variety of techniques have been proposed for limiting the range of covariance computation [72, 76], of which the most frequently used are the so-called *autocorrelation method* and the *covariance method* [6].

Here we follow the approach proposed by Makhoul [77], Rabiner and Schaefer [6], Haykin [72], Salami *et al.* [71] and briefly highlight the *autocorrelation method*, where the prediction error term of Equation (2.11) is now minimised over the finite interval of $0 \leq n \leq L_a - 1$, rather than $-\infty < n < \infty$. Hence the covariance coefficients $C(i,k)$ are now computed from the following short-term expected value expression:

$$C(i,k) = \sum_{n=0}^{L_a+p-1} s(n-i)s(n-k), \quad i = 1,\ldots,p,\ k = 0,\ldots,p. \tag{2.17}$$

Upon setting $m = n - i$, Equation (2.17) can be expressed as

$$C(i,k) = \sum_{m=0}^{L_a-1-(i-k)} s(m)s(m+i-k), \tag{2.18}$$

which suggests that $C(i,k)$ is the short-time autocorrelation of the input signal $s(m)$ evaluated at a displacement of $(i-k)$, giving

$$C(i,k) = R(i-k), \tag{2.19}$$

where

$$R(j) = \sum_{n=0}^{L_a-1-j} s(n)s(n+j) = \sum_{n=j}^{L_a-1} s(n)s(n-j), \tag{2.20}$$

and $R(j)$ represents the speech autocorrelation coefficients. Hence the set of p Equations (2.16) can now be reformulated as

$$\sum_{k=1}^{p} a_k R(|i-k|) = R(i), \quad i = 1, \ldots, p. \tag{2.21}$$

Alternatively, Equation (2.21) can be re-written in a matrix form as

$$\begin{pmatrix} R(0) & R(1) & R(2) & \ldots & R(p-1) \\ R(1) & R(0) & R(1) & \ldots & R(p-2) \\ R(2) & R(1) & R(0) & \ldots & R(p-3) \\ \vdots & \vdots & \vdots & \ddots & \vdots \\ R(p-1) & R(p-2) & R(p-3) & \ldots & R(0) \end{pmatrix} \cdot \begin{pmatrix} a_1 \\ a_2 \\ a_3 \\ \vdots \\ a_p \end{pmatrix} = \begin{pmatrix} R(1) \\ R(2) \\ R(3) \\ \vdots \\ R(p) \end{pmatrix}. \tag{2.22}$$

The $p \times p$ autocorrelation matrix above has a so-called Toeplitz structure, where all the elements along a certain diagonal are identical. Hence Equation (2.22) can be solved without matrix inversion that would imply a computational complexity cubically related to p. There is a variety of efficient recursive algorithms that have a complexity proportional to the square of p for the solution of Toeplitz-type systems. The most well-known ones are the Berlekamp–Massey algorithm [74] favoured in error correction coding or the recursive Levinson–Durbin algorithm, which can be stated as follows [6, 71, 77]:

$E(0) = R(0)$

For $i = 1$ to p do

$$k_i = \left[R(i) - \sum_{j=1}^{i-1} a_j^{(i-1)} R(i-j) \right] / E(i-1) \tag{2.23}$$

$a_i^{(i)} = k_i$

For $j = 1$ to $i-1$ do

$$a_j^{(i)} = a_j^{(i-1)} - k_i a_{i-j}^{(i-1)} \tag{2.24}$$

$$E(i) = (1 - k_i^2) E(i-1). \tag{2.25}$$

The final solution after p iterations is given by

$$a_j = a_j^{(p)}, \quad j = 1, \ldots, p, \tag{2.26}$$

where $E(i)$ in Equation (2.25) is the prediction error of an ith-order predictor. The flowchart of the Levinson–Durbin algorithm is depicted in Figure 2.3 in order to augment its exposition.

It is beneficial to define the so-called *prediction gain*, which is the ratio of the expected value of the input signal's energy, namely $R_s(0)$, and that of the prediction error energy $R_e(0)$ expressed in terms of the corresponding autocorrelation coefficients as follows:

$$G = \frac{R_s(0)}{R_e(0)}. \tag{2.27}$$

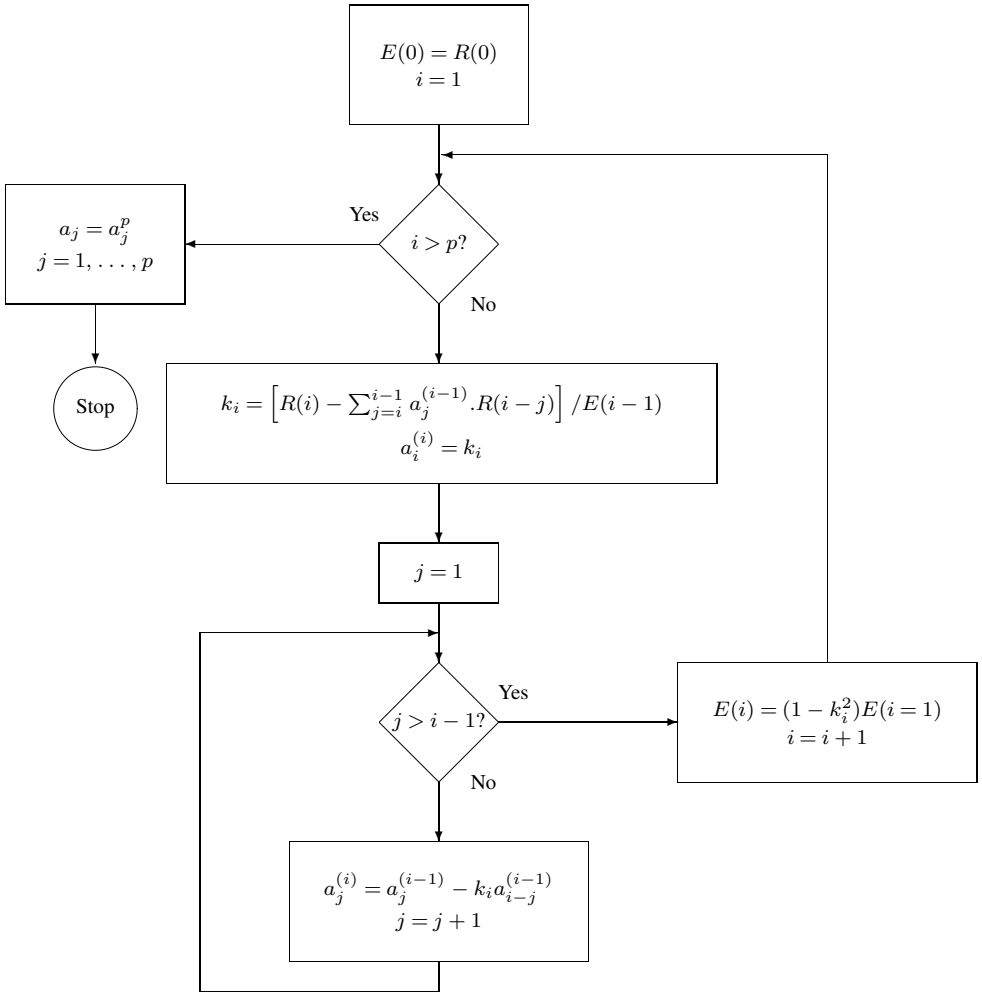

Figure 2.3: Flowchart of the Levinson–Durbin algorithm.

Note also that the prediction gain is often expressed in terms of dB. Let us now invoke a simple example to augment the above concepts.

Example. *The long-term one-step autocorrelation coefficient of the input signal was found to be* $R_s(1)/R_s(0) = 0.9$*. Determine the prediction gain in the case of using the optimum one-tap predictor and with the aid of non-optimum prediction using the previous sample as the predicted value. Express these gains in dB.*

From Equation (2.11) the prediction error variance can be expressed as

$$E[e^2(n)] = E[[s(n) - a_1 s(n-1)]^2], \tag{2.28}$$

yielding

$$R_e(0) = R_s(0) - 2a_1R_s(1) + a_1^2R_s(0), \tag{2.29}$$

where $R(0)$ and $R(1)$ represent the correlation coefficients at offsets of 0 and 1 sample, respectively. Upon setting the derivative of the above equation with respect to a_1 to zero we get

$$a_1 = \frac{R_s(1)}{R_s(0)}, \tag{2.30}$$

which is the *normalised one-step correlation* between adjacent input samples. Finally, upon substituting the optimum coefficient from Equation (2.30) into Equation (2.29) we arrive at

$$\begin{aligned} R_e(0) &= R_s(0) - 2\frac{R_s(1)}{R_s(0)}R_s(1) + a^2R_s(0) \\ &= R_s(0)(1 - a_1^2) \end{aligned} \tag{2.31}$$

which gives the prediction gain as

$$G = \frac{R_s(0)}{R_e(0)} = 1/(1 - a_1^2). \tag{2.32}$$

For $a_1 = 0.9$ we have $G = 1/(1 - 0.81) = 5.26$, corresponding to 7.2 dB. When using $a_1 = 1$ in Equation (2.30) – which corresponds to using the previous sample to predict the current one – we get $G = 1/0.2 = 5$, which is equivalent to about 7 dB. This result is very similar to the 7.2 dB gain attained when using the optimum tap, which is due to the high adjacent-sample correlation. For lower correlation values the prediction gain difference becomes more substantial, eroding to $G < 1$ for uncorrelated signals, where $R_s(1)/R_s(0) < 0.5$.

Returning to the Levinson–Durbin algorithm, the internal variable k_i has a useful physical interpretation when applying the Levinson–Durbin algorithm to speech signals. Namely, they are referred to as the so-called *reflection coefficients* and $-1 < k_i < 1$ are defined as

$$k_i = \frac{A_{i+1} - A_i}{A_{i+1} + A_i}, \tag{2.33}$$

where $A_i, i = 1, \ldots, p$, represents the area of an acoustic tube section, assuming that the vocal tract can be modelled by a set of p concatenated tubes of different cross section. The above definition of k_i implies that they physically represent the area ratios of the consecutive sections of the lossless acoustic tube model of the vocal tract [6, 71]. Rabiner and Schafer [6] have shown that the $-1 < k_i < 1$ condition is necessary and sufficient for all the roots of the polynomial $A(z)$ to be inside the unit circle in the z-domain, thereby guaranteeing the stability of the system transfer function $H(z)$. It has been shown that the autocorrelation method always leads to a stable filter $H(z)$. These issues will be re-visited in Chapter 4, where the statistical properties of the a_i and k_i parameters will be characterised in terms of their PDFs in Figures 4.1 and 4.2 along with those of a range of other equivalent spectral parameters, which are more amenable to quantisation for transmission.

The rectangular windowing of the input signal at the LPC analysis frame edges corresponds in the spectral domain to convolving the signal's spectrum with a sinc-function,

which results in the so-called *Gibbs oscillation*. In time domain the rectangular windowing results in a high prediction error at the beginning and at the end of the segment, since the signal outside the interval was zero. This undesirable phenomenon can be mitigated by using smooth, tapering windows, such as the time-domain Hamming windowing, which employs the function

$$w(n) = 0.54 - 0.46\cos(2\pi n/(L_a - 1)), \quad 0 \leq n \leq L_a - 1, \tag{2.34}$$

where the Hamming windowing frame length L_a is often longer than the length L of the input signal update frame. The LPC coefficients are typically interpolated between adjacent LPC frames in order to smooth the abrupt signal envelope changes at frame edges.

On the basis of the previously introduced adaptive predictor, which can adjust the predictor coefficients in order to accommodate signal statistics variations, we can modify the DPCM codec schematic of Figure 2.2 to portray these added features, as seen in Figure 2.4. Clearly, the filter coefficients $a_k, k = 1, \ldots, p$, must be computed, as highlighted earlier in this section using for example the autocorrelation method and the Levinson–Durbin algorithm, before encoding and transmitting them at the cost of an increased bitrate to the decoder. Furthermore, it is necessary to scale the input signal with the help of its variance in order to maintain near-unity input variance and hence achieve best quantisation performance. To this effect, a simple but efficient adaptive quantisation technique was proposed by Jayant [78], which introduces the notion of memory in the quantisation process in order to use the previously quantised sample to control the quantiser's step-size. This method, which can be employed in both PCM and DPCM codecs, will be the subject of our next section.

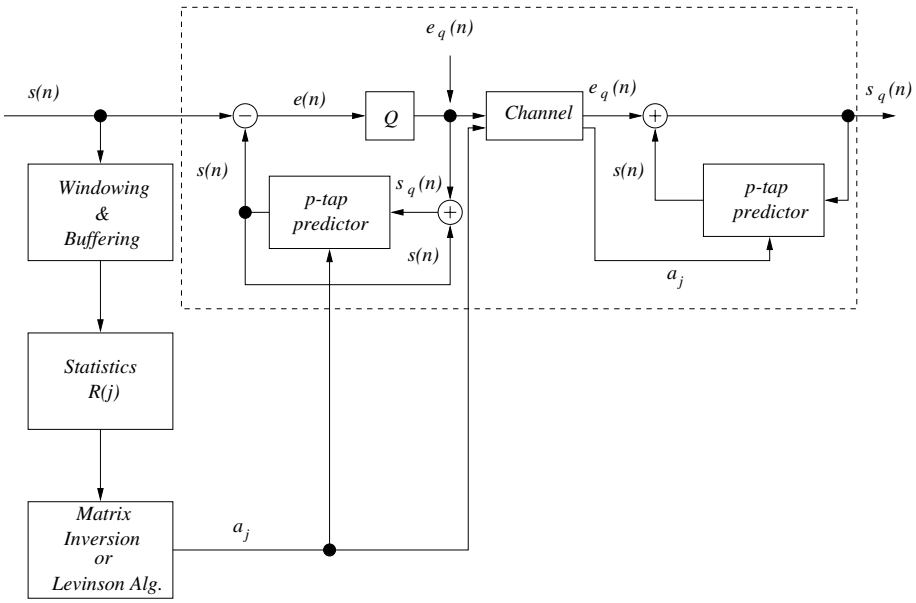

Figure 2.4: Adaptive forward-predictive DPCM codec schematic.

2.4 Adaptive One-word-memory Quantisation [78]

Adaptive one-word-memory quantisation is a form of adaptive pulse code modulation (APCM) due to Jayant [78], where the quantiser's instantaneous step-size is adjusted on the basis of the previous quantised sample in order to minimise the quantisation distortion. The schematic of the quantiser is displayed in Figure 2.5. The philosophy behind this scheme is that if the previous quantised sample $s_q(n-1)$ is near the top level of the quantiser characteristic, then action must be taken to increase the quantiser's step-size Δ_n, since in the case of correlated samples the forthcoming samples are similar to the current one and hence there is a danger of quantiser characteristic overload or saturation. Similarly, if the previous quantised sample $s_q(n-1)$ is near the lowest quantisation level, then too high a granular noise is inflicted, since the step-size is too small. This problem can then be mitigated by increasing the step-size. It is plausible, however, that the speed of step-size adaptation is critical, since various source signals have different statistical and spectral domain properties, which result in a different rate of change. Furthermore, the number of quantisation bits R is also an important factor in determining the required step-size control parameters, since in the case of $R = 1$, for example, no magnitude information is available, only the sign of the signal, which precludes the employment of this technique. The higher the number of bits R, the finer the step-size control.

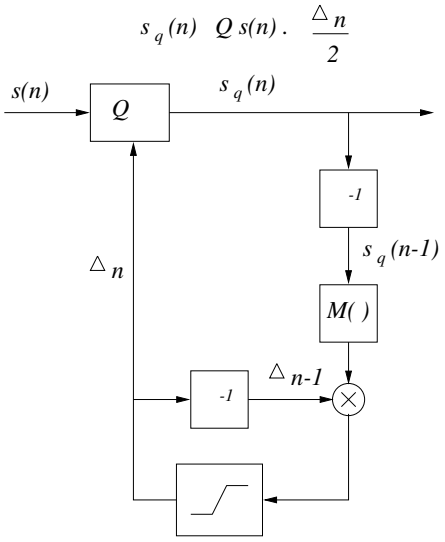

Figure 2.5: Schematic of Jayant's one-word-memory quantiser, where the current step-size depends on the previous one, scaled by a multiplier, which is a function of the previous quantised sample.

Formulating the algorithm displayed in Figure 2.5 more rigorously, the Jayant quantiser [78] adapts its step-size Δ_n at each sampling instant. The quantised output $s_q(n)$ of an R-bit quantiser $(R > 1)$ is of the form [78]

$$s_q(n) = Q\{s(n)\}\frac{\Delta_n}{2}, \tag{2.35}$$

where $|Q\{s(n)\}| = 1, 3, \ldots, 2^R - 1$, and $\Delta_n > 0$. The step-size Δ_n is given by the previous step-size Δ_{n-1} multiplied by a statistics-dependent, optimised time-invariant function of the code-word magnitude $|Q\{s_q(n-1)\}|$,

$$\Delta_n = \Delta_{n-1} M(|Q\{s_q(n-1)\}|). \tag{2.36}$$

In practical terms the step-size Δ_n can vary only over a limited dynamic range, from the minimum step-size $\Delta_{\min}$ to the maximum step-size $\Delta_{\max}$, which is expressed more formally as

$$\Delta_n = \begin{cases} \Delta_{\min} & \Delta_n < \Delta_{\min} \\ \Delta_{\max} & \Delta_n > \Delta_{\max} \\ \Delta_n & \text{otherwise.} \end{cases} \tag{2.37}$$

The multiplier function $M(\cdot)$ determines the rate of adaption for the step-size. For PCM and DPCM-encoded speech and video signals Jayant [78] tabulated these multiplier values for a range of quantiser resolutions $R = 2, \ldots, 5$, which are shown in Table 2.1 for PCM codecs. The values in brackets refer to video signals and similar multipliers apply to DPCM codecs [78] as well. It is also interesting to observe that the step-size increment associated with $M > 1$ is typically more rapid than the corresponding step-size reduction corresponding to $M < 1$, since the on-set of speech signals, for example, is more rapid than their decay.

Table 2.1: Jayant-multipliers for R-bit PCM quantisers.

R	Multiplier $M(\cdot)$
2	0.6, 2.20
3	0.85, 1.00, 1.00, 1.50 (0.9, 0.95, 1.50, 2.5 – for video)
4	0.80, 0.80, 0.80, 0.80, 1.20, 1.60, 2.00, 2.40
5	0.85, 0.85, 0.85, 0.85, 0.85, 0.85, 0.85, 0.85, 1.20, 1.40, 1.60, 1.80, 2.00, 2.20, 2.40, 2.60

Having highlighted the concept of adaptive one-word-memory quantisation let us now characterise the expected performance of DPCM codecs in contrast to PCM.

2.5 DPCM Performance

In this brief performance analysis we follow the approach proposed by Jain [69] and note that in contrast to PCM, where $s(n)$ is subjected to quantisation, in the case of DPCM the quantiser operates on the prediction error signal $e(n)$ having a variance of $\sigma_e^2 = E\{[e(n)]^2\}$, while the quantisation error variance is assumed to be σ_q^2. Then applying the rate-distortion

formula of Equation (1.5), the DPCM coding rate is given by

$$R_{\mathrm{DPCM}} = \frac{1}{2}\log_2\frac{\sigma_e^2}{\sigma_q^2}\ [\text{bits/pixel}]. \tag{2.38}$$

When compared to PCM and assuming the same quantiser for both PCM and DPCM we have a constant quantisation distortion of σ_q^2, although the quantiser is applied in the former case to quantise the input signal $s(n)$, while in the latter to $e(n)$. Since typically $\sigma_s < \sigma_q$, the coding rate reduction due to using DPCM is yielded as [69]

$$\triangle R = R_{\mathrm{PCM}} - R_{\mathrm{DPCM}} = \frac{1}{2}\log_2\frac{\sigma_s^2}{\sigma_q^2} - \frac{1}{2}\log_2\frac{\sigma_e^2}{\sigma_q^2} = \frac{1}{2}\log_2\frac{\sigma_s^2}{\sigma_e^2} \tag{2.39}$$

giving a coding rate gain of

$$\triangle R \approx 1.66 \cdot \log_{10}\left(\frac{\sigma_s}{\sigma_e}\right)^2\ [\text{bits/pixel}]. \tag{2.40}$$

For example, if $\sigma_s = 10 \cdot \sigma_e$, then we have $\triangle R = 3.332$, which means that a PCM codec having the same quantisation error variance as a DPCM codec would require more than three additional quantisation bits per sample, or the DPCM codec ensures in excess of three bits/sample transmission rate saving. In general, the coding rate reduction $\triangle R = (\sigma_s/\sigma_e^2)$ due to DPCM coding depends on the ability to predict the input signal $s(n)$, that is on the intersample correlation. We have seen before that for minimum prediction error variance σ_e^2 the optimum one-tap predictor coefficient is given by the adjacent-sample correlation.

For the variance of the feed-forward prediction error we have $\sigma_\varepsilon \leq \sigma_e$, since the prediction based on the locally decoded signal contaminated by quantisation noise cannot be better than that based on the original signal. This fact does not contradict the previously argued statement that the reconstruction error variance of the DPCM codec is typically lower than that of the feed-forward codec. If the number of quantisation bits is high, we have $\sigma_\varepsilon \approx \sigma_e$. Hence, *the lower bound* on the DPCM coding rate is given by [69]

$$R_{\min} = \frac{1}{2}\log_2\frac{\sigma_\varepsilon^2}{\sigma_q^2} \leq R_{\mathrm{DPCM}}. \tag{2.41}$$

The SNR of the DPCM codec can be written as

$$\mathrm{SNR}_{\mathrm{DPCM}} = 10\log_{10}\frac{\sigma_s^2}{\sigma_q^2} = 10\log_{10}\frac{\sigma_s^2}{\sigma_e^2 \cdot f(R)} \tag{2.42}$$

leading to

$$\mathrm{SNR}_{\mathrm{DPCM}} \leq 10\log_{10}\frac{\sigma_s^2}{\sigma_\varepsilon^2 \cdot f(R)}, \tag{2.43}$$

where $f(R)$ is the quantiser mean square distortion function for R number of quantisation bits in the case of a unit variance input signal [69]. For an equal number of quantisation bits

the SNR improvement of DPCM over PCM is then given by

$$\begin{aligned}\triangle \text{SNR} &= \text{SNR}_{\text{DPCM}} - \text{SNR}_{\text{PCM}} \\ &= 10 \log_{10} \frac{\sigma_s^2}{\sigma_q^2} - 10 \log_{10} \frac{\sigma_d^2}{\sigma_q^2} \\ &= 10 \log_{10} \frac{\sigma_s^2}{\sigma_d^2} \leq 10 \log_{10} \frac{\sigma_s^2}{\sigma_{\tilde{\varepsilon}}^2}. \end{aligned} \tag{2.44}$$

Again, assuming for example that $\sigma_s = 10 \cdot \sigma_e$, we have a 20 dB SNR improvement over PCM, while maintaining the same coding rate. In general, the gains achievable will depend on the signal's statistics, as well as on the predictor (P) and quantiser (Q) designs. Usually Lloyd–Max quantisation (MLQ) is used, which is designed to match the prediction error's PDF by allocating more bits, where the PDF is high and less bits, where the probability of occurrence is low. Ideally, the integral of the PDF over each quantisation interval is constant.

If the prediction error's PDF matches a Gaussian, Laplacian or Gamma distribution, the analytic quantiser designs tabulated in the literature [69] can be invoked. Otherwise specially trained Lloyd–Max quantisers must be employed, which can be designed using the training algorithm highlighted in Section 1.4.6. Having considered forward-adaptive predictive coding, in the next section we explore some of the features of backward-adaptive predictive schemes.

2.6 Backward-adaptive Prediction

2.6.1 Background

In the preceding sections we have considered forward adaptive prediction, where the predictor coefficients must be transmitted to the decoder. Hence they reserve some of the channel capacity available and their computation requires buffering a segment of the input signal, over which spectral analysis can take place. These factors limit the affordable rate of predictor updates. In contrast, in backward-adaptive predictive schemes the predictor coefficients are determined from the previously recovered speech and the frequency of the LPC update is practically only limited by the affordable codec complexity. During our later discourse we will consider a variety of such backward-adaptive standard and non-standard codecs, including the CCITT G.721, G.727, G.726 and G.728 codecs.

In this subsection following Jayant's deliberations [10] we will introduce a predictor update technique, which is used in a range of standard ADPCM codecs, including the G.721, G.726 and G.727 schemes. The expected value of the mean squared prediction error of Equation (2.6) can also be expressed as

$$\begin{aligned}\sigma_e^2 &= E[e^2(n)] = E[(s(n) - \tilde{s}(n))^2] \\ &= E\left[\left(s(n) - \sum_{k-1}^{p} a_k s(n-k)\right)^2\right], \end{aligned} \tag{2.45}$$

where σ_e^2 is the variance of the prediction error $e(n)$. This formulation has led us to Equation (2.22), referred to as the Wiener–Hopf equation. Once the matrix has been inverted either by Gauss–Jordan elimination or, for example, by the recursive Levinson–Durbin algorithm, the optimum predictor coefficient set becomes known and the actual achievable minimum expected value of the prediction residual energy can be computed. Using a convenient vectorial notation the predictor coefficient vector and the speech vector used in the prediction process can be expressed as

$$\mathbf{a}^{\mathrm{T}} = [a_{1,2}, \ldots, a_p]$$
$$\mathbf{s}^{\mathrm{T}} = [s(n-1), s(n-2), \ldots, s(n-k)].$$

Upon using this notation Equation (2.45) can be rewritten as

$$\begin{aligned}\sigma_e^2 &= E\left[\left(s(n) - \sum_{k=1}^{p} a_k s(n-k)\right)^2\right] \\ &= E[(s(n) - \mathbf{a}^{\mathrm{T}} \cdot \mathbf{s})(s(n) - \mathbf{s}^{\mathrm{T}} \cdot \mathbf{a})] \\ &= E[s^2(n) - s(n) \cdot \mathbf{s}^{\mathrm{T}} \cdot \mathbf{a} - \mathbf{a}^{\mathrm{T}} \cdot \mathbf{s} \cdot s(n) + \mathbf{a}^{\mathrm{T}} \cdot \mathbf{s} \cdot \mathbf{s}^{\mathrm{T}} \cdot \mathbf{a}]. \end{aligned} \tag{2.46}$$

Upon taking the expected value of the individual terms and using the notation of Equations (2.22) and (2.46) we arrive at

$$\sigma_e^2(\mathbf{a}) = \sigma_s^2 - 2 \cdot \mathbf{a}^{\mathrm{T}} \cdot \mathbf{r} + \mathbf{a}^{\mathrm{T}} \cdot \mathbf{R} \cdot \mathbf{a}, \tag{2.47}$$

where $r = E\{s(n)\mathbf{s}^{\mathrm{T}}\}$ and $R = E\{\mathbf{s}\mathbf{s}^{\mathrm{T}}\}$.

Explicitly, Equation (2.47) quantifies the expected value of the mean squared prediction error as a function of the predictor coefficient vector **a** and the optimum vector can be computed from Equation (2.22) by matrix inversion or using a recursive solution. However, since the input speech has a time-variant statistical behaviour, the optimum coefficient vector is also time-variant. Given an initial vector $\mathbf{a}^{\mathrm{opt}}$, it is possible to devise an adaptation algorithm which seeks to modify the coefficient vector in a sense to reduce $\sigma_e^2(\mathbf{a})$ in Equation (2.47). The gradient of $\sigma_e^2(\mathbf{a})$ with respect to the coefficient vector is an indicator of the required changes in **a** in order to minimise $\sigma_e^2(\mathbf{a})$. This can be written more formally using Equation (2.47) as

$$\frac{\mathrm{d}\sigma_e^2(\mathbf{a})}{\mathrm{d}\mathbf{a}} = 2\mathbf{R} \tag{2.48}$$

$$\begin{aligned}\Delta\sigma_e^2(\mathbf{a}) &\approx 2\mathbf{R} \cdot \Delta\mathbf{a} \\ &\approx 2\mathbf{R} \cdot (\mathbf{a} - \mathbf{a}^{\mathrm{opt}}), \end{aligned} \tag{2.49}$$

which demonstrates that the deviation of $\sigma_e^2(\mathbf{a})$ from its minimum value depends on both the speech signal's correlation quantified by **R** and the difference between the optimum and current coefficient vector, namely $(\mathbf{a} - \mathbf{a}^{\mathrm{opt}})$. The predictor coefficients can be updated on a sample-by-sample basis or block-by-block basis using techniques, such as the method of *steepest descent* or Kalman filtering [10], etc.

Here we consider a so-called *pole-zero predictor*, which is depicted in Figure 2.6, where $A(z)$ and $B(z)$ represent the all-pole and all-zero filters, respectively. Their transfer functions are given by

$$A(z) = \sum_{k=1}^{N_f} a_i z^{-k}$$
$$B(z) = \sum_{k=0}^{N_z} b_i z^{-k} \tag{2.50}$$

and a_k, b_k represent the filter coefficients, while N_f and N_z the filter orders. This predictor is studied in more depth in the next section.

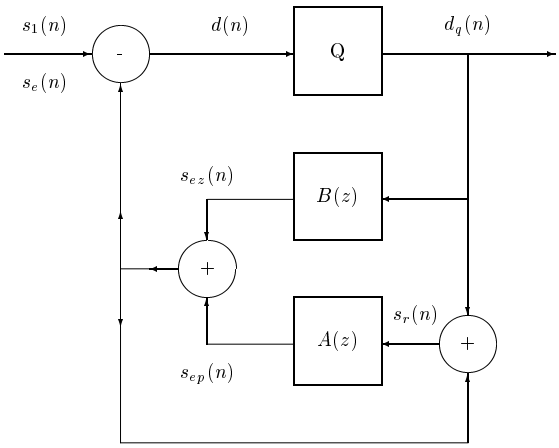

Figure 2.6: Pole-zero predictor schematic.

2.6.2 Stochastic Model Processes

In order to better understand the behaviour of this predictor, we have to embark on a brief discourse concerning stochastic model processes. Our pole-zero predictor belongs to the family of the so-called *autoregressive* (AR), *moving average* (MA) processes, which are jointly referred to as ARMA processes. An all-pole model or autoregressive model is usually derived from the previously introduced predictor formula of Equation (2.5), which is usually presented in the form

$$s(n) = \sum_{k=1}^{p} a_k \cdot s(n-k) + e(n) \; \forall_n, \tag{2.51}$$

where $e(n)$ is an uncorrelated, zero-mean, random input sequence with variance σ^2, as one would expect from a reliable predictor, removing all the predictable redundancy. The schematic of an AR process is displayed in Figure 2.7.

From Equation (2.51) the *transfer function of the all-pole AR model* can be derived as

$$e(n) = s(n) - \sum_{k=1}^{p} a_k \cdot s(n-k)$$

$$E(z) = S(z) - \sum_{k=1}^{p} a_k \cdot S(z) z^{-k}$$

$$= S(z)\left[1 - \sum_{k=1}^{p} a_k \cdot z^{-k}\right]$$

leading to

$$H(z) = \frac{S(z)}{E(z)} = \frac{1}{1 - \sum_{k=1}^{p} a_k \cdot z^{-k}} = \frac{1}{A(z)}. \tag{2.52}$$

As expected, this transfer function exhibits poles at the z values, where $A(z)$ becomes zero.

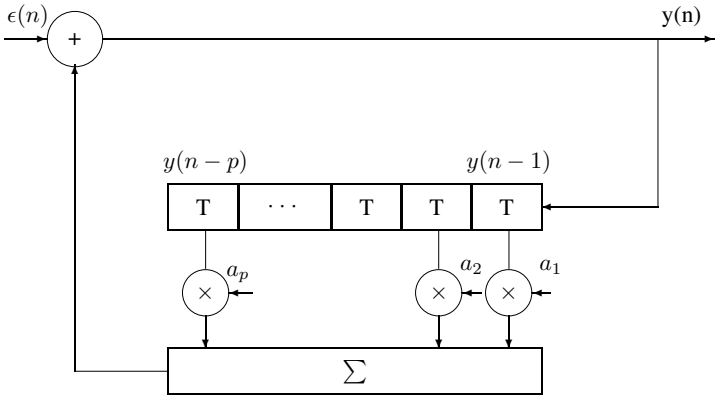

Figure 2.7: Markov model of order p.

By contrast, a *MA process is defined as*

$$s(n) = \sum_{k=0}^{q} b_k e(n-k), \tag{2.53}$$

expressing the random sequence $s(n)$ as a weighted sliding sum of the previous q samples of $e(n)$, where again $e(n)$ is a zero-mean, uncorrelated random sequence with a variance σ^2. The transfer function of a MA model can be expressed as

$$B(z) = \frac{S(z)}{E(z)} = \sum_{k=0}^{q} b_k z^{-k}, \tag{2.54}$$

which is shown in Figure 2.8.

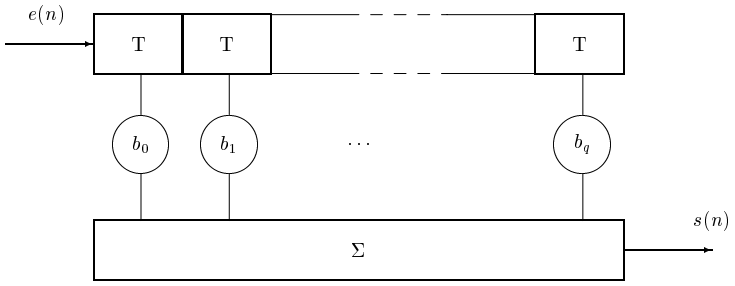

Figure 2.8: MA process generation.

Upon returning to our pole-zero predictor of Figure 2.6, we have

$$s_{ep}(n) = \sum_{k=1}^{p} a_k s_r(n-k) \tag{2.55}$$

and

$$s_{ez}(n) = \sum_{k=0}^{q} b_k d_q(n-k) \tag{2.56}$$

and the reconstructed signal $s_r(n)$ of Figure 2.6 can be written as the sum of the quantised prediction residual $d_q(n)$ and the estimated signal $s_e(n)$ as

$$s_r(n) = s_e(n) + d_q(n),$$

while the estimated signal is the sum of the two predictors, giving

$$s_e(n) = s_{ez}(n) + s_{ep}(n).$$

Both the all-zero and all-pole predictor coefficients can be updated using the *gradient or steepest descent* algorithm, which modifies each of the pole-zero predictor's coefficients in every iteration by an amount proportional to the error gradient with respect to the specific coefficient concerned, but opposite in terms of its sign, in order to reduce the error variance at each iteration yielding

$$\begin{aligned} a_k(i+1) &= a_k(i) - C(i) \cdot \frac{d\sigma_e^2(a_k)}{da_k}, \quad k = 1, \ldots, p \\ b_k(i+1) &= b_k(i) - C(i) \frac{d\sigma_e^2(b_k)}{db_k}, \quad k = 1, \ldots, q. \end{aligned} \tag{2.57}$$

Clearly, the coefficients at iteration $(i+1)$ are derived by subtracting the $C(i)$ scaled gradient of the prediction error variance from the coefficients at iteration i, where $C(i)$ is an adaptation-speed control factor. As expected, the adaptation-speed control factor $C(i)$ has a strong influence on the properties of the predictor adaptation loop. If a larger value is selected, the algorithm achieves a faster convergence at the cost of a higher steady-state tracking error

and *vice versa*. Furthermore, in Equation (2.57) it is possible to use the prediction error itself, rather than its longer-term variance. Here we curtail our discussions concerning various practical implementations of the gradient-algorithm based predictor adaptation and we will revisit this issue in our discourse on the G.721 standard ADPCM codec. Our deliberations concerning backward adaptive predictive codecs will be further extended at a later stage in the context of the vector-quantised CCITT G.728 low-delay 16 kbps codec in Chapter 8.

Following this rudimentary introduction to backward-adaptive predictive coding let us now embark on highlighting the details of a specific standardised speech codec, namely the 32 kbps CCITT G.721 *adaptive differential pulse code modulation* (ADPCM) codec, which has become popular in recent years due to its very low implementational complexity and high speech quality. It has also been adopted by a number of wireless communications standards, such as the British CT2 cordless telephone system [79, 80], the Digital European Cordless Telephone (DECT) system [81, 82] and the Japanese Personal Handy Phone (PHP) system [83].

2.7 The 32 kbps G.721 ADPCM Codec [84]

2.7.1 Functional Description of the G.721 Codec

As mentioned, the 32 kbps transmission rate ADPCM codec was specified in the CCITT G.721 Recommendation. The encoder/decoder pair is shown in Figure 2.9 and since it is essentially a waveform codec, apart from speech, it is also capable of transmitting data signals.

As seen in the figure, the A-law or μ-law companded PCM signal is first converted into linear PCM format, since all signal processing steps take place in the linear PCM domain. The input signal's estimate produced by the *adaptive predictor* is subtracted from the input in order to produce a difference signal having a lower variance. This lower-variance difference signal can then be adaptively quantised with lower noise variance than the original signal, using a 4-bit adaptive quantiser. Assuming a sampling frequency of 8 kHz, an 8-bit PCM sample is represented by a 4-bit ADPCM sample, giving a transmission rate of 32 kbps. This ADPCM stream is transmitted to the decoder. Furthermore, it is locally decoded, using the *inverse adaptive quantiser in the G.721 codec*, to deliver the locally reconstructed quantised difference signal, which is added to the previous signal estimate in order to yield the locally reconstructed signal. Based on the quantised difference signal and the locally reconstructed signal the adaptive predictor derives the subsequent signal estimate, etc.

The ADPCM decoder is constituted by the local decoder part of the encoder, and additionally it comprises the linear PCM to A-law or μ-law converter. The synchroneous coding adjustment block attempts to eliminate the cumulative tandem distortion occurring in subsequent synchroneous PCM/ADPCM operations. Further specific implementational details of the G.721 Recommendation will be described with reference to Figure 2.9, where the notation of the G.721 standard [84] has been adopted in order to avoid confusion.

2.7.2 Adaptive Quantiser

A 16-level or $R = 4$-bit adaptive quantiser is used to quantise the prediction error or difference signal $d(k) = s_1(k) - s_e(k)$, which is converted to base 2 logarithmic representation

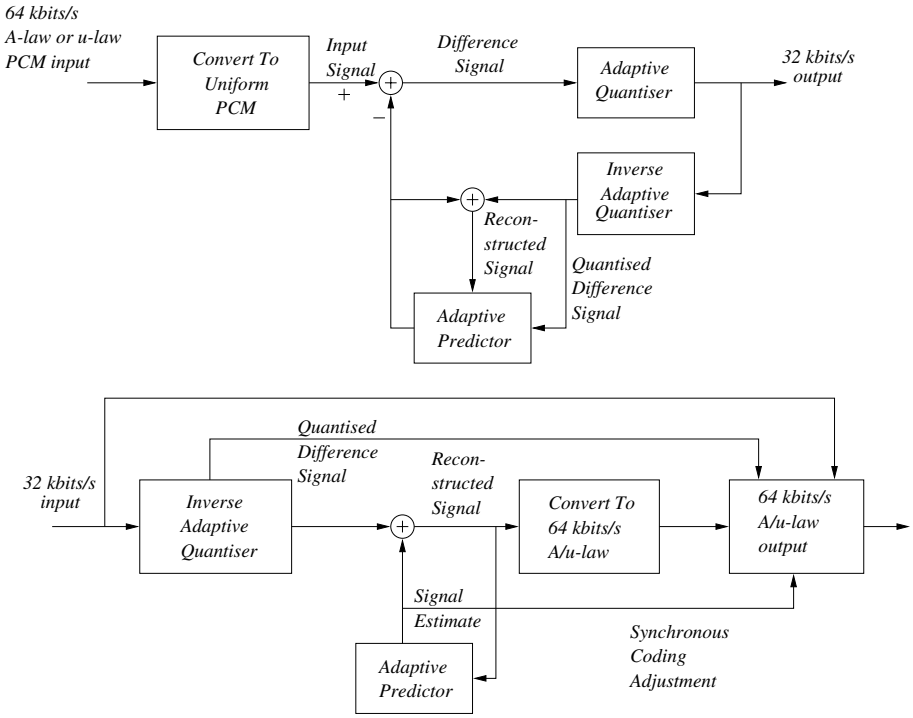

Figure 2.9: Detailed G.721 ADPCM encoder/decoder schematic.

prior to quantisation and scaled by the signal $y(k)$, which is output by the quantiser scale factor adaptation block seen in the schematic of Figure 2.9. Note that scaling in the logarithmic domain corresponds to subtracting the scaling factor $y(k)$. The scaled quantiser input/output ranges are given in Table 2.2, where the quantiser output is represented by a 4-bit number $I(k)$ and in its 4-bit binary representation the first bit determines the sign of $d(k)$. The 4-bit sequence $I(k)$ is both transmitted and locally decoded, using the inverse adaptive quantiser reconstruction values in the right-hand column of Table 2.2. This delivers the quantised prediction error samples $d_q(k)$. Observe, furthermore, in Figure 2.9 that $I(k)$ is also input to *the adaptation speed control* and *quantiser scale factor adaptation* blocks, which are considered in more depth below.

2.7.3 G.721 Quantiser Scale Factor Adaptation

The quantiser scale factor adaptation block derives the scaling factor $y(k)$ of Table 2.2. Its inputs are the 4-bit $I(k)$ values and the so-called adaptation speed control parameter $a_l(k)$. The quantiser scaling is rapidly changing for signals characterised by large fluctuations, such as speech signals. By contrast, the scaling is slowly varying for signals resulting in slowly changing difference signals, such as voice band data or signalling tones. The so-called fast scale factor $y_u(k)$ is recursively computed from the previously introduced logarithmic scale

Table 2.2: Scaled adaptive quantiser characteristic. Copyright © CCITT G.721.

Scaled quantiser input range $\log_2 \lvert d(k)\rvert - y(k)$	$\lvert I(k)\rvert$	Scaled quantiser output range $\log_2 \lvert d_q(k)\rvert - y(k)$
3.16–∞	7	3.34
2.78–3.16	6	2.95
2.42–2.78	5	2.59
2.04–2.42	4	2.23
1.58–2.04	3	1.81
0.96–1.58	2	1.29
-0.05–0.96	1	0.53
$-\infty$–0.05	0	-1.05

factor $y(k)$ in the base 2 logarithmic domain using

$$\begin{aligned} y_u(k) &= (1 - 2^{-5})y(k) + 2^{-5}W[I(k)], \\ y_u(k) &\approx 0.97y(k) + 0.03 \cdot W[I(k)], \end{aligned} \tag{2.58}$$

where $y_u(k)$ is restricted to the range

$$1.06 \leq y_u(k) \leq 10.00.$$

In other words, $y_u(k)$ is a weighted sum of $y(k)$ and $I(k)$, where the dominant part is usually $y(k)$. The leakage factor $(1 - 2^{-5}) \approx 0.971$ allows for the decoder to 'forget' the effect of eventual transmission errors. The factor $W(I)$ is specified in the G.721 Recommendation as seen in Table 2.3.

Table 2.3: Definition of the factor $W(I)$. Copyright © CCITT G.721.

$\lvert I\rvert$	7	6	5	4	3	2	1	0
$W(I)$	69.25	21.25	11.50	6.12	3.12	1.69	0.25	-0.75

The current value of the slow quantiser scale factor $y_l(k)$ is derived from the fast scale factor $y_u(k)$ and from the slow scaling factor's previous value $y_l(k-1)$, using

$$\begin{aligned} y_l(k) &= (1 - 2^{-6})y_l(k-1) + 2^{-6}y_u(k), \\ y_l(k) &\approx 0.984y_l(k-1) + 0.016y_u(k). \end{aligned} \tag{2.59}$$

Then, according to the G.721 Recommendation, the fast and slow scale factors are combined to form the scale factor $y(k)$:

$$y(k) = a_l(k)y_u(k-1) + [1 - a_l(k)]y_l(k-1), \tag{2.60}$$

where the *adaptation speed control factor* is constrained to the range $0 \leq a_l \leq 1$, and we have $a_l \approx 1$ for speech signals, whereas $a_l \approx 0$ for data signals. Therefore for speech signals the fast scaling factor $y_u(k)$ dominates, while for data signals the slow scaling factor $y_l(k)$ prevails.

2.7.4 G.721 Adaptation Speed Control

The computation of the adaptation speed control is based on two measures of the average value of $I(k)$. Namely, d_{ms} describes the relatively short term average of $I(k)$, while d_{ml} constitutes a relatively long term average of it, which are defined by the G.721 standard as

$$d_{ms}(k) = (1 - 2^{-5})d_{ms}(k-1) + 2^{-5}F[I(k)] \tag{2.61}$$

and

$$d_{ml}(k) = (1 - 2^{-7})d_{ml}(k-1) + 2^{-7}F[I(k)], \tag{2.62}$$

where $F[I(k)]$ is given in the G.721 Recommendation as specified by Table 2.4. Explicitly, due to the higher scaling factor of 2^{-5} the short-term average is more dependent on the current value of $I(k)$ than the long-term average, although both averages are more resemblant of their own 2^{-7} scaled previous values due to the near-unity scaling of their preceding values. As a result of the zero-valued weighting function $F[I(k)]$ these averages in fact do not take into account the value of $I(k)$, if it happens to be small.

Table 2.4: Definition of the factor $F[I(k)]$. Copyright © CCITT G.721.

$\lvert I(k)\rvert$	7	6	5	4	3	2	1	0
$F[I(k)]$	7	3	1	1	1	0	0	0

From the above averages, the variable $a_p(k)$ – which will be used in the definition of the adaptation speed control factor – was defined by the G.721 Recommendation as

$$a_p(k) = \begin{cases} (1 - 2^{-4})a_p(k-1) + 2^{-3} & \text{if } |d_{ms}(k) - d_{ml}(k)| \geq 2^{-3}d_{ml}(k) \\ (1 - 2^{-4})a_p(k-1) + 2^{-3} & \text{if } y(k) < 3 \\ (1 - 2^{-4})a_p(k-1) & \text{otherwise.} \end{cases} \tag{2.63}$$

More explicitly, the adaption speed control factor $a_p(k)$ is increased and in the long term tends towards the value 2, if the normalised short- and long-term average difference $[d_{ms}(k) - d_{ml}(k)]/d_{ml}(k) \geq 2^{-3}$, that is if the magnitude of $I(k)$ is changing. Although it is not obvious at first sight, this is because of the factor two difference between the positive and negative scaling factors of 2^{-3} and 2^{-4} in Equation (2.63). By contrast, the adaption speed control factor a_p is decreased and tends to zero if the difference of the above short- and long-term prediction error averages is relatively small, that is if $I(k)$ is near constant. This is due to the continuous decrementing action of the 2^{-4} factor in the third line of Equation (2.63). Furthermore, for an idle channel, where no significant scaling is required and the scaling

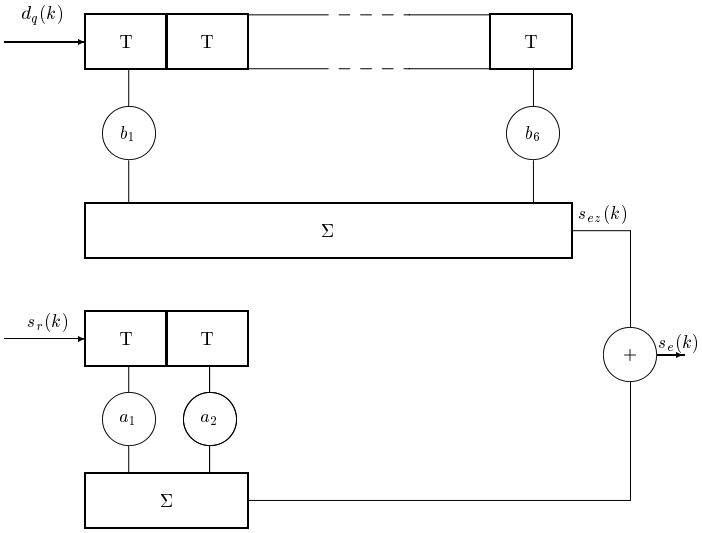

Figure 2.10: Adaptive six-zero, two-pole predictor in the G.721 32 kbp in APPCM codec.

factor satisfies $y(k) < 3$, the quantity $a_p(k)$ is increased and also tends to 2, irrespective of the value of the above normalised difference.

Finally, the adaptation speed control factor a_l used in Equation (2.60) is derived by limiting a_p according to the G.721 Recommendation, as

$$a_l(k) = \begin{cases} 1 & \text{if } a_p(k-1) > 1 \\ a_p(k-1) & \text{if } a_p(k-1) \leq 1. \end{cases} \tag{2.64}$$

This limiting operation renders the actual value of $a_p(k)$ irrelevant, as long as it is larger than one. By keeping $a_l(k)$ constant until $a_p(k)$ falls below one, this condition postpones the premature start of a fast to slow transition, if the differences in the average value of $I(k)$ were low only for a limited period of a few sampling intervals.

2.7.5 G.721 Adaptive Prediction and Signal Reconstruction

Let us now concentrate our attention on the action of the adaptive predictor of Figure 2.9, which generates the signal estimate $s_e(k)$ from the quantised difference signal $d_q(k)$, as seen also in Figure 2.10. Much of this adaptive predictor design research is due to Jayant [78]. Explicitly, the predictor's transfer function is characterised by six zeros and two poles. This pole-zero predictor models the spectral envelope of a wide variety of input signals efficiently. Note, however, that the previously described Levinson–Durbin algorithm was applicable to the problem of an all-pole model only. The reconstructed signal is given by

$$s_r(k-i) = s_e(k-i) + d_q(k-i), \tag{2.65}$$

where the signal estimate $s_e(k-i)$ seen in Figure 2.9 is derived from a linear combination of the previous reconstructed samples and that of the previous quantised differences d_q, using

$$s_e(k) = \sum_{i=1}^{2} a_i(k-1)s_r(k-i) + \sum_{i=1}^{6} b_i(k-1)d_q(k-i), \tag{2.66}$$

where the factors $a_i,\ \ i = 1, \ldots, 2$, and $b_i,\ \ i = 1, \ldots, 6$, represent the corresponding predictor coefficients. Both sets of predictor coefficients – $a_i(k)$ and $b_i(k)$ – are recursively computed using a somewhat complex gradient algorithm, which we will describe first in analytical terms following the G.721 Recommendation and then provide a brief verbal interpretation of the expressions. Explicitly, the first of the second-order predictor coefficients is specified as

$$a_1(k) = (1 - 2^{-8})a_1(k-1) + (3 \cdot 2^{-8})\,\mathrm{sgn}[p(k)]\,\mathrm{sgn}[p(k-1)], \tag{2.67}$$

where $a_1(k)$ depends strongly on $a_1(k-1)$ as well as on the coincidence of the polarity of two consecutive samples of the variable $p(k)$, where

$$p(k) = d_q(k) + \sum_{i=1}^{6} b_i(k-1)d_q(k-i)$$

represents the sum of the current quantised prediction error $d_q(k)$ and the estimated or predicted signal contribution at the output of the sixth-order zero-section of the predictor due to previous values of $d_q(k)$, while using the coefficients $b_i(k-1)$. Specifically, when updated, a_1 is increased by the second term of Equation (2.67), if the polarity of two consecutive $p(k)$ values coincides, and decreased otherwise. Note, however, that this adaptation is a slow process due to the scaling factor of $(3-1) \cdot 2^{-8}$.

A similar adaptation process is applied, in order to control the second coefficient of the predictor's zero section, as follows:

$$\begin{aligned} a_2(k) = (1 - 2^{-7})a_2(k-1) + 2^{-7}\{&\mathrm{sgn}[p(k)]\,\mathrm{sgn}[p(k-1)] \\ &- f[a_1(k-1)]\,\mathrm{sgn}[p(k)]\,\mathrm{sgn}[p(k-1)]\}, \end{aligned} \tag{2.68}$$

where the function $f(a_1)$ is given by

$$f(a_1) = \begin{cases} 4a_1 & \text{if } |a_1| \leq 1/2 \\ 2\,\mathrm{sgn}(a_1) & \text{if } |a_1| > 1/2 \end{cases}$$

and where $\mathrm{sgn}(0) = +1$. Note that Equation (2.68) is similar to Equation (2.67), but the effect of the third term governed by the value of a_1 is more dominant, since it is not scaled down by the factor 2^{-7}. If $|a_1| < 0.5$, then $a_2(k)$ is decreased by the third term, when the adjacent $p(k)$ samples have an identical polarity. If, however, $|a_1| > 0.5$, the polarity of a_1 also enters the complex interplay of parameters. Lastly, there are two stability constraints, which have to be satisfied, namely

$$|a_2(k)| \leq 0.75 \wedge |a_1(k)| \leq 1 - 2^{-4} - a_2(k). \tag{2.69}$$

The sixth-order predictor is updated using the following equation:

$$b_i(k) = (1 - 2^{-8})b_i(k-1) + 2^{-7}\,\mathrm{sgn}[d_q(k)]\,\mathrm{sgn}[d_q(k-i)] \quad \text{for } i = 1, \ldots, 6, \quad (2.70)$$

where the predictor coefficients are constrained to the range $-2 \leq b_i(k) \leq 2$. Observe in Equation (2.70) that $b_i(k)$ is increased upon updating, if the polarity of the current and previous quantised prediction error samples $d_q(k)$ and $d_q(k-i)$, $i = 1, \ldots, 6$, coincides, and decreased otherwise. This is because the 2^{-7} scaling factor of the second term outweighs the reduction caused by the leakage factor of 2^{-8} in the first term.

The ADPCM decoder uses identical functional blocks to those of the encoder, as seen in Figure 2.9. We point out that when transmitting ADPCM-coded speech, the bit-sensitivity within each four-bit symbol monotonically decreases from the most significant bit (MSB) towards the least significant bit (LSB), since the corruption of the MSB inflicts the largest waveform distortion, while the LSB inflicts the smallest. After this rudimentary description of the G.721 ADPCM codec, we first offer a short introduction to speech quality evaluation, which will be followed by a brief account of two closely related standardised ADPCM based codecs, namely the CCITT G.726 and G.727 schemes.

2.8 Subjective and Objective Speech Quality

In order to be able to assess and compare the speech quality of various speech codecs, here we introduce a few speech-quality measures, while a more in-depth treatment is offered in Chapter 18. In general the speech quality of communications systems is difficult to assess and quantify. The most reliable quality evaluation methods are subjectively motivated, such as the so-called *mean opinion score* (MOS), which uses a five-point scale ranging between one and five. MOS tests facilitate the direct evaluation of arbitrary speech impairments by untrained listeners, but their results depend on the test conditions. Specifically, the selection and ordering of the test material, the language and listener expectations all influence their outcome. A variety of other subjective measures is discussed in references [85–87], but subjective measures are tedious to derive and difficult to quantify during system development.

By contrast, *Objective speech-quality* measures do not provide results that could be easily converted into MOS values, but they facilitate quick comparative measurements during research and development. Most objective speech-quality measures quantify the distortion between the speech communications system's input and output either in time or in frequency domain. The conventional SNR can be defined as

$$\mathrm{SNR} = \frac{\sigma_{\mathrm{in}}^2}{\sigma_e^2} = \frac{\sum_n s_{\mathrm{in}}^2(n)}{\sum_n [s_{\mathrm{out}}(n) - s_{\mathrm{in}}(n)]^2}, \quad (2.71)$$

where $s_{\mathrm{in}}(n)$ and $s_{\mathrm{out}}(n)$ are the sequences of input and output speech samples, while σ_{in}^2 and σ_e^2 are the variances of the input speech and that of the error signal, respectively. A major drawback of the conventional SNR is its inability to give equal weighting to high- and low-energy speech segments, since its value will be dominated by the SNR of the higher-energy voiced speech segments. Therefore the reconstruction fidelity of voiced speech is

given higher priority than that of low-energy unvoiced sounds when computing the arithmetic mean of the SNR, which can be expressed in dB as $\mathrm{SNR}^{\mathrm{dB}} = 10\log_{10}\mathrm{SNR}$. Hence a system optimised for maximum SNR usually is suboptimum in terms of subjective perceptual speech quality.

Some of the ills of speech SNR computation mentioned above can be mitigated by defining the so-called *segmental SNR* (SEGSNR) objective measure as

$$\mathrm{SEG-SNR}^{\mathrm{dB}} = \frac{1}{M}\sum_{m=1}^{M} 10\log_{10}\frac{\sum_{n=1}^{N} s_{\mathrm{in}}^2(n)}{\sum_{n=1}^{N}[s_{\mathrm{out}}(n)-s_{\mathrm{in}}(n)]^2}, \tag{2.72}$$

where N is the number of speech samples within a segment of typically 15–25 ms, i.e. 120–200 samples at a sampling rate of 8 kHz, while M is the number of 15–25 ms segments, over which $\mathrm{SEGSNR}^{\mathrm{dB}}$ is evaluated. Clearly, the SEGSNR relates the ratio of the *segmental signal energy* to the *segmental noise energy*, computed over 15–25 ms segments and, after expressing this ratio in terms of dB, averages the corresponding values in the logarithmic domain. The advantage of using $\mathrm{SEGSNR}^{\mathrm{dB}}$ over the conventional SNR is that by averaging the $\mathrm{SNR}^{\mathrm{dB}}$ values in the logarithmic domain it gives a more 'fair' weighting to low-energy unvoiced segments by effectively computing the geometric mean of the SNR values instead of the arithmetic mean. Hence the SEGSNR values correlate better with subjective speech quality measures, such as the MOS. Further speech quality measures are discussed in depth in Chapter 18.

2.9 Variable-rate G.726 and Embedded G.727 ADPCM

2.9.1 Motivation

In recent years two derivatives of the G.721 Recommendation have been approved by the CCITT (now known as the International Telecommunication Union (ITU)). Namely, the G.726 and G.727 Standards, both of which can operate at rates of 16, 24, 32 and 40 kbps. The corresponding number of bits/sample is 2, 3, 4 and 5. The latter scheme also has the attractive feature that the decoder can operate without prior knowledge of which transmission rate was used by the encoder. This is particularly useful in packetised speech systems, such as those specified by the ITU G.764 Standard which is referred to as the *packetised voice protocol (PVP)*. Accordingly, congested networks can be relieved by discarding some of the LSBs of the packets at packetisation or intermediate nodes.

The schematic of the G.726 codec is identical to that of the previously described G.721 codec, which was shown in Figure 2.9. This is also reflected in the identical structure of the two standard documents. Note, however, that at its various rates different definition tables and constants must be invoked by the G.726 scheme. Hence, Tables 2.2–2.4 are appropriately modified in the G.726 and G.727 Standards for the 2, 3 and 5 bits/sample modes of operation, respectively, and the reader is referred to the standards for their in-depth study. Here we refrain from discussing the G.726 Recommendation in depth and focus our attention on the G.727 codec in order to be able to describe the principle of *embedded ADPCM coding*.

2.9.2 Embedded G.727 ADPCM Coding

A specific feature of embedded ADCM coding is that the decision levels of the lower-rate codecs constitute a subset of those of the higher-rate codecs. In other words, the embedded codec produces a codeword which consists of so-called *core bits* that cannot be dropped and *enhancement bits* which can be neglected at the decoder. The corresponding codec arrangement is portrayed in Figure 2.11, where the *bit masking block* ensures that the local decoder relies only on a more coarse estimate $I_c(k)$ of the quantised prediction error $I(k)$. Explicitly, only the core bits are used in the computation of the locally reconstructed signal and to control the adaptive predictor, since the enhancement bits may not be available at the decoder. The decoder in Figure 2.11 generates both the lower-resolution reconstructed signal used to control the adaptive predictor at both ends, and the full-resolution signal based on the assistance of the enhancement bits.

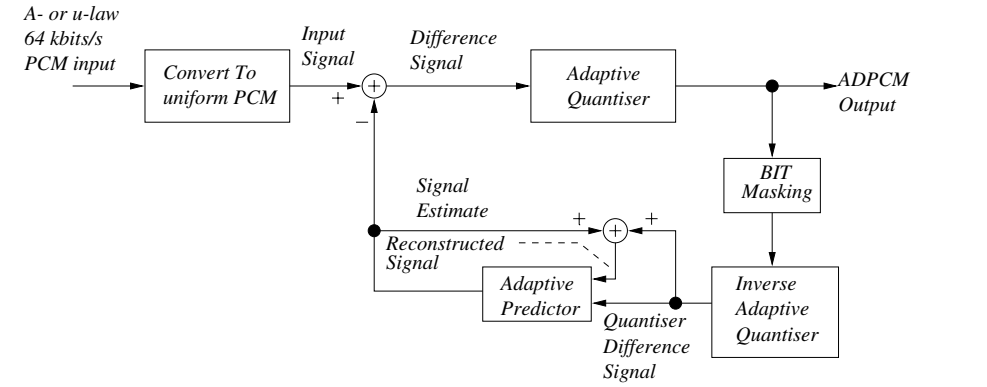

a) Encoder

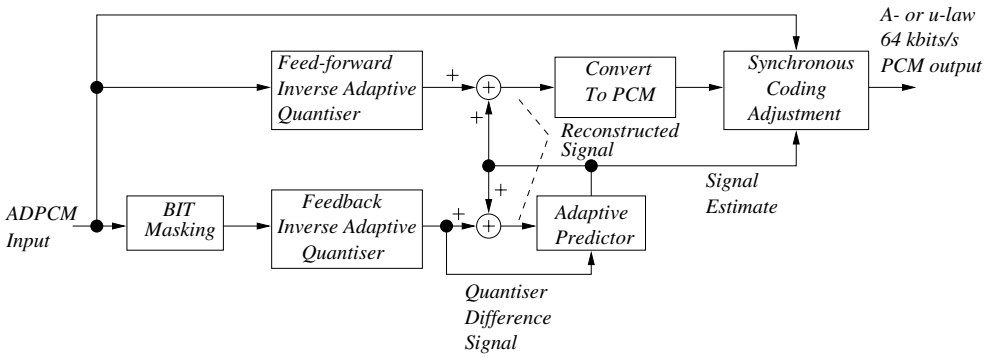

b) Decoder

Figure 2.11: G.727 embedded ADPCM codec schematic, where only the core bits are used for prediction, while the enhancement bits, when retained, are used to enhance the reconstructed signal quality.

The corresponding ADPCM coding algorithms can be specified with the help of the number of core bits y and enhancement bits x as (x, y). The possible combinations are: $(5, 2)$, $(4, 2)$, $(3, 2)$, $(2, 2)$, $(5, 3)$, $(4, 3)$, $(5, 4)$ and $(4, 4)$.

Example. *By referring to a* $(3, 2)$ *embedded scheme show how the embedded principle can be exploited to drop enhancement bits without unacceptably impairing the speech quality.*

The normalised quantisation intervals for the 16 kbps and 24 kbps modes are shown in Tables 2.5 and 2.6, respectively.

Table 2.5: Quantiser normalised input/output characteristic for 16 kbps embedded operation of the G.727 codec.

Normalised quantiser input range $\log_2 \lvert d(k)\rvert - y(k)$	$\lvert I(k)\rvert$ $\lvert I_c(k)\rvert$	Normalised quantiser output $\log_2 \lvert d_q(k)\rvert - y(k)$
$(-\infty, 2.04)$	0	0.91
$[2.04, \infty)$	1	2.85

Table 2.6: Quantiser normalised input/output characteristic for 24 kbps embedded operation, where the decision thresholds seen in Table 2.5 constitute a subset.

Normalised quantiser input range $\log_2 \lvert d(k)\rvert - y(k)$	$\lvert I(k)\rvert$ $\lvert I_c(k)\rvert$	Normalised quantiser output $\log_2 \lvert d_q(k)\rvert - y(k)$
$(-\infty, 0.96)$	0	-0.09
$[0.96, 2.04)$	1	1.55
$[2.04, 2.78)$	2	2.40
$[2.78, \infty)$	3	3.09

In Tables 2.5 and 2.6, '[' indicates that the endpoint value is included in the range, and '(' or ')' indicates that the endpoint value is excluded from the range. Observe in the first columns of the tables that in the higher resolution 3-bit mode both the lower and higher quantiser input ranges of the 2-bit mode are split into two further intervals and, in order to differentiate between these intervals, the 24 kbps codec assigns an extra bit to improve the quantiser's resolution. When this enhancement bit is dropped in the network, the decoder will be unable to use it in order to output a reconstruction level, which is in the centre of one of the eight quantisation intervals of the 24 kbps codec. Instead, it will output a reconstruction level, which is at the centre of one of the four quantisation intervals of the 16 kbps codec.

2.9.3 Performance of the Embedded G.727 ADPCM Codec

In what follows, we will characterise the expected performance of the well-established standard G.727 ADPCM speech codec at a range of bitrates. Initially the efficiency of the adaptive predictor is characterised with the help of the prediction residual and its statistical parameters, the PSD and the ACF, which are portrayed in Figures 2.12–2.15 for the voiced and unvoiced speech segments used earlier in Figures 1.2–1.5.

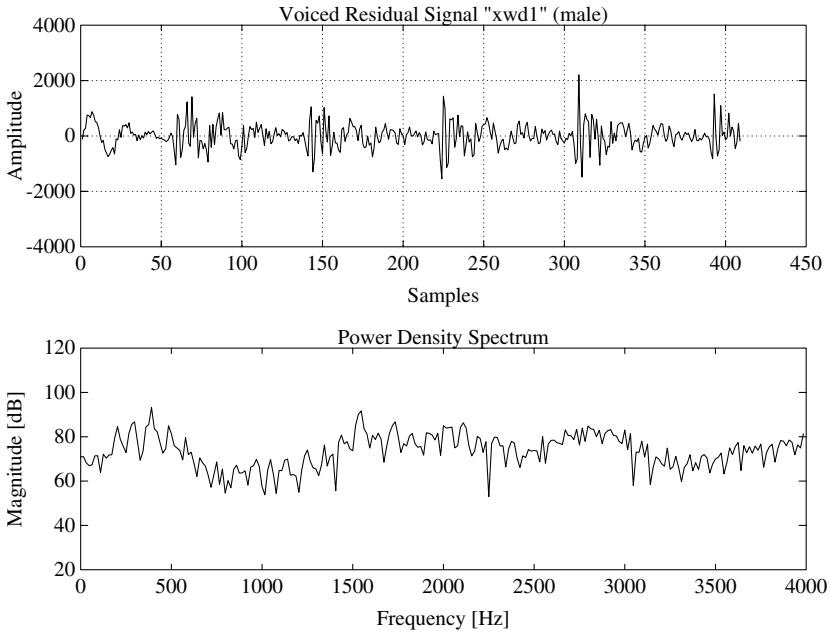

Figure 2.12: Prediction residual of the typical voiced speech segment of Figure 1.2 (top trace) and its PSD for a male speaker (bottom trace).

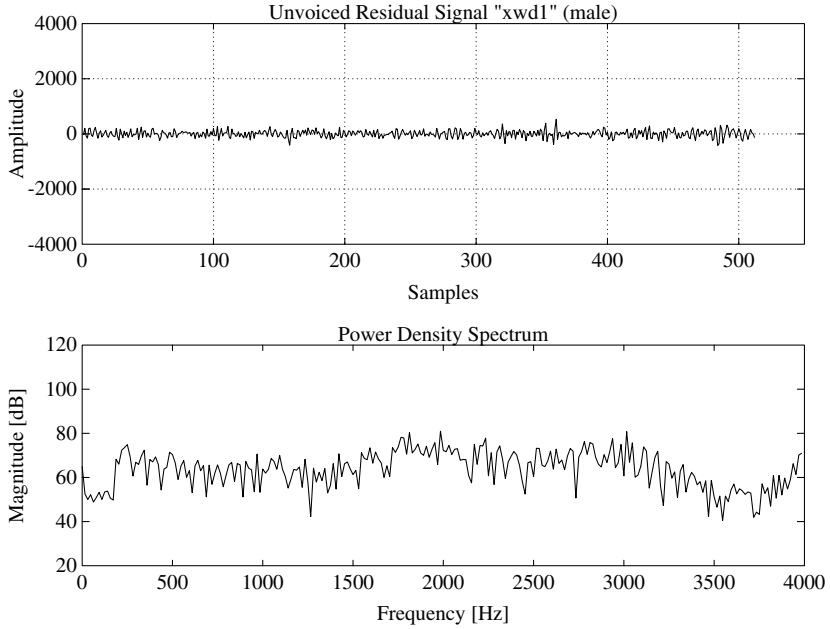

Figure 2.13: Prediction residual of the typical unvoiced speech segment of Figure 1.3 (top trace) and its PSD for a male speaker (bottom trace).

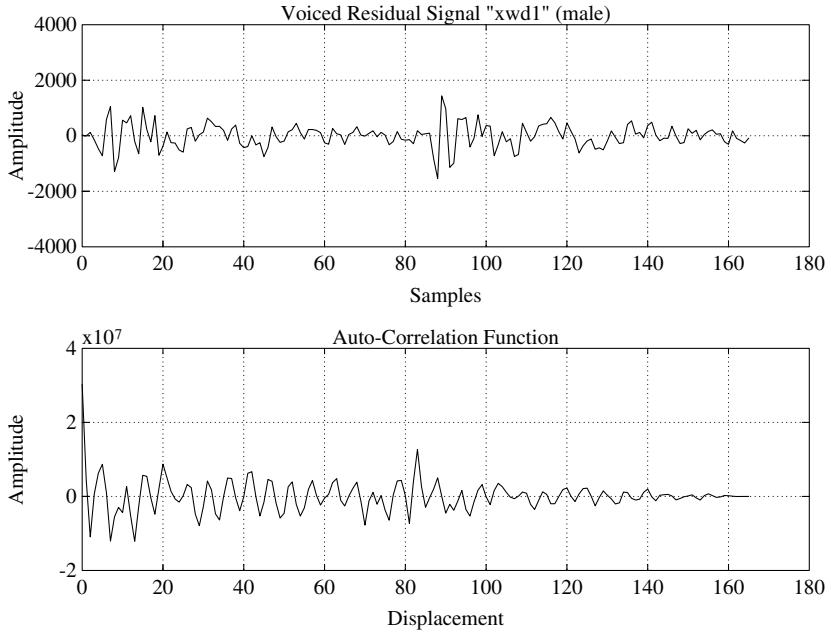

Figure 2.14: Prediction residual of the typical voiced speech segment of Figure 1.4 (top trace) and its ACF for a male speaker (bottom trace).

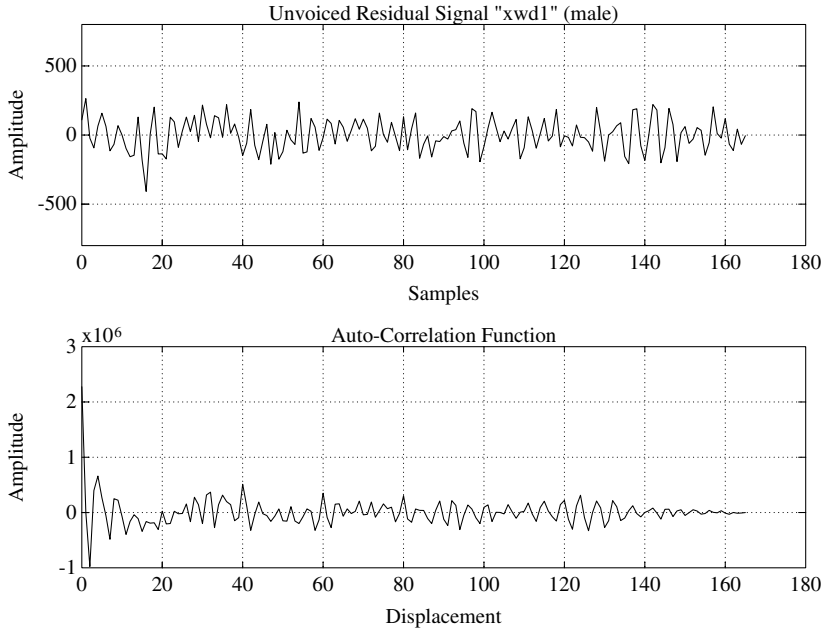

Figure 2.15: Prediction residual of the typical unvoiced speech segment of Figure 1.5 (top trace) and its ACF for a male speaker (bottom trace).

It becomes clear from the pair-wise comparison of Figures 1.2 and 2.12 that in the case of voiced speech the prediction residual has a substantially reduced variance, although it still retains some high values in the region of the highest time-domain peaks of the original speech signal. This is due to the fact that the predictor is attempting to predict an ever-increasing signal on the basis of its past samples, while the signal has actually started to recede. The PSD of the prediction residual is much flatter than that of the original signal and it becomes similar to that of band-limited white noise.

The unvoiced speech segment of Figure 1.3 and its corresponding residual signal of Figure 2.13 are both noise-like, but the associated PSD functions show that the spectrum of the unvoiced speech segment has also been further flattened. These tendencies are also confirmed by comparing Figures 1.4 and 2.14 in the case of the voiced segment using an expanded scale, where the ACF became substantially narrower in the case of the voiced residual signal. The unvoiced ACF shown in Figure 1.5 exhibited virtually no correlation and hence the prediction residual's ACF is also quite similar, as is demonstrated by Figure 2.15. A consequence of this is that in the case of unvoiced speech segments, predictive coding does not significantly improve the coding efficiency. However, since human speech is voiced for significantly longer periods of time than it is unvoiced and also due to the typically higher voiced energy, the perceived speech quality is more dependent on that of voice segments, and hence substantial coding efficiency is achieved by predictive codecs.

Figure 2.16 characterises the codec's performance in time domain by portraying both a voiced and an unvoiced speech segment along with the corresponding reconstruction error signal between the original and the reconstructed speech for bitrates of 32, 24 and 16 kbps, that is using 4, 3 and 2 bits/symbol.

In order to characterise the various operating modes of the G.727 codec in more formal terms the fluctuation of the segmental signal energy and segmental residual energy are plotted in Figure 2.17 as a function of the frame index for a male speaker using our test file 'xwd1' at 32 kbps using 4 core bits and no enhancement bits. Each frame was constituted by 20 ms speech, corresponding to 160 samples at a sampling rate of 8 kHz. Observe in the figure that both functions exhibit a high dynamic range, and a bimodal nature, corresponding to high energy in the case of voiced segments and low energy for unvoiced segments. In the vicinity of very low-energy voiced segments the residual energy is not significantly lower than the signal's energy, but in the case of voiced segments there is typically at least a 10 dB energy reduction due to the employment of predictive coding, exceeding 30 dB occasionally.

Similar tendencies can be inferred from Figure 2.18, where the fluctuation of the segmental speech energy, SEGSNR and prediction gain are displayed as a function of the frame index for the 40 kbps mode of operation of the G.727 codec, when employing 4 core bits and one enhancement bit. The SEGSNR fluctuates around 30 dB, but occasionally reaches 50 dB, which is associated with perceptually unimpaired, transparent speech quality.

The objective speech quality of a representative subset of the possible modes of operation of the G.727 codec, namely that of the $(5, 4)$, $(4, 4)$, $(3, 3)$ and $(2, 2)$ modes is shown in Figure 2.19 in terms of a set of SEGSNR versus frame index plots for our 'xwd1' male test file. All curves follow the same tendencies and the corresponding average SEGSNR values can be read from Figure 2.20 for bitrates between 16 and 40 kbps. Observe that the associated SEGSNR versus bitrate curves are nearly linear and the SEGSNR improvement

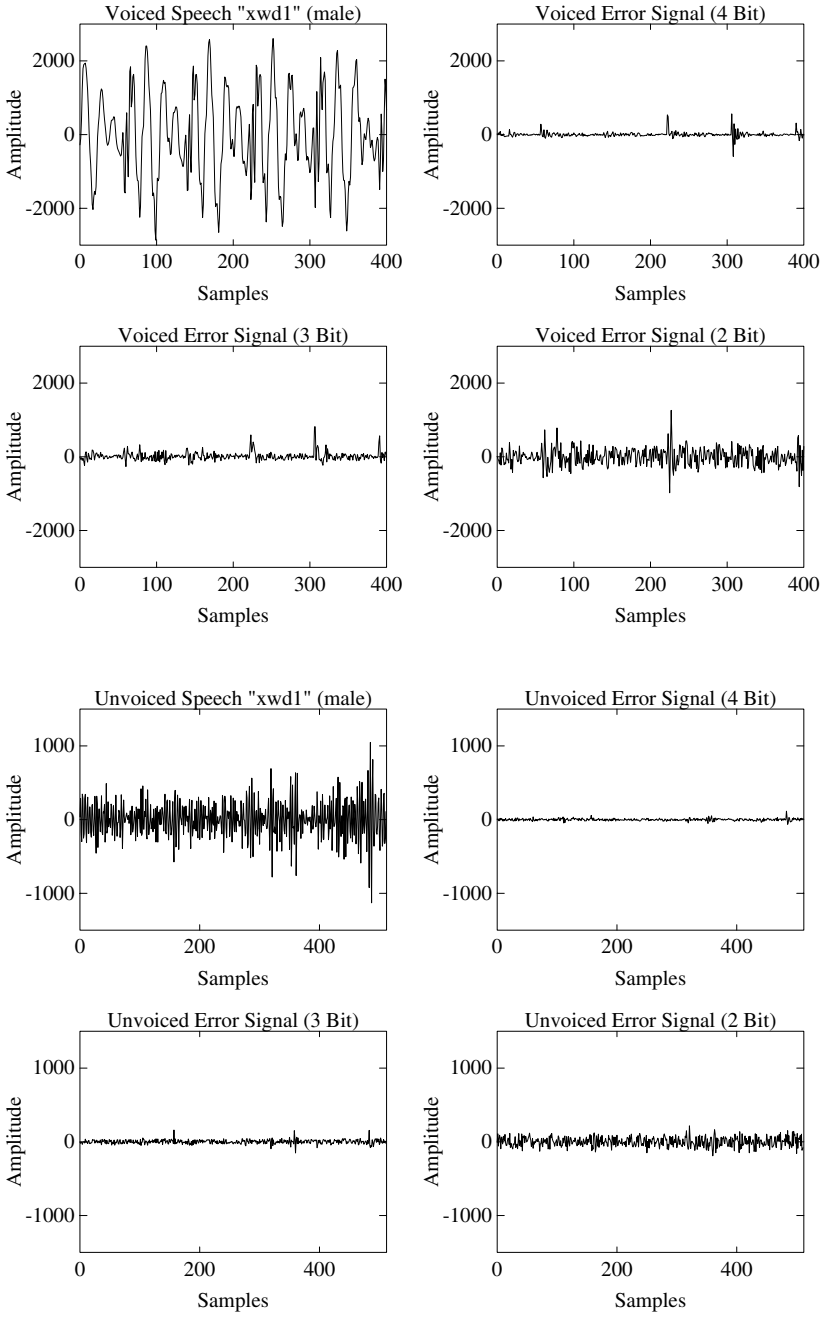

Figure 2.16: Typical voiced and an unvoiced speech segment and the corresponding reconstruction error signal between the original and the reconstructed speech generated by the G.727 codec for bitrates of 32, 24 and 16 kbps, that is using 4, 3 and 2 bits/symbol.

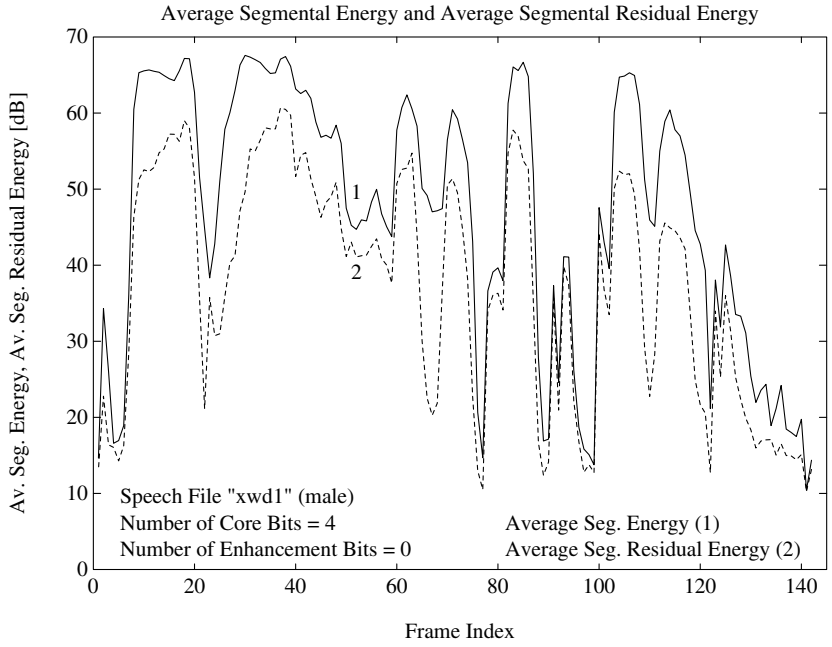

Figure 2.17: Segmental speech energy (1) and segmental residual energy (2) versus frame index for a male speaker at 32 kbps using 4 core bits and no enhancement bits.

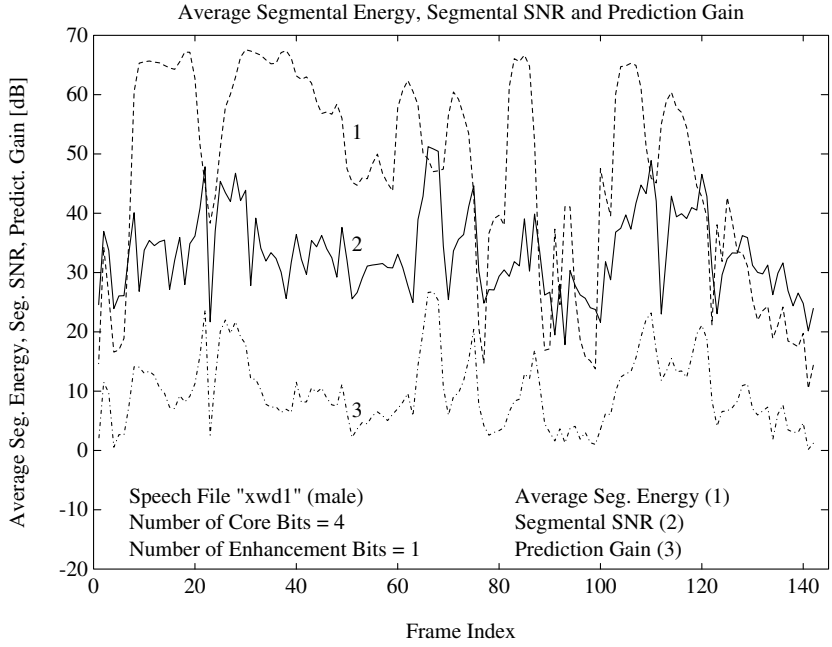

Figure 2.18: Segmental speech energy (1), SEGSNR (2) and prediction gain (3) versus frame index for a male speaker at 40 kbps using 4 core bits and 1 enhancement bit.

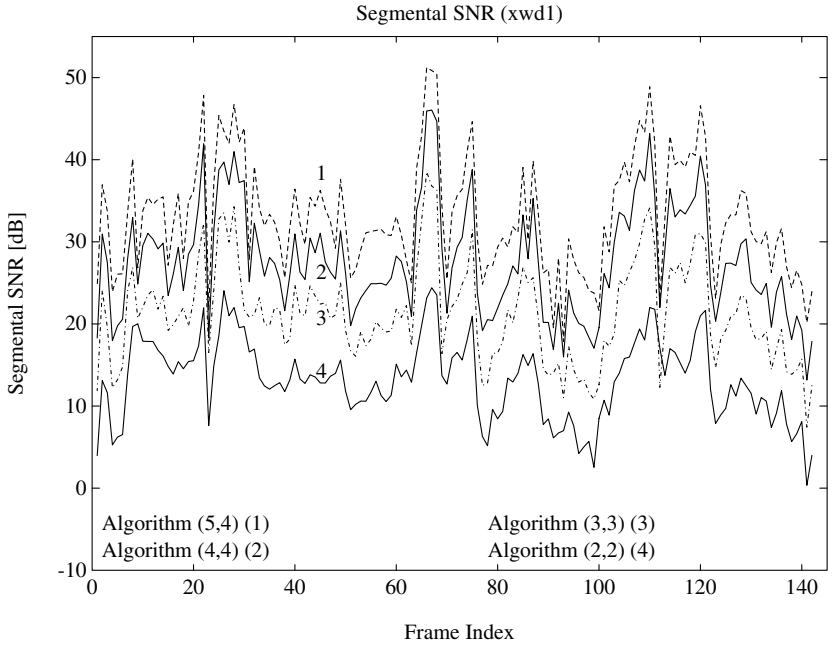

Figure 2.19: SEGSNR versus frame index for a male speaker using the G.727 algorithms $(5, 4)$ (1), $(4, 4)$ (2), $(3, 3)$ (3) and $(2, 2)$ (4).

due to increasing the bitrate is approximately 15 dB per octave. For example, when doubling the bitrate from 16 to 32 kbps, the SEGSNR improves from about 15 to around 30 dB for a female speaker and from 13 to around 28 dB for a male speaker.

Before concluding this chapter, in the next section we briefly consider the performance estimates provided by the application of rate-distortion theory for the family of predictive codecs.

2.10 Rate-distortion Theory in Predictive Coding

In Section 1.4.3 we applied rate-distortion theory to conventional waveform codecs in order to derive performance estimates. In this section we will attempt to provide similar results for the family of predictive codecs. In general, the rate-distortion function is not known in a closed form for arbitrary source distributions and distortion measures. However, for the MSE distortion function some results are known, and we consider only this measure. For convenience we repeat Equation (1.5) from Section 1.4.3, stating that for a memoryless Gaussian distributed source x having a variance σ_x^2 the rate-distortion function can be expressed as

$$R_D = \begin{cases} \frac{1}{2}\log_2 \sigma_x^2/D & 0 \leq D \leq \sigma_x^2 \\ 0 & D > \sigma_x^2. \end{cases} \tag{2.73}$$

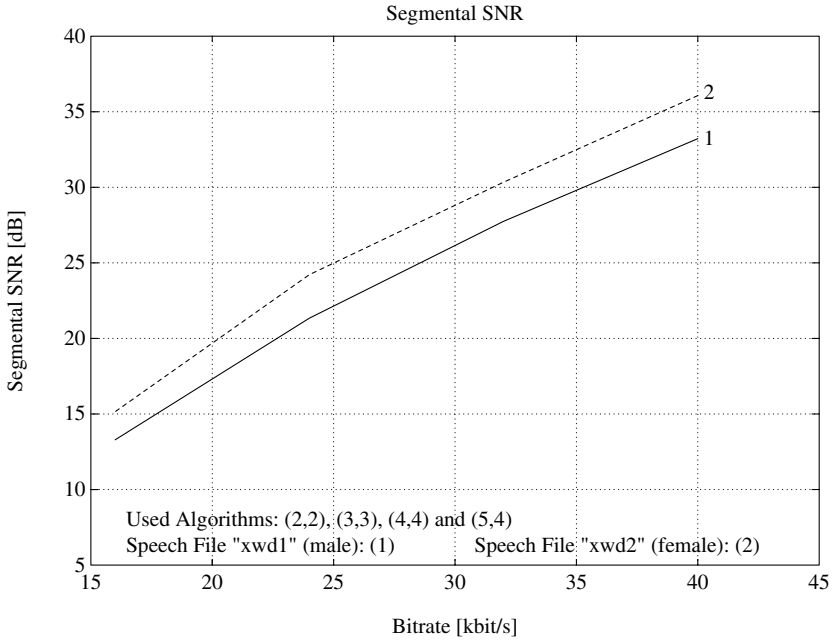

Figure 2.20: SEGSNR versus bitrate performance of the G.727 codec for female (2) and male (1) speakers using the algorithms $(2, 2)$, $(3, 3)$, $(4, 4)$ and $(5, 4)$.

For other memoryless sources, $R(D)$ curves can be calculated numerically, and it can be shown that the rate distortion function for a Gaussian source upper bounds $R(D)$ for all other sources with the same variance. For example, a memoryless source with the Gamma PDF (which is a close approximation to the long-term PDF of speech signals) can be coded with an SNR of 8.53 dB at the rate of 1 bpsample [88], compared to an SNR of 6.02 dB for a Gaussian source at the same rate.

For sources exhibiting memory, the rate necessary for reproducing the source signal with a given distortion is always less than the rate for a similar source with no memory. This is because sources having memory are predictable, hence they can be more accurately represented at a given bitrate. Predictability exhibits itself in terms of a non-flat PSD, as was mentioned before. For a coloured, that is spectrally non-flat Gaussian source having a power spectral density $S(\omega)$, $R(D)$ can be calculated as

$$D(\phi) = \frac{1}{2\pi} \int_{-\pi}^{\pi} \min(\phi, S(\omega))\, \mathrm{d}\omega$$
$$R(\phi) = \frac{1}{2\pi} \int_{-\pi}^{\pi} \max\left(0, \frac{1}{2} \log_2 \frac{S(\omega)}{\phi}\right)\, \mathrm{d}\omega, \tag{2.74}$$

since in the low-energy speech spectral bands of Figures 2.21 and 2.22 below the dashed lines the PSD is set to zero.

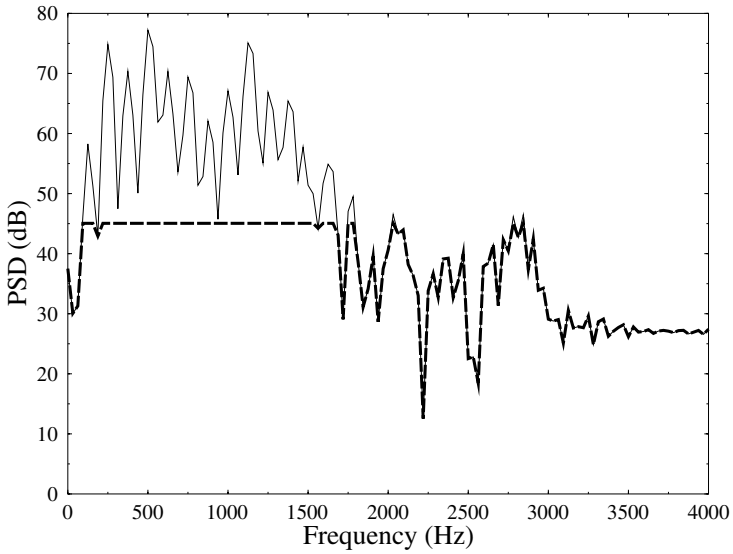

Figure 2.21: Power spectrum density for a segment of voiced speech as well as $\min[\phi, S(\omega)]$ shown using a dashed line.

This implies that the threshold level ϕ is chosen according to the required rate/distortion. In the frequency regions, where the speech PSD dips below ϕ, that is where $\phi \geq S(\omega)$, no information is transmitted. For these regions – known as the stop-bands – the decoder should set the reconstructed power spectral density to zero, in order to minimise the average rate R. Therefore, in the stop-bands the average distortion is equal to the original PSD $S(\omega)$. By contrast, in the frequency regions where $S(\omega) \geq \phi$, known as the pass-bands, the distortion is equal to ϕ and the transmission rate is $\log_2 \sqrt{S(\omega)/\phi}$.

For small distortions, that is if ϕ is such that $S(\omega) \geq \phi$ for all ω, Equation (2.74) can be simplified to

$$R(D) = \frac{1}{2} \log_2 \frac{\sigma^2 \gamma^2}{D}, \tag{2.75}$$

where σ^2 is the variance and γ^2 is the so-called spectral flatness measure of the source signal. For a memoryless source we have a flat spectrum associated with $\gamma^2 = 1$ and Equation (2.75) is simplified accordingly.

The SNR (in dB) of the reconstructed signal is given by $10 \log_{10}(\sigma^2/D)$ and hence using Equation (2.75) we see that the maximum achievable SNR when coding at a rate of R bits/sample and using a high R value is given by

$$\begin{aligned} \mathrm{SNR}_{\max} &= 2R * 10 \log_{10}(2) - 10 \log_{10} \gamma^2 \\ &= T_B + T_P, \end{aligned} \tag{2.76}$$

where

$$T_B = 2R * 10 \log_{10}(2) \approx 6R \tag{2.77}$$

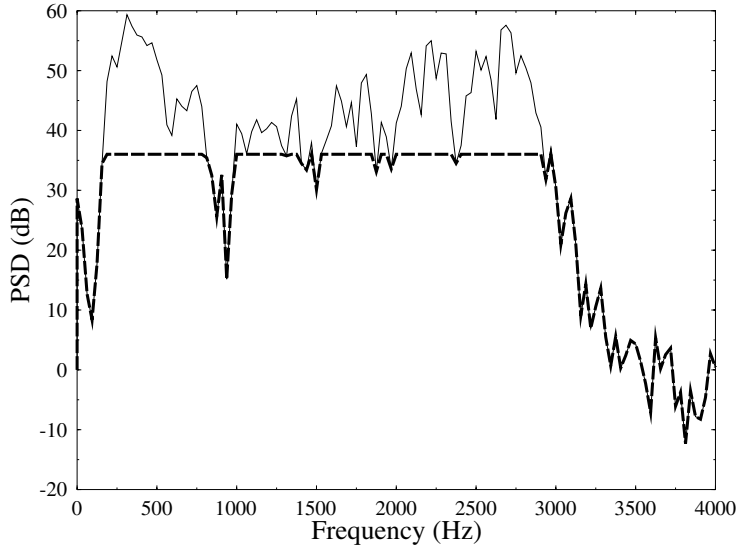

Figure 2.22: Power spectrum density for a segment of unvoiced speech as well as $\min[\phi, S(\omega)]$ shown using a dashed line.

and

$$T_P = 10 \log_{10} \frac{1}{\gamma^2}. \tag{2.78}$$

From Equation (2.78) we see that T_P can be thought of as the best possible gain (in dB) that can be produced by linear prediction of the signal.

As in the memoryless case, for non-Gaussian sources the exact form of $R(D)$ is not known. However, it can be shown that for a source having a given power spectral density, the distortion $R(D)$ will be less than or equal to the rate distortion function for a Gaussian source with the same PSD.

Rate distortion theory assumes that the source we are coding is stationary, with a power spectral density known at both the encoder and decoder. Speech, however, is non-stationary and can only be considered to be quasi-stationary for short periods of time, of the order of 20 ms. Furthermore, explicit rate distortion functions are known only for sources having a Gaussian distribution, which is not a good model for the long-term PDF of speech signals. Nevertheless, we can use simplified theory in order to give some idea of the optimum performance achievable by a speech codec, and as to how such an optimum coder will behave. For example, in [89] the predictions of rate-distortion theory, assuming a Gaussian source, are shown to agree reasonably well with the performance of practical speech codecs.

Equation (2.76) gives the maximum possible SNR for a stationary Gaussian source (for small distortions) in terms of the data rate (per sample) and the maximum possible prediction gain T_P of the signal. This gain was taken by O'Neal in [90] to be 21 dB (following suggestions by Atal and Schroeder). Thus, if speech was a stationary Gaussian source we

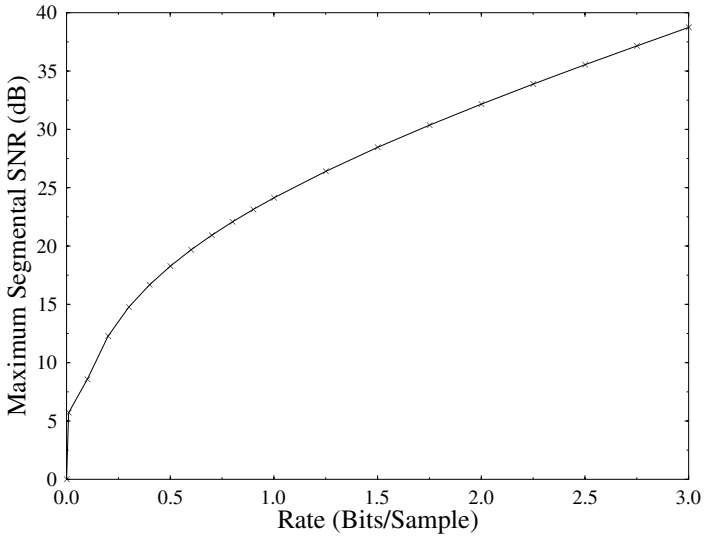

Figure 2.23: Predicted maximum possible SEGSNR.

could write for large rates R that

$$\mathrm{SNR}_{\max} \approx 21 + 6R \text{ (dB)}. \tag{2.79}$$

For lower rates – where $\phi > \min S(\omega)$) – the above equation will not be valid, and hence we have to use Equation (2.74) in order to calculate the achievable SNR for a given rate. We carried out this experiment using about seven seconds of speech, sampled at 8 kHz, obtained from two male and two female speakers. The speech signal was split into 256 sample segments, and we used the fast Fourier transform (FFT) of the Hamming-windowed samples in order to find the power spectrum $S(\omega)$ for each segment. Then for each segment an iterative procedure was used, invoking Equation (2.74) to find ϕ and hence D for a given rate.

The spectra of two typical segments, one voiced and the other unvoiced, are shown in Figures 2.21 and 2.22. Also shown in these figures in dashed lines are the functions $\min(\phi, S(\omega))$, which give the power spectra of the noise in an optimum encoder. The values of ϕ have been set to give a rate of one bpsample, and we found that at this rate the SNRs were about 21 dB for the voiced speech, and 14 dB for the unvoiced speech. The voiced segment can be encoded with a lower distortion than the unvoiced segment because of its greater predictability – we found that $T_P = -10 \log_{10} \gamma^2$ was 20 dB for the voiced speech and 15 dB for the unvoiced speech.

Figure 2.23 shows the predicted maximum SEGSNR against the data rate. This was calculated by finding the SNR in decibels for each speech segment as described above, and then averaging over the test file's duration. We also calculated the maximum prediction gain T_P in a similar way and found that it was 20.9 dB, agreeing well with the value used in [90]. Notice that for rates above about 1.5 bits/sample the curve in Figure 2.23 becomes approximately a straight line, as predicted by Equation (2.79).

In the discussion above we have considered each 256 sample (32 ms) segment of speech to be a stationary Gaussian signal. We now discuss how these assumptions are likely to affect our results. Firstly, although the long-term statistics of speech closely match the Gamma PDF, the short-term statistics are approximately Gaussian [91]. Therefore assuming the 32 ms segments of speech to be Gaussian will probably not affect the validity of our results too gravely. The non-stationarity will have a more significant effect, and will result in the true 'maximum SNR' function for speech lying somewhere below that drawn in Figure 2.23. Thus the maximum SNR values we have calculated give an upper bound for the SNR that could be obtained with the aid of a practical speech codec.

We can produce a tighter bound by evaluating, how the non-stationary nature of speech will affect our results. The first difference will be that for a speech codec to obtain a prediction gain close to T_P it will have to send side information about the current spectrum of the signal to the decoder. The rate necessary for this side information (say $\hat{R}$ bits/sample) will reduce the effective rate R of the codec. The side information necessary to support short-term linear prediction at the current state-of-the-art is about 20 bits per 20 ms or 160 speech samples, requiring on average about 1/8 bits per sample, and we take this as the necessary rate $\hat{R}$. Secondly, the prediction gain possible will be reduced below T_P because of the non-stationary nature of speech, and also because only limited information about the present correlations in the signal is sent in the side information (that is the gain will be dependent on $\hat{R}$). For example, for the speech file referred to earlier, the calculated value of T_P is 21 dB, but the gain achieved with the aid of short-term linear prediction (of order 10) is only 17 dB.

At bitrates above about 1.5 bits per sample, Equation (2.79) gives a good approximation to the maximum SEGSNR possible for a speech codec, provided that we take into account the effects mentioned above. For a 16 kbps codec the bitrate is 2 bits per sample and hence the effective rate R is about 1.875 bits per sample. Thus, using 4 dB as the reduction of the prediction gain T_p, the maximum SEGSNR predicted for a 16 kbps speech codec is about 28 dB. At rates below 1 bit per sample Equation (2.79) is no longer accurate, and hence we have to use Figure 2.23, in order to estimate the maximum SEGSNR of speech codecs at these rates. Furthermore, the effect of the reduction in T_p will be less significant than the 4 dB figure used above, because of the fall of the maximum SNR figures below $T_p + 6R$. We take a decrease of about 2 dB to be typical at low rates. These assumptions mean that the effective rate R for a 4.7 kbps codec will be about 0.45 bits/sample, giving a maximum SEGSNR of around $17.5 - 2 = 15.5$ dB. Similarly, we predict a maximum possible SEGSNR of about 19 dB at 7.1 kbps. It is interesting to compare these figures with those obtained for a range of CELP speech codecs that are to be described later in Chapter 6, which operate at the same rates. It is equally instructive to compare these estimates with the experimentally evaluated results of the G.727 codec in Figure 2.20.

2.11 Chapter Summary

In this chapter we initially highlighted the basic principles of forward-predictive as well as DPCM-based coding. This was followed by the design principles of the optimum linear predictor invoking the Levinson–Durbin algorithm. Jayant's adaptive one-word-memory quantiser was then characterised, leading to our discussions on AR, MA and ARMA processes. The associated predictors were then invoked in the context of the ITUs G.721,

G.726 and G.727 Standard codes. Finally, the performance of predictive codecs was characterised.

Having considered a range of low-complexity predictive codecs in this chapter, in the next chapter we will concentrate on the family of lower bitrate, higher complexity AbS speech codecs. These AbS codecs are widely used in most existing mobile radio systems at the time of writing.

Part II

Analysis-by-Synthesis Coding

Chapter 3

Analysis-by-Synthesis Principles

3.1 Motivation

Recall from Section 1.2 that we argued that human speech can be adequately described with the help of the linearly separable speech production model of Figure 1.1, where the excitation signal is filtered through a slowly varying spectral shaping system in order to generate the speech signal. In a simple inverse approach one could view speech production as filtering the excitation $E(z)$ through the spectral shaping system $H(z) = 1/A(z)$ in order to generate the speech signal $S(z)$.

In Chapter 2 we showed in the context of the G.727 codec, how a slowly varying two-zero, six-pole predictor can be used to estimate the incoming signal's spectrum and the corresponding spectral coefficients were determined in Section 2.3.3. It was also demonstrated how this so-called short-term predictor can be rendered adaptive, in order to accommodate changes in the incoming signal's statistics and it was stated that the predictor coefficients must be transmitted to the decoder in a forward-adaptive predictive codec.

In Sections 2.5 and 2.9.3 we showed how efficient predictive coding was in terms of removing redundancy and reducing the signal's variance. As a result, the prediction residual signal characterised in both time- and frequency-domains in Section 2.9.3 became nearly unpredictable, which we described with the help of waveform coding techniques using an adaptive quantiser. In the G.727 codec no predictor coefficients were transmitted, but the number of bits required for the adequate encoding of the near-random prediction residual was quite high, requiring bitrates up to 40 kbps, when using 5 bits/sample in order to maintain a high speech quality.

Although the high-quality encoding of the prediction residual is a sufficient criterion for perceptually high speech quality, it is not a necessary condition. In Section 2.8 we have already alluded to the fact that the conventional SNR is not a reliable speech quality measure. In this section we will endeavour to improve the bitrate economy, while maintaining perceptually high speech quality.

Voice and Audio Compression for Wireless Communications Second Edition
L. Hanzo, F. C. A. Somerville and J. P. Woodard

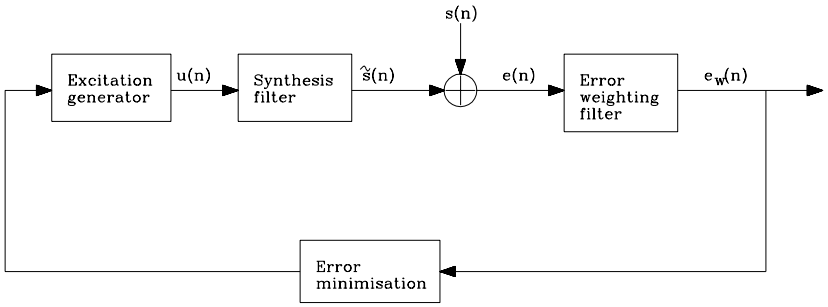

(a) ABS Encoder

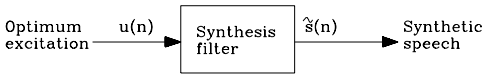

(b) ABS Decoder

Figure 3.1: General analysis-by-synthesis codec schematic.

3.2 Analysis-by-Synthesis Codec Structure

A number of measures will assist us in achieving the above goals, which are incorporated in the so-called analysis-by-synthesis (AbS) codec structure shown in Figure 3.1. In order to improve the coding efficiency, so-called *vector-quantisation* techniques are invoked, where the synthesis filter is excited by an excitation vector of typically 5 ms or 40 samples length. A further important feature is that a *closed-loop structure* is used. Accordingly, the prediction error between the original input signal and the synthesised speech signal is evaluated for each candidate excitation vector and the specific excitation vector minimising the so-called *weighted error*, rather than the conventional MSE, is deemed to produce the best synthetic speech quality. Following this rudimentary introduction to the philosophy of AbS codecs we will elaborate on their salient features during our further discussions.

As seen in Figure 3.1 the slowly varying synthesis filter(s) are excited by the so-called innovation sequences $u(n)$ of the excitation generator in order to produce the synthetic speech $\hat{s}(n)$, which is compared with the input speech $s(n)$ about to be encoded. The prediction error residual $e(n) = s(n) - \hat{s}(n)$ is formed and weighted by the error-weighting filter, which will be described during our further discourse, in order to produce the *perceptually weighted error* $e_w(n)$.

An important feature of these AbS codecs is that instead of minimising the usual MSE term in an effort to provide best waveform reproduction, they minimise the perceptually weighted error $e_w(n)$. Thereby they actually degrade the waveform representation in favour of better subjective speech quality. The high speech quality of AbS speech codecs is

achieved at the cost of relatively high complexity, since the synthetic speech is computed for all legitimate innovation sequences, sometimes several thousand times. A fundamental property of closed-loop AbS codecs is that the prediction residual is encoded by minimising the perceptually weighted error between the original and reconstructed speech rather than minimising the MSE between the residual and its quantised version as in open-loop structures. The error-weighting filter will be derived from the short-term predictor filter and it is designed to de-emphasise the weighted error in the vicinity of formant regions, where the speech signal's spectral prominances successfully mask the effects of allowing a higher reconstruction error. This renders the SNR more or less constant over the speech signal's frequency range, rather than aiming for a near-constant quantised noise PSD.

The so-called *short-term synthesis filter* determined in Section 2.3.3 is responsible for modelling the spectral envelope of the speech waveform. Its coefficients are computed by minimising the error of predicting a speech sample from a few, typically 8–10, previous samples, where minimisation is carried out over a quasi-stationary period of some 20 ms or 160 samples, when the sampling frequency is 8 kHz. The synthesis filter might incorporate an additional so-called *long-term synthesis filter* modelling the fine structure of the speech spectrum, which predicts the long-term periodicity of speech persisting after short-term prediction, reflecting the pitch periodicity of the residual.

As seen in Figure 3.1, the decoder uses an identical structure to that of the encoder for generating the synthetic speech. However, its complexity is considerably lower, since the innovation sequence that minimised the perceptual error is transmitted to the decoder and it is the only sequence to which the synthesis filter's response is computed.

As detailed in Section 2.3.3, the short-term synthesis filter parameters are determined by minimising the prediction error over a quasi-stationary interval of about 20 ms outside the optimisation loop. The 'remainder' of the speech information is carried by the prediction residual, which is not modelled directly, instead the best excitation for this short-term synthesis filter is determined by minimising the weighted error between the input and the synthetic speech. The excitation optimisation interval is typically 5 ms, which is a quarter of the 20 ms short-term filter update interval. The 20 ms duration speech frame is therefore divided into, typically, four subsegments and the optimum excitation is determined individually for each 5 ms subsegment. The quantised filter parameters and the vector-quantised excitation are transmitted to the decoder, where the synthesised speech is generated by filtering the decoded excitation signal through the synthesis filter(s). Let us now consider the effects of choosing different parameters for the short-term synthesis filter.

3.3 The Short-term Synthesis Filter

As mentioned before, the vocal tract can be modelled as a series of uniform lossless acoustic tubes [5, 6]. It can then be shown that for a digital all-pole synthesis filter to approximate the effect of such a model of the vocal tract, its delay should be at least twice the time required for sound waves to travel along the tract. For a vocal tract of length 17 cm, voice velocity of 340 m/sec and a sampling rate of 8 kHz this corresponds to the order p of the filter being at least 8 taps or $8.125\ \mu\text{s} = 1\ m\text{s}$. Generally, a few extra taps are added, in order to help the filter cope with effects not allowed for in the lossless tube model, such as spectral zeros and losses in the vocal tract. We simulated the effect of changing the order p on the prediction gain

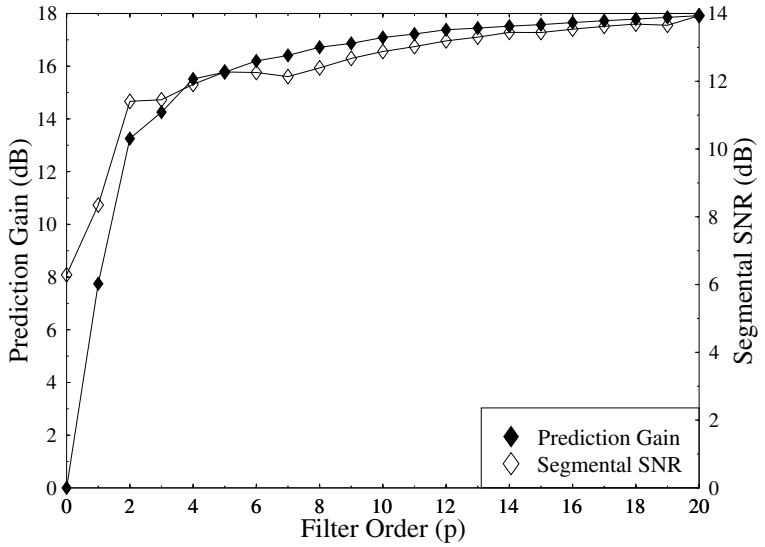

Figure 3.2: Variation of LPC performance as a function of the predictor order p for 20 ms duration speech frames using no error weighting and the 7.1 kbps CELP codec of Section 6.2.

of the inverse filter $A(z)$. We used about eleven seconds of speech data obtained from two male and two female speakers. The speech was sampled at 8 kHz and split into 20 ms frames. For each frame the filter coefficients were calculated using the autocorrelation approach applied to the Hamming-windowed speech signal, and the prediction gain was calculated and converted into decibels. Here the prediction gain is defined as the energy of the original speech samples $s(n)$ divided by the energy of the prediction error samples $e(n)$. The overall prediction gain was taken as the average of the decibel gains for all the 20 ms frames in the speech file.

The results of our simulations are shown in Figure 3.2. Also shown in this figure is the variation of the SEGSNR of a CELP codec as a function of the order p of its synthesis filter. The filter coefficients were calculated for 20 ms frames as described above, and were left unquantised. The excitation parameters for the codec were determined identically to our 7.1 kbps CELP codec to be described later in Section 6.2, except no error weighting was used. It can be seen that both the prediction gain of the inverse filter and the SEGSNR of the codec increase, as the order of the synthesis filter is increased. However, in a forward adaptive system, each synthesis filter coefficient used requires side information to be sent to the decoder, and hence we wish to keep their number to a minimum. We chose $p = 10$ as a sensible compromise between a high prediction gain and a low bitrate.

The rate required to transmit information about the synthesis filter coefficients also depends on how often this information is updated, that is on the LPC analysis frame length L.

We carried out similar simulations to those described above, in order to quantify how the frame length affected the prediction gain of the inverse filter and the segmental SNR of a CELP codec. The order p of the filter was fixed at $p = 10$ and the coefficients were calculated using Hamming-windowed speech frames of length L samples. However, the prediction gain and the SEGSNR were calculated using frames 20 ms long to find the gains/SNRs, which were converted into decibels and averaged. This was carried out in order to ensure a fair comparison within our results, which are shown in Figure 3.3. It can be seen that for very short analysis frame lengths both the prediction gain and the SEGSNR are well below the best values found. This is probably because we have used the autocorrelation method of analysis, and for small values of L we do not have $L \gg p$ and hence inaccuracies are introduced due to the windowing of the input speech signal. The best values of the prediction gain and the SEGSNR are given for $L = 160$, which corresponds to a 20 ms frame length. For larger frames there is a gradual decrease in the performance of the filter due to the non-stationary nature of speech.

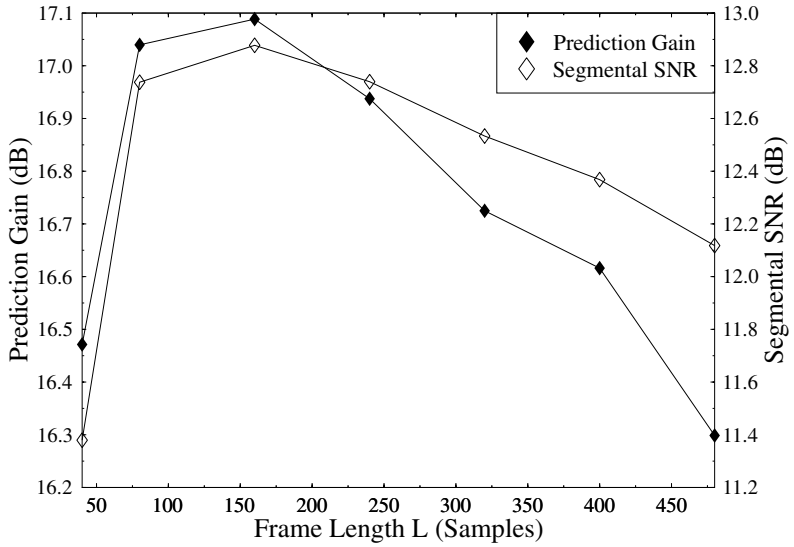

Figure 3.3: Variation of LPC performance versus the analysis frame length L.

The synthesis filter coefficients must be quantised in order to be sent to the decoder. Unfortunately, the filter coefficients themselves are not suitable for quantisation because the frequency response of the synthesis filter is very sensitive to changes in them. This means even a small change in the values of the coefficients when they are quantised can lead to a large change in the spectrum of the synthesis filter. Furthermore, after quantisation it is difficult to ensure that a given set of coefficients will produce a stable synthesis filter. Thus although the autocorrelation approach guarantees a stable filter, this stability could be easily

lost through direct quantisation of the filter coefficients. Therefore before quantisation the coefficients are converted into another set of parameters from which they can be recovered, but which are less sensitive to quantisation noise and which allow stability to be easily guaranteed. Some schemes use the so-called reflection coefficients, which are related to the lossless acoustic tube model of the vocal tract and are calculated as a by-product of using the Levinson–Durbin algorithm of Figure 2.3 to solve Equation (2.16). Using these coefficients, the stability of the synthesis filter can be readily ensured by limiting the magnitude of all the coefficients to be less than one. Typically the reflection coefficients are transformed, using the so-called inverse-sine transformation or log-area ratios, before quantisation. These issues will be discussed in the next chapter in detail. Let us now introduce long-term prediction in the AbS codec of Figure 3.1.

3.4 Long-term Prediction

3.4.1 Open-loop Optimisation of LTP Parameters

As mentioned earlier, most AbS speech codecs incorporate a so-called long-term predictor (LTP) in order to improve the speech quality and bitrate economy by further reducing the variance of the prediction residual. This can be achieved by predicting and removing the long-term redundancy of the speech signal. While the short-term predictor (STP) removes the adjacent sample correlation and models the spectral envelope, that is the formant structure, it still leaves some long-term peaks in the STP residual, since at the on-set of quasi-periodic waveform segments of voiced sounds it fails to predict the signal adequately. This is clearly demonstrated by Figure 3.4 for an 800 sample or 100 ms long speech segment. The pitch-related, quasi-periodic LPC prediction error peaks can be efficiently reduced by the LTP, as seen in Figure 3.4(c).

The operation of the LTP can be explained in a first approximation as subtracting a 'pitch-synchronously' positioned or delayed segment of the previous LPC residual from the current segment. If the pitch periodicity is quasi-stationary, that is near time-invariant, then the properly positioned previous segment will have co-located pitch pulses with the current segment. Hence after subtracting the previous LPC segment the pitch-synchronous prediction residual pulses of Figure 3.4(b) can be eliminated, as evidenced by Figure 3.4(c) portraying the LTP residual. We will show shortly that the performance of the above-mentioned simple LTP can be improved if, before subtracting the previous 'history', we scale the previous segment by a gain factor G, which can be optimised to minimise the energy of the LTP residual, which will be made explicit in the context of Equation (3.1). Both the LTP delay and the gain factor will have to be transmitted to the decoder in order to be able to reconstruct the LPC residual. Furthermore, since at the decoder only the previous reconstructed residual is available, which is based on the transmitted innovation sequence and LTP parameters, such as the delay and gain, the encoder also uses the previously reconstructed LPC residual segments, rather than the original ones.

Since periodic signals exhibit a line-spectrum, the quasi-periodic prediction residual's spectrum seen in Figure 2.12 has a periodic fine structure showing peaks and valleys, which is the manifestation of the time-domain long-term periodicity. Hence the LTP models the spectral fine-structure of the speech signal that is similar to the line spectrum of a periodic signal. This pitch-related periodicity is strongly speaker- and gender-dependent. Its typical

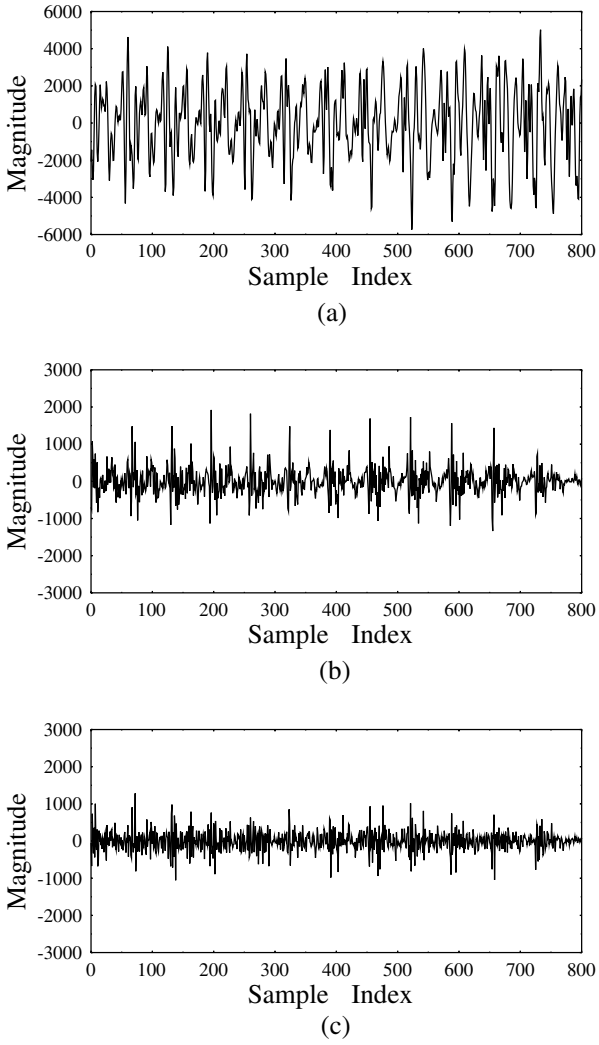

Figure 3.4: Typical 100 ms segment of (a) voiced speech signal, (b) LPC residual and (c) LTP residual.

values are in the range of 100–300 Hz or about 3–10 ms. When employing a LTP, the LTP residual error becomes truly unpredictable. This noise-like process is hence often modelled by innovation sequences of a zero-mean, unit-variance random Gaussian code book, yielding an extremely efficient vector quantiser. This concept leads to CELP coding, constituting the most prominent member of the family of AbS codecs, which will be treated in depth during our further discourse.

As we have seen in Figure 3.1, the decoder reconstructs the speech signal by passing the specific innovation sequence through the synthesis filter. The best innovation sequence does not necessarily closely resemble the LTP residual, nor does it guarantee the best waveform

match between the original speech and synthetic speech. It rather endeavours to produce the perceptually best speech quality.

In order to augment our exposition, we now describe the LTP in analytical terms, as follows. When using a so-called one-tap LTP, the LTP residual $e_L(n)$ is computed as

$$e_L(n) = r(n) - G_1 r(n-\alpha), \tag{3.1}$$

where $r(n)$ is the STP residual. To interpret Equation (3.1) physically, the STP residual $r(n)$ is delayed by α samples to create its delayed version $r(n-\alpha)$ which is then subtracted from $r(n)$ after being scaled by an optimum gain factor G_1, where G_1 was computed by minimising the LTP residual error. The z-transform of Equation (3.1) is given by

$$E_L(z) = R(z)[1 - G_1 z^{-\alpha}], \tag{3.2}$$

which can be re-arranged in the following form:

$$R(z) = \frac{E_L(z)}{[1 - G_1 z^{-\alpha}]} = \frac{E_L(z)}{P(z)}, \tag{3.3}$$

where $P(z) = [1 - G_1 z^{-\alpha}]$ is the z-domain transfer function of the LTP.

The total mean-squared LTP residual error E_L computed over a segment of N samples can be formulated as

$$\begin{aligned} E_L &= \sum_{n=0}^{N-1} e_L^2(n) \\ &= \sum_{n=0}^{N-1} [r(n) - G_1 r(n-\alpha)]^2 \\ &= \sum_{n=0}^{N-1} r^2(n) - \sum_{n=0}^{N-1} 2G_1 r(n) r(n-\alpha) + \sum_{n=0}^{N-1} G_1^2 r^2(n-\alpha). \end{aligned} \tag{3.4}$$

Setting $\partial E_L / \partial G_1 = 0$ gives

$$\sum_{n=0}^{N-1} -2r(n)r(n-\alpha) + \sum_{n=0}^{N-1} 2G_1 r^2(n-\alpha) = 0, \tag{3.5}$$

yielding the optimum LTP gain factor G_1 in the following form:

$$G_1 = \frac{\sum_{n=0}^{N-1} r(n) r(n-\alpha)}{\sum_{n=0}^{N-1} [r(n-\alpha)]^2}. \tag{3.6}$$

Observe that the computed gain factor can be interpreted as the normalised cross correlation of $r(n)$, where the normalisation factor in the denominator represents the energy of the STP residual segment. If the previous and current segments are identical, they are perfectly correlated and $G_1 = 1$, yielding $e_L = 0$ in Equation (3.1), which corresponds to perfect long-

term prediction. If there is practically no correlation between $r(n)$ and $r(n-\alpha)$, as in the case of unvoiced sounds, $G_1 \approx 0$ and no LTP gain is achieved.

In general, upon substituting the optimum LTP gain G_1 back into Equation (3.4), the minimum LTP residual energy is given by

$$E_{L,\min} = \sum_{n=0}^{N-1} r^2(n) - \frac{[\sum_{n=0}^{N-1} r(n)r(n-\alpha)]^2}{\sum_{n=0}^{N-1}[r(n-\alpha)]^2}. \tag{3.7}$$

Again, in harmony with our previous argument, minimising E is equivalent to maximising the second term in Equation (3.7), which physically represents the normalised correlation between the residual $r(n)$ and its delayed version $r(n-\alpha)$. Hence the optimum LTP parameters can be determined by computing this term for all possible values of α over its specified range of typically $N = 20 - 147$ samples, when the sampling rate is 8 kHz. The delay α which maximises the second term is the optimum LTP delay.

The effect of both the STP and LTP becomes explicit by comparing the PDF of a typical speech signal, as well as that of both the STP residual and the LTP residual as shown in Figure 3.5. Note that the speech signal has a long-tailed PDF, while the STP and LTP have substantially reduced the signal's variance. Since the LTPs action is to reduce the relatively low-probability pitch pulses, this effect becomes more explicit from Figure 3.6, where the PDFs were plotted on a logarithmic axis in order to magnify the long low-probability PDF tails. This effect may not appear dramatic, but invoking a LTP typically improves the speech quality sufficiently, in order to justify its added complexity.

When using a LTP, our AbS speech codec schematic seen in Figure 3.1 can be re-drawn as portrayed in Figure 3.7. The choice of the appropriate error-weighting filter is crucial to the codec's performance [70, 92] and its transfer function is based on findings derived from the theory of auditory masking. Experience shows that when generating, for example, a sinusoidal signal, often referred to as a single tone due to its single spectral line in the frequency domain, it is capable of masking a high-energy, but spectrally more spread noise signal residing within the same frequency band. This is due to the inability of the human ear to resolve the two signals. Due to the speech signal's spectral prominancies in the frequency regions of the formants, this property can be exploited by allowing more quantisation noise to be concentrated around them. Clearly, an adaptive quantisation noise spectrum shaping filter is required, which de-weights the quantisation noise in the formant regions, thereby allowing more quantisation noise to reside in these frequency bands than without filtering.

It is plausible that the filter's transfer function has to depend on the momentary signal spectrum, which is evaluated in the codec in terms of the filter coefficients a_i, describing the polynomial $A(z)$. A convenient choice is to define the error weighting filter's transfer function as [92, 93]

$$W'(z) = \frac{A(z)}{A(z/\gamma)} = \frac{1 - \sum_{k=1}^{p} a_k z^{-k}}{1 - \sum_{k=1}^{p} a_k \gamma^k z^{-k}}, \tag{3.8}$$

where the constant γ determines to what extent the error spectrum is de-emphasised in the formant regions. Typical values of γ are in the range of 0.6–0.85. The schematic diagram of Figure 3.7 can also be re-arranged in the form shown in Figure 3.8, which is an often favoured equivalent configuration.

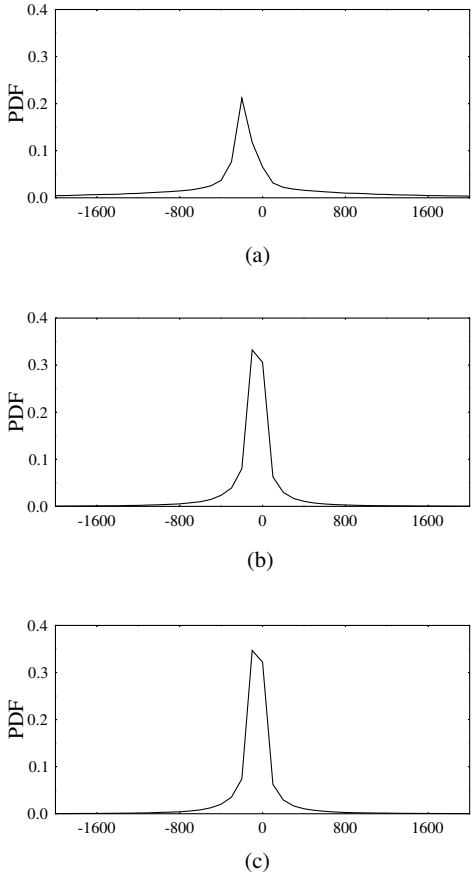

Figure 3.5: PDF of (a) typical speech signal (b) LPC residual and (c) LTP residual.

Recently, other forms of error weighting have been suggested for speech codecs. For example, in the 16 kbps G.728 codec [94] the filter

$$W(z) = \frac{A(z/\gamma_1)}{A(z/\gamma_2)} \tag{3.9}$$

is used where $\gamma_1 = 0.9$ and $\gamma_2 = 0.6$. We also employed this weighting filter later in the book in the context of the low-delay codecs of Chapter 8. In [95] an explicit auditory model is used in order to take account of our knowledge about psychoacoustics and auditory masking.

3.4.2 Closed-loop Optimisation of LTP Parameters

According to our previous approach the LTP parameters were computed from the LPC residual signal using a simple correlation technique, as suggested by Equation (3.7), in a sub-optimum two-stage approach often referred to as open-loop optimisation. However, it

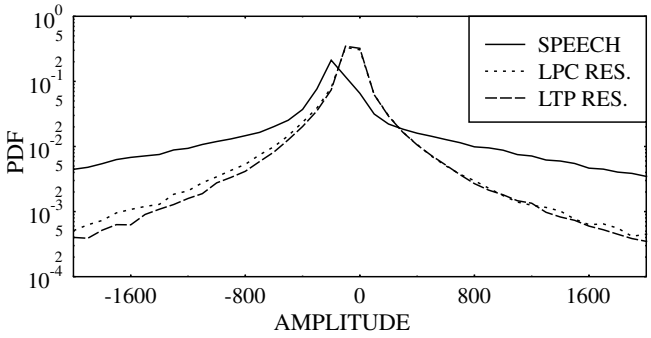

Figure 3.6: Logarithmic PDF of a typical speech signal, (top) LPC residual (middle) and LTP residual (bottom).

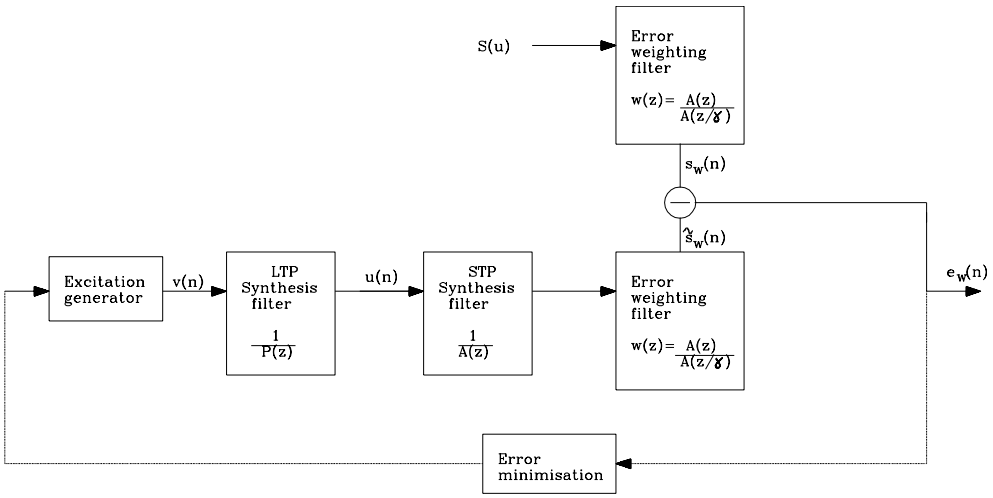

Figure 3.7: Analysis-by-synthesis codec schematic using a LTP.

was suggested by Singhal and Atal [96] that a substantially improved speech quality can be attained at the cost of a higher complexity, if the LTP parameters are computed inside the AbS loop, which leads to the so-called *adaptive codebook* approach featured in the schematic of Figure 3.9 that will be described below. This terminology is justified by the fact that the adaptive codebook is replenished regularly using the previous composite excitation patterns $u(n)$ after a delay of one subsegment duration, which will be made more explicit during our forthcoming deliberations following Salami's approach [70, 71].

The composite excitation signal $u(n)$ in Figure 3.9 is given by

$$u(n) = v(n) + G_1 u(n - \alpha) \tag{3.10}$$

which is the superposition of the appropriately delayed G_1-scaled adaptive codebook entry $u(n - \alpha)$ and the excitation $v(n)$, while $v(n)$ is recomputed for each excitation

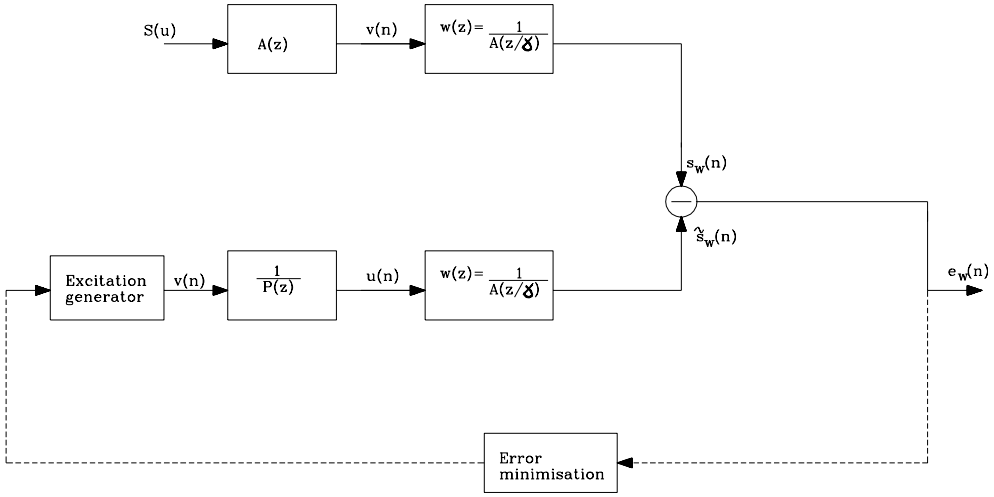

Figure 3.8: Modified analysis-by-synthesis codec schematic with LTP.

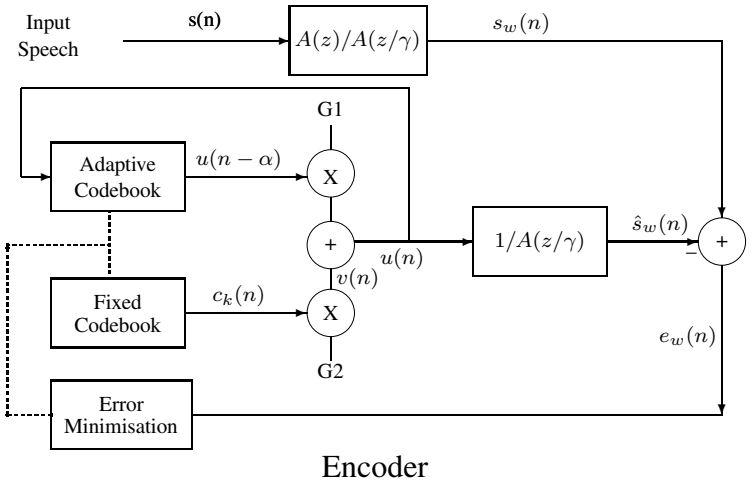

Figure 3.9: Adaptive codebook approach in the context of AbS CELP codecs.

optimisation subsegment. In conventional forward adaptive AbS codecs the subsegment length is typically 5–7.5 ms and hence in an LPC update frame of 10–30 ms there are usually 2–6 excitation optimisation subsegments. This provides extra flexibility for the codec to adapt to the changing nature of the speech signal in spite of the LPC parameters and the corresponding spectral envelope being fixed for 10–30 ms due to transmission bitrate constraints. By contrast, in the so-called backward adaptive codecs the corresponding intervals can be significantly shorter, since the LPC coefficients are extracted from the

previously recovered speech signal, rather than being transmitted. This will be elaborated on in the context of the ITU low-delay G.728 16 kbps standard codec in Chapter 8.

In forward-predictive codecs the excitation signal $u(n)$ is then determined by minimising the mean squared weighted error (mswe) E_w for a typical duration of a subframe of $N = 40$–60 samples or 5–7.5 ms. Ideally, according to the closed-loop AbS approach the optimum excitation and the adaptive codebook parameters resulting in the perceptually best synthetic speech quality would have to be found jointly – testing each possible combination of the two – in order to minimise E_w. Unfortunately, this would inflict an unacceptable complexity penalty and hence usually a suboptimal approach is invoked, where initially the adaptive codebook parameters are computed first, assuming that no excitation is input to the synthesis filter, i.e. $v(n) = 0$. This is because the excitation $v(n)$ is not known at this stage, yielding $u(n) \approx G_1 u(n - \alpha)$.

At this stage we have not yet specified the set of legitimate excitation patterns, but one might expect that the more attention is devoted to designing these sequences and the larger this set, the better the quality of the synthetic speech. During the process of determining the best excitation sequence $u(n)$ from the set of legitimate sequences, which results in the best synthetic speech segment, each excitation segment is filtered through the so-called *weighted synthesis filter* $1/A(z/\gamma)$ of Figure 3.8, which is an infinite impulse response (IIR) system. Hence, following Salami's deliberations [70, 71], the weighted synthetic speech in the current optimisation interval can be described as the superposition of the filter's response due to the current excitation sequence and that due to all previous actual optimum excitation sequences. It is important to note that this memory contribution is not influenced by the current excitation sequence. Hence, it is also often referred to as the IIR filter's *zero input response*. Treating this memory contribution adequately is extremely important in order to ensure that in spite of filtering all the candidate excitations tentatively through this IIR filter, the synthesis filter's output signal becomes a seemless, close replica of the weighted input speech due to the sequence of actual optimum excitation sequences.

There are two alternative solutions to treating these memory contributions adequately during the excitation optimisation process. According to the first technique, once all candidate excitations were tested and the optimum excitation for the current interval was found, the zero input filter response due to the sequence of all concatenated previous optimum excitations can be updated to include the contribution by the current one. This updated memory contribution is then stored in order to be able to add it to the synthesis filter's output due to the set of all candidate excitations during the next optimisation interval, before they are compared to the corresponding weighted input speech segment. The disadvantage of this approach is that the zero input response has to be added to all candidate synthetic speech segments, before they are compared to the weighted original speech.

It is therefore usually more efficient to invoke the second approach and subtract this filter memory contribution from the weighted original speech, before pattern matching, since this operation takes place only once per optimisation interval, rather than for each candidate excitation pattern. After subtracting the memory contribution of the weighted synthesis filter from the weighted original speech vector we arrive at the so-called *target vector*, to which then all filtered candidate excitation sequences are compared. However, according to this approach the IIR filter's memory must be set to zero each time, before a new excitation is tentatively filtered through it, because the effect of the filter memory was taken into account now by modifying the weighted original speech signal. Following the latter approach, the

synthetic speech can be described as [70, 71]

$$\hat{s}_w(n) = \sum_{i=0}^{n} u(i)h_w(n-i) + \hat{s}_0(n), \tag{3.11}$$

where $h_w(n)$ denotes the IIR of the weighted synthesis filter $W(z) = 1/A(z/\gamma)$ and $\hat{s}_0(n)$ is the so-called zero-input response of the weighted synthesis filter, which is equivalent to the filter's memory contribution due to previous excitations. Hence the weighted error between the original and synthetic speech can be written as

$$e_w(n) = x'(n) - \sum_{i=0}^{n} u(i)h_w(n-i), \tag{3.12}$$

where

$$x'(n) = s_w(n) - \hat{s}_0(n) \tag{3.13}$$

represents the weighted input speech after subtracting the memory contribution of the IIR weighted synthesis filter due to previous excitations and the notation $x'(n)$ is used for later notational convenience.

Having found a solution to treating the IIR filter memory during the excitation optimisation process let us now return to finding the closed-loop LTP parameters. Recall that since $v(n)$ is unknown initially, it is set to zero and hence upon substituting $u(n) \approx Gu(n-\alpha)$ into the weighted error expression of Equation (3.12) we arrive at

$$\begin{aligned} e_w(n) &= x'(n) - G\sum_{i=0}^{n} u(i-\alpha)h_w(n-i) \\ &= x'(n) - Gu(n-\alpha) * h_w(n) \\ &= x'(n) - Gy_\alpha(n), \end{aligned} \tag{3.14}$$

where we used the short-hand

$$y_\alpha(n) = u(n-\alpha) * h_w(n) = \sum_{i=0}^{n} u(i-\alpha)h_w(n-i). \tag{3.15}$$

The mswe for the excitation optimisation subsegment of N samples is given by

$$E_w = \sum_{n=0}^{N-1} [x'(n) - Gy_\alpha(n)]^2. \tag{3.16}$$

Upon expanding the above equation in analogy to Equations (3.4)–(3.7) and setting $\partial E_w/\partial G = 0$ leads to [70, 71]

$$G = \frac{\sum_{n=0}^{N-1} x'(n)y_\alpha(n)}{\sum_{n=0}^{N-1} [y_\alpha(n)]^2}. \tag{3.17}$$

Observe that whilst the optimum open-loop gain in Equation (3.6) was based on the normalised correlation $r(n)$ of the LPC residual, the closed-loop gain of Equation (3.17) is based on the more elaborate operations summarised in Equations (3.12)–(3.17).

Since the optimum closed loop LTP gain is now known, the minimum weighted error is computed by substituting Equation (3.17) into Equation (3.16), which yields

$$E_w = \sum_{n=0}^{N-1} [x'(n)]^2 - \frac{[\sum_{n=0}^{N-1} x'(n) y_\alpha(n)]^2}{\sum_{n=0}^{N-1} [y_\alpha(n)]^2}. \tag{3.18}$$

Clearly, the closed-loop LTP delay α is found by maximising the second term of Equation (3.18), while the optimum LTP gain factor G is determined from Equation (3.17). In conclusion we note that Salami [70, 71] also proposed a computationally efficient recursive procedure for the successive evaluation of y_α, which is highlighted below.

Salami commenced his elaborations by noting that the past excitation signal $u(n-\alpha)$ is only available for $n - \alpha < 0$. When $n - \alpha > 0$, the 'past excitation' is part of the excitation for the current sub-frame and hence it is not yet known. Thus, for delays less than the sub-frame length N only the first α values of $u(n-\alpha)$ are available. We make up the rest of the values by repeating the available pattern, that is taking $u(n-2\alpha)$ for $\alpha < n < 2\alpha - 1$ etc, until the range $0 \leq n \leq N-1$ has been covered.

The computational load required to calculate the convolution $y_\alpha(n)$ for all possible values of the delay α would be large if they were all calculated independently. Fortunately, this can be avoided by calculating the convolution for the lowest value of α and then using an iterative procedure to find $y_\alpha(n)$ for all the other necessary values of α [71]. This iterative procedure is possible because the adaptive codebook codeword for a delay α is merely the codeword for the delay $\alpha - 1$ shifted by one sample, with one new value $u(-\alpha)$ introduced, and one old value $u(N-\alpha)$ discarded. This is true except for delays less than the sub-frame length N, for which the iterative procedure becomes slightly more complicated because of the repetition described above used to construct the codewords.

In summary, we gave a rudimentary introduction to AbS speech coding and showed that the synthetic speech is the output signal of the optimum synthesis filter when excited by the innovation sequence. Once the STP and LTP analysis and synthesis filters are described by the coefficients a_k, G and delay α, the central problem of achieving a good compromise in terms of speech quality and bitrate hinges on modelling the prediction residual. A variety of methods for modelling the prediction residual are described in references [70] and [71]. In the next section we will briefly highlight a number of techniques, including the so-called regular pulse excitation (RPE) described in depth in Chapter 5, which is used in the Pan-European mobile radio system known as GSM [97, 98], as well as CELP that will be detailed in the context of Chapter 6.

3.5 Excitation Models

Again, the differences between RPE and CELP codecs arise from the representation of the excitation signal $u(n)$ used. In the so-called multi-pulse excited (MPE) codecs proposed in 1982 by Atal and Remde [9], $u(n)$ is given by a fixed number of non-zero pulses for every frame of speech. The positions of these non-zero pulses within the frame, and their

amplitudes, must be determined by the encoder and transmitted to the decoder. In theory it would be possible to find the very best values for all the pulse positions and amplitudes, but this is not practical due to the excessive complexity it would entail. In practice, some sub-optimal method of finding the pulse positions and amplitudes must be used. Usually the positions are found one at a time as follows. Initially all the pulses are assumed to have zero amplitude except one. The position and amplitude of this first pulse can then be found by tentatively allocating the pulse to all possible positions and then finding its magnitude in order to minimise the associated perceptually weighted error. Finally, the pulse position and the associated magnitude yielding the lowest weighted error are confirmed. Then using this information the position and amplitude of the second pulse can be determined similarly. This procedure continues, until all the pulses have been found. Once a pulse position is determined it is fixed. However, the amplitudes of the previously found pulses can be re-optimised at each stage of the algorithm [99] when a new pulse was allocated. The quality of the reconstructed speech produced by MPE codecs is largely determined by how many non-zero pulses are used in the excitation. However, this is constrained by the bitrate necessary to transmit information about the pulse positions and amplitudes. Typically about 4 pulses per 5 ms are used, and this leads to good quality reconstructed speech and a bitrate of around 10 kbps.

Similar to the MPE codec, the RPE codec uses a number of non-zero pulses in order to generate the excitation signal $u(n)$. However, in RPE codecs the pulses are regularly spaced with a certain separation. Hence the encoder only has to determine the position of the first pulse and the amplitude of all the pulses. Therefore less information has to be transmitted concerning the pulse positions, and hence for a given bitrate the RPE codec can benefit from using many more non-zero pulses than MPE codecs. For example, as will become clear during our forthcoming discussions, at a bitrate of about 10 kbps around 10 pulses per 5 ms can be used in RPE codecs, compared to 4 pulses for MPE codecs. This allows RPE codecs to give slightly higher quality reconstructed speech than that of the MPE codecs. However, RPE codecs also tend to be more complex. The Pan-European GSM mobile telephone system [98] uses a simplified RPE codec, in conjunction with long-term prediction, operating at 13 kbps to provide toll quality speech.

Although MPE and RPE codecs can provide high-quality speech at bitrates around 10 kbps and higher, they are unsuitable for significantly lower rates. This is due to the large amount of information that must be transmitted about the excitation pulses' positions and amplitudes. If we attempt to reduce the bitrate by using fewer pulses, or by coarsely quantising their amplitudes, the reconstructed speech quality deteriorates rapidly. Currently the most commonly used algorithm for producing good quality speech at rates below 10 kbps is CELP. This approach was proposed by Schroeder and Atal in 1985 [16], and differs from MPE and RPE in that the excitation signal is vector quantised. Explicitly, the excitation is given by an entry from a large vector quantiser codebook, and by a multiplicative gain term invoked in order to control its power. Typically the codebook index is represented with the aid of about 10 bits (to give a codebook size of 1024 entries) and the codebook gain is coded using about 5 bits. Thus the bitrate necessary to transmit the excitation information is significantly reduced, namely to around 15 bits compared to the 47 bits used for example in the GSM RPE codec.

Originally [16] the codebook used in CELP codecs contained white Gaussian sequences. This was because it was assumed that the long- and short-term predictors would be able to remove nearly all the redundancy from the speech signal in order to produce a

random noise-like residual. Furthermore, it was shown that the short-term PDF of this residual was nearly-Gaussian. Schroeder and Atal found that using such a codebook to produce the excitation for long- and short-term synthesis filters could produce high quality speech. However, each codebook entry had to be passed through the synthesis filters in order to assess how similar the reconstructed speech it produced would be to the original. This implied that the complexity of the original CELP codec was excessive for it to be implemented in real-time – it took 125 seconds of Cray-1 CPU time to process 1 second of the speech signal. Since 1985 significant research efforts have been invested into reducing the complexity of CELP codecs – mainly through optimising the structure of the codebook. Furthermore, significant advances have been made in the design of digital signal processor (DSP) chips, so that at the time of writing it is relatively easy to implement a real-time CELP codec on a single, low cost, DSP chip. Several important speech coding standards have been defined based on the CELP principle: for example, the US Department of Defence (DoD) 4.8 kbps codec [100], and the ITUs G.728 16 kbps low-delay codec [94]. We give a detailed description of CELP codecs in the next chapter.

The CELP coding principle has been very successful in producing communications to toll-quality speech at bitrates between 4.8 and 16 kbps. The ITUs G.728 standard 16 kbps codec produces speech which is almost indistinguishable from 64 kbps log-PCM coded speech, while the DoDs 4.8 kbps codec gives good communications-quality speech. Recently, much research has been conducted in the field of codecs operating at rates below 4.8 kbps, with the aim of producing a codec at 2.4 or 3.6 kbps, while having a speech quality equivalent to that of the 4.8 kbps DoD CELP. We will briefly describe a few of the approaches which seem promising in contriving such a codec, noting that the last part of this book is dedicated to this codec family.

The original CELP codec's structure can be further improved and used at rates below 4.8 kbps by classifying speech segments into a number of classes (for example, voiced, unvoiced and 'transitory' frames) [101]. The different speech segment types are then coded differently with a specially designed encoder for each type. For example, for unvoiced frames the encoder will not use any long-term prediction, whereas for voiced frames such prediction is vital but the fixed codebook may be less important. Such class-dependent codecs have been shown to be capable of producing reasonable quality speech at rates down to 2.4 kbps [102]. Multi-band excitation (MBE) codecs [103] analyse the speech frequency bands and declare some regions in the frequency domain as voiced and others as unvoiced. They transmit for each frame a pitch period, spectral magnitude and phase information, as well as voiced/unvoiced decisions for the bands related to the harmonics of the fundamental frequency. Originally it was shown that such a structure was capable of producing good quality speech at 8 kbps, and since then this rate has been significantly reduced (see, for example, [104]). Finally, Kleijn has suggested an approach for coding voiced segments of speech, which he referred to as prototype waveform interpolation (PWI) [105]. This codec operates by sending information about a single pitch cycle every 20–30 ms, and using interpolation between these instances in order to reproduce a smoothly varying quasi-periodic waveform for voiced speech segments using similar principles. Excellent quality reproduced speech can be obtained for voiced speech at rates as low as 3 kbps. Such a codec can be combined with a CELP-type coding regime for the unvoiced segments in order to attain good quality speech at rates below 4 kbps.

Having highlighted a variety of excitation models used in various previously proposed codecs, in the next section we will provide a brief treatise on post-filtering which has successfully been employed in a range of standard codecs in order to improve their perceptual speech quality.

3.6 Adaptive Short-term and Long-term Post-Filtering

Post-filtering was originally proposed by Jayant and Ramamoorthy [106, 107] for 32 kbps ADPCM coding using the two-pole six-zero synthesis filter of the G.721 codec of Figure 2.10, and later Chen *et al.* also adopted this technique in order to improve the performance of low-rate CELP codecs [108] as well as that of the CCITT G.728 16 kbps low-delay backward-adaptive CELP codec [94, 109]. The basic principle of post-filtering is to further emphasise the spectral peaks of the speech signal, while slightly reducing their bandwidth and attenuating spectral valleys between these prominances. This spectral shaping procedure inevitably alters the waveform shape of the speech signal to a certain extent, which constitutes an undesirable impairment. Nonetheless, the enhancement of the spectral peaks – and in particular the concomitant attenuation of the potentially noise-contaminated low-energy spectral valleys – results in subjective quality improvement. Hence the advantage of reducing the effect of quantisation noise in the subjectively important spectral valleys outweighs the waveform distortion penalty inflicted. This is necessary, since despite allocating a reduced amount of quantisation noise to the spectral valleys after perceptual error weighting, these low-energy frequency bands remain vulnerable to contamination. This effect can be mitigated by retrospectively attenuating these partially contaminated frequency bands.

During the initial phases of its development the G.728 codec did not employ adaptive post-filtering, since it was believed that it would result in the accumulation of quantisation noise in the speech spectral valleys, when tandeming several codecs. However, tandeming experiments showed that in conjunction with post-filtering the coding noise due to concatenating three asynchronously operated codecs became about 4.7 dB higher than in the case of using no tandeming, that is when using just one codec. Chen *et al.* concluded [94, 109] that this effect of introducing post-filtering was a consequence of optimising the extent of post-filtering for maximum noise masking at a concomitant minimum speech distortion for the scenario using no tandeming, that is when employing a single coding stage. Therefore upon concatenating up to three asynchronously operated codecs the amount of post-filtering became exaggerated. These findings prompted a new postfilter design, which was optimised for three stages and, as a consequence, the corresponding speech quality over three tandemed codec stages improved by a MOS of 0.81 to 3.93.

Modern post-filters [110] operate by emphasising both the formant and pitch peaks in the frequency-domain representation of speech, and simultaneously attenuating the spectral valleys between these peaks. This reduces the audible noise in the reconstructed speech, which persists even after the noise shaping action of the error-weighting filter, since it is in the valleys between the formant and pitch peaks where the noise energy is most likely to cross the masking threshold and become audible. Therefore attenuating the speech in these regions reduces the audible noise, and – since our ears are not overly sensitive to the speech intensity in these valleys – only minimal distortion is introduced to the speech signal.

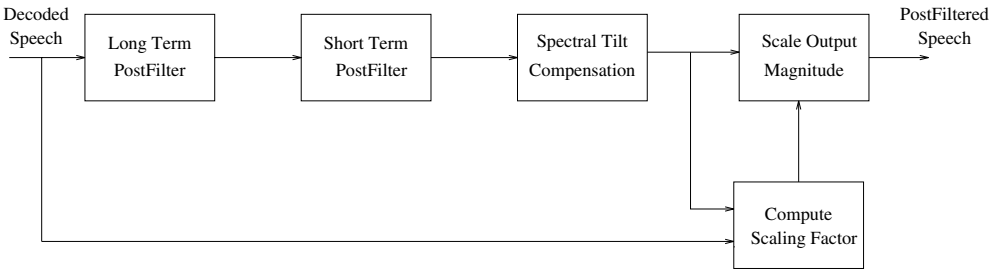

Figure 3.10: The G.728 adaptive postfilter arrangement.

The simplified block diagram of the postfilter arrangement used in the G.728 codec and in our variable rate codecs proposed in Chapter 8 is shown in Figure 3.10. The components of this schematic will be highlighted below. Further specific details concerning the G.728 adaptive postfilter can be found in Section 8.4.6. The long-term postfilter (LTPF) has a transfer function of

$$H_l(z) = \frac{1}{1+b}(1 + bz^{-p}), \tag{3.19}$$

where p is the backward adapted estimate of the pitch period, which must not be confused with the STP order p. The calculation of the backward-adapted pitch is based on the past encoded speech, as highlighted in Section 8.6, and the coefficient b is given by

$$b = \begin{cases} 0 & \text{if } \beta < 0.6 \\ \lambda\beta & \text{if } 0.6 \leq \beta \leq 1 \\ \lambda & \text{if } \beta > 1, \end{cases} \tag{3.20}$$

where λ is a parameter which controls the amount of LTPF and β is the tap weight of a single-tap long-term predictor having a delay of p, where β is given by

$$\beta = \frac{\sum_{n=-100}^{-1} \hat{s}(n)\hat{s}(n-p)}{\sum_{n=-100}^{-1} \hat{s}^2(n-p)}. \tag{3.21}$$

Note that here β was used instead of the previously introduced conventional forward-adapted LTP delay α. If β is less than 0.6, then the speech is assumed to be unvoiced and b is set to zero, effectively turning off the LTPF.

The short-term postfilter is given by

$$H_s(z) = \frac{1 - \sum_{i=1}^{10} \tilde{a}_i \gamma_1^i z^{-i}}{1 - \sum_{i=1}^{10} \tilde{a}_i \gamma_2^i z^{-i}}, \tag{3.22}$$

where γ_1 and γ_2 are tunable parameters which control the short-term post-filtering (STPF). Furthermore, $\tilde{a}_i,\ i = 1, 2, \ldots, 10$, are the backward adapted short-term synthesis filter parameters for a filter of order 10, which are derived as a by-product during the calculation of the coefficients for the actual 50th-order synthesis filter. Again, this backward adapted STP calculation process is detailed in Section 8.4. The all-pole section of $H_s(z)$, which is

constituted by its denominator, emphasises the formants in the reconstructed speech, and attenuates the valleys between these formants. However, this filtering operation introduces an undesirable spectral tilt in the post-filtered speech, which leads to a somewhat muffled speech perception. This spectral tilt is partially offset by the all-zero section of $H_s(z)$, namely by its numerator.

The all-zero section of $H_s(z)$ significantly reduces the muffling effect of the postfilter. However, the post-filtered speech is still slightly muffled, and hence a *spectral tilt compensation* block is used to further reduce this effect. This is a first-order filter with a transfer function of $1 - \mu k_1 z^{-1}$, where μ is a tunable parameter between 0 and 1, and k_1 is the first reflection coefficient calculated from the LPC analysis of the reconstructed speech. During voiced speech the postfilter introduces a low-pass spectral tilt to the speech, but simultaneously k_1 is close to -1 and hence the spectral tilt compensation block introduces high-pass filtering in order to offset this spectral tilt. During unvoiced speech the postfilter tends to introduce a high-pass spectral tilt to the speech, but k_1 becomes positive and therefore the spectral tilt compensation block automatically changes to a low-pass filter and again, offsets the spectral tilt.

The final section of the postfilter in Figure 3.10 scales the output so that it has approximately the same power as the original decoded speech. The LTPF has its own gain control because of the factor $1/(1 + b)$ in $H_l(z)$. However, the STPF tends to amplify the post-filtered speech, when the prediction gain of the short-term filter is high, and this leads to the output speech sounding un-natural. The output scaling blocks remove this effect by estimating the average magnitudes of the decoded speech and the output from the spectral tilt compensation block, and determining a scaling factor based on the ratio of these average magnitudes.

The tunable parameters λ, γ_1, γ_2 and μ must be chosen appropriately in order to control the amount of post-filtering used. We want to introduce sufficient post-filtering in order to attenuate the audible coding noise as much as possible, without introducing too much distortion to the post-filtered speech. In the G.728 codec the parameters were chosen to minimise the coding noise after three tandemed codec stages [94], since the ITU allows a maximum of three consecutive tandeming stages. The parameters were set to $\lambda = 0.15$, $\gamma_1 = 0.65$, $\gamma_2 = 0.75$ and $\mu = 0.15$.

In conclusion, post-filtering is important and sophisticated in state-of-the-art codecs. A variety of further solutions will be discussed in Chapter 7 in the context of existing standard codecs. Having considered the basic elements of the AbS structure, namely the issues of short- and long-term prediction and various excitation models, in closing this chapter an alternative technique of linear predictive AbS coding is presented in the next section, which is referred to as lattice-based short-term prediction. This will also allow us to further familiarise ourselves with the reflection coefficients introduced in the Levinson–Durbin algorithm, as well as with other equivalent ways of describing the speech signal's spectrum and to consider the effect of quantising these spectral parameters.

3.7 Lattice-based Linear Prediction

In order to augment our exposition of the linear prediction problem we note that several authors, including Itakura and Saito [111, 112], Kitawaki *et al.* [113], Makhoul [76], Rabiner

and Schaefer [6], Gordos and Takacs [15] as well as a number of other authors showed how the key relationship of LPC analysis given by Equation (2.22) can be formulated using the so-called *lattice approach* by combining the correlation computation with an iterative solution for the predictive coefficients.

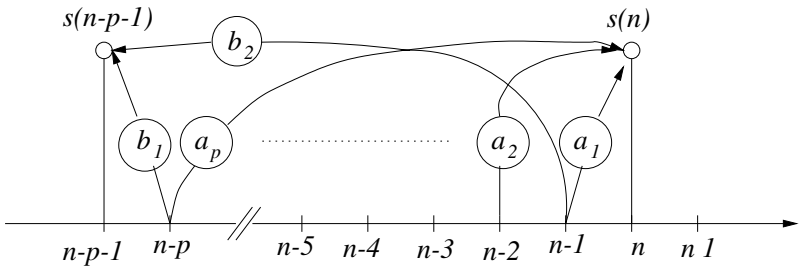

Figure 3.11: Forward and backward prediction of samples in the lattice approach, where $s(n)$ is forward predicted using $a_i, i = 1, \ldots, p$, while $s(n-p-1)$ is backward predicted using $b_i, i = 1, \ldots, p$.

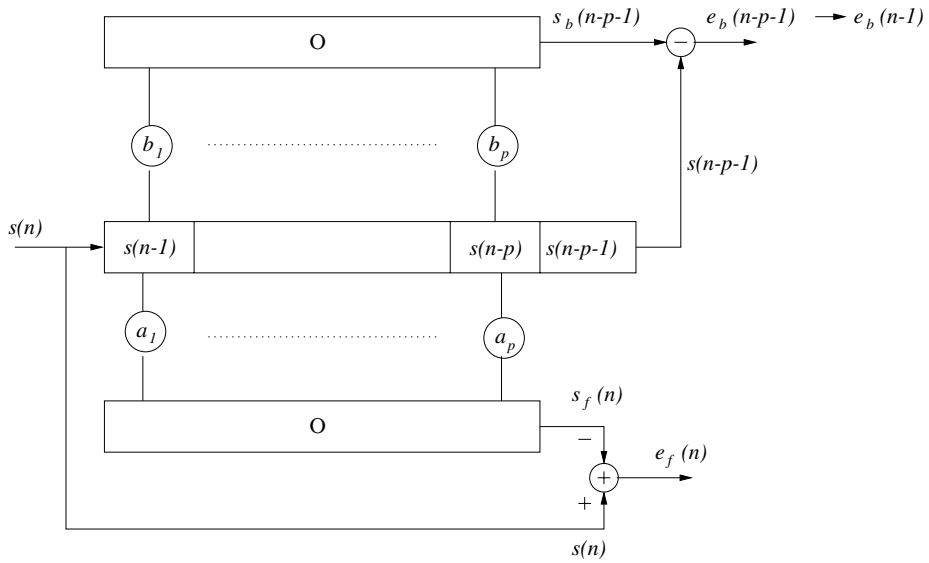

Figure 3.12: Forward and backward prediction schematic using the lattice approach, where $s(n)$ is forward predicted using $a_i, i = 1, \ldots, p$, while $s(n-p-1)$ is backward predicted using $b_i, i = 1, \ldots, p$.

In order to be able to deduce the linear predictive lattice structure, let us first highlight the analogy between the concept of backwards prediction and forward prediction, which relies on a set of symmetric equations. Specifically, let us refer to Figures 3.11 and 3.12, where the current sample $s(n)$ is predicted using the previous p number of samples and coefficients a_i,

$i = 1, \ldots, p$, and the forward-prediction error is given by the usual expression of

$$e_f(n) = s(n) - \sum_{k=1}^{p} a_k s(n-k) = \sum_{k=0}^{p} a_k s(n-k), \quad a_0 \equiv 1 \tag{3.23}$$

or in the z-domain as

$$E(z) = A(z) \cdot S(z). \tag{3.24}$$

Similarly, the sample $s(n-p-1)$ can be predicted in a backwards-oriented fashion on the basis of the samples $s(n-p), \ldots, s(n-1)$, which arrived later than $s(n-p-1)$, using the prediction coefficients b_i, $i = 1, \ldots, p$. The associated backwards-prediction error is given by

$$e_b(n-p-1) = s(n-p-1) - \sum_{k=1}^{p} b_k s(n-k). \tag{3.25}$$

It is convenient, however, to relate the backward-prediction error to the instant $(n-1)$, since this is the time of the latest sample influencing its value. Hence we rewrite Equation (3.25) as

$$e_b(n-1) = s(n-p-1) - \sum_{k=1}^{p} b_k s(n-k), \tag{3.26}$$

which allows us to define a causal system, generating $e_b(n-1)$ on the basis of $s(n-p-1), \ldots, s(n-1)$. Again, in an analogy to the previously outlined forward predictive approach, the predictor coefficients b_i, $i = 1, \ldots, p$ can be determined by minimising the total squared backward prediction error of

$$\begin{aligned} E_b &= \sum_{N} e_b^2(n-p-1) \\ &= \sum_{N} \left[s(n-p-1) - \sum_{k=1}^{p} b_k s(n-k) \right]^2. \end{aligned} \tag{3.27}$$

Upon expanding Equation (3.27), similar to our approach previously described by Equation (2.21) in the context of forward prediction, we arrive at

$$\begin{pmatrix} R(0) & R(1) & \ldots & R(p-1) \\ R(1) & R(0) & \ldots & R(p-2) \\ \vdots & & & \\ R(p-1) & R(p-2) & \ldots & R(0) \end{pmatrix} \begin{pmatrix} b_1 \\ b_2 \\ \vdots \\ b_p \end{pmatrix} = \begin{pmatrix} R(p) \\ R(p-1) \\ \vdots \\ (R(1) \end{pmatrix}, \tag{3.28}$$

giving a solution of

$$b_i = a_{p+1-i}, \tag{3.29}$$

which, in accordance with Figure 3.11, is symmetric with respect to the forward-oriented predictor.

We can also express this relationship in terms of the corresponding all-zero polynomials $A(z)$ and $B(z)$ upon z-transforming Equation (3.26), yielding [15]

$$E_b(z)z^{-1} = S(z)z^{-p-1} - S(z)\left[\sum_{k=1}^{p} b_i z^{-k}\right]. \tag{3.30}$$

This allows us to express the backward-oriented all-zero polynomial $B(z)$ as

$$\begin{aligned} B(z) = \frac{E_b(z)}{S(z)} &= z^{-p} - \sum_{k=1}^{p} b_k z^{-k+1} \\ &= z^{-p}\left[1 - \sum_{k=1}^{p} b_k z^{-k+1+p}\right] \end{aligned} \tag{3.31}$$

and upon exploiting Equation (3.29) we arrive at

$$\begin{aligned} B(z) &= z^{-p}\left[1 - \sum_{k=1}^{p} a_{p+1-k} z^{-k+1+p}\right] \\ &= z^{-p}[1 - a_p z^p - a_{p-1}z^{p-1} - \cdots - a_1 z]. \end{aligned} \tag{3.32}$$

Lastly, since

$$\begin{aligned} A(z) &= 1 - a_1 z^{-1} - a_2 z^{-2} - \cdots - a_p z^{-p} \\ &= 1 - a_1 \frac{1}{z} - a_2 \frac{1}{z^2} - \cdots - a_p \frac{1}{z^p} \end{aligned} \tag{3.33}$$

and

$$A(z^{-1}) = A\left(\frac{1}{z}\right) = 1 - a_1 z^1 - a_2 z^2 - \cdots - a_p z^p \tag{3.34}$$

we get the plausible relationship of

$$B(z) = z^{-p} A(z^{-1}) \tag{3.35}$$

between the backwards- and forwards-oriented all-zero polynomials. Clearly, the physical interpretation of Equation (3.35) suggests that the optimum backward-prediction polynomial is a close relative of $A(z^{-1})$. The z-domain representation of the backward-prediction error is given by

$$E_b(z) = B(z) \cdot S(z) = z^{-p} A(z^{-1}) S(z). \tag{3.36}$$

In order to proceed with the formulation of the lattice-based prediction approach, let us now derive a recursion for the generation of the ith order all-zero polynomial from the $(i-1)$st order system, where

$$A^{(i)}(z) = 1 - a_1^{(i)} z^{-1} - a_2^{(i)} z^{-2} - \cdots - a_{i-1}^{(i)} z^{-i+1} - a_i^{(i)} z^{-i}. \tag{3.37}$$

Upon exploiting from the Levinson–Durbin algorithm of Figure 2.3 that for the coefficients of the ith order system we have

$$\begin{aligned} a_j^{(i)} &= a_j^{(i-1)} - k_i a_{i-j}^{(i-j)} \quad \text{for } j = 1, \ldots, i-1 \\ a_i^{(i)} &= k_i \end{aligned} \tag{3.38}$$

we arrive at

$$\begin{aligned} A^{(i)} &= 1 - (a_1^{(i-1)} - k_i a_{i-1}^{(i-1)})z^{-1} - (a_2^{(i-1)} - k_i a_{i-2}^{(i-1)})z^{-2} - \cdots \\ &\quad - (a_{i-1}^{(i-1)} - k_i a_{i-i+1}^{(i-1)})z^{-i+1} \\ &= 1 + k_i(a_{i-1}^{(i-1)}z^{-1} + a_{i-2}^{(i-1)}z^{-2} + \ldots + a_1^{(i-1)}z^{-i+1} - z^{-i}) \\ &\quad - a_1^{(i-1)}z^{-1} - a_2^{(i-1)}z^{-2} - \cdots - a_{i-1}^{(i-1)}z^{-i+1}. \end{aligned} \tag{3.39}$$

Due to Equation (3.37) we have

$$A^{(i-1)}(z) = 1 - a_1^{(i-1)}z^{-1} - a_2^{(i-1)}z^{-2} - \cdots - a_{i-1}^{(i-1)}z^{-i+1} \tag{3.40}$$

and

$$A^{(i-1)}(z^{-1}) = 1 - a_1^{(i-1)}z - a_2^{(i-1)}z^2 - \cdots - a_{i-1}^{(i-1)}z^{i-1} \tag{3.41}$$

hence the required recursion is given by

$$\begin{aligned} A^{(i)}(z) &= A^{(i-1)}(z) + k_i(a_{i-1}^{(i-1)}z^{-1} + \cdots + a_1^{(i-1)}z^{-i+1} - z^{-i}) \\ &= A^{(i-1)}(z) + k_i z^{-i}(a_{i-1}^{(i-1)}z^{i-1} + \cdots + a_1^{(i-1)}z^1 - 1) \\ &= A^{(i-1)}(z) - k_i z^{-i}A^{(i-1)}(z^{-1}). \end{aligned} \tag{3.42}$$

As an example, for $i = 2$ we have

$$\begin{aligned} A^{(1)}(z) &= A^{(0)}(z) - k_1 z^{-1}A^{(0)}(z^{-1}) = 1 - k_1 z^{-1} \\ A^{(2)}(z) &= A^{(1)}(z) - k_2 z^{-2}A^{(1)}(z^{-1}); \end{aligned}$$

upon exploiting that $A^{(1)}(z^{-1}) = 1 - k_1 z$ we arrive at

$$\begin{aligned} A^{(2)}(z) &= (1 - k_1 z^{-1}) - k_2 z^{-2}(1 - k_1 z) \\ &= 1 - k_1 z^{-1} - k_2 z^{-2} + k_1 k_2 z^{-1} \\ &= 1 - k_1 z^{-1}(1 - k_2) - k_2 z^{-2}. \end{aligned} \tag{3.43}$$

Observe, however, in both Equation (3.41) and in the above example that the function $A^{(i-1)}(z^{-1})$ represents an unrealisable, non-causal system. Nonetheless, upon using an $(i-1)$st order predictor in Equation (3.35) and invoking Equation (3.42), we can rectify

this problem, leading to

$$\begin{aligned} A^{(i)}(z) &= A^{(i-1)}(z) - k_i z^{-1} z^{(i-1)} A^{(i-1)}(z^{-1}) \\ &= A^{(i-1)}(z) - k_i z^{-1} B^{(i-1)}(z). \end{aligned} \tag{3.44}$$

When substituting the recursion of Equation (3.44) into Equation (3.24), the forward-oriented prediction error of the ith order predictor is yielded as

$$\begin{aligned} E_f^{(i)}(z) &= A^{(i)}(z) S(z) \\ &= A^{(i-1)}(z) S(z) - k_i z^{-1} B^{(i-1)}(z) S(z). \end{aligned} \tag{3.45}$$

Observe in Equation (3.45) that the first term is the forward-prediction error of the $(i-1)$st order predictor, while the second term can be interpreted in an analogous fashion after transforming Equation (3.45) back to the time-domain:

$$e_f^{(i)}(n) = e_f^{(i-1)}(n) - k_i e_b^{(i-1)}(n-1). \tag{3.46}$$

Clearly, this expression generates the forward-prediction error of the ith order predictor as a linear combination of the forward- and backward-prediction errors of the $(i-1)$st order forward and backward predictors.

In order to arrive at a complete set of recursive formulae it is also possible to generate the ith order backward-prediction error $e_b^{(i)}(n)$ from that of the $(i-1)$st order forward and backward predictors using the following approach. The ith order backward predictor's prediction error is given in the z-domain by

$$E_b^{(i)}(z) = B^{(i)}(z) \cdot S(z) \tag{3.47}$$

which can be rewritten with the help of Equation (3.35) as

$$E_b^{(i)}(z) = z^{-i} A^{(i)}(z^{-1}) \cdot S(z), \tag{3.48}$$

which in turn is reformulated using the recursion of Equation (3.42) as

$$\begin{aligned} E_b^{(i)}(z) &= z^{-i} S(z) [A^{(i-1)}(z^{-1}) - k_i z^i A^{(i-1)}(z)] \\ &= z^{-i} A^{(i-1)}(z^{-1}) S(z) - k_i A^{(i-1)}(z) S(z). \end{aligned} \tag{3.49}$$

Exploiting the relationship of Equation (3.35) again and introducing the z-transform of the forward-prediction error leads to

$$\begin{aligned} E_b^{(i)}(z) &= B^{(i)} \cdot S(z) \\ &= z^{-1} B^{(i-1)}(z) S(z) - k_i A^{(i-1)}(z) S(z) \\ &= z^{-1} E_b^{(i-1)}(z) - k_i E_f^{(i-1)}(z). \end{aligned} \tag{3.50}$$

Finally, after transforming the above equation back to time-domain, we arrive at

$$e_b^{(i)}(n) = e_b^{(i-1)}(n-1) - k_i e_f^{(i-1)}(n), \tag{3.51}$$

expressing the ith order backward-prediction error as a combination of the $(i-1)$st order forward- and backward-prediction errors. Furthermore, from the 1st and 2nd line of Equation (3.50) we can also infer the recursive relationship of

$$B^{(i)}(z) = z^{(-1)} b^{(i-1)}(z) - k_q A^{(i-1)}(z), \tag{3.52}$$

producing the optimum ith order backward-oriented all-zero polynomial from the $(i-1)$st order $B(z)$ and $A(z)$ functions.

The recursions in Equations (3.46) and (3.51) now define the *lattice analysis structure*, delivering both the forward- and backward-prediction errors from $s(n)$. For the zero-order predictor we have $e_f^{(0)}(n) = e_b^{(0)}(n) = s(n)$, implying that the forward predictor generates $s(n)$ from $s(n)$, while the backward predictor produces $s(n-1)$ from $s(n-1)$. Using Equations (3.46) and (3.51), it is now easy to confirm that the corresponding schematic obeys the structure of Figure 3.13, which constitutes an alternative implementation of the all-zero analysis filter $A(z)$ without relying on the coefficients a_i, $i = 1, \ldots, p$.

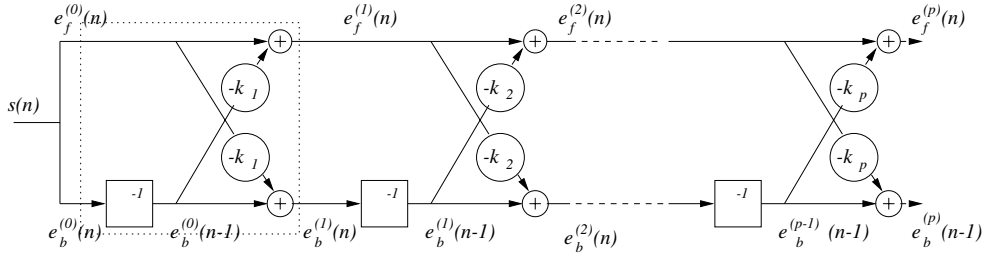

Figure 3.13: Lattice analysis scheme.

The corresponding *synthesis lattice structure* can be readily constructed by adopting an inverse approach in order to generate $s(n)$ from $e_f^{(p)}(n)$. Hence Equation (3.46) can be rearranged to reflect this approach as [15]

$$e_f^{(i-1)}(n) = e_f^{(i)}(n) + k_i e_b^{(i-1)}(n-1), \tag{3.53}$$

while

$$\begin{aligned} e_b^{(i)}(n) &= e_b^{(i-1)}(n-1) - k_i e_f^{(i-1)}(n) \\ &= e_b^{(i-1)}(n-1) - k_i e_f^{(i-1)}(n) + k_i^2 e_b^{(i-1)}(n-1) \\ &\quad - k_i^2 e_b^{(i-1)}(n-1) \\ &= e_b^{(i-1)}(n-1) - k_i [e_f^{(i-1)}(n) - k_i e_b^{(i-1)}(n-1)] \\ &\quad - k_i^2 e_b^{(i-1)}(n-1). \end{aligned} \tag{3.54}$$

Upon recognising that the square-bracketed term corresponds to the right-hand side of Equation (3.46), we arrive at

$$\begin{aligned} e_b^{(i)}(n) &= e_b^{(i-1)}(n-1) - k_i e_f^{(i)}(n) - k_i^2 e_b^{(i-1)}(n-1) \\ &= -k_i e_f^{(i)}(n) + (1-k_i^2) e_b^{(i-1)}(n-1). \end{aligned} \tag{3.55}$$

Equations (3.53) and (3.55) are directly realizable, as portrayed in Figure 3.14, which is easily verified by the interested reader. Observe that this circuit contains three multipliers. It is possible to find arithmetically equivalent representations, while requiring two or just one multiplier, which usually require a higher number of adders [6, 15].

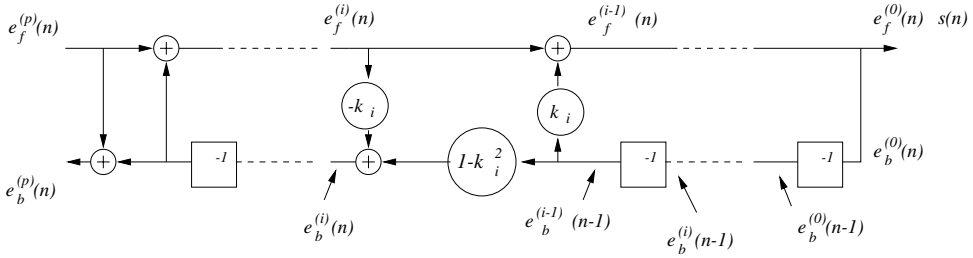

Figure 3.14: Lattice synthesis scheme.

3.8 Chapter Summary

In this chapter the AbS structure was introduced and its building blocks were detailed. The concept of perceptual error weighting was introduced, in order to mask the effects of quantisation errors in the most vulnerable spectral valleys of the speech signal between the high-energy formant regions. Both open-loop and closed-loop LTPs were analysed and studied. The latter guarantees a better performance at the cost of a higher complexity. Practical codecs often combine these techniques by invoking an initial coarse open-loop LTP analysis and then a more accurate closed-loop procedure in the vicinity of the pitch value determined by the open-loop search.

These LTP-oriented discussions were followed by a brief discourse on post-filters, which further enhance the perceptual speech quality. Finally, having introduced the reflection coefficients and having studied their characteristics let us now focus our attention on a range of other spectral coefficients, which are more amenable to quantisation. In other words, we are seeking alternative ways of representing the speech signal's spectral envelope, which exhibit a higher robustness against transmission errors inflicted by hostile channels.

Chapter 4

Speech Spectral Quantisation

4.1 Log-area Ratios

In Section 2.3.3 the filter coefficients $a_i,\ i = 1, \ldots, p$ and their equivalent representations, the so-called reflection coefficients $k_i,\ i = 1, \ldots, p$, were introduced in order to describe the speech signal's spectral envelope. Here we characterise their statistical properties in terms of their experimentally evaluated PDFs, which are portrayed in Figures 4.1 and 4.2, respectively. Experience shows that in the case of the a_i coefficients an extremely fine-resolution quantisation is necessary in order to guarantee the stability of the synthesis filter $H(z) = 1/A(z)$. Clearly, this is undesirable in terms of bitrate.

As discussed in the context of the Levinson–Durbin algorithm of Section 2.3.3, the reflection coefficients have a more limited amplitude range and the stability of $H(z)$ can be ensured by checking the physically tangible condition of

$$|k_i| = \left| \frac{A_{i+1} - A_i}{A_{i+1} + A_i} \right| < 1, \tag{4.1}$$

where again, $A_i,\ i = 1, \ldots, p$ represents the area of the ith acoustic tube section modelling the vocal tract [6,71] and $|k_i| > 1$ would imply a tube cross-section of $A_i \leq 0$. If the computed or transmitted value of k_i is outside the unit circle, it can be reduced to below one, which does modify the computed spectrum, but in exchange ensures filter stability. It was shown [114] that for values of $|k_i| \approx 1$ a very fine quantiser resolution must be ensured, requiring a densely spaced Lloyd–Max quantiser, since the filter transfer function $H(z)$ is very sensitive to the quantisation errors for values of $|k_i| \approx 1$.

The so-called *log-area ratios* (LAR) defined as

$$\mathrm{LAR}_i = \log \frac{1 - k_i}{1 + k_i} \tag{4.2}$$

constitute a nonlinear transformation of the reflection coefficients or area ratios and have better quantisation properties. Their PDFs are plotted in Figure 4.3. Observe that the

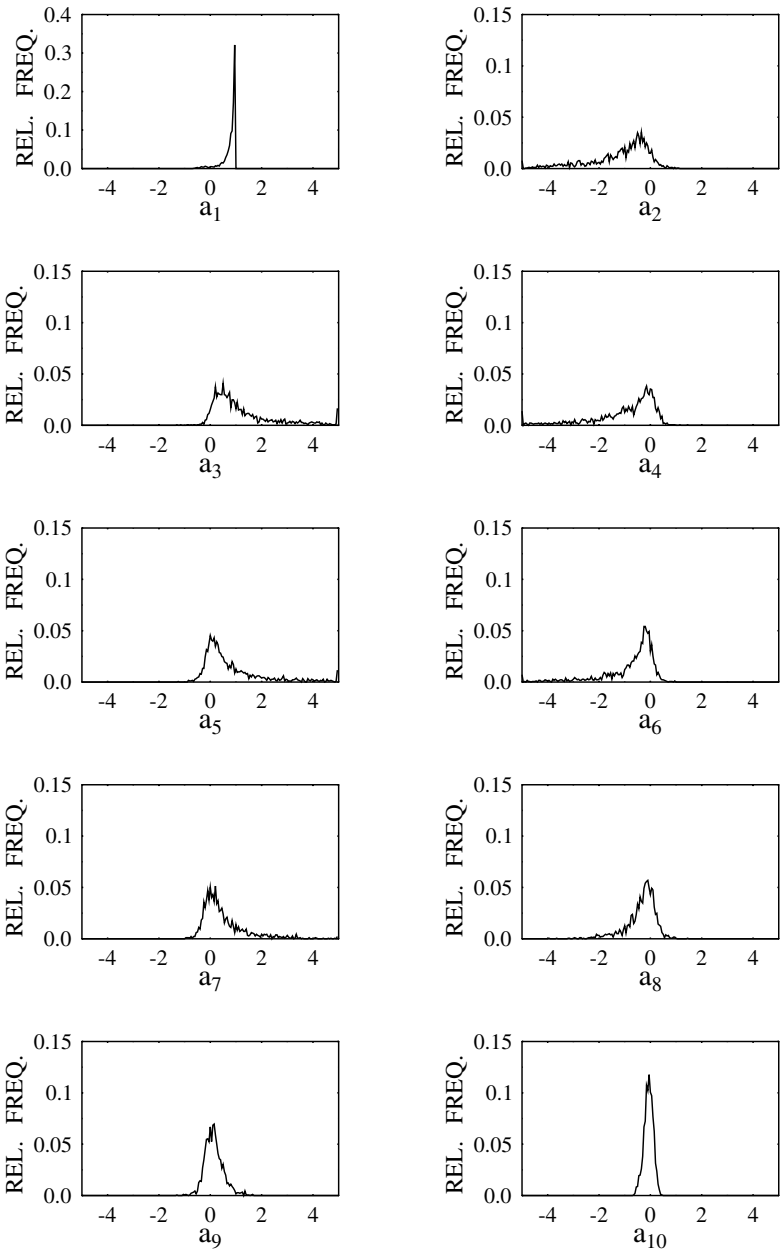

Figure 4.1: Relative frequency plots of the filter coefficients $a_i,\ i = 1, \ldots, 10$, for a typical mixed-gender speech segment.

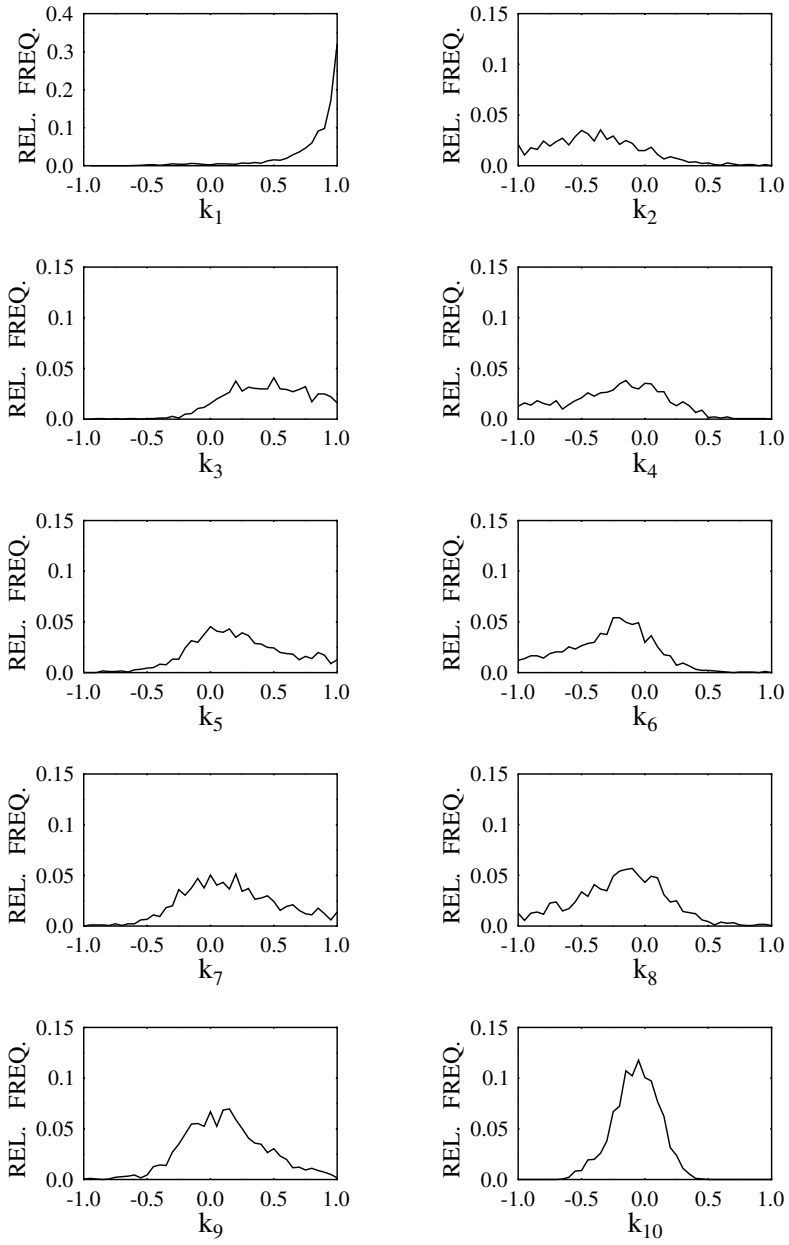

Figure 4.2: Relative frequency plots of the reflection coefficients k_i, $i = 1, \ldots, 10$, for a typical mixed-gender speech segment.

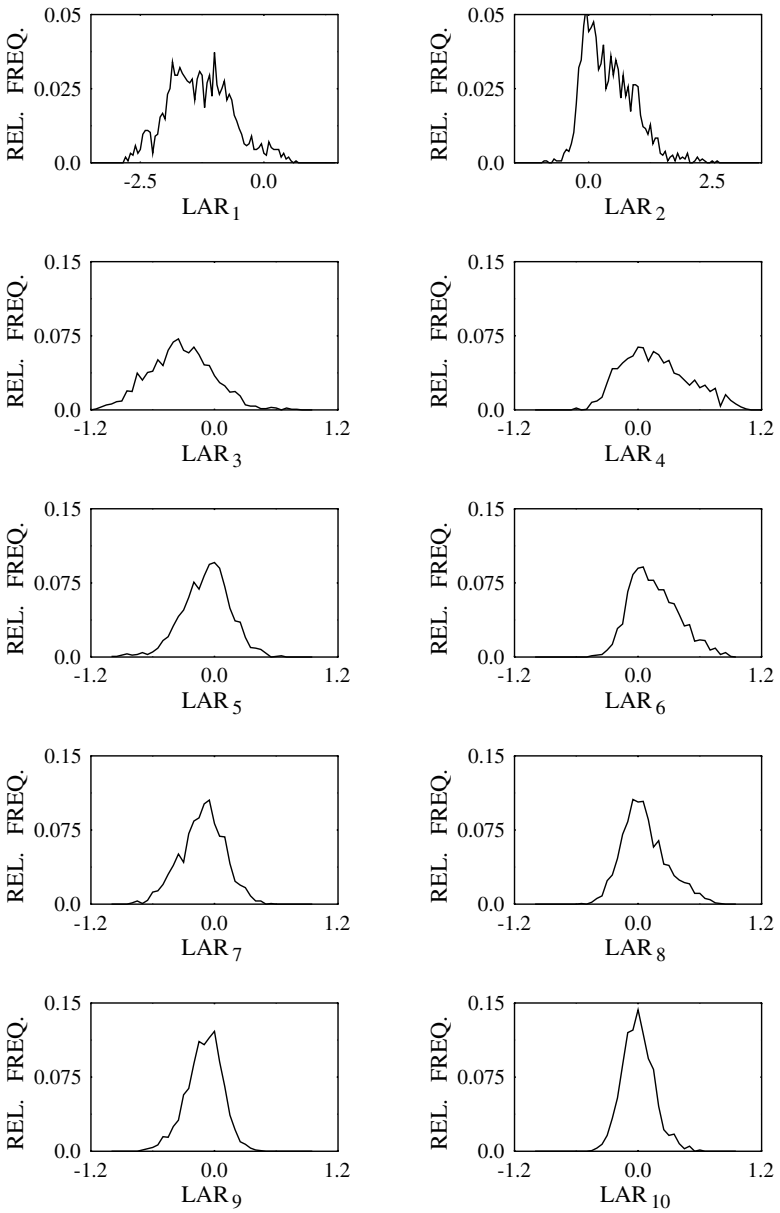

Figure 4.3: Relative frequency plots of the LAR filter coefficients $\mathrm{LAR}_i,\ i = 1, \ldots, 10$, for a typical mixed-gender speech segment.

range of the LAR coefficients is becoming more limited towards higher-order coefficients. This property was exploited, for example, in the Pan-European digital mobile radio system known as GSM [98], where 6, 6, 5, 5, 4, 4, 3 and 3 bits were used to quantise the first eight LAR coefficients, requiring a total of 36 bits per 20 ms LPC analysis frame.

4.2 Line Spectral Frequencies

4.2.1 Derivation of the Line Spectral Frequencies

Another derivative of the reflection coefficients and the all-zero filter $A(z)$ is the set of *line spectrum frequencies* (LSF) [115, 116], which are often also referred to as *line spectrum pairs* (LSP). In our forthcoming discourse we will introduce the LSFs using a detailed mathematical description for the more advanced reader. Then a simple numerical procedure will be proposed for their computation and their statistical properties will be contrasted with those of the a_i, k_i and LAR_i parameters.

Recall from Equation (3.42) in Section 3.7, which is repeated here for convenience, that $A^{(i)}(z)$ associated with the ith iteration of the pth order prediction obeys the recursion

$$A^{(i)}(z) = A^{(n-i)}(z) - k_i z^{-i} A^{(i-1)}(z^{-1}), \quad i = 1, \ldots, p, \tag{4.3}$$

where $A^{(0)}(z) = 1$ and the polynomial $A(z^{-1})$ is physically related to the optimum backward-oriented all-zero polynomial $B(z)$ through Equation (3.35). Upon artificially extending the filter order to $i = p + 1$, Equation (4.3) can be formally re-written as

$$A^{(p+1)}(z) = A^{(p)}(z) - k^{p+1} z^{-p+1} A^{(p)}(z^{-1}). \tag{4.4}$$

Soong and Juang [117] argued that this extension is legitimate, if no unknown information is exploited, which can be ensured by setting $k_{p+1} = \pm 1$. Then the lattice analysis and synthesis schemes defined by Equations (3.46), (3.51) as well as by Equations (3.53), (3.55) and portrayed in Figures 3.13 as well as 3.14, respectively, are fully described, since they do not contain unknown quantities. When considering the lattice analysis scheme of Figure 3.13, which generates the prediction residual signal at the output of its $(p + 1)$st stage, $k_{p+1} = \pm 1$ corresponds to perfect reflection or, in other words, to a complete closure and complete opening of the acoustic tube model at the glottis. From Equation (3.42) according to $k_{p+1} = \pm 1$, at iteration $p + 1$ we can write

$$A^{(p+1)} = A^{(p)} \pm z^{-}(p + 1) A^{(p)}(z^{-1}). \tag{4.5}$$

Specifically, for $k_{p+1} = 1$ the corresponding polynomial defined by Soong and Juang [117] is given by

$$\begin{aligned} P(z) &= A^{(p+1)}(z) - z^{-(p+1)} A^{(p+1)}(z^{-1}) \\ &= 1 - a_1 z^{-1} - a_2 z^{-2} + \cdots - a_p z^{-p} \\ &\quad - [1 - a_1 z^{1} - a_2 z^{2} + \cdots - a_p z^{p}] \ldots z^{-(p+1)}, \end{aligned} \tag{4.6}$$

which is accordingly referred to as the *difference filter*. Similarly, for $k_{p+1} = -1$ we can derive the so-called *sum filter* as follows:

$$\begin{aligned} Q(z) &= A^{(p+1)}(z) + z^{-(p+1)} A^{(p+1)}(z^{-1}) \\ &= 1 - a_1 z^{-1} - a_2 z^{-2} + \cdots - a_p z^{-p} \\ &\quad + [1 - a_1 z^1 - a_2 z^2 + \cdots - a_p z^p \ldots z^{-(p+1)}]. \end{aligned} \tag{4.7}$$

It is plausible from our discussions on forward- and backward-oriented prediction in Section 3.7 and specifically from Figure 3.11 and Equation (3.35) that the backward-oriented predictor's impulse response is a time-reversed version of that of the forward-oriented one. In Figure 4.4 a hypothetical all-zero filter impulse response is portrayed together with its appropriately time-reversed and shifted version and with the impulse responses of the sum- and difference filters. Observe that while the impulse response of the sum filter $Q^{(p+1)}(z)$ is symmetric with respect to its centre point, that of the difference filter $P^{(p+1)}(z)$ is anti-symmetric or odd-symmetric. From the above two equations the all-zero analysis filter can then be expressed as

$$A^p(z) = \tfrac{1}{2}[P^{(p+1)}(z) + Q^{p+1)}(z)]. \tag{4.8}$$

This particular formulation is not specific to the linear predictive coding of speech, it is valid for arbitrary finite response filters in general.

From Equation (4.6) we can collect the terms which correspond to the same power of z, or to the same delay in the impulse response of Figure 4.4, which ensues that

$$\begin{aligned} P^{(p+1)}(z) &= 1 - a_1 z^{-1} + a_p z^{-1} - a_2 z^{-2} + a_{p-1} z^{-2} - \cdots \\ &\quad - a_{p/2} z^{-p/2} + a_{(p/2-1)} z^{-p/2} \\ &\quad + a_{p/2} z^{-p/2+1} - a_{(p/2-1)} z^{-p/2+1} + \cdots \\ &\quad + a_2 z^{-p+1} - a_{p-1} z^{-p+1} + \cdots \\ &\quad + a_1 z^{-p} - a_p z^{-p} - z^{-(p+1)} \\ &= 1 + (a_p - a_1) z^{-1} + (a_{p-1} - a_2) z^{-2} + \cdots \\ &\quad + (a_{(p/2-1)} - a_{p/2}) z^{-p/2} \\ &\quad - (a_{(p/2-1)} - a_{p/2}) z^{-p/2+1} - \cdots \\ &\quad - (a_{p-1} - a_2) z^{-p+1} - (a_p - a_1) z^{-p} - z^{-(p+1)}. \end{aligned} \tag{4.9}$$

In harmony with Figure 4.4, Equation (4.9) now explicitly shows the odd symmetry of coefficients. Explicitly, for the first and last terms these coefficients have an absolute value of one. By contrast, for the second and last but one terms we have $|a_p - a_1|$, etc. Upon rewriting Equation (4.9) in a more compact form, we arrive at [118]

$$\begin{aligned} P^{(p+1)}(z) &= 1 + p_1 z^{-1} + p_2 z^{-2} + \cdots + p_{p/2} z^{-p/2} \\ &\quad - p_{p/2} z^{-p/2+1} - \cdots - p_2 z^{-p+1} - p_1 z^{-p} - z^{-(p+1)}, \end{aligned} \tag{4.10}$$

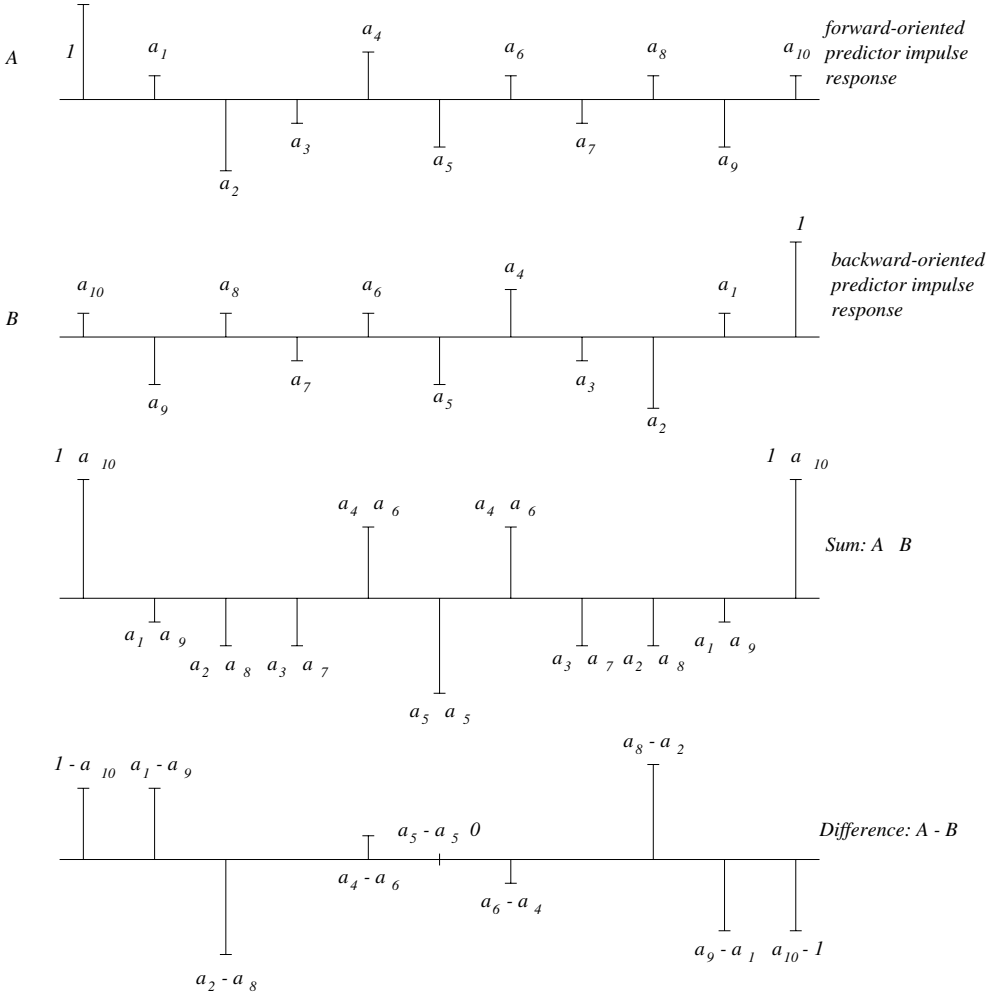

Figure 4.4: From top to bottom: (A) stylised impulse response of the all-zero filter $A(z)$; (B) the stylised time-reversed shifted impulse response; (Sum: A + B) stylised impulse response of the sum filter; (Difference: A - B) stylised impulse response of the difference-filter.

where only $p/2$ coefficients are necessary in order to describe $P^{(p+1)}(z)$, and the coefficients are given by

$$p_1 = (-a_1 + a_p), \quad p_2 = (-a_2 + a_{p-1}) \ldots p_{p/2} = (-a_{p/2} + a_{p/2-1}). \tag{4.11}$$

Since any odd-symmetric polynomial has a zero at $z = 1$, Equation (4.10) can be rewritten to express this explicitly as [118]

$$P^{(p+1)}(z) = (1 - z^{-1})[1 + c_1 z^{-1} + c_2 z^{-2} + \cdots + c_{p/2-1} z^{-p/2-1} + c_{p/2} z^{-p/2} + \cdots$$

$$+ c_2 z^{-p+2} + c_1 z^{-p+1} + z^{-p}]$$
$$= (1 - z^{-1}) \cdot C(z), \tag{4.12}$$

where the coefficients $c_1 \ldots c_{p/2}$ can be determined with the help of simple polynomial division. Clearly, the resulting polynomial $C(z)$ now has a total of p coefficients, rather than $(p+1)$, but due to its even symmetry only $p/2$ are different. Soong and Juang showed [117] that the roots of such a polynomial occur in complex conjugate pairs on the unit circle and hence it is sufficient to determine only those on the upper half circle. Explicitly, the roots of $P^{(p+1)}(z)$ are: 1, $\pm e^{j\Theta_1}$, $\pm e^{j\Theta_2}, \ldots, \pm e^{j\Theta_{p/2}}$, which allows us to express $P^{(p+1)}(z)$ as [118]

$$\begin{aligned} P^{(p+1)}(z) &= (1 - z^{-1}) \prod_{i=1}^{p/2} (1 - e^{j\Theta_i} z^{-1})(1 - e^{-j\Theta_i} z^{-1}) \\ &= (1 - z^{-1}) \prod_{i=1}^{p/2} [1 - z^{-1}(e^{-j\Theta_i} + e^{j\Theta_i}) + z^{-2}] \\ &= (1 - z^{-1}) \prod_{i=1}^{p/2} [1 - 2z^{-1} \cos 2\pi f_i t_s + z^{-2}], \end{aligned} \tag{4.13}$$

where f_i defines the so-called LSF or LSP, while t_s corresponds to the sampling instants. When using the shorthand

$$d_i = -2 \cos 2\pi f_i t_s \tag{4.14}$$

we arrive at

$$P^{(p+1)}(z) = (1 - z^{-1}) \prod_{i=1}^{p/2} [1 + d_i z^{-1} + z^{-2}]. \tag{4.15}$$

Following the same approach, a similar expression can be derived for the polynomial $Q^{(p+1)}(z)$:

$$\begin{aligned} Q^{(p+1)}(z) &= (1 + z^{-1}) \prod_{i=1}^{p/2} [1 - 2z^{-1} \cos 2\pi f_i t_s + z^{-2}] \\ &= (1 + z^{-1}) \prod_{i=1}^{p/2} [1 + d_i z^{-1} + z^{-2}]. \end{aligned} \tag{4.16}$$

Using Equation (4.8), Kang and Fransen [118] proposed a simple analysis filter implementation on the basis of Equations (4.15) and (4.16). Although this scheme is not wide-spread in current codec implementations, its portrayal in Figure 4.5 conveniently concludes our previous discourse on the derivation of LSFs. Observe in the figure that it obeys the structure of Equations (4.15) and (4.16), implementing each multiplicative term as a block surrounded by dotted lines.

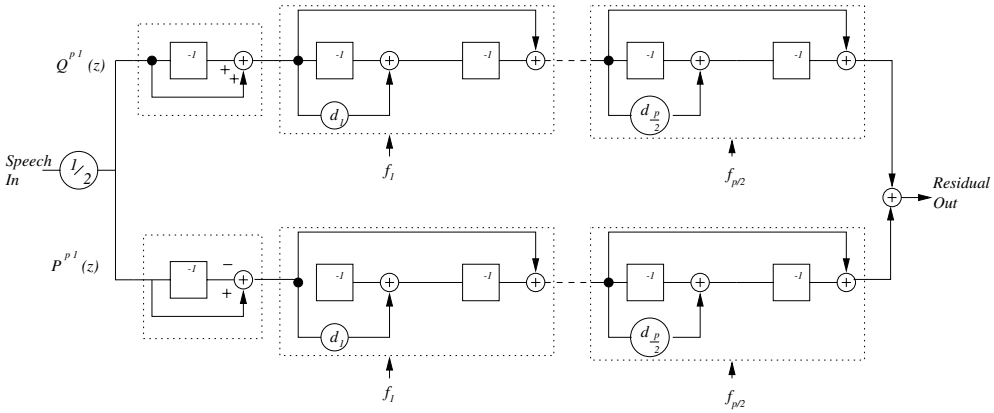

Figure 4.5: Schematic of a pth order LSF-based analysis filter according to Equations (4.15) and (4.16). Copyright © Kang, Fransen 1984 [118].

Assuming that the LSFs are known, the coefficients a_i, $i = 1, \ldots, p$, can be recovered upon substituting Equations (4.15) and (4.16) in Equation (4.8) and collecting the terms multiplying the appropriate powers of z.

In practical codec implementations the lattice based structures of Figures 3.13 and 3.14 are often favoured, and the LSFs are computed from the coefficients a_i, $i = 1, \ldots, p$, or k_i, $i = 1, \ldots, p$, in order to be able to exploit their more attractive quantisation properties. More explicitly, in many practical codecs the LSFs are computed by determining the roots of the polynomials $P_{(z)}^{(p+1)}$ and $Q_{(z)}^{(p+1)}$, which are then quantised for transmission to the decoder. At the decoded we have to recover the coefficients a_i. Hence, in what follows we will highlight how the predictor coefficients a_i, $i = 1, \ldots, p$, can be converted to LSF parameters, and then we will summarise the most salient features of LSFs.

4.2.2 Computation of the Line Spectral Frequencies

A number of different techniques have been suggested for the computation of the LSFs [117–121] which have different strengths and weaknesses. Soong and Juang [117] expressed the sum and difference filters $P^{(p+1)}(z)$ and $Q^{(p+1)}(z)$ as

$$P^{(p+1)}(z) = A(z)\left[1 + z^{-(p+1)}\frac{A(z^{-1})}{A(z)}\right] = A(z)[1 + R(z)]$$
$$Q^{(p+1)}(z) = A(z)\left[1 - z^{-(p+1)}\frac{A(z^{-1})}{A(z)}\right] = A(z)[1 - R(z)], \tag{4.17}$$

where they referred to

$$R(z) = z^{-(p+1)} \cdot \frac{A(z^{-1})}{A(z)} \tag{4.18}$$

as the *ratio-filter*.

Equation (4.18) takes the general form of a so-called *all-pass system*, which has a unity magnitude for all frequencies associated with a phase response. Hence an all-pass filter is also often referred to as a phase shifter or phase corrector, since it may be invoked to correct the undesirable phase response of the rest of the system. Accordingly, the transfer function of the ratio-filter of Equation (4.18) can also be formulated as [117]

$$R(\omega) = e^{j\phi(\omega)}, \tag{4.19}$$

where $\phi(\omega)$ represents the phase of $R(\omega)$. It is clear from Equations (4.17) and (4.18) that in order for $P^{(p+1)}(z)$ and $Q^{(p+1)}(z)$ to disappear, $R(z) = \pm 1$ must be maintained, which clearly implies that the zeros of $P^{(p+1)}(z)$ and $Q^{(p+1)}(z)$ must be on the unit circle. Furthermore, the roots are conjugate complex and symmetric to the origin. These facts were already alluded to earlier.

Note that it is possible to invoke general factorisation techniques in order to find the roots of $P^{(p+1)}(z)$ as well as $Q^{(p+1)}(z)$ and in possession of the roots we can compute the corresponding LSFs f_i using Equation (4.14). However, upon exploiting our *a priori* knowledge as regards to their locations on the unit circle, more efficient methods can be devised, which is the topic of our forthcoming discussion.

The polynomial $C(z)$ in Equation (4.12) can be rewritten in order to reflect the conjugate complex symmetry of its roots explicitly as

$$C(z) = z^{p/2}[(z^{p/2} + z^{-p/2}) + c_1(z^{p/2-1} + z^{-(p/2-1)}) + \cdots + c_{p/2}]. \tag{4.20}$$

The equivalent of Equation (4.12) for the polynomial $Q^{(p+1)}(z)$ is

$$\begin{aligned} Q^{(p+1)}(z) &= (1 + z^{-1})[1 + d_1 z^{-1} + d_2 z^{-2} + \cdots + d_{p/2-1} z^{-p/2-1} \\ &\quad + d_{p/2} z^{-p/2} + \cdots + d_2 z^{-p+2} + d_1 z^{-p+1} + z^{-p}] \\ &= (1 + z^{-1}) \cdot D(z), \end{aligned} \tag{4.21}$$

yielding the symmetrical formula of

$$D(z) = z^{p/2}[(z^{p/2} + z^{-p/2}) + d_1(z^{p/2-1} + z^{-(p/2-1)}) + \cdots + d_{p/2}]. \tag{4.22}$$

If we now exploit the *a priori* knowledge that the roots of $C(z)$ and $D(z)$ are on the unit circle, that is $z = e^{j\omega}$, we can express Equations (4.20) and (4.21) in a real form employing

$$\begin{aligned} z^{+1} + z^{-1} &= e^{j\omega} + e^{-j\omega} = 2\cos\omega \\ z^{+2} + z^{-2} &= e^{j2\omega} + e^{-j2\omega} = 2\cos 2\omega \\ &\vdots \\ z^{+p/2} + z^{-p/2} &= e^{j(p/2)\omega} + e^{-j(p/2)\omega} = 2\cos p\omega/2, \end{aligned} \tag{4.23}$$

leading to

$$C(z) = 2e^{j(p/2)\omega}[\cos(p/2)\omega + c_1 \cos(p/2-1)\omega + \cdots + c_{p/2-1}\cos\omega + 1/2c_{p/2}] \quad (4.24)$$

$$D(z) = 2e^{j(p/2)\omega}[\cos(p/2)\omega + d_1 \cos(p/2-1)\omega + \cdots + d_{p/2-1}\cos\omega + 1/2d_{p/2}]. \quad (4.25)$$

If we can factorise the polynomials $C(z)$ and $D(z)$, then according to Equations (4.12) and (4.21) the roots of $P_{(z)}^{(p+1)}$ and $Q_{(z)}^{(p+1)}$ have also been found, which determine the LSFs sought.

For the factorization of Equations (4.24) and (4.25) a number of techniques have been proposed. The conceptually most straightforward method is to evaluate the above expressions on a sufficiently fine grid in terms of ω, and observe the abscissa values at which the first expression of Equations (4.24) and (4.25) changes its polarity [117]. Between these positive and negative values there exists a root, which can then be identified more accurately recursively, halving the interval every time, in order to arrive at the required resolution.

The philosophy behind one of the approaches proposed by Kang and Fransen was to calculate the power spectra of $C(z)$ and $D(z)$ in order to be able to locate the frequencies at which these polynomials had local minima. Their alternative proposal was to exploit in Equations (4.17) and (4.18) that when the phase $\phi(\omega)$ of the ratio filter $R(z)$ of Equation (4.18) is a multiple of 2π, we have $Q^{(P+1)}(z) = 0$, since $|R(z)| = 1$. Alternatively, when $\phi(\omega)$ is an odd multiple of π, $P^{(p+1)}(z) = 0$. Hence, the LSFs can be determined by evaluating the phase spectrum $\phi(\omega)$ of the ratio filter $R(z)$ in Equation (4.19). A deficiency of the above procedures is that they rely on various trigonometric functions of the LSFs, which is an impediment in real-time codecs, since these functions must be pre-stored and hence require memory. Kabal and Ramachandran [119] suggested an approach, which is based on expressing $C(z)$ and $D(z)$ in Equations (4.24) and (4.25) in terms of Chebyshev polynomials, which remedies these ills.

4.2.3 Chebyshev Description of Line Spectral Frequencies

Upon introducing the cosinusoidal frequency transformation of $x = \cos\omega$, for the LSFs Kabal and Ramachandran [119] noted that Equations (4.24) and (4.25) can be reformulated in terms of the so-called *Chebyshev polynomials*, which constitute a set of functions that can be generated recursively from lower-order members of the family. This will have implementational advantages. In general, an nth order Chebyshev polynomial is defined by

$$T_n(x) = \cos[n \cdot \arccos x] \quad (4.26)$$

and the recursion generating successive members of the family can be derived by substituting our frequency transformation of $x = \cos\omega$ into Equation (4.26), which yields [122]

$$T_n(x) = \cos n\omega. \quad (4.27)$$

Upon formally extending this to $(n-1)$ and $(n+1)$, we arrive at

$$T_{(n+1)}(x) = \cos(n+1)\omega = \cos n\omega \cos\omega - \sin n\omega \sin\omega \tag{4.28a}$$

$$T_{(n-1)}(x) = \cos(n-1)\omega = \cos n\omega \cos\omega + \sin n\omega \sin\omega. \tag{4.28b}$$

When adding Equations (4.28a) and (4.28b) and using Equation (4.27), we have $T_{(n+1)}(x) + T_{(n-1)}(x) = 2\cos n\omega \cos\omega = 2xT_n(x)$, yielding the required recursion as

$$T_{(n+1)}(x) = 2xT_n(x) - T_{(n-1)}(x). \tag{4.29}$$

From Equation (4.26), for $n = 0$ we have

$$T_0(x) = 1 \tag{4.30}$$

$$T_1(x) = x \tag{4.31}$$

and from Equation (4.29),

$$T_2(x) = 2x^2 - 1 \tag{4.32}$$

$$T_3(x) = 4x^3 - 3x \tag{4.33}$$

$$T_4(x) = 8x^4 - 8x^2 + 1, \quad \text{etc.} \tag{4.34}$$

Upon substituting the corresponding Chebyshev polynomials into Equation (4.24) and (4.25) and neglecting the multiplicative linear-phase term $e^{j(p/2)\omega}$, we arrive at [119]

$$C'(x) = 2T_{p/2}(x) + 2c_1T_{p/2-1}(x) + \cdots + 2c_{p/2-1}T_1(x) + c_{p/2} \tag{4.35a}$$

$$D'(x) = 2T_{p/2}(x) + 2d_1T_{p/2-1}(x) + \cdots + 2d_{p/2-1}T_1(x) + d_{p/2}. \tag{4.35b}$$

In order to determine the LSFs from Equations (4.35a) and (4.35b), first the roots $x_i = \cos\omega_1$ of $C'(x)$ and $D'(x)$ must be computed, which are then converted to LSFs using $\omega_i = \arccos x_i$. While ω sweeps the range $0, \ldots, \pi$ along the positive half of the unit circle, $x = \cos\omega$ takes on values in the range of $[-1, +1]$, implying that for the roots x_i we have $-1 \leq x_i \leq +1$. At $\omega_i = 0$ we have $x_i = 1$ and the mapping $x = \cos\omega$ ensures that the lowest LSF ω_i is associated with the root x_i closest to unity.

Therefore Kabal and Ramachandran proposed the following numerical solution for finding the LSF values ω_i at which $C'(x)$ and $D'(x)$ become zero. The principle applied is to a certain extent similar to that suggested by Soong and Juang [117], whereby the intervals in which the sign of the function changes are deemed to contain a single zero. The search is initiated from $x = 1$, since as argued in the previous paragraph, $C'(x)$ has the root closest to unity. Once the region of sign change is located, the corresponding zero-crossing or change of polarity is identified more accurately by recursively halving the interval.

An attractive property of the Chebyshev polynomials is that rather than evaluating all independent terms of Equations (4.24) and (4.25) for a high number of abscissa values using, for example, a cosine table, the recursion of Equation (4.29) can be invoked. Hence, during the evaluation of the equivalent set of Equations (4.35a) and (4.35b) only two lower-order Chebyshev polynomials have to be remembered, as suggested by Equation (4.29).

Upon exploiting the so-called *ordering property of the LSFs* [117], which states that $f_0 < f_1 < f_2 < f_3, \ldots, f_p < f_{p+1}$, the search then proceeds to trace the first root of $D'(x)$, commencing from the previously located $C'(x)$ root. This procedure is continued, interchanging the functions $C'(x)$ and $D'(x)$, until all LSFs $f_i,\ i = 1, \ldots, p$, are found. Since $f_0 = 0$ and $f_{p+1} = 0.5$, they are known *a priori* and hence never transmitted.

The convergence speed of the above procedure is strongly dependent on the choice of the initial evaluation interval δ_1, which has to be sufficiently short in order to avoid that more than one root is contained in an interval over which the polarity of $C'(z)$ and $D'(z)$ changes. Kabal and Ramachandran [119] suggested that $\delta_1 = 0.02$ is an adequate value to use, which implies a resolution of 100 intervals for $-1 \leq x_i \leq +1$.

The refined root search invoking interval halving required typically an accuracy of $\delta = 0.0015$, demanding four consecutive interval halving steps. When converting these x-domain root-location ambiguities to ω-domain, the LSF inaccuracy becomes nonlinearly frequency-dependent due to the $\omega_i = \arccos x_i$ conversion. However, several authors, e.g. [118], reported that an LSF resolution ambiguity of 10 Hz does not cause any perceptual speech degradation.

In summary of our discourse on LSFs, we note that the odd-symmetric $P^{(p+1)}(z)$ and symmetric $Q^{(p+1)}(z)$ polynomials were defined by Equations (4.6) and (4.7) as the sum and difference polynomials, respectively. They led to the definition of LSFs through Equations (4.15) and (4.16). Assuming that the decoder is informed of the quantised LSFs, Equation (4.8) can be used to reconstruct the all-zero analysis filter $A(z)$. Section 4.2.2 was dedicated to highlighting procedures for the derivation of explicit formulae for the computation of LSFs, while Section 4.2.3 introduced a simple numerical technique for their computation, using a recursive formula for the efficient updating of the associated Chebyshev polynomial coefficients.

In conclusion, the basic properties of LSFs are summarised as follows.

1. The roots of $P(z)$ and $Q(z)$, which are constituted by the LSFs $\omega_i,\ i = 1, \ldots, p$, obey the ordering property on the unit circle.

2. The stability of the all-pole synthesis filter $H(z) = 1/A(z)$ is retained upon quantising the roots of $P(z)$ and $Q(z)$, as long as the ordering property is not violated.

3. The ordering property can also be invoked in order to detect and mitigate the effect of transmission errors in the LSP parameters by re-establishing their right ordering, when transmission errors were inflicted.

4. Experience shows that a concentration of LSFs in a frequency region implies the presence of a spectral peak [123–125].

5. The LSFs evolve smoothly over consecutive frames, as seen in Figure 4.8, which stimulated research in order to further reduce the associated bitrate by exploiting this redundancy using predictive- or vector-quantisation techniques.

Figure 4.6 portrays the PDFs of the LSFs for a 10th-order spectral shaping filter, while the relative frequency histogram of a 35-bit Lloyd–Max quantisation scheme is shown in Figure 4.7. Observe that the first three and last two LSFs were quantised using a 3-bit or eight-level Lloyd–Max quantiser, while the other LSFs employed 4-bit or 16-level Lloyd–Max quantisation. Accordingly, the latter schemes have a finer resolution or a more dense

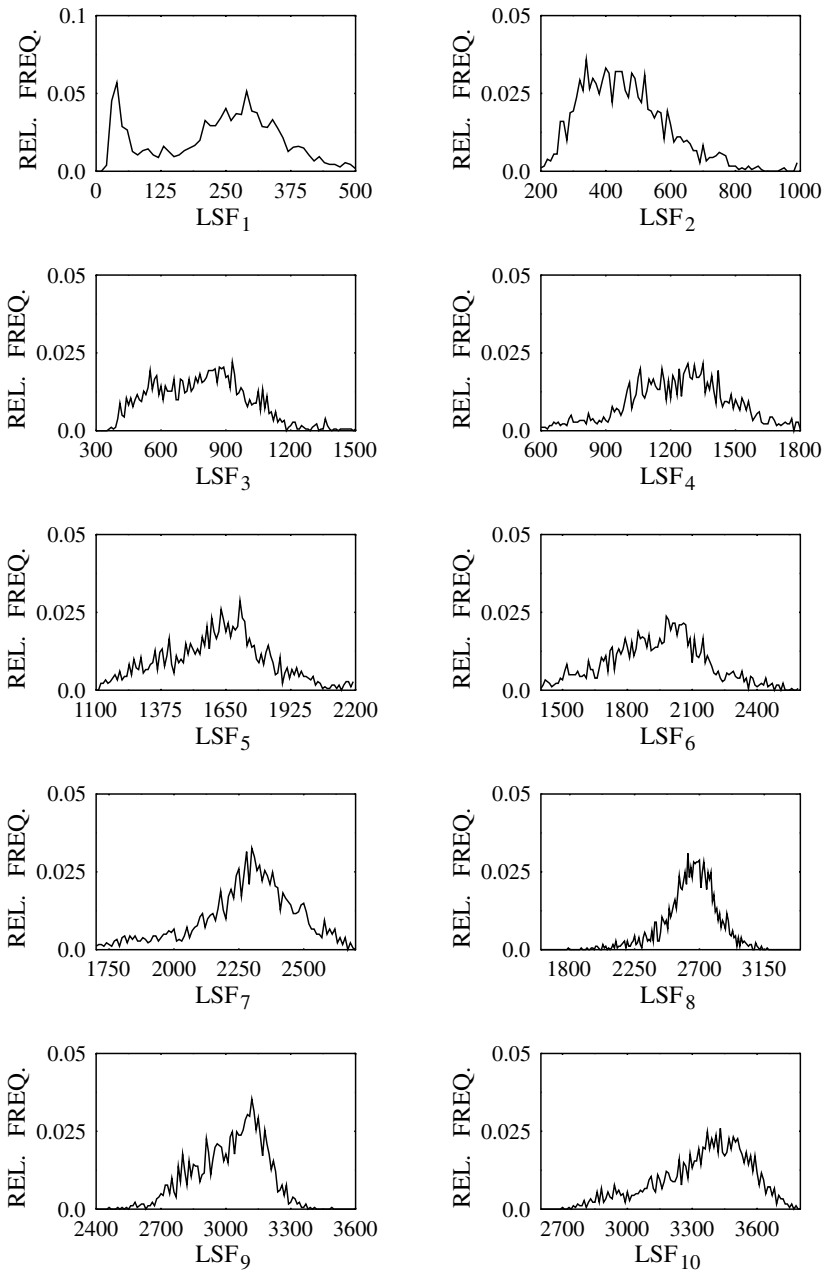

Figure 4.6: Relative frequency plots of the LSF filter coefficients $\mathrm{LSF}_i,\ i = 1, \ldots, 10$, for a typical mixed-gender speech segment.

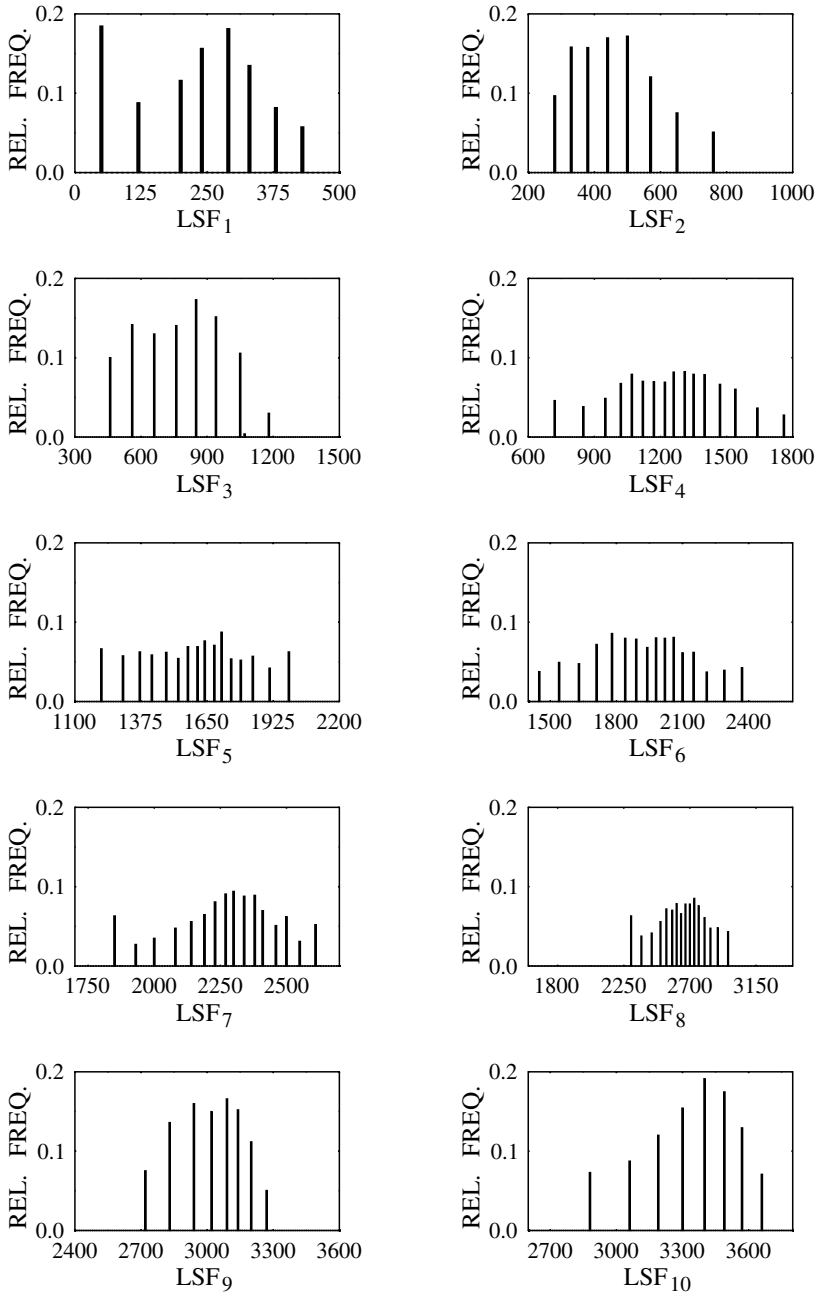

Figure 4.7: Relative frequency plots of the Lloyd–Max quantised LSF filter coefficients LSF_i, $i = 1, \ldots, 10$, for a typical mixed-gender speech segment.

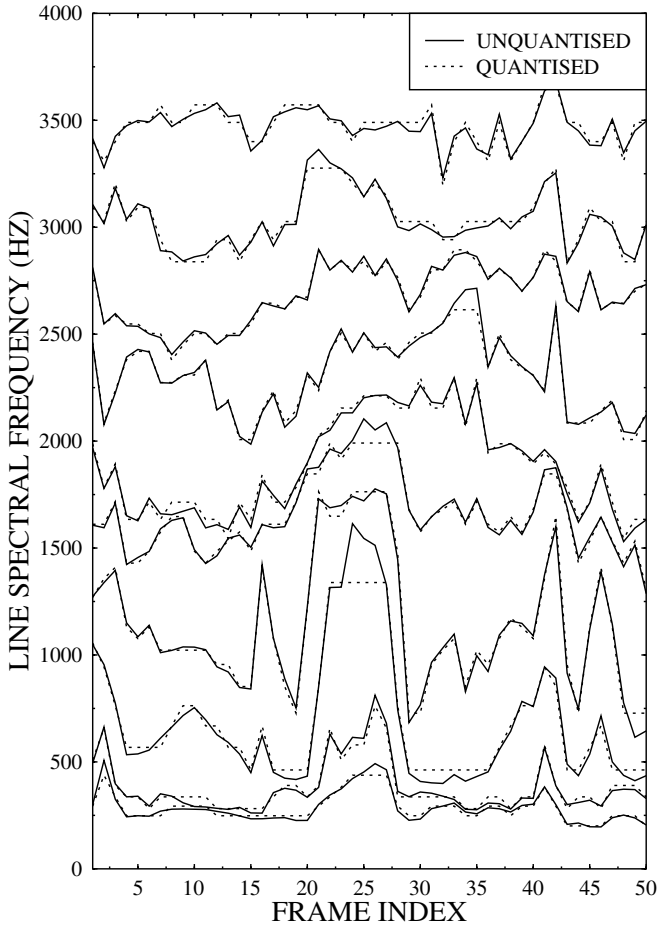

Figure 4.8: Evolution of the LSF filter coefficients $\mathrm{LSF}_i,\ i = 1, \ldots, 10$, for a typical 100 ms speech segment using the scalar quantiser of Figure 4.7.

spacing. Furthermore, in the regions of higher relative frequency the Lloyd–Max quantiser allocated the reconstruction levels more closely than in the lower-probability intervals. In Figure 4.8 we portrayed a typical segment of the evolution of consecutive LSFs for 50 speech frames of 20 ms duration, which corresponds to 1 s of speech. Observe that the LSF profiles never cross and this so-called ordering property is often exploited in error-resilient codecs in order to detect and mitigate the effects of transmission errors, which may have violated this condition. Observe, furthermore, that the quantised profiles closely follow the pattern of the ideal unquantised functions. Finally, in order to motivate the next section, we observe in Figure 4.8 that the LSFs at any instant can be viewed as components of a ten-dimensional LSF vector. A specific feature of the consecutive LSF vectors derived for each consecutive 20 ms speech segment is that their corresponding components are similar to each other. The physical explanation of this observation is that the human vocal apparatus does not change

its time- and frequency-domain characteristics abruptly. Hence the spectral envelope of the consecutive 20 ms speech segments is similar, which can be exploited by quantising the LSF vectors with the aid of vector quantisers, as will be outlined in the next section.

4.3 Vector Quantisation of Spectral Parameters

4.3.1 Background

Vector quantisation of various source signals has grown in popularity over the years and a vast body of research has been incorporated in a range of excellent review papers, e.g. by Makhoul, Roucos and Gish [91] and in a monograph by Gersho and Gray [126]. For speech coding with bitrates around 10–16 kbps, the LAR or the LSF are usually quantised with 30–40 bits per 20 ms LPC update frame. Below 5 kbps encoding rates either the LPC update frame has to be extended to around 30 ms, or vector quantisation of the LPC parameters with at most 25 bits per 20 ms speech frame has to be employed. Conventional vector quantisers (VQ) [91] use trained codebooks, which usually lack robustness over speakers outside the training sequence. Shoham [127] attempted to exploit the similarities among successive spectral envelopes by employing vector predictive coding, where trained codebooks are needed for the predictor and residual vectors. A range of various LPC parameter quantisers have been proposed by Paliwal and Atal [116], Shoham [127], Lee *et al.* [128], Yong *et al.* [133], Ramachandran *et al.* [129] and Xydeas and So [130].

A specific low-complexity speaker-adaptive LSF VQ scheme proposed by Lee *et al.* [128] will be highlighted in the next section which is followed by a discussion on a high-complexity vector quantiser arrangement using two consecutive random, stochastic codebooks [131,132].

4.3.2 Speaker-adaptive Vector Quantisation of LSFs

According to the scheme portrayed in Figure 4.9 proposed by Lee *et al.* [128] the inter-frame redundancy, which is inherent in consecutive LSF vectors, as evidenced by Figure 4.8, is exploited in order to reduce the number of bits required by scalar quantisation. As seen in Figure 4.9, each LSF vector is modelled by a codebook, CB1, containing the previously quantised vectors and hence the authors refer to this scheme as a *speaker adaptive vector quantiser* (SAVQ).

Due to the high interframe correlation of the LSFs this predictive process provides a good estimate of the current frame's LSF vector and hence the residual error of $E_i > S_i^{K_i}$ from this first stage becomes rather unpredictable. This random prediction error can be quantised using a random Gaussian codebook, namely CB2. Specifically, the unquantised LSF vector $S_i,\ i = 1, \ldots, p$, is represented by that particular quantised LSF vector $\hat{V}_i,\ i = 1, \ldots, p$, from CB1, which minimises the squared and component-wise accumulated error of

$$ER = \sum_{i=1}^{p} [S_i - \hat{V}_i]^2. \tag{4.36}$$

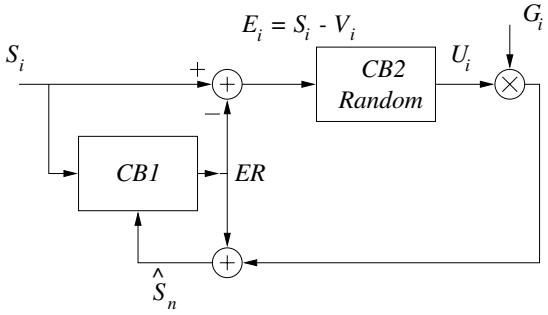

Figure 4.9: LSF vector quantiser schematic.

Then the prediction-error vector $E_i = S_i - \hat{V}_i,\ i = 1, \ldots, p$, is quantised with the help of CB2 by minimising the quantisation error term of

$$e = \sum_{i=1}^{p} [G \cdot U_i - E_i]^2. \tag{4.37}$$

Observe in Figure 4.9 that the codebook gain factor G allows the process to match the power of the codebook entries to that of the LSF prediction residual error. The optimum gain is computed for each entry. In order to find an expression for the gain factor we set $\partial e / \partial G = 0$, yielding

$$\sum_{i=1}^{p} 2[G \cdot U_i - E_i] \cdot U_i = 0, \tag{4.38}$$

which gives

$$G_i = \frac{\sum_{i=1}^{p} [E_i \cdot U_i]}{\sum_{i=1}^{p} [U_i]^2}. \tag{4.39}$$

Observe that this is physically the normalised cross-correlation of the input and output of CB_2, hence a high gain factor is assigned, if E_i and U_i are similar. The effect of using the gain G_i is equivalent to extending the size of the codebook, without increasing the pattern-matching complexity. The codebook indices for CB1 and CB2 along with the quantised gain factor are transmitted to the decoder and the encoder also uses the quantised gain in its pattern matching process. It is essential for the operation of this scheme that the ordering property is always checked, before an encoded vector is accepted. Notice in Figure 4.9 that the two codebooks' outputs are superimposed in order to produce the quantised LSF vector, which is then written in CB1 for future use. This scheme has a low complexity, but it has a deficiency in terms of propagating channel errors.

Let us now embark on considering a more complex VQ scheme, which uses stochastic codebook entries and hence requires no training. This has the advantage of exhibiting a similar performance, irrespective of the speaker's gender, mother tongue, etc. This VQ scheme transforms the original stochastic codebook entries in vectors exhibiting similar statistical properties to the original LSFs to be encoded, as will be discussed in the next section.

4.3.3 Stochastic VQ of LPC Parameters

In this section an academically interesting stochastic VQ scheme is presented for the advanced reader, noting that the practically motivated reader may skip this section and proceed to consider a range of more moderate-complexity LSF quantisers in Section 4.3.4.

4.3.3.1 Background

In reference [133] a switched-adaptive method was suggested by Yong *et al*. which exploits the correlation between adjacent LSF vectors in a different fashion. In this section we will assume that the reader is familiar with the statistical properties of stochastic processes and the so-called Karhunen–Loeve transform [69] and propose a stochastic VQ method based on an approach published by Atal [131]. In the original approach, the covariance matrix of the LARs was computed from a buffer containing the previously quantised LAR vectors. Then the covariance matrix of the LARs was decomposed into its eigenvectors and eigenvalues [75], following a procedure which is not detailed here. This decomposition was carried out for every new LPC update frame, which is a computationally rather demanding task. Furthermore, the eigenvalue solution requires an iterative algorithm, for example the so-called QR algorithm [75], which makes the processing time data dependent. This is undesirable in real-time applications.

According to the approach proposed by Salami *et al.* [132], an LPC parameter vector, such as the vector of 10 LAR or LSF parameters of an LPC update frame, which possess certain correlation properties, can be quantised using an uncorrelated Gaussian or stochastic codebook by transforming the uncorrelated codebook entries into vectors having correlations similar to those of the LPC parameter vectors. This technique is attractive, since the employment of random or stochastic codebooks ensures speaker independent performance, which is often a deficiency associated with trained codebooks that may not be robust to speakers outside the training set. In general a vector $\mathbf{x}$ of dimension N having jointly correlated components can be transformed into a vector $\mathbf{u}$ exhibiting uncorrelated components using a so-called *orthogonal rotation* with the help of an $N \times N$ matrix $\mathbf{A}$ according to

$$\mathbf{u} = \mathbf{A}\mathbf{x}. \tag{4.40}$$

Such orthogonal rotations have been extensively used in source coding in order to remove redundancy from the source signal [69]. The effect of orthogonal rotations can be easily made plausible by referring to the *Wiener–Khintchin theorem*, which states that the ACF and PSD are Fourier transform pairs. A manifestation of this is that the Dirac-delta ACF of AWGN is associated with an infinite bandwidth flat PSD. For example, when correlation is introduced in the uncorrelated AWGN signal by limiting the maximum rate of change at which the source signal can fluctuate using low-pass filtering, the band-limited AWGN has a sinc-function shaped ACF, exhibiting low correlation. In general, the more correlated the signal, the narrower the spectrum. This has been exploited, for example, in the context of *discrete cosine transformation* (DCT) [69] based coding of speech and video signals, since after discrete cosine transforming the correlated source signal to the frequency domain, typically only a small fraction of the signal's spectral coefficients has to be encoded, namely those that exhibit a high magnitude. By contrast, the remaining low-energy spectral coefficients are neglected without significant loss of energy.

For a correlated source vector $\mathbf{x}$, which is, for example, in our case the vector of 10 LSFs, it was shown that the best decorrelating rotation $\mathbf{A}$ is given by a matrix, whose rows are the normalised eigenvectors of $\mathbf{\Gamma_x}$, the covariance matrix of $\mathbf{x}$ [134]. This transformation is usually referred to as the *Karhunen–Loeve transform* (KLT) [69], and it can be applied to some extent also to non-Gaussian sources [91]. The impediment of the KLT is its high computational complexity, which is due to the fact that the optimum decorrelating rotation matrix $\mathbf{A}$ is dependent on the source signal's correlation properties expressed in terms of $\mathbf{\Gamma_x}$. It can be shown [69] that other time- and data-invariant orthogonal transforms, such as the DCT, have similar decorrelating or energy-compaction properties, while ensuring lower system complexity.

In what follows we will describe an inverse approach. Specifically, instead of decorrelating the correlated source vectors in order to achieve better compression, here we will use uncorrelated stochastic codebook vectors and impose the required correlation properties in order to be able to model the LPC spectral components adequately.

In general, the covariance matrix $\mathbf{\Gamma_x}$ of a source $\mathbf{x}$ is often used to characterise the source's statistical properties, which can be computed as

$$\mathbf{\Gamma_x} = E[(\mathbf{x} - \bar{\mathbf{x}})(\mathbf{x} - \bar{\mathbf{x}})^{\mathrm{T}}], \tag{4.41}$$

where $E(\bullet)$ denotes the expected value of $\bullet$, the mean value of $\mathbf{x}$ is given by $\bar{\mathbf{x}} = E(\mathbf{x})$ and the superscript T represents matrix transposition.

Before proceeding, we briefly introduce the concept of the previously mentioned *eigenvectors* and *eigenvalues* [69]. The eigenvalues γ_k of the matrix $\mathbf{\Gamma_x}$ are defined as the roots of

$$|\mathbf{\Gamma_x} - \gamma_k \mathbf{I}| = 0, \tag{4.42}$$

where $\mathbf{I}$ represents the identity matrix having unity diagonal elements, while all other elements are zero. The eigenvectors $\phi_{\mathbf{k}}$ are defined by all the solutions of

$$\mathbf{\Gamma_x}\phi_{\mathbf{k}} = \gamma_k \phi_{\mathbf{k}}. \tag{4.43}$$

4.3.3.2 The Stochastic VQ Algorithm

With the above preliminaries we now proceed to describe Atal's stochastic VQ algorithm. The covariance matrix $\mathbf{\Gamma_x}$ of the source vector $\mathbf{x}$ can be decomposed into three matrices according to [75] as follows:

$$\mathbf{\Gamma_x} = \mathbf{S} \cdot \boldsymbol{\lambda} \cdot \mathbf{S}^{\mathrm{T}}, \tag{4.44}$$

where $\mathbf{S}$ is a matrix whose columns are the normalised eigenvectors of $\mathbf{\Gamma_x}$ and $\boldsymbol{\lambda}$ is a diagonal matrix whose elements are the eigenvalues of $\mathbf{\Gamma_x}$. Equation (4.44) can also be written as

$$\boldsymbol{\lambda} = \mathbf{S}^{\mathrm{T}} \cdot \Gamma_x \cdot \mathbf{S}. \tag{4.45}$$

Therefore, the rotated vector $\mathbf{u}$ in Equation (4.40) is given by

$$\mathbf{u} = \mathbf{S}^{\mathrm{T}}\mathbf{x}. \tag{4.46}$$

Upon exploiting Equation (4.45) the covariance matrix $\mathbf{\Gamma_u}$ of $\mathbf{u}$ can be formulated as

$$\begin{aligned}\mathbf{\Gamma_u} &= E[(\mathbf{u}-\bar{\mathbf{u}})(\mathbf{u}-\bar{\mathbf{u}})^{\mathrm{T}}] \\ &= \mathbf{S}^{\mathrm{T}} \cdot \mathbf{\Gamma_x} \cdot \mathbf{S} = \boldsymbol{\lambda},\end{aligned} \tag{4.47}$$

which is the diagonal matrix $\boldsymbol{\lambda}$, implying that $\mathbf{u}$ has uncorrelated components. The variances of the components of the uncorrelated vector $\mathbf{u}$ are the eigenvalues of $\mathbf{\Gamma_x}$, and their means are given by

$$\bar{\mathbf{u}} = \mathbf{S}^{\mathrm{T}}\bar{\mathbf{x}}. \tag{4.48}$$

In order to turn the uncorrelated vector $\mathbf{u}$ into a vector having unity covariance matrix and zero mean, its mean value $\bar{\mathbf{x}}$ is subtracted from it, then the decorrelating transformation using $\mathbf{S}^{\mathrm{T}}$ is carried out and lastly this quantity is normalised by $\boldsymbol{\lambda}^{-1/2}$ according to

$$\mathbf{u} = \boldsymbol{\lambda}^{-1/2}\mathbf{S}^{\mathrm{T}}(\mathbf{x}-\bar{\mathbf{x}}). \tag{4.49}$$

Hence, upon exploiting Equation (4.45) again we have

$$\begin{aligned}\mathbf{\Gamma_u} &= E[(\mathbf{u}-\bar{\mathbf{u}})(\mathbf{u}-\bar{\mathbf{u}})^{\mathrm{T}}] \\ &= E[\boldsymbol{\lambda}^{-1/2}\mathbf{S}^{\mathrm{T}}(\mathbf{x}-\bar{\mathbf{x}})\boldsymbol{\lambda}^{-1/2}\mathbf{S}^{\mathrm{T}}(\mathbf{x}-\bar{\mathbf{x}})^{\mathrm{T}}] \\ &= \boldsymbol{\lambda}^{-1/2}\mathbf{S}^{\mathrm{T}}\mathbf{\Gamma_x}\boldsymbol{\lambda}^{-1/2}\mathbf{S}^{\mathrm{T}} \\ &= \boldsymbol{\lambda}^{-1/2}\boldsymbol{\lambda}\boldsymbol{\lambda}^{-1/2} = \mathbf{I},\end{aligned} \tag{4.50}$$

which explicitly states that the process $\mathbf{u}$ is uncorrelated, since its covariance matrix is the identity matrix.

Now the stochastic vector quantisation method accrues from rearranging Equation (4.49). Specifically, the LPC parameter vector $\mathbf{x}$ is quantised using the uncorrelated vectors $\mathbf{u}^{(k)},\ k=1,\ldots,K$, chosen from a codebook, – which contains K number of zero mean, unity variance Gaussian entries – through the following transformation:

$$\hat{\mathbf{x}} = \bar{\mathbf{x}} + \beta\mathbf{S}\boldsymbol{\lambda}^{1/2}\mathbf{u}^{(k)}. \tag{4.51}$$

Equation (4.51) above is derived directly from Equation (4.49) with the scalar β introduced in order to allow more flexibility in terms of matching the powers of $\mathbf{x}$ and $\hat{\mathbf{x}}$. The MSE between the original and quantised vectors $\mathbf{x}$ and $\hat{\mathbf{x}}$ is given by

$$\begin{aligned}E_x &= (\mathbf{x}-\hat{\mathbf{x}})^{\mathrm{T}}(\mathbf{x}-\hat{\mathbf{x}}) \\ &= \parallel (\mathbf{x}-\hat{\mathbf{x}})^{\mathrm{T}} \parallel^2 \\ &= \parallel \mathbf{y} - \beta\boldsymbol{\lambda}^{1/2}\mathbf{u}^{(k)} \parallel^2,\end{aligned} \tag{4.52}$$

where $\parallel \bullet \parallel$ denotes the Euclidean norm of $\bullet$ and

$$\mathbf{y} = \mathbf{S}^{\mathrm{T}}(\mathbf{x}-\bar{\mathbf{x}}). \tag{4.53}$$

The optimum codebook gain β is computed by setting $\partial E_x/\partial\beta = 0$. The codebook of K Gaussian vectors $\mathbf{u}^{(k)},\ k=1,\ldots,K$, is exhaustively searched for the index k, which

minimises the error in Equation (4.52), and the quantised vector is then computed from Equation (4.51). The long-term covariance matrix $\mathbf{\Gamma_x}$ is precomputed from a large data base of LPC vectors. Hence, the decomposition specified in Equation (4.44) is precomputed saving the effort of decomposing the covariance matrix for every new LPC analysis frame. In fact, no improvement was achieved when we attempted to update the covariance matrix for every LPC analysis frame.

The quality of VQ schemes is typically evaluated in terms of the so-called spectral deviation (SD) metric, which is defined as [86]

$$\begin{aligned} \mathrm{SD} &= \frac{1}{2\pi}\int_{-\pi}^{\pi}\left(10\log|H(\omega)|^2 - 10\log|\hat{H}(\omega)|^2\right)^2 \,\mathrm{d}\omega \quad [\mathrm{dB}]^2 \\ &= \frac{1}{2\pi}\int_{-\pi}^{\pi}\left(10\log\frac{\left|\hat{A}(\omega)\right|^2}{|A(\omega)|^2}\right)^2 \,\mathrm{d}\omega \quad [\mathrm{dB}]^2, \end{aligned} \tag{4.54}$$

and $\hat{H}(z)$ and $\hat{A}(z)$ are the quantised synthesis and analysis filters, respectively. The SD is typically computed for each LPC update frame of 20–30 ms and averaged over a number of speech frames in terms of dB. Although SD = 1 dB is considered as the spectral distortion limen for perceptually transparent coding of the LPC parameters [115], it is also very important to consider its distribution evaluated in terms of its PDF, since the probability of extreme outliers associated with SD values in excess of 2 dB must be very low [116].

Low average spectral deviation values were achieved, when this method was used to quantise the LAR parameters with the aid of 25 bits per LPC update frame. A two-stage VQ approach was adopted in order to reduce the complexity of the error minimisation procedure. Exploiting the high correlation between the LSFs in adjacent frames, the method has given better results when the vector $\mathbf{x}$ to be quantised was the difference between the present LSF vector and the previously quantised one. In order to reduce the search complexity from 2^B comparisons, where B is the total number of codebook address bits, a computationally more attractive two-stage approach was employed. Specifically, two codebooks associated with two gain factors were employed, as we have seen in Section 4.3.2 for the SAVQ scheme. For example, when using $B = 20$ bits, initially the first 256-entry codebook was searched in order to find the best entry and its size was, virtually, expanded by a factor of four using a 2-bit quantised gain factor, which was computed similar to Equation (4.39). Then the error of this first matching process was further encoded using the second 256-entry codebook and 2-bit quantised gain. In a first approximation this process reduced the search-complexity from an unacceptable 2^{20} comparisons to around 2×2^8.

The performance of this VQ scheme can be further improved by employing a *switched-adaptive vector quantisation* approach according to the scheme suggested by Yong *et al.* [133], where a number of fixed covariance matrices are used for different classes of speech. The performance of this approach was characterised by Salami *et al.* in [135].

We now proceed to consider two recently suggested VQ schemes [116, 129], which have a moderate implementational complexity and apart from minimising the average SD they also limit the probability of high peak SD values [136].

4.3.4 Robust Vector Quantisation Schemes for LSFs

Paliwal and Atal [116] have proposed a moderate complexity 24-bit vector quantisation arrangement for the LSFs. They noted that the individual LSFs have a localised effect in terms of spectral distortion in the spectral domain, which facilitates splitting the 10-component LSF vector into shorter vectors, while limiting the spectral distortion spillage from one region to another. They also defined an LSF-based spectral distortion measure and on the basis of the limited distortion spillage to other frequency domains the most important LSFs were allocated a higher weight during the quantisation process and *vice versa*. In contrast, LARs have a rather wide-spread effect in the frequency domain.

Specifically, the weighted Euclidean distance measure $d(\mathbf{f}, \hat{\mathbf{f}})$ between the original and quantised LSF vectors was defined as [116]

$$d(\mathbf{f}, \hat{\mathbf{f}}) = \sum_{i=1}^{10} [c_i w_i (\mathbf{f} - \hat{\mathbf{f}})]^2, \tag{4.55}$$

where the weighting factor $w_i,\ i = 1, \ldots, 10$, is assigned to the ith component of the LSF vector, which is defined as

$$w_i = [|H(f_i)|^2]^r. \tag{4.56}$$

Specifically, in Equation (4.56) $|H(f_i)|^2$ represents the LPC power spectrum at frequency f_i and the experimentally optimised constant r, allowing Paliwal and Atal to attribute different weights to different LSFs, was 0.15. Lastly, the additional weighting factor c_i was 1.0 for $i = 1, \ldots, 8$, while a choice of $c_9 = 0.8$ and $c_{10} = 0.4$ allowed the measure to de-emphasise high-frequency LSFs.

It is plausible that the VQ complexity is reduced at a concomitant lower performance, if the original 10-component LSF vector is split into smaller vectors and Paliwal and Atal found that a good compromise was to employ a two-way split. An extreme case would be to use 10-way splitting, which is equivalent to scalar quantisation. Hence, assuming a total of 24 bits, two 12-bit VQ schemes were employed. There are three basic requirements, which must be satisfied in order to achieve transparent LSF quantisation: (1) the average SD is lower than 1 dB; (2) there are no frames having a SD above 4 dB; and (3) the probability of SD values between 2 and 4 dB is below 2%. Experimental results showed that best overall SD performance in terms of the above three criteria was guaranteed, when 5 LSFs were quantised by both 12-bit or 4096-entry codebooks. The LSFs' ordering property can be satisfied by ensuring that only those vectors of the second segment of the codebook are invoked, for which the lowest quantised LSF value within the vector, namely LSF_6, is higher than the quantised value of the highest frequency component, namely that of LSF_5, of the first VQ segment. The proposed quantisation scheme was shown to have an impressive robustness against channel errors, which was shown to be similar to that of scalar arrangements.

In a further attempt to improve the overall LSF quantiser design Ramachandran *et al.* [129] have proposed a hybrid scheme, which employs a combination of vector and scalar quantisation. The design constraints and objectives were similar to those in Atal's former work reported above, but the weighting factor of Equation (4.56) was modified according to [137]:

$$w_i = \frac{1}{f_i - f_{i-1}} + \frac{1}{f_{i+1} - f_i}, \tag{4.57}$$

which attributed higher weights to frequency regions where the LSFs were grouped closer, indicating a dominant spectral peak. The proposed scheme is memoryless, which improves its robustness against channel errors. Further important design constraints were to reduce the complexity and memory requirements.

The proposed arrangement quantised the differences between consecutive LSFs of the same frame, rather than the LSFs themselves [117], since these differences have a lower dynamic range than the LSFs. Initially an independent vector and a scalar quantiser was designed, both using 29 bits. The authors' conclusion was that the best performance was achieved when each set of 10 LSFs was both scalar and vector quantised and the specific scheme minimising the distortion measure was actually used. A further one-bit flag was then allocated to indicate which scheme was used. A three-way split VQ scheme using $(3, 3, 4)$ LSF vectors was designed using $(10, 9, 10)$ bits, respectively. The associated scalar quantiser employed $(3, 3, 3, 3, 3, 3, 3, 3, 3, 2)$ bits for the individual LSFs.

The benefits of using this combined scheme were interpreted by analysing the quantised vectors. Namely, the two schemes complement each other in that the VQ caters for those LSF sets where some components are clipped by the scalar arrangement. In contrast, the scalar quantiser can encode the sparse regions of the VQ more efficiently. Lastly, the coding performance can be further improved by employing a codebook adaptation procedure. Specifically, it can be intelligently exploited that due to the LSFs' ordering property, a subset of the second codebook whose lowest LSF component is lower than the highest one of the first 3-component subvector becomes illegitimate. This fact can be capitalised upon. Namely, rather than restricting the search to that area, the entire codebook can be remapped to the legitimate frequency region, thereby providing a finer quantiser resolution. Specific algorithmic details of this procedure are beyond the scope of our treatment here, the interested reader is referred to [129] for a full description of the associated dynamic programming technique employed.

4.3.5 LSF VQs in Standard Codecs

In recent years a range of sophisticated, error-resilient, high-quality, low-rate speech codecs emerged, such as, for example, the ITUs 8 kbps G.729 scheme of Section 7.8, the dual-rate G.723.1 scheme of Section 7.12, the 5.6 kbps half-rate GSM codec portrayed in Section 7.7, the enhanced full-rate GSM scheme described in Section 7.10, the 7.4 kbps IS-136 codec arrangement of Section 7.11 or some of the other schemes of Chapter 7. Most of these state-of-the-art codecs employ LSF vector-quantisation techniques, which will be detailed in more depth in Chapter 7, but it is beneficial here to put some of the previously detailed principles into practice. Hence, below we provide a rudimentary introduction to the split LSF VQ of the recently standardised 7.4 kbps enhanced full-rate IS-136 codec approved in the US, which will be the subject of Section 7.11.

The IS-136 scheme requires a bitrate contribution of 26 bits/20 ms for the quantisation of the 10 LSFs. The corresponding LSF VQ scheme is shown in Figure 4.10, which is schematically identical to the 24-bit LSF VQ of the G.723.1 dual-rate codec of Section 7.12. Observe in Figures 7.33 and 4.10 that only the codebook sizes are slightly different, since the 7.4 kbps IS-136 codec allocates 26, rather than 24 bits to LSF quantisation. As was pointed out above, usually split VQ is employed, since it reduces the search complexity although at the cost of some performance degradation. In the IS-136 LSF VQ the first 3 LSFs are

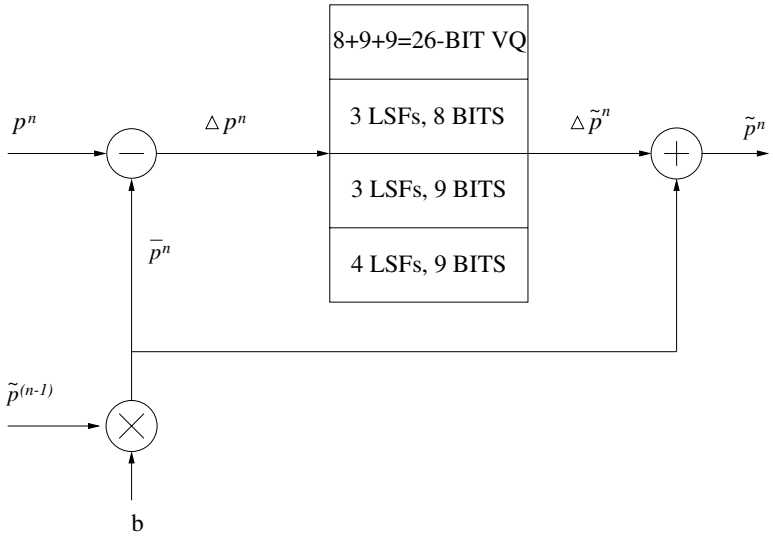

Figure 4.10: The 26-bit IS-136 LSF quantisation schematic.

grouped together and vector-quantised using 8 bits, or 256 entries, while the two other groups of LSF quantisers are constituted by 3 and 4 LSFs, employing 9 and 9 bits, respectively. Observe in Figure 4.10 that the nth unquantised LSF vector p^n is predicted first on the basis of the previous quantised LSF vector $\tilde{p}^{(n-1)}$, after multiplying it with a scaling factor b, which is proportional to the long-term correlation between consecutive LSF vectors. This is often termed as first-order moving-average prediction, since it relies on a simple first-order prediction model. The estimated LSF vector $\bar{p}^n$ is then subtracted from the original unquantised LSF vector in order to generate their difference vector, namely δp^n, which is split into sub-vectors of 3, 3 and 4 LSFs and quantised. Finally, the quantised LSF difference vector $\Delta\tilde{p}^n$ is added to the predicted value $\bar{p}^n$, in order to generate the current quantised LSF vector $\tilde{p}^n$. Again, a range of similar LSF VQ schemes can be found in specific sections of Chapter 7 in the context of other state-of-the-art standard codecs.

4.4 Spectral Quantisers for Wideband Speech Coding[1]

G. Guibé, H.T. How and L. Hanzo

4.4.1 Introduction to Wideband Spectral Quantisation

In wideband speech codecs a high number of spectral coefficients – typically 16 – has to be quantised in order to represent the spectrum up to frequencies of 7 kHz. However, the LSF coefficients above 4 kHz are less amenable to VQ than their low-frequency counterparts.

[1]This section is based on G. Guibé, H.T. How and L. Hanzo © European Transactions on Telecommunications.

Table 4.1: Overview of wideband LPC quantisers.

	Quantisation scheme	No. of bits per frame
Harborg *et al.* [138]	Scalar	60, 70 and 80
Lefebvre *et al.* [139]	Split VQ	49
Paulus and Schitzler [140]	Predictive VQ	44
Chen and Wang [141]	Split VQ	49
Ubale and Gersho [142]	Multi-stage VQ	28
Combescure *et al.* [143]	Multi-stage	33 at 16 kbps
	Split VQ	43 at 24 kbps

Table 4.1 summarises most of the recent approaches to wideband speech spectral quantisation found in the literature. The approach employed by Harborg *et al.* [138] is based on scalar quantisation (SQ). However, the resulting bitrate is excessive, requiring 3 or 4 bits for each LSF. Chen and Wang [141] as well as Lefebvre *et al.* [139] utilised low-dimensional split VQ. For instance, a $(2, 2, 2, 2, 2, 3, 3)_{7777777}$ split VQ is invoked in their approach, where only two- or three-dimensional VQs are used, employing 7 bits – i.e. 128 codebook entries – per sub-vector. This reduces the number of bits allocated to the LSF quantisation compared to SQ, although the resulting number of bits still remains somewhat high, namely $7 \cdot 7 = 49$. Clearly, these approaches are simple, but a large number of bits is required.

Paulus and Schaitzler [140] proposed a coding scheme based on sub-band analysis of the speech signal. The speech signal was split into two unequal sub-bands, namely 0–6 kHz and 6–7 kHz. LPC analysis was only invoked in the lower band, using 14 LSF coefficients quantised with 44 bits per 15 ms. The quantisation scheme employed inter-frame moving-average prediction and split vector quantisation. In the 6–7 kHz higher sub-band only the signal energy was encoded using 12 additional bits. Following a similar approach Combescure *et al.* [143] described a system based on two sub-bands, where the lower band (0–5 kHz) applied a 12th order LP filter with its coefficients quantised using 33 bits. The upper band (5–7 kHz) uses an 8th order LP filter encoded with 10 bits, but these coefficients were only transmitted in the higher bitrate mode of the coder, namely at 24 kbps. The lower-band coefficients were quantised using predictive multi-stage split vector quantisation (MSVQ). These types of LSF quantisers are not directly amenable to employment in fullband wideband speech codecs. However, the approach using separate coding of the higher- and lower-band LSFs can be helpful in general for LPC quantisation.

Finally, Ubale and Gersho [142] proposed a scheme using predictive MSVQ of seven stages employing four bits each. This method employed a so-called multiple survivor method, where four – rather than one – residual survivors were retained at each pattern-matching stage and were then tested at the next pattern-matching stage. The final decision was taken at the last VQ stage as to which of the split vector combinations gave the lowest quantisation error. In addition, the MSVQ was designed by a joint optimisation procedure, clearly demonstrating the advantages of using schemes which predictively exploit the knowledge of the signal's past history, in order to improve the coding efficiency.

Having reviewed the background of wideband speech spectral quantisation, we now focus our attention on the statistical properties of the wideband speech LSFs, which render it attractive for vector quantisation.

4.4.1.1 Statistical Properties of Wideband LSFs

The employment of the LSF [117, 144, 145] representation for quantisation of the LPC parameters is motivated by their statistical properties. Figure 4.11 shows the PDFs of 16 wideband speech LSFs over the interval of 0–8 kHz. Their different PDFs have to be taken into account in the design of the quantisers.

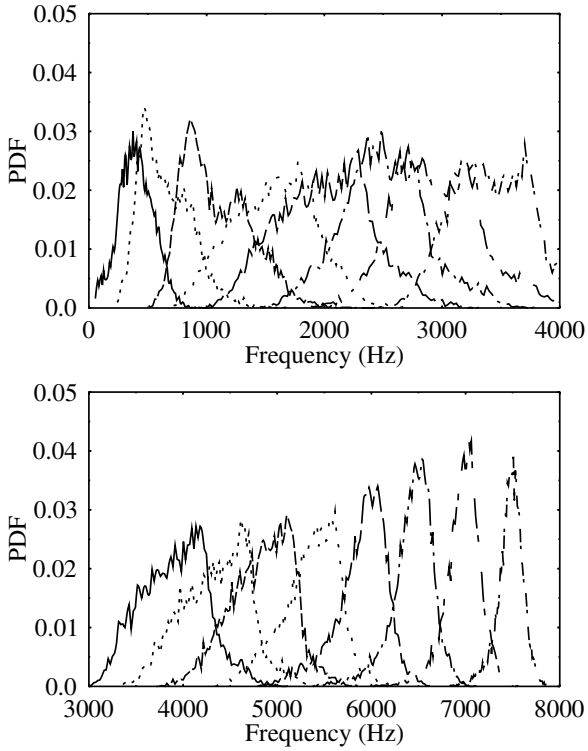

Figure 4.11: PDFs of the LSFs using LPC analysis with a filter order of 16, demonstrating the ordering property of the LSFs.

The essential motivation of vector quantisation is the exploitation of the relationship between the LSFs in both the frequency and the time domain. Figure 4.12 shows the time-domain evolution of the wideband speech LSF traces, demonstrating their strong correlation in consecutive frames in the time domain, which is often referred to as their inter-frame correlation. Similarly, it demonstrates within each speech frame the ordering property of neighbouring LSF values, which is also referred to as intra-frame correlation.

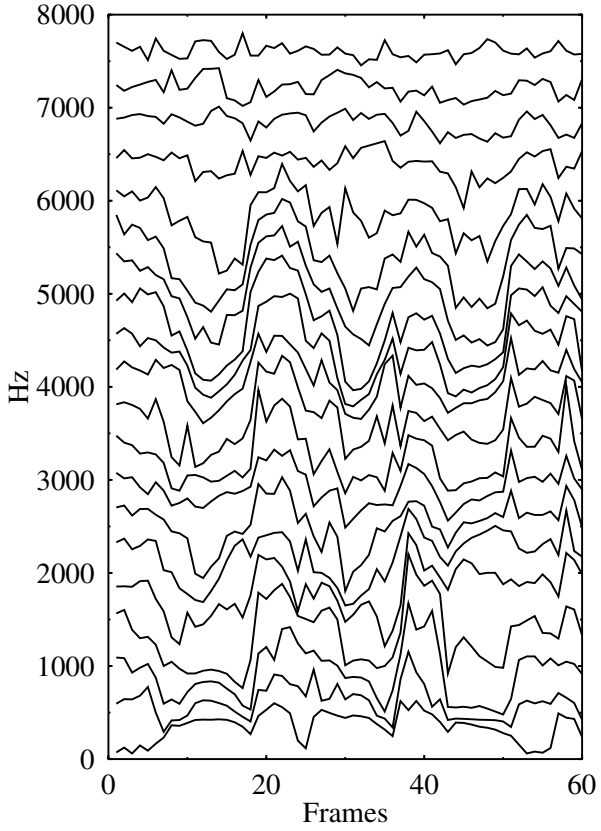

Figure 4.12: Traces of 16 wideband LSFs, demonstrating their inter- and intra-frame correlations.

Intra-frame correlation motivates the employment of vector quantisation, since it enables a mapping that matches the multi-dimensional LSF distribution. We observe at the top of Figure 4.12 that the correlation of the individual LSFs within a given speech frame tends to decrease, as the frequency increases, i.e. higher frequency LSFs are more statistically independent of each other, although they still obey the ordering property. This clearly manifests itself, for example, around frame 18 in Figure 4.12. The highest frequency LSFs describe the noisy high-frequency bands of the speech signal, which typically appear to be noise-like. This characteristic will mostly be exploited in the design of memoryless VQ schemes.

Inter-frame correlation of the LSFs can be exploited by interframe predictive vector quantisation schemes having memory, where predictions of the current LSF values are employed, in order to reduce the variance of the vector we want to quantise. Finally, when rapid spectral changes are observed in the LSF traces, affecting both their intra- and inter-

frame correlation, various multimode schemes can be invoked, as we will show during our further discourse.

4.4.1.2 Speech Codec Specifications

The design of speech codecs is based, in general, on a trade-off between the conflicting factors of perceptual speech quality, the required bitrate, the channel error resilience and the implementational complexity. Wideband speech coding [146] aims to provide a better perceptual quality than narrowband speech codecs. Hence, a fine quantisation of the LPC parameters is required.

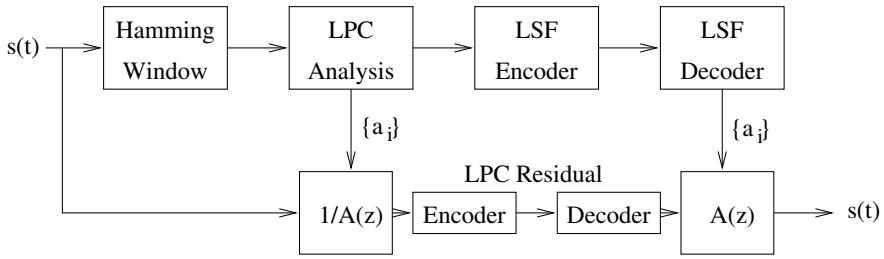

Figure 4.13: Evaluation of the perceptual speech quality after applying LSF vector quantisation.

Listening tests using the scheme depicted in Figure 4.13 indicate that the transparency criterion formulated by Paliwal and Atal [116] in the context of narrowband speech codecs is also relevant in wideband scenarios. This criterion uses a SD measure given by

$$\mathrm{SD}^2 = \frac{1}{f_s} \int_0^{f_s} [10 \log_{10}(P(f)) - 10 \log_{10}(\widehat{P}(f))]^2 \, \mathrm{d}f,$$

where $P(f)$ and $\widehat{P}(f)$ are the amplitude spectra of the original and reconstructed signal, respectively. The required criteria are satisfied if an average SD of about 1 dB is maintained and there are only a few 'outliers' between $\mathrm{SD} = 2$ and 4 dB, while there are no outliers in excess of $\mathrm{SD} = 4$ dB. In addition, an important issue in speech quality terms is the preservation of the stability of the STP. The STP filter's stability has a dramatic influence on the reconstructed speech quality, which is guaranteed by preserving the ordering property of the LSFs.

Every codec designed for transmission over noisy channels has to exhibit a good robustness against channel errors. The effect of transmission errors is characterised by their immediate effect on both the present speech frame and also on the forthcoming frames. Complexity reduction is also of high importance for real time applications. The codebook storage requirements and codebook search complexity are the main factors to be taken into consideration in the field of vector quantisation. In the next section we examine a few wideband LSF vector quantisation schemes.

4.4.2 Wideband LSF VQs

4.4.2.1 Memoryless Vector Quantisation

The so-called nearest neighbour vector quantisation (NNVQ) scheme [126] theoretically constitutes the optimal memoryless solution for VQ. However, the high number of LSFs – typically 16 – required for wideband speech spectral quantisation results in a complexity that is not realistic for a real-time implementation, unless the 16-component LSF vector is split into subvectors. As an extreme alternative, low complexity scalar quantisation constitutes the ultimate splitting of the original LSF vector into reduced-dimension sub-vectors. This method exhibits a low complexity and a good SD performance can be achieved using 16-entry or 4-bit codebooks. Nevertheless, the large number of LSFs required in wideband speech codecs implies a requirement of $4 \cdot 16 = 64$ or $5 \cdot 16 = 80$ bits per 10 ms speech frame. As a result, the contribution of the scalar quantised LSFs to the codec's bitrate is 6.4 or 8 kbps. Slight improvements can be achieved using a non-uniform bit allocation, when more bits are allocated to the perceptually most significant LSFs.

Between the above extreme cases, split vector quantisation (SVQ) aims to define a split configuration that minimises the average SD within a given total complexity. Specifically, SVQ operates on sub-vectors of dimensions that can be vector quantised within the given constraints of complexity, following the schematic of Figure 4.14.

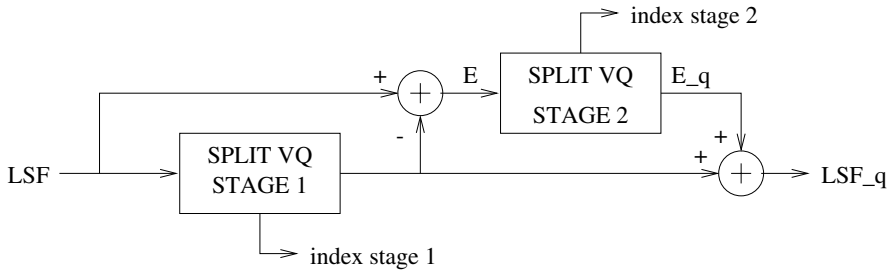

Figure 4.14: Schematic of the multi-stage split VQ.

One of the main issues in split LSF VQ is defining the best possible partitioning of the initial LSF vector into sub-vectors. Since the high-frequency LSFs typically exhibit a different statistical behaviour from their low-frequency counterparts, they have to be encoded separately. For linear predictive filters of order 16 the three highest-order LSFs behave differently from the other LSFs, as exemplified by Figure 4.12. Hence, this leads naturally to a $(13, 3)$-split VQ scheme. Figure 4.15 shows the PDF of the SD using a $(6, 7, 3)$-split LSF VQ scheme, where the lower frequency 13-component sub-vector is split into two further 6- and 7-component sub-vectors, in order to reduce the implementational complexity. Seven bits, i.e. 128 codebook entries, were used for each sub-vector. In addition, a $(4, 4, 4, 4)$-split second stage VQ was applied according to Figure 4.14 using five bits, i.e. 32 codebook entries, for each sub-vector. We refer to this scheme as the $[(6, 7, 3)_{777}; (4, 4, 4, 4)_{5555}]$ 41-bit regime.

The lower intra-frame correlation of the higher frequency LSFs imposes a high bitrate requirement on the SVQ in light of the relatively low energy contained in the corresponding

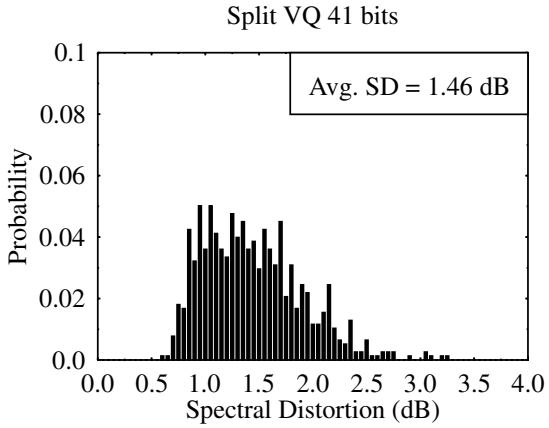

Figure 4.15: PDF of the SD for the 41-bit split VQ scheme using the $[(6, 7, 3)_{777}; (4, 4, 4, 4)_{5555}]$ two-stage regime (compare to Figures 4.20 and 4.23).

speech band (typically less than 1%). Although split VQ schemes are attractive in complexity terms and can preserve the LSFs ordering property, they often fail to reach the target SD within a low bitrate budget.

The introduction of LSF classified vector quantisation (CVQ) [126] aims to assign the LSF vectors into classes having a particular statistical behavior, in an effort to improve the coding efficiency.

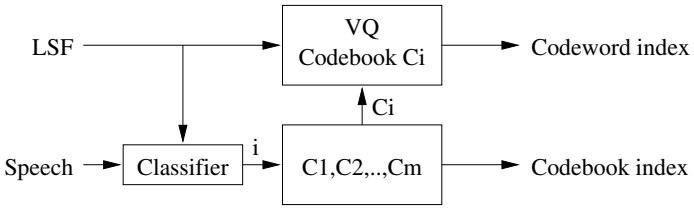

Figure 4.16: Schematic of the CVQ.

In Figure 4.16 the LSF vectors are classified into one of m categories $C_1, \ldots, C_m$ and then a reduced-size codebook C_m, which reflects the statistical properties of class m that is searched in order to find the best matching codebook entry for the unquantised LSF vector. Clearly, this scheme searches a reduced-size codebook, reducing the matching complexity and the quantisation precision in comparison to a VQ using no pre-classification before quantisation. In the context of wideband speech LSF quantisation, we wish to find a classification of the LSFs which can provide a more efficient representation of the vector to be quantised, than the previous SVQ. Accordingly, the main issue in CVQ is the design of an accurate classifier. In this context, we briefly investigate the performance of a voiced/unvoiced classifier.

The problem of voicing detection can be solved upon invoking an autocorrelation based pitch detector [55], exploiting the waveform similarities between the original speech and its pitch-duration shifted version. The highest correlation between these two signals is registered when their displacement corresponds to the pitch. Figure 4.17(a) shows a low-pass filtered speech waveform band-limited to 900 Hz, which was subjected to autocorrelation-based voicing-strength evaluation and thresholding at a normalised cross-correlation of 0.5, in order to generate the binary voiced/unvoiced (V/UV) decisions seen in Figure 4.17(b).

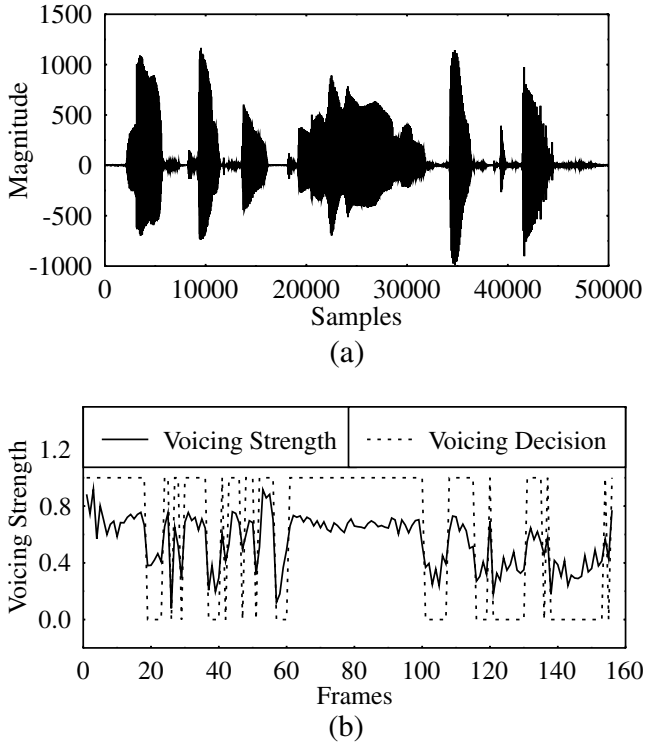

Figure 4.17: V/UV speech classification using low-pass filtering of the speech to 900 Hz and autocorrelation based pitch detection. (a) Low-pass filtered speech signal; (b) voicing strength and the associated binary voicing decisions.

Figure 4.18 demonstrates the relevance of this approach, portraying – as an illustrative example – the scatter diagrams of the first two LSFs after classification. For both diagrams, the unoccupied bottom right corner region manifests the dependency between the LSFs due to their ordering property. The first two LSFs of voiced frames in Figure 4.18(a) are centred around two clusters. One corresponding to the low-frequency LSF 1 occurrences, where LSF 2 appears near constant. The other voiced frame cluster corresponds to frames where LSF 1 and 2 exhibit similar values, creating a near-linear cluster along the 'ordering property border'. The unvoiced frames in Figure 4.18(b) appear more scattered, although they also exhibit an apparent, but less pronounced clustering along the ordering property border.

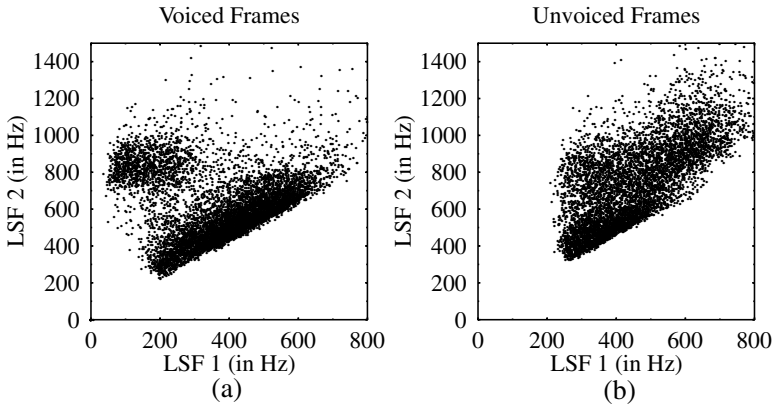

Figure 4.18: Scatter diagrams of the first two LSFs for wideband (a) voiced and (b) unvoiced frames.

Voiced and unvoiced LSFs do not necessarily exhibit a totally different statistical behavior in their clusters along the ordering property border in Figure 4.18. However, the typically more concentrated clusters of the voiced LSF frames can be typically more accurately vector quantised, whereas the somewhat more scattered occurrences of the unvoiced frames' LSFs are expected to be less amenable to CVQ. Similar scatter diagrams can be obtained also for higher frequency LSFs, although the pronounced difference between voiced and unvoiced frames tends to decrease, as the frequency increases. This is directly related to the less pronounced correlation between neighbouring LSFs for the higher frequencies of the 8 kHz range.

Although our simulations using this CVQ gave better SD results than the previously discussed SVQ, the overall scheme presents shortcomings. Specifically, if the speech frame classification is carried out before the LSF quantisation, classification errors at the V/UV speech boundaries increase the average SD, as well as the number of outliers. At the decoder, this method has to rely on the V/UV information extracted from the excitation signal in order to reconstruct the LSF coefficients, unless the V/UV mode is explicitly signalled to the decoder. Alternatively, if the V/UV classification is processed after LSF quantisation upon selecting the mode having the lower SD, no classification errors occur, although one bit per speech frame is required for transmitting the V/UV mode selection. When using the $[(6, 7, 3)_{777}; (4, 4, 4, 4)_{5555}]$ 41-bit split LSF VQ for each mode, an average SD of 1.15 dB is obtained upon invoking a mode selection bit, whereas an average SD of 1.35 dB is achieved using the pitch-detection based classification.

In addition, it is difficult to proceed to a joint optimisation of both the voiced and the unvoiced codebooks, since there are regions of the LSF domain where both types of LSFs can be located. The LSF clusters, which are encountered in both modes, are quantised independently by the voiced codebook and the unvoiced codebooks. Hence the same sub-domain of the LSF space is mapped twice by the quantisation cells of both modes. This leads to a sub-optimal quantisation of this area. Let us now consider predictive VQ schemes.

4.4.2.2 Predictive Vector Quantisation

In this section our discussions evolve from memoryless vector quantisation to more efficient vector quantisation schemes exploiting the time-domain inter-frame correlation of LSFs. According to this approach we typically quantize a *sequence of vectors*, where successive vectors may be statistically dependent. In contrast to the more conventional memoryless scalar quantisers, these vector quantisers are capable of exploiting the predictability of consecutive LSF vectors and hence may achieve further bitrate economies.

Predictive vector quantisation (PVQ) constitutes a vector-based extension of traditional scalar predictive quantisation. Its schematic is shown in Figure 4.19. PVQ schemes aim to exploit the correlation between the current vector and its past values in order to reduce the variation range of the signal to be quantised. Provided that there is sufficient correlation between consecutive vectors and the predictor is efficient, the vector components to be quantised are expected to be unpredictable, random noise-like signals, exhibiting a reduced dynamic range. Hence, for a given number of codebook entries, PVQ is expected to give a lower SD, than non-predictive VQ.

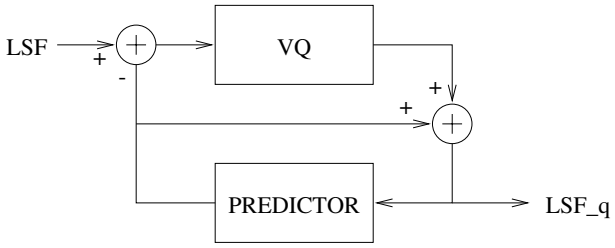

Figure 4.19: Schematic of a PVQ.

AR predictors use recursive reconstruction of the LSFs, hence they potentially suffer from severe propagation of channel errors over consecutive frames. By contrast, a MA predictor can typically limit the error propagation to a lower number of frames, given by the predictor order. Here, however, we restricted our experiments to first-order AR vector predictors.

PVQ does not necessarily preserve the LSFs' ordering property. This may results in instability of the STP filter, deteriorating the perceptual quality. In order to counteract this problem, an LSF rearrangement procedure [147] can be introduced, ensuring a minimum distance of 50 Hz between neighbouring LSFs in the frequency domain.

Figure 4.20 shows the PDF of the SD using $(4, 4, 4, 4)_{9999}$ 36-bit split vector quantisation of the prediction error, employing a 9-bit codebook per 4-LSF sub-vector. Hence this quantiser requires a total of $4 \cdot 9 = 36$ bits per LSF vector. Based on the above experience we concluded that the 36-bit PVQ provides a gain of 5 bits per LSF vector in comparison to our previous 41-bit memoryless SVQ having a similar complexity. Equivalently, PVQ generates an average SD gain of approximatively 0.3 dB for a given bitrate. A deficiency of this method is its higher sensitivity to channel error propagation, although this problem can be mitigated by using MA prediction instead of AR prediction. During our investigations we noted that this scheme was sensitive to unpredictable LSF vectors generated by rapid speech spectral

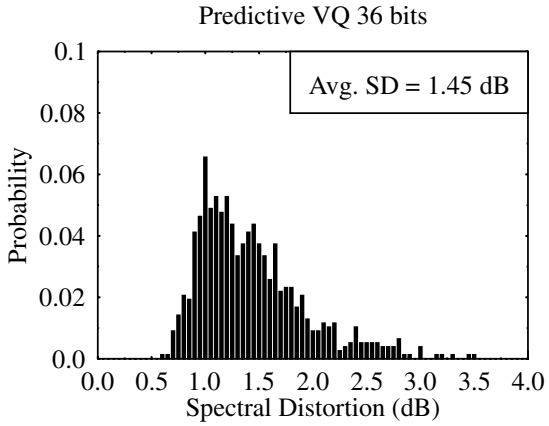

Figure 4.20: PDF of the SD for the 36-bit PVQ scheme (compare to Figures 4.15 and 4.23).

changes, which increase both the average SD as well as the number of SD outliers beyond $\mathrm{SD} = 2\,\mathrm{dB}$. This problem is addressed in the next section.

4.4.2.3 Multimode Vector Quantisation

Our previous CVQ scheme has primarily endeavored to define V/UV correlation modes. When we observe these V/UV speech transitions in the time domain, they result in the rapid changes of the LSF traces seen in Figure 4.12, for example, around frame 20. Several methods exist for differentiating between these modes. Switched prediction is widely employed [55, 147]. In this section, we will investigate the separate encoding of the unpredictable frames due to rapid spectral changes and that of the highly-correlated frames. This can be achieved by the combination of a PVQ and a fixed memoryless SVQ, referred to as the so-called safety-net VQ (SNVQ) scheme [148–150]. In this context, we invoke a full search using both the PVQ and the fixed memoryless SVQ schemes for every speech frame, and the better candidate with respect to a mean-squared distortion criterion is chosen.

The SNVQ improves the overall robustness against outliers, which are typically due to input LSF vectors having a low correlation with the previous LSF vectors. In addition, the SNVQ allows the PVQ to concentrate on the predictable, highly correlated frames. Hence, the variance of the LSF prediction error is reduced and a higher-resolution LSF prediction error codebook can be designed. The advantage of this method is that when the inter-frame correlation cannot be successfully exploited in a PVQ scheme, the intra-frame correlation is capitalised on instead.

Figure 4.21 shows the structure of the SNVQ scheme. Again, the input LSF vector is quantised using both predictive and memoryless quantisers, then both quantised vectors are compared to the input vector in order to select the better quantisation scheme. The codebook index selected is transmitted to the decoder, along with a signalling bit that indicates the selected mode. The specific transmitted quantised vector is finally used by the PVQ in order to predict the LSF vector of the next frame.

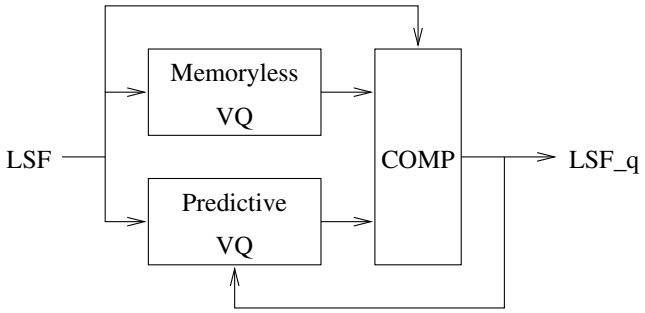

Figure 4.21: Schematic of the Safety Net Vector Quantiser (SNVQ) constituted by a memoryless- and a predictive-VQ.

The performance difference between the memoryless SVQ and PVQ sections of the SNVQ suggests the employment of variable bitrate schemes, where the lower performance of the memoryless SVQ can be compensated by using a larger codebook. In our experiments below – as before – a memoryless SVQ 41-bit codebook was used. Hence, the SNVQ is characterised by its average bitrate, depending on the proportion of vectors quantised by the predictive and memoryless VQ, respectively. Eriksson *et al.* [149] argued that the optimum performance is attained, when 50–75% of frames invoke the PVQ.

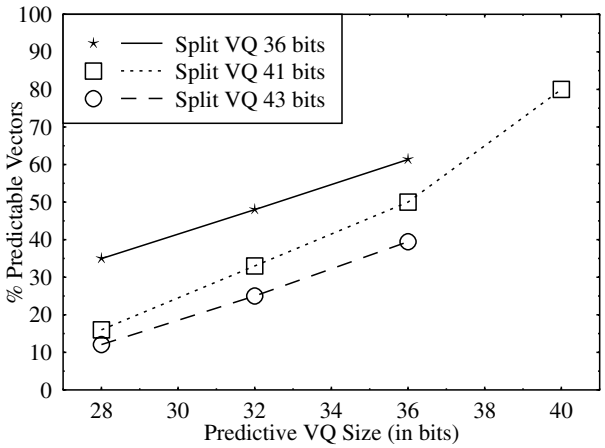

Figure 4.22: Proportion of frames using PVQ in various SNVQ schemes, employing memoryless SVQs of 36, 41 and 43 bits.

Figure 4.22 shows the proportion of frames quantised using the 28-, 32- and 36-bit PVQs in the context of SNVQ schemes employing 36-, 41- and 43-bit SVQs. We observe in Figure 4.22 that for a PVQ codebook size of 28 and 32 bits a relatively low proportion of the LSF vectors was quantised using the PVQ and this indicated that its codebook size was too small, failing to outperform the memoryless 36-, 41- or 43-bit SVQs. Accordingly, only the 36-bit PVQ was deemed suitable. This figure illustrates that if the PVQ exhibits low performance compared to the memoryless SVQ, i.e. the proportion of its utilization tends

to zero, the SNVQ will tend to behave like a simple memoryless SVQ. Alternatively, if the memoryless SVQ exhibits low performance compared to the PVQ, i.e. the proportion of PVQ LSF vectors tends to 100%, the SNVQ will tend to behave like a PVQ.

The individual PVQ and memoryless SVQ schemes employed so far were designed independently from each other, hence the resulting scheme is sub-optimal. Furthermore, both quantisers were designed without distinction between predictable and unpredictable LSF vectors. Hence, their optimisation will aim, on one hand, to have the PVQ focussing on predictable frames which generate LSF prediction errors with a low variation range. On the other hand, the memoryless SVQ codebook is to be matched to the distribution of the unpredictable LSF vectors in the p-dimensional LSF space. In order to obtain an optimal SNVQ we will proceed as follows.

(1) The original training sequence T is passed through our previously used individual sub-optimum codebook based SNVQ, in order to generate the sub-training sequences $T_{\rm PVQ}$ and $T_{\rm SN}$ of vectors, quantised using either the PVQ or the memoryless SVQ, respectively, depending on which generated a lower SD.

(2) Then codebooks for both the PVQ and the memoryless SVQ are designed using the sub-training sequences generated above.

Our results to be highlighted with reference to Table 4.2 show that the optimised PVQ results in significant improvements, but only a modest further gain was obtained with the aid of the safety-net approach, invoking the optimised memoryless SVQ. Clearly, optimisation is the main issue in SNVQ design, requiring the joint design of both parts of the SNVQ. We designed a $[36, 36]$-bit and a $[36, 41]$-bit scheme, where the first bracketed number indicates the number of bits assigned to the PVQ, while the second one that of the memoryless SVQ. Again, the performance of these schemes is summarised in Table 4.2. In both cases a SD gain of about 0.15 dB was obtained upon the joint optimisation of the component VQs, as seen in Table 4.2. In addition, the number of outliers between 2 and 4 dB was substantially reduced and all the outliers over 4 dB were removed.

Table 4.2: Optimisation effects for the $[36, 36]$ and $[36, 41]$ SNVQ schemes.

Scheme	Avg. SD (dB)	Outliers (%) 2–4 dB	Outliers (%) >4 dB
[36, 36] SNVQ scheme			
Non-optimised	1.34	7.19	0.12
Optimized	1.17	2.18	0
[36, 41] SNVQ scheme			
Non-optimised	1.25	4.5	0.12
Optimized	1.09	0.38	0

We found that the optimisation slightly increased the proportion of frames quantised using the PVQ. For our $[36, 36]$ SNVQ scheme, this proportion increased from 67% to 74%. Similarly, for the $[36, 41]$ SNVQ scheme constituted by the 36-bit PVQ and 41-bit

memoryless SVQ, respectively, this proportion increased from 50% to 60%. Hence, in the case of such switched variable bitrate schemes, the optimisation tends to reduce the average SNVQ bitrate, since the PVQ requires less bits than the memoryless SVQ.

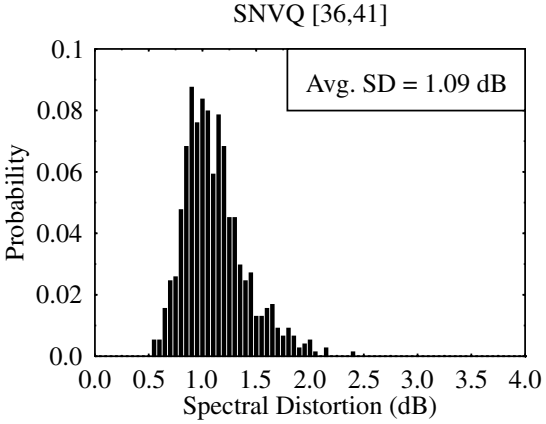

Figure 4.23: PDF of the SD for the $[36, 41]$ bit SNVQ scheme (compare to Figures 4.15 and 4.20).

Figure 4.23 shows the PDF of the SD for the $[36, 41]$ SNVQ scheme, indicating a significant SD PDF enhancement compared to both the memoryless SVQ and the PVQ. In addition, this system improves the robustness against channel errors, since the propagation of bit errors was limited due to the low number of consecutive employment of the PVQ. Clearly, the SNVQ enabled an efficient exploitation of both the inter-frame correlation and the intra-frame correlation of LSF vectors. Its main deficiency is the increased complexity of the codebook search procedure, requiring twice as many comparisons as the memoryless SVQ or the PVQ.

4.4.3 Simulation Results and Subjective Evaluations

Figure 4.24 summarises the performance of the split memoryless SVQ, the PVQ and the SNVQ. As observed in the figure, the SD results for the memoryless SVQ are more modest and, in general, a better performance was obtained by using the predictive quantisation schemes. This figure illustrates a difference of 4 or 5 bits between the memoryless SVQ and the PVQ for the same SD. The three SD curves corresponding to the SNVQ schemes using 28-, 32- and 36-bit PVQs in conjunction with various associated memoryless SVQ configurations are also shown in Figure 4.24. For the SNVQ using 28- and 32-bit PVQs, the lines crossing the PVQ performance curve drawn using a solid line indicate that at this stage the PVQ starts to attain a better performance than the SNVQ for the equivalent bitrate. Hence, in this scenario there is no benefit from employing SNVQ schemes using 28- and 32-bit PVQs beyond this cross-over point. A consistent SD gain in comparison to the PVQ is only ensured for the SNVQ using the 36-bit PVQ. In this case a 2-bit reduction in the number of required coding bits was obtained. Informal listening tests have shown that the best perceptual performance was obtained by employing the $[36, 41]$ SNVQ scheme.

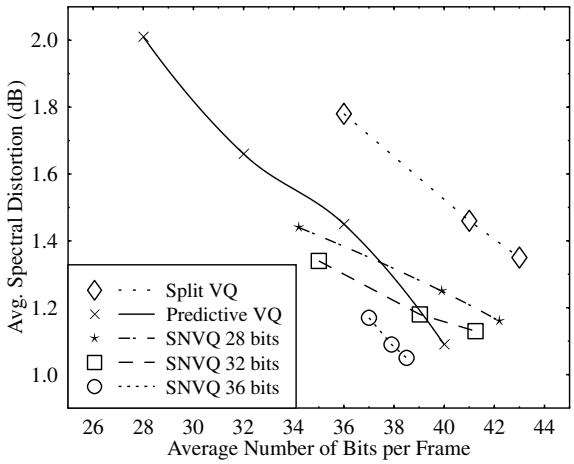

Figure 4.24: Average SD of the various vector quantisers considered in this study.

Table 4.3: Transparent quantisation schemes.

Scheme	No. of bits	Avg. SD (dB)	Outliers (%)	
			2–4 dB	>4 dB
PVQ	40	1.09	4.24	0
SNVQ	38	1.09	0.38	0

Table 4.3 details the characteristics of two high-quality quantisation schemes. The first configuration utilised a $(4, 4, 4, 4)_{10,10,10,10}$ PVQ scheme employing $4 \cdot 10 = 40$ bits and the second scheme used a $[36, 41]$ SNVQ arrangement with an average of 38 bits. Although both schemes have a similar average SD, the SNVQ provides a large reduction in the number of SD outliers between 2 and 4 dB, which have a significant effect on the perceptual speech quality. A high speech quality was also obtained for the $[36, 36]$ fixed bitrate SNVQ, as shown in Table 4.2.

4.4.4 Conclusions on Wideband Spectral Quantisation

In this section we have comparatively studied various predictive and memoryless VQ. In the context of memoryless vector quantisation, a $[(6, 7, 3)_{777}; (4, 4, 4, 4)_{5555}]$ 41-bit multi-stage SVQ was designed. This method enabled a simple implementation. In order to improve the performance of this initial memoryless scheme, we introduced V/UV classification. This approach gave about 0.2 dB SD improvement, but increased the complexity. Nonetheless, both of these sub-optimum approaches maintained a low computational complexity, as well as a high error resilience.

In the context of 41-bit PVQ a SD quality enhancement was achieved compared to memoryless schemes, or alternatively the number of bits could be reduced to 36,

while maintaining a similar average SD. The associated SD PDFs were portrayed in Figures 4.15, 4.20 and 4.23, while their salient features were summarised in Tables 4.2 and 4.3. Unfortunately, the channel error sensitivity increased due to potential error propagation. Lastly, we combined both the memoryless and the predictive approaches in a SNVQ scheme. Even though the SNVQ scheme increased the complexity, it significantly improved the SD performance and mitigated the propagation of channel errors. Our future research considers the design trade-offs of wideband backwards adaptive speech codecs and transform codecs.

4.5 Chapter Summary

In this chapter a range of parameters were introduced which can be invoked for the error-resilient representation of the speech signal's spectral envelope. Specifically, the LARs and the LSFs were discussed in more details and their PDFs were exemplified. These elaborations were followed by the portrayal of a suit of spectral quantisers. VQs were found to be particularly efficient due to the inherent correlation of the LSFs both versus time and versus frequency. Finally, a comparative study of various wideband spectral quantisers was provided.

Having treated the issues of spectral representation, in the spirit of the linearly separable speech generation model of Figure 1.1, let us now concentrate our attention on a range of techniques which can be used to represent the prediction residual. However, recall from Section 3.2 and Figure 3.1 that having determined the spectral coefficients of the current segment of speech the aim in AbS coding is not to find a good waveform replica of the prediction residual, but to find a model of it which results in the *perceptually* best synthetic speech quality. A plethora of techniques have been suggested in the literature which are based on a range of different design trade-offs in terms of speech quality, bitrate, implementational complexity, robustness against transmission errors, etc, that will be characterised in the forthcoming sections.

Let us initially concentrate on the RPE technique in the next section, which constitutes an attractive design trade-off at a bitrate of 13 kbps in terms of low complexity and high speech quality characterised by a MOS of about four. In an international comparative test [151] it outperformed a range of other codecs and hence it was selected for the Pan-European mobile radio system known as the Global System of Mobile Communications or GSM [97, 98].

Chapter 5

Regular Pulse Excited Coding

5.1 Theoretical Background

The schematic of the RPE speech codec is based on the AbS structure of Figure 3.8. The typically $N = 40$ samples or 5 ms duration excitations or innovation sequences $v(n)$ are filtered through the LTP synthesis filter $1/P(z)$, STP synthesis filter $1/A(z)$ and perceptual weighting filter $W'(z) = A(z)/A(z/\gamma)$, where the STP synthesis filter $1/A(z)$ and the numerator of $W'(z)$ cancel, yielding the simplified weighting filter $W(z) = 1/A(z/\gamma)$ seen in the figure. Hence the weighted synthetic speech $\tilde{s}_w(n)$ is given by the convolution

$$\tilde{s}_w(n) = v(n) * h_p(n) * h_w(n) = v(n) * h_c(n), \tag{5.1}$$

where $h_p(n)$ and $h_w(n)$ are the impulse responses of the filters $1/P(z)$ and $W(z) = 1/A(z/\gamma)$, respectively, and $h_c(n)$ is that of the cascaded filter complex $1/P(z)$, $W(z)$. Similarly, a 5 ms input speech segment about to be encoded is weighted by the identical perceptual weighting filter, and their difference is computed for each legitimate innovation sequence in order to find the particular one yielding the minimum weighted error and hence the subjectively best 5 ms duration synthetic speech segment.

As mentioned above, depending on the construction of the innovation vectors, rather different complexities, bitrates and speech qualities arise. Historically one of the most important excitation description models is constituted by the MPE codec invented by Atal and Remde [9,71], since it was the first AbS codec yielding good speech quality between 9.6 kbps and 16 kbps at a moderate complexity. Variants of the typically low-bitrate (4.8–8 kbps) CELP codec yield medium quality at a high complexity, while the moderate complexity, medium bitrate (13 kbps) RPE codec also used in the GSM system provides high speech quality (MOS ≈ 4.0). Spectrally, it is almost three times more efficient than the previously described 32 kbps ADPCM G.721 ITU codec, while also maintaining a higher robustness against channel errors.

In RPE codecs the innovation sequence $v(n)$ holds M equidistant excitation samples with amplitudes β_k and positions m_k, yielding a set of legitimate excitation sequences $v(n)$ in the

form

$$v(n) = \sum_{k=0}^{M-1} \beta_k \delta(n - m_k). \tag{5.2}$$

Since the excitation model $v(n)$ is now given by Equation (5.2), we can embark on determining the optimum excitation parameters β_k, m_k. It is plausible that for LTP delay values longer than the excitation optimisation sub-segment length we have $\alpha > N$, implying that the pitch synthesis filter's impulse response $h_p(n)$ is zero inside the current excitation optimisation sub-segment. Hence, for $n < N$ we have $h_c(n) = h_w(n)$, that is the composite impulse response is identical to the weighted synthesis filter's impulse response. Hence, if we impose the condition $\alpha > N$ by restricting the LTP delay to values exceeding the excitation frame length N, the LTP synthesis filter will not contribute to the composite synthesis filter's impulse response $h_c(n)$, but it will have to be considered during the computation of the zero-input response of the combined synthesis filter. Assuming that the LTP synthesis filter is replaced by an adaptive G-scaled codebook $Gu(n - \alpha) = Gc_\alpha$, where the adaptive codebook entry is denoted by c_α, the composite excitation is given by

$$u(n) = v(n) + Gu(n - \alpha) = v(n) + Gc_\alpha. \tag{5.3}$$

The computation of the LTP parameters α and G was highlighted in Sections 3.4.1 and 3.4.2 and the weighted synthetic speech can now be expressed as the convolution of the excitation with the impulse response of the composite synthesis filter as

$$\begin{aligned} \hat{s}_w(n) &= u(n) * h_w(n) \\ &= v(n) * h_w(n) + Gc_\alpha(n) * h_w(n) + \hat{s}_0(n), \end{aligned} \tag{5.4}$$

where the convolution is a memoryless process since the filter memory is treated separately, and $\hat{s}_0(n)$ represents the zero-input response of the weighted synthesis filter in the lower branch of Figure 3.8. For details as to the analytical description of the zero-input response $\hat{s}_0(n)$ the interested reader is referred to Salami's work [70, 71].

When substituting the excitation model of Equation (5.2) into Equation (5.4), the synthetic speech is yielded in the form

$$\begin{aligned} \hat{s}_w(n) &= \sum_{i=0}^{n} \left(\sum_{k=0}^{M-1} \beta_k \delta(n - m_k) \right) h_w(n - i) \\ &\quad + Gc_\alpha(n) * h_w(n) + \hat{s}_0(n), \\ &= \sum_{k=0}^{M-1} \beta_k h_w(n - m_k) + Gy_\alpha(n) + \hat{s}_0(n), \end{aligned} \tag{5.5}$$

where

$$y_\alpha(n) = c_\alpha(n) * h_w(n)$$

is referred to as the *zero-state response* of the weighted synthesis filter $h_w(n)$, when after resetting its memory to zero, it is excited by the codeword c_α chosen from the adaptive codebook. Now, the weighted error between the original speech and the synthetic speech is

given by

$$\begin{aligned} e_w(n) &= s_w(n) - \hat{s}_w(n) \\ &= s_w(n) - Gy_\alpha(n) - \hat{s}_0(n) - \sum_{k=0}^{M-1} \beta_k h_w(n - m_k) \\ &= x(n) - \sum_{k=0}^{M-1} \beta_k h_w(n - m_k), \end{aligned} \tag{5.6}$$

where now

$$x(n) = s_w(n) - Gy_\alpha(n) - \hat{s}_0(n), \tag{5.7}$$

implying that now not only the zero-input response $\hat{s}_0(n)$ of $W(z)$, but also the effect of the scaled adaptive codebook entry $Gy_\alpha(n)$ is subtracted from the weighted original speech in order to generate the *target vector*, to which the candidate synthesis filter responses are then compared in response to the candidate excitation patterns. Explicitly, the target vector $x(n)$ is now computed by updating $x'(n)$ of Equation (3.13):

$$x(n) = x'(n) - Gy_\alpha(n). \tag{5.8}$$

From Equation (5.6) the total weighted MSE (WMSE) can now be written as

$$\begin{aligned} E_w &= \sum_{n=0}^{N-1} e_w^2(n) \\ &= \sum_{n=0}^{N-1} \left[x(n) - \sum_{k=0}^{M-1} \beta_k h_w(n - m_k) \right]^2 . \end{aligned} \tag{5.9}$$

Following Kroon *et al.*'s [11] and Salami's deliberations [70, 71] the optimum pulse amplitudes β_k and the pulse positions m_k minimising the WMSE can be determined by setting $\partial E_w / \partial \beta_i = 0$ for $i = 0, \ldots, M-1$, which yields

$$\frac{\partial E_w}{\partial \beta_i} = -2 \sum_{n=0}^{N-1} \left[x(n) - \sum_{k=0}^{M-1} \beta_k h_w(n - m_k) \right] h_w(n - m_i) = 0. \tag{5.10}$$

Upon rearranging the above formula we arrive at

$$\sum_{n=0}^{N-1} x(n) h_w(n - m_i) = \sum_{n=0}^{N-1} \left[\sum_{k=0}^{M-1} \beta_k h_w(n - m_k) \right] h_w(n - m_i). \tag{5.11}$$

Upon exchanging the order of summations on the right-hand side of Equation (5.11) we get

$$\sum_{k=0}^{M-1} \beta_k \sum_{n=0}^{N-1} h_w(n - m_k) h_w(n - m_i) = \sum_{n=0}^{N-1} x(n) h_w(n - m_i), \quad i = 0, \ldots, M-1. \tag{5.12}$$

Observe in the above equation that

$$\Phi(m_i, m_k) = \sum_{n=0}^{N-1} h_w(n - m_i)h_w(n - m_k) \tag{5.13}$$

represents the autocorrelation of $h_w(n)$, and

$$\Psi(m_i) = \sum_{n=0}^{N-1} x(n)h_w(n - m_i) = x(n) * h_w(-n) \tag{5.14}$$

the cross-correlation between $x(n)$ and $h_w(n)$, then Equation (5.12) can be simplified to

$$\sum_{k=0}^{M-1} \beta_k \Phi(m_i, m_k) = \Psi(m_i), \quad i = 0, \ldots, M-1. \tag{5.15}$$

The above set of M equations can be written in a more explicit matrix form as:

$$\begin{pmatrix} \Phi(m_0, m_0) & \Phi(m_0, m_1) & \ldots & \Phi(m_0, m_{M-1}) \\ \Phi(m_1, m_0) & \Phi(m_1, m_1) & \ldots & \Phi(m_1, m_{M-1}) \\ \vdots & \vdots & \ddots & \vdots \\ \Phi(m_{M-1}, m_0) & \Phi(m_{M-1}, m_1) & \ldots & \Phi(m_{M-1}, m_{M-1}) \end{pmatrix} \begin{pmatrix} \beta_0 \\ \beta_1 \\ \vdots \\ \beta_{M-1} \end{pmatrix} \begin{pmatrix} \Psi(m_0) \\ \Psi(m_1) \\ \vdots \\ \Psi(m_{M-1}) \end{pmatrix}. \tag{5.16}$$

Equation (5.16) represents a set of M equations that should be solved for M pulse positions plus M pulse amplitudes, which is not possible. A computationally attractive, high quality sub-optimum solution was proposed by Kroon *et al.* [11] that was also portrayed in Salami's work [70, 71], which will be highlighted below.

According to Kroon *et al.*, the innovation sequence can be derived as a sub-sampled version of the STP residual. The excitation pulses are d samples apart and there are d decimated candidate excitation sequences according to the d possible initial grid-positions. If a frame of N prediction residual samples is processed, the number of excitation pulses is given by $M = (N) \div (d)$, where $\div$ implies integer division. The legitimate excitation pulse positions are $m[k, i] = k + (i - 1)d$, $i = 1, 2, \ldots, M$, where $k = 0, 1, \ldots, (d - 1)$ are the initial grid-positions. With the pulse-positions fixed, Equation (5.16) is solved d times for each candidate excitation pattern, yielding d sets of M pulse amplitudes. Upon expanding Equation (5.9) we arrive at

$$\begin{aligned} E_w = & \sum_{n=0}^{N-1} x^2(n) - 2 \sum_{n=0}^{N-1} x(n) \sum_{k=0}^{M-1} \beta_k h_w(n - m_k) \\ & + \sum_{n=0}^{N-1} \left[\sum_{k=0}^{M-1} \beta_k h_w(n - m_k) \right]^2 \end{aligned}$$

$$= \sum_{n=0}^{N-1} x^2(n) - 2 \sum_{k=0}^{M-1} \beta_k \Psi(m_k) + \sum_{i=0}^{M-1} \sum_{k=0}^{M-1} \beta_i \beta_k \Phi(m_i, m_k). \tag{5.17}$$

The second term of the above expression can be rewritten with the help of Equation (5.15) as

$$\begin{aligned} \sum_{i=0}^{M-1} \beta_i \Psi(m_i) &= \sum_{i=0}^{M-1} \beta_i \sum_{k=0}^{M-1} \beta_k \Phi(m_i, m_k) \\ &= \sum_{i=0}^{M-1} \sum_{k=0}^{M-1} \beta_i \beta_k \Phi(m_i, m_k), \end{aligned} \tag{5.18}$$

which allows us to simplify Equation (5.17) to

$$E_w = \sum_{n=0}^{N-1} x^2(n) - \sum_{k=0}^{M-1} \beta_k \Psi(m_k), \tag{5.19}$$

where E_w is minimised if the second term of Equation (5.19) is maximised.

Again, the set of M Equations (5.15) or (5.16) contains twice as many unknowns as the number of independent equations and hence there exists no direct solution to the problem. It would be possible to solve it, however, assuming a particular legitimate combination of the pulse positions, find the associated optimum excitation pulse amplitudes and remember the corresponding total WMSE E_w from Equation (5.19). This operation could then be continued for all legitimate pulse position combinations, until the optimum one resulting in the minimum E_w term was found. In order to be able to assess the associated computational complexity we note that the matrix of impulse response autocorrelations can be inverted using Gaussian elimination or employing Cholesky-decomposition [71], which has a complexity proportional to M^3. For the typical values of $N = 40$ and $d = 4$ a total of $M = 10$ equations would have to be solved four times for each 5 ms excitation optimisation sub-segment. Equation (5.13) and Equation (5.14) would have to be evaluated as well.

The computational complexity incurred in solving Equation (5.16) can be significantly reduced, while maintaining high speech quality. Specifically, substantial algorithmic simplification is achieved at almost imperceptible speech quality degradation assuming that the speech is stationary, rendering the covariance $\Phi(i, j)$ to become $\Phi(|i - j|) = \Phi(k)$. With this assumption the key equation Equation (5.16), is simplified to

$$\begin{pmatrix} \Phi(0) & \Phi(d) & \Phi(2d) & \dots & \Phi[(M-1)d] \\ \Phi(d) & \Phi(0) & \Phi(d) & \dots & \Phi[(M-2)d] \\ \vdots & & & & \\ \Phi[(M-1)d] & & & \dots & \Phi(0) \end{pmatrix} \begin{pmatrix} \beta(k,1) \\ \beta(k,2) \\ \vdots \\ \beta(k,M) \end{pmatrix} = \begin{pmatrix} \Psi[m(k,1)] \\ \Psi[m(k,2)] \\ \vdots \\ \Psi[m(k,M)] \end{pmatrix} \tag{5.20}$$

where the correlation matrix $\mathbf{\Phi}$ becomes a Toeplitz matrix. Hence, Equation (5.20) can again be solved with the help of the Levinson–Durbin algorithm.

It has been reported by Kroon *et al.* [11] and Salami *et al.* [70, 71] that $h_w(n)$ is a sharply decaying function, therefore its covariance of

$$\Phi(i) = \sum_{n=i}^{N-1} h_w(n)h_w(n-i) \tag{5.21}$$

decays even faster. This allows us to set all off-diagonal elements in the covariance matrix $\mathbf{\Phi}$ to zero, resulting in a dramatically reduced complexity when solving Equation (5.16), since it can now be written as

$$\Phi(0) \begin{pmatrix} \beta(k,1) \\ \beta(k,2) \\ \vdots \\ \beta(k,M) \end{pmatrix} = \begin{pmatrix} \Psi[m(k,1)] \\ \Psi[m(k,2)] \\ \vdots \\ \Psi[m(k,M)] \end{pmatrix} \tag{5.22}$$

giving the optimum pulse amplitudes in the form of

$$\beta(k,i) = \frac{\Psi[m(k,i)]}{\Phi(0)}. \tag{5.23}$$

In order to further simplify the computation of the optimum excitation pulse amplitudes we briefly return to Equation (5.7). As seen in Figure 3.8, the weighted original speech signal $s_w(n)$ can be expressed as the convolution of the prediction residual $r(n)$ and the weighting filter's response as

$$s_w(n) = \sum_{i=-\infty}^{n} r(i)h_w(n-i) = \sum_{i=0}^{n} r(i)h_w(n-i) + s_0(n), \tag{5.24}$$

where $s_0(n)$ is the zero-input response of the filter $W(z)$ in the upper branch of Figure 3.8, processing the original speech signal. Then upon substituting $s_w(n)$ from Equation (5.24) into Equation (5.7) we arrive at

$$\begin{aligned} x(n) &= r(n) * h_w(n) - Gy_\alpha(n) + s_0(n) - \hat{s}_0(n) \\ &= r(n) * h_w(n) - Gc_\alpha(n) * h_w(n) + s_0(n) - \hat{s}_0(n) \\ &= [r(n) - Gc_\alpha(n)] * h_w(n) + s_0(n) - \hat{s}_0(n) \\ &= d(n) * h_w(n) + s_0(n) - \hat{s}_0(n), \end{aligned} \tag{5.25}$$

where the shorthand

$$d(n) = [r(n) - Gc_\alpha] \tag{5.26}$$

was used to denote the LTP residual.

Now, assuming equal memory contributions in the original and synthetic speech paths, since both paths are filtering similar signals, we then have $s_0(n) = \hat{s}_0(n)$. This enables us to compute $\Psi(m_i)$ in Equation (5.14) with the aid of Equation (5.25) as

$$\Psi(n) = x(n) * h_w(-n) = d(n) * h_w(n) * h_w(-n) = d(n) * \Phi(n). \tag{5.27}$$

Substituting $\Psi(m_i)$ from Equation (5.27) into Equation (5.23) gives the optimum excitation pulse amplitudes as

$$\beta(k,i) = d[m(k,i)] * \frac{\Phi[m(k,i)]}{\Phi(0)} = d[m(k,i)] * \varphi[m(k,i)]. \tag{5.28}$$

Note that according to Equation (5.28) the derivation of the optimum excitation pulses can be interpreted as filtering the samples of the decimated signal $d[m(k,i)]$ employing a filter described with the help of the impulse response $\varphi[m(k,i)]$. This impulse response was given by Equation (5.21) in the form of the covariance of the weighting filter's impulse response, which is naturally a speech spectrum dependent, time-variant function akin to the impulse response of a LPF, which is also often termed as a 'smoother'.

Further algorithmic simplifications accrue without significant speech quality degradation, if we derive a time-invariant 'compromise smoother' from the long-term averaged weighting filter covariances or employ simple and ideal LPF. For a pulse-spacing or decimation factor of $d = 3$, as in the GSM-standard RPE codec, a cutoff frequency of $f_c = 1.3\,\text{kHz}$ has to be used. For an ideal 'rectangular' low-pass finite impulse response (FIR)-filter of order 11 the symmetric impulse response coefficients are simply derived from the Hamming-windowed sinc function samples of $\varphi(0) = \varphi(10) = -0.016256$, $\varphi(1) = \varphi(9) = -0.045649$, $\varphi(2) = \varphi(8) = 0$, $\varphi(3) = \varphi(7) = 0.250793$, $\varphi(4) = \varphi(6) = 0.70079$, $\varphi(5) = 1$.

In conclusion, the simplified RPE codec's operation can be summarised as follows. Initially the STP coefficients $a_i,\ i = 1, \ldots, p$, are determined and the STP residual $r(n)$ is computed by filtering the original input speech $s(n)$ through the filter $A(z)$. Then the LTP filter parameters G and α are computed and the LTP residual $d(n)$ is determined using Equation (5.26), which is then smoothed or low-pass (LP) filtered, before it is decomposed into d candidate excitation sequences. In the case of $d = 3$ candidate excitation sequences, $d(n)$ is decimated by a factor of $d = 3$, hence the LPFs cutoff frequency is $4/3 \approx 1.33\,\text{kHz}$. The specific excitation pulses of each of the d candidate excitation sequences are given by Equation (5.28), which are derived from the smoothed and decimated LTP residual $d(n)$.

The specific candidate excitation sequence minimising the WMSE of Equation (5.19) is then finally selected to generate the synthetic speech by exciting the synthesis filters. Explicitly, the total WMSE $E_w^{(j)}$ for the jth candidate excitation vector is computed using Equation (5.28) as

$$E_w^{(j)} = \sum_{n=0}^{N-1} x^2(n) - \Phi(0) \sum_{k=1}^{M} \beta^2(k,i) = \sum_{n=0}^{N-1} s_w^2(n) - \Phi(0) E(j), \tag{5.29}$$

where $E(j)$ is the energy of the jth candidate excitation vector. It now becomes plausible that the specific excitation vector having the highest energy, in other words the one maximising the second term of Equation (5.29), minimises E_w. This is in harmony with our expectations, since after smoothing the LTP residual was decomposed into d candidate excitations, but the highest-energy vector is expected to give the best representation of the prediction residual $r(n)$ and hence to generate the closest synthetic speech replica of the original speech segment.

Before we embark on describing the specific implementational details of the standardised GSM speech codec [98] we note that while the original RPE codec as proposed by Kroon *et al.* [11] was a true AbS codec, the simplified RPE codec deduced above and used by the

GSM system is actually an open-loop system. This open-loop codec constitutes an attractive design trade-off in terms of bitrate, complexity and speech quality. The performance of the RPE codec was studied by Salami *et al*. [70,71] varying a range of parameters, including the sub-segment length N, the number of pulses M per sub-segment, the decimation factor d, etc.

5.2 The 13 kbps RPE-LTP GSM Speech Encoder

The selection of the most appropriate speech codec for the GSM system from the set of candidate codecs was based on extensive comparative tests at various operating conditions. The rigorous comparisons published in [151] are interesting and offer deep insights for system designers as regards to the pertinent trade-offs in terms of speech quality, robustness against channel errors, complexity, system delay, etc. The codecs participating in the final comparative tests were two different sub-band codecs: a MPE codec and the RPE codec, which was finally selected for standardisation on the basis of the overall comparison tests. The average MOS of the RPE codec on a five-point scale over the various test conditions was found to be four, which is hardly distinguishable from the original uncoded speech at normal operating conditions.

The schematic diagram of the RPE-LTP encoder is shown in Figure 5.1, where the following functional parts can be recognised [12,13,97]: (1) pre-processing; (2) STP analysis filtering; (3) LTP analysis filtering; (4) RPE computation.

5.2.1 Pre-processing

Pre-emphasis can be employed to increase the numerical precision in computations by emphasising the high-frequency, low-power part of the speech spectrum. This can be carried out with the help of a one-pole filter with the transfer function of

$$H(z) = 1 - c_1 z^{-1}, \tag{5.30}$$

where $c_1 \approx 0.9$ is a practical value. The pre-emphasised speech $s_p(n)$ is segmented into blocks of 160 samples in a buffer, where they are windowed by a Hamming-window to counteract the spectral domain Gibbs oscillation, caused by truncating the speech signal outside the analysis frame. The Hamming-window has a tapering effect towards the edges of a block, while it has no influence in its middle ranges:

$$s_{psw}(n) = s_{ps}(n) \cdot c_2 \cdot \left(0.54 - 0.46 \cos 2\pi \frac{n}{L}\right), \tag{5.31}$$

where $s_{ps}(n)$ represents the pre-emphasised, segmented speech, $s_{psw}(n)$ is its windowed version and the constant $c_2 = 1.5863$ is determined from the condition that the windowed speech must have the same power as the non-windowed.

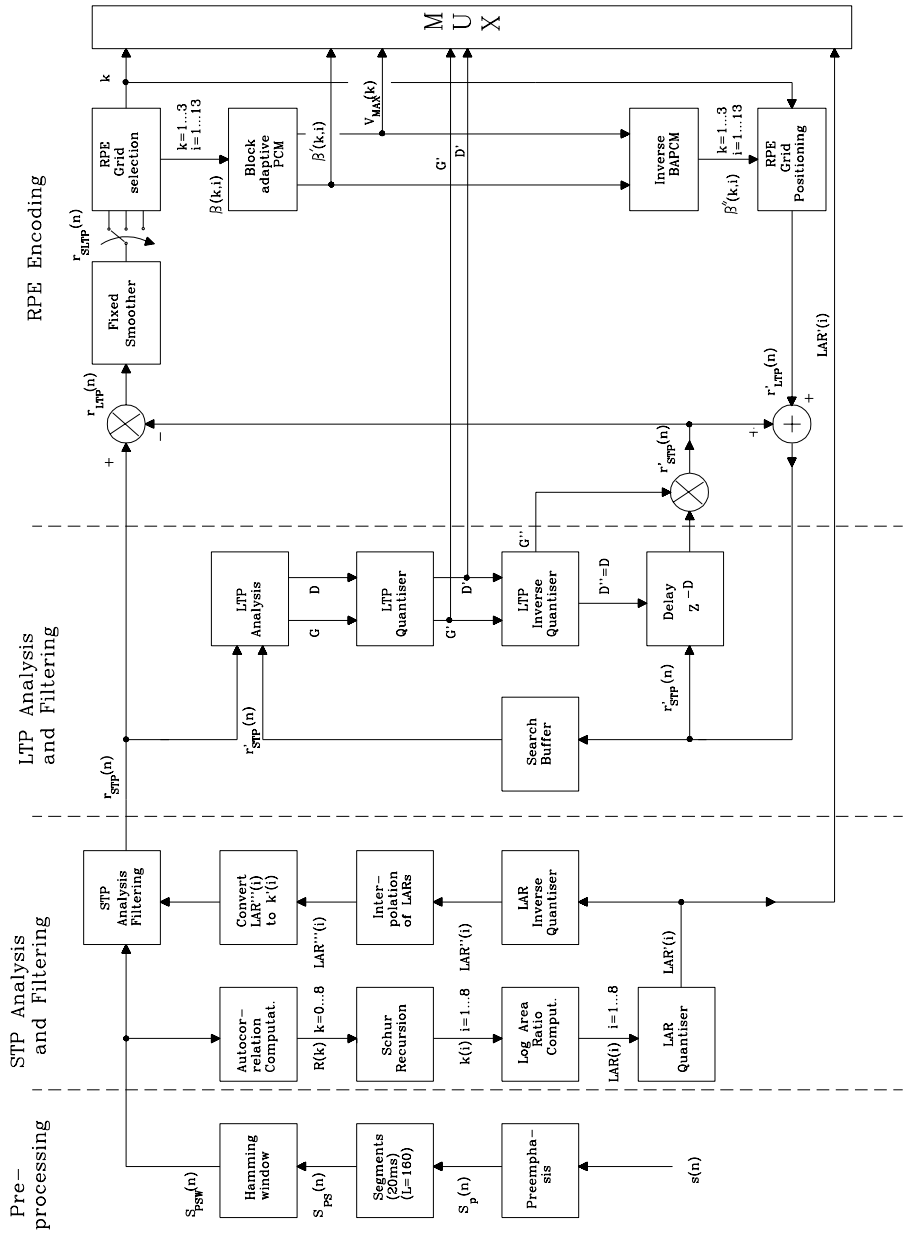

Figure 5.1: Block-diagram of the RPE-LTP encoder.

5.2.2 STP Analysis Filtering

For each segment of $L = 160$ samples, nine autocorrelation coefficients $R(k)$ are computed from $s_{psw}(n)$ by

$$R(k) = \sum_{n=0}^{L-1-k} s_{psw}(k)s_{psw}(n+k), \quad k = 0, \ldots, 8. \tag{5.32}$$

From the speech autocorrelation coefficients $R(k)$, eight reflection coefficients k_i are computed according to the Schur-recursion [152], which is an equivalent method to the Durbin algorithm used for solving the LPC key equations to derive the reflection coefficients k_i, as well as the STP filter coefficients a_i. However, the Schur-recursion delivers the reflection coefficients k_i only. The reflection coefficients k_i are converted to logarithmic area ratios $\mathrm{LAR}(i)$, because the logarithmically companded LARs have better quantisation properties than the coefficients k_i:

$$\mathrm{LAR}(i) = \log_{10}\left(\frac{1+k(i)}{1-k(i)}\right), \tag{5.33}$$

where a piecewise linear approximation with five segments is used to simplify the real-time implementation:

$$\mathrm{LAR}'(i) = \begin{cases} k(i) & \text{if } 0|k(i)| < 0.675 \\ \mathrm{sign}[k(i)][2|k(i)| - 0.675] & \text{if } 0.675 < |k(i)| < 0.95 \\ \mathrm{sign}[k(i)][8|k(i)| - 6.375] & \text{if } 0.975 < |k(i)| < 1.0. \end{cases} \tag{5.34}$$

The various $\mathrm{LAR}(i), i = 1, \ldots, 8$, filter parameters have different dynamic ranges and differently shaped PDFs, as we have seen in Chapter 4. This justifies the allocation of 6, 5, 4 and 3 bits to the first, second, third and fourth pairs of LARs, respectively. The quantised $\mathrm{LAR}(i)$ coefficients $\mathrm{LAR}'(i)$ are locally decoded into the set $\mathrm{LAR}''(i)$, as well as transmitted to the speech decoder. So as to mitigate the abrupt changes in the nature of the speech signal envelope around the STP analysis frame edges, the LAR parameters are linearly interpolated, and towards the edges of an analysis frame the interpolated $\mathrm{LAR}'''(i)$ parameters are used. Now the locally decoded reflection coefficients $k'(i)$ are computed by converting $\mathrm{LAR}'''(i)$ back into $k'(i)$, which are used to compute the STP residual $r_{\mathrm{STP}}(n)$ in a so-called PARCOR (partial correlation) structure. The PARCOR scheme directly uses the reflection coefficients $k(i)$ in order to compute the STP residual $r_{\mathrm{STP}}(n)$, and it constitutes the natural analogy to the acoustic tube model of human speech production.

5.2.3 LTP Analysis Filtering

As we have seen in Chapter 3, the LTP prediction error is minimised by that LTP delay D, which maximises the cross-correlation between the current residual $r_{\mathrm{STP}}(n)$ and its previously received and buffered history at delay D, i.e. $r_{\mathrm{STP}}(n-D)$. To be more specific, the $L = 160$ samples long STP residual $r_{\mathrm{STP}}(n)$ is divided into four $N = 40$ samples long subsegments, and for each of them one LTP is determined by computing the cross-correlation

between the presently processed sub-segment and a continuously sliding $N = 40$ samples long segment of the previously received 128 samples long STP residual segment $r_{\mathrm{STP}}(n)$. The maximum of the correlation is found at a delay D, where the currently processed sub-segment is the most similar to its previous history. This is most probably true at the pitch periodicity or at a multiple of the pitch periodicity. Hence the most redundancy can be extracted from the STP residual if this highly correlated segment is subtracted from it, multiplied by a gain factor G, which is the normalised cross-correlation found at delay D. Once the LTP filter parameters G and D have been found, they are quantised to give G' and D', where G is quantised only by two bits, while to quantise D' seven bits are sufficient.

The quantised LTP parameters (G', D') are locally decoded into the pair (G'', D'') so as to produce the locally decoded STP residual $r'_{\mathrm{STP}}(n)$ for use in the forthcoming sub-segments to provide the previous history of the STP residual for the search buffer, as shown in Figure 5.1. Observe that since D is integer, we have $D = D' = D''$. With the LTP parameters just computed the LTP residual $r_{\mathrm{LTP}}(n)$ is calculated as the difference of the STP residual $r_{\mathrm{STP}}(n)$ and its estimate $r''_{\mathrm{STP}}(n)$, which has been computed with the help of the locally decoded LTP parameters (G'', D) as

$$r_{\mathrm{LTP}}(n) = r_{\mathrm{STP}}(n) - r''_{\mathrm{STP}}(n) \tag{5.35}$$

$$r''_{\mathrm{STP}}(n) = G'' r'_{\mathrm{STP}}(n - D). \tag{5.36}$$

Here $r'_{\mathrm{STP}}(n - D)$ represents an already known segment of the past history of $r'_{\mathrm{STP}}(n)$, stored in the search buffer. Finally, the content of the search buffer is updated by using the locally decoded LTP residual $r'_{\mathrm{LTP}}(n)$ and the estimated STP residual $r''_{\mathrm{STP}}(n)$ to form $r'_{\mathrm{STP}}(n)$

$$r'_{\mathrm{STP}}(n) = r'_{\mathrm{LTP}}(n) + r''_{\mathrm{STP}}(n). \tag{5.37}$$

5.2.4 Regular Excitation Pulse Computation

The LTP residual $r_{\mathrm{LTP}}(n)$ is weighted with the fixed smoother, which is essentially a gracefully decaying band-limiting LP filter with a cutoff frequency of 4/3 kHz $= 1.33$ kHz according to a decimation by three about to be employed, as argued in Section 5.1. The impulse response of this filter was also given in Section 5.1. The smoothed LTP residual $r_{\mathrm{SLTP}}(n)$ is decomposed into three excitation candidates, by actually discarding the 40th sample of each sub-segment, since the three candidate sequences can host 39 samples only. Then the energies E1, E2, E3 of the three decimated sequences are computed, and the candidate with the highest energy is chosen to be the best representation of the LTP residual. The excitation pulses are afterwards normalised to the highest amplitude $v_{\max}(k)$ in the sequence of the 13 samples, and they are quantised by a three-bit uniform quantiser, whereas the logarithm of the block maximum $v_{\max}(k)$ is quantised with six bits. According to three possible initial grid positions k, two bits are needed to encode the initial offset of the grid for each sub-segment. The pulse amplitudes $\beta(k, i)$, the grid positions k and the block maxima $v_{\max}(k)$ are locally decoded to give the LTP residual $r'_{\mathrm{LTP}}(n)$, where the 'missing pulses' in the sequence are filled with zeros.

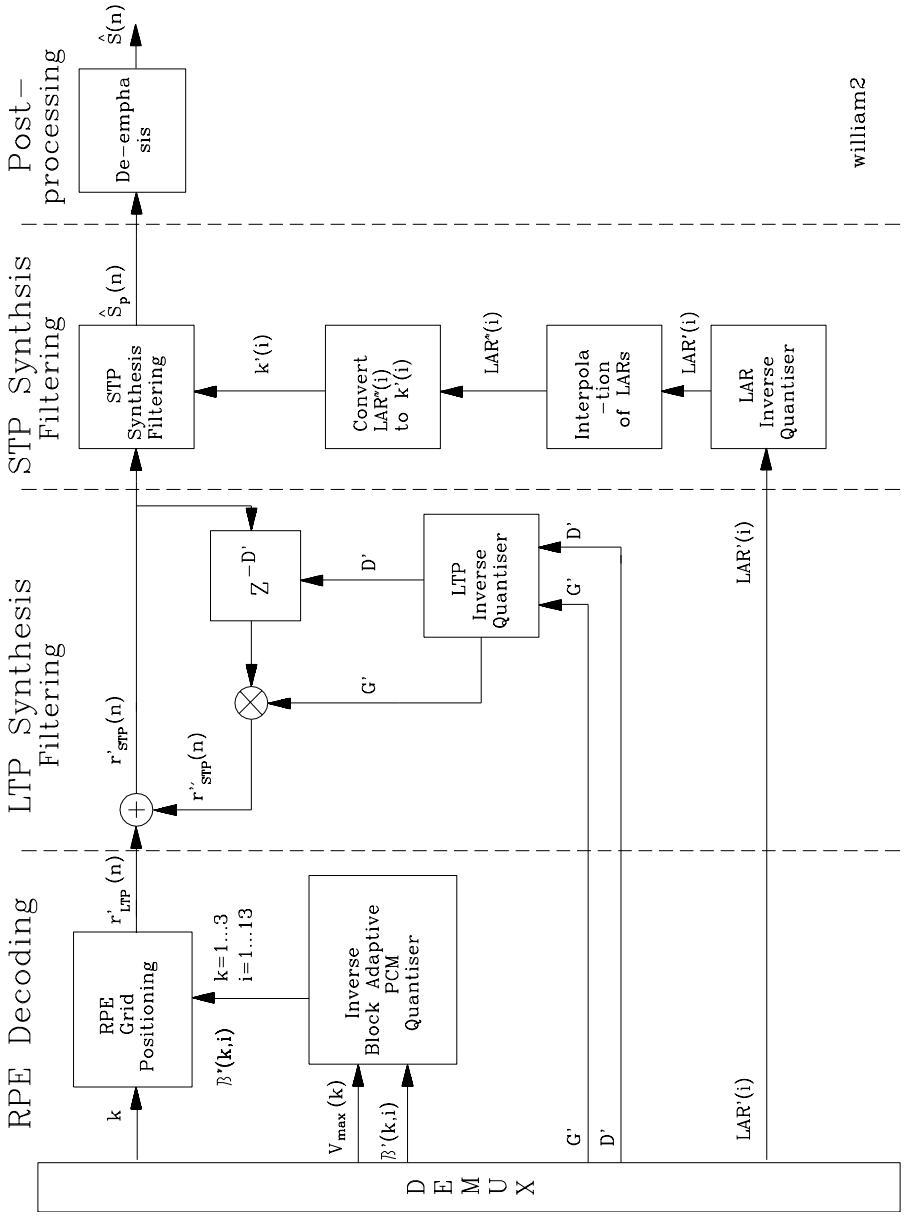

Figure 5.2: Block-diagram of the RPE-LTP decoder.

5.3 The 13 kbps RPE-LTP GSM Speech Decoder

The block-diagram of the RPE-LTP decoder is shown in Figure 5.2, which exhibits an inverse structure, constituted by the functional parts of: (1) RPE decoding; (2) LTP synthesis filtering; (3) STP synthesis filtering; (4) post-processing.

RPE decoding. In the decoder the grid position k, the sub-segment excitation maxima $v_{\max}(k)$ and the excitation pulse amplitudes $\beta'(k,i)$ are inverse quantised, and the actual pulse amplitudes are computed by multiplying the decoded amplitudes with their corresponding block maxima. The LTP residual model $r'_{\rm LTP}(n)$ is recovered by properly positioning the pulse amplitudes $\beta(k,i)$ according to the initial offset k.

LTP synthesis filtering. Firstly the LTP filter parameters (G', D') are inverse quantised to derive the LTP synthesis filter. Then the recovered LTP excitation model $r'_{\rm LTP}(n)$ is used to excite this LTP synthesis filter (G', D') to recover a new subsegment of length $N = 40$ of the estimated STP residual $r'_{\rm STP}(n)$. To do so, the past history of the recovered STP residual $r'_{\rm STP}(n)$ is used, properly delayed by D' samples and multiplied by G' to deliver the estimated STP residual $r''_{\rm STP}(n)$

$$r''_{\rm STP}(n) = G' r'_{\rm STP}(n - D'), \tag{5.38}$$

and then $r''_{\rm STP}(n)$ is used to compute the most recent sub-segment of the recovered STP residual

$$r'_{\rm STP}(n) = r''_{\rm STP}(n) + r'_{\rm LTP}(n). \tag{5.39}$$

STP synthesis filtering. In order to compute the synthesised speech $\hat{s}(n)$ the PARCOR synthesis is used, where – similar to STP analysis filtering – the reflection coefficients $k(i) i = 1, \ldots, 8$, are required. The $\mathrm{LAR}'(i)$ parameters are decoded by using the LAR inverse quantiser to give $\mathrm{LAR}''(i)$, which are again linearly interpolated towards the analysis frame edges between parameters of the adjacent frames to prevent abrupt changes in the character of the speech spectral envelope. Finally, the interpolated parameter set is transformed back into reflection coefficients, where filter stability is guaranteed, if recovered reflection coefficients, which fell outside the unit circle are reflected back into it, by taking their reciprocal values. The inverse formula to convert $\mathrm{LAR}(i)$ back into $k(i)$ is

$$k(i) = \frac{10^{\mathrm{LAR}(i)} - 1}{10^{\mathrm{LAR}(i)} + 1}. \tag{5.40}$$

Post-processing is constituted by the de-emphasis, using the inverse of the filter $H(z)$ in Equation (5.30).

The RPE-LTP bit allocation scheme is summarised in Table 5.1 for a period of 20 ms, which is equivalent to the encoding of $L = 160$ samples, while the detailed bit-by-bit allocation is given in the GSM Standard [97].

The 260 bits derived have to be reordered according to their subjective importances before error correction coding, as proposed by GSM, and classified into categories of Class 1a, Class 1b and Class 2 in descending order of prominence to facilitate a three-level error protection scheme. We note that the true sensitivity order has to be based on subjective tests. Objective bit-sensitivity analysis based on a combination of segmental signal-to-noise ratios

Table 5.1: Summary of the RPE-LTP bit-allocation scheme.

Parameter to be encoded	No. of bits
8 STP LAR coefficients	36
4 LTP gains G	$4 \times 2 = 8$
4 LTP delays D	$4 \times 7 = 28$
4 RPE grid positions	$4 \times 2 = 8$
4 RPE block maxima	$4 \times 6 = 24$
$4 \times 13 = 52$ pulse amplitudes	$52 \times 3 = 156$
Total number of bits per 20 ms	260
Transmission bitrate	13 kbps

and cepstrum distance measures, as defined in Chapter 18, results in a similar significance order [153]. During our experiments we also designed a modified version of the standard scheme [153, 154], since we found that when using LSF instead of the standardised LARs we obtained a slightly better performance, while encoding them using 36 bits. This is mainly due to their so-called ordering property, as we discussed in Chapter 4, implying that the LSF parameters are monotonically increasing with increasing parameter index. This property allows the detection of channel errors that violate the ordering property and the speech quality can be improved by LSF extrapolation invoked over consecutive frames. A further difference in this modified RPE-LTP codec was that we used four bits to encode the LTP gain instead of the standard two bits, which resulted in a speech quality improvement. Therefore the total number of bits was 268 per 20 ms frame and the overall bitrate was increased to 13.4 kbps. The final bit allocation scheme of the 13.4 kbps RPE-LTP codec is summarised in Table 5.2.

Table 5.2: 13.4 kbps RPE codec bit allocation.

Parameter	Bit no.	Bitpos. in frame
8 LSFs	36	1–36
RPE gridpos.	2	37,38
Block max.	6	39–44
RPE exc. pulses	$13 \times 3 = 39$	45–83
LTP delay (LTPD)	7	84–90
LTP gain (LTPG)	4	91–94
Per sub-segment	58	
Total bitrate: $36 + 4 \times 58 = 268/20$ ms $= 13.4$ kbps		

In comparison, the 32 kbps ADPCM waveform codec has a segmental SNR (SSNR) of about 28 dB, while the 13 kbps AbS RPE-LTP codec has a lower SSNR of about 16 dB, associated with similar subjective quality rated as a MOS of about four. This discrepancy in SSNR is because the RPE-LTP codec utilises perceptual error weighting. The cost of the

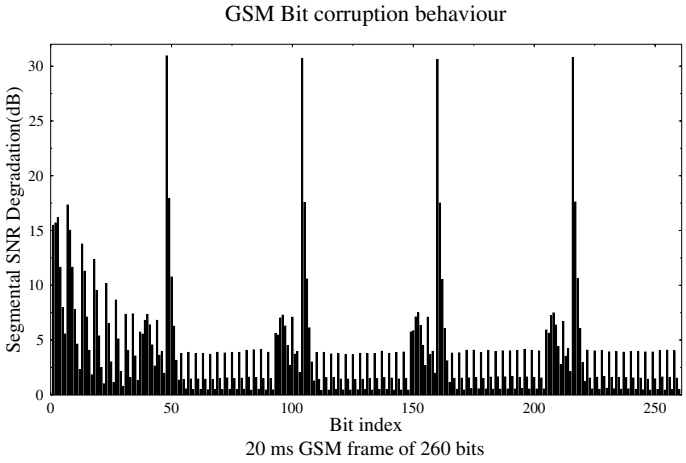

Figure 5.3: Bit-sensitivity in the 260-bit, 20 ms RPE-LTP GSM speech frame.

RPE-LTP codec's significantly lower bitrate and higher robustness compared to ADPCM is its increased complexity and encoding delay. In the next section we consider the bit-sensitivity issues of this codec.

5.4 Bit-sensitivity of the 13 kbps GSM RPE-LTP Codec

The bit allocation of the standard GSM speech codec was summarised in Table 5.1, while the sensitivity of each bit in the 260-bit, 20 ms frame is characterised by Figure 5.3. This figure provides an overview of the SEGSNR degradation inflicted by consistently corrupting one out of the 260 bits of each frame, while keeping the others in the frame intact. This technique masks the effects of error propagation across frame boundaries, since instead of quantifying this potential degradation over a number of consecutive frames, over which it results in observable SEGSNR degradation, the bit concerned is corrupted in each frame. Nonetheless, due to its simplicity and adequate accuracy, this technique is often used in practice.

Observe in Figure 5.3 that the repetitive structure reflects the periodicity due to the four 5 ms, 40-sample excitation optimisation subsegments, while the left-hand side section corresponds to the 36 LAR coefficients. Focusing more closely on the sensitivity of these LAR bits, the MSB to LSB hierarchy is clearly recognised in Figure 5.4. Furthermore, the higher-order LARs, corresponding to the last stages of the acoustic tube model of the vocal tract are less important and, accordingly, exhibit a lower sensitivity. This is also reflected by the fact that the first, second, third and fourth pairs of LARs are allocated 6, 5, 4 and 3 bits, respectively. Since the LAR coefficients are re-computed each 20 ms, despite mild error propagation due to LAR-interpolation between consecutive frames their corruption is not as detrimental as that of the excitation pulse block maxima seen in Figure 5.5.

By observing Figure 5.5 we note that the MSB–LSB structure of the block maximum bits and normalised excitation pulse magnitude bits is conspicuous. Again, these bits do not

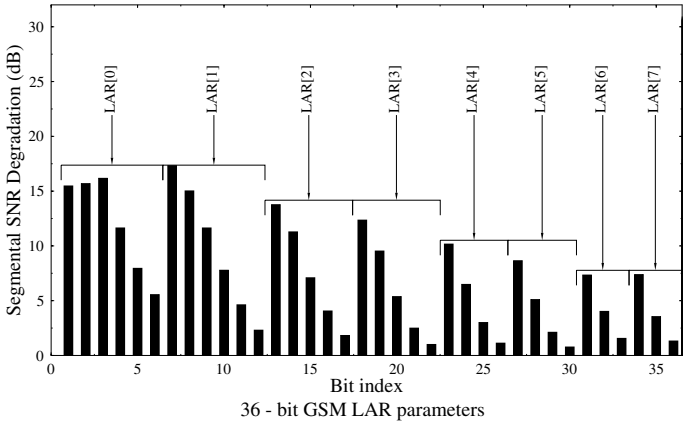

Figure 5.4: Bit-sensitivity of the LARs in the 260-bit, 20 ms RPE-LTP GSM speech frame.

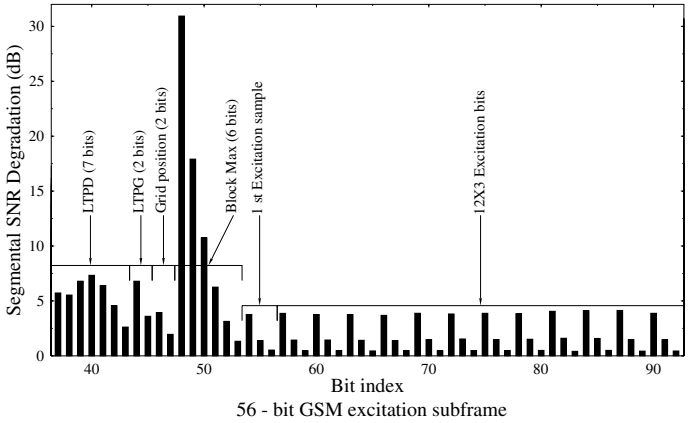

Figure 5.5: Bit-sensitivity of the excitation subsegment in the 260-bit, 20 ms RPE-LTP GSM speech frame.

result in serious error propagation. This is not true for the long-term predictor delay (LTPD) and long-term predictor gain (LTPG) bits, whose sensitivity in practice is more critical, when taking into account the associated error propagation effects.

Having portrayed the concept and algorithmic details of RPE codecs and described their most important representative, namely the 13 kbps GSM codec, in the next section we consider a reconfigurable, tool-box based speech transceiver and its performance.

5.5 Application Example: A Tool-box Based Speech Transceiver [155]

In the comparative study [155] Williams *et al.* presented simulation results giving BER, bandwidth occupancy and an estimate of complexity for 4 bit/symbol 16-Star QAM modems

in order to characterise the potential of an ambitious multi-level system, that of a 2 bit/symbol $\pi/4$-shifted differential quadrature phase-shift keying ($\pi/4$-DQPSK) modems, since they are used in the Pan-American IS-54 [156] and the Japanese JDC [157] systems as well as binary Gaussian minimum-shift keying (GMSK) modems. Packet reservation multiple access (PRMA) was used, since it provided substantial improvements over Time Division Multiple Access (TDMA) in terms of the number of users supported.

Specifically, GMSK [158], $\pi/4$-DQPSK and 16-Star QAM modems [159] were used. These transmission schemes were combined with the unprotected low-complexity 32 kbps ADPCM codec, as in the DECT system, the Japanese Handyphone system, known as PHS and in the British CT2 system. Furthermore, the same modems were also combined with the 13 kbps RPE-LTP GSM codec and a twin-class forward error correcting (FEC). Each modem had the option of either a low- or a high-complexity demodulator. The high-complexity demodulator for the GMSK modem was a maximum likelihood sequence estimator based on the Viterbi algorithm [93], while the low complexity one was a frequency discriminator. For the two multilevel modems either low complexity non-coherent differential detection or a maximum likelihood correlation receiver (MLH-CR) was invoked. Synchronous transmissions and perfect channel estimation were used in evaluating the relative performances of the systems listed in Table 5.3. Our results represent performance upper bounds, allowing relative performance comparisons under identical circumstances.

The system performances applied to microcellular conditions. The carrier frequency was 2 GHz, the data rate 400 kBd, and the mobile speed 15 m/s. At 400 kBd in microcells the fading is flat and usually Rician. The best and worst Rician channels are the Gaussian and Rayleigh fading channels, respectively, and we performed our simulations for these channels to obtain upper- and lower-bound performances. Our conditions of 2 GHz, 400 kBd and 15 m/s are arbitrary. They correspond to a fading pattern that can be obtained for a variety of different conditions, for example, at 900 MHz, 271 kBd and 23 m/s. The performance of the various systems is summarised in Table 5.3.

Returning to Table 5.3, the first column shows the system classification letter, the next the modulation used, the third the demodulation scheme employed, the fourth the FEC scheme and the fifth the speech codec employed. The sixth column gives the estimated relative order of the complexity of the schemes, where the most complex one having a complexity parameter of 12 is the 16-Star QAM, MLH-CR, Bose–Chaudhuri–Hocquenghem (BCH), RPE-LTP arrangement. All the BCH-coded RPE-LTP schemes have complexity parameters larger than six, while the unprotected ADPCM systems are characterised by values of one to six, depending on the complexity of the modem used. The speech Baud rate and the TDMA user bandwidth are given next.

An arbitrary signalling rate of 400 kBd was chosen for all our experiments, irrespective of the number of modulation levels, in order to provide a fair comparison for all the systems under identical propagation conditions. Again, these propagation conditions can be readily converted to arbitrary Bd-rates upon scaling the vehicular speed appropriately. The 400 kBd systems have a total bandwidth of $400/1.35 = 296$ kHz, $2 \cdot 400/1.62 = 494$ kHz and $4 \cdot 400/2.4 = 667$ kHz, respectively. When computing the user bandwidth requirements we took account of the different bandwidth constraints of GMSK, $\pi/4$-DQPSK and 16-QAM, assuming an identical Baud rate.

In order to establish the speech performance of systems A–L (summarised in Table 5.3) their SEGSNR and cepstral distance (CD), both defined in Chapter 18, versus channel

Table 5.3: System parameters [155]. Copyright © IEEE, 1994, Williams *et al.*

1 Syst.	2 Modulator	3 Detector	4 FEC	5 Speech codec	6 Comp-lexity order	7 Baud rate (KBd)	8 TDMA user bandw. (kHz)	9 No. of TDMA users per carrier	10 No. of PRMA users per carrier	11 No. of PRMA users per slot	12 PRMA user bandw. (kHz)	13 Min SNR (dB) AWGN	14 Min SNR (dB) Rayleigh
A	GMSK	Viterbi	No	ADPCM	2	32	23.7	11	18	1.64	14.5	7	∞
B	GMSK	Freq. discr.	No	ADPCM	1	32	23.7	11	18	1.64	14.5	21	31
C	$\pi/4$-DQPSK	MLH-CR	No	ADPCM	4	16	19.8	22	42	1.91	10.4	10	28
D	$\pi/4$-DQPSK	differential	No	ADPCM	3	16	19.8	22	42	1.91	10.4	10	28
E	16-StQAM	MLH-CR	No	ADPCM	6	8	13.3	44	87	1.98	6.7	20	∞
F	16-StQAM	differential	No	ADPCM	5	8	13.3	44	87	1.98	6.7	21	31
G	GMSK	Viterbi	BCH	RPE-LTP	8	24.8	18.4	12	22	1.83	10.1	1	15
H	GMSK	Freq. discr.	BCH	RPE-LTP	7	24.8	18.4	12	22	1.83	10.1	8	18
I	$\pi/4$-DQPSK	MLH-CR	BCH	RPE-LTP	10	12.4	15.3	24	46	1.92	8	5	20
J	$\pi/4$-DQPSK	differential	BCH	RPE-LTP	9	12.4	15.3	24	46	1.92	8	6	18
K	16-StQAM	MLH-CR	BCH	RPE-LTP	12	6.2	10.3	48	96	2.18	4.7	13	25
L	16-StQAM	differential	BCH	RPE-LTP	11	6.2	10.3	48	96	2.18	4.7	16	24

GMSK: Gaussian minimum-shift keying
$\pi/4$-DQPSK: differential phase-shift keying
16-StQAM: 16-level quadrature amplitude modulation
MLH-CR: Maximum likelihood correlation receiver
BCH: Bose Chaudhuri Hocquenghem FEC coding
ADPCM: Adaptive differential pulse code modulation
RPE-LTP: Regular pulse excited speech codec with long-term prediction
TDMA: Time division multiple access
PRMA: Packet reservation multiple access

SNR characteristics were evaluated. These experiments yielded 24 curves for AWGN, and 24 curves for Rayleigh fading channels, constituting the best and worst case channels, respectively. Then for the twelve different systems and two different channels we derived the minimum required channel SNR value for near-unimpaired speech quality in terms of both CD and SEGSNR. These values are listed in columns 13 and 14 of Table 5.3.

We note, that the bandwidth efficiency gains tabulated are reduced in signal-to-interference ratio-limited scenarios due to the less dense frequency reuse of multilevel modems [73]. Nevertheless, multilevel modulation schemes result in higher PRMA gains than their lower level counterparts.

5.6 Chapter Summary

In this chapter the family of RPE speech codecs was characterised. RPE codecs are historically important, since they constitute the first AbS codec employed in a public mobile radio system. While the AbS coding principle relies on a closed-loop assisted excitation optimisation, the 13 kbps GSM speech codec is strictly speaking an open-loop excitation optimisation assisted codec, striking a good trade-off between speech quality and implementational complexity. In this chapter we also provided some discussions on the bit-sensitivity issues and transmission aspects of a mobile radio system transmitting over fading mobile channels.

Having characterised the family of RPE speech codecs, let us now focus our attention on another prominent class of AbS codecs referred to as code excited linear predictive (CELP) schemes.

Chapter 6

Forward-Adaptive Code Excited Linear Prediction

6.1 Background

Since Schroeder and Atal suggested the basic CELP codec in 1985 [16] it went through a quick evolution and has developed into the most prominent speech codec over a wide bitrate range from 4.18–16 kbps. The original CELP codec was a *forward-adaptive* predictive scheme, requiring the transmission of spectral envelope and spectral fine-structure information to the decoder. In order to maintain a low bitrate, while using about 36 bits per LPC analysis frame for scalar short-term spectral quantisation, the framelength was constrained to be in excess of 20 ms. Then the associated channel capacity requirement becomes 36 bits/20 ms = 1.8 kbps and even upon extending the framelength to 30 ms, 1.2 kbps has to be allocated to the LPC coefficients. When using an ingenious so-called split vector-quantisation scheme, Salami *et al.* [147, 160] succeeded in reducing the forward-adaptive frame-length and delay to 10 ms, which is an important advance in the state-of-the-art. They used 18 bits/10 ms LPC analysis frame and the associated coefficients were invoked for the second of its two 5 ms excitation optimisation subframes, while those for the first one were inferred by interpolating the two adjacent subframes' LSF parameters. This scheme was discussed in Chapter 4 and will be discussed also in the context of the 8 kbps CCITT G.729 10 ms delay codec in Section 7.8.

The CCITT G.728 Standard codec [109] also employs a CELP-type excitation, but its philosophy has moved substantially from the original CELP concept in many respects. Firstly, constrained by the low-delay requirement of 2 ms, forward-adapted LPC analysis was not a realistic option for the design team at AT&T. Hence, backward-adaptive prediction was employed, recovering the LPC coefficients from previously decoded speech segments. This was possible at 16 kbps, since the decoded speech quality was very good and hence the quantisation effects did not inflict serious speech degradation, which would have led to precipitated error propagation. In fact, we showed experimentally that the effect of using past decoded speech, rather than the current unencoded speech for LPC analysis manifested

Voice and Audio Compression for Wireless Communications Second Edition
L. Hanzo, F. C. A. Somerville and J. P. Woodard

itself more adversely due to the inherent time-lag, rather than due to quantisation effects. Therefore a frequent LPC filter coefficient update was necessary, which was essentially only restricted by the codec's complexity, but did not have any ramifications as regards to the bitrate. Specifically, an LPC update interval of 20 samples or 2.5 ms was found acceptable in terms of complexity, when using a high filter order of 50.

A second significant deviation from the original CELP principle is that the choice of the above exceptionally high filter order was justified by a strong preference for avoiding the employment of a LTP. This was justified by the argument that the LTP would only have been realistic in terms of frequent up-dates without the requirement of added channel capacity, that is if it was a backwards-adaptive LTP, which is sensitive against channel errors due to its long-term memory, re-implanting previous transmission error effects in the adaptive codebook. The presence of a LTP constitutes a particular problem, for example, in packet networks, where the loss of a transmission cell would inflict a long-term speech degradation. The LPC filter order of 50 can remove long-term speech periodicities of up to $50 \times 0.125\,\mathrm{ms} = 6.25\,\mathrm{ms}$, catering for the pitch-periodicities of female speakers having pitch frequencies as low as 160 Hz, for whom LTPs have a typically substantial conducive effects. Thirdly, instead of the original 1024 40-sample, 5 ms random vectors, the G.728 codec uses a smaller 128-entry, 5-sample, 0.625 ms codebook filled with trained, rather than stochastic entries. These measures were introduced with reduced implementational complexity, robustness against channel errors, high speech quality and potential frame-loss in transmission networks in mind.

Over the years there have also been a number of attractive wideband CELP-based coding schemes, endeavouring to provide improved intelligibility and naturalness using 16 kHz-sampled 7 kHz-bandwidth speech signals. In some proposals a split-band CELP codec was advocated, which allowed greater flexibility in terms of controlling and localizing the frequency-domain effects of quantisation noise [161], while maintaining as low a bitrate as 16 kbps. This codec had a similar performance to the CCITT G.722 Standard sub-band-ADPCM codec at 48 kbps [146]. Laflamme *et al.* [162] and Salami *et al.* [163] proposed full-band wideband CELP codecs using vast codebooks combined with focussed search, in order to reduce the associated implementational complexity, while maintaining bitrates of 16 and 9.6 kbps, respectively. Unfortunately, it is unknown whether, for example, either of the above 16 kbps wideband codecs perceptually outperformed the 16 kbps narrowband G.728 codec. Following the above brief overview of the advantages and disadvantages of the various CELP codecs let us now dedicate the rest of this chapter to the classic Schroeder–Atal forward-adaptive codec [16]. The above-mentioned trade-offs and issues will be revisited in depth during our further discussions.

A plethora of computationally efficient approaches has been proposed in order to reduce the excessive complexity of the original CELP codec and ease its real-time implementation. A comprehensive summary of these algorithmic details has been published by Salami *et al.* [70, 71], Kondoz [55], etc. Here we give a rudimentary description of CELP coding.

6.2 The Original CELP Approach

In CELP codecs a Gaussian process having a slowly varying power spectrum is used for representing or modelling the prediction residual signal after short-term and long-term prediction. The synthetic speech waveform is generated by filtering Gaussian distributed

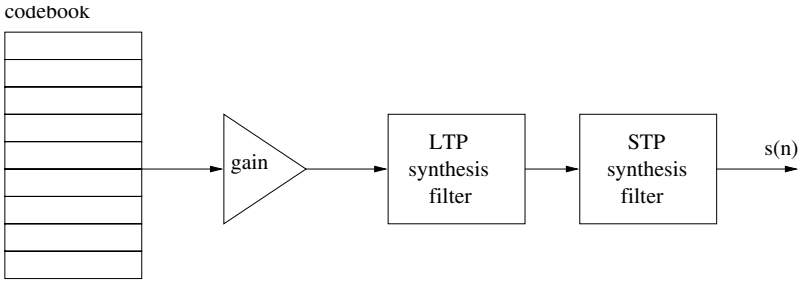

Figure 6.1: Simplified CELP codec schematic.

excitation vectors stored in a read-only memory through the slowly time-varying linear LTP synthesis or pitch synthesis filter and the LPC synthesis filters, as seen in Figure 6.1. This schematic mimics the previously detailed AbS speech codec structures portrayed in Figures 3.7 and 3.8, the only difference is again that the random excitation is pre-stored in a memory.

Specifically, in the original CELP codec [16], Gaussian distributed zero-mean, unit-variance random excitation vectors of dimension $N = 40$ were stored in a codebook of 1024 entries and the optimum excitation sequence was determined by the exhaustive search of the excitation codebook. This scheme essentially followed the schematic of Figure 3.8, where in contrast to the regularly spaced decimated prediction residual of the RPE codec, the excitation generator was constituted by a fixed stochastic codebook and the long-term predictor's schematic was made explicit.

As argued before, in state-of-the-art high-quality CELP codecs the majority of information to be transmitted to the decoder is determined in a closed-loop fashion so that the signal reconstructed by the decoder is perceptually as close as possible to the original speech. Full closed-loop optimisation of all the codec parameters is usually unrealistic in terms of real-time implementations, but we will attempt to document the range of complexity, speech quality, robustness and delay trade-offs. The adaptive codebook-based schematic of CELP codecs is shown in Figure 6.2, which explicitly reflects the closed-loop optimised LTP principle in contrast to Figure 6.1. The adaptive codebook-based schematic differs from the general AbS codec structure shown in Figure 3.8 and from its CELP-oriented interpretation given in Figure 6.1. Here the excitation signal $u(n)$ is given by the sum of the outputs from two codebooks. The adaptive codebook is used to model the long-term periodicities present in voiced speech, while the fixed codebook models the random noise-like residual signal which remains after both long- and short-term prediction. Recall that the difference between Figures 3.1 and 3.8 was that the error weighting filter of Figure 3.1 had been moved so that the input speech signal $s(n)$ and the reconstructed speech signal $\hat{s}(n)$ are both separately weighted before their difference is found. This is permissible because of the linear nature of the weighting filter, and is done because it makes the determination of the codebook parameters less complex. With a synthesis filter of the form $1/A(z)$, and an error weighting filter $A(z)/A(z/\gamma)$, we arrive at the schematic of Figure 6.2. The filter $1/A(z/\gamma)$ in the encoder is referred to as the *weighted synthesis filter* – when fed with an excitation signal it produces a weighted version $\hat{s}_w(n)$ of the reconstructed speech $\hat{s}(n)$.

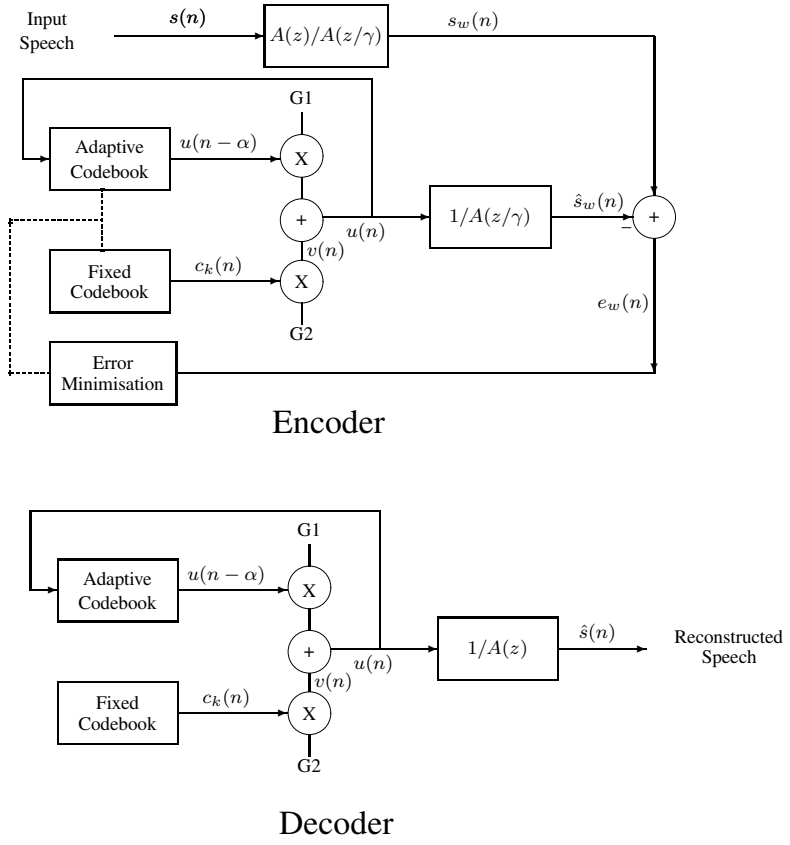

Figure 6.2: Adaptive codebook assisted CELP codec structure.

In this chapter we consider only systems in which forward-adaptive filtering is used. For such systems the input speech is split up into frames for processing, where a frame is of the order of 20 ms long. The frames are usually further divided into sub-frames, with around 4 sub-frames per frame. The short-term synthesis filter coefficients are determined and transmitted once per frame, while the adaptive and fixed codebook parameters are updated once per sub-frame. The 4.7 kbps codec we have simulated has a frame length of 30 ms with 4 sub-frames of 7.5 ms each, while our 7.1 kbps codec has a frame length of 20 ms with 5 ms long sub-frames.

The encoding procedure generally takes place in three stages. First the coefficients of the short-term synthesis filter $1/A(z)$ are determined for the frame by minimising the residual energy obtained when the input speech is passed through the inverse filter $A(z)$. Then for each sub-frame, first the adaptive and then the fixed codebook parameters are calculated using a closed-loop approach. The determination of the synthesis filter was detailed in Section 2.3, its quantisation was addressed in Chapter 4, while the computation of the closed-loop optimised adaptive codebook entry in Section 3.4.2. Let us therefore concentrate our attention in the next section on the fixed codebook-search.

6.3 Fixed Codebook Search

In the final stage of its calculations the coder finds the fixed codebook index and gain which minimise E_w. Following Salami *et al.* [70, 71] and taking the fixed codebook contribution into account, which was ignored in the last section, we arrive at

$$\begin{aligned} e_w(n) &= s_w(n) - \hat{s}_w(n) \\ &= s_w(n) - (\hat{s}_o(n) + G_1 y_\alpha(n)) - G_2 c_k(n) * h(n) \\ &= \tilde{x}(n) - G_2 c_k(n) * h(n), \end{aligned} \tag{6.1}$$

where

$$\tilde{x}(n) = s_w(n) - \hat{s}_o(n) - G_1 y_\alpha(n) \tag{6.2}$$

is the target for the fixed codebook search, $c_k(n)$ is the codeword from the fixed codebook and G_2 is the fixed codebook gain. Thus

$$\begin{aligned} E_w &= \frac{1}{N} \sum_{n=0}^{N-1} e_w^2(n) \\ &= \frac{1}{N} \sum_{n=0}^{N-1} (\tilde{x}(n) - G_2[c_k(n) * h(n)])^2. \end{aligned} \tag{6.3}$$

Setting $\partial E_w / \partial G_2 = 0$ gives the optimum gain for a given codeword $c_k(n)$ as

$$\begin{aligned} G_2 &= \frac{\sum_{n=0}^{N-1} \tilde{x}(n)[c_k(n) * h(n)]}{\sum_{n=0}^{N-1} [c_k(n) * h(n)]^2} \\ &= \frac{\tilde{C}_k}{\xi_k}, \end{aligned} \tag{6.4}$$

where

$$\tilde{C}_k = \sum_{n=0}^{N-1} \tilde{x}(n)[c_k(n) * h(n)] \tag{6.5}$$

and

$$\xi_k = \sum_{n=0}^{N-1} [c_k(n) * h(n)]^2. \tag{6.6}$$

Physically, ξ_k is the energy of the filtered codeword and $\tilde{C}_k$ is the correlation between the target signal $\tilde{x}(n)$ and the filtered codeword. In the search for the fixed codebook parameters the values of ξ_k and $\tilde{C}_k$ are calculated for every codeword k and the optimum gain for that codeword is calculated using Equation (6.4). The gain is quantised to give $\hat{G}_2$, which is substituted back into Equation (6.3) to give

$$E_w = \frac{1}{N} \sum_{n=0}^{N-1} \left(\tilde{x}(n) - \hat{G}_2[c_k(n) * h(n)] \right)^2$$

$$= \frac{1}{N}\left(\sum_{n=0}^{N-1}\tilde{x}^2(n) - 2\hat{G}_2\sum_{n=0}^{N-1}\tilde{x}(n)[c_k(n)*h(n)] + \hat{G}_2^2\sum_{n=0}^{N-1}[c_k(n)*h(n)]^2\right)$$

$$= \frac{1}{N}\left(\sum_{n=0}^{N-1}\tilde{x}^2(n) - 2\hat{G}_2\tilde{C}_k + \hat{G}_2^2\xi_k\right). \tag{6.7}$$

The term $T_k = \hat{G}_2(2\tilde{C}_k - \hat{G}_2\xi_k)$ is calculated for every codeword and the index which maximises it is chosen. This index along with the quantised gain is then sent to the decoder.

Traditionally, the major part of a CELP coder's complexity comes from calculating the energy ξ_k of the filtered codeword, and the correlation $\tilde{C}_k$ between the target signal $\tilde{x}(n)$ and the filtered codeword for every codebook entry. From Equations (6.5) and (6.6) these are given by

$$\begin{aligned}\tilde{C}_k &= \sum_{n=0}^{N-1}\tilde{x}(n)[c_k(n)*h(n)] \\ &= \sum_{n=0}^{N-1}\psi(n)c_k(n)\end{aligned} \tag{6.8}$$

and

$$\begin{aligned}\xi_k &= \sum_{n=0}^{N-1}[c_k(n)*h(n)]^2 \\ &= \sum_{i=0}^{N-1}c_k^2(i)\phi(i,i) + 2\sum_{i=0}^{N-2}\sum_{j=i+1}^{N-1}c_k(i)c_k(j)\phi(i,j),\end{aligned} \tag{6.9}$$

where

$$\begin{aligned}\psi(i) &= \tilde{x}(i)*h(-i) \\ &= \sum_{n=i}^{N-1}\tilde{x}(n)h(n-i), \quad \text{for } i = 0,\ldots,N-1\end{aligned} \tag{6.10}$$

and

$$\phi(i,j) = \sum_{n=\max(i,j)}^{N-1}h(n-i)h(n-j), \quad \text{for } i,j = 0,\ldots,N-1. \tag{6.11}$$

The functions $\psi(i)$ and $\phi(i,j)$ can be calculated once per sub-frame, but then ξ_k and $\tilde{C}_k$ must be calculated for each codeword. This involves a large number of additions and multiplications by the elements of $c_k(n)$. Several schemes, for example *binary pulse excitation* [135] and *transformed binary pulse excitation* (TBPE) were proposed by Salami *et al*. [71] and *vector sum excited linear prediction* (VSELP) by Gerson and Jasiuk [164] in order to simplify these calculations. Typically, CELP codecs use codebooks where most of the entries $c_k(n)$ are zero, which are referred to as *sparse codebooks*, thus greatly reducing

the number of additions necessary to find ξ_k and $\tilde{C}_k$. Furthermore, if the non-zero elements of the codebook are equal to $+1$ or -1 then no multiplications are necessary and $\tilde{C}_k$ and ξ_k can be calculated by a series of additions and subtractions. Having highlighted the fixed codebook search procedure of CELP codecs, in our next section we will elaborate on the choice of the specific CELP excitation model.

6.4 CELP Excitation Models

6.4.1 Binary-pulse Excitation

Instead of choosing the excitation pulses in a sparse excitation vector from a Gaussian random process, the pulses can be randomly chosen to be either -1 or 1 without any perceived deterioration in the quality of the CELP reconstructed speech. Using binary-pulse excitation vectors populated by the duo-binary values of -1 or 1, efficiently structured codebooks can be designed, where the codebook structure can be exploited to obtain fast codebook search algorithms [165, 166].

In a further step we will totally eliminate the codebook storage and its corresponding computationally demanding search procedure by utilising a very simple approach in computing the optimum positions of the duo-binary -1 or 1 excitation pulses. Assuming that M pulses are allocated over the excitation optimisation subsegment of N sample positions, the excitation vector is given by

$$u(n) = \sum_{i=1}^{M} b_i \delta(n - m_i), \quad \text{for } n = 0, \ldots, N-1, \tag{6.12}$$

where b_i represents the duo-binary pulse amplitudes taking values -1 or 1 and m_i are the pulse positions. Having M binary excitation pulses per N-sample excitation vector and assuming that their positions are known is equivalent to a codebook of size 2^M, but when they can be allocated to any arbitrary positions, the number of position combinations is given by $C_M^N = N!/((N-M)!M!)$. This approach has yielded a performance similar to that of the original CELP system with the advantage of having a very simple excitation determination procedure characterised by about 10 multiplications per speech sample.

Xydeas *et al.* [167] and Adoul *et al.* [168] have invoked a useful geometric representation of various CELP excitation codebooks, arguing that irrespective of their statistical distribution they result in similar perceptual speech quality. This is because they represent a vector quantiser, where all codebook entries populate the surface of a unit-radius N-dimensional sphere and 2^N is the maximum possible number of legitimate codebook entries on the sphere's surface. When assuming a sufficiently dense population of the sphere's surface, the subjective speech quality will be rather similar for different codebooks, although the coding complexity may vary enormously. In this vector quantiser each codebook entry constitutes a vector centroid, defining a particular subset of the full codebook. Taking into account the arbitrary positions of the pulses and assuming for the sake of illustration that there are 5 non-zero pulses, which can take any of the $N = 40$ positions, the total number of combinations in which these can be allocated is $C_5^4 0 = 40!/(35! \cdot 5!) = 658\,008$. Since the total number of

possible duo-binary excitations is $2^{40} \approx 1.1 \cdot 10^{12}$, on average there are about $2^{40}/658\,008 \approx 1.67 \cdot 10^6$ possible excitation vectors per actual excitation vectors.

6.4.2 Transformed Binary-pulse Excitation

6.4.2.1 Excitation Generation

The attraction of TBPE codecs when compared to CELP codecs accrues from the fact that the excitation optimisation can be achieved in a direct computation step. The sparse Gaussian excitation vector is assumed to take the form of

$$\mathbf{c} = \mathbf{A}\mathbf{b}, \tag{6.13}$$

where the binary vector $\mathbf{b}$ has M elements of ± 1, while the $M \cdot M$ matrix $\mathbf{A}$ represents an orthogonal transformation. Due to the orthogonality of $\mathbf{A}$ the binary excitation pulses of $\mathbf{b}$ are transformed into independent, unit variance Gaussian components of $\mathbf{c}$. The set of $2M$ binary excitation vectors gives rise to $2M$ Gaussian vectors of the original CELP codec.

Having found the optimum codebook gain G_2 given in Equation (6.4) the minimum mean square weighted error expression of Equation (6.3) can be expressed following Salami *et al.* [70, 71] as

$$E_{\min} = \sum_{n=0}^{N-1} x^2(n) - \frac{[\sum_{i=0}^{N-1} \psi(i) c_k(i)]^2}{\sum_{i=0}^{N-1} c_k^2(i)\phi(i,i) + 2\sum_{i=1}^{N-2}\sum_{j=i+1}^{N-1} c_k(i)c_k(j)\phi(i,j)}, \tag{6.14}$$

and upon using Equations (6.5) and (6.6) the above expression can be simplified as

$$E_{\min} = \sum_{n=0}^{N-1} x^2(n) - \frac{(\tilde{C}_k)^2}{\xi_k}, \tag{6.15}$$

where, again, most of the complexity of conventional CELP codecs is due to the computation of the energy ξ_k of the filtered codeword, and to the correlation $\tilde{C}_k$ between the target signal $\tilde{x}(n)$ and the filtered codeword, which must be evaluated for all codebook entries.

The direct excitation of the TBPE codec accrues from the matrix representation of Equation (6.14) using Equation (6.13), i.e.

$$E = \mathbf{x}^{\mathrm{T}}\mathbf{x} - \frac{(\mathbf{\Psi}^{\mathrm{T}}\mathbf{A}\mathbf{b})^2}{\mathbf{b}^{\mathrm{T}}\mathbf{A}^{\mathrm{T}}\mathbf{\Phi}\mathbf{A}\mathbf{b}}. \tag{6.16}$$

The denominator in Equation (6.16) is nearly constant over the entire codebook and hence plays practically no role in the excitation optimisation. This is due to the fact that the autocorrelation matrix $\mathbf{\Phi}$ is strongly diagonal, since the impulse response $h(n)$ decays sharply. Due to the orthogonality of $\mathbf{A}$ we have $\mathbf{A}^{\mathrm{T}}\mathbf{A} = \mathbf{I}$, where $\mathbf{I}$ is the identity matrix, causing the denominator to be constant.

Closer scrutiny of Equation (6.16) reveals that its second term reaches its maximum if the binary vector element $b(i) = -1$, whenever the vector element $\mathbf{\Psi}^{\mathrm{T}}\mathbf{A}$ is negative, and *vice versa*, i.e. $b(i) = +1$ if $\mathbf{\Psi}^{\mathrm{T}}\mathbf{A}$ is positive. The numerator of Equation (6.16) is then

constituted by exclusively positive terms, i.e. it is maximum, and the WMSE is minimum. The optimum Gaussian excitation is computed from Equation (6.13) in both the encoder and decoder. Only the M-bit index representing the optimum binary excitation vector $\mathbf{b}$ has to be transmitted. The evaluation of the vectors $\mathbf{\Psi}^{\mathrm{T}}\mathbf{A}$ and $\mathbf{c} = \mathbf{A}\mathbf{b}$ requires a mere $2M^2$ number of multiplications/additions, which gives typically 5 combined operations per output speech sample, a value 400 times lower than the complexity of the equivalent quality CELP codec.

Table 6.1: Bit allocation of 4.8 kbps TBPE codec.

Parameter	Bit number
10 LSFs	36
LTPD	$2 \cdot 7 + 2 \cdot 5$
LTPG	$4 \cdot 3$
GP	$4 \cdot 2$
EG	$4 \cdot 4$
Excitation	$4 \cdot 12$
Total: 144	

The bit allocation of the TBPE codec is summarised in Table 6.1, while its schematic is portrayed in Figure 6.3. The spectral envelope is represented by ten LSFs which are scalar quantised using 36 bits. The 30 ms long speech frames having 240 samples are divided into four 7.5 ms subsegments having 60 samples. The subsegment excitation vectors $\mathbf{b}$ have 12 transformed duo-binary samples with a pulse-spacing of $D = 5$. The LTP delays (LTPD) are quantised with seven bits in odd and five bits in even indexed subsegments, while the LTP gain (LTPG) is quantised with three bits. The excitation gain (EG) factor is encoded with four bits, while the grid position (GP) of candidate excitation sequences by two bits. A total of 28 or 26 bits per subsegment were used for quantisation, which yields $36 + 2 \cdot 28 + 2 \cdot 26 = 144$ bits/30 ms, resulting in a bitrate of 4.8 kbps.

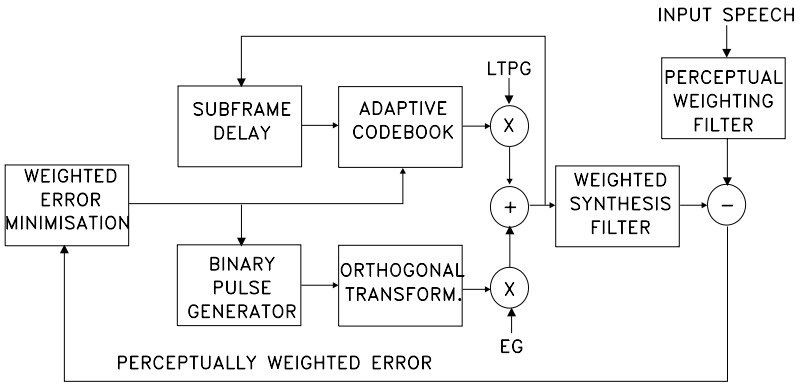

Figure 6.3: Block diagram of the 4.8 kbps TBPE codec.

6.4.2.2 Bit-sensitivity Analysis of the 4.8 Kbps TBPE Speech Codec

In the bit-sensitivity investigations each bit of a 144 bit TBPE frame was systematically corrupted and the SEGSNR and CD degradation were evaluated. The associated results are depicted for the first 63 bits of a TBPE frame in terms of SEGSNR (dB) in Figure 6.4, and in terms of CD (dB) in Figure 6.5. For the sake of completeness we note that we previously reported our findings on a somewhat more sophisticated sensitivity evaluation technique in [169]. According to this procedure the effects of error propagation across speech frame boundaries due to filter memories was also taken into account by integrating or summing these degradations over all consecutive frames, where the error propagation inflicted measurable SEGSNR and CD reductions. However, for simplicity at this stage we refrain from using this technique and demonstrate the principles of source sensitivity-matched error protection using a less complex procedure. We recall from Table 6.1 that the first 36 bits represent the 10 LSFs describing the speech spectral envelope. The SEGSNR degradations shown in Figure 6.4 indicate the most severe waveform distortions for the first 10 bits describing the first 2–3 LSFs. The CD degradation, however, was quite severe for all LSFs, particularly for the MSBs of the individual parameters. This was confirmed by our informal subjective tests. Whenever possible, all LSF bits should be protected against corruption.

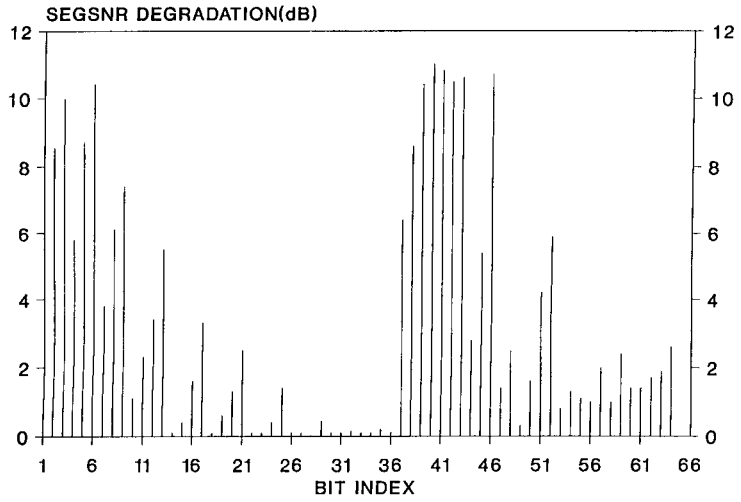

Figure 6.4: Bit sensitivities for the 4.8 Kbps codec expressed in terms of SEGSNR (dB).

The situation is practically reversed for the rest of the 144 bits in the TBPE frame, which represents the LTPD, LTPG, GP, EG and excitation parameters for the subsegments. We highlight our findings for the case of the first 27-bit subsegment only, as the other subsegments have identical behaviours. Bits 37–43 represent the LTP delays and bits 44–47 the LTP gains. Their errors are more significant in terms of SEGSNR than in CD, as demonstrated by Figure 6.5. This is because the LTPD and LTPG parameters describe the spectral fine structure and do not seriously influence the spectral envelope, although they seriously degrade the recovered waveform. As the TBPE codec is a stochastic codec with

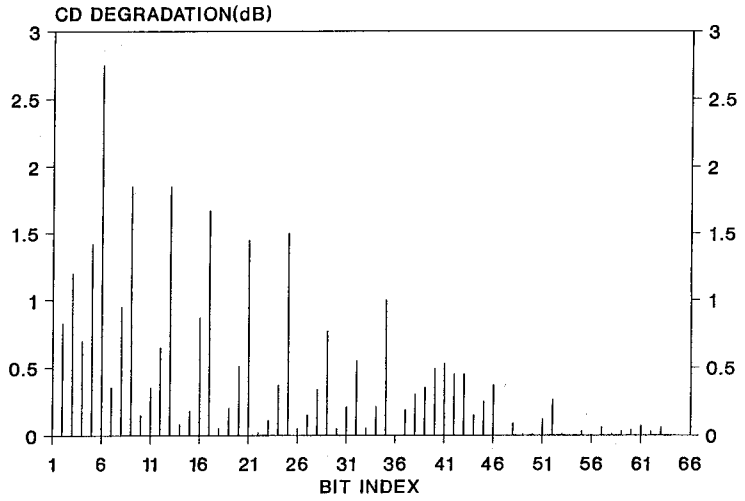

Figure 6.5: Bit sensitivities for the 4.8 Kbps codec expressed in terms of CD (dB).

random excitation patterns, the bits 48–63 assigned to the excitations and their gains are not particularly vulnerable to transmission errors. This is because the redundancy in the signal is removed by the long-term and short-term predictors. Furthermore, the TBPE codec exhibits exceptional inherent excitation robustness, as the influence of a channel error in the excitation diminishes after the orthogonal transformation $\mathbf{c} = \mathbf{A}\mathbf{b}$. In conventional CELP codecs this is not the case, as a codebook address error causes the decoder to select a different excitation pattern from its codebook causing considerably more speech degradation than encountered by the TBPE codec.

In general, most robust performance is achieved if the bit protection is carefully matched to the bit sensitivities, but the SEGSNR and CD sensitivity measures portrayed in Figures 6.4 and 6.5 often contradict. Therefore, we combine the two measures to give a sensitivity figure S, representing the average sensitivity of a particular bit. The bits must be first ordered both according to their SEGSNR and CD degradations given in Figures 6.4 and 6.5, respectively, to derive their 'grade of prominence' with 1 representing the highest and 63 the lowest sensitivity. Observe that the highest CD degradation is caused by bit 6, which is the MSB of the second LSF in the speech frame, while the highest SEGSNR degradation is due to bit 40 in the group of bits 37–43, representing the LTP delay. Furthermore, bit 6 is the seventh in terms of its SEGSNR degradation, hence its sensitivity figure is $S = 1 + 7 = 8$, as seen in the first row of Table 6.2. On the other hand, the corruption of bit 40, the most sensitive in terms of SEGSNR, results in a relatively low CD degradation, as it does not degrade the spectral envelope representation characterised by the CD, but spoils the pitch periodicity and hence the spectral fine-structure. This bit is the 19th in terms of its SEGSNR degradation, giving a sensitivity figure contribution of 19 plus 1 due to CD degradation, i.e. the combined sensitivity figure is $S = 20$, as shown by row 6 of Table 6.2. The combined sensitivity figures for all the LSFs and the first 27-bit subsegment are similarly summarised in ascending order in column 3 of Table 6.2, where column 2 represents the bit index in the first 63-bit segment of the 144-bit TBPE frame.

Table 6.2: Bit sensitivity figures for the 4.8 kbps TBPE codec.

Bit no. in frame	Bit index in frame	Sensit. figure	Bit no. in frame	Bit index in frame	Sensit. figure
1	6	8	33	48	69
2	9	14	34	24	71
3	5	16	35	63	76
4	3	16	36	57	76
5	41	19	37	10	79
6	40	20	38	28	80
7	13	21	39	19	80
8	2	23	40	61	80
9	43	24	41	59	82
10	8	25	42	62	84
11	46	25	43	15	85
12	42	26	44	60	88
13	17	27	45	34	89
14	39	31	46	50	91
15	4	31	47	31	92
16	21	32	48	55	95
17	12	37	49	27	95
18	38	38	50	23	97
19	25	43	51	14	97
20	16	44	52	47	98
21	52	45	53	58	102
22	7	45	54	54	103
23	1	45	55	53	105
24	37	48	56	56	105
25	45	49	57	18	105
26	11	55	58	33	108
27	20	58	59	49	109
28	51	60	60	26	109
29	29	60	61	30	110
30	35	60	62	22	119
31	44	63	63	36	125
32	32	68			

Having studied the family of TBPE codecs, the next section is dedicated to VSELP [164], which is another successful coding technique. It was standardized not only for the 8 kbps Pan-American dual-mode mobile radio system referred to as IS-54, but also in the 5.6 kbps half-rate Pan-European system GSM [98].

6.4.3 Dual-rate Algebraic CELP Coding

6.4.3.1 ACELP Codebook Structure

Algebraic Code Excited Linear Predictive (ACELP) codecs have recently conquered the battle-field of speech codec standardisation, winning extensive comparative tests aimed at

finalizing the 8 kbps CCITT G.729 Recommendation. One of the two operating modes of the new CCITT G.723/H.324 codec is also based on ACELP principles and it is also the most likely candidate for the Pan-European private mobile radio system known as TETRA. The algebraic codebook structure was originally proposed by Adoul *et al.* in reference [168]. In this section we briefly introduce the ACELP principle and design a dual-rate ACELP codec, which can be conveniently used in a range of systems. The above-mentioned standard coding schemes will be detailed in Chapter 7.

In the proposed codec each excitation codeword $c_k(n)$ has only four non-zero pulses, which have amplitudes of either $+1$ or -1. In its lower-rate mode the dual codec allocates these excitation pulses over an excitation optimisation subframe of 60 samples or 7.5 ms, while in its higher-rate mode over 40 samples or 5 ms. Also each non-zero pulse has a limited number of positions within the codeword where it can lie. The amplitudes and possible positions within the codeword for each of the four pulses are shown in Table 6.3 for our sub-frame size 60, 4.7 kbps codec, and in Table 6.4 for our sub-frame size 40, 7.1 kbps codec. In both codecs each pulse can take up eight positions, and so the chosen positions can be represented with three bits each, giving a total of twelve bits per sub-frame to represent the codebook index. The gain sign is represented with one bit and its magnitude is quantised with four bits using logarithmic quantisation. This gives a total of 17 bits per sub-frame for the fixed codebook information.

Table 6.3: Pulse amplitudes and positions for the 4.7 kbps codec. Copyright © IEEE Adoul *et al.* [168].

Pulse number i	Amplitude	Possible position m_i
0	$+1$	0, 8, 16, 24, 32, 40, 48, 56
1	-1	2, 10, 18, 26, 34, 42, 50, 58
2	$+1$	4, 12, 20, 28, 36, 44, 52
3	-1	6, 14, 22, 30, 38, 46, 54

Table 6.4: Pulse amplitudes and positions for the 7.1 kbps codec.

Pulse number i	Amplitude	Possible position m_i
0	$+1$	1, 6, 11, 16, 21, 26, 31, 36
1	-1	2, 7, 12, 17, 22, 27, 32, 37
2	$+1$	3, 8, 13, 18, 23, 28, 33, 38
3	-1	4, 9, 14, 19, 24, 29, 34, 39

The algebraic codebook structure has several advantages: it does not require any codebook storage, since the excitation vectors are generated in real-time and it is robust against channel errors, since a single error corrupts the excitation vector only in one position, leading to a similar excitation vector at the decoder. Most importantly, however, it allows the values $\tilde{C}_k$ and ξ_k to be calculated very efficiently. From Equations (6.8) and (6.9) the

correlation and energy terms can be computed for the four excitation pulses of Table 6.3:

$$\tilde{C}_k = \psi(m_0) - \psi(m_1) + \psi(m_2) - \psi(m_3) \tag{6.17}$$

and

$$\begin{aligned}\xi_k = &\phi(m_0, m_0) \\ &+ \phi(m_1, m_1) - 2\phi(m_1, m_0) \\ &+ \phi(m_2, m_2) + 2\phi(m_2, m_0) - 2\phi(m_2, m_1) \\ &+ \phi(m_3, m_3) - 2\phi(m_3, m_0) + 2\phi(m_3, m_1) - 2\phi(m_3, m_2),\end{aligned} \tag{6.18}$$

where m_i is the position of the pulse number i. By changing only one pulse position at a time $\tilde{C}_k$ and ξ_k can be calculated using four nested loops associated with the four excitation pulses used. In the inner loop, $\tilde{C}_k$ is updated with one addition and ξ_k with three multiplications and four additions. This allows for a very efficient codebook search.

A pair of appropriately extended equations analogous to (6.17) and (6.18) can be written for five and more pulses, leading to a corresponding number of encapsulated search loops, which will be exploited during our discussions on the 8 kbps CCITT G.729 10 ms delay codec in Section 7.8 as well as in Section 9.4. A further major attraction of the ACELP principle is that Salami *et al.* [160] proposed a computationally efficient focussed search technique, which was also advocated by Kataoka *et al.* [147, 170]. The proposed algorithm invokes a few threshold tests during subsequent search phases upon adding the individual excitation pulses one-by-one, in order to decide whether a particular subset of vectors characterised by the so far incorporated pulses is likely to lead to the lowest weighted error over the codebook for the subsegment about to be encoded. As we will highlight in Section 9.4, this facilitates a search complexity reduction around a factor of 100 or more without inflicting any significant performance degradation, while searching codebooks of 32 000 entries or even up to 10^6 entries.

In the decoder, the codebook information received from the encoder is used to find an excitation signal $u(n)$. If there are no channel errors this will be identical to the excitation signal $u(n)$ in the encoder. It is then passed through a synthesis filter $1/A(z)$ to give the reconstructed speech signal $\hat{s}(n)$ as shown in Figure 6.2. The parameters of the synthesis filter are determined from the line spectrum frequencies transmitted from the encoder, using interpolation between adjacent frames.

6.4.3.2 Dual-rate ACELP Bit Allocation

As mentioned, the excitation signal $u(n)$ is determined for each 5 or 7.5 ms subsegment of a 30 ms speech frame, depending on the targeted output bitrate, and it is described in terms of the following parameters, as summarised in Table 6.5.

- The adaptive codebook delay α that can take any integer value between 20 and 147 and hence is represented using 7 bits.

- The adaptive codebook gain G_1 which is non-uniformly quantised with 3 bits.

- The index of the optimum fixed codebook entry $c_k(n)$, which is represented with 12 bits.

- The fixed codebook gain G_2 which is quantised with a 4-bit logarithmic quantiser and an additional sign bit.

Thus a total of 27 bits are needed to represent the subsegment excitation signal $u(n)$, and for the low-rate mode we have a total of $(34 + 4 \times 27) = 142$ bits per 30 ms frame, or a rate of about 4.73 kbps, while in the high-rate mode the bitrate becomes 142 bits/20 ms $= 7.1$ kbps.

A slightly different higher-rate mode can also be contrived by keeping the 30 ms frame-length constant, which may become important in networks operating, for example, on the basis of a fixed 30 ms framelength. In this case the lower-rate mode's bit allocation remains unchanged, while in the higher-rate mode six, rather than four 5 ms excitation optimisation subsegments can be used. Then the number of bits per frame becomes $(34 + 6 \times 27) = 196$, yielding a bitrate of 196 bits/30 ms $= 6.54$ kbps.

6.4.3.3 Dual-rate ACELP Codec Performance

In this chapter, so far we have described in detail the general framework of CELP codecs and considered binary-pulse excitation, transformed binary-pulse excitation, vector sum excitation as well as ACELP codebook structures which allowed an efficient codebook search. Table 6.6 shows the approximate complexity, in terms of millions of floating point operations per second (MFLOPs), of the various stages of the encoding procedure for our 7.1 kbps ACELP codec. Also shown is the complexity for a non-sparse 12-bit conventional CELP codebook search. As can be seen from the table, the fixed codebook search accounts for the majority of the complexity in the encoder, and the algebraic codebook structure gives a huge reduction in this complexity. In total the encoding procedure we have described requires approximately 23 MFLOPs, with most operations being spent on the two codebook searches. The decoder does not have to do any codebook searches but merely filters the selected excitation through the synthesis filter. As a result it is much less complex and requires only about 0.2 MFLOPs.

Table 6.5: Bits allocated per frame for the dual-rate ACELP codec.

Line spectrum frequencies	34
Adaptive codebook delays	28 (4*7)
Adaptive codebook gains G_1	12 (4*3)
Fixed codebook index k	48 (4*12)
Fixed codebook gains G_2	20 (4*5)
Total	142

The two codecs described here were tested with the speech file described earlier. The 4.7 kbps codec produced good communications quality speech with a SEGSNR of 10.5 dB while the 7.1 kbps codec produced speech which was noticeably more transparent and had a SEGSNR of 12.1 dB. An important issue in the design of low bitrate speech codecs

Table 6.6: CELP and ACELP encoder complexity (MFLOPs).

CELP codebook search	300 000
ACELP codebook search	15
LPC analysis	0.75
Adaptive codebook search	7

is their robustness to background noise. We tested this aspect of our codec's performance using a speech correlated noise source called the modulated noise reference unit, as described in [71]. This method was proposed by Law and Seymour [171] in 1962 and standardised by the CCITT. Figure 6.6 shows how the SEGSNR of our 4.7 kbps codec varies with the signal to modulated noise ratio. It can be seen that the ACELP codec is not seriously affected by the background noise until the signal to modulated noise ratio falls below about 20 dB.

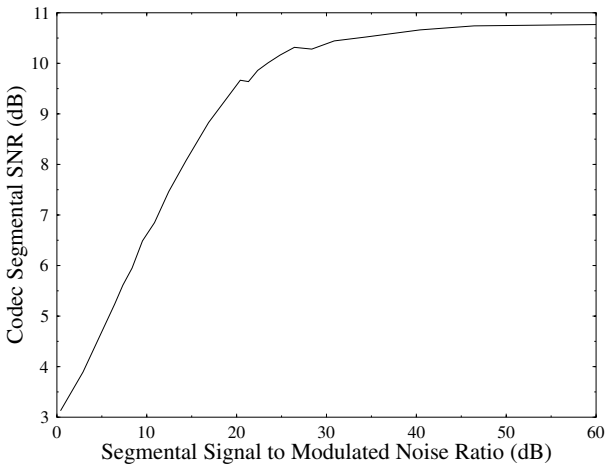

Figure 6.6: Performance of 4.7 kbps ACELP codec for noisy input signals.

Here we curtail our discourse on the performance of various ACELP codecs, although we will return to the issue of codec robustness in section 6.6. In the next section we will revisit the general AbS codec structure in the context of CELP coding in order to identify areas where the codec performance could be improved at the cost of acceptable implementational complexity.

6.5 Optimisation of the CELP Codec Parameters

6.5.1 Introduction

In the previous chapter we discussed the general structure of CELP codecs. This largely closed-loop structure is used in order to produce reconstructed speech which is as close as

possible to the original speech. However, there are two exceptions to an entirely closed-loop approach which are used in most CELP codecs. The first is in the determination of the synthesis filter $H(z)$, which is simply assumed to be the inverse of the short-term linear prediction error filter $A(z)$ which minimises the energy of the prediction residual. This means that although the excitation signal $u(n)$ is derived taking into account the form of the synthesis filter, no account is taken of the form of the excitation signal when the synthesis filter parameters are determined. This seems like an obvious deficiency and means, for example, that the synthesis filter may attempt to take account of long-term periodicities which would be better left to the adaptive codebook to deal with.

The second departure from a strict closed-loop approach in most CELP codecs is in the determination of the codebook parameters. Rather than the adaptive and fixed codebook parameters being determined together to produce an overall minimum in the weighted error signal, the adaptive codebook delay and gain are determined first by assuming that the fixed codebook signal is zero. Then, given the adaptive codebook signal, the fixed codebook parameters are found. This approach is taken in order to reduce the complexity of CELP codecs to a reasonable level. However, it seems obvious that it must lead to some degradation in the reconstructed speech quality.

In this chapter we discuss ways of overcoming the two exceptions to the closed-loop approach described above, and attempt to improve the quality of the reconstructed speech from our codecs while maintaining a reasonable level of complexity. We have concentrated our studies on the 4.7 kbps forward adaptive ACELP codec described in the previous chapter, although the techniques described will be applicable to other AbS codecs.

6.5.2 Calculation of the Excitation Parameters

In this section we discuss the procedure traditionally used for the adaptive and fixed codebook searches in CELP codecs, and ways in which this procedure can be improved. First the theory behind a full search procedure is given. Then we describe how the equations derived for a full search reduce to those in Section 6.3 derived for the usual sequential determination of the codebook parameters. In Section 6.5.2.3 we describe the full search procedure, its complexity and the results it gives. Section 6.5.2.4 describes various sub-optimal approaches which can be used, and finally Section 6.5.2.5 describes the quantisation of the codebook gains.

6.5.2.1 Full Codebook Search Theory

Consider the weighted error $e_w(n)$ between the weighted input speech and the weighted reconstructed speech. This is given by

$$\begin{aligned} e_w(n) &= s_w(n) - \hat{s}_w(n) \\ &= s_w(n) - \hat{s}_o(n) - G_1 y_\alpha(n) - G_2[c_k(n) * h(n)], \end{aligned} \tag{6.19}$$

where the symbols used here have the same meaning as before and throughout Chapter 6. Explicitly, $s_w(n)$ is the weighted input speech, $\hat{s}_o(n)$ is the zero input response of the weighted synthesis filter due to its input in previous sub-frames, G_1 is the adaptive codebook gain, $y_\alpha(n) = h(n) * u(n-\alpha)$ is the filtered adaptive codebook signal, G_2 is the fixed

codebook gain, $c_k(n)$ is the fixed codebook codeword and $h(n)$ is the impulse response of the weighted synthesis filter.

The search procedure attempts to find the values of the adaptive codebook gain G_1 and delay α and the fixed codebook index k and gain G_2 which minimise the MSE E_w taken over the sub-frame length N. This is given by

$$\begin{aligned}
E_w &= \frac{1}{N}\sum_{n=0}^{N-1} e_w^2(n) \\
&= \frac{1}{N}\sum_{n=0}^{N-1} \left(x(n) - G_1 y_\alpha(n) - G_2[c_k(n) * h(n)]\right)^2 \\
&= \frac{1}{N}\Bigg(\sum_{n=0}^{N-1} x^2(n) + G_1^2 \sum_{n=0}^{N-1} y_\alpha^2(n) + G_2^2 \sum_{n=0}^{N-1} [c_k(n) * h(n)]^2 \\
&\quad - 2G_1 \sum_{n=0}^{N-1} x(n) y_\alpha(n) - 2G_2 \sum_{n=0}^{N-1} x(n)[c_k(n) * h(n)] \\
&\quad + 2G_1 G_2 \sum_{n=0}^{N-1} y_\alpha(n)[c_k(n) * h(n)]\Bigg),
\end{aligned} \tag{6.20}$$

where $x(n) = s_w(n) - \hat{s}_o(n)$ is the target signal for the codebook search, referred to as the LTP target. We can rewrite this formula as

$$\begin{aligned}
E_w &= \frac{1}{N}\Bigg(\sum_{n=0}^{N=1} x^2(n) + G_1^2 \xi_\alpha + G_2^2 \xi_k - 2G_1 C_\alpha - 2G_2 C_k + 2G_1 G_2 Y_{\alpha k}\Bigg) \\
&= \frac{1}{N}\Bigg(\sum_{n=0}^{N-1} x^2(n) - T_{\alpha k}\Bigg),
\end{aligned} \tag{6.21}$$

where

$$T_{\alpha k} = 2(G_1 C_\alpha + G_2 C_k - G_1 G_2 Y_{\alpha k}) - G_1^2 \xi_\alpha - G_2^2 \xi_k \tag{6.22}$$

is the term to be maximised by the codebook search. Here,

$$\xi_\alpha = \sum_{n=0}^{N-1} y_\alpha^2(n) \tag{6.23}$$

is the energy of the filtered adaptive codebook signal and

$$C_\alpha = \sum_{n=0}^{N-1} x(n) y_\alpha(n) \tag{6.24}$$

is the correlation between the filtered adaptive codebook signal and the codebook target $x(n)$. Similarly, ξ_k is the energy of the filtered fixed codebook signal $[c_k(n) * h(n)]$, and C_k is the correlation between this and the target signal. Finally,

$$Y_{\alpha k} = \sum_{n=0}^{N-1} y_\alpha(n)[c_k(n) * h(n)] \tag{6.25}$$

is the correlation between the filtered signals from the two codebooks. With this notation we intend to emphasise what codebook the variables are dependent on. For example, once the weighted synthesis filter parameters are known, ξ_α depends only on which delay α is chosen for the adaptive codebook, whereas $Y_{\alpha k}$ depends on the indices α and k used for both the adaptive and fixed codebooks.

The codebook search must find the values of the indices α and k, and the gains G_1 and G_2, which maximise $T_{\alpha k}$ and so minimise E_w. For a given pair of indices α and k we can find the optimum values for G_1 and G_2 by setting the partial derivatives of $T_{\alpha k}$ with respect to G_1 and G_2 to zero. This gives

$$\frac{\partial T_{\alpha k}}{\partial G_1} = 2C_\alpha - 2G_2 Y_{\alpha k} - 2G_1 \xi_\alpha = 0 \tag{6.26}$$

and

$$\frac{\partial T_{\alpha k}}{\partial G_2} = 2C_k - 2G_1 Y_{\alpha k} - 2G_2 \xi_k = 0. \tag{6.27}$$

Solving these two linear simultaneous equations gives the optimum values of the gains for given codebook indices:

$$G_1 = \frac{C_\alpha \xi_k - C_k Y_{\alpha k}}{\xi_\alpha \xi_k - Y_{\alpha k}^2} \tag{6.28}$$

and

$$G_2 = \frac{C_k \xi_\alpha - C_\alpha Y_{\alpha k}}{\xi_\alpha \xi_k - Y_{\alpha k}^2}. \tag{6.29}$$

The full search procedure has to find – for every pair of codebook indices α, k – the terms ξ_α, ξ_k, C_α, C_k, and $Y_{\alpha k}$, and use these to calculate the gains G_1 and G_2. These gains can then be quantised and substituted into Equation (6.22) to give $T_{\alpha k}$ which the coder must maximise by the proper choice of α and k.

6.5.2.2 Sequential Search Procedure

In this section we discuss how the equations derived above relate to those in Section 6.3 for the sequential search procedure which is usually employed in CELP codecs. In this sequential search the adaptive codebook parameters are determined first by assuming $G_2 = 0$. Substitution of this into Equation (6.26) gives

$$G_1 = \frac{C_\alpha}{\xi_\alpha} = \frac{\sum_{n=0}^{N-1} x(n) y_\alpha(n)}{\sum_{n=0}^{N-1} y_\alpha^2(n)}. \tag{6.30}$$

If we then substitute the values $G_1 = C_\alpha/\xi_\alpha$ and $G_2 = 0$ into Equation (6.22), the term to be maximised becomes

$$T_{\alpha k} = \frac{C_\alpha^2}{\xi_\alpha} = \frac{(\sum_{n=0}^{N-1} x(n)y_\alpha(n))^2}{\sum_{n=0}^{N-1} y_\alpha^2(n)}. \tag{6.31}$$

Once the adaptive codebook parameters have been determined they are assumed constant during the fixed codebook search. The LTP target $x(n)$ is updated to give the fixed codebook target $\tilde{x}(n)$, where

$$\tilde{x}(n) = x(n) - G_1 y_\alpha(n), \tag{6.32}$$

and for each codebook index k the energy ξ_k and the correlation $\tilde{C}_k$ between $\tilde{x}(n)$ and the filtered codewords are found. The correlation term $\tilde{C}_k$ is given by

$$\begin{aligned}\tilde{C}_k &= \sum_{n=0}^{N-1} \tilde{x}(n)[c_k(n) * h(n)] \\ &= \sum_{n=0}^{N-1} (x(n) - G_1 y_\alpha(n))[c_k(n) * h(n)] \\ &= C_k - G_1 Y_{\alpha k}.\end{aligned} \tag{6.33}$$

Substitution of this into Equation (6.27) gives

$$G_2 = \frac{\tilde{C}_k}{\xi_k} \tag{6.34}$$

as in Equation (6.4), and the term to be maximised becomes

$$\begin{aligned}T_{\alpha k} &= 2G_1 C_\alpha + 2G_2(C_k - G_1 Y_{\alpha k}) - G_1^2 \xi_\alpha - G_2^2 \xi_K \\ &= 2G_1 C_\alpha - G_1^2 \xi_\alpha + 2G_2 \tilde{C}_k - G_2^2 \xi_k.\end{aligned} \tag{6.35}$$

Now as G_1 and α are fixed we can ignore the first two terms above and write the expression to be maximised by the fixed codebook search as $G_2(2\tilde{C}_k - G_2\xi_k)$, as in Section 6.3.

6.5.2.3 Full Search Procedure

We describe here the procedure used to perform a full codebook search to find the minimum possible weighted error E_w. Although such a full search is not a practical method for use in real speech coders, it does give us an upper bound to the improvements which can be obtained over the sequential search approach.

In order to perform a full search of the two codebooks the coder must calculate the value of $T_{\alpha k}$ using Equation (6.22) for every possible pair of codebook indices α and k, and select the indices which maximise $T_{\alpha k}$. This means that we must calculate ξ_α and C_α for every adaptive codebook codeword, ξ_k and C_k for every fixed codebook codeword, and $Y_{\alpha k}$ for every pair of codewords. All the necessary values of C_α, ξ_α, C_k and ξ_k are calculated in the normal sequential search procedure. The extra complexity of the full search comes from calculating $Y_{\alpha k}$ for all values of α and k.

Using a similar approach to that used to find $\tilde{C}_k$ in the normal search, $Y_{\alpha k}$ can be written as

$$\begin{aligned} Y_{\alpha k} &= \sum_{n=0}^{N-1} y_\alpha(n)[c_k(n) * h(n)] \\ &= \sum_{n=0}^{N-1} c_k(n)[y_\alpha(n) * h(-n)] \\ &= \sum_{n=0}^{N-1} c_k(n)\Omega_\alpha(n), \end{aligned} \tag{6.36}$$

where $\Omega_\alpha(n)$ is given by

$$\Omega_\alpha(n) = \sum_{i=n}^{N-1} y_\alpha(i)h(i-n). \tag{6.37}$$

Thus, once $\Omega_\alpha(n)$ is known, using the algebraic codebook structure allows $Y_{\alpha k}$ to be calculated using four additions for each fixed codebook index k. Using four nested loops and updating the position of one pulse only in each loop allows us to find $Y_{\alpha k}$ very efficiently. Also, because of the nature of the filtered adaptive codebook signal $y_\alpha(n)$ we can find $\Omega_\alpha(n)$ efficiently using an iterative procedure.

We simulated a full search codec in order to evaluate the degradation, inflicted by the sequential approach compared to the ideal full search. We measured the performance of the codec using the conventional SEGSNR and the weighted SNR measures, where the SNR weighting was implemented using the perceptual weighting filter $A(z)/A(z/\gamma)$, averaging the SNR over the entire measurement duration. The delay α of the adaptive codebook was allowed to take any integer value between 20 and 147, and a twelve bit algebraic fixed codebook was used as described in Section 6.3. We found that quantising the codebook gains with quantisers designed for the normal codec masked the improvements obtained with the full search. Therefore for all our simulation results reported here and in the next section neither G_1 nor G_2 were quantised. We consider quantisation of the gains in Section 6.5.2.5.

We found – for four speech-files containing speech from two male and two female speakers – that the full search procedure improved the average SEGSNR of our 4.7 kbps ACELP codec from 9.7 dB to 10.8 dB. A similar improvement was seen in the average weighted SNR – it increased from 7.3 dB to 8.2 dB. The reconstructed speech using the full search procedure sounded more full and natural than that obtained using the sequential search procedure.

However, these gains are obtained only at the expense of a huge increase in the complexity of the codec. Even with the techniques described above to allow the full search to be carried out efficiently, such a codec is almost sixty times more computationally demanding than a codec using the standard approach. Therefore in the next section we describe some sub-optimal approaches to the codebook search, with the aim of keeping the improvement in the reconstructed speech quality we have seen with the full codebook search, but reducing the complexity of the search to a reasonable level.

6.5.2.4 Sub-optimal Search Procedures

The full search procedure described in the previous section allows us to find the best combination of the codebook indices α and k. However, this method is unrealistically complex, and in this section we describe some sub-optimal search strategies.

Such a feasible search procedure, which we refer to here as 'Method A', is to follow the sequential approach and find G_1 and α by assuming $G_2 = 0$, and then find G_2 and k, while assuming that G_1 and α are fixed. Then – once α and k have been determined – we can use Equations (6.28) and (6.29) in order to jointly optimise the values of the codebook gains. In order to accomplish this we have to know C_α, ξ_α, C_k, ξ_k and $Y_{\alpha k}$ for the chosen indices. The values of C_α, ξ_α and ξ_k will be known from the codebook searches, and C_k can be found from $Y_{\alpha k}$ and $\tilde{C}_k$ using Equation (6.33). The main computational requirement for the update of the gains is therefore the calculation of $Y_{\alpha k}$ for the given α and k, and this is relatively undemanding. In fact, updating of the codebook gains given the codebook indices increases the complexity of the codec by about only two percent. Using the same speech files described earlier we found this update of the gains increased the average SEGSNR of the codec from 9.7 dB to 10.1 dB, and the average weighted SNR from 7.3 dB to 7.5 dB.

Another possible sub-optimal approach to the codebook searches is to find the adaptive codebook delay α using the usual approach (i.e. by assuming $G_2 = 0$), and then use only this value of α during the fixed codebook search in which G_1, G_2 and k are all determined. This is similar to an approach suggested in [172] where a very small (32 entries) fixed codebook was used, and a one-tap IIR filter was used instead of the adaptive codebook. For our codec we find ξ_k, C_k and $Y_{\alpha k}$ for every fixed codebook index k using the approach with four nested loops described in Sections 6.3 and 6.5.2.3. The values of ξ_α and C_α are known from the adaptive codebook search, and so we can use Equations (6.28) and (6.29) to find G_1 and G_2, and then calculate $T_{\alpha k}$ using Equation (6.22). The value of k which maximises $T_{\alpha k}$ is chosen as the fixed codebook index. We refer to this joint codebook search procedure as 'Method B'.

This 'Method B'-based search allows the fixed codebook entry to be selected taking full account of the possible variations in the magnitude of the adaptive codebook signal. If we could trust the initial value of α calculated assuming $G_2 = 0$ to be correct, then it would give identical results to the full search procedure. However, it is much less computationally demanding than the full codebook search, and increases the complexity of the normal codec by only about 30%. In our simulations we found that it increased the average SEGSNR from 9.7 dB to 10.3 dB. Similarly, the average weighted SNR increased from 7.3 dB to 7.8 dB. Thus this approach gives significant gains over the normal sequential search, but still does not match the results of the codec using the full search procedure.

The differences between the results using the full codebook search, and those described above, must be due to differences in the chosen adaptive codebook delay α. We therefore investigated a procedure recalculating or updating this delay, once the fixed codebook index k is known. We refer to this final sub-optimal search procedure as 'Method C', which operates as follows. The adaptive codebook delay is initially chosen assuming $G_2 = 0$. Then the fixed codebook index is found by calculating G_1, G_2 and $T_{\alpha k}$ for every k, and choosing the index k which maximises $T_{\alpha k}$ as in the Method B search. Then once k is known we update the delay α by finding G_1, G_2 and $T_{\alpha k}$ for each possible α, and choosing the delay α which maximises $T_{\alpha k}$. To do this we need to know ξ_α, C_α, ξ_k, C_k and $Y_{\alpha k}$ for all values of α and the value of

Table 6.7: Performance and complexity of various search procedures.

	Segmental SNR	Weighted SNR	Complexity
Sequential search	9.7	7.3	1
Method A	10.1	7.5	1.02
Method B	10.3	7.8	1.3
Method C	10.6	7.8	1.4
Full search	10.8	8.2	60

k chosen during the fixed codebook search. As explained previously, ξ_α, C_α, ξ_k and C_k will all be known already, and so we must calculate $Y_{\alpha k}$ for all possible values of α and a fixed k.

This procedure to update the adaptive codebook delay once the fixed codebook index is known increases the complexity of the codec by about a further 10% relative to the complexity of the normal codec. It improved the average SEGSNR for our four speech files to 10.6 dB, and the average weighted SNR to 7.8 dB.

The performance of the search procedures we have described in this section, along with the normal and the full search methods, is shown in Table 6.7 in terms of the average segmental and weighted SNRs. Also shown are the complexities of codecs using these search procedures relative to a codec using the normal sequential search. It can be seen that the joint codebook search Method A gives a significant improvement in the codec's performance with very little extra complexity. Furthermore, we can see that Method C – the most complex sub-optimal search procedure investigated – increases the codec's complexity by only 40% but gives reconstructed speech, in terms of the SEGSNR at least, very similar to that using the much more complex full search procedure.

The investigations we have reported in this section have ignored the effects of quantisation of the codebook gains G_1 and G_2. However, in any real coder we must somehow quantize these gains for transmission to the decoder. This is discussed in the next section.

6.5.2.5 Quantisation of the Codebook Gains

In this section we study ways of quantising the codebook gains G_1 and G_2 to attempt maintaining the improvements achieved without quantisation due to our various codebook search procedures. This was necessary because we noticed, especially for female speakers, quantisation of the gains had a much more serious effect in the codecs with improved search procedures than for the normal codec. This meant that the improvement which arose from the new search procedures was largely lost when quantisation was considered. For example, for one of our speech files containing the sentence 'To reach the end he needs much courage' spoken by a woman, the SEGSNR of the normal codec with no quantisation was 11.45 dB. With quantisation of both gains this was only slightly reduced to 11.38 dB. The codec using the joint search procedure Method C gave a SEGSNR with no quantisation of 12.45 dB. However, with quantisation this fell to 11.67 dB, meaning that the increase in the SEGSNR due to the improved search procedure fell from 1 dB without quantisation to 0.3 dB with quantisation.

There are several possible reasons for this effect. The most obvious is that when the gains are calculated in a different way their distributions change and so quantisers designed

using the old distributions will be less effective. Also, it may just be that the gains calculated with the improved search procedures are more sensitive to quantisation than those calculated normally.

Notice that Equation (6.28) gives the optimum value of G_1 only, if G_2 is given by Equation (6.29). When we quantize G_2 the optimum value of G_1 will change. We can find the best value of G_1 by substituting the quantised value of G_2, i.e. $\hat{G}_2$, into Equation (6.26). This gives

$$G_1 = \frac{C_\alpha - \hat{G}_2 Y_{\alpha k}}{\xi_\alpha}. \tag{6.38}$$

Similarly, if the adaptive codebook gain has been quantised to give $\hat{G}_1$ then the optimum value of G_2 becomes

$$G_2 = \frac{C_k - \hat{G}_1 Y_{\alpha k}}{\xi_k}. \tag{6.39}$$

We set about improving the quantisation of the gains for the codec using our best sub-optimal search procedure, namely Method C. A speech file, containing about eleven seconds of speech spoken by two men and two women was used to train our quantisers. None of the speakers, or the sentences spoken, were the same as those used to measure the performance of the codec. Distributions for the two gains were measured using our training data when neither of the gains were quantised. We were then able to train quantisers using the Lloyd–Max algorithm [10].

There is a problem with the adaptive codebook gain G_1 because while most values of G_1 are between $+1.5$ and -1.5, a few values are very high. If we use all these values with the Lloyd–Max algorithm then the resulting quantiser will have several reconstruction levels which are very high and rarely used. We found that for an eight level quantiser trained using all the unquantised values of G_1, half the reconstruction levels were greater than 3 or less than -3. Using such a quantiser gives a serious degradation in the SEGSNR of the reconstructed speech. To overcome this problem the values of G_1 must be cut down to some reasonable range. The DoD [100] codec uses the range -1 to $+2$, hence we invoked these values, additionally also experimenting with the range of -1.5 to $+1.5$, which was suggested by the PDF of our own experimental data.

Another problem when using the Lloyd–Max algorithm to design a quantiser for G_1 is that one reconstruction level tends to get allocated very close to zero where the PDF of the gains is low. We overcame this problem by splitting the values of G_1 into positive and negative values, and running the Lloyd–Max algorithm separately on each half of the data. Using these techniques we were able to design quantisers for G_1 which outperformed the quantiser designed for the normal codec.

Our normal codec used a four bit logarithmic quantiser for the magnitude of G_2, with the sign being allocated an additional bit. We also used the Lloyd–Max algorithm to design a five bit quantiser for G_2 using the distribution derived from our training data.

We conducted our simulations of the codec with G_1 calculated using Equation (6.28) and quantised, and then G_2 calculated using Equation (6.39). Using this technique we were able to derive distributions for G_2 when G_1 was quantised with various quantisers. Similarly, we were able to find distributions for G_1 when G_2 was quantised with various quantisers. These distributions were then used to train quantisers for G_1 to use in conjunction with those already designed for G_2 and *vice versa*. We attempted quantising G_1 first using various

Table 6.8: Performance of search procedures with quantisation.

	Segmental SNR	Weighted SNR
Normal codec	9.5	7.1
Improved search and quantisation	10.0	7.5

different quantisers, and then using the specially trained quantiser for G_2. Similarly, we also attempted quantising G_2 first and then using various specially trained quantisers for G_1. The best results were obtained when G_2 was calculated first and quantised with the normal logarithmic quantiser, before G_1 was calculated using Equation (6.38) and quantised using a Lloyd–Max quantiser trained with gains cut to the range -1 to $+2$. Such a quantisation scheme improved the SEGSNR for the female speech file described earlier from 11.67 dB to 11.97 dB. The improvement was less significant for the two male speech files, but on average using the improved quantisation scheme gave a SEGSNR of 10.0 dB and a weighted SNR of 7.5 dB. These figures should be compared to an average SEGSNR of 9.9 dB, and an average weighted SNR of 7.4 dB, when using the normal quantisers.

The average SEGSNR and weighted SNR for our four speech files using the codec with the normal search procedure and gain quantisers, and the codec with the improved search procedure (Method C) and quantisation, are shown in Table 6.8. It can be seen that on average the improved search procedure and quantisation gives an increase in the SEGSNR of about half a decibel, and the weighted SNR increases by 0.4 dB. The improvements are similar for both the male and female speech files, and in informal listening tests we found that the reconstructed speech for the improved search procedure again sounded more full and natural than that for the normal search procedure.

Next we discuss methods of improving the performance of our 4.7 kbps forward adaptive ACELP codec by re-calculating the synthesis filter parameters after the excitation signal $u(n)$ has been determined. However, in Section 8.9 we will return to joint codebook search procedures, and discuss using Method A and Method B described earlier to improve the performance of low-delay backward-adaptive CELP codecs.

6.5.3 Calculation of the Synthesis Filter Parameters

In the previous section we discussed ways of improving the determination of the codebook parameters which give the excitation signal $u(n)$. At the decoder this excitation signal is passed through the synthesis filter $H(z)$ in order to generate the reconstructed speech $\hat{s}(n)$. As stated before, $H(z)$ is usually simply assumed to be the inverse of the prediction error filter $A(z)$ which minimises the energy of the prediction residual. It is well known that this is not the ideal way to determine the synthesis filter parameters. For example, when the pitch frequency is close to the frequency of the first formant, which commonly happens for high-pitched speakers, the spectral analysis tends to give spectral envelopes with sharp and narrow resonances [173]. This leads to amplitude booms in the reconstructed speech which can be annoying.

In this section we discuss ways of improving the synthesis filter $H(z)$, in order to maximise the SNR of the reconstructed speech. Initially, for simplicity, the filter coefficients were not quantised. In these endeavours no overlapping of the LPC analysis frames was implemented and interpolating the LSF of Section 4.2.1 between frames was not used. Discarding of inter-frame interpolation implies that the filter coefficients for the weighted synthesis filter change only once per frame, rather than every sub-frame. Therefore the energy of the filtered fixed codebook signals, namely ξ_k, has to be computed only once per frame, and hence the complexity of the fixed codebook search is dramatically reduced. This reduces the overall complexity of the codec by about 40%.

6.5.3.1 Bandwidth Expansion

One well known and relatively simple way of improving the synthesis filter parameters is to use bandwidth expansion [173]. In this technique the filter coefficients a_k, produced by the autocorrelation or covariance analysis of the input speech, are replaced by $a_k\gamma^k$ where γ is some constant less than one. This has the effect of expanding the bandwidth of the resonances in the transfer function of the synthesis filter and, therefore, helps reduce the problems mentioned above which occur when the pitch frequency is close to the first formant frequency.

The constant γ can be expressed as [173]

$$\gamma = \exp(-\sigma\pi T) \tag{6.40}$$

where T is the sampling interval and σ is the bandwidth expansion in Hertz. We attempted this using a 15 Hz expansion, which corresponds to $\gamma = 0.9941$, and found that this improved the SEGSNR of our 4.7 kbps codec (with no LSF quantisation or interpolation) from 9.90 dB to 10.59 dB. Also, it is reported [174] that such an expansion improves the robustness of a codec to channel errors, and so we used bandwidth expansion in our studies on error sensitivity in Section 6.6. Note that like all the results quoted in this section, those above were obtained for a speech file containing one sentence each from two male and two female speakers.

6.5.3.2 Least Squares Techniques

Given an excitation signal $u(n)$ and a set of filter coefficients $a_k,\ k = 1, 2 \cdots p$, the reconstructed speech signal $\hat{s}(n)$ will be given by

$$\hat{s}(n) = u(n) + \sum_{k=1}^{p} a_k \hat{s}(n-k). \tag{6.41}$$

We wish to minimise E, the energy of the error signal $e(n) = s(n) - \hat{s}(n)$, where $s(n)$ is the original speech signal. E is given by

$$\begin{aligned} E &= \sum_n (s(n) - \hat{s}(n))^2 \\ &= \sum_n \left(s(n) - u(n) - \sum_{k=1}^{p} a_k \hat{s}(n-k) \right)^2 \\ &= \sum_n \left(x(n) - \sum_{k=1}^{p} a_k \hat{s}(n-k) \right)^2, \end{aligned} \tag{6.42}$$

where $x(n) = s(n) - u(n)$ is the 'target' signal. For a given frame this target is fixed once the excitation signal has been determined. The problem with Equation (6.42) is that E is given in terms of not only the filter coefficients but also the reconstructed speech signal $\hat{s}(n)$ which, of course, also depends on the filter coefficients. Therefore we cannot simply set the partial derivatives $\partial E/\partial a_i$ to zero and obtain a set of p simultaneous linear equations for the optimal set of coefficients.

A feasible approach – which has been used in MPE codecs [175, 176] – is to make the approximation

$$\hat{s}(n-k) \approx s(n-k) \tag{6.43}$$

in Equation (6.42), which then gives

$$E \approx \sum_n \left(x(n) - \sum_{k=1}^{p} a_k s(n-k) \right)^2. \tag{6.44}$$

We can then set the partial derivatives $\partial E/\partial a_i$ to zero for $i = 1, 2, \ldots, p$, to obtain a set of p simultaneous linear equations:

$$\frac{\partial E}{\partial a_i} = -2 \sum_n \left(x(n) - \sum_{k=1}^{p} a_k s(n-k) \right) s(n-i) = 0 \tag{6.45}$$

so

$$\sum_{k=1}^{p} a_k \sum_n s(n-i)s(n-k) = \sum_n x(n)s(n-i) \tag{6.46}$$

for $i = 1, 2, \ldots, p$. Similar to our earlier elaborations in this chapter, two different approaches are possible depending on the limits of the summations in Equation (6.46). If we consider $s(n)$ and $u(n)$ to be of infinite duration and minimise the energy of the error signal $e(n)$ from $n = 0$ to $n = L - 1$, where L is the analysis frame length, the summations in Equation (6.46) are from $n = 0$ to $L - 1$ and we have a covariance like approach [93]. Alternatively we can consider $s(n)$ and $u(n)$ to be non-zero only for $0 \leq n \leq L - 1$, which leads to an autocorrelation like approach [93] where the simultaneous equations to be solved become

$$\sum_{k=1}^{p} a_k \sum_{n=0}^{L-1-|k-i|} s(n)s(n + |k-i|) = \sum_{n=0}^{L-1-i} s(n)x(n+i). \tag{6.47}$$

We investigated these two approaches, both with and without windowing of $s(n)$ and $u(n)$, in our 4.7 kbps codec. We found that the updated filter coefficients were, in terms of the SNR of the reconstructed speech, usually worse than the original coefficients. This is because of the inaccuracy of the approximation in Equation (6.43). To obtain any improvement in the SEGSNR of the reconstructed speech it was necessary in each frame to find the output of the synthesis filter with the original and updated filter coefficients, and transmit the set of coefficients which gave the best SNR for that frame. Using this technique we found that the updated filter coefficients were better than the original coefficients in only about 15% of frames, and the SEGSNR of the codec was improved by about 0.25 dB.

These results were rather disappointing, hence we attempted to find an improved method of updating the synthesis filter parameters. One possibility comes to light if we write

Equation (6.42) in a matrix notation

$$E = |\underline{x} - \underline{\underline{\hat{S}}}\,\underline{a}|^2, \tag{6.48}$$

where

$$\underline{x} = \begin{pmatrix} s(0) - u(0) \\ s(1) - u(1) \\ \vdots \\ s(L-1) - u(L-1) \end{pmatrix} \tag{6.49}$$

$$\underline{\underline{\hat{S}}} = \begin{pmatrix} \hat{s}(-1) & \hat{s}(-2) & \cdots & \hat{s}(-p) \\ \hat{s}(0) & \hat{s}(-1) & \cdots & \hat{s}(-p+1) \\ \vdots & \vdots & \ddots & \vdots \\ \hat{s}(L-2) & \hat{s}(L-3) & \cdots & \hat{s}(L-1-p) \end{pmatrix} \tag{6.50}$$

and

$$\underline{a} = \begin{pmatrix} a_1 \\ a_2 \\ \vdots \\ a_p \end{pmatrix}. \tag{6.51}$$

Note that here we have set the elements of $\underline{x}$ and $\underline{\underline{\hat{S}}}$ assuming that we are using the covariance-like approach, but similar equations can be written for the autocorrelation approach. We have to attempt to find a set of coefficients $\underline{a}$ such that

$$\underline{\underline{\hat{S}}}\,\underline{a} \approx \underline{x}. \tag{6.52}$$

Similar problems occur in many areas of science and engineering and are solved using least squares (LS) methods [177]. The usual technique is to assume that the 'data' matrix $\underline{\underline{\hat{S}}}$ is known perfectly, and that the 'observation' vector $\underline{x}$ is known only approximately. Then a set of coefficients $\underline{a}$ are found such that

$$\underline{\underline{\hat{S}}}\,\underline{a} = \underline{x} + \underline{\Delta x} \tag{6.53}$$

and $|\underline{\Delta x}|^2$ is minimised. One method of solving the LS problem is to use what are called the 'normal equations':

$$\underline{\underline{\hat{S}}}^{\mathrm{T}}\,\underline{\underline{\hat{S}}}\,\underline{a} = \underline{\underline{\hat{S}}}^{\mathrm{T}}\,\underline{x}. \tag{6.54}$$

These equations are equivalent to those in Equation (6.46). However, in our problem it is the data matrix $\underline{\underline{\hat{S}}}$ which is known only approximately, and the observation vector $\underline{x}$ which is known exactly. Therefore it seems obvious that the usual LS technique will not be ideal for our purposes.

In recent years a relatively new technique called total least squares (TLS) [178] has been applied to several problems, see for instance [179]. In this method, errors are assumed to exist

in both $\underline{\underline{\hat{S}}}$ and $\underline{x}$ and we find a set of coefficients $\underline{a}$ such that

$$(\underline{\underline{\hat{S}}} + \underline{\underline{\Delta \hat{S}}})\underline{a} = \underline{x} + \underline{\Delta x}, \tag{6.55}$$

where $|(\underline{\underline{\Delta \hat{S}}} \;||\; \underline{\Delta x})|_F^2$ is minimised. Here $|\cdot|_F^2$ denotes the squared Frobenius norm of a matrix, namely the sum of the squares of the matrix's elements, and $(\underline{\underline{\Delta \hat{S}}} \;||\; \underline{\Delta x})$ is a matrix constructed by adding $\underline{\Delta x}$ to $\underline{\underline{\hat{S}}}$ as the $(p+1)$th column of the new matrix.

The solution $\underline{a}$ of the TLS problem can be found using the singular value decomposition of $(\underline{\underline{\hat{S}}} \;||\; \underline{x})$ [178]. We invoked this technique, but found that it was not useful, since a high fraction (about 95%) of the sets of filter coefficients it delivered resulted in unstable synthesis filters.

One final LS method we investigated was the data least squares (DLS) technique [180]. Here all the errors are assumed to lie in the data matrix $\underline{\underline{\hat{S}}}$, and a set of coefficients are found such that

$$(\underline{\underline{\hat{S}}} + \underline{\underline{\Delta \hat{S}}})\;\underline{a} = \underline{x}. \tag{6.56}$$

This is much closer to what we want in our situation, and again the solution can be found using singular value decomposition. However, we found that the filter coefficients produced were very similar to those given by the TLS technique with, again, about 95% of the updated synthesis filters being unstable. Therefore, unfortunately, neither the TLS nor the DLS update are practical solutions for our problem.

6.5.3.3 Optimisation via Powell's Method

Given our input speech signal $s(n)$, the filter's excitation $u(n)$ and the reconstructed speech memory $\hat{s}(-p), \hat{s}(-p+1), \ldots, \hat{s}(-1)$, the error energy E is a function of the p filter coefficients. Thus we can consider E as a p-dimensional function which we wish to minimise. There are many different methods [177] for the minimisation of multidimensional functions, and we attempted this using the direction set, or Powell's method [177]. This method operates by iteratively carrying out a series of one-dimensional line minimisations, and attempting to find a series of 'conjugate' directions for these minimisations so that the minimum along one direction is not spoiled by subsequent movement along the others. At each iteration a line minimisation is carried out along each of the p directions, and then the p directions are updated in an effort to obtain the ideal conjugate directions (see [177] for details). The process ends when the decrease in E during a particular iteration is less than some given fractional tolerance. When this happens it is assumed that we have settled into a minimum, which we hope is the global minimum of E. In our simulations the line minimisations were carried out using Brent's method [177]. This does a series of evaluations of E for various sets of filter coefficients and hunts down the minimum along a particular direction using either a golden section search or parabolic interpolation.

We invoked Powell's optimisation for various values of the fractional tolerance which controls when the process of iterations should end. A good indicator of the complexity of minimisation procedures, such as Powell's method, is the number of times the function E to be minimised is evaluated. Every 100 evaluations are approximately as complex as the whole encoding process in our standard ACELP codec. Figure 6.7 shows how the SEGSNR of our 4.7 kbps codec with a Powell optimisation of the synthesis filter varies with the number of

evaluations of E carried out. The best SNR we were able to obtain was 11.85 dB, which was about 2 dB better than the SEGSNR of the codec without interpolation of the LSFs. However, as shown in Table 6.9 this difference is much reduced if we use bandwidth expansion and interpolation of the LSFs in the codec, and these methods are much less complex than the Powell update. The Powell optimisation is not a realistic option for a real codec, but it does give us an idea of the absolute best performance we can expect from updating the synthesis filter parameters. We see that without LSF quantisation this is only about half a decibel better than a codec with LSF interpolation and bandwidth expansion.

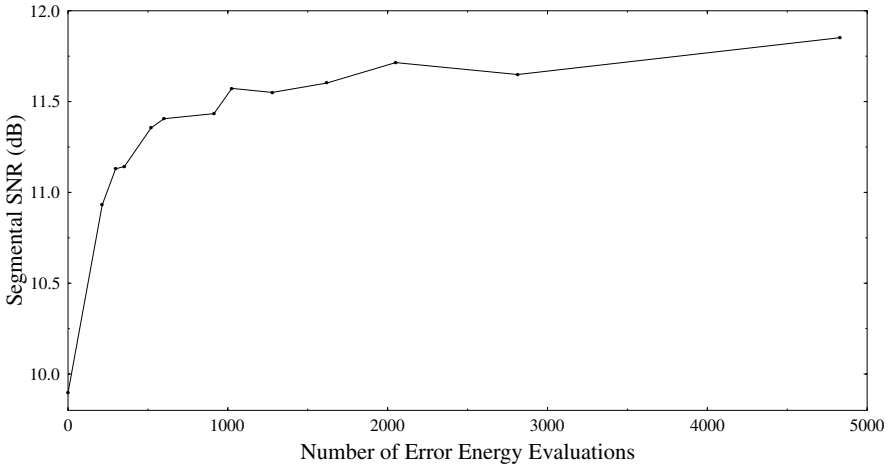

Figure 6.7: Powell optimisation performance.

Table 6.9: Performance of various synthesis filter determination techniques.

	Segmental SNR
Codec with no interpolation or bandwidth expansion	9.90
Codec with least squares optimisation	10.13
Codec with LSF interpolation only	10.49
Codec with bandwidth expansion only	10.59
Codec with interpolation and bandwidth expansion	11.29
Codec with Powell optimisation	11.85

6.5.3.4 Simulated Annealing and the Effects of Quantisation

In any real coder it is necessary to quantize the synthesis filter parameters for transmission to the decoder. It is not clear whether this need for quantisation will make updating the LPC parameters more or less worthwhile. On one hand the quantisation may mask and reduce the improvement due to the update, but on the other hand the updating algorithm can take

account of the quantisation when it is choosing a set of filter parameters and this may lead to the update having more effect.

We decided to start our investigation of the effects of updating the synthesis filter parameters with quantisation of the LSFs by finding an upper limit to the possible improvement. The Powell optimisation method was designed to operate on functions of continuous variables and so is not suitable when we consider quantisation of the LSFs. Instead, we used the technique of simulated annealing [177] which is more suitable for discrete optimisation.

Simulated annealing operates – as the termonology suggests – in analogy to the annealing (or slow cooling) of metals. When metals cool slowly from their liquid state they start in a very disordered and high-energy state and reach equilibrium in an extremely ordered crystalline state. This crystal is the minimum energy state for the system, and simulated annealing similarly allows us to find the global minimum of a complex function with many local minima. The procedure is as follows. The system starts in an initial state, which in our situation is an initial set of quantised LSFs. A temperature like variable T is defined, and possible changes to the state of the system are randomly generated. For each possible change the difference ΔE in the error energy between the present state and the possible new state is evaluated. If this is negative, in other words the new state has a lower energy than the old state, then the system always moves to the new state. If on the other hand ΔE is positive then the new state has higher energy than the old state, but the system may still change to this new state. The probability of this happening is given by the Boltzmann distribution

$$\text{prob} = \exp\left(\frac{-\Delta E}{kT}\right) \tag{6.57}$$

where k is a constant. The initial temperature is set so that kT is much larger than any ΔE that is likely to be encountered, so that initially most offered moves will be taken. As the optimisation proceeds the 'temperature' T is slowly decreased, and the number of moves to states with higher energy reduces. Eventually kT becomes so small that no moves with positive ΔE are taken, and the system comes to equilibrium in what is hopefully the global minimum of its energy.

The advantage of simulated annealing over other optimisation methods is that it should not be deceived by local minima and should slowly make its way towards the global minimum of the function to be minimised. In order to guarantee that this happens it is important to ensure that the temperature T starts at a high enough value and is reduced suitably slowly. We followed the suggestions in [177] and reduced T by 10% after every $100p$ offered moves, or every $10p$ accepted moves. The initial temperature was set so that kT was equal to ten times the highest value of ΔE that was initially encountered. The random changes in the state of the system were generated by randomly choosing an LSF and then moving it up or down by one quantisation level, provided that this did not lead to an LSF overlap, as it is necessary to avoid unstable synthesis filters.

We found that we were able to improve the SEGSNR of our 4.7 kbps codec with quantisation of the LSFs from 9.86 dB to 10.92 dB. Note, furthermore, that we were able to achieve almost the same improvement with a much simpler search technique described below. Rather than choose an LSF at random to modify and accept some changes which increase the error energy as well as all those which reduce the energy, we cycled sequentially through all p LSFs in turn. Each LSF was moved up and down one quantiser level to see if we

could reduce the error energy. Any changes which reduced the error energy, but none which increased it, were accepted. This process can be repeated any number of times, with every testing of all p LSFs counting as one iteration. The SEGSNR of our codec against the number of update iterations used is shown in Figure 6.8.

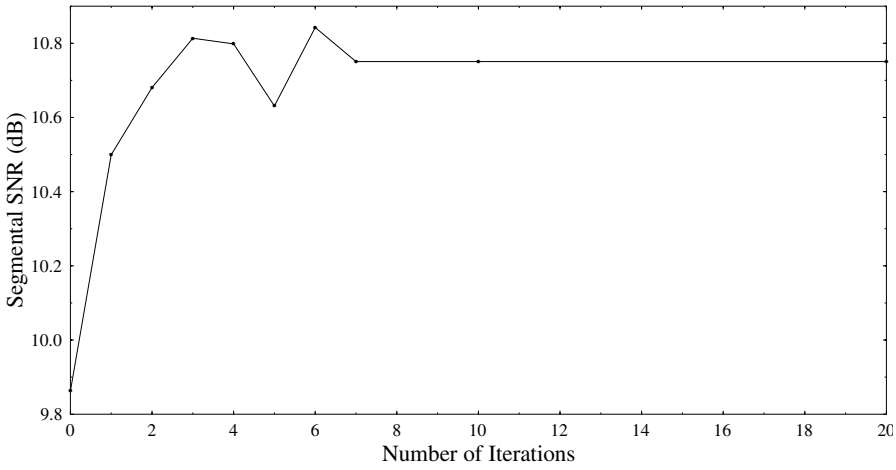

Figure 6.8: Performance of quantized LSF update scheme.

We see that this method of updating the quantised synthesis filter parameters produces a SEGSNR of 10.8 dB after just three iterations. This is almost equal to the improvement produced by simulated annealing of the LSFs, and yet the complexity of the codec is increased by only about 80%. The improvement obtained (about 1 dB) is similar to that quoted in [176] of 10% in multi-pulse codecs at SEGSNRs of around 10 dB. However, the method used in [176] required the recalculation of the excitation after the update of the synthesis filter parameters, and so approximately doubled the complexity of the codec.

As mentioned in [176], not only does updating of the synthesis filter help to increase the average SEGSNR, but it also helps remove the very low minima in SNR that occur for some frames. This effect is shown in Figure 6.9 which shows the variation of SNR for a sequence of fifty frames for 4.7 kbps codecs with and without update of the synthesis filter. The update used three iterations of the scheme described above. These low minima that occur can be subjectively annoying and so it is helpful if they can be partially removed.

It is also possible to update the synthesis filter in an attempt to increase the weighted SNR for each frame. We attempted this using the iterative scheme described above, and found that the improvement in the weighted SEGSNR due to the update saturated after just one iteration. The weighted SEGSNR increased from 7.18 dB to 7.43 dB, and the conventional SEGSNR increased from 9.86 dB to 10.08 dB.

The results described above comparing codecs with updated synthesis filter parameters to a codec with no update are reasonably good. However, as noted earlier for the codecs with no quantisation of the LSFs, the results are not so impressive when compared to codecs using the techniques of bandwidth expansion and interpolation of the LSFs. This is shown in Table 6.10. Using both bandwidth expansion and interpolation of the LSFs gives a SEGSNR almost identical to that achieved using the iterative update algorithm. Also, the

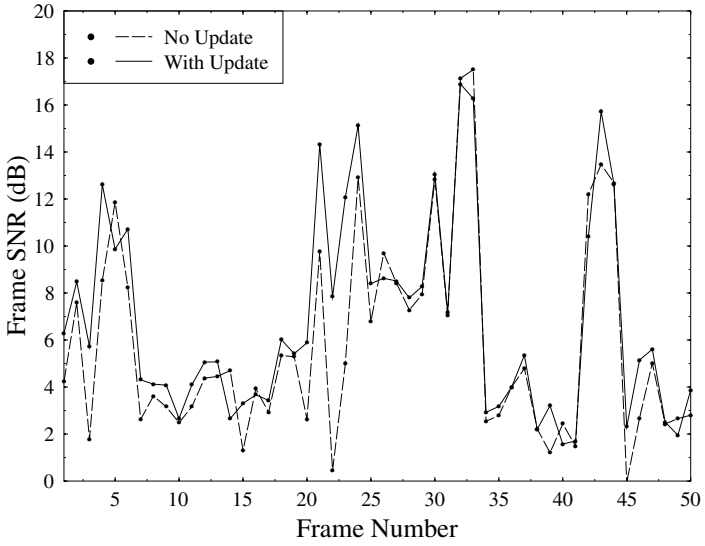

Figure 6.9: Effect of update on variation of SNR.

Table 6.10: Performance of synthesis filter techniques with quantisation.

	Segmental SNR
Codec with no interpolation or bandwidth expansion	9.86
Codec with bandwidth expansion only	9.89
Codec with LSF interpolation only	10.31
Codec with interpolation and bandwidth expansion	10.76
Codec with iterative update	10.75
Codec with simulated annealing update	10.92

interpolation and bandwidth expansion help remove the very low minima in the SNR in the same way that the update does. Although several papers [176, 181, 182] have reported reasonable improvements using various methods of update, to our knowledge none of them have considered the effects of LSF interpolation and bandwidth expansion. Our codec with the iterative update of the LSFs is about 10% more complex than the codec with interpolation and bandwidth expansion. However, the LSF interpolation scheme employed increases the delay of the codec by two sub-frames, or 15 ms. Both interpolation (when used along with bandwidth expansion) and the iterative update scheme give very similar improvements in the performance of the codec. If a 15 ms increase in the delay of the codec is not important then the LSF interpolation can be invoked. However, our iterative update scheme provides an alternative which gives similar results without increasing the delay of the codec, and is only slightly more complex.

The research reported here was summarised in [183]. In the next section we move on to investigating the error sensitivity of our 4.7 kbps ACELP codec.

6.6 The Error Sensitivity of CELP Codecs

6.6.1 Introduction

As we have previously argued, CELP codecs are capable of producing good toll quality speech at low bitrates with reasonable complexity. However, almost equally important for a codec which is to be used over a radio channel is its ability to cope with random bit errors between the encoder and decoder. A mobile radio channel is particularly hostile [93] and when there is no line of sight path between the receiver and transmitter, multi-path propagation leads to a channel which can be described by the Rayleigh distribution. Such a channel is not memory-less and deep fades of -20 dB, or more, are common. Such fades lead to error bursts and therefore it is necessary to use either interleaving, which attempts to randomise the bit errors, or a channel coder with good burst error correcting abilities. In any case, a channel coder is essential for any speech coder which is to be used over a mobile radio channel at reasonable channel SNR. However, no channel coder will be able to remove all the bit errors without requiring an unreasonable bandwidth, and so even with channel coding it is important that the speech codec should be as robust as possible to errors.

In this section we describe several methods for improving the bit error sensitivity of our coder, and also how to measure the error sensitivity of the speech encoder output bits so that the matching channel coder can be carefully designed to give most protection to the bits which are most sensitive. The results of simulations which are reported refer to our 4.7 kbps codec, and similar results were found to apply to the 7.1 kbps codec.

6.6.2 Improving the Spectral Information Error Sensitivity

It has been noted [184, 185] that the spectral parameters in CELP coders are particularly sensitive to errors. There are many different ways to represent these parameters, but LSFs [117] offer some definite advantages in terms of error robustness. One advantage is that the spectral sensitivities of the LSFs are localised [116], so that an error in a given LSF produces a change in the resulting spectrum only in the neighbourhood of the corrupted LSF. Another advantage is the ordering property of the LSFs. This means that for the synthesis filter to be stable, it is a necessary and sufficient condition that the LSFs from which it was derived are ordered, satisfying the condition $\mathrm{LSF}_1 < \mathrm{LSF}_2 < \mathrm{LSF}_3$, etc. Therefore, if a set of LSFs are received which are not ordered, the decoder infers that there must be at least one error in the bits that represent these LSFs, and some action must be taken to rectify this error and produce a stable synthesis filter. It is this action which is studied here.

6.6.2.1 LSF Ordering Policies

There is a high correlation between the LSFs of successive frames. This means that, as reported in [185], occasionally the LSF set for a given frame can be replaced by the set from the previous frame without introducing too much audible distortion. Therefore one possible

policy for dealing with frames where non-monotonic LSFs are received is to completely discard the LSFs which were received for that frame, and use those from the previous frame.

A better policy is to attempt replacing those LSFs which have to be, rather than all of them. In [186] when a non-monotonic set of LSFs is received, the two particular frequencies which cross over are replaced by the corresponding frequencies from the previous frame. Only if the resulting set of LSFs is still not ordered is the whole set replaced.

Several attempts have been made in order to attempt identifying which particular LSF is causing the instability, and then replace only it. In [187] use is made of the long-term statistics of the differences between adjacent LSFs in the same frame. If two frequencies cross over then an attempt is made to guess which one was corrupted and, in general, the guess is correct about 80% of the time. This 'hit ratio' can be improved by including a voicing decision – in a frame of voiced speech the formants are sharper than in unvoiced frames, and so the spacings between adjacent LSFs are generally smaller.

Instead of attempting to guess which LSF from a non-monotonic set is corrupted and then replacing this LSF with the corresponding frequency from a previous frame, we attempted to produce a monotonic set of LSFs by inverting various bits in the received bitstream. Initially we endeavour to determine which set of bits should be examined. For example, if $\mathrm{LSF}_i > \mathrm{LSF}_{i+1}$ then we know that either LSF_i or LSF_{i+1} has been corrupted. When such a cross-over is found we take the following steps.

(1) We check to see if $\mathrm{LSF}_i > \mathrm{LSF}_{i+2}$. If it is we assume that LSF_i is corrupt and select the bits representing this LSF as those to be examined.

(2) We check to see if $\mathrm{LSF}_{i-1} > \mathrm{LSF}_{i+1}$. If it is we assume LSF_{i+1} is in error and select these bits to be examined.

(3) If neither of the checks above indicate whether it is LSF_i or LSF_{i+1} which is corrupt then the bits representing both these LSFs are selected to be examined.

(4) We attempt to correct the LSF cross-over by inverting each bit, one at a time, from those to be examined. After each bit inversion the new value of LSF_i or LSF_{i+1} is decoded and checked to see if the cross-over has been removed and no new cross-overs introduced. If several possible codes are found then the one which gives the corrected LSFs as close as possible to their values in the previous frame is chosen.

(5) If, as occasionally happens at high bit error rates, no single bit inversion can be found which corrects the LSF cross-over, and introduces no new cross-over, then we adopt the policy which is recommended in [70]. First LSF_i, then LSF_{i+1}, then both, and finally the entire LSF set, is replaced by those in the previous frame until a monotonic set is found.

We simulated the effect of the error correction scheme described above over a set of four sentences spoken by different speakers. The predictor coefficients were determined in a 4.7 kbps coder using the autocorrelation approach and a 15 Hz bandwidth expansion was used. The LSFs were non-uniformly quantised with 34 bits. The CD [85] degradation produced by errors in the bits representing the LSFs is shown in Figure 6.10. The dotted curve represent the effect of the scheme described in [186]. As can be seen our correction

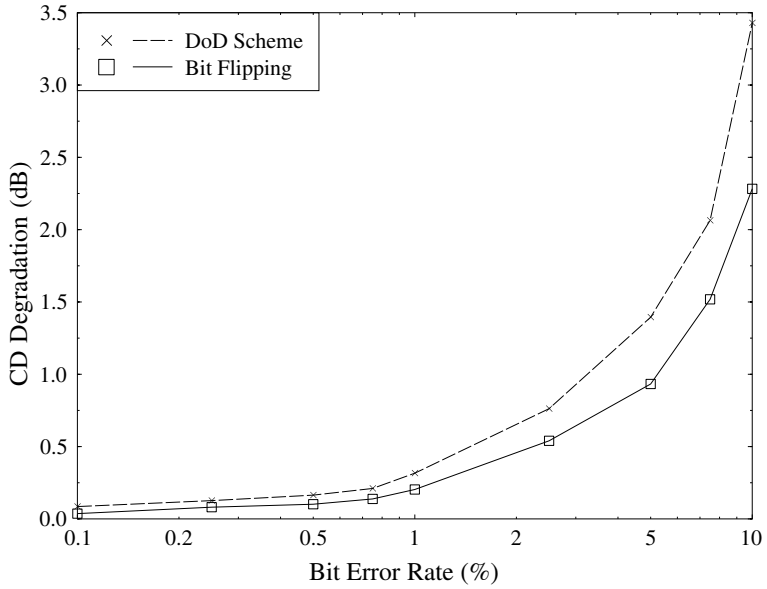

Figure 6.10: The CD degradation produced by random corruption of LSF bits.

policy gives consistently better results, and a definite subjective improvement was heard in informal listening tests.

Table 6.11: Hit ratios for various algorithms.

Bit error rate (%)	0.1	1	2	2.5	3	4
Atungsiri's scheme	100	80	80	82	79	80
Our scheme	100	88	92	93	93	92
Correct bit hit	83	81	80	77	78	78

Also in [187], a table of 'Hit ratio' figures is included to indicate how often the correct LSF for replacement was chosen at various bit error rates. The figures for the improved hit ratio which resulted when the voicing decision was used are reproduced in Table 6.11. Also shown in this table is the hit ratio for our scheme, quantifying as to how often the bit which was inverted was part of the codeword for the LSF which had actually been corrupted. As can be seen, our scheme performs significantly better than that reported in [187]. In the final row of Table 6.11 are the figures for how often the correct bit is inverted when a non-monotonic set of LSFs is received. As can be seen, the bit causing the LSF overlap is corrected about 80% of the time, and when this happens the effect of the bit error is completely removed. As about 30% of corrupted LSF bits produce LSF cross-overs, this means that about 25% of all LSF errors can be entirely removed by the decoder.

6.6.2.2 The Effect of FEC on the Spectral Parameters

Although our scheme described above can remove the effect of channel errors on the LSF bits about 25% of the time, the reconstructed speech is unacceptably distorted if the bit error rate among the LSF bits is above about 1%. Therefore some sort of error correction code is necessary if the coder is to be used at higher bit error rates. We found which of the LSF bits were most susceptible to errors by taking one LSF bit at a time and corrupting it 10% of the time. The resulting degradations in the SEGSNR and the CD of the reconstructed speech were noted. The 13 bits which were least sensitive in terms of CD degradation all gave a degradation of less than 0.05 dB when corrupted 10% of the time, and were left unprotected. The remaining 21 bits were protected with a $(31, 21, 2)$ BCH code which was simulated as follows. If two or less errors were generated in the 31 bit code word then they were corrected, and if more than two errors were generated then we assumed that although the BCH code would be unable to correct these errors, it would at least be able to detect that the protected 21 bits may contain errors. Then in the decoding of the speech if an LSF cross-over was found the decoder attempts to put it right by examining only unprotected bits, unless the BCH code indicates that the 21 protected bits may contain an error.

Thus the effect of including FEC on some of the LSF bits is not only that the most sensitive bits are completely protected (unless the code fails), but also when an LSF cross-over occurs because of an error in one of the less sensitive bits, the bit flipping algorithm is much more likely to select the correct bit to toggle. In fact, we found that for frames where the FEC had not failed, if an LSF cross-over occurred it was correctly fixed almost 100% of the time. In informal listening tests we found that for a bit error rate of 2.5% among the LSF bits the distortions produced were barely noticeable, and at 5% although the distortions were noticeable the reproduced speech was still of acceptable quality.

An alternative means of improving the performance of speech and channel codecs, based on similar ideas, has been proposed [188]. This uses the ordering property of the LSFs, along with a specific property of multi-band excited codecs to feed back information from the speech decoder to the channel decoder. The speech decoder indicates to the channel decoder if a set of received bits results in an LSF cross-over, or is otherwise unlikely to be correct. The channel decoder can then use this information to help it decode the correct information from the received bitstream. Good results, in terms of the error correcting capability of the source aided channel decoder, are reported.

6.6.2.3 The Effect of Interpolation

In our codec the usual practice of employing interpolation between the present and the previous set of LSFs is used. This helps minimise sudden sharp changes in the short-term predictor filter coefficients between one frame and the next. However, as can be seen from Figure 6.11, it also leads to increased propagation of the effect of an LSF error from one frame to the next. The upper graph shows the average effect, in terms of degradation of the frame SNR and CD, of an error in one of the LSF bits in the coder with LSF interpolation.The bit is corrupted in frame 0 and the graph shows how the resultant degradation dies out from one frame to the next. In frame 1 the corrupted set of LSFs is used along with the present set to form the interpolated LSFs. Hence the effect of the error is almost as serious in the frame following the error as it is in the corrupted frame. After this the effect of the error quickly disappears.

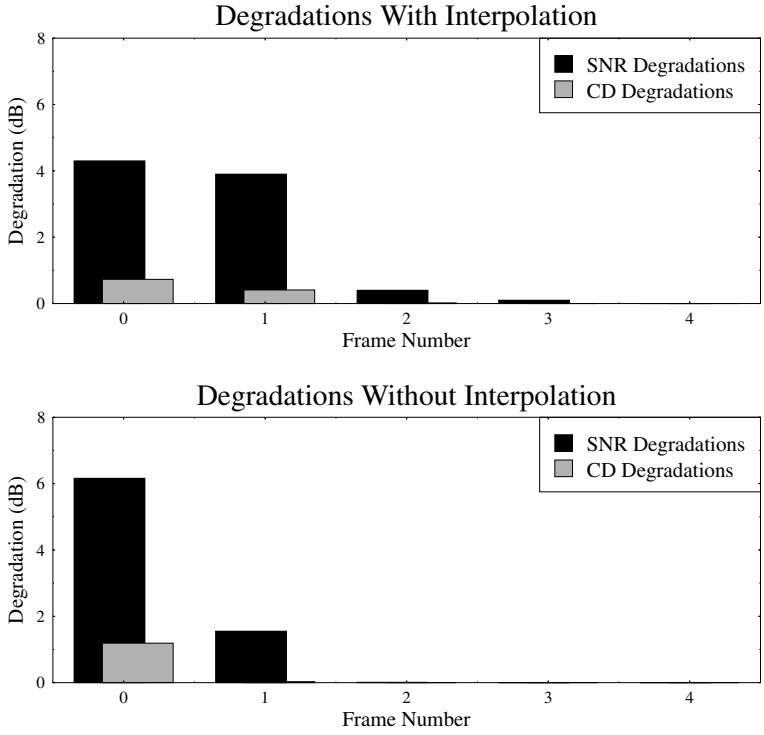

Figure 6.11: The effect of interpolation on error propagation.

Because of this error propagation it might be expected that the error sensitivity of the bits representing the LSFs could be improved by removing the interpolation. However, we found that removing interpolation from the codec reduced its clear channel SEGSNR by about 0.5 dB, and at various error rates between 0.1% and 10% the resultant degradations are almost identical to those found in the coder with interpolation. The lower graph in Figure 6.11 shows the effect of an error (on the same LSF bit as was used in the upper graph) in the coder in which interpolation is not used. It can be seen that although the error propagation is reduced, the degradation in the frame which was corrupted is increased. This is because interpolation helps to smooth out the effect of an LSF error in the corrupted frame.

6.6.3 Improving the Error Sensitivity of the Excitation Parameters

Most of the bits transmitted by a CELP coder are used to represent the excitation for the synthesis filter. In our coder the information which must be sent to the decoder is as follows.

(1) The fixed codebook index. Twelve bits per sub-frame are used.

(2) The fixed codebook gain. Four bits are used to represent the magnitude, which is logarithmically quantised, and one bit is used to represent the sign.

(3) The adaptive codebook delay. The delay can vary between 20 and 147 samples and so seven bits per sub-frame are needed to represent this information.

(4) The adaptive codebook gain. Three bits per sub-frame are used.

The error sensitivity of this information, and ways of improving it, are discussed below.

6.6.3.1 The Fixed Codebook Index

The algebraic codebook structure used in our codec is inherently quite robust to channel errors. This is because if one of the codebook index bits is corrupted, the codebook entry selected at the decoder will differ from that used in the encoder only in the position of one of the four non-zero pulses. Hence the corrupted codebook entry will be similar to the original. This is in contrast to traditional CELP coders which use a non-structured, randomly filled, codebook. In such codecs when a bit of the index is corrupted a new codebook address is decoded and the codebook entry used is entirely different to the original. Hence errors in the codebook index in such coders will be more significant than in ours. Such a codebook is used in [185] where SNR degradations of about 8 dB are recorded when a codebook index bit is corrupted in every frame. In our coder the corresponding degradation is only about 4 dB.

It is generally reported [70, 186] that errors in the fixed codebook index produce reconstructed speech in which the degradations are not perceptually annoying. Therefore the fixed codebook index is often left unprotected.

6.6.3.2 The Fixed Codebook Gain

The magnitude of the fixed codebook gain tends to vary quite smoothly from one sub-frame to the next. Therefore errors in the codebook gain can be spotted using a smoother to indicate, from the neighbouring gains, what range of values the present codebook gain should lie within. If a codebook gain is found which is not in this range then it is assumed to be corrupted, and replaced with some other gain.

We want a scheme which will spot as many errors in the codebook gain as possible, without introducing too many new errors by replacing gains which were not originally corrupted by the channel. After careful investigation of the effects of bit errors on the fixed codebook gain magnitude we implemented the following scheme. Every codebook gain quantiser level at the decoder is checked by calculating the mean and standard deviation of its two nearest neighbours. If the standard deviation of these neighbours is less than two quantiser levels then it is set equal to two. We then check to see if the present level is within 2.25 standard deviations of the mean calculated from its neighbours. If not it is assumed to be corrupt. When the codebook gain bits are corrupt with an error rate of 2.5% then this scheme spots almost 90% of the errors in the MSB of the gain level, while in error-free conditions it falsely spots errors in only about 0.5% of the sub-frames. This false error spotting produces a small degradation in the decoder performance at zero bit error rate. However, if some feedback between the channel decoder and the speech decoder is implemented so that the smoother is disabled in error-free conditions, as suggested in [185], then this degradation is removed.

Another important aspect of the smoother is how gains which are thought to be corrupt are replaced. In [185] when a gain magnitude is thought to be in error it is replaced with the

mean of its neighbours' magnitudes. However, we found that a bit flipping scheme, similar to that used to correct LSF cross-overs, produced better results. When an error is spotted the decoder inverts all four bits, one at a time, in the received codeword for the gain magnitude. The single bit inversion which produces a decoded gain level as close as possible to the mean of its neighbours is chosen.

The effect of our smoother on the error sensitivity of the four bits per sub-frame representing the fixed codebook gain magnitude is shown in Table 6.12. This table shows the SNR degradation produced in 4.7 kbps codecs with and without smoothing when the bits shown are corrupt in every frame (the bits are corrupt for one sub-frame only per frame). As can be seen the smoothing improves the error sensitivity of all the bits, most especially the MSB in which most of the errors are spotted and corrected by the smoother.

Table 6.12: SNR degradations for fixed codebook gain bits with and without smoothing.

Gain bit	SNR degradations (dB) without smoothing	SNR degradations (dB) with smoothing
LSB	1.4	1.3
Bit 2	3.0	2.8
Bit 3	6.2	4.8
MSB	10.5	2.1

The fixed codebook gain sign shows erratic behaviour and is not suitable for smoothing. This bit is among the most sensitive of the coder and should be well protected by the channel codec.

6.6.3.3 Adaptive Codebook Delay

Seven bits per sub-frame are used to encode the adaptive codebook delay, and most of these are extremely sensitive to channel errors. An error in one of these bits produces a large degradation not only in the frame in which the error occurred, but also in subsequent frames, and generally it takes more than ten frames before the effect of the error dies out.

If the adaptive codebook delay is chosen by the encoder by merely minimising the weighted MSE of the reconstructed speech, its behaviour will be erratic and not suitable for smoothing. The delay can be forced to take on smooth behaviour by modifying the encoder to choose slightly sub-optimal delays. This then allows the decoder to use smoothing to minimise the effect of errors. However, there is a noticeable clear channel degradation due to the sub-optimal delays chosen by the encoder.

Another approach [185, 189] is to use simulated annealing to assign codewords to delays so that common codewords have good neighbours. This means that when a common codeword is corrupted the new delay selected is such that the resultant degradation is minimised. This approach, along with smoothing, is used in the DoD 4.8 kbps standard [100], but as it has already been studied extensively we have not attempted this.

6.6.3.4 Adaptive Codebook Gain

The pitch gain is much less smooth than the fixed codebook gain, and is not suitable for smoothing. However, its error sensitivity can be slightly increased by coding the quantiser level with a Gray code rather than the natural binary code (NBC). The effect off this is shown in Table 6.13, which gives the SNR degradation for the two codes caused by bit errors (at a rate of 10%) in the three bits used to represent the gain in one sub-frame.

Table 6.13: The effect of using a gray code for the LTP gain.

Gain bit	SNR degradations (dB) NBC	SNR degradations (dB) Gray code
Bit 1	1.9	1.9
Bit 2	3.0	1.7
Bit 3	5.3	4.8

6.6.4 Matching Channel Codecs to the Speech Codec

It is very clear that some bits are much more sensitive to channel errors than others, and so should be more heavily protected by the channel coder. However, it is not obvious how the sensitivity of different bits should be measured. One commonly used approach [185] is, for a given bit, to invert this bit in every frame and measure the SEGSNR degradation which results. The error sensitivity of various bits for our coder measured in this way is shown in Figure 6.12. What information various bits represent is given in Table 6.14. Another similar approach [184] is to measure the degradations in both the SNR and the CD which result from systematic inversion of a given bit in every frame, and combine these measures to give an overall sensitivity measure.

The problem with these approaches is that they do not take adequate account of the different error propagation properties of different bits. This means that if instead of corrupting a bit in every frame it is corrupted randomly with some error probability then the relative sensitivity of different bits will change. We propose a new measure of error sensitivity. For each bit a graph similar to that in Figure 6.11 is found; in other words, we find the

Table 6.14: Bit numbering.

Bit numbers	Represents
1–34	LSFs
35–41	Adaptive codebook delay (sub-frame 1)
42–44	Adaptive codebook gain (sub-frame 1)
45–56	Fixed codebook index (sub-frame 1)
57	Fixed codebook gain sign (sub-frame 1)
58–61	Fixed codebook gain (sub-frame 1)

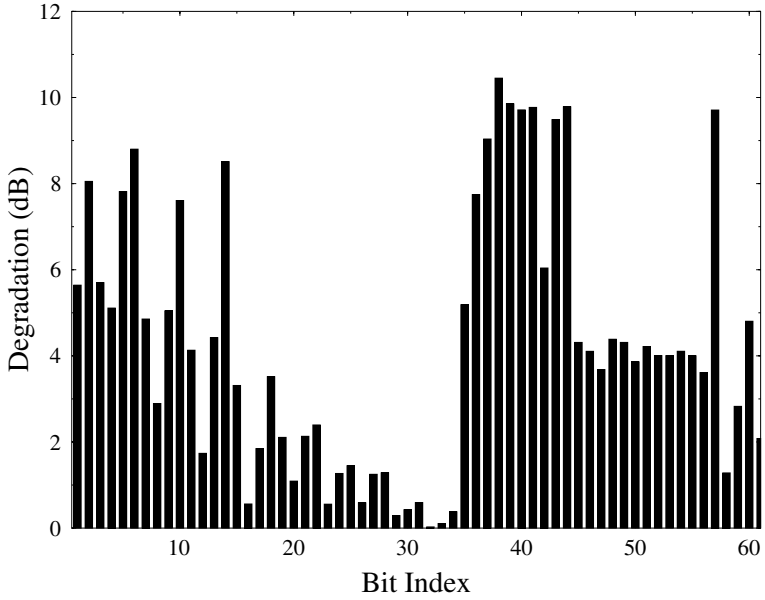

Figure 6.12: The SNR degradations due to consistently corrupting the bit studied.

average SNR degradation for a single bit error in the frame in which the error occurs and in the following frames. The total SNR degradation is then found by adding together the degradations in frames $0, 1, 2$, etc. This total degradation is equivalent to the average SNR degradation which will be produced by a single error in a given bit. Of course, the effect of a single error on the SEGSNR will be averaged out over all the frames of the speech file so that, for example, if a bit with a total SNR degradation of 10 dB is corrupted once in a speech file of 100 frames then the overall degradation in the SEGSNR will on average be 0.1 dB. The exact degradation depends very much on which frame the bit is corrupted in – corrupting a given bit in one frame of a speech file can produce a much larger degradation in the SEGSNR for that file than corrupting the same bit in a different frame. This is shown in Figure 6.13 which gives the degradation in the SEGSNR produced by a single bit corruption versus the frame in which the corruption takes place, for various different bits.

Figure 6.14 shows, for various bits, the average effect of a bit error in the frame in which the error occurred and in the following frames. The different error-propagation properties of different bits can be clearly seen. For example, an error in a bit representing an LSF has a significant effect only in the frame in which the error occurred and in the next two frames. Conversely, an error in a bit representing the LTP delay gives a large degradation in the frame SNR, and this degradation is still significant 10 frames later. Figure 6.15 shows the total SNR degradation for single bit errors of the various bits. This graph is significantly different to that in Figure 6.12, in particular the importance of the adaptive codebook delay bits, because of their memory propagation properties, is much clearer.

Our error-sensitivity figure is based on the total SNR degradation described above and on a similar measure for the total CD degradation. The two sets of degradation figures are

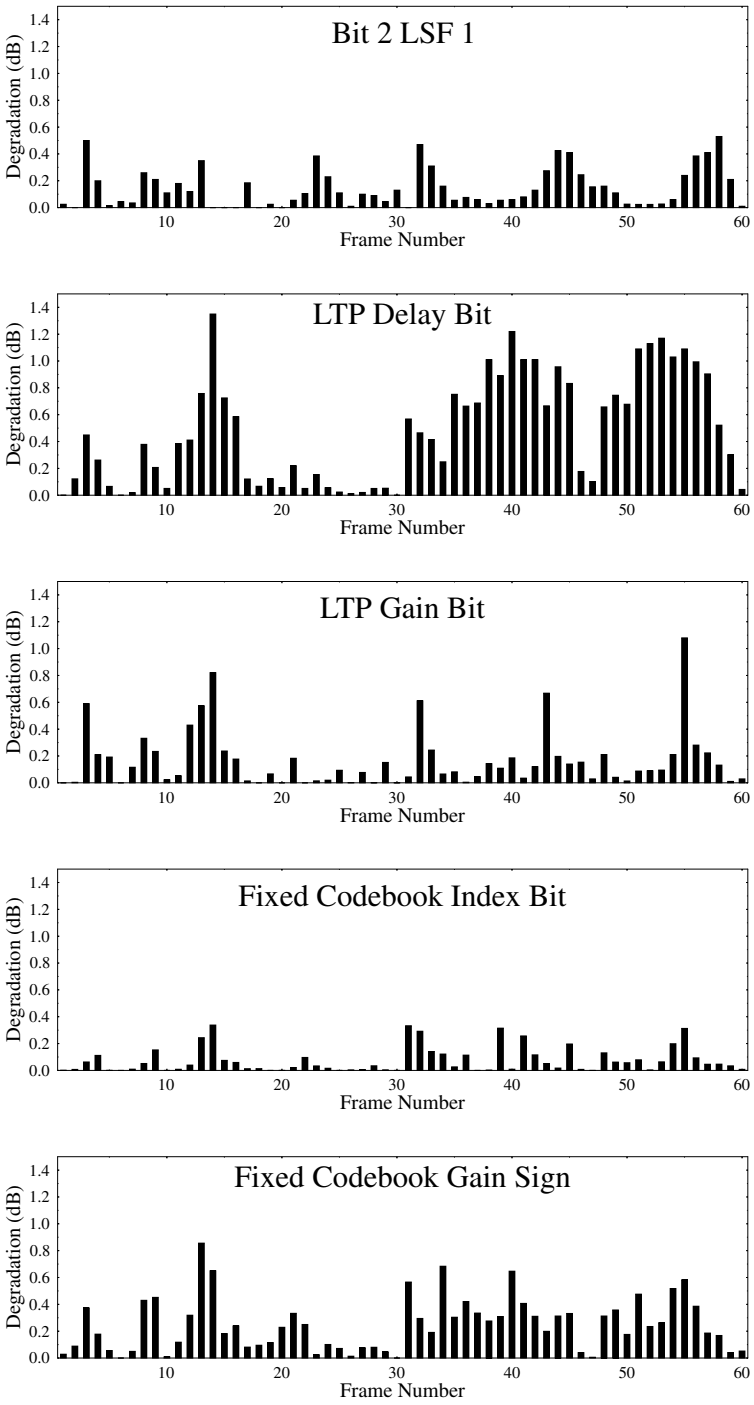

Figure 6.13: The degradation caused by bit errors in different frames.

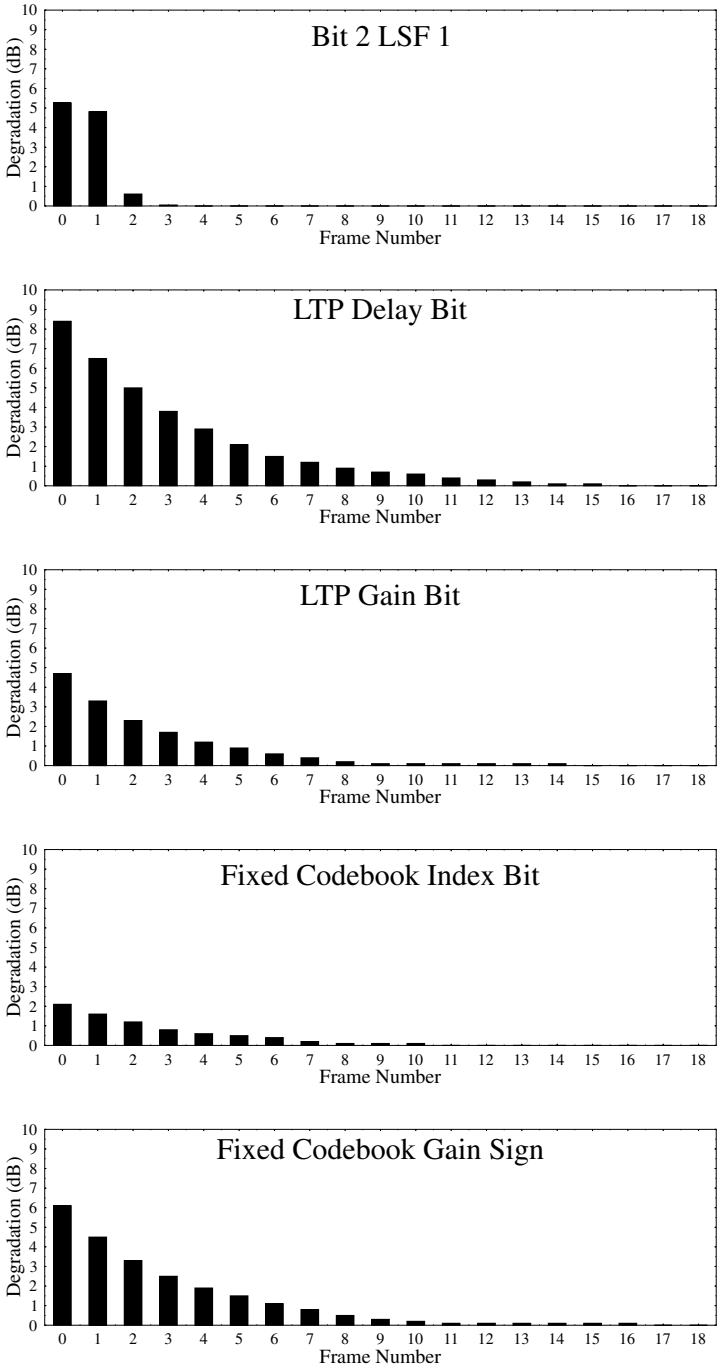

Figure 6.14: The SNR degradation propagation for various bits.

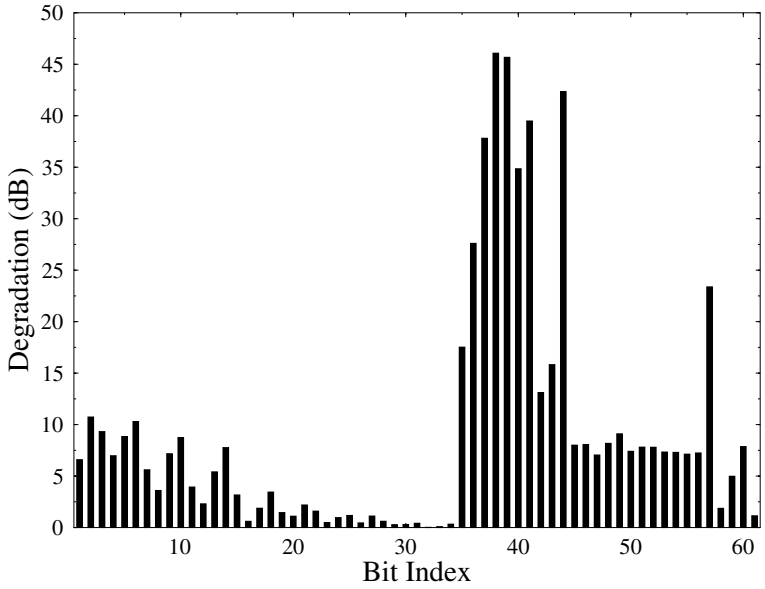

Figure 6.15: Total SNR degradation due to single errors in various bits.

combined and given equal weight by scaling each total SNR degradation by the maximum such degradation, and similarly for the total CD figures. The two sets of scaled degradation figures are then added together to give an overall sensitivity figure between 0 and 2. The higher this figure is, the more sensitive the bit is deemed to be.

Our new scheme was tested as follows. The twelve most sensitive bits were determined using our scheme and that reported in [184]. These two sets of twelve bits contained four in common, which were removed to give two sets of eight bits. The two different sets were corrupted at a 5% bit error rate for various different speech files, and in all cases we found that both objectively (CD and SNR degradations) and in informal listening tests, the bits our scheme predicted would be most sensitive were much more sensitive than those predicted using the approach in [184].

6.6.5 Error Resilience Conclusions

In this section we have discussed the error sensitivity of the forward adaptive ACELP codec described earlier in this chapter. We investigated various ways of improving the error sensitivity of the codec, and how the sensitivity of different bits could be compared in order to correctly match a channel coder to the speech coder. We have also shown how the degradations produced by errors propagate from one frame to another, and may persist for more than ten frames, and how the sensitivity of a given bit can vary significantly from frame to frame.

The error sensitivity improvement and evaluation techniques we have described in this chapter were used to match our 4.7 kbps speech codec with a set of BCH error-correcting codes. The speech and error-correction codecs were used in conjunction with 16-level

QAM and a PRMA scheme to simulate a complete multiple-user mobile communication system [169]. Similar studies were also carried out for a 6.5 kbps codec, which was similar to our 7.1 kbps codec described in Section 6.4.3, except it used six 5 ms sub-frames to make up a 30 ms frame instead of using four sub-frames per 20 ms frame. This extension of the frame length of the higher-rate codec to be equal to the frame length of the low-rate codec was carried out for reasons of ease of implementation of the PRMA scheme [169, 190], as will become clear in the next section, focussing on a variety of application examples.

6.7 Application Example: A Dual-mode 3.1 kBd Speech Transceiver

6.7.1 The Transceiver Scheme

The schematic diagram of the proposed re-configurable transceiver is portrayed in Figure 6.16. A Voice Activity Detector (VAD) similar to that of the Pan-European GSM system [98] enables or disables the ACELP encoder [191] and queues the active speech frames in the PRMA [192] slot allocator (SLOT ALLOC) for transmission to the base station (BS). The 4.7 or 6.5 kbps (kbps) ACELP coded active speech frames are mapped according to their error sensitivities to n number of protection classes by the Bit Mapper (BIT MAP), as shown in the figure and source sensitivity-matched binary BCH encoded [158] by the BCHE1, . . . ,BCHEn encoders. The 'Map & PRMA Slot Allocator' block converts the binary bitstream to 4- or 6-bit symbols, injects pilot symbols [159] and ramp symbols, and allows the packets to contend for a PRMA slot reservation. After BCH encoding the 4.7 and 6.5 kbps speech bits they are mapped to 4- or 6-bit symbols, which are modulating a re-configurable 16- or 64-level QAM scheme.

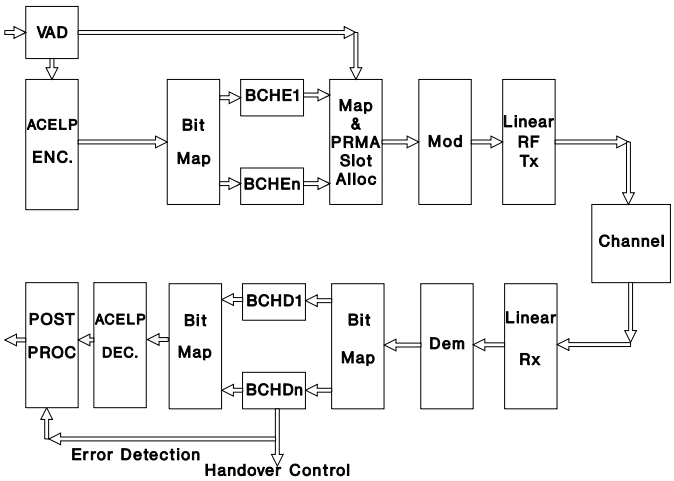

Figure 6.16: Transceiver schematic.

We have arranged for the 4.7 kbps/16-QAM and 6.5/64-QAM schemes to have the same signaling rate and bandwidth requirement. Therefore, this transmission scheme can provide higher speech quality, if high channel SNR and signal-to-interference ratios (SIR) prevail, while it can be reconfigured under network control to deliver lower but unimpaired speech quality amongst lower SNR and SIR conditions. Indoors pico-cellular cordless systems have typically friendly, high-SNR and high-SIR non-dispersive propagation channels and the partitioning walls also contribute towards attenuating co-channel interferences. Furthermore, the PRMA time-slots can be classified according to the prevailing interference levels evaluated during idle slots and if sufficiently high SIRs prevail, the higher speech quality mode can be invoked, otherwise the more robust lower speech quality mode of operation must be used.

The modulated signal is then transmitted using the linear radio frequency (RF) transmitter (Tx) over the friendly indoors channel, received by the linear receiver (Rx), demodulated (DEM) and the received speech bits are mapped back to their original bit protection classes by the bit mapper. The n-class BCH decoder BCHD1, . . . ,BCHDn carries out error correction before ACELP decoding and post-processing can take place. Observe that the error detection capability of the strongest BCH decoder, which is more reliable than that of its weaker counterparts, can be used to assist in controlling handovers to a less interfered PRMA time slot on any other available carrier or to activate speech post-processing in order to conceal the subjective effects of BCH decoding errors.

6.7.2 Re-configurable Modulation

The choice of the modulation scheme is a critical issue and it has wide-ranging ramifications as regards to the system's robustness, bandwidth efficiency, power consumption, whether to use an equaliser, etc. In [155] we have shown that due to the fact that GMSK, π/4-shifted quaternary phase shift keying ($\pi/4$-DQPSK) and 16-QAM have bandwidth efficiencies of 1.35 bps/Hz, 1.64 bps/Hz and 2.4 bps/Hz, respectively, 16-QAM achieves the highest PRMA gain. This is explained by the fact that 16-QAM allows us to generate the highest number of time slots amongst them, given a certain bandwidth, and therefore the statistical multiplexing gain of PRMA can approach the reciprocal of the voice activity factor. These findings prompted us to opt for multi-level modulation.

In our proposed re-configurable transceiver the different source rates of the 4.7 and 6.5 kbps ACELP codecs will be equalised using a combination of appropriately designed FEC codecs and 4 bits/symbol or 6 bits/symbol modulators. When the channel SNR and SIR are high, as in friendly indoors pico-cells, 64-level QAM (64-QAM) is used to convey the 196 bits of the 6.5 kbps ACELP codec. In contrast, for worse channel conditions, for example after a hand-over to an outdoors micro-cell, the 142 bits of the lower quality 4.7 kbps codec are delivered by a more robust 16-QAM modem in the same bandwidth as the 64-QAM scheme.

Non-coherent QAM modems [159] are less complex to implement, but typically require higher SNR and SIR values than their coherent counterparts. Hence in our proposed scheme, second-order switched-diversity assisted coherent pilot symbol assisted modulation (PSAM) using the maximum-minimum-distance square QAM constellation is preferred. For the 16-QAM scheme it was shown in [159] that it has two independent subchannels exhibiting different integrities, depending on the position of the bits in a four-bit symbol. On the same

note, our 64-QAM modem possesses three different subchannels having different bit error rates. This property naturally lends itself to un-equal error protection, if the source sensitivity-matched integrity requirements are satisfied by the QAM subchannel integrities.

Therefore, we have evaluated the C1 and C2 bit error rate (BER) versus channel SNR performance of our 16-QAM modem using a pilot spacing of $P = 10$ over both the best-case AWGN channel and over the worst-case Rayleigh-fading channel with and without second-order diversity. The C1 and C2 BER results are shown in Figure 6.17 for the experimental conditions characterised by a pedestrian speed of 4 mph, propagation frequency of 1.9 GHz, pilot symbol spacing of $P = 10$ and a signaling rate of 100 kBd. Observe in the figure that over Rayleigh-fading channels (RAY) there is an approximately factor three BER difference between the two subchannels both with and without diversity (D). Due to the violent channel phase fluctuations our modem was unable to remove the residual BER floor exhibited at higher channel SNR values, although diversity reception reduced its value by nearly an order of magnitude. The diversity receiver operated on the basis of the minimum channel phase shift within a pilot period, since this condition was found more effective in terms of reducing the BER than the maximum received power condition. Note that in the case of the chosen 100 kBd signaling rate the modulated signal will fit in a bandwidth of 200 kHz when using a 100% excess bandwidth. Since this coincides with the bandwidth of the Pan-European GSM system [98], we will be able to make direct comparisons in terms of the number of users supported. This will allow us to assess the potential benefits of using multimode terminals constituted by third generation system components in terms of the increased number of users supported.

How this BER difference between the two subchannels can be exploited in order to provide source-matched FEC protection for the 4.7 kbps ACELP codec will be described in the next section. Following a similar approach for the 6.5 kbps/64-QAM scheme leads to the system proposed as a re-configurable alternative, which will also be introduced in the next section. Suffice to say here that the BER versus channel SNR performance of this more vulnerable but higher speech quality 64-QAM scheme is portrayed under the same propagation conditions as in the case of the 16-QAM modem in Figure 6.18, when using a pilot spacing of $P = 5$. As expected, this diversity and pilot-assisted modem also exhibits a residual BER floor and there is a characteristic BER difference of about a factor of two between the C1 and C2, as well as the C2 and C3 subchannels, respectively. Rather than equalising these BER differences we will design an un-equal error-protection scheme for the speech bits, which capitalises on this property.

6.7.3 Source-matched Error Protection

6.7.3.1 Low-quality 3.1 kBd Mode

In this section we will exploit the subchannel integrity differences highlighted in the previous section in Figures 6.17 and 6.18, and protect these subchannels with source-sensitivity matched binary BCH FEC codecs [158]. Both convolutional [158] and block codes [158] can be successfully employed over bursty mobile channels and convolutional codes have found favour in systems, such as the Pan-European GSM system [98], where the complexity of soft-decisions is acceptable. Their disadvantage is that they cannot reliably detect decoding errors and hence they are typically combined with an external error detecting block code,

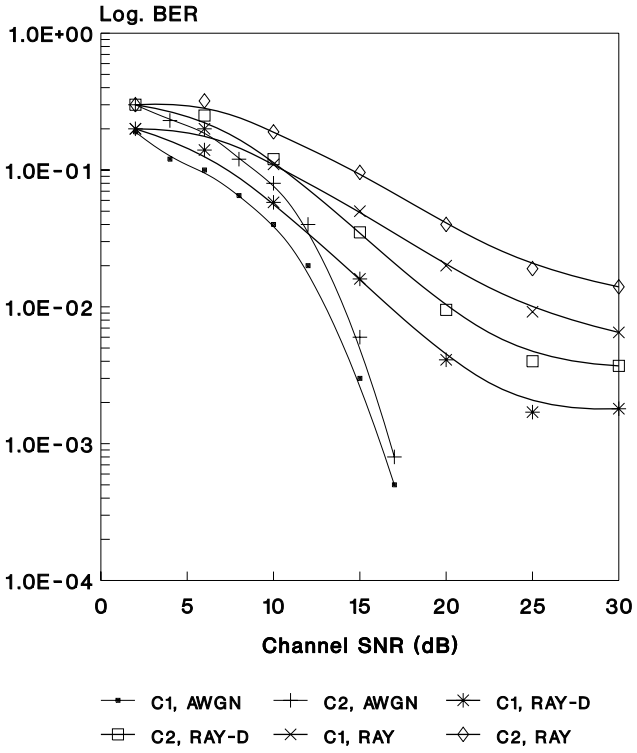

Figure 6.17: C1 and C2 BER versus channel SNR performance of PSAM-assisted 16-QAM using a pilot spacing of $P = 10$ over AWGN and Rayleigh channels at 4 mph, 100 kBd and 1.9 GHz with and without diversity.

as in the GSM system. In contrast, powerful block codes have an inherent reliable error-detection capability in addition to their error-correction capability, which can be exploited to invoke error concealment or to initiate handovers, when the average bit error rate is high, as portrayed in Figure 6.16.

The error sensitivity of the 4.7 kbps ACELP source bits was evaluated in Figures 6.14 and 6.15, but the number of bit protection classes n still remains to be resolved. Intuitively, one would expect that the more closely the FEC protection power is matched to the source sensitivity, the higher the robustness. In order to limit the system's complexity and the variety of candidate schemes, in the case of the 4.7 kbps ACELP codec we have experimented with a full-class BCH codec, a twin-class and a quad-class scheme, while maintaining the same coding rate.

For the full-class system we decided to use the approximately half-rate BCH$(127, 71, 9)$ codec in both subchannels, which can correct 9 errors in each 127-bits block, while encoding 71 primary information bits. The coding rate is $R = 71/127 \approx 0.56$ and the error correction capability is about 7%. Observe that this code curtails BCH decoding error propagation across the speech frame boundaries by encoding each 142-bit speech frame using two

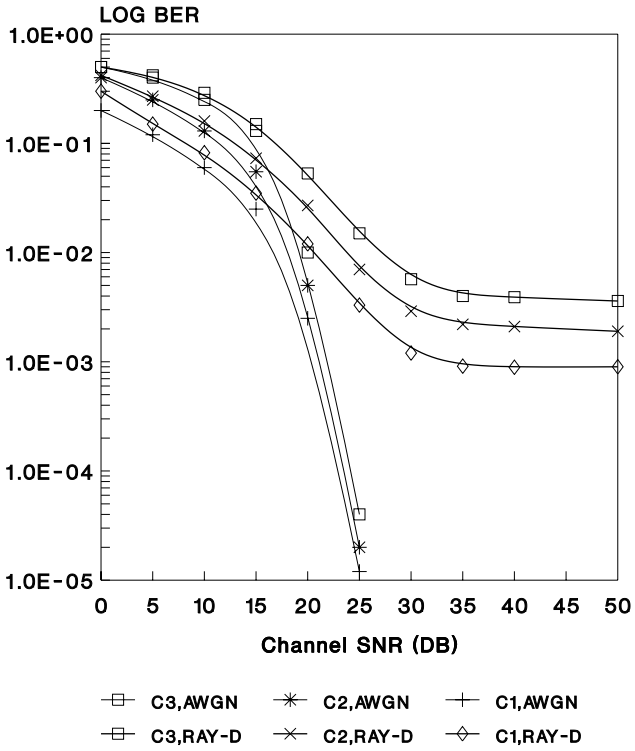

Figure 6.18: C1, C2 and C3 BER versus channel SNR performance of PSAM-assisted 64-QAM using a pilot spacing of $P = 5$ over AWGN and Rayleigh channels with diversity at 4 mph, 100 kBd and 1.9 GHz.

BCH$(127, 71, 9)$ frames, although even a single BCH decoding error will inflict prolonged speech impairments, as portrayed in Figure 6.14.

In order to design the twin-class system, initially we divided the ACELP bits into two sensitivity classes, Class One and Class Two, which are distinct from the C1 and C2 16-QAM subchannels. Both Class One and Two contained 71 bits. Then we evaluated the SEGSNR degradation inflicted by certain fixed channel BERs maintained in each of the classes using randomly distributed errors, while keeping bits of the other class intact. These experiments suggested that an approximately five times lower BER was required by the more sensitive Class One bits in order to restrict the SEGSNR degradations to similar values to those of the Class Two bits.

Recall from Figure 6.17 that the 16-QAM C1 and C2 subchannel BER ratio was limited to about a factor of three. Hence we decided to employ a stronger FEC code to protect the Class One ACELP bits transmitted over the 16-QAM C1 subchannel than for the Class Two speech bits conveyed over the lower integrity C2 16-QAM subchannel, while maintaining the same number of BCH-coded bits in both subchannels. However, the increased number of redundancy bits of stronger BCH codecs requires that a higher number of sensitive ACELP bits are directed to the lower integrity C2 16-QAM subchannel, whose coding power must be

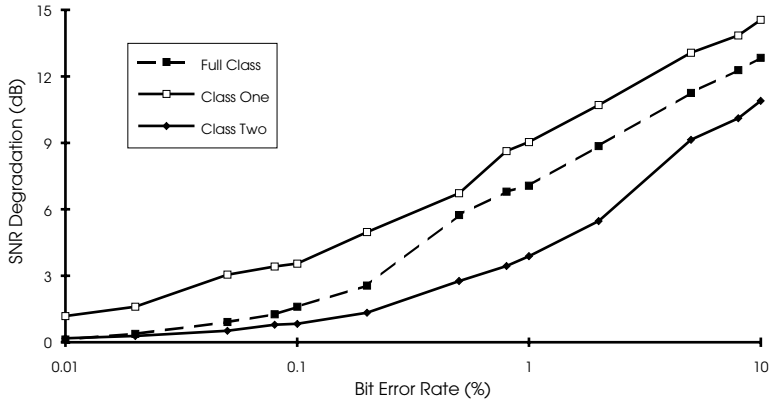

Figure 6.19: SEGSNR degradation versus BER for the 4.7 kbps ACELP codec when mapping 71 ACELP bits to both Classes One and Two in the full-class system and 57 as well as 85 bits to Classes One and Two in the twin-class scheme, respectively.

concurrently reduced in order to accommodate more source bits. This nonlinear optimisation problem can only be solved experimentally, assuming a certain sub-division of the source bits, which would match a given pair of BCH codecs.

Based on our previous findings as regards to the C1 and C2 16-QAM BERs and taking account of the practical FEC correcting power limitations we then decided to increase the C1–C2 16-QAM subchannel BER ratio from about three by about a factor of two so that the Class One ACELP bits were guaranteed a BER advantage of about a factor of six over the more robust Class Two bits. After some experimentation we found that the BCH$(127, 57, 11)$ and BCH$(127, 85, 6)$ codes employed in the C1 and C2 16-QAM subchannels provided the required integrity. The SEGSNR degradation caused by a certain fixed BER assuming randomly distributed errors is portrayed in Figure 6.19 for both the full-class and the above twin-class system, where the number of ACELP bits in the protection classes One and Two is 57 and 85, respectively. Note that the coding rate of this system is the same as that of the full-class scheme and each 142-bit ACELP frame is encoded by two BCH codewords. This yields again $2 \cdot 127 = 254$ encoded bits and curtails BCH decoding error propagation across speech segments, although the speech codec's memory will still be corrupted and hence will prolong speech impairments. The FEC-coded bitrate became ≈ 8.5 kbps.

The BER versus channel SNR performance of our twin-class C1, BCH$(127, 57, 11)$-protected and C2, BCH$(127, 85, 6)$-protected diversity-assisted 16-QAM modem is shown in Figure 6.20 along with the curves C1, Ray-D and C2, Ray-D characteristic of the diversity-assisted no-FEC Rayleigh-fading scenarios, which are repeated here from Figure 6.17 for ease of reference. Observe that between the SNR values of 15–20 dB there is about an order of magnitude BER difference between the FEC-coded subchannels, as required by the 4.7 kbps speech codec.

With the incentive of perfectly matching the FEC coding power and the number of bits in the distinct protection classes to the ACELP source sensitivity requirements we also designed a quad-class system, while maintaining the same coding rate. We used the BCH$(63, 24, 7)$, BCH$(63, 30, 6)$, BCH$(63, 36, 5)$ and BCH$(63, 51, 2)$ codes and transmitted the most sensitive

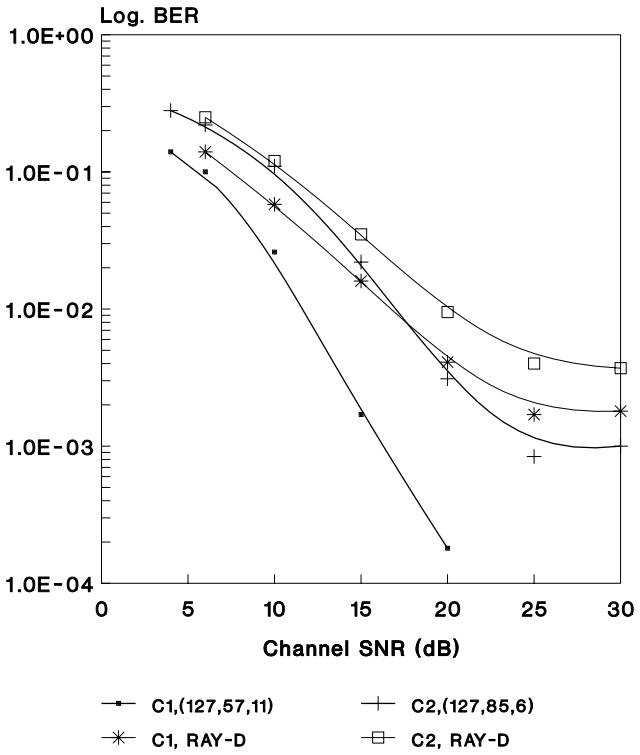

Figure 6.20: C1 and C2 BER versus channel SNR performance of PSAM-assisted 16-QAM using a pilot spacing of $P = 10$ over Rayleigh channels at 4 mph, 100 kBd and 1.9 GHz with diversity and FEC coding.

bits over the C1 16-QAM subchannel using the two strongest codes and relegated the rest of them to the C2 subchannel, protected by the two weaker codes.

The PRMA control header [192] was for all three schemes allocated a BCH$(63, 24, 7)$ code and hence the total PRMA framelength became 317 bits, representing 30 ms speech and yielding a bitrate of ≈ 10.57 kbps. The 317 bits give 80 16-QAM symbols and 9 pilot symbols as well as $2 + 2 = 4$ ramp symbols, resulting in a PRMA framelength of 93 symbols per 30 ms slot. Hence the signaling rate becomes 3.1 kBd. Using a PRMA bandwidth of 200 kHz, similar to the Pan-European GSM system [98] and a filtering excess bandwidth of 100% allowed us to accommodate 100 kBd/3.1 kBd ≈ 32 PRMA slots.

6.7.3.2 High-quality 3.1 kBd Mode

Following the approach proposed in the previous subsection we designed a triple-class source-matched protection scheme for the 6.5 kbps ACELP codec. The C1, C2 and C3 64-QAM subchannel performance was characterised by Figure 6.18, when using second-order switched-diversity and pilot-symbol assisted coherent square-constellation 64-QAM [73]

amongst our previously stipulated propagation conditions with a pilot-spacing of $P = 5$. The BER ratio of the C1, C2 and C3 subchannels was about 1:2:4.

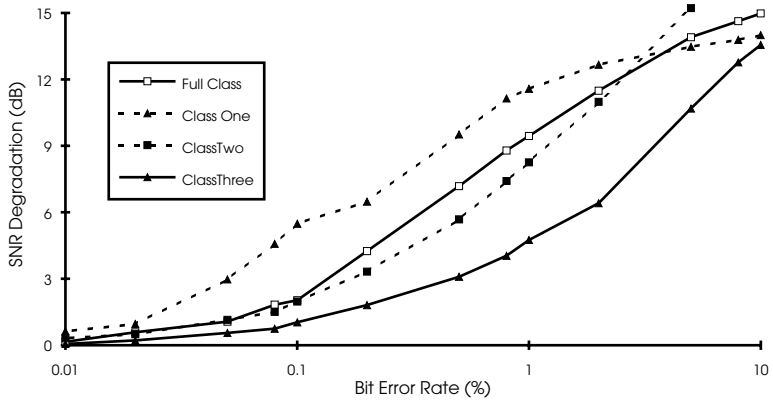

Figure 6.21: SEGSNR degradation versus BER for the 6.5 kbps ACELP codec when using either the full-class scheme or mapping 49, 63 and 84 ACELP bits to Classes One, Two and Three in the triple-class scheme, respectively.

The SEGSNR degradation versus channel BER performance of the 6.5 kbps higher-quality mode is portrayed in Figure 6.21, when using randomly distributed bit errors and assigning 49, 63 and 84 bits to the three sensitivity classes. For reference we have also included the sensitivity curve for the full-class codec. As we have seen for the lower-quality 16-QAM mode of operation, the modem subchannel BER differences had to be further emphasised using stronger FEC codes for the transmission of the more vulnerable speech bits.

The appropriate source sensitivity-matched codes for the C1, C2 and C3 subchannels were found to be the shortened 13-error correcting BCH13 = BCH$(126, 49, 13)$, the 10-error correcting BCH10 = BCH$(126, 63, 10)$ and the 6-error correcting BCH6 = BCH$(126, 84, 6)$ codes, while the packet header was again allocated a BCH$(63, 24, 7)$ code. The corresponding BER versus channel SNR curves are presented for our standard propagation conditions in Figure 6.22, where the non-protected diversity-assisted Rayleigh BER curves are also repeated for convenience. These codes allowed us to satisfy both the integrity and the bit packing requirements, while curtailing bit-error propagation across speech frame boundaries.

The total number of BCH-coded bits becomes $3 \times 126 + 63$=441/30 ms, yielding a bitrate of 14.7 kbps. The resulting 74 64-QAM symbols are amalgamated with 15 pilot and 4 ramp symbols, giving 93 symbols/30 ms, which is equivalent to a signaling rate of 3.1 kBd, as in the case of the low-quality mode of operation. Again, 32 PRMA slots can be created, as for the low-quality system, accommodating more than 50 speech users in a bandwidth of 200 kHz and yielding a speech user bandwidth of about 4 kHz, while maintaining a packet dropping probability of about 1%.

6.7.4 Voice Activity Detection and Packet Reservation Multiple Access

In the modulation section we have noted that multi-level modulation conveniently increases the number of time slots, which in turn results in higher PRMA statistical multiplexing

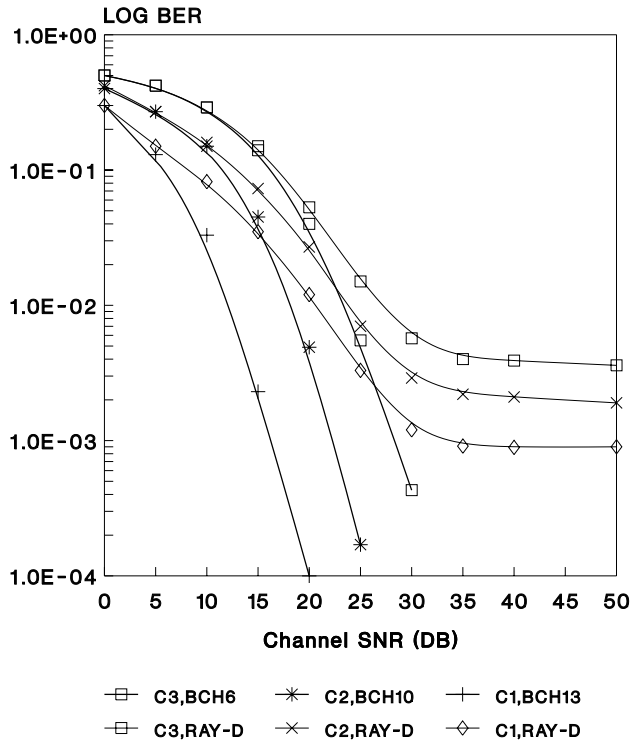

Figure 6.22: C1, C2 and C3 BER versus channel SNR performance of PSAM-assisted 64-QAM using a pilot spacing of $P = 5$ over Rayleigh channels at 4 mph, 100 kBd and 1.9 GHz with diversity and FEC coding.

gain than in the case of binary modulation. The operation of the VAD [98] has a profound effect as regards to the overall subjective speech quality. The fundamental design problem is that on one hand the VAD must respond to an active speech spurt almost instantaneously in order to queue the active speech packet for transmission to the BS and hence minimise front-end speech spurt clipping. On the other hand, it has to have a low false triggering rate even in the presence of high-level acoustic background noise, which imposes a taxing design problem, since the input signal's statistics must be observed for some length of time in order to differentiate between speech and noise reliably. In our GSM-like VAD [98] a combination of signal power, stationarity and spectral envelope-based decisions is carried out before speech is deemed to be present. In order to prevent prematurely curtailing active spurts during low-energy voiced sounds a so-called hangover switch-off delay of one speech frame length or 30 ms was also imposed. The GSM VAD was designed and extensively tested by an international expert body and for further details on it the interested reader is referred to [98].

PRMA was designed for conveying speech signals on a flexible demand basis via time division multiple access (TDMA) systems [192]. In our system a VAD similar to that of the GSM system [98] queues the active speech spurts to contend for an up-link TDMA time-

slot for transmission to the BS. Inactive users' TDMA time slots are offered by the BS to other users, who become active and are allowed to contend for the un-used time slots with a given permission probability $P_{\rm perm}$. In order to prevent colliding users from consistently colliding in their further attempts to attain a time-slot reservation we have $P_{\rm perm} < 1$. If several users attempt to transmit their packets in a previously free slot, they collide and none of them will attain a reservation. In contrast, if the BS receives a packet from a single user, or succeeds to decode an un-corrupted packet despite a simultaneous transmission attempt, then a reservation is granted. When the system is heavily loaded, the collision probability is increased and hence a speech packet might have to keep contending in vain, until its life-span expires due to the imminence of a new speech packet's arrival after 30 ms. In this case the speech packet must be dropped, but the packet dropping probability must be kept below 1%. Since packet dropping is typically encountered at the beginning of a new speech spurt, its subjective effects are perceptually insignificant.

Our transceiver used a signaling rate of 100 kBd, in order for the modulated signal to fit in a 200 kHz GSM channel slot, when using a QAM excess bandwidth of 100%. The number of time-slots created became TRUNC(100 kBd/3.1 kBd) $= 32$, where TRUNC represents truncation to the nearest integer, while the slot duration was 30/32 ms $= 0.9375$ ms. One of the PRMA users was transmitting speech signals recorded during a telephone conversation, while all the other users generated negative exponentially distributed speech spurts and speech gaps with mean durations of 1 and 1.35 s. These PRMA parameters are summarised in Table 6.15.

Table 6.15: Summary of PRMA parameters.

PRMA parameters	
Channel rate	100 kBd
Source rate	3.1 kBd
Frame duration	30 ms
No. of slots	32
Slot duration	0.9375 ms
Header length	63 bits
Maximum packet delay	30 ms
Permission probability	0.2

In conventional TDMA systems the reception quality degrades due to speech impairments caused by call blocking, hand-over failures and corrupted speech frames due to noise, as well as co- and adjacent-channel interference. In PRMA systems calls are not blocked due to the lack of an idle time-slot. Instead, the number of contending users is increased by one, slightly inconveniencing all other users, but the packet dropping probability is increased only gracefully. Hand-overs will be performed in the form of contention for an un-interfered idle time slot provided by the specific BS offering the highest signal quality amongst the potential target BSs.

If the link degrades before the next active spurt is due for transmission, the subsequent contention phase is likely to establish a link with another BS. Hence this process will have a favourable effect on the channel's quality, effectively simulating a diversity system having

independent fading channels and limiting the time spent by the MS in deep fades, thereby avoiding channels with high noise or interference.

This attractive PRMA feature can be capitalised upon in order to train the channel segregation scheme proposed in reference [193]. Accordingly, each BS evaluates and ranks the quality of its idle physical channels constituted by the un-used time slots on a frame-by-frame basis and identifies a certain number of slots, N, with the highest quality, i.e. lowest noise and interference. The slot-status is broadcast by the BS to the portable stations (PSs) and top-grade slots are contended for using the less robust, high speech quality 64-QAM mode of operation, while lower quality slots attract contention using the lower speech quality, more robust 16-QAM mode of operation. Lastly, the lowest quality idle slots currently impaired by noise and interference can be temporarily disabled. When using this algorithm, the BS is likely to receive a signal benefiting from high SNR and SIR values, minimising the probability of packet corruption due to interference and noise. However, due to disabling the lowest SNR and SIR slots the probability of packet dropping due to collision is increased, reducing the number of users supported. When a successful, uncontended reservation takes place using the high speech quality 64-QAM mode, the BS promotes the highest quality second-grade time slot to the set of top-grade slots, unless its quality is unacceptably low. Similarly, the best temporarily disabled slot can be promoted to the second-grade set in order to minimise the collision probability, if its quality is adequate for 16-QAM transmissions.

With the system elements described we now focus our attention on the performance of the re-configurable transceiver proposed.

6.7.5 3.1 kBd System Performance

The number of speech users supported by the 32-slot PRMA system becomes explicit from Figure 6.23, where the packet dropping probability versus number of users is displayed. Observe that more than 55 users can be served with a dropping probability below 1%. The effect of various packet dropping probabilities on the objective speech SEGSNR quality measure is portrayed in Figure 6.24 for both the 4.7 kbps and the 6.5 kbps mode of operation. This figure implies that packet dropping due to PRMA collisions is more detrimental in the case of the higher quality 6.5 kbps codec, since it has an originally higher SEGSNR. In order to restrict the subjective effects of PRMA-imposed packet dropping, according to Figure 6.23 the number of users must be below 60. However, in generating Figure 6.24 packets were dropped on a random basis and the same 1% dropping probability associated with initial clipping only imposes much less subjective annoyance or speech quality penalty than intra-spurt packet loss would. As a comparative basis it is worth noting that the 8 kbps CCITT/ITU ACELP candidate codec's target was to inflict less than 0.5 MOS degradation in the case of a speech frame error rate of 3%.

The overall SEGSNR versus channel SNR performance of the proposed speech transceiver is displayed in Figure 6.25 for the various systems studied, where no packets were dropped, as in a TDMA system supporting 32 subscribers. Observe that the source sensitivity-matched twin-class and quad-class 4.7 kbps ACELP-based 16-QAM systems have a virtually identical performance, suggesting that using two appropriately matched protection classes provides adequate system performance, while maintaining a lower complexity than the quad-class scheme. The full-class 4.7 kbps/16-QAM system was outperformed by both source-matched schemes by about 4 dB in terms of channel SNR, the latter systems requiring an SNR

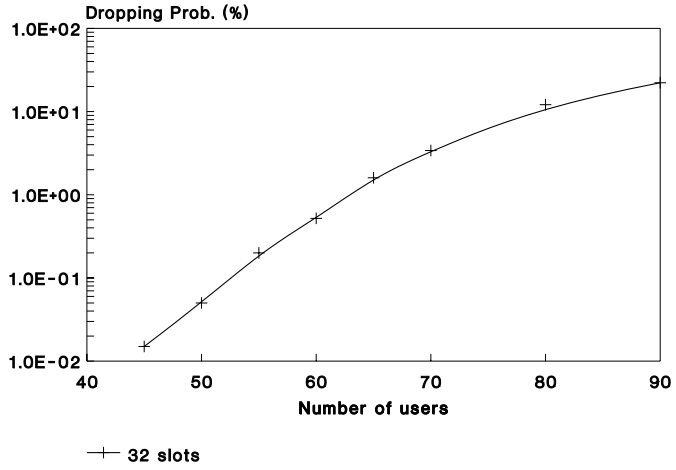

Figure 6.23: Packet dropping probability versus number of users for 32-slot PRMA.

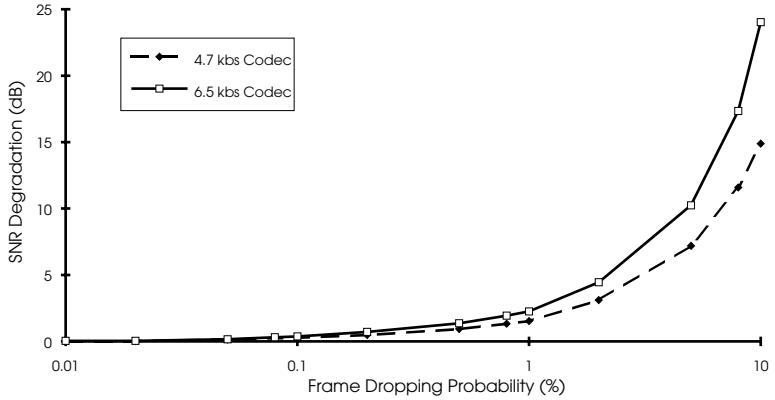

Figure 6.24: Speech SEGSNR degradation versus packet dropping probability for the 4.7 and 6.5 kbps ACELP codecs.

in excess of about 15 dB for nearly un-impaired speech quality over our pedestrian Rayleigh-fading channel. When the channel SNR was in excess of about 25 dB, the 6.5 kbps/64-QAM system outperformed the 4.7/16-QAM scheme in terms of both objective and subjective speech quality. When the proportion of corrupted speech frames due to channel-induced impairments and due to random packet dropping as in Figure 6.24 was identical, similar objective and subjective speech degradations were experienced. Furthermore, at around a 25 dB channel SNR, where the 16-QAM and 64-QAM SEGSNR curves cross each other in Figure 6.25 it is preferable to use the inherently lower quality but unimpaired mode of operation.

When supporting more than 32 users, as in our PRMA-assisted system, speech quality degradation is experienced due to packet corruption caused by channel impairments and packet dropping caused by collisions. These impairments yield different subjective perceptual

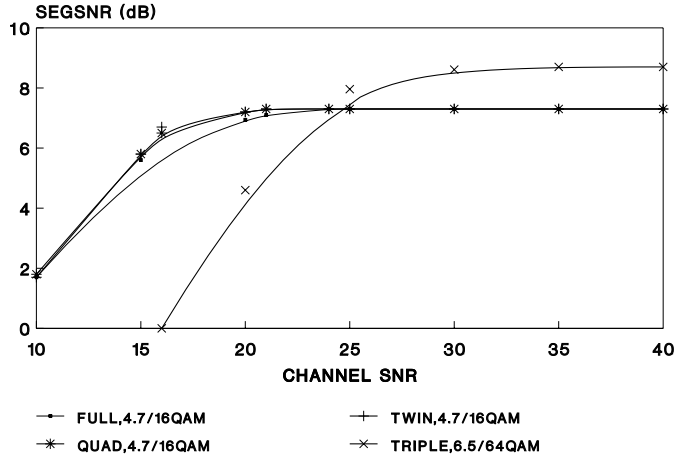

Figure 6.25: SEGSNR versus channel SNR performance of the proposed 100 kBd transceiver using 32-slot TDMA.

degradation, which we will attempt to compare in terms of the objective SEGSNR degradation. Quantifying these speech imperfections in relative terms in contrast to each other will allow system designers to adequately split the tolerable overall speech degradation between packet dropping and packet corruption. The corresponding SEGSNR versus channel SNR curves for the twin-class 4.7 kbps/16-QAM and the triple-class 6.5 kbps/64-QAM operational modes are shown in Figure 6.26 for various numbers of users between 1 and 60. Observe that the rate of change of the SEGSNR curves is more dramatic due to packet corruption caused by low-SNR channel conditions than due to increasing the number of users.

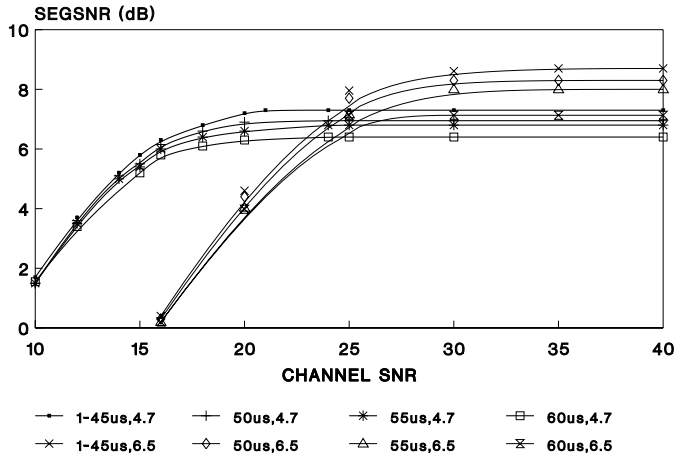

Figure 6.26: SEGSNR versus channel SNR performance of the re-configurable 100 kBd transceiver using 32-slot PRMA for different number of conversations.

As long as the number of users does not significantly exceed 50, the subjective effects of PRMA packet dropping show an even more benign speech quality penalty than that suggested by the objective SEGSNR degradation, because frames are typically dropped at the beginning of a speech spurt due to a failed contention.

6.7.6 3.1 kBd System Summary

In conclusion, our re-configurable transceiver has a single-user rate of 3.1 kBd, and can accommodate 32 PRMA slots at a PRMA rate of 100 kBd in a bandwidth of 200 kHz. The number of users supported is in excess of 50 and the minimum channel SNR for the lower speech quality mode is about 15 dB, while for the higher quality mode about 25 dB. The number of time slots can be further increased to 42, when opting for a modulation access bandwidth of 50%, accommodating a signaling rate of 133 kBd within the 200 kHz system bandwidth. This will inflict a slight bit error rate penalty, but pay dividends in terms of increasing the number of PRMA users by about 20. The parameters of the proposed transceiver are summarised in Table 6.16. In order to minimise packet corruption due to interference, the employment of a time-slot quality ranking algorithm is essential for invoking the appropriate mode of operation. When serving 50 users the effective user bandwidth becomes 4 kHz which guarantees the convenience of wireless digital speech communication in a bandwidth similar to conventional analogue telephone channels.

Table 6.16: Transceiver parameters.

Parameter	Low/high quality mode
Speech codec	4.7/6.5 kbps ACELP
FEC	Twin-/triple-class binary BCH
FEC-coded rate	8.5/12.6 kbps
Modulation	Square 16-QAM/64-QAM
Demodulation	Coherent diversity PSAM
Equaliser	No
User's signaling rate	3.1 kBd
VAD	GSM-like [98]
Multiple access	32-slot PRMA
Speech frame length	30 ms
Slot length	0.9375 ms
Channel rate	100 kBd
System bandwidth	200 kHz
No. of users	> 50
Equiv. user bandwidth	4 kHz
Min. channel SNR	15/25 dB

Our future research in the field of speech coding and modulation will be targeted at creating a more finely graded set of re-configurable sub-systems in terms of speech quality, transmission rate and robustness. These new sub-systems will enable us to match the mode of operation more closely with the prevailing channel quality. Further algorithmic research is required in order to define specific control algorithms to accommodate various operating

conditions, in particular in the area of appropriate time-slot classification algorithms to invoke the best matching mode of operation and find the best compromise between packet dropping due to collision and packet corruption due to channel impairments.

In the next section we will invoke a similar re-configurable transceiver, but we will employ a modem-mode dependent number of PRMA slots for conveying the speech information.

6.8 Multi-slot PRMA Transceiver [194]

6.8.1 Background and Motivation

In another study by Williams *et al*. [194] PRMA assisted adaptive modulation using 1, 2 and 4 bit/symbol transmissions was proposed as an alternative to dynamic channel allocation (DCA) in order to maximise the number of users supported in a traffic cell. The cell was divided into three concentric rings and in the central high SNR region 16-level star quadrature amplitude modulation (16-StQAM) was used, in the first ring DQPSK was invoked, while in the outer ring differential phase shift keying (DPSK) was utilised. In our diversity-assisted modems a channel SNR of about 7, 10 and 20 dB, respectively, was required in order to maintain a BER of about 1%, which can then be rendered error free by the binary BCH error correction codes used. Our previously designed 4.7 kbps ACELP speech codec of section 6.4.3 was assumed, protected by the quad-class source-sensitivity matched BCH coding scheme of Section 6.7.3, yielding a total bitrate of 8.4 kbps. A GSM-like VAD [98] controls the PRMA-assisted adaptive system, which ensures a capacity improvement of a factor of 1.78 over PRMA-aided binary schemes.

DCA and PRMA are techniques which potentially allow large increases in capacity over a FCA TDMA system. Although both DCA and PRMA can offer a significant system capacity improvement, their capacity advantages typically cannot be jointly exploited, since the rapid variation of slot occupancy resulting from the employment of PRMA limits the validity of interference measurements, which are essential for the reliable operation of the DCA algorithm. One alternative to tackle this problem is to have mixed fixed and dynamic frequency re-use patterns, but this has the disadvantage of reducing the number of slots per carrier for the PRMA scheme, thus decreasing its efficiency.

In this study we proposed diversity-assisted adaptive modulation as an alternative to DCA. The cells must be frequency planned as in a FCA system using a binary modulation scheme. When adaptive modulation is employed, the throughput is increased by permitting high level modulation schemes to be used by the mobiles roaming near to the centre of the cell, which therefore will require a lower number of PRMA slots to deliver a fixed number of channel encoded speech bits to the BS. In contrast, mobile stations (MS) near the fringes of the cell will have to use binary modulation in order to cope with the prevailing lower SNR and hence will occupy more PRMA slots for the same number of speech bits. Specifically, our adaptive system uses three modulation schemes: namely, binary DPSK transmitting one bit per symbol at the cell boundary; DQPSK transmitting two bits per symbol at medium distances from the BS; and 16-StQAM [73] which carries four bits per symbol close to the centre of the cell.

6.8.2 PRMA-assisted Multi-slot Adaptive Modulation

Standard PRMA schemes [192] have been discussed, for example, in [159]. However, in the proposed PRMA-assisted adaptive modulation scheme, MSs can reserve more than one slot in order to deliver up to four bursts per speech frame, when DPSK is invoked towards the cell edges. When a free slot appears in the frame, each mobile that requires a new reservation contends for it based on a permission probability, P_p. If the slot is granted to a 16-StQAM user, that slot is reserved in the normal way. If the slot is granted to a DQPSK user, then the next available free slot is also reserved for that user. Lastly, if the slot is granted to a DPSK user, then the next three free slots must also be reserved for this particular user. In this way, users that require more than one slot are not disadvantaged by forcing them to contend for each slot individually. If, however, there are less than three slots available, DQPSK or 16-StQAM users still may be able to exploit the remaining slots.

Again, we found that the difference in SNR required for the different diversity-assisted modulation schemes in order to maintain similar BER was approximately 3 dB between DPSK and DQPSK, and 12dB between DPSK and StQAM, when transmitting over Rayleigh-fading channels in our GSM- and DECT-type systems. The BER curves for these modulation schemes in narrowband Rayleigh channels with second-order diversity, a propagation frequency of 2 GHz and a vehicular speed of 15 m/s are shown in Figures 6.27 and 6.28 in the case of the GSM- and DECT-type systems, respectively.

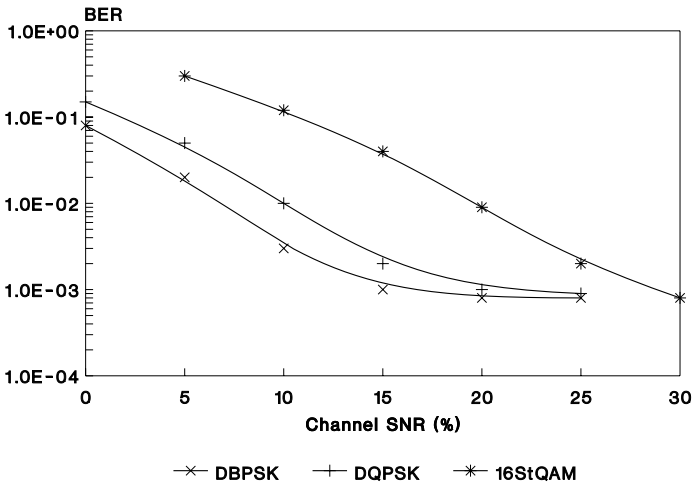

Figure 6.27: BER performance of our modulation schemes in Rayleigh fading with second-order diversity at a symbol rate of 133 kBd, carrier frequency 2 GHz and mobile velocity of 15 m/s. Copyright © IEE, Williams *et al*. 1995 [194].

Thus, using an inverse fourth power pathloss law, DPSK was invoked between radii $0.84R$ and the cell boundary, R, which is one quarter of the cell area. StQAM was used between the cell centre and $0.5R$, which is a further quarter of the cell area and DQPSK in the remaining area, which constitutes half of the total cell area. Accordingly, considering the number of slots needed by the various modulation schemes invoked and assuming a uniform traffic density,

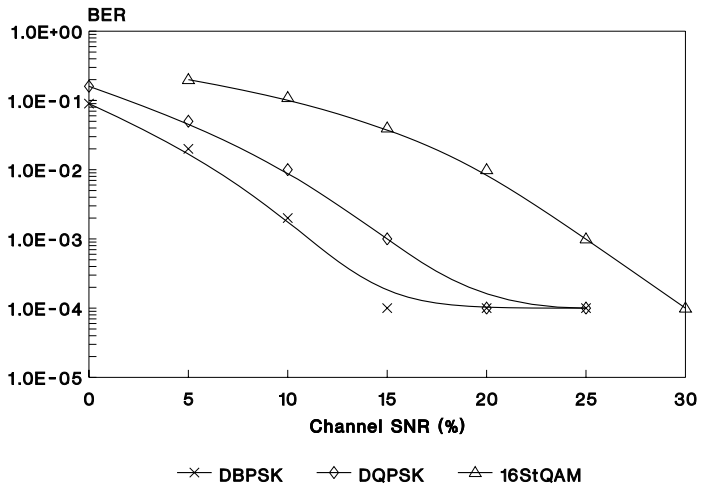

Figure 6.28: BER performance of our modulation schemes in Rayleigh fading with second-order diversity at a symbol rate of 1152 kBd, carrier frequency 2 GHz and mobile velocity of 15 m/s. Copyright © IEE, Williams *et al*. 1995 [194].

we can calculate the expected number of required slots per call as

$$E(n) = \frac{1}{4}4 + \frac{1}{2}2 + \frac{1}{4}1 = 2.25 \text{ slots}.$$

Since a binary user would require 4 slots, this implies a capacity improvement of a factor of $4/2.25 \approx 1.78$.

6.8.3 Adaptive GSM-like Schemes

The basic systems features are summarised in Table 6.17, where all modulation schemes assumed an excess bandwidth of 50%, resulting in a symbol rate which is 2/3 of the total bandwidth. The 8.4 kbps channel-coded rate after accommodating the packet header allowed us to create 48 or 416 slots per 30 ms frame in the GSM-like and DECT-like systems respectively, as shown in the table. Specifically, when using the 133.33 kBd GSM-like adaptive PRMA schemes, we can create 48 slots per 30 ms speech frame, which is equivalent to 12 slots for a binary-only system, since four slots are required for the transmission of a 30 ms speech packet. When the quaternary system is used, 24 pairs of slots can be created. Note that when fixed channel allocation is used, the adaptive scheme and the binary-only scheme can use the same cluster size. A quaternary-only system requires a 3 dB greater SIR than the binary scheme. According to Lee [195] we have

$$\frac{D}{R} = \sqrt{3K}, \tag{6.58}$$

Table 6.17: Parameters of the GSM-like and DECT-like adaptive modulation PRMA systems.

Parameter	GSM	DECT	Unit
Channel bandwidth	200	1728	kHz
Symbol rate	133	1152	kBd
Bursts per frame	48	416	

where D is the distance to the closest interferer, R is the cell radius and K is the cluster size. The prevailing SIR can be expressed as

$$\mathrm{SIR} \approx \left(\frac{D}{R}\right)^{\gamma}, \tag{6.59}$$

where γ is the path-loss exponent and hence

$$K = \tfrac{1}{3}(\mathrm{SIR})^{2/\gamma}. \tag{6.60}$$

In this study we have used a path-loss exponent of $\gamma = 4$, and therefore increasing the SIR by 3 dB requires that the cluster size be increased by a factor of $\sqrt{2}$. The packet dropping versus number of users performance of the 12 slot binary scheme is shown in Figure 6.29 together with the 24 slot quaternary and the 48 slot adaptive scheme. For all schemes their associated optimum permission probability was used, which allowed us to support the highest number of users, assuming a packet-dropping probability of 1%. We found that a maximum of 19 simultaneous calls can be supported at a packet-dropping probability of 1%, when using the binary scheme with a PRMA permission probability of 0.5. In contrast, the 24 slot quaternary scheme can support 44 simultaneous calls when using a permission probability of 0.4. Lastly, our 48 slot adaptive scheme can accommodate 36 simultaneous calls with a permission probability of 0.5. The capacity improvements attainable by the proposed GSM-like scheme are presented in Table 6.18.

Table 6.18: Improvements in capacity possible with adaptive modulation PRMA with 48 slots. Copyright © IEE, Williams *et al*. 1995 [194].

System	Slots	P_p	Simult. calls	Normalised by cluster size K	Improvement over binary with PRMA	Improvement over binary without PRMA
DBPSK	12	0.5	19	19	—	58%
DQPSK	24	0.4	44	31.1	64%	159%
Adaptive	48	0.5	36	36	89%	200%

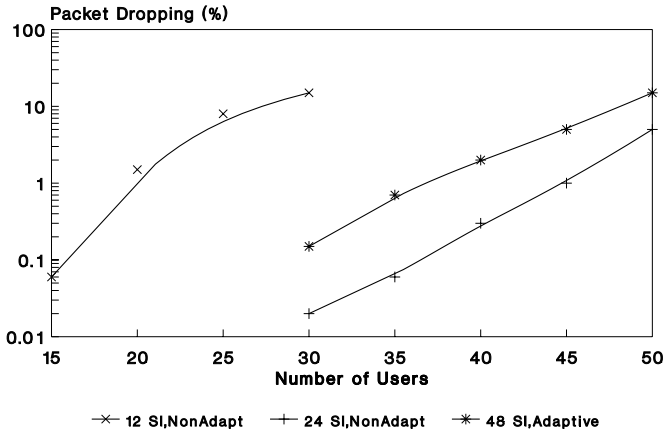

Figure 6.29: Packet dropping performance of the GSM-like PRMA schemes. Copyright © IEE, Williams *et al*. 1995 [194].

6.8.4 Adaptive DECT-like Schemes

In our DECT-like schemes we have INT{1152/2.77 kBd} $= 416$ slots per frame for the adaptive PRMA system. This is equivalent to 104 slots for a binary-only system and 216 slots for a quaternary-only system. Note that when fixed channel allocation is used, the adaptive scheme and the binary-only scheme can use the same cluster size. Again, a quaternary-only system requires a 3 dB greater SIR than the binary scheme and so the cluster size should be increased by a factor of $\sqrt{2}$.

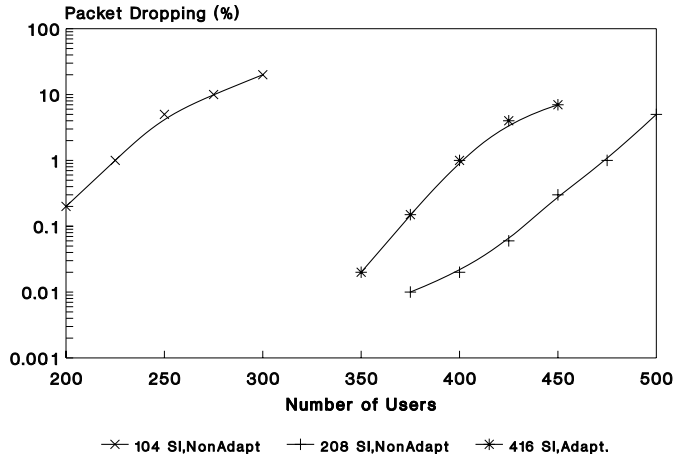

Figure 6.30: Packet dropping performance of the DECT-like PRMA schemes. Copyright © IEE, Williams *et al*. 1995 [194].

The packet dropping versus number of users performance of the 104 slot binary scheme is portrayed in Figure 6.30 when using a permission probability of 0.1. Observe

from the figure that the binary scheme can support up to 220 simultaneous calls at a packet dropping probability of 1%. When opting for the 208 slot quaternary scheme, the packet dropping versus number of users performance curve reveals that this system can accommodate 470 simultaneous calls with a permission probability of 0.1. Finally, the packet dropping performance of the 416 slot adaptive scheme suggests that the number of supported simultaneous conversations is about 400, when opting for a permission probability of 0.1. The achievable capacity improvements for our DECT-like system are displayed in Table 6.19.

Table 6.19: Achievable capacity improvements for the adaptive modulation PRMA with 416 slots. Copyright © IEE, Williams *et al*. 1995 [194].

System	Slots	P_p	Simult. calls	Normalised by cluster size K	Improvement over binary with PRMA	Improvement over binary without PRMA
DBPSK	104	0.1	220	200	—	112%
DQPSK	208	0.1	470	332	51%	219%
Adaptive	416	0.1	400	400	82%	285%

6.8.5 Summary of Adaptive Multi-slot PRMA

In conclusion, adaptive modulation with PRMA gives the expected three- to four-fold capacity increase over the binary scheme without PRMA. Generally, the greater the number of slots, the greater the advantage of PRMA over non-PRMA systems, since the statistical multiplexing gain approaches the reciprocal of the speech activity ratio. Furthermore, PRMA-assisted adaptive modulation achieves an additional 80% capacity increase over PRMA-assisted binary modulation. The speech performance of our adaptive system evaluated in terms of SEGSNR and CD is unimpaired by channel effects for SNR values in excess of about 8, 10 and 20 dB, when using diversity-assisted DPSK, DQPSK and 16-StQAM, respectively, although in dispersive environments a reduced performance is expected.

6.9 Chapter Summary

In this chapter the design principles of forward adaptive CELP codecs were highlighted and various CELP excitation models proposed over the years were reviewed. The philosophy of ACELP codecs was detailed in more depth, since these codecs have been successful at various rates and hence have found their way into various standardised codecs.

The sensitivity of these schemes against transmission errors was also analysed and a new sensitivity measure was proposed, which was capable of quantifying the effects of error propagation inflicted upon the codec. Finally, a PRMA-assisted dual-rate system design example was offered, which was capable of operating at two different speech coding rates, whilst maintaining a constant system bandwidth. This was achieved by adjusting the number of bits per symbol conveyed by the transceiver as a function of the channel quality experienced.

Having introduced the concept of CELP codecs, in the next chapter we attempt to provide a review of most of the forward-adaptive CELP-based standard speech codecs that have emerged during recent years.

Chapter 7

Standard Speech Codecs

7.1 Background

Due to the rapid development of DSP technology on one hand and with the advent of recent speech compression advances on the other hand, the late eighties and nineties witnessed the emergence of a whole host of new speech coding standards. Some of these are summarised in this chapter, in order to put our earlier theoretical elaborations into practice. There have been considerable improvements in terms of both speech quality and robustness against channel errors, partially rendered affordable by more capable DSPs. The ITUs 8 kbps G.729 codec, for example, maintains a similar speech quality to that of the 32 kbps G.726 ADPCM codec, which is equivalent to wire-line quality, while maintaining a high robustness against transmission errors. More explicitly, over the years the speech quality of 64 kbps standard PCM codecs has been maintained by various newer codecs, which gradually reduced this rate to 8 kbps, at the cost of ever increasing implementational complexity. At the time of writing researchers endeavour to further halve the 8 kbps rate of the G.729 codec to 4 kbps, an initiative referred to as the ITU 4 codec development. Further important factors are that modern codecs tolerate both background noise, such as engine noise in cars, and tandeming in mobile-to-mobile connections. We note that since the standard codecs are reviewed here in a chronological order, this chapter also constitutes a historical portrayal of the advances in the field. The objective and subjective performance of most existing standard codecs will be compared in Chapter 18. Let us commence our discourse by considering the first CELP-based standard codec, namely the US DoD 4.8 kbps codec, in the next section.

7.2 The US DoD FS-1016 4.8 kbps CELP Codec [100]

7.2.1 Introduction

In 1984 the US DoD launched a programme to develop a third generation secure telephone unit, in order to supplement the 2.4 kbps LPC-10 vocoder. The latter vocoder produced speech *almost* as intelligible as natural speech [196], but it sounded synthetic and lacked any speaker

Voice and Audio Compression for Wireless Communications Second Edition
L. Hanzo, F. C. A. Somerville and J. P. Woodard

recognisability. In 1988 a survey of 4.8 kbps codecs was conducted, and a CELP codec [186], jointly developed by the DoD and AT&T Bell Laboratories, was selected. This codec, which was later enhanced and standardised as Federal Standard 1016 (FS-1016) [100], was very advanced for its time and outperformed all US government standard codecs at rates below 16 kbps [197]. We describe it in this section.

The FS-1016 codec uses a standard CELP structure, with both a fixed and an adaptive codebook producing the excitation to an all-pole synthesis filter. A frame length of 30 ms is used, and each frame is split into four 7.5 ms sub-frames. The filter coefficients for a 10th order all pole synthesis filter are determined for each frame using forward-adaptive LPC analysis, and are converted to LSFs and scalar quantised with 34 bits. The excitation to this filter is coded every sub-frame, using a 512 entry ternary valued overlapping fixed codebook, and a 256 entry adaptive codebook with fractional delays. Both codebooks are searched by the encoder using a closed loop search to minimise the weighted squared error between the original and the reconstructed speech, and the codebook gains are scalar quantised with 5 bits each. In odd sub-frames the adaptive codebook index is coded with 8 bits but, to reduce the complexity and the bitrate of the codec, in even sub-frames this delay is differentially encoded with 6 bits. One bit per frame is used for synchronisation, and 4 bits per frame are used to provide simple forward error correction for the most sensitive bits transmitted by the codec. Finally, one bit per frame is allocated for future expansion of the codec. This bit is intended to ensure that the standard does not become obsolete as technology advances. It could be used, for example, to indicate that some, as yet unknown, improved decoding technique should be used. The bit allocation for the codec is summarised in Table 7.1.

Table 7.1: Bit allocation scheme of the FS-1016 codec.

Parameter	Per sub-frame	Total per frame
LPC coefficients	—	34
Adaptive codebook delay	8 or 6	28
Fixed codebook index	9	36
Adaptive codebook gain	5	20
Fixed codebook gain	5	20
Forward error correction	—	4
Synchronisation	—	1
Expansion bit	—	1
Total	—	144

At the decoder the received bitstream is used to give filter coefficients for the synthesis filter, and to select codebook entries form the adaptive and fixed codebooks to excite this filter and produce the reconstructed speech. Adaptive post-filtering can then be applied to this reconstructed speech to improve its perceptual quality.

An interesting aspect of the FS-1016 standard is that it allows some flexibility in both encoders and decoders that comply with the standard. For example, the encoder can search only a subset of the fixed or adaptive codebook in order to reduce its complexity. Also, the postfilter recommended at the decoder is optional. However, we now describe in more detail the blocks outlined above that would be required for a full implementation of the standard.

7.2.2 LPC Analysis and Quantisation

LPC analysis is carried out for every 30 ms frame at the encoder to derive filter coefficients for use in the synthesis and weighting filters. A 30 ms Hamming window covering the last two sub-frames of the current frame and the first two sub-frames of the next frame is used, as shown in Figure 7.1. Autocorrelation coefficients are found from the windowed speech signal, which can then be used to calculate a set of 10 filter coefficients, a_i. A bandwidth expansion of 15 Hz is applied to the filter by replacing the original coefficients a_i with $a_i\gamma^i$, where $\gamma = 0.994$. This bandwidth expansion improves the reconstructed speech quality of the codec, and also aids the quantisation of the coefficients.

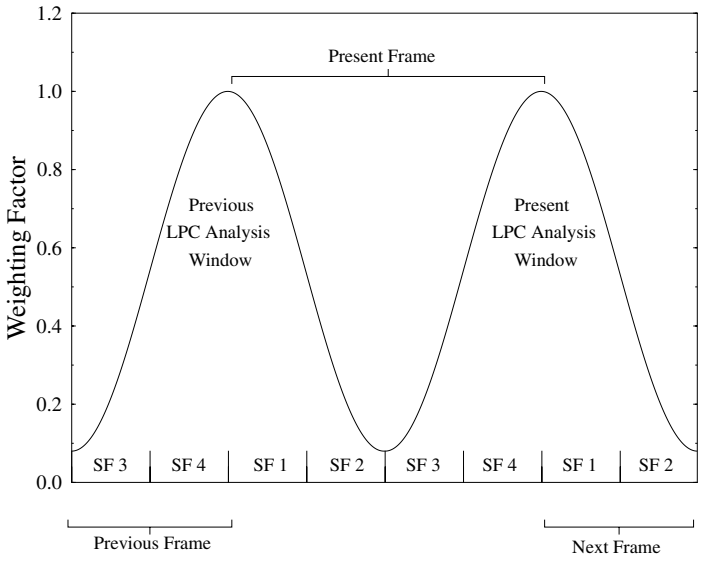

Figure 7.1: LPC analysis window used in FS-1016.

The expanded filter coefficients are converted to LSFs and scalar quantised with 34 bits. Interpolation between the quantised LSFs from the previous frame and those from the present frame is then used to give a set of LSFs for each sub-frame. The interpolation coefficients used are shown in Table 7.2. The interpolated LSFs for each sub-frame are then converted back to give the filter coefficients to be used in that sub-frame.

A simple weighting filter of the form

$$W(z) = \frac{A(z)}{A(z/\gamma)}, \tag{7.1}$$

where $\gamma = 0.8$, is used at the encoder. It is then the squared weighted error which is minimised by the adaptive and fixed codebook searches, as described below.

Table 7.2: LSF interpolation used in the FS-1016 codec.

Sub-frame	Contribution of LSFs from previous frame	Contribution of LSFs from present frame
1	7/8	1/8
2	5/8	3/8
3	3/8	5/8
4	1/8	7/8

Table 7.3: Delay resolutions used in the FS-1016 codec.

Delay range	Resolution
20–25 2/3	1/3 sample
26–33 3/4	1/4 sample
34–79 2/3	1/3 sample
80–147	1 sample

7.2.3 The Adaptive Codebook

A 256 entry adaptive codebook is used in the FS-1016 codec to model the long-term periodicities present in voiced speech. The adaptive codebook delay ranges between 20 and 147, and non-integer as well as integer delays are used. Different delay resolutions are used for different delay ranges as shown in Table 7.3. These resolutions were chosen to give the highest resolutions for typical female speakers, where the improvements in reconstructed speech quality given by non-integer pitch resolution are especially significant [198]. Adaptive codebook codewords for non-integer delays are formed using interpolation with Hamming windowed sinc functions. Interpolating functions at least 8 points long are recommended for the codebook search, and 40 points long for the synthesis of the selected adaptive codebook codeword.

The entire adaptive codebook is searched and an index coded with 8 bits in the first and third sub-frame, whereas in the second and fourth sub-frame the delay is delta encoded, relative to the previous sub-frame's delay, using only 6 bits. This was found to reduce the bitrate and the complexity of the encoder while causing no perceivable loss in the codec's reconstructed speech quality. Sub-multiples of the delay value which gives the minimum weighted squared error between the original and the weighted speech are checked, and favoured if they give a match to the original speech which is almost as good. This results in a smoothly varying pitch contour, which is important for the delta coding of the speech in odd sub-frames. It also enables the receiver to use a smoother to check for channel errors in the received adaptive codebook index.

Once the adaptive codebook delay has been chosen, the corresponding gain term is calculated and scalar quantised using 5 bit non-uniform quantisation between -1 and $+2$.

This gives an adaptive codebook signal which is filtered through the synthesis and weighting filters and subtracted from the target for the adaptive codebook search to give the target signal for the fixed codebook search. This fixed codebook and its search is described next.

7.2.4 The Fixed Codebook

The fixed codebook in the FS-1016 codec contains 512 sparse, ternary valued, overlapped codewords. The codewords are overlapped by -2 so that each codeword contains all but two samples of the previous codeword plus two new samples. This overlapping dramatically reduces the storage necessary for the fixed codebook as only $N + 2(L - 1) = 1082$, rather than $LN = 30\,720$, elements need to be stored at the encoder and decoder. Here $L = 512$ is the number of entries in the codebook and $N = 60$ is the dimension of each entry. The overlapped nature of the codebook also allows fast calculation of the energy and correlation terms which must be calculated for each codebook entry to allow the fixed codebook search to be carried out, and it is reported in [199] to give performance equivalent to that of a non-overlapped codebook.

The 1082 codebook entries are derived using a zero-mean unit variance white Gaussian sequence. This sequence is centre-clipped at 1.2, and all values which are greater than 1.2, or less than -1.2, are set equal to $+1$ or -1. This gives a ternary valued codebook which is approximately 77% sparse, and whose non-zero elements are either $+1$ or -1. The sparse ternary valued nature of the codebook gives a further reduction in the storage necessary for the codebook and further simplifies the codebook search procedure.

A novel feature of the FS-1016 codec is in the calculation of the fixed codebook gain. This gain is non-uniformly quantised with 5 bits, and initially is calculated and quantised for each codebook entry as in most CELP codecs. It is reported in [197] that this joint optimisation of the codebook index and quantised gain is subjectively similar to searching twice as large a fixed codebook without joint optimisation. However, once the fixed codebook gain and index have been determined the fixed codebook gain is adaptively attenuated or amplified depending on the efficiency of the adaptive codebook. This is similar to Shoham's constrained excitation idea [200] and attenuates the stochastic element of the excitation during voiced segments of speech. This reduces roughness heard during sustained voiced segments of speech, and hence significantly improves the subjective quality of the reconstructed speech. Also during unvoiced segments of speech the stochastic element of the excitation signal is increased, which provides a more subjectively pleasing match between the reconstructed and the input speech.

The efficiency of the adaptive codebook is measured using the normalised cross-correlation R between the target signals for the fixed and adaptive codebook searches. This is given by

$$R = \frac{\sum_{n=0}^{N-1} x(n)y(n)}{\sum_{n=0}^{N-1} x^2(n)}, \tag{7.2}$$

where $x(n)$ is the target signal for the adaptive codebook search and $y(n)$ is the target signal for the fixed codebook search. The quantised codebook gain $\hat{G}_2$ is then modified to $\tilde{G}_2$

depending on the value of R as

$$\tilde{G}_2 = \begin{cases} 0.2\,\hat{G}_2 & |R| < 0.04 \\ 1.4\,\hat{G}_2\sqrt{|R|} & |R| > 0.81 \\ \hat{G}_2\sqrt{|R|} & \text{otherwise.} \end{cases} \tag{7.3}$$

This modification of the stochastic excitation component has a negligible effect on the complexity of the codec, but as stated above gives a significant improvement in the subjective quality of the codec.

Once the fixed and adaptive codebook indices and gains have been found at the encoder, locally reconstructed speech can be calculated at the encoder and used to update the filter memories. Also, indices representing the fixed and adaptive codebook signals are coded and sent to the decoder, allowing it to find the reconstructed speech. The decoder also incorporates a simple postfilter to further improve the subjective quality of the reconstructed speech, and error detection and concealment techniques to improve the robustness of the codec to channel errors. These blocks of the decoder are described below.

7.2.5 Error Concealment Techniques

The FS-1016 codec uses several techniques to improve its performance over noisy channels. A Hamming $(15, 11, 1)$ FEC code is used to protect the 11 most sensitive bits of each frame, and this together with careful assignment of binary indices to codebook indices and the use of adaptive smoothers at the decoder yields a codec that is reasonably resilient to channel errors.

The power of the Hamming code is concentrated on the adaptive codebook information because of the sensitivity of this information to channel errors as described in section 6.6. The three most significant bits of the index representing the two absolute adaptive codebook delays are protected by the FEC. The two absolute delays are heavily protected in this way, whereas the two delta coded delays are not protected at all, because of the importance of correctly decoding the absolute delays in order for the delta coded delays to be received correctly. Also, the most significant bit representing the adaptive codebook gain for each sub-frame is protected. This gives a total of 10 bits to be protected per frame, and the final protected bit is the 'Bishnu' expansion bit described earlier.

Along with the FEC code described above, the indices of the adaptive codebook delay are assigned using simulated annealing to minimise the effect of a single bit error in the 8 bits representing each absolute adaptive codebook delay. Adaptive smoothers, which are disabled when the decoding of the $(15, 11, 1)$ Hamming code indicate error free conditions, operate on both the fixed and adaptive codebook gains, as well as the adaptive codebook index. Finally, when an error in the 34 bits representing the quantised LSFs causes adjacent LSFs to overlap, this error can be detected by the decoder and action taken to mitigate it. When overlapping LSFs are detected at the decoder an attempt is made to correct them by repeating the two corresponding LSFs from the previous frame. If this does not result in a monotonic set of LSFs then the entire set of 10 LSFs is replaced with the set from the previous frame. The combination of the measures described above allow the FS-1016 to provide reasonable speech quality at bit error rates as high as 1%.

7.2.6 Decoder Post-filtering

A traditional short term pole-zero filter with adaptive spectral tilt compensation, as suggested by Chen and Gersho [108], is recommended for use at the FS-1016 decoder. Cautious application of the postfilter is suggested, especially in situations where the codec is used in tandem or in noisy conditions. When the codec is used in noisy environments the postfilter may enhance the noise because it is based on the LPC coefficients. Also, post-filtering can be detrimental when the codec is used several times in tandem, and in such circumstances it is suggested that all the post-filters are disabled except for that operating at the final decoder.

7.2.7 Conclusion

The FS-1016 standard provided the first use of the CELP principle in a standard codec, and provided reconstructed speech of communications quality for the first time at a bitrate as low as 4.8 kbps. It also showed reasonable resilience to channel errors, and operated well in the presence of acoustic background noise. The use of a ternary-valued overlapped fixed codebook meant that the codec could be implemented in real time using readily available DSP chips. Also, the standard was flexible enough to allow only segments of either the fixed or the adaptive codebook to be searched at the encoder, and so allowed the complexity of the codec to be reduced if lower reconstructed speech quality was acceptable. More recently, a dynamic partial search scheme has been proposed [201] for the fixed codebook which reduces the codebook search complexity significantly without degrading the reconstructed speech quality.

In closing, we note that this scheme, denoted by FS1016, is compared to various existing standard codecs in Figure 18.4 of Chapter 18. Following the above rudimentary introduction to the 4.8 kbps DoD codec, which was the first standardised CELP-based scheme, let us now concentrate on the 7.95 kbps Pan-American IS-54 coding arrangement.

7.3 The 7.95 kbps Pan-American Speech Codec – Known as IS-54 DAMPS Codec [156]

This section gives a rudimentary overview of the operation of the 7.95 kbps Pan-American Advanced Mobile Phone System's (DAMPS) [156] speech codec. Similar to the half-rate Pan-European system, known as GSM, which will be detailed in Section 7.7, the DAMPS' speech codec is also based on the so-called vector sum excited linear predictive (VSELP) principle proposed by Gerson and Jasiuk [202, 203], which will be briefly highlighted below. Hence its schematic portrayed in Figure 7.2 is also similar to the half-rate GSM codec's schematic seen in Figure 7.12, in that the fixed codebook entry is a linear combination of two scaled vectors. This allows for a high grade of flexibility in terms of the excitation vector shape, as is also argued in more depth in Section 7.7. We note that this scheme will be compared to a range of existing standard codecs in Figure 18.4 of Chapter 18.

The codec's bit allocation scheme is shown in Table 7.4, while the reasons for using the specified number of bits will be detailed during our later discussions. Similar to other medium-rate speech codecs, 38 spectral quantisation bits per 20 ms are allocated for the reflection coefficients, corresponding to a 1.9 kbps bitrate contribution. The specific number of bits used for the individual reflection coefficients is 6, 5, 5, 4, 4, 3, 3, 3, 3 and 2, starting

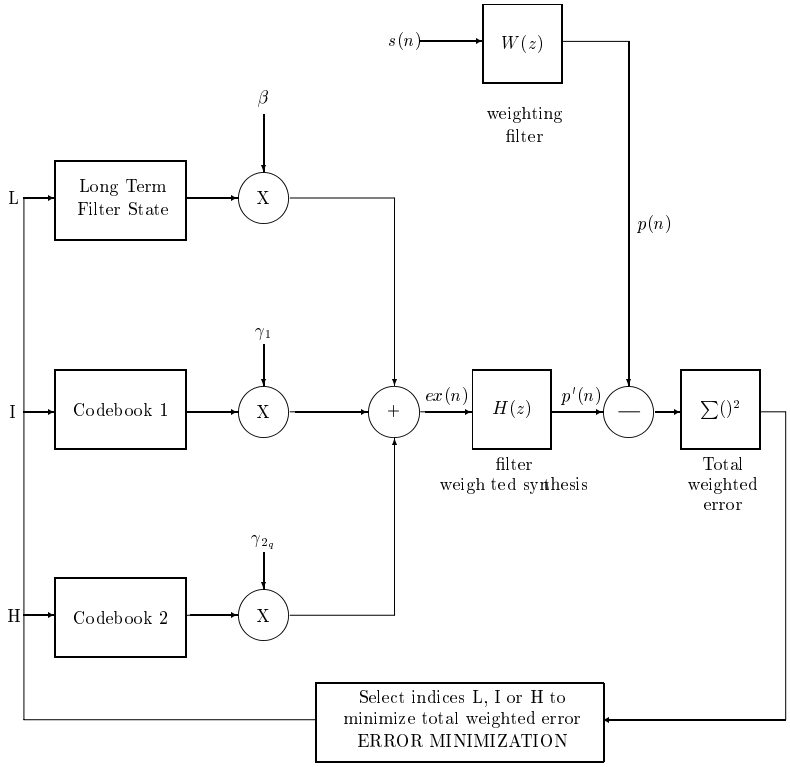

Figure 7.2: The 7.95 kbps DAMPS VSELP encoder's schematic. Copyright © TIA, 1992 [156].

Table 7.4: 7.95 kbps IS-54 VSELP Codec Bit Allocation. Copyright © TIA, 1992 [156].

Parameter	Bit/subframe	Bit/frame
Reflection coefficient		38
Frame energy $R(0)$		5
Pitch-lag L	7	$4 \times 7 = 28$
CB-entries I, H	$7 + 7$	$4 \times 14 = 56$
Gains, $\beta, \gamma_1, \gamma_2$	8	32
Total		159/20 ms

from the first one. Similar to the half-rate GSM codec, the so-called fixed point lattice technique (FLAT) [204, 205] was proposed for the IS-54 standard by Gerson. The lattice-based prediction algorithms were the subject of Section 3.7, while for the implementational details the interested reader is referred to the standard itself [156]. Suffice to say here that the technique computes the reflection coefficients iteratively, always producing the optimum jth order predictor at each stage of the iteration which can be quantised, before the next

coefficient is determined. Hence each forthcoming predictor stage can compensate for the quantisation error of the optimum reflection coefficient determined at the previous stage.

Five bits are used to quantise the energy of the speech frame, as we will see for the half-rate VSELP GSM codec's bit allocations scheme in Table 7.8, which was also partially designed by Gerson and Jasiuk [202, 203]. The gains, $\beta, \gamma_1, \gamma_2$ in Figure 7.2 are quantised using a total of 8 bits/5 ms subframe, contributing 32 bits/20 ms frame. The adaptive codebook index or pitch-lag is represented by 7 bits/5 ms subframe, corresponding to 128 possible pitch values. For reasons of robustness against channel errors no differential coding of the pitch-lag was used. Lastly, both fixed codebook entries are represented by a 128-entry, 7-bit codebook. When combining all possible codebook entries and gain factors, the total number of legitimate excitation patterns per subsegment becomes $128 \times 128 \times 128 \times 256 = 536\,870\,912$, while maintaining an acceptable computational complexity. This is achieved using a sub-optimum solution, whereby the three codebooks are searched through consecutively, identifying the best entry of the adaptive codebook first and then the fixed entries. The decoder's operation is characterised by Figure 7.3, which is essentially constituted by synthesiser section of the encoder, extended by the spectral postfilter.

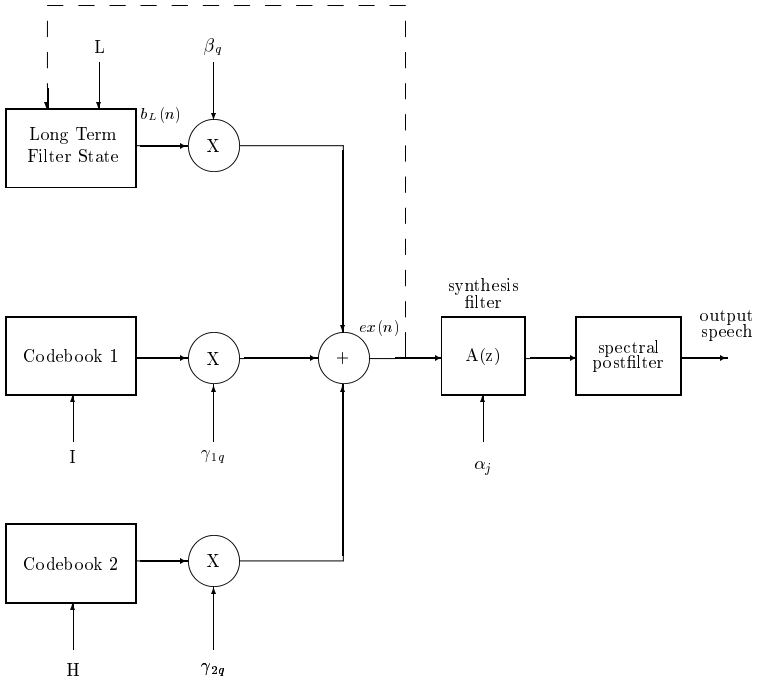

Figure 7.3: The 7.95 kbps DAMPS VSELP decoder's schematic. Copyright © TIA, 1992 [156].

In order to provide source-sensitivity matched error protection for the speech bits, similar to most mobile radio speech transmission schemes, the 159 speech bits are divided into a number of protection classes. The most sensitive 12 bits are assigned a 7-bit cyclic redundancy checking (CRC) pattern, which is used by the decoder for invoking bad frame

masking, as shown in Figure 7.4. This could be due to channel errors, or due to the so-called fast associated control channel stealing a speech frame for conveying a very urgent control message, such as a hand-over request. In this case the speech frame is obliterated and at the decoder it has to be replaced by a repeated speech segment. However, this simple post-processing can only mitigate the frame loss for periods below 100 ms or five consecutive frames.

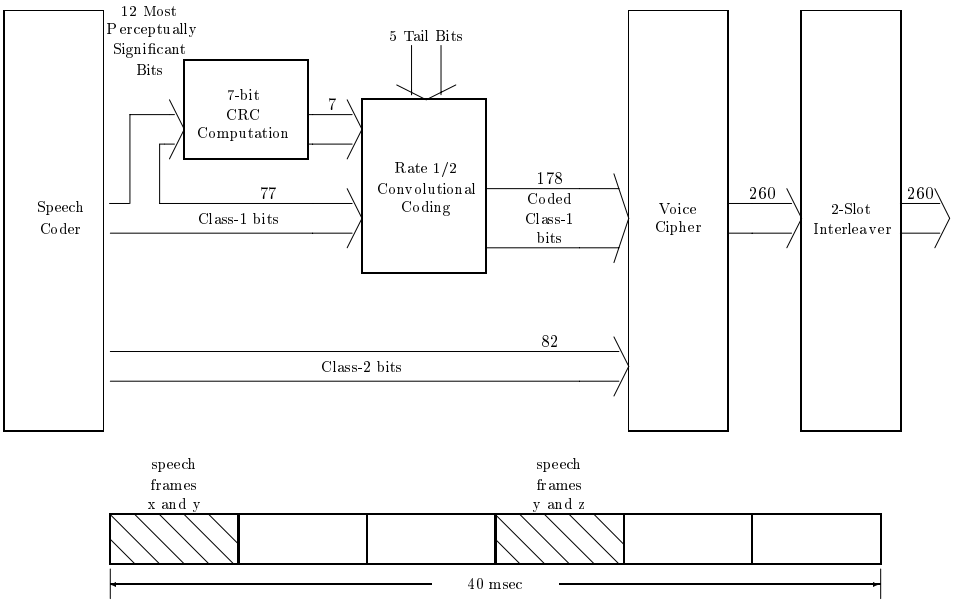

Figure 7.4: The 7.95/13 kbps DAMPS VSELP error protection schematic. Copyright © TIA 1992 [156].

As portrayed in Figure 7.4, the 159 speech bits are subdivided into 77 so-called Class-1 bits and 82 Class-2 bits. The more important Class-1 bits are half-rate convolutionally encoded, while the remaining 82 bits are transmitted unprotected. This implies that the Class-2 bits are always more prone to errors. The convolutional encoder processes $77 + 7 + 5 = 89$ bits, where the 5 tailing bits are required by the so-called constraint-length five code to flush its buffer before the transmission of the next speech frame. This allows us to curtail the propagation of transmission errors across frame boundaries, which would otherwise result in prolonged speech degradation due to the decoder's deviation from the error-free trellis path. There will, however, still be error propagation through the codec's adaptive codebook. The $2 \times 89 = 178$ protected Class-1 bits and the 82 Class-2 bits are then ciphered for the sake of confidentiality and 260 bits/20 ms are transmitted to the decoder. The resulting error-protected bitrate is incidentally the same as the unprotected full-rate RPE-coded GSM rate. Lastly, interleaving over two consecutive speech frames takes place, in order to disperse bursty channel errors which have a tendency to overload the error correction capability of the channel decoder. As displayed in Figure 7.4, there are three time-slots per transmission frame in IS-54 and the channel coded Class-1 bits are dispersed over two consecutive 20 ms

speech frames. Hence each transmission packet contains bits from two consecutive speech frames, namely frame x, y and y, z, respectively.

Again, this scheme is compared to a range of existing standard codecs in Figure 18.4 of Chapter 18 in subjective speech quality terms. Let us now turn our attention to the 6.7 kbps Japanese codec, which is essentially a reduced-rate derivative of the IS-54 codec.

7.4 The 6.7 kbps Japanese Digital Cellular System's Speech Codec [157]

Similar to the 7.95 kbps IS-54 Pan-American codec of Section 7.3, the Japanese Digital Cellular (JDC) system's 6.7 kbps speech codec [157] is also based on the VSELP excitation optimisation principle introduced by Gerson and Jasiuk [202, 203]. The schematic of the JDC codec is also quite similar to that of the IS-54 arrangement's shown in Figures 7.2 and 7.3, apart from the fact that in the JDC system only one codebook is used. This naturally restricts the number of different excitation vectors, and hence results in a somewhat lower bitrate and speech quality. The corresponding bitrate allocation is summarised in Table 7.5, while the associated subjective speech quality of this scheme will be compared to a range of existing standard codecs in Figure 18.4 of Chapter 18.

Table 7.5: 6.7 kbps JDC codec bit allocation. Copyright © R&D Centre for Radio Systems, Japan [157].

Parameter	Bit/Subframe	Bit/frame
Reflection coefficient		36
Frame energy $R(0)$		5
Pitch-lag L	7	$4 \times 7 = 28$
CB-entries I	9	$4 \times 9 = 36$
Gains, β, γ_1	7	$4 \times 7 = 28$
Soft-interpolation bit		1
Total		134/20 ms

As seen in Table 7.5, a total of 36 bits are used for spectral quantisation, where the specific number of bits used for the individual reflection coefficients is 5, 5, 4, 4, 4, 3, 3, 3, 3 and 2. Similar to the 5.6 kbps half-rate GSM codec and the 7.95 kbps IS-54 codec, the so-called FLAT [204, 205] was proposed by Gerson. Recall that lattice-based prediction algorithms were detailed in Section 3.7 and the implementational aspects can be found in the standard [157]. We remind the reader here that the reflection coefficients are determined iteratively, generating the optimum jth order lattice-based predictor at each stage of the iteration which can be quantised, before the next coefficient is determined. Therefore, as argued for both the half-rate GSM codec and the IS-54 scheme, the effect of the quantisation errors of the reflection coefficients of each predictor stage can be taken into account during the computation of the next reflection coefficient.

Similar to the IS-54 codec characterised by Table 7.4 and to the half-rate GSM scheme of Table 7.8, five bits are used to quantise the energy of the speech frame. The adaptive-

and fixed-codebook gains β, γ_1 of Figure 7.2 are jointly vector-quantised using a total of 7 bits/5 ms subframe, requiring 28 bits/20 ms frame. The adaptive codebook index or pitch-lag is represented by 7 bits/5 ms subframe, encoding 128 possible pitch values. Despite the low bitrate constraint, for error-resilience reasons no differential coding of the pitch-lag was employed. Lastly, the 512-entry fixed codebook address is encoded using 9 bits/5 ms subframe. When combining all the codebook entries and gain factors, the total number of excitations per subsegment becomes $128 \times 128 \times 512 = 8\ 388\ 608$, which is substantially lower than the corresponding number of $128 \times 128 \times 128 \times 256 = 536\ 870\ 912$ used by the higher-rate IS-54 codec. Naturally, for complexity reasons a full-search is impractical and hence a sub-optimum solution is to search through the three codebooks consecutively. Firstly, the best entry of the adaptive codebook is found and then the fixed entry.

The soft-interpolation flag of Table 7.5 is used to signal for the decoder which of two specific sets of filter coefficients was used by the encoder, where the first one is generated without interpolation, while the second one with interpolation. Explicitly, this bit is used to inform the decoder whether the current frame's prediction residual energy was lower with or without interpolating the direct form LPC coefficients. We will see from Table 7.8 that this technique was also employed in the half-rate GSM codec. For details of the codebook construction and other algorithmic issues the interested reader is referred to the recommendation [157]. Let us now consider the associated channel coding aspects.

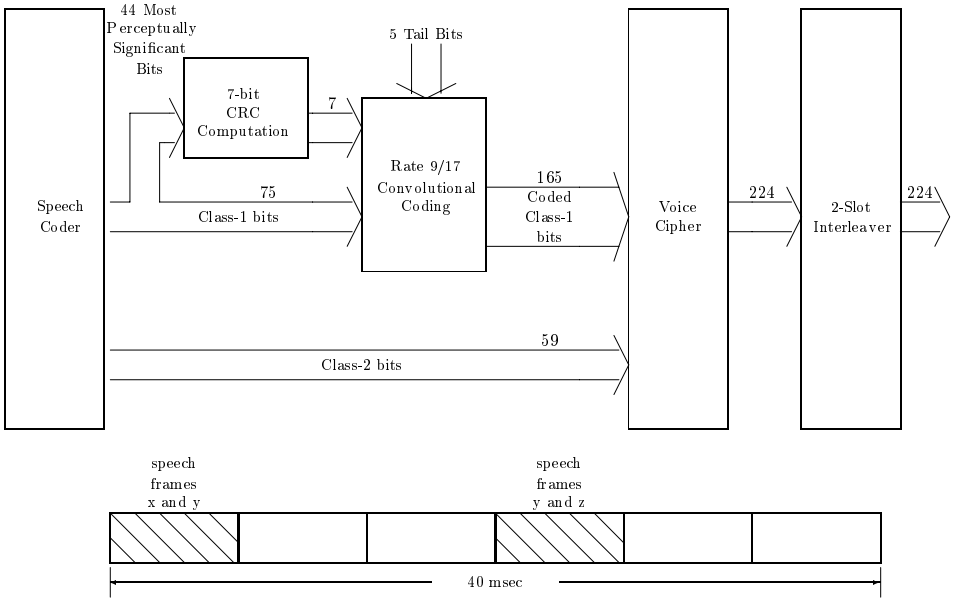

Figure 7.5: The 6.7/11.4 kbps JDC VSELP error protection schematic. Copyright © R&D Centre for Radio Systems, Japan [157].

The JDC system's channel coding scheme seen in Figure 7.5 exhibits a similar structure to that of the IS-54 arrangement portrayed in Figure 7.4. The 134/20 ms speech bits are divided in two main protection classes. The perceptually most sensitive 44 bits are assigned a 7-bit

CRC segment, which is again invoked by the decoder for activating bad frame masking. As displayed in Figure 7.5, the 134 speech bits are grouped in 75 so-called Class-1 bits and 59 Class-2 bits. The perceptually more significant Class-1 bits are 9/17-rate convolutionally encoded, while the 59 Class-2 bits remain unprotected. This implies that the Class-2 bits are always more prone to errors. The $75 + 7 + 5 = 87$ input bits are convolutionally encoded, where the 5 tailing bits are necessitated by the so-called constraint-length five code to clear its buffer, before the next speech frame is transmitted. Due to this, both the encoder and the decoder commence their operation from an identical known state, which is beneficial in error-resilience terms.

The $(9/17) \times 87 = 164.33$ encoded bits are represented naturally by 165 protected Class-1 bits and the 59 Class-2 bits are then ciphered for the sake of confidentiality and 224 bits/20 ms are transmitted to the decoder. The resulting error-protected bitrate of 11.2 kbps is very close to that of the 11.4 kbps half-rate GSM rate, although the latter has a lower speech rate of 5.6 kbps, yet exhibiting an improved speech quality. Interleaving is carried out over two consecutive speech frames or 40 ms, in order to randomize the bursty channel error statistics and hence to improve the scheme's error resilience. Again, similar to the IS-54 systems three-slot per channel structure seen in Figure 7.4, there are three time-slots per transmission frame also in the JDC system and the channel coded Class-1 bits are dispersed over two consecutive 20 ms speech frames, each transmission packet hosting bits from two consecutive speech frames, namely frame x, y and y, z, respectively.

Due to the advances in speech compression technology recently it became realistic to further reduce the bitrate of the first VSELP-based codecs, such as the 7.95 kbps IS-54 and the 6.7 kbps JDC codecs, which led to the development of the 5.6 kbps half-rate GSM codec of Section 7.7. The subjective speech quality of the previously discussed IS-54 and JDC coding arrangements is compared to a range of existing standard codecs in Figure 18.4 of Chapter 18. In the next section we will consider the variable-rate Qualcomm CELP codec.

7.5 The Qualcomm Variable Rate CELP Codec [206]

7.5.1 Introduction

Amongst the several different digital cellular mobile phone systems in use around the world most, including the European GSM, the Japanese JDC and the American IS-54 standards, use TDMA to allow groups of several users to share the same frequency. However, in July 1993 the US Telecommunications Industry Association (TIA) gave approval to a code division multiple access (CDMA) system known as IS-95, designed to offer an alternative digital system to IS-54. This system was designed by Qualcomm and claims to offer large increases in capacity over IS-54 [206]. Qualcomm designed a speech codec, known as Qualcomm CELP (QCELP) [206], for use in IS-95 and this speech codec is described here. A more detailed description can be found in the IS-95 standard [207].

QCELP is a variable rate CELP codec which operates at one of 4 data rates for every 20 ms frame. Which data rate the codec uses is determined by the encoder depending on the input signal. The four possible data rates are 8,4,2 kbps and 800 bits/s. These different rates are known as full rate, 1/2 rate, 1/4 rate and 1/8 rate. The speech encoder tries to determine the nature of the input signal and codes active speech frames at full rate and background noise and silence at one of the lower rates. Testing has shown that for a typical conversation the QCELP

codec operates at an average bitrate of under 4 kbps, but provides speech quality equivalent to the 8 kbps VSELP codec used in IS-54. As CDMA is used in IS-95 this reduction in the average bitrate of the speech codec is easily exploited to improve the capacity of the system.

In the next section we give an overview of the coding used in the QCELP codec, and the bit allocation used at its various rates. Then we describe how the encoder determines at which rate to code a given speech frame. Finally, we give details of the various components used in the QCELP codec.

7.5.2 Codec Schematic and Bit Allocation

A schematic of the QCELP codec is shown in Figure 7.6. For all the data rates except the 1/8 rate the codec uses a relatively standard CELP codec structure with a fixed codebook, a pitch filter and a short term synthesis filter. At the 1/8 rate the codec structure is modified so as to code background noise, which is what the 1/8 rate is used for, more efficiently. No pitch filter is used, and instead of an entry chosen by AbS techniques from a fixed codebook, a gain scaled pseudo-random series from a random-noise generator is used as the excitation to the synthesis filter. At the decoder, post-filtering is used to improve the perceptual quality of the reconstructed speech.

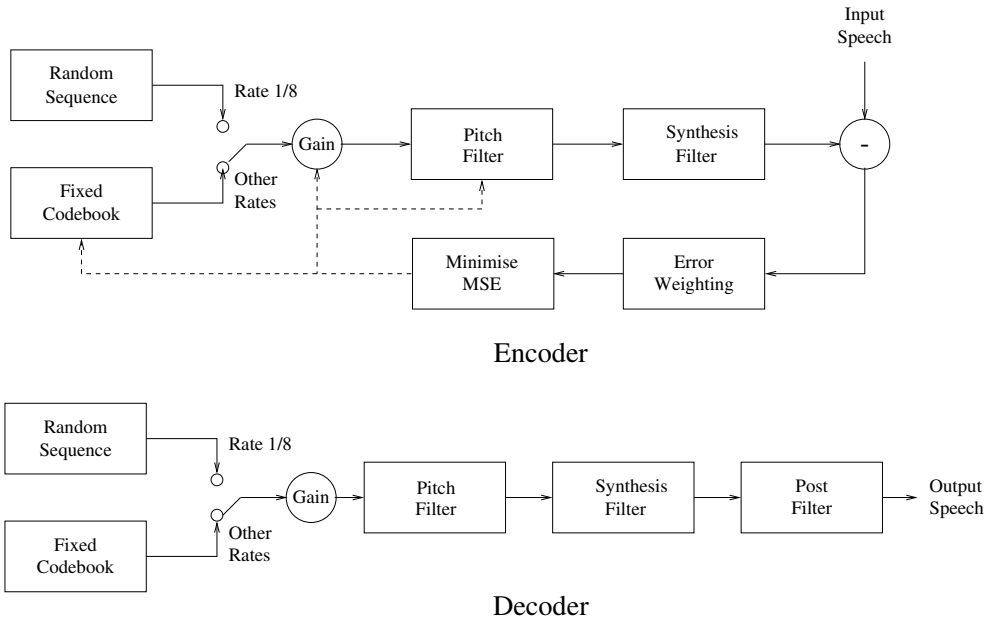

Figure 7.6: QCELP codec.

The bit allocation for the various data rates is shown in Table 7.6. For each rate this table shows how many bits are used to code the LPC, pitch and fixed codebook parameters, and how many times per frame these parameters are determined and coded. At all the rates the LPC coefficients are determined and transmitted once per 20 ms frame, but at lower rates fewer bits are used for their quantisation. Both the pitch filter (when used) and the fixed

codebook parameters are coded with 10 bits at all rates, but at different rates these parameters are coded more or less frequently.

Table 7.6: Bit allocation scheme of the QCELP codec.

Bitrate	8 kbps	4 kbps	2 kbps	800 bits/s
LPC	40 bits once	20 bits once	10 bits once	10 bits once
Pitch	10 bits four times	10 bits twice	10 bits once	0 bits
Code book	10 bits eight times	10 bits four times	10 bits twice	6 bits once
Total	160 bits per frame	80 bits per frame	40 bits per frame	16 bits per frame

In the next section we briefly describe how the encoder decides which of the four codec rates to use to encode a given frame.

7.5.3 Codec Rate Selection

For most frames at the encoder the QCELP codec decides which of its four data rates to use by comparing the energy of its input over the 20 ms frame to an estimate of the background noise energy. This estimate of the background noise energy is updated each frame depending on whether the current input frame has a lower or higher energy than the estimate. If the estimate is higher than the current input energy then the estimate is reset to the input energy. If on the other hand the estimate is lower than the input energy then it is slightly increased. This means that when no speech is present the estimate of the background noise energy follows the input energy. When speech is present the estimate slowly increases, but the fluctuations inherent in the input speech energy cause it to be frequently reset. An example of the variations in the input speech energy and the background noise estimate can be found in [206].

To select which of the four data rates to use the encoder uses a set of three thresholds which 'float' above the running estimate of the background noise energy. If the energy of the input signal is higher than all three thresholds then the encoder selects the full rate, otherwise one of the lower rates is selected.

This comparison of the input signal's energy to three floating thresholds is how the encoder data rate is selected for most frames. However, the encoder can also be instructed to generate a blank packet to allow for 'blank and burst' transmission of signalling information. Also, the encoder can be instructed not to code at the full rate for certain given frames. This allows the network to reduce the average data rate of its existing users and hence increase its capacity to accommodate extra users. This means that the CDMA system has a 'soft capacity' – when the number of users is greater than the usual system capacity extra users can be accommodated by slightly decreasing each user's codec data rate and hence voice quality.

In the following sections we describe the formant and pitch filters used in the QCELP codec, the excitation used for these filters, the post-filtering used at the decoder to improve the perceptual quality of the reconstructed speech and finally the error protection and concealment techniques used.

7.5.4 LPC Analysis and Quantisation

A tenth order LPC synthesis filter is used in the QCELP codec. The filter coefficients are determined from the input speech using the autocorrelation method. A 160 sample Hamming window, centred between the 139th and the 140th sample of the current 160 sample frame, is used to calculate autocorrelation values. These are then converted to filter coefficients using the Levinson–Durbin algorithm, and a 15 Hz bandwidth expansion is applied before the coefficients are converted to LSPs. The 10 LSPs are quantised using a scalar predictive quantiser as shown in Figure 7.7.

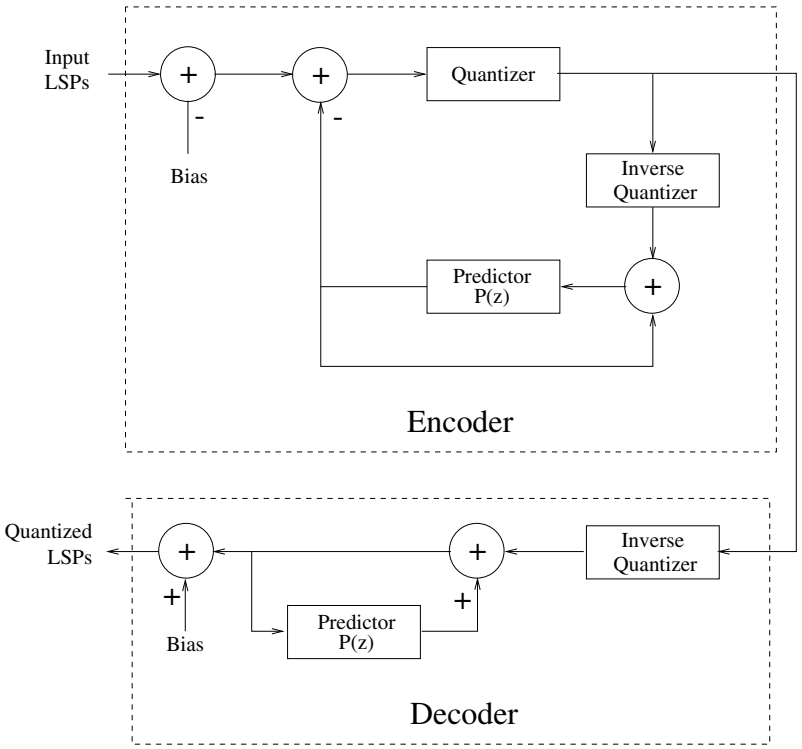

Figure 7.7: LSP quantisation.

This predictive quantiser operates as follows. Initially each LSP has an offset or a 'bias' value subtracted. These bias values are the values of the LSPs when the input speech has flat spectrum. The bias used for LSP_i is given by

$$\text{Bias} = \frac{0.5i}{p+1}(0.0454545\ldots)i, \quad 1 \leq i \leq 10, \tag{7.4}$$

where $p = 10$ is the order of the filter. The bias offset LSPs then have a predicted value for the offset LSP subtracted, and the difference between the actual offset LSP and the predicted offset LSP is quantised with either $4, 2$ or 1 bits, depending on the codec rate. The predicted values for the offset LSPs are simply given by the value of the quantised offset LSP for the

previous frame multiplied by 29/32, implying that the predictor has a transfer function $P(z)$ given by

$$P(z) = 0.90625z^{-1}. \tag{7.5}$$

At the decoder, and also in the local decoder in the encoder, the LSPs are reconstructed by inverse quantising the transmitted quantiser index, adding the predicted offset LSP and then adding the bias value to give the quantised LSPs. The stability of the synthesis filter is then ensured by forcing the LSPs to be ordered. The decoder also ensures that the frequencies are separated by at least 80 Hz in order to avoid unusually large peaks in the frequency response of the synthesis filter. For rates below the full rate only 1 or 2 bits are used to quantize each LSP, so the quantisation is very noisy. In order to remove some of this quantisation noise for codec rates below the full rate the LSPs are low-pass filtered. The extent of this filtering is set depending on the current rate of the codec. Also, if 10 or more consecutive rate 1/4 or 1/8 frames are received, or a frame erasure occurs, then the extent of the filtering is dramatically increased. Finally, before converting the LSPs back to filter coefficients, LSP interpolation between the quantised LSPs for the current and the previous frame is used to determine LSPs for each pitch and fixed codebook sub-frame. At different rates the QCELP codec has different numbers of sub-frames per 20 ms frame, and so the interpolation used depends on the rate of the codec.

Having determined the synthesis filter coefficients to use, the encoder next calculates the pitch filter coefficient and delay as described below.

7.5.5 The Pitch Filter

The QCELP codec uses a pitch filter of the form

$$\frac{1}{1 - bz^{-L}} \tag{7.6}$$

to represent the long-term periodicities present in voiced speech, where the pitch gain b and lag L are determined once per pitch sub-frame by AbS techniques in the encoder, and transmitted to the decoder. The pitch sub-frames are 5 ms, 10 ms and 20 ms long for full, 1/2 and 1/4 rate frames respectively. In 1/8 rate frames the pitch filter is not used. The pitch-lag L is represented with 7 bits, and can take integer values between 17 and 143. This means that it can take only 127 different values, rather than the 128 distinct values that can be represented with 7 bits. The 128th value ($L = 16$) is used to denote a pitch gain b of 0. The gain b has nine possible values, uniformly spaced in the range $0 \leq b \leq 2$ with steps of 0.25. Three bits are used to code the chosen value of b when this value is greater than 0, and $b = 0$ is coded by setting $L = 16$.

The pitch delay and gain L and b are determined using AbS techniques to minimise the weighted error between the original speech and the synthesised speech. When these parameters are determined the output from the fixed codebook is unknown, and so is assumed to be zero. A weighting filter of the form

$$W(z) = \frac{\hat{A}(z)}{\hat{A}(z/\gamma)} \tag{7.7}$$

is used for the determination of both the pitch filter and fixed codebook parameters. Here $\hat{A}(z)$ is the inverse synthesis filter using the quantised interpolated filter coefficients, and γ is a constant (0.8). In the AbS search for the best pitch-lag L and gain b each possible value of L *and* b is tested to see which pair of values minimises the weighted error between the synthesised and the original speech. This is in contrast to the more usual approach in determining the pitch parameters where the best delay is chosen using AbS techniques, but the quantisation of the gain is carried done outside the AbS loop.

Another difference between the representation of the voicing information in QCELP and in most CELP-type codecs is that a pitch filter is used instead of an adaptive codebook. Using a pitch filter gives the same excitation signal to the synthesis filter as an adaptive codebook except for pitch delays L shorter than the pitch sub-frame. To re-cap, using the notation of Section 3.4, the output from an adaptive codebook is given by $G_1 * u(n-\alpha)$, where $u(n)$ is the excitation to the synthesis filter, G_1 is the codebook gain and α is the delay. When the adaptive codebook parameters G_1 and α, which are equivalent to b and L for the pitch filter in the QCELP codec, are determined the excitation signal $u(n)$ is known only for the previous sub-frames. Hence $u(n-\alpha)$ cannot be determined for $n \geq \alpha$. This problem is most often overcome by repeating the available excitation signal in the adaptive codebook; in other words by using $u(n-\alpha)$ for $0 \leq n < \alpha$, $u(n-2\alpha)$ for $\alpha \leq n < 2\alpha$, etc.

In the QCELP pitch filter an alternative approach is taken. In the AbS determination of the pitch-lag L and gain b for lags L shorter than the sub-frame length the available past excitation $u(n-L)$ is extended for $n \geq L$ using the delayed 'formant residual' as an estimate. This formant residual is given by the original speech signal $s(n)$ filtered through the inverse synthesis filter $\hat{A}(z)$. This estimate is used only when determining L and b – for the determination of the fixed codebook parameters and in the decoder when generating the synthesised speech this estimate is not needed.

Once the pitch filter parameters L and b have been determined, the fixed codebook parameters are found as described next.

7.5.6 The Fixed Codebook

For all the coding rates except the 1/8 rate a fixed codebook searched using AbS techniques is used to provide the excitation to the pitch and synthesis filters. This codebook is described in this section. For the 1/8 rate the codec uses a pseudo-random sequence for the excitation, and this process is described in the next section.

For the full, 1/2 and 1/4 coding rates the fixed codebook is searched every 2.5, 5 or 10 ms. This means that there are two fixed codebook sub-frames for every pitch sub-frame. A 7-bit Gaussian vector codebook is used, together with a 3-bit gain codebook. This gives a total of 10 bits per sub-frame to represent the fixed codebook information. In order to reduce the complexity of the codebook search a circular recursive codebook with 128 entries $c(0), c(1), \ldots, c(127)$ is used. The kth codebook entry $c_k(n)$ is then given by $c([n-k]_{\mathrm{mod}\,128})$. This means the $(k+1)$th codebook entry is equal to the kth entry shifted by one place, with one new sample added at $c_{k+1}(0)$ and one sample dropped at $c_{k+1}(L_c-1)$, where L_c is the fixed codebook sub-frame length (20, 40 or 80 samples depending on the coding rate). The recursive nature of the codebook then allows the convolutions of $c_k(n)$ with the impulse response $h(n)$ of the weighted synthesis filter, which are carried out during the AbS search of the codebook, to be calculated recursively.

This significantly reduces the complexity of the codebook search. To further simplify this search the 128 entries of the recursive codebook are centre clipped so that approximately 80% of them of zero.

Like the AbS search for the pitch filter parameters, the fixed codebook parameters are determined by searching for both the best codebook entry k and the best quantised gain G within the AbS loop. This codebook gain is quantised with three bits, one for its sign and two for its magnitude. The magnitude is quantised in the log domain using a scalar predictive quantiser similar to that used for the LSPs and shown in Figure 7.7. However, the gain quantiser does not subtract a bias value before the quantisation, and uses a second-order nonlinear predictor function rather than the simple first-order predictor $P(z)$ given in Equation (7.5) used in the LSP quantiser.

7.5.7 Rate 1/8 Filter Excitation

At the 1/8 rate the excitation to the synthesis filter (the pitch filter is not used at this rate) is modified to allow the codec to encode background noise more efficiently. Instead of using the recursive centre clipped Gaussian codebook used at the higher rates and described in the previous section, a pseudo-random number generator is used to give the filter excitation. This excitation is scaled by a gain, which is always positive but has its magnitude quantised with two bits in the same way as the codebook gain is quantised for the higher-rate frames. For rate 1/8 packets only the gain that is then used is the average of the gain magnitude for the previous frame (or sub-frame if the previous frame was at a higher rate than 1/8) and the quantised gain for the present frame. This effectively low-pass filters the gain, and prevents burstiness in the level of the background noise. The gain is also interpolated during the length of the frame to give a smooth variation in the level of the reconstructed background noise.

To ensure the encoder and decoder use the same pseudo-random sequence, and hence keep the memory of their filters identical, the random number generators in both the encoder and decoder use the transmitted 16 bit packet as their seed. As well as the ten bits used to represent the LSPs for the frame, and the two bits used to quantize the gain for the frame, the encoder adds four pseudo-random bits to ensure that the 16 bit packet that is transmitted is random.

Having described the synthesis and pitch filters used in the QCELP codec, and the excitation generated as the input to these filters, we now describe the postfilter used at the decoder to improve the perceptual quality of the decoded speech.

7.5.8 Decoder Post-filtering

At the decoder a postfilter similar to those described for other codecs is used. The postfilter has a transfer function $PF(z)$ given by

$$PF(z) = B(z)\frac{\hat{A}(z/\alpha)}{\hat{A}(z/\beta)}, \tag{7.8}$$

where $\hat{A}(z)$ is the inverse synthesis filter and α and β are constants, equal to 0.5 and 0.8 respectively. $B(z)$ is a spectral tilt compensation filter which is described below, and the filter $\hat{A}(z/\alpha)/\hat{A}(z/\beta)$ gives a short-term postfilter which emphasises the formant peaks in

the reconstructed speech and attenuates the valleys between these peaks. This renders the coding noise less audible and so improves the perceptual quality of the reconstructed speech. However, this filter also introduces a spectral tilt to the reconstructed speech which can result in the speech sounding muffled. This effect is corrected using the spectral tilt compensation filter $B(z)$, which is given by

$$B(z) = \frac{1 - gz^{-1}}{1 + gz^{-1}}, \tag{7.9}$$

where g is determined based on the average of the ten interpolated LSPs.

Finally, gain compensation is applied at the output of the postfilter to ensure that the energy of its input and output are roughly equal. A scaling factor given by the square root of the ratio of the energies of the input and the output from $PF(z)$ is calculated, and filtered with a first-order IIR filter before being used to scale the output from $PF(z)$ to give the decoded speech.

7.5.9 Error Protection and Concealment Techniques

For full rate frames the 18 most perceptually sensitive bits (the most significant bits from the 10 LSPs and the 8 fixed codebook gain magnitudes) are protected with 11 parity bits from a $(29, 18)$ cyclic code. This code allows the decoder to provide error detection and correction for these 18 most sensitive bits. The decoder is also able to deal with packets that are declared 'erased'. Such packets occur when the decoder has been unable to satisfactorily determine the coding rate or when the decoder determines that a full-rate frame was sent, but the $(29, 18)$ cyclic code protecting the 18 most sensitive bits of the frame is overloaded. When such erasures occur the decoder takes the following steps:

(1) the LSPs are decayed towards their white-noise 'bias' values;

(2) the previous pitch-lag L is used;

(3) the pitch gain b is decayed towards zero;

(4) a random codebook index is chosen;

(5) the fixed codebook gain is decayed towards zero.

By decaying these parameters towards their background levels annoying squeaks or whistles, which can occur in the reconstructed speech when bit errors occur, are avoided. It is stated in [206] that when operating under typical conditions in a CDMA system the quality of the reconstructed speech in the QCELP codec is very close to that achieved over an error-free channel.

7.5.10 Conclusion

In this section we have described the techniques used in the QCELP variable rate speech codec. This codec produces speech quality equivalent to that of the 7.95 kbps IS-54 VSELP codec of Section 7.3, but at an average bitrate of less than 4 kbps. This reduction in the average bitrate of the codec is exploited by the CDMA system used in IS-95 to almost double the user capacity of the system. This codec marks the end of the first generation CELP-based

codecs. CELP schemes and their relatives, such as VSELP codecs, constituted an important milestone in the history of speech compression, reaching bitrates as low as 4.8 kbps in the DoD codec.

However, for rates below 4.8 kbps further advances were required. These advances were fuelled by two factors. Firstly, the ever increasing demand for accommodating more speech users in the allocated bandwidth of existing mobile radio systems led to the development of so-called half-rate coding standard, doubling the number of users supported. This trend is hallmarked by the 3.6 kbps half-rate Japanese codec of the next section as well as by the 5.6 kbps half-rate Pan-European GSM standard of Section 7.7. The second trend was the arrival of a range of so-called enhanced full-rate codecs, such as that of the Pan-American Qualcomm system and the enhanced version of the IS-54 system's speech codec, referred to as the IS-136 standard arrangement, which is the subject of Section 7.11. The Pan-European GSM system was also endowed with a new enhanced full-rate scheme, which will be discussed in Section 7.7. As the first representative of this new generation of CELP-based schemes, in the next section we consider the 3.6 kbps half-rate Japanese codec.

7.6 Japanese Half-rate Speech Codec [157]

7.6.1 Introduction

Recall from Section 7.4 that the Japanese full-rate speech codec [157] was developed by Ohya *et al.* [208, 209], which employed VSELP-based coding at 6.7 kbps. This speech coded rate was increased by 4.5 kbps of error protection, giving a total channel coded rate of 11.2 kbps. Thus, the half-rate speech codec is expected to operate at a rate beneath 4 kbps. In order to achieve a bitrate below 4 kbps, the excitation vector length passed to the synthesis filter has to be increased to about 8 to 10 ms. Hence the excitation vector may contain several pitch period cycles. The random nature of the conventional CELP code vectors, described in Chapter 6, poorly represents these excitations and hence employing purely random excitations seriously degrades the performance of any CELP-based speech codec operating at rates beneath 4 kbps. The Japanese half-rate speech codec [157] overcomes these excitation vector problems by employing the pitch synchronous innovation code excited linear prediction (PSI-CELP) principle [210]. This PSI-CELP codec operates at a rate of 3.45 kbps with an additional 2.1 kbps allocated for error protection, producing a channel coded rate of 5.55 kbps. This codec is described in detail next.

7.6.2 Codec Schematic and Bit Allocation

The Japanese half-rate speech codec operates on the basis of 40 ms speech frames, processing an input speech bandwidth of 0.3 kHz to 3.4 kHz, and a sampling frequency of 8 kHz. The encoder and decoder schematics are given in Figures 7.8 and 7.9, respectively. Four 10 ms subframes are used within each 40 ms speech frame. Initially the power of each subframe is vector quantised using a total of 7 bits/frame. The ten LPC coefficients are then vector quantised in the LSP domain for the second and fourth subframe, while the first and third subframes' parameters are not explicitly transmitted, they are regenerated at the decoder with the aid of interpolation between the transmitted subframes' parameters. In the second and

fourth subframes a moving average predictor and two-stage vector quantisation are employed for each subframe, using a total of 31 bits/frame for LSP quantisation.

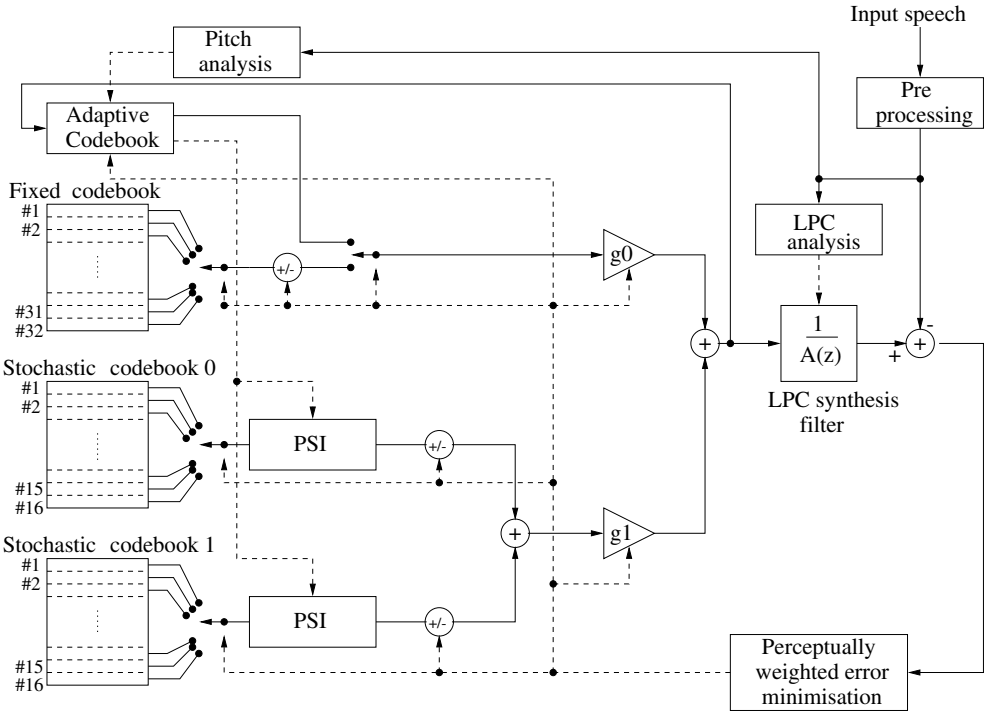

Figure 7.8: The Japanese half-rate speech encoder's schematic.

Similar to traditional CELP codecs [100], the PSI-CELP speech codec uses two excitation vectors in order to represent the excitation for each subframe. The first excitation vector is chosen either from the 192-entry adaptive codebook seen at the top left-hand corner of Figure 7.10 using fractional delays, or from the 32-entry fixed random codebook portrayed below the adaptive codebook in Figure 7.10. Since the 32-entry fixed codebook also has a polarity bit, it can produce 64 different vectors. The total number of entries hosted by the first excitation vector is hence $192 + 64 = 256$, which is encoded with the aid of 8 bits. Hence, if the input excitation has insufficient periodicity in order to warrant the employment of the adaptive codebook, which would be typically used in voiced segments, then the first excitation vector is automatically generated by the 32-entry fixed codebook. The encoding of the excitation vectors will be further detailed in Section 7.6.6.

The second excitation vector is generated by the superposition of two fixed codebooks, as will be detailed in Section 7.6.7. As regards to the construction of the second excitation vector, if the first excitation vector was selected from the fixed 32-entry codebook, then the two 16-entry subcodebooks operate as in a typical CELP system in order to form the composite excitation. Since they both also have a polarity bit, these codebook entries are encoded with a total of 10 bits.

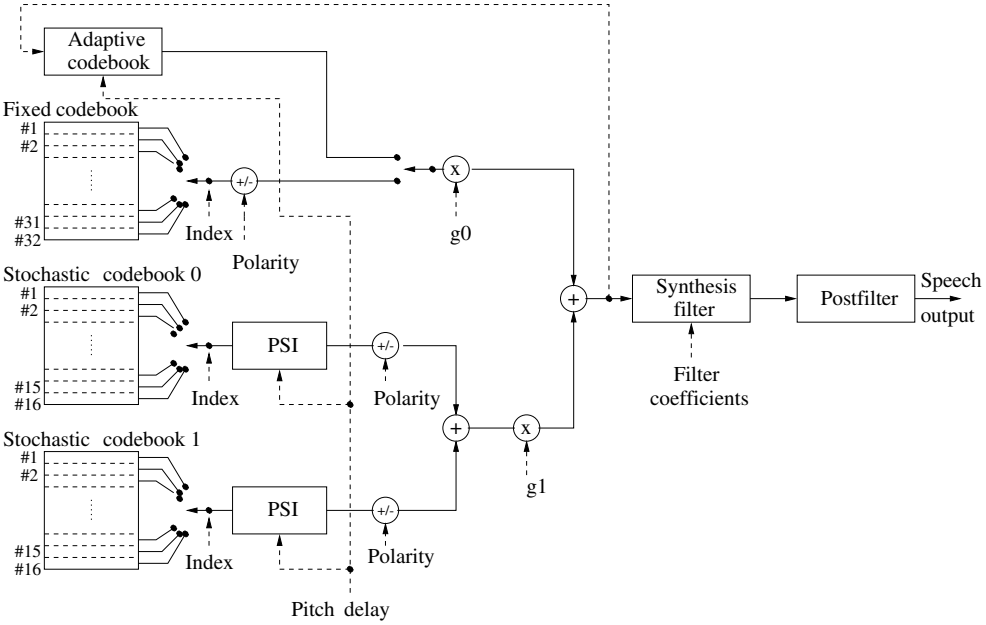

Figure 7.9: The Japanese half-rate speech decoder's schematic.

However, if the first excitation vector was generated by the 192-entry adaptive codebook, then the second excitation vector is constituted by a sequence having the length of the pitch determined by the adaptive codebook. Such a sequence is selected from each subcodebook, which are then combined into one sequence. This pitch-duration segment is then repeated in order to create the second 10 ms duration excitation vector. This unique feature of the PSI-CELP codec enhances the periodicity of voiced speech, and this principle is often used in speech codecs operating at rates beneath 4 kbps. For each excitation optimisation subframe the gains of the excitation vectors are vector quantised using a 7-bit codebook. The entries constituting the two excitation vectors and the codebook gains are optimised for each subframe using an AbS search in order to minimise the weighted error between the original and reconstructed speech.

At the decoder the transmitted parameters are decoded in order to produce the filter coefficients for the synthesis filter and to select the codebook entries for the excitation vectors and gain codebooks. Adaptive post-filtering [110] is used to improve the perceptual quality of the reconstructed speech. The bit-allocation scheme of the Japanese half-rate speech codec is summarised in Table 7.7. We now describe in more detail the various blocks shown in Figures 7.8 and 7.9.

7.6.3 Encoder Pre-processing

The input speech signal is band-limited to the frequency range of 0.3 kHz–3.4 kHz. Subsequently, the power of each 10 ms subframe is computed, transformed to the logarithmic domain and stored in a four-dimensional vector. Since the energy levels of the consecutive

Table 7.7: Bit allocation for the 40 ms duration LPC frame of the Japanese half-rate speech codec, which is constituted by four 10 ms duration subframes.

Parameter	Bits/frame
LSP parameters	31
Power	7
Excitation vector 1	8×4
Excitation vector 2	10×4
Gain vector	7×4
Total/40 ms	138 (3.45 kbps)

10 ms speech subsegments are similar, vector quantisation of these values results in coding economy. A total of 7 bits per 40 ms speech frame was found to be adequate for their quantisation, which corresponds to a codebook size of 128 entries, as seen in Table 7.7.

7.6.4 LPC Analysis and Quantisation

For the Japanese half-rate speech codec, 10th-order LPC analysis is performed and the LPC coefficients are transformed to the LSP domain, as highlighted in Chapter 4. The LPC coefficients are calculated twice for every 40 ms duration speech frame, namely for the second and fourth 10 ms subframes. By contrast, for the first subframe the LPC coefficients are calculated from the average of the LSPs of the fourth subframe in the previous speech frame and from those of the second subframe in the current 40 ms speech frame. Concerning the third subframe, the LPC coefficients are determined from the average of the LSPs in the second and fourth subframes of the current speech frame. For the second and fourth subframes the window employed during the LPC analysis is a non-symmetric window of 35.8 ms, which is calculated from the impulse response of an AR filter. This non-symmetric window ensures that no future samples are required for the LPC analysis.

The LSP vector quantisation process allocates a total of 30 bits per 40 ms speech frame, as is shown in Table 7.7. The LSP vector to be quantised is initially estimated by MA prediction. This MA prediction exploits the high correlation between the LSPs in adjacent frames, while ensuring that channel errors only propagate to a fixed number of frames. For details of the specific MA predictor the interested reader is referred to [157]. Suffice to say here that a one-bit flag is used by the codec in order to differentiate between two different MA predictor coefficients.

7.6.5 The Weighting Filter

The weighting filter used by the Japanese half-rate speech codec is based on the unquantised LPC filter coefficients α_i. The transfer function of the weighting filter is comprised of a spectral weighting filter $W'_f(z)$ and a pitch weighting filter $W_p(z)$, which is formulated as

$$W(z) = W_f(z) \cdot W_p(z) \approx W'_f(z) \cdot W_p(z), \tag{7.10}$$

where the individual filter transfer functions are given by

$$W_f(z) = \frac{1 + \sum_{i=1}^{p} \alpha_i \gamma_1^i z^{-i}}{1 + \sum_{i=1}^{p} \alpha_i \gamma_2^i z^{-i}}, \quad (0 \leq \gamma_2 \leq \gamma_1 \leq 1) \tag{7.11}$$

$$W'_f(z) = \sum_{i=0}^{m} a_i z^{-i} \tag{7.12}$$

$$W_p(z) = 1 + \epsilon_1 \sum_{i=-1}^{1} \beta_i z^{-L-i} \tag{7.13}$$

and $p = 10$, $m = 11$, $\gamma_1 = 0.9$, $\gamma_2 = 0.4$ and $\epsilon_1 = 0.4$. The calculation of the filter $W_f(z)$ is computationally complex, hence it is approximated by the FIR filter $W'_f(z)$.

7.6.6 Excitation Vector 1

For the Japanese half-rate speech codec the structure of the first excitation vector is portrayed at the top left-hand corner of Figure 7.10. Specifically, the first excitation vector contains the adaptive codebook entry used in the traditional CELP codecs described in Chapter 6, together with an entry from a fixed random codebook. This first excitation vector is encoded with a total of 8 bits, resulting in 256 different possible excitations. The adaptive codebook is constituted by 192 entries, while the fixed random codebook has 32 entries, each of which can be multiplied by ± 1 – again, yielding a total of $192 + 64 = 256$ excitation patterns.

For the adaptive codebook non-integer pitch delays are used in the range of $L_{\min} = 16$ and $L_{\min} = 97$, invoking the closed-loop search described in Section 3.4.2. The fixed codebook-based section of the first excitation vector was designed to improve the representation quality of the uncorrelated portions of speech, namely that of silence, unvoiced and transient segments. This choice of codebooks follows the technique often used in low bitrate speech codecs, where voiced and unvoiced speech, as described in Section 1.2, are encoded separately.

The selection between the adaptive codebook and the fixed random codebook is based on a perceptually weighted distortion metric given by

$$D = \|W(X^* - Y)\|^2, \tag{7.14}$$

where W is a matrix constituted by the impulse response of the perceptual error-weighting filter, X^* is the input speech vector containing the current speech subframe and Y is the corresponding vector containing the synthesised speech.

Initially for the adaptive codebook, six pitch delay candidates are selected, using an open-loop technique. These six candidates are eventually reduced to two candidates following an AbS-based closed-loop search. An additional two candidate excitations are selected from the fixed codebook. Finally, from these four candidate excitations the best two candidate excitations are selected for the first excitation vector, amalgamating the best vector of both codebooks.

7.6.7 Excitation Vector 2

The structure of the second excitation vector is portrayed in the lower left portion of Figure 7.10. Each 16-entry subcodebook is assigned 5 bits, which includes 1 bit for their polarity. The outputs of the two subcodebooks are then combined in order to create the second excitation vector.

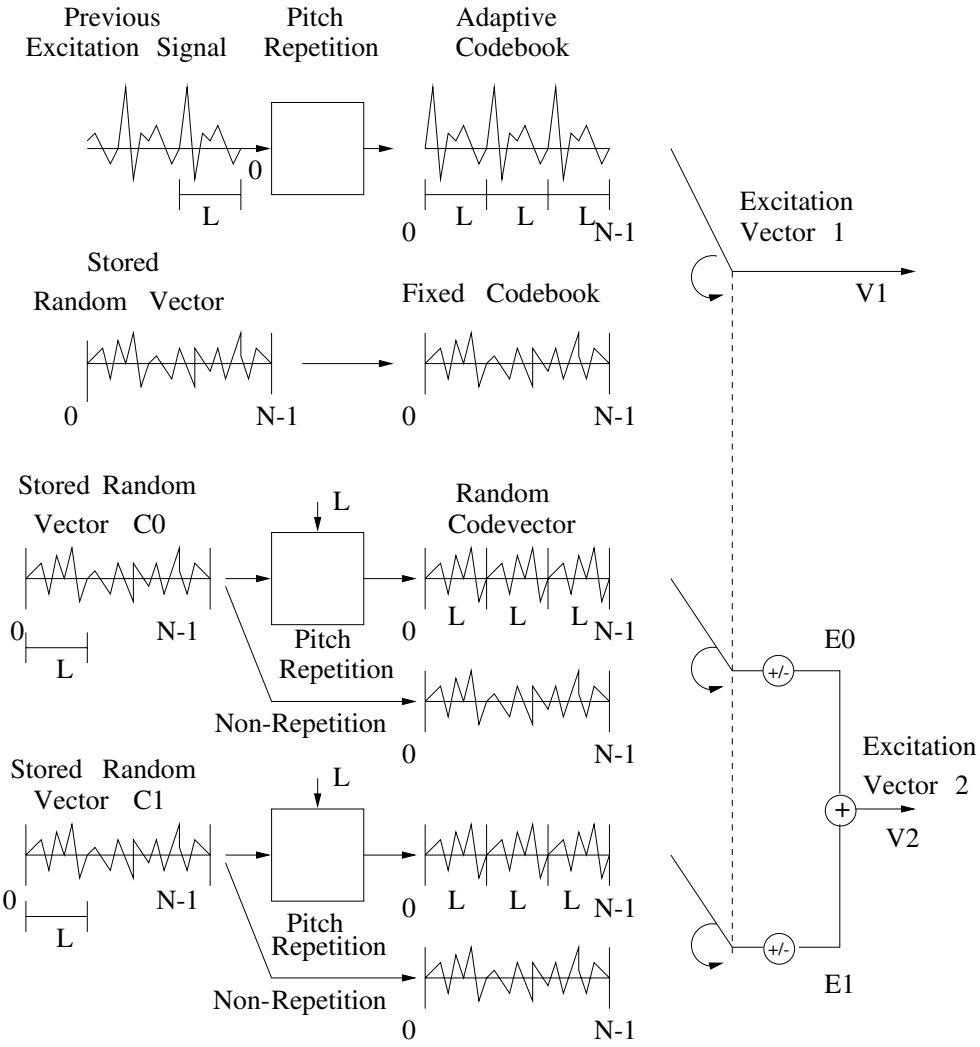

Figure 7.10: Excitation formulation for the Japanese half-rate speech codec.

During the determination of the second excitation vector, initially the result of optimising the first excitation is examined, and if the fixed codebook was selected, then the two 10 ms duration excitation vectors output by the 6-bit subcodebooks are combined in order to produce the second excitation vector, which is encoded with the aid of 10 bits. However,

if the adaptive codebook was selected for generating the first excitation vector, then the length of the excitation vectors generated by the subcodebooks is limited to the duration of the associated pitch delay, as seen at the bottom of Figure 7.10. These pitch-duration fixed codebook vector segments are than repeated a number of times until the subframe is filled. Thus, when encountering voiced speech segments, pitch synchronous excitation vectors are produced by each subcodebook. Hence, for uncorrelated portions of speech, such as unvoiced speech segments, the combined excitation vector will contain only random signals. By contrast, for predictable portions of speech, such as voiced speech, the combined excitation vector will contain two pitch synchronous vectors. The employment of the adaptive codebook and fixed random codebooks follows the philosophy of conventional CELP codecs, while the separate encoding of predictable and unpredictable portions of speech reflects the principles of a vocoder. Thus, the PSI-CELP Japanese half-rate speech codec constitutes a hybrid of traditional CELP codecs and traditional vocoders.

7.6.8 Channel Coding

The Japanese half-rate speech codec was designed to cope with a maximum of 3% burst error rate inflicted by the transmission channel. It has been found that the power parameter, the first excitation vector, some of the LSP parameters and the most significant gain signalling bit are particularly sensitive to noisy channels.

Figure 7.11 shows the channel coding scheme protecting the different bits generated by the encoder. Specifically, the 66 most sensitive bits are protected bits, while the remaining 72 bits are left unprotected. Initially, the protected bits are assigned a 9-bit CRC code for error detection. Subsequently, the protected bits and the output of the CRC code are passed to a half-rate convolutional code having a memory of 7. Finally, interleaving is performed to randomise the effect of channel error bursts. In the next section we consider the operations of the speech decoder.

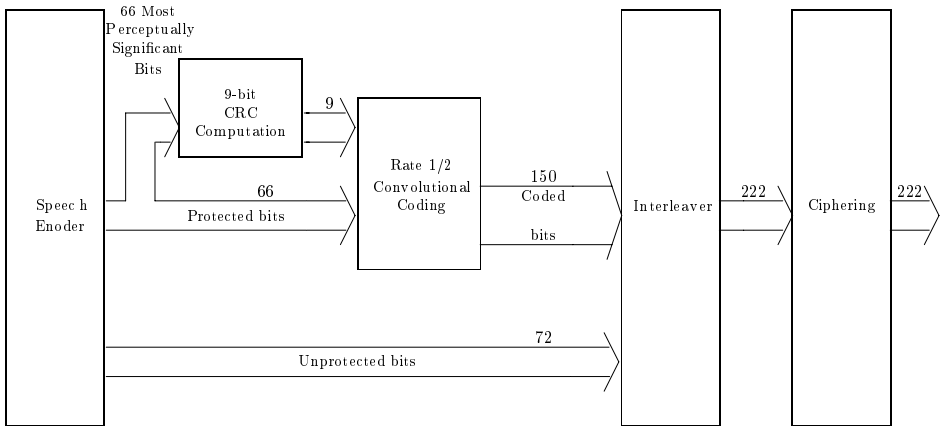

Figure 7.11: Channel coding employed by the Japanese half-rate speech codec.

7.6.9 Decoder Post-processing

The initial process at the decoder is to check whether the transmitted frame has been lost due to channel errors. If a lost frame has occurred then a parameter recovery process is activated, with the lost parameters interpolated from the previous frames' corresponding parameters, that have been successfully received. The power is attenuated depending on the current and past frame error events. For a lost speech coded frame the LPC coefficients, the first excitation vector, and the gain parameters are replaced by the previous correctly received values. However, in a lost frame, for the second excitation vector no form of error recovery was undertaken. Following the determination of the parameters the reconstructed speech is formed, and subsequently passed to a postfilter [110].

The postfilter $F(z)$ used in the Japanese half-rate speech decoder is adaptive, and it was designed to improve the perceptual quality of the reconstructed speech. The postfilter's transfer function is described by

$$F(z) = F_f(z) \cdot F_p(z) \cdot F_h(z), \tag{7.15}$$

where the individual filters are given by

$$F_f(z) = \frac{1 + \sum_{i=1}^{p} \alpha_{qi} \gamma_3^i z^{-i}}{1 + \sum_{i=1}^{p} \alpha_{qi} \gamma_4^i z^{-i}} \quad (0 \leq \gamma_3 \leq \gamma_4 \leq 1) \tag{7.16}$$

$$F_p(z) = \frac{1}{1 + \epsilon_2 \sum_{i=-L}^{1} v_i z^{-L-i}} \tag{7.17}$$

$$F_h(z) = 1 - \eta z^{-1} \tag{7.18}$$

and the individual parameters are given by $p = 10$, $\gamma_3 = 0.5$, $\gamma_4 = 0.8$, $\epsilon_2 = 0.7$ and $\eta = 0.4$.

Specifically, the filter $F_f(z)$ is based on the LPC filter coefficients and was designed to augment the spectral domain formants in the speech spectrum, hence it is effectively a short-term postfilter. By contrast, the filter $F_p(z)$ is a three-tap pitch comb-filter, which was designed to enhance the pitch harmonics in the speech spectrum, and hence it constitutes a long-term postfilter. The third filter described by $F_h(z)$ is a single-tap differential high-pass filter, designed to combat the muffling effect of the long-term and short-term post-filters. If a speech frame loss occurs at the decoder, then the postfilter parameters are changed to $\epsilon_2 = 0.4$ and $\eta = 0.0$, reducing the effect of long-term post-filtering and removing the high-pass filter. Following the post filter, automatic gain control is employed in order to restore the original speech energy level.

As in the context of the other speech codecs considered, this coding arrangement will be compared in subjective speech quality terms to a range of existing standard codecs in Figure 18.4 of Chapter 18, where it is denoted by JDC/2.

In the next section we will consider the 5.6 kbps half-rate GSM codec, which is based on a refined VSELP codec, a principle that was used in the 7.95 kbps IS-54 and the 6.7 kbps JDC codecs.

7.7 The Half-rate GSM Speech Codec [211]

7.7.1 Half-rate GSM Codec Outline and Bit Allocation

In what follows we briefly highlight the techniques proposed by Gerson *et al*. [211], which led to the definition of the half-rate GSM standard codec employing a 5.6 kbps VSELP codec [202, 203]. The codec's schematic is shown in Figure 7.12, where two different block-diagrams characterise its operation in four different operational modes. In Mode 0 the codec obeys the schematic portrayed at the top of Figure 7.12, while in the remaining three modes, Mode 1, 2 and 3 it is configured as seen at the bottom of Figure 7.12. The analysis synthesis filter's coefficients are determined every 20 ms and this interval is divided in four 5 ms excitation optimisation subsegments, corresponding to 160 and 40 samples, respectively, when using a sampling frequency of 8 kHz. In our forthcoming discussion we focus our attention on the above-mentioned different operating modes and the corresponding schematics.

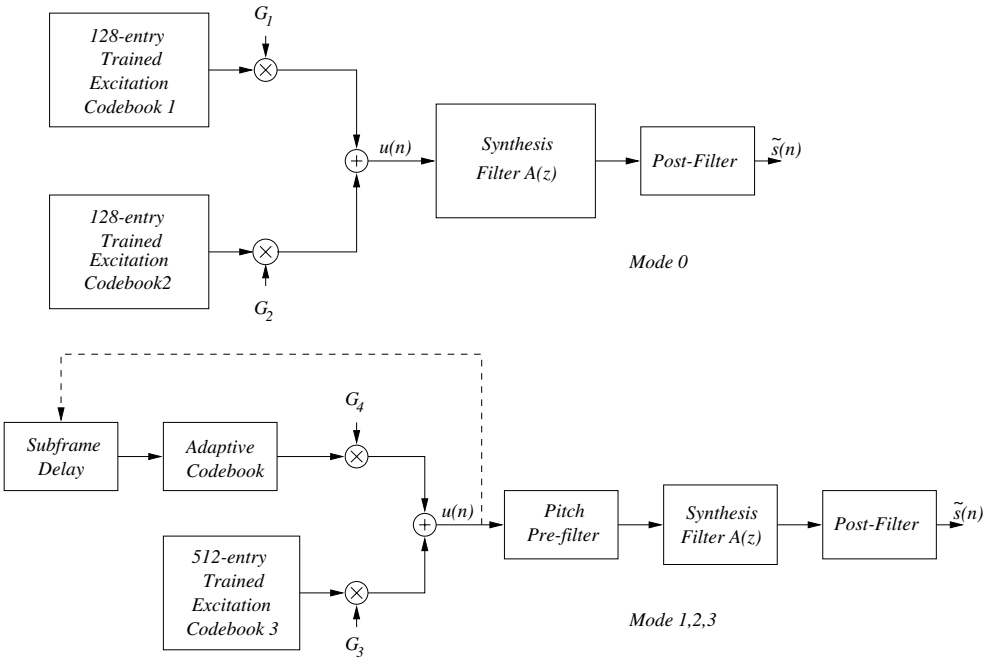

Figure 7.12: Schematic of the 5.6 kbps VSELP half-rate GSM codec, portraying the unvoiced Mode 0 and the voiced Modes 1, 2 and 3.

The codec's bit allocation scheme is summarised in Table 7.8 for the synthesis modes of 0–3. The speech spectral envelope is encoded by allocating 28 bits/20 ms synthesis frames for the vector quantisation of the reflection coefficients. A so-called soft interpolation bit is used to inform the decoder whether the current frame's prediction residual energy was lower with or without interpolating the direct form LPC coefficients.

As mentioned before, there are four different synthesis modes corresponding to different excitation modes, implying the presence of different grades of voicing in the speech signal.

Table 7.8: Bit allocation scheme of the 5.6 kbps VSELP half-rate GSM codec.

Parameter	Bits/frame
LPC coefficients	28
LPC interpolation flag	1
Excitation mode	2
Mode 0 :	
Codebook 1 index	$4 \times 7 = 28$
Codebook 2 index	$4 \times 7 = 28$
Modes 1, 2, 3	
LTPD (subframe 1)	8
Δ LTPD (subframes 2, 3, 4)	$3 \times 4 = 12$
Codebook 3 index	$4 \times 9 = 36$
Frame energy E_F	5
Excitation gain-related quantity $[E_s E_1]$	$4 \times 5 = 20$
Total no of bits	112/20 ms
Bitrate	5.6 kbps

As seen in the table, two bits/frame are used for excitation mode selection. The decisions as to what amount of voicing is present and hence which excitation mode has to be used are based on the LTP gain, which is typically high for highly correlated voiced segments and low for noise-like, uncorrelated unvoiced segments.

In the unvoiced Mode 0 the schematic at the top of Figure 7.12 is used, where the speech is synthesised by superimposing the G_1- and G_2-scaled outputs of two 128-entry trained codebooks in order to generate the excitation signal, which is then filtered through the synthesis filter $A(z)$ and the spectral postfilter. Accordingly, both excitation Codebook 1 and 2 have a 7-bit address in each of the 4 subsegments, as shown in Table 7.8.

In Modes 1–3, where the input speech exhibits some grade of voicing, the schematic at the bottom of Figure 7.12 is used. The excitation is now generated by superimposing the G_3-scaled 512-entry trained codebook's output onto that of the G_4-scaled so-called adaptive codebook. The fixed codebook in these modes requires a 9-bit address, yielding a total of $4 \times 9 = 36$ coding bits for the 20 ms frame, as seen in Table 7.8. The adaptive codebook delay or LTPD is encoded in the first subsegment using 8 bits, allowing for 256 integer and non-integer delay positions. In consecutive subframes the LTPD is encoded differentially, with respect to the previous subframe's delay, which we indicated as ΔLTPD in Table 7.8. The 4 encoding bits allow for a maximum difference of $[-8, +7]$ positions with respect to the previous LTPD value. The legitimate LTPD values are listed in Table 7.9.

Observe in the table that for low LTPD values a finer resolution is used and the highest resolution is assigned for the range 23 – $(34 + 5/6)$, corresponding to a pitch-lag of between 2.875 – 4.35 ms or pitch frequency of 230–348 Hz.

Returning to Table 7.8, the overall frame energy is encoded with 5 bits, which allows spanning a dynamic range of 64 dB when using a stepsize of 2 dB and 32 steps. The excitation gains G_1–G_4 are not directly encoded. Instead, the energy of each subframe E_s is expressed

Table 7.9: Legitimate non-integer LTPD values and LTP resolution in the 5.6 kbps VSELP half-rate GSM codec.

LTPD range	Resolution
21–(22 + 2/3)	1/3
23–(34 + 5/6)	1/6
35–(49 + 2/3)	1/3
50–(89 + 1/2)	1/2
90–142	1

normalised by the frame energy E_F, which is then jointly vector quantised with another parameter about to be introduced. Specifically, it was found advantageous to express the relative contribution E_1 of the first excitation component constituted by Codebook 1 at the top of Figure 7.12 in Mode 0, and by the adaptive codebook at the bottom of Figure 7.12 in Modes 1–3 to the overall excitation. Clearly, this relative contribution must be limited to the range of 0–1. Then the parameter pair $[E_s, E_1]$ is vector quantised using 5 bits/5 ms subsegment, which allowed for 32 possible combinations. Accordingly, Table 7.8 assigns a total of 20 bits/20 ms frame for the encoding of this gain-related information.

7.7.2 Spectral Quantisation in the Half-rate GSM Codec

According to Table 7.8, the codec employs 28-bit VQ of the so-called reflection coefficients, where the best set is deemed to be the one which minimises the prediction residual energy. A reduced-complexity version of the FLAT [204, 205] was proposed for the standard, which will be briefly highlighted below.

It would be impractical to use a 2^{28}-entry codebook for both search-complexity and storage-capacity reasons, whence a suboptimum three-way split-vector implementation was proposed by Gerson [204], where the reflection coefficients $k_1 - k_3$, $k_4 - k_6$ and $k_7 - k_{10}$ are stored in separate codebooks. The number of quantisation or codebook address bits is $Q_1 = 11, Q_2 = 9$ and $Q_3 = 8$ bits, respectively. A particularly attractive property of the reflection coefficient-based lattice-type predictors is that in the case of the above so-called split-vector quantisers the choice of the current acoustic tube model segment's reflection coefficient quantiser can partially compensate for the quantisation effects of the preceding tube section quantiser.

To elaborate on these issues Gerson *et al.* [211] introduced the ingenious concept of pre-quantisation, where in each of the three split codebooks a so-called pre-quantiser using $P_1 = 6, P_2 = 5$ and $P_3 = 4$ bits is invoked. Each vector of the pre-quantiser is associated with a set of vectors in the actual quantiser. For example, each of the $P_1 = 6$ bit quantiser entries is associated with $n_1 = 2^{Q_1}/2^{P_1} = 2^{11}/2^6 = 2^5 = 32$ vectors in the first actual VQ codebook, etc. In order to reduce the overall complexity, the prediction residual error is computed for each of the prequantiser vectors at a given acoustic tube model segment and the four vectors resulting in the four lowest error energy values are earmarked. These four vectors are then used as pointers to identify four sets of vectors, which are associated with the earmarked

pre-quantiser vectors. The four sets of actual quantised vectors are then exhaustively searched in order to find the set, which minimises the prediction residual energy.

This technique results in a substantial complexity reduction. Specifically, instead of searching the $2^{Q_1} = 2^{11}$ = 2048-entry codebook storing the reflection coefficients $(k_1 - k_3)$, initially the $2^{P_1} = 2^6$ = 64-entry pre-quantiser codebook is searched to find the best four 'pointers', around each of which then the prediction residual is evaluated 32 times, requiring its computation 128 times. For simplicity, assuming an identical evaluation complexity for both steps, the complexity of the full search was reduced by a factor of $2048/(64 + 128) \approx 10.67$. The corresponding factors for the $(k_4 - k_6)$ and $(k_7 - k_{10})$ codebooks are $2^9/(32 + 64) \approx 5.3$ and $2^8/(16 + 64) = 3.2$, respectively.

The reflection coefficients themselves have been reported to have a high spectral sensitivity in the vicinity of the unit circle, when $k_i \approx 1$. This may result in a large speech spectrum variation due to the quantisation of the reflection coefficients. Hence a very fine Lloyd–Max quantiser would be required for their quantisation in this domain, instead of uniform quantisation. Therefore two widely used nonlinear transformations have been proposed for circumventing this problem, namely the LAR and the inverse sine transformation $S_i = \sin^{-1}(k_i)$, which are more amenable to uniform quantisation. The GSM half-rate codec uses the latter, employing an efficient 8-bit representation for the codebook entries which were generated by uniformly sampling their so-called inverse-sine representations. Let us now briefly consider the error protection strategy used.

7.7.3 Error Protection

The error control strategy used is based on the schematic of Figure 7.13, which is quite similar in terms of its philosophy to that of other mobile radio systems such as, for example, the full-rate or the enhanced full-rate GSM schemes or the IS-54 system, portrayed in Figure 7.4. The 112 bits/20 ms are divided into 95 more sensitive Class-1 bits and 17 more robust Class-2 bits. The most sensitive 22 Class-1 bits are assigned a 3-bit CRC pattern, which is then invoked by the decoder for initiating bad frame masking. Bad frames may be encountered due to channel errors or due to fast associated control channel messages replacing a speech frame; for example, in order to signal an urgent hand-over request. In this case the speech frame is wiped out by this fast associated control channel message and at the decoder it has to be replaced by a post-processed speech segment.

As displayed in Figure 7.13, the 17 robust Class-2 bits are unprotected, while the 95 Class-1 bits are 1/3-rate, constraint-length 7 convolutionally encoded. Here we note that the definition of constraint length in this case includes the current input bit of the encoder plus the six shift-register stages. Hence six tailing bits are necessary for flushing the encoder's shift-registers after each transmission burst in order to prevent error propagation across transmission frame boundaries. We note, however, that a so-called punctured code was employed, where the effective coding rate becomes 1/2 due to puncturing. More explicitly, puncturing implies obliterating some of the encoded bits. The 95 Class-1 bits and the 6 tailing bits yield 101 bits, which generate 202 punctured convolutionally coded bits, while the 3 CRC bits are 1/3-rate coded, yielding a total of 211 bits. After concatenating the 17 unprotected bits the total rate becomes 228 bits/20 ms $= 11.4$ kbps, which is exactly half of that of the full-rate and enhanced full-rate systems.

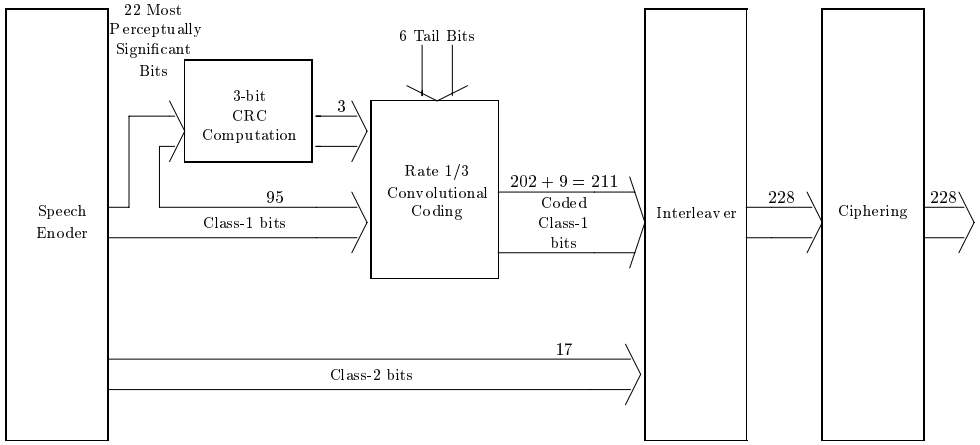

Figure 7.13: The 5.6/11.4 kbps GSM half-rate error protection schematic.

Having highlighted the basic features of the 5.6 kbps half-rate GSM codec, in the next section we address some of the issues specific to the 8 kbps ITU G.729 scheme.

7.8 The 8 kbps G.729 Codec [147]

7.8.1 Introduction

In 1990 the CCITT (recently renamed the ITU-T) invited candidate codecs for a low delay 8 kbps speech coding standard. Requirements regarding speech quality, robustness to channel errors and frame length were specified. However, no candidate codec submitted by the July 1991 deadline satisfied all the requirements, and so in November 1991 the frame length requirement was relaxed from the original 5 ms to 16 ms. In November 1992 two candidate codecs were submitted. One, from NTT in Japan, used conjugate structure CELP (CS-CELP) with a frame length of 13ms. The other was designed by France Telecom and the University of Sherbrooke in Canada, and used ACELP with a frame length of 12 ms. It was decided that considering potential applications a 10 ms frame length would be preferable, and so both groups agreed to reduce the frame length of their codecs to 10 ms. Aspects of both the CS-CELP codec [212] and the ACELP codec [160, 213] were used in the final standardised codec, which uses conjugate structure algebraic CELP (CS-ACELP), and provides toll quality speech at 8 kbps with a 10 ms frame length. This codec is described in detail below.

7.8.2 Codec Schematic and Bit Allocation

Schematics of the G.729 encoder and decoder are shown in Figures 7.14 and 7.15. It can be seen that the structure of this codec is similar to that of other forward-adaptive codecs described earlier. Forward adaption is used to determine the synthesis filter parameters once per 10 ms frame. These filter coefficients are then converted to LSFs and quantised with 18 bits using predictive two stage vector quantisation. Each 10 ms frame is split into two 5 ms

sub-frames, and the excitation for the synthesis filter is determined for each sub-frame. The long term correlations in the speech are modelled using an adaptive codebook with fractional delays, using 8 bits to represent the delay in the first sub-frame, and 5 bits to differentially encode the delay in the second sub-frame. Also, to improve the robustness of the codec to channel errors, the six most significant bits of the adaptive codebook index in the first sub-frame have a parity bit added. This allows most errors in these bits to be detected at the decoder, and when such errors are detected an error concealment procedure is applied. A 17-bit algebraic codebook with a focussed search procedure is used as the fixed codebook. Finally, the adaptive and fixed codebook gains are vector quantised with 7 bits using a two stage conjugate structured codebook, with fourth-order moving average prediction applied to the fixed codebook gain to aid the efficiency of the quantiser. The entries from the fixed, adaptive and gain codebooks are chosen every sub-frame using an AbS search to minimise the weighted error between the original and the reconstructed speech.

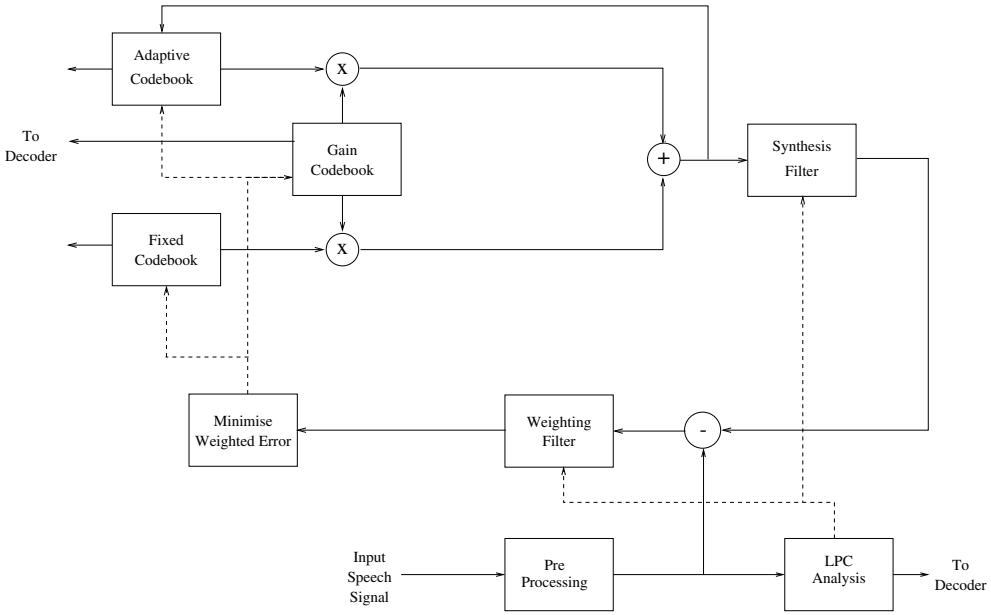

Figure 7.14: 8 kbps low-delay CCITT G.729 encoder.

At the decoder the transmitted parameters are used to give the filter coefficients for the synthesis filter, and to select entries from the fixed, adaptive and gain codebooks to represent the excitation to this filter. The reconstructed speech is then post-processed to improve its perceptual quality. The bit allocation of the G.729 codec is summarised in Table 7.10. We now describe in more detail the various blocks shown in the G.729 encoder and decoder.

7.8.3 Encoder Pre-processing

Simple pre-processing is applied to the input speech signal in the G.729 encoder. The input signal is assumed to be a 16 bit linear PCM signal, and is initially divided by a factor of 2 to

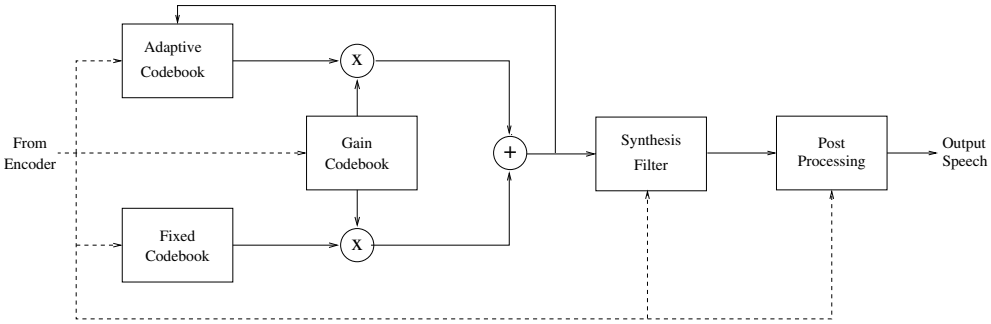

Figure 7.15: 8 kbps low-delay CCITT G.729 decoder.

Table 7.10: Bit allocation scheme of the G.729 codec.

Parameter	Sub-Frame 1	Sub-Frame 2	Total/frame
LPC: LSPQ1–LSPQ4			$1+7+5+5=18$
Pitch-delay: PD1, PD2	8	5	13
Parity for pitch-delay: PPD	1	0	1
Fixed codebook ind.: FC1, FC2	$3\times 3+4=13$	$3\times 3+4=13$	26
Sign of fixed codebook: SFC1, SFC2	4	4	8
Codebook gains (stage 1): GC1A, GC2A	3	3	6
Codebook gains (stage 2): GC1B, GC2B	4	4	8
Total			80

reduce the possibility of overflows in fixed-point implementations of the codec. The signal is also high-pass filtered using a second-order pole-zero filter with a cutoff frequency of 140 Hz. This acts as a precaution against undesired low-frequency components in the input signal. The pre-processed speech signal acts as the input to the speech encoder, and is referred to as the input speech in our descriptions below.

7.8.4 LPC Analysis and Quantisation

LPC analysis is carried out in the G.729 encoder to derive filter coefficients to be used by the 10th order synthesis and weighting filters. The coefficients for these filters are calculated at the encoder for every 10 ms frame, using the autocorrelation method with a 30 ms asymmetric window. This window is shown in Figure 7.16, where the sample indices $0, 1, \ldots, 79$ correspond to the present 10 ms frame. The window consists of half a Hamming window for 25 ms, and a quarter of a cosine cycle for the final 5 ms of the window. It can be seen that although the frame length of the codec is 10 ms, a 5 ms lookahead is used which increases the total delay of the codec by 5 ms.

The windowed speech signal is used to compute 11 autocorrelation coefficients $R(k)$, $k = 0, 1, \ldots, 10$. These autocorrelations are then slightly modified as follows. $R(0)$ is given a lower bound of 1.0 to avoid arithmetic problems with low-level input signals. A 60 Hz

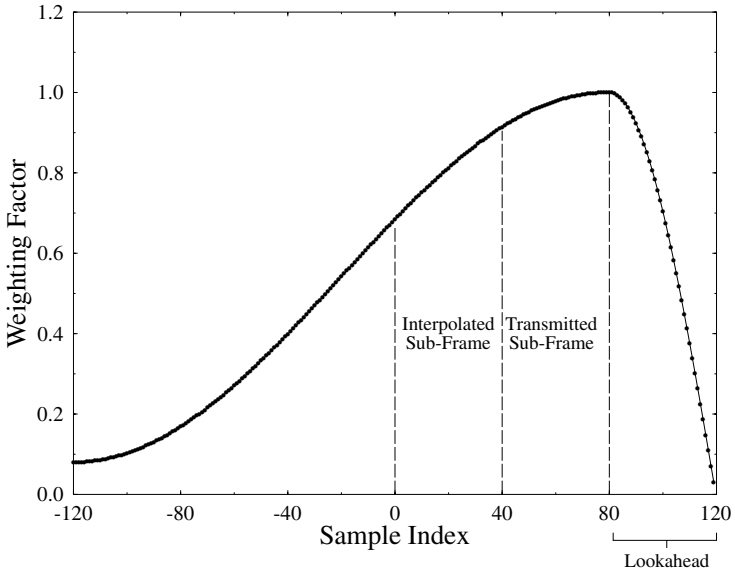

Figure 7.16: LPC analysis window used in G.729.

bandwidth expansion is applied to the filters by multiplying the autocorrelation coefficients $R(k)$ by

$$\exp\left[-\frac{1}{2}\left(\frac{2\pi f_o k}{f_s}\right)^2\right] \quad \text{for } k = 1, 2, \ldots, 10.$$

Here, $f_o = 60$ Hz and f_s is the sampling frequency of 8000 Hz. Finally, $R(0)$ is multiplied by a white-noise correction factor of 1.001.

These modified autocorrelation coefficients are used to calculate the filter coefficients a_i, $i = 1, 2, \ldots, 10$, using the Levinson–Durbin algorithm. Then the filter coefficients are converted into LSFs before quantisation and interpolation. The synthesis filter coefficients to be used are derived from the quantised set of LSFs. Interpolation is used on these LSFs so that in the first sub-frame the LSFs used are the average of the quantised LSFs from the present and the previous frames, whereas in the second sub-frame the quantised LSFs from the present frame are used.

The simplified block diagram of the 18 bit predictive two stage LSF vector quantiser used in G.729 is shown in Figure 7.17, which will be elaborated on below. Here we exploit the fact that due to the inherent correlation between consecutive sets of LSF vectors the previous quantised LSS vector provides a good estimate of the current vector to be quantised, resulting in a lower-variance quantity to be quantised. Hence the number of LSF quantisation bits required by the prediction error is reduced. The switched fourth-order MA predictor seen in the figure is constituted by a pair of predictors, which in not explicitly shown in the figure. Both of these predictors are tentatively invoked and the one minimising the LSF prediction error of Figure 7.17 is actually employed in the prediction, which is signalled to the decoder using the 1 bit flag at its output. This MA predictor is used to predict the set of LSFs for the current frame on the basis of the previous quantised LSFs, and then the LSF prediction error

between the resultant LSF vector prediction and the actual set of zero-mean LSFs is quantised using a two-stage vector quantiser. According to the set of ten LSFs, in the first stage a 10-dimensional, 7-bit, 128-entry codebook is used in order to crudely estimate the LSF vector and to derive the Stage 1 LSF prediction error of Figure 7.17. The Stage 1 LSF prediction error is then modelled by invoking the Stage 2 LSF vector quantiser, which attempts to match the five-dimensional split LSF vectors using the 5-bit or 32-entry codebooks. Together with the one-bit flag at the output of the MA predictor of Figure 7.17 that is used to specify which of the pair of LSF predictors implicit in this block should be employed, this gives a total of $7 + 5 + 5 + 1 = 18$ bits per frame for the quantisation of the LSFs.

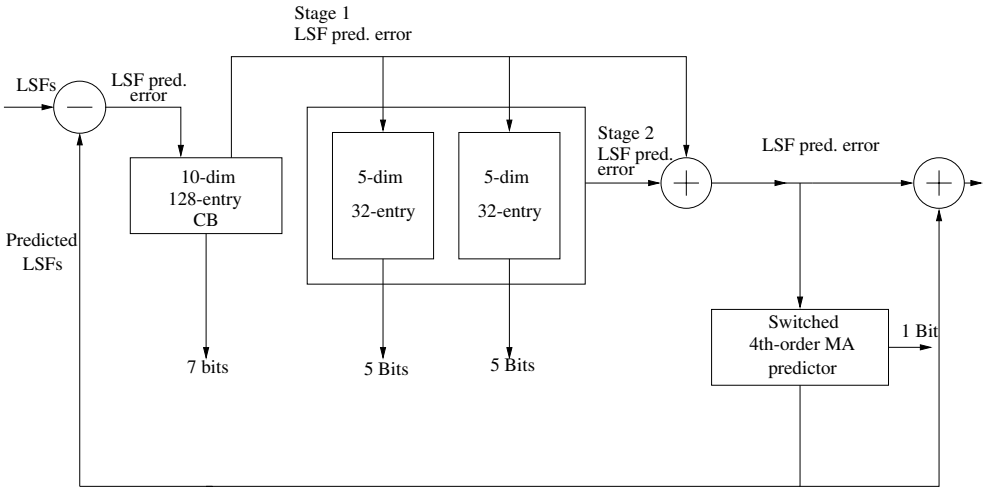

Figure 7.17: G.729 LSF vector quantiser.

To elaborate further on the inner working of the G.729 LSF vector quantiser, for each speech frame both possible LSF MA predictors give a set of predicted LSFs, yielding two sets of LSF prediction errors, which must be vector quantised. Then for each set of LSF prediction errors the following procedure is carried out. Initially the first stage, 7-bit, 10-dimensional codebook is searched to find the codebook entry which gives the closest match to the set of zero-mean LSF prediction errors. This closeness of match is measured using the simple squared-error measure. Then the difference between the codebook entry selected from the first codebook and the set of prediction errors to be quantised is itself quantised in the second stage of the vector quantiser. The second stage is a 10-bit quantiser but, in order to reduce the complexity of the quantiser, it is split into two. One 5-bit, five-dimensional, quantiser is used to code the first five LSFs, and the other 5-bit quantiser codes the final five LSFs. Entries from the two codebooks are chosen to minimise the weighted squared error E_{LSF}, where

$$E_{\mathrm{LSF}} = \sum_{i=1}^{i=10} W_i(\omega_i - \hat{\omega}_i)^2 \tag{7.19}$$

and ω_i are the set of input LSFs, $\hat{\omega}_i$ are the quantised LSFs and W_i are a set of weighting coefficients derived from the input LSFs. Thus for each of the two sets of predictors a 7-bit

index for the first stage quantiser is chosen to minimise the squared quantisation error, and then two 5-bit indices are chosen for the second-stage quantiser to minimise the weighted squared error E_{LSF}. The LSF predictor which gives the lowest weighted squared error E_{LSF} is chosen as the predictor to be used, and one bit is sent to the decoder to indicate which predictor to use. The stability of the synthesis and weighting filters are guaranteed by ensuring the quantised LSFs are ordered, and that adjacent LSFs are separated by at least a given minimum distance.

7.8.5 The Weighting Filter

The weighting filter used in the G.729 encoder is based upon the unquantised filter coefficients a_i derived from the LPC analysis described above. The transfer function of the weighting filter is given by

$$\begin{aligned} W(z) &= \frac{A(z/\gamma_1)}{A(z/\gamma_2)} \\ &= \frac{1+\sum_{i=1}^{10}\gamma_1^i a_i z^{-i}}{1+\sum_{i=1}^{10}\gamma_2^i a_i z^{-i}}, \end{aligned} \tag{7.20}$$

where γ_1 and γ_2 control the amount of weighting. This amount of weighting is made adaptive, to improve the performance of the codec for input signals with a flat frequency response, by adapting γ_1 and γ_2 based on the spectral shape of the input signal. This adaption is done for every 10 ms frame, but interpolation is used in the first sub-frame to smooth the adaption process. The adaption is based on LAR coefficients obtained as a by-product of the LPC analysis carried out on the input speech. The LARs of a second-order filter are used to characterise the input speech as either flat or tilted, and the values of γ_1 and γ_2 are adjusted depending on this classification. We note here that in the G.729 standard the Levinson–Durbin algorithm delivers a set of LPC coefficients which have the opposite sign in comparison to the G.723.1 standard, for example. This is why there is a positive sign in front of the summation in the weighting filter of Equation (7.51), while the G.723.1 weighting filter, for example, has a negative sign in the weighting filter.

7.8.6 The Adaptive Codebook

For each sub-frame an adaptive codebook index must be chosen which minimises the weighted error between the input speech and the reconstructed speech. In AbS codecs, such as G.729, the best adaptive codebook index is determined using a closed-loop search as described in Section 3.4.2. However, in order to reduce the complexity of this closed-loop search, in the G.729 encoder the search range is limited to around a candidate delay T_{op} which is obtained by an open-loop pitch analysis on the input weighted speech $s_w(n)$. This open-loop pitch analysis is carried out over the 10 ms frame and attempts to maximise the autocorrelation $R_w(k)$ of the weighted input speech. This correlation is given by

$$R_w(k) = \sum_{n=0}^{79} s_w(n)s_w(n-k) \tag{7.21}$$

and its maximum is found in the following three ranges: 20–39, 40–79, and 80–143. These three maxima in $R_w(k)$ are normalised and the open-loop pitch value $T_{\rm op}$ is selected from amongst the three values of k which give a local maxima by favouring the delays with values in the lower ranges. Dividing the delay range into sections, and favouring the choice of delays in the lower sections is invoked in order to avoid inadvertently opting for pitch multiples as the open-loop pitch $T_{\rm op}$.

Once the open-loop pitch has been determined the closed-loop search for the adaptive codebook index T_1 in the first sub-frame is limited to the six samples around $T_{\rm op}$. This index is coded with 8 bits and takes fractional values with resolution 1/3 in the range $19\frac{1}{3}$–$84\frac{2}{3}$ and integer values only in the range 85–143. In the second sub-frame the closed loop search for the adaptive codebook index T_2 is limited to delays around the delay T_1 chosen in the first sub-frame. A codebook index with resolution 1/3 is selected in the range between $({\rm int}(T_1) - 5\frac{2}{3})$ and $({\rm int}(T_1) + 4\frac{2}{3})$, where ${\rm int}(T_1)$ is the integer part of T_1. This index T_2 is coded with 5 bits.

The closed-loop pitch search for T_1 and T_2 is achieved by maximising the term

$$\chi_\alpha = \frac{\sum_{n=0}^{39} x(n) y_\alpha(n)}{\sum_{n=0}^{39} y_\alpha(n) y_\alpha(n)}, \tag{7.22}$$

where $x(n)$ is the target for the filtered adaptive codebook signal and $y_\alpha(n)$ is the past filtered excitation at delay α. The fractional pitch search is carried out, when necessary, using interpolated values of χ_α. This interpolation is done using an FIR filter based on a Hamming windowed $\sin(x)/x$ function.

Once the adaptive codebook index T_1 or T_2 for the sub-frame has been determined, the resulting output from the adaptive codebook must be calculated at both the encoder and decoder. This adaptive codebook signal is the delayed past excitation signal, but if a fractional delay has been selected then interpolation must be carried out on this past excitation signal. Again, a FIR-filter based on a Hamming windowed $\sin(x)/x$ function is used for this interpolation.

At the encoder once the adaptive codebook signal has been determined the fixed codebook is searched, again using a closed-loop search designed to minimise the weighted error between the reconstructed and the input speech signals. The structure of this fixed codebook, and the techniques used to search it, are described below.

7.8.7 The Fixed Algebraic Codebook

G.729 uses a 17-bit fixed codebook. Using traditional random codebooks the closed-loop search of such a large codebook would be extremely complex and render the use of such a codebook in a real-time speech codec unrealistic. However, in G.729 an algebraic codebook is used, with only four non-zero pulses per sub-frame, and this allows the codebook to be searched efficiently using a series of four nested loops. Also a focussed search is used to further simplify the determination of the codebook parameters. These measures mean that the huge 17-bit codebook can be searched with reasonable complexity, and thus used in the G.729 codec which is intended for real-time operation on a single DSP.

The structure of the algebraic codebook used in G.729 is shown in Table 7.11. Each codeword contains only four non-zero pulses, each of which has its amplitude fixed to either

Table 7.11: Pulse amplitudes and positions for the G.729 codec.

Pulse number i	Amplitude	Possible positions m_i
0	± 1	0, 5, 10, 15, 20, 25, 30, 35
1	± 1	1, 6, 11, 16, 21, 26, 31, 36
2	± 1	2, 7, 12, 17, 22, 27, 32, 37
3	± 1	3, 8, 13, 18, 23, 28, 33, 38
		4, 9, 14, 19, 24, 29, 34, 39

$+1$ or -1 and coded with one bit. The first three non-zero pulses have eight possible positions, and have their positions coded with three bits each. The final pulse has 16 possible positions, and its position is coded with four bits. Thus a total of 17 bits are used to represent the fixed codebook index. The fixed codebook signal is then given by

$$c_k(n) = s_0\delta(n - m_0) + s_1\delta(n - m_1) + s_2\delta(n - m_2) + s_3\delta(n - m_3), \tag{7.23}$$

where s_i is the sign and m_i the position of pulse i.

A special feature of the codebook used in G.729 is that for pitch delays less than 40 the codebook signal $c_k(n)$ is modified according to

$$c_k(n) = \begin{cases} c_k(n) & n = 0, \ldots, T-1 \\ c_k(n) + \beta c_k(n - T) & n = T, \ldots, 39, \end{cases} \tag{7.24}$$

where T is the integer part of the pitch delay used in the current sub-frame, and the value of β is based on the quantised pitch gain of the previous sub-frame. This modification is incorporated into the codebook search by modifying the impulse response $h(n)$ of the synthesis and weighting filters used in the codebook search. It is equivalent to including an adaptive pre-filter in the codebook, and enhances the harmonic components in the reconstructed speech and improves the performance of the codec.

The fixed codebook search is carried out as follows. The target signal $\tilde{x}(n)$ for the filtered fixed codebook signal is given by the target signal $x(n)$ from the pitch search with the filtered adaptive codebook contribution subtracted, i.e.

$$\tilde{x}(n) = x(n) - G_1 y_\alpha(n), \tag{7.25}$$

where G_1 is the unquantised pitch gain given by

$$G_1 = \frac{\sum_{n=0}^{39} x(n)y_\alpha(n)}{\sum_{n=0}^{39} y_\alpha^2(n)} \quad \text{bounded by } 0 \leq G_1 \leq 1.2 \tag{7.26}$$

and $y_\alpha(n)$ is the filtered adaptive codebook signal. As was explained in Chapter 6, the best codebook vector is then found by determining which vector k maximises the term $T_k = C_k^2/\xi_k$. Here C_k is the correlation between the filtered fixed codebook signal and the target signal $\tilde{x}(n)$, and ξ_k is the energy of the filtered fixed codebook signal. As there are only

four non-zero pulses per codeword with positions m_i and amplitudes s_i, these terms can be written as

$$\begin{aligned} C_k &= \sum_{n=0}^{39} \tilde{x}(n)[c_k(n) * h(n)] \\ &= \sum_{n=0}^{39} \psi(n) c_k(n) \\ &= \sum_{i=0}^{3} s_i \psi(m_i), \end{aligned} \tag{7.27}$$

where

$$\begin{aligned} \psi(i) &= \tilde{x}(i) * h(-i) \\ &= \sum_{n=i}^{39} \tilde{x}(n) h(n-i) \quad \text{for } i = 0, \ldots, 39, \end{aligned} \tag{7.28}$$

and

$$\begin{aligned} \xi_k &= \sum_{n=0}^{39} [c_k(n) * h(n)]^2 \\ &= \sum_{i=0}^{39} c_k^2(i)\phi(i,i) + 2\sum_{i=0}^{38}\sum_{j=i+1}^{39} c_k(i)c_k(j)\phi(i,j) \\ &= \sum_{i=0}^{3} \phi(m_i, m_i) + 2\sum_{i=0}^{2}\sum_{j=i+1}^{3} s_i s_j \phi(m_i, m_j), \end{aligned} \tag{7.29}$$

where

$$\phi(i,j) = \sum_{n=\max(i,j)}^{39} h(n-i)h(n-j) \quad \text{for } i, j = 0, \ldots, 39. \tag{7.30}$$

The functions $\psi(i)$ and $\phi(i,j)$ can be calculated once per sub-frame, but then ξ_k and C_k must be calculated for each codeword. To simplify the search procedure for a given set of pulse positions m_i the signs of the four pulses s_i are set equal to the signs of $\psi(m_i)$ at the pulse positions. This means that the correlation term C_k will be maximised for the given set of pulse positions, and is given by

$$C_k = |\psi(m_0)| + |\psi(m_1)| + |\psi(m_2)| + |\psi(m_3)|. \tag{7.31}$$

It also allows the calculation of the energy term ξ_k to be simplified by modifying $\phi(i,j)$. The sign information is included in $\phi(i,j)$ by modifying it to $\tilde{\phi}(i,j)$ as follows:

$$\tilde{\phi}(i,j) = |\psi(i)||\psi(j)|\phi(i,j). \tag{7.32}$$

Also, the diagonal elements in ϕ are scaled so as to remove the factor of two in Equation (7.29), i.e.

$$\tilde{\phi}(i,i) = \tfrac{1}{2}\phi(i,j), \tag{7.33}$$

so that the energy term ξ_k which must be calculated for every codeword k is simplified to

$$\xi_k/2 = \sum_{i=0}^{3} \tilde{\phi}(m_i, m_i) + \sum_{i=0}^{2} \sum_{j=i+1}^{3} \tilde{\phi}(m_i, m_j), \tag{7.34}$$

which is significantly less complex to calculate than the expression in Equation (7.29).

The codebook search is further simplified using a focussed search procedure. As usual in algebraic CELP codecs a series of four nested loops are used to test the value of T_k for each set of pulse positions. However, in G.729 the final loop, which is the largest because of the 16 possible positions of the fourth pulse, is entered only if the correlation C_k due to the first three pulses exceeds a certain threshold Thr_3. This threshold is precomputed before the codebook search commences for each sub-frame, and is set to

$$\text{Thr}_3 = \text{av}_3 + 0.4 * (\text{max}_3 - \text{av}_3) \tag{7.35}$$

where av_3 is the average correlation due to the first three pulses, and max_3 is the maximum value of the correlation due to the first three pulses. Also, the maximum number of times the final loop can be entered is set to 180 per frame, to give a definite upper bound to the complexity of the codebook search.

Using the methods described above, at most 180×16 codebook entries per frame are tested to see if they maximise T_k. This is only about 1% of the total number of tests of 2×2^{17} per frame that would be necessary if all possible pulse positions and signs were tested. However, the performance of the codec using such focussed search procedures is reported [162] to be close to that which would be achieved using the much more complex full search.

Once the adaptive and fixed codebook indices have been determined by the decoder the two codebook gains are vector quantised with 7 bits as described below.

7.8.8 Quantisation of the Gains

The two codebook gains in G.729 are quantised using a predictive, two stage, conjugate structured vector quantiser. Fourth-order moving average prediction, based on the energies (in the logarithmic domain) of the previous gain-scaled fixed codebook signals, is used to find a predicted fixed codebook gain $\tilde{G}_2$. The optimum gain G_2 is then given by

$$G_2 = \gamma \tilde{G}_2, \tag{7.36}$$

where γ is a correction factor which is quantised along with the adaptive codebook gain G_1.

The quantised values of G_1 and γ are chosen from a two stage codebook. The first stage consists of a 3-bit two-dimensional codebook, while the second stage is a 4-bit two-dimensional codebook. Thus the quantised values $\hat{G}_1$ and $\hat{G}_2$ of the adaptive and fixed codebook gains are given by

$$\hat{G}_1 = G_1 CB_1(k_1) + G_1 CB_2(k_2) \tag{7.37}$$

and

$$\hat{G}_2 = \tilde{G}_2(G_2CB_1(k_1) + G_2CB_2(k_2)), \tag{7.38}$$

where k_1 and k_2 are the chosen indices from the two codebooks, G_1CB_1 and G_2CB_1 are the entries from the first stage codebook, and G_1CB_2 and G_2CB_2 are the entries from the second codebook.

The indices k_1 and k_2 from the two codebooks must be chosen so as to minimise the weighted squared error between the input and the reconstructed speech. As explained previously in Section 6.5.2.1, this is equivalent to maximising $T_{\alpha k}$, where

$$T_{\alpha k} = 2(\hat{G}_1 C_\alpha + \hat{G}_2 C_k - \hat{G}_1 \hat{G}_2 Y_{\alpha k}) - \hat{G}_1^2 \xi_\alpha - \hat{G}_2^2 \xi_k. \tag{7.39}$$

The definitions and interpretations of the terms C_α, ξ_α, C_k, ξ_k and $Y_{\alpha k}$ were given in Section 6.5, hence suffice to say that here they are all fixed, once the adaptive and fixed codebook indices have been selected. Hence the gain vector quantisation must simply select codebook indices which give values of $\hat{G}_1$ and $\hat{G}_2$ which maximise $T_{\alpha k}$ above.

The conjugate structure of the codebooks simplifies this search procedure as follows. The two codebooks are arranged so that, in general, the first codebook contains entries in which the elements corresponding to $\hat{G}_2$ are larger than those corresponding to $\hat{G}_1$. Similarly, in the second codebook the elements corresponding to $\hat{G}_1$ are generally larger than those corresponding to $\hat{G}_2$. When the codebooks are searched a pre-selection process is applied to simplify the search. The optimum value of G_2, derived from Equation (7.39), is used to select the 4 from 8 codebook entries of the first codebook whose values of $\hat{G}_2$ are closest to the optimum. Similarly, the optimum value of G_1 is used to select 8 from the 16 values of the second codebook whose values of $\hat{G}_1$ are closest to the optimum. Then an exhaustive search of the $4 \times 8 = 32$ possible codebook index combinations is carried out, and the indices k_1 and k_2 which maximise $T_{\alpha k}$ are chosen. The quantised gains $\hat{G}_1$ and $\hat{G}_2$ are then given by Equations (7.37) and (7.38).

We have described above how the encoder finds codebook indices from an 18-bit LSF vector quantiser, a 17-bit algebraic codebook, the adaptive codebook and a 7-bit vector gain quantiser. These indices are transmitted to the decoder which uses them to determine the coefficients for the synthesis filter, the excitation signal for this filter, and hence the reconstructed speech signal $\hat{s}(n)$. The decoder also applies post-filtering to the speech to improve its perceptual quality, and uses error concealment techniques to improve the robustness of the codec to channel errors. The post-processing and error-concealment techniques used at the decoder are described below.

7.8.9 Decoder Post-processing

After the reconstructed speech signal $\hat{s}(n)$ is calculated at the decoder, post-processing is applied. The reconstructed speech is passed through an adaptive postfilter, which is described below, to improve its perceptual quality. It is then high-pass filtered using a second-order pole-zero filter with a cutoff frequency of 100 Hz, and finally the filtered signal is multiplied by a factor of two to restore the input signal level.

The adaptive post-filtering used in G.729 is similar to the post-filtering used in G.728. It improves the perceptual quality of the decoded speech [110] by emphasising the formant and pitch peaks in the speech, and attenuating the valleys between these peaks. This reduces the

audible noise in the reconstructed speech because, even with the noise shaping of the error weighting filter, it is in the valleys between the formant and pitch peaks that the noise energy is most likely to cross the masking threshold and become audible. Therefore attenuating the speech in these regions reduces the audible noise, and because our ears are not very sensitive to the speech intensity in these valleys only minimal distortion is introduced to the speech signal.

A block diagram of the postfilter used in G.729 is shown in Figure 7.18. It consists of both a long- and a short-term postfilter, together with a spectral tilt compensation filter and adaptive gain scaling. We describe here the blocks shown in Figure 7.18, but for more information on the ideas behind post-filtering see the excellent paper by Chen and Gersho [110] as well as Section 8.4.6.

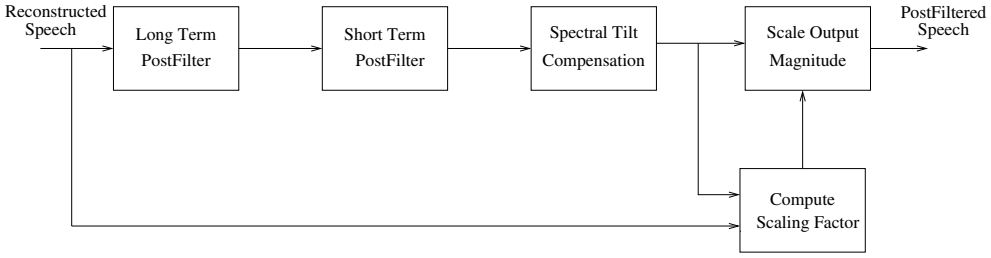

Figure 7.18: The G.729 adaptive postfilter.

The long-term postfilter has a transfer function

$$H_p(z) = \frac{1}{1+\gamma_p g_l}(1+\gamma_p g_l z^{-T}), \tag{7.40}$$

where γ_p is a constant which controls the amount of post-filtering and is set to 0.5, T is the pitch delay, and g_l is the gain coefficient. Both T and g_l are derived from the residual signal $\hat{r}(n)$ obtained by filtering the reconstructed speech $\hat{s}(n)$ through $\hat{A}(z/\gamma_n)$, which is the numerator of the short-term postfilter. The delay T is calculated with resolution 1/8, using a two-pass procedure, by searching for the maximum of the correlation of $\hat{r}(n)$ around the integer part of the delay T_1 in the first sub-frame. Once the delay T is found the gain g_l is calculated, again using the residual signal $\hat{r}(n)$. This gain term is bounded by $0 \leq g_l \leq 1.0$, and is set to zero (to disable the long-term post-filtering) if the long-term prediction gain is less than 3 dB.

After the long-term post-filtering a short-term postfilter $H_f(z)$ is used. This filter has a transfer function

$$\begin{aligned} H_f(z) &= \frac{1}{g_f}\frac{\hat{A}(z/\gamma_n)}{\hat{A}(z/\gamma_d)} \\ &= \frac{1}{g_f}\frac{1+\sum_{i=1}^{10}\gamma_n \hat{a}_i z^{-i}}{1+\sum_{i=1}^{10}\gamma_d \hat{a}_i z^{-i}}, \end{aligned} \tag{7.41}$$

where $\hat{A}(z)$ is the quantised inverse synthesis filter, $\gamma_n = 0.55$ and $\gamma_d = 0.7$ are constants which control the amount of short-term post-filtering, and g_f is a gain term given by

$$g_f = \sum_{n=0}^{19} |h_f(n)|, \tag{7.42}$$

where $h_f(n)$ is the impulse response of the filter $\hat{A}(z/\gamma_n)/\hat{A}(z/\gamma_d)$. Because the short-term postfilter numerator $\hat{A}(z/\gamma_n)$ is used to calculate the residual signal $\hat{r}(n)$ used in the determination of the long-term postfilter parameters, to reduce the complexity of the postfilter the all-zero section of the short term postfilter $\hat{A}(z/\gamma_n)$ is in fact used before the long-term postfilter. It is then the residual signal $\hat{r}(n)$ which is passed though the long-term postfilter and the all-pole section $1/(g_f\hat{A}(z/\gamma_d))$ only of the short-term postfilter. However, this moving of the all-zero section of the short-term postfilter does not, of course, affect the transfer function of the overall postfilter, but merely reduces the complexity of the post-filtering.

After the short-term post-filtering, tilt compensation is used to compensate for the spectral tilt introduced by $H_f(z)$. The tilt compensation filter $H_t(z)$ is a first-order all-zero filter with a transfer function

$$H_t(z) = \frac{1}{1 - |\gamma_t k_1|}(1 + \gamma_t k_1 z^{-1}), \tag{7.43}$$

where k_1 is the first reflection coefficient derived from the impulse response $h_f(n)$ of $\hat{A}(z/\gamma_n)/\hat{A}(z/\gamma_d)$, and γ_t is set to 0.9 if k_1 is negative and 0.2 if k_1 is positive.

The final block in the postfilter is adaptive gain control, used to compensate for energy differences between the reconstructed speech signal $\hat{s}(n)$ and the post-filtered signal $sf(n)$. For each sub-frame a gain factor G is calculated according to

$$G = \frac{\sum_{n=0}^{39} |\hat{s}(n)|}{\sum_{n=0}^{39} |sp(n)|}. \tag{7.44}$$

Then each sample $sf(n)$ is scaled by a factor $g(n)$ which is updated on a sample by sample basis according to

$$g(n) = 0.9875\, g(n-1) + 0.125\, G. \tag{7.45}$$

This results in a smoothly varying gain scaling factor $g(n)$. The signal $g(n) \times sf(n)$ is then high-pass filtered and multiplied by a factor of two as explained earlier to give the output speech from the decoder.

7.8.10 G.729 Error-concealment Techniques

An important part of any speech codec which is to be used over channels subject to errors is that it should be resilient to these errors. Two measures are used in G.729 to help improve its error resilience: a parity bit is used to protect the adaptive codebook index T_1 in the first subframe, and a frame-erasure concealment procedure is used to improve the decoder performance when frame erasures occur in the received bitstream. These two measures are described below.

As noted in Section 6.6, the bits representing the adaptive codebook index in CELP codecs are extremely sensitive to channel errors. This is particularly true of the delay T_1

from the first sub-frame in G.729, because the second sub-frame delay T_2 is calculated and coded relative to T_1. Therefore a parity bit is added at the encoder to the six most significant bits representing T_1. When a single error occurs in one of the six most significant bits of T_1, or in the parity bit itself, this error is detected by the decoder based on the parity information transmitted by the encoder. When such an error is detected the decoded value of T_1 is considered to be incorrect, and is replaced by the integer part of the delay T_2 from the previous sub-frame. This helps reduce the impact of errors among the bits representing T_1.

The G.729 decoder also employs a frame-erasure concealment technique. The method of detecting which frames have been erased is not specified, but depends on the application in which the codec is used. However, when the decoder is told that a frame of 80 bits has not been received correctly, because for example a packet of information has been dropped by the transmission system, it employs techniques to reconstruct the current frame based on previously received information. Both the synthesis filter and the excitation to this filter must be derived, and also the memory of the LSF and the fixed codebook gain predictors must be updated.

The coefficients of synthesis filter for an erased frame are simply set equal to those from the last good frame. Also, the LSF predictor, which uses the output of the two stage 17-bit vector quantiser as its input, has its memory updated. This is done using the set of quantised LSFs from the last good frame to derive an output from the vector quantiser which would have lead to this set of LSFs in the current frame. This derived codebook output is then used to update the memory of the LSF predictor.

In an erased frame the two codebook gains $\hat{G}_1$ and $\hat{G}_2$ are given by attenuated versions of the gains used in the previous sub-frame. $\hat{G}_2$ is attenuated by a factor of 0.98 each sub-frame, and $\hat{G}_1$ is bounded by $\hat{G}_1 < 0.9$ and is attenuated by a factor of 0.9 each sub-frame. The adaptive codebook delay is based on the integer part of the delay in the last good sub-frame. This delay is then used in any following erased frames, but to avoid excessive periodicity the delay is increased by one for each sub-frame (but bounded by 143).The fixed codebook index is randomly generated. The excitation signal to use in erased frames is then determined based on whether the frame is considered to be periodic or non-periodic. This decision is made based on the long-term prediction gains derived when calculating the long-term postfilter coefficients g_l in the previous frame. If this long-term prediction gain in either of the previous two sub-frames is greater than 3 dB then the present frame is considered to be periodic. Otherwise the frame is classified as non-periodic. In periodic frames the excitation signal to be used is taken entirely from the adaptive codebook. In other words, the fixed codebook contribution is set to zero, whereas in non-periodic frames it is taken entirely from the fixed codebook. These methods allow the G.729 decoder to cope well with frame erasures in the received bitstream.

7.8.11 G.729 Bit-sensitivity

The bit-sensitivity of the G.729 scheme was characterised using the previously introduced 'consistent corruption technique' and was plotted in terms of SEGSNR degradation versus bit index in Figure 7.19. Observe in the figure that while the LSP predictor choice flag-bit LSPQ1 of Table 7.10 and the higher-order second-stage 5-bit, 32-entry VQ address bits LSPQ4 appear quite robust to transmission errors, the vulnerability of the first-stage 10-dimensional, 128-entry address bits LSPQ2 is quite pronounced. This is as expected, since

corruption of any of these bits will affect all 10 LSFs. The sensitivity of the low-frequency second-stage 5 bits LSPQ3 is lower than that of the 7 LSPQ2 bits, but higher than that of the high-frequency bits LSPQ4. Clearly, these findings are in harmony with our expectations.

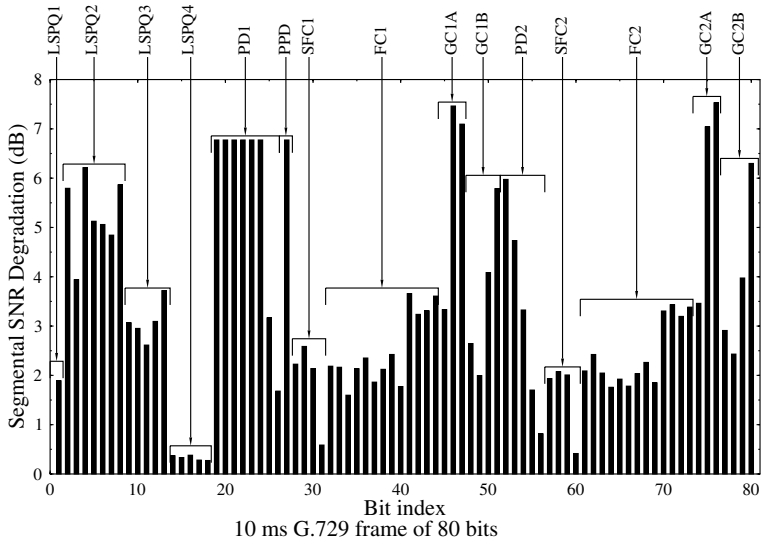

Figure 7.19: Bit-sensitivity of the forward-adaptive 8 kbps ACELP G.729 speech frame.

The pitch delay (PD) parameters PD1 and PD2 are both quite sensitive, in particular the 8 bits of PD1, since due to the differential encoding of PD2 any errors in PD1 automatically corrupt PD2 as well. Similar comments apply to the jointly vector-quantised fixed and adaptive codebook gains, where the more important 3-bit first-stage indices GC1A and GC2A of both subsegments exhibit a very pronounced error sensitivity, while the second-stage VQ address bits GC1B and GC2B have a somewhat more mitigated sensitivity. There also appears to be a more robust category of bits, which is mainly constituted by the set of 13 fixed codebook index bits FC1 and FC2 and their corresponding sign bits, namely bits SFC1 and SFC2. This excitation robustness is an attractive property of ACELP codecs, where corrupting one of the pulses does not vitally affect the shape of the excitation vector and the synthesised speech quality.

7.8.12 Turbo-coded Orthogonal Frequency Division Multiplex Transmission of G.729 Encoded Speech [214]

7.8.12.1 Background

In this section we study the performance of a range of so-called parallel concatenated or turbo codecs (TC) in conjunction with various interleavers, which profoundly affect the TC performance over wideband orthogonal frequency division multiplexing (OFDM) systems, which were highlighted in [159]. Due to their diversity effect, wideband propagation channels provide similar gains for OFDM modems to those of equalised narrowband channels [73], resulting in substantial coding gains when combined with turbo coding.

In the proposed system the source and channel coded bits are transmitted using a wideband OFDM system in the framework of the Mode-I FRAMES proposals [215]. We illustrate the benefits of using OFDM with channel coding to alleviate some of the problems associated with wideband fading channels. Furthermore, we discuss how OFDM can be used in conjunction with the G.729 speech codec and half-rate channel coding in order to utilise one speech/data FRAMES sub-burst. Finally some of the issues and problems associated with using turbo coded OFDM in speech transmission systems are considered using the system characterised in Table 7.12. We will show in Figure 7.25 that a channel SNR of 6dB appears sufficiently high under the stipulated system conditions for near-unimpaired speech transmission.

Table 7.12: Turbo-coded OFDM system for speech transmission – system parameters. Copyright © Woodard, Keller and Hanzo, 1997 [214].

System parameters	
Carrier frequency	2 GHz
Sampling rate:	1.3 Mhz
Channel	
Impulse response	COST207 BU
Normalised Doppler frequency	$6.7664 \cdot 10^{-5}$
OFDM	
Number of sub-carriers	64
Cyclic extension	24 samples
Data sub-carriers	43
Pilot sub-carriers	21
Modulation scheme	coherent QPSK
Turbo channel coding	
Constraint length	3
Generator polynomials	7, 5
Interleaver length	169
Decoding algorithm	MAP
Number of iterations	8

7.8.12.2 System Overview

The system model employed in this study is depicted in Figure 7.20. At the transmitter, a G.729 speech coder generates data packets of 80 bits per 10 ms from a speech file, and this speech data is encoded by a half-rate channel encoder. The encoded bits are modulated by a quadrature phase shift keying (QPSK) modulator and the resulting signals are transmitted using an OFDM modem to the receiver. During transmission, the signal is corrupted in the frequency-selective time-varying channel, and white Gaussian noise is added at the receiver's input stage. At the receiver, the OFDM signal is demultiplexed and demodulated, and the resulting bits are passed to the channel decoder. The received bits are decoded by the G.729 decoder, and the SEGSNR degradation of the recovered speech is evaluated.

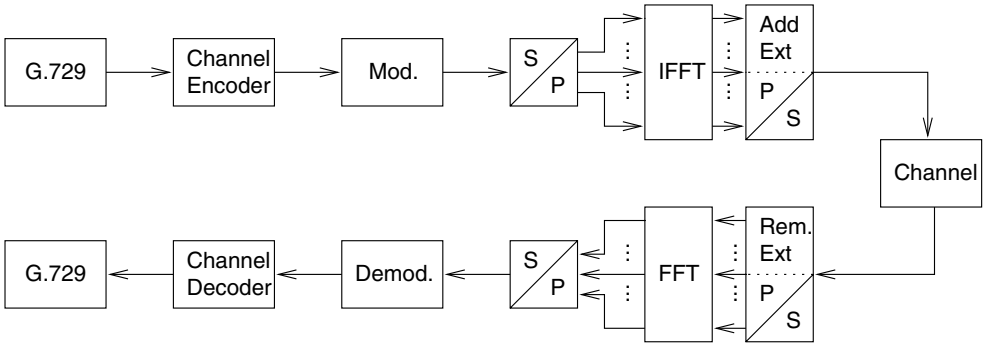

Figure 7.20: Schematic model of the G.729 OFDM system.

7.8.12.3 Turbo Channel Encoding

Turbo coding is a novel form of channel coding, reported to produce excellent results [216, 217]. The information sequence is encoded twice, with an interleaver between the two encoders serving to make the two encoded data sequences approximately statistically independent of each other. In our simulations we have used half-rate recursive systematic convolutional (RSC) encoders, but turbo coding is also possible with other constituent codes [218]. Each constituent RSC encoder produces a systematic output, which is equivalent to the original information sequence, as well as a stream of parity information. The two parity sequences are then punctured before being transmitted along with the original information sequence to the decoder. This puncturing of the parity information allows a wide range of coding rates to be realised. We have chosen to use the commonly adopted scheme of sending alternative parity bits from each encoder. Along with the original data sequence this results in an overall coding rate of 1/2.

The original, near-Shannonian, performance results for turbo codes were achieved using a very long block length L of 65,536 bits. It is well known that the performance of the codes decreases as the frame length L decreases, but that good performance is still achievable with relatively short frame lengths. It is also well known that the design of the interleaver used within the turbo coder has a vital influence on its performance. For long frame lengths random interleavers are used, but for shorter frame lengths of 100 or 200 bits, such as in a speech transmission system, Jung and Naßhan [219] reported that block interleavers should be used. However, Jung and Naßhan used a 12×16 block interleaver in their work, while we have found that block interleavers with an odd number of rows and columns significantly out-perform those with an even number of rows or columns. This is because, as noted by Barbulescu and Pietrobon [220], with an odd number of rows and columns the odd and even data bits are kept separate. When alternate puncturing from each constituent encoder is used, as it most often is, this ensures that for each information bit one and only one parity bit is transmitted. This 'odd–even' separation improves the performance of the turbo code [220], especially for short frame-length systems in our experience.

As mentioned above, the G.729 speech codec provides 80 coded speech bits per 10 ms frame. All our simulations have used two constraint-length three RSC constituent encoders, with generator polynomials expressed in octal form as 7 and 5. The maximum *a posteriori*

(MAP) [221] algorithm has been used with 8 decoding iterations. For each 10 ms G.729 frame to be turbo encoded separately we need to convey 80 information bits, plus two bits for trellis termination, where the number of trellis terminating bits required to flush the encoder's shift-register corresponds to the number of shift-register stages in the encoder. This gives a required interleaver length of 82, which is very close to the interleaver length of 81 given by a 9×9 square interleaver.

For BER comparisons we have simulated systems using both a square $L = 81$ interleaver, which can transport 79 data bits per turbo coded frame, and a system with an $L = 82$ interleaver. Because of the known benefit of using block interleavers for short frame transmission systems [219] we generated this length-82 interleaver by merely copying the elements of a square 81 interleaver, and leaving the final additional element in the $L = 82$ interleaver un-interleaved. We have also simulated a system with $L = 169$, using a 13×13 square interleaver. As described later this turbo encoder is used to code the 160 bits from two 10 ms G.729 frames. Finally, in order to characterise the near-optimum performance that can be achieved with turbo coding, we have simulated a system using a random interleaver with $L = 10{,}000$. Naturally, such an encoder could not be used for speech systems because of the delay it would introduce, but it may be useful for video or data transmission. Let us now consider the frame structure of the proposed system.

7.8.12.4 OFDM in the FRAMES Speech/Data Sub-burst

The emerging UMTS standard will have to accommodate a wide range of user profiles and data rates. The Advanced Communications Technologies and Services (ACTS) programme's FRAMES project [215] aims to propose such a system, incorporating a wide variety of possible system parameters. For these experiments, the FRAMES Mode 1 speech/data sub-burst was chosen, offering sufficient data bandwidth for half-rate coded speech transmission. Figure 7.21 shows the timing of the frame and the chosen time slot, where the frame and the speech/data sub-burst durations are 4.615 μs and 72.1 μs, respectively, and the channel symbol rate is 1.3 MHz. Originally, the FRAMES proposal specified offset-QPSK as the modulation scheme in these slots, leading to a channel bitrate of 2.6 Mbits/s.

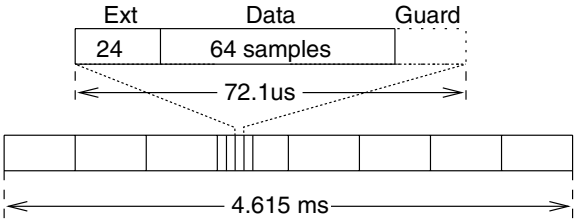

Figure 7.21: ACTS FRAMES Mode 1 frame and speech/data sub-burst. The sub-burst has been modified to hold a 64-sub-carrier OFDM signal and a 24 samples cyclic extension. The symbol rate and the guard time duration have not been altered.

The FRAMES Speech/Data sub-burst offers a convenient environment for 64 sub-carrier OFDM transmission, as is demonstrated in Figure 7.21. The 64 data samples of the OFDM symbol are preceded by a 24-sample cyclic extension, which allows operation in wideband

channels with an impulse response length of up to 24 samples or $18.5\ \mu$s without inter-burst interference. In the next section we consider our wideband channel model.

7.8.12.5 Channel Model

All experiments were conducted utilising the COST207 bad urban (BU) compliant impulse response [222]. The continuous COST207 BU impulse response was discretised to a seven–path model exhibiting a delay spread of $2.45\ \mu$s and a maximum delay of $7.7\ \mu$s, as seen in Figure 7.22. Each of the paths constituting the impulse response was faded independently, employing a Rayleigh fading channel. The carrier frequency and the vehicular velocity were set to 2 GHz and 50 km h^{-1}, respectively, which leads to a Doppler frequency of 92.6 Hz for the Rayleigh channel. The normalised Doppler frequency is therefore $6.7664 \cdot 10^{-5}$.

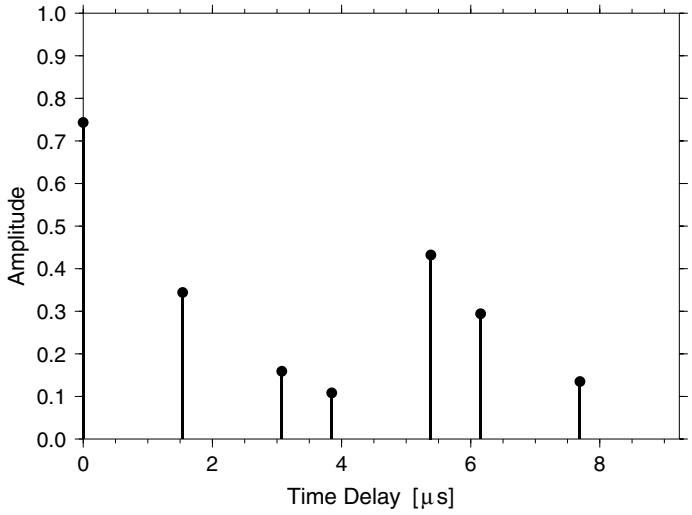

Figure 7.22: COST207 BU compliant seven-path impulse response.

The magnitude of the resulting time- and frequency-variant channel transfer function for a duration of 200 frames or 0.923 seconds is shown in Figure 7.23. Although the transfer function exhibits considerable variations in the frequency domain, the average received sub-carrier energy per OFDM symbol, indicated by the bold line, shows little fluctuation. This relative stability of the OFDM symbol energy, over a period of time substantially longer than the inverse of the Doppler frequency, is an effect of the inherent multipath diversity. This leads to a more even distribution of errors, which enables the channel codec to work more efficiently.

7.8.12.6 Turbo-coded G.729 OFDM Parameters

Since the end-to-end delay of speech transmission should be less than 100 ms, the speech frame length should ideally not exceed 20–30 ms. The performance of a turbo decoder, on the other hand, improves with an increasing number of coded bits per block. As a compromise, a

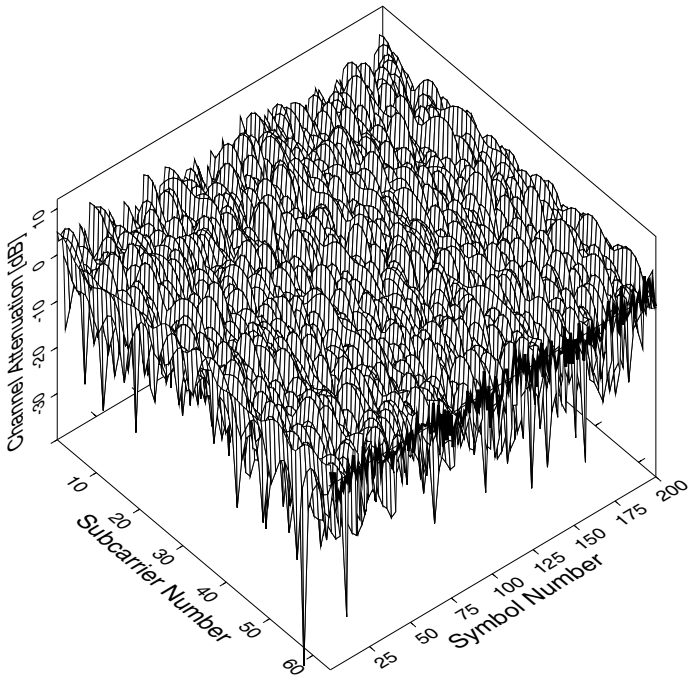

Figure 7.23: Amplitude plot of the frequency and time varying channel impulse response for 200 OFDM symbols. Copyright © Woodard, Keller and Hanzo, 1997 [214].

20 ms speech block size was chosen. The G.729 speech codec produces 80 data bits per 10 ms input speech, resulting in a total of 160 data bits per speech block. We will demonstrate that the performance of turbo codes is very dependent on the internal interleaver's algorithm and latency. For short block lengths, as stated earlier, square interleavers with an odd number of rows and columns exhibit the best performance. The smallest square interleaver holding 160 input bits is $13 \times 13 = 169$ bits long, allowing for the transmission of 160 data, two termination and seven unused padding bits.

The 169 uncoded data bits produce 338 coded output bits, which are transmitted using OFDM in one time slot over four consecutive frames. Employing QPSK as the modulation scheme for the OFDM sub-carriers, only 43 of the 64 sub-carriers in each OFDM symbol are employed for data transmission. The 21 remaining sub-carriers are used for PSAM, allowing coherent detection of the symbols at the receiver. This PSAM was not simulated, but instead perfect channel estimation was used at the receiver. This means that both the demodulator and the turbo decoder operated with perfect estimates of both the fading amplitude and the noise variance. Having described the system, let us now focus our attention on the results.

7.8.12.7 Turbo-coded G.729 OFDM Performance

Figure 7.24 shows the BER performance of our system for the various turbo-encoder/ interleaver combinations described earlier, as well as for a constraint-length three convolu-

tional code for comparison. It can be seen that the $L = 10\,000$ turbo code gives an extremely impressive performance even in the Rayleigh fading channel. The $L = 81$ and $L = 169$ turbo decoded systems both give performances significantly better than the convolutional coded system, showing that turbo codes can be useful in speech transmission schemes. However, disappointingly, the $L = 82$ system performs much worse than the $L = 81$ system, illustrating the importance of choosing a good interleaver for use with turbo encoders.

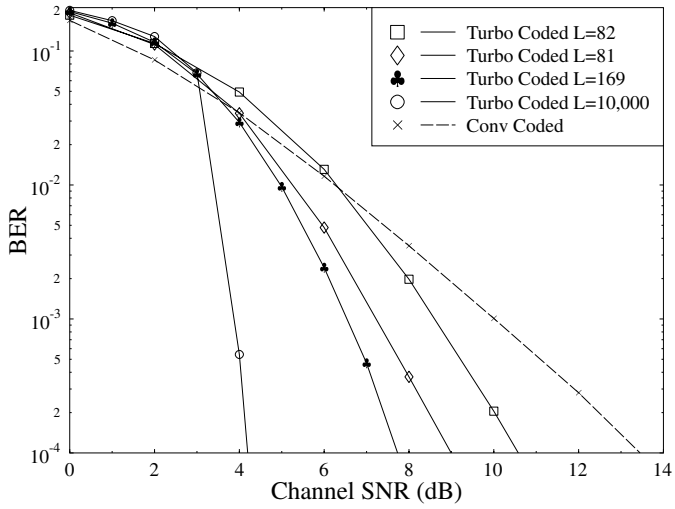

Figure 7.24: The effect of frame length on BER. Copyright © Woodard, Keller and Hanzo, 1997 [214].

The $L = 169$ turbo coded system described above was used to transmit G.729 coded speech. The SEGSNR degradation relative to the performance of G.729 over a perfect channel, against channel SNR for both this and the convolutional coded system is shown in Figure 7.25. It can be seen that the turbo-coded system gives a gain of about 3 dB in channel SNR over the convolutional coded system in SEGSNR degradation region of less than 1 dB, which corresponds to near-unimpaired speech quality. We note, however, that this is achieved at the cost of an increased decoding complexity due to the eight decoding iterations employed.

7.8.12.8 Turbo-coded G.729 OFDM Summary

In conclusion, the attractive G.729 speech codec can be advantageously combined with turbo coding and OFDM transmission using the system of Table 7.12. Due to the multipath diversity of wideband channels the OFDM modem performance is quite impressive. Furthermore, the error distribution is less bursty than over narrowband channels and hence the channel codec is less frequently overloaded by channel errors. In Figure 7.25 a channel SNR of 6 dB appears sufficiently high under the stipulated system conditions for near-unimpaired speech transmission.

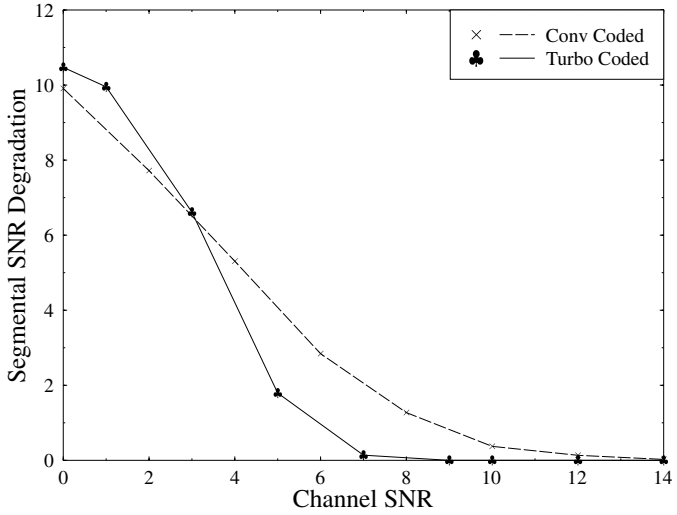

Figure 7.25: The SEGSNR degradation with convolutional and turbo encoding. Copyright © Woodard, Keller and Hanzo, 1997 [214].

7.8.13 G.729 Summary

In this section we have described the ITUs G.729 scheme. This codec operates at 8 kbps with a 10 ms frame length and gives output speech of quality equivalent to the 32 kbps ADPCM G.726 codec in error-free conditions. In the presence of channel errors the G.729 codec significantly outperforms G.726. As described above, various techniques are used to reduce the complexity of the codec, and implementations on single fixed point DSPs are available already. This codec looks set to become very widely used in many applications. In the previous section we also provided an application example for the G.729 codec.

Similar to the other coding schemes considered, the G.729 arrangement is compared in subjective speech quality terms to the family of existing standard codecs in Figure 18.4 of Chapter 18. In the next section we briefly highlight the techniques used in the reduced complexity G.729A codec.

7.9 The Reduced Complexity G.729 Annex A Codec

7.9.1 Introduction

In this section we describe the recently adopted ITU-T Recommendation G.729 Annex A (also known as G.729A) [223, 224]. This codec is a modification of the standard 8 kbps G.729 codec described previously, with significantly reduced complexity and only a slight degradation in performance.

G.729A grew from the interest in digital simultaneous voice and data (DSVD) applications in 1995. Although several standard low bitrate speech codecs existed or were being finalised at the time it was felt that, in order for speech coding and modem algorithms to be integrated on the same processor, a lower complexity speech codec was needed. A limit of

10 million instructions per second (MIPS) was set on the complexity of the codec, which was required to give speech quality as good as G.726 at 32 kbps in most conditions, and operate at a bitrate of 11.4 kbps or lower. In the summer of 1995 five candidate codecs were submitted for subjective testing, including one from the University of Sherbrooke in Canada which was based on G.729. This University of Sherbrooke codec had the advantage of being bitstream inter-operable with G.729. In other words, speech encoded using G.729 could be decoded with the new algorithm, and *vice versa*. This was considered important by the study group of the ITU-T, and so the Sherbrooke codec was chosen to be used in DSVD applications. Rather than forming a new recommendation it was decided to make the reduced complexity version of G.729 a new Annex to the original G.729 recommendation. Hence G.729 Annex A was formed.

G.729A operates at 8 kbps and gives speech quality equivalent to G.729 and G.726 at 32 kbps in most conditions, with only a small degradation in performance over G.729 in the case of three tandems and in the presence of background noise. It is approximately 50% less complex than G.729 and has been implemented on a fixed point DSP (Texas Instruments TMS320C50) using only 12 MIPS for full-duplex operation (compared to 22 MIPS for G.729) [223]. Most of the codec is identical to G.729, with changes made to the following aspects of the codec to reduce complexity:

(1) the perceptual weighting filter;

(2) the open-loop search for the pitch delay;

(3) the closed-loop pitch search;

(4) the algebraic codebook search;

(5) the decoder post-processing.

Details of these changes are given below.

7.9.2 The Perceptual Weighting Filter

In G.729, as described in Section 7.8.5, an error weighting filter of the form $W(z) = A(z/\gamma_1)/A(z/\gamma_2)$ is used. The unquantised LPC filter coefficients a_i are used to form $A(z)$, and both γ_1 and γ_2 are adapted. In G.729A a more traditional error weighting filter $W(z)$, where

$$W(z) = \frac{\hat{A}(z)}{\hat{A}(z/\gamma)}, \tag{7.46}$$

is used. The quantised LPC filter coefficients $\hat{a}_i$, identical to those used in the synthesis filters in the encoder and decoder, are used to form $\hat{A}(z)$ so that the concatenation of the synthesis filter $1/\hat{A}(z)$ and the weighting filter $W(z)$ becomes $W(z)/\hat{A}(z) = 1/\hat{A}(z/\gamma)$. This simplifies the filtering operations involved in the speech encoding. Also, the weighting factor γ used in G.729A is constant (0.75), and so the adaption procedures for γ_1 and γ_2 used in G.729 are not needed.

7.9.3 The Open-loop Pitch Search

In both G.729 and G.729A the adaptive codebook search is simplified by first finding an open-loop pitch delay value $T_{\rm op}$ for each 10 ms frame, and then doing a closed-loop search around $T_{\rm op}$ in each 5 ms sub-frame to find the optimum adaptive codebook delay. The open-loop pitch search attempts to maximise the autocorrelation $R_w(k)$ of the weighted input speech $s_w(n)$ in three ranges of k: 20–39, 40–79 and 80–143. In G.729A the calculation of the autocorrelation function $R_w(k)$ is simplified by using only even samples of $s_w(n)$, so that $R_w(k)$ is given by

$$R_w(k) = \sum_{n=0}^{39} s_w(2n) * s_w(2n-k), \tag{7.47}$$

rather than $\sum_{n=0}^{79} s_w(n) * s_w(n-k)$ as in G.729 (see Equation (7.21)). The search for the best open-loop pitch is also further simplified by initially only testing even values of k in the third range ($80 \leq k \leq 143$), and then testing the two odd values of k around the chosen even value. This almost halves the number of calculations of $R_w(k)$ which must be carried out in the third range.

7.9.4 The Closed-loop Pitch Search

In G.729A the closed-loop search for the best adaptive codebook indices T_1 and T_2 for the two sub-frames is also simplified. In the G.729 codec in the first sub-frame χ_α, as given in Equation (7.22), is calculated for values around $T_{\rm op}$ to find the value of α which maximises χ_α. This value of α is chosen as the adaptive codebook index T_1 for the first sub-frame. Similarly, in the second sub-frame values of χ_α around $\mathrm{int}(T_1)$ are calculated to find the index T_2. In G.729A these search operations are simplified by considering only the numerator of Equation (7.22) giving χ_α; in other words instead of χ_α the term $\tilde{\chi}_\alpha$ is maximised, where

$$\begin{aligned} \tilde{\chi}_\alpha &= \sum_{n=0}^{39} x(n) y_\alpha(n) \\ &= \sum_{n=0}^{39} x_b(n) u(n-\alpha). \end{aligned} \tag{7.48}$$

Here $x(n)$ is the target for the filtered adaptive codebook signal, $u(n-\alpha)$ is the past excitation signal, $y_\alpha(n)$ is the filtered version of $u(n-\alpha)$ and $x_b(n)$ is the backward filtered target signal.

This change to the closed-loop adaptive codebook search results in some degradation compared to G.729 – the chosen adaptive codebook delay sometimes differs by $1/3$ from that chosen in G.729. However, calculating $\tilde{\chi}_\alpha$ rather than χ_α approximately halves the complexity of the closed-loop pitch search [224].

7.9.5 The Algebraic Codebook Search

Both G.729 and G.729A employ a huge 17-bit algebraic codebook. Exhaustively searching such a large codebook would be unrealistic for a real-time speech codec. The codebook search

is simplified using an algebraic structure – each codebook entry consists of only four non-zero pulses. Each pulse can be either $+1$ or -1, and has its sign encoded with one bit per pulse. The possible positions of the pulses are shown in Table 7.11, and are encoded with a total of 13 bits for the four pulses. Both codecs pre-determine the sign of the four pulses depending on the sign of the backward filtered target signal $\psi(m_i)$ at the pulse positions m_i. This leaves effectively a 13-bit codebook to be searched – still too large to be realistic for a real-time codec.

In G.729 the codebook search is further simplified using a series of four nested loops and a focussed search procedure as described in Section 7.8.7. This results in a maximum of 2880 codebook entries being tested per frame – only about 1% of the total number of tests that would be necessary to exhaustively search the entire 17-bit codebook (if the signs were not pre-determined). In G.729A the algebraic codebook search is further simplified using a depth-first tree search. In this approach only 320 codebook entries are tested per sub-frame (i.e. 640 per frame), reducing the number of tested codebook entries by a factor of 4.5 relative to G.729.

The depth-first tree search used in G.729A is responsible for about 50% of the reduction in complexity of G.729A relative to G.729. Using this technique the algebraic codebook search consumes about 3 MIPS, as opposed to about 8.5 MIPs for the search technique used in G.729. The simpler codebook search technique gives only a slight degradation in the codec's performance – about a 0.2 dB drop in the SNR [223, 224].

7.9.6 The Decoder Post-processing

In both G.729 and G.729A at the decoder the reconstructed speech signal is passed through an adaptive postfilter to improve its perceptual quality. This postfilter consists of both short- and long-term filters, spectral tilt compensation and gain scaling. The post-filtering operations used in G.729 are described in Section 7.8.9, and use about 2.5 MIPS. In G.729A several changes are implemented to simplify the post-filtering. The main change is in the adaptive long-term post-filtering. In G.729 the delay T of the long-term postfilter in each sub-frame is calculated with $1/8$ sample resolution using a two-stage search around the integer part of the transmitted adaptive codebook delay T_1 for the first sub-frame. In G.729A the delay T is always an integer, and is computed by searching the range $T_{cl} - 3$ to $T_{cl} + 3$, where T_{cl} is the integer part of the transmitted adaptive codebook delay for the current sub-frame. This, along with several other minor modifications, reduces the complexity of the decoder post-filtering to about 1 MIPS.

7.9.7 Conclusions

In this section we have described the G.729A 8 kbps codec. This codec is very similar to, and is bitstream compatible with, the G.729 codec described in Section 7.8. However, due to several complexity-reducing modifications it has a full duplex complexity of only about 12 MIPS, compared to about 22 MIPS for G.729. This reduction in complexity is achieved at the expense of a small degradation in the performance of the codec in the case of three tandems and in the presence of background noise. The codec was originally conceived for use in DSVD applications, but is suitable for use in many other applications as well. Indeed,

because of its bitstream compatibility it can be used as a direct replacement for G.729, when complexity reduction is necessary.

In the next two sections we will consider a pair of ACELP-based codecs, which essentially also originated from the University of Sherbrooke speech compression team. Hence many of the attractive features of the G.729 scheme can be recognised in different incarnations. We note, furthermore, that these schemes were contrived in order to improve the perceived speech quality of the existing GSM and IS-54 systems, in an attempt to render the wireless service quality similar to that of wireline based systems. Let us commence this excursion by considering the enhanced full-rate GSM codec.

7.10 The 12.2 kbps Enhanced Full-rate GSM Speech Codec [225, 226]

7.10.1 Enhanced Full-rate GSM Codec Outline

This section gives a brief account of the operation of the 12.2 kbps enhanced full-rate GSM speech codec, which will replace the 13 kbps RPE speech codec. This scheme was standardised by the European Telecommunications Standardisation Institute (ETSI) in 1996. Here we follow the approach of Salami *et al.* [225, 226] and the interested reader is referred to [226] for a more in-depth discussion. The codec employs the successful ACELP excitation model invented in 1987 by Adoul *et al.* at Sherbrooke University [168], which was detailed in Section 6.3. The enhanced full-rate GSM scheme uses a bitrate of 10.6 kbps for channel coding, resulting in a channel coded rate of 22.8 kbps, similar to the 13 kbps RPE GSM codec which was the topic of Chapter 5 and was characterised by the schematics of Figures 5.1 and 5.2.

The enhanced full-rate GSM (EFR-GSM) encoder schematic is portrayed in Figure 7.26, while that of the decoder is displayed in Figure 7.29, both of which will be detailed below. Similar to the RPE GSM encoder of Figure 5.1, the input speech is initially pre-emphasised using a high-pass filter, in order to augment the low-energy, high-frequency components, before the speech signal is processed. Observe in Figure 7.26 that as usual, the spectral quantisation is carried out on a frame-by-frame basis, while the excitation optimisation is on a subsegment-by-subsegment basis, although we note at this early stage that the spectral quantisation is quite original.

The codec's bit-allocation scheme is summarised in Table 7.13, while the rationale behind using the specified number of bits will be detailed during our forthcoming discourse. The 38 LSF quantisation bits per 20 ms constitute a 1.9 kbps bitrate contribution, which is typical for medium-rate codecs, although the quantisation scheme to be highlighted below is unconventional. The fixed ACELP codebook gains are quantised using 5 bits/subframe, while the fixed ACELP codes are represented by 35 bits per subframe which, again, will be justified below with reference to Table 7.13. The adaptive codebook index, corresponding to the pitch-lag, is represented by 9 bits, catering for 512 possible positions in the first and third subframes using a very fine over-sampling by a factor of six in the low-delay region. In the second and fourth subframes the pitch-lag is differentially encoded with respect to the odd subframes, again, employing an oversampling by six in the low-delay domain.

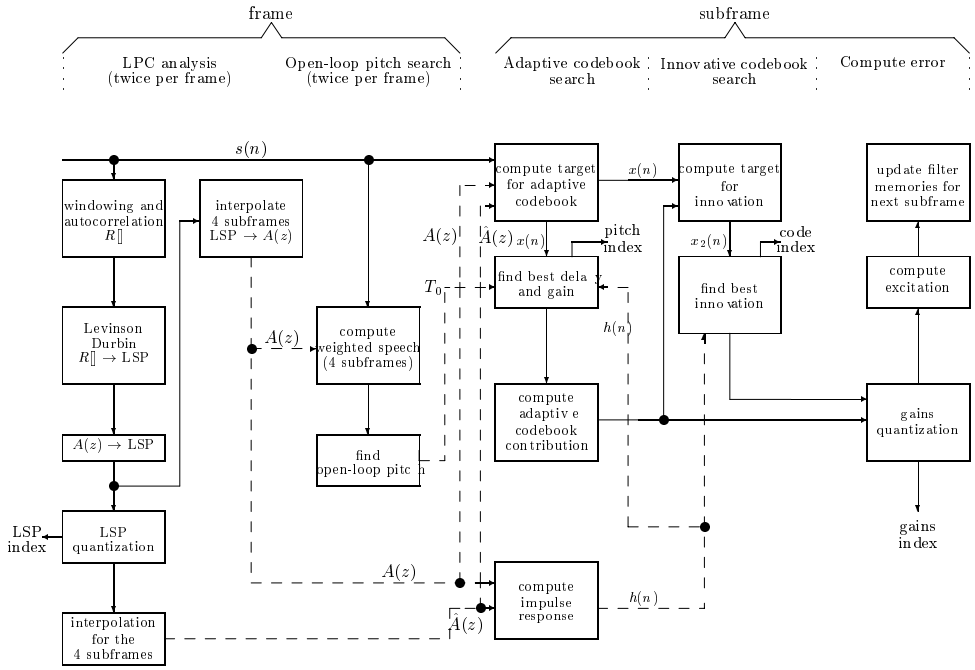

Figure 7.26: Enhanced full-rate 12.2 kbps GSM encoder schematic.

Table 7.13: 12.2 kbps enhanced full-rate GSM codec bit allocation.

Parameter	First and third subframe	Second and fourth subframe	No. of bits	Total (kbps)
Two LSF sets			38	1.9
Fixed codebook gain	5	5	4·5=20	1
ACELP code	35	35	$4 \cdot 35 = 140$	7
Adaptive codebook index	9	6	$2 \cdot 9 + 2 \cdot 6 = 30$	1.5
Adaptive codebook gain	4	4	16	0.8
Total			244/20 ms	12.2

We note that historically the DoD codec was the first scheme to invoke the above mentioned differential coding of the pitch-lag and oversampling in the low-lag pitch domain. These measures became fairly widely employed in state-of-the-art codecs, despite the inherent error sensitivity of differential coding. The high resolution pitch-lag coding of low values is important, since it is beneficial to ensure a more-or-less constant relative pitch resolution, rather than a constant absolute resolution, as in case of uniformly applied 125 μs sample-spaced pitch encoding. Lastly, the pitch-gains are encoded using four bits per

subframe. Below we will consider most of the above-mentioned operations of Figure 7.26 in more depth.

7.10.2 Enhanced Full-rate GSM Encoder

7.10.2.1 Spectral Quantisation and Windowing in the Enhanced Full-rate GSM Codec

Let us initially consider the spectral quantisation employed in the EFR-GSM codec, where tenth-order LPC analysis is invoked twice for each 20 ms speech frame, upon using two different 30 ms duration asymmetric windows, which will be justified below. In contrast to the 8 kbps ITU G.729 ACELP codec's window function shown in Figure 7.16, where a 5 ms or 40-sample look-ahead was used, the EFR-GSM codec employs no 'future speech samples', or – synonymously – no look-ahead in the filter coefficient computation and both asymmetric window functions act on the same set of 240 speech samples, corresponding to the 30 ms analysis interval. Whereas in the 10 ms framelength G.729 codec an additional 5 ms look-ahead delay was deemed acceptable in exchange for a smoother speech spectral envelope evolution, in the 20 ms framelength EFR-GSM scheme this was deemed unacceptable. This implies that there is a 10 ms or 80-sample 'look-back' interval in the window functions.

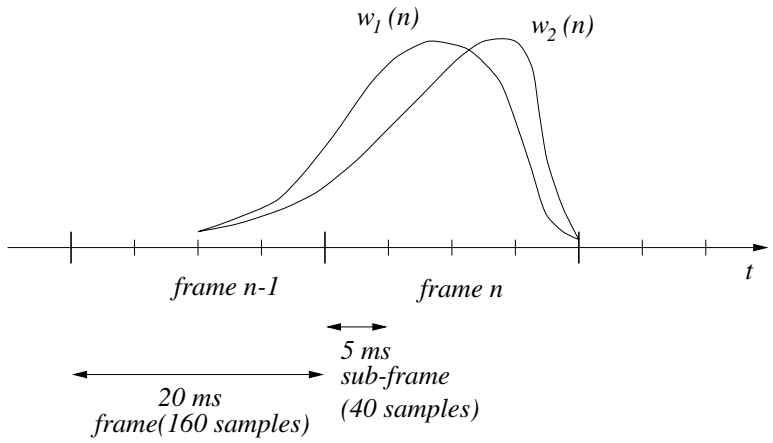

Figure 7.27: Stylised enhanced full-rate GSM window functions.

Before specifying the shape of the window functions, let us state the rationale behind using two LSF sets, which are used for the second and fourth subframes, respectively. Accordingly, the peak of the first window $w_1(n)$ of Figure 7.27 is concentrated near the centre of the second subframe, while that of the second window $w_2(n)$ is near the centre of the fourth subframe. Hence the latter has to exhibit a rapidly decaying slope, given that no look-ahead is employed. For the first and third subframes the LSFs are interpolated on the basis of the surrounding subframes. Specifically, the first window $w_1(n)$ is constituted by two

Hamming-window segments of different sizes, which is given as

$$w_1(n) = \begin{cases} 0.54 - 0.46 \cdot \cos \dfrac{\pi n}{L_1 - 1} & n = 0, \ldots, L_1 - 1 \\ 0.54 - 0.46 \cdot \cos \dfrac{\pi (n - L_1)}{L_2 - 1} & n = L_1, \ldots, L_1 + L_2 - 1, \end{cases} \tag{7.49}$$

where the parameters $L_1 = 160$ and $L_2 = 80$ were standardised. Although this window is asymmetric, it is gently decaying towards both ends of the current 20 ms frame, as seen in Figure 7.27. By contrast, since the centre of gravity of the second window is close to the beginning of the frame, it has to be tapered more abruptly, which is facilitated by using a short raised-cosine segment

$$w_2(n) = \begin{cases} 0.54 - 0.46 \cdot \cos \dfrac{\pi n}{L_1 - 1} & n = 0, \ldots, L_1 - 1 \\ \cos \dfrac{2\pi (n - L_1)}{4L_2 - 1} & n = L_1, \ldots, L_1 + L_2 - 1, \end{cases} \tag{7.50}$$

where the parameters $L_1 = 232$ and $L_2 = 8$ were employed.

As seen in Figure 7.26, the autocorrelation coefficients are computed from the windowed speech and the Levinson–Durbin algorithm is employed in order to derive both the reflection and the linear predictive coefficients, which describe the speech spectral envelope with the help of the $A(z)$ polynomial. Further details of Figure 7.26 concerning, for example, the pitch lag search and excitation optimisation will be unravelled during our later discussions. The LPC coefficients are then converted to LSFs and quantised using the so-called split matrix quantiser (SMQ) of Figure 7.28, which is considered next.

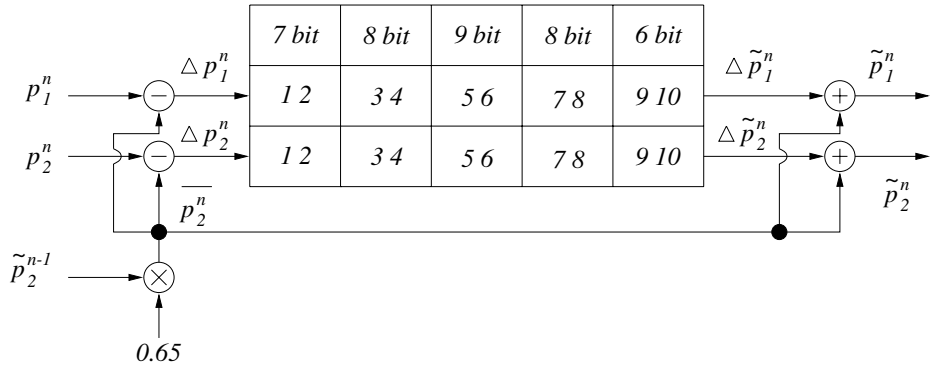

Figure 7.28: The 38-bit split matrix LSF quantisation of the sets generated using windows $w_1(n)$ and $w_2(n)$ of Figure 7.27 in the 12.2 kbps enhanced full-rate GSM codec.

First the long-term mean of both LSF vectors is removed, yielding the zero-mean LSF vectors p_1^n and p_2^n for frame n, corresponding to the two windows in Figure 7.27. Then both LSF sets of frame n are predicted from the previous quantised LSF set $\tilde{p}_2^{n-1}$, taking into account their long-term correlation of 0.65, as portrayed in Figure 7.28. Both LSF difference vectors are then input to the SMQ. Specifically, the LSFs of both vectors are paired, as suggested by Figure 7.28, creating a 2×2 submatrix from the first two LSFs of both LSF

vectors and quantising them by searching through a 7-bit, 128-entry codebook. Similarly, the third and fourth LSFs of both LSF vectors are paired and quantised using the 8-bit, 256-entry codebook of Figure 7.28, etc. Observe that the most important LSFs corresponding to the medium frequency range are quantised using a larger codebook than those towards the lower and higher frequencies. Finally, after finding the best-matching codebook entries for all 2×2 submatrices the previous subtracted predicted values are added to them, in order to produce both quantised LSF vectors, namely $\tilde{p}_1^n$ and $\tilde{p}_2^n$, respectively.

7.10.2.2 Adaptive Codebook Search

A combined open- and closed-loop pitch analysis is used, which is similar to that employed in the G.729 codec discussed in Section 7.8. Salami *et al.* [225] summarised the procedure as follows.

- As seen in Figure 7.26, based on the weighted speech an open-loop pitch search is carried out twice per 20 ms frame or once every two subframes, favouring low pitch values in order to avoid pitch doubling. In this search integer sample-based search is used and the open-loop lag T_o is identified.
- Then a closed-loop search for integer pitch values is conducted on a subframe basis. This is restricted to the range $[T_o \pm 3]$ in the first and third subframes, in order to maintain a low search complexity. As to the second and fourth subframes, the closed-loop search is concentrated around the pitch values of the previous subframe, in the range of $[-5 - +4]$.
- Finally, fractional pitch delays are also tested around the best closed-loop lag value in the second and fourth subframes, although only for the pitch delays below 95 in the first and third subframes, corresponding to pitch frequencies in excess of about 84 Hz.
- Having determined the optimum pitch lag, the adaptive codebook entry is uniquely identified, while its gain is restricted to the range of [0 – 1.2] and quantised using four bits, as seen in Table 7.13.

In the next subsection we consider the optimisation of the fixed codebook.

7.10.2.3 Fixed Codebook Search

Again, the principles of ACELP coding [168] were detailed in Section 6.3, hence here only a rudimentary overview is given. As shown in Table 7.13, 35 bits per subsegment are allocated to the ACELP code. The 5 ms, 40-sample excitation vector hosts 10 non-zero excitation pulses, each of which can take the values ± 1. Salami *et al.* [225] subdivided the 40-sample subframe into five so-called tracks, each comprising two excitation pulses. The two pulses in each track are allowed to be co-located, potentially resulting in pulse amplitudes of ± 2. The standardised pulse positions are summarised in Table 7.14. Since there are eight legitimate positions for each excitation pulse, three bits are necessary for signalling each pulse position. Given that there are ten excitation pulses, a total of 30 bits are required for their transmission. Furthermore, the sign of the first pulse of each of the five tracks is encoded using one bit, yielding a total of 35 bits per subsegment. The sign of the second pulse is inherently

determined by the order of the pulse positions, an issue elaborated on in [225, 226]. The 3-bit pulse positions were also Gray-coded, implying that adjacent pulse positions are different only in one bit position. Hence a bit-error results in the closest possible excitation pulse position to the one that was transmitted. This ACELP codebook is then invoked in order to generate the 20 ms synthetic speech frame, which is compared to the original speech segment in order to identify the best excitation vector.

Table 7.14: 12.2 kbps enhanced full-rate GSM codec's ACELP pulse allocation. Copyright © IEEE, Salami *et al.*, 1997 [225].

Track	Pulses	Positions
1	p_0, p_1	0, 5, 10, 15, 20, 25, 30, 35
2	p_2, p_3	1, 6, 11, 16, 21, 26, 31, 36
3	p_4, p_5	2, 7, 12, 17, 22, 27, 32, 37
4	p_6, p_7	3, 8, 13, 18, 23, 28, 33, 38
5	p_8, p_9	4, 9, 14, 19, 24, 29, 34, 39

At the decoder portrayed in Figure 7.29 the received codec parameters are recovered and the synthetic speech is reconstructed. Specifically, the decoded LSF parameters are interpolated for the individual subframes. Both the fixed and adaptive codebook vectors are regenerated and with the aid of the corresponding gain factors the excitation signal is synthesised. The excitation is then filtered through the synthesis filter and the postfilter in order to generate the synthetic speech.

Following the above brief description of the EFR-GSM codec, in the next section we consider another enhanced full-rate codec namely that of the IS-54 system, which was standardised as the IS-136 scheme.

7.11 The Enhanced Full-rate 7.4 kbps IS-136 Speech Codec [228, 229]

7.11.1 IS-136 Codec Outline

In this section we provide a rudimentary introduction to the operation of the 7.4 kbps IS-136 speech codec, which is a successor of the 7.95 kbps IS-54 DAMPS speech codec [156]. This scheme was standardised in the IS-641 recommendation [227], as part of the enhanced IS-136 standard in the US [228]. This new scheme was the result of a collaboration between Nokia and Sherbrooke University and here we follow the approach of Honkanen *et al.* [229]. The interested reader is referred to [227] for a more detailed overview. Similar to a number of other standard schemes, the codec employs the ACELP excitation model contrived in 1987 by Adoul *et al.* at Sherbrooke University [168], which was described in depth in Section 6.3. The original IS-54 VSELP codec was discussed in Section 7.3. This scheme is, however, more similar to the enhanced full-rate ACELP GSM codec. In fact, the schematic of these schemes is quite similar and hence here we do not duplicate the corresponding block diagrams, we simply refer the reader to Figures 7.26 and 7.29, which are briefly highlighted below. We note,

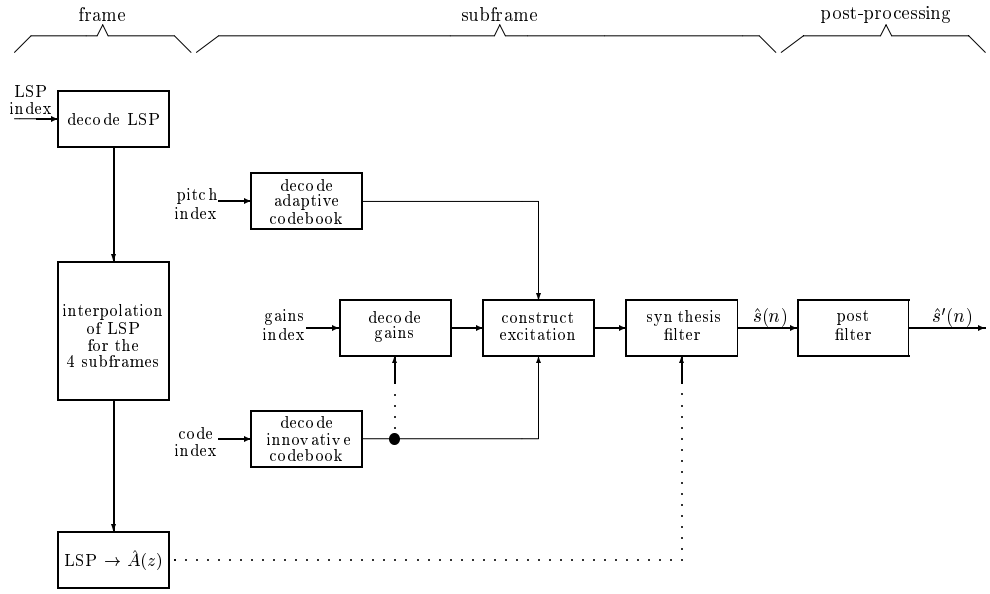

Figure 7.29: EFR-GSM decoder schematic.

however, that the spectral quantisation, windowing and interpolation regime is, for example, radically different from that of the enhanced full-rate GSM codec, since a more stringent bitrate constraint has been imposed. Further differences are inevitable in terms of the number of bits allocated to the various codec parameters.

As, for example, in the full-rate and EFR-GSM encoders, the input speech is initially pre-emphasised using a high-pass filter, in order to boost the low-energy, high-frequency components and hence mitigate the associated number representation problems. As seen in Figure 7.26 for the enhanced GSM codec, the spectral quantisation is carried out on a frame-by-frame basis, while the excitation optimisation is on a subsegment-by-subsegment basis. The codec's bit-allocation scheme is presented in Table 7.15. Below we provide some rudimentary justification for the specific parameter quantisation schemes used.

Table 7.15: The 7.4 kbps enhanced full-rate IS-136 codec's bit allocation.

Parameter	First and third subframes	Second and fourth subframes	No. of bits	Bitrate (kbps)
10 LSFs			$8+9+9=26$	1.3
Gain VQ	7	7	28	1.4
ACELP code	17	17	68	3.4
Pitch-lag	8	5	26	1.3
Total			148/20 ms	7.4

7.11.2 IS-136 Bit-allocation Scheme

In comparison to the schematically similar ACELP EFR-GSM codec, there is a reduced bitrate contribution by the 10 LSFs due to using only one set of LSFs per 20 ms, as opposed to two. For each 20 ms speech frame a 30 ms duration asymmetric windows is applied. Whereas for the EFR-GSM codec, for example, no window-look-ahead was used, in the IS-136 codec a 5 ms or 40-sample look-ahead was employed, similar to the 8 kbps ITU G.729 ACELP codec. Bitrate savings are achieved by VQ, requiring a total 26 bits/20 ms, which constitutes a 1.3 kbps bitrate contribution. The corresponding LSF VQ scheme is shown in Figure 7.30, which is very similar to the corresponding arrangement of the G.723.1 dual-rate codec of Section 7.12. By comparing Figures 7.33 and 7.30 it becomes clear that, essentially, only the codebook sizes are slightly different, since the 7.4 kbps IS-136 scheme invests a total of 26, rather than 24 bits in spectral quantisation, due to its slightly less stringent bitrate budget. Explicitly, split VQ is used for reasons of complexity reduction, where the first 3 LSFs are grouped together and vector-quantised using 8 bits, or 256 entries, while the two other groups of LSF quantisers are constituted by 3 and 4 LSFs, employing 9 and 9 bits, respectively. As seen in Figure 7.30, the nth unquantised LSF vector p^n is predicted first on the basis of the previous quantised LSF vector $\tilde{p}^{(n-1)}$, after multiplying it with a scaling factor b, which is proportional to the long-term correlation between adjacent LSF vectors. The predicted LSF vector $\bar{p}^n$ is then subtracted from the original unquantised LSF vector in order to generate their difference vector, namely δp^n, which is split in sub-vectors of 3, 3 and 4 LSFs and quantised. Finally, the quantised LSF difference vector $\Delta\tilde{p}^n$ is added to the predicted value $\bar{p}^n$, in order to generate the current quantised LSF vector $\tilde{p}^n$.

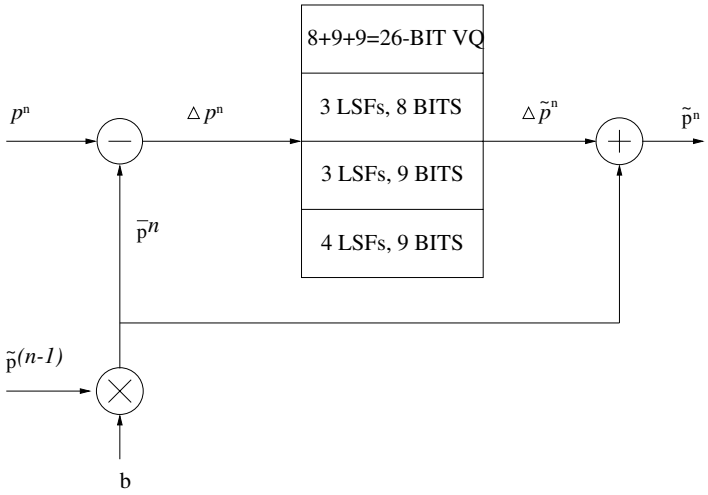

Figure 7.30: The 26-bit IS-136 LSF quantisation schematic.

The fixed ACELP codebook gains and adaptive codebook gains are jointly vector quantised using 7 bits/5 ms subframe, hence contributing 1.4 kbps to the total bitrate. The fixed ACELP codes are assigned 17 bits per subframe, which will be justified in the context of Table 7.16. As seen in the table, the adaptive codebook index or pitch-lag is encoded using

8 bits, corresponding to 256 positions in the first and third subframes. In the second and fourth subframes the pitch-lag is differentially encoded by 5 bits with respect to the corresponding lags in subframes 1 and 3, allowing 32 possible positions. Similar to the G.729 and to the EFR-GSM codecs, Salami *et al.* [160,213] employed a combination of open- and closed-loop search for the pitch-lag in the sample index range of [19 1/3 – 143], implying that, as in most modern codecs, in the low-delay range on oversampling is used. Specifically, the 1/3-sample based search is carried out over the interval [19 1/3 – 85]. This guarantees a similar relative resolution to the high-delay lag range, where integer-sampling is sufficiently accurate. The open-loop search is explicitly shown in the schematic of Figure 7.26, which is found from the perceptually weighted input speech.

Table 7.16: 7.4 kbps enhanced full-rate IS-136 Codec's ACELP pulse allocation. Copyright © IEEE, Honkanen *et al.*, 1997 [229].

Track	Pulses	Positions
1	p_0	0, 5, 10, 15, 20, 25, 30, 35
2	p_1	1, 6, 11, 16, 21, 26, 31, 36
3	p_2	2, 7, 12, 17, 22, 27, 32, 37
4	p_3	3, 8, 13, 18, 23, 28, 33, 38
5		4, 9, 14, 19, 24, 29, 34, 39

In order to ensure a smooth evolution of the pitch-lag and hence also to aid the operation of the differential pitch-lag coding in even subframes, the open-loop pitch-lag is determined once per 10 ms, in other words in every other subframe. This implies giving preference to low pitch-lag values and hence preventing opting for pitch-harmonics, rather than for the true pitch values. This initial pitch-lag search is then followed by a sub-frame based closed-loop pitch search in the range of $[\pm 3]$ around the open-loop values for subframes 1 and 3. Finally, the pitch-lag of the even-indexed subframes is found by restricting the closed-loop search to the range $[-5 - +4]$ around the previous odd-indexed subframe. Again, these measures ensure the well-behaved evolution of the pitch-lag over time.

7.11.3 Fixed Codebook Search

As noted before, the principles of ACELP coding proposed by Adoul *et al.* [168] were outlined in Section 6.3, and the fixed codebook search of this scheme is akin to that of the EFR-GSM codec of Section 7.10. The ACELP codebook of Table 7.16 is also similar to that of Table 7.13. However, instead of allocating two pulses per excitation track in each 40 ms subsegment, due to the lower bitrate constraint of 7.4 kbps here only one pulse per excitation track is employed. The corresponding bitrate contribution was reduced from 35 bits per 40-sample subsegment to 17 bits.

Explicitly, the 5 ms, 40-sample excitation vector hosts four non-zero excitation pulses, each of which can take the values ± 1. Salami *et al.* [225] and Honkanen *et al.* [229] subdivided the 40-sample subframe into 5 tracks. Each of the first three tracks hosts an excitation pulse, while tracks 4 and five share a pulse. Since there are eight possible positions for each pulse in the first three tracks, their encoding requires 9 bits, while the encoding of

the fourth pulse necessitates 4 bits, yielding a total of 13 bits per subsegment for the pulse positions, while another bit is used to encode the sign of the bit. Hence a total of 17 bits/5 ms subsegment are required for the ACELP code. Honkanen *et al.* employed focussed search strategies similar to those first proposed by Salami *et al.* for the G.729 codec [160]. According to the 13-bit ACELP code, a total of 8192 entries per subsegment have to be tested for identifying the optimum one, which was reduced to about 9% of the total range at the cost of low perceptual penalty. The decoder's operations are also similar to those of the EFR-GSM decoder, which was portrayed in Figure 7.29. Let us now consider some of the channel coding aspects of the IS-136 codec.

7.11.4 IS-136 Channel Coding

Source-sensitivity matched error protection is provided for the IS-136 codec by dividing the speech bits in two protection classes, Class-1 and Class-2. The codec itself is more robust against channel errors than the original 7.95 kbps IS-54 scheme and due to the reduced speech-rate more robust channel coding can be assigned. The schematic of the channel coding and mapping scheme is very similar to that of the IS-54 arrangement of Figure 7.4, only the number of associated bits has changed, as seen in Figure 7.31. The most sensitive 48 bits are allocated a 7-bit CRC pattern, which can assist the decoder for activating bad-frame masking.

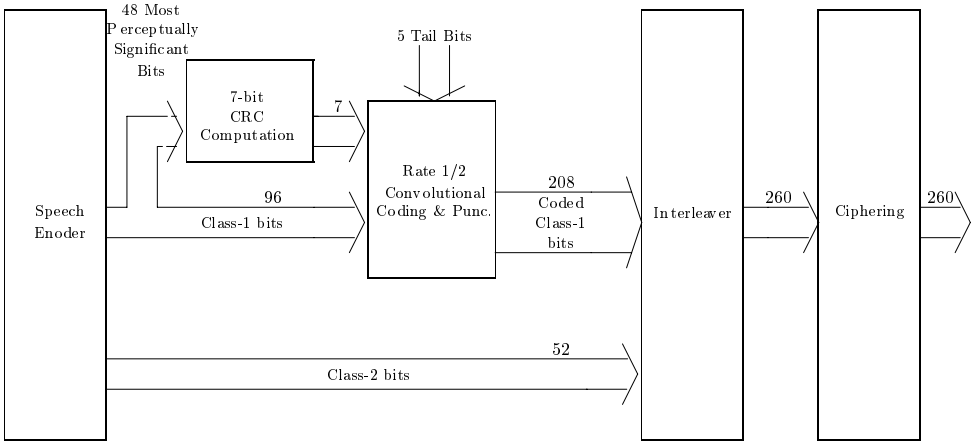

Figure 7.31: The 7.4/13 kbps IS-136 ACELP error protection schematic. Copyright © TIA 1996, [228].

As indicated by Figure 7.31, the 148 speech bits are classified as 96 so-called Class-1 bits and 52 Class-2 bits. The more error-prone Class-1 bits are half-rate, constraint-length five convolutionally encoded, while the remaining 52 bits are transmitted unprotected. The convolutional encoder processes $96 + 7 + 5 = 108$ bits, where the 5 tailing bits are, again, necessitated by the constraint-length five code to flush its buffer before the transmission of the next speech frame. This prevents the propagation of channel errors across speech-frame boundaries, which would otherwise result in prolonged speech degradation due to the convolutional decoder's deviation from the error-free trellis path. The $2 \times 108 = 216$

protected Class-1 bits have to undergo light puncturing, since only 260 channel coded bits can be transmitted in the current IS-136 transmission burst structure. Figure 7.31 shows that a total of 208 bits are generated after puncturing, which are then amalgamated with the 52 unprotected bits to yield the required 260 channel coded speech bits. These are then interleaved and ciphered, before they are transmitted over the channel.

Having considered the family of recent enhanced full-rate codecs, which were based on the ACELP principle, we now focus our attention on another ITU scheme, namely the dual-rate G.723 codec.

7.12 The ITU G.723.1 Dual-rate Codec [230]

7.12.1 Introduction

The ITU G.723.1 dual-rate codec was contrived to form part of the H.324 multimedia compression and transmission standard, which also includes the well-known H.263 video codec. Initially this speech codec was referred to as G.723, but since there exists on older ADPCM-based G.723 standard, this scheme was renamed as G.723.1 in order to avoid confusion. The G.723.1 encoding and decoding processes are based on linear prediction carried out for 30 ms or 240-sample speech segments with a look ahead of 7.5 ms giving a total delay of 37.5 ms. AbS excitation optimisation is used on the basis of four 60-sample subsegments. The G.723.1 scheme is a dual-rate speech codec, which employs ACELP at 5.3 kbps, a technique also adopted by the 8 kbps ITU G.729 codec. For its 6.3 kbps mode of operation multi-pulse maximum likelihood quantisation (MP-MLQ) excitation is utilised. The codec's bit allocation is shown in Table 7.18 in its 5.3 kbps mode of operation, while that of the 6.3 kbps mode is portrayed in Table 7.19, both of which will be elaborated on at a later stage. This dual-rate principle has been demonstrated to be a useful system design option for intelligent multimode transceivers [169], which facilitate a transceiver reconfiguration at each speech-frame boundary in order to provide, for example, a more robust but lower speech quality mode of operation or a higher speech quality and higher speech rate associated with weaker error correction. The G.723.1 codec is also amenable to voice-activity controlled discontinuous transmission and comfort noise injection during untransmitted passive speech spurts. A further feature of this scheme is that it was designed to require a relatively low implementational complexity.

7.12.2 G.723.1 Encoding Principle

The schematic of the G.723.1 encoder is shown in Figure 7.32, which will be detailed during our further discourse. Similar to other ITU speech codecs, the G.723.1 scheme band-limits the speech signal to the conventional 300–3400 Hz telephone band, samples it at 8 kHz and then converts it to 16-bit linear PCM for further processing. Hence this scheme actually constitutes a transcoder. Before further processing, the speech signal is high-pass filtered which removes any residual DC-offset and excitation optimisation is carried out on the basis of 7.5 ms or 60-sample segments.

As seen in Figure 7.32, the original speech signal $y(n)$ is segmented to yield the 240-sample speech $s(n)$ before it is subjected to LPC analysis. The LPC filter order is ten and, similar to most forward-adaptive LPC-based schemes, its coefficients are determined from

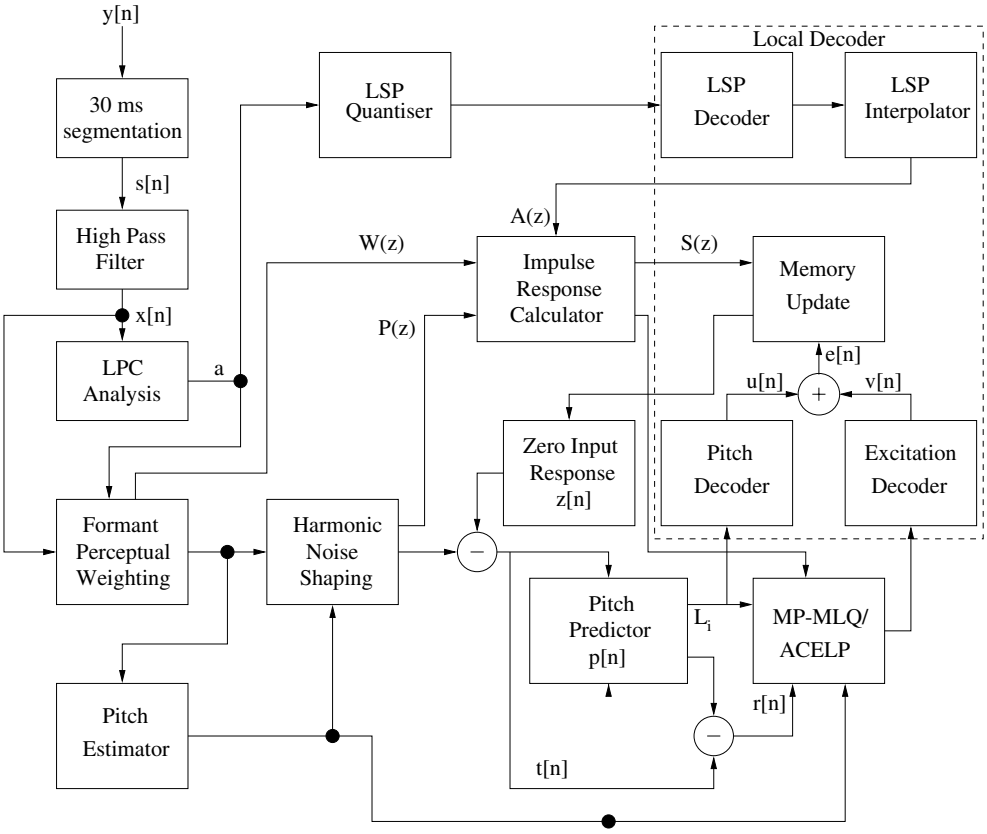

Figure 7.32: G.723 encoder schematic.

the original speech signal. A 180-sample duration Hamming window is centered on each subsegment and 11 autocorrelation coefficients are determined before invoking the Levinson–Durbin algorithm, in order to compute four LPC sets per subsegment. These coefficients are then used in the formant-based perceptual weighting filter. The LPC coefficients used in the last of the four excitation optimisation subsegments are quantised using a technique referred to as predictive split vector quantisation (PSVQ), which will be highlighted during our further elaborations. Suffice to say here with reference to Figure 7.32 that the LPC coefficients are transformed to LSP format before quantisation in the LSP-quantiser block of Figure 7.32. Observe, furthermore, in the figure that as in most state-of-the-art codecs, the LSP parameters are locally decoded and interpolated across subsegments.

The conventional formant-based perceptual error weighting filter of Figure 7.32 is followed by a so-called harmonic noise shaping filter, which, as suggested by its name, relies on the harmonic pitch estimate delivered by the corresponding block of Figure 7.32. For a detailed discourse on the mathematical description of this filter the interested reader is referred to the G.723.1 standard [230]. In order to maintain a low complexity, this pitch-lag estimate L_{ol} is derived from the formant-weighted speech signal initially in an open-loop

search in the range of 18 to 142 samples on the basis of two consecutive subsegments. This open-loop pitch estimate can then be used for a more accurate closed-loop AbS search in a limited range, which takes place in the corresponding 'Pitch Predictor' block of Figure 7.32, operating on the weighted speech signal following the formant-based and harmonic-based filtering blocks and the deduction of the filters' zero-input response. As in all other AbS codecs, the zero-input response of the synthesis filter corresponds to its memory from the previous excitation optimisation cycle.

An unusually high, fifth-order pitch predictor is employed. For the first and third subframes the pitch lag is refined around the open-loop estimate within the range of ± 1 and its value is transmitted using 7 bits. For the second and fourth subframes the pitch delay is differentially encoded using 2 bits, allowing a deviation in the range of $[-1 - +2]$. The pitch-predictor gains are vector quantised employing a 170-entry codebook for the 5.3 kbps mode of operation and an additional 85-entry codebook for the 6.3 kbps mode. The 85-entry codebook is activated for quantising open-loop pitch gains, when the associated pitch lag is below 58, while the 170-entry codebook is dedicated to quantising the pitch gains related to high pitch-delay scenarios. The effect of the refined pitch predictor can then be deducted from the speech signal and depending on the required bitrate, the resultant residual signal is consecutively subjected to either MP-MLQ or ACELP excitation optimisation in the MP-LPQ/ACELP block of Figure 7.32. As usual, the local decoder decodes the pitch, excitation as well LSP parameters in order to ensure that the encoder and decoder rely on the same set of parameters in reconstructing the speech. The 'Impulse Response Calculator' block determines the response of the combined closed-loop synthesis filter, constituted by the formant-based perceptual weighting filter and the harmonic noise-shaping filter.

7.12.3 Vector-quantisation of the LSPs

The previously mentioned PSVQ LSP-quantisation scheme is depicted in Figure 7.33. Initially the long-term average $\mathbf{P}_{\text{mean}}$ of the unquantised LSP parameters is subtracted from the current set of unquantised LSP, in order to arrive at the set $\mathbf{P}_n$, although this subtraction step is not shown in the figure. Due to the inherent correlation between consecutive LSPs the previous quantised LSP vector $\tilde{\mathbf{P}}_{n-1}$ provides a good estimate of the current vector to be quantised. Their long-term adjacent-vector correlation was found to be 12/32, which is used here in a simple first-order predictor to produce an estimate $\bar{\mathbf{P}}_n$ of the current vector $\mathbf{P}_n$ that has to be quantised. As portrayed in the figure, the difference ΔP_n of the estimate and the original vector is computed, which is now likely to exhibit a more uncorrelated behaviour. This vector could be scalar quantised, but better performance is achieved using vector quantisation at the cost of higher complexity. However, the vector quantisation of a ten-dimensional vector may become excessively high, if a low quantisation distortion has to be maintained, requiring a large trained codebook. A good compromise is to use the so-called split vector quantisation principle also advocated by the G.729 codec, for example. The G.723.1 scheme employs a three-way split LSP VQ, constituted by three sub-vectors which have dimensions of 3, 3 and 4, respectively. Having found the best-matching codebook entry for the three sub-vectors, the quantised LSP vector is determined by adding the predicted value $\bar{\mathbf{P}}_n$ to the codebook entry and superimposing the previously subtracted mean value, as portrayed in the figure.

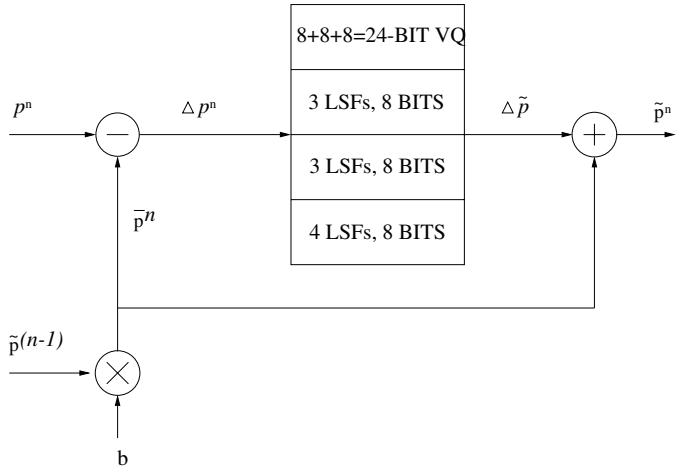

Figure 7.33: The 24-bit G.723.1 LSF quantisation schematic.

As mentioned before, the LSPs are then interpolated across the subframes for maintaining a seamless spectral envelope evolution. If $\mathbf{P}^n_{\text{quant}}$ is the quantised LPC vector in the present frame and $\mathbf{P}^{n-1}_{\text{quant}}$ is the quantised LPC vector from the past frame, then the interpolated LSP vector for the four subframes is given by

$$\begin{aligned}
\mathbf{P}^n_{\text{quant},1} &= 0.75\mathbf{P}^{n-1}_{\text{quant}} + 0.25\mathbf{P}^n_{\text{quant}} \\
\mathbf{P}^n_{\text{quant},2} &= 0.5\mathbf{P}^{n-1}_{\text{quant}} + 0.5\mathbf{P}^n_{\text{quant}} \\
\mathbf{P}^n_{\text{quant},3} &= 0.25\mathbf{P}^{n-1}_{\text{quant}} + 0.75\mathbf{P}^n_{\text{quant}} \\
\mathbf{P}^n_{\text{quant},4} &= 0.75\mathbf{P}^n_{\text{quant}}.
\end{aligned}$$

7.12.4 Formant-based Weighting Filter

The weighting filter employed in the G.723.1 encoder is similar to that of the G.729 scheme and it is based upon the unquantised LPC filter coefficients a_i, which are updated for each subsegment on the basis of a 180-sample Hamming-windowed speech segment. The transfer function of the weighting filter is given by

$$\begin{aligned}
W_j(z) &= \frac{A_j(z/\gamma_1)}{A_j(z/\gamma_2)} \\
&= \frac{1 - \sum_{i=1}^{10} \gamma_1^i a_{ij} z^{-i}}{1 - \sum_{i=1}^{10} \gamma_2^i a_{ij} z^{-i}}, \quad 0 \le j \le 3,
\end{aligned} \tag{7.51}$$

where $\gamma_1 = 0.9$ and $\gamma_2 = 0.5$ determine the amount of spectral weighting. In the G.729 codec the amount of weighting, i.e. the factors γ_1 and γ_2, was adaptively controlled in order to improve the performance of the codec for input signals with a flat frequency response. We

note, furthermore, that in the G.729 standard, for example, the Levinson–Durbin algorithm delivers a set of LPC coefficients which have the opposite sign in comparison to the G.723.1 LPC coefficients. Hence the negative sign before the summation in the weighting filter of Equation (7.51), while the G.729 weighting filter contains a positive sign in the weighting filter.

7.12.5 The 6.3 kbps High-rate G.723.1 Excitation

The target vector modelling is carried out in the MP-MLQ/ACELP block of Figure 7.32 using the convolution

$$r'(n) = \sum_{j=0}^{n} h(j) \cdot v(n-j), \quad 0 \leq n \leq 59, \tag{7.52}$$

where $v(n)$ is the excitation vector and $h(n)$ is the impulse response of the combined formant-based perceptual filter and harmonic noise filter. The excitation vector is of the form

$$v(n) = G \cdot \sum_{m=0}^{M-1} \alpha_m \cdot \delta(n - n_m), \quad 0 \leq n \leq 59, \tag{7.53}$$

where G is the excitation gain factor, allowing the excitation's energy to fluctuate and hence to cater for speech segments exhibiting different energy; α_m, $m = 0, \ldots, M$, represents the sign of the Dirac-delta excitation pulses, while n_m, $m = 0, \ldots, M$, denote the positions of the excitation pulses. The number of excitation pulses in the 6.3 kbps mode is $M = 6$ in even subframes and 5 in odd ones. The pulse positions are restricted to either be all odd or even, which is encoded using a so-called grid-position bit, as seen in the bit-allocation scheme of Table 7.18. Given that the odd or even positions are preselected by the grid-position bit, there are 30 possible pulse locations and the six excitation pulses of the even subframes hence can take

$$\binom{30}{6} = 593775$$

different positions. Similarly, in the odd subframes

$$\binom{30}{5} = 142506$$

position combinations can be encountered. Since $2^{20} = 1048576$ and $2^{18} = 262144$, the required number of bit using the so-called enumerative coding technique is 20 and 18 in the even and odd subframes, respectively.

It is also noted in the recommendation, however, that the resultant bitrate can be further reduced if the pulse positions are not separately represented for the individual subframes. This is plausible, since we noted above that $2^{20} = 1048576$ and $2^{18} = 262144$, allowing us to represent by nearly a factor of two more than the potential possible numbers of 593775 and 142506 excitation pulse positions of the two modes. Hence it was recommended to combine the first four MSBs from each subframe pulse position index and employ 13 bits to encode these 16 bits. This reduces the total number of bits from 192 to 189/30 ms, yielding a bitrate of 6.3 kbps This bitrate reduction is not reflected in the bit-allocation scheme of Table 7.18 for

the sake of simplicity. However, in the bit-sensitivity plot of Figure 7.35 this bitrate reduction becomes explicit, portraying the 13-bit pulse position MSBs (POS MSB) and the 16-bit, 14-bit, 16-bit and 14-bit position indices.

The excitation is found using the classic approach, in other words by minimising the MSE between the target vector and the candidate excitation vectors over the set of legitimate excitation patterns, where the error term concerned is formulated as

$$\begin{aligned} e(n) &= r(n) - r'(n) \\ &= r(n) - G \cdot \sum_{m=0}^{M-1} \alpha_m \cdot h(n - n_m), \quad 0 \leq n \leq 59. \end{aligned} \tag{7.54}$$

Minimising the MSE term of

$$E = \sum_{0}^{59} e^2(n) \tag{7.55}$$

for all the previously stipulated legitimate excitation patterns leads to the following optimum excitation gain expression:

$$G_{\max} = \frac{\max |d(j)|_{j=0,\ldots,59}}{\sum_{n=0}^{59} h^2(n)}, \tag{7.56}$$

where we have

$$d(j) = \sum_{n=j}^{59} r(n) \cdot h(n - j), \quad 0 \leq n \leq 59. \tag{7.57}$$

The optimum excitation gain $G_{\max}$ is then logarithmically scalar-quantised using 24 quantisation steps, which are spaced by 3.2 dB. Taking the logarithm of a quantity which exhibits a highly non-uniform PDF compresses the large values to be quantised and expands the range of lower values, hence rendering the PDF typically more uniform and hence more amenable to uniform quantisation on the resulting logarithmic scale. In order to further improve the speech quality, the optimum quantised gain $G_{\max}$ is tentatively reduced by one 3.2 dB step and increased by two such steps and the excitation pulses are re-optimised to find the best combination of these parameters, resulting in the minimum MSE. Finally, these parameters are encoded and transmitted to the decoder.

7.12.6 The 5.3 kbps Low-rate G.723.1 Excitation

ACELP codecs have been discussed in depth earlier in both general terms as well as in the context of the 8 kbps G.729 codec, hence here we refrain from detailing the excitation optimisation procedure. Suffice to say here that a 17-bit ACELP codebook is used in the 5.3 kbps mode, where the innovation vector is constituted by at most four non-zero pulses, which can have the signs and positions summarised as in Table 7.17.

As mentioned before, the pulses can occupy either even or odd positions in the subframe, which is ensured by testing the MSE associated with the set of pulses shifted by one position with respect to that indicated in Table 7.17. This is signalled to the decoder using the grid-position bit. Observe, furthermore, from the table that the bracketed pulse positions

Table 7.17: G.723.1 ACELP excitation pulses in the 5.3 kbps mode.

Sign	Positions
± 1	0, 8, 16, 24, 32, 40, 48, 56
± 1	2, 10, 18, 26, 34, 42, 50, 58
± 1	4, 12, 20, 28, 36, 44, 52, (60)
± 1	6, 14, 22, 30, 38, 46, 54, (62)

are actually outside the subframe limits and hence they are not used. According to the three legitimate positions of the excitation pulses their position is signalled to the decoder using 3 bits, while their sign is transmitted using a fourth bit. Hence for the four excitation pulses 16 bits are required, totalling 17 with the additional grid-position bit. The excitation optimisation is structured in four nested loops, according to identifying the best position for each of the four excitation pulses.

The computational complexity of the codec is further reduced by applying a so-called focussed search strategy, similar to the G.729 8 kbps ACELP codec. Explicitly, before entering the last of the four nested loops a thresholding operation is invoked, in order to test whether it is sufficiently promising to continue the search in terms of synthesised speech quality. This loop is then searched only if the thresholding condition is met. Furthermore, the maximum number entering this loop is also fixed for the sake of setting a maximum for the search complexity, which is an important aspect for real-time implementations. Specifically, the last loop is entered a maximum of 150 times per subsegment. Before the commencement of the excitation optimisation for the next subsegment the memory of the concatenated synthesis-filter, formant-based perceptual weighting filter and harmonic noise filter has to be updated both at the encoder and decoder. This operation is carried out by filtering the optimum excitation through this cascaded filter complex both at the encoder and decoder and storing it until it is invoked as the so-called 'zero input response' or 'filter memory' during the optimisation of the next subsegment excitation. Let us now summarise the bit allocation of both codecs.

7.12.7 G.723.1 Bit Allocation

The bit-allocation schemes of the two modes of operation are summarised in Tables 7.18 and 7.19. Since the innovation sequences of the two modes are different, the encoding of the excitation pulses is different, but the remaining parameters are encoded identically. Hence the bitrate reduction accrues from the lower number of excitation quantisation bits in the 5.3 kbps ACELP mode. Explicitly, instead of the $76 + 22 = 98$ bits/30 ms ≈ 3.27 kbps pulse position and pulse sign excitation bitrate contribution of the 6.3 kbps scheme, the 5.3 kbps codec requires $48 + 16 = 64$ bits/30 ms ≈ 2.13 kbps, resulting in a bitrate reduction of about 1.1 kbps.

In order to elaborate further on gain quantisation, we note that 12 gain-quantisation bits are allocated for encoding the 24 3.2 dB-spaced excitation gain levels and the 5-tap pitch predictor gains, using 170 levels for the latter. The associated quantisation schemes

Table 7.18: Bit-allocation scheme of the 5.3 kbps mode of the G.723.1 codec.

Parameter	Subframe 1	Subframe 2	Subframe 3	Subframe 4	Total/30 ms
LPC indices					$3 \cdot 8 = 24$
Adaptive codebook lag: ACL0–ACL3	7	2	7	2	18
Excitation and pitch gains combined: GAIN0–GAIN3	12	12	12	12	48
Pulse positions: POS0–POS3	12	12	12	12	48
Pulse signs: PSIG0–PSIG3	4	4	4	4	16
Grid index: GRID0–GRID3	1	1	1	1	4
Total					158/30 ms

are identical in both operational modes. There is a total of $170 \times 24 = 4080$ possible combinations of the excitation and pitch gains, which is less than 4096 and hence can be jointly encoded using 12 bits. However, this is not a robust quantisation, since a single bit error in the 12 bit index will affect all gains. Alternatively, it would have been possible to employ 8 bits for the pitch gains, implementing a finer, 256-level quantiser and 5 bits for the excitation gain, again ensuring a somewhat finer 32-level quantisation scheme. Quantising the two gains separately would have required a total of 13 bits, only requiring one additional bit, while ensuring a higher error resilience. A similar combinatorial coding was also used for the excitation pulse locations.

There is a further fine detail concerning the 6.3 kbps gain quantisation.[1] Namely, if the pitch lag in the first or in the third subframe is less than 58, then the number of levels for pitch gains is 85 instead of 170 for two consecutive subframes. This will save one gain quantisation bit, since $85 \times 24 = 2040 < 2048$, and hence 11 bits will suffice. This saved bit is used to signal whether so-called pitch sharpening is invoked in the excitation code. If pitch sharpening is employed, then an excitation pulse is replaced with a series of excitation pulses, separated by the pitch period within the limits of the subframe boundary, as will be illustrated using the following example. Let us assume that there are three excitation pulses at the pulse positions of 0, 20, and 30 and the pitch period is 25, corresponding to $25 \times 125\ \mu\text{s} = 3.125$ ms or to a pitch frequency of 320 Hz.

[1] The authors are grateful to Redwan Salami for this private communication.

Table 7.19: Bit-allocation scheme of the 6.3 kbps mode of the G.723.1 codec.

Parameter	Subframe 1	Subframe 2	Subframe 3	Subframe 4	Total/30 ms
LPC indices					$3 \cdot 8 = 24$
Adaptive codebook lag: ACL0–ACL3	7	2	7	2	18
Excitation and pitch gains combined: GAIN0–GAIN3	12	12	12	12	48
Pulse positions: POS0–POS3	20	18	20	18	76
Pulse signs: PSIG0–PSIG3	6	5	6	5	22
Grid index: GRID0–GRID3	1	1	1	1	4
Total					192/30 ms

When invoking pitch sharpening, the above three pulses will be replaced by the following pitch-spaced pulses: 0, 25, 50; 20, 45; 30, 55, while using the previously determined excitation gains. We note, however, that the pitch-spaced pulses are not extended beyond the subframe boundary at position 60. Hence there are still three excitation gains but six excitation pulses in this case. Both the original and the pitch-sharpened excitation configurations will be tentatively invoked and the one which minimises the error criterion will be selected. The 1 bit flag saved in the modified gain quantisation will be used to indicate the presence or absence of pitch sharpening.

Since the quantisation and encoding philosophies of the various remaining parameters were discussed during our earlier discourse, here we refrain from detailing these bit-allocation tables further. The encoded bitstream is transmitted to the decoder, where the individual parameters are reconstructed and they are employed in reconstructing the synthesised speech signal similar to the local decoder, which was briefly summarised during our description of the encoder schematic. With the main G.723.1 algorithms known, let us now consider the error sensitivity of the codec.

7.12.8 G.723.1 Error Sensitivity

The bit-allocation scheme of the G.723.1 codec was summarised in Tables 7.18 and 7.19. In this section, knowledge of these tables is assumed and only a brief summary of the associated bit-sensitivity issues is offered with reference to Figures 7.34 and 7.35.

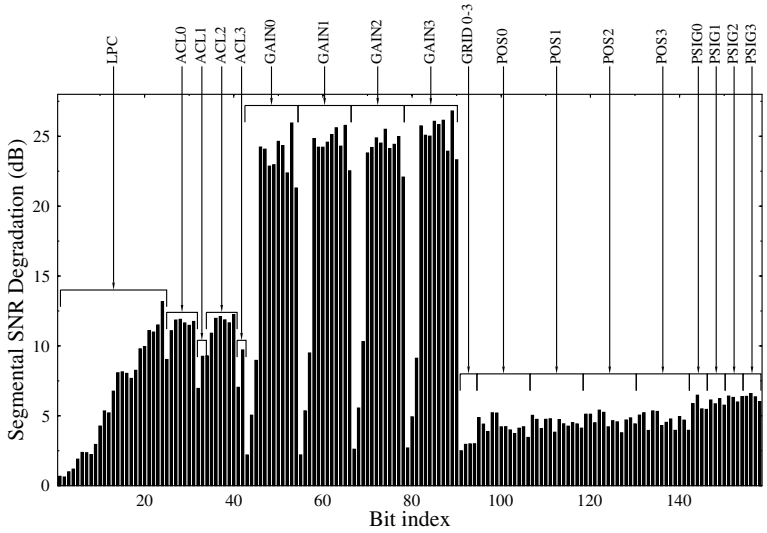

Figure 7.34: Bit-sensitivity of the 5.3 kbps G.723 speech frame.

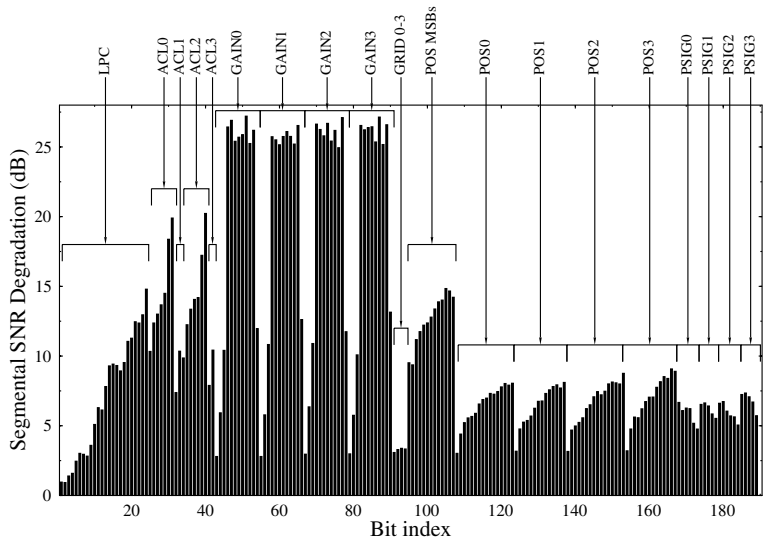

Figure 7.35: Bit-sensitivity of the 6.3 kbps G.723 speech frame.

Considering the sensitivity of the 5.3 kbps codec first, the first 24 bits of the frame illustrated in Figure 7.34 represent the LPC vector quantiser address bits, which exhibit a gradually increasing SEGSNR degradation for the more significant address bits. This suggests that the codebook is structured by allocating codebook entries representing spectral envelopes similar to each other in each others vicinity, since corrupting the LSBs of the codebook

address results in small SEGSNR degradations. By contrast, when corrupting the MSBs, a high SEGSNR degradation is experienced. The non-differentially encoded 7-bit adaptive codebook lag bits exhibit more or less uniform bit sensitivities, while the differentially coded 2-bit lags are less sensitive. This is intuitively expected, since the corruption of the non-differential values also corrupts the differential values. The highest sensitivity is exhibited by the jointly quantised 12-bit gain-indices. As expected, similar observations can also be made with respect to the corresponding bits of the 6.3 kbps codec, as seen in Figure 7.35.

Focusing our attention on excitation pulse parameters, the 5.3 kbps ACELP excitation bits of Figure 7.34 show a rather flat sensitivity as a function of the bit index. This is in harmony with our expectations for ACELP codecs, since corrupting one pulse position does not dramatically change the whole of the excitation vector. This is also valid for the excitation pulse sign, although the associated SEGSNR degradation is slightly higher than that due to the position bits.

The 6.3 kbps excitation encoding relies on the enumerative technique of the multi-pulse excitation. The sensitivity of the excitation grid bits is relatively low, while that of the jointly encoded four subsegment excitation pulse position MSBs is significantly higher. The observed stair-case effect suggests, again, that similar excitation pulse positions are encoded using similar indices. Hence, if one of the index LSBs is corrupted, its SEGSNR effects are more mitigated than in case of some of the MSBs. The excitation pulse signs, again, exhibit similar sensitivities to the pulse position index bits.

As with most other coding schemes discussed, the G.723.1 codec is also compared in subjective speech-quality terms to the set of standard codecs in Figure 18.4 of Chapter 18.

7.13 Advanced Multirate JD-CDMA Transceiver

H.T. How, T.H. Liew, E.L. Kuan and L. Hanzo[2]

7.13.1 Multirate Codecs and Systems

Recently, the Adaptive Multi-Rate (AMR) speech codec has been standardised by ETSI [28, 231]. The codec is capable of operating in the full-rate and half-rate speech traffic channels of GSM. It is also amenable to adapting the source coding and channel coding bitrates according to the quality of the radio channel. Most speech codecs employed in communication systems – such as, for example, the existing GSM speech codecs (full rate, half rate and enhanced full rate) – operate at a fixed bitrate, with a trade-off between source coding and channel coding. However, estimating the channel quality and adjusting the bitrate adaptively according to the channel conditions has the potential of improving the error resilience and the speech quality over wireless channels.

The AMR concept is amenable to a range of intelligent configurations. When the instantaneous channel quality is low, the speech encoder operates at low bitrates, thus

[2]This section is based on: H.T. How, T.H. Liew, E.L Kuan and L. Hanzo," A redundant residue number system coded burst-by-burst adaptive joint-detection based CDMA speech transceiver", from Vehicular Technology, Vol. 65, Issue 1, Jan. 2006 pp. 387–397 IEEE.

facilitating the employment of more powerful forward error control within a fixed bitrate budget or using a more robust but lower-rate transceiver mode. By contrast, under favourable channel conditions the speech encoder may use its highest bitrate, implying high speech quality, since in this case weaker error protection is sufficient or a less robust, but higher bitrate transceiver mode can be invoked. However, the system must be designed for seamless switching between rates without encountering annoying perceptual artifacts.

Das *et al.* provided an extensive review of multimode and multirate speech coding in [232]. Some of the earlier contributors in multimode speech coding include those by Taniguchi *et al.* [233], Kroon and Atal [234], Yong *et al.* [133], DeJaco *et al.* [235], Paksoy *et al.* [236] and Cellario *et al.* [237]. Further recent work on incorporating multirate speech coding into wireless systems was covered in a vast body of literature [238, 239]. Specifically, Yuen *et al.* [238] in their paper employed embedded and multimode speech coders based on the CELP technique in combination with channel coders using rate compatible punctured convolutional RCPC codes. The combined speech and channel coding resulted in a gross bitrate of 12.8 kbps and 9.6 kbps, with the assumption of possible transmission using either TDMA or CDMA techniques. The investigations showed that multimode CELP coders performed better than their embedded counterparts, and that adaptive schemes were superior to fixed-rate schemes.

LeBlanc *et al.* in [240] developed a low complexity, low delay, multirate coder suitable for indoor wireless communications. The speech coder was a modified version of the G.728 LD-CELP standard coder, employing multi-stage excitation configuration together with an adaptive codebook. A lower LPC predictor order of 10 was used, rather than 50 as in G.728, and a higher bandwidth expansion factor of 0.95, rather than 0.9883 was employed, which resulted in a more robust performance in noisy channels. In [241], Kleider and Campbell proposed an adaptive speech system utilising a multirate sinusoidal transform coder (MRSTC), in conjunction with convolutional coding and pulse position modulation (PPM). The MRSTC is based on the sinusoidal transform coding proposed by McAulay and Quatieri [242]. This codec was investigated further by McAulay in the context of wireless and Internet applications in [243], using a range of bitrates between 1.2 kbps and 9.6 kbps. Upon employing convolutional coding and a fixed BPSK modulation scheme, it was reported to give a reduction of nearly 9 dB in average spectral distortion over the fixed rate 9.6 kbps benchmarker.

In a contribution from the speech coding team at Qualcomm, Das *et al.* [244] illustrated using a multimode coder having four modes (full rate, half rate, quarter rate and eighth rate) that the diverse characteristics of the speech segments can be adequately captured using variable rate codecs. It was shown that a reduced average rate can be obtained, achieving equivalent speech quality to that of a fixed full-rate codec. Specifically, a multimode codec with an average rate of 4 kbps achieved significantly higher speech quality than that of the equivalent fixed-rate codec. An excellent example of a recent standard variable-rate codec is the enhanced variable rate coder (EVRC), standardized by the TIA as IS-127 [245]. This codec operates at a maximum rate of 8.5 kbps and an average rate of about 4.1 kbps. The EVRC incorporates three coding modes that are all based on the CELP model. Selection among the three modes is source-controlled, based on the estimation of the input signal state.

Multimode speech coding was also evaluated in an ATM-based environment by Beritelli *et al.* in [246]. The speech codec possessed seven coding rates, ranging from 0.4–16 kbps. Five different bitrates were allocated for voiced/unvoiced speech encoding, while two lower

bitrates were generated for inactive speech periods, depending on the stationarity of the background noise. The variable-rate voice source was modelled using a Markov-based process. The multimode coding scheme was compared to the 12 kbps CS-ACELP standard coder [247] using the traditional ON–OFF voice generation model. It was found that the multimode coder performed better than the CS-ACELP ON–OFF scheme, succeeding in minimising the required transmission rate by exploiting the local characteristics of the speech waveform. Furthermore, it was also capable of realistically synthesising the background noise.

Thus far we have focussed our attention on source-controlled multirate coders, where the coding algorithm responds to the time-varying local character of the speech signal in order to determine the required speech rate. An additional capacity enhancement can be achieved by introducing network control, which implies that the speech codec has to respond to a network-originated control signal for switching the speech rate to one of a predetermined set of possible rates. The network control procedure, for example, was addressed by Hanzo and Woodard [169] and Kawashima *et al.* [239]. Specifically, in [169] a novel high-quality, low-complexity dual-rate 4.7 kbps and 6.5 kbps ACELP codec was proposed for indoor communications, which was capable of dropping the associated source rate and speech quality under network control, in order to invoke a more resilient modem mode, amongst less favourable channel conditions. Source-matched binary BCH channel codecs combined with un-equal protection diversity and pilot-assisted 16-level quadrature amplitude modulation (16-QAM) and 64-level quadrature amplitude modulation (64-QAM) was employed, in order to accommodate both the 4.7 and the 6.5 kbps coded speech bits at a signalling rate of 3.1 kBd. Good communications quality speech was reported in an equivalent bandwidth of 4 kHz, if the channel SNR and SIR of the benign indoors cordless channels were in excess of about 15 and 25 dB for the lower and higher speech quality 16-QAM and 64-QAM systems, respectively. In [239], Kawashima *et al.* proposed network control procedures for CDMA systems, focussing only on the downlink from the base to the mobile station, where the base station can readily coordinate the coding rate of all users without any significant delay. This network control scheme was based on the so-called M/M/∞/M queueing model applied to a cell under heavy traffic conditions. A modified version of the QCELP coder [235] was used, employing the fixed rates of 9.6 and 4.8 kbps.

Focussing our attention on the associated transmission aspects, significant research interest has also been devoted to burst-by-burst adaptive quadrature amplitude modulation (BbB-AQAM) transceivers [248, 249]. The transceiver reconfigures itself on a burst-by-burst basis, depending on the instantaneous perceived wireless channel quality. More explicitly, the associated channel quality of the next transmission burst is estimated and the specific modulation mode which is expected to achieve the required BER performance target at the receiver is then selected for the transmission of the current burst. Modulation schemes of different robustness and of different data throughput have also been investigated [248, 250, 251]. The BbB-AQAM principles have also been applied to joint detection code division multiple access (JD-CDMA) [252, 253] and OFDM [248, 254, 255].

Against the above background, in this section we propose and characterise a dual-mode burst-by-burst adaptive speech transceiver scheme, based on the AMR speech codec, redundant residue number system (RRNS) assisted channel coding [256] and JD-CDMA [253]. The mode switching is controlled by the channel quality fluctuations imposed by the time-variant channel, which is not a desirable scenario. However, we will endeavour to

contrive measures in order to mitigate the associated perceptual speech-quality fluctuations. The underlying trade-offs associated with employing two speech modes of the AMR standard speech codec in conjunction with a reconfigurable, unequal error protection BPSK/4QAM modem are investigated.

This discussion is structured as follows. Subsection 7.13.2 provides a brief system overview. Subsection 7.13.3 details the structure of the AMR speech codec, while the associated bit sensitivity issues are discussed in Subsection 7.13.4. Subsection 7.13.5 describes the RRNS channel codes applied in our system and the associated source-matched error protection scheme is discussed in Subsection 7.13.5.2. The BbB-AQAM JD-CDMA scheme is detailed in Subsection 7.13.6. Finally, before concluding, our system performance results are summarised in Subsection 7.13.7.

7.13.2 System Overview

The schematic of the proposed adaptive JD-CDMA speech transceiver is depicted in Figure 7.36. The encoded speech bits generated by the AMR codec at the bitrate of 4.75 or 10.2 kbps are first mapped according to their error sensitivities into three protection classes, although for simplicity this is not shown explicitly in the figure. The sensitivity-ordered speech bits are then channel encoded using the RRNS encoder [256] and modulated using a re-configurable BPSK or 4QAM based JD-CDMA scheme [248]. We assigned the 4.75 kbps speech codec mode to the BPSK modulation mode, and the 10.2 kbps speech codec mode to the 4QAM mode. Therefore, this transmission scheme can provide higher speech quality at 10.2 kbps, provided that sufficiently high channel SNRs and SIRs prevail. Furthermore, it can be reconfigured under transceiver control to provide an inherently lower, but unimpaired speech quality amongst lower SNR and SIR conditions at the speech rate of 4.75 kbps.

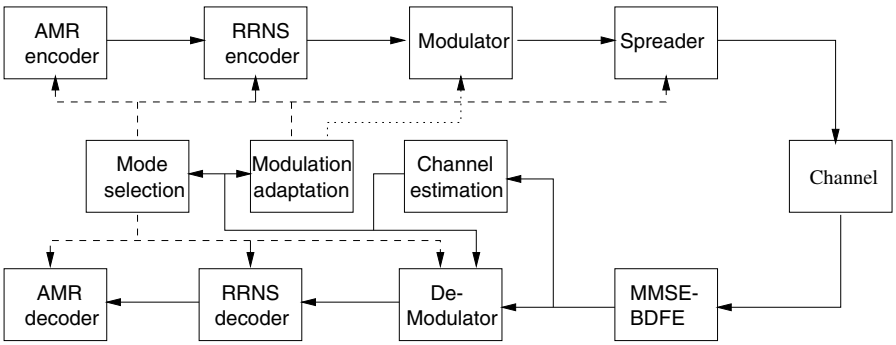

Figure 7.36: Schematic of the adaptive dual-mode JD-CDMA system.

Subsequently, the modulated symbols are spread in Figure 7.36 by the spreading sequence assigned to the user, where a random spreading sequence is employed. The minimum mean squared error block decision feedback equaliser (MMSE-BDFE) is used as the multiuser detector [253], where perfect channel impulse response (CIR) estimation and perfect decision feedback are assumed. The soft outputs for each user are obtained from the MMSE-BDFE and passed to the RRNS channel decoder. Finally, the decoded bits are mapped back to their

original bit protection classes by using a bit-mapper (not shown in Figure 7.36) and the speech decoder reconstructs the original speech information.

In BbB-AQAM/CDMA, in order to determine the best choice of modulation mode in terms of the required trade-off between the BER and throughput, the near instantaneous quality of the channel has to be estimated. The channel quality is estimated at the receiver and the chosen modulation mode and its corresponding speech mode are then communicated using explicit signalling to the transmitter in a closed-loop scheme, as depicted in Figure 7.36. Specifically, the channel estimation is obtained by using the metric of signal-to-residual interference plus noise ratio (SINR), which can be calculated at the output of MMSE-BDFE [253].

7.13.3 The Adaptive Multirate Speech Codec

7.13.3.1 AMR Codec Overview

The AMR codec employs the ACELP model [16,160] shown in Figure 7.37. Here we provide a brief overview of the AMR codec following the approach of [28, 231, 257]. The AMR codec's complexity is relatively low and hence it can be implemented cost-efficiently. This codec operates on a 20 ms frame of 160 speech samples, and generates encoded blocks of 95, 103, 118, 134, 148, 159, 204 and 244 bits/20 ms. This leads to bitrates of 4.75, 5.15, 5.9, 6.7, 7.4, 7.95, 10.2 and 12.2 kbps, respectively. Explicitly, the AMR speech codec provides eight different modes. Multirate coding [56] allows a variation in the total allocation of bits for a speech frame, adapting the rate to the local phonetic character of the speech signal to the channel quality or to network traffic conditions. This is particularly useful in digital cellular communications, where one of the major challenges is that of designing a codec that is capable of providing high-quality speech for a wide variety of channel conditions. Ideally, a good solution must provide the highest possible quality under perfect channel conditions, while also maintaining good quality in hostile channel environments. The codec mode adaptation is a key feature of the new AMR standard that has not been used in any prior mobile standard. At a given fixed gross bitrate, this mechanism of adapting the source coding rate has the potential of altering the partitioning between the speech source bitrate and the redundancy added for error protection. Alternatively, the AMR codec can be invoked in our BbB-AQAM/CDMA transceiver.

As shown in Figure 7.37, the encoder operates on the sampled input speech signal $s(n)$ and linear prediction (LP) is applied to each speech segment. The coefficients of this predictor are used to construct a LPC synthesis filter $1/(1 - A(z))$, which describes the spectral envelope information of the speech segment [56, 158]. An AbS procedure is employed in order to find the excitation that minimises the weighted mmse between the reconstructed and original speech signal. The weighting filter is derived from the LPC synthesis filter and takes into account the psycho-acoustic quantisation noise masking effect, namely that the quantisation noise in the spectral neighbourhood of the spectrally prominent speech formants is less perceptible [56, 158]. In order to reduce the complexity, adaptive and fixed excitation codebooks are searched sequentially for the best codebook entry; namely, first for the adaptive contribution and then for the fixed codebook entry. The adaptive codebook consists of time-shifted versions of past excitation sequences and describes the long-term characteristics of the speech signal [56, 158].

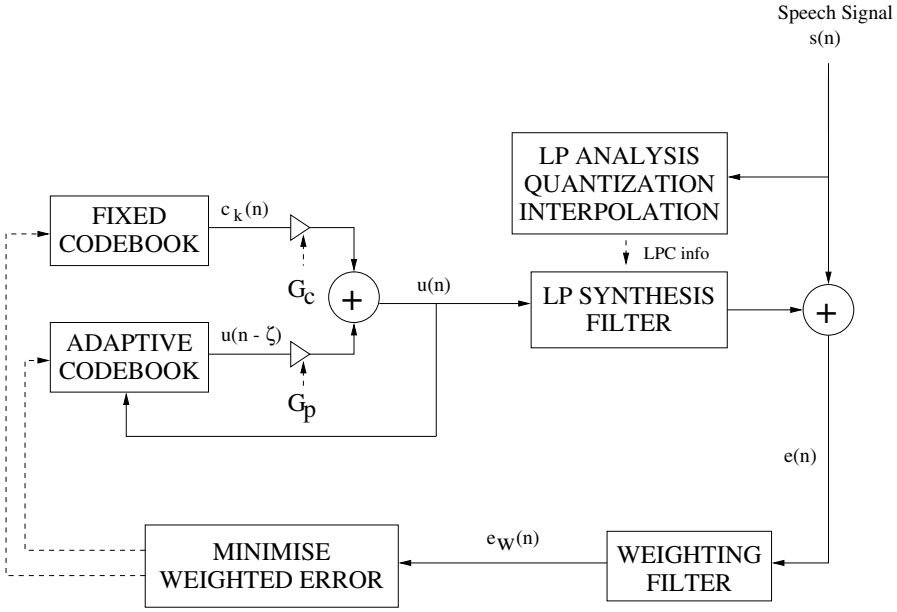

Figure 7.37: Schematic of ACELP speech encoder.

Three of the AMR coding modes correspond to existing standards, which renders communication systems employing the new AMR codec interoperable with other systems. Specifically, the 12.2 kbps mode is identical to the GSM EFR standard, the 12.2 and 7.4 kbps modes correspond to the US1 and EFR (IS-641) codecs of the TDMA (IS-136) system, and the 6.7 kbps mode is equivalent to the EFR codec of the Japanese PDC system [56]. For each of the codec modes, there exist corresponding channel codecs which perform the mapping between the speech source bits and the fixed number of channel coded bits.

In the forthcoming subsections, we will give a functional description of the codec operating in the 4.75 and 10.2 kbps modes. These two bitrates will be used in our investigations in order to construct a dual-mode speech transceiver.

7.13.3.2 Linear Prediction Analysis

A tenth order LPC analysis filter is employed to model the short-term correlation of the speech signal $s(n)$. Short-term prediction, or linear predictive analysis is performed once for each 20 ms speech frame using the Levinson–Durbin algorithm [158]. The LP coefficients are transformed to the LSF for quantisation and interpolation. The employment of the LSF [144] representation for quantisation of the LPC coefficients is motivated by their statistical properties. Within each speech frame, there is a strong intra-frame correlation due to the ordering property of neighbouring LSF values [158]. This essentially motivates the employment of vector quantisation. The interpolated quantised and unquantised LSFs are converted back to the LP filter coefficients in order to construct the synthesis and weighting

filters at each subframe. The synthesis filter shown in Figure 7.37 is used in the decoder to produce the reconstructed speech signal from the received excitation signal $u(n)$.

7.13.3.3 LSF Quantisation

In the AMR codec, the LSFs are quantised using prediction and SVQ [28]. The SVQ aims to split the ten-dimensional LSF vector into a number of reduced-dimension LSF subvectors, which simplifies the associated search complexity. Specifically, the proposed configuration minimises the average SD [116] within a given total complexity. Predictive vector quantisation is used [28] and the ten-component LSF vectors are split into three subvectors of dimension 3, 3 and 4. The bit allocations for the three subvectors will be described in Section 7.13.3.7 for the 4.75 and 10.2 kbps speech coding modes.

7.13.3.4 Pitch Analysis

Pitch analysis using the adaptive codebook approach models the long-term periodicity, i.e. the pitch of the speech signal. It produces an output which is a scaled version of the adaptive codebook of Figure 7.37 based on previous excitations. The excitation signal $u(n) = G_p u(n-\alpha) + G_c c_k(n)$ seen in Figure 7.37 is determined from its G_p-scaled history after adding the G_c-scaled fixed algebraic codebook vector c_k for every 5 ms subframe. The optimum excitation is chosen on the basis of minimising the MSE E_w over the subframe.

In an optimal codec, the fixed codebook index and codebook gain as well as the adaptive codebook parameters would all be jointly optimised in order to minimise E_w [169]. However, in practice this is not possible due to the associated excessive complexity. Hence, a sequential sub-optimal approach is applied in the AMR codec, where the adaptive codebook parameters are determined first under the assumption of zero fixed codebook excitation component, i.e. $G_c = 0$, since at this optimisation stage no fixed codebook entry was determined. Then, given that the adaptive codebook parameters were found which consist of the delay and gain of the pitch filter, the fixed codebook parameters are determined.

Most CELP codecs employ both so-called open-loop and closed-loop estimation of the adaptive codebook delay parameters, as is the case in the AMR codec. The open-loop estimate of the pitch period is used to narrow down the range of the possible adaptive codebook delay values and then the full closed-loop AbS procedure is used to find a high-resolution delay around the approximate open-loop position.

7.13.3.5 Fixed Codebook with Algebraic Structure

Once the adaptive codebook parameters are found, the fixed codebook is searched by taking into account the now known adaptive codebook vector. This sequential approach constitutes a trade-off between the optimal performance and the affordable computational complexity. The fixed codebook is searched by using an efficient non-exhaustive AbS technique, which is similar to that of the G.729 codec, minimising the MSE between the weighted input speech and the weighted synthesised speech.

The fixed or algebraic codebook structure is specified in Tables 7.20 and 7.21 for the 4.75 and 10.2 kbps codec modes, respectively [28]. The algebraic structure is based on the so-called interleaved single-pulse permutation (ISPP) code design [169]. The computational complexity of the fixed codebook search is substantially reduced when the codebook entries

Table 7.20: Pulse amplitudes and positions for 4.75 kbps AMR codec mode [28]. There are two excitation pulses in each track.

Subframe	Track	Pulse: Positions
1	1	i_0: 0,5,10,15,20,25,30,35
		i_1: 2,7,12,17,22,27,32,37
	2	i_0: 1,6,11,16,21,26,31,36
		i_1: 3,8,13,18,23,28,33,38
2	1	i_0: 0,5,10,15,20,25,30,35
		i_1: 3,8,13,18,23,28,33,38
	2	i_0: 2,7,12,17,22,27,32,37
		i_1: 4,9,14,19,24,29,34,39
3	1	i_0: 0,5,10,15,20,25,30,35
		i_1: 2,7,12,17,22,27,32,37
	2	i_0: 1,6,11,16,21,26,31,36
		i_1: 4,9,14,19,24,29,34,39
4	1	i_0: 0,5,10,15,20,25,30,35
		i_1: 3,8,13,18,23,28,33,38
	2	i_0: 1,6,11,16,21,26,31,36
		i_1: 4,9,14,19,24,29,34,39

$c_k(n)$ used are mostly zeros. The algebraic structure of the excitation having only a few non-zero pulses allows for a fast search procedure. The non-zero elements of the codebook are equal to either $+1$ or -1, and their positions are restricted to the limited number of excitation pulse positions, as portrayed in Tables 7.20 and 7.21 for the speech modes of 4.75 and 10.2 kbps, respectively.

Table 7.21: Pulse amplitudes and positions for 10.2 kbps AMR codec mode [28]. Each track contains two excitation pulses.

Track	Pulse	Positions
1	i_0, i_4	0, 4, 8, 12, 16, 20, 24, 28, 32, 36
2	i_1, i_5	1, 5, 9, 13, 17, 21, 25, 29, 33, 37
3	i_2, i_6	2, 6, 10, 14, 18, 22, 26, 30, 34, 38
4	i_3, i_7	3, 7, 11, 15, 19, 23, 27, 31, 35, 39

More explicitly, in the 4.75 kbps codec mode, the excitation codebook contains two non-zero pulse positions, denoted by i_0 and i_1 in Table 7.20. Again, all pulses can have the amplitudes $+1$ or -1. The 40 positions in a 5 ms duration subframe are divided into four so-called tracks. Two tracks are used for each 5 ms duration subframe with one pulse in each track. Different tracks may be used for each subframe as shown in Table 7.20 and hence one bit is needed to encode the track used. The two pulse positions, i_0 and i_1 are encoded

with 3 bits each, since both have eight legitimate positions in Table 7.20. Furthermore, the sign of each pulse is encoded with 1 bit. This gives a total of $1 + 2(3) + 2(1) = 9$ bits for the algebraic excitation encoding in a subframe.

In the 10.2 kbps codec mode of Table 7.21 there are four tracks, each containing two pulses. Hence, the excitation vector contains a total of $4 \times 2 = 8$ non-zero pulses. All the pulses can have amplitudes of $+1$ or -1 and the excitation pulses are encoded using a total of 31 bits.

Table 7.22: Bit allocation of the AMR speech codec at 4.75 and 10.2 kbps [28]. The bit positions for the 4.75 kbps mode, which are shown in round bracket, assist in identifying the corresponding bits in Figure 7.38 and 7.40.

Mode	Parameter	First subframe	Second subframe	Third subframe	Fourth subframe	Total per frame
4.75 kbps	LSFs					$8 + 8 + 7 = 23$ (1–23)
	Pitch delay	8 (24–31)	4 (49–52)	4 (62–65)	4 (83–86)	20
	Fixed codebook index	9 (32–40)	9 (53–61)	9 (66–74)	9 (87–95)	36
	Codebook gains	8 (41–48)		8 (75–82)		16
	Total					95/20 ms = 4.75 kbps
10.2 kbps	LSFs					$8 + 9 + 9 = 26$
	Pitch delay	8	5	8	5	26
	Fixed codebook index	31	31	31	31	124
	codebook gains	7	7	7	7	28
	Total					204/20 ms = 10.2 kbps

For the quantisation of the fixed codebook gain, an energy gain predictor is used in order to exploit the correlation between the fixed codebook gains in adjacent frames [28]. The fixed codebook gain is expressed as the product of the predicted gain based on previous fixed codebook energies and a correction factor. The correction factor is the parameter which is coded together with the adaptive codebook gain for transmission over the channel. In the 4.75 kbps mode the adaptive codebook gains and the correction factors are jointly vector quantised for every 10 ms, while this process occurs every subframe of 5 ms in the 10.2 kbps mode.

7.13.3.6 Post-processing

At the decoder, an adaptive postfilter [110] is used to improve the subjective quality of the reconstructed speech. The adaptive postfilter consists of a formant-based postfilter and a spectral tilt-compensation filter [28]. Adaptive gain control (AGC) is also used in order to compensate for the energy difference between the synthesised speech signal, which is the output from the synthesis filter and the post-filtered speech signal.

7.13.3.7 The AMR Codec's Bit Allocation

The AMR speech codec's bit allocation is shown in Table 7.22 for the speech modes of 4.75 and 10.2 kbps. For the 4.75 kbps speech mode, 23 bits are used to encode the LSFs by employing SVQ. As stated before, the LSF vector is split into three subvectors of dimension 3, 3 and 4, and each subvector is quantised using 8, 8 and 7 bits, respectively. This gives a total of 23 bits for the LSF quantisation of the 4.75 kbps codec mode.

The pitch delay is encoded using 8 bits in the first subframe and the relative delays of the other subframes are encoded using 4 bits. The adaptive codebook gain is quantised together with the above-mentioned correction factor of the fixed codebook gain for every 10 ms using 8 bits. As a result, 16 bits are used to encode both the adaptive- and fixed codebook gains. As described in Section 7.13.3.5, 9 bits were used to encode the fixed codebook indices for every subframe, which resulted in a total of 36 bits per 20 ms frame for the fixed codebook.

For the 10.2 kbps mode, the three LSF subvectors are quantised using 8, 9 and 9 bits, respectively. This implies that 26 bits are used to quantize the LSF vectors at 10.2 kbps, as shown in Table 7.22. The pitch delay is encoded with 8 bits in the first and third subframes and the relative delay of the other subframes is encoded using 5 bits. The adaptive codebook gain is quantised together with the correction factor of the fixed codebook gain using a 7-bit non-uniform vector quantisation scheme for every 5 ms subframe. The fixed codebook indices are encoded using 31 bits in each 5 ms duration subframe, in order to give a total of 124 bits for a 20 ms speech frame.

7.13.3.8 Codec Mode Switching Philosophy

In the AMR codec, the mode adaptation allows us to invoke a subset of at most four modes out of the eight available modes [258]. This subset is referred to as the active codec set (ACS). In the proposed BbB-AQAM/CDMA system the codec mode adaptation is based on the channel quality, which is expressed as the MSE at the output of the multi-user CDMA detector [253]. The probability of switching from one mode to another is typically lower than the probability of sustaining a specific mode.

Intuitively, frequent mode switching is undesirable due to the associated perceptual speech quality fluctuations. It is more desirable to have a mode selection mechanism that is primarily source-controlled, assisted by a channel-quality-controlled override. During good channel conditions the mode switching process is governed by the local phonetic character of the speech signal and the codec will adapt itself to the speech signal characteristics in an attempt to deliver the highest possible speech quality. When the channel is hostile or the network is congested, transceiver control or external network control can take over the mode selection and allocate less bits to source coding in order to increase the system's robustness or user capacity. By amalgamating the channel-quality motivated or network- and source-controlled processes, it results in a robust, high-quality system. Surprisingly, we found from our informal listening tests that the perceptual speech quality was not affected by the rate of codec mode switching, as will be demonstrated in Section 7.13.7. This is due to the robust ACELP structure, whereby the main bitrate reduction is related to the fixed codebook indices, as shown in Table 7.22 for the codec modes of 4.75 and 10.2 kbps.

As expected, the performance of the AMR speech codec is sensitive to transmission errors of the codec mode information. The corruption of the codec mode information that describes which codec mode has to be used for decoding leads to complete speech-frame losses,

since the decoder is unable to apply the correct mode for decoding the received bitstream. Hence, robust channel coding is required in order to protect the codec mode information and the recommended transmission procedures were discussed, for example, by Bruhn *et al.* [257]. Furthermore, in transceiver-controlled scenarios the prompt transmission of the codec mode information is required to react to sudden changes of the channel conditions. In our investigations we assume that the signalling of the codec mode information is free from corruption, so that we can concentrate on other important aspects of the system.

Let us now briefly focus our attention on the robustness of the AMR codec against channel errors.

7.13.4 The AMR Speech Codec's Error Sensitivity

In this section, we will demonstrate that some bits are significantly more sensitive to channel errors than others, and hence have to be better protected by the channel codec [169]. A commonly used approach in quantifying the sensitivity of a given bit is to invert this bit consistently in every speech frame and evaluate the associated SEGSNR degradation. The error sensitivity of various bits for the AMR codec determined in this way is shown in Figure 7.38 for the bitrate of 4.75 kbps. Again, Figure 7.38 shows more explicitly the bit sensitivities in each speech subframe for the bitrate of 4.75 kbps, with the corresponding bit allocations shown in Table 7.22. For the sake of visual clarity, Subframe 4 (bit positions 83–95) was not shown explicitly above, since it exhibited identical SEGSNR degradations to Subframe 2.

It can be observed from Figure 7.38 that the most sensitive bits are those of the LSF subvectors, seen at positions 1–23. The error sensitivity of the adaptive codebook delay is the highest in the first subframe, commencing at bit 24, as shown in Figure 7.38, which was encoded using 8 bits in Table 7.22. By contrast, the relative adaptive codebook delays in the next three subframes are encoded using 4 bits each, and a graceful degradation of the SEGSNR is observed in Figure 7.38 at bit positions 49–52, 62–65 and 83–86. The next group of bits is constituted by the 8 codebook gains in decreasing order of bit sensitivity, as seen in Figure 7.38 at bit positions 41–48 for Subframe 1 and 75–82 for Subframe 3. The least sensitive bits are related to the fixed codebook pulse positions, which were shown, for example, at bit positions 54–61 in Figure 7.38. This is because if one of the fixed codebook index bits is corrupted, the codebook entry selected at the decoder will differ from that used in the encoder only in the position of one of the non-zero excitation pulses. Hence the corrupted codebook entry will be similar to the original one. Therefore, the algebraic codebook structure used in the AMR codec is inherently quite robust to channel errors. The information obtained here will be used to design the bit-mapping procedure in order to assign the channel encoders according to the bit error sensitivities.

Despite its appealing conceptual simplicity, the above approach used for quantifying the error sensitivity of the various coded bits does not illustrate the error-propagation properties of different bits over consecutive speech frames. In order to obtain a better picture of the error-propagation effects, we also employed a more elaborate error-sensitivity measure. Here, for each bit we find the average SEGSNR degradation due to a single bit error both in the frame in which the error occurs and in consecutive frames. These effects are exemplified in Figure 7.39 for five different bits, where each of the bits belongs to a different speech codec parameter. More explicitly, Bit 1 represents the first bit of the first LSF subvector,

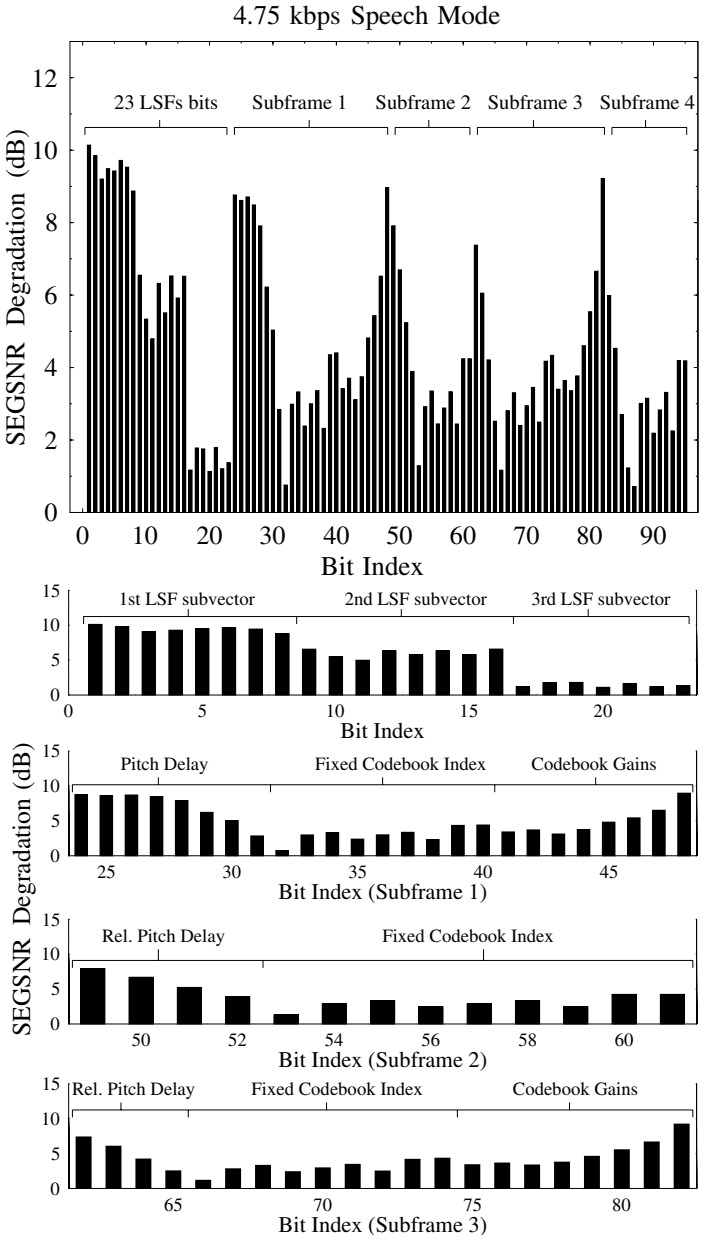

Figure 7.38: The SEGSNR degradations due to 100% bit error rate in the 95-bit, 20 ms AMR speech frame. The associated bit allocation can be seen in Table 7.22.

which shows some error propagation effects due to the interpolation between the LSFs over consecutive frames. The associated SEGSNR degradation dies away over six frames. Bit 24 characterised in Figure 7.39 is one of the adaptive codebook delay bits and the corruption of this bit has the effect of a more prolonged SEGSNR degradation over 10 frames. The fixed codebook index bits of Table 7.22 are more robust, as was shown in Figure 7.38 earlier. This argument is supported by the example of Bit 33 in Figure 7.39, where a small and insignificant degradation over consecutive frames is observed. A similar observation also applies to Bit 39 in Figure 7.39, which is the sign bit for the fixed codebook. By contrast, Bit 41 of the codebook gains produced a high and prolonged SEGSNR degradation profile.

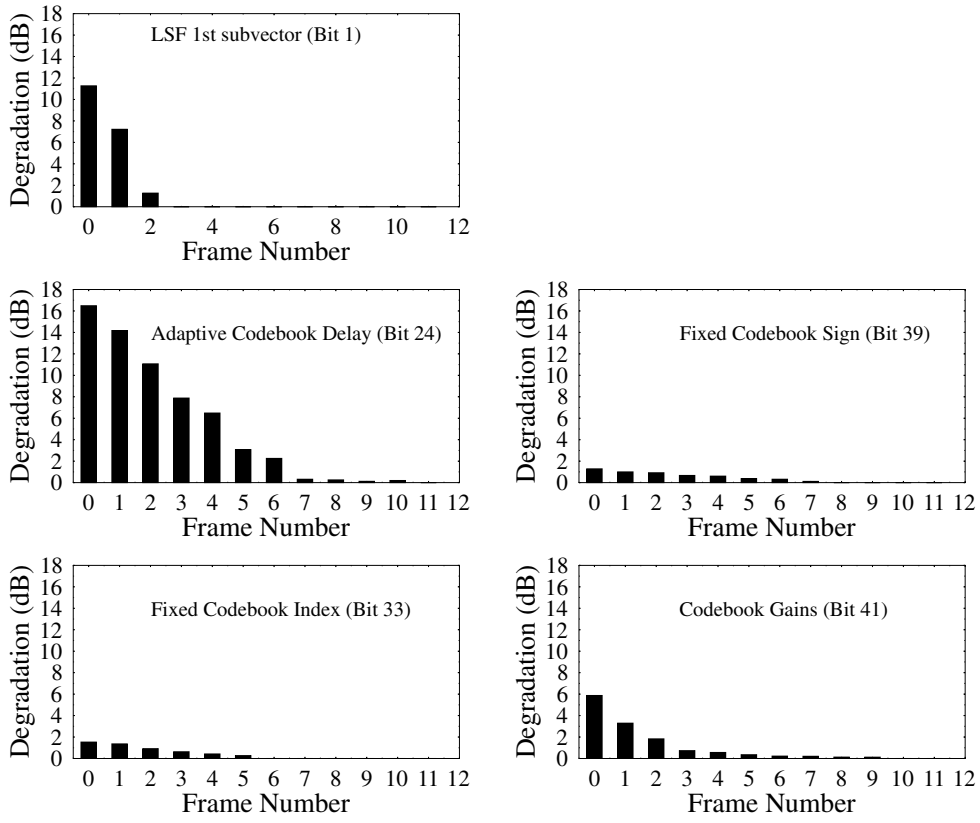

Figure 7.39: The SEGSNR degradation versus speech frame index for various bits.

We recomputed our bit-sensitivity results of Figure 7.38 using this second approach in order to obtain Figure 7.40, taking into account the error-propagation effects. More explicitly, these results were calculated by summing the SEGSNR degradations over all frames which were affected by the error. Again, these results are shown in Figure 7.40 and the associated bit positions can be identified with the aid of Table 7.22. The importance of the adaptive codebook delay bits became more explicit. By contrast, the significance of the LSFs was reduced, although still requiring strong error protection using channel coding.

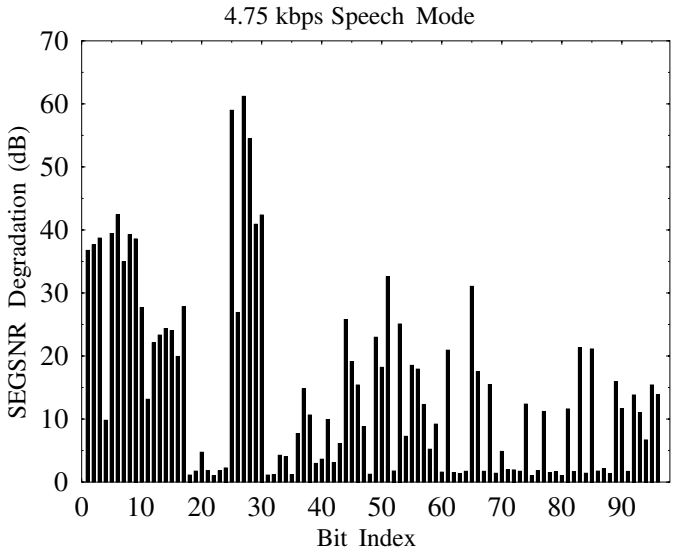

Figure 7.40: Average SEGSNR degradation due to single bit errors in various speech coded bits.

Having characterised the error sensitivity of the various speech bits, we will capitalise on this knowledge in order to assign the speech bits to various bit protection classes, as will be discussed in Section 7.13.5.2. In the next section we consider the channel coding aspects of our transceiver.

7.13.5 RRNS-based Channel Coding

7.13.5.1 RRNS Overview

In order to improve the performance of the system, we employ the novel family of RRNS codes for protecting the speech bits unequally, depending on their respective error sensitivities.

Since their introduction, RRNSs have been used for constructing fast arithmetics [259, 260]. In this section we exploit the error-control properties of non-binary systematic RRNS codes, which – similar to Reed–Solomon (RS) codes – exhibit maximum minimum distance properties [261,262]. Hence, RRNS codes are similar to RS codes [158]. However, the RRNS codes chosen in our design are more amenable to implementing short codes. More explicitly, in the context of RS codes, short codes are derived by inserting dummy symbols into full-length codes. This, however, requires the decoding of the full-length RS code. By contrast, RRNS codes simply add the required number of redundant symbols. Furthermore, RRNS codes allow us to use the low-complexity technique of residue dropping [262]. Both of these advantages will be augmented during our further discourse.

An RRNS(n, k) code has k so-called residues which host the original data bits and the additional $(n - k)$ redundant residues can be employed for error correction at the decoder. The coding rate of the code is k/n and the associated error-correction capability of the code

is $t = \lfloor (n-k)/2 \rfloor$ non-binary residues [261, 262]. At the receiver, soft decision [256] and residue dropping [263] decoding techniques are employed.

The advantages of the RRNS codes are simply stated here without proof due to lack of space [256, 263]. Since the so-called residues of the RRNS [259] can be computed independently from each other, additional residues can be added at any stage of processing or transmission. This has the advantage that the required coding power can be adjusted according to the prevalent BER of the transmission medium. For example, when the protected speech bits enter the wireless section of the network – where higher BERs than in the fixed network prevail – a number of additional redundant residues are computed and concatenated to the message for providing extra protection.

In our design, RRNS codes employing 5 bits per residue have been chosen. Three different RRNS codes having different code rates are used to protect the three different classes of speech bits. In addition, the RRNS codes employed are also switched in accordance with the modulation modes and speech rates used in our system. In Table 7.23, we have two sets of RRNS codes for the BPSK and 4QAM modes. For the most sensitive class I speech bits, we used a RRNS$(8, 4)$ code, which has a minimum free distance of $d_{\min} = 5$ [256] and a code rate of $1/2$. At the receiver, the soft metric of each received bit was calculated and soft decoding was applied. An extra information residue was added to the RRNS$(8, 4)$ code to generate the RRNS$(8, 5)$ code for the protection Class II. The extra residue enables us to apply one residue dropping [263] and soft decision decoding. The Class III bits are least protected, using the RRNS$(8, 6)$ code which has a minimum free distance of $d_{\min} = 3$ and a code rate of $2/3$. Only soft decision decoding is applied to this code.

Table 7.23: RRNS codes designed for two different modulation modes.

Class	RRNS code	Number of codewords	Databits	Total data bits	Total coded bits
		4.75 kbps/BPSK			
I	RRNS$(8, 4)$	2	40		
II	RRNS$(8, 5)$	1	25	95	160
III	RRNS$(8, 6)$	1	30		
		10.2 kbps/4QAM			
I	RRNS$(8, 4)$	3	60		
II	RRNS$(8, 5)$	1	25	205	320
III	RRNS$(8, 6)$	4	120		

7.13.5.2 Source-matched Error Protection

The error sensitivity of the 4.75 kbps AMR codec's source bits was evaluated in Figures 7.38 and 7.40. The same procedures were applied in order to obtain the error sensitivity for the source bits of the 10.2 kbps AMR codec. Again, in our system we employed RRNS channel coding and three protection classes were deemed to constitute a suitable trade-off between the system's complexity and performance. As shown in Table 7.23, three different RRNS codes

having different code rates are used to protect the three different classes of speech bits in a speech frame.

For the 4.75 kbps AMR speech codec, we divided the 95 speech bits into three sensitivity classes, Class I, II and III. Class I consists of 40 bits, while Classes II and III were allocated 25 and 30 bits, respectively. Then we evaluated the associated SEGSNR degradation inflicted by certain fixed channel BERs maintained in each of the classes using randomly distributed errors, while keeping bits of the other classes intact. The results of the SEGSNR degradations applying random errors are portrayed in Figure 7.41 for both the full-class and the triple-class system. It can be seen that Class I, which consists of the 40 most sensitive bits, suffers the highest SEGSNR degradation. Classes II and III – which are populated mainly with the fixed codebook index bits – are inherently more robust to errors. Note that in the full-class scenario the associated SEGSNR degradation is higher than that of the individual protection classes. This is due to having more errors in the 95-bit frame at a fixed BER, compared to the individual protection classes, since upon corrupting a specific class using a fixed BER, the remaining classes were intact. Hence the BER averaged over all the 95 bits was lower than that of the full-class scenario. For the sake of completeness, we decreased the BER of the full-class scheme so that on average the same number of errors were introduced into the individual classes as well as in the full-class scheme. In this scenario, it can be seen from Figure 7.41 that, as expected, the Class I scheme has the highest SEGSNR degradation, while the sensitivity of the full-class scheme is mediocre.

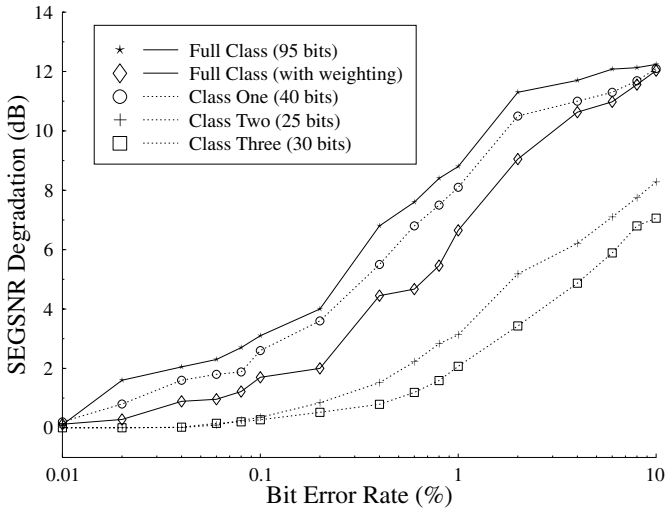

Figure 7.41: SEGSNR degradation versus average BER for the 4.75 kbps AMR codec for full-class and triple-class protection systems. When the bits of a specific class were corrupted, bits of the other classes were kept intact.

Similarly, the 204 bits of a speech frame in the 10.2 kbps AMR speech codec mode are divided into three protection classes. Class I is allocated the 60 most sensitive bits, while 25 and 119 bits are distributed to Classes II and III, in decreasing order of error sensitivity. Their respective SEGSNR degradation results against the BER are presented in Figure 7.42. Due to the fact that the number of bits in Class III is five times higher than in Class II, the

error sensitivity of Class III compared to Class II appeared higher. This occurs due to the non-trivial task of finding appropriate channel codes to match the source sensitivities, and as a result, almost 60% of the bits are allocated to Class III. Note that after the RRNS channel coding stage, an additional dummy bit is introduced in Class III, which contains 119 useful speech bits, as shown in Table 7.23. The extra bit can be used as a CRC bit for the purpose of error detection. Having considered the source and channel coding aspects, let us now focus our attention on transmission issues.

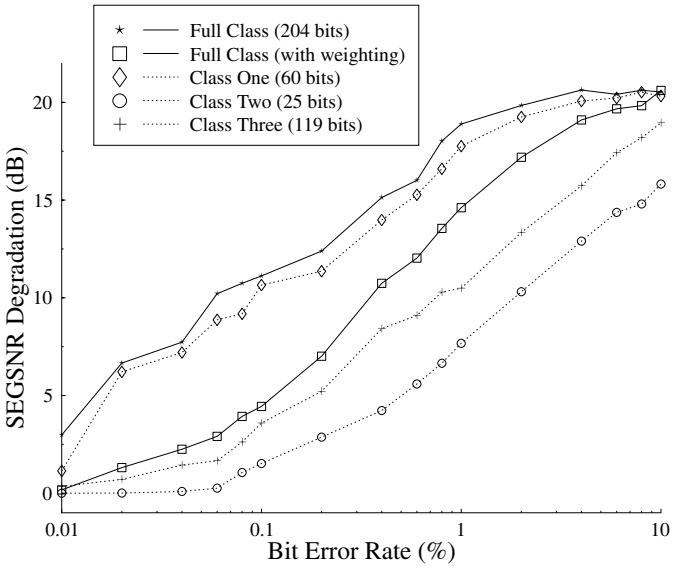

Figure 7.42: SEGSNR degradation versus average BER for the 10.2 kbps AMR codec for full class and triple-class protection systems. When the bits of a specific class were corrupted, bits of the other classes were kept intact.

7.13.6 Joint Detection Code Division Multiple Access

7.13.6.1 Overview

Joint detection receivers [264] constitute a class of multiuser receivers that were developed based on conventional equalization techniques [248] used for mitigating the effects of inter-symbol interference (ISI). These receivers utilise the CIR estimates and the knowledge of the spreading sequences of all the users in order to reduce the level of multiple-access interference (MAI) in the received signal.

By concatenating the data symbols of all CDMA users successively, as though they were transmitted by one user, we can apply the principles of conventional TDMA-oriented channel equalization [248] to multiuser detection. In our investigations, we have used the MMSE-BDFE proposed by Klein *et al.* [264], where the multiuser receiver aims to minimise the MSE between the data estimates and the transmitted data. A feedback process is incorporated, where the previous data estimates are fed back into the receiver in order to remove the residual interference and assist in improving the BER performance.

7.13.6.2 Joint Detection Based Adaptive Code Division Multiple Access

In QAM [248], n bits are grouped to form a signalling symbol and $m = 2^n$ different symbols convey all combinations of the n bits. These m symbols are arranged in a constellation to form the m-QAM scheme. In the proposed system we used the BbB-AQAM/CDMA modes of BPSK (2-QAM) and 4QAM, conveying 1 and 2 bits per symbol, respectively. However, for a given channel SNR, the BER performance degrades upon switching from BPSK to 4QAM, whilst doubling the throughput,

Previous research BbB-AQAM schemes for TDMA transmissions has been carried out by Webb and Steele [265], Sampei *et al*. [249], Goldsmith and Chua [266], as well as Torrance and Hanzo [267]. This work has been extended to wideband channels, where the received signal also suffers from ISI in addition to amplitude and phase distortions due to the fading channel. The received signal strength is not a good indicator of the wideband channel's quality, since the signal is also contaminated by ISI. Wong and Hanzo [268] proposed a wideband BbB-AQAM scheme, where a channel equalizer was used to mitigate the effects of ISI on the CIR estimate.

Here we propose to combine joint detection CDMA [264] with AQAM, by modifying the approach used by Wong and Hanzo [268]. Joint detection is particularly suitable for combining with AQAM, since the implementation of the joint detection algorithm does not require any knowledge of the modulation mode used [253]. Hence the associated complexity is independent of the modulation mode used.

In order to choose the most appropriate BbB-AQAM/CDMA mode for transmission, the SINR at the output of the MMSE-BDFE was estimated by modifying the SINR expression given in [264] exploiting the knowledge of the transmitted signal amplitude, g, the spreading sequence and the CIR. The data bits and noise values were assumed to be uncorrelated. The average output SINR was calculated for each transmission burst of each user. The conditions used to switch between the two AQAM/JD-CDMA modes were set according to their target BER requirements as

$$\text{Mode} = \begin{cases} \text{BPSK} & \text{SINR} < t_1 \\ \text{4QAM} & t_1 \leq \text{SINR}, \end{cases} \tag{7.58}$$

where t_1 represents the switching threshold between the two modes.

With the system elements described, we now focus our attention on the overall performance of the adaptive transceiver proposed.

7.13.7 System Performance

The simulation parameters used in our AQAM/JD-CDMA system are listed in Table 7.24. The channel profile used was the COST 207 BU channel [269] consisting of seven paths, where each path was faded independently at a Doppler frequency of 80 Hz.

The BER performance of the proposed system is presented in Figures 7.43, 7.44 and 7.45. Specifically, Figure 7.43 portrays the BER performance using the 4QAM modulation mode and employing the RRNS codes of Table 7.23 for a two-user JD-CDMA speech transceiver. As seen in Table 7.23, three different RRNS codes having different code rates are used to protect the three different classes of speech bits in the speech codec. The BER of the

Table 7.24: Transceiver parameters.

Parameter	Value
Channel type	COST 207 BU
Paths in channel	7
Doppler frequency	80 Hz
Spreading factor	16
Chip rate	2.167 MBaud
JD block size	26 symbols
Receiver type	MMSE-BDFE
AQAM type	Dual-mode (BPSK, 4QAM)
Channel codec	Triple-class RRNS
Channel-coded rate	8/16 kbps
Speech codec	AMR (ACELP)
Speech rate	4.75/10.2 kbps
Speech frame length	20 ms

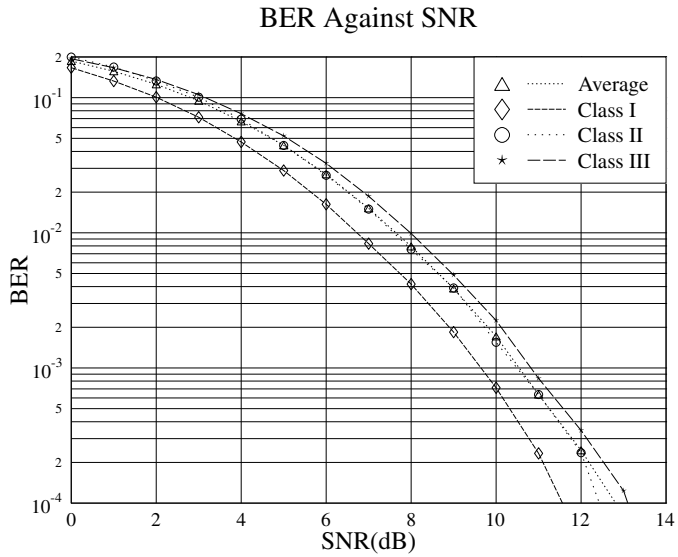

Figure 7.43: BER performance of 4QAM/JD-CDMA over the COST 207 BU channel of Table 7.24 using the RRNS codes of Table 7.23.

three protection classes is shown together with the average BER of the channel coded bits versus the channel SNR. The number of bits in these protection classes was 60, 25 and 120, respectively. As expected, the Class I subchannel exhibits the highest BER performance, followed by the Class II and Class III subchannels in decreasing order of BER performance. The corresponding BER results for the BPSK/JD-CDMA mode are shown in Figure 7.44.

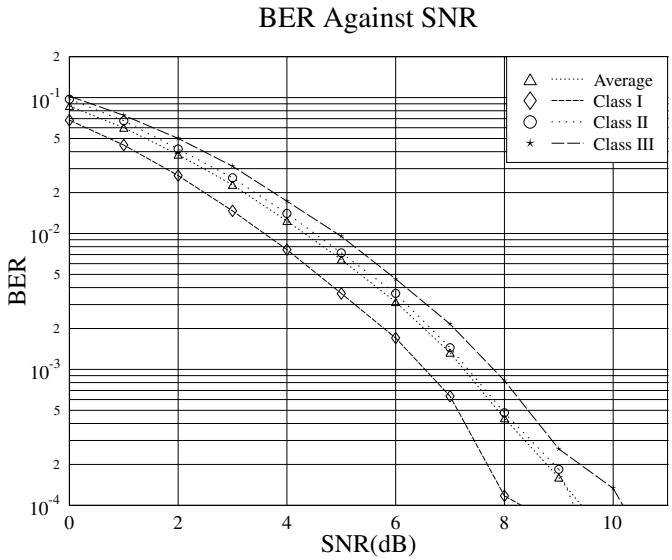

Figure 7.44: BER performance of BPSK/JD-CDMA over the COST 207 BU channel of Table 7.24 using the RRNS codes of Table 7.23.

In Figure 7.45, the average BER performance of the coded fixed-mode BPSK/JD-CDMA and 4QAM/JD-CDMA systems is presented along with that of the twin-mode AQAM/JD-CDMA system supporting two users and assuming zero-latency modem mode signalling. The performance of the AQAM scheme was evaluated by analyzing the BER and the throughput expressed in terms of the average number of bits per symbol (BPS) transmitted. The BER curve has to be read by referring to the vertical axis at the left of the figure, while the BPS throughput curve is interpreted by referring to the vertical axis at the right that is labelled BPS. At low channel SNRs the BER of the AQAM/JD-CDMA scheme mirrored that of BPSK/JD-CDMA, which can be explained using Figure 7.46. In Figure 7.46, the PDF of the AQAM/JD-CDMA modes versus channel SNR are plotted. As mentioned earlier, the results were obtained using an SINR switching threshold of 10.5 dB. We can see from the figure that at low *average* channel SNRs ($<$ 6dB), the threshold of 10.5 dB *instantaneous* SNR was seldom reached, and therefore BPSK/JD-CDMA was the predominant mode. Hence, the performance of the AQAM/JD-CDMA scheme was similar to BPSK/JD-CDMA. However, as the channel SNR increased, the BER performance of AQAM/JD-CDMA became better than that of BPSK/JD-CDMA, as shown in Figure 7.45. This is because the 4QAM mode is employed more often, reducing the probability of using BPSK, as shown in Figure 7.46. Since the mean BER of the system is the ratio of the total number of bit errors to the total number of bits transmitted, the mean BER will decrease with a decreasing number of bit errors or with an increasing number of transmitted bits. For a fixed number of symbols transmitted, the total number of transmitted bits in a frame is constant for fixed mode BPSK/JD-CDMA, while for AQAM/JD-CDMA the total number of transmitted bits increased when the 4QAM/JD-CDMA mode was used. Consequently, the average BER of the AQAM/JD-CDMA system was lower than that of the fixed-mode BPSK/JD-CDMA scheme.

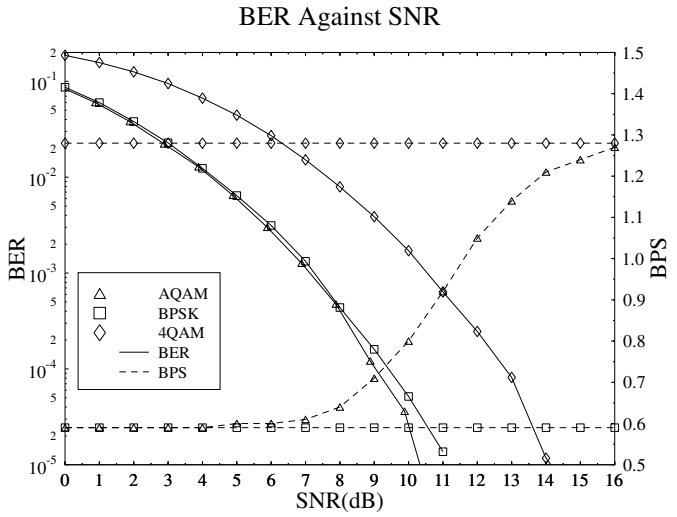

Figure 7.45: BER and BPS comparisons for fixed mode BPSK and 4QAM as well as for the AQAM/JD-CDMA system, using the RRNS codes of Table 7.23. The switching threshold for AQAM was set to 10.5 dB and the simulation parameters are listed in Table 7.24.

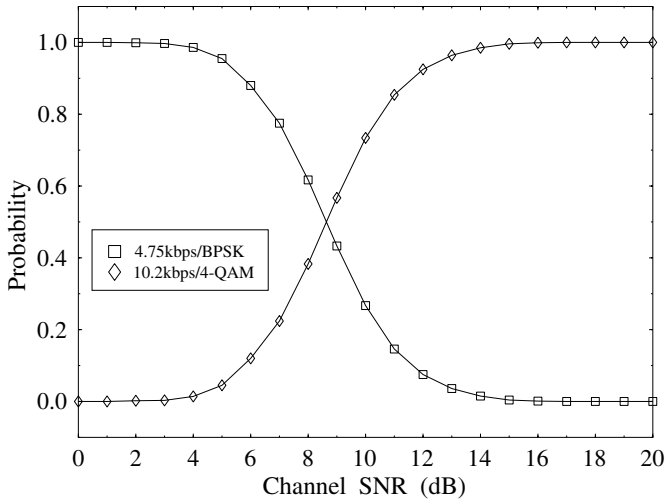

Figure 7.46: The probability of each modulation mode being chosen for transmission in a twin-mode (BPSK, 4QAM), two-user AQAM/JD-CDMA system using the parameters of Table 7.24.

The BPS throughput performance curve is also plotted in Figure 7.45. As expected, the number of BPS of both BPSK and 4QAM is constant for all channel SNR values. The BPS throughput is limited by the modulation scheme used and the coding rate of the RRNS codes seen in Table 7.23. For example, for 4QAM we have 2 BPS, but the associated channel code rate is $205/320$, as shown in Table 7.23, hence the effective throughput

of the system is $2 \times (205/320) = 1.28$ BPS. For AQAM/JD-CDMA, we can see from Figure 7.45 that the throughput is similar to that of BPSK/JD-CDMA at low channel SNRs. However, as the average channel SNR increased, more and more frames were transmitted using 4QAM/JD-CDMA and the average throughput increased gradually. At high average SNRs, the throughput of AQAM/JD-CDMA became similar to that of the 4QAM/JD-CDMA scheme.

The overall SEGSNR versus channel SNR performance of the proposed speech transceiver is displayed in Figure 7.47. Observe that the source sensitivity-matched triple-class 4.75 kbps BPSK/JD-CDMA system requires a channel SNR in excess of about 8 dB for nearly unimpaired speech quality over the COST207 BU channel of Table 7.24. When the channel SNR was in excess of about 12 dB, the 10.2 kbps 4QAM/JD-CDMA system outperformed the 4.75 kbps BPSK/JD-CDMA scheme in terms of both objective and subjective speech quality. Furthermore, at channel SNRs around 10 dB, where the BPSK and 4QAM SEGSNR curves cross each other in Figure 7.47, it was preferable to use the inherently lower quality but unimpaired mode of operation. In light of these findings, the application of the AMR speech codec in conjunction with AQAM constitutes an attractive trade-off in terms of providing users with the best possible speech quality under arbitrary channel conditions. Specifically, the 10.2 kbps 4QAM/JD-CDMA scheme has the highest source bitrate and thus exhibits the highest SEGSNR under error-free conditions. The 4.75 kbps BPSK/JD-CDMA scheme exhibits a lower source bitrate and correspondingly lower speech quality under error-free conditions. However, due to its less robust modulation mode, the 10.2 kbps 4QAM/JD-CDMA scheme is sensitive to channel errors and breaks down under hostile channel conditions where the 4.75 kbps BPSK/JD-CDMA scheme still exhibits robust operation, as illustrated in Figure 7.47.

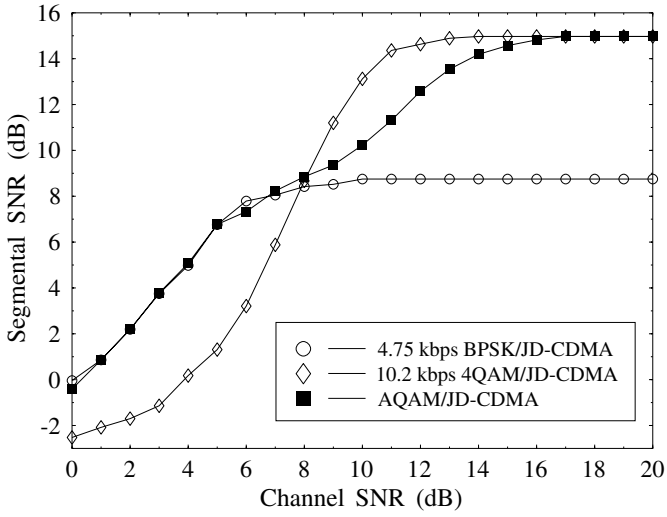

Figure 7.47: SEGSNR versus channel SNR.

In the context of Figure 7.47, ideally a system is sought that achieves a SEGSNR performance which follows the envelope of the SEGSNR curves of the individual BPSK/JD-

CDMA and 4QAM/JD-CDMA modes. The SEGSNR performance of the AQAM system is also displayed in Figure 7.47. We observe that AQAM provides a smooth evolution across the range of channel SNRs. At high channel SNRs in excess of 12–14 dB, the system operates predominantly in the 4QAM/JD-CDMA mode. As the channel SNR degrades below 12 dB, some of the speech frames are transmitted in the BPSK/JD-CDMA mode, which implies that the lower-quality speech rate of 4.75 kbps is employed. This results in a slightly degraded average speech quality, while still offering a substantial SEGSNR gain compared to the fixed-mode 4.75 kbps BPSK/JD-CDMA scheme. At channel SNRs below 10 dB, the performance of the 10.2 kbps 4QAM/JD-CDMA mode deteriorates due to the occurrence of a high number of errors, inflicting severe SEGSNR degradations. In these hostile conditions, the 4.75 kbps BPSK/JD-CDMA mode provides a more robust performance associated with a better speech quality. With the advent of the AQAM/JD-CDMA mode-switching regime the transceiver exhibits a less bursty error distribution than that of the conventional fixed-mode 4QAM modem, as it can be seen in Figure 7.48, where the error events of the BPSK/JD-CDMA scheme are also displayed.

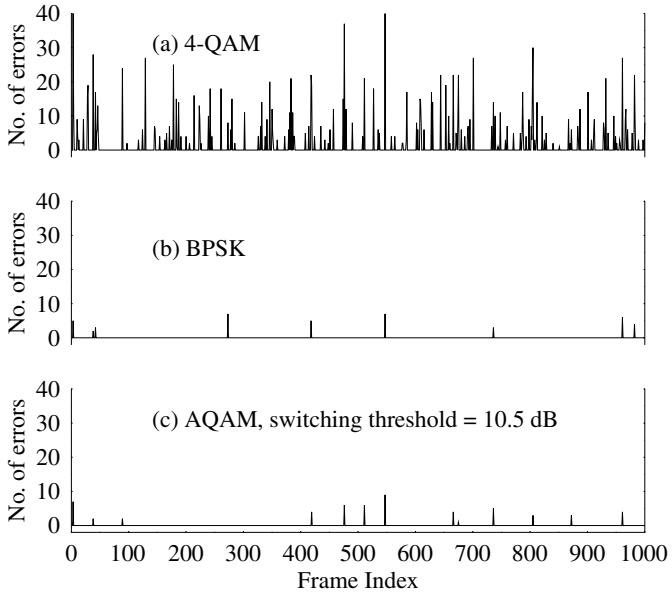

Figure 7.48: The comparison of the number of errors per frame versus 20 ms frame index for the (a) 4QAM, (b) BPSK and (c) AQAM/JD-CDMA systems with a switching threshold of 10.5 dB at channel SNR = 10 dB for 1000 frames over the COST207 BU channel of Table 7.24.

The benefits of the proposed dual-mode transceiver are further demonstrated in Figure 7.49, consisting of three graphs plotted against the speech-frame index, giving an insightful characterisation of the adaptive speech transceiver. Figure 7.49(a) shows a speech segment of 30 frames. In the AMR codec, a speech frame corresponds to a duration of 20 ms. In Figure 7.49(b), the SEGSNR versus frame index performance curves of the BPSK, 4QAM and AQAM/JD-CDMA schemes are shown, in both error-free and channel-impaired

scenarios. The SINR at the output of the MMSE-BDFE is displayed in Figure 7.49(c). The adaptation of the modulation mode is also shown in Figure 7.49(c), where the transceiver switches to the BPSK or 4QAM mode according to the estimated SINR using the switching threshold set to 10.5 dB.

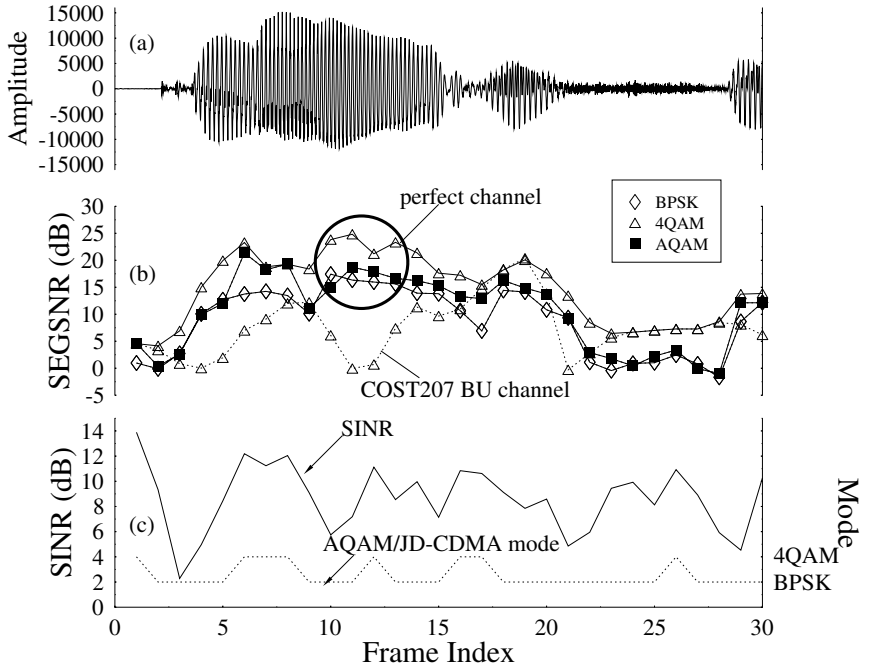

Figure 7.49: Characteristic waveforms of the adaptive system. (a) Time-domain speech signal; (b) SEGSNR in various transceiver modes; (c) SINR versus time and transceiver modes versus time over the COST207 BU channel of Table 7.24.

When transmitting in the less robust 4QAM mode using the higher-rate speech mode of 10.2 kbps, a sudden steep drop in the channel conditions – as portrayed at Frame 1 in Figure 7.49 – results in a high number of transmission errors, as also illustrated in Figure 7.48(a). This happens to occur during the period of voice onset in Figure 7.49, resulting in the corruption of the speech frame which has the effect of inflicting impairments to subsequent frames due to the error propagation effects of various speech bits, as alluded to in Section 7.13.4. It can be seen in Figure 7.49 that the high number of errors inflicted in the 4QAM mode during voiced speech segments caused a severe SEGSNR degradation at frame index 10 and the 10.2 kbps speech codec never fully recovered until the channel conditions expressed in terms of the SINR in Figure 7.49(c) improved. On the other hand, the significantly more robust 4.75 kbps BPSK/JD-CDMA scheme performed well under these hostile channel conditions, encountering a low number of errors in Figure 7.48(b), while transmitting at a lower speech rate, hence at an inherently lower speech quality. For the sake of visual clarity, the performance curves of BPSK/JD-CDMA and AQAM/JD-CDMA were not displayed in Figure 7.49(b) for the channel-impaired scenarios, since their respective graphs are almost identical to that of the error-free speech SEGSNR curves.

7.13.7.1 Subjective Testing

Informal listening tests were conducted in order to assess the performance of the AQAM/JD-CDMA scheme in comparison to the fixed-mode BPSK/JD-CDMA and 4QAM/JD-CDMA schemes. It is particularly revealing to investigate how the AQAM/JD-CDMA scheme performs in the intermediate channel SNR region between 7 dB and 11 dB. The speech quality was assessed using pairwise comparison tests. The listeners were asked to express a preference between two speech files A or B or neither. A total of 12 listeners were used in the pairwise comparison tests. Four different utterances were employed during the listening tests, where the utterances were a mixture of male and female speakers having American accents. Table 7.25 details some of the results of the listening tests.

Table 7.25: Details of the listening tests conducted using the pairwise comparison method, where the listeners were given a choice of preference between two speech files coded in different transmission scenarios.

		Preference (%)		
Speech material A	Speech material B	A	B	Neither
4.75 kbps (error free)	10.2 kbps (error free)	4.15	66.65	29.2
AQAM (9 dB)	4QAM (9 dB)	100	0.00	0.00
AQAM (9 dB)	4QAM (11 dB)	8.3	50.0	41.7
AQAM (9 dB)	BPSK (9 dB)	37.5	16.65	45.85
AQAM (12 dB)	4QAM(12 dB)	4.15	20.85	75.0
AQAM (12 dB)	4QAM(13 dB)	8.3	25.0	66.7
AQAM (12 dB)	BPSK(12 dB)	41.65	8.3	50.05

Through the listening tests we found that for the fixed-mode BPSK/JD-CDMA scheme, unimpaired perceptual speech quality was achieved for channel SNRs in excess of 7 dB. With reference to Figure 7.47, when the channel conditions degraded below 7 dB, the speech quality became objectionable due to the preponderance of channel errors. For the fixed mode 4QAM/JD-CDMA scheme, the channel SNR threshold was 11 dB, below which the speech quality started to degrade. The perceptual performance of AQAM/JD-CDMA was found superior to that of 4QAM/JD-CDMA at channel SNRs below 11 dB. Specifically, it can be observed from Table 7.25 that all the listeners preferred the AQAM/JD-CDMA scheme at a channel SNR of 9 dB due to the associated high concentration of channel errors in the less robust 4QAM/JD-CDMA scheme at the same channel SNR, resulting in a perceptually degraded reconstructed speech quality.

More explicitly, we opted for investigating the AQAM/JD-CDMA scheme at a channel SNR of 9 dB since – as shown in Figure 7.46 – it switches between BPSK/JD-CDMA and 4QAM/JD-CDMA according to the ratio of about 50:50. As the channel conditions improved to an SNR in excess of 11 dB, the 4QAM/JD-CDMA scheme performed slightly better, than AQAM/JD-CDMA due to its inherently higher SEGSNR performance under error-free conditions. Nonetheless, the AQAM/JD-CDMA scheme provided a good perceptual performance, as exemplified in Table 7.25 at a channel SNR of 12 dB, in comparison to the 4QAM/JD-CDMA scheme at the channel SNRs of both 12 dB and 13 dB. Here, only

about 20% of the listeners preferred the 4QAM/JD-CDMA scheme to the AQAM/JD-CDMA scheme, while the rest suggested that both sounded very similar. It can also be observed from Table 7.25 that the AQAM/JD-CDMA scheme performed better than BPSK/JD-CDMA for a channel SNR of 7 dB and above, while in the region below 7 dB, AQAM/JD-CDMA has a similar perceptual performance to that of BPSK/JD-CDMA. As shown in Table 7.26, we found that changing the mode switching frequency for every 1, 10 or 100 frames does not impair the speech quality either in objective SEGSNR terms or in terms of informal listening tests.

Table 7.26: Frame switching frequency versus SEGSNR.

Frame switching frequency	SEGSNR (dB)
1	11.38
10	11.66
100	11.68

7.13.8 Conclusions

In this section a joint-detection assisted adaptive CDMA speech transceiver has been designed that allows the system to switch between a set of different source and channel coders as well as transmission parameters, depending on the overall instantaneous channel quality. More explicitly the system was capable of dropping its source coding rate and speech quality under transceiver control in order to invoke a more error-resilient modem mode amongst less favourable channel conditions. The novel, high-quality AMR speech codec was operated at bitrates of 4.75 and 10.2 kbps and it was combined with source-sensitivity-matched RRNS-based channel codes.

The benefits of the multimode speech transceiver clearly manifest themselves in terms of supporting unimpaired speech quality under time-variant channel conditions, where a fixed-mode transceiver's quality would become severely degraded by channel effects. Hence the AQAM/JD-CDMA scheme achieved the best compromise between unimpaired error-free speech quality and robustness, which has also been verified by informal listening tests.

Future research in this area might be focussed on improving the performance of BbB-AQAM/CDMA transceivers using wideband speech codecs operated at multiple modes. Furthermore, more robust, turbo space–time coded multi-carrier, frequency-hopped BbB-AQAM/CDMA transceivers may be invoked for enhancing the system's performance.

7.14 Chapter Summary

In Sections 7.2–7.12 we described many CELP-related forward-adaptive standard speech codecs. We remind the reader of the stylised Figure 1.6, which was refined by Cox [1, 2], portraying the associated formally evaluated subjective quality in Figure 18.4 of Chapter 18.

Over the years many standard speech codecs have emerged, each of which characterised a certain state-of-the-art. The ultimate aim has been to find the best quality, complexity, delay

and robustness trade-off at the given stage of development. The standard codecs considered can be broadly divided in two classes, namely mobile radio speech codecs and ITU schemes. As seen in Figure 18.4, the G.-series ITU codecs endeavoured always to maintain a subjective speech quality in excess of a MOS of 4, while reducing the bitrate by a factor of two, which was only possible at the cost of increasing the implementational complexity. By contrast, the mobile radio codecs often had to accept a compromise associated with a lower speech quality, compromised, for example, by the complexity constraints imposed by limited battery-consumption.

The first standard CELP-based codec was the 4.8 kbps DoD scheme of Section 7.2, where differential pitch-lag encoding and oversampled lag representation was first invoked, in an attempt to minimise the prediction residual and to ensure near-constant relative lag-representation error across the entire legitimate lag range. This scheme invoked scalar quantisation of the LPC coefficients.

This arrangement was followed by the family of VSELP codecs, such as the 7.95 kbps IS-54 and the 6.7 kbps JDC schemes of Sections 7.3 and 7.4, which are closely related to each other. However, whereas the IS-54 codec possessed two fixed codebooks, the JDC codec had only one. Hence the former had a significantly higher combination of fixed codebook vectors and a higher associated complexity and speech quality. Similar to the DoD scheme, both of these codecs employed scalar quantisation of the LPC coefficients, which required in excess of 30 bits per LPC frame. The variable-rate Qualcomm codec of Section 7.5 also represented a similar stage of development to these codecs, using scalar quantisation of the LPC coefficients.

The half-rate codec family was spawned by the 3.45 kbps Japanese PSI-CELP scheme of Section 7.6, which was the first codec to invoke pitch-synchronous excitation. Another half-rate codec is the 5.6 kbps GSM coding arrangement of Section 7.7, which followed similar VSELP coding principles of the IS-54 and JDC codecs. However, in order to operate at such low rate, it employed four different excitation modes. In the unvoiced mode the combination of two 7-bit excitation codebooks were employed, but no long-term prediction was utilised. In voiced speech segments, long-term prediction was invoked and a larger single codebook of 512 entries was used. Furthermore, the reflection coefficients were quantised using a three-way SVQ, reducing the number of LPC quantisation bits below 30 per LPC frame. An advantageous feature of the reflection-coefficient based lattice predictors was that the quantisation error of the previous quantisation stages was partially taken into account by the later quantiser stages. The half-rate GSM codec also employed a multi-resolution long-term predictor.

Perhaps the most prominent speech codec to date is the G.729 scheme of Section 7.8 and its reduced-complexity version described in Section 7.9, employing ACELP principles. For the sake of maintaining a low delay it employs asymmetric windowing with a short, 40 samples or 5 ms look-ahead and differentially encoded pitch-lag. A sophisticated 18-bit LSF vector-quantiser is employed along with a refined perceptual error weighting filter. Both short-term and long-term post-filtering as well as spectral tilt compensation are invoked at the output of the decoder in order to improve the perceived speech quality. Strong consideration was given to the error concealment aspects in order to tolerate high error rates and frame loss rates. Similar techniques dominated the design of the enhanced full-rate GSM codec of Section 7.10 and that of the enhanced Pan-American codec referred to as the IS-136 scheme. The G.723.1 dual-rate codec of Section 7.12 also used ACELP coding in one of its operational

modes, while multipulse excited techniques were utilised in its other mode. The chapter was concluded by portraying the AMR speech codec in the context of an advanced burst-by-burst adaptive JD-CDMA speech transceiver.

Following the above brief chronological overview of the speech codec standardisation scene, in the next chapter we consider backward-adaptive codecs.

Chapter 8

Backward-adaptive Code Excited Linear Prediction

8.1 Introduction

In the previous chapter a range of medium- to high-delay forward-adaptive CELP codecs were described, which constituted different trade-offs in terms of speech quality, bitrate, delay and implementational complexity. In this chapter our work moves on to low delay, backward adaptive, codecs.

The outline of this chapter is as follows. In the next section we discuss why the delay of a speech codec is an important parameter, methods of achieving low-delay coding and problems with these methods. Much of the material presented is centered around the recently standardised 16 kbps G728 low-delay CELP codec [94, 109], and the associated algorithmic issues are described in Section 8.4. We then describe our attempts to extend the G728 codec in order to propose a low delay, programmable bitrate codec operating between 8 kbps and 16 kbps. In Section 8.6 we describe the potential speech quality improvements that can be achieved in such a codec by adding a LTP, albeit at the cost of increased error sensitivity due to error-propagation effects introduced by the backward-adaptive LTP. These error-propagation effects can be mitigated at system level, for example by introducing reliable error-control mechanisms, such as automatic repeat request (ARQ), an issue to be discussed in a system context at a later stage. In Section 8.7 we discuss means of training the codebooks used in our variable-rate codec to optimise its performance. Section 8.8 describes an alternative variable-rate codec which has a constant vector size. Finally, in Section 8.4.6 we describe the post-filtering which is used to improve the perceptual quality of our codecs.

8.2 Motivation and Background

The delay of a speech codec can be an important parameter for several reasons. In the public switched telephone network, four to two wire conversions lead to echoes, which will be

Voice and Audio Compression for Wireless Communications Second Edition
L. Hanzo, F. C. A. Somerville and J. P. Woodard

subjectively annoying if the echo is sufficiently delayed. Experience shows that the 57.5 ms speech coding and interleaving delay of the Pan-European GSM system already introduces an undesirable echoing effect and this value can be considered as the maximum tolerable margin in toll-quality communications. Even if echo cancellers are used, a high-delay speech codec makes the echo cancellation more difficult. Therefore if a codec is to be connected to the telephone network it is desirable that its delay should be as low as possible. If the speech codec used has a lower delay, then other elements of the system, such as bit interleavers, will have more flexibility and should be able to improve the overall quality of the system.

The one-way *coding delay* of a speech codec is defined as the time from when a sample arrives at the input of the encoder to when the corresponding sample is produced at the output of the decoder, assuming the bitstream from the encoder is fed directly to the decoder. This one-way delay is typically made up of three main components [94]. The first is the *algorithmic buffering delay* of the codec – the encoder operates on frames of speech, and must buffer a frame-lengths worth of speech samples before it can start encoding. The second component of the overall delay is the *processing delay* – speech codecs typically operate in just real time, and so it takes almost one frame length in time to process the buffered samples. Finally, there is the bit *transmission delay* – if the encoder is linked to the decoder by a channel with capacity equal to the bitrate of the codec then there will be a further time delay equal to the codec's frame length while the decoder waits to receive all the bits representing the current frame.

From the above description the overall one-way delay of the codec will be equal to about three times the frame length of the codec. However, it is possible to reduce this delay by careful implementation of the codec. For example, if a faster processor is used the processing delay can be reduced. Also, it may not be necessary to wait until the whole speech frame has been processed before we can start sending bits to the decoder. Finally, a faster communications channel, for example in a time division multiplexed system, can dramatically reduce the bit transmission delay. Other factors may also result in the total delay being increased. For example, the one sub-frame look-ahead used to aid the interpolation of the LSFs in our ACELP codecs described earlier will increase the overall delay by one sub-frame. Nonetheless, typically the one-way coding delay of a speech codec is assumed to be about 2.5 to 3 times the frame length of the codec.

It is obvious from the discussion above that the most effective way of producing a low-delay speech codec is to use as short a frame length as possible. Traditional CELP codecs have a frame length of 20 to 30 ms, leading to a total coding delay of at least 50 ms. Such a long frame length is necessary because of the forward adaption of the short-term synthesis filter coefficients. As explained in Chapter 6, a frame of speech is buffered, LPC analysis is performed and the resulting filter coefficients are quantised and transmitted to the decoder. As we reduce the frame length, the filter coefficients must be sent more often to the decoder and so more and more of the available bitrate is taken up by LPC information. Although efficient speech windowing and LSF quantisation schemes have allowed the frame length to be reduced to 10 ms (with a 5 ms look-ahead) in a candidate codec [160] for the CCITT 8 kbps standard, a frame length of between 20 and 30 ms is more typical. If we want to produce a codec with delay of the order of 2 ms, which was the objective for the CCITT 16 kbps codec [109], it is obvious that we cannot use forward adaption of the synthesis filter coefficients.

The alternative is to use backward adaptive LPC analysis. This means that rather than window and analyse present and future speech samples in order to derive the filter coefficients, we analyse previous quantised and locally decoded signals to derive the coefficients. These past quantised signals are available at both the encoder and decoder, and so no side information about the LPC coefficients needs to be transmitted. This allows us to update the filter coefficients as frequently as we like, with the only penalty being a possible increase in the complexity of the codec. Thus we can dramatically reduce the codec's frame length and delay.

As explained above, backward adaptive LPC analysis has the advantages of allowing us to dramatically reduce the delay of our codec, and removing the information about the filter coefficients that must be transmitted. This side information is usually about 25% of the bitrate of a codec, and so it is very helpful if it can be removed. However, backward adaption has the disadvantage that it produces filter coefficients which are typically degraded in comparison to those used in forward adaptive codecs. The degradation in the coefficients comes from two sources [270]:

(1) *Noise feedback*. In a backward-adaptive system the filter coefficients are derived from a quantised signal, and so there will be a feedback of quantisation noise into the LPC analysis which will degrade the performance of the coefficients produced.

(2) *Time mismatch*. In a forward-adaptive system the filter coefficients for the current frame are derived from the input speech signal for the current frame. In a backward-adaptive system we only have signals available from previous frames to use, and so there is a time mismatch between the current frame and the coefficients we use for that frame.

The effects of noise feedback especially increases dramatically as the bitrate of the codec is reduced and means that traditionally backward adaption has only been used in high bitrate, high quality, codecs. Recently, however, as researchers have attempted to reduce the delay of speech codecs, backward-adaptive LPC analysis has been used at bitrates as low as 4.8 kbps [271].

Clearly, the major design challenge associated with the ITU G728 codec was due to the complexity of its specifications, which are summarised in Table 8.1. Although many speech codecs can produce good speech quality at 16 kbps, at such a low rate most previous codecs have inflicted significantly higher delays than the targeted 2 ms. This is due to the fact that in order to achieve such a low rate in linear predictive coding, the up-date interval of the LPC coefficients must be around 20–30 ms. We have argued before in Section 4 that in the case of scalar LPC parameter coding, typically 36 bits/20 ms $= 1.8$ kbps channel capacity is required for their encoding. Hence, in the case of a 2 ms delay, forward-predictive coding is not a realistic alternative. We have also seen in Section 2.9 that low-complexity, low-delay ADPCM coding at 16 kbps is possible, which would satisfy the first two criteria of Table 8.1, but the last three requirements are not satisfied.

Chen *et al*. have contributed a major development to the state-of-art of speech coding [94], which satisfied all the design specifications and was standardised by the ITU [109]. In this section we will follow their discussions from [94] and [109, pp. 625–627], in order to describe the operation of their proposed backward-adaptive codec. The ITUs call for proposals stimulated a great deal of research, and a variety of candidate codecs were proposed, which typically satisfied some but not all requirements of Table 8.1.

Table 8.1: G 728 codec specifications.

Parameter	Specification
Bitrate	16 kbps
One-way delay	< 2 ms
Speech quality at BER $= 0$	< 4 QDU for one codec
	< 14 QDU for three tandems
Speech quality at	Better than that of
BER $= 10^{-3}$ and 10^{-2}	G721 32 kbps ADPCM
Additional requirement	Pass DTMF and CCITT
	No. 5, 6 and 7 signalling

Nonetheless, a range of endeavours – amongst others those of [106, 272] – have contributed in various ways towards the standardisation process.

CELP coding emerged as the best candidate, which relied on backward prediction using a filter order of 50. The coefficients of this high-order filter did not have to be transmitted, since they were extracted from the past decoded speech. As a benefit of using this high-order STP there was no need to include an error-sensitive LTP. The importance of adaptive post-filtering was underlined by Jayant and Ramamoorthy in [106, 107], where the quality of 16 kbps ADPCM-coded speech was reportedly improved, which was confirmed by Chen and Gersho [108].

The delay and high speech quality criteria were achieved by using a short STP-update interval of 20 samples or $20 \cdot 125\ \mu$s $= 2.5$ ms and an excitation vector length of 5 samples or $5 \cdot 125\ \mu$s $= 0.625$ ms. The speech quality was improved using a trained codebook rather than a stochastic one, which was 'virtually' extended by a factor of eight using a 3-bit codebook gain factor. Lastly, a further novel element of the codec is the employment of backward-adaptive gain scaling [273, 274], which will be discussed in more depth during our further discourse. In the next section we will describe the 16 kbps G728 low-delay CELP codec, and in particular the ways it differs from the ACELP codecs we have used previously. We will also attempt to quantify the effects of both noise feedback and time mismatch on the backward-adaptive LPC analysis used in this codec. Let us now focus our attention on specific details of the codec.

8.3 Backward-adaptive G728 Codec Schematic [94, 109]

The G728 encoder and decoder schematics are portrayed in Figures 8.1 and 8.2, respectively. The input speech segments are compared with the synthetic speech segments as in any AbS codec, and the error signal is perceptually weighted before the specific codebook entry associated with the lowest error is found in an exhaustive search procedure. For the G728 codec a vector size of 5 samples corresponding to $5 \cdot 125\ \mu$s $= 0.625$ ms was found appropriate in order to curtail the overall speech delay to 2 ms.

Having fixed the length of the excitation vectors, let us now consider the size of the excitation codebook. Clearly, the larger the codebook size, the better the speech quality, but

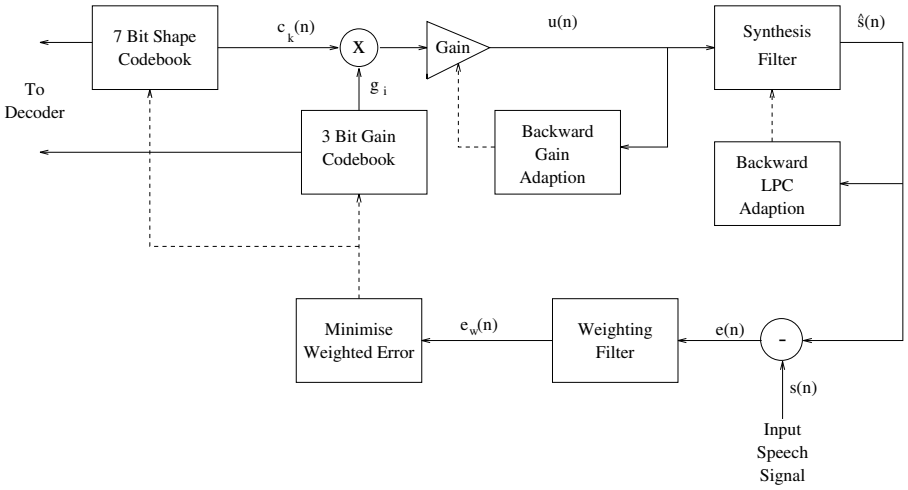

Figure 8.1: 16 kbps low-delay CCITT G728 encoder.

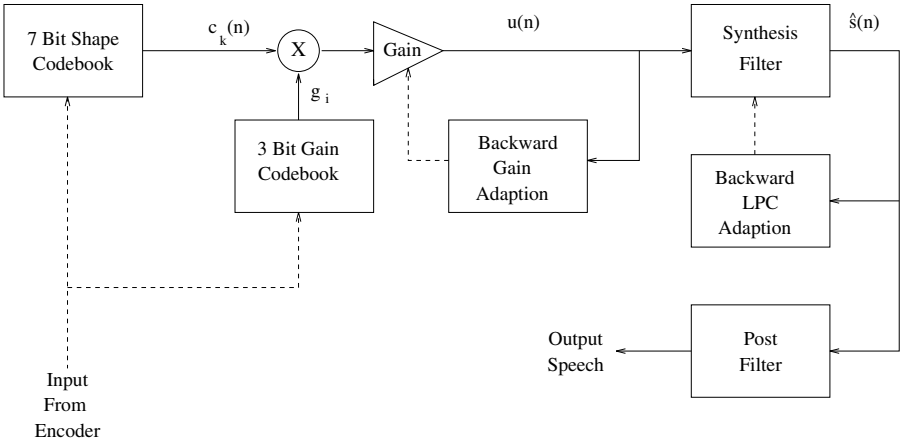

Figure 8.2: 16 kbps low-delay CCITT G728 decoder.

the higher the computational complexity and the bitrate. An inherent advantage of backward-adaptive prediction is that the LPC coefficients are not transmitted, hence a high-order filter can be used and we can dispense with using an LTP. Therefore, a design alternative is to allocate all bits transmitted to the codebook indices. Assuming a transmission rate of 16 kbps and an 8 kHz sampling rate, we are limited to a coding rate of 2 bits/sample or 10 bits/5 samples. Logically, the maximum possible codebook size is then $2^{10} = 1024$ entries. Recall that in the case of forward-predictive codecs the codebook gain was typically quantised using 4–5 bits, which allowed a degree of flexibility in terms of excitation envelope fluctuation. In this codec it is unacceptable to dedicate such a high proportion of the bitrate budget to the gain quantisation. Chen and Gersho [274] noted that this slowly

fluctuating gain information is implicitly available and hence predictable on the basis of previously scaled excitation segments. This prompted them to contrive a *backward-adaptive gain predictor*, which infers the required current scaling factor from its past values using predictive techniques. The actual design of this gain predictor will be highlighted at a later stage. Suffice to say here that this allowed the total of 10 bits to be allocated to the codebook index, although the codebook finally was trained as a 128–entry scheme in order to reduce the search complexity by a factor of eight, and the remaining three bits were allocated to quantise another multiplicative gain factor. This two-stage approach is suboptimum in terms of coding performance, since it replaces eight independent codebook vectors by eight identically shaped, different magnitude excitation vectors. Nonetheless, the advantage of the eight-fold reduced complexity outweighed the significance of a slight speech degradation.

As mentioned before, Chen and Gersho [274] decided to opt for a fiftieth-order backward-adaptive STP filter in order to achieve the highest possible prediction gain, and to be able to dispense with LTP filtering, without having to transmit any LPC coefficients. However, the complexity of the Levinson–Durbin algorithm used to compute the LPC coefficients is proportional to the square of the filter order $p = 50$, which constitutes a high complexity. This is particularly so if the LPC coefficients are updated for each 5-sample speech vector. In order to compromise, an update interval of 20 samples or 2.5 ms was deemed to be appropriate. This implies that the LPC parameters are kept constant for the duration of four excitation vectors, which is justifiable since the speech spectral envelope does not vary erratically.

A further ramification of extending the LPC update interval is that the time-lag between the speech segment to be encoded and the spectral envelope estimation is increased. This is a disadvantage of backward-adaptive predictive systems, since in backward-adaptive schemes the current speech frame is used for the speech spectral estimation. On the same note, backward-adaptive arrangements have to infer the LPC coefficients from the past decoded speech, which is prone to quantisation effects. In the case of high-rate, high-quality coding this is not a significant problem, but it is aggravated by error-propagation effects, inflicting future impairments in future LPC coefficients. Hence, at low bitrates, below 8 kbps, backward-adaptive schemes found only limited favour in the past. These effects can be readily quantified using the unquantised original delayed speech signal and the quantised but not delayed speech signal to evaluate the codec's performance. Woodard and Hanzo [183] found that the above factors degraded the codec's SEGSNR performance by about 0.2 dB due to quantisation noise feedback, and by about 0.7 dB due to the time mismatch, yielding a total of 0.9 dB SEGSNR degradation. At lower rates and higher delays these degradations become more dominant. Let us now concentrate our attention on specific algorithmic issues of the codec schematics given in Figures 8.1 and 8.2.

8.4 Backward-adaptive G728 Coding Algorithm [94, 109]

8.4.1 G728 Error Weighting

In contrast to the more conventional *error weighting filter* introduced in Equation (3.8), the G728 codec employs the filter [108]

$$W(z) = \frac{1 - A(z/\gamma_1)}{1 - A(z/\gamma_2)} = \frac{1 - \sum_{i=1}^{10} a_i \gamma_1^i}{1 - \sum_{i=1}^{10} a_i \gamma_2^i}, \tag{8.1}$$

where $\gamma_1 = 0.9$ and $\gamma_2 = 0.6$, and the filter is based on a tenth-order LPC analysis carried out using the unquantised input speech. This was necessary to prevent the introduction of spectral distortions due to quantisation noise. Since the error weighting filter is only used at the encoder, where the original speech signal is available, this error weighting procedure does not constitute any problem at all. The choice of the parameters $\gamma_1 = 0.9$ and $\gamma_2 = 0.6$ was motivated by the requirement of optimising the tandemised performance for three asynchronous coding operations. Explicitly, listening tests proved that the pair $\gamma_1 = 0.9$ and $\gamma_2 = 0.4$ gave a better single-coding performance, but for three tandemed codec $\gamma_2 = 0.6$ was found to exhibit a superior performance. The coefficients of this weighting filter are computed from the windowed input speech, and the particular choice of the window function will be highlighted in the next section.

8.4.2 G728 Windowing

The choice of the windowing function plays an important role in capturing the time-variant statistics of the input speech which in turn influences the subsequent spectral analysis. In contrast to more conventional Hamming windowing, Chen *et al.* [94] proposed using a hybrid window, which is constituted by an exponentially decaying long-term past history section and a non-recursive section, as depicted in Figure 8.3.

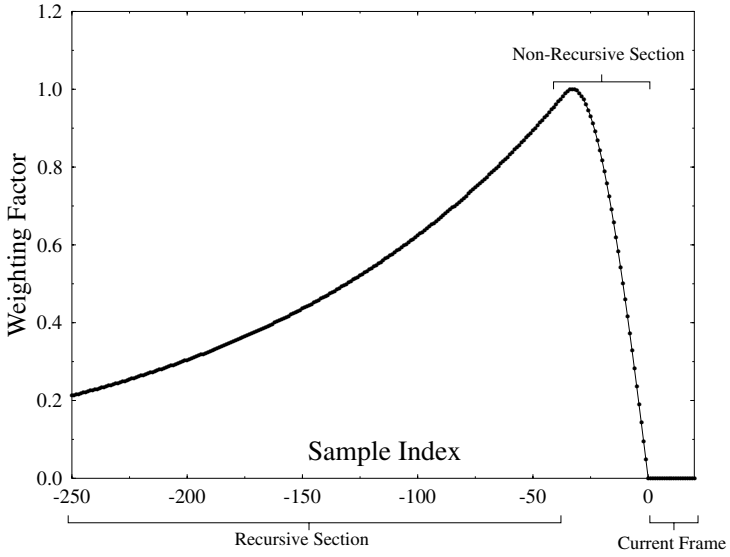

Figure 8.3: Windowing function used in the backward-adaption of the synthesis filter.

Let us assume that the LPC analysis frame size is $L = 20$ samples, which hosts the samples $s(m)$, $s(m+1), \ldots, s(m+L-1)$, as portrayed in Figure 8.3. The N-sample window section immediately preceding the current LPC frame of L samples is then termed as the non-recursive portion, since it is described mathematically with the help of a sinusoid non-recursive function of $w(n) = -\sin[c(n-m)]$, where the sample index n is limited to the previous N samples $(m - N \leq n \leq (m-1))$. In contrast, the recursive section of the

window function weights the input speech samples preceding $(m - N)$, as suggested by Figure 8.3, using a simple negative exponential function given by

$$w(n) = b \cdot \alpha^{-[n-(m-N-1)]} \quad \text{if } n \leq (m - N - 1), \tag{8.2}$$

where $0 < b$, $\alpha < 1$. Evaluating Equation (8.2) for sample index values at the left of $n = (m - N)$ in Figure 8.3 yields weighting factors of $b, b \cdot \alpha, b \cdot \alpha^2, \ldots$. In summary, the hybrid window function can be written as

$$w_m(n) = \begin{cases} f_m(n) = b \cdot \alpha^{-[n-(m-N-1)]} & \text{if } n \leq (m - N - 1) \\ g_m(n) = -\sin[c(n - m)] & \text{if } (m - N) \leq n \leq (m - 1) \\ 0 & \text{if } n \geq m. \end{cases} \tag{8.3}$$

It is important to maintain a seamless transition between the recursive and non-recursive section of the window function in order to avoid introducing spectral sidelobes which would be incurred in the case of a non-continuous derivative at $n = (m - N)$ [275], where the two sections are joined.

Chen *et al.* also specify in the Recommendation [109] how this recursive windowing process can be exploited to calculate the required autocorrelation coefficients, using the windowed speech signal given by

$$s_m(n) = s(n) \cdot w_m(n), \tag{8.4}$$

where the subscript m indicates the commencement of the current L-sample window in Figure 8.3.

In the case of an Mth order LPC analysis at instant m, the autocorrelation coefficients $R_m(i)$ $i = 0, 1, 2, \ldots, M$ are required by the Levinson–Durbin algorithm, where

$$\begin{aligned} R_m(i) &= \sum_{n=-\infty}^{m-1} s_m(n) \cdot s_m(n - i) \\ &= \sum_{n=-\infty}^{m-N-1} s_m(n) \cdot s_m(n - i) + \sum_{n=m-N}^{m-1} s_m(n) \cdot s_m(n - i). \end{aligned} \tag{8.5}$$

Upon taking into account Equations (8.3) and (8.4) in Equation (8.5), the first term of Equation (8.5) can be written as

$$r_m(i) = \sum_{n=-\infty}^{m-N-1} s(n) \cdot s(n - i) \cdot f_m(n) \cdot f_m(n - i), \tag{8.6}$$

which constitutes the recursive component of $R_m(i)$, since it is computed from the recursively weighted speech segment. The second term of Equation (8.5) relates to the section given by $(m - N) \leq n \leq (m - 1)$ in Figure 8.3, which is the non-recursive section. The N-component sum of the second term is computed for each new N-sample speech segment, while the recursive component can be calculated recursively following the procedure proposed by Chen *et al* [94, 109] as outlined below.

Assuming that $r_m(i)$ is known for the current frame we proceed to the frame commencing at sample position $(m + L)$, which corresponds to the next frame in Figure 8.3, and express $r_{m+L}(i)$ in analogy with Equation (8.5) as

$$\begin{aligned} r_{m+L}(i) &= \sum_{n=-\infty}^{m-1} s_m(n) \cdot s_m(n-i) \\ &= \sum_{n=-\infty}^{m-N-1} s_m(n) \cdot s_m(n-i) + \sum_{n=m-N}^{m-1} s_m(n) \cdot s_m(n-i) \\ &= \sum_{n=-\infty}^{m-N-1} s(n) \cdot f_m(n) \cdot \alpha^L \cdot s(n-i) f_m(n-i) \alpha^L \\ &\quad + \sum_{n=m-N}^{m+L-N-1} s_{m+L}(n) \cdot s_{m+L}(n-i) \\ &= L^{2L} r_m(i) + \sum_{n=,-N}^{m+L-N-1} s_{m+L}(n) \cdot s_{m+L}(n-i). \end{aligned} \tag{8.7}$$

This expression is the required recursion which facilitates the computation of $r_{m+L}(i)$ on the basis of $r_m(i)$. Finally, the total autocorrelation coefficient $R_{m+L}(i)$ is generated with the help of Equation (8.5). When applying the above general hybrid windowing process to the LPC analysis associated with the error weighting, the following parameters are used: $M = 10$, $L = 20$, $N = 30$, $\alpha = (1/2)40 \approx 0.983$, yielding $\alpha^{2L} = \alpha^{40} = 1/2$. Then the Levinson–Durbin algorithm is invoked in the usual manner, as described by Equation (2.25) and by the flow chart of Figure 2.3.

The performance of the synthesis filter in terms of its prediction gain and the SEGSNR of the G728 codec using this filter, is shown against the filter order p in Figure 8.4 for a single sentence spoken by a female. Also shown in Table 8.2 is the increase in performance obtained when p is increased above 10, which is the value most commonly used in AbS codecs. It can be seen that there is a significant performance gain due to increasing the order from 10 to 50, but little additional gain is achieved as p is further increased.

Table 8.2: Relative performance of the synthesis filter as p is increased.

Filter order p	Δ Prediction gain (dB)	Δ SEGSNR (dB)
10	0.0	0.0
25	+0.68	+0.70
50	+1.05	+1.21
75	+1.12	+1.41
100	+1.11	+1.46
150	+1.10	+1.42

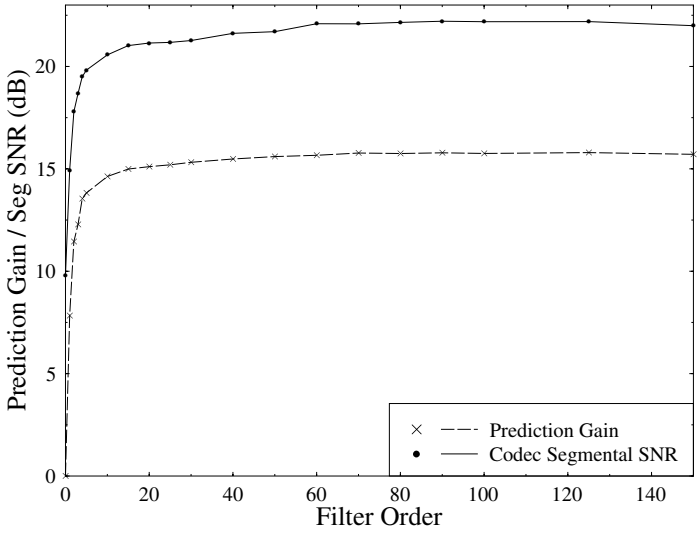

Figure 8.4: Performance of the synthesis filter in a G728-like codec.

We also tested the degradations in the synthesis filter's performance at $p = 50$ due to backward adaption being used. This was done as follows. To measure the effect of quantisation noise feedback we updated the synthesis filter parameters exactly as in G728 except we used the previous speech samples rather than the previous reconstructed speech samples. To measure the overall effect of backward adaption we updated the synthesis filter using both past and present speech samples. The improvements obtained in terms of the SEGSNR of the codec and the filter's prediction gain are shown in Table 8.3. We see that due to the high SNR of the G728 codec, noise feedback has relatively little effect on the performance of the synthesis filter. The time mismatch gives a more significant degradation in the codec's performance. Note, however, that the forward-adaptive figures given in Table 8.3 could not be obtained in reality because they do not include any effects of the LPC quantisation that must be used in a real forward-adaptive system.

Table 8.3: Effects of backward adaption of the synthesis filter.

	Δ Prediction gain (dB)	Δ SEGSNR (dB)
No noise feedback	$+0.50$	$+0.18$
No time mismatch	$+0.74$	$+0.73$
Use forward adaption	$+1.24$	$+0.91$

Having familiarised ourselves with the hybrid windowing process in general terms we note that this process is invoked during three different stages of the G728 codec's operation. The next scheme, where it is employed using a different set of parameters, is the code book gain adaption arrangement, which will be elaborated on in the next section.

8.4.3 Codebook Gain Adaption

Let us describe the codebook vector scaling process at iteration n with the help of

$$e(n) = \delta(n) \cdot y(n), \tag{8.8}$$

where $y(n)$ represents one of the 1029 5-sample codebook vectors, $\delta(n)$ the scaling gain factor and $l(n)$ the scaled excitation vector. The associated RMS values are denoted by $\delta_e(n)$ and $\delta_y(n)$, respectively. As regards to the RMS values we also have

$$\delta_e(n) = \delta(n) \cdot \delta_y(n) \tag{8.9}$$

or in logarithmic domain,

$$\log[\delta_e(n)] = \log[\delta(n)] + \log[\delta y(n)].$$

The philosophy of the gain prediction scheme is to exploit the correlation between the current required value of $\delta(u)$ and its past history, which is a consequence of the slowly varying speech envelope. Chen and his colleagues suggested using a tenth-order predictor operating on the sequence $\log[\delta_e(n-1)], \log[\delta_e(n-2)], \ldots, \log[\delta_e(n-10)]$ in order to predict $\log[\delta(n)]$. This can be written more formally as

$$\log[\delta(n)] = \sum_{i=1}^{10} p_i \log[\delta_e(n-i)], \tag{8.10}$$

where the coefficient p_i, $i = 1, \ldots, 10$, are the predictor coefficients.

When using a tenth-order predictor relying on 10 gain estimates derived for 5 speech samples each, the memory of this scheme is 50 samples, which is identical to that of the STP. This predictor, therefore, analyses the same time interval as the STP and assists in modelling any latent residual pitch periodicity. The excitation gain is predicted for each speech vector n from the 10 previous gain values on the basis of the current set of predictor coefficients p_i, $i = 1, \ldots, 10$. These coefficients are then updated using conventional LPC analysis every fourth 5-sample speech vector, or every 20 samples.

The schematic of the gain prediction scheme is depicted in Figure 8.5, where the gain-scaled excitation vector $e(n)$ is buffered and the logarithm of its RMS value is computed in order to express it in terms of dB. At this stage the average excitation gain of voiced speech, namely an offset of 32 dB, is subtracted in order to remove the bias of the process, before hybrid windowing and LPC analysis takes place.

The *bandwidth expansion* module modifies the predictor coefficients $\hat{\alpha}_i$ computed according to

$$\alpha_i = \left(\frac{29}{32}\right)^i \hat{\alpha} = 0.90625^i \hat{\alpha}_i, \quad i = 1, \ldots, 10. \tag{8.11}$$

It can be shown that this process is equivalent in the z-domain to moving all the poles of the corresponding synthesis filter towards the origin according to the factor $(29/32)$. Poles outside the unit circle imply instability, while those inside but close to the unit circle are associated with narrow but high spectral prominances. Moving these poles further away from the unit circle expands their bandwidth and mitigates the associated spectral peaks.

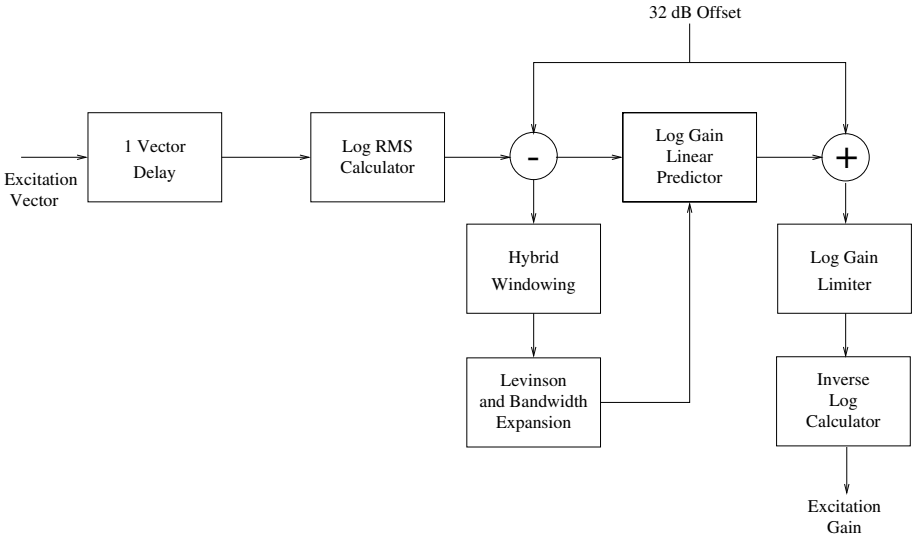

Figure 8.5: G728 excitation gain predictor scheme.

If the encoder and decoder are misaligned, for example because the decoder selected the wrong codebook vector due to channel errors, both the speech synthesis filter and the gain prediction scheme will be 'deceived'. The above bandwidth expansion process assists in reducing the error sensitivity of the predictive coefficients by artificially modifying them at both the encoder and decoder using a near-unity leakage factor.

Returning to Figure 8.5, finally the modified predictor coefficients of Equation (8.11) are employed to predict the required logarithmic gain $\log[\sigma(n)]$. Before the gain factor is used in the current frame, its 32 dB offset must be restored, while its extreme values are limited to the range of 0–60 dB and finally $\sigma(n)$ is restored from the logarithmic domain. The linear gain factor is limited accordingly to the range 1–1000.

The efficiency of the backward gain adaption can be seen from Figure 8.6. This shows the PDFs, on a log scale for clarity, of the excitation vector's optimum gain both with and without gain adaption. Here the optimum vector gain is defined as

$$\sqrt{\frac{1}{vs}\sum_{n=0}^{vs} g^2 c_k^2(n)}, \tag{8.12}$$

where g is the unquantised gain chosen in the codebook search. For a fair comparison both PDFs were normalised to have a mean of one. It can be seen that gain adaption produces a PDF which peaks around one and has a shorter tail and a reduced variance. This makes the quantisation of the excitation vectors significantly easier. Figure 8.7 shows the PDFs of the optimum unquantised codebook gain g and its quantised value when backward gain adaption is used. It can be seen that most of the codebook gain values have a magnitude less than or close to one, but it is still necessary to allocate two gain quantiser levels for the infrequently used high magnitude gain values.

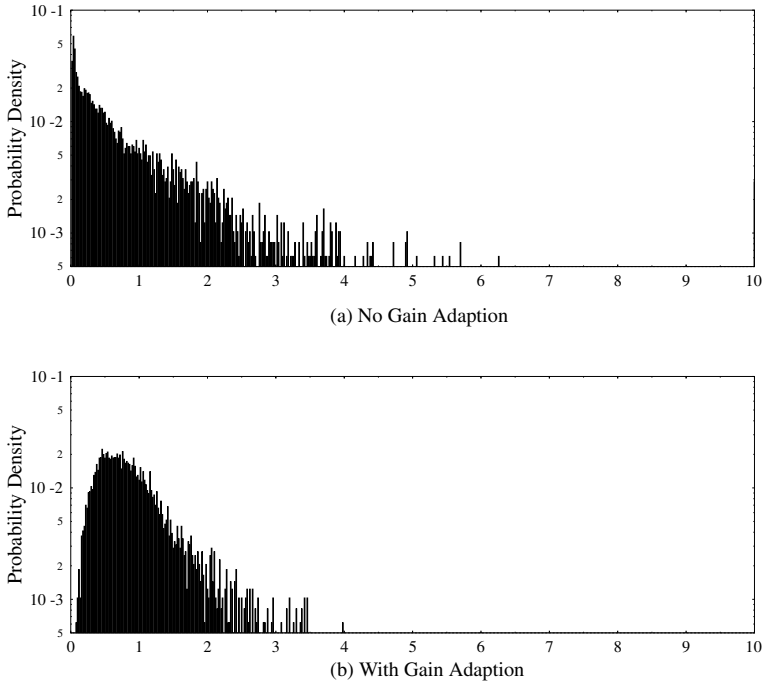

Figure 8.6: PDFs of the normalised codebook gains (a) with and (b) without backward gain adaption.

By training a split 7/3 bit shape/gain codebook, as described in Section 8.7, for G728-like codecs both with and without gain adaption we found that the gain adaption increased the SEGSNR of the codec by 2.7 dB, and the weighted SEGSNR by 1.5 dB. These are very significant improvements, especially when it is considered that the gain adaption increases the encoder complexity by only about 3%.

8.4.4 G728 Codebook Search

The standard recognised technique of finding the optimum excitation in CELP codecs is to generate the so-called *target vector* for each input speech vector to be encoded and match the filtered candidate excitation sequences to the target, as will be explained in our forthcoming discourse. During synthesising the speech signal using each codebook vector, the excitation vectors are filtered through the concatenated LPC synthesis filter and the error weighting filter, which are described by their combined impulse response as seen in Figure 8.1. Since this filter complex is an IIR system, upon exciting it with a new codebook entry its output signal will be the super-position of the response due to the current entry plus the response due to all previous entries. We note that the latter contribution is not influenced by the current input vector and hence this *filter memory contribution* plays no role in identifying the best codebook vector for the current 5-sample frame. Therefore the filter memory contribution due to previous inputs has to be buffered before a new excitation is input and subtracted from the current input speech frame in order to generate the target vector $x(n)$, to which all filtered

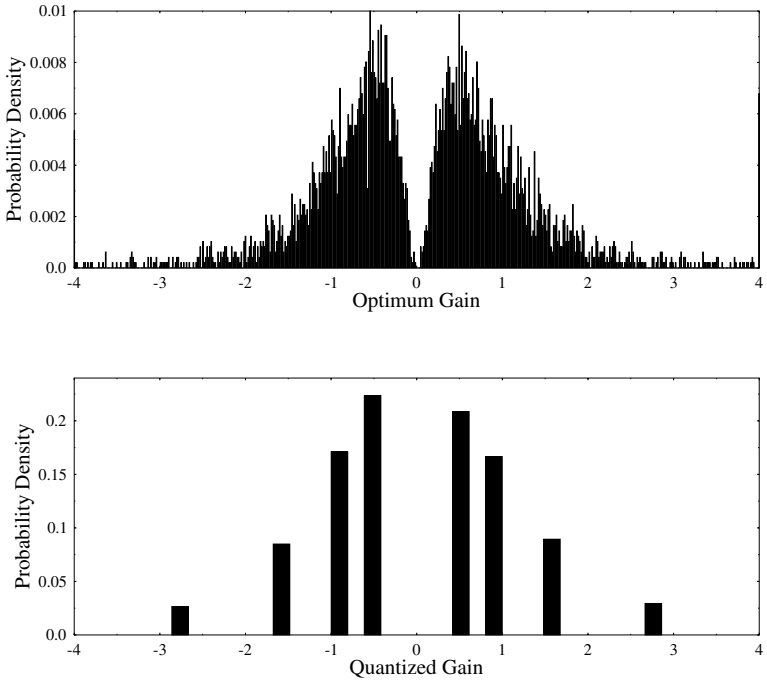

Figure 8.7: PDFs of the optimum and quantized codebook gain values.

codebook entries are compared in order to find the best innovation sequence resulting in the best synthetic speech segment. A preferred alternative to subtracting the filter memory from the input speech in generating the target vector is to set the filter memory to zero before a new codebook vector is fed into it. Since the backward-adaptive gain $\sigma(n)$ is known at frame n, before the codebook search commences, the normalised target vector $x(n) = x(n)/\sigma(n)$ can be used during the optimisation process.

Let us follow the notation used in the G728 Recommendation and denote the codebook vectors by $y_j, j = 1, \ldots, 128$, and the associated gain factor by $g_i, i = 1, \ldots, 8$. Then the filtered and gain-scaled codebook vectors are given by the convolution

$$\hat{x}_{ij} = \sigma(n) \cdot g_i[h(n) * y_j], \tag{8.13}$$

where, again, $\sigma(n)$ represents the codebook gain determined by the backward-adaptive gain recovery scheme of Figure 8.5. With the help of the lower triangle convolution matrix of

$$\mathbf{H} = \begin{bmatrix} h_0 & 0 & 0 & 0 & 0 \\ h_1 & h_0 & 0 & 0 & 0 \\ h_2 & h_1 & h_0 & 0 & 0 \\ h_3 & h_2 & h_1 & h_0 & 0 \\ h_4 & h_3 & h_2 & h_1 & h_0 \end{bmatrix}, \tag{8.14}$$

Equation (8.13) can be expressed in a more terse form as:

$$\hat{x}_{ij} = \mathbf{H}\sigma(n)g_i y_j. \tag{8.15}$$

The best innovation sequence is deemed to be the one which minimises the MSE distortion expression

$$D = \|x(n) - \hat{x}_{ij}\|^2 = \sigma^2(n)\|\hat{x}(n) - g_i \cdot \mathbf{H}y_j\|^2, \tag{8.16}$$

where, again, $\hat{x}(n) = x(n)/\sigma(n)$ is the normalised target vector. Upon expanding the above term we arrive at

$$D = \sigma^2(n)[\|\hat{x}(n)\|^2 - 2g_i\hat{x}^{\mathrm{T}}\mathbf{H}y_j + g_i^2\|\mathbf{H}g_j\|^2]. \tag{8.17}$$

Since the normalised target vector energy $\|\hat{x}(n)\|^2$ and the codebook gain $\sigma(n)$ are constant for the duration of scanning the codebook, minimising D in Equation (4.35a) is equivalent to

$$\hat{D} = -2g_i \cdot p^{\mathrm{T}}(n) \cdot y_j + g_i^2 E_j, \tag{8.18}$$

where the notation $p(n) = \mathbf{H}^{\mathrm{T}} \cdot \hat{x}(n)$ and $E_j = \|\mathbf{H}y_j\|^2$ was employed. Notice that E_j represents the energy of the filtered codebook entry y_j, and since the filter coefficients are only updated every 20 samples, E_j, $j = 1, \ldots, 128$, is computed once per LPC update frame.

The optimum codebook entry can now be found by identifying the best g_i, $i = 1, \ldots, 8$. A computationally more efficient technique is to compute the optimum gain factor for each entry and then quantise it to the closest prestored value. Further specific details of the codebook search procedure are given in [94, 109], while the codebook training algorithm was detailed in [276].

In the original CELP codec proposed by Schroeder and Atal a stochastic codebook populated by a zero-mean unit-variance Gaussian vector was used. The G728 codec uses a 128-entry trained codebook.

In a conceptually simplistic but suboptimum approach, the codebook could be trained by simply generating the prediction residual using a stochastic codebook and then employ the *pairwise nearest neighbour* or the *pruning method* [126] to cluster the excitation vectors in order to arrive at a trained codebook. It is plausible, however, that upon using this trained codebook the prediction residual vectors generated during the codec's future operation will now be different, necessitating the re-training of the codebook recursively a number of times. This is particularly true in the case of backward-adaptive gain recovery, because the gain factor will be dependent on the codebook entries, which in turn again will depend on the gain values. According to Chen [276] the codec performance is dramatically reduced if no closed-loop training is invoked. The robustness against channel errors was substantially improved following the proposals by De Marca and Jayant [277] as well as Zeger and Gersho [278] using pseudo-Gray coding of the codebook indices, which ensured that in the case of a single channel error the corresponding codebook entry was similar to the original one.

8.4.5 G728 Excitation Vector Quantisation

At 16 kbps there are 10 bits which can be used to represent every 5 sample vector, and as the LPC analysis is backward adaptive these bits are used entirely to code the excitation

signal $u(n)$ which is fed to the synthesis filter. The 5-sample excitation sequences are vector quantised using a 10-bit split shape-gain codebook. Seven bits are used to represent the vector shapes, and the remaining 3 bits are used to quantize the vector gains. This splitting of the 10-bit vector quantiser is done to reduce the complexity of the closed-loop codebook search. To measure the degradations that were introduced by this splitting we trained codebooks for a 7/3 bit shape/gain split vector quantiser, and a pure 10-bit vector quantiser. We found that the 10-bit vector quantiser gave no significant improvement in either the SEGSNR or the segmental weighted SNR of the codec, and increased the complexity of the codebook search by about 550% and the overall codec complexity by about 300%. Hence this splitting of the vector quantiser is a very efficient way to significantly reduce the complexity of the encoder.

The closed-loop codebook search is carried out as follows. For each vector the search procedure finds values of the gain quantiser index i and the shape codebook index k which minimise the squared weighed error E_w for that vector. E_w is given by

$$E_w = \sum_{n=0}^{vs-1} (s_w(n) - \hat{s}_o(n) - \hat{\sigma} g_i h(n) * c_k(n))^2, \tag{8.19}$$

where $s_w(n)$ is the weighted input speech, $\hat{s}_o(n)$ is the zero-input response of the synthesis and weighting filters, $\hat{\sigma}$ is the predicted vector gain, $h(n)$ is the impulse response of the concatenated synthesis and weighting filters and g_i and $c_k(n)$ are the entries from the gain and shape codebooks. This equation can be expanded to give

$$\begin{aligned} E_w(n) &= \hat{\sigma}^2 \sum_{n=0}^{vs-1} (x(n) - g_i[h(n) * c_k(n)])^2 \\ &= \hat{\sigma}^2 \sum_{n=0}^{vs-1} x^2(n) \; + \; \hat{\sigma}^2 g_i^2 \sum_{n=0}^{vs-1} [h(n) * c_k(n)]^2 \qquad (8.20) \\ &\quad - 2\hat{\sigma}^2 g_i \sum_{n=0}^{vs-1} x(n)[h(n) * c_k(n)] \\ &= \hat{\sigma}^2 \sum_{n=0}^{vs-1} x^2(n) + \hat{\sigma}^2 (g_i^2 \xi_k - 2 g_i C_k), \qquad (8.21) \end{aligned}$$

where $x(n) = (s_w(n) - \hat{s}_o(n))/\hat{\sigma}$ is the codebook search target,

$$C_k = \sum_{n=0}^{vs-1} x(n)[h(n) * c_k(n)] \tag{8.22}$$

is the correlation between this target and the filtered codeword $h(n) * c_k(n)$, and

$$\xi_k = \sum_{n=0}^{vs-1} [h(n) * c_k(n)]^2 \tag{8.23}$$

is the energy of the filtered codeword $h(n) * c_k(n)$. Note that this is almost identical to the form of the term in Equation (6.7) which must be minimised in the fixed codebook search in our ACELP codecs.

In the G728 codec the synthesis and weighting filters are changed only once every four vectors. Hence ξ_k must be calculated for the 128 codebook entries only once every four vectors. The correlation term C_k can be rewritten as

$$\begin{aligned} C_k &= \sum_{n=0}^{vs-1} x(n)[h(n) * c_k(n)] \\ &= \sum_{n=0}^{vs-1} c_k(n)\psi(n), \end{aligned} \tag{8.24}$$

where

$$\psi(n) = \sum_{i=n}^{vs-1} x(i)h(i-n) \tag{8.25}$$

is the reverse convolution between $h(n)$ and $x(n)$. This means that we need to carry out only one convolution operation for each vector to find $\psi(n)$ and then we can find C_k for each codebook entry k with a relatively simple series of multiply–add operations.

The codebook search finds the codebook entries $i = 1$–8 and $k = 1$–128 which minimise E_w for the vector. This is equivalent to minimising

$$D_{ik} = g_i^2 \xi_k - 2g_i C_k. \tag{8.26}$$

For each codebook entry k, C_k is calculated and then the best quantised gain value g_i is found. The values g_i^2 and $2g_i$ are pre-computed and stored for the 8 quantised gains, and these values along with ξ_k and C_k are used to find D_{ik}. The codebook index k which minimises this, together with the corresponding gain quantiser level i, are sent to the decoder. These indices are also used in the encoder to produce the excitation and reconstructed speech signals which are used to update the gain predictor and the synthesis filter.

The decoder's schematic was portrayed in Figure 8.2, which carries out the inverse operations of the encoder seen in Figure 8.1. Without delving into specific algorithmic details of the decoder's functions, in the next section we briefly describe the operation of the postfilter at its output stage.

Post-filtering was originally proposed by Jayant and Ramamoorthy [106, 107] in the context of ADPCM coding using the two-pole six-zero synthesis filter of the G721 codec of Figure 2.10 to improve the preceptual speech quality.

8.4.6 G728 Adaptive Post-filtering

Since post-filtering was shown to improve the perceptual speech quality in the G721 ADPCM codec, Chen and Gersho [108] have also adopted this technique in order to improve the performance of CELP codecs. The basic philosophy of post-filtering is to augment spectral prominances, while slightly reducing their bandwidth and attenuating spectral valleys between them. This procedure naturally alters the waveform shape to a certain extent, which

constitutes an impairment, but its perceptual advantage in terms of reducing the effect of quantisation noise outweighs the former disadvantage.

Early versions of the G728 codec did not employ adaptive post-filtering in order to prevent the accumulation of speech distortion during tandeming several codecs. However, without post-filtering the coding noise due to concatenating three asynchronously operated codecs became about 4.7 dB higher than in the case of one codec. Chen and Gersho found that this was due to optimising the extent of post-filtering for maximum noise masking at a concomitant minimum speech distortion, while using a single coding stage. Hence the amount of post-filtering became excessive in case of tandeming. This then led to a design which was optimised for three concatenated coding operations and the corresponding speech quality improved by a MOS point of 0.81 to 3.93.

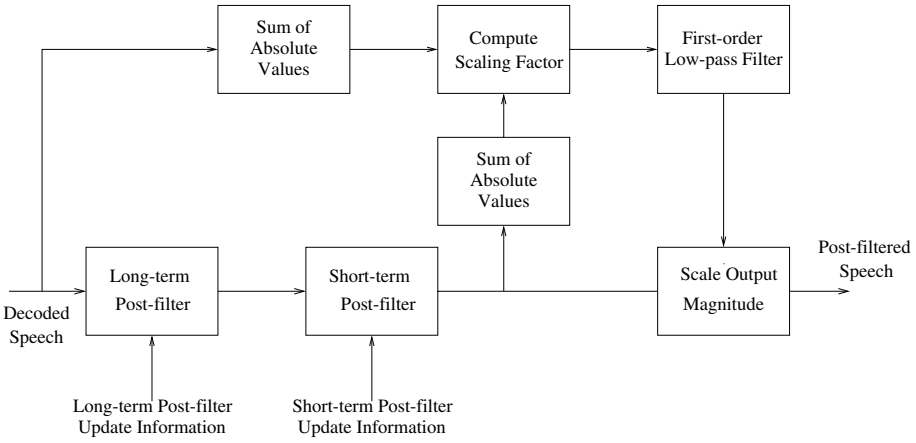

Figure 8.8: G.728!Postfilter Schematic.

8.4.6.1 Adaptive Long-term Post-filtering

The schematic of the G728 adaptive postfilter is shown in Figure 8.8. The *long-term postfilter* is a comb filter which enhances the spectral needles in the vicinity of the upper harmonics of the pitch frequency. Albeit the G728 codec dispenses with using LTP or pitch predictor for reasons of error resilience, the pitch information is recovered in the codec using a pitch detector to be described at a later stage. Assuming that the true pitch periodicity p is known, the LT postfilter can be described with the help of the transfer function

$$H_l = g_l(1 + bz^{-p}), \tag{8.27}$$

where the coefficients g_l, b and p are updated during the third 5-sample speech segment of each 4-segment, or 2.5 ms duration LPC update frame, as suggested by Figure 8.8.

The *postfilter adapter* schematic is displayed in Figure 8.9. A tenth-order LPC inverse filter and the *pitch detector* act in unison in order to extract the pitch periodicity p. Chen and Gersho also proposed a possible implementation for the pitch detector. The tenth-order LPC

inverse filter of

$$\tilde{A}(z) = 1 - \sum_{i=1}^{10} \tilde{a}_i z^{-i} \tag{8.28}$$

employs the filter coefficients $\tilde{a}_i, i = 1, \ldots, 10$, computed from the synthetic speech in order to generate prediction residual $d(k)$. This signal is fed to the pitch detector of Figure 8.9, which buffers a 240-sample history of $r(k)$. It would now be possible to determine the pitch periodicity using the straightforward evaluation of Equation (3.7) for all possible delays in the search scope, which was stipulated in the G78 codec to be $[20, \ldots, 140]$, employing a summation limit of $N = 100$. However, the associated complexity would be unacceptably high.

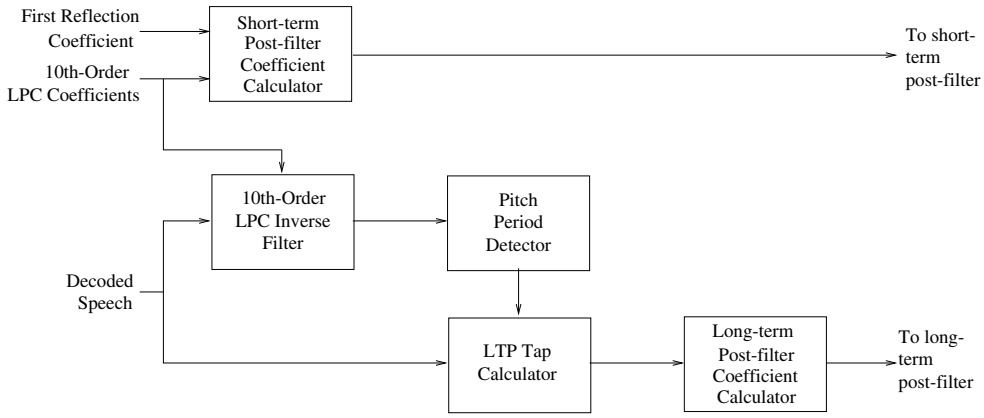

Figure 8.9: Post-filter adapter schematic.

Therefore, the Recommendation suggests to low-pass filter $d(k)$ using a third-order elliptic filter to a bandwidth of 1 kHz and then decimate it by a factor of four, allowing a substantial complexity reduction. The second term of Equation (3.7) is maximised over the search scope of $\alpha = [20, 21, \ldots, 140]$, but in the decimated domain this corresponds to the range $[5, 6, \ldots, 35]$. Now Equation (3.7) only has to be evaluated for 31 different delays and the $\log \alpha_1$ maximising the second term of Equation (3.7) is inferred as an initial estimate of the true pitch periodicity p. This estimate can then be refined to derive a better estimate α_3 by maximising the above mentioned second term of Equation (3.7) over the undecimated $r(k)$ signal within the log range of $[\alpha_1 \pm 3]$. In order to extract the true pitch periodicity, it has to be established whether the refined estimate α_2 is not a multiple of the true pitch. This can be ascertained by evaluating the second term of Equation (3.7) also in the range $[\alpha_3 \pm 6]$, where α_3 is the pitch determined during the previous 20-sample LPC update frame. Due to this frequent pitch-picking update, at the beginning of each talk-spurt the scheme will be able to establish the true pitch lag, since the true pitch lag is always longer than 20 samples or 2.5 ms and hence no multiple-length lag values will be detected. This will allow the codec to recursively check in the absence of channel error, whether the current pitch lag is within a range of ± 6 samples or 1.5 ms of the previous one, namely α_3. If this is not the case, the

lag $(\alpha_3 - 6) < \alpha_4 < (\alpha_3 + 6)$ is also found, for which the second term of Equation (3.7) is maximum.

Now a decision must be taken as to whether α_4 or α_2 constitutes the true pitch lag and this can be established by ranking them on the basis of their associated gain terms $G = \beta$ given by Equation (3.6), which is physically the normalised cross-correlation of the residual segments at delays 0 and α, respectively. The higher this correlation, the more likely that α represents the true pitch lag. In possession of the optimum LTP lag α and gain β, Chen and Gersho defined the LT postfilter coefficients b and g_e in Equation (8.27) as

$$b = \begin{cases} 0 & \text{if } \beta < 0.6 \\ 0.15\beta & \text{if } 0.6 \leq \beta \leq 1 \\ 0.15 & \text{if } \beta = 1 \end{cases} \tag{8.29}$$

$$g_e = \frac{1}{1+b}, \tag{8.30}$$

where the factor 0.15 is an experimentally determined constant controlling the weighting of the LT postfilter. If the LTP gain of Equation (3.6) is close to unity, the signal $v(k)$ is almost perfectly periodic. If, however, $\beta < 0.6$, the signal is unvoiced, exhibiting almost no periodicity, hence the spectrum has no quasi-periodic fine-structure. Therefore, according to $b = 0$ no long-term post-filtering is employed, since $H_l(z) = 1$ represents an all-pass filter. Lastly, in the range of $0.6 \leq \beta \leq 1$ we have $b = 0.5\beta$, i.e. β controls the extent of long-term post-filtering, allowing a higher degree of weighting in the case of highly correlated $r(k)$ and speech signals.

Having described the adaptive long-term post-filtering let us now turn our attention to details of the short-term (ST) post-filtering.

8.4.6.2 G.728 Adaptive Short-term Post-filtering

The adaptive ST postfilter standardised in the G728 Recommendation is constituted by a tenth-order pole-zero filter concatenated with a first-order single-zero filter:

$$H_s(z) = \frac{1 - \sum_{i=1}^{10} \overline{b_i} z^{-i}}{1 - \sum_{i=1}^{10} \overline{a_i} z^{-i}} [H \mu z^{-1}], \tag{8.31}$$

where the filter coefficients are specified as

$$\begin{aligned} \overline{b_i} &= \tilde{a}_i (0.65)^i, \quad i = 1, 2, \ldots, 10 \\ \overline{a_i} &= \tilde{a}_i (0.75)^i, \quad i = 1, 2, \ldots, 10 \\ \mu &= 0.15.k_i. \end{aligned} \tag{8.32}$$

The coefficients $\tilde{a}_i, i = 1, \ldots, 10$, are obtained in the usual fashion as by-products of the fiftieth-order LPC analysis at iteration $i = 10$, while k_1 represents the first reflection coefficient in the Levison–Durbin algorithm of Figure 2.3. Observe in Equation (8.33) that the coefficients $\overline{a_i}$ and $\overline{b_i}$ are derived from the progressively attenuated $\tilde{a}_i$ coefficients. The pole-zero section of this filter emphasises the formant structure of the speech signal, while

attenuating the frequency regions between formants. The single-zero section has a high-pass characteristic and was included in order to compensate for the low-pass nature or spectral delay of the pole-zero section.

Returning to Figure 8.8, observe that the output signal of the adaptive postfilter is scaled in order for its input and output signals to have the same power. The sum of the postfilter's input and output samples is computed, the required scaling factor is calculated and low-pass filtered in order to smooth its fluctuation, before the output scaling takes place.

Here we conclude our discussions on the standard G728 16 kbps codec with a brief performance analysis, before we embark on contriving a range of programmable-rate 8–16 kbps codecs.

8.4.7 Complexity and Performance of the G728 Codec

In the previous subsections we have described the operation of the G728 codec. The associated implementational complexities of the various sections of the codec are shown in Table 8.4 in terms of millions of arithmetic operations (mostly multiplies and adds) per second. The weighting filter and codebook search operations are carried out only by the encoder, which requires a total of about 12.4 million operations per second. The post-filtering is carried out only by the decoder which requires about 8.7 million operations per second. The full duplex codec requires about 21 million operations per second.

Table 8.4: Millions of operations per second required by the G728 codec.

Synthesis filter	5.1
Backward gain adaption	0.4
Weighting filter	0.9
Codebook search	6.0
Post-filtering	3.2
Total encoder complexity	12.4
Total decoder complexity	8.7

We found that the codec gave an average SEGSNR of 20.1 dB, and an average weighted SEGSNR of 16.3 dB. The reconstructed speech was difficult to distinguish from the original, with no obvious degradations. In the next section we discuss our attempts to modify the G728 codec in order to produce a variable bitrate 8–16 kbps codec which gives a graceful degradation in speech quality as the bitrate is reduced. Such a programmable-rate codec is useful in intelligent systems, where the transceiver may be reconfigured under network control, in order to invoke a higher or lower speech quality mode of operation, or to assign more channel capacity to error correction coding in various traffic loading or wave propagation scenarios.

8.5 Reduced-rate G728-like Codec: Variable-length Excitation Vector

Having detailed the G728 codec in the previous section we now describe our work in reducing the bitrate of this codec and producing an 8–16 kbps variable rate low-delay codec. The G728

codec uses 10 bits to represent each 5-sample vector. It is obvious that to reduce the bitrate of this codec we must either reduce the number of bits used for each vector or increase the number of speech samples per vector. If we were to keep the vector size fixed at 5 samples then in an 8 kbps codec we would have only 5 bits to represent both the excitation shape and gain. Without special codebook training this leads to a codec with unacceptable performance. Therefore, initially we concentrated on reducing the bitrate of the codec by increasing the vector size. In Section 8.8 we discuss the alternative approach of keeping the vector size constant and reducing the size of the codebooks used.

In this section at all bitrates we use a split 7/3 bit shape/gain vector quantiser for the excitation signal $u(n)$. The codec rate is varied by changing the vector size vs used, from $vs = 5$ for the 16 bits/s codec to $vs = 10$ for the 8 kbps codec. For all the codecs we used the same 3-bit gain quantiser as in G728, and for the various shape codebooks we used randomly generated Gaussian codebooks with the same variance as the G728 shape codebook. Random codebooks with a Gaussian PDF were used for simplicity and because in the past such codebooks have been shown to give a relatively good performance [16]. We found that replacing the trained shape codebook in the G728 codec with a Gaussian codebook reduced the SEGSNR of the codec by 1.7 dB, and the segmental weighted SNR by 2 dB. However, these losses in performance are recovered in Section 8.7 when we consider closed-loop training of our codebooks.

In the G728 codec the synthesis filter, weighting filter and the gain predictor are all updated every four vectors. With a vector size of 5 this means the filters are updated every 20 samples or 2.5 ms. Generally, the more frequently the filters are updated the better the codec will perform, and we found this to be true for our codec. However, updating the filter coefficients more frequently significantly increases the complexity of the codec. Therefore, we decided to keep the period between filter updates as close as possible to 20 samples as the bitrate of our codec is reduced by increasing the vector size. This means reducing the number of vectors between filter updates as the vector size is increased. For example, at 8 kbps the vector size is 10 and we updated the filters every 2 vectors, which again corresponds to 2.5 ms.

The SEGSNR of our codec against its bitrate as the vector size is increased from 5 to 10 is shown in Figure 8.10. Also shown in this figure is the segmental prediction gain of the synthesis filter at the various bitrates. It can be seen from this figure that the SEGSNR of our codec decreases smoothly as its bitrate is reduced, falling by about 0.8 dB for every 1 kbps drop in the bitrate.

As explained in the previous section, an important part of the codec is the backward-adaptive synthesis filter. It can be seen from Figure 8.10 that the prediction gain of this filter falls by only 1.3 dB as the bitrate of the codec is reduced from 16 to 8 kbps. This suggests that the backward-adaptive synthesis filtering copes well with the reduction in bitrate from 16 to 8 kbps. We also carried out tests at 16 and 8 kbps, similar to those used for Table 8.3, to establish how the performance of the filter would be improved if we were able to eliminate the effects of using backward adaption, i.e. the noise feedback and time mismatch. The results are shown in Tables 8.5 and 8.6 for the 16 kbps codec (using the Gaussian codebook rather than the trained G728 codebook used for Table 8.3) and the 8 kbps codec. As expected the effects of noise feedback are more significant at 8 rather than 16 kbps, but the overall effects on the codec's SEGSNR of using backward adaption are similar at both rates.

It has been suggested [270] that high-order backward-adaptive linear prediction is inappropriate at bitrates as low as 8 kbps. However, we found that this was not the case for

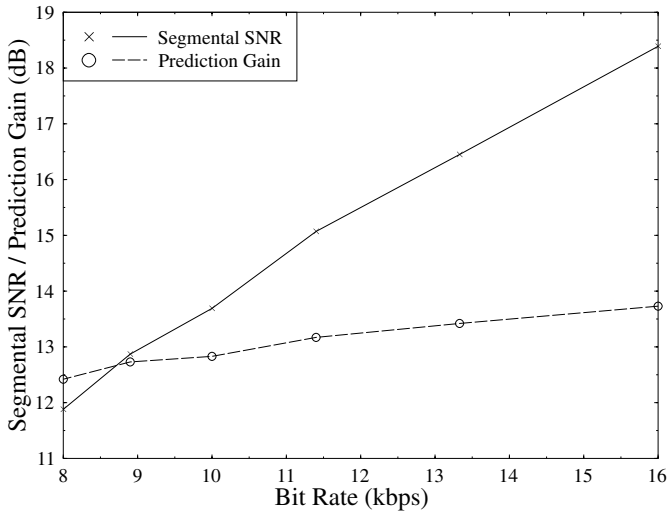

Figure 8.10: Performance of the reduced-rate G728-like codec with variable-length excitation vectors.

Table 8.5: Effects of backward adaption of the synthesis filter at 16 kbps.

	Δ Prediction gain (dB)	Δ SEGSNR (dB)
No noise feedback	$+0.74$	$+0.42$
No time mismatch	$+0.85$	$+0.83$
Use forward adaption	$+1.59$	$+1.25$

Table 8.6: Effects of backward adaption of the synthesis filter at 8 kbps.

	Δ Prediction gain (dB)	Δ SEGSNR (dB)
No noise feedback	$+2.04$	$+0.75$
No time mismatch	$+0.85$	$+0.53$
Use forward adaption	$+2.89$	$+1.28$

our codec and that increasing the filter order from 10 to 50 gave almost the same increase in the codec performance at 8 kbps as at 16 kbps. This is shown in Table 8.7.

Another important part of the G728 codec is the backward gain adaption. Figure 8.6 shows how at 16 kbps this backward adaption makes the optimum codebook gains cluster around one, and hence become easier to quantize. We found that the same was true at 8 kbps.

Table 8.7: Relative performance of the synthesis filter as p is increased at 8 and 16 kbps.

	Δ Prediction gain (dB)	Δ SEGSNR (dB)
8 kbps $p = 10$	0.0	0.0
8 bits/s $p = 50$	+0.88	+1.00
16 kbps $p = 10$	0.0	0.0
16 kbps $p = 50$	+1.03	+1.04

To quantify the performance of the gain prediction we defined the SNR

$$\mathrm{SNR}_{\mathrm{gain}} = \frac{\sum \sigma_o^2}{\sum (\sigma_o - \hat{\sigma})^2}. \tag{8.33}$$

Here, σ_o is the optimum excitation gain given by

$$\sigma_o = \sqrt{\frac{1}{vs} \sum_{n=0}^{vs} (\hat{\sigma} g c_k(n))^2}, \tag{8.34}$$

where g is the unquantised gain chosen by the codebook search and $\hat{\sigma}$ is the predicted gain value. We found that this gain prediction SNR was on average 5.3 dB for the 16 kbps codec, and 6.1 dB for the 8 kbps codec. Thus the gain prediction is even more effective at 8 kbps than at 16 kbps.

In the next section we discuss the addition of long-term prediction to our variable-rate codec.

8.6 The Effects of Long-term Prediction

In this section we describe the improvements in our variable-rate codec that can be obtained by adding backward-adaptive LTP. This work was motivated by the fact that we found that significant long-term correlations remained in the synthesis filter's prediction residual, even when the pitch period was lower than the order of this filter. This can be seen from Figure 8.11, which shows the prediction residual for a segment of voiced female speech with a pitch period of about 45 samples. It can be seen that the residual has clear long-term redundancies, which could be exploited by a long-term prediction filter.

In a forward-adaptive system the short-term synthesis filter coefficients are determined by minimising the energy of the residual signal found by filtering the original speech through the inverse synthesis filter. Similarly for open-loop LTP, we minimise the energy of the long-term residual signal which is found by filtering the short-term residual through the inverse long-term predictor. If $r(n)$ is the short-term residual signal, then for a one-tap long-term predictor we want to determine the delay L and gain β which minimise the long-term residual energy

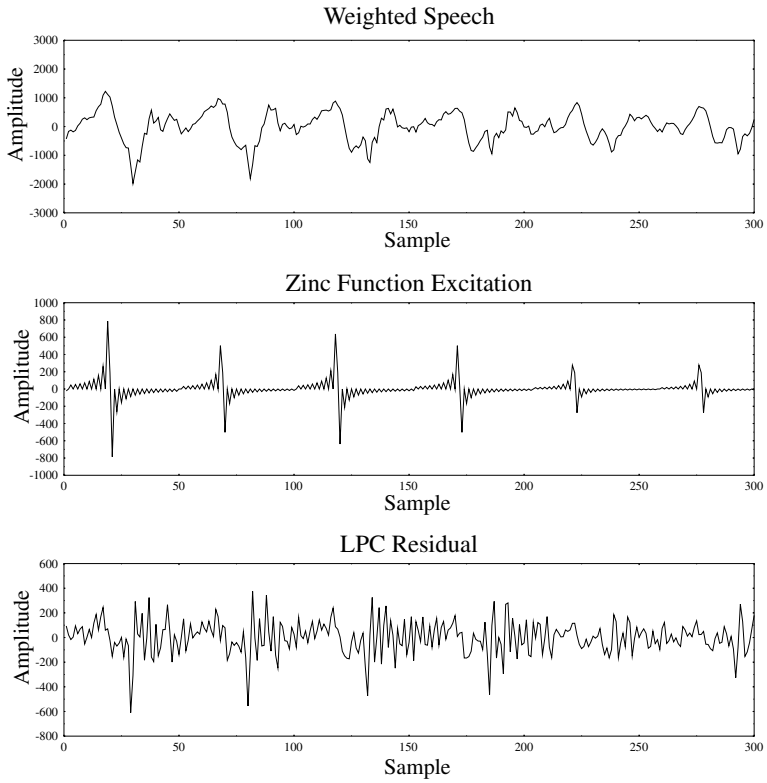

Figure 8.11: Short-term synthesis-filter prediction residual in G728.

E_{LT} given by

$$E_{\mathrm{LT}} = \sum_n (r(n) - \beta r(n-L))^2. \tag{8.35}$$

The best delay L is found by calculating

$$X = \frac{(\sum_n r(n)r(n-L))^2}{\sum_n r^2(n-L)} \tag{8.36}$$

for all possible delays, and choosing the value of L which maximises X. The best long-term gain β is then given by

$$\beta = \frac{\sum_n r(n)r(n-L)}{\sum_n r^2(n-L)}. \tag{8.37}$$

In a backward-adaptive system the original speech signal $s(n)$ is not available, so instead we use the past reconstructed speech signal $\hat{s}(n)$ to find the short-term synthesis filter coefficients. These coefficients can then be used to filter $\hat{s}(n)$ through the inverse filter to find the 'reconstructed residual' signal $\hat{r}(n)$. This residual signal can then be used in Equations (8.36) and (8.37) to find the LTP delay and gain. Alternatively we can use the

past excitation signal $u(n)$ in Equations (8.36) and (8.37). This approach is slightly simpler than using the reconstructed residual signal because the inverse filtering of $\hat{s}(n)$ to find $\hat{r}(n)$ is not necessary, and we found in our codec that the two approaches gave almost identical results.

Initially we used a one-tap LTP in our codec. The best delay L was found by maximising

$$X = \frac{(\sum_{n=-100}^{-1} u(n)u(n-L))^2}{\sum_{n=-100}^{-1} u^2(n-L)} \tag{8.38}$$

over the range of delays 20 to 140 every frame. The LTP gain β was updated every vector by solving

$$\beta = \frac{\sum_{n=-100}^{-1} u(n)u(n-L)}{\sum_{n=-100}^{-1} u^2(n-L)}. \tag{8.39}$$

We found that this backward-adaptive LTP improved the average SEGSNR of our codec by 0.6 dB at 16 kbps, and 0.1 dB at 8 kbps. However, the calculation of X as given in Equation (8.38) for 120 different delays every frame dramatically increases the complexity of the codec. The denominator $\sum u^2(n-L)$ for delay L need not be calculated independently, but instead can be simply updated from the equivalent expression for delay $L-1$. Even so, if the frame size is 20 samples then to calculate X for all delays increases both the encoder and the decoder complexity by almost 10 million arithmetic operations per second, which is clearly unacceptable.

Fortunately, the G728 postfilter requires an estimate of the pitch period of the current frame. This is found by filtering the reconstructed speech signal through a tenth-order short-term prediction filter to find a reconstructed residual-like signal. This signal is then low-pass filtered with a cutoff frequency of 1 kHz and 4:1 decimated, which dramatically reduces the complexity of the pitch determination. The maximum value of the autocorrelation function of the decimated residual signal is then found to give an estimate τ_d of the pitch period. A more accurate estimate τ_p is then found by maximising the autocorrelation function of the undecimated residual between $\tau_d - 3$ and $\tau_d + 3$. This lag could be a multiple of the true pitch period, and to guard against this possibility the autocorrelation function is also maximised between $\tau_o - 6$ and $\tau_o + 6$, where τ_o is the pitch period from the previous frame. Finally, the pitch estimator chooses between τ_p and the best lag around τ_o by comparing the optimal tap weights β for these two delays.

This pitch estimation procedure requires only about 2.6 million arithmetic operations per second, and is carried out at the decoder as part of the post-filtering operations anyway. So using this method to find a LTP delay has no effect on the decoder complexity and increases the encoder complexity by only 2.6 million arithmetic operations per second. We also found that not only was this method of calculating the LTP delay much simpler than finding the maximum value of X from Equation (8.38) for all delays between 20 and 140, it also gave better results. This was due to the removal of pitch doubling and tripling by the checking of pitch values around that used in the previous frame. The average SEGSNR and segmental weighted SNR for our codec at 16 kbps both with and without 1-tap LTP using the pitch estimate from the postfilter is shown in Table 8.8. Similar figures for the codec at 8 kbps are given in Table 8.9. We found that when LTP was used, there was very little gain in having a

filter order any higher than 20. Therefore the figures in Tables 8.8 and 8.9 have a short-term filter order of 20 when LTP is used.

Table 8.8: Performance of LTP at 16 kbps.

	SEGSNR (dB)	Segmental weighted SNR (dB)
No LTP	18.43	14.30
1-tap LTP	19.08	14.85
3-tap LTP	19.39	15.21
5-tap LTP	19.31	15.12

Table 8.9: Performance of LTP at 8 kbps.

	SEGSNR (dB)	Segmental weighted SNR (dB)
No LTP	11.86	8.34
1-tap LTP	12.33	8.64
3-tap LTP	12.74	9.02
5-tap LTP	12.49	8.81

Tables 8.8 and 8.9 also give the performance of our codec at 16 and 8 kbps when we use multi-tap LTP. As the LTP is backward adaptive we can use as many taps in the filter as we like, with the only penalty being a slight increase in complexity. Once the delay is known, for a $(2p+1)$th order predictor the filter coefficients $b_{-p}, b_{-p+1}, \ldots, b_0, \ldots, b_p$ are given by solving the following set of simultaneous equations:

$$\sum_{j=-p}^{j=p} b_j \sum_{n=-100}^{n=-1} u(n-L-j)u(n-L-i) = \sum_{n=-100}^{-1} u(n)u(n-L-i) \tag{8.40}$$

for $i = -p, -p+1, \ldots, p$. The LTP synthesis filter $H_{\mathrm{LTP}}(z)$ is then given by

$$H_{\mathrm{LTP}}(z) = \frac{1}{1 - b_{-p}z^{-L+p} - \cdots - b_0 z^{-L} - \cdots - b_p z^{-L-p}}. \tag{8.41}$$

It can be seen from Tables 8.8 and 8.9 that at both 16 and 8 kbps the best performance is given by a 3-tap filter which improves the SEGSNR at both bitrates by almost 1 dB. Also, because when LTP is used the short-term synthesis filter order was reduced to 20, the complexity of the codecs is not significantly increased by the use of a long-term prediction filter.

We found that it was possible to slightly increase the performance of the codec with LTP by modifying the signal $u(n)$ used to find the filter coefficients in Equation (8.40). This modification involves simply repeating the previous vector's excitation signal once. Hence instead of using the signal $u(-1), u(-2), \ldots, u(-100)$ to find the LTP coefficients, we

use $u(-1), u(-2), \ldots, u(-vs), u(-1), u(-2), \ldots, u(-100+vs)$. This single repetition of the previous vector's excitation in the calculation of the LTP coefficients increased both the segmental and the weighted SNR of our codec at 16 kbps by about 0.25 dB. It also improved the codec performance at 8 kbps, although only by about 0.1 dB. The improvements that this repetition brings in the codec's performance seem to be due to the backward adaptive nature of the LTP - no such improvement is seen when a similar repetition is used in a forward-adaptive system.

Figure 8.12 shows the variation in the codec's SEGSNR as the bitrate is reduced from 16 to 8 kbps. The codec uses 3-tap LTP with the repetition scheme described above and a short-term synthesis filter of order 20. Also shown in this figure is the equivalent variation in SEGSNR for the codec without LTP, repeated here from Figure 8.10. It can be seen that the addition of long-term prediction to the codec gives a uniform improvement in its SEGSNR of about 1 dB from 8 to 16 kbps. The effectiveness of the LTP can also be seen from Figure 8.13 which shows the long-term prediction residual in the 16 kbps codec for the same segment of speech as was used for the short-term prediction residual in Figure 8.11. It is clear that the long-term correlations have been significantly reduced. It should be noted, however, that the addition of backward-adapted long-term prediction to the codec will degrade its performance over noisy channels [279].

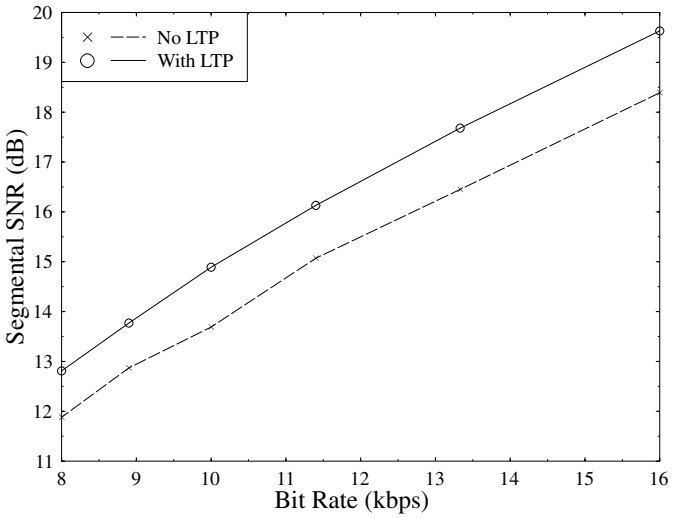

Figure 8.12: Performance of a 8–16 kbps low-delay codec with LTP.

Finally, we tested the degradations in the performance of the long-term prediction due to backward adaption being used. To measure the effect of quantisation noise feedback we used past values of the original speech signal rather than the reconstructed speech signal to find the LTP delay and coefficients. To measure the overall effect of backward adaption as opposed to open-loop forward adaption we used both past and present speech samples to find the LTP delay and coefficients. The improvements obtained in terms of the SEGSNR and the segmental weighted SNR are shown in Table 8.10 for the codec at 16 kbps and Table 8.11 for the codec at 8 kbps. It can be seen that the use of backward adaption degrades the codecs

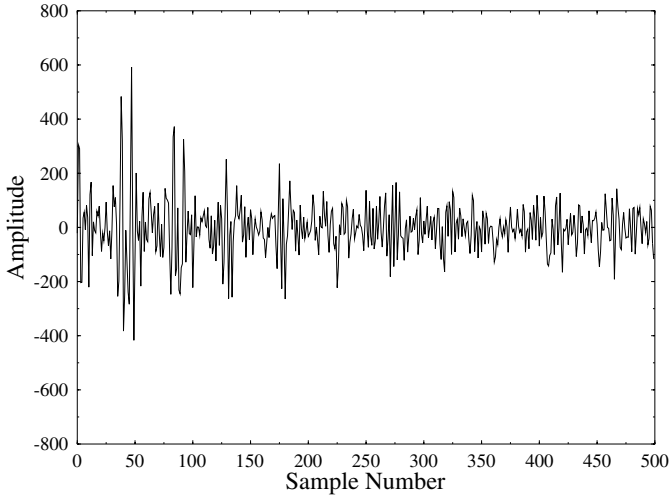

Figure 8.13: Long-term filter prediction residual at 16 kbps.

performance by just under 1 dB at 16 kbps and just over 1 dB at 8 kbps. At both bitrates noise feedback has very little effect, with most of the degradation coming from the time mismatch inherent in backward adaption.

Table 8.10: Effects of backward adaption of the LTP at 16 kbps.

	Δ Segmental weighted SNR (dB)	Δ SEGSNR (dB)
No noise feedback	-0.03	$+0.01$
No time mismatch	$+0.87$	$+0.85$
Use forward adaption	$+0.84$	$+0.86$

Table 8.11: Effects of backward adaption of the LTP at 8 kbps.

	Δ Segmental weighted SNR (dB)	Δ SEGSNR (dB)
No noise feedback	-0.18	$+0.02$
No time mismatch	$+1.17$	$+1.17$
Use forward adaption	$+0.99$	$+1.19$

8.7 Closed-loop Codebook Training

In this section we describe the training of the shape and gain codebooks used in our codec at its various bitrates. In Sections 8.5 and 8.6, Gaussian shape codebooks were used together

with the G728 gain codebook. These codebooks were used for simplicity and in order to provide a fair comparison between the different coding techniques used.

Due to the backward-adaptive nature of the gain and synthesis filter and LTP adaption used in our codec it is not sufficient to generate a training sequence for the codebooks and use the Lloyd algorithm [280] to design the codebooks. This is because the codebook entries required from the shape and gain codebooks depend very much upon the effectiveness of the gain adaption and the LTP and synthesis filters used. However, because these are backward adapted, they depend on the codebook entries that have been selected in the past. Therefore, the effective training sequence needed changes as the codebooks are trained. Thus, it is reported in [273], for example, that in a gain-adaptive vector quantisation scheme unless the codebook is properly designed, taking into account the gain adaption, the performance is worse than simple non-adaptive vector quantisation.

We used a closed-loop codebook design algorithm similar to that described in [276]. A long speech file consisting of four sentences spoken by two males and two females is used for the training. Both the sentences spoken and the speakers are different from those used for the performance figures quoted in this chapter. The training process commences with an initial shape and gain codebook and codes the training speech as usual. The total weighted error E_k from all the vectors that used the codebook entry $c_k(n)$ is then given by

$$E_k = \sum_{m \in N_k} \left(\hat{\sigma}_m^2 \sum_{n=0}^{vs-1} (x_m(n) - g_m[h_m(n) * c_k(n)])^2 \right), \tag{8.42}$$

where N_k is the set of vectors that use $c_k(n)$, $\hat{\sigma}_m$ is the backward-adapted gain for vector m, g_m is the gain codebook entry selected for vector m and $h_m(n)$ is the impulse response of the concatenated weighting filter and the backward-adapted synthesis filter used in vector m. Finally, $x_m(n)$ is the codebook target for vector m, which with $(2p+1)$th-order LTP is given by

$$x_m(n) = \frac{s_{wm}(n) - \hat{s}_{om}(n) - \sum_{j=-p}^{j=p} b_{jm} u_m(n - L_m - j)}{\hat{\sigma}_m}. \tag{8.43}$$

Here, $s_{wm}(n)$ is the weighted input speech in vector m, $\hat{s}_{om}(n)$ is the zero input response of the weighting and synthesis filters, $u_m(n)$ is the previous excitation and L_m and b_{jm} are the backward-adapted LTP delay and coefficients in vector m.

Equation (8.42) giving E_k can be expanded to yield

$$\begin{aligned} E_k &= \sum_{m \in N_k} \left(\hat{\sigma}_m^2 \sum_{n=0}^{vs-1} (x_m(n) - g_m[h_m(n) * c_k(n)])^2 \right) \\ &= \sum_{m \in N_k} \left(\hat{\sigma}_m^2 \sum_{n=0}^{vs-1} x_m^2(n) + \hat{\sigma}_m^2 g_m^2 \sum_{n=0}^{vs-1} [h_m(n) * c_k(n)]^2 \right. \\ &\quad \left. - 2\hat{\sigma}_m^2 g_m \sum_{n=0}^{vs-1} x_m(n)[h_m(n) * c_k(n)] \right) \end{aligned}$$

$$= \sum_{m \in N_k} \left(\hat{\sigma}_m^2 \sum_{n=0}^{vs-1} x_m^2(n) + \hat{\sigma}_m^2 g_m^2 \sum_{n=0}^{vs-1} [h_m(n) * c_k(n)]^2 - 2\hat{\sigma}_m^2 g_m \sum_{n=0}^{vs-1} p_m(n) c_k(n) \right), \tag{8.44}$$

where $p_m(j)$ is the reverse convolution between $h_m(n)$ and the target $x_m(n)$. This expression can be partially differentiated with respect to element $n = j$ of the codebook entry $c_k(n)$ to give

$$\frac{\partial E_k}{\partial c_k(j)} = \sum_{m \in N_k} \left(2\hat{\sigma}_m^2 g_m^2 \sum_{n=0}^{vs-1} c_k(n) H(n, j) - 2\hat{\sigma}_m^2 g_m p_m(j) \right), \tag{8.45}$$

where $H_m(n, j)$ is the autocorrelation of the delayed impulse response $h_m(n)$ and is given by

$$H_m(i, j) = \sum_{n=0}^{vs-1} h_m(n - i) h_m(n - j). \tag{8.46}$$

Setting these partial derivatives to zero gives the optimum codebook entry $c_k^*(n)$ for the cluster of vectors N_k as the solution of the set of simultaneous equations

$$\sum_{m \in N_k} \left(\hat{\sigma}_m^2 g_m^2 \sum_{n=0}^{vs-1} c_k^*(n) H_m(n, j) \right) = \sum_{m \in N_k} (\hat{\sigma}_m^2 g_m p_m(j)), \quad \text{for } j = 0, 1, \ldots, vs - 1. \tag{8.47}$$

A similar expression for the total weighted error E_i from all the vectors that use the gain codebook entry g_i is

$$\begin{aligned} E_i &= \sum_{m \in N_i} \left(\hat{\sigma}_m^2 \sum_{n=0}^{vs-1} (x_m(n) - g_i [h_m(n) * c_m(n)])^2 \right) \\ &= \sum_{m \in N_i} \left(\hat{\sigma}_m^2 \sum_{n=0}^{vs-1} x_m^2(n) + g_i^2 \hat{\sigma}_m^2 \sum_{n=0}^{vs-1} [h_m(n) * c_m(n)]^2 - 2 g_i \hat{\sigma}_m^2 \sum_{n=0}^{vs-1} x_m(n) [h_m(n) * c_m(n)] \right), \end{aligned} \tag{8.48}$$

where N_i is the set of vectors that use the gain codebook entry g_i, and $c_m(n)$ is the shape codebook entry used by the mth vector. Differentiating this expression with respect to g_i gives

$$\frac{\partial E_i}{\partial g_i} = \sum_{m \in N_i} \left(2 g_i \hat{\sigma}_m^2 \sum_{n=0}^{vs-1} [h_m(n) * c_m(n)]^2 - 2\hat{\sigma}_m^2 \sum_{n=0}^{vs-1} x_m(n) [h_m(n) * c_m(n)] \right) \tag{8.49}$$

and setting this partial derivative to zero gives the optimum gain codebook entry g_i^* for the cluster of vectors N_i as

$$g_i^* = \frac{\sum_{m \in N_i} (\hat{\sigma}_m^2 \sum_{n=0}^{vs-1} x_m(n)[h_m(n) * c_m(n)])}{\sum_{m \in N_i} (\hat{\sigma}_m^2 \sum_{n=0}^{vs-1} [c_m(n) * h_m(n)]^2)}. \tag{8.50}$$

The summations in Equations (8.47) and (8.50) over all the vectors that use $c_k(n)$ or g_i are carried out for all 128 shape codebook entries and all 8 gain codebook entries as the coding of the training speech takes place. At the end of the coding the shape and gain codebooks are updated using Equations (8.47) and (8.50), and then the codec starts coding the training speech again with the new codebooks. This closed loop codebook training procedure is summarised as follows.

(1) Start with an initial gain and shape codebook.

(2) Code the training sequence using the given codebooks. Accumulate the summations in Equations (8.47) and (8.50).

(3) Calculate the total weighted error of the coded speech. If this distortion is less than the minimum distortion so far keep a record of the codebooks used as the best codebooks so far.

(4) Calculate new shape and gain codebooks using Equations (8.47) and (8.50).

(5) Return to step 2.

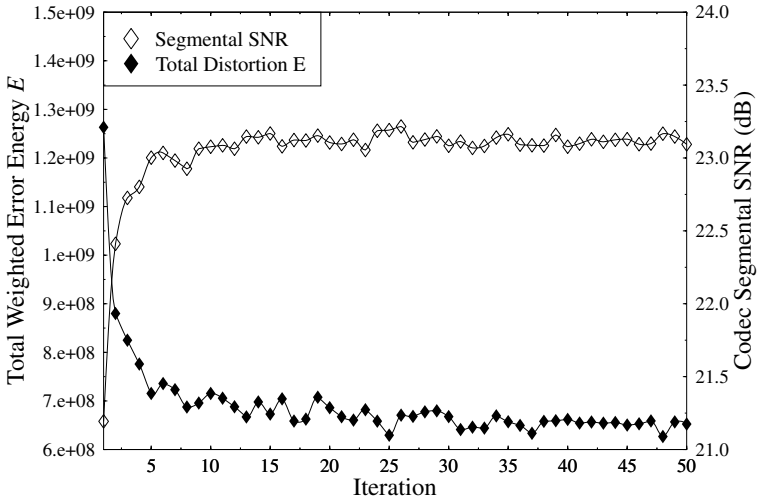

Figure 8.14: Codec's performance as the codebooks are trained.

Each entire coding of the training speech file counts as one iteration, and Figure 8.14 shows the variation in the total weighted error energy E and the codec's SEGSNR as the

training progresses for the 16 kbps codebooks. From this figure it can be seen that this closed-loop training sequence does not give a monotonic decrease in the total weighted error from one iteration to the next. This is because of the changing of the codebook target $x_m(n)$, as well as the other backward-adapted parameters, from one iteration to the next. However, it is clear from Figure 8.14 that the training does give a significant improvement in the codec's performance. Due to the non-monotonic decrease in the total weighted error energy it is necessary during the codebook training to keep a record of the lowest error energy achieved so far, and the corresponding codebooks. If a certain number of iterations passes without this minimum energy being improved then the codebook training can be terminated. It can be seen from Figure 8.14 that we get close to the minimum within about 20 iterations.

An important aspect in vector quantiser training can be the initial codebook used. In Figure 8.14 we used the G728 gain codebook and the Gaussian shape codebook as the initial codebooks. We also tried using other codebooks such as the G728 fixed codebook, and Gaussian codebooks with different variances, as the initial codebooks. However, although these gave very different starting values of the total weighted error E, and took different numbers of iterations to give their optimum codebooks, they all resulted in codebooks which gave very similar performances. Therefore, we concluded that the G728 gain codebook, and the Gaussian shape codebook, are suitable for use as the initial codebooks.

We trained different shape and gain codebooks for use by our codec at all of its bitrates between 8 and 16 kbps. The average SEGSNR given by the codec using these codebooks is shown in Figure 8.15 for the four speech sentences which were not part of the training sequence. Also shown in this figure for comparison is the curve from Figure 8.12 for the corresponding codec with the untrained codebooks. It can be seen that the codebook training gives an improvement of about 1.5 to 2 dB across the codec's range of bitrates.

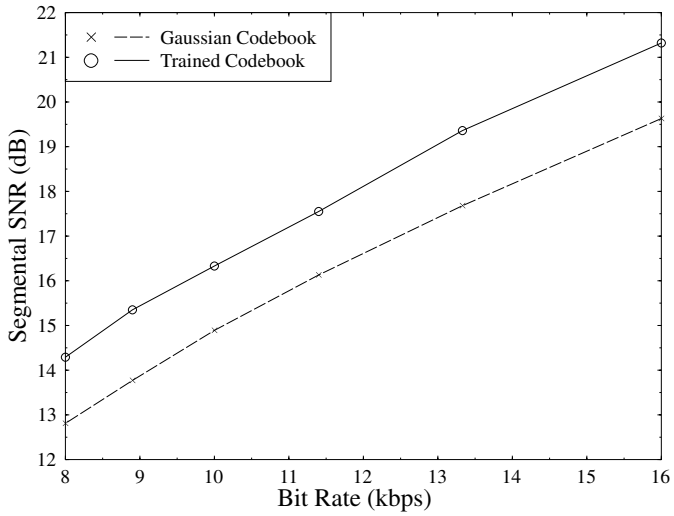

Figure 8.15: Performance of the 8–16 kbps codec with trained codebooks.

It can be seen from Figure 8.14 that a decrease in the total weighted error energy E does not necessarily correspond to an increase in the codec's SEGSNR. This is also true for the

codec's segmental weighted SNR, and is because the distortion D calculated takes no account of the different signal energies in different vectors. We tried altering the codebook training algorithm described above to take account of this, hoping that it would result in codebooks which gave lower SEGSNRs. However, the codebooks trained with this modified algorithm gave very similar performances to those trained by minimising E.

We also attempted training different codebooks at each bitrate for voiced and unvoiced speech. The voicing decision can be made backward adaptive based on the correlations in the previous reconstructed speech. A voiced/unvoiced decision like this is made in the G728 postfilter to determine whether to apply pitch post-filtering. We found, however, that although an accurate determination of the voicing of the speech could be made in a backward-adaptive manner, no significant improvement in the codec's performance could be achieved by using separately trained voiced and unvoiced codebooks. This agrees with the results in [270] when fully backward-adaptive LTP is used.

8.8 Reduced-rate G728-like Codec: Constant-length Excitation Vector

In the previous sections we discussed a variable-rate codec based on G728 which varied its bitrate by changing the number of samples in each vector. The excitation for each vector was coded with 10 bits. In this section we describe the alternative approach of keeping the vector size constant and varying the number of bits used to code the excitation. The bitrate of the codec is varied between 8 and 16 kbps with a constant vector size of 5 samples by using between 5 and 10 bits to code the excitation signal for each vector. We used a structure for the codec identical to that described earlier, with backward gain adaption for the excitation and backward-adapted short- and long-term synthesis filters. With 10, 9 or 8 bits to code the excitation we used a SVQ, similar to that used in G728, with a 7-bit shape codebook and a 3, 2 or 1-bit gain codebook. For the lower bitrates we used a single 7, 6 or 5-bit vector quantiser to code the excitation. Codebooks were trained for the various bitrates using the closed-loop codebook training technique described in Section 8.7.

The SEGSNR of this variable rate codec is shown in Figure 8.16. Also shown in this graph is the SEGSNR of the codec with a variable vector size, copied here from Figure 8.15 for comparison. At 16 kbps the two codecs are of course identical, but at lower rates the constant vector size codec performs worse than the variable vector size codec. The difference between the two approaches increases as the bitrate decreases, and at 8 kbps the SEGSNR of the constant vector size codec is about 1.75 dB lower than that of the variable vector size codec.

However, although the constant vector size codec gives lower reconstructed speech quality, it does have certain advantages. The most obvious is that it has a constant delay equal to that of G728, i.e. less than 2 ms. Also, the complexity of its encoder, especially at low bitrates, is lower than that of the variable vector size codec. This is because of the smaller codebooks used – at 8 kbps the codebook search procedure has only to examine 32 codebook entries. Therefore, for some applications this codec may be more suitable than the higher speech quality variable vector size codec.

In this chapter, so far we have described the G728 16 kbps low-delay codec and investigated a variable-rate low-delay codec, which is compatible with the 16 kbps G728 codec at

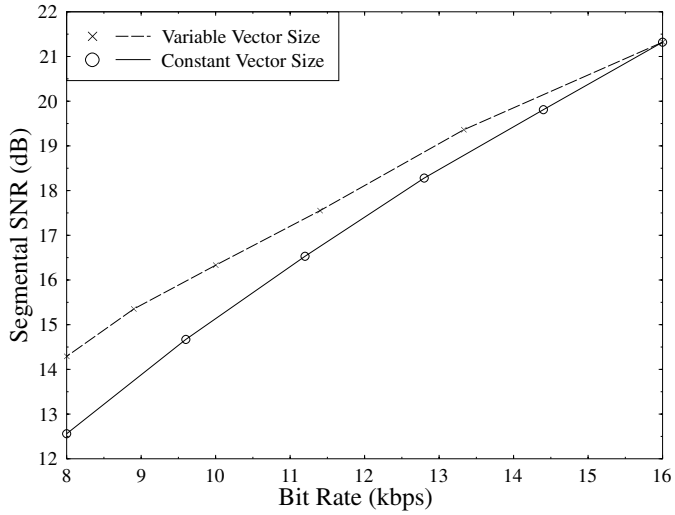

Figure 8.16: Performance of the reduced-rate G728-like codec with constant-length excitation vectors.

its highest bitrate, and exhibits a graceful degradation in speech quality down to 8 kbps. The bitrate can be reduced while the buffering delay is kept constant at 5 samples (0.625 ms) or, alternatively, better speech quality is achieved if the buffering delay is increased gradually to 10 samples as the bitrate is reduced down to 8 kbps.

8.9 Programmable-rate 8–4 kbps Low-delay CELP Codecs

8.9.1 Motivation

Having discussed low-delay 8–16 kbps programmable-rate coding in the previous section, in this section we consider methods of improving the performance of the proposed 8 kbps backward-adaptive predictive codec, while maintaining as low a delay and complexity as possible. Our proposed 8 kbps codec developed in Sections 8.5 and 8.8 uses a 3-bit gain codebook and a 7-bit shape codebook with backward adaption of both the long- and the short-term synthesis filters, and gives an average SEGSNR of 14.29 dB. In Section 8.9.2 we describe the effect of increasing the size of the gain and shape codebooks in this codec while keeping a vector length of 10 samples. This is followed by Sections 8.9.3 and 8.9.4 where we consider the improvements that can be achieved, again while maintaining a vector length of 10 samples, by using forward adaption of the short- and long-term synthesis filters. Then in Section 8.9.5 we show the performance of three codecs, based on those developed in the earlier sections, operating at bitrates between 8 and 4 kbps. Finally, as an interesting benchmarker, in Section 8.9.6 we describe a codec with a vector size of 40 samples based on the algebraic codebook structure we described in Section 6.4.3. The performance of this codec is compared to the previously introduced low-delay codecs from Section 8.9.5 and the higher-delay forward-adaptive predictive ACELP codec described in Section 6.4.3.

8.9.2 8–4 kbps Codec Improvements Due to Increasing Codebook Sizes

In this section we use the same structure for the codec as before, but increase the size of the shape and the gain codebooks. This codec structure is shown in Figure 8.17, and we refer to it as 'Scheme One'. We used 3-tap backward-adapted LTP and a vector length of 10 samples with a 7-bit shape codebook, and varied the size of the gain codebook from 3 to 4 and 5 bits. Then in our next experiments we used a 3-bit gain codebook and trained 8 and 9 bit shape codebooks. Finally, we attempted increasing the size of both the shape and the gain codebooks by one bit. In each case the new codebooks were closed-loop trained using the technique described in Section 8.7.

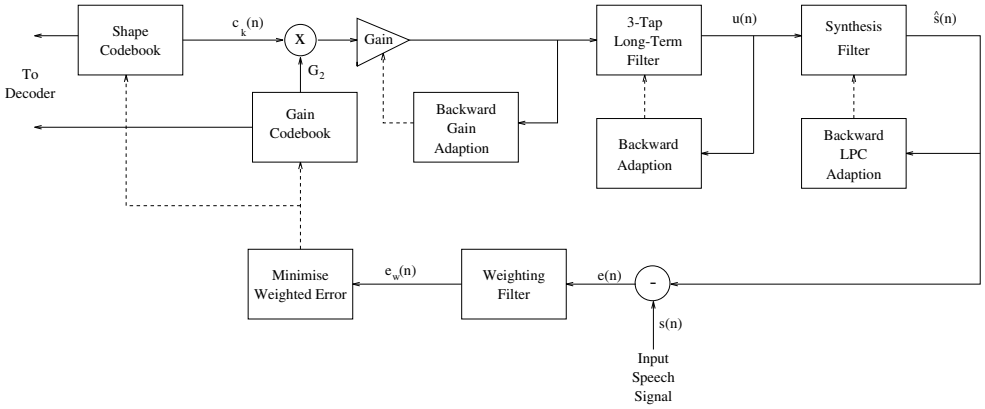

Figure 8.17: Scheme one low-delay CELP codec.

The SEGSNRs of this Scheme One codec with various size shape and gain codebooks is shown in Table 8.12. It can be seen that adding one bit to either the gain or the shape codebook increases the SEGSNR of the codec by about 1 dB. Adding two extra bits to the shape codebook, or one bit each to both codebooks, increases the SEGSNR by almost 2 dB.

Table 8.12: Performance of the scheme one codec with various size gain and shape codebooks.

Gain codebook bits	Shape codebook bits	SEGSNR (dB)
3	7	14.29
4	7	15.24
5	7	15.62
3	8	15.33
3	9	16.12
4	8	16.01

8.9.3 8–4 kbps Codecs – Forward Adaption of the Short-term Synthesis Filter

In this section we consider the improvements that can be achieved in the vector size 10 codec by using forward adaption of the short-term synthesis filter. In Table 8.6 we examined the effects of backward adaption of the synthesis filter at 8 kbps. However, these figures gave the improvements that can be achieved by eliminating the noise feedback and time mismatch that are inherent in backward adaption when using the same recursive windowing function and update rate as the G728 codec. In this section we consider the improvements that could be achieved by significantly altering the structure used for the determination of the synthesis filter parameters.

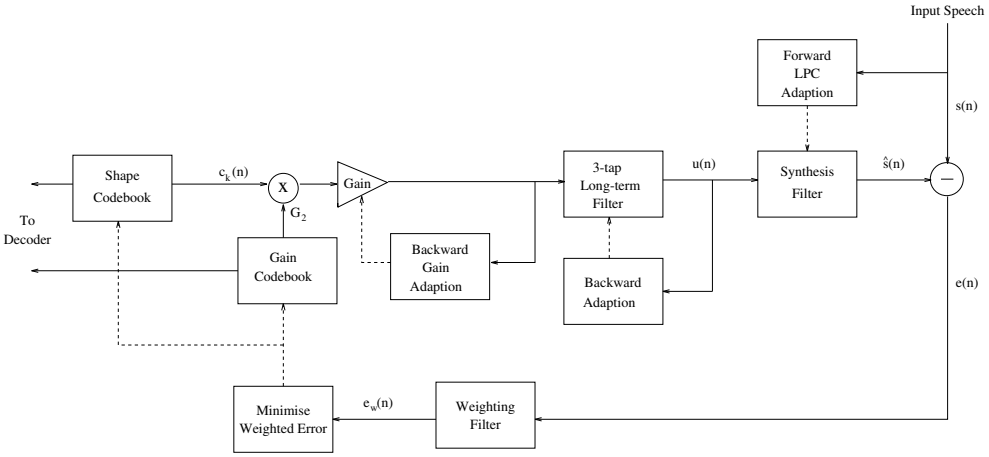

Figure 8.18: Scheme Two low-delay CELP codec.

The codec structure used is shown in Figure 8.18, and we refer to it as 'Scheme Two'. Its only difference from our previously developed 8 kbps backward-adaptive codec is that we replaced the recursive windowing function shown in Figure 8.3 with an asymmetric analysis window which was used in a candidate codec for the CCITT 8 kbps standard [160, 213]. This window, which is shown in Figure 8.19, is made up of half a Hamming window and a quarter of a cosine function cycle. The windowing scheme uses a frame length of 10 ms (or 80 samples), with a 5 ms look-ahead. The 10 ms frame consists of two sub-frames, and a LSF interpolation scheme similar to that described in Section 6.4.3 is used.

We implemented this method of deriving the LPC coefficients in our codec. The vector length was kept constant at 10 samples, but instead of the synthesis filter parameters being updated every 20 samples, as in the Scheme One codec, they were updated every 40 samples using either the interpolated or transmitted LSFs. In the candidate 8 kbps CCITT codec [160] a filter order of ten is used and the ten LSFs are quantised with 19 bits using differential SVQ. However, for simplicity, and in order to see the best performance gain possible for our codec by using forward adaption of the short-term synthesis filter, we used the ten unquantised LSFs to derive the filter coefficients. A new 3-bit gain codebook and 7-bit shape codebook were derived for this codec using the codebook training technique described in Section 8.7.

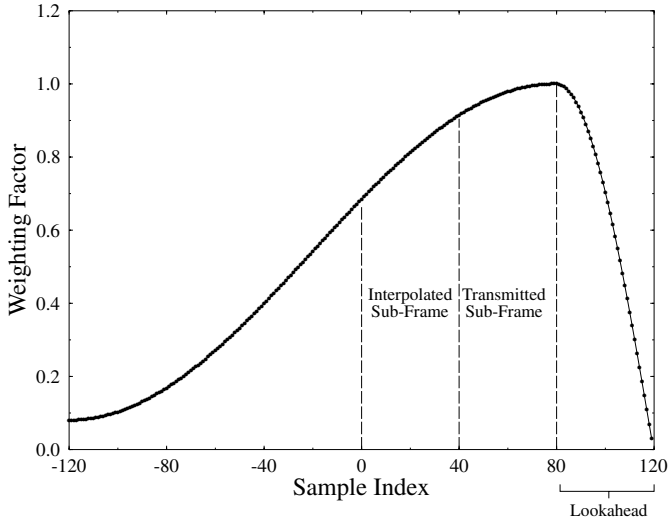

Figure 8.19: LPC windowing function used in candidate CCITT 8 kbps codec.

We found that this forward adaption increased the SEGSNR of the codec by only 0.8 dB, and even this rather small improvement would, of course, be reduced by the quantisation of the LSFs. Using a 19-bit quantisation scheme to transmit a new set of LSFs every 80 sample frame would mean using on average about 2.4 bits per 10 sample vector.

Traditionally, codecs employing forward-adaptive LPC are more resilient to channel errors than those using backward-adaptive LPC. However, a big disadvantage of using such a forward-adaptive LPC scheme is that it would increase the delay of the codec by almost an order of magnitude. Instead of a vector length of 10 samples we would need to buffer a frame of 80 speech samples, plus a 40 sample look-ahead, to calculate the LPC information. This would increase the overall delay of the codec from under 4 ms to about 35 ms.

8.9.4 Forward Adaption of the Long-term Predictor

8.9.4.1 Initial Experiments

In this section we consider the gains in our codec performance which can be achieved using forward adaption of the LTP gain. Although forward adaption of the LTP parameters would improve the codec's robustness to channel errors, we did not consider forward adaption of the LTP delay because to transmit this delay from the encoder to the decoder would require around 7 extra bits per vector. However, we expected to be able to improve the performance of the codec, at the cost of significantly fewer extra bits, by using forward adaption of the LTP gain.

Previously we employed a 3-tap LTP with backward-adapted values for the delay and filter coefficients. Initially we replaced this LTP scheme with an adaptive codebook arrangement, where the delay was still backward adapted but the gain was calculated as in forward-adaptive CELP codecs, which was detailed in Section 6.5. This calculation assumes

that the fixed codebook signal, which is not known until after the LTP parameters are calculated, is zero. The 'optimum' adaptive codebook gain G_1 which minimises the weighted error between the original and reconstructed speech is then given by

$$G_1 = \frac{\sum_{n=0}^{vs-1} x(n)y_\alpha(n)}{\sum_{n=0}^{vs-1} y_\alpha^2(n)}. \tag{8.51}$$

Here $x(n) = s_w(n) - \hat{s}_o(n)$ is the target for the adaptive codebook search, $s_w(n)$ is the weighted speech signal, $\hat{s}_o(n)$ is the zero input response of the weighted synthesis filter, and

$$y_\alpha(n) = \sum_{i=0}^{n} u(i-\alpha)h(n-i) \tag{8.52}$$

is the convolution of the adaptive codebook signal $u(n-\alpha)$ with the impulse response $h(n)$ of the weighted synthesis filter, where α is the backward-adapted LTP delay.

Again, we trained new 7/3-bit shape/gain fixed codebooks, and used the unquantised LTP gain G_1 as given by Equation (8.51). However, we found that this arrangement improved the SEGSNR of our codec by only 0.1 dB over the codec with 3-tap backward-adapted LTP. Therefore we decided to invoke some of the joint adaptive and fixed codebook optimisation schemes described in Section 6.5.2.4. These joint optimisation schemes are described below.

The simplest optimisation scheme – Method A from Section 6.5.2.4 – involves calculating the adaptive and fixed codebook gains and indices as usual, and then updating the two gains for the given codebook indices k and α using Equations (6.28) and (6.29), which are repeated here for convenience:

$$G_1 = \frac{C_\alpha \xi_k - C_k Y_{\alpha k}}{\xi_\alpha \xi_k - Y_{\alpha k}^2} \tag{8.53}$$

$$G_2 = \frac{C_k \xi_\alpha - C_\alpha Y_{\alpha k}}{\xi_\alpha \xi_k - Y_{\alpha k}^2}. \tag{8.54}$$

Here G_1 is the LTP gain, G_2 is the fixed codebook gain,

$$\xi_\alpha = \sum_{n=0}^{vs-1} y_\alpha^2(n) \tag{8.55}$$

is the energy of the filtered adaptive codebook signal and

$$C_\alpha = \sum_{n=0}^{vs-1} x(n)y_\alpha(n) \tag{8.56}$$

is the correlation between the filtered adaptive codebook signal and the codebook target $x(n)$. Similarly, ξ_k is the energy of the filtered fixed codebook signal $[c_k(n) * h(n)]$, and C_k is the correlation between this and the target signal. Finally,

$$Y_{\alpha k} = \sum_{n=0}^{vs-1} y_\alpha(n)[c_k(n) * h(n)] \tag{8.57}$$

is the correlation between the filtered signals from the two codebooks.

We studied the performance of this gain update scheme in our vector length 10 codec. A 7-bit fixed shape codebook was trained, but the LTP and fixed codebook gains were not quantised. We found that the gain update improved the SEGSNR of our codec by 1.2 dB over the codec with backward-adapted 3-tap LTP and no fixed codebook gain quantisation. This is a much more significant improvement than that reported in Section 6.5.2.4 for our 4.7 kbps ACELP codec, because of the much higher update rate for the gains used in our present codec. In our low-delay codec the two gains are calculated for every 10 sample vector, whereas in the 4.7 kbps ACELP codec used in Section 6.5 the two gains are updated only every 60 sample sub-frame.

Encouraged by these results we also invoked the second sub-optimal joint codebook search procedure described in Section 6.5.2.4. In this search procedure the adaptive codebook delay α is determined first by backward adaption in our present codec, and then for each fixed codebook index k the optimum LTP and fixed codebook gains G_1 and G_2 are determined using Equations (8.53) and (8.54) above. The index k which maximises $T_{\alpha k}$,

$$T_{\alpha k} = 2(G_1 C_\alpha + \hat{\sigma} G_2 C_k - \hat{\sigma} G_1 G_2 Y_{\alpha k}) - G_1^2 \xi_\alpha - \hat{\sigma}^2 G_2^2 \xi_k, \tag{8.58}$$

will minimise the weighted error between the reconstructed and the original speech for the present vector, and is transmitted to the decoder. This codebook search procedure was referred to as Method B in Section 6.5.2.4.

We trained a new 7-bit fixed shape codebook for this joint codebook search algorithm, and the two gains G_1 and G_2 were left unquantised. We found that this scheme gave an additional improvement in the performance of the codec so that its SEGSNR was now 2.7 dB higher than the codec with backward-adapted 3-tap LTP and no fixed gain quantisation. Again, this is a much more significant improvement than that which we found for our 4.7 kbps ACELP codec.

8.9.4.2 Quantisation of Jointly Optimized Gains

The improvements quoted above for our vector size 10 codec when we use an adaptive codebook arrangement with joint calculation of the LTP and fixed codebook gains, and no quantisation of either gain, are quite promising. Next we considered the quantisation of the two gains G_1 and G_2. In order to minimise the number of bits used we decided to use a vector quantiser for the two gains. A block diagram of the coding scheme used is shown in Figure 8.20. We refer to this arrangement as 'Scheme Three'.

This Scheme Three codec with forward-adaptive LTP was tested with 4, 5, 6 and 7-bit vector quantisers for the fixed and adaptive codebook gains and a 7-bit shape codebook. The vector quantisers were trained as follows. For a given vector quantiser level i the total weighted energy E_i for speech vectors using this level will be

$$E_i = \sum_{m \in N_i} \left(\sum_{n=0}^{vs-1} (x_m(n) - G_{1i} y_{\alpha m}(n) - G_{2i} \hat{\sigma}_m [h_m(n) * c_m(n)])^2 \right). \tag{8.59}$$

Here $x_m(n)$, $y_{\alpha m}(n)$, and $h_m(n)$ are the signals $x(n)$, $y_\alpha(n)$ and $h(n)$ in the mth vector, $\hat{\sigma}_m$ is the value of the backward adapted gain $\hat{\sigma}$ in the mth vector, $c_m(n)$ is the fixed codebook

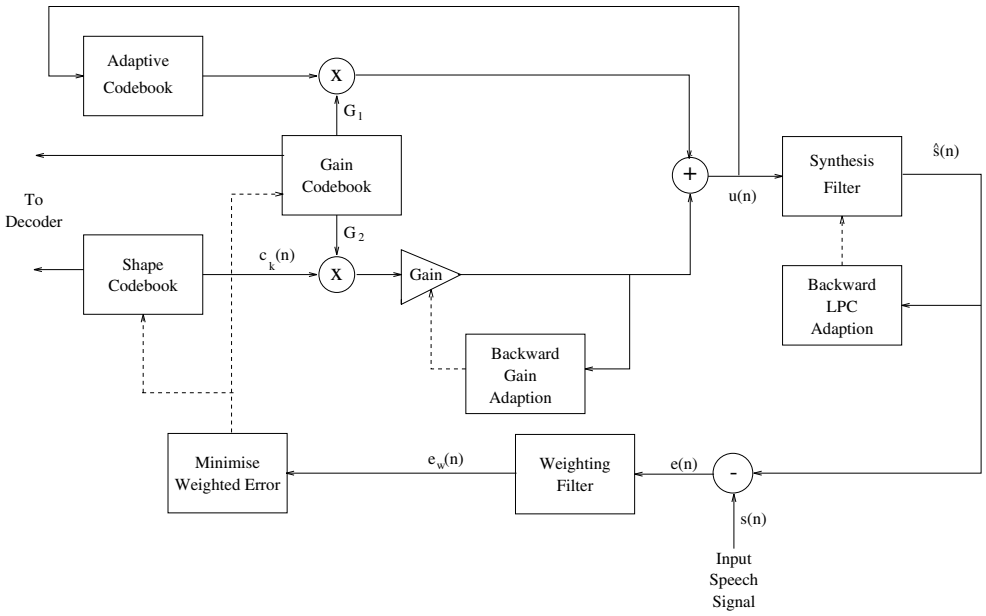

Figure 8.20: Scheme Three low-delay CELP codec.

entry $c_k(n)$ used in the mth vector, G_{1i} and G_{2i} are the values of the two gains in the ith entry of the joint vector quantiser, and N_i is the set of speech vectors that use the ith entry of the vector quantiser. As before, vs is the vector size used in the codec, which in our present experiments is ten.

Expanding Equation (8.59) gives

$$E_i = \sum_{m \in N_i} (X_m + G_{1i}^2 \xi_{\alpha m} + G_{2i}^2 \hat{\sigma}_m^2 \xi_{km} - 2G_{1i} C_{\alpha m} - 2\hat{\sigma}_m G_{2i} C_{km} + 2\hat{\sigma}_m G_{1i} G_{2i} Y_{\alpha km}), \tag{8.60}$$

where $X_m = \sum_{n=0}^{vs-1} x_m^2(n)$ is the energy of the target signal $x_m(n)$, and $\xi_{\alpha m}$, ξ_{km}, $C_{\alpha m}$, C_{km} and $Y_{\alpha km}$ are the values in the mth vector of ξ_α, ξ_k, C_α, C_k and $Y_{\alpha k}$ defined earlier.

Differentiating Equation (8.60) with respect to G_{1i} and setting the result to zero gives

$$\frac{\partial E_i}{\partial G_{1i}} = \sum_{m \in N_i} (2G_{1i}\xi_{\alpha m} - 2C_{\alpha m} + 2\hat{\sigma}_m G_{2i} Y_{\alpha km}) = 0 \tag{8.61}$$

or

$$G_{1i} \sum_{m \in N_i} \xi_{\alpha m} + G_{2i} \sum_{m \in N_i} \hat{\sigma}_m Y_{\alpha m} = \sum_{m \in N_i} C_{\alpha m}. \tag{8.62}$$

Similarly, differentiating with respect to G_{2i} and setting the result to zero gives

$$G_{1i} \sum_{m \in N_i} \hat{\sigma}_m Y_{\alpha km} + G_{2i} \sum_{m \in N_i} \hat{\sigma}_m^2 \xi_{km} = \sum_{m \in N_i} \hat{\sigma}_m C_{km}. \tag{8.63}$$

Solving these two simultaneous equations gives the optimum values of G_{1i} and G_{2i} for the cluster of vectors N_i as

$$G_{1i} = \frac{(\sum_{m \in N_i} C_{\alpha m})(\sum_{m \in N_i} \hat{\sigma}_m^2 \xi_{km}) - (\sum_{m \in N_i} \hat{\sigma}_m C_{km})(\sum_{m \in N_i} \hat{\sigma}_m Y_{\alpha km})}{(\sum_{m \in N_i} \xi_{\alpha m})(\sum_{m \in N_i} \hat{\sigma}_m^2 \xi_{km}) - (\sum_{m \in N_i} \hat{\sigma}_m Y_{\alpha km})^2} \tag{8.64}$$

and

$$G_{2i} = \frac{(\sum_{m \in N_i} \hat{\sigma}_m C_{km})(\sum_{m \in N_i} \xi_{\alpha m}) - (\sum_{m \in N_i} C_{\alpha m})(\sum_{m \in N_i} \hat{\sigma}_m Y_{\alpha km})}{(\sum_{m \in N_i} \xi_{\alpha m})(\sum_{m \in N_i} \hat{\sigma}_m^2 \xi_{km}) - (\sum_{m \in N_i} \hat{\sigma}_m Y_{\alpha km})^2}. \tag{8.65}$$

Using Equations (8.64) and (8.65) we performed a closed-loop training of the vector quantiser gain codebook along with the fixed shape codebook, similar to the training of the shape and single gain codebooks described in Section 8.7. However, we found a similar problem to that which we encountered when training scalar codebooks for G_1 and G_2 in Section 6.5.2.5. Specifically although almost all values of G_1 have magnitudes less than 2, a few values have very high magnitudes. This leads to a few levels in the trained vector quantisers having very high values, and being very rarely used. Following an in-depth investigation into this phenomenon we solved the problem by excluding all vectors for which the magnitude of G_1 was greater than 2 or the magnitude of G_2 was greater than 5 from the training sequence. This approach solved the problems of the trained gain codebooks having some very high and very rarely used levels.

We trained vector quantisers for the two gains using 4, 5, 6 and 7 bits. The values of the 4-bit trained vector quantiser for G_1 and G_2 are shown in Figure 8.21. It can be seen that when G_1 is close to zero, the values of G_2 have a wide range of values between -3 and $+3$, but when the speech is voiced and G_1 is high the fixed codebook contribution to the excitation is less significant, and the quantised values of G_2 are closer to zero.

Our trained joint gain codebooks are searched as follows. For each fixed codebook entry k the optimum gain codebook entry is found by tentatively invoking each pair of gain values in Equation (8.58), in order to test which level maximises $T_{\alpha k}$ and hence minimises the weighted error energy. The SEGSNR of our Scheme Three codec with a trained 7-bit shape codebook and trained 4, 5, 6 and 7-bit joint $G1/G_2$ vector quantisers is shown in Table 8.13. The SEGSNRs in this table should be compared with the value of 14.29 dB obtained for the Scheme One codec with a 3-bit scalar quantiser for G_2 and 3-tap backward-adapted LTP.

It can be seen from Table 8.13 that the joint G_1/G_2 gain codebooks give a steady increase in the performance of the codec as the size of the gain codebook is increased. In the next section we describe the use of backward-adaptive voiced/unvoiced switched codebooks to further improve the performance of our codec.

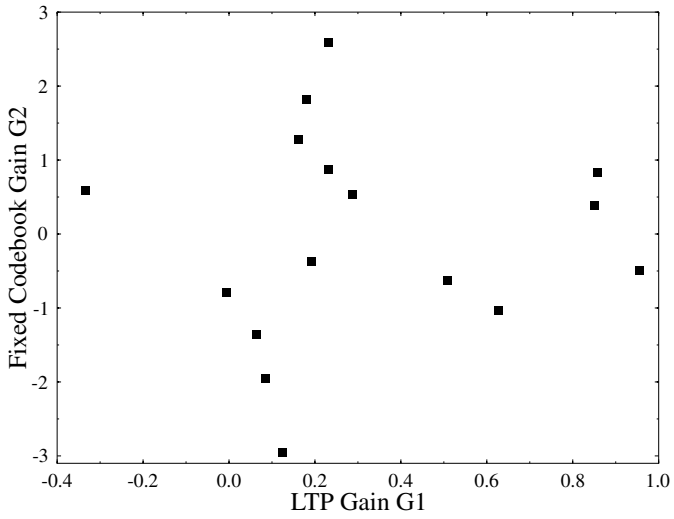

Figure 8.21: Values of G_1 and G_2 in the 4-bit gain quantiser.

Table 8.13: Performance of the Scheme Three codecs.

Gain codebook bits	SEGSNR (dB)
4 bits	14.81
5 bits	15.71
6 bits	16.54
7 bits	17.08

8.9.4.3 8–4 kbps Codecs – Voiced/Unvoiced Codebooks

In Section 8.7 we discussed using different codebooks for voiced and unvoiced segments of speech, and using a backward-adaptive voicing decision to select which codebooks to use. However, we found that in the case of a codec with fully backward-adaptive LTP no significant improvement in the codec's performance was achieved by using switched codebook excitation. In this section we discuss using a similar switching arrangement in conjunction with our Scheme Three codec described above.

The backward-adaptive voiced/unvoiced switching is based on the voiced/unvoiced switching used in the postfilter employed in the G728 codec [109]. In our codec the switch uses the normalised autocorrelation value of the past reconstructed speech signal $\hat{s}(n)$ at the delay α which is used by the adaptive codebook. This normalised autocorrelation value β_α is given by

$$\beta_\alpha = \frac{\sum_{n=-100}^{-1} \hat{s}(n)\hat{s}(n-\alpha)}{\sum_{n=-100}^{-1} \hat{s}^2(n-\alpha)}, \tag{8.66}$$

and when it is greater than a set threshold the speech is classified as voiced; otherwise the speech is classified as unvoiced. In our codec, as in the G728 postfilter, the threshold is set to 0.6.

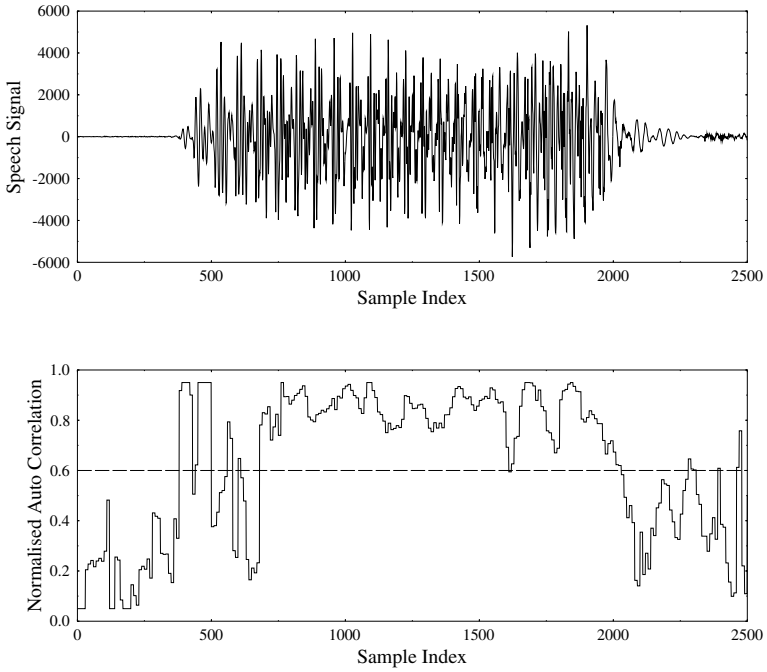

Figure 8.22: Normalised autocorrelation value β_α during voiced and unvoiced speech.

Figure 8.22 shows a segment of the original speech and the normalised autocorrelation value β_α calculated from the reconstructed speech of our 8 kbps codec. To aid the clarity of this graph the values of β_α have been limited to lie between 0.05 and 0.95. It can be seen that the condition $\beta_\alpha > 0.6$ gives a good indication of whether the speech is voiced or unvoiced.

The backward-adaptive voicing decision described above was incorporated into our Scheme Three codec shown in Figure 8.20 to produce a new coding arrangement which we referred to as 'Scheme Four'. Shape and joint gain codebooks were trained as described earlier for both the voiced and unvoiced modes of operation in a vector length 10 codec. The quantised values of G_1 and G_2 in both the 4-bit voiced and unvoiced codebooks are shown in Figure 8.23. It can be seen that similar to Figure 8.21, when G_1 is high the range of values of G_2 is more limited than when G_1 is close to zero. Furthermore, as expected, the voiced codebook has a group of quantiser levels with G_1 close to one, whereas the values of the LTP gain in the unvoiced codebook are closer to zero.

The results we achieved with 7-bit shape codebooks and joint gain codebooks of various sizes are shown in Table 8.14. It can be seen by comparing this to Table 8.13 that the voiced/unvoiced switching gives an improvement in the codec's performance of about 0.25 dB for the 4- and the 5-bit gain quantisers, and a smaller improvement for the 6- and 7-bit gain quantisers.

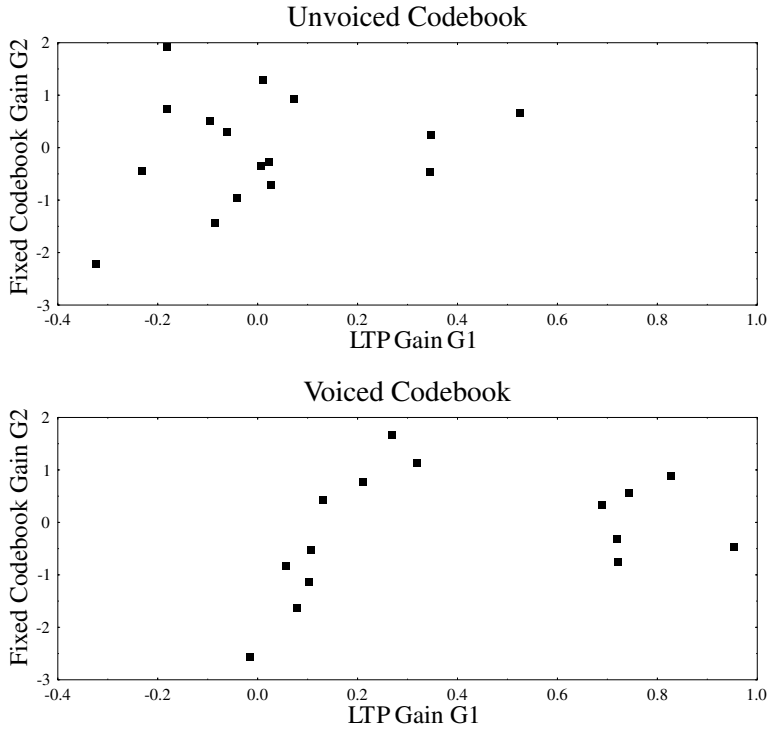

Figure 8.23: Values of G_1 and G_2 in the 4-bit voiced and unvoiced gain quantisers.

Table 8.14: Performance of the Scheme Four codecs.

Gain codebook bits	SEGSNR (dB)
4 bits	15.03
5 bits	15.92
6 bits	16.56
7 bits	17.12

8.9.5 Low-delay Codecs at 4–8 kbps

In the previous three sections we have considered the improvements that can be achieved in our vector size 10 codec by increasing the size of the shape and gain codebooks, and by using forward adaption of the short-term predictor coefficients and the long-term predictor gain. The improvements obtained by these schemes are summarised in Table 8.15, which shows the various gains in the codec's SEGSNR against the number of extra bits used to represent each ten sample vector.

In this table the Scheme One codec (see Section 8.9.2) is the vector size 10 codec, with 3-tap backward-adapted LTP and a 20-tap backward-adapted short-term predictor. The table

Table 8.15: Improvements obtained using schemes one to four.

	Synthesis filter	Long-term predictor	Shape C.B.	Gain C.B.	Extra bits	Δ SEGSNR
Scheme One	Backward adapted $p = 20$	3-tap backward adapted	7 bits	3 bits	0	0 dB
			7 bits	4 bits	1	$+0.95$ dB
			8 bits	3 bits	1	$+1.04$ dB
			7 bits	5 bits	2	$+1.33$ dB
			8 bits	4 bits	2	$+1.72$ dB
			9 bits	3 bits	2	$+1.83$ dB
Scheme Two	Forward adapted $p = 10$	3-tap backward adapted	7 bits	3 bits	≈ 2.4	$\leq +0.82$ dB
Scheme Three	Backward adapted $p = 20$	Forward adapted	7 bits	4 bits	1	$+0.52$ dB
			7 bits	5 bits	2	$+1.42$ dB
			7 bits	6 bits	3	$+2.25$ dB
			7 bits	7 bits	4	$+2.79$ dB
Scheme Four	Backward adapted $p = 20$	Switched forward adapted	7 bits	4 bits	1	$+0.74$ dB
			7 bits	5 bits	2	$+1.63$ dB
			7 bits	6 bits	3	$+2.27$ dB
			7 bits	7 bits	4	$+2.83$ dB

shows the gains in the SEGSNR of the codec that are achieved by adding one or two extra bits to the shape or the scalar gain codebooks.

The Scheme Two codec (see Section 8.9.3) also uses 3-tap backward-adapted LTP, but uses forward adaption to determine the short term synthesis filter coefficients. Using these coefficients without quantisation gives an improvement in the codecs SEGSNR of 0.82 dB, which would be reduced if quantisation were applied. In [160], where forward adaption is used for the LPC parameters, 19 bits are used to quantize a set of LSFs for every 80 sample frame; this quantisation scheme would require us to use about 2.4 extra bits per 10 sample vector.

The Scheme Three codec (see Section 8.9.4) uses backward adaption to determine the short-term predictor coefficients and the long-term predictor delay. However, forward adaption is used to find the LTP gain, which is jointly determined along with the fixed codebook index and gain. The LTP gain and the fixed codebook gain are jointly vector quantised using 4, 5, 6 or 7-bit quantisers, which implies using between 1 and 4 extra bits per 10 sample vector.

Finally, the Scheme Four codec uses the same coding strategy as the Scheme Three codec, but also implements a backward-adapted switch between specially trained shape and vector gain codebooks for the voiced and unvoiced segments of speech.

It is clear from Table 8.15 that, for our vector size 10 codec, using extra bits to allow forward adaption of the synthesis filter parameters is the least efficient way of using these extra bits. If we were to use two extra bits the largest gain in the codec's SEGSNR is given if we simply use the Scheme One codec and increase the size of the shape codebook by 2 bits.

This gain is almost matched if we allocate one extra bit to both the shape and gain codebooks in the Scheme One codec, and this would increase the codebook search complexity less dramatically than allocating both extra bits to the shape codebook.

In order to give a fair comparison between the different coding schemes at bitrates between 4 and 8 kbps we tested the Schemes One, Three and Four codecs using 8-bit shape codebooks, 4-bit gain codebooks and vector sizes of 12, 15, 18 and 24 samples. This gave three different codecs at 8, 6.4, 5.3 and 4 kbps. Note that as the vector size of the codecs increase, their complexity also increases. Methods of reducing this complexity are possible [281], but have not been studied in our work. The SEGSNRs of our three 4–8 kbps codecs against their bitrates is shown in Figure 8.24.

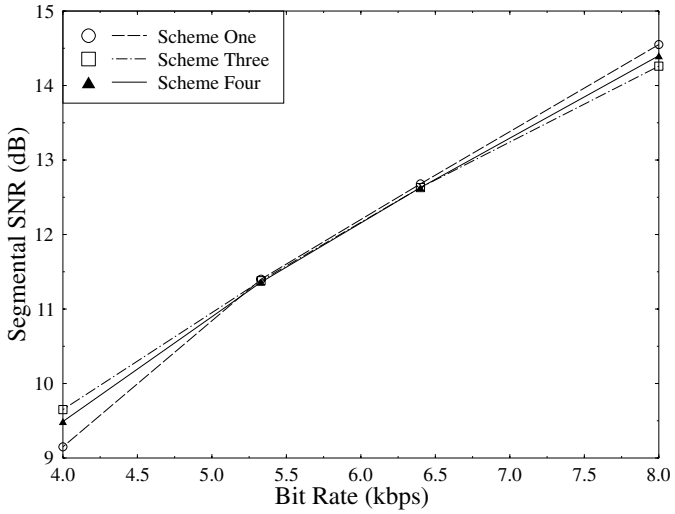

Figure 8.24: Performance of Schemes One, Three and Four codecs at 4–8 kbps.

Several observations can be made from this graph. At 8 kbps, as expected from the results in Table 8.15, the Scheme One codec gives the best quality reconstructed speech, with a SEGSNR of 14.55 dB. However, as the vector size is increased and hence the bitrate reduced it is the Scheme One codec whose performance is most badly affected. At 6.4 kbps and 5.3 kbps all three codecs give very similar SEGSNRs, but at 4 kbps the Scheme One codec is clearly worse than the other codecs, which use forward adaption of the LTP gain. This indicates that although the 3-tap backward-adapted LTP is very effective at 8 kbps and above, it is less effective as the bitrate is reduced. Furthermore, the backward-adaptive LTP scheme is more prone to channel error propagation.

Similarly, as indicated in Table 8.15, the backward-adaptive switching between specially trained voiced and unvoiced gain and shape codebooks improves the performance of our Scheme Four codec at 8 kbps so that it gives a higher SEGSNR than the Scheme Three codec. However, as the bitrate is reduced the gain due to this codebook switching is eroded, and at 4 kbps the Scheme Four codec gives a lower SEGSNR than the Scheme Three codec. This is due to inaccuracies in the backward-adaptive voicing decisions at the lower bitrates. Figure 8.25 shows the same segment of speech as was shown in Figure 8.22, and the

normalised autocorrelation value β_α calculated from the reconstructed speech of our Scheme Four codec at 4 kbps. It can be seen that the condition $\beta_\alpha > 0.6$ no longer gives a good indication of the voicing of the speech. Again, for clarity of display the values of β_α have been limited to between 0.05 and 0.95 in this figure.

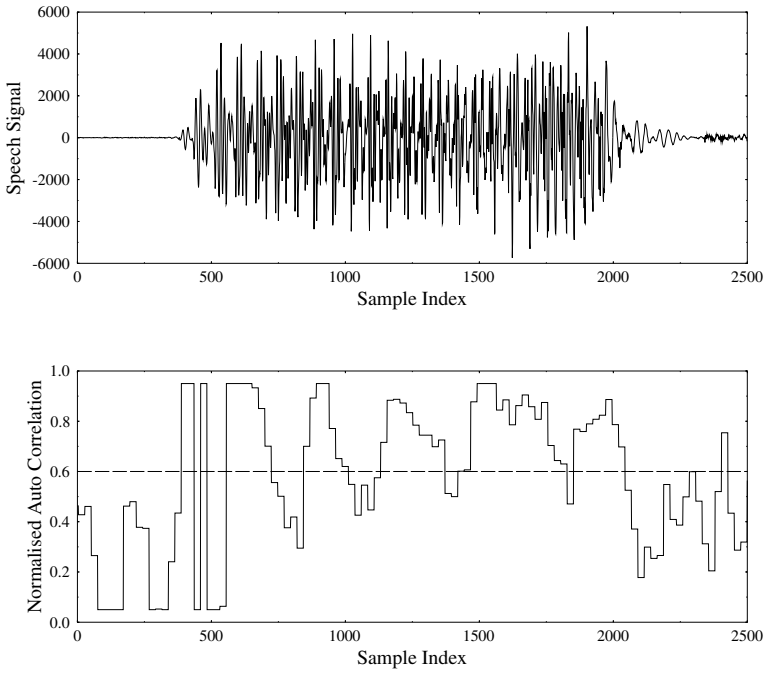

Figure 8.25: Normalised autocorrelation value β_α during voiced and unvoiced speech.

In listening tests we found that all three codecs gave near toll quality speech at 8 kbps, with differences between the codecs being difficult to distinguish. However, at 4 kbps the Scheme Two codec sounded clearly better than the Scheme One codec, and gave reconstructed speech of communications quality.

8.9.6 Low-delay ACELP Codec

In this section of our work on low-delay CELP codecs operating between 4 and 8 kbps we implemented a low-delay version of our ACELP codec which was described in Section 6.4.3. We developed a series of low-delay codecs with a frame size of 40 samples or 5 ms, and hence a total delay of about 15 ms, and with various bitrates between 5 and 6.2 kbps. All of these codecs use backward adaption with the recursive windowing function described in Section 8.4.2 in order to determine the coefficients for the synthesis filter, which has an order of $p = 20$. Furthermore, they employ the same weighting filter, which was described in Section 8.4.1, as our other low-delay codecs. However, apart from this they have a structure similar to the codecs described in Section 6.4.3. An adaptive codebook is used to represent the long-term periodicities of the speech, with possible delays taking all integer values between

20 and 147 and being represented using 7 bits. As described in Section 6.4.3 the best delay is calculated once per 40 sample vector within the AbS loop at the encoder, and then transmitted to the decoder.

Initially we used the 12-bit ACELP fixed codebook structure shown in Table 6.4 which is repeated here in Table 8.16. Each 40 sample vector has a fixed codebook signal given by four non-zero pulses of amplitude $+1$ or -1, whose possible positions are shown in Table 8.16. Each pulse position is encoded with 3 bits giving a 12-bit codebook. As was explained in Section 6.3, the pulse positions can be found using a series of four nested loops, leading to a very efficient codebook search algorithm [93, 162].

Table 8.16: Pulse amplitudes and positions for the 12-bit ACELP codebook.

Pulse number i	Amplitude	Possible position m_i
0	$+1$	1, 6, 11, 16, 21, 26, 31, 36
1	-1	2, 7, 12, 17, 22, 27, 32, 37
2	$+1$	3, 8, 13, 18, 23, 28, 33, 38
3	-1	4, 9, 14, 19, 24, 29, 34, 39

In our first low-delay ACELP codec, which we refer to as Codec A, we used the same 3- and 5-bit scalar quantisers as were used in the codecs in Section 6.4.3 to quantize the adaptive and fixed codebook gains G_1 and G_2. This meant that 12 bits were required to represent the fixed codebook index, 7 bits for the adaptive codebook index and a total of 8 bits to quantize the two codebook gains. This gave a total of 27 bits to represent each 40 sample vector, giving a bitrate for this codec of 5.4 kbps. We found that this codec gave an average SEGSNR of 10.20 dB, which should be compared to the average SEGSNRs for the same speech files of 9.83 dB, 11.13 dB and 11.42 dB for our 4.7 kbps, 6.5 kbps and 7.1 kbps forward-adaptive ACELP codecs described in Section 6.4.3. All of these codecs have a similar level of complexity, but the backward-adaptive 5.4 kbps ACELP codec has a frame size of only 5 ms, compared to the frame sizes of 20 or 30 ms for the forward-adaptive systems. Furthermore, it can be seen from Figure 8.26 that, upon interpolating the SEGSNRs between the three forward-adaptive ACELP codecs, the backward-adaptive ACELP codec at 5.4 kbps gives a very similar level of performance to the forward-adaptive codecs. In this figure we have marked the SEGSNRs of the three forward-adaptive ACELP codecs with circles, and the SEGSNR of our low-delay ACELP codec at 5.4 kbps with a diamond. Also marked with diamonds are the SEGSNRs and bitrates of other backward-adaptive ACELP codecs which will be described later. For comparison, the performance of the Scheme One low-delay codec, described in Section 8.9.5 and copied from Figure 8.24, is also shown.

It can be seen from Figure 8.26 that although the 5.4 kbps low-delay backward-adaptive ACELP codec described above gives a similar performance in terms of SEGSNR to the higher-delay forward-adaptive ACELP codecs, it performs significantly worse than the Scheme One codec of Table 8.15, which uses a shorter vector size and a trained shape codebook. We therefore attempted to improve the performance of our low-delay ACELP codec by introducing vector quantisation and joint determination of the two codebook gains G_1 and G_2. Note that similar vector quantisation and joint determination of these gains was

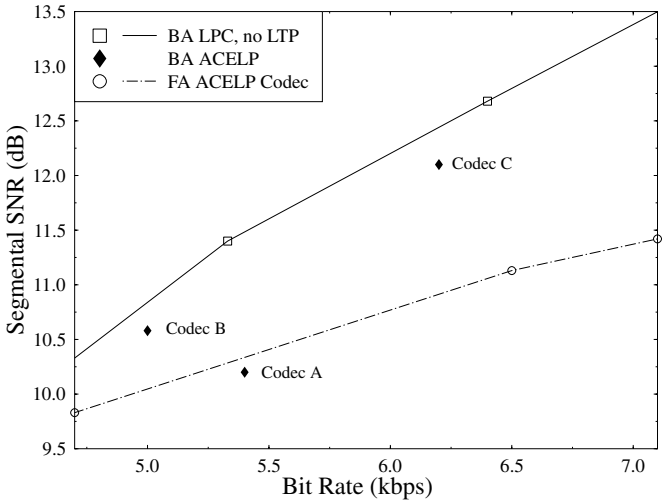

Figure 8.26: Performance of low-delay ACELP codecs.

used in the Schemes Three and Four codecs described in Section 8.9.5. We also re-introduced the backward adaption of the fixed codebook gain G_2 – as known from the schematic of the G.728 decoder seen in Figure 8.2, which was used in our other low-delay codecs as detailed in Section 8.4.3. We replaced the 3- and 5-bit scalar quantisers for G_1 and G_2 with a 6-bit joint vector quantiser for these gains, which resulted in a total of 25 bits being used to represent each 40 sample vector and therefore gave us a 5 kbps codec. We refer to this as Codec B. The joint 6-bit vector quantiser for the gains was trained as described in Section 8.9.4.2. A joint codebook search procedure was used so that for each fixed codebook index k the joint gain codebook was searched to find the gain codebook index which minimised the weighted error for that fixed codebook index. The best shape and gain codebook indices are therefore determined together. This codebook search procedure results in a large increase in the complexity of the codec, but also significantly increases the performance of the codec.

We found that our 5 kbps Codec B, using joint vector quantisation of G_1 and G_2 and backward adaption of G_2, gave an average SEGSNR of 10.58 dB. This is higher than the SEGSNR of the codec with scalar gain quantisation, i.e. Codec A, despite Codec B having a lower bitrate. The performance of this Codec B is marked with a diamond in Figure 8.26, which shows that it falls between the SEGSNRs of the ACELP codecs with scalar gain quantisation and the Scheme One codecs.

Next, we replaced the 12-bit algebraic codebook detailed in Table 8.16 with the 17-bit algebraic codebook used in the G.729 ACELP codec described in Section 7.8. Also, the 6-bit vector quantisation of the two gains was replaced with 7-bit vector quantisation. This gave a 6.2 kbps codec, referred to as Codec C, which is similar to the G.729 codec. The main difference between G.729 and our Codec C is that G.729 uses forward adaption to determine the LPC coefficients, whereas Codec C uses backward adaption. This implies that it does not transmit the 18 bits per 10 ms that G.729 uses to represent the LPC parameters, and hence it operates at a bitrate 1.8 kbps lower. Also, its buffering delay is halved to only 5 ms.

We found that this Codec C gave reconstructed speech with a SEGSNR of 12.1 dB, as shown in Figure 8.26. It can be seen that our G.729-like codec gives a better SEGSNR than the forward-adaptive ACELP codecs described earlier. This is because of the more advanced 17-bit codebook, together with the joint determination and vector quantisation of the fixed and the adaptive codebook gains used in the backward-adaptive ACELP codec. It is also clear from Figure 8.26 that Codec C gives a similar performance to the backward-adaptive variable-rate codecs with trained codebooks. Subjectively, we found that Codec C gave speech of good communications quality but significantly lower than that of the toll quality produced by the forward-adaptive G729. Even so, this codec may be preferred to G.729 in situations where a lower bitrate and delay are required, and the lower speech quality can be accepted.

The characteristics of our low-delay ACELP codecs are summarised in Table 8.17. In the next section we discuss error sensitivity issues relating to the low-delay codecs described in this chapter.

Table 8.17: Performance and structure of low-delay ACELP codecs.

	Algebraic codebook	Gain quantisation	Bitrate (kbps)	SEGSNR
Codec A	12 bit	$3+5$ bit scalar	5.4	10.2 dB
Codec B	12 bit	6 bit vector	5	10.6 dB
Codec C	17 bit	7 bit vector	6.2	12.1 dB

8.10 Backward-adaptive Error Sensitivity Issues

Traditionally, one serious disadvantage of using backward adaption of the synthesis filter is that it is more sensitive to channel errors than forward adaption. In this section we first consider the error sensitivity of the 16 kbps G728 codec described earlier. We then discuss the error sensitivity of the 4-8 kbps low-delay codecs described earlier, and means of improving this error sensitivity. Finally, we investigate the error sensitivity of our low-delay ACELP codec described above, and compare this to the error sensitivity of a traditional forward-adaptive ACELP codec.

8.10.1 The Error Sensitivity of the G728 Codec

As described earlier, for each five sample speech vector the G728 codec produces a 3-bit gain codebook index, and an 8-bit shape codebook index. Figure 8.27 shows the sensitivity to channel errors of these ten bits. The error sensitivities were measured for each bit, by corrupting the given bit only with a 10% BER. This approach was taken, rather than the more usual method of corrupting the given bit in every frame, to allow account to be taken of the possible different error propagation properties of different bits [169]. Bits 1 and 2 in Figure 8.27 represent the magnitude of the excitation gain, bit 3 represents the sign of this gain, and the remaining bits are used to code the index of the shape codebook entry chosen to represent the excitation. It can be seen from this figure that not all ten bits are equally

sensitive to channel errors. Notice for example that bit 2, representing the most significant bit of the excitation gain's magnitude, is particularly sensitive.

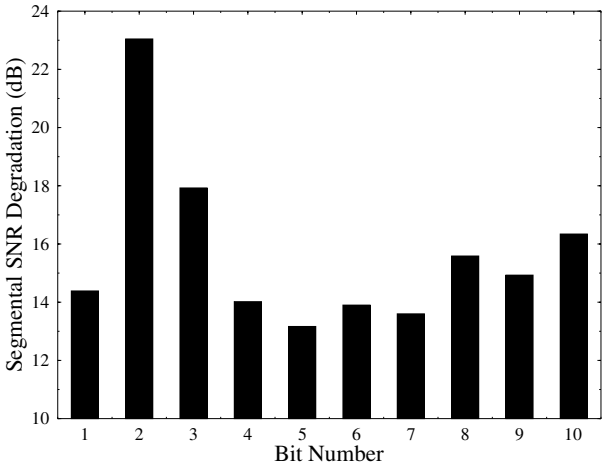

Figure 8.27: Degradation in G728 SEGSNR caused by 10% BER in given bits.

This unequal error sensitivity can also be seen from Figure 8.28, which shows the SEGSNR of the G728 codec for channel BERs between 0.001% and 1%. The solid line shows the performance of the codec when the errors are equally distributed amongst all ten bits, whereas the dashed lines show the performance when the errors are confined only to the five most sensitive bits (the so called 'Class One' bits) or the five least sensitive bits (the 'Class Two' bits). The ten bits were arranged into these two groups based on the results shown in Figure 8.27 – bits 2, 3, 8, 9 and 10 formed Class One and the other five bits formed Class Two. It can be seen that the Class One bits are about two or three times more sensitive than the Class Two bits. Therefore, it is clear that when the G728 codec is employed in an error-prone transmission scheme, for example in a mobile radio transmission system, the error resilience of the system will be improved if un-equal error protection is employed [279]. The use of un-equal error protection for speech codecs is discussed in detail later.

8.10.2 The Error Sensitivity of our 4–8 kbps Low-delay Codecs

We now consider the error sensitivity of some of our 4–8 kbps codecs which were described in Section 8.9.5. It is well known that codecs using backward adaption for both the LTP delay and gain are very sensitive to bit errors, and this is why LTP was not used in G728 [94]. Thus, as expected, we found that the Scheme One codec gave a very poor performance, when subjected to even a relatively low BER. Unfortunately, we also found similar results for the Schemes Three and Four codecs, which, although they used backward adaption for the LTP delay, used forward adaption for the LTP gain. We therefore decided that none of these codecs are suitable for use over error-prone channels. However, the Scheme One codec can be easily modified by removing its entirely backward-adapted 3-tap LTP and increasing the order of its short-term filter to 50 as in G728, to make it less sensitive to channel errors. Although this impairs the performance of the codec, as can be seen from Figure 8.29 the resulting

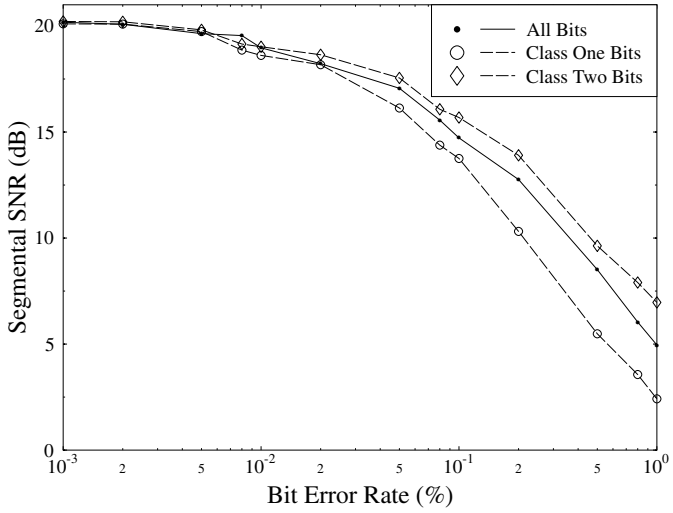

Figure 8.28: SEGSNR of the G728 Codec versus channel BER.

degradation in the codec's SEGSNR is not too serious, especially at low bitrates. Therefore, in this section we detail the error sensitivity of the Scheme One codec with its LTP removed, and describe a means of making this codec less sensitive to channel errors. For simplicity, only the error sensitivity of the codec operating with a frame length of 15 samples and a bitrate of 6.4 kbps are considered in this section. However, similar results also apply at the other bitrates.

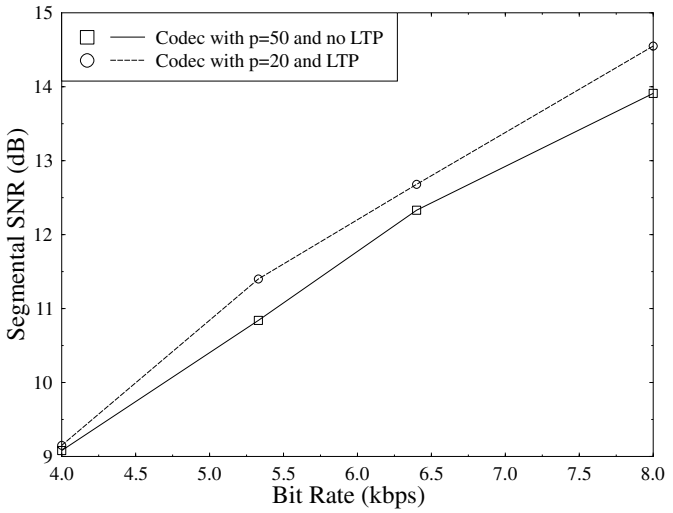

Figure 8.29: SEGSNR of the G728 codec versus channel BER.

At 6.4 kbps our codec transmits only 12 bits per 15 sample frame from the encoder to the decoder. Of these 12 bits, 8 are used to represent the index of the shape codebook and the remaining 4 bits are used to represent the index of the gain codebook entry used. The error resilience of these bits can be significantly improved by careful assignment of codebook indices to the various codebook entries. Ideally, each codebook entry would be assigned an index so that corruption of any of the bits representing this index will result in another entry being selected in the decoder's codebook which is in someway 'close' to the intended codebook entry. If this ideal can be achieved, then the effects of errors in the bits representing the codebook indices will be minimised.

Consider first the 8-bit shape codebook. Initially, the 256 available codebook indices are effectively randomly distributed amongst the codebook entries. We seek to rearrange these codebook indices so that when the index representing a codebook entry is corrupted, the new index will represent a codebook entry that is 'close' to the original entry. In our work we chose to measure this 'closeness' by the squared error between the original and the corrupted codebook entries. We considered only the effects of single bit errors among the 8 codebook bits because at reasonable BERs the probability of two or more errors occurring in 8 bits will be small. Thus for each codebook entry the 'closeness' produced by a certain arrangement of codebook entries is given by the sum of the squared errors between the original codebook entry and the eight corrupted entries that would be produced by inverting each of the 8 bits representing the entry's index. The overall 'cost' of a given arrangement of codebook indices is then given by the closeness for each codebook entry, weighted by the probability of that codebook entry being used. Thus the cost we seek to minimise is given by

$$\text{Cost } = \sum_{j=0}^{255} P(j) \left[\sum_{i=1}^{8} \left(\sum_{n=1}^{15} (c_j(n) - c_j^i(n))^2 \right) \right], \tag{8.67}$$

where $P(j)$ is the probability of the jth codebook entry being used, $c_j(n)$, $n = 1, \ldots, 15$, is the jth codebook entry and $c_j^i(n)$ is the entry that will be received if the index j is transmitted but the ith bit of this index is corrupted.

The problem of choosing the best arrangement of the 256 codebook indices among the codebook entries is similar to the famous travelling salesman problem. In this problem the salesman must visit each of N cities, and must choose the order in which he visits the cities so as to minimise the total distance he travels. As N becomes large it becomes impractical to solve this problem using an exhaustive search of all possible orders in which he could visit the cities – the complexity of such a search is proportional to $N!$ Instead, a non-exhaustive search must be used which we hope will find the best order possible in which to visit the N cities.

The minimisation method of simulated annealing has been successfully applied to this problem [177], and has also been used by other researchers as a method of improving the error resilience of quantisers [282]. Simulated annealing works, as its name suggests, in analogy to the annealing (or slow cooling) of metals. When metals cool slowly from their liquid state they start in a very disordered and high-energy state and reach equilibrium in an extremely ordered crystalline state. This crystal is the minimum energy state for the system, and simulated annealing similarly allows us to find the global minimum of a complex function with many local minima. The procedure works as follows. The system starts in an initial state, which in our situation is an initial assignment of the 256 codebook indices to the codebook

entries. A temperature-like variable T is defined, and possible changes to the state of the system are randomly generated. For each possible change the difference ΔCost in the cost between the present state and the possible new state is evaluated. If this is negative, i.e. the new state has a lower cost than the old state, then the system always moves to the new state. If on the other hand ΔCost is positive then the new state has a higher cost than the old state, but the system may still change to this new state. The probability of this happening is given by the Boltzmann distribution

$$\text{prob} = \exp\left(\frac{-\Delta\text{Cost}}{kT}\right), \tag{8.68}$$

where k is a constant. The initial temperature is set so that kT is much larger than any ΔCost that is likely to be encountered, so that initially most offered moves will be taken. As the optimisation proceeds the 'temperature' T is slowly decreased, and the number of moves to states with higher costs reduces. Eventually kT becomes so small that no moves with positive ΔCost are taken, and the system comes to equilibrium in what is hopefully the global minimum of its cost.

The advantage of simulated annealing over other optimisation methods is that it should not be deceived by local minima and should slowly make its way towards the global minimum of the function to be minimised. In order to make this likely to happen it is important to ensure that the temperature T starts at a high enough value, and is reduced suitably slowly. We followed the suggestions in [177] and reduced T by 10% after every $100N$ offered moves, or every $10N$ accepted moves, where N is the number of codebook entries (256). The initial temperature was set so that kT was equal to ten times the highest value of ΔCost that was initially encountered. The random changes in the state of the system were generated by randomly choosing two codebook entries and swapping the indices of these two entries.

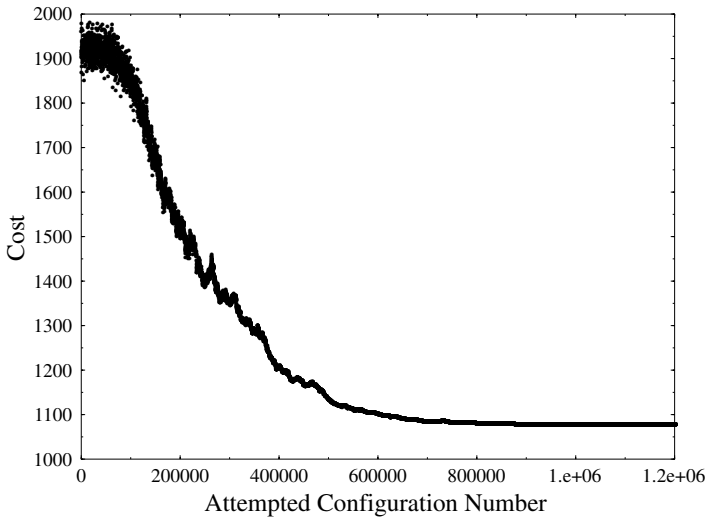

Figure 8.30: Reduction in cost using simulated annealing.

The effectiveness of the simulated annealing method in reducing the cost given in Equation (8.67) is shown in Figure 8.30. This graph shows the cost of the present arrangement of codebook indices versus the number of arrangements of codebook indices which have been tried by the minimisation process. The initial randomly assigned arrangement of indices to codebook entries gives a cost of 1915. As can be seen in Figure 8.30, initially the temperature T is high and so many index assignments which have a higher cost than this are accepted. However, as the number of attempted configurations increases, the temperature T is gradually decreased. Hence only a reduced number of re-arrangements are accepted which would increase the cost of the present arrangement. Thus, as seen in Figure 8.30, the cost of the present arrangement slowly falls. The resultant curve narrows as the temperature increases and less re-arrangements which increase the cost of the present arrangement are accepted. The cost of the final arrangement of codebook indices to codebook entries is 1077, which corresponds to a reduction in the cost of about 44%.

The effectiveness of this re-arrangement of codebook indices in increasing the resilience of the codec to errors in the bitstream between its encoder and decoder can be seen in Figure 8.31. This graph shows the variation in the SEGSNR of our 6.4 kbps low-delay codec with the BER between its encoder and decoder. The solid line shows the performance of the codec with the original codebook index assignment, and the lower dashed line shows the performance when the shape codebook indices are re-arranged as described above. It can be seen that at BERs of between 0.1% and 1% the codec with the re-arranged codebook indices has a SEGSNR about 0.5 to 1 dB higher than the original codec.

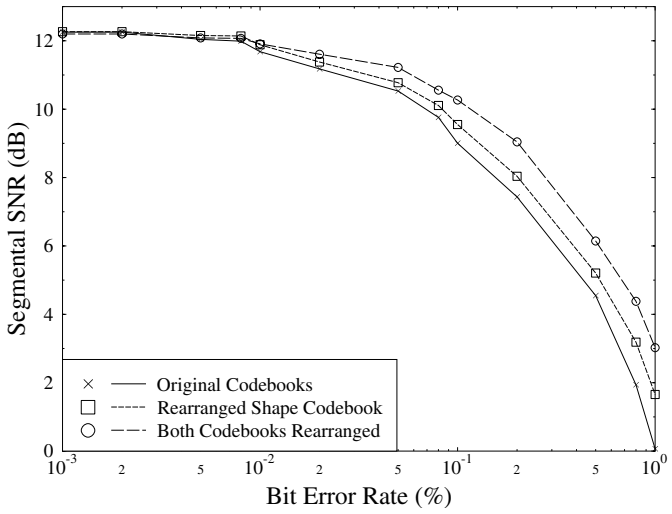

Figure 8.31: The error sensitivity of our low-delay 6.4 kbps codec.

Apart from the 8 shape codebook bits which the codec transmits from its encoder to the decoder, the only other information that is explicitly transmitted are the 4 bits representing the gain codebook entry selected. Initially, indices were assigned to the 16 gain codebook entries using the simple natural binary code (NBC). However, because the gain codebook levels do not have an equi-probable distribution this simple assignment can be improved

upon in a similar way to that described for the shape codebook described above. Again, we defined a cost function that was to be minimised. This cost function was similar to that given in Equation (8.67) except because the gain codebook is scalar, whereas the shape codebook has a vector dimension of 15, no summation over n is needed in the cost function for the gain codebook index arrangement. We used simulated annealing again to reduce the cost function over that given using a NBC and found that we were able to reduce the cost by over 60%. The effect of this re-arrangement of the gain codebook indices is shown by the upper curve in Figure 8.31 which gives the performance of the Scheme One codec with LTP removed, with both the gain and shape codebooks re-arranged. It can be seen that the re-arrangement of the gain codebook indices gives a further improvement in the error resilience of the codec, and that the codec with both the shape and gain codebooks re-arranged has a SEGSNR more than 1 dB higher than the original codec at BERs around 0.1%.

8.10.3 The Error Sensitivity of our Low-delay ACELP Codec

The SEGSNR of our 6.2 kbps low-delay ACELP codec described in Section 8.9.6 is shown in Figure 8.32. Also shown in this figure are the error sensitivities of our 6.4 kbps Scheme One codec with no LTP, and of a traditional 6.5 kbps forward-adaptive ACELP codec. As noted above, at 0% BER the two backward-adaptive codecs give similar SEGSNRs, but the forward-adaptive codec gives a SEGSNR of about 1 dB lower. However, in subjective listening tests the better spectral match provided by the forward-adaptive codec, which is not adequately reflected in the SEGSNR distortion measure, results in it providing better speech quality than the two backward-adaptive codecs. As the BER is increased the backward-adaptive ACELP is the worst affected, but surprisingly the other backward-adaptive codec is almost as robust to channel errors as the forward-adaptive ACELP codec. Both these codecs give a graceful degradation in their reconstructed speech quality at BERs up to about 0.1%, but provide impaired reconstructed speech for BERs much above this.

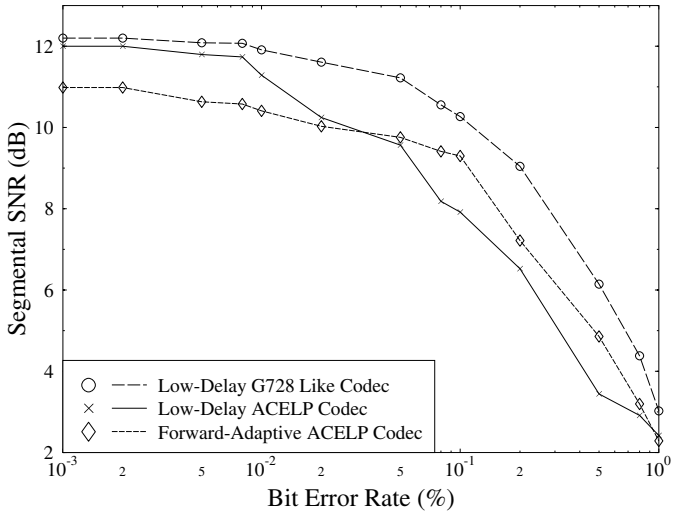

Figure 8.32: A comparison of the bit error sensitivities of backward- and forward-adaptive codecs.

In the next section we provide an application scenario for employing the previously designed G.728-like 8–16 kbps speech codecs and evaluate the performance of the transceiver proposed.

8.11 A Low-delay Multimode Speech Transceiver

8.11.1 Background

The intelligent, adaptively reconfigurable wireless systems of the near future require programmable source codecs in order to optimally configure the transceiver to adapt to time-variant channel and traffic conditions. Hence we designed a flexible transceiver for the previously portrayed programmable 8–16 kbps low-delay speech codec, which is compatible with the G728 16 kbps ITU codec at its top rate and offers a graceful trade-off between speech quality and bitrate in the range 8–16 kbps. Source-matched BCH codecs combined with un-equal protection pilot-assisted 4- and 16-QAM are employed in order to transmit both the 8 and the 16 kbps coded speech bits at a signalling rate of 10.4 kBd. In a bandwidth of 1728 kHz, which is used by the DECT system, 55 duplex or 110 simplex time slots can be created. We will show that good toll quality speech is delivered in an equivalent user bandwidth of 15.71 kHz, if the channel SNR and SIR are in excess of about 18 and 26 dB for the lower and higher speech quality 4-QAM and 16-QAM modes, respectively.

8.11.2 8–16 kbps Codec Performance

The SEGSNR versus bitrate performance of our 8–16 kbps codec was shown in Figure 8.16. The unequal bit error sensitivity of the codec becomes explicit in Figure 8.28, showing the SEGSNR of the G728 codec for channel BERs between 0.001% and 1%. The ten bits were arranged into these two groups based on the results shown in Figure 8.27 – bits 2, 3, 8, 9 and 10 formed Class One and the other five bits formed Class Two. It can be seen that the Class One bits are about two or three times more sensitive than the Class Two bits, and therefore should be more strongly protected by the error correction and modulation schemes. For robustness reasons we have refrained from using a LTP.

We also investigated the error sensitivity of the 8 kbps mode of our low-delay codec. LTP was not invoked, but the codec with a vector size of ten was used because, as was seen earlier, it gave a SEGSNR almost 2 dB higher than the 8 kbps mode of the codec with a constant vector size of five. As discussed in Section 8.7, the vector codebook entries for our codecs were trained as described in [276]. However, the 7-bit indices used to represent the 128 codebook entries are effectively randomly assigned. This assignment of indices to codebook entries does not affect the performance of the codec in error-free conditions, but it is known that the robustness of vector quantisers to transmission errors can be improved by the careful allocation of indices to codebook entries [277]. This can be seen from Figure 8.33 which shows the SEGSNR of the 8 kbps codec for BERs between 0.001% and 1%. The solid line shows the performance of the codec using the codebook with the original index assignment, whereas the dashed line shows the performance of the codec when the index assignment was modified to improve the robustness of the codebook. A simple, non-optimum, algorithm was used to perform the index assignment and it is probable that the codec's robustness could be further improved by using a more effective minimisation algorithm such as simulated

annealing. Also, as in the G728 codec, a NBC was used to represent the eight quantised levels of the excitation gain. It is likely that the use, for example, of a Gray code to represent the eight gain levels could also improve the codec's robustness.

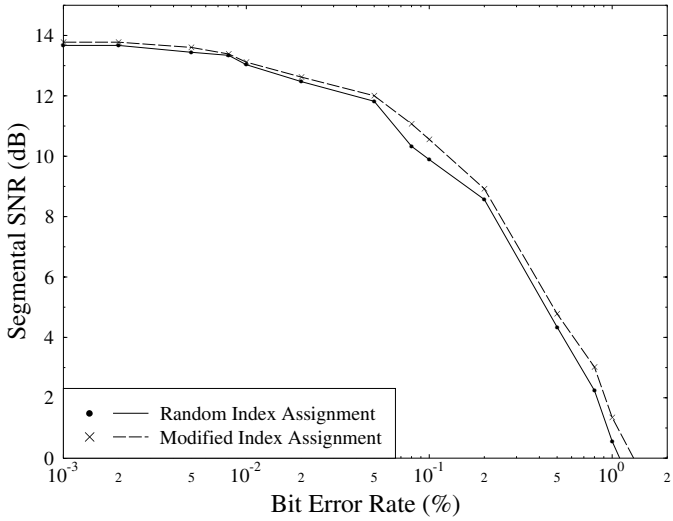

Figure 8.33: SEGSNR of 8 kbps codec versus channel BER for original and rearranged codebooks.

The sensitivity of the ten bits used to represent each ten speech sample vector in our 8 kbps codec is shown in Figure 8.34. Again, bits 1, 2 and 3 are used to represent the excitation gain, and the other 7 bits represent the index of the codebook entry chosen to code the excitation shape. As in the case of the G728 codec the unequal error resilience of different bits can be clearly seen. Note, in particular, how the least significant of the 3 bits representing the excitation gain is much less sensitive than the 7 bits representing the codebook index, but that the two most sensitive gain bits are more sensitive than the codebook index bits.

Figure 8.35 shows the SEGSNR of the 8 kbps codec for BERs between 0.001% and 1%. Again, the solid line shows the performance of the codec when the errors are equally distributed amongst all ten bits, whereas the dashed lines show the performance when the errors are confined only to the five most sensitive Class One bits or the five least sensitive Class Two bits. The need for the more sensitive bits to be more protected by the FEC and modulation schemes is again apparent. These schemes, and how they are used to provide the required unequal error protection, are discussed in the next section.

8.11.3 Transmission Issues

8.11.3.1 Higher-quality Mode

Based on the bit-sensitivity analysis presented in the previous section we designed a sensitivity-matched transceiver scheme for both the higher and lower quality speech coding modes. Our basic design criterion was to generate an identical signalling rate in both modes

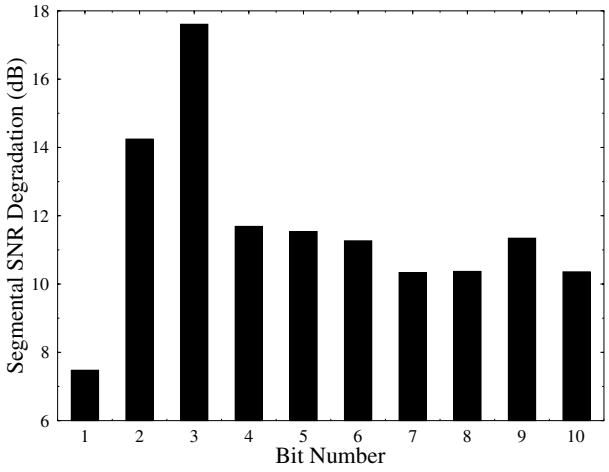

Figure 8.34: Degradation in 8 kbps SEGSNR caused by 10 % BER in given bits.

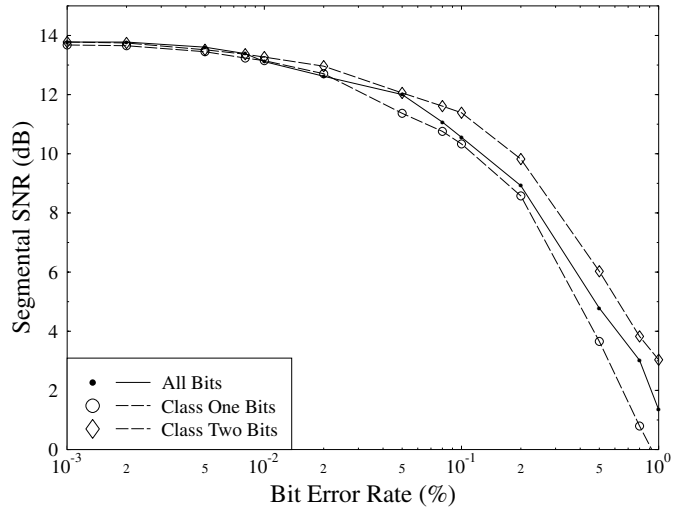

Figure 8.35: SEGSNR of 8 kbps codec versus channel BER.

in order to facilitate the transmission of speech within the same bandwidth, while providing higher robustness at a concomitant lower speech quality, if the channel conditions degrade.

Specifically, in the more vulnerable, higher-quality mode, 16-level pilot symbol assisted quadrature amplitude modulation (16-PSAQAM) [159] was used for the transmission of speech encoded at 16 kbps. In the more robust, lower-quality mode the 8 kbps encoded speech is transmitted using 4-PSAQAM at the same signalling rate. In our former work [169] we have found that, typically, it is sufficient to use a twin-class un-equal protection scheme, rather than more complex multi-class arrangements. It was also shown [73] that the maximum minimum

distance square 16-QAM constellation exhibits two different-integrity subchannels; namely the better quality C1 and lower quality C2 subchannels, where the BER difference is about a factor two in our operating SNR range. This was also argued in [159].

Hence we would require a FEC code of twice the correction capability for achieving a similar overall performance of both subchannels over Gaussian channels, where the errors have a typically random, rather than bursty distribution. Over bursty Rayleigh channels an even stronger FEC code would be required in order to balance the differences between the two subchannels. After some experimentation we opted for the binary BCH$(127, 92, 5)$ and BCH$(124, 68, 9)$ codes [158] for the protection of the 16 kbps encoded speech bits. The weaker code was used in the lower BER C1 subchannel and the stronger in the higher BER C2 16-QAM subchannel. Upon evaluating the BERs of the coded subchannels over Rayleigh channels, which are not presented here due to lack of space, we found that a ratio of two in terms of coded BER was maintained.

Since the 16 kbps speech codec generated 160 bits/10 ms frame, the 92 most vulnerable speech bits were directed to the better BCH$(127, 92, 5)$ C1 16-QAM subchannel, while the remaining 68 bits to the other subchannel. Since the C1 and C2 subchannels have an identical capacity, after adding some padding bits, 128 bits of each subchannel were converted to 32 4-bit symbols. A control header of 30 bits was BCH$(63, 30, 6)$ encoded, which was transmitted employing the more robust 4-QAM mode of operation using 32 2-bit symbols. Finally, two ramp symbols were concatenated at both ends of the transmitted frame, which also incorporated four uniformly-spaced pilot symbols. A total of 104 symbols/10 ms therefore represented 10 ms speech, yielding a signalling rate of 10.4 kBd. When using a bandwidth of 1728 kHz, as in the DECT system and an excess bandwidth of 50%, the multi-user signalling rate becomes 1152 kBd. Hence a total of INT[1152/104] $= 110$ time-slots can be created, which allows us to support 55 duplex conversations in Time Division Duplex (TDD) mode. The timeslot duration becomes 10 ms/(110 slots) ≈ 90.091 μs.

8.11.3.2 Lower-quality Mode

In the lower-quality 8 kbps mode of operation 80 bits/10 ms are generated by the speech codecs, but the 4-QAM scheme does not have two different integrity subchannels. Here we opted for the BCH$(63, 36, 5)$ and BCH$(62, 44, 3)$ codes in order to provide the required integrity subchannels for the speech codec. Again, after some padding the 64-bit coded subchannels are transmitted using 2-bit/symbol 4-QAM, yielding 64 symbols. After incorporating the same 32-symbol header block, 4 ramp and 4 pilot symbols, as in case of the higher-quality mode, we arrive at a transmission burst of 104 symbols/10 ms, yielding an identical signalling rate of 10.4 kBd.

8.11.4 Speech Transceiver Performance

The SEGSNR versus channel SNR performance of the proposed multimode transceiver is portrayed in Figure 8.36 for both 10.4 kBd modes of operation. Our channel conditions were based on the DECT-like propagation frequency of 1.9 GHz, signalling rate of 1152 kBd and pedestrian speed of 1 m/s $= 3.6$ km h^{-1}, which yielded a normalised Doppler frequency of 6.3 Hz/1152 kBd $\approx 5.5 \cdot 10^{-3}$. Observe in the figure that unimpaired speech quality was experienced for channel SNRs in excess of about 26 and 18 dBs in the less and more robust

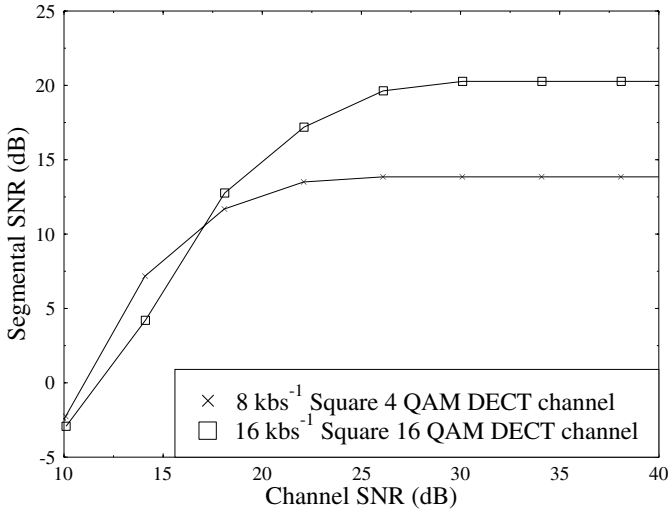

Figure 8.36: SEGSNR versus channel SNR performance of the proposed multimode transceiver.

modes, respectively. When the channel SNR degrades substantially below 22 dB, it is more advantageous to switch to the inherently lower quality, but more robust and essentially error-free speech mode, demonstrating the advantages of the multimode concept. The effective single-user simplex bandwidth is 1728 kHz/110 slots ≈ 15.71 kHz, while maintaining a total transmitter delay of 10 ms. Our current research is targeted at increasing the number of users supported using PRMA.

8.12 Chapter Summary

In this chapter we highlighted the operation of the CCITT G728 16 kbps standard codec and proposed a range of low-delay coding schemes operating between 16–8 and 8–4 kbps. While in the higher bitrate range entirely backward-adaptive predictive arrangements were used, in the lower range codecs using both forward- and backward-adaption of the long-term filter have been considered, but all the codecs use backward adaption of the short-term synthesis filter and so have frame sizes of at most 5 ms. Both relatively small trained shape codebooks and large algebraic codebooks were used. We found that the resulting codecs offered a range of reconstructed speech qualities between communications quality at 4 kbps to near-toll quality at 8 kbps. Lastly, an application example was given, demonstrating the practical applicability of the codecs portrayed. In the next chapter we concentrate our attention on high-quality wideband speech compression.

Part III

Wideband Speech, MPEG-4 Audio and Their Transmission

Chapter 9

Wideband Speech Coding

9.1 Sub-band-ADPCM Wideband Coding at 64 kbps [283]

9.1.1 Introduction and Specifications

In our previous chapters we have assumed that the speech signal was band limited to 0.3–3.4 kHz and sampled according to the Nyquist principle at 8 kHz. This filtering process, however, removes some of the energy of the speech signal, which amounts to about 1%. This does not significantly reduce the perceived quality of reproduction but, nonetheless, in many applications, such as in so-called commentatory quality channels, a better quality is desirable. Therefore the CCITT standardised a so-called wideband codec, referred to as G722, which filters the signal to 50–7000 Hz, before sampling at 16 kHz takes place. We commence our discourse on wideband speech coding by considering the specifications and algorithmic details of the G722 sub-band-split adaptive differential pulse code modulated (SB-ADPCM) speech codec. In our discourse we follow the G722 Recommendation and Maitre's deliberations [283]. The range of requirements to be satisfied by the standardised G722 codec encompassed the following specifications [283].

(1) A speech quality better than that of 128 kbps PCM was aimed for and the encoding quality of music signals was not considered of highest priority.

(2) There was no consideration given to the transmission of voiceband data or in-band signaling.

(3) A total of four tandemed sections, including digital transcoding to and from linear PCM were considered a realistic requirement.

(4) The codec was required to have no significant quality degradation at a BER of 10^{-4} and to have a better performance at 10^{-3} than 128 kbps linear PCM.

(5) The total delay was specified to be less than 4 ms.

Voice and Audio Compression for Wireless Communications Second Edition
L. Hanzo, F. C. A. Somerville and J. P. Woodard

(6) There was a need to accommodate a data channel at the cost of a reduced speech quality, which was satisfied by defining the following three modes of operation: Mode 1 – speech only at 64 kbps; Mode 2 – 56 kbps speech plus 8 kbps data; and Mode 3 – 48 kbps speech plus 16 kbps data, which are also summarised in Table 9.1. Two candidate codecs emerged, a full-band ADPCM codec and a sub-band-ADPCM scheme. Comparative tests have shown that the latter significantly outperformed the full-band codec at the lower rates of 48 and 56 kbps, which justified its standardisation.

Table 9.1: G722 codec specification.

Mode	Speech-rate (kbps)	Data-rate (kbps)
1	64	0
2	56	8
3	48	16

9.1.2 G722 Codec Outline

The basic codec schematic is shown in Figure 9.1, where the full-band input signal $x(n)$ is split in to two sub-band signals, namely the higher-band component $X_h(n)$ and the lower-band component $X_L(n)$. The band-splitting operation is carried out by the aliasing-free *quadrature mirror filter* (QMF), which will be characterised in analytical terms in the next section.

The QMF stage is constituted by two linear-phase FIR filters, whose impulse responses are symmetric. These filters split the 0–8000 Hz frequency band to 0–4000 Hz and 4000–8000 Hz, which now can be sampled at 8 kHz due to halving their bandwidths.

The 0–4000 Hz lower band retains a significantly higher proportion of the signal energy than the higher band. Furthermore, it is more important subjectively than the 4000–8000 Hz higher band. Hence it is encoded using 6 bits/sample ADPCM coding, at 8 ksamp $\cdot$ 6 bits/sample $= 48$ kbps in Mode 1. The lower-significance 4–8 kHz band is encoded using 2 bits/sample, i.e., at 16 kbps. The resulting signals are denoted in Figure 9.1 by I_L and I_M, which are then multiplexed for transmission over the digital channel. It is important to note that the 6-bit lower-band ADPCM quantiser could generate 64 reconstruction levels, but only 60 levels are actually generated.

This is explained as follows. As mentioned before, the codec can drop its rate to 48 kbps, in which case the lower-band ADPCM codec transmits at 32 kbps or 4 bits/sample. In certain systems the all-zero code-word's transmission must be avoided in order to refrain from generating long strings of zeros, which may result in synchronisation problems. Hence in Mode 3 only 15 levels are used for quantisation. Similarly, adding a further bit to the quantiser output generates 30 levels and including two additional bits allows us to differentiate amongst 60 levels.

The principle of *embedded ADPCM* coding was detailed with reference to the CCITT G727 codec. Similar principles are followed in the G722 codec in order to support the

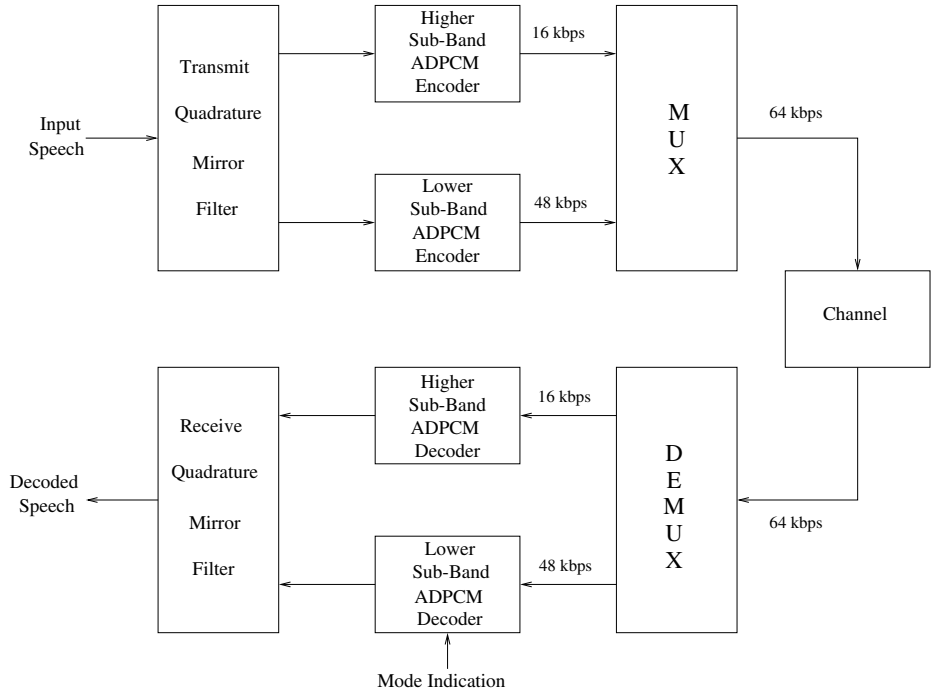

Figure 9.1: G722 SB-ADPCM codec schematic.

synchronous operation of the encoder and decoder in the event of dropping one or two bits from the transmitted sequence for the sake of supporting 8 or 16 kbps data transmission.

Explicitly, the two LSBs of the lower-band signal I_L are punctured in the predictive feedback loop, to produce the truncated representation $I_{Lt}(n)$ in Figure 9.2. The coarsely quantised prediction residual $d_{Lt}(n)$ and the reconstructed, truncated-precision lower-band signal $r_{Lt}(n)$ are input to the pole-zero predictor, which was featured in the G727 codec, in order to produce the predicted signal $s_L(n)$. Clearly, using 4 bits, rather than 6 bits in the encoder's prediction loop allows the decoder's prediction loop to be synchronised with that of the encoder even in the event when data bits are transmitted along with 48 kbps-coded speech. The operation of the higher-band ADPCM encoder depicted in Figure 9.3 is very similar to that of the lower-band scheme, except that it uses 2 bits/sample, 15-level quantisation without deleting any bits from the predictor loop. For further details on the embedded ADPCM codec the interested reader is referred to Section 2.9.2.

The schematic of the SB-ADPCM decoder shown in Figure 9.1 follows the inverse structure of the encoder. After demultiplexing the higher and lower sub-band bits these sequences are decoded using the decoders of Figures 9.4 and 9.5, respectively. The 16 kbps higher band signal I_H is input to the decoder of Figure 9.4 and its reconstructed signal is r_H. The operation of the adaptive quantiser and that of the adaptive predictor is identical to those of the encoder and these will be described during our further discussions.

The lower-band's schematic is somewhat more complex due to the embedded tri-modal operation. The received 48 kbps bitstream is processed according to the 'Mode Indication'

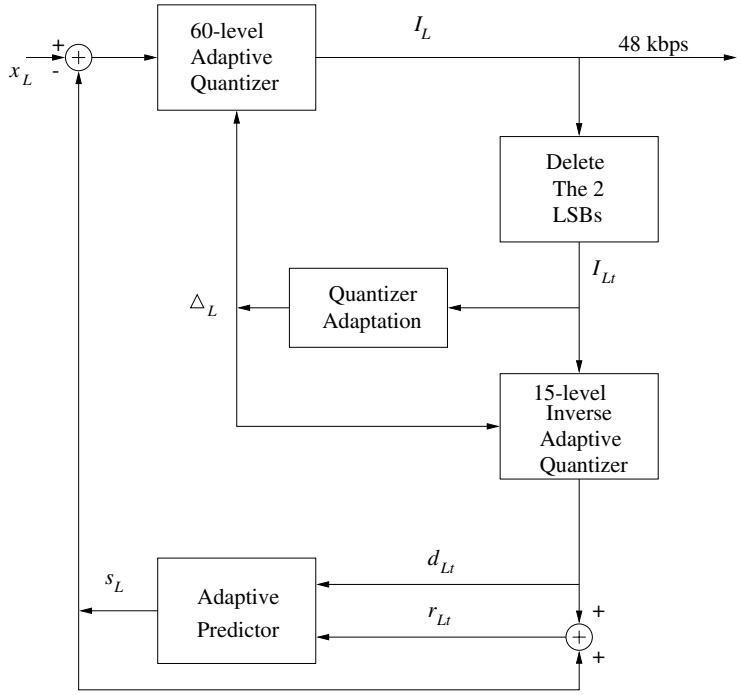

Figure 9.2: Schematic of the lower-band G722 SB-ADPCM encoder.

signal and the corresponding decoded signal is assigned into the low-band decoded residual d_L. In the highest-quality Mode 1 the 60-level inverse adaptive quantiser is used, while in Mode 2 the LSB delivering the 8 kbps data-signal is deleted from each received 6-bit sample and the remaining 5 bits are input to the 30-level inverse quantiser. Lastly, in Mode 3 the two LSBs conveying the 16 kbps data signal are removed from the signal, before invoking the 15-level inverse quantiser for their decoding. Observe at the bottom of Figure 9.5 that the truncated low-band signal I_{Lt} is also input to the quantiser adaptation block to be described later. The lower-band quantiser stepsize ΔL is then used by all three increase adaptive quantisers. Note, furthermore, that due to the embedded operation the adaptive predictor, which is the subject of our later discussions, uses the truncated 4-bit resolution decoded residual d_{Lt} and the resulting truncated reconstructed signal $v_{Lt} = d_{Lt} + s_L$, where S_L is the estimate of the low-band input signal x_L seen in Figure 9.2. In the absence of transmission errors, s_L produced by the 'Adaptive Predictor' of Figure 9.4 is identical to that of Figure 9.2 and the transmission of data in Modes 2 and 3 does not affect this estimate. Finally, the low-band reconstructed signal r_L is generated by adding the estimate s_L to the decoded residual d_L to yield $r_L = s_L + d_L$.

In our deliberations so far we have not considered the operation of the adaptive predictors, quantiser adaption processes and QMF-based band-pass splitting. In the forthcoming sections we will concentrate on these issues.

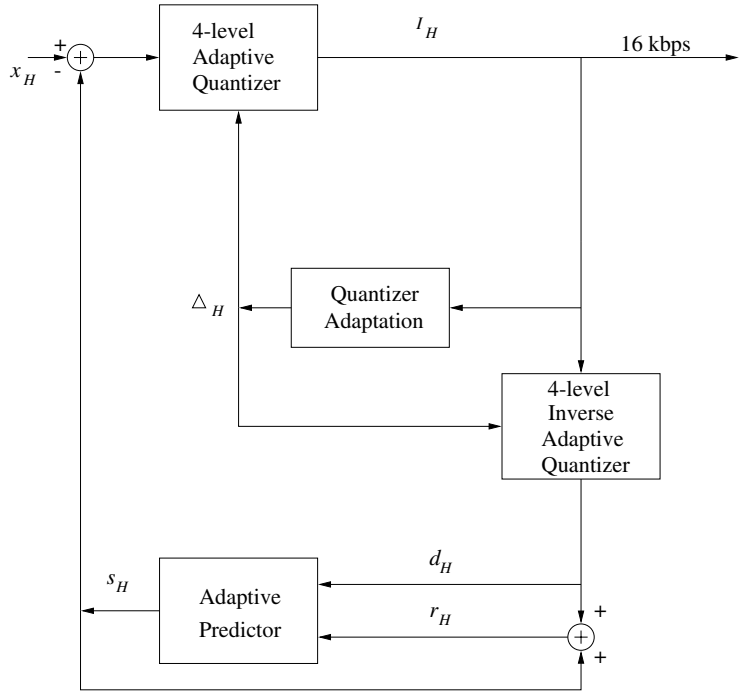

Figure 9.3: Schematic of the higher-band G722 SB-ADPCM encoder.

9.1.3 Principles of Sub-band Coding

Let us briefly introduce the operation of sub-band codecs (SBC) [284, 285], where the speech signal is initially split into a number of sub-bands, which are separately encoded. The main attraction of sub-band codecs is that they allow an arbitrary bit allocation to be applied to each sub-band according to their perceptual importance, thereby confining the corresponding quantisation noise to the sub-bands concerned. Then output bits generated by the sub-band encoders are multiplexed and transmitted to the receiver, where after demultiplexing and decoding each sub-band signal the original full-band signal is reconstructed by combining the individual sub-band components.

The success of this technique hinges on the design of appropriate band-splitting analysis and synthesis filters, which do not interfere with each other in their transition bands, i.e. avoid the introduction of the so-called *aliasing distortion* induced by sub-band overlapping due to an insufficiently high sampling frequency, i.e. sub-sampling. If, on the other hand, the sampling frequency is too high, or for some other reason the filter bank employed generates a spectral gap, again, the speech quality suffers. In a simplistic approach this would imply employing filters having a zero-width transition band, associated with an infinite-steepness cutoff slope. Clearly, this would require an infinite filter order, which is impractical. As a practical alternative, an ingenious band-splitting structure referred to as QMF was proposed by Esteban and Galand [286], which will be detailed at a later stage. QMFs have a finite filter order and remove aliasing effects by cancellation in the overlapping transition bands.

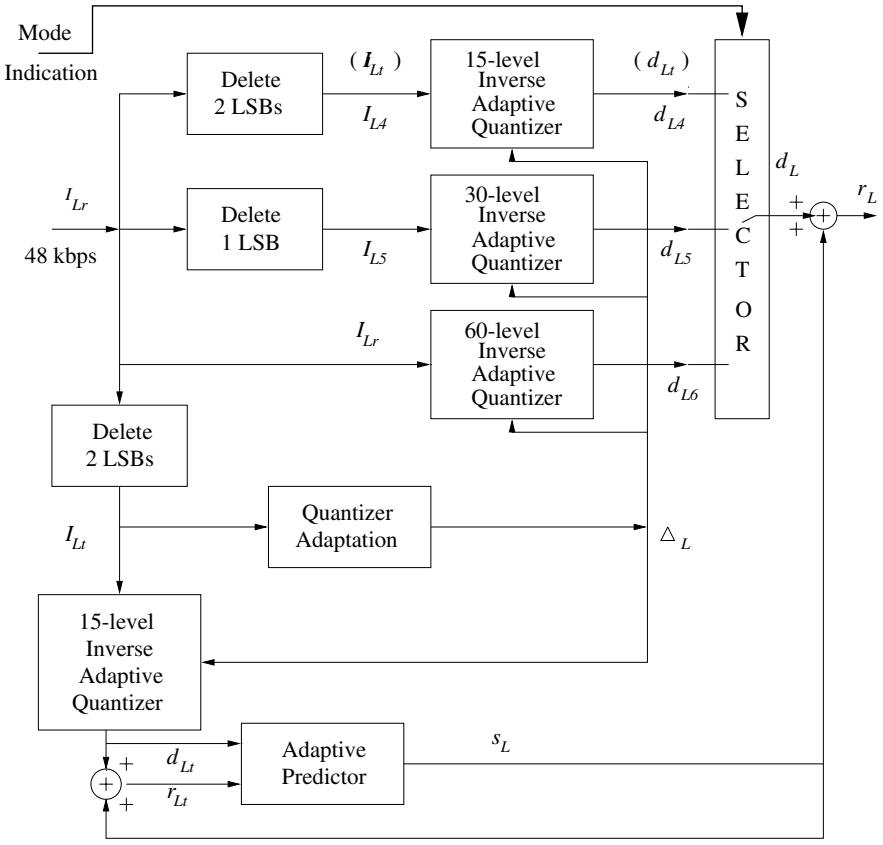

Figure 9.4: Schematic of the lower-band G722 SB-ADPCM decoder.

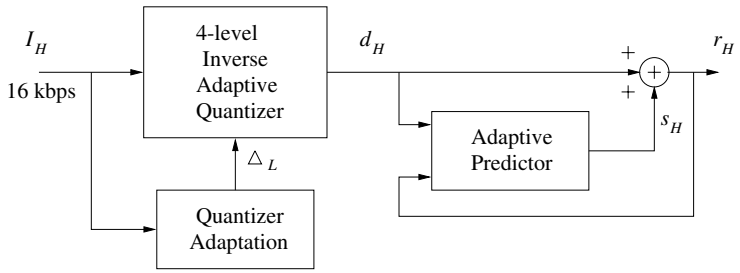

Figure 9.5: Schematic of the lower-band G722 SB-ADPCM decoder.

9.1.4 Quadrature Mirror Filtering [71, 286]

9.1.4.1 Analysis Filtering

As mentioned above, QMFs were introduced by Esteban and Galand [286], while Johnston [287] designed a range of QMFs for a variety of applications. The principle of QMF

analysis/synthesis filtering can be highlighted following their deliberations and considering the twin-channel scheme portrayed in Figure 9.6, where the sub-band signals are initially unquantised for the sake of simplicity. The corresponding spectral-domain operations can be viewed in Figure 9.7. If most of the energy of the speech signal is confined to the frequency $f_s/2$, it can be band-limited to this range and sampled at $f_s = 1/T = \omega_s/2\pi$, to produce the QMFs input signal $x_{\rm in}(n)$, which is input to the QMF analysis filter of Figure 9.6. As seen in the figure, this signal is filtered by the low-pass filter $H_1(z)$ and the high-pass filter $H_2(z)$ in order to yield the low-band signal $x_1(n)$ and the high-band signal $x_2(n)$, respectively. Since the energy of $x_1(n)$ and $x_2(n)$ is now confined to half of the original bandwidth of $x(n)$, the sampling rate of the sub-bands can be halved by discarding every second sample to produce the so-called *decimated signals* $y_1(n)$ and $y_2(n)$.

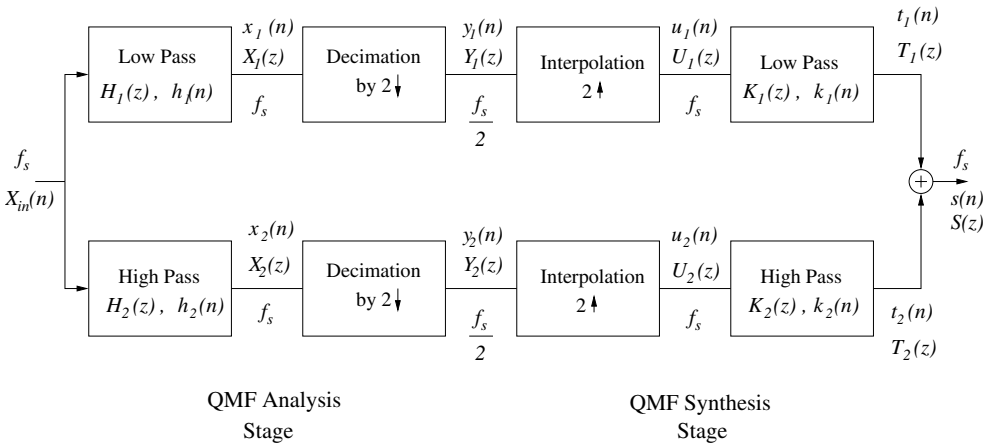

Figure 9.6: QMF analysis/synthesis arrangement.

In the sub-band synthesis stage of Figure 9.6 the decimated signals $y_1(n)$ and $y_2(n)$ are *interpolated* by inserting a zero-valued sample between adjacent samples in order to generate the up-sampled sequences $u_1(n)$ and $u_2(n)$. These are then filtered using the z-domain transfer functions $K_1(z)$ and $K_2(z)$ in order to produce the discrete-time sequences $t_1(n)$ and $t_2(n)$, which, again, now have a sampling frequency of f_s and the filtering operation re-introduced non-zero samples in the positions of the previously injected zero in the process of interpolation. Finally, the $t_1(n)$ and $t_2(n)$ are superimposed onto each other, delivering the recovered speech $s(n)$.

Esteban and Galand [286] have shown that if the LP filter transfer functions $H_1(z)$, $K_1(z)$ and their high-pass (HP) counterparts $H_2(z)$, $K_2(z)$ satisfy certain conditions, perfect signal reconstruction is possible, provided the sub-band signals are unquantised. Let us assume that the transfer functions obey the following constraint:

$$|H_1(e^{j\omega T})| = |H_2(e^{j(\omega_s/2-\omega)T})|, \tag{9.1}$$

where ω is the angular frequency, $2\pi = \omega_s$ and the imposed constraint implies a mirror-symmetric magnitude response around $f_s/4$, where the 3 dB down frequency responses, corresponding to $|H(\omega)| = 0.5$, cross at $f_s/4$. This can be readily verified by the following

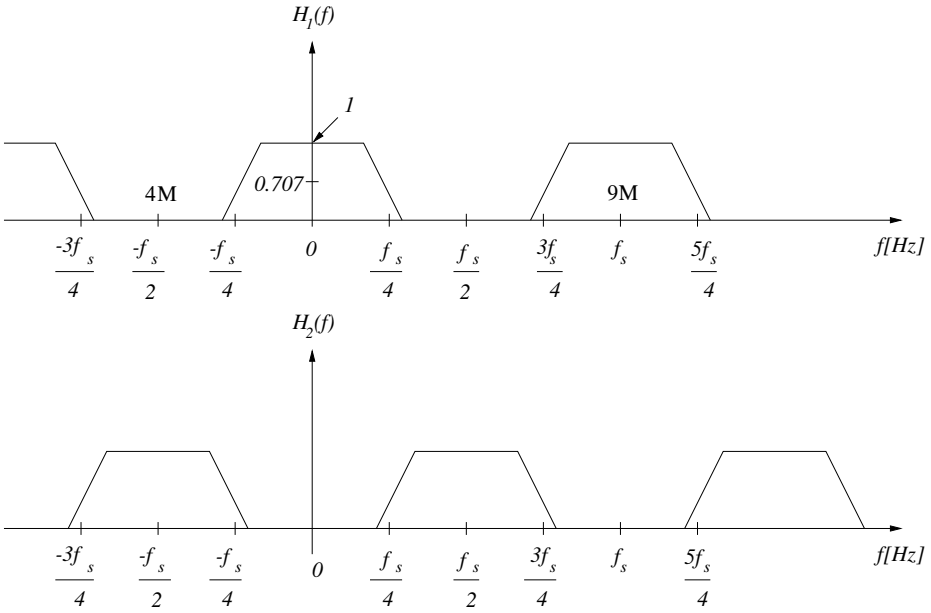

Figure 9.7: Stylised spectral domain transfer function of the lower- and higher-band QMFs.

argument referring to Figure 9.7. Observe that $H_1(\omega)$ is equal to the $\omega_s/2 = \pi$-shifted version of the mirror image $H_2(-\omega)$, which becomes explicit by shifting $H_2(-\omega)$ to the right by $\omega_s/2 = \pi$ at the bottom of the figure. Furthermore, it can also be verified in the figure that by shifting $H_1(\omega)$ to the left by $\omega_s/2 = \pi$ the following relationship holds:

$$|H_2(e^{j\omega T})| = |H_1(e^{-j(\omega_s/2-\omega)T})|. \tag{9.2}$$

Upon exploiting the fact that

$$\begin{aligned} e^{-j(\omega_s/2-\omega)T} &= e^{-j(\pi-\omega T)} \\ &= \cos(\pi - \omega T) - j\sin(\pi - \omega T) \\ &= -\cos(\omega T) - j\sin(\omega T) \\ &= -e^{j\omega T}, \end{aligned} \tag{9.3}$$

Equation (9.2) can also be written as

$$|H_2(e^{j\omega T})| = |H_1(-e^{j\omega T})|, \tag{9.4}$$

and upon taking into account the fact that $z = e^{j\omega T}$, in the z-domain we have $H_1(z) = H_2(-z)$. Following a similar argument it can also be easily shown that the corresponding HP filters $K_1(z)$ and $K_2(z)$ also satisfy Equation (9.4).

Let us now show how the original full-band signal can be reproduced using the required filters. The z-transform of the LP-filtered signal $x_1(n)$ can be expressed as

$$X_1(z) = H_1(z)X(z) \tag{9.5}$$

or alternatively as

$$X_1(z) = a_0 + a_1 z^{-1} + a_2 z^{-2} + a_3 z^{-3} + a_4 z^{-4} + \cdots , \tag{9.6}$$

where a_i, $i = 1, 2, \ldots$, are the z-transform coefficients. Upon decimating $x_1(n)$ we arrive at $y_1(n)$, which can be written in the z-domain as

$$Y_1(z) = a_0 + a_2 z^{-1} + a_4 z^{-2} + \cdots , \tag{9.7}$$

where every other sample has been discarded and the previous even samples now become adjacent samples, which corresponds to halving the sampling rate. Equation (9.7) can also be decomposed into the following expression:

$$\begin{aligned} Y_1(z) &= \tfrac{1}{2}[a_0 + a_1 z^{-1/2} + a_2 (z^{-1/2})^2 + a_3 (z^{-1/2})^3 + a_4 (z^{-1/2})^4 + \cdots] \\ &\quad + \tfrac{1}{2}[a_0 + a_1 (-z^{-1/2}) + a_2 (-z^{-1/2})^2 + a_3 (-z^{-1/2})^3 + \cdots] \qquad (9.8) \\ &= \tfrac{1}{2}[X_1(z^{1/2}) + X_1(-z^{1/2})], \qquad (9.9) \end{aligned}$$

which represents the decimation operation in the z-domain.

9.1.4.2 Synthesis Filtering

The original full-band signal is reconstructed by interpolating both the low-band and high-band signals, filtering them and adding them, as shown in Figure 9.6. Considering the low-band signal again, $y_1(n)$ is interpolated to give $u_1(n)$, whereby the injected new samples are assigned zero magnitude, yielding

$$\begin{aligned} U_1(z) &= a_0 + 0 \cdot z^{-1} + a_2 z^{-2} + 0 \cdot z^{-3} + a_4 z^{-4} + \cdots \\ &= Y_1(z^2). \end{aligned} \tag{9.10}$$

From Figure 9.6 the reconstructed low-band signal is given by

$$T_1(z) = K_1(z)U_1(z). \tag{9.11}$$

When using Equations (9.5)–(9.11), we arrive at

$$\begin{aligned} T_1(z) &= K_1(z)U_1(z) \\ &= K_1(z)Y_1(z^2) \\ &= K_1(z)\tfrac{1}{2}[X_1(z) + X_1(-z)] \\ &= \tfrac{1}{2}K_1(z)[H_1(z)X(z) + H_1(-z)X(-z)]. \end{aligned} \tag{9.12}$$

Following similar arguments in the lower branch of Figure 9.6 as was done for the high-band signal we arrive at

$$T_2(z) = \tfrac{1}{2}K_2(z)[H_2(z)X(z) + H_2(-z)X(-z)]. \tag{9.13}$$

Upon adding the low-band and high-band signals we arrive at the reconstructed signal

$$\begin{aligned} S(z) &= T_1(z) + T_2(z) \\ &= \tfrac{1}{2}K_1(z)[H_1(z)X(z) + H_1(-z)X(-z)] \\ &\quad + \tfrac{1}{2}K_2(z)[H_2(z)X(z) + H_2(-z)X(-z)]. \end{aligned}$$

This formula can be rearranged in order to reflect the partial system responses due to $X(z)$ and $X(-z)$:

$$\begin{aligned} S(z) = &\tfrac{1}{2}[H_1(z)K_1(z) + H_2(z)K_2(z)]X(z) \\ &+ \tfrac{1}{2}[H_1(-z)K_1(z) + H_2(-z)K_2(z)]X(-z), \end{aligned} \tag{9.14}$$

where the second term reflects the aliasing effects due to decimation-induced spectral overlap around $f_s/4$, which can be eliminated following Esteban and Galand [286] if we satisfy the following constraints:

$$K_1(z) = H_1(z) \tag{9.15}$$

$$K_2(z) = -H_1(-z) \tag{9.16}$$

and invoke Equation (9.4), satisfying the following relationship:

$$H_2(z) = H_1(-z). \tag{9.17}$$

Upon satisfying these conditions Equation (9.14) can be written as

$$\begin{aligned} S(z) = &\tfrac{1}{2}[H_1(z)H_1(z) - H_1(-z)H_1(-z)]X(z) \\ &+ \tfrac{1}{2}[H_1(-z)H_1(z) - H_1(z)H_1(-z)]X(-z), \end{aligned}$$

simplifying the aliasing-free reconstructed signal's expression to

$$S(z) = \tfrac{1}{2}[H_1^2(z) - H_1^2(-z)]X(z). \tag{9.18}$$

If we exploit the fact that $z = e^{j\omega T}$, we arrive at

$$S(e^{j\omega T}) = \tfrac{1}{2}[H_1^2(e^{j\omega T}) - H_1^2(-e^{j\omega T})]X(e^{j\omega T})$$

and from Equation (9.3) by symmetry we have

$$-e^{-j\omega T} = e^{j(\omega_s/2+\omega)T}, \tag{9.19}$$

leading to

$$S(e^{j\omega T}) = \tfrac{1}{2}[H_1^2(e^{j\omega T}) - H_1^2(e^{j(\omega_s/2+\omega)T})]X(e^{j\omega T}). \tag{9.20}$$

9.1.4.3 Practical QMF Design Constraints

Having considered the analysis/synthesis filtering, the elimination of aliasing becomes more explicit in this subsection. Let us now examine how the imposed filter design constraints can be satisfied. Esteban and Galand [286] have proposed an elegant solution in the case of FIR filters, having a z-domain transfer function given by

$$H_1(z) = \sum_{n=0}^{N-1} h_1(n) z^{-n}, \tag{9.21}$$

where N is the FIR filter order. Since $H_2(z)$ is the mirror-symmetric replica of $H_1(z)$, below we show that its impulse response can be derived by inverting every other tap of the filter impulse response $h_1(n)$. Explicitly, from Equation (9.17) we have

$$\begin{aligned} H_2(z) &= H_1(-z) \\ &= \sum_{n=0}^{N-1} h_1(n)(-z)^{-n} \\ &= \sum_{n=0}^{N-1} h_1(n)(-1)^{-n} z^{-n} \\ &= \sum_{n=0}^{N-1} h_1(n)(-1)^{n} z^{-n}, \end{aligned} \tag{9.22}$$

which obeys the above stated symmetry relationship between the low-band and high-band impulse responses.

According to Esteban and Galand the low-band transfer function $H_1(z)$, which is a symmetric FIR filter, can be expressed by its magnitude response $H_1(\omega)$ and a linear phase term, corresponding to the filter-delay $(N-1)$, as follows:

$$H_1(e^{j\omega T}) = H_1(\omega) e^{-j(N-1)\pi(\omega/\omega_s)}. \tag{9.23}$$

Upon substituting this linear-phase expression into the reconstructed signal's expression in Equation (9.20) and taking into account the fact that $2\pi/\omega_s = 2\pi/(2\pi f_s) = T$ we arrive at

$$\begin{aligned} S(e^{j\omega T}) &= \frac{1}{2}\left[H_1^2(\omega) e^{-j2(N-1)\pi(\omega/\omega_s)} - H_1^2\left(\omega + \frac{\omega_s}{2}\right) e^{-j2(N-1)\pi(\omega/\omega_s + 1/2)}\right] X(e^{j\omega T}) \\ S(e^{j\omega T}) &= \frac{1}{2}\left[H_1^2(\omega) - H_1^2\left(\omega + \frac{\omega_s}{2}\right) e^{-j(N-1)\pi}\right] e^{-j(N-1)2\pi(\omega/\omega_s)} X(e^{j\omega T}). \end{aligned} \tag{9.24}$$

As to whether the aliasing can be perfectly removed, we have to consider two different cases depending on whether the filter order N is even or odd.

(1) *The filter-order N is even*. In this case we have:

$$e^{-j(N-1)\pi} = -1, \tag{9.25}$$

since the expression is evaluated at odd multiples of π on the unit circle. Hence the reconstructed signal's expression in Equation (9.24) can be formulated as

$$S(e^{j\omega T}) = \frac{1}{2}\left[H_1^2(\omega) + H_1^2\left(\omega + \frac{\omega_s}{2}\right)\right] e^{-j(N-1)\omega T} X(e^{j\omega T}). \tag{9.26}$$

In order to satisfy the condition of a perfect all-pass system we have to maintain

$$H_1^2(\omega) + H_1^2\left(\omega + \frac{\omega_s}{2}\right) = 1 \tag{9.27}$$

yielding

$$S(e^{j\omega T}) = \tfrac{1}{2} e^{-j(N-1)\omega T} X(e^{j\omega T}), \tag{9.28}$$

which can be written in the time domain as

$$s(n) = \tfrac{1}{2} x(n - N + 1). \tag{9.29}$$

In conclusion, if the FIR QMF filter order N is even, the reconstructed signal is an $(N-1)$-sample delayed and 1/2-scaled replica of the input speech, implying that all aliasing components have been removed.

(2) *The filter-order N is odd.* For an odd filter-order N we have

$$e^{-j(N-1)\pi} = 1, \tag{9.30}$$

since the exponential term is evaluated now at even multiples of π, hence the reconstructed signal's expression is now formulated as

$$S(e^{j\omega T}) = \frac{1}{2}\left[H_1^2(\omega) - H_1^2\left(\omega + \frac{\omega_s}{2}\right)\right] e^{-j(N-1)\omega T} X(e^{j\omega T}). \tag{9.31}$$

Observe that due to the symmetry of $H_1(\omega)$ we have $H_1(\omega) = H_1(-\omega)$ and hence the square-bracketed term becomes zero at $\omega = -\omega_s/4$ and therefore the reconstructed signal $S(e^{j\omega T})$ is now different from the transmitted signal. As a consequence, perfect-reconstruction QMFs have to use even filter orders.

The conditions for perfect reconstruction QMFs are summarised in Table 9.2. Johnston [287] has proposed a range of perceptually optimised so-called real QMF filter designs, which process real-time signals. A range of so-called complex quadrature mirror filters (CQMF) potentially halving the associated computational complexity have been suggested by Nussbaumer and Galand [288, 289].

Let us now apply the above results to the G722 codec. The G722 analysis QMF stage is shown in Figure 9.8, where a joint tapped delay-line is used by the LP and HP stages. The filter coefficients are tabulated in Table 9.3 and the symmetry of the LP impulse response becomes explicit in the table. The anti-symmetric HP impulse response of Table 9.2 is implemented using a single (-1) multiplier in Figure 9.8, which is an attractive implementation suggested by Maitre [283]. The input speech is clocked into the shift-register

Table 9.2: Conditions for perfect reconstruction QMF.

$H_1(z)$ is a symmetric FIR filter of even order: $h_1(n) = h_1(N-1-n), n = 0 \ldots (N-1)$
$H_2(z)$ is an anti-symmetric FIR filter of even order: $h_2(n) = -h_2(N-1-n), n = 0 \ldots (N/2)-1$
Mirror-symmetry: $H_2(z) = H_1(-z)$ $h_2(n) = (-1)^n h_1(n)$ $n = 0, \ldots, (N-1)$
$K_1(z) = H_1(z)$
$K_2(z) = -H_2(z)$
All-pass criterion: $H_1^2(\omega) + H_1^2\left(\omega + \frac{\omega_s}{2}\right) = 1$

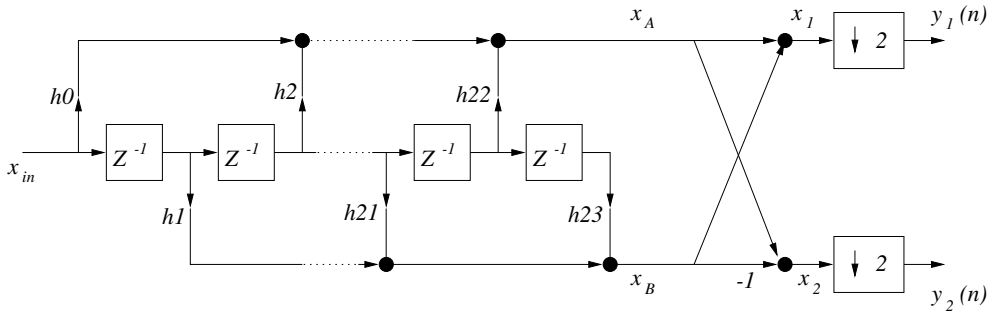

Figure 9.8: G722 QMF analysis stage.

at a rate of 16 kHz and decimation is implemented by outputting the split-band signals x_L and x_M at 8 kHz.

The structure of the QMF synthesis stage is shown in Figure 9.9, which also obeys the conditions summarised in Table 9.2, requiring $K_1(z) = H_1(z)$ in the lower band and $K_2(z) = -H_2(z)$ in the higher band.

Following Maitre's approach [283], the above operations can be summarised as

$$\begin{aligned} x_1(j) &= x_A(j) + x_B(j) \\ x_2(j) &= x_A(j) - x_B(j), \end{aligned} \tag{9.32}$$

Table 9.3: Transmit and receive QMF coefficient values.

h0	,	h23	0.366211E−03
h1	,	h22	−0.134277E−02
h2	,	h21	−0.134277E−02
h3	,	h20	0.646973E−02
h4	,	h19	0.146484E−02
h5	,	h18	−0.190430E−01
h6	,	h17	0.390625E−02
h7	,	h16	0.441895E−01
h8	,	h15	−0.256348E−01
h9	,	h14	−0.982666E−01
h10	,	h13	0.116089E+00
h11	,	h12	0.473145E+00

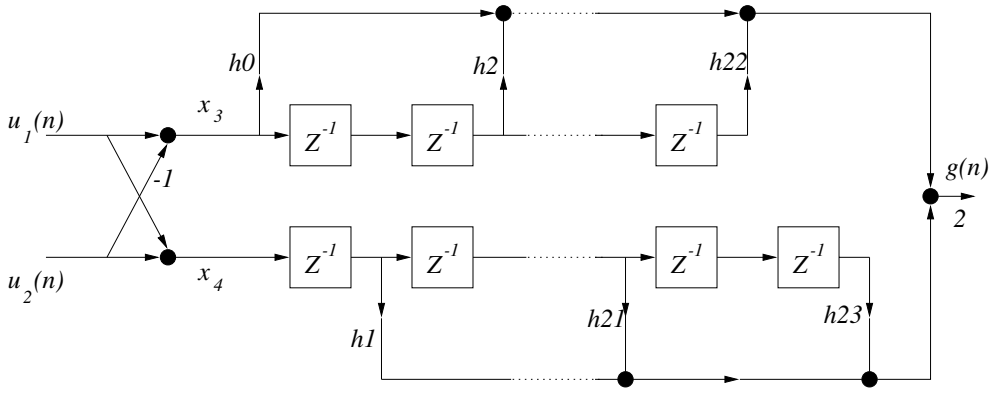

Figure 9.9: G722 QMF synthesis stage.

where we have

$$
\begin{aligned}
x_A(j) &= \sum_{i=0}^{11} h(2i)x_{\text{in}}(j-2i) \\
x_B(j) &= \sum_{i=0}^{11} h(2i+1)x_{\text{in}}(j-2i-1).
\end{aligned}
\tag{9.33}
$$

Substituting Equation (9.33) into Equation (9.32) yields

$$\begin{aligned} x_1(j) &= \sum_{i=0}^{11} h(2i)x_i(j-2i) + \sum_{i=0}^{11} h(2i+1)\cdot x_{\text{in}}(j-2i-1) \\ &= \sum_{i=0}^{23} h(i)x_{\text{in}}(j-i) \\ x_2(j) &= \sum_{i=0}^{23}(-1)^i h(i)\cdot x_{\text{in}}(j-i). \end{aligned} \tag{9.34}$$

In the z-domain we have

$$X_1(z) = \sum_{i=0}^{23} h(i)z^{-1}X_{\text{in}}(z) = H_1(z)x_{\text{in}}(z), \tag{9.35}$$

where

$$H_1(z) = \sum_{i=0}^{23} h(i)z^{-1} \tag{9.36}$$

and

$$X_2(z) = \sum_{i=0}^{23}(-1)^i h(i)z^{-1} = H_2(z)\cdot X_{\text{in}}(z), \tag{9.37}$$

where

$$H_2(z) = \sum_{i=0}^{23}(-1)^i h(i)z^{-1}. \tag{9.38}$$

Recall from Equation (9.9) that the decimated signals can be written as

$$\begin{aligned} Y_1(z) &= \tfrac{1}{2}[X_1(z^{1/2}) + X_1(-z^{1/2})] \\ Y_2(z) &= \tfrac{1}{2}[X_2(z^{1/2} + X_2(-z^{1/2})] \end{aligned} \tag{9.39}$$

and in the case of no transmission errors we get

$$\begin{aligned} U_1(z) &= Y_1(z^2) = \tfrac{1}{2}[X_1(z) + X_1(-z)] \\ U_2(z) &= Y_2(z^2) = \tfrac{1}{2}[X_2(z) + X_2(-z)]. \end{aligned} \tag{9.40}$$

Upon substituting Equations (9.35) and (9.37) into Equation (9.40) we arrive at

$$\begin{aligned} U_1(z) &= \tfrac{1}{2}[H_1(z)\cdot X_{\text{in}}(z) + H_1(-z)\cdot X_{\text{in}}(-Z)] \\ U_2(z) &= \tfrac{1}{2}[H_2(z)\cdot X_{\text{in}}(z) + H_2(-z)\cdot X_{\text{in}}(-z)]. \end{aligned} \tag{9.41}$$

As seen in Figure 9.6 the original speech is reconstructed as

$$\begin{aligned} S(z) &= T_1(z) + T_2(z) \\ &= K_1(z) \cdot U_1(z) + K_2(z) \cdot U_2(z) \end{aligned} \tag{9.42}$$

and taking into account Equation (9.41) and the conditions $K_1(z) = H_1(z)$ and $K_2(z) = -H_2(z)$ in Table 9.2 we have

$$S(z) = H_1(z)U_1(z) - H_2(z)U_2(z). \tag{9.43}$$

The equivalent expression in time-domain using Equations (9.36) and (9.38) is

$$\begin{aligned} s(j) &= 2\left[\sum_{i=0}^{23} h(i)u_1(j-i) - \sum_{i=0}^{23}(-1)^i h(i)u_2(j^{-i})\right] \\ &= 2\sum_{i=0}^{23} h(i)[u_1(j-i) - (-1)^i u_2(j-i)] \\ &= 2\sum_{i=0}^{11} h(2i)[u_1(j-2i) - u_2(j-2i)] \\ &\quad + 2\sum_{i=0}^{11} h(2i+1)[u_1(j-2i-1) + u_2(j-2i-1)] \\ &= 2\sum_{i=0}^{11} h(2i)x_3(i) + 2\sum_{i=0}^{11} h(2i+1)x_4(i), \end{aligned} \tag{9.44}$$

where

$$\begin{aligned} x_3(i) &= u_1(j-2i) - u_2(j-2i) \\ x_4(i) &= u_1(j-2i-1) + u_2(j-2i-1). \end{aligned} \tag{9.45}$$

In summary, the above operations justify the simplified QMF analysis/synthesis operations portrayed in Figures 9.8 and 9.9, which now necessitate two filters only. Having considered the QMF stages let us now concentrate on the operation of the adaptive quantisers.

9.1.5 G722 Adaptive Quantisation and Prediction

Let us now consider the quantisation of the low-band and high-band prediction error signals $e_L(n)$ and $e_H(n)$, respectively, which are generated by subtracting the corresponding estimates $s_L(n)$ and $s_H(n)$ from the respective low-band and high-band QMF outputs:

$$\begin{aligned} e_L(n) &= x_L(n) - s_L(n) \\ e_H(n) &= x_H(n) - s_H(n). \end{aligned}$$

Then, as mentioned before, in the low-band 60-, 30- or 15-level quantisation is used in order to avoid transmitting long strings of the all-zero codeword, while the high-band

is quantised with 2 bits/sample. For the sake of brevity, here we refrain from detailing the quantisation tables containing the output codewords and decision levels for both sub-bands, the interested reader is referred to the Recommendation G722 for specific details on these issues.

In the embedded codec the truncated 4-bit low-band codeword I_{Lt} is converted to the truncated locally decoded low-band difference d_{Lt} using the 4-bit low-band inverse quantiser Q_{L4}^{-1} of Figure 9.10 and Table 9.4 and scaling it by $\Delta_L(u)$ as follows:

$$d_{Lt}(n) = Q_{L4}^{-1}[I_{Lt}(n)] \cdot \Delta_L(n) \cdot \text{sgn}[I_{Lt}(n)],$$

where the $\text{sgn}[I_{Lt}(n)]$ function indicates the sign of the low-band prediction error $e_L(n)$. The untruncated high-band difference signal is regenerated similarly using an analogous formula.

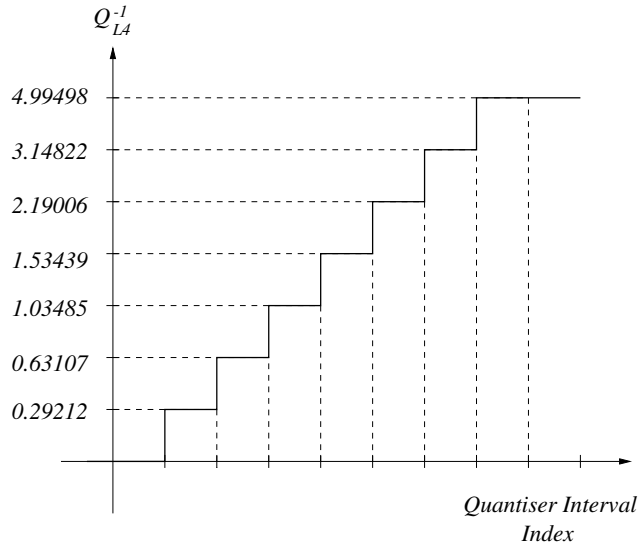

Figure 9.10: The 4-bit low-band inverse quantiser Q_{L4}^{-1}.

The quantiser scaling factors are up-dated in the logarithmic domain in order to maintain a high dynamic range and then they are converted to the linear domain using a look-up table. The logarithmic scaling factors $\nabla_L(n)$ and $\nabla_H(n)$ are computed using the following recursive relationships:

$$\nabla_L(n) = \frac{127}{128} \cdot \nabla_L(n-1) + W_L[I_{Lt}(n-1)]$$
$$\nabla_H(n) = \frac{127}{128} \cdot \nabla_H(u-1) + W_H[_H(n-1)],$$

where W_L and W_H are the *logarithmic scaling factors* and the low-band factor W_L is given in Table 9.4. This expression is similar to the corresponding scaling factor update formula of Equation (2.4) used in the previously detailed G721 32 kbps ADPCM codec, although the logarithmic scalers of Tables 2.3 and 9.4 are different. On the same note, the G722

Table 9.4: Lower-band inverse quantiser (Q_{L4}^{-1}) and logarithmic scale-factor (W_L) characteristic.

Quantiser interval index	Q_{L4}^{-1}	W_L
1	0	-0.02930
2	0.29212	-0.01465
3	0.63107	0.02832
4	1.03485	0.08398
5	1.53439	0.16309
6	2.19006	0.26270
7	3.14822	0.58496
8	4.99498	1.48535

codec uses a *leakage factor* of $p = (127/128)$, while the G721 scheme used $\beta = 31/32$, implying a somewhat higher innate robustness or tolerable BER in the case of the latter. The logarithmic scaling factors are limited to the range $0 \leq \nabla_L(n) \leq g, 0 \leq \nabla_H(n) \leq 11$ and they are converted to the linear domain using an approximation to the inverse of the $\log_2(\cdot)$ function; namely,

$$\Delta_L(n) = 2^{(\nabla_L(n)+2)} \cdot \Delta_{\min}$$
$$\Delta_H(n) = 2^{\nabla_H(n)} \cdot \Delta_{\min},$$

where $\Delta_{\min}$ was set to half the step-size of the 14-bit A/D converter used, which minimised the codecs idle noise.

The *adaptive predictor* used in the G722 codec is identical to the G721 two-pole, six-zero ARMA arrangement which was detailed in Section 2.7. Specifically, Equations (2.66)–(2.70) have to be used in order to periodically update the predictors using a simplified gradient algorithm.

In closing, we note that the low-band decoder can make use of the mode information, which can be inferred by the data extraction unit preceding the G722 decoder. The G722 codec can operate without the availability of this side-information, albeit at the cost of some performance degradation.

9.1.6 G722 Coding Performance

Since the standardisation of the G722 codec, compression technology has made substantial advances, although it has not led to lower-rate wideband speech coding standards as yet. In our forthcoming discussion we will highlight a range of research results reducing the wideband bitrate to 32 kbps and even to 9.6 kbps.

9.2 Wideband Transform-coding at 32 kbps [290]

9.2.1 Background

In this section we will briefly consider a scheme proposed by Quackenbush [290], which processes 7 kHz bandwidth speech sampled at 16 kHz. This codec achieves a compression of 8:1 when compared to the near-transparent quality 16-bit PCM input signal and hence transmits at 2 bits/sample or 32 kbps. In his contribution, Quackenbush adopted the transform-coding approach proposed by Johnston [291] for audio signals and reduced the bitrate required.

9.2.2 Transform-coding Algorithm

The codec's schematic is shown in Figure 9.11, which processes 240-sample blocks, corresponding to 15 ms at a sampling rate of 16 kHz and concatenates 16 samples from the previous block, yielding an overall block length of 256 samples. This block is then windowed, smoothing the first 16 samples of the block at both ends. This 256-sample real signal is then transformed to 128 complex coefficients using the FFT, where the coefficients are quantised for transmission.

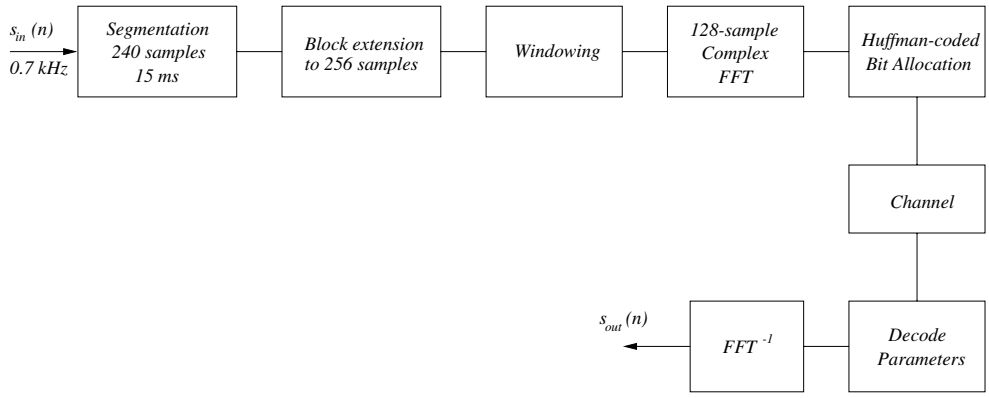

Figure 9.11: Transform-coded wideband speech codec schematic.

The codec distributes the quantisation noise in the spectral domain such that its perceptual effects are minimised by adjusting the signal-to-quantisation noise ratio appropriately across the frequency band. This process could also be conveniently carried out using a QMF stage to split the frequency band into the required width sub-bands, as we have seen in the case of the G722 codec. Quackenbush [290] followed Scharf's suggestions [8] in order to determine the tolerable noise threshold T_i for the frequency band i, were i is the so-called *critical band* index. Quackenbush opted for a fixed rather than dynamically adjusted critical band energy evaluation, determining the energy C_i for band i from the long-term analysis of speech. According to Scharf's suggestion the noise threshold can be adjusted to

$$T_i = 14.5 + i[\text{dB}]$$

below the signal energy C_i, while inflicting negligible perceptual distortion. This simple masking model allows us to determine the required bit allocation as a function of frequency, which is carried out dynamically using an iterative procedure.

In each frame, 26 bits have a time-invariant assignment, allocating 16 bits to the lowest-frequency FFT bin, 4 bits to indicate the number of iterations during the bit-allocation process, which can be accordingly 16, 2 bits for the selection of one of four Huffman codebooks and 4 bits for frame-synchronisation. Therefore, assuming 2 bits/sample coding, there are $480 - 76 = 454$ bits for dynamic spectral-domain coding of the FFT coefficients. The bit allocation scheme is summarised in Table 9.5.

Table 9.5: Bit allocation table for 32 kbps wideband transform codec.

Parameter	No. of bits/15 ms
Lowest frequency FFT bin	16
No of bit allocation iterations	4
Selection of Huffman codebook	2
Frame synchronisation	2
FFT coefficients	454
Total	480 bits/15 ms = 32 kbps

Following an initial tentative bit allocation the iterative bit allocation is activated. The FFT spectrum is subdivided into 16 frequency bands and 'sub-bands' $k = 1, \ldots, 11$ are assigned 6 FFT spectral lines, while 'sub-bands' $k = 12, \ldots, 16$ are allocated 12 spectral lines. The above $11 \cdot 6 + 5 \cdot 12 = 126$ spectral lines are encoded by the iterative technique to be highlighted, line 0 has a fixed allocation of 16 bits and line 127 is not encoded. Then the maximum spectral magnitude M_k of each 'sub-band' k is found and quantised logarithmically, yielding

$$m_k = \{\log_2 M_k\}, \quad k = 1, \ldots, 16,$$

where $\{\cdot\}$ indicates the smallest integer greater than or equal to $\cdot$ and an m_k-bit quantiser is needed in 'sub-band' k.

Once the 'sub-band' spectral maxima and the spectral lines are encoded, the bitrate economy can be further improved using Huffman coding, as will be highlighted during our further discourse. Two sets of codebooks are used both for the maxima and for the spectral lines. Quackenbush argues that this technique does not dramatically improve the average bitrate overall, but it reduces the peak rate.

Huffman coding has been treated in a range of classic books; for example, [10] by Jayant and Noll. Suffice to say here that Huffman coding is a simple, practical technique which arranges the messages to be encoded in descending order and assigns a variable-length code to them on the basis of their probability of occurrence. Specifically, more frequent messages are encoded using a low number of bits, while infrequent ones can be transmitted using longer codes. Overall, if the source-message probabilities vary over a wider range, the average bitrate is significantly reduced at the cost of some coding complexity and delay.

Returning to the process of Huffman coding the spectral maxima, for the 16 'sub-bands' Quackenbush trained a separate codebook. For the spectral lines a more complex scheme was used, where 1, 2 or 3 complex spectral lines were concatenated into a single word before invoking a specific Huffman coding table. The choice of the Huffman coding table was governed by the value of m_k and hence no side-information had to be sent to the decoder since m_k was transmitted for all 'sub-bands'. The choice of Huffman codebooks is summarised in Table 9.6.

Table 9.6: Dependence of Huffman coding scheme on 'sub-band' maxima. Copyright © IEEE, Quackenbush, 1991.

Condition	No. of quantisation levels	Codebook	Complex vector length
$15 < \|m_k\|$	1771	5	1 (real)
$7 < \|m_k\| \leq 15$	31	4	1
$3 < \|m_k\| \leq 7$	15	3	1
$1 < \|m_k\| \leq 3$	7	2	2
$0 < \|m_k\| \leq 1$	3	1	3

Specifically, one of the five Huffman codebooks involved in Table 9.6 is invoked in each of the 'sub-bands'. All the spectral lines belonging to this band are encoded by the same book, which is one of the five choices provided in Table 9.6. If $|m_k| = 0$, no bits are allocated to the given band. Furthermore, observe in the table that if $|m_k| > 15$, then the real and imaginary spectral lines are encoded separately by Codebook 5, which is similar to Codebook 4, but the encoded values are limited to $[7 \ldots 14]$.

Quackenbush used the following iterative codebook design approach. Initially a set of simple linear scalar quantisers was used in order to generate a histogram of the quantities to be encoded, such as the 'sub-band' maxima and the spectral line, and the generated bitrate was estimated. Then Huffman codebooks were generated on the basis of these tentative histograms for both the 'sub-band' maxima and spectral lines. These codebooks were then used in a subsequent session to estimate the bitrate again, and lastly a new set of histograms was generated again. These iterations can be repeated a number of times in order to arrive at a near-optimum set of Huffman codebooks.

As mentioned before, there are two Huffman codebooks for both the 'sub-band' maxima and the spectral lines. First, m_k is encoded tentatively invoking both codebooks for each 'sub-band' maxima and the one resulting in a lower bitrate is selected. This side-information flag is also signalled to the decoder. Then depending on $|m_k|$, the corresponding set of twin codebooks of Table 9.6 is used, checking the generated number of bits due to both of the twin codebooks. The number of bits generated is also stored.

Quackenbush also suggested an iterative bitrate control mechanism for maintaining a rate of 32 kbps or 480 bits/15 ms. If after the first encoding pass the bitrate is not between 1.9 and 2 bits/sample, corresponding to $456 \ldots 480$ bits per frame, then a new coding cycle ensues. An integer scaling factor m was introduced to control the number of quantiser levels used and on each iteration the quantised spectral lines are scaled by a factor of $2^{(1/m)}$, until the

number of bits generated is between 456 and 480. Explicitly, if the number of bits generated is too low, the number of quantisation levels is increased and *vice versa*.

The value of the scaling factor m is determined as follows. If the number of bits produced by the initial spectral line quantisation is below 456, m is set to 1, otherwise to -1. This would imply a spectral-line quantiser up- or down-scaling by a factor of 2 or $1/2$ respectively. During the subsequent iterations, it is observed whether the direction of scaling is maintained and if so the preceding value of m is retained. If, however, the direction of scaling has to change, since due to a previous correction step now the number of bits generated deviates from the target in the opposite direction, the value of m is doubled and the sign of it is toggled, before the next iteration takes place.

As an example, let us assume that $m = 1$ was used in the last iteration, and as an effect of scaling by $2^{1/m} = 2$ the number of bits became too high. Now it would not improve the bitrate iteration to set $m = -1$ again, since that would reduce the bitrate exactly to that value, which activated the choice of $m = 1$, requiring a bitrate increase. Hence m is doubled to $m = 2$ and its sign is toggled, leading to a scaling by $2^{(1/m)} = 2^{-1/2} = 1/\sqrt{2} = \sqrt{2} \approx 1.41$. This sequence of iterative scaling operations is encoded using four bits, allowing for a selection of 16 possible consecutive scaling protocols to take place. The iterative bit-allocation process is concluded when either the number of bits falls between 456 and 480 or the maximum allowed number of iterations took place. The total bitrate can be maintained at 32 kbps, but in some cases the total bitrate budget may not be fully exploited.

9.3 Sub-band-split Wideband CELP Codecs

9.3.1 Background

In the previous sections we have considered the G722 64 kbps, SB-ADPCM wideband codec and a transform-coding-based 32 kbps codec. Since CELP codecs are so successful in coding narrowband speech signals, they have also been employed in wideband coding. A simple and realistic alternative is to invoke the previously described CCITT G728 16 kbps low-delay narrowband codec and operate it at an increased sampling rate of 16 kHz, rather than at 8 kHz, which would result in a bitrate of 32 kbps. However, better results can be achieved, if the codec is designed specifically for wideband applications, since the efficient encoding of high frequencies present in the 4–7 kHz band requires special attention. Ordentlich and Shoham [292] proposed a low-delay CELP-based 32 kbps wideband codec, which achieved a similar speech quality to the G722 64 kbps codec at a concomitant higher complexity.

A philosophy similar to that of the backwardly adaptive G728 16 kbps codec was proposed by Ordentlich and Shoham, and two codec versions were tested: one with and one without LTP, although their preferred codec refrained from using LTP. The backward-adaptive LPC filter had an order of 32, which was significantly lower than the filter order of 50 used in the G728 codec. Recall that the G728 filter order of 50 was able to cater for long-term periodicities of up to 6.25 ms, corresponding to pitch frequencies down to 160 Hz without a LTP, allowing better reconstruction for female speakers. The filter order of 32 at a sampling frequency of 16 kHz cannot cater for long-term periodicities.

In contrast to the G728 codebook of 128 entries, here 1024 entries were used to model the 5-sample excitations. Let us now examine how the bitrate can be further reduced using split-band coding.

9.3.2 Sub-band-based Wideband CELP Coding

9.3.2.1 Motivation

One of the problems associated with full-band coding of wideband speech is the codec's inability to treat the less predictable high-frequency, low-energy speech band, which was tackled by the G722 codec using split-band coding. Although this band is important for maintaining an improved intelligibility and naturalness, it only contains a small fraction of the speech energy and therefore its bitrate contribution has to be limited appropriately. In a contribution by Black *et al*. [161] the backward-adaptive principle was retained for the sake of low delay, but it was combined with a split-band approach. This is mainly motivated by the fact that in a full-band CELP codec the excitation is typically chosen on the basis of providing good low-frequency regeneration, since the majority of the energy resides in that band. Hence, the lower-energy high-frequency region may not be treated adequately in full-band CELP codecs, unless appropriate measures are taken, such as choosing vast codebooks, which then require sophisticated measures in order to mitigate their complexity.

It is well understood that in backward-adaptive narrowband codecs, such as the G728 scheme, an LPC frame update rate of 2 ms is sufficiently frequent in order to achieve similar LPC prediction gains to forward-adaptive arrangements. However, when using a similar update rate in wideband coding, the high-frequency spectrum above 4 kHz was reported to have been distorted [161] due to the abovementioned dominantly low-frequency-matched synthesis process. Black *et al*. have found that the backward-adaptive LPC spectrum, better to say the spectral envelope, often exhibited a higher energy towards high frequencies than the forward-adaptive spectrum, which was again attributable to the predominantly low-frequency matching. All in all, the sub-band approach has a number of advantages for wideband coding, allowing the codec to restrict quantisation error spillage from one band to the other and hence Black *et al.* [161] favoured this technique. The previously described G722 standard QMF band-splitting scheme was used and the proposed low-band and high-band schemes are depicted in Figures 9.12 and 9.13, both of which now operate independently at an 8 kHz sampling rate.

9.3.2.2 Low-band Coding

The low-band was encoded by a backward-adaptive CELP codec using a tenth-order LPC filter updated over 14, 8 kHz-sampled samples or 1.75 ms. This narrowband LPC analysis was free from the high-band (>4 kHz) spectral envelope distortion problem of backward-adaptive wideband codecs. For the preferred innovation sequence length of 14 samples Black *et al.* argued that it was necessary to incorporate a forward-adaptive LTP in order to counteract the potentially damaging error feedback effect of the backward-adaptive LPC analysis. A conventional perceptual weighting filter was employed and non-integer LTP delays were incorporated. Specifically, a resolution of $1/3 \cdot 1/8\,\text{kHz} \approx 41.67\ \mu\text{s}$ was used between LTP delays of $19\frac{1}{3}$ and $84\frac{2}{3}$, while in the range $85 \ldots 143$ no oversampling was utilised. The LTP delay was represented by 8 bits. Black *et al.* first initiated a closed-loop synthesis for all integer delays and if the delay found fell in the high-resolution region, a range of fractional delays surrounding the identified integer position were also tested, which was found to improve the codec performance for female speakers. In contrast to the G728 trained 128-

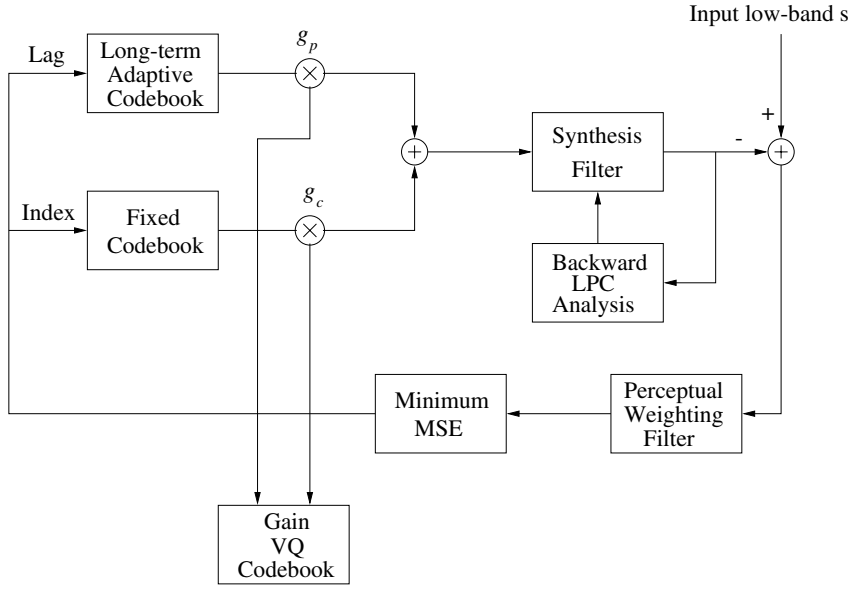

Figure 9.12: Low-band encoder in 16 kbps sub-band-CELP wideband codec. Copyright © Black *et al.* [161].

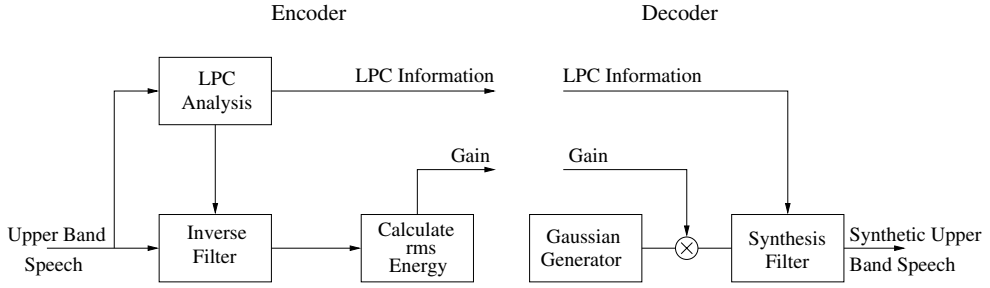

Figure 9.13: High-band encoder/decoder in 16 kbps sub-band-CELP wideband codec. Copyright © Black *et al.* [161].

entry codebook, here a 256-entry fixed stochastic codebook was used in the low-band, which contained overlapping entries.

9.3.2.3 High-band Coding

The upper-band typically contains a less structured, noise-like signal, which has a slowly varying dynamic range. Black *et al.* proposed the use of a sixth-order forward-adaptive predictor updated over a 56-sample interval, which is quadrupled in comparison to the low-band. Backward-adaptive prediction would be unsuitable for this less accurately quantised band, which would precipitate the effect of quantisation errors in future segments. This crude LPC analysis did not attempt to give a waveform-matching representation of the upper-

band signal, it merely endeavored to model its spectral envelope. Therefore the decoder regenerated the high-band signal by exciting the LPC synthesis filter using a scaled random zero-mean, unit variance excitation pattern. The magnitude of this vector was determined by the encoder upon inverse-filtering the high-band signal using the above sixth-order LPC filter and calculating the energy of the residual over 56 samples. Listening tests confirmed, however, that the excitation gain determined above was typically too high, in particular for voiced sounds and hence this gain factor was scaled by 0.5, which was then quantised and transmitted to the decoder. Let us now consider the parameter quantisation schemes proposed by Black *et al*.

9.3.2.4 Bit-allocation Scheme

In the backward-predictive low-band no LPC spectral information is transmitted and hence all the bits are assigned to the frequently updated fixed codebook and adaptive codebook parameters. The fixed codebook gain can be predicted by a technique proposed by Soheili *et al*. [293], which was referred to as backward average mean smoothing, where the current gain is predicted by the average of the preceding three quantised gains. This predicted gain G_p was then used to normalize the current stochastic codebook gain determined during the excitation optimisation. This normalised fixed codebook gain was then jointly vector-quantised with the LTP gain in a closed-loop optimisation process. Similar schemes were discussed in Section 6.5.2.5. Black *et al.* then used the Linde–Buzo–Gray (LBG) [276, 280] clustering algorithm for training the joint gain codebook.

The six high-band LPC coefficients were transformed to LSFs and vector quantised with a total of 12 bits, while the random excitation vector gains were quantised with 4 bits. The overall bit-allocation scheme is portrayed in Table 9.7.

Table 9.7: Bit allocation of 16 kbps SB-CELP wideband codec. Copyright © Black *et al.* [161].

Parameter	Bits	Update (ms)	Bitrate (bps)
Low-band			
LTP delay	8	1.75	4571.4
Codebook index	8	1.75	4571.4
Gain VQ	8	1.75	4571.4
High-band			
LSFs	12	7	1714.4
Gain	4	7	571.4
Total			16000

Informal listening tests showed that the codec had a similar performance to the G722 scheme at 48 kbps.

A range of further attractive wideband schemes were proposed by the prestigious speech coding group at Sherbrooke University, who have contributed a plethora of successful narrowband and wideband ACELP codecs.

9.4 Fullband Wideband ACELP Coding

9.4.1 Wideband ACELP Excitation [162]

One of the difficulties associated with wideband CELP coding without band splitting is that upon doubling the sampling rate and hence the bitrate, while maintaining the same relative bitrate contribution for all parameters, as in narrowband schemes, the codec's complexity would become excessively high. For example, assuming a forward adaptive codec and a 10-bit codebook for narrowband coding, the corresponding 20-bit wideband codec would be unrealisably complex, requiring the generation of synthetic speech for $2^{20} = 1048576$ codebook entries. Hence, suboptimum approaches, such as multi-stage codebooks or split-band coding must be used, as we highlighted in the previous sections.

However, in reference [162], Laflamme *et al.* argued that ACELP codecs are amenable to wideband coding, when employing a *focussed codebook search strategy* using a number of encapsulated search loops as detailed in Section 6.3. This technique facilitates searching only a fraction of a vast codebook, while achieving a similar performance to that of a full-search. Without repeating the algorithmic details, suffice to say here that this technique was also proposed by the authors for the CCITT G729 8 kbps low-delay codec using a 15-bit ACELP codebook and five encapsulated loops, which we described earlier in Section 7.8.

As one would expect, according to the 16 kHz sampling frequency the authors doubled the length of the excitation vectors to 80 samples, corresponding to a 5 ms excitation optimisation subframe. A codebook size of 2^{20} was proposed, which can be realistically invoked with the proviso of using the focussed search strategy, and the excitation pulse magnitudes were fixed to $1, -1, 1, -1, 1$ implying that five pulses per excitation vector were used. Assuming that each pulse can occupy 16 legitimate interlaced positions, the five pulses are encoded by a total of $4 \cdot 5 = 20$ bits, yielding a 20-bit codebook. The codebook structure can be described more explicitly as [162]

$$c(n) = \sum_{i=0}^{4} b_i \delta(u - m_i), \quad n = 0, \ldots, 79,$$

where

$$b_i = \begin{cases} +1 & \text{for } i = \text{even} \\ -1 & \text{for } i = \text{odd} \end{cases} \tag{9.46}$$

are the excitation pulse amplitudes and m_i the legitimate pulse locations given by

$$m_i^{(j)} = i + 5j, \quad i = 0, \ldots, 4, \; j = 0, \ldots, 16. \tag{9.47}$$

As mentioned before, Adoul *et al.* [168] and Xydeas *et al.* [167] offered a plausible geometric interpretation of different CELP codebooks by allocating the zero-mean unit-variance codebook vector to the surface of a unit-radius sphere. They invoked this useful 'visual aid' in supporting the 'perceptual equivalence' of different excitation models, populating the surface of the N-dimensional hyper-sphere by randomly- or uniformly-spaced excitation vectors, where N represents the length of the excitation patterns used. Since due to Equation (9.47) any of the 80 excitation pulse positions can host a pulse, Laflamme *et al.* [162] noted that for $N = 80$ and 5 pulses per vector the synthesised number of 5 ms

audio segments becomes $C_5^{80} = 80!/75!5! \approx 24.04 \cdot 10^6$ out of the potentially possible $2^{80} \approx 1.21 \cdot 10^{24}$ segments which would be generated by the full-search of a fully populated, i.e. non-sparsed 80-pulse binary excitation codebook. The proposed ACELP codebook ensures a sufficiently dense coverage of the excitation vector space, while reducing the number of search operations by a factor of $\sim 5 \cdot 10^{16}$.

The ACELP codebook search is inherently structured, which alleviates its real-time implementation by referring to Equations (6.8) and (6.9). In Section 6.4.3 it was argued that updating $\tilde{C}_k$ and ξ_k for the testing of a new excitation vector becomes very efficient, if always only one pulse position is updated upon cycling through the legitimate set of excitation vectors. In general, when there are p legitimate pulse positions for each pulse, p nested loops can be created for this recursive search technique. Nonetheless, even this efficient up-date technique is excessively complex for a codebook of 2^{20} entries and hence Laflamme *et al.*'s [162] ACELP codec in their 16 kbps wideband suggested a similar focussed search strategy to that which the Sherbrooke Laboratory, CNET and NTT proposed for the G729 codec.

Although this focussed search technique was highlighted in Section 7.8, here we briefly note that the philosophy behind it is to quantify the chances of each of a range of particular excitation subsets to contain the optimum excitation vector. Upon testing the incremental effect of each newly included excitation pulse from the set of p pulses of a vector as regards to the overall weighted error of this specific excitation vector, it becomes possible to quantify the chances of this vector leading to the minimum error over the whole codebook without actually adding all p pulses. Specifically, after adding say 3–4 pulses the weighted error can be tested against an experimentally optimised threshold inferred from the statistical evaluation of the weighted error of the best vectors after entering 3–4, rather than 5 nested loops.

In order to be more explicit, the error term of Equations (6.14) and (6.15) must be minimised over the codebook by maximising its second term, given by [71, 163]

$$\tau_k = \frac{(\tilde{C}_k)^2}{\xi_k}.$$

Clearly, the higher the ratio $\tilde{C}_k$ in Equation (6.15), the lower the WMSE, which facilitates the focussed search. Equations (6.17) and (6.18) that were valid for $b_i = +1, -1, +1, -1$, $p = 4$ pulses and four nested loops per excitation vector can be reformulated to reflect the situation $b_i = +1, -1, +1, -1, +1$, $p = 5$ pulses and five loops as

$$\tilde{C}_k = 4(m_0) - 4(m_1) + 4(m_2) - 4(m_3) + 4(m_5) \tag{9.48}$$

$$\begin{aligned}\xi_k = {} & \phi(m_0, m_0) \\ & + \phi(m_{11}m_1) - 2\phi(m_1m_0) \\ & + \phi(m_{21}m_2) + 2\phi(m_{21}m_0) - 2\phi(m_{21}m_1) \\ & + \phi(m_3, m_3) - 2\phi(m_3, m_0) + 2\phi(m_{31}m_1) - 2\phi(m_{31}m_2) \\ & + \phi(m_{41}m_4) + 2\phi(m_{41}m_0) - 2\phi(m_{41}m_1) + 2\phi(m_41m_2) - 2\phi(m_{41}m_3).\end{aligned} \tag{9.49}$$

Recall that physically C_k is the cross-correlation between the target vector $\mathbf{X}$ and the filtered excitation vector $\mathbf{HC}_k$, while ξ_k is the energy of the filtered codeword $\mathbf{HC}_k$.

Laflamme *et al.* [162] evaluated the ratio $\tau_k = (\tilde{C}_k)^2/\xi_k$ in Equation (6.15) at every stage, when considering the cumulative effect of including one pulse at a time out of the p legitimate pulses, which allowed the authors to derive a set of thresholds for the consecutive search stages. The proportion of the total set of legitimate excitation vectors over which the search is carried out can be controlled by eliminating particular vector subsets from further search if they fail to produce 'promising' $\tau_k = (\tilde{C}_k)^2/\xi_k$ ratios after adding 3–4 excitation pulses. Clearly, the higher this statistically optimised threshold at stages 3–4, the higher the proportion of eliminated vectors and the lower the search complexity. This naturally increases the chances of occasionally prematurely eliminating certain excitation subsets, but in most cases the second best vector will still be retained and the reward of reduced complexity far outweighs the inflicted slight performance penalty.

Laflamme *et al.* [162] quantified the associated wideband speech quality degradation, which is shown in Table 9.8 for various proportions of the codebook, which the authors adjusted using two statistically optimised thresholds at stage 3 and 4. Observe in the table that upon searching a mere 0.05% of the $2^{20} \approx 10^6$ entry codebook a relatively low SNR degradation of 0.4 dB was inflicted, while reducing the search-complexity by a factor of 2000. This would correspond to the full-search of a 512-entry, 9-bit address codebook, while maintaining a SNR in excess of 21 dB. It is important to note that, in general, the number of threshold-controlled search operations varies on a frame by frame basis, which results in a time-variant implementational complexity. In order not to hamper real-time implementations the search must be curtailed, once a predefined maximum number of operations was reached.

Table 9.8: Wideband ACELP speech degradation versus the fraction of codebook searched. Copyright © IEEE Laflamme *et al.* [162].

Search complexity (%)	SNR dB
100	22.2
4	22.14
1.6	22.0
0.2	22.05
0.15	21.83
0.05	21.8
0.03	21.5

Although following the above thoughts on excitation optimisation, Laflamme *et al.* [162] outlined a tentative bit-allocation scheme in their treatise, their work has moved on to propose slightly different wideband ACELP codecs [294].

9.4.2 Backward-adaptive 32 kbps Wideband ACELP [294]

In [294] the Sherbooke-team attempted to contrive a backward-adaptive predictive CELP codec which used a conventional backward-adaptive CELP schematic, except for the fact that two excitation generators were employed. Both excitation generators had a separate gain

factor and were constituted by a modified ACELP-type codebook where each binary pulse could take an arbitrary sign. Hence the excitation vector retained a higher flexibility in terms of pulse amplitudes and the codebook search required $2d$ nested loops in order to arrive at the optimum excitation.

In their backward-adaptive ACELP codec the authors used a 32nd-order LPC filter and a 3-tap pitch-predictor, both of which were updated every 2 ms, corresponding to 32 samples at a sampling rate of 16 kHz, using a windowing function similar to that of the 16 kbps G728 codec of Chapter 8. The input speech was also pre-emphasised. The excitation frame-length was 16 samples or 1 ms, hosting 4 pulses per excitation vector, each having four legitimate locations encoded by 2 bits and magnitudes of ± 1. Therefore, each pulse required a total of 3 bits, and each vector holding 4 pulses needed 12 encoding bits. The two codebook gains were assigned 4 bits each. Therefore, the two codebooks were allocated a total of $2 \times (12 + 4) = 32$ bits, 1 ms, yielding a bitrate of 32 kbps, while maintaining a delay of 1 ms. The codecs bit-allocation scheme is summarised in Table 9.9. Sanchez-Calle *et al.* noted that the achieved speech quality was similar to that maintained by the previously described 16 kbps scheme of [162] but the ability of the low-delay 32 kbps backward-adaptive scheme to encode music, rather than speech was superior. The achieved SEGSNR of the 32 kbps codec was in the range of 20–22 dB for wideband speech signals.

Table 9.9: Bit allocation of 32 kbps backward-adaptive fullband wideband ACELP codec. Copyright © IEEE Sanchez-Calle *et al.* 1992 [294].

Parameter	No. of bits/1 ms	Bitrate (kbps)
Codebook index 1	$4 \cdot (2 + 1) = 12$	12
Codebook index 2	$4 \cdot (2+) = 12$	12
Codebook gain 1	4	8
Codebook gain 2	4	8
Total	32	32

9.4.3 Forward-adaptive 9.6 kbps Wideband ACELP [163]

In a further contribution, Salami *et al.* [163] returned to the forward-adaptive ACELP philosophy, while using the previously described dual-codebook ACELP structure. A range of innovative techniques were proposed in order to mitigate the codec's complexity escalating due to the doubled sampling rate. Specifically, the real-time wideband codec has half the time, namely 1/(16 kHz) $= 62.5$ μs to process twice as many samples in comparison to conventional narrowband codecs, assuming a certain fixed analysis interval duration.

Here we restrict ourselves to the portrayal of the proposed bit-allocation scheme which is summarised in Table 9.10. The LPC update frame-length was 30 ms and a filter-order of 16 was used, quantising the LSFs with a total of 54 bits using a channel capacity of 54/30 ms $= 1.8$ kbps. There were five 6 ms excitation optimisation subsegments constituted by 96, 62.5 μs-spaced samples. The pitch-delay was restricted to the range 40–295 and accordingly 8 bits were used for its encoding. The LTP gain was quantised with 4 bits.

Table 9.10: Bit-allocation scheme of wideband forward-adaptive fullband ACELP codec. Copyright © IEEE Salami, 1992 [163].

Parameter	Update (ms)	No. of bits	Bitrate (kbps)
LPC filter	30	54	1.8
LTP delay	6	8	1.33
LTP gain	6	4	0.67
Codebook index 1	6	12	2
Codebook index 2	6	13	2.17
Codebook gain 1	6	6	1
Codebook gain 2	6	3	0.5
Padding bits	30	4	0.13
Total	30	$54 + (5 \cdot 46)$ $+4 = 288$	9.6

The two codebooks in this scheme are different from each other. The first one contains four conventional $+1, -1, +1, -1$ interlaced pulses per 6 ms or 96 sample excitation optimisation vector, where the pulse positions m_i were defined as [163]

$$m_i^{(j)} = 3i + 12j, \quad i = 0, \ldots, 3, \ j = 0, \ldots, 7.$$

As can be inferred from the above equation, there are eight possible positions for each of the interlaced pulses and hence a total of $4 \cdot 3 = 124$ bits per 6 ms excitation vector are needed for their encoding. The associated bitrate contribution is 12 bits/6 ms $= 2$ kbps. In order to maintain a near-constant implementational complexity, the fourth encapsulated loop is entered at most 64 times and a maximum total of 512 excitation vectors are used out of the possible $2^{12} = 4096$ sequences. The first codebook gain was encoded using 6 bits/6 ms, yielding a bitrate contribution of 1 kbps.

After taking into account the contribution of the above ACELP codebook, the second codebook has to model an essentially random process. Hence this codebook has a simple structure, populated with regularly spaced binary pulses. In order to incorporate some flexibility in this codebook, the excitation pulses ± 1 were spaced at positions $k + 9 \cdot n$, where the initial grid-position k can take the values $k = 0, 1, 2$ and 3 and $n = 0, 1, 2, \ldots, 10$. Hence there are four possible initial grid positions and a total of 11 pulses are allocated with a spacing of 9. Therefore, the second codebook requires a total of $(11 + 2) = 13$ coding bits per 96-bit subsegment, yielding a bitrate contribution of 2.17 kbps. The second codebook gain was quantised relative to the first gain, using 3 bits per subsegment, requiring a channel capacity of 0.5 kbps. Finally, 4 padding bits per 30 ms LPC update frame were used, giving a total of $54 + (5 \cdot 46) + 4 = 288$ bits per 30 ms, corresponding to a bitrate of 9.6 kbps. This codec was reported to have an SNR of around 17 dB, while in perceptual terms a higher rate, 14 kbps version of it was formally found equivalent to the G722 SB-ADPCM codec operated at 56 kbps. Recall that the 16 kbps SB-CELP codec proposed by Black *et al.* [161], which was described earlier in this chapter, was deemed to have a similar performance to the 48 kbps G722 operating mode.

It is also interesting to note that Roy and Kabal in [295] comparatively studied a conventional single- and a dual-codebook CELP codec for wideband speech coding. In harmony with Salami *et al.* [163] they also found that the dual-codebook arrangement was more natural-sounding, although their findings were mainly based on experiments carried out without quantisation of the filter parameters.

Before offering our conclusions on wideband speech compression in Table 9.11 we summarise the basic features of the various wideband codecs considered and in the next section we will provide an audio system design example, highlighting the associated design trade-offs.

9.5 A Turbo-coded Burst-by-burst Adaptive Wideband Speech Transceiver[1]

T. Keller, M. Münster and L. Hanzo

9.5.1 Background and Motivation

Burst-by-burst adaptive quadrature amplitude modulation (AQAM) transceivers [159] have recently generated substantial research interest in the wireless communications community [265, 266, 296–302]. The transceiver reconfigures itself on a burst-by-burst basis, depending on the instantaneous perceived wireless channel quality. More explicitly, the associated channel quality of the next transmission burst is estimated and the specific modulation mode which is expected to achieve the required performance target is then selected for the transmission of the current burst. In other words, modulation schemes of different robustness and of different data throughput are invoked. In the event of expected error burst due to a low expected instantaneous channel quality the transmitter can also be temporarily disabled, while the data is delayed and buffered, until the channel quality improves, provided that the associated delay is not excessive for the service supported. Due to this feature the distribution of channel errors becomes typically less bursty than in conjunction with non-adaptive modems. This is an attractive feature in conjunction with channel codecs, resulting in potentially increased coding gains [268,303,304]. Furthermore, the soft-decision channel codec metrics can also be invoked in estimating the instantaneous channel quality. Block turbo-coded AQAM transceivers have also been proposed for dispersive wideband channels in conjunction with conventional decision feedback equalisers (DFE) [268, 303, 304], where the MSE at the DFEs output was used as the channel quality metric, controlling the choice of modes. An alternative neural-network radial basis function (RBF) DFE-based AQAM modem design was proposed in [251], where the RBF DFE provided the channel quality estimates for the modem mode switching regime.

Further work on combining various conventional channel coding schemes with adaptive modulation has been reported by Matsuoka *et al.* [305], Lau and Macleod [306] and Goldsmith and Chua [307]. For data transmission systems which do not necessarily require a low transmission delay, variable-throughput adaptive schemes can be devised, which operate

[1]This section is based on: T. Keller, M. Münster and L. Hanzo, A Turbo-coded Burst-by-burst Adaptive Wideband Speech Transceiver; *IEEE JSAC*, November 2000, Vol. 18, No. 11 pp. 2363–2372.

Table 9.11: Basic wideband codec features.

	Coding algorithm	Bitrate (kbps)	Encoding delay (ms)	Bit allocation
G722	SB-ADPCM 0–4 kHz: 4–6 bit ADPCM, 4–8 kHz: 2-bit ADPCM	64	1.5	
Quackenbush [290]	Adaptive 256-FFT	32	16	
Laflamme *et al*. [162]	Full band Forward-adaptive ACELP	16	15	Not available
Sanchez-Calle *et al*. [294]	Full band Backward-adaptive ACELP	32	1	Table 9.9
Salami *et al*. [163]	Full band Forward-adaptive ACELP	9.6–14	30	Table 9.10
Black *et al*. [161]	Split-band 0–4 kHz: 13.7 kbps Backward-adaptive CELP, 4–8 kHz: 2.3 kbps Vocoder	16	7	Table 9.7

efficiently in conjunction with powerful error-correction codecs, such as long block length turbo codes [216,217]. By contrast, fixed rate burst-by-burst adaptive systems, which sacrifice a guaranteed BER performance for the sake of maintaining a fixed data throughput, are more amenable to employment in the context of low-delay interactive speech and video communications systems. The above burst-by-burst adaptive principles can also be extended to adaptive orthogonal frequency division multiplexing (AOFDM) schemes [308], and to adaptive joint-detection-based code division multiple access (ACDMA) arrangements [309].

OFDM was first proposed by Chang in his 1966 paper [310], revived by Cimini's often cited paper [311], but was developed to its full potential in the 1990s, when a whole host of contributions appeared; for example in [312]. Other developments were due to May and Rohling [313] at the University of Hamburg, Müller and Huber at Erlangen University [314], Classen and Meyr [315,316] at Aachen University, Shepherd *et al*. [317] and Jones *et al*. [318] in the UK, di Benedetto and Mandarini at the University of Rome [319] to name just a few of the key contributors without completeness. Further significant advances over more benign,

slowly varying dispersive Gaussian fixed links are due to Chow *et al*. [320] from the USA, where OFDM became the dominant solution for asymmetric digital subscriber loop (ADSL) applications, potentially up to a bitrate of 54 Mbps. In Europe, OFDM has been favoured for both digital audio broadcasting (DAB) and digital video broadcasting (DVB) [321, 322] as well as for high-rate wireless asynchronous transfer mode (WATM) systems due to its ability to combat the effects of highly dispersive channels [323]. The notion of adaptive bit allocation in the context of OFDM was proposed as early as 1989 by Kalet [324], which was further developed by Chow *et al.* [320] and was refined for duplex wireless links in, for example, [308]. Lastly, an OFDM-based narrowband speech system was proposed in [214]. The co-channel interference sensitivity of OFDM can be mitigated with the aid of adaptive beam-forming [325, 326]

Against this backcloth, in this section we propose a burst-by-burst adaptive 7 kHz bandwidth audio transceiver scheme, based on turbo-coded multimode constant throughput OFDM. The rationale behind proposing this system was that non-adaptive OFDM was also a contender for the Pan-European universal mobile telecommunications system (UMTS) and hence it was beneficial to explore the potential of a substantially enhanced turbo-coded fixed-rate AQAM wideband audio arrangement. Firstly, OFDM provides a powerful framework for exploiting both the time- and frequency-domain channel properties by adapting the bit-allocation to subcarriers, as we will demonstrate. Secondly, OFDM is amenable to powerful soft-decision based turbo coding [214, 327, 328]. Thirdly, although our adaptive transceiver requires a programmable-rate speech or audio codec, to date only a limited number of such codecs have been proposed in the literature. Specific examples are the lower-quality 4 kHz bandwidth – i.e. narrowband – advanced multirate (AMR) speech codec, which was designed for UMTS, and the higher quality 7 kHz bandwidth G.722.1 codec, which can be programmed to operate between 10 kbps and 32 kbps.

We will explore the design trade-offs and show that the AOFDM bitrate can be adaptively controlled in an effort to find the best compromise in terms of loading the AOFDM subcarriers more heavily in an effort to increase the available throughput bitrate for maintaining a higher speech coding rate and higher speech quality, while also maintaining a high robustness against transmission errors. A further trade-off is that although the more heavily loaded, higher-throughput AOFDM modem is more vulnerable against transmission errors due to using more corrupted subcarriers, the longer turbo interleaving improves the turbo codecs performance.

The proposed AOFDM system is constituted by two adaptation loops, namely an inner constant throughput transmission regime, and an outer switching control regime, which jointly maintain the required target bitrate of the system, while employing a set of distinct operating modes. This system was contrived in order to highlight the system design aspects of joint burst-by-burst adaptive modulation, channel coding and source coding. This system design section is structured as follows. Subsection 9.5.2 provides a brief system overview, also listing our experimental conditions. Subsection 9.5.4 details the philosophy of our constant throughput burst-by-burst adaptive OFDM modem. Subsection 9.5.6 investigates the multimode modem adaptation regime proposed, leading to a discussion on the adaptive audio source codec employed in Subsection 9.5.8. Our system performance results are summarised in Subsection 9.5.10 along with our future research endeavours.

9.5.2 System Overview

The structure of the proposed adaptive OFDM transceiver is depicted schematically in Figure 9.14. The top half of the diagram is the transmitter chain, which consists of the source and channel coders, a channel interleaver to de-correlate the channel's frequency-domain fading, an adaptive modulator, a multiplexer adding signalling information to the transmitted data, and an inverse fast Fourier transform/radio frequency (IFFT/RF) OFDM stage. The receiver, seen in the lower half of the figure, consists of a RF/FFT OFDM receiver, a demultiplexer extracting the signalling information, an adaptive demodulator, a de-interleaver/channel decoder, and the source decoder. The parameter adaptation linking the receiver- and transmitter-chain consists of a channel quality estimator and the mode selection, as well as the modulation adaptation blocks.

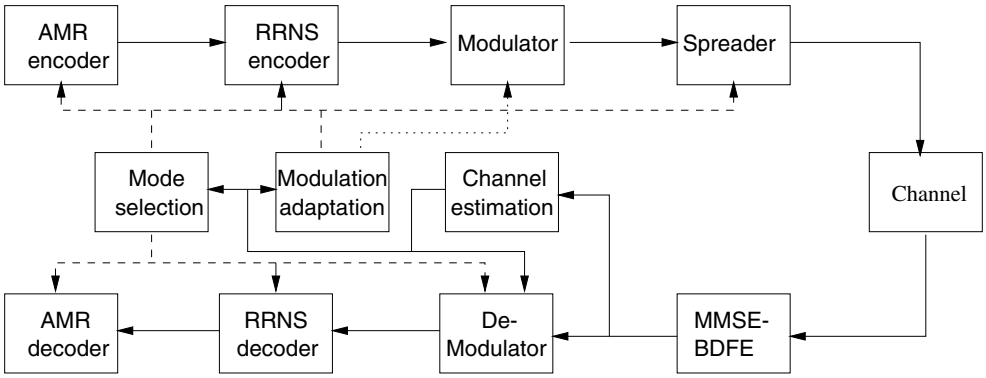

Figure 9.14: Schematic model of the multi-mode adaptive OFDM system.

The open-loop control structure of the adaptation algorithms can be observed in the figure, where the receiver's operation is controlled by the signalling information that is contained in the received OFDM symbol, while the channel quality information estimated by the receiver is employed in order to determine the parameter set to be employed by the transmitter. The two distinct adaptation loops distinguished by dotted and dashed lines are the inner and outer adaptation regimes, respectively. The outer adaptation loop controls the overall throughput of the system, so that a fixed–delay decoding of the received data packets becomes possible. This controls the packet size of the channel codec, the block length of the channel encoder and interleaver, as well as the target throughput of the inner adaptation loop. The operation of the adaptive modulator, controlled by the inner loop, is transparent to the rest of the system. The operation of the adaptation loops is described in more detail below.

9.5.3 System Parameters

The transmission parameters have been adopted from the TDD–mode of the Pan-European UMTS system [329], having a carrier frequency of 1.9 GHz and a TDD frame and time slot duration of 4.615 ms and 122 μs, respectively. The sampling rate is assumed to be 3.78 MHz, leading to a 1024-subcarrier OFDM symbol, having a cyclic extension of 64 samples in each time slot. In order to assist in the spectral shaping of the OFDM signal, there are a total

of 96 virtual subcarriers at the bandwidth boundaries. Table 9.12 gives an overview of the transmission parameters employed for this system.

Table 9.12: OFDM system parameters of adaptive system.

OFDM FFT length	1024
Active subcarriers	928
Guard interval length	64 samples
Sampling rate	3.78 MHz
TDD frame duration	4.615 ms
TDD slot duration	122 μs

The 7 kHz bandwidth G.722.1 audio codec [330] designed by the PictureTel company has been chosen for this system because of its good audio quality, robustness to packet dropping and adjustable bitrate, which will be discussed in more detail later.

The channel encoder/interleaver combination is a convolutional constituent coding-based turbo encoder [216, 217] employing block interleavers with a subsequent pseudo-random channel interleaver. The constituent RSC encoders are of constraint length 3, with octal generator polynomials of $(7, 5)$ and eight iterations are performed at the decoder, utilising the MAP algorithm [221] and the log-likelihood ratio soft inputs provided by the demodulator.

The channel model consists of a four path COST 207 typical urban impulse response [331], where each impulse is subjected to independent Rayleigh fading having a normalised Doppler frequency of $2.25 \cdot 10^{-6}$, corresponding to a pedestrian scenario with a walking speed of 3 mph. The unfaded channel impulse response as well as the magnitude and phase of the corresponding frequency-domain channel transfer function are shown in Figure 9.15. The grey shaded areas in Figure 9.15(b) represent the virtual subcarriers.

9.5.4 Constant Throughput Adaptive Modulation

The constant throughput adaptive OFDM algorithm attempts to allocate the required number of bits for transmission to the specific OFDM subcarriers exhibiting a low BER due to their unattenuated spectral envelope as shown in Figure 9.15(b), while the use of high BER subcarriers is minimised. We assume an open-loop adaptive system, basing the decision on the next transmit OFDM symbol's modulation scheme allocation on the channel estimation gained at the reception of the most recent OFDM symbol by the local station. Sub-band adaptive modulation [308], where the modulation scheme is adapted not on a subcarrier-by-subcarrier basis, but for blocks of adjacent subcarriers, is employed in order to simplify the adaptive OFDM modem mode signalling requirements.

If the impulse response of the channel $h(t, \tau)$ varies slowly compared to the OFDM symbol duration, then the Fourier transform of the impulse response during the OFDM symbol exists, and the data symbols transmitted in the subcarriers $n \in [0, \ldots, N]$ are exposed to the frequency-domain fading determined by the instantaneous channel transfer function $H(t, n \cdot \Delta f) = H_n$.

The allocation of bits to subcarriers is based on the estimated frequency-domain channel transfer function $\hat{H}_n$. On the basis of this and the overall SNR γ, the local SNR in each

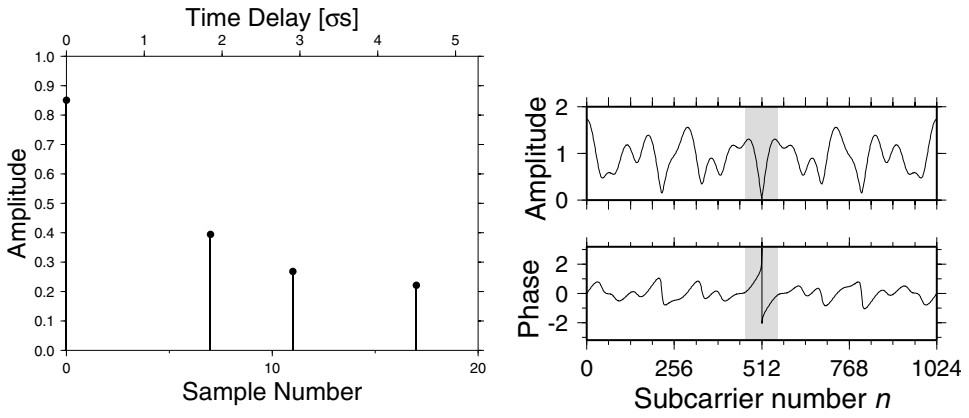

(a) COST 207 impulse response

(b) channel frequency response

Figure 9.15: Channel model: (a) COST 207 impulse response; (b) unfaded frequency-domain channel transfer function $H(n)$. The grey shaded areas represents the virtual subcarriers.

subcarrier n can be calculated as $\gamma_n = \gamma/|\hat{H}_n|^2$. The predicted BER $p_e(\gamma_n, m)$ in each subcarrier n and each of the possible modulation schemes $m \in [0, \ldots, M]$ can now be computed and summed over the N_j sub-carriers in sub-band j in order to yield the expected number of bit errors for each sub-band and for each modulation scheme, which is given by

$$e(j, m) = \sum_i p_e(\gamma_i, m)$$

for all subcarrier indices i in sub-band j. In our case, four modulation schemes are employed for $m = 0, \ldots, 3$, which are 'no transmission', BPSK, QPSK and 16-QAM, respectively. Clearly, $e(j, 0) = 0$, and the other bit error probabilities can be evaluated using the Gaussian Q-function [332]. The number of bits transmitted in sub-band j when using modulation scheme m is denoted by $b(j, m)$.

The bit-allocation regime operates iteratively, allocating bits to subcarriers by choosing the specific subcarriers for transmitting the next bit to be assigned for transmission, which increases the system's BER by the smallest amount. In other words, the bits to be transmitted are allocated consecutively, commencing by assigning bits to the highest channel quality subcarriers, gradually involving the lower channel quality carriers.

More explicitly, for each sub-band a state variable s_j is initialised to 0, and then the sub-band index j, for which the differential BER increment $(e_{s_j+1} - e_{s_j})/(b_{s_j+1} - b_{s_j})$ due to assigning the next bit to be transmitted is the lowest is found. The state variable s_j is incremented from 0, if it is not yet set to the index of the highest-order modulation mode, i.e. to 16-QAM. This search for the lowest BER 'cost' or BER penalty, when allocating additional bits is repeated until the total number of bits allocated to the current OFDM symbol is equal or higher than the target number of bits to be transmitted. Clearly, the higher the target number

of bits to be transmitted by each OFDM symbol, the higher the BER, since gradually lower and lower channel quality subcarriers have to be involved.

The transmitter modulates the subcarriers using the specific modulation schemes indexed by the state variables s_j, eventually padding the data with dummy bits in order to maintain the required constant data throughput. The specific modulation schemes chosen for the different sub-bands have to be signalled to the receiver for demodulation. Alternatively, blind sub-band modem mode detection algorithms can be employed at the receiver [328]. For the scope of these investigations we assume 32 sub-bands of 32 subcarriers in each 1024-subcarrier OFDM symbol. Perfect channel estimation and sub-band modem mode signalling were assumed.

9.5.5 Adaptive Wideband Transceiver Performance

Figure 9.16 shows an example of the fixed throughput adaptive modulation scheme's performance under the channel conditions characterised above, for a block length of 578 coded bits. As a comparison, a fixed BPSK modem transmitting the same number of bits in the same channel, employing 578 out of 1024 subcarriers, is depicted. The number of bits per OFDM symbol is based on a 200 bit useful data throughput, which corresponds to 10 kbps data rate, padded with 89 bits which can contain a checksum for error detection and high-level signalling information, as well as half-rate channel coding.

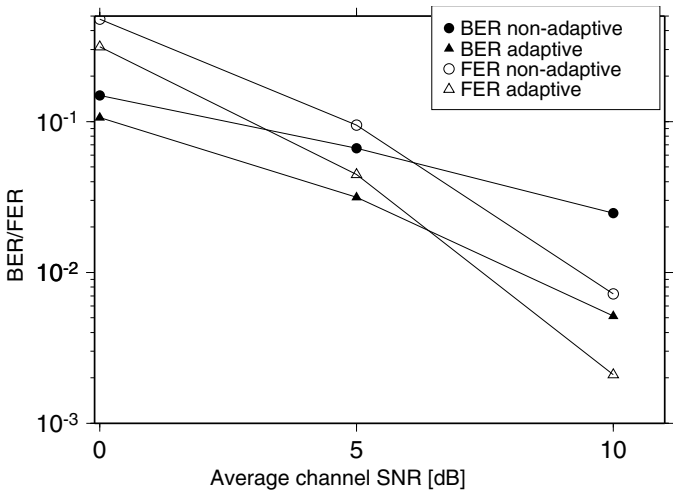

Figure 9.16: FER and uncoded BER for fixed throughput adaptive and non-adaptive modulation in the fading time dispersive channel of Figure 9.15 for a block length of 578 coded bits per 1024 subcarrier for the system of Table 9.12.

The BER plotted in the figure is the hard decision BER at the receiver before channel decoding. It can be seen that the adaptive modulation yields a significantly improved performance, which is reflected also in the frame error rate (FER). This FER is the probability of a decoded block containing errors, in which case it is unusable for the source decoder and

hence it is dropped. This error event can be detected by using the checksum of the data symbol.

The modulation scheme allocation for the 578 data bit adaptive modem for an average channel SNR of 5 dB is given in Figure 9.17(a) for 100 consecutive OFDM symbols. The unused sub-bands with indices 15 and 16 contain the virtual carriers and, therefore, do not transmit any data. It can be seen that the adaptation algorithm allocates data to the better quality subcarriers on a symbol-by-symbol basis, while keeping the total number of bits per OFDM symbol constant. As a comparison, Figure 9.17(b) shows the equivalent overview of the modulation schemes employed for the fixed bitrate of 1458 bits per OFDM symbol. It can be seen that in order to hit the throughput target, hardly any sub-bands are in 'no transmission' mode, and overall higher-order modulation schemes have to be employed.

Figure 9.18 shows the subcarrier SNR for the first transmitted frame over the channel of Figure 9.15 for a long-term SNR of 5 dB. It can be seen that the subcarrier SNR experienced by the modem varies greatly both across the overall OFDM bandwidth, as well as within the sub-bands, delineated by the dotted vertical lines. The different shades of grey markers at the bottom of the graph indicate the modem mode employed for each sub-band, and the circular markers indicate the expected BER averaged over the subcarriers of each sub-band. Figure 9.18(a) gives the modem mode allocation and BER for the 10 kbps mode, corresponding to the first column of Figure 9.17(a), while Figure 9.18(b) depicts the same information for the 32 kbps mode, which corresponds to the first column of Figure 9.17(b).

9.5.6 Multi-mode Transceiver Adaptation

While the fixed throughput adaptive algorithm described above copes well with the frequency-domain fading of the channel, there is also a medium-term time-domain variation of the overall channel capacity. Hence, in addition to the previously proposed fixed-rate frequency-domain bit-allocation scheme, in this section we propose the employment of a time-variant bitrate scheme in order to gauge its additional performance potential benchmarked against the fixed-rate schemes. We will then also contrive appropriate matching audio transceivers at a later stage. However, our experience demonstrated that it was an arduous task to employ powerful block-based turbo channel coding schemes in conjunction with variable throughput adaptive schemes for real-time applications, such as voice or video telephony. Nonetheless, a multi-mode adaptive system can be designed that allows us to switch between a set of different source and channel coders as well as transmission parameters, depending on the overall instantaneous channel quality. We have investigated the employment of the estimated overall BER at the output of the receiver, which is the sum of all the $e(j, s_j)$ sub-band BER contributions after modem mode adaptation. On the basis of this expected input error rate of the channel decoder, the probability of a frame error must be estimated, and compared with the expected FER of the other modem modes. Then, the mode having the lowest FER is selected and the source coder, the channel coder and the adaptive modem are set up accordingly.

We have defined four different operating modes which correspond to the uncoded audio data rates of 10, 16, 24 and 32 kbps at the source encoder's output. With half-rate channel coding and allowing for checksum and signalling overheads, the number of transmitted coded bits per OFDM symbol is 578, 722, 1058 and 1458 for the four source-coded modes, respectively.

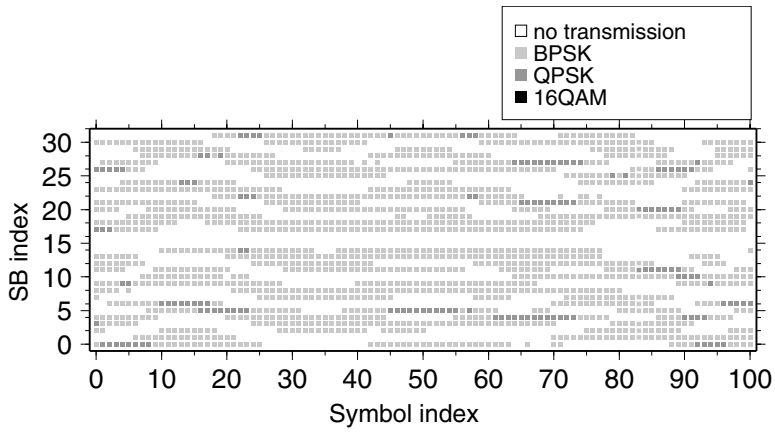

(a) 578 data bits per OFDM symbol

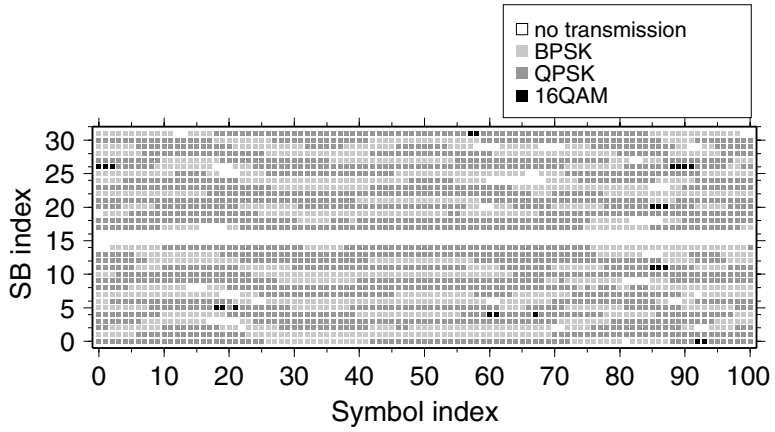

(b) 1458 data bits per OFDM symbol

Figure 9.17: Overview of modulation scheme allocation for the 578-bit (top) and 1458-bit (bottom) fixed throughput adaptive modem over the fading time-dispersive channel of Figure 9.15 at 5 dB average channel SNR.

9.5.7 Transceiver Mode Switching

Figure 9.19 shows the observed FER for all four modes versus the uncoded BER that was predicted at the transmitter during the channel estimation and modem mode adaptation. The predicted BER was discretised into intervals of 1%, and the FER was averaged over these intervals. It can be seen that for estimated BER values below 5% no frame errors were observed for any of the modes. For higher estimated BER values, the higher throughput

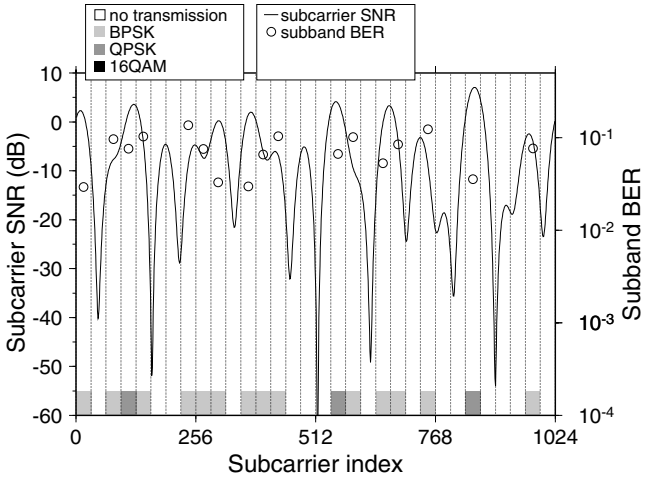

(a) 578 data bits per OFDM symbol

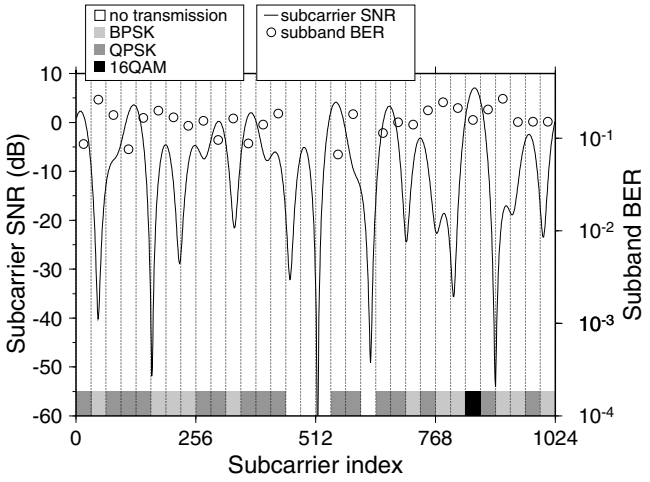

(b) 1458 data bits per OFDM symbol

Figure 9.18: Subcarrier SNR versus subcarrier index for the first transmitted frame in the channel of Figure 9.15 for a long-term SNR of 5 dB, with selected modem mode and average estimated sub-band BER for the 32 sub-bands. The two sub-bands around carrier 512 are virtual carriers. (a) 10 kbps mode; (b) 32 kbps mode.

modes exhibited a lower FER than the lower throughput modes, which was consistent with the turbo coder's performance increase for longer block lengths. A FER of 1% was observed for a 7% predicted input error rate for the 10 kbps mode, while BERs of 8% to 9% were allowed for the longer blocks.

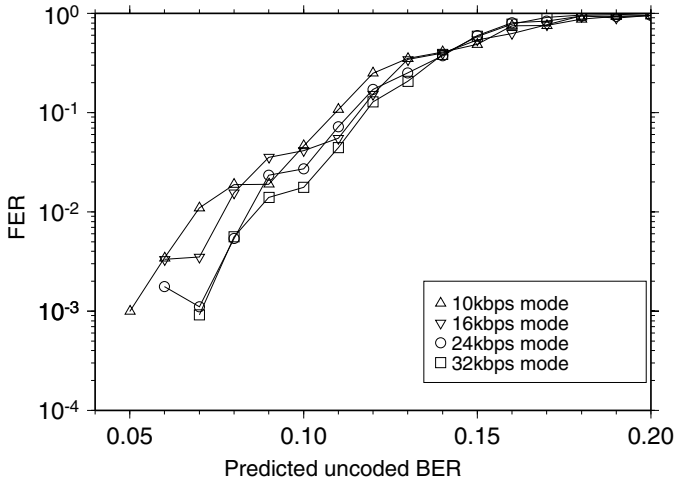

Figure 9.19: FER versus the predicted uncoded BER for 10, 16, 24 and 32 kbps modes.

In this study we assumed the best-case scenario of using the measured FER statistics of Figure 9.19 for the mode switching algorithm. In this case, the FER corresponding to the predicted overall BER values for the different modes are compared, and the mode with the lowest FER is chosen for transmission. The mode switching sequence for the first 500 OFDM symbols at 5 dB channel SNR is depicted in Figure 9.20. It can be seen that in this segment of the sequence, 32 kbps transmission is the most frequently employed mode, followed by the 10 kbps mode. The intermediate modes are mostly transitory, as the improving or deteriorating channel conditions render switches between the 10 kbps and 32 kbps modes necessary. This behaviour is consistent with Table 9.13, for the 'Switch-I' scheme, which will be discussed in depth during our forthcoming discourse. Let us now briefly consider the 7 kHz bandwidth audio codec, which can be reconfigured in a range of different quality and bitrate modems and hence can exploit the time-variant bitrate of the AOFDM modem.

9.5.8 The Wideband G.722.1 Codec

9.5.8.1 Audio Codec Overview

In recent years speech coding research has been focussed on coding 7 kHz bandwidth, rather than 3.4 kHz bandwidth, speech signals in an effort to increase the perceived speech quality [140, 143]. The challenge in this context has been the encoding of the speech components above 3.4 kHz, which on average account for less than 1% of the speech energy, yet they substantially influence the perceived speech quality. A plausible approach is to separate these two bands, which allows the designer to independently control the number of bits allocated to them. A more refined approach is to invoke frequency-domain

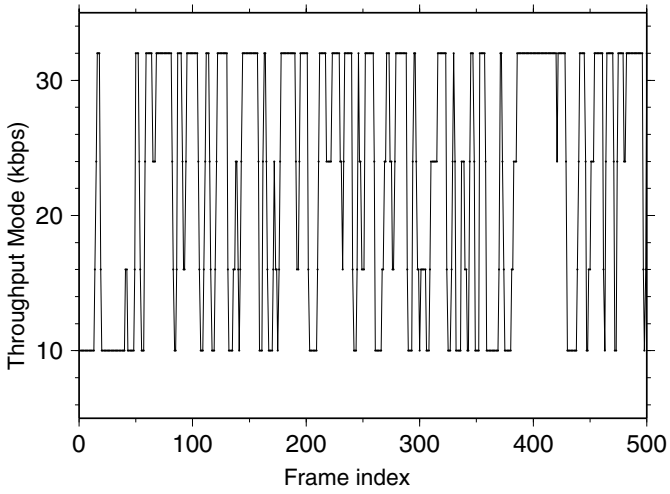

Figure 9.20: Mode switching pattern at 5 dB channel SNR over the WATM channel of Figure 9.15(b).

Table 9.13: FER and relative frequency (Rel.fr) of different bitrates in the fixed bitrate and in the burst-by-burst switching schemes (successfully transmitted frames) for an SNR of 5 dB.

Scheme	FER (%)	Rel.fr.: (%) 10 kbps	Rel.fr.: (%) 16 kbps	Rel.fr.: (%) 24 kbps	Rel.fr.: (%) 32 kbps
Fixed 10 kbps	4.45	95.55	0.0	0.0	0.0
Fixed 16 kbps	5.58	0.0	94.42	0.0	0.0
Fixed 24 kbps	10.28	0.0	0.0	89.72	0.0
Fixed 32 kbps	18.65	0.0	0.0	0.0	81.35
Switch I	4.44	21.87	13.90	11.59	48.20
Switch II	5.58	0.0	34.63	11.59	48.20

coding techniques, such as transform coding [143, 330], which allows a more intelligent, finely-grained distribution of the available coding bits to the most important audio signal frequencies. Furthermore, the bitrate can be adaptively controlled in an effort to find the best compromise in terms of loading the AOFDM subcarriers more heavily in an effort to increase the available bitrate for maintaining a higher speech coding rate and higher speech quality, while also maintaining a high robustness against transmission errors.

The current 64 kbps G.722 ITU standard wideband speech codec [146] is becoming antiquated and the PictureTel transform codec (PTC) was selected for the new ITU-T G.722.1 wideband audio coding standard [330]. It is based on the so-called modulated lapped transform (MLT) [333], followed by a quantisation stage using a perceptually motivated psychoacoustic quantisation model and Huffman coding for encoding the residual frequency domain coefficients.

At its input the G.722.1 expects frames of 320 PCM audio samples, obtained by sampling an audio signal at a frequency of 16 kHz with a quantiser resolution of 14, 15 or 16 bit. Furthermore, the input samples are assumed to contain frequency components up to 7 kHz. At the time of writing the G.722.1 standard recommends operating the codec at output bitrates of 16, 24 or 32 kbps, generating output frame lengths of 320, 480 or 640 bits per 20 ms, respectively, for which the codec was optimised. The total delay encountered by an audio frame, when passing through the codec (consisting of encoder and decoder) can be estimated to be of the order of about 60 ms, which is a result of the time domain frame overlapping technique and the computational delay inherent in the codec.

Since the PTC employs Huffman coding for encoding the frequency domain coefficients, the decoding is very sensitive to bit errors. Hence, a single bit error can render the whole audio frame undecodable. The PTCs standard reaction to such a frame error is simply to repeat the previous frame of coefficients, as long as they occur relatively rarely. For bursts of frame errors the output signal is gradually muted after decoding the first erroneous frame.

9.5.9 Detailed Description of the Audio Codec

We now want to give a brief description of the signal processing stages incorporated in the PTC, which is supported by the block diagram of the encoder depicted in Figure 9.21. In the first processing step, the PCM input signal is mapped from the time domain into the frequency domain, using the MLT, a derivative of the DCT [333]. It is well known that the MLT can be effectively employed in applications where blocking effects can cause severe signal distortion. The latest 320 time-domain samples form a block, which is fed together with the previous block of 320 coefficients into the MLT. As an output, the MLT then produces a block of 320 frequency-domain samples, which yields a frequency resolution of 8000 Hz/320 $= 25$ Hz. As mentioned previously, only signal components with frequencies up to 7 kHz are encoded, which correspond to frequency coefficients with an index lower than 280 – the other coefficients are discarded.

The remaining MLT coefficients are further grouped into 14 equal-width *regions*, each representing a frequency range of 500 Hz, and hosting $280/14 = 20$ coefficients. For each frequency region, the RMS of the power is calculated in Figure 9.21, which gives an estimate of the spectral envelope. With the help of these RMS values, which are transformed to the logarithmic domain in Figure 9.21, the MLT coefficients are then quantised using different step sizes according to a *perceptual model*. This task is performed by calculating an initial *categorisation*, in which a certain set of quantisation and coding parameters referred to as the *category* is assigned to each region. As portrayed in Figure 9.21, a total of 16 tentative categorisations and bit allocations are calculated, of which finally only the one that makes use of the available bits in the most efficient way is used. After the best bit allocation has been determined, the MLT coefficients are quantised and Huffman coded along with the parameters of the associated categories. During the last computational step the output data of the described signal processing stages is multiplexed into a data frame. The 'macroscopic' bit allocation which we encounter in a typical data frame at the output of the PTC encoder is illustrated in Figure 9.22 for the case of 320 frame bits, i.e. 16 kbps. As shown in Figure 9.21, the multiplexer (MUX) arranges the *RMS code bits*, the *rate-control bits*, and finally the *MLT code bits* into a bitstream. The exact frame structure is given in Figure 9.22, together with the typical number of bits needed for encoding the spectral

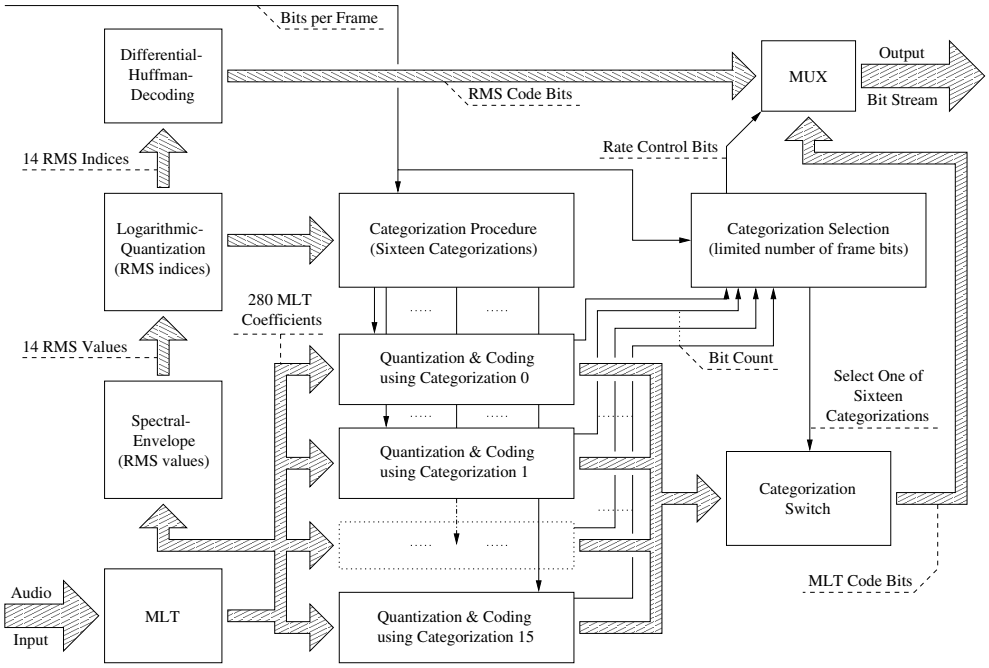

Figure 9.21: Block diagram of the PictureTel G.722.1 encoder.

envelope and the transform coefficients. In every frame, the first 5 bits are occupied by the value RMS_index(0), followed by the Huffman codes of the differentially coded RMS indices $1, \ldots, 13$ in spectral frequency order. The next 4 bits of every frame are occupied by the so-called rate control bits. Then the MLT code vector indices are transmitted, beginning with frequency region 0. Directly after a vector index's variable length code, the associated MLT coefficient sign bits are transmitted, in spectral frequency order.

The signal processing stages which constitute the G.722.1 decoder [330] are essentially the inverse operations of the encoder shown in Figure 9.21. The decoding of a frame starts with the reconstruction of the spectral envelope. Next, the four rate control bits are decoded, in order to determine which of the 16 possible categorisations has been used for encoding the MLT coefficients. In the same way, as 16 categorisations are generated in the encoder, they are now also generated in the decoder. Finally, the particular categorisation used at the encoder is also employed by the decoder. The frequency regions, where category 7 has been applied, are treated differently. Since no MLT coefficients have been transmitted for these frequency regions, a specific technique, referred to as *noise-filling* is used to prevent the associated MLT coefficients being set to zero. This technique is also applied to categories 5 and 6, since most of their coefficients are quantised to zero. The coefficients, which were quantised to non-zero values are reconstructed using a predetermined decoding table. After de-normalisation by multiplying all coefficients of a frequency region by their decoded RMS values, the MLT coefficients are rearranged into blocks of 320 coefficients, where the upper 40 coefficients are set to zero, since they belong to frequencies above 7 kHz. Then, the

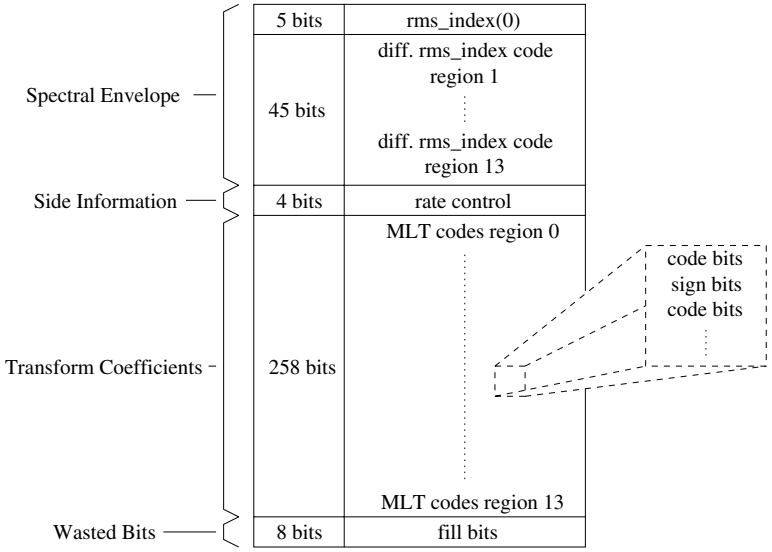

Figure 9.22: Structure of a typical coded frame at a bitrate of 16 kbps (320 bits per 20 ms frame); the number of bits needed for encoding the differential RMS indices and the transform coefficients varies in each frame together with the number of wasted bits.

inverse MLT (IMLT) is applied to the coefficients, generating 320 time-domain samples at the output. Both the MLT and the IMLT can be decomposed into a computationally efficient so-called discrete cosine transform (DCT) DCT type-IV and inverse DCT (IDCT) IDCT type-IV implementation [334], followed by a window, overlap and add operation [333]. Due to the Huffman coding which is applied to the values of the spectral envelope as well as to the MLT coefficients, the information carried by those codewords is extremely sensitive to bit errors. If the channel decoder is unable to correct all transmissions errors, the PTC decoder's recommended behaviour [330] is to repeat the MLT coefficients of the previous frame in case of a single erroneous frame, or to set the MLT coefficients to zero, which corresponds to muting the output signal, provided that the previous frame had also been contaminated by channel errors. For further details concerning the G.722.1 transform codec, the interested reader is referred to [330].

9.5.10 Wideband Adaptive System Performance

Our discussions related to the associated system design trade-offs and the impact of an automatic bitrate selection scheme on the audio quality of the system will be mainly based on measurements performed around channel SNR values of 5 dB, since for very low SNRs of around 0 dB the frame dropping rate is excessive, yielding an unacceptable audio quality. By contrast, for high channel SNRs around 10 dB the FER is too low to allow us to illustrate the trade-offs between the audio quality and FER effectively. A tentative estimate of the average quality of the reconstructed audio signal is provided by audio SEGSNR calculations, which provide an approximate measure of the subjectively perceived audio quality, especially in the

presence of frame dropping in conjunction with perceptual masking assisted transform-based audio coding.

9.5.11 Audio Frame Error Results

The basic trade-off between the system throughput and audio frame dropping-rate is illustrated for the 5 dB channel SNR scenario with the aid of our four fixed bitrate modes in Table 9.13. The first column reflects for each bitrate the associated frame dropping rate that we will encounter.

As expected, by increasing the required throughput bitrate, the FER will also increase, since a high proportion of reduced-quality subcarriers has to be used for conveying the increased number of audio bits, although the performance of the turbo channel codec improves. Experiments have shown that a frame dropping rate of around 5% in conjunction with the 16 kbps fixed bitrate mode is still sufficiently low in order to provide a perceptually acceptable audio quality. In the third to fifth columns of Table 9.13, the relative frequency of encountering error-free audio frames for the different audio bitrates is portrayed. Observe, furthermore, in the table that the same performance figures were also summarised for two different transmission schemes denoted by *Switch I* and *Switch II*. These schemes invoked a system philosophy allowing the bitrate to become time-variant and controlling the audio source codec and channel codec on a time-variant basis, in order to take this time-variant behaviour into account, as will be highlighted below.

Specifically, both of our experimental switching regimes, namely Switch I and Switch II employed the same switching algorithm as described in Section 9.5.7 with the only difference being that Switch I incorporated in addition to the three standard bitrates of 16, 24 and 32 kbps, proposed by the PictureTel company, a 10 kbps mode, with the intention of lowering the frame dropping rate further due to the more modest 'loading' of the OFDM symbols. For these switching schemes the 5 dB SNR related results in Table 9.13 underline that, for example, in comparison to the 16 kbps fixed-rate mode the system throughput was very much improved, conveying $(11.59 + 48.20)\%$ of the audio frames in the 24 and 32 kbps mode, rather than in the 16 kbps mode, while maintaining the same frame dropping rate of 5.58% as the 16 kbps mode. Although exhibiting a slightly lower frame dropping rate, the Switch I scheme was shown to produce an audio quality inferior to that of the Switch II scheme. This was due to the employment of the 10 kbps bitrate mode in the Switch I scheme, which produced a relatively low subjective audio quality. In this context it is interesting to see that although the Switch I scheme assigns about 22% percent of all frames to the 10 kbps transmission mode, the frame dropping rate was increased only by about 1.1% when disabling this subjectively low-quality but error resilient mode in the Switch II scheme. This is an indication of the conservative decision regime of our bitrate selector. The relative frequency of invoking the different bitrates in conjunction with the Switch II scheme has been evaluated additionally for channel SNRs of 0 dB and 10 dB, which characterises the operation of the bitrate selector once again. The associated results are presented in Table 9.14, which become plausible in light of our previous discussions.

Table 9.14: FER and relative frequency (Rel.fr.) of different bitrates in the Switch II scheme (successfully transmitted frames) for channel SNRs of 0, 5 and 10 dB.

Scheme	FER (%)	Rel.fr.: (%) 10 kbps	Rel.fr.: (%) 16 kbps	Rel.fr.: (%) 24 kbps	Rel.fr.: (%) 32 kbps
0	37.69	0.0	37.79	14.42	10.10
5	5.58	0.0	34.63	11.59	48.20
10	0.34	0.0	7.81	5.61	86.24

9.5.12 Audio SEGSNR Performance and Discussions

In addition to our previous results Figure 9.23 displays the CDF of the SEGSNR of consecutive 20 ms duration audio segments obtained from the reconstructed signal of an audio test signal at the output of the PTC decoder for the schemes described above. These CDFs were recorded at a channel SNR of 5 dB. The step function-like CDF discontinuity at a SEGSNR of 0 dB corresponds to the frame dropping rate of the associated transmission scheme which was summarised in Table 9.14 for the various systems. As expected, for any given SEGSNR value it is desirable to maintain as low a proportion of the audio frames' SEGSNRs below a given abscissa value as possible. Hence we concluded that the best SEGSNR CDF was attributable to the Switch II scheme, while the worst to the fixed 10 kbps arrangement, as suggested before. In the range of high audio SEGSNRs the preference order of the various fixed schemes followed our expectations, i.e. the fixed 32 kbps scheme performed best in SEGSNR terms when neglecting frame drops. The trade-off was that although due to its highest audio bitrate of 32 kbps the scheme exhibited the inherently highest SEGSNR, due to its high throughput requirement this scheme was forced to invoke a high proportion of partially impaired, low-quality OFDM subcarriers, which often resulted in corrupted and dropped audio frames. Since the fixed 10 kbps scheme exhibited the lowest audio SEGSNR performance, this scheme was excluded from the Switch II arrangement. However, FERs in excess of 10% result in distinctively audible artifacts, which – despite their high error-free SEGSNRs – virtually rendered the fixed-rate 24 kbps and 32 kbps modes unacceptable. Hence, our proposed switching scheme – Switch II – which is based on the 16, 24 and 32 kbps bitrates, achieved at medium SNRs the best compromise between average error-free audio quality and frame dropping rate, which has been verified by our informal listening tests.

As outlined in Section 9.5.7, the mode-switching algorithm operates on the basis of statistically evaluated experimental results for the prediction of the FER. A robust, channel-independent switching regime on the basis of the turbo coder's quality perceptions can overcome this dependence. Furthermore, a target-FER driven switching scheme instead of the minimal-FER algorithm employed for this series of experiments will be investigated in the future.

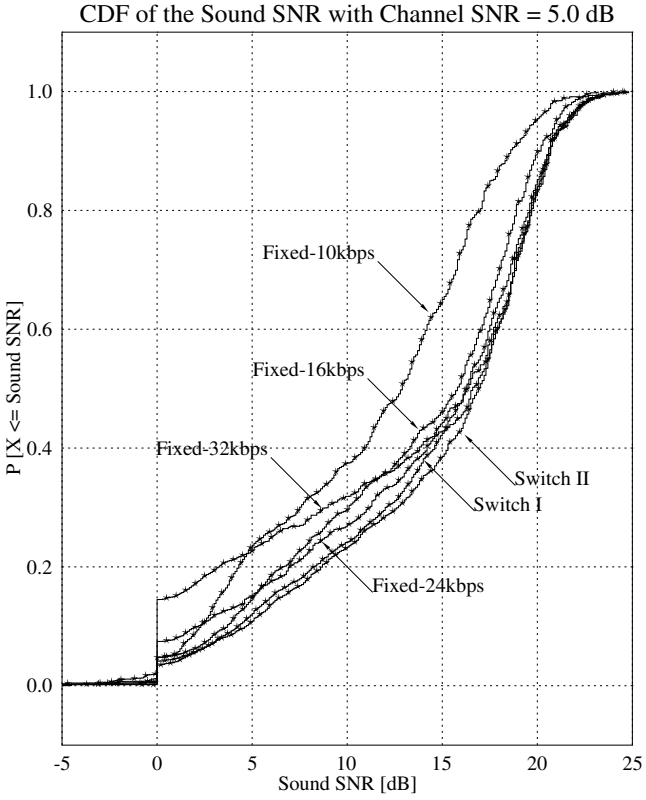

Figure 9.23: Typical CDF of the SEGSNR of a reconstructed audio signal transmitted over the fading time dispersive channel.

9.5.13 G.722.1 Audio Transceiver Summary and Conclusions

The design trade-offs of turbo-coded burst-by-burst (AOFDM) wideband speech transceivers were analysed. A constant throughput adaptive OFDM transceiver was designed and benchmarked against a time-variant rate scheme. The proposed joint adaptation of source codec, channel codec and modulation regime resulted in attractive, robust, high-quality audio candidate systems, capable of conveying near-unimpaired wideband audio signals over fading dispersive channels for SNRs in excess of about 5 dB.

9.6 Turbo-detected Unequal Error Protection Irregular Convolutional Coded AMR-WB Transceivers

J. Wang, N. S. Othman, J. Kliewer, L. L. Yang and L. Hanzo

9.6.1 Introduction

Recent speech coding research efforts have been successful in creating a range of both narrow- and wideband multimode and multirate coding schemes, many of which have found

their way into standardised codecs, such as the advanced multirate (AMR) codec and its wideband version known as the AMR-WB scheme proposed for employment in the third-generation wireless systems. Other multimode solutions have been used in the MPEG-4 codec, which will be investigated in the next chapter. In multimode coding schemes [335, 336], a mode selection process is invoked and the specific coding mode best suited to the local character of the speech signal is selected from a predetermined set of modes. This technique dynamically tailors the coding scheme to the widely varying local acoustic-phonetic character of the speech signal.

Multirate coding, on the other hand, facilitates the assignment of a time-variant number of bits for a frame, adapting the encoding rate on the basis of the local phonetic character of the speech signal or the network conditions. This is particularly useful in digital cellular communications, where one of the major challenges is that of designing an encoder that is capable of providing high-quality speech for a wide variety of channel conditions. Ideally, a good solution must provide the highest possible speech quality under perfect channel conditions, while maintaining an error-resilient behaviour in hostile channel environments. Traditionally, existing digital cellular applications have employed a single coding mode where a fixed source/channel bit allocation provides a compromise solution between the perfect and hostile channel conditions. Clearly, a coding solution which is well suited for high-quality channels would use most of the available bits for source coding in conjunction with only minimal error protection, while a solution designed for poor channels would use a lower-rate speech encoder along with more powerful forward error protection. Due to the powerful combination of channel equalization, interleaving and channel coding, near-error-free transmission can be achieved down to a certain threshold of the carrier to interferer ratio (C/I). However, below this threshold, the error correction code is likely to fail in removing the transmission errors, with the result that the residual errors may cause annoying artifacts in the reconstructed speech signal.

Therefore, in existing systems typically a worst case design is applied, where the channel coding scheme is sufficiently powerful to remove most transmission errors, as long as the system operates within a reasonable C/I range. However, the drawback of this solution is that the speech quality becomes lower than necessary under good channel conditions, since a high proportion of the gross bitrate is dedicated to channel coding.

The Advanced Multi-Rate (AMR) concept [28] solves this 'resource allocation' problem in a more intelligent way. Specifically, the ratio between the speech bitrate and the error protection-oriented redundancy is adaptively adjusted according to the prevalent channel conditions. While the channel quality is inferior, the speech encoder operates at low bitrates, thus accommodating powerful forward error control within the total bitrate budget. By contrast, under high channel conditions the speech encoder may benefit from using the total bitrate budget, yielding high speech quality, since in this high-rate case low-redundancy error protection is sufficient. Thus, the AMR concept allows the system to operate in an error-resilient mode under poor channel conditions, while benefitting from a better speech quality under good channel conditions. This is achieved by dynamically splitting the gross bitrate of the transmission system between source and channel coding according to the instantaneous channel conditions. Hence, the source coding scheme must be designed for seamless switching between rates available without annoying artifacts.

The employment of the AMR-WB codec has been under discussion in both GSM networks [337, 338] as well as in the 3G systems [339]. With the aim of providing a system-

design example for these intelligent systems, in this section we will characterise the error sensitivity of the AMR-WB encoder's output bits so that the matching channel encoder can be carefully designed to provide the required protection for the speech bits, in particular for those which are most sensitive to transmission errors.

Furthermore, in the context of turbo detection the channel codes should also match the characteristics of the channel for the sake of attaining a good convergence performance. In this section we address this design dilemma by using irregular convolutional codes (IRCCs) which constitute a family of different-rate subcodes. We will demonstrate the benefit of the high design flexibility of IRCCs and hence excellent convergence properties are maintained while having unequal error protection capabilities matched to the requirements of the source. An EXIT chart-based design procedure is proposed and used in the context of protecting the different sensitivity speech bits of the wideband AMR speech codec. As a benefit, the unequal-protection system using IRCCs exhibits an SNR advantage of about 0.4 dB over the equal-protection system employing regular convolutional codes when communicating over a Gaussian channel. We will also demonstrate that IRCCs exhibit excellent convergence properties in the context of iterative decoding, whilst having an unequal error protection capability, which is exploited here to protect the different sensitivity speech bits of the wideband AMR speech codec. As a benefit, the unequal-protection system exhibits an SNR advantage of about 0.3 dB over the equal-protection system when communicating over a Gaussian channel.

Source encoded information sources, such as speech, audio or video, typically exhibit a non-uniform error sensitivity where the effect of a channel error may significantly vary from one bit to another. Hence unequal error protection (UEP) is applied to ensure that the perceptually more important bits benefit from more powerful protection. In [340], the speech bits were protected by a family of rate-compatible punctured convolutional (RCPC) codes [341] whose error protection capabilities had been matched to the bit sensitivity of the speech codec. Different rate RCPC codes were obtained by puncturing the same mother code, while satisfying the rate-compatibility restriction. However, they were not designed in the context of turbo detection. Other schemes using a serially concatenated system and turbo processing were proposed in [342, 343], where the UEP was provided by two different rate convolutional codes.

Tüchler and Hagenauer [344, 345] studied the construction of IRCCs and proposed several design criteria. These IRCCs consisted of a family of convolutional codes having different code rates and were specifically designed with the aid of extrinsic information transfer (EXIT) charts [346] invoked for the sake of improving the convergence behaviour of iteratively decoded serially concatenated systems. In general, EXIT chart analysis assumes having long interleaver block lengths. However, it was shown in [345] that by using an appropriate optimisation criterion, the concatenated system is capable of performing well even for short interleaver block lengths. Since the constituent codes have different coding rates, the resultant IRCC is capable of providing UEP.

A novel element of this section is that UEP and EXIT chart-based code optimisation will be jointly carried out and successfully applied to improve the achievable robustness of speech transmission. We propose a serially concatenated turbo transceiver using an IRCC as the outer code for the transmission of AMR-WB coded speech. Rather than being decoded separately, the constituent codes of the IRCC are decoded jointly and iteratively by exchanging extrinsic information with the inner code. The IRCC is optimised to match the characteristics of both

the speech source codec and those of the channel, so that UEP is achieved while maximising the iteration gain attained.

The error sensitivity of the AMR-WB speech codec will be characterised in Section 9.6.2, while our system model will be introduced in Section 9.6.3. Section 9.6.4, will describe the design procedure of IRCCs. An IRCC design example is provided in Section 9.6.5. Our performance results are presented in Section 9.6.6, while Section 9.6.7 concludes the discussion.

9.6.2 The AMR-WB Codec's Error Sensitivity

The AMR-WB speech codec is capable of supporting bitrates varying from 6.6 to 23.85 kbps and it has become a 3GPP and ITU-T standard which provides a superior speech quality in comparison to the conventional telephone-bandwidth voice codecs [347]. Each AMR-WB frame represents 20 ms of speech, producing 317 bits at a bitrate of 15.85 kbps plus 23 bits of header information per frame. The codec parameters in each frame include the so-called immittance spectrum pairs (ISPs), the adaptive codebook delay (pitch delay), the algebraic codebook excitation index and the jointly vector quantised pitch gains as well as algebraic codebook gains.

Most source coded bitstreams contain certain bits that are more sensitive to transmission errors than others. A common approach used for quantifying the sensitivity of a given bit is to consistently invert this bit in every speech frame and evaluate the associated SEGSNR degration. The error sensitivity of the various encoded bits in the AMR-WB codec determined in this way is shown in Figure 9.24. The results are based on speech samples taken from the EBU SQAM (Sound Quality Assessment Material) CD, sampled at 16 kHz and encoded at 15.85 kbps. It can be observed that the bits representing the ISPs, the adaptive codebook delay, the algebraic codebook index and the vector quantised gain are fairly error sensitive. By contrast, the least sensitive bits are related to the fixed codebook's excitation pulse positions. Statistically, about 10% (35/340) of the bits in a speech frame will cause a SEGSNR degration in excess of 10 dB, and about 8% (28/340) of the bits will inflict a degration between 5 and 10 dB. Furthermore, the error-free reception of the 7% (23/340) header information is, in general, crucial for the adequate detection of speech.

9.6.3 System Model

Fig. 9.25 shows the system's schematic diagram. At the transmitter, each of the K-bit speech frames is protected by a serially concatenated channel code consisting of an outer code (Encoder I) and an inner code (Encoder II) before transmission over the channel, resulting in an overall coding rate of R. At the receiver, iterative decoding is performed with the advent of extrinsic information exchange between the inner code (Decoder II) and the outer code (Decoder I). Both decoders employ the *a posteriori* probability (APP) decoding algorithm, e.g. the BCJR algorithm [348]. After F iterations, the speech decoder is invoked in order to reconstruct the speech frame.

According to the design rules of [349], the inner code of a serially concatenated system should be recursive to enable interleaver gain. Furthermore, it has been shown in [350] that for binary erasure channels (BECs) and block lengths tending to infinity, the inner code should have rate-1 to achieve capacity. Experiments have shown that this approximately holds also

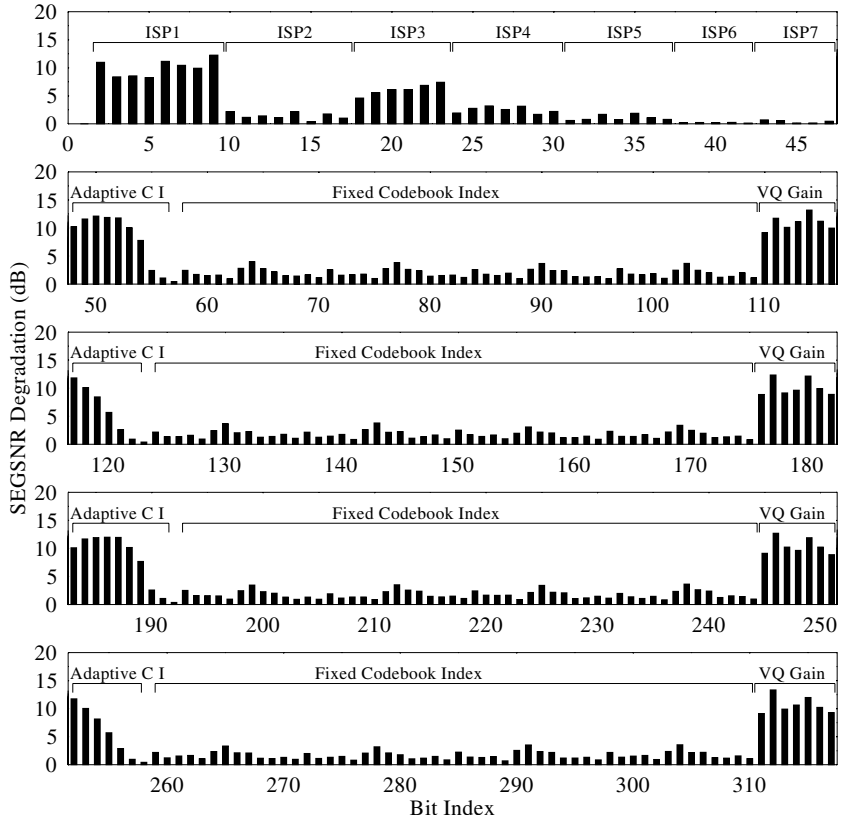

Figure 9.24: SEGSNR degrations versus bit index due to inflicting 100% BER in the 317-bit, 20 ms AMR-WB frame.

for AWGN channels [344,345]. For the sake of simplicity, we opted for employing a memory-1 recursive convolutional code having a generator polynomial of $1/(1+D)$, which is actually a simple accumulator. Hence the decoding complexity of the inner code is extremely low. In the proposed system, we use an IRCC as the outer code, while in the benchmarker system we use a regular non-systematic convolutional (NSC) code as the outer code. BPSK modulation and encountering an AWGN channel are assumed.

9.6.4 Design of Irregular Convolutional Codes

An IRCC is constructed from a family of P subcodes. First, a rate-r convolutional mother code C_1 is selected and the other $(P-1)$ subcodes C_k of rate $r_k > r$ are obtained by puncturing. Let L denote the total number of encoded bits generated from the K input information bits. Each subcode encodes a fraction of $\alpha_k r_k L$ information bits and generates $\alpha_k L$ encoded bits. Given the target code rate of $R \in [0,1]$, the weighting coefficient α_k has

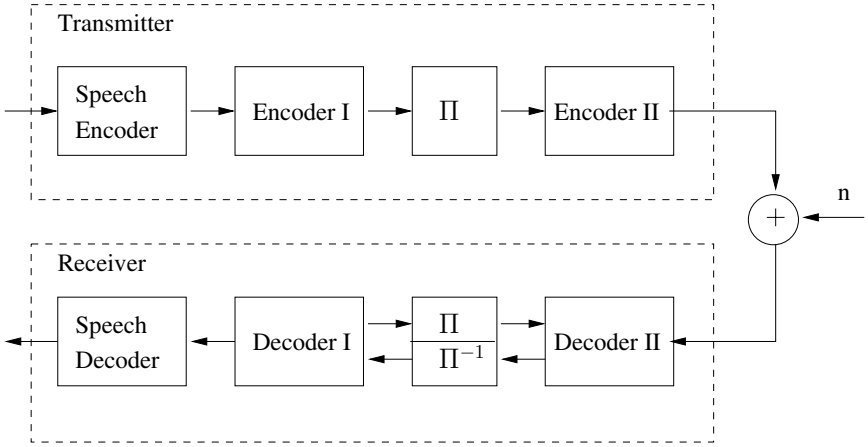

Figure 9.25: System model.

to satisfy

$$1 = \sum_{k=1}^{P} \alpha_k, \quad R = \sum_{k=1}^{P} \alpha_k r_k, \quad \alpha_k \in [0, 1], \ \forall k. \tag{9.50}$$

For example, in [345] a family of $P = 17$ subcodes were constructed from a systematic, rate-1/2, memory-4 mother code defined by the generator polynomial $(1, g_1/g_0)$, where $g_0 = 1 + D + D^4$ is the feedback polynomial and $g_1 = 1 + D^2 + D^3 + D^4$ is the feedforward polynomial. Higher code rates may be obtained by puncturing, while lower rates are created by adding more generators and by puncturing under the constraint of maximising the achievable free distance. The two additional generators used are $g_2 = 1 + D + D^2 + D^4$ and $g_3 = 1 + D + D^3 + D^4$. The resultant 17 subcodes have coding rates spanning from $0.1, 0.15, 0.2, \ldots, 0.9$.

The constructed IRCC has the advantage that the decoding of all subcodes may be performed using the same mother code trellis, except that at the beginning of each block of $\alpha_k r_k L$ trellis sections corresponding to the subcode C_k, the puncturing pattern has to be restarted. Trellis termination is necessary only after all of the K information bits have been encoded.

We now optimise the iterative receiver by means of EXIT charts [346], which are capable of predicting the performance of an iterative receiver by examining the extrinsic information transfer function of each of the component devices independently.

For the outer decoder (Decoder I), denote the mutual information between the *a priori* input A and the transmitted code bits C as $I_{A1} = I(C; A)$, while the mutual information between the extrinsic output E and the transmitted code bits C is denoted as $I_{E1} = I(C; E)$. Then the transfer function of Decoder I can be defined as

$$I_{E1} = T_I(I_{A1}), \tag{9.51}$$

which maps the input variable I_{A1} to the output variable I_{E1}. Similarly, for the inner decoder (Decoder II) we denote the mutual information between the *a priori* input A and

the transmitted information bits X as $I_{A2} = I(X; A)$. Furthermore, we denote the mutual information between the extrinsic output E and the transmitted information bits X as $I_{E2} = I(X; E)$. Note that the extrinsic output of the inner code also depends on the channel SNR or E_b/N_0. Hence the transfer function of the inner code is defined as

$$I_{E2} = T_{II}(I_{A2}, E_b/N_0). \tag{9.52}$$

The transfer functions can be obtained by using the histogram-based log-likelihood (LLR) measurements as proposed in [346] or the simplified method as proposed in [351].

When using IRCCs, the transfer function of an IRCC can be obtained from those of its subcodes. Denote the transfer function of the subcode k as $T_{I,k}(i)$. Assuming that the trellis fractions of the subcodes do not significantly interfere with each other, which might change the associated transfer characteristics, the transfer function $T_I(i)$ of the target IRCC is the weighted superposition of the transfer function $T_{I,k}(i)$ [345], yielding

$$T_I(i) = \sum_{k=1}^{P} \alpha_k T_{I,k}(i). \tag{9.53}$$

Note that in iterative decoding, the extrinsic output $E2$ of Decoder II becomes the *a priori* input $A1$ of Decoder I and *vice versa*. Given the transfer function, $T_{II}(i, E_b/N_0)$, of the inner code, and that of the outer code $T_I(i)$, the extrinsic information I_{E1} at the output of Decoder I after the ith iteration can be calculated using the recursion of

$$\mu_i = T_I(T_{II}(\mu_{i-1}, E_b/N_0)), \quad i = 1, 2, \ldots, \tag{9.54}$$

with $\mu_0 = 0$, i.e. assuming the absence of *a priori* input for Decoder II at the commencement of iterations.

Generally, interactive speech communication systems require a low delay, and hence a short interleaver block length. The number of iterations for the iterative decoder is also limited due to the constraint of complexity. It has been found [345] that EXIT charts may provide a reasonable convergence prediction for the first couple of iterations even in the case of short block lengths. Hence, we fixed the transfer function of the inner code for a given E_b/N_0 value yielding $T_{II}(i) = T_{II}(i, E_b/N_0)$, and optimised the weighting coefficients $\{\alpha_k\}$ of the outer IRCC for the sake of obtaining a transfer function $T_I(i)$ that specifically maximises the extrinsic output after exactly F iterations [345], which is formulated as

$$\text{maximise } \mu_i = T_I(T_{II}(\mu_{i-1})), \quad i = 1, 2, \ldots, F, \tag{9.55}$$

with $\mu_0 = 0$.

In addition, considering the non-uniform error sensitivity of the speech source bits characterised in Figure 9.24, we may intentionally enhance the protection of the more sensitive source data bits by using strong subcodes, thus imposing the source constraints of

$$\sum_{k=k_1}^{k_2} \alpha_k r_k / R \geq x\%, \quad 1 \leq k_1 \leq k_2 \leq P, \;\; 0 \leq x \leq 100, \tag{9.56}$$

which implies that the percentage of the speech source bits protected by the subcodes k_1 to k_2 is at least $x\%$.

Finally, our task is to find a weight vector $\boldsymbol{\alpha} = [\alpha_1, \alpha_2, \ldots, \alpha_P]^{\mathrm{T}}$, so that Equation (9.55) is maximised, while satisfying the constraints of Equations (9.50) and (9.56). This optimisation problem can be solved by slightly modifying the procedure proposed in [345], as will be illustrated by the following example.

9.6.5 An Irregular Convolutional Code Example

We assume the overall system coding rate to be $R = 0.5$. As stated in Section 9.6.3, the inner code has a unitary code rate, hence all the redundancy is assigned to the outer code. We use a half-rate, memory-4, maximum free distance NSC code having the generator polynomials of $g_0 = 1 + D + D^2 + D^4$ and $g_1 = 1 + D^3 + D^4$. The extrinsic information transfer functions of the inner code and the outer NSC code are shown in Figure 9.26. It can be seen that the minimum convergence SNR threshold for the benchmarker system using the NSC outer code is about 1.2 dB, although we note that these curves are based on the assumption of having an infinite interleaver length and a Gaussian LLR distribution. In the case of short block lengths, the actual SNR convergence threshold might be higher.

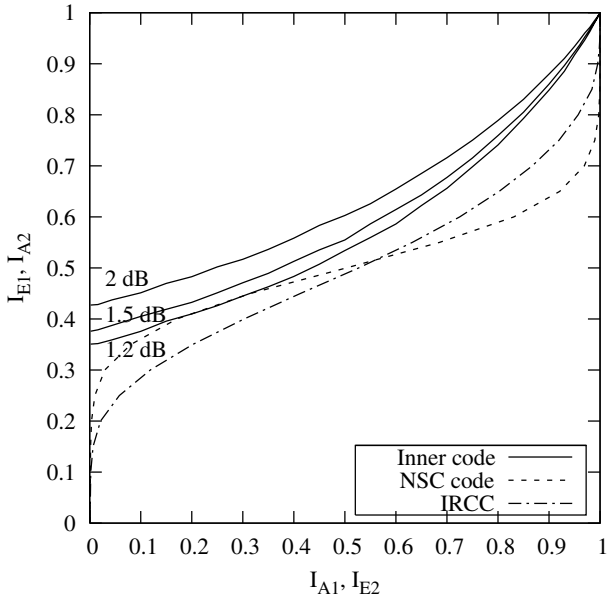

Figure 9.26: Extrinsic information transfer functions of the outer NSC code and the designed IRCC, as well as those of the inner code at $E_b/N_0 = 1.2$, 1.5 and 2 dB.

Hence, when constructing the IRCC we choose the target inner code transfer function $T_{II}(i)$ at E_b/N_0 = 1.5 dB, and the number of iterations $F = 6$. For the constituent subcodes we use those proposed in [345] except that code rates of $r_k > 0.75$ are excluded from our design for the sake of avoiding significant error floors. The resultant code rates of the subcodes span the range of $r_1 = 0.1, r_2 = 0.15, \ldots, r_{14} = 0.75$.

Initially the source constraint of Equation (9.56) was not imposed. By using the optimisation procedure of [345], we arrive at the weight vector of $\boldsymbol{\alpha}_0 = [0\ 0\ 0\ 0\ 0.01\ 0.13\ 0.18\ 0.19\ 0.14\ 0.12\ 0.10\ 0.01\ 0.03\ 0.10]^{\mathrm{T}}$, and the percentage of the input speech data bits protected by the different subcodes becomes [0, 0, 0, 0, 0.6%, 9.0%, 14.4%, 16.7%, 14.0%, 13.0%, 11.5%, 1.6%, 4.2%, 15.0%]$^{\mathrm{T}}$. The extrinsic output of Decoder I after 6 iterations becomes $\mu_6 = 0.98$.

Observe in the context of the vector containing the corresponding speech bit fractions that only 0.6% of the source bits are protected by the $r_5 = 0.3$-rate subcode, whereas a total of 23.4% of the speech bits is protected by the $r_6 = 0.35$ and $r_7 = 0.4$-rate subcodes. In order to enhance the protection of the more sensitive speech bits, we now impose the source constraint of Equation (9.56) by requiring all the header information bits in a speech frame to be protected by the relatively strong $r_5 = 0.3$-rate subcode. More explicitly, we impose the constraint of $\alpha_5 r_5 / 0.5 \geq 7\%$, resulting in a new weight vector of $\boldsymbol{\alpha}_1 = [0\ 0\ 0\ 0\ 0.12\ 0.06\ 0.14\ 0.16\ 0.13\ 0.12\ 0.10\ 0.02\ 0.04\ 0.11]^{\mathrm{T}}$, and the new vector of speech bit fractions becomes [0, 0, 0, 0, 7.1%, 4.0%, 10.9%, 14.8%, 13.5%, 13.3%, 12.2%, 2.7%, 5.5%, 16%]$^{\mathrm{T}}$. The extrinsic output after 6 iterations is now slightly reduced to $\mu_6 = 0.97$, which is close to the maximum value of 0.98. Furthermore, now 14.9% of the speech bits is protected by the $r_6 = 0.35$ and $r_7 = 0.4$-rate subcodes.

The extrinsic information transfer function of this IRCC is also shown in Figure 9.26. As seen from the EXIT chart, the convergence SNR threshold for the system using the IRCC is lower than 1.2 dB and there is a wider EXIT chart tunnel between the inner code's curve and the outer code's curve which is particularly so at the low I_A values routinely encountered during the first couple of iterations. Hence, given a limited number of iterations, we would predict that the system using the IRCC may be expected to perform better than that using the NSC outer code in the range of $E_b/N_0 = 1.5$–2 dB.

9.6.6 UEP AMR IRCC Performance Results

Finally, the achievable system performance was evaluated for a $K = 340$ speech bit per 20 ms transmission frame, resulting in an interleaver length of $L = 688$ bits, including 8 tail bits. This wideband-AMR speech coded [347] frame was generated at a bitrate of 15.85 kbps in the codec's mode 4. Before channel encoding, each frame of speech bits is rearranged according to the descending order of the error sensitivity of the bits by considering Figure 9.24, so that the more important data bits are protected by stronger IRCC subcodes. An S-random interleaver [352] was employed with $S = 15$, where all of the subcodes' bits are interleaved together, and 10 iterations were performed by the iterative decoder.

The BER performance of the UEP system using IRCCs and that of the equal error protection (EEP) benchmarker system using the NSC code are depicted in Figure 9.27. It can be seen that the UEP system outperforms the EEP system in the range of $E_b/N_0 = 1.5$–2.5 dB, which matches our performance prediction inferred from the EXIT chart analysis of Section 9.6.4.

The actual decoding trajectories of both the UEP system and the EEP system recorded at $E_b/N_0 = 1.5$ and 2 dB are shown in Figures 9.28 and 9.29, respectively. These are obtained by measuring the evolution of mutual information at the input and output of both the inner decoder and the outer decoder as the iterative decoding algorithm is simulated. Due to the relatively short interleaver block length of 688 bits, the actual decoding trajectories do not

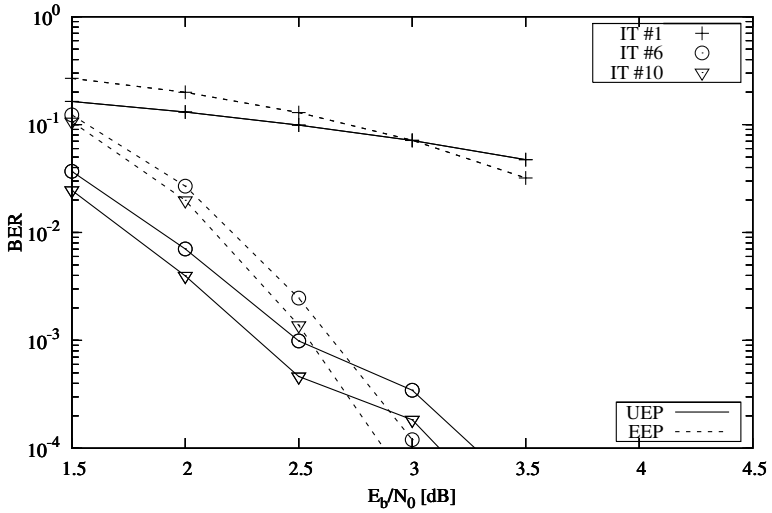

Figure 9.27: BER performance of both the UEP system employing the IRCC and the EEP system using the NSC code.

closely follow the transfer functions especially when increasing the number of iterations. Nonetheless, the UEP system does benefit from having a wider open tunnel during the first couple of iterations and hence it is capable of reaching a higher extrinsic output in the end, resulting in a lower BER.

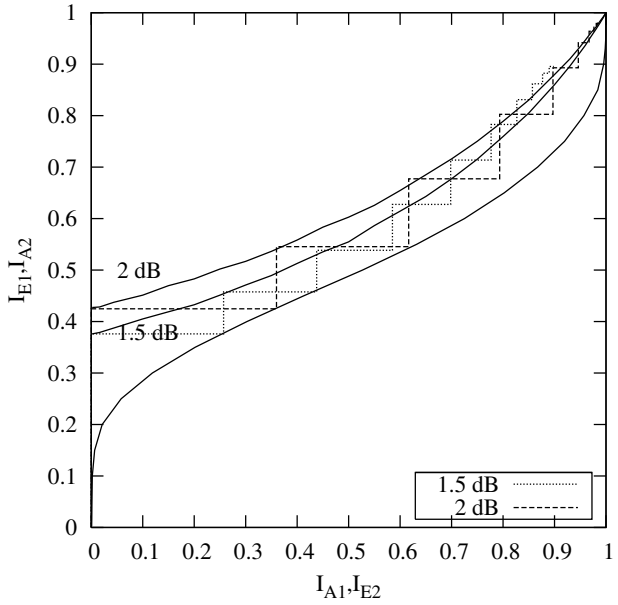

Figure 9.28: The EXIT chart and the simulated decoding trajectories of the UEP system using our IRCC as the outer code and a rate-1 recursive code as the inner code at both $E_b/N_0 = 1.5$ and 2 dB.

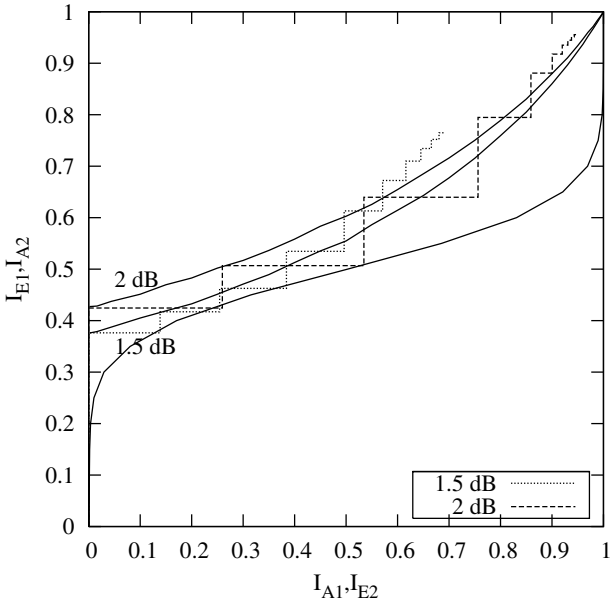

Figure 9.29: The EXIT chart and the simulated decoding trajectories of the EEP system using our NSC code as the outer code and a rate-1 recursive code as the inner code at both $E_b/N_0 = 1.5$ and 2 dB.

The BER profiles of the UEP system at $E_b/N_0 = 1.5$, 2 and 2.5 dB are plotted in Figure 9.30. As intended, different fractions of the speech frame benefitted from different degrees of IRCC-aided protection. The first 60 bits represent the header information bits and the most sensitive speech bits, which require the lowest BER.

The SEGSNR performances of both the UEP and EEP system are depicted in Figure 9.31. The UEP system is seen to outperform the EEP system at $E_b/N_0 \leq 2.5$ dB. Above this E_b/N_0 point, the two systems attained almost the same SEGSNRs. To achieve a good speech quality associated with SEGSNR > 9 dB, the UEP system requires $E_b/N_0 \geq 2$ dB, about 0.3 dB less than the EEP system.

9.6.7 UEP AMR Conclusions

In Figure 9.24 of Section 9.6.2 we briefly exemplified the error sensitivity of the AMR-WB codec and then investigated the application of IRCCs for the sake of providing UEP for the AMR-WB speech codec. The IRCCs were optimised with the aid of EXIT charts and the design procedure used was illustrated with the aid of an example.

In the design of IRCCs, we aimed for matching the extrinsic information transfer function of the outer IRCC to that of the inner code, where that of the latter is largely determined by the channel SNR. At the same time, we imposed certain source constraints determined by the error sensitivity of the AMR-WB source bits. Hence the design method proposed here may be viewed as an attractive joint source/channel codec optimisation.

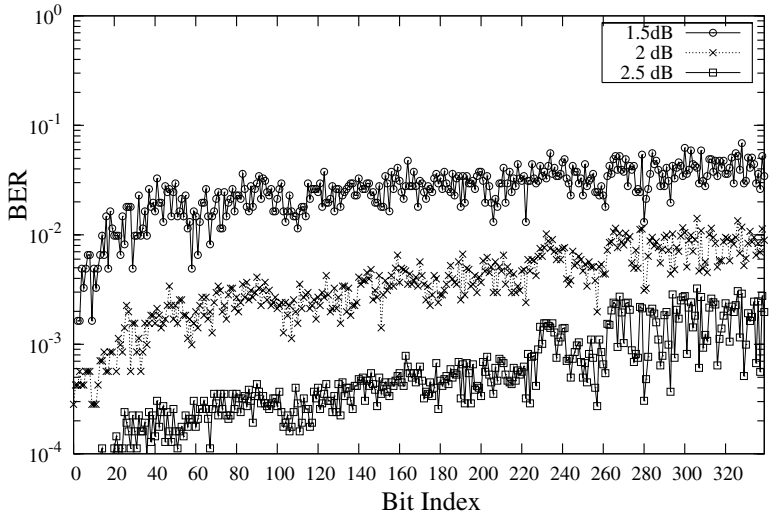

Figure 9.30: BER of the different speech bits after ten iterations at $E_b/N_0 = 1.5$, 2 and 2.5 dB recorded by transmitting 10^5 speech frames.

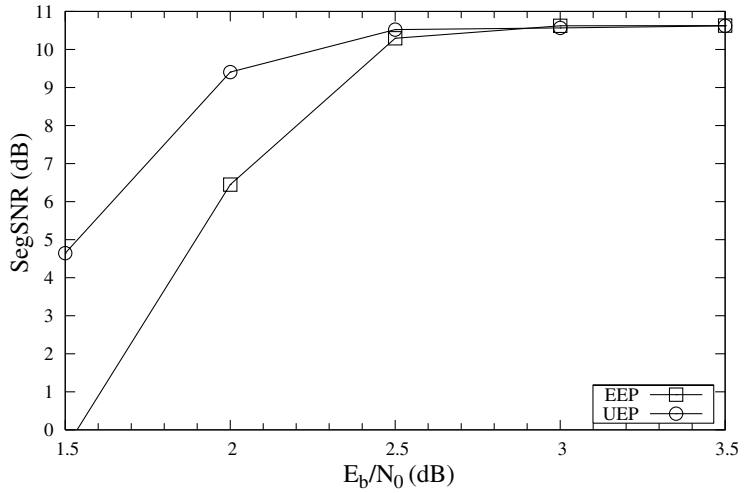

Figure 9.31: Comparison of SEGSNRs of the AMR-WB speech codec using both EEP and UEP.

The concatenated system using an IRCC benefits from having a low convergence SNR threshold. Owing to its design flexibility, various transfer functions can be obtained for an IRCC. We have shown that our IRCC was capable of achieving better convergence than a regular NSC code having the same constraint length and code rate. Hence the system using IRCCs has the potential of outperforming the corresponding arrangement using regular NSC codes in the low SNR region.

Furthermore, IRCCs are capable of providing UEP, since it is constituted by various subcodes having different code rates and hence different error protection capabilities. Multimedia source information, such as speech, audio and video source can benefit from this property, when carefully designing the IRCC to match the source's bit sensitivity. Our future research aims at exchanging soft speech bits between the speech and channel decoders.

It is worth noting that an ISI channel can also be viewed as a rate-1 convolutional code, and the transfer function of an equalizer for a precoded ISI channel [353] is similar to that of the inner code here. Hence the proposed design method can be easily extended to ISI channels.

9.7 The AMR-WB+ Audio Codec[2]

9.7.1 Introduction

This section introduces the architecture and characterises the achievable performance as well as a range of potential application scenarios for the AMR-WB+ code, which is also often referred to as the extended AMR-WB audio codec. This state-of-the-art coding arrangement is capable of achieving high audio quality at exceptionally low rates. This codec was recently selected by 3GPP and DVB for supporting low bitrate audio and audiovisual applications on mobile networks. The impressive recent advances in both source compression as well as in wireless networking and in mobile device technologies have enabled the introduction of innovative multimedia services delivered to wireless devices. Marketing studies conducted around the globe demonstrates the growing popularity of mobile multimedia services, such as the streaming, downloading and uploading of audio and audiovisual content. The provision of high-quality mobile multimedia services imposes challenging requirements on both the design of an error-resilient stereophonic source codec as well as on the wireless network, when aiming for a high perceptual audio quality. The 3GPP has defined a range of high-quality mobile multimedia services for both the Generic Packet Radio System (GPRS) and for the 3G networks, both of which benefit from the increased effective throughput and potentially reduced error rates of these advanced wireless networks. More explicitly, the corresponding 3GPP standards specify the following advanced services, which exhibit a number of common elements, such as the media types and media formats, where the content conveyed may be a combination of audio and video clips, graphics, images as well as text.

- *Multimedia messaging services (MMS) [3GPP TS 22.140].* To elaborate a little further, the multimedia message service may be used between mobile terminals as well as for downloading information from a content server to a mobile terminal and *vice versa*. As the density of sophisticated multimedia terminals is increasing, this imposes challenges on the interoperability of the various networks.

- *Packet-switched streaming services (PSS) [3GPP TS 22.233].* PSS provide a framework for point to point multimedia streaming services with the aid of the real-time transport protocol (RTP) for the transport of real-time interactive audio and video.

[2]This section is based on R. Salami, R. Lefebvre, A. Lakaniemi, K. Kontola, S. Bruhn and A. Taleb: Extended AMR-WB for high-quality audio on mobile devices, IEEE Communications Magazine, Volume 44, Issue 5, May 2006, pp. 90–97.

- *Multimedia broadcast/multicast services (MBMS) [3GPP TS 22.246].* MBMS constitute point-to-multipoint services, where typically RTP-based streaming and downloading is employed.
- *IP multimedia subsystem (IMS) messaging [3GPP TS 22.340].*
- *Presence service [3GPP TS 22.141].*[3]

The challenge faced by the design of the AMR-WB+ codec is that these services include the transmission of music, speech and speech mixed with diverse audio types as in sports casts, news and movies, while the bitrates available in the context of GPRS networks may be as low as 10 kbps. Therefore, the 3GPP body has standardized audio codecs for supporting the interoperability of GPRS and 3G networks as well as that of mobile terminals. However, when 3GPP Release 5 was specified, no audio codec was readily capable of satisfying these challenging requirements because speech codecs tend to exploit the specific statistical properties of speech signals, while audio signals typically exhibit different statistical properties. This design challenge was tackled by the MPEG4 codec to be discussed in the next chapter by introducing a number of speech- and audio-specific coding modes, which naturally exhibited widely different properties. Therefore, in the 3GPP Release 5 the narrowband AMR [3GPP TS 26.071] and the AMR-WB [3GPP TS 26.171] codecs were standardised. By contrast, the low complexity advanced audio coding (AAC-LC) mode of MPEG-4 [354] was recommended for the more challenging audio services. The AMR-WB codec discussed in the previous section delivers high quality for 7 kHz bandwidth speech signals at bitrates as low as 12.65 kbps, but as expected, it does not perform well when encoding audio signals. On the other hand, the AAC-LC MPEG-4 coding mode achieves a high perceptual audio quality, but requires bitrates in excess of 48 kbps. As expected, the attainable audio quality degrades as the bitrate is reduced, which motivated the development of the AMR-WB+ codec.

In the 3GPP Release 6 recommendation which was issued in December 2002, a new work item was approved with the goal of extending the AMR-WB speech codec for delivering perceptually high-quality speech, audio and mixed content. Hence this codec was termed the extended AMR-WB or AMR-WB+ scheme. Almost concomitantly the advanced coding mode of high-efficiency (HE) MPEG-4 (also known as MPEG-4 HE AAC) was standardized and it was suggested for adoption by 3GPP for supporting low bitrate audio services replacing AAC-LC. Hence, a process was launched in 3GPP for testing and selecting audio codecs for employment in Release 6, in order to support multimedia services. One of the main requirements was to achieve a performance better than that of the Release 5 codecs, such as AMR-WB and AAC LC, regardless of the specific content delivered. The testing was divided into two categories, namely the handling of rates below 24 kbps and that of high-quality services at rates of 32 and 48 kbps.

The candidates shortlisted for the latter high-rate schemes included the so-called MPEG-4 aacPlus and Enhanced aacPlus (Eaac+) (also known as aacPlus v2) schemes, which are constituted by the combination of three different MPEG schemes, namely that of the advanced audio coding (AAC) mode, coupled with a technique referred to as spectral band replication (SBR) and parametric stereo (PS) techniques, both of which were proposed by 'Coding Technologies'. To expound a little further, the above-mentioned SBR technique

[3]The above-mentioned 3GPP technical specifications are publically available for download at www.3gpp.org.

allows audio codecs to operate at a given audio quality, while requiring a reduced bitrate. Similarly, the PS technique significantly increases the codec's efficiency when encoding stereophonic signals at a low rate. As a result, aacPlus is capable of delivering multi-channel audio at 128 kbps, near-CD-quality stereo audio at 32 kbps, while maintaining a high quality even at rates below 16 kbps for monophonic signals in the context of diverse mobile wireless and digital broadcast scenarios. With the addition of the PS mode of MPEG, aacPlus v2 became the most powerful low bitrate open standard audio codec.

By contrast, the codec candidates earmarked for the low-rate schemes included the above-mentioned aacPlus MPEG-4 versions and the AMR-WB+ codec. The test material used in both the low-rate and high-rate categories included voice and audio signals, as well as voice signals mixed with different audio content encountered in diverse application scenarios requiring various bitrates.

Following the extensive selection tests carried out in 2004 and involving eight different quality-testing laboratories, 3GPP selected both the AMR-WB+ codec [3GPP TS 26.290] and the Eaac+ arrangement [3GPP TS 26.401] as recommended audio codecs for the 3GPP Release 6 multimedia services. Both codecs have their particular merits in certain application scenarios. Specifically, Eaac+ exhibited good performance when encoding music signals at high rates, while at low rates the AMR-WB+ codec performed well for audio and provided a better performance for both speech and mixed content. The AMR-WB+ codec was later also selected for DVB applications as an optional codec. Therefore the AMR-WB+ codec was included in both the generic codec toolbox of the DVB standard for the delivery of audio signals using RTP packets over IP networks [355] and in the IP Datacast (IPDC) mode employed in the context of the DVB services conveyed to handheld devices using the DVB-H service [356].

This overview continues by discussing the requirements of mobile multimedia services in Section 9.7.2, including the above-mentioned PSS, MMS and MBMS services. The main features of the high-quality, low-rate 3GPP AMR-WB+ audio codec are discussed in Section 9.7.3, while in Section 9.7.4 the associated subjective listening test results are summarised.

9.7.2 Audio Requirements in Mobile Multimedia Applications

Let us now summarise the broad specifications to be met by the audio codec according to the 3GPP standardisation body, when communicating over GPRS or 3G networks.

- An attractive trade-off has to be found between the required bitrate and the audio quality maintained. For example, a typical 16-bit stereo PCM audio signal sampled at 48 kHz has to be compressed to bitrates as low as 10 to 24 kbps.

- The decoder has to be able to recover the audio signal at an unobjectionable quality even in the presence of transmission packet loss events imposed by the wireless channel.

- The decoders used by the battery-operated handsets have to exhibit a low complexity, particularly when additionally decoding video signals protected by complex FEC decoding.

Let us continue by considering the quality versus bitrate requirements of the various services considered.

9.7.2.1 Summary of Audiovisual Services

In Table 9.15 a range of diverse audio and audiovisual services, content types as well as their transport mechanism designed for supporting mobile media services are summarised in the context of the above-mentioned PSS, MBMS and MMS that may be supported by the forthcoming 3GPP systems of the near-future.

Table 9.15: Audio and audiovisual services, content types as well as their transport mechanism designed for supporting mobile media services. The term 'mixed' refers to voice mixed with other contents and N/A implies not applicable.

Service	Content	PSS	MMS	MBMS	Download
Information – news, sports, shares, traffic, weather	speech, mixed	Yes	Yes	Yes	Yes
Travel guides	speech, mixed	Yes	Yes	N/A	N/A
M-Commerce – online shopping, commercials	speech, mixed	Yes	Yes	N/A	N/A
Edutainment – training, instructional, corporate presentations	speech, mixed	Yes	Yes	Yes	Yes
TV, movies	speech, music, mixed	Yes	Yes	Yes	Yes
Person-to-person MMS	speech, mixed	N/A	Yes	N/A	N/A
Audio content distribution – audio books	speech, mixed	Yes	Yes	Yes	Yes
Audio content distribution – music	music	Yes	Yes	Yes	Yes

9.7.2.2 Bit Rates Supported by the Radio Network

Given the paucity and high price of the bandwidth available for high-quality multimedia services, the employment of efficient, yet low-complexity compression techniques is of high importance. A somewhat simplistic, but plausible statement is that if we can halve the bandwidth required for the transmission of an audio stream, we can potentially double the number of users supported. Naturally, this implies typically increasing both the complexity

and the delay of the codec. Table 9.16 offers a summary of the bitrates supported by the various GPRS and 3G bearers, where the third column indicates the total channel bitrate, while the fourth column represents the bitrate available for the audio codec without considering the additional overhead imposed by the transmission protocols, such as the Internet protocol.

Table 9.16: Available audio bitrates, or required download time, for audio and audiovisual media distribution depending on service and radio access technology.

		Audio content		Audiovisual content	
Transport & service	Radio access	Channel bandwidth or message size	Audio (net rate) or content length	Channel bandwidth or message size	Audio (net rate) or content length
PSS	GPRS	36 kbps	24 kbps	36 kbps	$\sim$ 10 kbps
	UMTS	64 kbps	48 kbps	64 kbps (128 kbps)	$\sim$14 kbps ($\sim$24 kbps)
MBMS streaming	GPRS	36 kbps	$<$24 kbps	36 kbps	$\sim$10 kbps
	UMTS	64 kbps	$<$48 kbps	64 kbps (128 kbps)	12–16 kbps ($\sim$ 24 kbps)
MMS	GPRS or UMTS	100 KB (audio)	0.5 min at 24 kbps or 1 min at 14 kbps	75 KB(video) + 25 KB(audio)	20 s at 10 kbps
MBMS download	GPRS or UMTS	300 KB (audio)	1.5 min at 24 kbps or 3 min at 14 kbps	225 KB(video) + 75 KB(audio)	60 s at 10 kbps

For the above-mentioned PSS and MBMS streaming of audio-only content over GPRS networks and using three time slots provides a maximum bitrate of approximately 24 kbps, while the 3G UMTS network is capable of offering an audio bitrate of about 48 kbps on a 64 kbps bearer. However, error correction coding has to be used for MBMS streaming and hence the effective audio bitrate is reduced to around 18 kbps when communicating over GPRS. An MMS message containing 100 KByte of audio-only content may require a period of about 0.5 minute at 24 kbps or 1 minute at 14 kbps. Correspondingly, a 300 KByte MBMS message may deliver about 1.5 minutes of audio at 24 kbps.

When transmitting audio-visual content, the bitrate required for the transmission of video further reduces the available audio bitrate. Head-and-shoulder videophone sequences require similar transmission rates to those of the audio signals, while high-dynamic sports scenes may require 75% of the available bitrate, leaving only 25% for audio. The latter assumption leads to the net audio rates seen in Table 9.16. Hence, only very low bitrates of 10 to 16 kbps

can be used for audio, which may be further reduced by the error correction coding. An audio bitrate of about 24 kbps may be achieved when using a 128 kbps bearer.

9.7.3 Overview of the AMR-WB+ Codec

The AMR-WB+ audio codec was designed to satisfy the requirements described in Section 9.7.2, by using a hybrid coding technique to deliver a consistently high quality for both speech and music signals at bitrates spanning from 6–48 kbps.

The AMR-WB+ scheme is an audio codec which contains the AMR-WB codec used in Section 9.6 as one of its possible coding modes, as well as a novel hybrid technique that combines the beneficial features of both audio and speech codecs. A detailed description of the algorithm can be found in 3GPP TS 26.290 [357]. The above-mentioned hybrid technique includes the classic ACELP coding technique optimised for handling speech signals and transform-based frequency-domain coding for efficiently representing audio and music signals. The AMR-WB+ encoder first decides upon the choice of the most appropriate coding mode, namely between CELP or transform coding on a per-frame basis. This allows the codec to provide a high reconstructed signal quality for a wide range of sounds at a low bitrate. In addition, AMR-WB+ integrates a parametric stereo model in order to enhance the end-user's perception of high-fidelity sound reproduction at remarkably low bitrates. Other key considerations behind the AMR-WB+ design are the inherent robustness to typical network impairments such as packet loss events and its ability to efficiently exploit the potentially time-variant high-speed down-link packet access (HSDPA)-style bitrate fluctuations.

The AMR-WB+ encoder is capable of compressing both mono and stereo signals. The decoder reproduces the original mono or stereo signal from the received bitstream, but it is also capable of outputting a mono signal based on the received stereo bitstream. Numerous sampling frequencies are supported by the encoder, ranging from 8–48 kHz. The sampling frequency and the associated audio bandwidth increases with the bitrate. In the mono mode, bitrates ranging from 6–36 kbps are supported, while in stereo the bitrate may span from 8–48 kbps.

The AMR-WB+ encoder operates at a nominal internal sampling frequency of 25.6 kHz. The audio input signal is first resampled at the internal sampling frequency, and then split into two equal-width bands, which are critically downsampled to 12.8 kHz. This allows the efficient integration of the original AMR-WB speech encoder which operates at a sampling frequency of 12.8 kHz.

Gradual bitrate and bandwidth scaling is realized by varying the internal sampling frequency from 0.5 to 1.5 times the nominal frequency of 25.6 kHz. Hence, the internal sampling frequency of the AMR-WB+ codec is in the range of 12.8–38.4 kHz. The corresponding audio bandwidth thus ranges from 6.4 kHz at the lowest bitrate to 19.2 kHz at the highest bitrates. Since the frame length expressed in terms of the number of samples is kept constant, varying the internal sampling frequency of the encoder changes the absolute frame duration expressed in terms of ms in an inversely proportional manner. For example, if the internal sampling frequency is doubled, then the frame duration is reduced by a factor of two.

The encoder processes the input signal in blocks of 2048 samples, independently of the internal sampling frequency. After band-splitting and critical downsampling, the lower band and the higher band are processed in blocks of 1024 samples. In the AMR-WB+

code a block of 1024 samples is referred to as a superframe. The superframe in the low band spanning from 0–6.4 kHz is encoded using the above-mentioned hybrid ACELP and transform coded excitation (TCX) model, which will be described in slightly more detail below. The superframe in the high band spanning from 6.4–12.8 kHz is encoded using 64 bits per 1024 samples, employing a bandwidth extension (BWE) method, where only the energy and spectral envelope are transmitted as mentioned earlier in this chapter.

Figure 9.32 shows high-level schematic diagrams of the AMR-WB+ encoder and decoder. When processing a mono input, the encoder and decoder schematics are restricted to the shaded area. By contrast, in the stereo mode of operation the entire schematic is activated, i.e. the dashed lines are removed. In Figure 9.32, the left, right and centre signals are labeled as L, R and M, respectively, where the centre signal is created from the left and right channels of the stereophonic signal. The low-frequency band's signals are denoted as LF and the high-frequency band's signals are represented by HF. In Figure 9.32(a), the preprocessing represents the conditioning filters and resampling operation, generating the signal required by the internal sampling frequency used. The analysis filterbank splits the input signal into the low- and high-band signals. The down-mixing operation produces a centre or mid- and a side-channel from the left and right channels of a stereo input signal. The low band of the mid (or mono) signal is encoded using the 'core' ACELP/TCX model, while the high band of the mid (or mono) signal is encoded using the above-mentioned BWE operation, which is denoted as HF encoding in Figure 9.32(a). In the specific case of stereo encoding, the 1–6.4 kHz band of the low band signal is encoded using a parametric model, which will be briefly described below. The lowest-frequency band spanning 0–1 kHz of the side signal is encoded using the 'core' ACELP/TCX model. By contrast, the high band of both the left and right channel of the stereo input signal is encoded separately using the above-mentioned BWE approach. After quantisation and encoding, the different parameters generate a bitstream, which is multiplexed for transmission. The decoder shown in Figure 9.32(b), demultiplexes the received bits, decodes them in order to obtain the quantised parameters and then performs the inverse operations of the encoder in order to recover the synthesised audio signal.

In the ACELP/TCX 'core', each 1024-sample superframe is divided in four frames of 256 samples. Each of the four frames can be encoded in one of four possible modes: (1) as a 256-sample AMR-WB frame; (2) as a 256-sample TCX frame; (3) as part of a 512-sample TCX frame in which case two consecutive frames are concatenated in a single longer frame before applying transform coding; and (4) or as part of a 1024-sample TCX frame in which case the entire superframe is encoded in a single transform coding operation. In the transform coded mode, the spectral coefficients are quantised using a technique referred to as scalable algebraic VQ [358]. Note that in the TCX mode the frame is extended with a 'look-ahead' segment, which is needed for overlapping the transform windows. The employment of the different encoding modes and frame lengths assists the codec in achieving a better encoding of different types of input signals, such as speech, sustained audio or sudden audio-type changes by facilitating a trade-off between time- and frequency-domain resolution. More details on this hybrid ACELP/TCX technique can be found, for example, in [359].

A key component of the encoder is the mode-selection schemes designed for choosing the most suitable encoding mode combination for each superframe. Mode selection can be performed in either a closed-loop or open-loop manner, depending on the complexity constraints imposed at the encoder. Closed-loop mode selection is more complex than open-

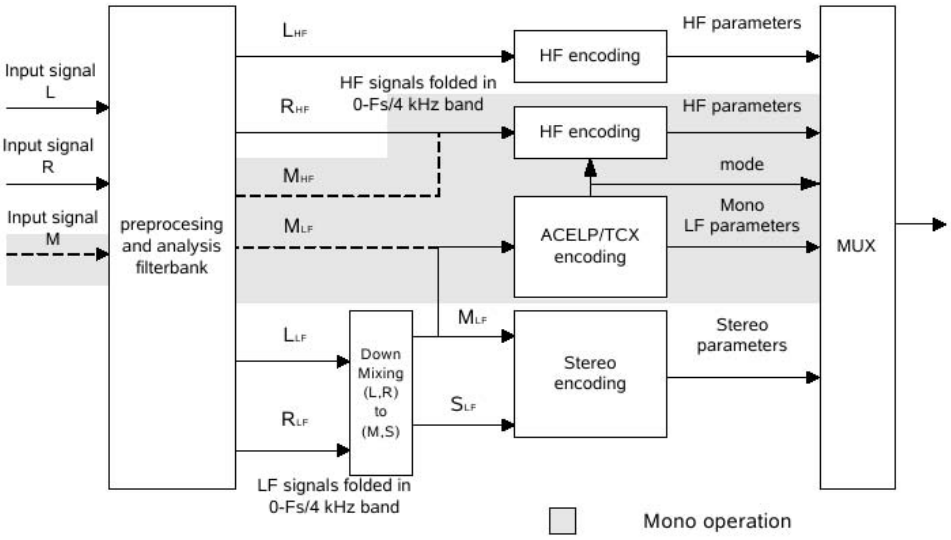

(a)

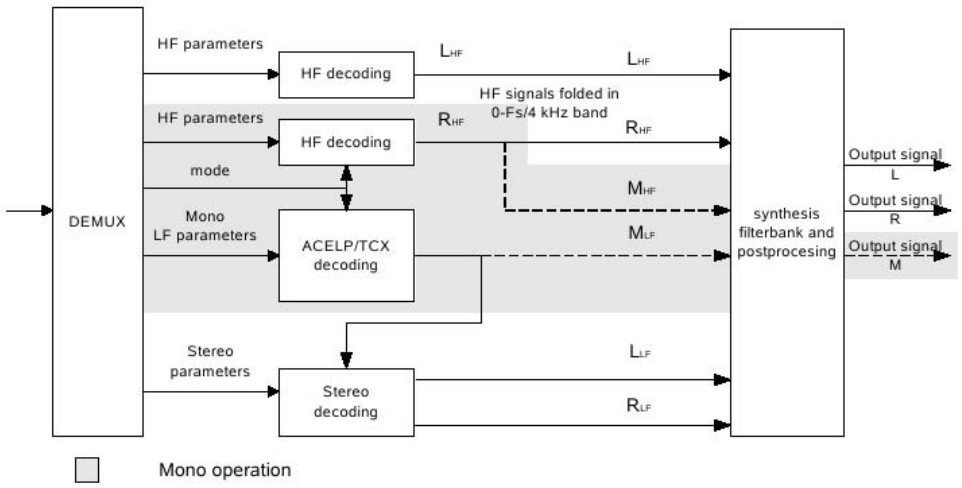

(b)

Figure 9.32: (a) Schematic of the AMR-WB+ encoder; (b) schematic of the AMR-WB+ decoder.

loop mode selection, since it involves encoding the input signal more than once before selecting the best mode. The low-complexity open-loop mode selection results in some quality degradation, especially when encoding non-speech signals.

The efficiency of the AMR-WB+ codec providing various encoding modes is illustrated by the following mode distributions measured for different content types. Typical stationary instrumental music: ACELP 1%, TCX-256 4%, TCX-512 15% and TCX-1024 80%. Pop music: ACELP 11%, TCX-256 17%, TCX-512 36% and TCX-1024 36%. Speech from several male and female talkers: ACELP 48%, TCX-256 25%, TCX-512 17% and TCX-1024 10%. This last example also shows that the TCX mode can be useful even for speech signals (stationary segments).

9.7.3.1 Encoding the High Frequencies

Recall from Figure 9.32(a) that the mono input audio signal or the down-converted stereo signal is divided in two bands. The 0–6.4 kHz band is sampled at 12.8 kHz and then encoded using the core ACELP/TCX model, as described above. By contrast, the signal above 6.4 kHz, which is denoted as M_{HF} in Figure 9.32(a) is encoded using the BWE approach. More explicitly, the BWE approach consists of extracting a parametric representation, namely the spectral envelope and gains, which are quantised and sent to the decoder. The spectral envelope is calculated only once for the entire frame, while the gains are recalculated for every new set of 64 samples. The spectral fine structure of the high-frequency signal is extrapolated at the decoder from the low-band excitation signal spanning the nominal range of 0–6400 Hz, which is generated from the encoded low-frequency signal M_{LF} of Figure 9.32(a).

9.7.3.2 Stereo Encoding

The AMR-WB+ codec employs a highly efficient parametric stereo coding technique. Since the encoder uses both time-domain and frequency-domain coding, a time-domain inter-channel prediction approach is used. Furthermore, perceptually important cues required for sound localisation are the low-frequency inter-channel time differences and the high-frequency inter-channel level differences. This suggests splitting the full-frequency band into at least a low-band and a high-band signal. The 0–1 kHz low-band signal is encoded according to a waveform coding technique. A stereo balance factor is derived first for representing the ratio between the mono and side signal levels. Subsequently, in order to maintain the perceptually important time resolution of the low-band stereo image, a critically downsampled representation of the normalised side signal is waveform encoded. The encoding operation is carried out in the frequency domain using a closed-loop variable-frame-length technique and algebraic VQ, invoking the TCX coding methods of the core ACELP/TCX algorithm.

In addition, a supplementary TCX mode using time-domain envelope shaping is employed in order to efficiently encode the perceptually important transient signals. Correspondingly, a number of frame-length candidates are chosen from the total length of a superframe, gradually reducing the frame-length to a quarter or half of the total length of the superframe. For the frequencies above 1 kHz the encoding merely aims to match a target spectral shape. Specifically, a band decomposition as in the mono scenario is used, where the frequency band spanning up to 6.4 kHz is encoded according to a shape/gain-constrained time-domain

filter approach. For the remaining high-band part of the stereo signal – which expands above 6.4 kHz – using a limited spectral resolution is sufficient. For this band it was found adequate to carry out the encoding operation according to the parametric BWE as described above and applied to each of the two stereo channels separately.

9.7.3.3 Complexity of AMR-WB+

The AMR-WB+ specifications within the 3GPP standardisation provide both floating-point and fixed-point reference C code. The latter is implemented using a set of basic operators which simulate generic DSP instructions. Each basic operator is assigned a particular weight, which reflects the number of cycles corresponding to that operator resulting in specific complexity estimates referred to as weighted million operations per second (WMOPS). The implementational complexity, when run on a DSP is measured in terms of million instructions per second (MIPS). The ratio between the estimated WMOPS and MIPS depends on the specific DSP used and on the level of software optimisation. For state-of-the-art DSPs, such as the TI C55, the number of WMOPS and MIPS is similar.

The estimated worst case decoder complexity imposed by the most complex 48 kbps stereo operation is 23.9 WMOPS, which resulted in 24 MIPS on a C55 DSP. The decoder's complexity at 24 kbps is 17 WMOPS for stereo and 11 WMOPS for mono operation [3GPP TR 26.936]. An important feature of the AMR-WB+ codec which renders its employment attractive in power-limited battery-powered devices is that its complexity can be scaled by adjusting the internal sampling frequency.

In specific applications, where only the decoder is needed in the mobile terminal, the encoder's complexity does not play a significant role. In some applications, such as terminal-generated messaging, it can be assumed that the signal will be encoded in a terminal at bitrates up to 24 kbps. For 24 kbps mono content creation the low-complexity, open-loop mode selection can be employed when the average complexity becomes about 38 WMOPS, which is similar to the complexity of the original AMR-WB codec. By comparison, in the closed-loop mode-selection aided mono mode of operation the encoder's complexity at 24 kbps is about 60 WMOPS [3GPP TR 26.936].

9.7.3.4 Transport and File Format of AMR-WB+

The RTP payload format for the AMR-WB+ codec including all the parameters required for session setup is defined in IETF RFC 4352 [360]. This format supports the encapsulation of multiple AMR-WB+ transport frames per packet and provides means for redundancy transmission as well as frame interleaving in order to improve the codec's robustness against packet loss events.

The AMR-WB+ audio encoded stream can be stored in a file using the ISO-based 3GPP file format defined in 3GPP TS 26.244, which has the media type audio/3GPP. Note that the 3GPP structure also supports the storage of many other multimedia formats, thereby allowing synchronised playback.

9.7.4 Performance of AMR-WB+

The AMR-WB+ audio codec has been extensively tested by numerous independent laboratories in order to assess its subjective performance in various application scenarios. The

relevant multimedia content types used included speech, speech over music and music. The test methodology used in most cases was the so-called MUSHRA methodology [361]. In the 2004 selection tests conducted by 3GPP, the AMR-WB+ codec was evaluated in the low-rate experiments in the bitrate range of 14–24 kbps in both mono and stereo modes of operation. The results showed that the AMR-WB+ codec exhibited the best audio quality at low rates, when considering all the different content types, compared to the competing algorithms aacPlus and Eaac+. As anticipated, the quality recorded for predominantly speech content is significantly better than that recorded for the audio codecs, but the tests also showed that the AMR-WB+ codec provides a consistently high reproduction quality for music.

Following the selection of AMR-WB+ and Eaac+ in 2004, 3GPP conducted characterisation tests using the fixed-point versions of the two codecs. These tests included a variety of content types, such as speech, music etc, at different bitrates. These extensive tests, including the results and conclusions, can be found in a 3GPP technical report [3GPP TR 26.936]. The report also contains information about the complexity and delay analysis of both codecs. As noted in the report, the codecs used in the characterisation test were different from the candidate codecs used in the earlier selection test, where the improvements included 'bug fixes', speed-optimised configurations, etc. Thus, these recent characterisation tests represent the actual performance of the 3GPP standardized audio codecs.

Figure 9.33 characterises the subjective performance of the AMR-WB+ codec and that of the Eaac+ scheme, which was reproduced from the 3GPP characterisation tests [3GPP TR 26.936]. For the results seen in Figure 9.33, the AMR-WB+ codec was used in its 'normal' mode of operation, when the closed-loop mode selection was activated. Figure 9.33(a) summarises the subjective performance of the AMR-WB+ and Eaac+ arrangements at bitrates between about 10 and 20 kbps, in its mono mode of operation. The advantage of using a hybrid encoding model in the AMR-WB+ codec become explicit from this figure. At an equivalent bitrate, the AMR-WB+ codec performed consistently better than the Eaac+ benchmarker scheme. This is particularly so for speech and mixed signals, but it is also the case for music. Figure 9.33(a) demonstrates that when considering very low rates, the subjective quality of the AMR-WB+ codec does not suffer as much from the rate reduction as a pure transform codec, such as the Eaac+ arrangement. At 9.75 kbps, the performance of the AMR-WB+ codec is close to that of the Eaac+ arrangement operated at 16 kbps.

The achievable performance recorded at low rates in stereo is shown in Figure 9.33(b). Again, at an equivalent bitrate the performance recorded for speech and mixed signals is better for the AMR-WB+ codec than for the Eaac+ scheme, while for music signals Eaac+ performs better at the higher rates.

Further results of the characterisation tests reported in the 3GPP TR 26.936 document show how the AMR-WB+ codec performs at rates up to 32 kbps. In Annex 1 of 3GPP TR 26.936, the results of an ITU-T characterisation test using the AMR-WB+ and Eaac+ codecs as reference codecs are given. The test was performed in mono, using the MUSHRA methodology, and includes both music as well as speech mixed with other audio content. In this test, the input signal was band-limited to 14 kHz. Figure 9.34 summarises the results obtained. In this test, the objective was to characterise Annex C of the ITU-T recommendation G.722.1, when encoding 32 kHz-sampled speech and audio band-limited to 14 kHz at rates between 24 and 48 kbps.

It can be clearly seen in Figure 9.34 that the AMR-WB+ codec delivers consistent quality across different content types.

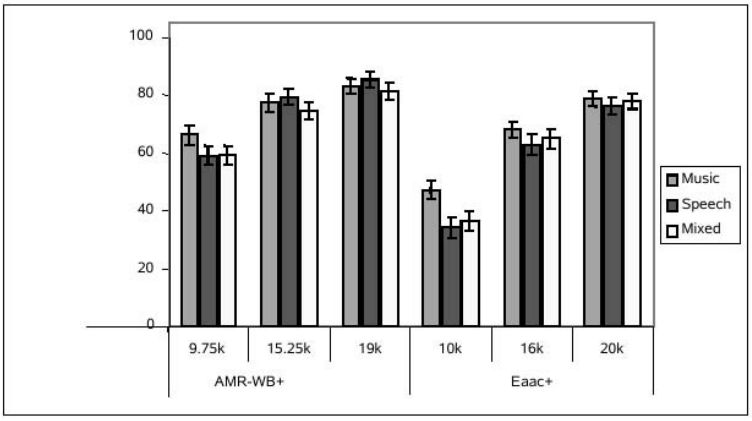

(a)

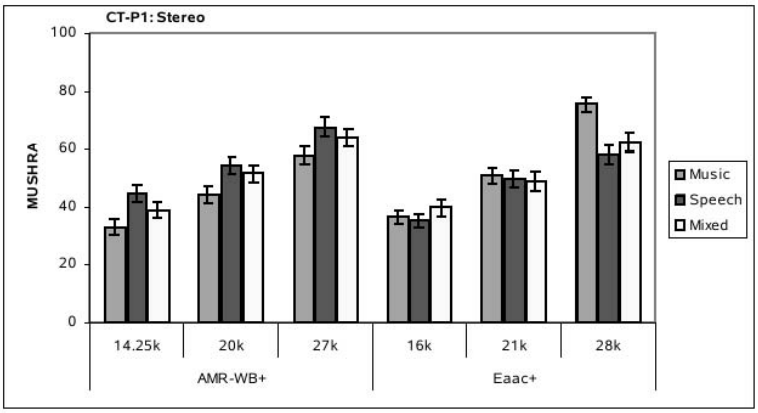

(b)

Figure 9.33: (a) Subjective evaluation at low rates in mono operation; (b) subjective evaluation at low rates in stereo operation.

9.7.5 Summary of the AMR-WB+ Codec

The rapid evolution of wireless communication systems has facilitated the employment of innovative applications and services, including the transmission of both audio and video content. Even with the increased data capacity supported by 3G wireless systems, delivering multimedia content requires a highly efficient exploitation of the available network capacity. This is particularly true for the compression of audio contents in order to additionally convey video signals and other data over wireless links. The AMR-WB+ codec has the ability to

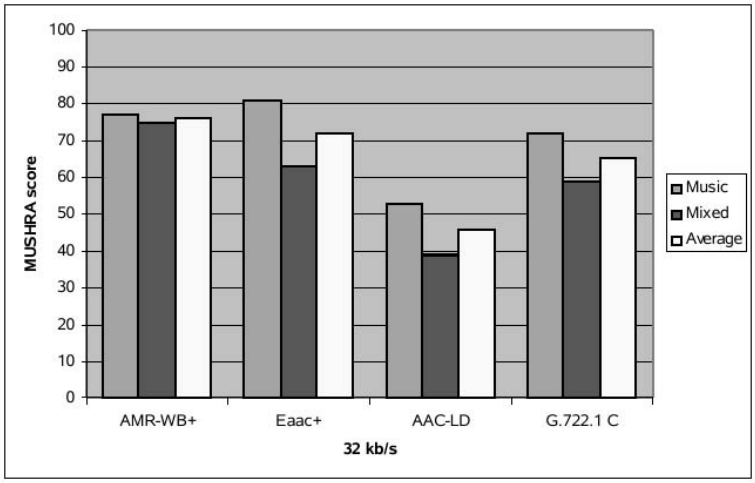

Figure 9.34: Summary of ITU-T characterisation tests in mono at 32 kbps.

consistently deliver high-quality audio across diverse content types, even at very low bitrates. In 2004, the 3GPP standardisation body has recommended the AMR-WB+ codec as one of the key enabling techniques for the transmission and storage of audio content over wireless links. The ability of the codec to near-instantaneously adjust its bitrate in the context of channel-quality dependent variable-rate HSDPA-style 3G transceivers is also an important benefit.

9.8 Chapter Summary

In this chapter a range of wideband speech codecs were described commencing in Section 9.1 with the mature G722 SB-ADPCM standard codecs, which employed QMFs in order to guarantee sufficient flexibility in allocating channel capacity to the low and high bands. The codec operated at 48, 56 and 64 kbps, which was achieved by dropping one or two of the six low-band ADPCM bits and this allowed the codec to incorporate an 8 or 16 kbps data channel. The basic codec features are summarised in Table 9.11. As an interesting alternative technique an FFT-based 32 kbps transform codec was reviewed in Section 9.2.

A similar sub-band-split philosophy was suggested by Black *et al.* [161] in Section 9.3.2, but the authors advocated a higher-complexity backward- and forward-adaptive CELP-type codec for the encoding of the lower- and higher-sub-band signals respectively, and they achieved a similar performance to the 48 kbps mode of the G722 codec at 16 kbps. In the author's view it was necessary to opt for a split-band scheme, since the full-band CELP optimisation places most of the emphasis on the representation of the higher-energy low-frequency band. The Sherbrooke team invoked their ubiquitous ACELP codecs in a variety of attractive wideband schemes both in forward- and backward-adaptive arrangements in the bitrate range of 9.6–32 kbps. Their forward-adaptive 14 kbps codec [163] has a similar performance to the G722 codec operated at 56 kbps.

As an important development in the field, the G.722.1 speech codec's basic features were also highlighted. This codec was then employed in our system design example, characterising the achievable performance of an intelligent adaptive OFDM transceiver.

In Section 9.6.2 the wideband AMR codec was investigated and in Figure 9.24 we briefly exemplified the error sensitivity of the AMR-WB codec. Then IRCCs were invoked for the sake of providing UEP for the AMR-WB speech codec, which were optimised with the aid of the novel tools of EXIT charts. More specifically, we aimed to match the EXIT transfer function of the outer IRCC to that of the inner code and we additionally imposed certain source constraints determined by the error sensitivity of the AMR-WB source bits. This design procedure may be readily extended to other joint source- and channel-coding schemes for the sake of attaining a near-capacity performance. Finally, the topic of Section 9.7 was the AMR-WB+ audio/speech codec, which has the ability to near-instantaneously adjust its bitrate in the context of channel-quality dependent variable-rate HSDPA-style 3G multimedia transceivers.

Following our discussions on wideband coding, in the next chapter of the book the MPEG4 audio codec is discussed.

Chapter 10

MPEG-4 Audio Compression and Transmission

H.-T. How and L. Hanzo

10.1 Overview of MPEG-4 Audio

The Moving Picture Experts Group (MPEG) was first established by the International Standard Organisation (ISO) in 1988 with the aim of developing a full audiovisual coding standard referred to as MPEG-1 [30–32]. The audio-related section MPEG-1 was designed to encode digital stereo sound at a total bitrate of 1.4–1.5 Mbps – depending on the sampling frequency, which was 44.1 kHz or 48 kHz – down to a few hundred kilobits per second [33]. The MPEG-1 standard is structured in layers, from Layer I to III. The higher layers achieve a higher compression ratio, albeit at an increased complexity. Layer I achieves perceptual transparency, i.e. subjective equivalence with the uncompressed original audio signal at 384 kbps, while Layers II and III achieve a similar subjective quality at 256 kbps and 192 kbps, respectively [34–38].

MPEG-1 was approved in November 1992 and its Layer I and II versions were immediately employed in practical systems. However, the MPEG Audio Layer III, MP3 for short, only became a practical reality a few years later when multimedia PCs were introduced having improved processing capabilities and the emerging Internet sparked off a proliferation of MP3 compressed teletraffic. This changed the face of the music world and its distribution of music. The MPEG-2 backward compatible audio standard was approved in 1994 [39], providing an improved technology that would allow those who had already launched MPEG-1 stereo audio services to upgrade their system to multichannel mode, optionally also supporting a higher number of channels at a higher compression ratio. Potential applications of the multichannel mode are in the field of quadraphonic music distribution or cinemas. Furthermore, lower sampling frequencies were also incorporated, which include 16, 22.05,

Voice and Audio Compression for Wireless Communications Second Edition
L. Hanzo, F. C. A. Somerville and J. P. Woodard

24, 32, 44.1 and 48 kHz [39]. Concurrently, MPEG commenced research into even higher-compression schemes, relinquishing the backward compatibility requirement, which resulted in the MPEG-2 advanced audio coding (AAC) standard in 1997 [40]. This enables those who are not constrained by legacy systems to benefit from an improved multichannel coding scheme. In conjunction with AAC, it is possible to achieve perceptual transparent stereo quality at 128 kbps and transparent multichannel quality at 320 kbps; for example in cinema-type applications.

The MPEG-4 audio recommendation is the latest standard completed in 1999 [41–45], which offers in addition to compression further unique features that will allow users to interact with the information content at a significantly higher level of sophistication than is possible today. In terms of compression, MPEG-4 supports the encoding of speech signals at bitrates from 2 kbps up to 24 kbps. For coding of general audio, ranging from very low bitrates up to high quality, a wide range of bitrates and bandwidths are supported, ranging from a bitrate of 8 kbps and a bandwidth below 4 kHz to broadcast quality audio, including monoaural representations up to multichannel configuration.

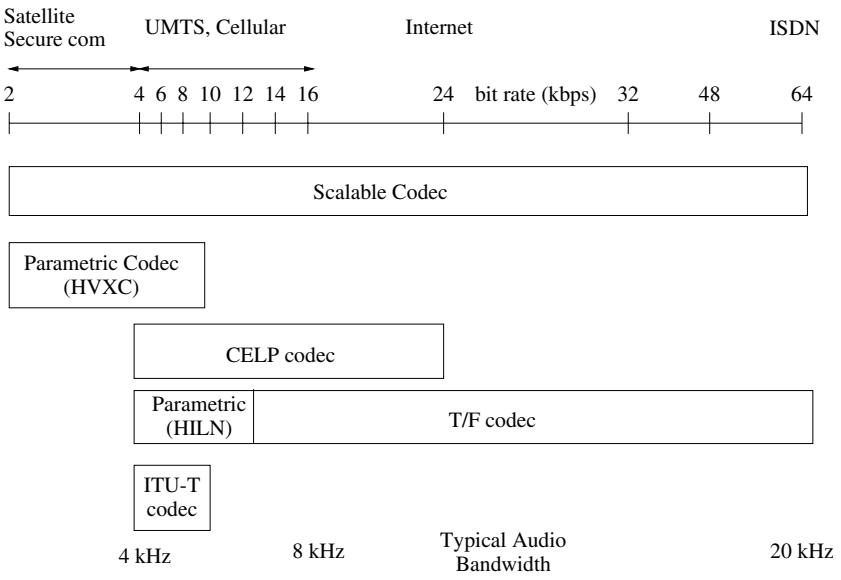

Figure 10.1: MPEG-4 framework [41].

The MPEG-4 audio codec includes coding tools from several different encoding families, covering parametric speech coding, CELP-based speech coding and Time/Frequency (T/F) audio coding, which are characterised in Figure 10.1. It can be observed that a parametric coding scheme, namely harmonic vector excitation coding (HVXC) was selected for covering the bitrate range from 2–4 kbps. For bitrates between 4 and 24 kbps, a CELP-coding scheme was chosen for encoding narrowband and wideband speech signals. For encoding general audio signals at bitrates between 8 and 64 kbps, a T/F coding scheme based on the MPEG-2 AAC standard [40] endowed with additional tools is used. Here, a combination of different techniques was established, because it was found that maintaining the required performance

for representing speech and music signals at all desired bitrates cannot be achieved by selecting a single coding architecture. A major objective of the MPEG-4 audio encoder is to reduce the bitrate, while maintaining a sufficiently high flexibility in terms of bitrate selection. The MPEG-4 codec also offers other new functionalities, which include bitrate scalability, object-based of a specific audio passage for example, played by a certain instrument representation, robustness against transmission errors and supporting special audio effects.

MPEG-4 consists of Versions 1 and 2. Version 1 [41] contains the main body of the standard, while Version 2 [46] provides further enhancement tools and functionalities that includes the issues of increasing the robustness against transmission errors and error protection, low-delay audio coding, finely grained bitrate scalability using the bit-sliced arithmetic coding (BSAC) tool, the employment of parametric audio coding, using the CELP-based silence compression tool and the 4 kbps extended variable bitrate mode of the HVXC tool. Due to the vast amount of information contained in the MPEG-4 standard, we will only consider some of its audio compression components, which include the coding of natural speech and audio signals. Readers who are specifically interested in text-to-speech synthesis or synthetic audio issues are referred to the MPEG-4 standard [41] and to the contributions by Scheirer *et al.* [47, 48] for further information. Most of the material in this chapter will be based on an amalgam of [34–38, 40, 41, 43, 44, 46, 49]. In the next few sections, the operations of each component of the MPEG-4 audio component will be highlighted in greater detail. As an application example, we will employ the transform-domain weighted interleaved vector quantisation (TWINVQ) coding tool, which is one of the MPEG-4 audio codecs in the context of a wireless audio transceiver in conjunction with space–time coding [50] and various QAM schemes [51]. The audio transceiver is introduced in Section 10.5 and its performance is discussed in Section 10.5.6.

10.2 General Audio Coding

The MPEG-4 general audio (GA) coding scheme employs the T/F coding algorithm, which is capable of encoding music signals at bitrates from 8 kbps per channel and stereo audio signals at rates from 16 kbps per stereo channel up to broadcast quality audio at 64 kbps per channel and higher. This coding scheme is based on the MPEG-2 AAC standard [40], enriched by the further addition of tools and functionalities. The MPEG-4 GA coding incorporates a range of state-of-the-art coding techniques, and in addition to supporting fixed bitrates it also accommodates a wide range of bitrates and variable rate coding arrangements. This was facilitated with the aid of the continuous development of the key audio technologies throughout the past decades. Figure 10.2 shows in a non-exhaustive fashion some of the important milestones in the history of perceptual audio coding, with emphasis on the MPEG standardisation activities. These important developments and contributions, which will be highlighted in more depth during our further discourse throughout this chapter, have also resulted in several well-known commercial audio coding standards, such as the Dolby AC-2/AC-3 [362], the Sony adaptive transform acoustic coding (ATRAC) for MiniDisc [363], the Lucent perceptual audio coder (PAC) [364] and Philips digital compact cassette (DCC) [365] algorithms. Advances in audio bitrate compression techniques can be attributed to four key technologies.

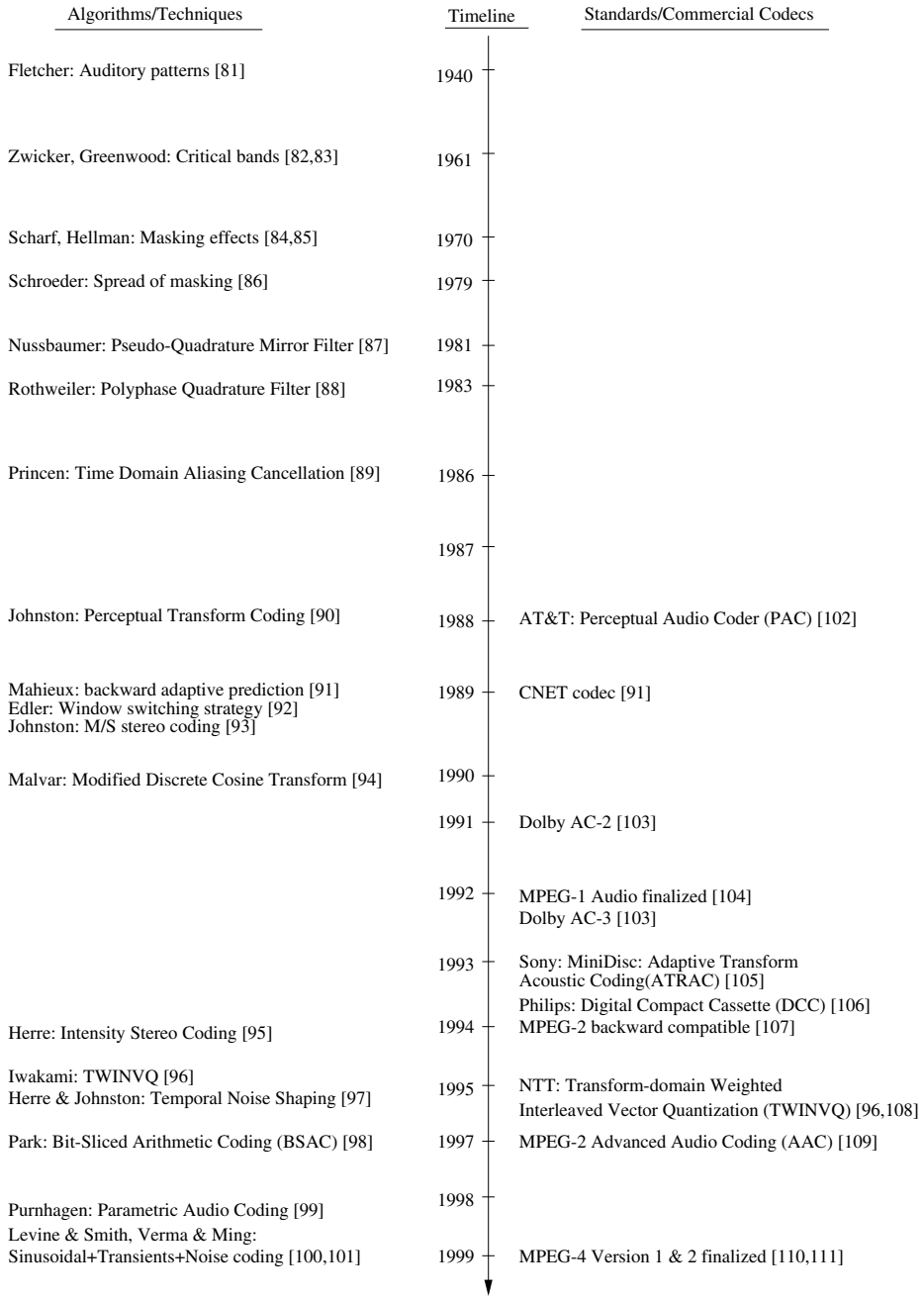

Figure 10.2: Important milestones in the development of perceptual audio coding.

(A) Perceptual Coding. Audio coders reduce the required bitrates by exploiting the characteristics of masking the effects of quantisation errors in both the frequency and time domains by the human auditory system, in order to render its effects perceptually inaudible [366–369]. The foundations of modern auditory masking theory were laid down by Fletcher's seminal paper in 1940 [370]. Fletcher suggested that the auditory system behaves like a bank of band-pass filters having continuously overlapping pass-bands. Research has shown that the ear appears to perceive sounds in a number of critical frequency bands, as shown by Zwicker [367] and Greenwood [371]. This model of the ear can be roughly described as a band-pass filterbank, consisting of overlapping band-pass filters having bandwidths of the order of 100 Hz for signal frequencies below 500 Hz. By contrast, the band-pass filter bandwidths of this model may be as high as 5000 Hz at high frequencies. There exists up to twenty five such critical bands in the frequency range up to 20 kHz [367]. Auditory masking refers to the mechanism by which a fainter but distinctly audible signal becomes inaudible when a louder signal occurs simultaneously (simultaneous masking), or within a very short time (forward or backward masking) [372]. More specifically, in the case of simultaneous masking the two sounds occur at the same time; for example in a scenario when a conversation (masked signal) is rendered inaudible by a passing train (the masker). Forward masking is encountered when the masked signal remains inaudible for a time after the masker has ended, while an example of this phenomenon in Backward masking takes place when the masked signal becomes inaudible even before the masker begins. An example is the scenario during abrupt audio signal attacks or transients, which create pre- and post-masking regions in time during which a listener will not be able to perceive signals beneath the audibility thresholds produced by a masker. Hence, specific manifestation of masking depends on the spectral composition of both the masker and masked signal and their variations as a function of time [373]. Important conclusions which can be drawn from all three masking scenarios [373, 374] are, firstly, that simultaneous masking is more effective when the frequency of the masked signal is equal to or higher than that of the masker. This result is demonstrated in Figure 10.3, where a masker rendered three masked signals inaudible, which occurred at both lower and higher frequencies than the masker. Secondly, while forward masking is effective for a considerable time after the masker has decayed, backward masking may only be effective for less than 2 or 3 ms before the onset of the masker [373].

A *masking threshold* can be determined, whereby signals below this threshold will be inaudible. Again, Figure 10.3 depicts an example of the masking threshold of a narrowband masker, having three masked signals in the neighbourhood. As long as the sound pressure levels of the three maskees are below the masking threshold, the corresponding signals will be masked. Observe that the slope of the masking threshold is steeper towards lower frequencies, which implies that higher frequencies are easier to mask. When no masker is present, a signal will be inaudible if its sound pressure level is below the *threshold in quiet*, as displayed in Figure 10.3. The *threshold in quiet* characterises the amount of energy required for a pure tone to be detectable by a listener in a noiseless environment. The situation discussed here only involved one masker, but in real life, the source signals may consist of many simultaneous maskers, each having its own masking threshold. Thus, a *global masking threshold* has to be computed, which describes the threshold of *just noticeable distortions* as a function of frequency [373].

(B) Frequency Domain Coding. The evolution of T/F mapping or filterbank-based techniques has contributed to rapid development in the area of perceptual audio coding. Some of the

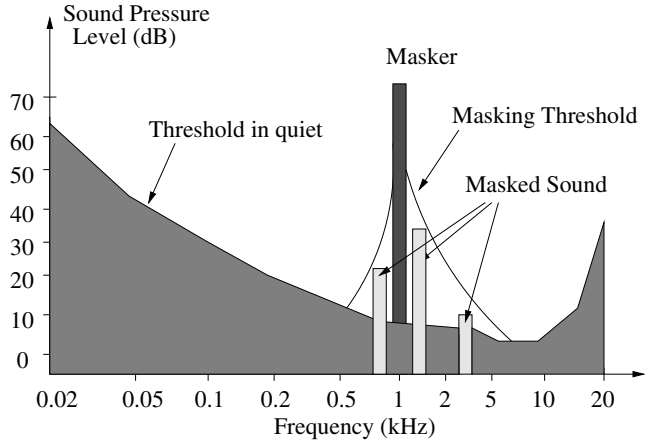

Figure 10.3: Threshold in quiet and masking threshold [375].

earliest frequency-domain audio coders include contributions from Brandenburg [376] and Johnston [377] although sub-band based narrow and wideband speech codecs were developed during the late 1970s and early 1980s [378–380]. Frequency-domain encoders [381, 382] which are employed in all MPEG codecs offer a convenient way of controlling the frequency-domain distribution of the quantisation noise, in conjunction with dynamic bit allocation applied to the quantisation of sub-band signals or transform coefficients. Essentially, the filterbank divides the spectrum of the input signal into frequency sub-bands, which host the contributions of the full-band signal in the sub-band concerned. Given the knowledge of an explicit perceptual model, the filterbank facilitates the task of perceptually motivated noise shaping and that of identifying the perceptually unimportant sub-bands. It is important to choose the appropriate filterbank for band-splitting. An adaptive filterbank exhibiting time-varying resolutions in both the time and frequency domain is highly desirable. This issue has motivated intensive research and experimentation with various switched or hybrid filterbank structures, where the switching decisions were based on the time-variant input signal characteristics [383].

Depending on the frequency-domain resolution, we can categorise frequency-domain coders as either transform coders [376, 377] or sub-band coders [384–386]. The basic principle of transform coders is the multiplication of overlapping blocks of audio samples with a smooth time-domain window function, followed by either the discrete Fourier transform (DFT) or the discrete cosine transform (DCT) [387], which transform the input time-domain signal into a high resolution frequency-domain representation, consisting of nearly uncorrelated spectral lines or transform coefficients. The transform coefficients are subsequently quantised and transmitted over the channel. At the decoder, the inverse transformation is applied. By contrast, in sub-band codecs the input signal is split into several uniform or non-uniform width sub-bands using critically sampled [385], perfect reconstruction (PR) [388] or non-PR [389] filter-banks. For example, as shown in Figure 10.4, when an input signal is split into M band-pass signals, critical decimation by a factor of M is applied. This means that every mth sample of each band-pass signal is retained, which

ensures that the total number of samples across the sub-bands equals the number of samples in the original input signal. At the synthesis stage, a summation of the M band-pass signals is performed, which leads to interpolation between samples at the output.

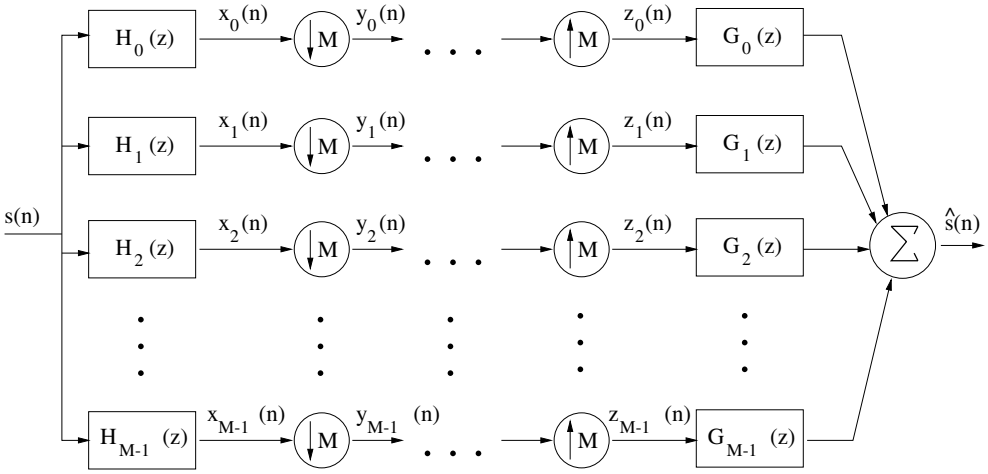

Figure 10.4: Uniform M-band analysis-synthesis filterbank [369].

The traditional categorisation into the families of sub-band and transform coders has been blurred by the emerging trend of combining both techniques in the codec design, as exemplified by the MPEG codecs which employ both techniques. In the contribution by Temerinac and Edler [390], it was shown mathematically that all transforms used today in the audio coding systems can be viewed as filter-banks. All uniform-width sub-band filter-banks can be viewed as transforms of splitting a full-band signal into n components [390]. One of the first filterbank structures proposed in the early 1980s was based on QMF [378]. Specifically, a near-PR QMF filter was proposed by Nussbaumer [391] and Rothweiler [389]. In order to derive the pseudo-QMF structure, firstly the AbS filters have to meet the mirror image condition of [389]:

$$g_k(n) = h_k(L-1-n). \tag{10.1}$$

In addition, the precise relationships between the analysis and synthesis filters h_k and g_k have to be established in order to eliminate aliasing. With reference to Figure 10.4, the analysis and synthesis filters which eliminate both aliasing and phase distortions are given by [385]

$$h_k(n) = 2w(n)\cos\left[\frac{\pi}{M}(k+0.5)\left(n-\frac{(L-1)}{2}\right)+\theta_k\right] \tag{10.2}$$

and

$$g_k(n) = 2w(n)\cos\left[\frac{\pi}{M}(k+0.5)\left(n-\frac{(L-1)}{2}\right)-\theta_k\right] \tag{10.3}$$

respectively, where

$$\theta_k = (-1)^k\frac{\pi}{4}. \tag{10.4}$$

The filterbank design is now reduced to the design of the time-domain window function, $w(n)$. The principles of pseudo-QMFs have been applied in both the MPEG-1 and MPEG-2 schemes, which employ a 32-channel pseudo-QMF for implementing spectral decomposition in both the Layer I and II schemes. The same pseudo-QMF filter was used in conjunction with a PR cosine-modulated filterbank in Layer III in order to form a hybrid filterbank [35]. This hybrid combination could provide a high-frequency resolution by employing a cascade of a filterbank and an modified discrete cosine transform (MDCT) transform that splits each sub-band further in the frequency domain [37].

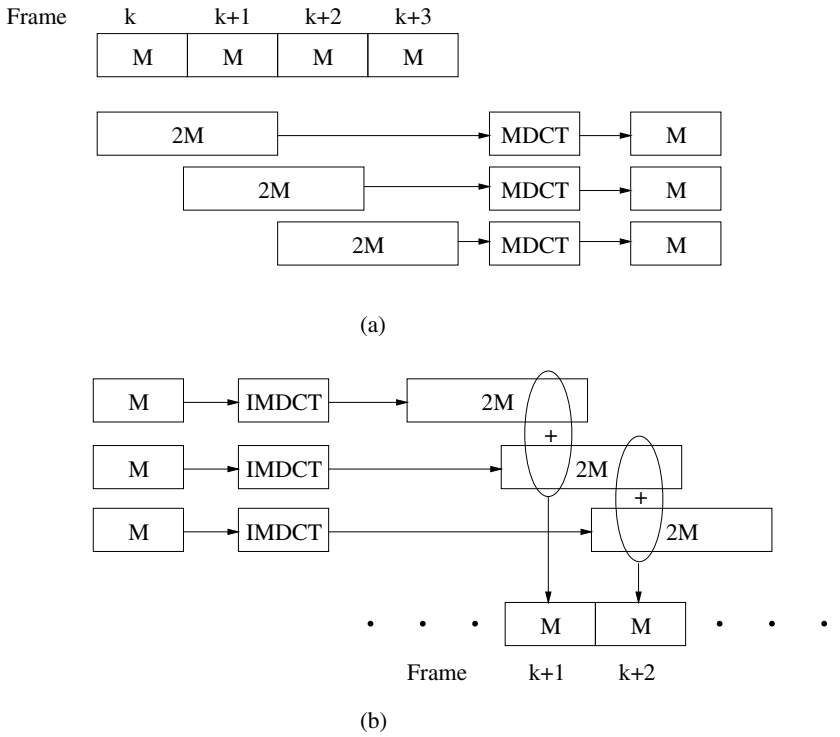

Figure 10.5: (a) MDCT analysis process: $2M$ samples are mapped into M spectral coefficients; (b) MDCT synthesis process: M spectral coefficients are mapped to a vector of $2M$ samples which is overlapped by M samples with the vector of $2M$ samples from the previous frame, and then added together to obtain the reconstructed output of M samples [369].

The MDCT [387], which has been defined in the current MPEG-2 and 4 codecs, was first proposed under the name of time domain aliasing cancellation (TDAC) by Princen and Bradley [392] in 1986. It is essentially a PR cosine modulated filterbank satisfying the constraint of $L = 2M$, where L is the window size and M is the transform length. In conventional block-based transformations, such as the DFT or DCT, blocks of input samples are processed independently. Hence the resultant decoded signal will exhibit discontinuities at the block boundaries, since in the context of conventional block-based transforms the time-domain signal is effectively multiplied by a rectangular time-domain window. Therefore, its sinc-shaped frequency domain representation is convolved with the spectrum of the audio signal.

This results in the well-known Gibbs phenomenon. This problem is mitigated by applying the MDCT, using a specific window function in combination with overlapping the consecutive time-domain blocks. As shown in Figure 10.5, a window of $2M$ samples collected from two consecutive time-domain blocks undergoes cosine transformation, which produces M frequency-domain transform coefficients. The time-domain window is then shifted by M samples for computing the next M transform coefficients. Hence, there will be a 50% overlap in each consecutive DCT transform coefficient computation. This overlap will ensure a more smooth evolution of the reconstructed time-domain samples, even though there will be some residual blocking artifacts due to the quantisation of the transform coefficients. Nonetheless, the MDCT virtually eliminates the problem of blocking artifacts that plague the reconstructed signal produced by non-overlapped transform coders. This problem often manifested itself as a periodic clicking in the reconstructed audio signals. Again, the processes associated with the MDCT-based overlapped analysis and the corresponding overlap-add synthesis are illustrated in Figure 10.5. At the analysis stage, the forward MDCT is defined as [393]

$$X(k) = \sum_{n=0}^{2M-1} x(n)h_k(n), \quad k = 0, \ldots, M-1, \tag{10.5}$$

where the M MDCT coefficients $X(k),\ k = 0, \ldots, M-1$, are generated by computing a series of inner products between the $2M$ samples $x(n)$ of the input signal and the corresponding analysis filter impulse response $h_k(n)$. The analysis filter impulse response, $h_k(n)$, is given by [393]

$$h_k(n) = w(n)\sqrt{\frac{2}{M}}\cos\left[\frac{(2n+M+1)(2k+1)\pi}{4M}\right], \tag{10.6}$$

where $w(n)$ is a window function, and the specific window function used in the MPEG standard is the sine window function given by [393]

$$w(n) = \sin\left[\left(n+\frac{1}{2}\right)\frac{\pi}{2M}\right]. \tag{10.7}$$

At the synthesis stage, the inverse MDCT is defined by [393]

$$x(n) = \sum_{k=0}^{M-1}[X(k)h_k(n) + X^P(k)h_k(n+M)]. \tag{10.8}$$

In Equation (10.8) we observe that the time-domain reconstructed sample $x(n)$ is obtained by computing a sum of the basis vectors $h_k(n)$ and $h_k(n+M)$ weighted by the transform coefficients $X(k)$ and $X^P(k)$ on the basis of the current and previous blocks as was also illustrated in Figure 10.5. More specifically, the first M-sample block of the kth basis vector, $h_k(n)$, for $0 \leq n \leq M-1$, is weighted by the kth MDCT coefficients of the current block. By contrast, the second M-sample block of the kth basis vector, $h_k(n)$, for $M \leq n \leq 2M-1$ is weighted by the kth MDCT coefficients of the previous block, namely by $X^P(k)$. The inverse MDCT operation is also illustrated in Figure 10.5.

(C) Window Switching. The window switching strategy was first proposed in 1989 by Edler [394], where a bitrate reduction method was proposed for audio signals based on overlapping transforms. More specifically, Edler proposed adapting the window functions and the transform lengths to the nature of the input signal. This improved the performance of the transform codec in the presence of impulses and rapid energy on-set occurrences in the input signal. The notion of applying different windows according to the input signal's properties has been subsequently incorporated in the MPEG codecs employing the MDCT; for example MPEG-1 Layer III and MPEG-2 AAC codecs [40].

Typically, a long time-domain window is employed for encoding the identifiable stationary signal segments while primarily a short window is used for localizing the pre-echo effects due to the occurrence of sudden signal on-sets, as experienced during transient signal periods, for example [40]. In order to ensure that the conditions of PR-based analysis and synthesis filtering are properly preserved, transitional windows are needed for switching between the long and short windows [393]. These transitional windows are depicted graphically in Figure 10.6, utilizing four window functions; namely long, short, start and stop windows, which are also used in the MPEG-4 GA coding standard.

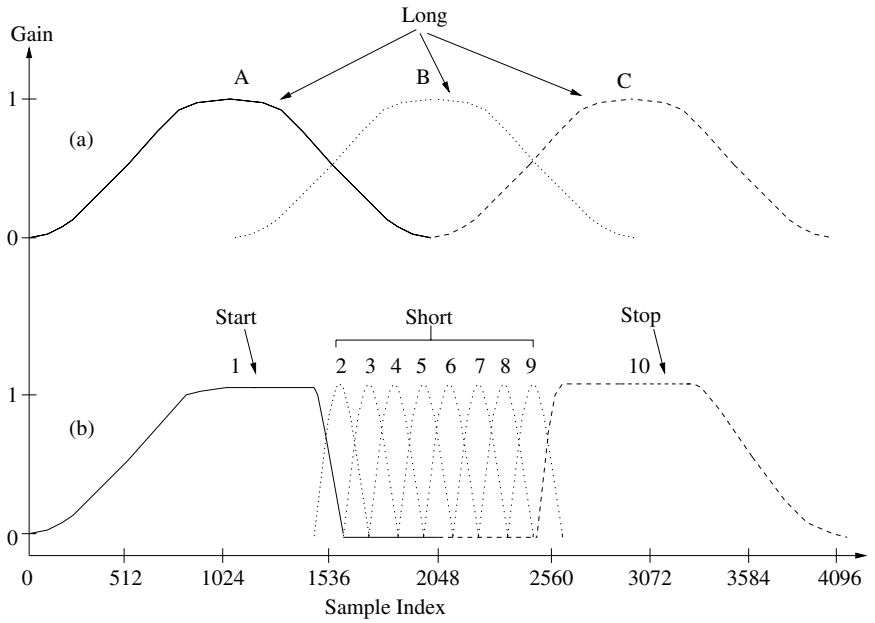

Figure 10.6: Window transition during (a) steady state using long windows and (b) transient conditions employing start, short, and stop windows [40].

(D) Dynamic Bit Allocation. Dynamic bit allocation aims to assign bits to each of the quantisers of the transform coefficients or sub-band samples in such a way that the overall perceptual quality is maximised [395]. This is an iterative process, where in each iteration the number of quantising levels is increased, while satisfying the constraint that the number of bits used must not exceed the number of bits available for that frame.

Furthermore, another novel bit-allocation technique referred to as the 'bit reservoir' scheme was proposed to accommodate the sharp signal on-sets which resulted in an increased number of required bits during the encoding of transient signals [395]. This is due to the fact that utilising the window switching strategy does not succeed in avoiding all audible pre-echos, in particular when sudden signal on-set occurs near the end of a transform block [369]. In block-based schemes like conventional transform codecs, the inverse transform spreads the quantisation errors evenly in time over the duration of the reconstruction block. This results in audible unmasked distortion throughout the low-energy signal segment at the instant of the signal attack [369]. Hence, the 'bit reservoir' technique was introduced for allocating more bits to those frames, which invoked pre-echo control. This 'bit reservoir' technique was employed in the MPEG Layer III and MPEG-2 AAC codecs [40].

10.2.1 Advanced Audio Coding

The MPEG-2 AAC scheme was declared an international standard by MPEG at the end of April 1997 [40]. The main driving factor behind the MPEG-2 AAC initiative was the quest for an efficient coding method for multichannel surround sound signals such as the five-channel (left, right, centre, left-surround and right-surround) system designed for cinemas. The main block diagram of the MPEG-4 T/F codec is as shown in Figure 10.7, which was defined to be backward compatible to the MPEG-2 AAC scheme [40].

In this section we commence with an overview of the AAC profiles based on Figure 10.7 and each block will be discussed in more depth in Sections 10.2.2–10.2.10. Following Figure 10.7, the T/F coder first decomposes the input signal into a T/F representation by means of an analysis filterbank prior to subsequent quantisation and coding. The filterbank is based on the MDCT [392] which is also known as the modulated lapped transform (MLT) [396]. In the case when the scalable sampling rate (SSR) mode is invoked, the MDCT will be preceded by a polyphase quadrature filter (PQF) [389] and a gain control module, which are not explicitly shown in Figure 10.7 but will be described in Section 10.2.2. In the encoding process, the filterbank takes in a block of samples, applies the appropriate windowing function and performs the MDCT within the filterbank block. The MDCT block length can be either 2048 or 256 samples, switched dynamically depending on the input signal's characteristics. This window switching mechanism was first introduced by Edler in [394]. Long block-transform processing (2048 samples) will improve the coding efficiency of stationary signals, but problems might occur when coding transients signals. Specifically, this gives rise to the problem of pre-echos which occur when a signal exhibiting a sudden sharp signal envelope rise begins near the end of a transform block [369]. In block-based schemes such as transform codecs, the inverse transform will spread the quantisation error evenly in time over the reconstructed block. This may result in audible unmasked quantisation distortion throughout the low-energy section preceding the instant of the signal attack [369]. By contrast, a shorter block length processing (256 samples) will be optimum for coding transient signals, although it suffers from inefficient coding of steady-state signals due to the associated poorer frequency resolution.

Figure 10.6 shows the philosophy of the block switching mechanisms during both steady state and transient conditions. Specifically, two different window functions, the Kaiser–Bessel-derived (KBD) window [362] and the sine window can be used for windowing the incoming input signal for the sake of attaining an improved frequency selectivity and for

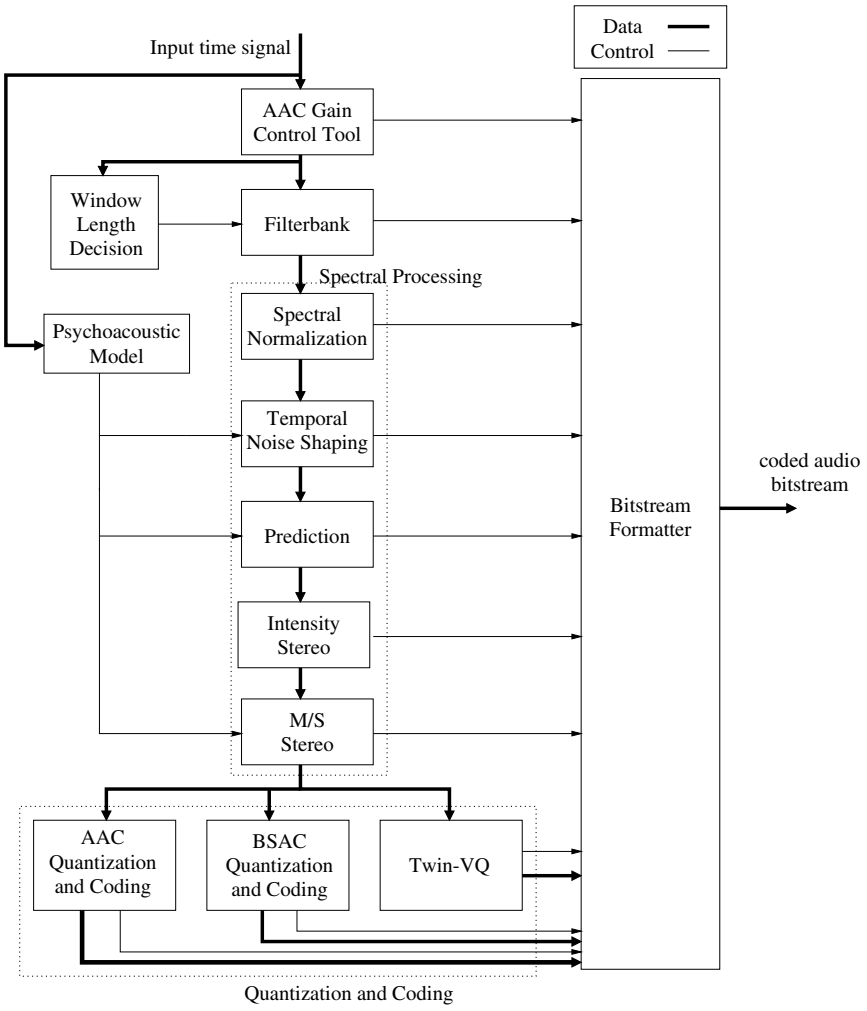

Figure 10.7: Block diagram of MPEG-4 T/F-based encoder [41].

mitigating the Gibb oscillation before the signal is transformed by the MDCT [362]. The potential problem of appropriate block alignment due to window switching is solved as follows. Two extra window shapes, the so-called start and stop windows, are introduced together with the long and short windows depicted in Figure 10.6. The long window consists of 2048 samples while a short window is composed of eight short blocks arranged to overlap by 50% with each other. At the boundaries between long and short blocks, half of the transform blocks overlap with the start and stop windows. Specifically, the *start* window enables the transition between the long and short window types. The left half of a *start* window seen at the bottom of Figure 10.6 has the same form as the left half of the long window depicted at the top of Figure 10.6. The right half of the *start* window

has the value of unity for one-third of the length and the shape of the right half of a short window for the central one-third duration of its total length, with the remaining one-third of the *start* window duration length set to zero. Figure 10.6(a) shows the steady-state condition where only long transform blocks are employed. By contrast, Figure 10.6(b) displays the block switching mechanism where we can observe that the start (#1) and stop (#10) window sequences ensure a smooth transition between long and short transforms. The start window can be either the KBD or the sine-window in order to match the previous long window type, while the stop window is the time-reversed version of the start window.

Like all other perceptually motivated coding schemes, the MPEG-4 AAC-based codec makes use of the signal masking properties of the human ear in order to reduce the required bitrate. By doing so, the quantisation noise is distributed to frequency bands in such a way that it is masked by the total signal and hence it remains inaudible. The input audio signal simultaneously passes through a psycho-acoustic model as shown in Figure 10.7 that determines the ratio of the signal energy to the masking threshold. An estimate of the masking threshold is computed using the rules of psycho-acoustics [34]. Here, a perceptual model similar to the MPEG-1 psycho-acoustic model II [40] is used (which will be described in Section 10.2.3). A signal-to-mask ratio is computed from the masking threshold which is used to decide on the bit allocation in an effort to minimise the audibility of the quantisation noise.

After the MDCT is carried out in the filterbank block of Figure 10.7, the spectral coefficients are passed to the spectral normalisation 'toolbox', if the TWINVQ mode is used. The spectral normalisation tool will be described in Section 10.2.9. For AAC-based coding, the spectral coefficients will be processed further by the temporal noise shaping (TNS) 'toolbox' of Figure 10.7, where TNS uses a prediction approach in the frequency domain for shaping and distributing the quantisation noise over time.

The time domain 'Prediction' block of Figure 10.7 or long-term prediction (LTP) is an important tool, which increases redundancy reduction of stationary signals. It utilises a second-order backward-adaptive predictor which is similar to the scheme proposed by Mahieux *et al.* [397]. In the case of multichannel input signals, 'intensity stereo' coding is also applied as seen in Figure 10.7, which is a method of replacing the left and right stereo signals by a single signal having embedded directional information. Mid/side (M/S) stereo coding, as described by Johnston and Ferreira [398], can also be used as seen in Figure 10.7, where instead of transmitting the left and right signals, the sum and difference signals are transmitted.

The data-compression based bitrate reduction occurs in the quantisation and coding stage, where the spectral values can be coded either using the AAC, (BSAC) [399] or TWINVQ [400] techniques as seen in Figure 10.7. The AAC quantisation scheme will be highlighted in Sections 10.2.6 while the BSAC and TWINVQ-based techniques will be detailed in Section 10.2.8 and 10.2.9, respectively. The AAC technique invokes an adaptive nonlinear quantiser and a further noise shaping mechanism employing scale factors is implemented. The allocation of bits to the spectral values is carried out according to the psycho-acoustic model, with the aim of suppressing the quantisation noise below the masking threshold. Finally, the quantised and coded spectral coefficients and control parameters are packed into a bitstream format ready for transmission. In the following sections, the individual components of Figure 10.7 will be discussed in further details.

10.2.2 Gain Control Tool

When the SSR mode is activated, which facilitates the employment of different sampling rates, the MDCT transformation taking place in the Filterbank block of Figure 10.7 is preceded by uniformly-spaced 4-band PQF [391], plus a gain control module [41]. The PQF splits the input signal into four frequency bands of equal width. When the SSR mode is invoked, lower bandwidth output signals and hence lower sampling rate signals can be obtained by neglecting the signals residing in the lower-energy upper bands of the PQF. In the scenario, when the bandwidth of the input signal is 24 kHz, equivalent to a 48 kHz sampling rate, output bandwidths of 18, 12 and 6 kHz can be obtained when one, two or three PQF outputs are ignored, respectively [40].

The purpose of the gain control module is to appropriately attenuate or amplify the output of each PQF band in order to reduce the potential Pre-echo effects [369]. The gain control module, which estimates and adjusts the gain factor of the sub-bands, according to the psycho-acoustic requirements, can be applied independently to each sub-band. At the encoder, the gain control 'toolbox' receives the time domain signals as its input and outputs the gain control data and the appropriately scaled signal whose length is equal to the length of the MDCT window. The 'gain control data' consists of the number of bands which experienced gain modification, the number of modified segments and the indices indicating the location and level of gain modification for each segment. Meanwhile, the 'gain modifier' associated with each PQF band controls the gain of each band. This effectively smoothes the transient peaks in the time domain prior to MDCT spectral analysis. Subsequently, the normal procedure of coding stationary signals using long blocks can be applied.

10.2.3 Psycho-acoustic Model

As argued in Section 10.2, the MPEG-4 audio codec and other perceptually optimised codecs reduce the required bitrate by taking advantage of the human auditory system's inability to perceive the quantisation noise satisfying the conditions of auditory masking. Again, perceptual masking occurs when the presence of a strong signal renders the weaker signals surrounding it in the frequency-domain imperceptible [373]. The psycho-acoustic model used in the MPEG-4 audio codec is similar to the MPEG-1 psycho-acoustic model II [34].

Figure 10.8 shows the flow chart of the psycho-acoustic model II. First a Hann window [41] is applied to the input signal and then the FFT provides the necessary time-frequency mapping. The Hann window is defined as [41]

$$w(n) = \frac{1}{2}\left[1 - \cos\left(\frac{2\pi n}{N}\right)\right], \tag{10.9}$$

where N is the FFT length. This windowing procedure is applied for the sake of reducing the frequency-domain Gibbs oscillation potentially imposed by a rectangular transform window. Depending on whether the signal's characteristics are of stationary or transient nature, FFT sizes of either 1024 or 128 samples can be applied. The FFT-based spectral coefficient values are then grouped according to the corresponding critical frequency band widths. This is achieved by transforming the spectral coefficient values into the 'partition index' domain, where the partition indices are related near-linearly to the critical bands that were summarised in Figure 10.9(a) recorded at the sampling rate of 44.1 kHz. At low frequencies, a single

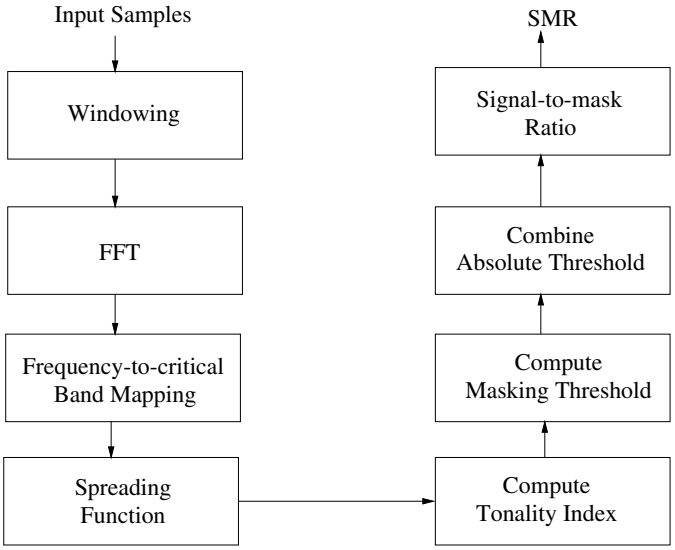

Figure 10.8: Flow diagram of the psycho-acoustic model II in MPEG-4 AAC coding.

spectral line constitutes a partition, while at high frequencies many lines will be combined in order to form a partition, as displayed in Figure 10.9(b). This facilitates the appropriate representation of the critical bands of the human auditory system [36]. Tables of the mapping functions between the spectral and partition domains and their respective values 'for the threshold in quiet' are supplied in the MPEG-4 standard for all available sampling rates [41].

During the FFT process of Figure 10.8, the polar representation of the transform-domain coefficients is also calculated. Both the magnitude and phase of this polar representation will be used for the calculation of the 'predictability measure', which is used for quantifying the predictability of the signal, as an indicator of the grade of tonality. The psycho-acoustic model identifies the tonal and noise-like components of the audio signal, because the masking abilities of the two types of signals differ. In this psycho-acoustic model, the masking ability of a tone masking the noise, which is denoted by $\mathrm{TMN}(b)$, is fixed at 18 dB in all the partitions, which implies that any noise within the critical band more than 18 dB below $\mathrm{TMN}(b)$ will be masked by the tonal component. The masking ability of noise masking tone, which is denoted by $\mathrm{NMT}(b)$, is set to 6 dB for all partitions. The previous two frequency-domain blocks are used for predicting the magnitude and phase of each spectral line for the current frequency-domain block via linear interpolation in order to obtain the 'predictability' values for the current block. Tonal components are more predictable and hence will have higher tonality indices. Furthermore, a spreading function [41] is applied in order to take into consideration the masking ability of a given spectral component, which could spread across its surrounding critical band.

The masking threshold is calculated in Figure 10.8 by using the tonality index and the threshold in quiet, T_q, which is known as the lower threshold bound above which a sound is audible. The masking threshold in each frequency-domain partition corresponds to the power

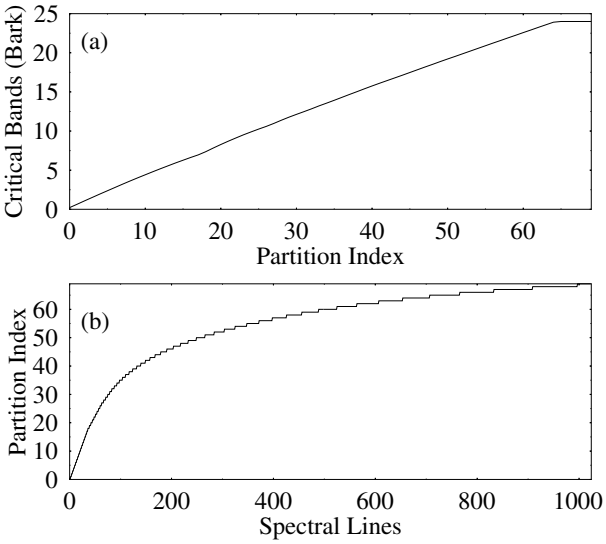

Figure 10.9: (a) The relationship between the partition index and critical bands. (b) The conversion from the FFT spectral lines to the partition index domain at the sampling rate of 44.1 kHz for a total of 1024 spectral lines per time-domain audio frame [34].

spectrum multiplied by an attenuation factor given by [41]

$$\textit{Attenuation\_Factor} = 10^{-\,\mathrm{SNR}(b)}, \tag{10.10}$$

implying that the higher the SNR, the lower the attenuation factor and also the masking threshold, where the SNR ratio is derived as

$$\mathrm{SNR}(b) = tb(b) \cdot \mathrm{TMN}(b) + (1 - tb(b)) \cdot \mathrm{NMT}(b), \tag{10.11}$$

where the masking ability of tone-masking-noise and noise-masking-tone is considered by exploiting the tonality index in each partition.

The masking threshold is transformed back to the linear frequency scale by spreading it evenly over all spectral lines corresponding to the partitions, as seen in Figure 10.10 in preparation for the calculation of the signal-to-mask ratios (SMR) for each sub-band. The minimum masking threshold, as shown in Figure 10.10, takes into account the value of the threshold in quiet, T_q, raising the masking threshold value to the value of T_q, if the masking threshold value is lower than T_q. Finally, the SMR is computed for each scalefactor band as the ratio of the signal energy within a frequency-domain scalefactor band to the minimum masking threshold for that particular band, as depicted graphically in Figure 10.10. The SMR values will then be used for the subsequent allocation of bits in each frequency band.

10.2.4 Temporal Noise Shaping

TNS in audio coding was first introduced by Herre and Johnston in [401]. The TNS tool seen in Figure 10.7 is a frequency-domain technique which operates on the spectral coefficients

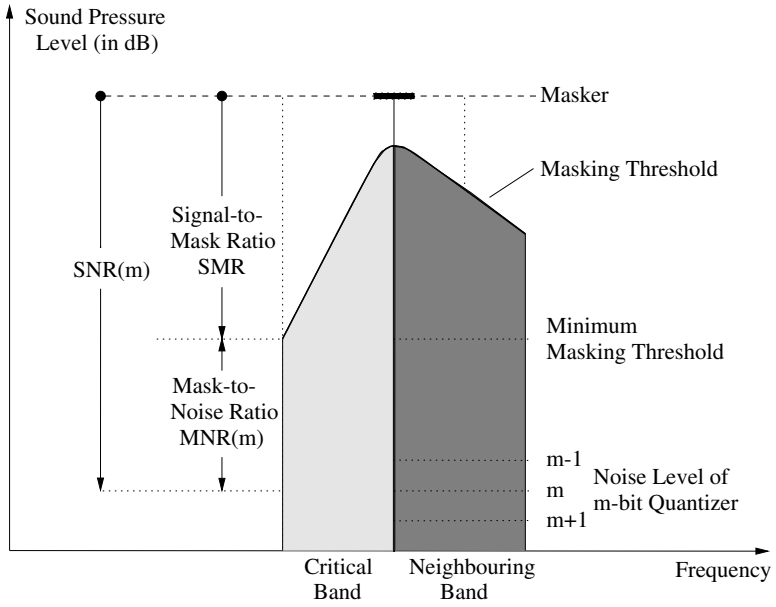

Figure 10.10: Masking effects and masking threshold calculation.

generated by the analysis filterbank. The idea is to employ linear predictive coding across the frequency range, rather than in the time domain. TNS is particularly important when coding signals that vary dynamically over time such as, for example, transient signals. Transform codecs often encounter problems when coding such signals since the distribution of the quantisation noise can be controlled over the frequency range but this spectral noise shaping is typically time invariant over a complete transform block. When a signal changes drastically within a time-domain transform block without activating a switch to shorter time-domain transform lengths, the associated time-invariant distribution of quantisation noise may lead to audible audio artifacts.

The concept of TNS is based upon the time- and frequency-domain duality of the LPC analysis paradigm [383], since it is widely recognized that signals exhibiting a non-uniform spectrum can be efficiently coded either by directly encoding the spectral-domain transform coefficients using transform coding, or by applying LPC methods to the time-domain input signal. The corresponding 'duality statement' relates to the encoding of audio signals exhibiting a time-variant time-domain behaviour, such as in the case of transient signals. Thus, efficient encoding of transient signals can be achieved by either directly encoding their time-domain representation or by employing predictive audio coding methods across the frequency domain.

Figure 10.11 shows the more detailed TNS filtering process seen in the centre of Figure 10.7. The TNS tool is applied to the spectral-domain transform coefficients after the filterbank stage of Figure 10.7. The TNS filtering operation replaces the spectral-domain coefficients with the prediction residual between the actual and predicted coefficient values, thereby increasing their representation accuracy. Similarly, at the decoder an inverse TNS

filtering operation is performed on the transform coefficient prediction residual in order to obtain the decoded spectral coefficients. TNS can be applied to either the entire frequency spectrum, or only to a part of the spectrum, such that the frequency-domain quantisation can be controlled in a time-variant fashion [40], again, with the objective of achieving agile and responsive adjustment of the frequency-domain quantisation scheme for sudden time-domain transients. In combination with further techniques such as window switching and gain control, the pre-echo problem can be further mitigated. In addition, the TNS technique enables the peak bitrate demand of encoding transient signals to be reduced. Effectively, this implies that an encoder may stay longer in the conventional and more bitrate efficient long encoding block.

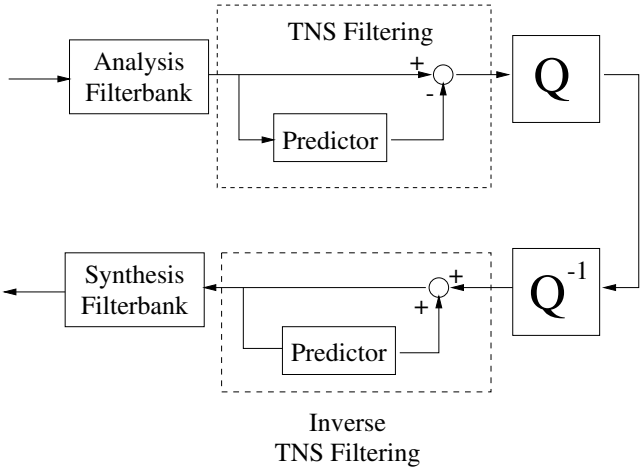

Figure 10.11: The TNS processing block also seen in Figure 10.7.

In addition, the long-term time-domain redundancy of the input signal may be exploited using the well-documented LTP technique, which is frequently used in speech coding [41, 335, 402].

10.2.5 Stereophonic Coding

The MPEG-4 scheme includes two specific techniques for encoding stereo coding of signals, namely intensity-based stereo coding [403] and M/S stereo coding [404], both of which will be described in this section. These coding strategies can be combined by selectively applying them to different frequency regions.

Intensity-based stereophonic coding is based on the analysis of high-frequency audio perception, as outlined by Herre *et al.* in [403]. Specifically, high-frequency audio perception is mainly based on the energy–time envelope of this region of the audio spectrum. It allows a stereophonic channel pair to share a single set of spectral intensity values for the high-frequency components with little or no loss in sound quality. Effectively, the intensity signal spectral components are used to replace the corresponding left channel spectral coefficients, while the corresponding spectral coefficients of the right channel are set to zero. Intensity-based stereophonic coding can also be interpreted as a simplified approximation to the idea of

directional coding. Thus, only the information of one of the two stereo channels is retained, while the directional information is obtained with the aid of two scalefactor values assigned to the left and right channels [405].

On the other hand, M/S stereo coding allows the pair of stereo channels to be conveyed as left/right (L/R) or as the M/S signals representing the M/S information on a block-by-block basis [404], where $M = (L + R)/2$ and $S = (L - R)/2$. Here, the M/S matrix takes the sum information $M + S$, and sends it to the left channel, and the difference information $M - S$, and sends it to the right channel. When the left and right signals are combined, $(M + S) + (M - S) = 2M$, the sum is M information only. The number of bits actually required to encode the M/S information and L/R information is then calculated. In cases where the M/S channel pair can be represented with the aid of fewer bits, while maintaining a certain maximum level of quantisation distortion, the corresponding spectral coefficients are encoded, and a flag bit is set for signalling that the block has utilised M/S stereo coding. During decoding the decoded M/S channel pair is converted back to its original left/right format.

10.2.6 AAC Quantisation and Coding

After all the pre-processing stages of Figure 10.7 using various coding tools, as explained in earlier sections, all parameters to be transmitted will now have to be quantised. The quantisation procedure follows an AbS process, consisting of two nested iteration loops which are depicted in Figure 10.12. This involves the non-uniform quantisation of the spectral-domain transform coefficients [40]. Transform-domain nonlinear quantisers have the inherent advantage of facilitating spectral-domain noise shaping in comparison to conventional linear quantisers [381]. The quantised spectral-domain transform coefficients are then coded using Huffman coding. In order to improve the achievable subjective audio quality, the quantisation noise is further shaped using scale factors [406], as is highlighted below.

Specifically, the spectrum is divided into several groups of spectral-domain transform coefficients, which are referred to as scale-factor bands (SFB). Each frequency-domain scale-factor band will have its individual scale-factor, which is used to scale the amplitude of all spectral-domain transform coefficients in that scale-factor band. This process shapes the spectrum of the quantisation noise according to the masking threshold portrayed in Figure 10.10, as estimated on the basis of the psycho-acoustic model. The width of the frequency-domain scale-factor bands is adjusted according to the critical bands of the human auditory system [372], seen in Figure 10.9. The number of frequency-domain scale-factor bands and their width depend on the transform length and sampling frequency. The spectral-domain noise shaping is achieved by adjusting the scale-factor using a step size of 1.5 dB. The decision as to which scale-factor bands should be amplified/attenuated relies on the threshold computed from the psycho-acoustic model and also on the number of bits available. The spectral coefficients amplified have high amplitudes and this results in a higher SNR after quantisation in the corresponding scale-factor bands. This also implies that more bits are needed for encoding the transform coefficients of the amplified scale-factor bands and hence the distribution of bits across the scale-factor bands will be altered. Naturally, the scale-factor information will be needed at the decoder, hence the scale factors will have to be encoded as efficiently as possible. This is achieved by first exploiting the fact that the scale factors

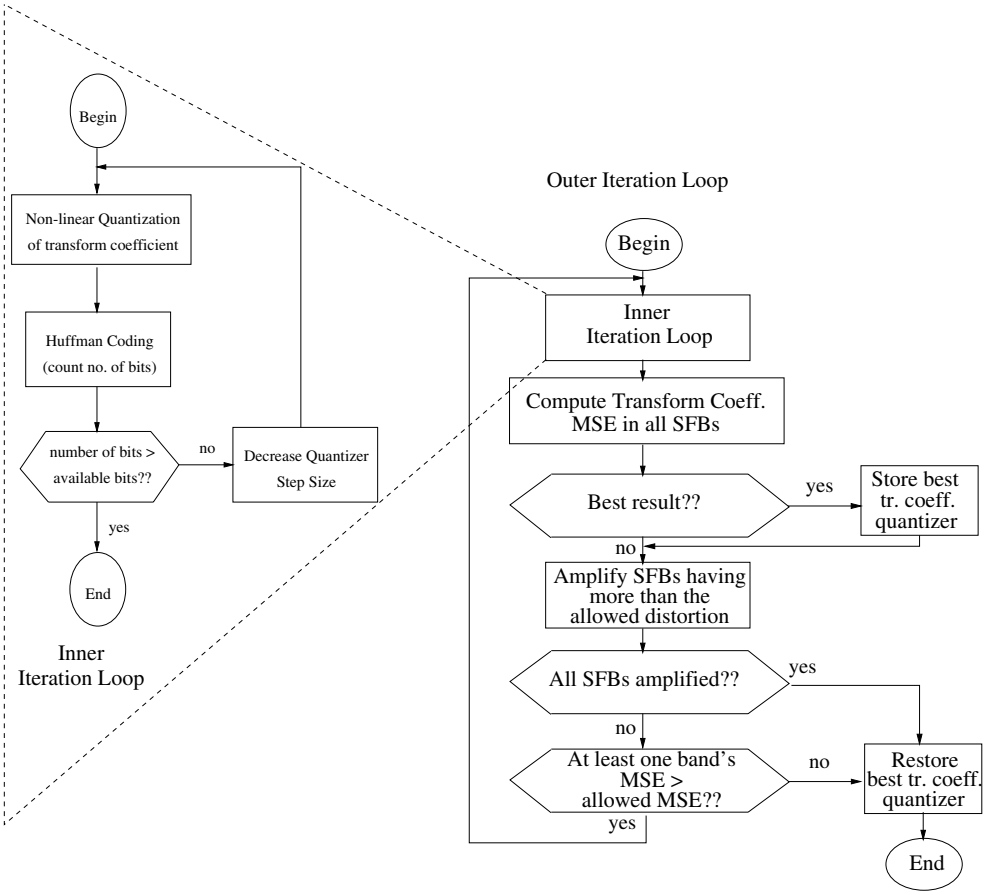

Figure 10.12: AAC inner and outer quantisation loops designed for encoding the frequency-domain transform coefficients.

usually do not change dramatically from one scale-factor band to another. Thus a differential encoding proved useful. Secondly, Huffman coding is applied, in order to further reduce the redundancy associated with the encoding of the scale factors [40].

Again, the AAC quantisation and coding process consists of two iteration loops: the inner and outer loops. The inner iteration loop shown in Figure 10.12 consists of a nonlinear frequency-domain transform coefficient quantiser and the noiseless Huffman coding module. The frequency-domain transform coefficient values are first quantised using a non-uniform quantiser, and further processing using the noiseless Huffman coding tool is applied to achieve a high coding efficiency. The quantiser step size is decreased until the number of bits generated exceeds the available bitrate budget of the particular scale-factor band considered. Once the inner iteration process is completed, the outer loop evaluates the MSE associated with all transform coefficients for all scale-factor bands. The task of the outer iteration loop is to amplify the transform coefficients of the scale-factor bands in order to satisfy the requirements of the psycho-acoustic model. The MSE computed is compared to

the masking threshold value obtained from the associated psycho-acoustic analysis. When the best result is achieved, i.e. the lowest MSE, the corresponding quantisation scheme will be stored in memory. Subsequently, the scale-factor bands having a higher MSE than the acceptable threshold are amplified, using a step size of 1.5 dB. The iteration process will be curtailed when all scale-factor bands have been amplified or it was found that the MSE of no scale-factor band exceeds the permitted threshold. Otherwise, the whole process will be repeated using new SFB amplification values, as seen in Figure 10.12.

10.2.7 Noiseless Huffman Coding

The noiseless Huffman coding tool of Figure 10.12 is used to further reduce the redundancy inherent in the quantised frequency-domain transform coefficients of the audio signal. One frequency-domain transform coefficient quantiser per scale-factor band is used. The step size of each of these frequency-domain transform coefficient quantisers is specified in conjunction with a global gain factor that normalizes the individual scale factors. The global gain factor is coded as an 8-bit unsigned integer. The first scale factor associated with the quantised spectrum is differentially encoded relative to the global gain value and then Huffman coded using the scale-factor codebook. The remaining scale factors are differentially encoded relative to the previous scale factor and then Huffman coded using the scale-factor codebook.

Noiseless coding of the quantised spectrum relies on partitioning the spectral coefficients into sets. The first partitioning divides the spectrum into scale-factor bands that contain an integer multiple of four quantised spectral coefficients. The second partitioning divides the quantised frequency-domain transform coefficients into sections constituted by several scale-factor bands. The quantised spectrum within such a section will be represented using a single Huffman codebook chosen from a set of twelve possible codebooks. This includes a particular codebook that is used for signalling that all the coefficients within that section are zero. Hence no spectral coefficients or scale factors will be transmitted for that particular band, and thus an increased compression ratio is achieved. This is a dynamic quantisation process, which varies from block to block such that the number of bits needed for representing the full set of quantised spectral coefficients is minimised. The bandwidth of the section and its associated Huffman codebook indices must be transmitted as side information, in addition to the section's Huffman coded spectrum.

Huffman coding creates variable length codes [381, 407], where higher probability symbols are encoded by shorter codes. The Huffman coding principles are highlighted in Figure 10.13. Specifically, column 0 in Figure 10.13 shows the set of symbols A, B, C and D, which are Huffman coded in the successive columns. At first, the symbols are sorted from top to bottom with decreasing probability. In every following step, the two lowest probability symbols at the bottom are combined into one symbol, which is assigned the sum of the single probabilities. The new symbol is then fitted into the list at the correct position according to its new probability of occurrence. This procedure is continued, until all codewords are merged, which leads to a coding tree structure as seen in Figure 10.13. The assignment of Huffman coded bits is carried out as follows. At every node, the upper branch is associated with a binary '1', and the lower branch with a binary '0', or the other way round. The complete binary tree can be generated by recursively reading out the symbol list, starting with symbol 'III'. As a result, symbol A is coded as '0', B with '1111', C as '10' and D with '110'; since none of the symbols constitutes a prefix of the other symbols, their decoding is unambiguous.

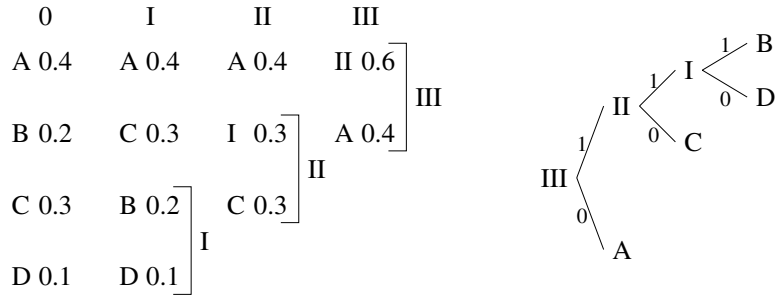

Figure 10.13: Huffman coding.

10.2.8 Bit-sliced Arithmetic Coding

The BSAC tool advocated by Park *et al.* [399] is an alternative to the AAC noiseless Huffman coding module of Section 10.2.7, while all other modules of the AAC-based codec remain unchanged, as shown earlier in Figure 10.7. BSAC is included in the MPEG-4 Audio Version 2 for supporting finely-grained bitstream scalability, and further reducing the redundancy inherent in the scale factors and in the quantised spectrum of the MPEG-4 T/F codec [408].

In MPEG-4 Audio Version 1, the GA codec supports coarse scalability where a base layer bitstream can be combined with one or more enhancement layer bitstreams in order to achieve a higher bitrate and thus an improved audio quality. For example, in a typical scenario we may utilise a 24 kbps base layer together with two 16 kbps enhancement layers. This gives us the flexibility of decoding in three modes, namely 24 kbps, $24 + 16 = 40$ kbps or $24 + 16 + 16 = 56$ kbps modes. Each layer carries a significant amount of side information and hence finely-grained scalability was not supported efficiently in Version 1.

The BSAC tool provides scalability in steps of 1 kbps per channel. In order to achieve finely-grained scalability, a 'bit-slicing' scheme is applied to the quantised spectral coefficients [399]. A simple illustration assisting us in understanding the operation of this BSAC algorithm is shown in Figure 10.14. Let us consider a quantised transform coefficient sequence, $x[n]$, each coefficient quantised with the aid of four bits, assuming the values of $x[0] = 5$, $x[1] = 1$, $x[2] = 7$ and $x[3] = 2$. Firstly, the bits of this group of sequences are processed in slices according to their significance, commencing with the MSB or LSB. Thus, the MSBs of the quantised vectors are grouped together yielding the bit-sliced vector of 0000, followed by the first significant vector (1010), second significant vector (0011) and the least significant vector (1110), as displayed in the top half of Figure 10.14.

The next step is to process the four bit-sliced vectors, exploiting their previous values, which are first initialized to zero. The MSB vector (0000) is first decomposed into two subvectors. Subvector 0 is composed of the bit values of the current vector whose previous state is 0, while subvector 1 consists of bit values of the current vector whose previous state is 1. Note that when a specific previous state bit is 0, the next state bit will remain 0 if the corresponding bit value of the current vector is 0 and it is set to 1 when either the previous state bit or the current vector's bit value, or both, is 1.

By utilising this BSAC scheme, finely-grained bitrate scalability can be achieved by employing first the most significant bits. An increasing number of enhancement layers can be

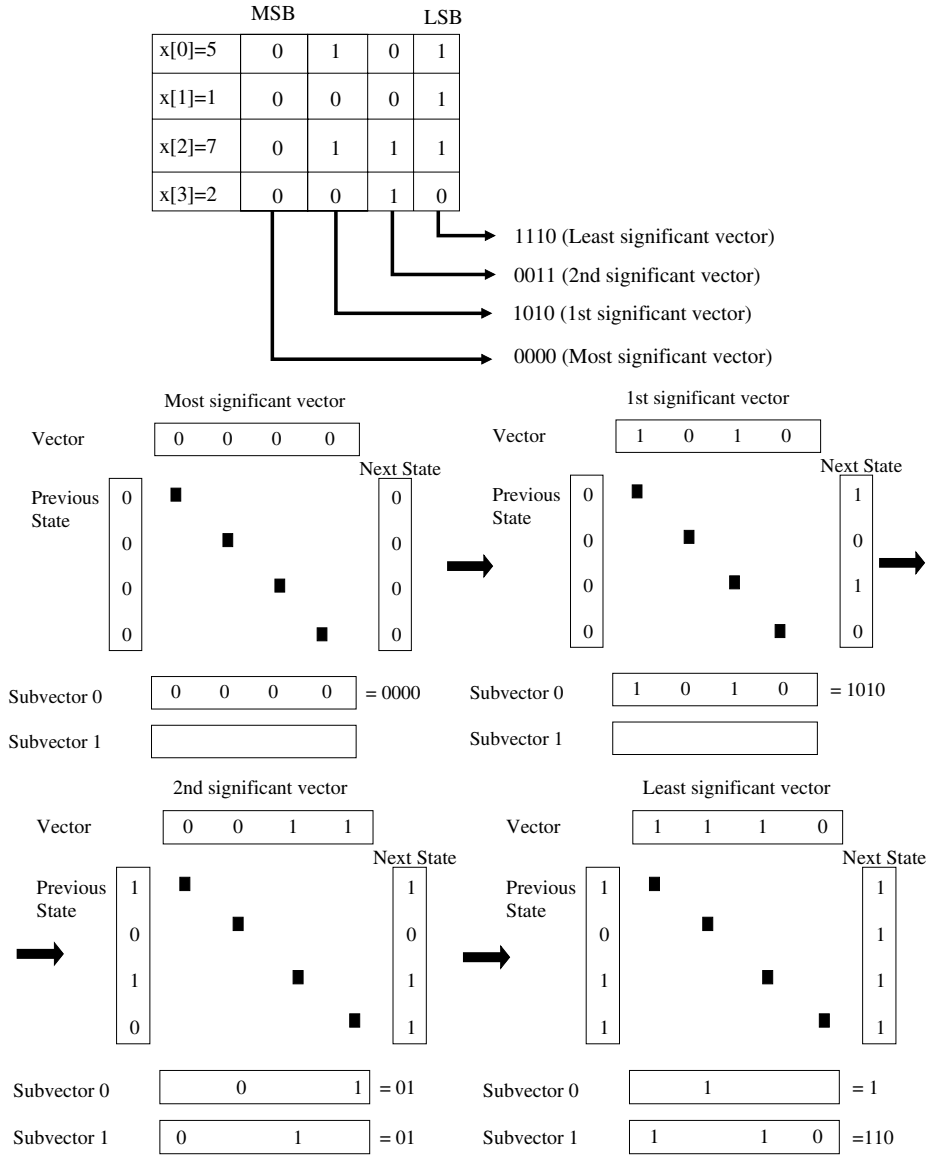

Figure 10.14: BSAC bit-sliced operations, where four quantised bit-sliced sequences are mapped into four 4-bit vectors.

utilised by using more of the less significant bits obtained through the bit-slicing procedure. The actively encoded bandwidth can also be increased by providing bit slices of the transform coefficients in the higher frequency bands.

10.2.9 Transform-domain Weighted Interleaved Vector Quantisation

As shown in Figure 10.7, the third quantisation and coding tool employed for compressing the spectral components is the TWINVQ [41] scheme. It is based on an interleaved vector quantisation and LPC spectral estimation technique, and its performance was superior in comparison to AAC coding at bitrates below 32 kbps per channel [400, 409–411]. TWINVQ invokes some of the compression tools employed by the G.729 8 kbps standard codec [412], such as LPC analysis and LSF parameter quantisation employing conjugate structure VQ [413]. The operation of the TWINVQ encoder is shown in Figure 10.15. Each block will be described during our further discourse in a little more depth. Suffice to say that TWINVQ was found to be superior for encoding audio signals at extremely low bitrates, since the AAC codec performs poorly at low bitrates, while the CELP mode of MPEG-4 is unable to encode music signals [414]. The TWIN-VQ scheme has also been used as a general coding paradigm for representing both speech and music signals at a rate of 1 bit per sample [415].

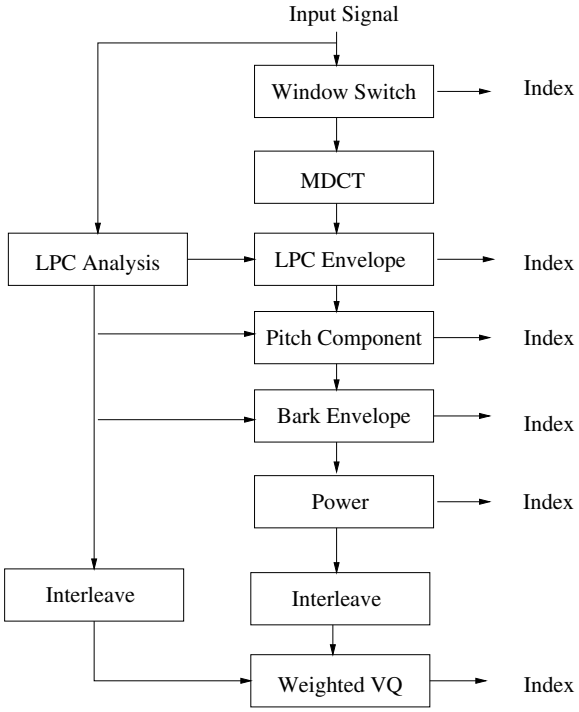

Figure 10.15: TWINVQ encoder [409].

More specifically, the input signal, as shown in Figure 10.15, is first transformed into the frequency domain using the MDCT. Before the transformation, the input signal is classified

into one of three modes, each associated with a different transform window size, namely a long, medium or short window. In the long-frame mode, the transform size is equal to the frame size of 1024. The transform operations are carried out twice in a 1024-sample frame with a half-transform size in the medium-frame mode, and eight times having a one-eighth transform size in the short-frame mode. These different window sizes cater for different input signal characteristics. For example, transient signals are best encoded using a small transform size, while stationary signals can be windowed employing the normal long-frame mode.

As shown in Figure 10.15, the spectral envelope of the MDCT coefficients is approximated with the aid of LPC analysis applied to the time-domain signal. The LPC coefficients are then transformed to the LSP parameters. A two-stage split vector quantiser with interframe moving-average prediction was used for quantising the LSPs, which was also employed in the G.729 8 kbps standard codec [412]. The MDCT coefficients are then smoothed in the frequency domain using this LPC spectral envelope. After the smoothing by the LPC envelope, the resultant MDCT coefficients still retain their spectral fine structure. In this case, the MDCT coefficients would still exhibit a high dynamic range, which is not amenable to vector quantisation. Pitch analysis is also employed in order to obtain the basic harmonic of the MDCT coefficients, although this is only applied in the long-frame mode. The periodic MDCT peak components correspond to the pitch period of speech or audio signal. The extracted pitch parameters are quantised by the interleaved weighted vector quantisation scheme [416], as will be explained later in this section.

As seen in Figure 10.15, the Bark envelope is then determined from the MDCT coefficients, which is smoothed by the LPC spectrum. This is achieved by first calculating the square-rooted power of the smoothed MDCT coefficients corresponding to each Bark-scale sub-band. Subsequently, the average MDCT coefficient magnitudes of the Bark-scale subbands are normalised by their overall average value in order to create the Bark-scale envelope. Before quantising the Bark-scale envelope, further redundancy reduction is achieved by employing interframe backward prediction, whereby the correlation between the Bark-scale envelope of the current 23.2 ms frame and that of the previous frame is exploited. If the correlation is higher than 0.5, the prediction is activated. Hence, an extra flag bit has to be transmitted. The Bark-scale envelope is then vector quantised using the technique of interleaved weighted vector quantisation, as seen at the bottom of Figure 10.15 [415] and augmented below.

At the final audio coding stage, the smoothened MDCT coefficients are normalised by a global frequency-domain gain value, which is then scalar quantised in the logarithmic domain, which takes place in the 'Weighted VQ' block of Figure 10.15. Finally, the MDCT coefficients are interleaved, divided into subvectors for the sake of reducing the associated matching complexity, and vector quantised using a weighted distortion measure derived from the LPC spectral envelope [416] as portrayed in Figure 10.16. The role of the weighting is that of reducing the spectral-domain quantisation errors in the perceptually most vulnerable frequency regions. Moriya and Honda [416] proposed this vector quantiser, since it constitutes a promising way of reducing the computational complexity incurred by vector quantisation [413], as will be highlighted below. Specifically, this two-stage MDCT VQ scheme uses two sets of trained codebooks for vector quantising the MDCT coefficients of a subvector, and the MDCT subvector is reconstructed by superimposing the two codebook vectors. In the encoder, a full-search is invoked for finding the combination of the code vector indices that minimises the distortion between the input and reconstructed MDCT subvector.

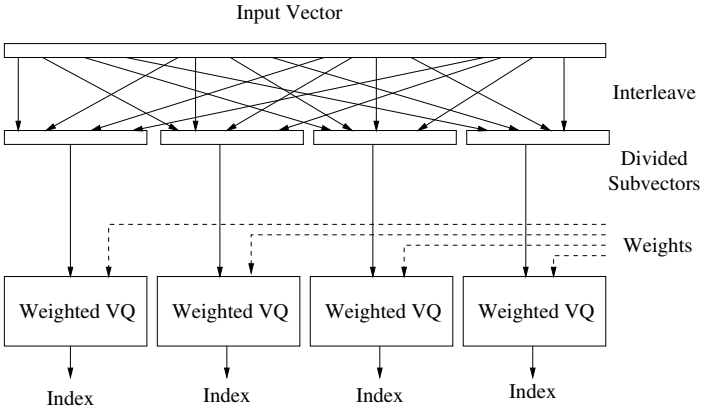

Figure 10.16: TWINVQ interleaved weighted vector quantisation process [41].

This two-stage MDCT VQ scheme constitutes a sub-optimal arrangement in comparison to a single-stage VQ; however it significantly reduces the memory and the computational complexity required. The employment of a fixed frame rate combined with the above vector quantiser improves its robustness against errors, since it does not use any error sensitive compression techniques, such as adaptive bit allocation or variable length codes [409].

The MPEG-4 TWINVQ bitstream structure is shown in Table 10.1 in its 16 kbps mode, which will be used in our investigations in order to construct a multimode speech transceiver, as detailed in Section 10.5. A substantial fraction of the bits were allocated for encoding the MDCT coefficients, which were smoothed by the LPC and Bark-scale spectra. Specifically, a total of 44 bits were allocated for vector quantising the Bark-scale envelope, while one bit is used for the interframe prediction flag. Nine bits were used for encoding the global spectral-domain gain value obtained from the MDCT coefficients and the LSF VQ requires 19 bits per 23.22 ms audio frame.

Table 10.1: MPEG-4 TWINVQ bit allocation scheme designed for a rate of 16 kbps, which corresponds to 372 bits per 23.22 ms frame.

Parameters	No. of bits
Window mode	4
MDCT coefficients	295
Bark-envelope VQ	44
Prediction switch	1
Gain factor	9
LSF VQ	19
Total bits	372

10.2.10 Parametric Audio Coding

An enhanced functionality provided by the MPEG-4 Audio Version 2 scheme is parametric audio coding, with substantial contributions from Purnhagen and Meine [417–419], Edler and Purnhagen [420], Levine *et al.* [421] and Verma and Meng [422]. This compression tool facilitates the encoding of audio signals at the very low bitrate of 4 kbps, using a parametric representation of the audio signal. Similar to the philosophy of parametric speech coding, instead of waveform coding here the audio signal is decomposed into audio objects, which are described by appropriate source models and the quantised models parameters are transmitted. This coding scheme is referred to as the harmonic and individual lines plus noise (HILN) technique, which includes object models for sinusoids, harmonic tones and noise components [418].

Due to the limited bitrate budget at low target bitrate, only the specific parameters that are most important for maintaining an adequate perceptual quality of the signal are transmitted. More specifically, in the context of the HILN technique, the frequency and amplitude parameters are quantised using existing masking rules from psycho-acoustics [373]. The spectral envelope of the noise and harmonic tones is described using LPC techniques. Parameter prediction is employed in order to exploit the correlation between the parameters across consecutive 23.22 ms frames. The quantised parameters are finally encoded using high-efficiency, but error-sensitive Huffman coding. Using a speech/music classification tool in the encoder, it is possible to automatically activate the coding of speech signals using the HVXC parametric encoder or the HILN encoder contrived for music signals.

The operating bitrate of the HILN scheme is at a fixed rate of 6 kbps in the mono, 8 kHz sampling rate mode and 16 kbps in the mono, 16 kHz sampling rate mode, respectively. In an alternative proposal by Levine and Smith III in [423], an audio codec employing switching between parametric- and transform-coding based representations was advocated. Sinusoidal signals and noise are modelled using multi-resolution sinusoidal modelling [421] and Bark-scale-based noise modelling, respectively, while the transients are represented by short-window-based transform coding. Verma and Meng in [422] extended the work of [421] by proposing an explicit transient model for sinusoidal-like signals and for noise. A slowly varying sinusoidal signal is impulse-like in the frequency domain. By contrast, transients are impulse-like in the time domain and cannot be readily represented with the aid of short-time Fourier transform (STFT) based analysis. However, due to the duality between time and frequency, transients which are impulse-like in the time domain appear to be oscillatory in the frequency domain. Hence, sinusoidal modelling can be applied after the transformation of the transient time-domain signals to sinusoidal-like signals in the frequency domain by quantising their DCT [422] coefficients.

10.3 Speech Coding in MPEG-4 Audio

While the employment of transform coding is dominant in coding music, audio and speech signals at rates above 24 kbps, its performance deteriorates as the bitrate decreases. Hence, in the MPEG-4 audio scheme, dedicated speech coding tools are included, operating at the bitrates in the range between 2 and 24 kbps [44, 49]. Variants of the CELP technique [424] are used for the encoding of speech signals at bitrates between 4 and 24 kbps, incorporating the additional flexibility of encoding speech represented at both 8 and 16 kHz sampling rates.

Below 4 kbps a sinusoidal technique, namely the so-called HVXC scheme, was selected for encoding speech signals at rates down to a bitrate of 2 kbps. The HVXC technique will be described in the next section, while CELP schemes will be discussed in Section 10.3.2.

10.3.1 Harmonic Vector Excitation Coding

HVXC is based on the signal classification of voiced and unvoiced speech segments, facilitating the encoding of speech signals at 2 kbps and 4 kbps [425, 426]. In addition, it also supports variable-rate encoding by including specific coding modes for both background noise and mixed voice generation in order to achieve an average bitrate as low as 1.2–1.7 kbps.

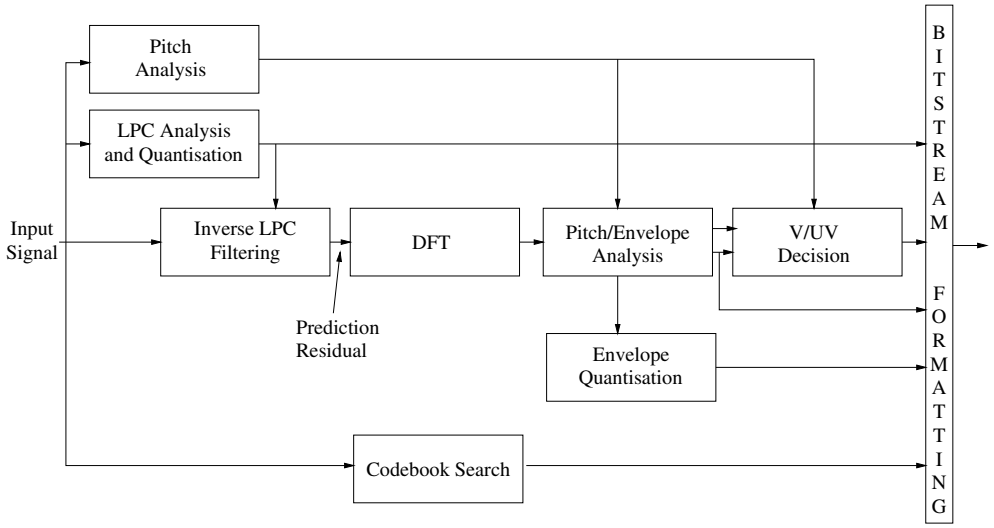

Figure 10.17: Harmonic vector excitation coding.

The basic structure of a HVXC encoder is shown in Figure 10.17, which first performs LPC analysis for obtaining the LPC coefficients. The LPC coefficients are then quantised and used in the inverse LPC filtering block in order to obtain the prediction residual signal. The prediction residual signal is then transformed into the frequency domain using the DFT and pitch analysis is invoked in order to assist in the V/UV classification process. Furthermore, the frequency-domain spectral envelope of the prediction residual is quantised by using a combination of two-stage shape vector quantiser and a scalar gain quantiser. For unvoiced segments, a closed-loop codebook search is carried out in order to find the best excitation vector.

Specifically, the HVXC codec operates on the basis of a 20 ms frame length for speech signals represented at an 8 kHz sampling rate. Table 10.2 shows the bit-allocation schemes of the HVXC codec at rates of 2 and 4 kbps [427]. Both voiced and unvoiced speech segments use the LSF parameters and the V/UV indicator flag. For 2 kbps transmission of voiced speech, the parameters include 18 bits for LSF quantisation using a two-stage split vector quantiser, which facilitates the reduction of the codebook search complexity by mitigating the VQ matching complexity. Furthermore, 2 bits are used for the V/UV mode indication,

where the extra one bit is used to indicate the background noise interval and mixed speech modes for variable rate coding, as will be explained later. Furthermore, 7 bits are dedicated to pitch encoding, while 8 and 5 bits are used for encoding the harmonic shape and gain of the prediction residual in Figure 10.17, respectively. Explicitly, for the quantisation of the harmonic spectral magnitudes/shapes of the prediction residual in Figure 10.17, a two-stage shape vector quantiser is used, where the size of both the shape codebooks is 16, both requiring a 4-bit index. The codebook gains are quantised using 3 and 2 bits, respectively. In the case of unvoiced speech transmission at 2 kbps, in addition to the LSF quantisation indices and the V/UV indication bits, the shape and gain codebook indices of the vector excitation (VXC) requires 6 and 4 bits, respectively, for a 10 ms frame length.

Table 10.2: MPEG-4 bit allocations at the fixed rates of 2.0 and 4.0 kbps using the HVXC coding mode [41].

	Voiced	Common	Unvoiced
LSF1 (2-stage split VQ at 2 kbps		18 bits/20 ms	
LSF2 (at 4 kbps)		8 bits/20 ms	
V/UV		2 bits/20 ms	
Pitch	7 bits/20 ms		
Harmonic 1 shape (at 2 kbps)	$4 + 4$ bits/20 ms		
Harmonic 1 gain (at 2 kbps)	5 bits/20 ms		
Harmonic 2 split (at 4 kbps)	32 bits/20 ms		
VXC1 shape (at 2 kbps)			6 bits/10 ms
VXV1 gain (at 2 kbps)			4 bits/10 ms
VXC2 shape (at 4 kbps)			5 bits/5 ms
VXC2 gain (at 4 kbps)			3 bits/5 ms
2 kbps mode	40 bits/20 ms		40 bits/20 ms
4 kbps mode	80 bits/20 ms		80 bits/20 ms

For 4 kbps transmission, a coding enhancement layer is added to the base layer of 2 kbps. In the case of LSF quantisation, a ten-dimensional vector quantiser using an 8-bit codebook is added to the 18 bits/20 ms LSF quantiser scheme of the 2 kbps codec mode seen at the top of Table 10.2. This results in an increased bitrate requirement for LSF quantisation, namely from 18 bits/20 ms to 26 bits/20 ms. A split VQ scheme, composed of four vector quantisers having addresses of 7, 10, 9 and 6 bits, respectively, is added to the two-stage vector quantiser required for the quantisation of the harmonic shapes of the prediction residual in Figure 10.17. This results in a total bitrate budget increase of 32 bits/20 ms, as seen in Table 10.2. For the sake of unvoiced speech segment encoding at 4 kbps, the excitation vectors of the enhancement layer are obtained by utilising codebook search and the specific gain/shape codebook indices, which minimise the weighted distortion are transmitted. Specifically, a 5-bit shape codebook as well as 3-bit gain codebook are used and this procedure, which are updated every 5 ms. For the unvoiced speech segments, the LPC coefficients of only the current 20 ms frame are used for two 10 ms subframes without any interpolation procedure using the LPC coefficients from the previous frame. Again, the codec's performance is summarised in Table 10.2.

Optional variable-rate coding can be applied to the HVXC codec, incorporating background noise detection, where only the mode bits are received during the 'background noise mode'. When the HVXC codec is in the 'background noise mode', the decoding is similar to the manner applied in an unvoiced (UV) frame, but in this scenario no LSF parameters are transmitted while only the mode bits are transmitted. Instead two sets of LSF parameters generated during the previous two UV frames will be used for the LPC synthesis process. During the background noise mode, fully encoded UV frames are inserted every nine 20 ms frames in order to transmit the background noise parameters. This means only eight consecutive 'background noise' frames are allowed to use the same two sets of LSF parameters from the previous UV frames. Hereafter, a new UV frame will be transmitted. This UV frame may or may not be a real UV frame indicating the beginning of active speech bursts. This is signalled by the transmitted gain factor. If the gain factor is smaller or equal to the previous two gain values, then this UV frame is regarded as background noise. In this case the most recent previously transmitted LSF parameters are used for maintaining the smooth variation of the LSF parameters. Otherwise, the currently transmitted LSFs are used, since the frame is deemed a real UV frame. During background noise periods, a gain-normalised Gaussian noise vector is used instead of the stochastic prediction residual shape codebook entry employed during UV frame decoding. The prediction residual gain value is encoded using an 8-bit codebook entry, as displayed in Table 10.3.

Table 10.3: Bit allocations for variable rate HVXC coding [41].

Mode	Background noise	Unvoiced	Mixed voiced/unvoiced
V/UV	2 bits/20 ms	2 bits/20 ms	2 bits/20 ms
LSF	0 bits/20 ms	18 bits/20 ms	18 bits/20 ms
Excitation	0 bits/20 ms	8 bits/20 ms (gain only)	20 bits/20 ms (pitch and harmonic spectral parameters)
Total	2 bits/20 ms $= 0.1$ kbps	28 bits/20 ms $= 1.4$ kbps	40 bits/20 ms $= 2.0$ kbps

Table 10.3 shows the bit-allocation scheme of variable rate HVXC coding for four different encoding modes, which are the modes dedicated to background noise, unvoiced, mixed voiced and unvoiced segments. The mixed voiced and unvoiced modes share the same bit allocation at 2 kbps. The unvoiced mode operates at 1.4 kbps, where only the gain parameter of the vector excitation is transmitted. Finally, for the background noise mode only the two voiced/unvoiced/noise signalling bits are transmitted.

10.3.2 CELP Coding in MPEG-4

While the HVXC mode of MPEG-4 supports the very low bitrate encoding of speech signals for rates below 4 kbps, the CELP compression tool is used for bitrates in excess of 4 kbps, as illustrated in Table 10.4. The MPEG-4 CELP tool enables the encoding of speech signals at two different sampling rates, namely at s8 and 16 kHz [428]. For narrowband speech coding the operating bitrates are between 3.85 and 12.0 kbps. Higher bitrates between 10.9 and

24 kbps are allocated for wideband speech coding, which cater for a higher speech quality due to their extended bandwidth of about 7 kHz. The MPEG-4 CELP codec supports a range of further functionalities, which include the possibility of supporting multiple bitrates, bitrate scalability, bandwidth scalability and complexity scalability. In addition, the MPEG-4 CELP mode supports both fixed and variable bitrate transmission. The bitrate is specified by the user's requirements, taking account of the sampling rate chosen and also of the type of LPC quantiser (scalar quantiser or vector quantiser) selected. The default CELP codec operating at 16 kHz sampling rate employs a scalar quantiser and in this mode the fine rate control (FRC) switch is also turned on. The FRC mode allows the codec to change the bitrate by skipping the transmission of the LPC coefficients, by utilising the Interpolation and the LPC_Present flags [429], as will be discussed in Section 10.3.3. By contrast, at the 8 kHz sampling rate, the default MPEG-4 CELP mode utilises vector quantiser and the FRC switch is turned off.

Table 10.4: Summary of various features of the MPEG-4 CELP codec [41].

	CELP	
Mode	Narrowband	Wideband
Sampling rate (kHz)	8	16
Bandwidth (Hz)	300–3400	50–7000
Bitrate (kbps)	3.85–12.2	10.9–24.0
Excitation scheme	MPE/RPE	RPE
Frame size (ms)	10–40	10–20
Delay (ms)	15–85	18.75–41.75
Features	Multi bitrate coding	
	Bitrate scalability	
	Bandwidth scalability	
	Complexity scalability	

As shown in Figure 10.18, first the LPC coefficients of the input speech are determined and converted to LARs or LSFs. The LARs or LSFs are then quantised and also inverse quantised in order to obtain the quantised LPC coefficients. These coefficients are used by the LPC synthesis filter. The excitation signal consists of the superposition of contributions by the adaptive codebook and one or more fixed codebooks. The adaptive codebook represents the periodic speech components, while the fixed codebooks are used for encoding the random speech components. The transmitted parameters include the LAR/LSF codebook indices, the pitch lag for the adaptive codebook, the shape codebook indices of the fixed codebook and the gain codebook indices of the adaptive as well as fixed codebook gains. MPE [430] or RPE [431] can also be used for the fixed codebooks. The difference among the two lies in the degree of freedom for pulse positions. MPE allows more freedom in the choice of the inter-pulse distance than RPE, which has a fixed inter-pulse distance. As a result, MPE typically achieves a better speech coding quality than RPE at a given bitrate. On the other hand, the RPE scheme imposes a lower computational complexity than MPE, which renders MPE a useful tool for wideband speech coding where the computational complexity is naturally higher than in narrowband speech coding due to the doubled sampling rate used.

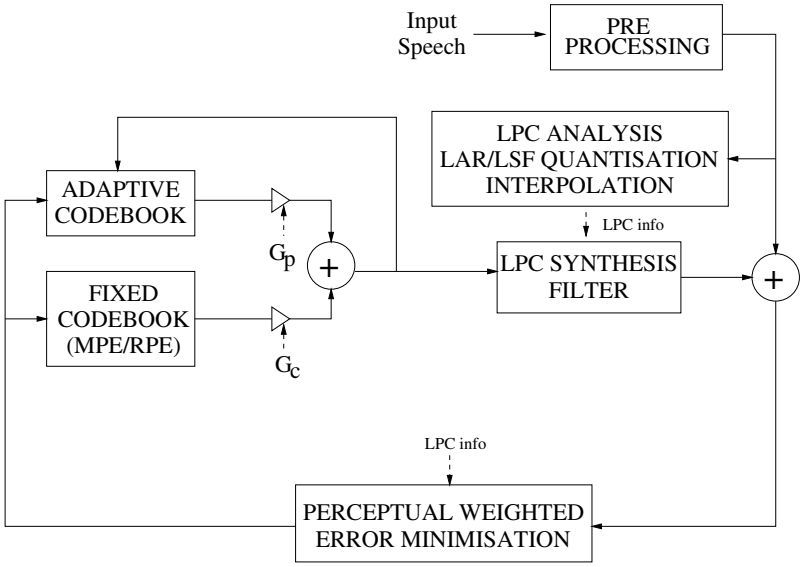

Figure 10.18: CELP encoder.

10.3.3 LPC Analysis and Quantisation

Depending on the tolerable complexity, the LPC coefficients can be quantised using either a scalar or a vector quantisation scheme. When a scalar quantiser is used, the LPC coefficients have to be transformed to the LAR parameters. In order to obtain the LAR parameters, the LPC coefficients are first transformed to the reflection coefficients [339]. The reflection coefficients are then quantised using a look-up table. The relationship between the LARs and the reflection coefficients are described by

$$\mathrm{LAR}[i] = \log((1 - q\_rfc[i])/(1 + q\_rfc[i])), \tag{10.12}$$

where q_rfc represents the quantised reflection coefficients. The necessity to transmit the LARs depends on the amount of change between the current audio/speech spectrum and the spectrum described by the LARs obtained by interpolation from the LARs of the adjacent frame. If the spectral change is higher than a pre-determined threshold, then the current LAR coefficients are transmitted to the decoder. The threshold is adaptive, depending on the desired bitrate. If the resultant bitrate is higher than the desired bitrate, the threshold is raised, otherwise, it is lowered. In order to reduce the bitrate further, the LAR coefficients can be losslessly Huffman coded. We note, however, that lossless coding will only be applied to the LARs but not to the LSF, since only the LARs are scalar quantised and there is no LAR VQ in the standard.

If vector quantisation of the LPC coefficients is used, the LPC coefficients are transformed into the LSF domain. There are two methods of quantising the LSFs in the CELP MPEG-4 mode. We can either employ a two-stage vector quantiser without interframe LSF prediction, or in combination with interframe LSF prediction, as shown in Figure 10.19. In the case

of using a two-stage vector quantiser without interframe LSF prediction, the second-stage VQ quantizes the LSF quantisation error of the first stage. When interframe LSF prediction is employed, the difference between the input LSFs and the predicted LSFs is quantised. At the encoder, both methods are applied and the better method is selected by comparing the LSF quantisation error obtained by calculating the weighted mean squared LSF error. In narrowband speech coding, the number of LSF parameters is 10, while it is 20 in the wideband MPEG-4 CELP speech encoding mode. The number of bits used for LSF quantisation is 22 for the narrowband case and 46 bits for the wideband scenario, which involves 25 bits used for quantising the first ten LSF coefficients and 21 bits for the ten remaining LSFs [41].

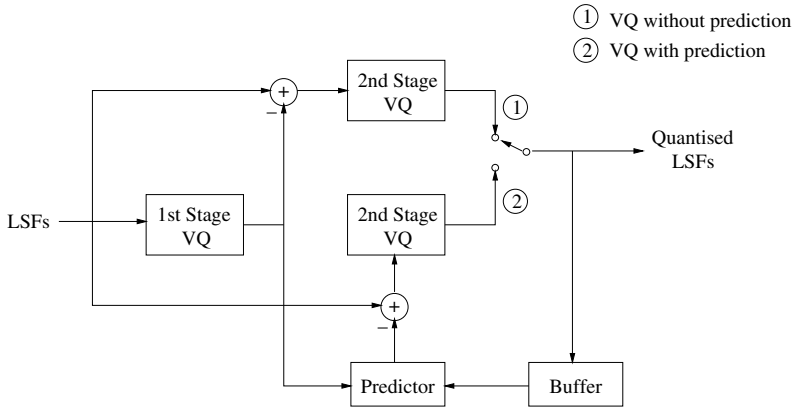

Figure 10.19: LSF VQ operating in two modes: with or without LSF prediction at the second stage VQ.

The procedure of spectral envelope interpolation can also be employed for interpolating both the LARs and LSFs. The Interpolation flag, together with the LPC_Present flag unambiguously describe how the LPC coefficients of the current frame are derived. The associated functionalities are summarised in Table 10.5. Specifically, if the Interpolation flag is set to one, this implies that the LPC coefficients of the current 20 ms frame are calculated by using the LPC coefficients of the previous and next frames. This would mean, in general, that the decoding of the current frame must be delayed by one frame. In order to avoid the latency of one frame delay at the decoder, the LPC coefficients of the next frame are enclosed in the current frame [41]. In this case, the LPC_Present flag is set. Since the LPC coefficients of the next frame are already present in the current frame, the next frame will contain no LPC information. When the Interpolation flag is zero and the LPC_Present flag is zero, the LPC parameters of the current frame are those received in the previous frame. When the Interpolation flag is zero and the LPC_Present flag is one, then the current frame is a complete frame and the LPC parameters received in the current frame belong to the current frame. Note that in order to maintain good subjective speech quality, it is not allowed to have consecutive frames without the LPC information. This means the Interpolation flag may not have a value of one in two successive frames.

Table 10.5: Fine rate control utilising the Interpolation and LPC_Present flags [41].

Interpolation	LPC_Present	Description
1	1	$\mathrm{LPC_{cur}} = \text{interpolate}(\mathrm{LPC_{prev}} + \mathrm{LPC_{next}})$
0	0	$\mathrm{LPC_{cur}} = \mathrm{LPC_{prev}}$
0	1	$\mathrm{LPC_{cur}} = \mathrm{LPC}$ received in current frame

10.3.4 Multi Pulse and Regular Pulse Excitation

In MPEG-4 CELP coding, the excitation vectors can be encoded using either the MPE [430] or RPE [431] techniques. MPE is the default mode used for narrowband speech coding while RPE is the default mode for wideband speech coding, due to its simplicity in comparison to the MPE technique.

In AbS based speech codecs, the excitation signal is represented by a linear combination of the adaptive code vector and the fixed code vector scaled by their respective gains. Each component of the excitation signal is chosen by an AbS search procedure in order to ensure that the perceptually weighted error between the input signal and the reconstructed signal is minimised [402]. The adaptive codebook parameters are constituted by the closed-loop delay and gain. The closed-loop delay is selected with the aid of a focussed search in the range around the estimated open-loop delay. The adaptive code vector is generated from a block of the past excitation signal samples associated with the selected closed-loop delay. The fixed code vector contains several non-zero excitation pulses. The excitation pulse positions obey an algebraic structure [402, 432]. In order to improve the achievable performance, after determining several sets of excitation pulse position candidates, a combined search based on the amalgamation of the excitation pulse position candidates and the pulse amplitudes is carried out.

For narrowband speech coding utilising MPE [430], the bitrate can vary from 3.85 to 12.2 kbps when using different configurations based on varying the frame length, the number of subframes per frame, and the number of pulses per subframe. These different configurations are shown in Tables 10.6 and 10.7 for narrowband MPE and wideband MPE, respectively.

Table 10.6: Excitation configurations for narrowband MPE.

Bitrate range (kbps)	Frame length (ms)	No. subframes per frame	No. pulses per subframe
3.85–4.65	40	4	3...5
4.90–5.50	30	3	5...7
5.70–7.30	20	2	6...12
7.70–10.70	20	4	4...12
11.00–12.20	10	2	8...12

Table 10.7: Excitation configurations for wideband MPE.

Bitrate range (kbps)	Frame length (ms)	No. subframes per frame	No. pulses per subframe
10.9–13.6	20	4	5...11
13.7–14.1	20	8	3...10
14.1–17.0	10	2	5...11
21.1–23.8	10	4	3...10

On the other hand, RPE [431, 433] enables implementations having significantly lower encoder complexity and only slightly reduced compression efficiency. The RPE principle is used in wideband speech encoding, replacing MPE as the default mode and supporting bitrates between 13 and 24 kbps. RPE employs fixed pulse spacing, which implies that the distance of subsequent excitation pulses in the fixed codebook is fixed. This reduces the codebook search complexity required for obtaining the best indices during the AbS procedure.

Having introduced the most important speech and audio coding modes of the MPEG-4 codec, in the next section we characterise its performance.

10.4 MPEG-4 Codec Performance

Figure 10.20 shows the achievable SEGSNR performance of the MPEG-4 codec at various bitrates applying various speech and audio coding modes. The MPE speech codec mode has been applied for bitrates between 3.85 kbps and 12.2 kbps for encoding narrowband speech while the RPE codec in the CELP 'toolbox' is employed for wideband speech encoding spans from 13 kbps to 24 kbps. The TWINVQ audio codec of Section 10.2.9 was utilised for encoding music signals for bitrates of 16 kbps and beyond. In Figure 10.20, the codecs were characterised in terms of their performance when encoding speech signals. As expected, the SEGSNR increases upon increasing the bitrate. When the RPE codec mode is used, the wideband speech quality is improved in terms of both the objective SEGSNR measure and the subjective quality. For the case of the TWINVQ codec mode of Section 10.2.9, the SEGSNR increases near-linearly with the bitrates. It is worth noting in Figure 10.20, that the RPE codec mode outperformed the TWINVQ codec mode over its entire bitrate range in the context of wideband speech encoding. This is because the RPE scheme is a dedicated speech codec while the TWINVQ codec is a more general audio codec, but also capable of encoding speech signals.

Figure 10.21 displays the achievable SEGSNR performance versus frame index for the three different narrowband speech coding bitrates of 3.85, 6.0 and 12.0 kbps, using the MPE tool of the MPEG-4 Audio standard. The MPE tool offers the option of multirate coding, which is very useful in adaptive transmission schemes that can adapt the source bitrate according to the near-instantaneous channel conditions.

The performance of various codecs of the MPEG-4 toolbox used for the encoding of music signals is shown in Figure 10.22 at a sampling rate of 16 kHz. We observe that, as

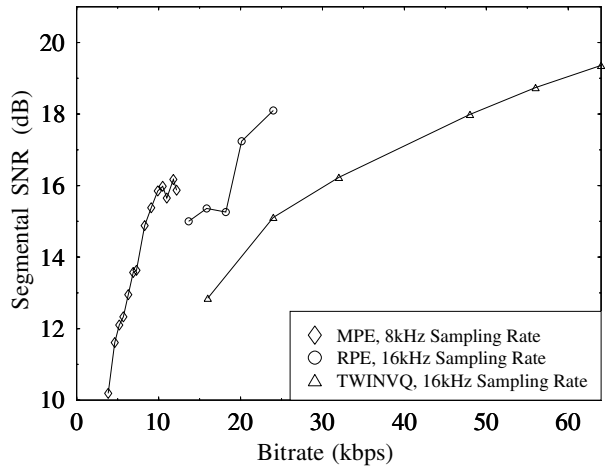

Figure 10.20: SEGSNR performance for the encoding of speech signals, with respect to three different MPEG-4 coding modes, where the MPE codec and the RPE codec are employed at the sampling rates of 8 kHz and 16 kHz, respectively, while the TWINVQ audio codec of Section 10.2.9 operates at 16 kHz sampling rate.

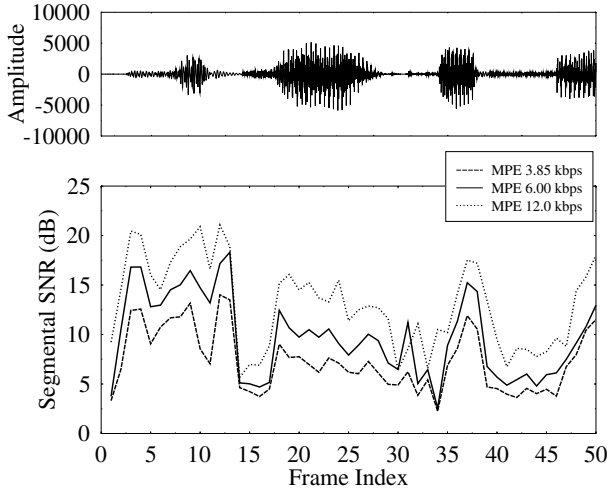

Figure 10.21: SEGSNR performances versus frame index for three different bitrates of 3.85, 6.0 and 12.0 kbps, using the CELP tool in MPEG-4 Audio at a sampling rate of 8 kHz for the speech file of five.bin.

expected, the TWINVQ codec of Section 10.2.9 performed better than the CELP codec when encoding music signals. The difference in SEGSNR performance can be as high as 2 dB at the same bitrate.

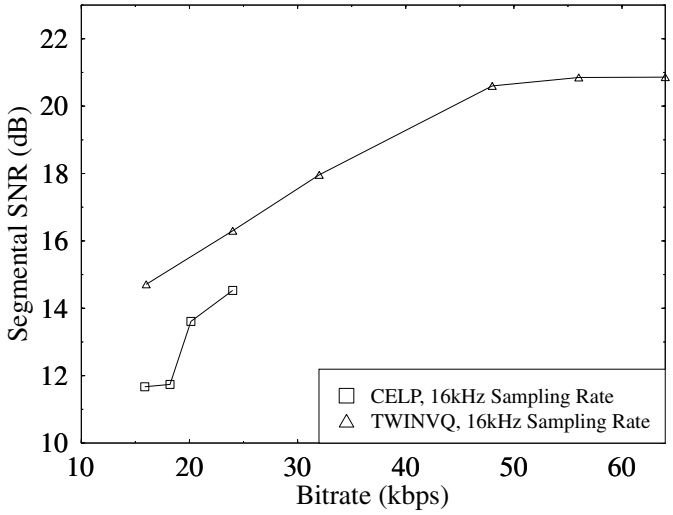

Figure 10.22: Comparing SEGSNR performances for CELP and TWINVQ codecs at 16 kHz sampling rate, for coding of the music file of moza.bin.

10.5 MPEG-4 Space–time Block Coded OFDM Audio Transceiver[1]

The 3G mobile communications standards [434] are expected to provide a wide range of bearer services, spanning from voice to high-rate data services, supporting rates of at least 144 kbps in vehicular, 384 kbps in outdoor-to-indoor and 2 Mbps in indoor as well as in picocellular applications.

In an effort to support such high rates, the bit/symbol capacity of band-limited wireless channels can be increased by employing multiple antennas [435]. The concept of space–time trellis codes (STTCs) was proposed by Tarokh *et al.* [436] in 1998. By jointly designing the FEC, modulation, transmit diversity and optional receive diversity scheme, they increased the effective bits/symbol (BPS) throughput of band-limited wireless channels, given a certain channel quality. A few months later, Alamouti [50] invented a low-complexity space–time block code (STBC), which imposes a significantly lower complexity at the cost of a slight performance degradation. Alamouti's invention motivated Tarokh *et al.* [437, 438] to generalise Alamouti's scheme to an arbitrary number of transmitter antennas. Then, Tarokh *et al.*, Bauch [439], Agrawal *et al.* [440], Li *et al.* [441] and Naguib *et al.* [442] extended the

[1]This section is based on How, Liew and Hanzo: A Space–time Coded OFDM based MPEG-4 Audio Transceiver, Proceedings of IEEE VTC, New Jersey, US, 7–10 October 2001, pp. 782–786 and it was based on collaborative research with the co-authors.

research of space–time codes from considering narrowband channels to dispersive channels [443]. The benefits of space–time coding in terms of mitigating the effects of channel fading are substantial and hence they were optionally adopted in the 3G cellular standards [444].

Substantial advances have been made in the field of OFDM, which was first proposed by Chang in his 1966 paper [445]. Research in OFDM was revived by, amongst others, Cimini in his often cited paper [446] and the field was further advanced during the 1990s, with a host of contributions documented for example, in [447]. In Europe, OFDM has been favoured for both DAB and DVB [448, 449] as well as for high-rate wireless asynchronous transfer mode (WATM) systems due to its ability to combat the effects of highly dispersive channels [450]. Most recently OFDM has also been proposed for the downlink of high-rate wireless Internet access [451].

At the time of writing we are witnessing the rapid emergence of intelligent multimode HSDPA-style mobile speech and audio communicators [339, 452, 453], that can adapt their parameters in response to rapidly changing propagation environments. Simultaneously, significant efforts have been dedicated to researching multirate source coding, which is required by the near-instantaneously adaptive transceivers [454]. The recent GSM AMR standardisation activities have prompted significant research interests in invoking the AMR mechanism in half-rate and full-rate channels [28]. Recently, ETSI also standardized the AMR-WB speech codec [337] for the GSM system, which provides a high speech quality due to representing the extra audio bandwidth of 7 kHz, instead of the conventional 3.1 kHz bandwidth. Finally, the further enhanced AMR-WB+ audio and speech codec was detailed in Section 9.7.

The standardisation activities within the framework of the MPEG-4 audio coding initiative [455] have also reached fruition, supporting the transmission of natural audio signals, including the representation of synthetic audio, such as musical instrument digital interface (MIDI) [48] and text-to-speech (TTS) systems [42]. A wide ranging set of bitrates spanning from 2 kbps per channel up to 64 kbps per channel are supported by the MPEG-4 audio codec.

Against this backcloth, in this section the underlying trade-offs of using the multirate MPEG-4 TWINVQ audio encoder of Section 10.2.9, in conjunction with a turbo-coded [456] and space–time coded [436], reconfigurable BPSK/QPSK/16-QAM OFDM system [51] are investigated, in order to provide an attractive system design example.

10.5.1 System Overview

Figure 10.23 shows the schematic of the turbo-coded and space–time-coded OFDM system. The source bits generated by the MPEG-4 TWINVQ encoder [41] are passed to the turbo encoder using the half-rate, constraint length three turbo convolutional encoder TC$(2, 1, 3)$, employing an octal generator polynomial of $(7, 5)$. The encoded bits were channel interleaved and passed to the modulator. The choice of the modulation scheme to be used by the transmitter for its next OFDM symbol is determined by the channel quality estimate of the receiver based on the current OFDM symbol. Here, perfect channel quality estimation and perfect signalling of the required modem modes were assumed. In order to simplify the task of signalling the required modulation modes from receiver A to transmitter B, we employed the sub-band-adaptive OFDM transmission scheme proposed by Hanzo *et al.* [51]. More specifically, the total OFDM symbol bandwidth was divided into equi-width sub-bands

having a similar channel quality, where the same modem mode was assigned. The modulated signals were then passed to the encoder of the space–time block code G_2 [50] which employs two transmitters and one receiver. The space–time encoded signals were OFDM modulated and transmitted by the corresponding antennas.

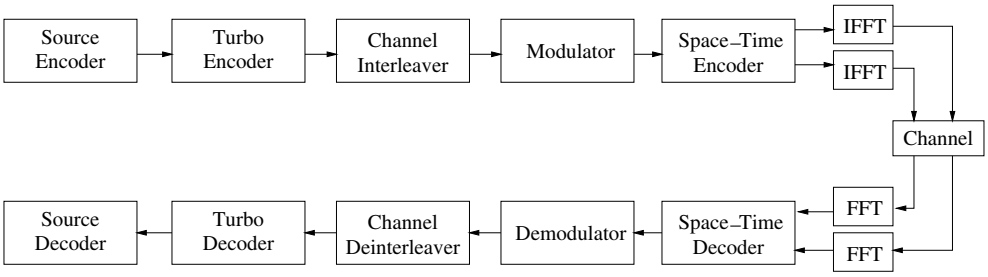

Figure 10.23: Schematic overview of the turbo-coded and space–time =-coded OFDM system.

The received signals were OFDM demodulated and passed to the space–time decoders. Logarithmic maximum *a posteriori* (Log-MAP) decoding [457] of the received space–time signals was performed in order to provide soft-outputs for the TC$(2, 1, 3)$ turbo decoder. The received bits were then channel de-interleaved and passed to the TC decoder which, again, employs the Log-MAP decoding algorithm. The decoded bits were finally passed to the MPEG-4 TWINVQ decoder to obtain the reconstructed audio signal.

10.5.2 System Parameters

Tables 10.8 and 10.9 gives an overview of the proposed system's parameters. The transmission parameters have been partially harmonised with those of the TDD-mode of the Pan-European UMTS system [444]. The sampling rate is assumed to be 1.9 MHz, leading to a 1024 subcarrier OFDM symbol. The channel model used was the four-path COST 207 TU CIR [458], where each impulse was subjected to independent Rayleigh fading having a normalised Doppler frequency of $2.25 \cdot 10^{-6}$, corresponding to a pedestrian scenario at a walking speed of 3 mph. CIR is shown in Figure 10.24.

The channel encoder is a convolutional constituent coding-based turbo encoder [456], employing block turbo interleavers and a pseudo-random channel interleaver. Again, the constituent RSC encoder employs a constraint length of 3 and the octal generator polynomial of $(7, 5)$. Eight iterations are performed at the decoder, utilising the MAP-algorithm and the LLR soft inputs provided by the demodulator.

The MPEG-4 TWINVQ audio coder has been chosen for this system, which can be programmed to operate at bitrates between 16 and 64 kbps. It provides a high audio quality at an adjustable bitrate and will be described in more depth in the next section.

10.5.3 Frame Dropping Procedure

For completeness, we investigated the bit sensitivity of the TWINVQ codec. A high robustness against bit errors inflicted by wireless channels is an important criterion for the design of a communication system. A commonly used approach in quantifying the sensitivity

Table 10.8: System parameters.

System parameters	Value
Carrier frequency	1.9 GHz
Sampling rate	3.78 MHz
Channel	
Impulse response	COST207
Normalised Doppler frequency	$2.25 \cdot 10^{-6}$
OFDM	
Guard period	64 samples
Modulation scheme	Fixed modulations
Number of subcarriers	1024
OFDM symbols/packet	1
OFDM symbol duration	$(1024 + 64) \times 1/(3.78 \cdot 10^6)$
Space–time coding	
Number of transmitters	2
Number of receivers	1
Channel coding	Turbo convolutional
Constraint length	3
Code rate	0.5
Generator polynomials	7, 5
Turbo interleaver length	464/928/1856/2784
Decoding algorithm	LogMAP
Number of iterations	8
Source coding	MPEG-4 TWINVQ
Bitrates (kbps)	16–64
Audio frame length (ms)	23.22
Sampling rate (kHz)	44.1

Table 10.9: System parameters.

Data + parity bits	928	1856	3712
Source coded bits/packet	372	743	1486
Source coding bitrate (kbps)	16	32	64
Modulation mode	BPSK	QPSK	16-QAM
Minimum channel SNR for 1% FER (dB)	4.3	7.2	12.4
Minimum channel SNR for 5% FER (dB)	2.7	5.8	10.6

of a given bit is to invert this bit consistently in every audio frame and to evaluate the associated SEGSNR degradation [452]. Figure 10.25 shows the bit-error sensitivity of the MPEG-4 TWINVQ encoder of Section 10.2.9 at 16 kbps. This figure shows that the bits representing the gain factors (bit 345–353), the LSF parameters (bit 354–372), and the Bark-

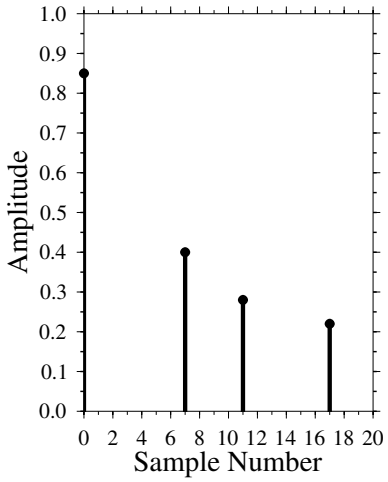

Figure 10.24: COST207 channel impulse response [458].

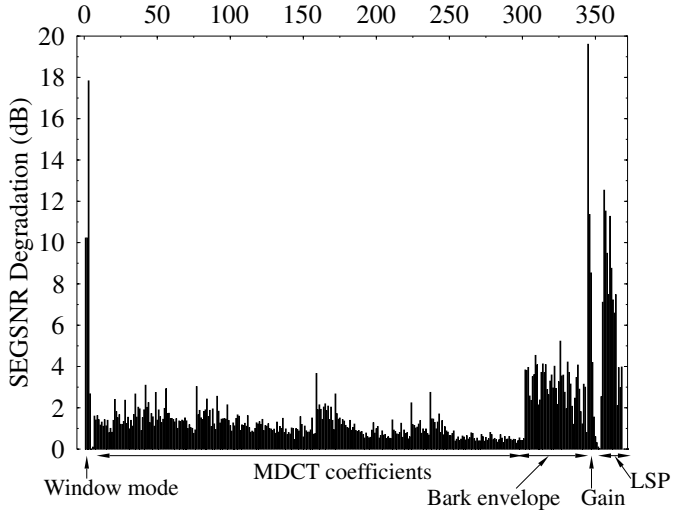

Figure 10.25: SEGSNR degradation versus bit index using MPEG-4 TWINVQ at 16 kbps. The corresponding bit allocation scheme was given in Table 10.1.

envelope (bit 302–343) are more sensitive to channel errors compared to the bits representing the MDCT coefficients (bit 7–301). The bits signalling the window mode used are also very sensitive to transmission errors and hence have to be well protected. The window modes were defined in Section 10.2.

In Section 7.13.5.2 we studied the benefits of invoking multi-class embedded error correction coding assigned to the narrowband AMR speech codec, and in Section 9.6 this was in the context of the AMR-WB codec. By contrast, in the wideband MPEG-4 TWINVQ

system studied here, erroneously received audio frames are dropped and replaced by the previous audio frame since the system is aiming to maintain a high audio quality and the error-infested audio frames would result in catastrophic inter-frame error propagation. Hence the system's audio quality is determined by the tolerable transmission FER, rather than by the BER. In order to determine the highest FER that can be tolerated by the MPEG-4 TWINVQ codec, it was exposed to random frame dropping and the associated SEGSNR degradation as well as the informally assessed perceptual audio degradation was evaluated. The corresponding SEGSNR degradation is plotted in Figure 10.26. Observe in the figure that at a given FER the higher rate modes suffer from a higher SEGSNR degradation. This is because their audio SEGSNR is inherently higher and hence, for example, obliterating one frame in 100 frames inevitably reduces the average SEGSNR more dramatically. We found that the associated audio quality expressed in terms of SEGSNR degradation was deemed to be perceptually objectionable for frame error rates in excess of 1%. Again, frame dropping was preferred, which was found to be more beneficial in audio quality terms than retaining corrupted audio frames.

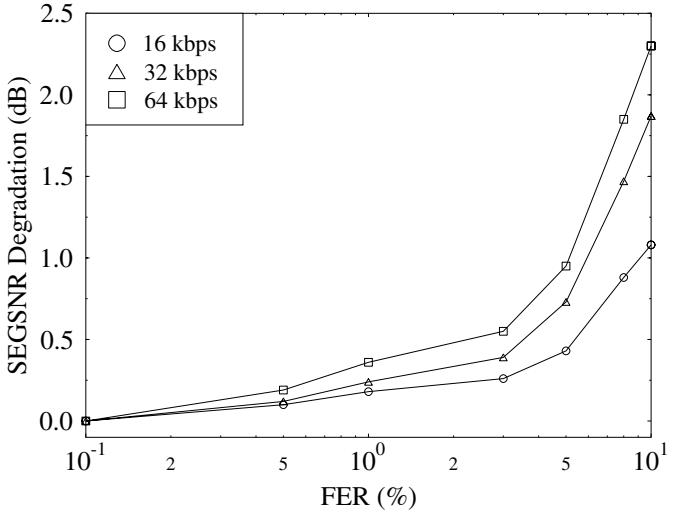

Figure 10.26: SEGSNR degradation versus FER for the MPEG-4 TWINVQ codec of Section 10.2.9, at bitrates of 16, 32 and 64 kbps. The SEGSNR degradation values were obtained, in conjunction with the employment of frame dropping.

For the sake of completeness, Figure 10.27 shows the SEGSNR degradation when inflicting random bit errors but retaining the corrupted audio frames. As expected, the highest bitrate mode of 64 kbps suffered the highest SEGSNR degradation upon increasing the BER, since a higher number of bits per frame was corrupted by errors which considerably degraded the audio quality.

10.5.4 Space–time Coding

Traditionally, the most effective technique of combating fading has been the exploitation of diversity [436]. Diversity techniques can be divided into three broad categories, namely:

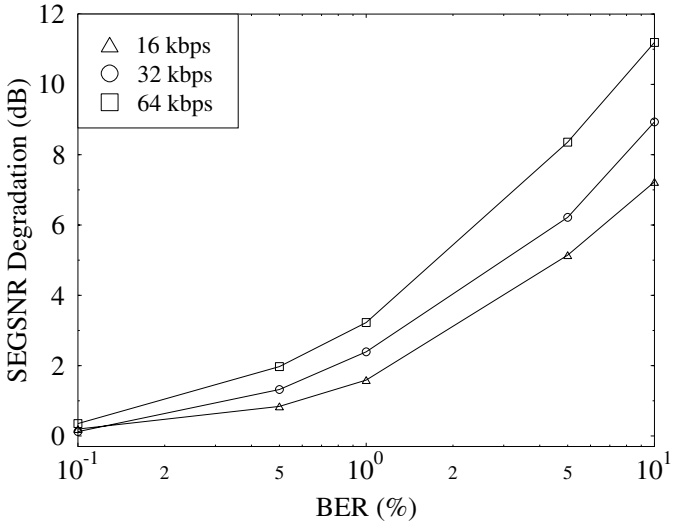

Figure 10.27: SEGSNR degradation versus BER for the MPEG-4 TWINVQ codec of Section 10.2.9 at bitrates of 16, 32 and 64 kbps.

temporal diversity, frequency diversity and spatial diversity. Temporal and frequency diversity schemes [50] introduce redundancy in the time and/or frequency domain, which results in a loss of bandwidth efficiency. Examples of spatial diversity are constituted by multiple transmit- and/or receive-antenna based systems [436]. Transmit-antenna diversity relies on employing multiple antennas at the transmitter and hence it is more suitable for downlink transmissions, since having multiple transmit antennas at the base station is certainly feasible. By contrast, receive-antenna diversity employs multiple antennas at the receiver for acquiring multiple copies of the transmitted signals, which are then combined in order to mitigate the channel-induced fading.

Space–time coding [50, 436] is a specific form of transmit-antenna diversity, which aims to usefully exploit the multipath phenomenon experienced by signals propagating through the dispersive mobile channel. This is achieved by combining multiple transmission antennas in conjunction with appropriate signal processing at the receiver in order to provide diversity and coding gain in comparison to uncoded single-antenna scenarios [442].

In the system investigated, we employ a two-transmitter and one-receiver configuration, in conjunction with turbo channel coding [456]. In Figure 10.28, we show the instantaneous channel SNR experienced by the 512-subcarrier OFDM modem for a one-transmitter, one-receiver scheme and for the space–time block code G_2 [50] using two transmitters and one receiver for transmission over the COST207 channel. The average channel SNR was 10 dB. We can see in Figure 10.28 that the variation of the instantaneous channel SNR for a one-transmitter, one-receiver scheme is severe. The instantaneous channel SNR may become as low as 4 dB due to the deep fades inflicted by the channel. On the other hand, we can see that for the space–time block code G_2 using one receiver the variation of the instantaneous channel SNR is less severe. Explicitly, by employing multiple transmit antennas in Figure 10.28, we have significantly reduced the depth of the channel fades. Whilst

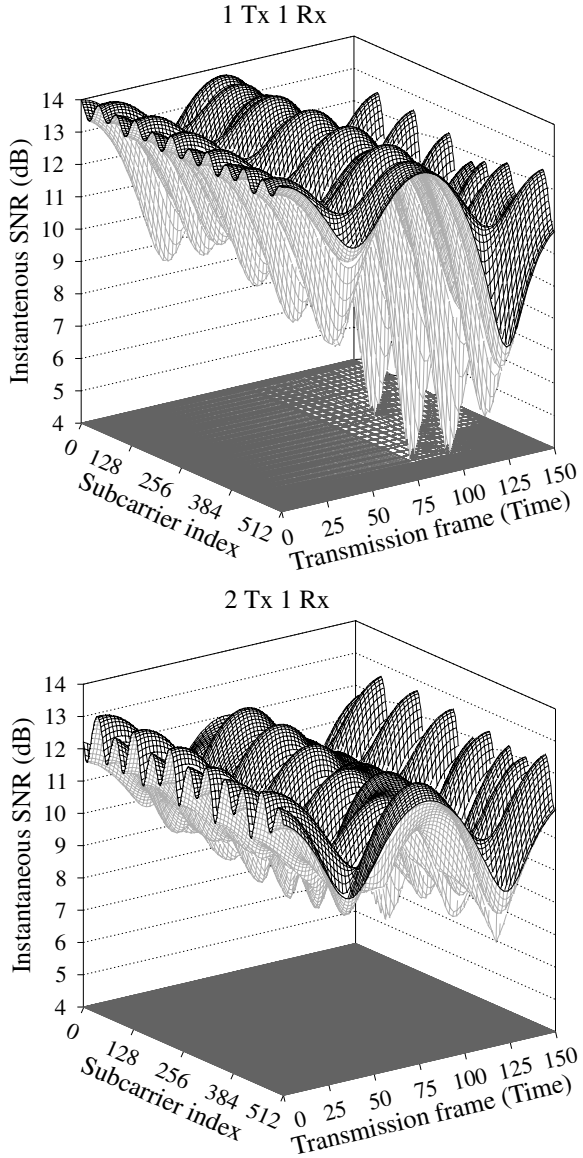

Figure 10.28: Instantaneous channel SNR of 512-subcarrier OFDM symbols for one-transmitter one-receiver (1Tx 1Rx) and for the space–time block code using two-transmitter one-receiver (2Tx 1Rx).

space–time coding endeavours to mitigate the fading-related time- and frequency-domain channel-quality fluctuations at the cost of increasing the transmitter's complexity, adaptive modulation attempts to accommodate these channel quality fluctuations, as will be outlined in the next section.

10.5.5 Adaptive Modulation

In order to accommodate the time- and frequency-domain channel-quality variations seen in case of the 1Tx 1Rx scenario of Figure 10.28, the employment of a multimode system is desirable, which allows us to switch between a set of different source and channel encoders as well as various transmission parameters, depending on the instantaneous channel quality [51].

In the proposed system, we have defined three operating modes which correspond to the uncoded audio bitrates of 16, 32 and 64 kbps. This corresponds to 372, 743 and 1486 bits per 23.22 ms audio frame. In conjunction with half-rate channel coding and also allowing for check sums and signalling overheads, the number of transmitted turbo-coded bits per OFDM symbol is 928, 1856 and 3712 for the three source-coded modes, respectively. Again, these bitrates are also summarised in Table 10.9. Each transmission mode uses a different modulation scheme, depending on the instantaneous channel conditions. It is beneficial if the transceiver can drop its source rate, for example from 64 kbps to 32 kbps and invoke QPSK modulation instead of 16-QAM, while maintaining the same bandwidth. Hence, during good channel conditions the higher throughput, higher audio quality but less robust modes of operation can be invoked, while the more robust but lower audio quality BPSK/16 kbps mode can be applied during degrading channel conditions.

Figure 10.29 shows the FER observed for all three modes of operation, namely for the 512, 1024 and 2048 versus the channel BER that was predicted by the OFDM receiver during the channel quality estimation process. Again, the rationale behind using the FER rather than the BER for estimating the expected channel-quality of the next transmitted OFDM symbol is because the MPEG-4 audio codec has to drop the turbo-decoded received OFDM symbols which contained transmission errors. This is because corrupted audio packets would result in detrimental MPEG-4 decoding error propagation and audio artifacts. A FER of 1% was observed for an estimated input bit error rate of about 4% for the 16 and 32 kbps modes, while a BER of over 5% was tolerable for the 64 kbps mode. This was because the number of bits per OFDM symbol was quadrupled in the 16-QAM mode over which turbo interleaving was invoked compared to the BPSK mode. The quadrupled interleaving length substantially increased the turbo codec's performance.

In Figure 10.30, we show our BPS throughput performance comparison between the sub-band-adaptive and fixed mode OFDM modulation schemes. From the figure we can see that at a low BPS throughput the adaptive OFDM modulation scheme outperforms the fixed OFDM modulation scheme. However, as the BPS throughput of the system increases, the fixed modulation schemes become preferable. This is because adaptive modulation is advantageous when there are high channel-quality variations in the one-transmitter, one receiver scheme. However, we have shown in Figure 10.28 that the channel-quality variations have been significantly reduced by employing two G_2 space–time transmitters. Therefore, the advantages of adaptive modulation eroded due to the reduced channel-quality variations in the space–time coded system. As a consequence, two different-complexity system design principles can be proposed. The first system is the lower-complexity one-transmitter, one receiver scheme, which mitigates the severe variation of the channel quality by employing sub-band adaptive OFDM modulation. By contrast, we can design a more complex G_2 space–time coded system, which employs fixed modulation schemes, since no substantial benefits accrue from employing adaptive modulation once the fading-induced channel-quality fluctuations have been sufficiently mitigated by the G_2 space–time code. In the remainder of

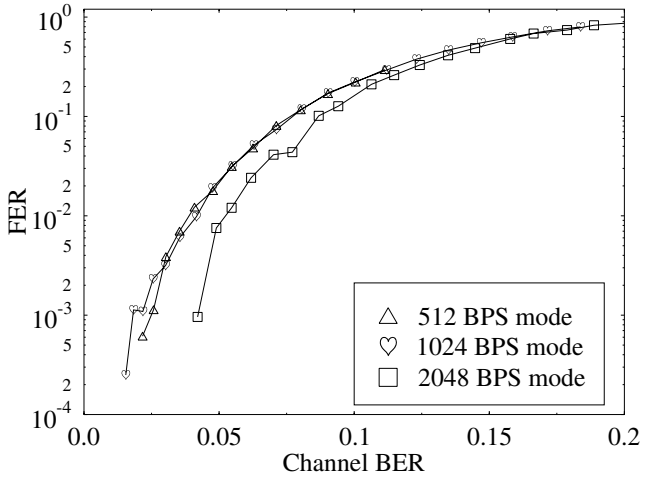

Figure 10.29: FER against channel BER performance of the adaptive OFDM modem conveying 512, 1024 and 2048 BPS for transmission over the channel model of Figure 10.24.

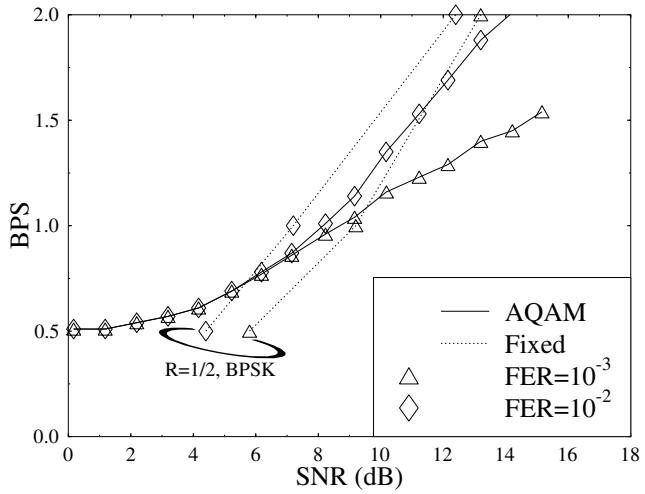

Figure 10.30: BPS performance comparison between the adaptive and fixed-mode OFDM modulation schemes when using space–time coding for transmission over the channel model of Figure 10.24.

this section, we have opted for investigating the performance of the more powerful space–time coded system, requiring an increased complexity.

10.5.6 System Performance

As mentioned before, the detailed subsystem parameters used in our space–time coded OFDM system are listed in Table 10.8. Again, the channel impulse response profile used

was the COST 207 TU channel [458] having four paths and a maximum dispersion of $4.5\ \mu$s, where each path was faded independently at a Doppler frequency of $2.25 \cdot 10^{-6}$ Hz.

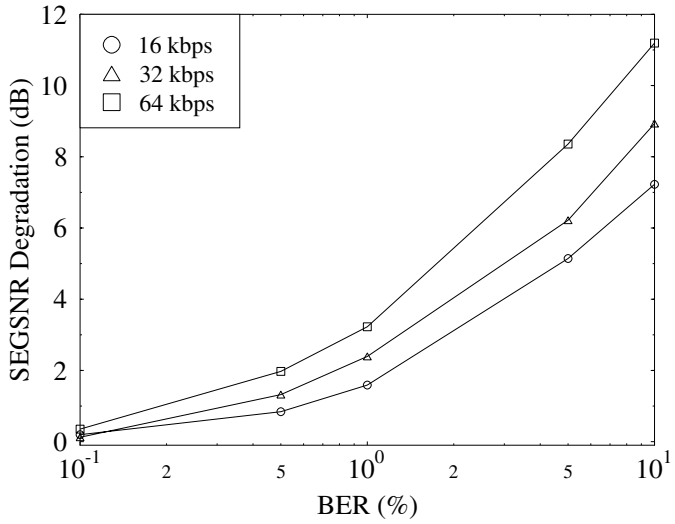

Figure 10.31: BER versus channel SNR performance of the fixed-mode OFDM transceiver of Table 10.8 in conjunction with and without space–time coding, in comparison to the conventional one-transmitter, one-receiver benchmarker for transmission over the channel model of Figure 10.24.

The BER is plotted versus the channel SNR in Figure 10.31 for the three different fixed modes of operation conveying 512, 1024 or 2048 bits per OFDM symbol both with and without space–time coding. The employment of space–time coding improved the system's performance significantly, giving an approximately 3 dB channel SNR improvement at a BER of 1%. As expected, the lowest throughput BPSK/16 kbps mode was more robust in BER terms than the QPSK/32 kbps and the 16-QAM/64 kbps configurations, albeit delivering a lower audio quality. Similar results were obtained in terms of FER versus the channel SNR, which are displayed in Figure 10.32, indicating that the most robust BPSK/16 kbps scheme performed better than the QPSK/32 kbps and 16-QAM/64 kbps configurations, albeit at a lower audio quality.

The overall SEGSNR versus channel SNR performance of the proposed audio transceiver is displayed in Figure 10.33, again employing G_2 space–time coding using two transmitters and one receiver. The lower-complexity benchmarker using the conventional one-transmitter, one-receiver scheme was also characterised in the figure. We observe again that the employment of space–time coding provides a substantial improvement in terms of maintaining an error-free audio performance. Specifically, an SNR advantage of 4 dB was recorded compared to the conventional lower-complexity one-transmitter, one-receiver benchmarker for all three modulation modes. Furthermore, focussing on the three different operating modes using space–time coding, namely on the curves drawn in continuous lines, the 16-QAM/64kbps mode was shown to outperform the QPSK/32kbps scheme in terms of both objective and subjective audio quality for channel SNRs in excess of about 10 dB. At a channel SNR of

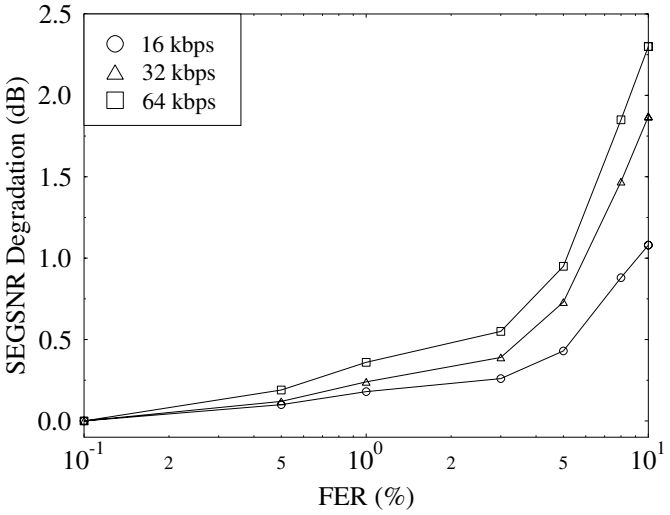

Figure 10.32: FER versus channel SNR performance of the fixed-mode OFDM transceiver of Table 10.8 in conjunction with and without space–time coding, in comparison with the conventional one-transmitter, one-receiver benchmarker for transmission over the channel model of Figure 10.24.

about 9 dB, where the 16-QAM and QPSK SEGSNR curves cross each other in Figure 10.33, it is preferable to invoke the inherently lower audio quality, but unimpaired QPSK mode of operation. Similarly, at a channel SNR around 5 dB, when the QPSK/32 kbps scheme's performance starts to degrade, it is better to invoke the unimpaired BPSK/16 kbps mode of operation in order to avoid the channel-induced audio artifacts.

10.6 Turbo-detected Space–time Trellis Coded MPEG-4 Audio Transceivers

N. S. Othman, S. X. Ng and L. Hanzo

10.6.1 Motivation and Background

In this section a jointly optimised turbo transceiver capable of providing unequal error protection is proposed for employment in an MPEG-4 coded audio transceiver. The transceiver advocated consists of STTC, trellis coded modulation (TCM) and two different-rate non-systematic convolutional codes (NSCs) used for unequal error protection. A benchmarker scheme combining STTC and a single-class protection NSC is used for comparison with the proposed scheme. The audio performance of both schemes will be evaluated when communicating over uncorrelated Rayleigh fading channels. We will demonstrate that the proposed unequal protection turbo-transceiver scheme requires about two dBs lower transmit power than the single-class turbo benchmarker scheme in the context of the MPEG-4 audio

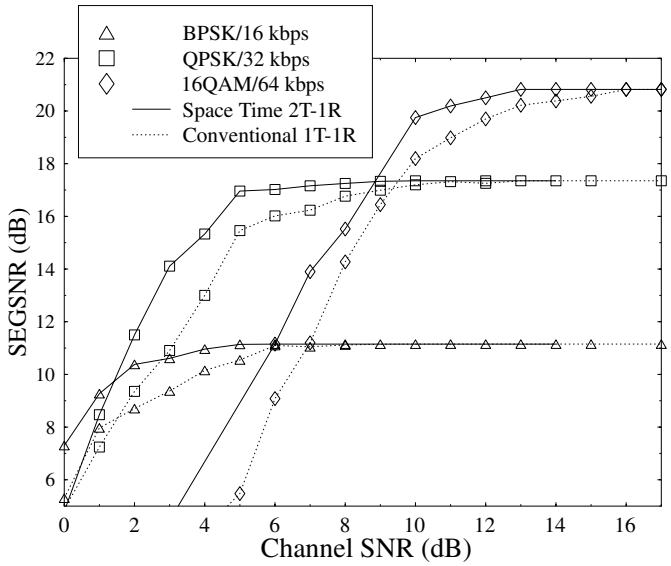

Figure 10.33: SEGSNR versus channel SNR of the MPEG-4 TWINVQ-based fixed-mode OFDM transceiver in conjunction with and without space–time coding, in comparison to the conventional one-transmitter, one-receiver benchmarker.

transceiver when aiming for an effective throughput of 2 bits/symbol, while exhibiting a similar decoding complexity.

The previously characterised MPEG-4 standard [459, 460] defines a comprehensive multimedia content representation scheme that is capable of supporting numerous applications such as: streaming multimedia signals over the Internet/intranet, content-based storage and retrieval, digital multimedia broadcast or mobile communications. The audio-related section of the MPEG-4 standard [461] defines audio codecs covering a wide variety of applications ranging from narrowband low-rate speech to high quality multichannel audio, and from natural sound to synthesised sound effects as a benefit of its object-based approach used for representing the audio signals.

The MPEG-4 GA encoder is capable of compressing arbitrary natural audio signals. One of the key components of the MPEG-4 GA encoder is the T/F compression scheme constituted by the AAC and TWINVQ, which is capable of operating at bitrates ranging from 6 kbps to broadcast quality audio at 64 kbps [459].

The MPEG-4 T/F codec is based on the MPEG-2 AAC standard, extended by a number of additional functionalities such as perceptual noise substitution PNS and LTP for enhancing the achievable compression performance, and combined with the TWINVQ for operation at extremely low bitrates. Another important feature of this codec is its robustness against transmission errors in error-prone propagation channels [462]. The error resilience of the MPEG-4 T/F codec is mainly attributed to the so-called virtual codebook tool (VCB11), reversible variable length coding tool (RVLC) and Huffman codeword reordering tool (HCR) [462, 463], which facilitate the integration of the MPEG-4 T/F codec into wireless systems.

In this study the MPEG-4 audio codec was incorporated in a sophisticated unequal-protection turbo transceiver using joint coding and modulation as inner coding, twin-class convolutional outer coding as well as space–time coding-based spatial diversity as seen in Figure 10.34. Specifically, maximal minimum distance NSCs [464, p. 331] having two different code-rates were used as outer encoders for providing unequal audio protection. On one hand, TCM [465–467] constitutes a bandwidth-efficient joint channel coding and modulation scheme, which was originally designed for transmission over AWGN channels. On the other hand, STTC [466, 468] employing multiple transmit and receive antennas is capable of providing spatial diversity gain. When the spatial diversity order is sufficiently high, the channel's Rayleigh fading envelope is transformed to a Gaussian-like near-constant envelope. Hence, the benefits of a TCM scheme designed for AWGN channels will be efficiently exploited when TCM is concatenated with STTC.

We will demonstrate that significant iteration gains are attained with the aid of the proposed turbo transceiver. The section is structured as follows. In Section 10.6.2 we describe the MPEG-4 audio codec, while in Section 10.6.3 the architecture of the turbo transceiver is described. We elaborate further by characterising the achievable system performance in Section 10.6.4 and conclude in Section 10.6.5.

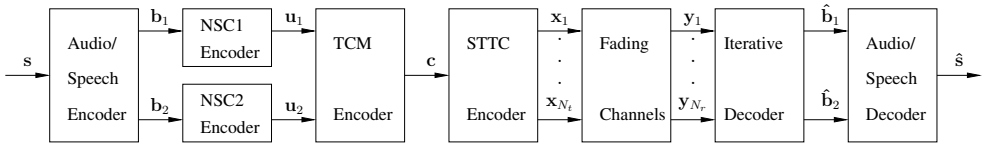

Figure 10.34: Block diagram of the serially concatenated STTC-TCM-2NSC assisted MPEG-4 audio scheme. The notation $\mathbf{s}$, $\hat{\mathbf{s}}$, $\mathbf{b}_i$, $\hat{\mathbf{b}}_i$, $\mathbf{u}_i$, $\mathbf{c}$, $\mathbf{x}_j$ and $\mathbf{y}_k$ denote the vector of the audio source symbol, the estimate of the audio source symbol, the class-i audio bits, the estimates of the class-i audio bits, the encoded bits of class-i NSC encoders, the TCM coded symbols, the STTC coded symbols for transmitter j and the received symbols at receiver k, respectively. Furthermore, N_t and N_r denote the number of transmitters and receivers, respectively. The symbol-based channel interleaver between the STTC and TCM schemes as well as the two bit-based interleavers at the output of NSC encoders are not shown for simplicity. The iterative decoder seen at the right is detailed in Figure 10.35.

10.6.2 Audio Turbo Transceiver Overview

As mentioned above, the MPEG-4 AAC is based on T/F audio coding which provides redundancy reduction by exploiting the correlation between subsequent audio samples of the input signal. Furthermore, the codec uses perceptual modelling of the human auditory system for masking the quantisation distortion of the encoded audio signals by allowing more distortion in those frequency bands where the signal exhibits higher energy peaks and *vice versa* [462, 463].

The MPEG-4 AAC is capable of providing an attractive audio quality versus bitrate performance, yielding high-fidelity audio reconstruction for bitrates in excess of 32 kbps per channel. In the proposed wireless system the MPEG-4 AAC is used for encoding the stereo audio file at a bitrate of 48 kbps. The audio input signal was sampled at 44.1 kHz

and hence results in an audio framelength of 23.22 ms which corresponds to 1024 audio input samples. The compressed audio information is formatted into a packetised bitstream which conveyed one audio frame. In our system, the average transmission frame size is approximately 1116 bits per frame. The audio SEGSNR of this configuration was found to be $S_0 = 16.28$ dB, which gives a transparent audio quality.

It is well recognised that in highly compressed audio bitstreams a low BER may lead to perceptually unacceptable distortion. In order to prevent the complete loss of transmitted audio frames owing to catastrophic error propagation, the most sensitive bits have to be well protected from channel errors. Hence, in the advocated system UEP is employed, where the compressed audio bitstream was partitioned into two sensitivity classes. More explicitly, an audio bit which resulted in a SEGSNR degradation above 16 dB upon its corruption was classified into protection class-1. A range of different audio files were used in our work and the results provided are related to a 60 seconds long excerpt of Mozart's 'Clarinet Concerto (2nd movement – Adagio)'. From the bit sensitivity studies using this audio file as the source, we found that approximately 50% of the total number of MPEG-4 encoded bits falls into class-1.

At the receiver, the output of the turbo transceiver is decoded using the MPEG-4 AAC decoder. During the decoding process, the erroneously received audio frames were dropped and replaced by the previous error-free audio frame for the sake of avoiding an even more dramatic error-infested audio-quality degradation [469, 470].

10.6.3 The Turbo Transceiver

The block diagram of the serially concatenated STTC-TCM-2NSC turbo scheme using a STTC, a TCM and two different-rate NSCs as its constituent codes is depicted in Figure 10.34. Since the number of class-1 audio bits is approximately the same as that of the class-2 audio bits and there are approximately 1116 bits per audio frame, we protect the 558-bit class-1 audio sequence using a rate-R_1 NSC encoder and the 558-bit class-2 sequence using a rate-R_2 NSC encoder. Let us denote the turbo scheme as STTC-TCM-2NSC-1 when the NSC coding rates of $R_1 = k_1/n_1 = 1/2$ and $R_2 = k_2/n_2 = 3/4$ are used. Furthermore, when the NSC coding rates of $R_1 = 2/3$ and $R_2 = 3/4$ are used, we denote the turbo scheme as STTC-TCM-2NSC-2. The code memory of the class-1 and class-2 NSC encoders is $L_1 = 3$ and $L_2 = 3$, respectively. The class-1 and class-2 NSC coded bit sequences are interleaved by two separate bit interleavers before they are fed to the rate $R_3 = 3/4$ TCM [465–467] scheme having a code memory of $L_3 = 3$. Code termination was employed for the NSCs, TCM [465–467] and STTC codecs [466, 468]. The TCM symbol sequence is then symbol-interleaved and fed to the STTC encoder. We invoke a 16-state STTC scheme having a code memory of $L_4 = 4$ and $N_t = 2$ transmit antennas, employing $M = 16$-QAM [467]. The STTC employing $N_t = 2$ requires one 16-QAM-based termination symbol. The overall coding rate is given by $R_{s1} = 1116/2520 \approx 0.4429$ and $R_{s2} = 1116/2152 \approx 0.5186$ for the STTC-TCM-2NSC-1 and STTC-TCM-2NSC-2 schemes, respectively. The effective throughput of the STTC-TCM-2NSC-1 and STTC-TCM-2NSC-2 schemes is $\log_2(M)R_{s1} \approx 1.77$ BPS and $\log_2(M)R_{s2} \approx 2.07$ BPS, respectively.

At the receiver, we employ $N_r = 2$ receive antennas and the received signals are fed to the iterative decoders for the purpose of estimating the audio bit sequences in both class-1 and class-2, as seen in Figure 10.34. The STTC-TCM-2NSC scheme's turbo decoder structure

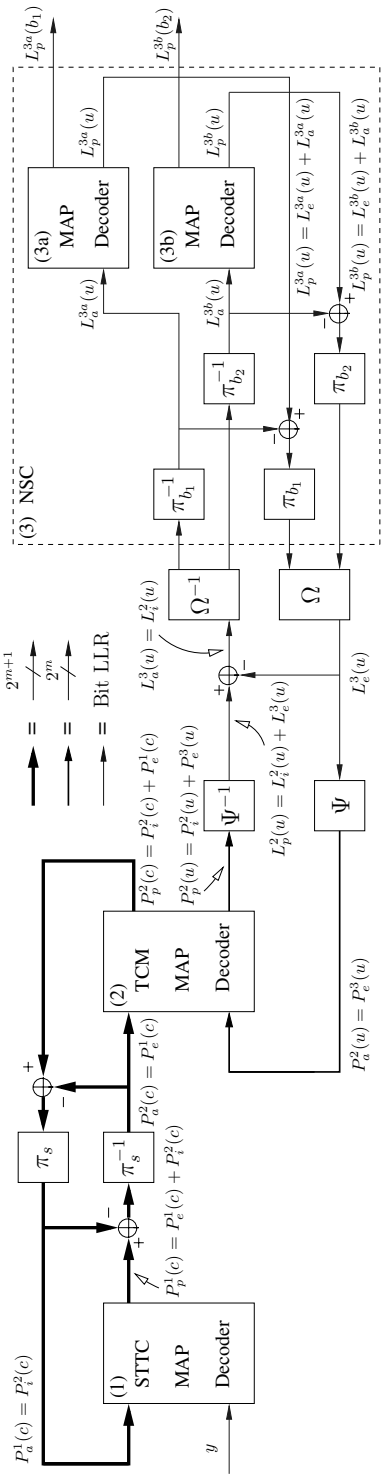

Figure 10.35: Block diagram of the STTC-TCM-2NSC turbo detection scheme seen at the right of Figure 10.40. The notations $\pi_{(s,b_i)}$ and $\pi_{(s,b_i)}^{-1}$ denote the interleaver and deinterleaver, while the subscript s denotes the symbol-based interleaver of TCM and the subscript b_i denotes the bit-based interleaver for class-i NSC. Furthermore, Ψ and Ψ^{-1} denote LLR-to-symbol probability and symbol probability-to-LLR conversion, while Ω and Ω^{-1} denote the parallel-to-serial and serial-to-parallel converter, respectively. The notation m denotes the number of information bits per TCM coded symbol. The thickness of the connecting lines indicates the number of non-binary symbol probabilities spanning from a single LLR per bit to 2^m and 2^{m+1} probabilities [471].

is illustrated in Figure 10.35, where there are four constituent decoders, each labelled with a round-bracketed index. The MAP algorithm [466] operating in the logarithmic-domain are employed by the STTC, TCM and the two NSC decoders, respectively. The notations $P(.)$ and $L(.)$ in Figure 10.35 denote the logarithmic-domain symbol probabilities and the LLR of the bit probabilities, respectively. The notations c, u and b_i in the round brackets $(.)$ in Figure 10.35 denote TCM coded symbols, TCM information symbols and the class-i audio bits, respectively. The specific nature of the probabilities and LLRs is represented by the subscripts a, p, e and i, which denote *a priori*, *a posteriori*, *extrinsic* and *intrinsic* information, respectively. The probabilities and LLRs associated with one of the four constituent decoders having a label of $\{1, 2, 3a, 3b\}$ are differentiated by the identical superscripts of $\{1, 2, 3a, 3b\}$. Note that the superscript 3 is used for representing the two NSC decoders of $3a$ and $3b$. The iterative turbo-detection scheme shown in Figure 10.35 enables an efficient information exchange between STTC, TCM and NSCs constituent codes for the purpose of achieving spatial diversity gain, coding gain, unequal error protection and a near-channel-capacity performance. The information exchange mechanism between each constituent decoders is detailed in [471].

For the sake of benchmarking the scheme advocated, we created a powerful benchmark scheme by replacing the TCM and NSC encoders of Figure 10.34 by a single NSC codec having a coding rate of $R_0 = k_0/n_0 = 1/2$ and a code memory of $L_0 = 6$. We will refer to this benchmarker scheme as the STTC-NSC arrangement. All audio bits are equally protected in the benchmarker scheme by a single NSC encoder and a STTC encoder. A bit-based channel interleaver is inserted between the NSC encoder and STTC encoder. Taking into account the bits required for code termination, the number of output bits of the NSC encoder is $(1116 + k_0 L_0)/R_0 = 2244$, which corresponds to 561 16-QAM symbols. Again, a 16-state STTC scheme having $N_t = 2$ transmit antennas is employed. After code termination, we have $561 + 1 = 562$ 16-QAM symbols or $4(562) = 2248$ bits in a transmission frame at each transmit antenna. The overall coding rate is given by $R = 1116/2248 \approx 0.4964$ and the effective throughput is $\log_2(16)R \approx 1.99$ BPS, both of which are very close to the corresponding values of the STTC-TCM-2NSC-2 scheme. A decoding iteration of the STTC-NSC benchmarker scheme is comprised of a STTC decoding and a NSC decoding step.

We will quantify the decoding complexity of the proposed STTC-TCM-2NSC scheme and that of the benchmarker scheme using the number of decoding trellis states. The total number of decoding trellis states per iteration for the proposed scheme employing 2 NSC decoders having a code memory of $L_1 = L_2 = 3$, TCM having $L_3 = 3$ and STTC having $L_4 = 4$ is given by $S = 2^{L_1} + 2^{L_2} + 2^{L_3} + 2^{L_4} = 40$. By contrast, the total number of decoding trellis states per iteration for the benchmarker scheme having a code memory of $L_0 = 6$ and STTC having $L_4 = 4$ is given by $S = 2^{L_0} + 2^{L_4} = 80$. Therefore, the complexity of the proposed STTC-TCM-2NSC scheme having two iterations is equivalent to that of the benchmarker scheme having a single iteration, which corresponds to 80 decoding states.

10.6.4 Turbo Transceiver Performance Results

In this section we evaluate the performance of the proposed MPEG-4 based audio transceiver schemes using both the achievable BER and the attainable SEGSNR.

Figures 10.36 and 10.37 depict the BER versus SNR per bit, namely E_b/N_0, performance of the 16-QAM-based STTC-TCM-2NSC-1 and STTC-TCM-2NSC-2 schemes, respectively, when communicating over uncorrelated Rayleigh fading channels. As we can observe from Figures 10.36 and 10.37, the gap between the BER performance of the class-1 and class-2 audio bits is wider for STTC-TCM-2NSC-1 compared to the STTC-TCM-2NSC-2 scheme. More explicitly, the class-1 audio bits of STTC-TCM-2NSC-1 have a higher protection at the cost of a lower throughput compared to the STTC-TCM-2NSC-2 scheme. However, the BER performance of the class-2 audio bits of the STTC-TCM-2NSC-1 arrangement is approximately 0.5 dB poorer than that of STTC-TCM-2NSC-2 at BER $= 10^{-5}$.

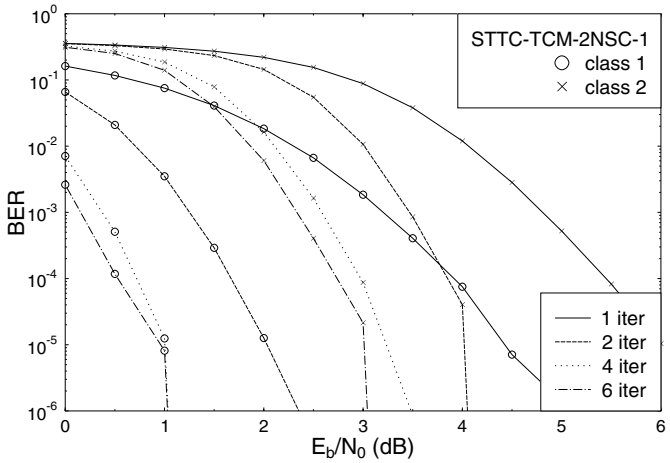

Figure 10.36: BER versus E_b/N_0 performance of the 16-QAM-based STTC-TCM-2NSC-1 assisted MPEG-4 audio scheme when communicating over uncorrelated Rayleigh fading channels. The effective throughput was 1.77 BPS.

Let us now study the audio SEGSNR performance of the schemes in Figures 10.38 and 10.39. As we can see from Figure 10.38, the SEGSNR performance of STTC-TCM-2NSC-1 is inferior in comparison to that of STTC-TCM-2NSC-2, despite providing a higher protection for the class-1 audio bits. More explicitly, STTC-TCM-2NSC-2 requires E_b/N_0 = 2.5 dB, while STTC-TCM-2NSC-1 requires E_b/N_0 = 3 dB, when having an audio SEGSNR in excess of 16 dB after the fourth turbo iteration. Hence, the audio SEGSNR performance of STTC-TCM-2NSC-1 is 0.5 dB poorer than that of STTC-TCM-2NSC-2 after the fourth iteration. Note that the BER of the class-1 and class-2 audio bits for the corresponding values of E_b/N_0, SEGSNR and iteration index is less than 10^{-7} and 10^{-4}, respectively, for the two different turbo schemes. After the sixth iteration, the SEGSNR performance of both turbo schemes becomes quite similar since the corresponding BER is low. These results demonstrate that the MPEG-4 audio decoder requires a very low BER for both class-1 and class-2 audio bits when aiming for a SEGSNR above 16 dB. In this context it is worth mentioning that RSCs [464–466] are capable of achieving a higher iteration gain, but suffer from an error floor. Due to this reason the SEGSNR performance of the schemes employing RSCs instead of NSCs was found to be poorer. The SEGSNR results of the turbo schemes

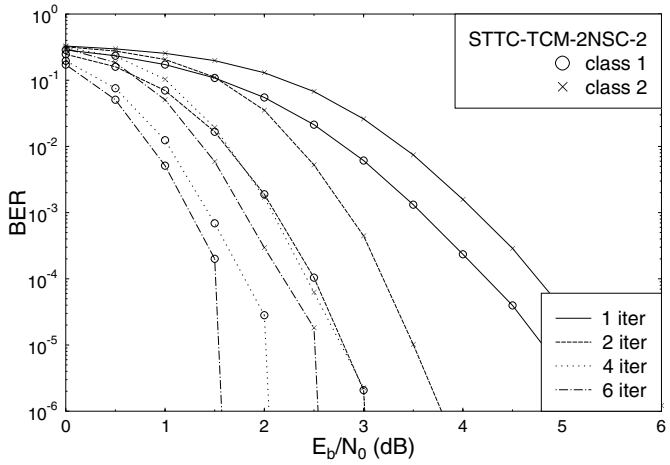

Figure 10.37: BER versus E_b/N_0 performance of the 16-QAM-based STTC-TCM-2NSC-2 assisted MPEG-4 audio scheme when communicating over uncorrelated Rayleigh fading channels. The effective throughput was 2.07 BPS.

employing RSCs instead of NSCs as the outer code were not shown here for reasons of space economy.

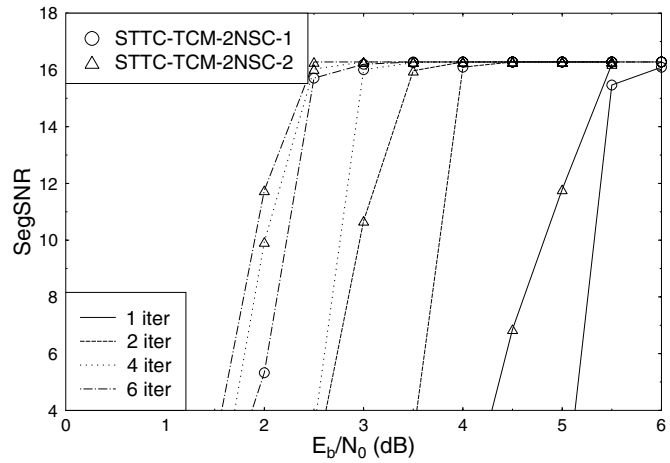

Figure 10.38: Average SEGSNR versus E_b/N_0 performance of the 16-QAM-based STTC-TCM-2NSC assisted MPEG-4 audio scheme when communicating over uncorrelated Rayleigh fading channels. The effective throughput of STTC-TCM-2NSC-1 and STTC-TCM-2NSC-2 was 1.77 and 2.07 BPS, respectively.

Figure 10.39 portrays the SEGSNR versus E_b/N_0 performance of the STTC-NSC audio benchmarker scheme, when communicating over uncorrelated Rayleigh fading channels. Note that if we reduce the code memory of the NSC constituent code of the STTC-NSC

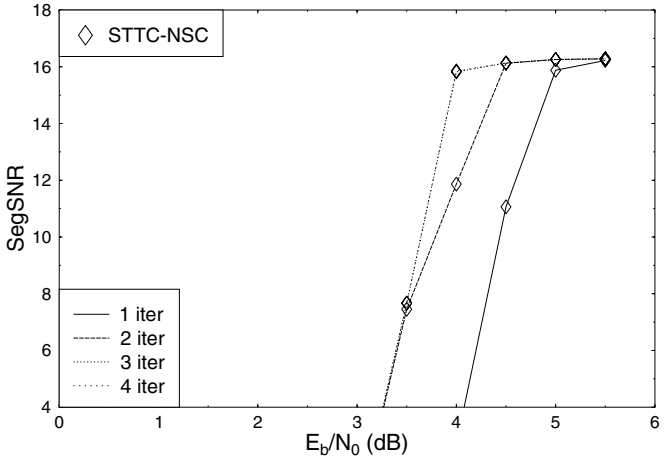

Figure 10.39: Average SEGSNR versus E_b/N_0 performance of the 16-QAM-based STTC-NSC assisted MPEG-4 audio benchmarker scheme when communicating over uncorrelated Rayleigh fading channels. The effective throughput was 1.99 BPS.

benchmarker arrangement from $L_0 = 6$ to 3, the achievable performance becomes poorer, as expected. If we increased L_0 from 6 to 7 (or higher), the decoding complexity would increase significantly, while the attainable best possible performance is only marginally increased. Hence, the STTC-NSC scheme having $L_0 = 6$ constitutes a good benchmarker scheme in terms of its performance versus complexity trade-offs. It is shown in Figures 10.38 and 10.39 that the first iteration-based performance of the STTC-NSC benchmarker scheme is better than that of the proposed STTC-TCM-2NSC arrangements. However, at the same decoding complexity of 160 or 240 trellis decoding states STTC-TCM-2NSC-2 having 4 or 6 iterations performs approximately 2 or 1.5 dB better than the STTC-NSC arrangement having 2 or 3 iterations, respectively.

It is worth mentioning that other joint coding and modulation schemes directly designed for fading channels such as, for example, bit interleaved coded modulation (BICM) [466,467, 472] were outperformed by the TCM-based scheme, since the STTC arrangement rendered the error statistics more Gaussian-like [473].

10.6.5 MPEG-4 Turbo Transceiver Summary

In conclusion, a jointly optimised audio source-coding, outer unequal protection NSC channel-coding, inner TCM and spatial diversity aided STTC turbo transceiver was proposed for employment in a MPEG-4 wireless audio transceiver. With the aid of two different-rate NSCs the audio bits were protected differently according to their error sensitivity. The employment of TCM improved the bandwidth efficiency of the system and by utilising STTC spatial diversity was attained. The performance of the proposed STTC-TCM-2NSC scheme was enhanced with the advent of an efficient iterative joint decoding structure. The high-compression MPEG-4 audio decoder is sensitive to transmission errors and hence it was found to require a low BER for both classes of audio bits in order to attain a perceptually

pleasing, artefact-free audio quality. The proposed twin-class STTC-TCM-2NSC scheme performs approximately 2 dB better in terms of the required E_b/N_0 than the single-class STTC-NSC audio benchmarker.

10.7 Turbo-detected Space–time Trellis Coded MPEG-4 Versus AMR-WB Speech Transceivers

N. S. Othman, S. X. Ng and L. Hanzo

10.7.1 Motivation and Background

The MPEG-4 TWINVQ audio codec and the AMR-WB speech codec are investigated in the context of the jointly optimised turbo transceiver of Figure 10.40, which is capable of providing unequal error protection. Apart from replacing the MPEG-4 codec by the AMR-WB scheme, the transceiver advocated follows the structure of Figure 10.34 and consists of serially concatenated STTC, TCM and two different-rate NSCs used for unequal error protection. A benchmarker scheme combining STTC and a single-class protection NSC is used for comparison with the proposed scheme. The audio and speech performance of both schemes is evaluated when communicating over uncorrelated Rayleigh fading channels. We will demonstrate that an E_b/N_0 value of about 2.5 (3.5) dB is required for near-unimpaired audio (speech) transmission, which is about 3.07 (4.2) dB from the capacity of the system.

Joint source-channel coding (JSCC) has been receiving significant research attention in the context of both delay- and complexity-constrained transmission scenarios. JSCC aims to design the source codec and channel codec jointly for the sake of achieving the highest possible system performance. As was argued in [473], this design philosophy does not contradict the classic Shannonian source and channel coding separation theorem. This is because instead of considering perfectly lossless Shannonian entropy coders for source coding and transmitting their bitstreams over Gaussian channels, we consider low-bitrate lossy audio and speech codecs, as well as Rayleigh-fading channels. Since the bitstreams of the speech and audio encoders are subjected to errors during wireless transmission, it is desirable to provide stronger error protection for the audio bits, which have a substantial effect on the objective or subjective quality of the reconstructed speech or audio signals. UEP is a particular manifestation of JSCC which offers a mechanism to match the error protection capabilities of channel coding schemes having different error correction capabilities to the differing bit-error sensitivities of the speech or audio bits [474].

Speech services are likely to remain the most important ones in wireless systems. However, there is an increasing demand for high-quality speech transmissions in multimedia applications, such as video-conferencing [469]. Therefore, an expansion of the speech bandwidth from the 300–3400 Hz range to a wider bandwidth of 50–7000 Hz is a key factor in meeting this demand. This is because the low-frequency enhancement ranging from 50–200 Hz contributes to the increased naturalness, presence and comfort, whilst the higher-frequency extension spanning from 3400–7000 Hz provides a better fricative differentiation and therefore a higher intelligibility. A bandwidth of 50–7000 Hz not only improves the intelligibility and naturalness of speech, but also adds an impression of

transparent communication and eases speaker recognition. The AMR-WB voice codec has become a 3GPP standard, which provides a superior speech quality [475].

Supporting high-quality multimedia services over wireless communication channels requires the development of techniques for transmitting not only speech, but also video, music and data. Therefore, in the field of audio-coding, high-quality, high-compression and highly error-resilient audio-coding algorithms are required. The MPEG-4 TWINVQ scheme is a low-bitrate audio-coding technique that achieves a high audio quality under error-free transmission conditions at bitrates below 40 kbps [461]. In order to render this codec applicable to wireless systems, which typically exhibit a high BER, powerful turbo transceivers are required.

TCM [465–467] constitutes a bandwidth-efficient joint channel coding and modulation scheme, which was originally designed for transmission over AWGN channels. STTC [466, 468] is a joint spatial diversity and channel coding technique. STTC may be efficiently employed in an effort to mitigate the effects of Rayleigh fading channels and render them Gaussian-like for the sake of supporting the operation of a TCM code. A sophisticated unequal-protection turbo transceiver using twin-class convolutional outer coding, as well as joint coding and modulation as inner coding combined with STTC-based spatial diversity scheme was designed for MPEG-4 video telephony in [471, 473]. Specifically, maximal minimum distance NSCs [464, p. 331] having two different code-rates were used as outer encoders for providing unequal MPEG-4 video protection. Good video quality was attained at a low SNR and medium complexity by the proposed transceiver. By contrast, in this section we study the achievable performance of the AMR-WB and the MPEG-4 TWINVQ speech and audio codecs in conjunction with the sophisticated unequal-protection turbo transceiver of [471, 473].

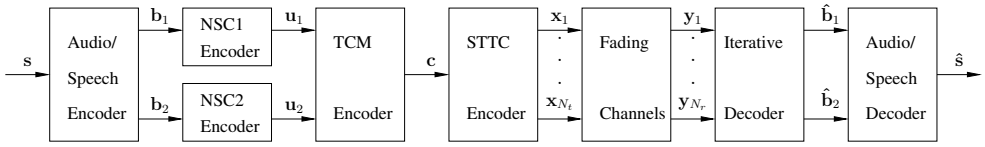

Figure 10.40: Block diagram of the serially concatenated STTC-TCM-2NSC assisted audio/speech scheme. The notation $\mathbf{s}$, $\hat{\mathbf{s}}$, $\mathbf{b}_i$, $\hat{\mathbf{b}}_\mathbf{i}$, $\mathbf{u}_i$, $\mathbf{c}$, $\mathbf{x}_j$ and $\mathbf{y}_k$ denote the vector of the audio/speech source symbol, the estimate of the audio/speech source symbol, the class-i audio/speech bits, the estimates of the class-i audio/speech bits, the encoded bits of class-i NSC encoders, the TCM coded symbols, the STTC coded symbols for transmitter j and the received symbols at receiver k, respectively. Furthermore, N_t and N_r denote the number of transmitters and receivers, respectively. The symbol-based channel interleaver between the STTC and TCM schemes as well as the two bit-based interleavers at the output of NSC encoders are not shown for simplicity. The iterative decoder seen at the right is detailed in Figure 10.43.

10.7.2 The AMR-WB Codec's Error Sensitivity

The synthesis filter's excitation signal in the AMR-WB codec is based on the ACELP algorithm, supporting nine different speech codec modes having bitrates of 23.85, 23.05, 19.85, 18.25, 15.85, 14.25, 12.65, 8.85 and 6.6 kbps [475]. Like most ACELP-based

algorithms, the AMR-WB codec interprets 20 ms segments of speech as the output of a linear synthesis filter synthesised from an appropriate excitation signal. The task of the encoder is to optimise the filter as well as the excitation signal and then represent both as efficiently as possible with the aid of a frame of binary bits. At the decoder, the encoded bit-based speech description is used to synthesise the speech signal by inputting the excitation signal to the synthesis filter, thereby generating the speech segment. Again, each AMR-WB frame represents 20 ms of speech, producing 317 bits at a bitrate of 15.85 kbps. The codec parameters that are transmitted over the noisy channel include the so-called ISPs, the adaptive codebook delay (pitch delay), the algebraic codebook excitation index and the jointly vector quantised pitch gains as well as algebraic codebook gains.

Most source coded bitstreams contain certain bits that are more sensitive to transmission errors than others. A common approach used for quantifying the sensitivity of a given bit is to consistently invert this bit in every speech or audio frame and evaluate the associated SEGSNR degradation [470]. The SEGSNR degradation is computed by subtracting from the SEGSNR recorded under error-free conditions the corresponding value when there are channel-induced bit-errors.

The error sensitivity of the various encoded bits in the AMR-WB codec determined in this way is shown in Figure 10.41. The results are based on samples taken from the EBU SQAM CD, sampled at 16 kHz and encoded at 15.85 kbps. It can be observed that the bits representing the ISPs, the adaptive codebook delay, the algebraic codebook index and the vector quantised gain are fairly error sensitive. The least sensitive bits are related to the fixed codebook's excitation pulse positions, as shown in Figure 10.41. This is because when one of the fixed codebook index bits is corrupted, the codebook entry selected at the decoder will differ from that used in the encoder only in the position of one of the non-zero excitation pulses. Therefore, the corrupted excitation codebook entry will be similar to the original one. Hence, the algebraic codebook structure used in the AMR-WB codec is quite robust to channel errors.

10.7.3 The MPEG-4 TWINVQ Codec's Error Sensitivity

The MPEG-4 TWINVQ scheme is a transform coder that uses the MDCT [461] for transforming the input signal into the frequency-domain transform coefficients. The input signal is classified into one of three modes, each associated with a different transform window size, namely a long, medium or short window, catering for different input signal characteristics. The MDCT coefficients are normalised by the spectral envelope information obtained through the LPC analysis of the signal. Then the normalised coefficients are interleaved and divided into sub-vectors by using the so-called interleave and division technique of [461], and all sub-vectors are encoded separately by the VQ modules.

Bit error sensitivity investigations were performed in the same manner, as described in the previous section. Figure 10.42 shows the error sensitivity of the various bits of the MPEG-4 TWINVQ codec for a bitrate of 32 kbps. The results provided are based on a 60 seconds long excerpt of Mozart's 'Clarinet Concerto (2nd movement – Adagio)'. This stereo audio file was sampled at 44.1 kHz and again, encoded at 32 kbps. Since the analysis frame length is 23.22 ms, which corresponds to 1024 audio input samples, there are 743 encoded bits in each frame. This figure shows that the bits representing the gain factors, the LSF parameters, and the Bark-envelope are more sensitive to channel errors, compared to the bits representing

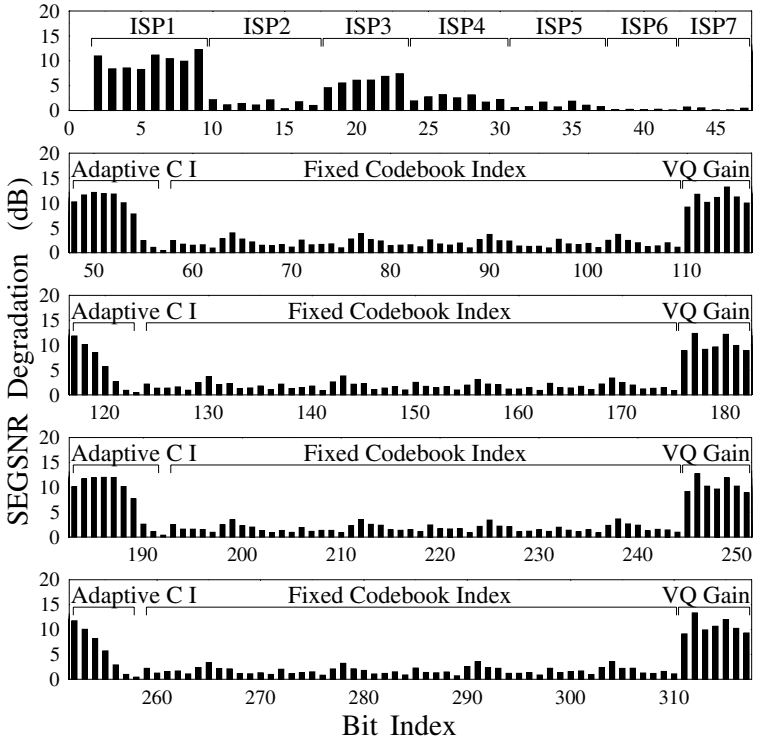

Figure 10.41: SEGSNR degradations versus bit index due to inflicting 100% BER in the 317-bit, 20 ms AMR-WB frame.

the MDCT coefficients. The bits signalling the window mode used are also very sensitive to transmission errors and hence have to be well protected. The proportion of sensitive bits was only about 10%. This robustness is deemed to be a benefit of the weighted vector-quantisation procedure which uses a fixed-length coding structure as opposed to using an error-sensitive variable-length structure, where transmission errors would result in a loss of synchronisation.

10.7.4 The Turbo Transceiver

Once the bit error sensitivity of the audio/speech codecs was determined, the bits of the AMR-WB and the MPEG-4 TWINVQ codec are protected according to their relative importance. Figure 10.40 shows the schematic of the serially concatenated STTC-TCM-2NSC turbo scheme using a STTC and a TCM scheme as well as two different-rate NSCs as its constituent codes. Let us denote the turbo scheme using the AMR-WB codec as STTC-TCM-2NSC-AMR-WB, whilst STTC-TCM-2NSC-TVQ refers to the turbo scheme using the MPEG-4 TWINVQ as the source codec. For comparison, both schemes protect 25% of the most sensitive bits in class-1 using an NSC code rate of $R_1 = k_1/n_1 = 1/2$. By contrast, the remaining 75% of the bits in class-2 are protected by an NSC scheme having a rate of $R_2 = k_2/n_2 = 3/4$. The code memory of the class-1 and class-2 encoders is $L_1 = 3$ and $L_2 = 3$, respectively. The class-1 and class-2 NSC coded bit sequences are interleaved by two

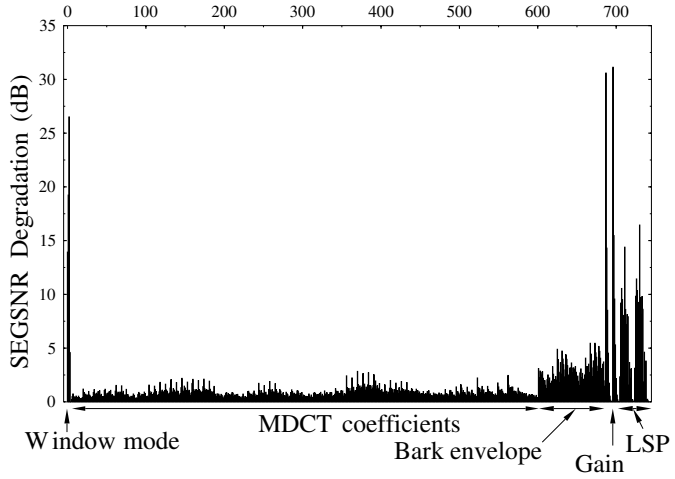

Figure 10.42: SEGSNR degradations due to inflicting a 100% BER in the 743-bit, 23.22 ms MPEG-4 TWINVQ frame.

separate bit interleavers before they are fed to the rate $R_3 = 3/4$ TCM scheme [465–467] having a code memory of $L_3 = 3$. Code termination was employed for the NSCs, as well as for the TCM [465–467] and STTC codecs [466, 468]. The TCM symbol sequence is then symbol-interleaved and fed to the STTC encoder as seen in Figure 10.43. We invoke a 16-state STTC scheme having a code memory of $L_4 = 4$ and $N_t = 2$ transmit antennas, employing $M = 16$-QAM [467]. The STTC scheme employing $N_t = 2$ requires a single 16-QAM-based termination symbol. In the STTC-TCM-2NSC-AMR-WB scheme, 25% of the bits that are classified into class-1 includes 23 header bits, which gives a total of 340 NSC1-encoded bits. In the ITU stream format [476], the header bits of each frame include the frame types and the window-mode used.

Hence, the overall coding rate of the STTC-TCM-2NSC-AMR-WB scheme becomes $R_{\rm AMRWB} = 340/720 \approx 0.4722$. By contrast, the overall coding rate of the STTC-TCM-2NSC-TVQ scheme is $R_{\rm TVQ} = 744/1528 \approx 0.4869$. The effective throughput of the STTC-TCM-2NSC-AMR-WB and STTC-TCM-2NSC-TVQ schemes is $\log_2(M) \cdot R_{\rm AMRWB} \approx 1.89$ BPS and $\log_2(M) \cdot R_{\rm TVQ} \approx 1.95$ BPS, respectively.

At the receiver, we employ $N_r = 2$ receive antennas and the received signals are fed to the iterative decoders for the purpose of estimating the audio bit sequences in both class-1 and class-2, as seen in Figure 10.40. The STTC-TCM-2NSC scheme's turbo decoder structure is illustrated in Figure 10.43, where there are four constituent decoders, each labelled with a round-bracketed index. The MAP algorithm [466] operating in the logarithmic-domain is employed by the STTC and TCM schemes as well as by the two NSC decoders, respectively. The iterative turbo-detection scheme shown in Figure 10.43 enables an efficient information exchange between the STTC, TCM and NSCs constituent codes for the purpose of achieving spatial diversity gain, coding gain, unequal error protection and a near-channel-capacity performance. The information exchange mechanism between each constituent decoders is detailed in [471].

For the sake of benchmarking both audio schemes advocated, we created a powerful benchmark scheme for each of them by replacing the TCM and NSC encoders of Figure 10.40

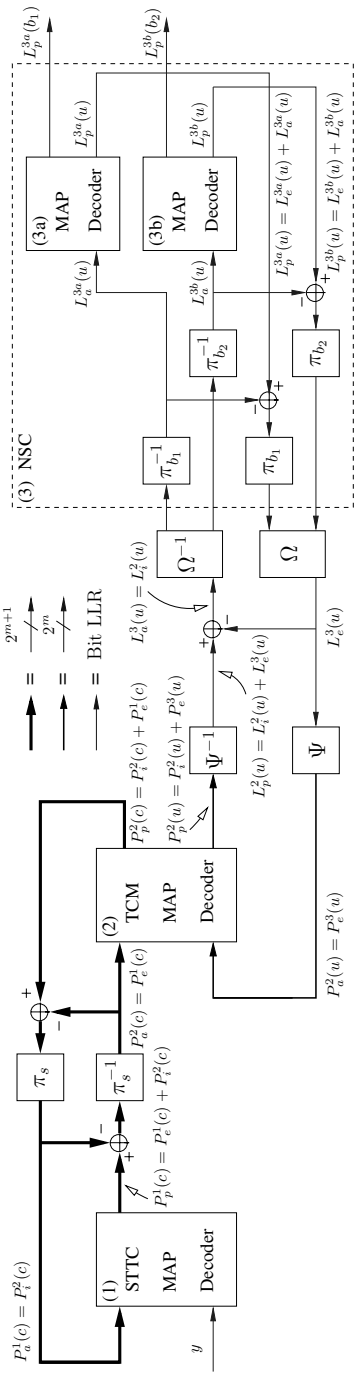

Figure 10.43: Block diagram of the STTC-TCM-2NSC turbo detection scheme seen at the right of Figure 10.40. The notations $\pi_{(s,b_i)}$ and $\pi_{(s,b_i)}^{-1}$ denote the interleaver and de-interleaver, while the subscript s denotes the symbol-based interleaver of TCM and the subscript b_i denotes the bit-based interleaver for class-i NSC. Furthermore, Ψ and Ψ^{-1} denote LLR-to-symbol probability and symbol probability-to-LLR conversion, while Ω and Ω^{-1} denote the parallel-to-serial and serial-to-parallel converter, respectively. The notation m denotes the number of information bits per TCM coded symbol [471].

by a single-class NSC codec having a coding rate of $R_0 = k_0/n_0 = 1/2$ and a code memory of $L_0 = 6$. Note that if we reduce the code memory of the NSC constituent code of the STTC-NSC benchmarker arrangement from $L_0 = 6$ to 3, the achievable performance becomes poorer, as expected. If we increased L_0 from 6 to 7 (or higher), the decoding complexity would double, while the attainable performance is only marginally increased. Hence, the STTC-NSC scheme having $L_0 = 6$ constitutes a good benchmarker scheme in terms of its performance versus complexity trade-offs. We will refer to this benchmarker scheme as the STTC-NSC-TVQ and the STTC-NSC-AMR-WB arrangement designed for the audio and the speech transceiver, respectively. Again, all audio and speech bits are equally protected in the benchmarker scheme by a single NSC encoder and a STTC encoder. A bit-based channel interleaver is inserted between the NSC encoder and STTC encoder. Taking into account the bits required for code termination, the number of output bits of the NSC encoder of the STTC-NSC-TVQ benchmarker scheme is $(744 + k_0 L_0)/R_0 = 1500$, which corresponds to 375 16-QAM symbols. By contrast, in the STTC-NSC-AMR-WB scheme the number of output bits after taking into account the bits required for code termination becomes $(340 + k_0 L_0)/R_0 = 692$, which corresponds to 173 16-QAM symbols. Again, a 16-state STTC scheme having $N_t = 2$ transmit antennas is employed. After code termination, we have $375 + 1 = 376$ 16-QAM symbols or $4(376) = 1504$ bits in a transmission frame at each transmit antenna for the STTC-NSC-TVQ. The overall coding rate is given by $R_{\mathrm{TVQ}-b} = 744/1504 \approx 0.4947$ and the effective throughput is $\log_2(16) R_{\mathrm{TVQ}-b} \approx 1.98$ BPS, both of which are very close to the corresponding values of the STTC-TCM-2NSC-TVQ scheme. Similarly, for the STTC-NSC-AMR-WB scheme, after code termination, we have $173 + 1 = 174$ 16-QAM symbols or $4(174) = 696$ bits in a transmission frame at each transmit antenna. This gives the overall coding rate as $R_{\mathrm{AMRWB}-b} = 340/696 \approx 0.4885$ and the effective throughput becomes $\log_2(16) R_{\mathrm{AMRWB}-b} \approx 1.95$ BPS. Again, both of the values are close to the corresponding values of the STTC-TCM-2NSC-AMR-WB scheme. A decoding iteration of each of the STTC-NSC benchmarker schemes is comprised of a STTC decoding and a NSC decoding step.

We will quantify the decoding complexity of the proposed STTC-TCM-2NSC schemes and that of its corresponding benchmarker schemes using the number of decoding trellis states. The total number of decoding trellis states per iteration of the proposed scheme employing two NSC decoders having a code memory of $L_1 = L_2 = 3$, using the TCM scheme having $L_3 = 3$ and the STTC arrangement having $L_4 = 4$, becomes $S = 2^{L_1} + 2^{L_2} + 2^{L_3} + 2^{L_4} = 40$. By contrast, the total number of decoding trellis states per iteration for the benchmarker scheme having a code memory of $L_0 = 6$ and for the STTC having $L_4 = 4$ is given by $S = 2^{L_0} + 2^{L_4} = 80$. Therefore, the complexity of the proposed STTC-TCM-2NSC scheme having two iterations is equivalent to that of the benchmarker scheme having a single iteration, which corresponds to 80 decoding states.

10.7.5 Performance Results

In this section we comparatively study the performance of the audio and speech transceiver using the SEGSNR metric.

Figures 10.44 and 10.45 depict the audio SEGSNR performance of the STTC-TCM-2NSC-TVQ and that of its corresponding STTC-NSC-TVQ benchmarker schemes, respectively, when communicating over uncorrelated Rayleigh fading channels. It can be seen from

Figures 10.44 and 10.45 that the non-iterative single-detection based performance of the STTC-NSC-TVQ benchmarker scheme is better than that of the STTC-TCM-2NSC assisted MPEG-4 TWINVQ audio scheme. However, at the same decoding complexity quantified in terms of the number of trellis decoding states the STTC-TCM-2NSC-TVQ arrangement performs approximately 0.5 dB better in terms of the required channel E_b/N_0 value than the STTC-NSC-TVQ benchmarker scheme, both exhibiting a SEGSNR of 13.8 dB. For example, at the decoding complexity of 160 trellis decoding states, this corresponds to the STTC-TCM-2NSC-TVQ scheme's fourth iteration, whilst in the STTC-NSC-TVQ scheme this corresponds to the second iteration. Therefore, we observe in Figures 10.44 and 10.45 that the STTC-TCM-2NSC-TVQ arrangement performs by 0.5 dB better in terms of the required channel E_b/N_0 value than its corresponding benchmarker scheme.

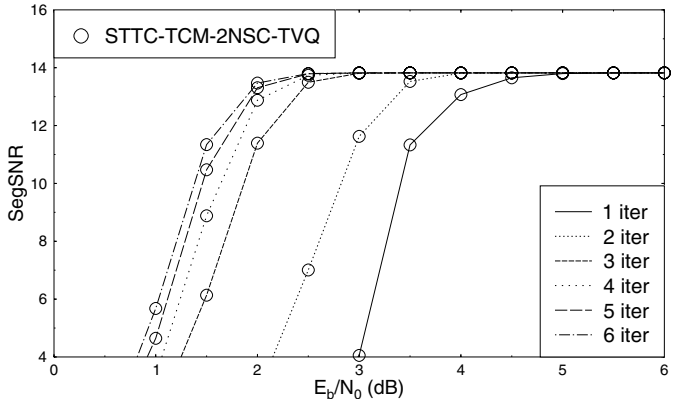

Figure 10.44: Average SEGSNR versus E_b/N_0 performance of the 16-QAM-based STTC-TCM-2NSC assisted MPEG-4 TWINVQ audio scheme when communicating over uncorrelated Rayleigh fading channels. The effective throughput was 1.95 BPS.

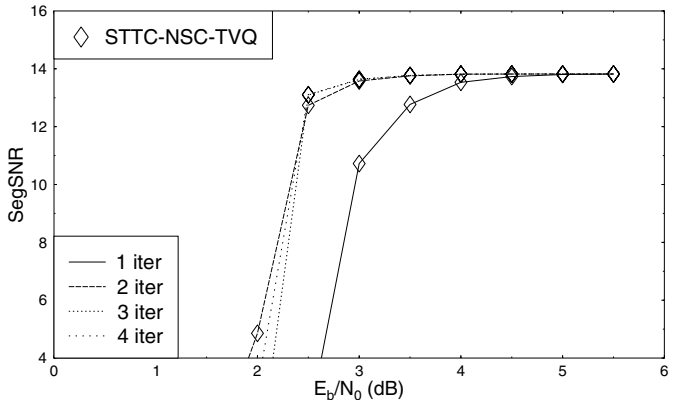

Figure 10.45: Average SEGSNR versus E_b/N_0 performance of the 16-QAM-based STTC-NSC assisted MPEG-4 TWINVQ audio benchmarker scheme when communicating over uncorrelated Rayleigh fading channels. The effective throughput was 1.98 BPS.

Similarly, it can be observed from Figures 10.46 and 10.47 that at the decoding complexity of 160 trellis decoding states the STTC-TCM-2NSC-AMR-WB arrangement performs 0.5 dB better in terms of the required channel E_b/N_0 value than the STTC-NSC-AMR-WB scheme when targeting a SEGSNR of 10.6 dB. By comparing Figures 10.44 and 10.46, we observe that the SEGSNR performance of the STTC-TCM-2NSC-AMR-WB scheme is inferior in comparison to that of STTC-TCM-2NSC-TVQ.

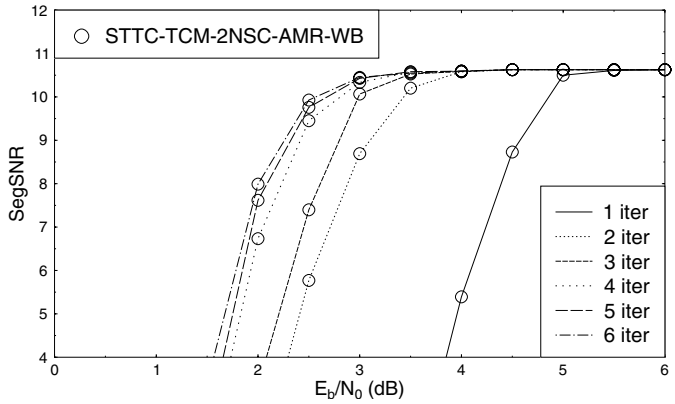

Figure 10.46: Average SEGSNR versus E_b/N_0 performance of the 16-QAM-based STTC-TCM-2NSC assisted AMR-WB speech scheme when communicating over uncorrelated Rayleigh fading channels. The effective throughput was 1.89 BPS.

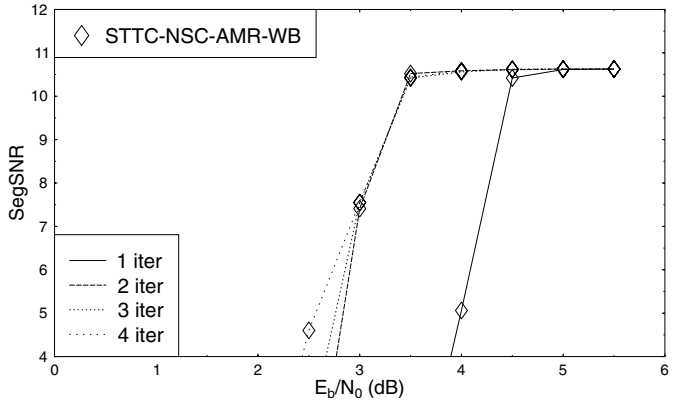

Figure 10.47: Average SEGSNR versus E_b/N_0 performance of the 16-QAM-based STTC-NSC assisted AMR-WB speech benchmarker scheme when communicating over uncorrelated Rayleigh fading channels. The effective throughput was 1.95 BPS.

More explicitly, the STTC-TCM-2NSC-TVQ system requires an E_b/N_0 value of 2.5 dB, while the STTC-TCM-2NSC-AMR-WB arrangement necessitates $E_b/N_0 = 3.0$ dB, when having their respective maximum attainable average SEGSNRs. The maximum attainable average SEGSNRs for STTC-TCM-2NSC-TVQ and STTC-TCM-2NSC-AMR-WB are 13.8 dB and 10.6 dB, respectively.

This discrepancy is due to the fact that both schemes map the most sensitive 25% of the encoded bits to class-1. By contrast, based on the bit error sensitivity study of the MPEG-4 TWINVQ codec outlined in Figure 10.42, only 10% of the MPEG-4 TwinVQ encoded bits were found to be gravely error sensitive. Therefore, the 25% class-1 bits of the MPEG-4 TWINVQ also includes some bits which were found to be only moderately sensitive to channel errors. However, in the case of the AMR-WB codec all the bits of the 25% partition were found to be quite sensitive to channel errors. Furthermore, the frame length of the STTC-TCM-2NSC-TVQ scheme is longer than that of the STTC-TCM-2NSC-AMR-WB arrangement and hence benefits from a higher coding gain.

It is worth mentioning that the channel capacity for the system employing the full-diversity STTC scheme with the aid of $N_t = 2$ transmit antennas and $N_r = 2$ receive antennas is 0.57 dB and 0.70 dB for the throughputs of 1.95 BPS and 1.89 BPS, respectively, when communicating over uncorrelated Rayleigh fading channels [477].

10.7.6 AMR-WB and MPEG-4 TWINVQ Turbo Transceiver Summary

In this section we comparatively studied the performance of the MPEG-4 TWINVQ and AMR-WB audio/speech codecs combined with a jointly optimised source-coding, outer unequal protection NSC channel-coding, inner TCM and spatial diversity aided STTC turbo transceiver. The audio bits were protected differently according to their error sensitivity with the aid of two different-rate NSCs. The employment of TCM improved the bandwidth efficiency of the system and by utilising STTC spatial diversity was attained. The performance of the STTC-TCM-2NSC scheme was enhanced with the advent of an efficient iterative joint decoding structure. Both proposed twin-class STTC-TCM-2NSC schemes perform approximately 0.5 dB better in terms of the required E_b/N_0 than the corresponding single-class STTC-NSC audio benchmarker schemes. This relatively modest advantage of the twin-class protected transceiver was a consequence of having a rather limited turbo-interleaver length. In the longer interleaver of the videophone system of [471, 473] an approximately 2 dB E_b/N_0 gain was achieved. For a longer-delay non-realtime audio streaming scheme a similar performance would be achieved to that of [471]. Our future work will further improve the achievable audio performance using the soft speech-bit decoding technique of [478].

10.8 Chapter Summary

In this chapter the MPEG-4 audio standard was discussed in detail. The MPEG-4 audio standard is constituted by a toolbox of different coding algorithms, designed for coding both speech and music signals in the range spanning from very low bitrates, such as 2 kbps to rates as high as 64 kbps. In Section 10.2, the important milestones in the field of audio coding were described and summarised in Figure 10.2. Specifically, four key technologies, namely perceptual coding, frequency domain coding, the window switching strategy and the dynamic bit-allocation technique were fundamentally important in the advancement of audio coding. The MPEG-2 AAC codec [40] as described in Section 10.2.1 forms a core part of the MPEG-4 audio codec. Various tools that can be used for processing the transform coefficients in order to achieve an improved coding efficiency were highlighted in Sections 10.2.2–

10.2.5. The AAC quantisation procedure was discussed in Section 10.2.6, while two other tools provided for encoding the transform coefficients, namely the BSAC and TWINVQ techniques were detailed in Sections 10.2.8 and 10.2.9, respectively. More specifically, the BSAC coding technique provides finely-grained bitstream scalability in order to further reduce the redundancy inherent in the quantised spectrum of the audio signal generated by the MPEG-4 codec. The TWINVQ codec [415] described in Section 10.2.9 was found to be capable of encoding both speech and music signals, which provides an attractive option for low bitrate audio coding.

In Section 10.3, which was dedicated to speech coding tools, the HVXC and CELP codecs were discussed. The HVXC codec was employed for encoding speech signals in the bitrate range spanning from 2 to 4 kbps, while the CELP codec is used at bitrates between 4 and 24 kbps, with the additional capability of encoding speech signals at the sampling rates of 8 and 16 kHz.

In Section 10.5, turbo coded and space–time coded adaptive as well as fixed modulation based OFDM assisted MPEG-4 audio systems have been investigated. The transmission parameters have been partially harmonised with the UMTS TDD mode [444] which provides an attractive system design framework. More specifically, we employed the MPEG-4 TWINVQ codec at the bitrates of 16, 32 and 64 kbps. We found that by employing space–time coding, the channel-quality variations have been significantly reduced and no additional benefits could be gained by employing adaptive modulation. However, adaptive modulation was found beneficial when it was employed in a low-complexity one-transmitter, one-receiver scenario when high channel-quality variations were observed. The space–time coded, two-transmitter, one-receiver configuration was shown to outperform the conventional one-transmitter, one-receiver scheme by about 4 dB in channel SNR terms over the highly dispersive COST207 TU channel.

In Section 10.7.6 we comparatively studied the performance of the MPEG-4 TWINVQ and AMR-WB audio/speech codecs combined with a jointly optimised source-coding, outer unequal protection NSC channel-coding, inner TCM and spatial diversity aided STTC turbo transceiver. The employment of TCM provided further error protection without expanding the bandwidth of the system and by utilising STTC, spatial diversity was attained, which rendered the error statistics experienced pseudo-random, as required by the TCM scheme, since it was designed for Gaussian channels inflicting randomly dispersed channel errors. Finally, the performance of the STTC-TCM-2NSC scheme was enhanced with the advent of an efficient iterative joint decoding structure. Both proposed twin-class STTC-TCM-2NSC schemes perform approximately 0.5 dB better in terms of the required E_b/N_0 than the corresponding single-class STTC-NSC audio benchmarker schemes. This relatively modest advantage of the twin-class protected transceiver was a consequence of having a rather limited turbo-interleaver length imposed by the limited tolerable audio delay. In the longer interleaver of the less delay-limited videophone system of [471,473] an approximately 2 dB E_b/N_0 gain was achieved. For a longer-delay non-realtime audio streaming scheme a similar performance would be achieved to that of [471].

Part IV

Very Low-rate Coding and Transmission

Chapter 11

Overview of Low-rate Speech Coding

11.1 Low-bitrate Speech Coding

Parts I–III of the book have provided extensive in-depth discussions on various aspects of characterising speech signals, portraying the spectral quantisation of speech, as well as various classes of low- to medium-rate codecs. The coding of wideband speech signals was considered in Part III. However, apart from the basics of vocoding, techniques applicable to coding of speech at rates below 4.8 kbps have not been considered. This is the objective of Part IV of the book.

This chapter endeavours to give a rudimentary overview of low-rate speech coding with a special emphasis on coding rates below 4.8 kbps and the techniques adopted in the associated codec designs.

Providing a brief very-low-rate-oriented introduction in this chapter allows the reader to delve directly into the intricacies of sophisticated low-rate techniques instead of having to work their way through the previous chapters. Further related information can be found in the excellent books edited by Kleijn and Paliwal [56] and Atal *et al*. [52], as well as in the monographs authored for example by Kondoz [55] and Jayant and Noll [10]. We commence with a historical perspective on the development of low-rate speech codecs, which is followed by a more in-depth review of 2.4 kbps speech coders. A brief glimpse at speech coders operating beneath 2 kbps is also offered. In addition, the methods of assessing a speech coder's performance are examined, with the greatest emphasis being placed upon subjective speech quality measures. Finally, the speech database used throughout this low-rate coding oriented part of the book is introduced.

Historically, the first speech coders were based on the now well-established waveform coding techniques [4–284], such as delta modulation (DM) [3] and SBC [284] which operate by directly quantising the speech waveform. However, their operating bitrate range is restricted, since they fail to produce communications quality speech at rates below 16 kbps. Instead, this niche is filled by the class of hybrid vocoders which employ LPC [481].

Voice and Audio Compression for Wireless Communications Second Edition
L. Hanzo, F. C. A. Somerville and J. P. Woodard

These hybrid vocoders operate by parameterising the speech signal and transmitting these parameters to the decoder. In the ubiquitous LPC schemes, this is performed through simulation of the human vocal system, thus, an understanding of the human speech production mechanism is desirable. The stylised human voice production system is shown in Figure 11.1. The human lung forces air through the glottis to the vocal tract, where quasi-periodic vocal fold vibration or constriction of the vocal tract creates voiced and unvoiced speech, respectively. Vowel sounds such as the front vowel /ε/ as in 'b*e*d' are voiced sounds, whereas the fricative /s/ as in '*s*ee' is an example of an unvoiced utterance. Examples of the time and frequency domain representation for 20 ms or 160 samples of voiced and unvoiced speech can be seen in Figure 11.2. The vocal tract can be labelled alternatively as the supra-glottal resonator, because it is the interaction of the air with the vocal tract that determines the spectrum of the speech. This resultant speech spectrum also depends on the vocal tract shape, which itself depends on the vocal tract articulators in Figure 11.1, namely the velum, lips, nostrils and tongue. Further explanation of speech processing and synthesis can be found in the book by Deller *et al.* [19], together with the book by O'Shaughnessy [17].

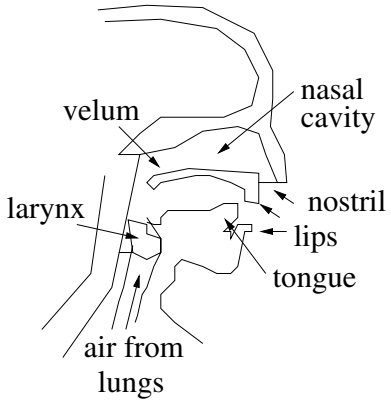

Figure 11.1: Human speech production system.

In their traditional form [196, 481], LPC schemes synthesise speech by passing an excitation signal through a spectral shaping filter to model the frequency domain shape produced by the vocal tract. The excitation signal mimics the glottal waveform using random noise for unvoiced speech and a sequence of periodic pulses for voiced speech. These periodic pulses are spaced according to the fundamental frequency of the speech waveform. Fundamental frequencies typically vary from 50–300 Hz for adult male speakers, and up to 500 Hz for adult female and child speakers, although the fundamental frequency can reach 1.5 kHz [20]. However, LPC schemes generally permit a fundamental frequency range of 54 to 400 Hz, because at an 8 kHz sampling rate this range covers 20 to 147 samples and can be quantised with 7 bits. Increasing the permitted fundamental frequency range to cover more of the female and child fundamental frequencies would increase both the coder's bitrate and complexity. For instance, if we would allow the fundamental frequencies 400 to 800 Hz, or 20 to 10 samples, the potential for the extra pitch period in each speech frame increases the associated bitrate.

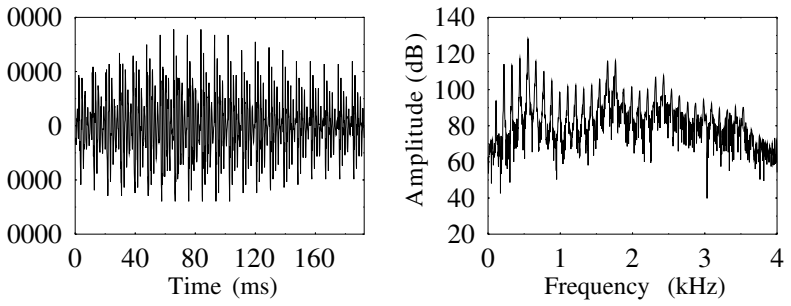

(a) Voiced speech

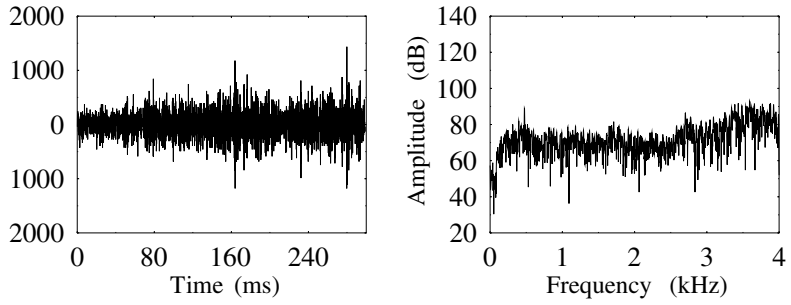

(b) Unvoiced speech

Figure 11.2: Voiced and unvoiced speech segments in both the time and frequency domain. In (a) the voiced sound is the front vowel /ɛ/ as in 'b*e*d', while for (b) the unvoiced sound is the fricative /s/ as in '*s*ee'.

In the speech coding community, the term pitch is often considered synonymous with fundamental frequency. Here it is noted that pitch actually refers to a perceived value and therefore is not a measure of the speech waveform. However, within this low-rate coding part of the book, the terms pitch and fundamental frequency are interchangeable, following the trend of the speech coding community.

The classical LPC vocoder schematic, where either a periodic pulse train or a Gaussian noise source is connected to the synthesis filter is shown in Figure 11.3. The spectral shaping arrangement is an all-pole filter that fully parameterises, and is analogous to, the shape of the vocal tract, albeit with the velum raised excluding the nasal cavity of Figure 11.1. This traditional vocoder form was proposed by Atal and Hanauer [481], and it is capable of encoding speech at 2 kbps. However, the resultant speech is of synthetic quality with a frequent 'buzziness' which will be explained later in Section 11.1.2.1.

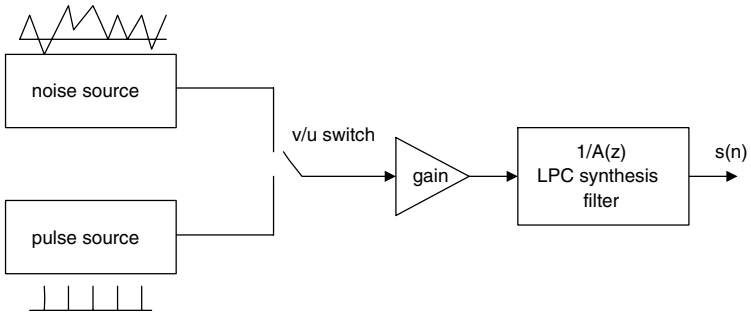

Figure 11.3: Schematic of the traditional LPC vocoder.

11.1.1 AbS Coding

A significant advance within the speech coding field was achieved with the introduction of AbS methods, such as the MPE-LPC developed by Atal and Remde [9]. For MPE-LPC, a selection of synthesised speech segments, of typically 5 ms length, are compared with the original segment and the best version is selected, where the criterion is the MMSE distance. In essence this is the addition of a synthetic ear to the voice production scheme, with many different versions of the utterance created and the one that is deemed to be most like the original selected. MPE-LPC locates several pulses with varying amplitudes in the optimum positions for each speech segment. The pulse positions and quantised amplitudes are subsequently sent to the decoder.

MPE-LPC preceded RPE developed by Kroon *et al.* [11], where the distance between excitation pulses was constrained to be regular. If each pulse is separated by a regular distance D_R, then for each frame only one pulse position is required as the other pulses are $D_R, 2D_R, 3D_R, \ldots$ further away. The lower number of parameters required results in a reduction in bitrate. This method of speech coding is used as the full-rate coder for the pan-European mobile radio system, known as GSM [97].

In order to achieve a further bitrate reduction, CELP [16] was introduced by Schroeder and Atal, where a codebook filled with vectors representing the excitation source is searched to find the best match for the speech segment, as demonstrated in Figure 11.4. Together with the spectral envelope parameters, the index for the relevant codebook entry is sent to the decoder. In order to allow the possible excitation signals to consist of random vectors, the periodicity of the speech signal must be removed, a task performed by the LTP. The LTP is frequently used in an adaptive codebook format, where each entry contains a past excitation signal with a particular delay. The excitation signal corresponds to the input of the LPC synthesis filter, where at each calculation of the LTP the adaptive codebook is filled with different overlapping vectors. The LTP parameters require updating more frequently than the LPC parameters, normally every 2.5–7.5 ms as opposed to every 20–30 ms. This frequent updating means that a large proportion of the CELP bitrate is consumed by the LTP parameters.

Methods to reduce the complexity of CELP coders generally involve the use of structured codebooks allowing efficient search procedures. However, to synthesise higher quality speech than the standard LPC-10 2.4 kbps [196] scheme at least 4 kbps is required, where this

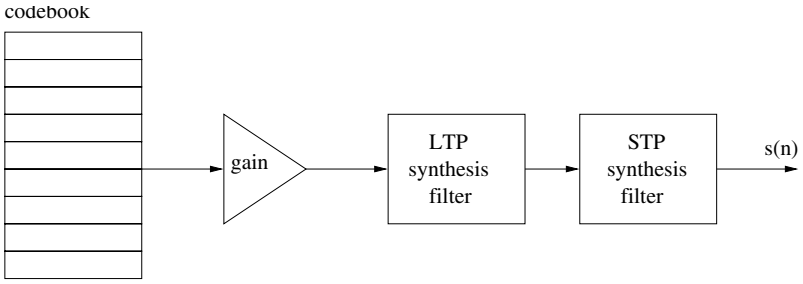

Figure 11.4: Schematic of a CELP arrangement.

assumes that about 20 bits per 20 ms speech frame are dedicated to coding the LPC filter coefficients. For coding rates below 4 kbps the excitation vector must be 8 to 10 ms in length to achieve the desired bitrate. It is then possible for several pitch period peaks to occur within a subframe, so subsequently the random code vectors lack the required pitch periodicity and the quality of the synthesised speech is degraded. A coder which can produce good quality speech at 3.6 kbps is the PSI-CELP scheme, which has been adopted for the Japanese mobile radio system's half-rate coder [210]. The PSI-CELP system produces quality speech for bitrates less than 4 kbps through exploitation of the periodicity which occurs in voiced speech. The use of periodicity in the CELP model reduces the overall SNR achieved by the coder, however, it improves the subjective quality of the speech signal.

Mano *et al.* [210] utilise pitch synchronous repetition of the random excitation to produce good quality voiced sections of speech. For the unvoiced, silent and transient sections of speech, a fixed codebook of random excitation is used in the coder instead of an adaptive codebook. This approach is returning to the classical LPC schemes where different excitation signals were used for voiced and unvoiced speech, as shown in Figure 11.5. The PSI-CELP excitation signal is of the form $G_1 v_1(n) + G_2 v_2(n)$ for $n = 1 \ldots N$, where $v_1(n)$ is equivalent to either an adaptive codebook or a fixed random codebook entry, and $v_2(n)$ is a combination of two random codebook vectors that for voiced speech contain a repetitious random vector synchronised to the pitch period. The superposition of two codebooks in generating $v_2(n)$ reduces the memory requirements of the coder. Initially, to select the excitation signal the most appropriate $v_1(n)$ vector is determined. If the $v_1(n)$ vector came from the adaptive codebook then the speech was deemed to be voiced, hence in constructing $v_2(n)$ the random vector will be repeated at pitch period intervals. If the fixed codebook is selected for $v_1(n)$, implying an unvoiced decision, then when selecting $v_2(n)$ unmodified random vectors are used.

Mano *et al.* [210] implemented a postfilter at the decoder, which enhances the pitch harmonics for the adaptive codebook and for the fixed codebook enhances the higher frequencies. The waveform shaping postfilter decreases the SNR of the coder, but improves the subjective quality of the speech. The PSI-CELP coder still requires over 3 kbps to produce good quality speech.

11.1.2 Speech Coding at 2.4 kbps

In order to produce good quality speech at less than 3 kbps different approaches must be pursued. An interesting review of these methods can be found in the recent selection

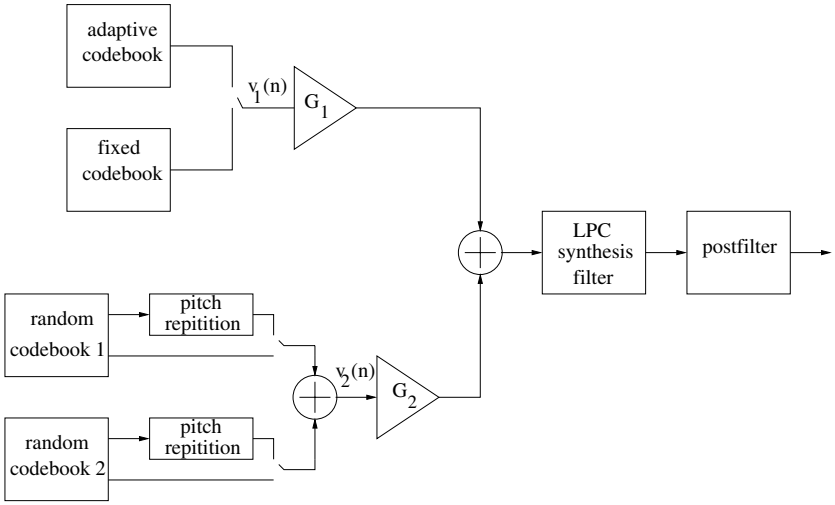

Figure 11.5: Schematic of the PSI-CELP arrangement. Copyright © IEEE.

procedure for the new US DoD 2.4 kbps standard. The new standard is designed to replace the old 2.4 kbps LPC-10 vocoder [196] and the 4.8 kbps DoD Federal Standard FS-1016 CELP coder [100].

11.1.2.1 Background to 2.4 kbps Speech Coding

Historically the first standard for 2.4 kbps speech coding using LPC was the LPC-10 recommendation, which has been in use since the late 1970s. The LPC-10 was later renamed as the Federal Standard FS-1015. An enhanced version of this standard, LPC-10e, was developed by the mid-1980s. However, even the enhanced version produces only synthetic quality speech, although state-of-the-art improvements in speech technology should allow significantly improved quality speech transmission. Thus, in May 1993 the United States DoD Digital Voice Processing Consortium (DDVPC) began the process of selecting a successor to the LPC-10e 2.4 kbps speech coding algorithm. Kohler *et al.* [482] described the workshops and general progression made in the selection process up to 1995. In May 1996, at the International Conference on Acoustics, Speech and Signal Processing (ICASSP) held in Atlanta, the winning speech compression algorithm was announced.

In this section the seven candidate speech coding algorithms are described and the successful candidate is revealed. The winning candidate selection method, employed by the DDVPC, is described in Section 11.3.3 where general information on speech coding performance is given.

The seven candidate coders fell, disproportionately, into two categories. The first group is the category of harmonic coders, which can be further subdivided into MBE [103, 483] and sinusoidal coders [484, 485]. Harmonic coders consider the frequency spectrum of a speech signal and encode the amplitudes of the harmonic frequencies. MBE speech coders have voiced–unvoiced excitation waveforms which are harnessed to represent different bands or harmonics within the frequency spectrum. Sinusoidal speech coders use an appropriate

sinusoid with amplitude and phase parameters for each harmonic, where the transmitted phase defines the sinusoid as either voiced or unvoiced. Four of the DoD candidate speech coders fell into the harmonic coder category, while two other coders [486, 487] also created a frequency spectrum consisting of voiced and unvoiced excitation. The primary aim of harmonic coders is to eliminate the frequent 'buzziness' of synthesised vocoder speech. This 'buzziness' will be inherent to any scheme which divides time-domain speech segments into the distinct categories of voiced and unvoiced.

The 'buzziness' occurs since speech is frequently a composite of voiced and unvoiced excitation sources, as demonstrated by voiced fricatives. In a voiced fricative, such as /v/ in '*v*alve', vocal cord vibration is accompanied by turbulence at a constriction in the vocal tract. Hence, a realistic harmonic excitation source must contain several voiced–unvoiced decisions in various frequency bands of the speech spectra [103]. Griffin and Lim [103] justify this principle with the observation that 'buzzy' speech, where the speech has been synthesised from a voiced source, tends to contain a spectrum with some regions dominated by the harmonics of the fundamental frequency and other regions dominated by noise. The introduction of harmonic excitation will degrade the waveform match between the original and reconstructed speech; this is indicative of low-bitrate speech coders that tend to neglect the objective speech quality and concentrate on the subjective quality of the reconstructed speech.

The final speech coder candidate [488] belonged to the waveform interpolation category. This class can also be further sub-divided, namely, into time and frequency domain interpolation. In waveform interpolation, a characteristic, or prototype, waveform is found periodically in the original speech signal which is then parameterised and transmitted, with interpolation between the selected prototypes producing a continuous synthesis signal. The interpolation can be performed in either the frequency or time domain, hence the two sub-categories. More explicitly, the aim of interpolation-based coders is to represent a small portion of the waveform accurately, then subsequently perform interpolation to reproduce the complete speech signal, thus, decreasing the required bitrate while maintaining the speech quality. Following this introduction, each individual candidate coder is now described in a little more detail.

11.1.2.2 Frequency Selective Harmonic Coder

The Frequency Selective Harmonic Coder (FSHC) [484] was proposed by the Communication Research Centre, Ontario, Canada. This candidate implements a harmonic coder, which extracts and encodes only the sections of the spectral envelope that are perceptually important. Selective encoding permits the reduction of the bitrate to 2.4 kbps while maintaining good quality speech.

For harmonic coders the frequency spectrum is divided into different bands, with each band being classed as voiced or unvoiced. The speech signal is modelled by a set of sine-waves representing the fundamental frequency and its harmonics, as follows:

$$\bar{s}(n;\omega_0;\theta) = \sum_{l=1}^{L(\omega_0)} A(l\omega_0)\exp[j(nl\omega_0+\theta_l)] \tag{11.1}$$

where n is the time sample domain index, $L(\omega_0)$ is the number of harmonics in the speech bandwidth, $A(l\omega_0)$ is the vocal tract envelope, ω_0 is the fundamental frequency and $\theta = \{\theta_1, \theta_2, \ldots, \theta_{L(\omega 0)}\}$ represents the phases of the harmonics. In order to achieve a bitrate as low as 2.4 kbps the phases θ are regenerated as minimum or zero phase at the decoder.

The extraction of perceptually important harmonics is performed by dynamic frequency band extraction (DFBE). The DFBE technique extracts the harmonics that are located at the spectral envelope peaks, but discards the harmonics situated in the spectral valleys. Elimination of the harmonics in the spectral envelope valleys by the DBFE exploits the human ear's reduced sensitivity in these regions. The overall structure of the FSHC speech coder is given in Figure 11.6, and it is described next.

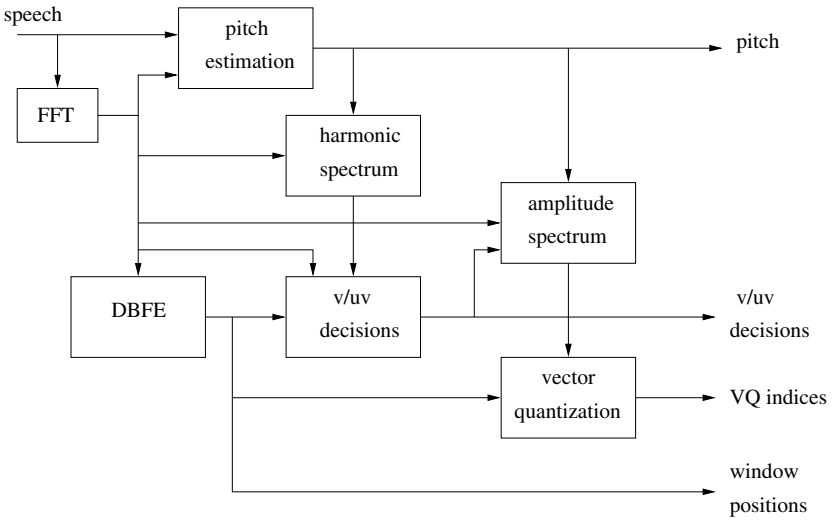

Figure 11.6: Schematic of the FSHC, proposed by Hassanein *et al.* [484]. Copyright © IEEE.

The selected pitch period of the speech frame is that which will generate a harmonic spectrum with the MMSE distance from the original spectrum. The DFBE algorithm is used to select the fraction of the spectrum whose spectral amplitudes are quantised for transmission. The window positions define the frequency bands that have been selected by the DFBE algorithm as containing perceptually important harmonics. The pitch-based amplitude spectrum, or spectral envelope, is then vector quantised and transmitted to the decoder.

11.1.2.3 Sinusoidal Transform Coder

The second candidate speech compression algorithm was the Sinusoidal Transform Coder (STC) [485, 489] developed by the Lincoln Laboratory at MIT. Similarly, to the above FSHC scheme, for this candidate a sinusoidal model is used to synthesise the speech signal, where the sinusoidal model is defined by amplitude, frequency and phase parameters. These components are determined by an analysis of the short-term Fourier transform (STFT) of the speech signal. Bitrate reduction is achieved through forcing the sinusoidal model to have

zero-phase, consequently the speech signal is defined in [489] by

$$\bar{s}(n) = \sum_{l=1}^{L(\omega_0)} A(l\omega_0)\cos[(n-n_0)l\omega_0 + \theta_l] \tag{11.2}$$

where $A(l\omega_0)$ is the vocal tract envelope, ω_0 is the fundamental frequency, n_0 is the onset time, which determines the location of the excitation pulse, and θ_l represents the voicing dependent phases, which are set to zero here.

Thus, the encoder parameters are the pitch period, voicing and the sine-wave amplitudes and are highlighted with reference to Figure 11.7. The sine-wave amplitudes were obtained from the magnitude of the harmonics of the fundamental frequency, where they determine the shape of the vocal tract spectral envelope. The amplitudes are encoded by fitting a set of cepstral coefficients to the envelope of the sine-wave amplitudes, which proved to be advantageous over an all-pole speech model [485]. Following unsuccessful attempts at encoding the cepstral coefficients directly at a low bitrate, instead they were passed through a cosine transformer and quantised for coding before transmission. The use of a cosine transformer permitted a simple pulse coded modulation (PCM) scheme to be used for the encoding of the cosine transformed cepstral coefficients. The output of the cosine transformer is a set of channel gains, where these channels divide up the frequency spectrum. Before the channel gains were encoded, a perceptually based scale was used to increase the efficiency of the encoding process by placing emphasis on the perceptually relevant lower frequencies. The STC candidate was found to produce good quality speech over the 2.4–4.8 kbps range.

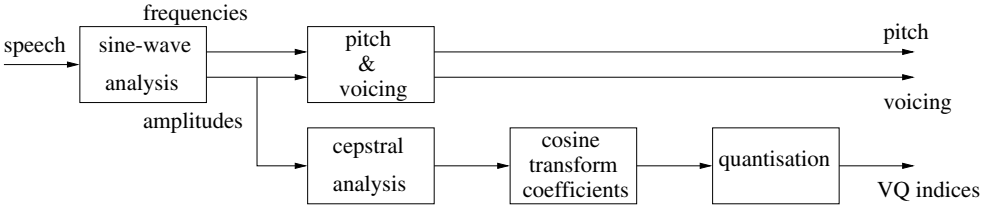

Figure 11.7: Schematic of the STC, proposed by McAulay and Quatieri [485]. Copyright © IEEE.

11.1.2.4 Multiband Excitation Coders

The next two candidate speech coders were the Advanced Multiband Excitation (AMBE) coder, developed by Digital Voice Systems Inc., and the Enhanced Multiband Excitation (EMBE) coder [483, 490], developed by Oklahoma State University. Both MBE models were based on the original MBE coder [103], which represents the spectral envelope $H_w(\omega)$ of a speech signal by a smoothed version of the original spectrum $\bar{S}_w(\omega)$. The excitation signal $|E_w(\omega)|$ is determined by a series of voiced–unvoiced decisions, either one decision for each harmonic or a decision for certain frequency bands spanning several harmonics. The synthesised speech signal is given by

$$\bar{S}_w(\omega) = H_w(\omega)|E_w(\omega)| \tag{11.3}$$

The excitation spectrum $|E_w(\omega)|$ consists of a combination of a periodic spectrum $|P_w(\omega)|$ and a random noise spectrum $|U_w(\omega)|$, where the periodic spectrum $|P_w(\omega)|$ can be viewed as the Fourier transform of the periodic pulse train used in the LPC-10 speech coder.

The quality of speech, synthesised from the MBE model, is dependent on the correct voiced–unvoiced decisions and on the accurate fundamental frequency calculation, where both were determined using methods similar to those employed by the FSHC of Section 11.1.2.2. The original MBE model [103] was designed to operate at 8 kbps, hence the EMBE and AMBE models must reduce the operating bitrate, while preserving the speech quality as much as possible.

For the EMBE coder [490], a 30 ms frame structure containing two subframes was introduced to help decrease the bitrate requirements. Some parameters are transmitted every subframe, while others are transmitted only once per frame and interpolated over the other subframe. The schematic of the EMBE encoder is given in Figure 11.8 which is described below.

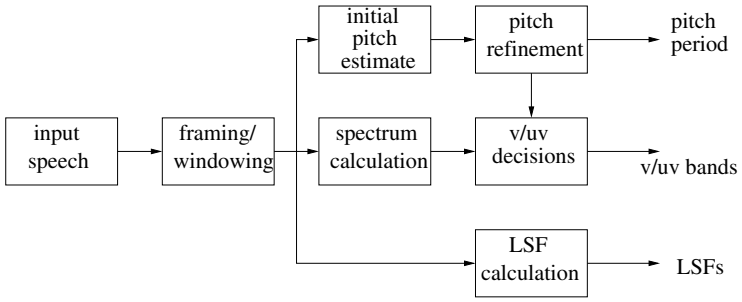

Figure 11.8: Schematic of the EMBE, proposed by Teague *et al*. [483]. Copyright © IEEE.

The speech waveform is divided into subframes of 15 ms, with the frequency spectrum calculated for each subframe. An integer estimate of the pitch period of the speech waveform from each subframe is also determined, with this initial estimate assessed for evidence of pitch doubling and halving. Since MBE coders use the pitch decision to search for evidence of voicing at the frequency harmonics this pitch period estimation is further refined to subsampled accuracy. A voiced–unvoiced decision is made concerning every harmonic in the speech spectrum, based on the closeness of match between the original spectrum and a fully voiced synthesised spectrum, created from the refined pitch period estimate. Four unequal voiced–unvoiced bands are created, based on the voiced–unvoiced decision for every harmonic within each band, with the division of the four unequal bands influenced by the pitch period and perceptual importance of different frequencies. For the EMBE coder the harmonic spectrum is not represented by the harmonic amplitudes, as in the original MBE, instead a detailed 18th-order linear prediction model is used. The LPC coefficients are transmitted once every 30 ms frame, while all other parameters are sent every 15 ms subframe.

11.1.2.5 Sub-band Linear Prediction Coder

The next speech coder candidate was the SBC LPC coder [487], suggested by Thomson CSF in France. This candidate uses the frequency division aspect of MBE coders, however, it also employs LPC techniques to produce an LPC synthesis filter. The schematic of this speech coder is given in Figure 11.9 and described next.

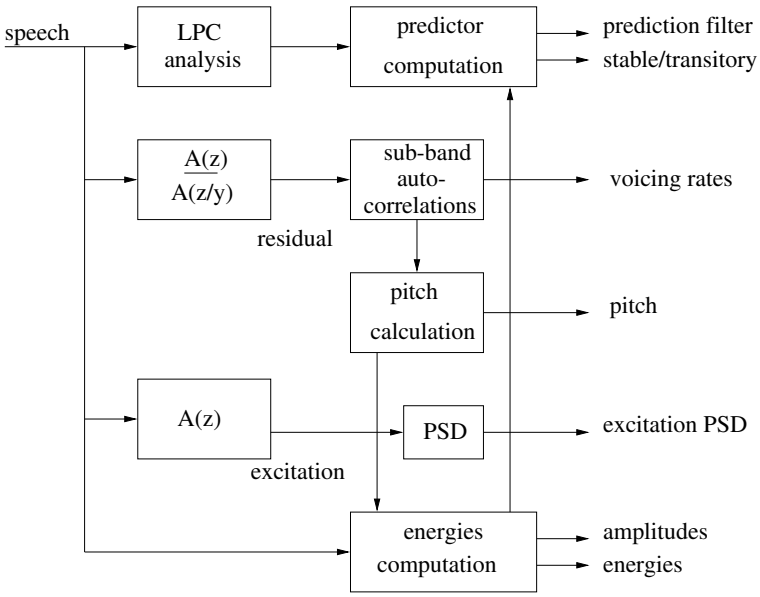

Figure 11.9: Schematic of the SBC LPC coder, proposed by Laurent and de La Noue [487]. Copyright © IEEE.

The SBC divides the frequency spectrum into five sub-bands with each sub-band being assigned a voicing strength, based on autocorrelation measurements. For speech which contains voicing in any of the sub-bands the fundamental frequency of the speech signal is found, again employing autocorrelation measures. For synthesis, the fundamental frequency and sub-band voicing strengths are utilised to create an excitation signal constructed of several excitation sources. This mixed excitation is used since it has been hypothesised that such a mixed excitation source, with combined pulses and noise, will remove much of the 'buzziness' of LPC speech [491]. Thus, the excitation signal in each sub-band can be either voiced, unvoiced, a mixture of voiced and unvoiced, or transitory, as shown in the stylised Figure 11.10, where the transitory excitation is used for speech with rapidly changing characteristics, which is typical of segments at the onset of voicing. The employment of a variety of excitation sources assists in synthesising improved quality speech at 2.4 kbps.

11.1.2.6 Mixed Excitation Linear Prediction Coder

The penultimate short-listed candidate speech coder was the Mixed Excitation Linear Prediction (MELP) coder [486, 492, 493], developed by Texas Instruments.

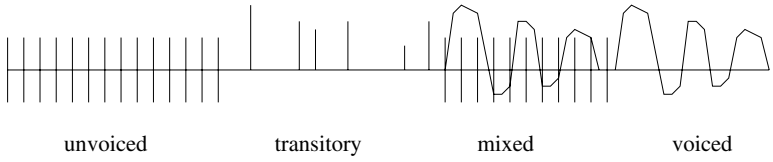

Figure 11.10: Excitation sources for the SBC LPC coder. Copyright © IEEE.

Similarly to the SBC LPC coder of Section 11.1.2.5, this speech coder also uses different combinations of voiced and unvoiced sources, which are determined for a series of frequency bands. The scheme proposed harnesses between four and ten frequency bands, with Figure 11.11 displaying its schematic. This candidate coder is based on the traditional LPC model, but features many functions designed to mimic elements of the human speech generation mechanism, which have previously been employed in formant vocoders [494].

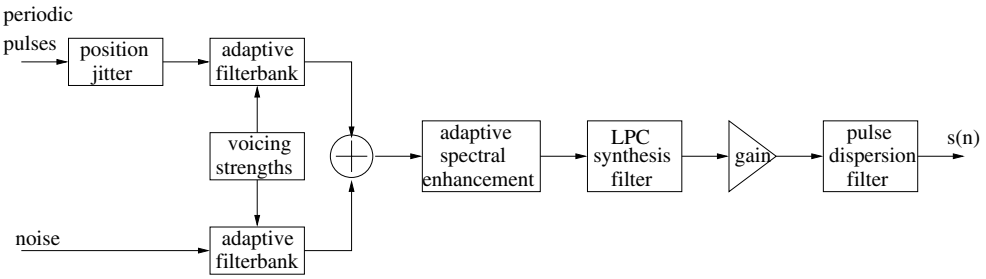

Figure 11.11: Schematic of the MELP coder arrangement, proposed by McCree and Barnwell [486]. Copyright © IEEE.

A multiband element is harnessed where voiced pulse excitation and Gaussian random excitation are passed through time-varying spectral shaping filters. These spectral shaping filters are combined to give the complete excitation as seen in Figure 11.11. The extent of voicing in a frequency band is determined by the strength of periodicity in that frequency band, while the amount of unvoiced excitation is chosen to keep the excitation power constant in each band.

In the scheme proposed by McCree and Barnwell [486] the vocoder model includes aperiodic pulses in order to simulate voicing transitions, which is similar to the excitation introduced by the SBC LPC of Section 11.1.2.5. These aperiodic pulses were created using a pulse position jitter uniformly distributed over $\pm 25\%$ of the pitch period, which was only included when weak correlation is apparent in the speech signal.

After the voiced and unvoiced excitation sources have been combined, adaptive spectral enhancement is performed, which helps the synthesised speech to match the spectrum of the original speech in the formant regions and is the short-term postfilter described later in Section 12.6. This enhancement is required since synthesised speech tends to reach a lower spectral valley between the time domain formant resonances than natural speech. The excitation signal is then passed to the LPC synthesis filter and finally to a pulse dispersion filter based on a typical male glottal pulse.

The pulse dispersion filter attempts to spread the excitation energy away from the periodic pulses of the speech coder in Figure 11.11. It models the occurrences when a fraction of the original excitation is concentrated away from the instant of glottal closure, thus the pulse dispersion filter simulates the effect of this time domain spread. This pulse dispersion filter has a time domain spread based on a typical male pitch period.

11.1.2.7 Waveform Interpolation Coder

The final candidate speech coder was the Waveform Interpolation (WI) coder [105, 488, 495], developed by AT&T, which is portrayed in Figure 11.12 and described next.

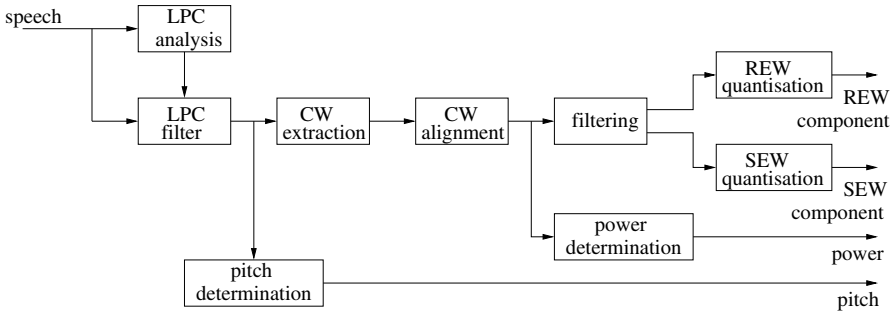

Figure 11.12: Schematic of the WI coder, proposed by Kleijn and Haagen [488]. Copyright © IEEE.

The WI method periodically selects a prototype, or characteristic waveform (CW), which characterises the speech signal over a given duration. The length of the CW is the pitch period of the input signal. The remainder of the encoding process is performed in the frequency domain, thus, the fast Fourier transform (FFT) of the CW is calculated. The current CW is then circularly time-shifted to ensure that the CW is aligned with the previous CWs, producing smoothly evolving CWs. The power of the CW is encoded and transmitted, enabling the CW to be normalised to unit magnitude. If the CW is determined at least once per pitch period then the speech signal can be perfectly reconstructed, but as the CW refreshing interval is extended in an attempt to reduce the bitrate, reconstruction errors will appear. The CW is divided into two signals, the slowly evolving waveform (SEW) for voiced speech and the rapidly evolving waveform (REW) for unvoiced speech, as these two types of waveforms have different characteristics and can be most efficiently encoded separately.

Filtering is employed to divide the speech signal into its voiced and unvoiced components, where high-pass filtering reveals the components of the REW and low-pass filtering produces the SEW. A high sampling rate is used to encode the REW, however, only a rough description of the waveform is encoded as unvoiced speech is not perceptually important. The SEW signal is initially down-sampled to the prototype, which is then accurately described, with the decoder reconstructing the complete signal using interpolation between consecutive CWs.

Following this review of the seven candidate speech coders for the new 2.4 kbps DoD standard we can now reveal that the winning candidate speech coder was the MELP scheme, developed by Texas Instruments. As mentioned before, the MELP is a basic vocoder with many additional features in order to more closely model the human speech

production mechanism. The procedure by which the MELP coder was selected is described in Section 11.3.3.

11.1.3 Speech Coding Below 2.4 kbps

Speech coding is also progressing below 2.4 kbps, with an example given below which employs WI in the time domain and was introduced by Hiotakakos and Xydeas [496]. It has a small portion, typically a pitch period, of the speech segment encoded in each frame, which is referred to as a prototype segment. The coder schematic is demonstrated by Figure 11.13. Smooth interpolation between the prototypes is performed at the decoder producing a slow evolution of the excitation signal. The time domain interpolation scheme represents the unvoiced speech separately using random Gaussian noise, thus as in any vocoder a robust pitch detector will be integral to the model.

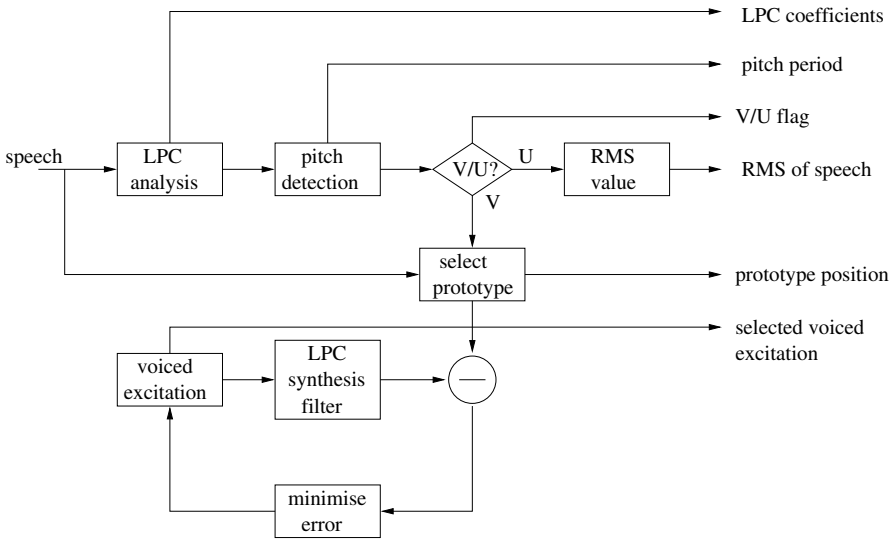

Figure 11.13: Schematic of the prototype WI arrangement, proposed by Hiotakakos and Xydeas [496].

For the model proposed by Hiotakakos and Xydeas [496] an orthogonal excitation model which utilises zinc basis functions [497] was employed. The excitation model's typical shape is shown by Figure 11.14, where the coefficients A and B describe the function's amplitude and λ defines its position. Sukkar *et al.* [497] compared the zinc functions to other excitation models, notably to the Fourier series description of the excitation. They found the zinc functions to be superior at modelling the LPC residual, which is partially due to their pulse-like shape being able to mimic the pitch-related residual pulses of voiced speech that remain after LPC analysis. The zinc functions are found to remove some of the 'buzziness', described in Section 11.1.2.1, from the synthesised speech.

The 2 kbps Interpolated Zinc Function Prototype Excitation (IZFPE) scheme proposed by Hiotakakos and Xydeas [496], detailed also in Chapter 14.2, uses a closed loop AbS model that encodes voiced and unvoiced speech separately. It processes 20 ms speech frames.

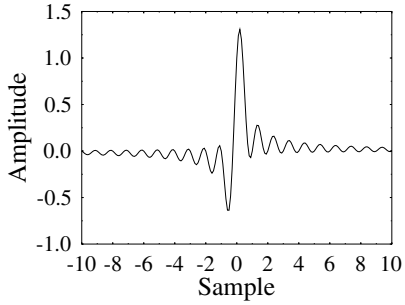

Figure 11.14: Typical shape of a zinc basis function, using the expression $z(n) = A_1 \cdot \text{sinc}(n - \lambda_1) + B_1 \cdot \text{cosc}(n - \lambda_1)$.

As seen in the block diagram of Figure 11.13, after the LPC analysis the pitch period of the speech frame is determined, where for voiced frames a pitch prototype segment is located. The voiced speech frames have their prototype segments modelled with the zinc basis functions characterised by Figure 11.14, and detailed in Section 14.2, while unvoiced speech frames are modelled by a Gaussian random process. At the voiced–unvoiced boundaries individual pitch periods are examined for evidence of voicing, which improves the coder's performance during rapidly evolving voicing onsets.

During a voiced sequence of frames the phase of the zinc function excitation (ZFE) must be constant, thus permitting the interpolation to be performed in the time domain, which is explained in more detail in Section 14.3.4. The phase of the ZFE sequence is determined by the second voiced frame in a sequence, since according to Hiotakakos and Xydeas [496] the second voiced frame typically represents the voiced sequence better than the first voiced frame. The selection of the phase by the second voiced frame and the consideration of voicing during the last unvoiced frame implies that a delay of 60 ms can be encountered in the coder.

This introductory section has reviewed some of the milestones in low-rate speech coding, dedicated to reducing the bitrate requirements while improving the synthesised speech quality. Special attention has been afforded to the lower bitrates, with particular interest paid to the recent developments at 2.4 kbps.

Following this overview of speech coders, particularly low-bitrate speech coders, a short discussion on the LPC model is presented.

11.2 Linear Predictive Coding Model

LPC has become a standard model for speech coders. Typically it uses an all-pole filter to describe the transfer function of the vocal tract. The derivation of this approach can be found in Rabiner and Schafer [6]. An all-pole filter is generally an adequate model of the vocal tract although the introduction of zeros refines the accuracy of the model, notably when the velum is lowered to introduce nasal coupling. However, the introduction of zeros in the model would prevent the separate optimisation of the synthesis filter coefficients and excitation model. It would also increase the bits for encoding and transmission, and hence in practical schemes it is avoided. It is claimed that the appropriate positioning of the poles can mimic the effect of

the neglected zeros, making the necessity for zeros redundant, thus reducing the complexity of the filter.

The all-pole or autoregressive model [6] represents the transfer function of the vocal tract by

$$H(z) = \frac{1}{1 - \sum_{k=1}^{p} a_k z^{-k}} = \frac{1}{A(z)} \tag{11.4}$$

where a_k are the coefficients from linear prediction and p is the order of the predictor filter. This modelling of the vocal tract shape is designated STP as described next.

11.2.1 Short-term Prediction

The schematic of STP within a basic AbS model is given in Figure 11.15 and described here. Within the encoder section the input speech is compared with the output of an LPC synthesis filter, whose coefficients a_k have previously been optimised. The excitation source which results in the minimum error between the original and synthesised speech is selected. At the decoder the excitation source and LPC synthesis filter coefficient parameters are received from the encoder. Passing the excitation source through the LPC synthesis filter produces the synthesised speech.

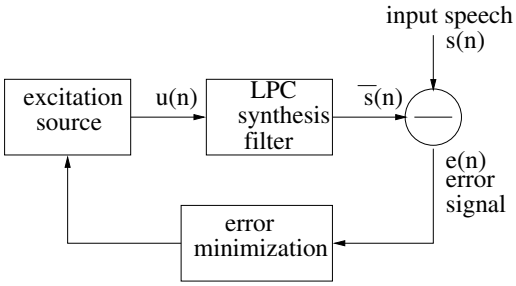

(a) Encoder

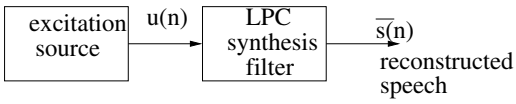

(b) Decoder

Figure 11.15: The AbS approach to LPC.

Linear prediction is useful as it predicts the next sample based on a weighted sum of previous samples, thus,

$$\bar{s}(n) = \sum_{k=1}^{p} a_k s(n-k) \tag{11.5}$$

where $\bar{s}(n)$ is the predicted sample and $s(n-k)$ is the kth previous sample. Appropriate values for a_k produce good predictions for $\bar{s}(n)$. Any inaccuracies in the prediction result in an error signal when the synthesised and original speech are compared.

The selection of the number of past speech samples, or filter order p, is a compromise between a low bitrate and high spectral accuracy. There should be a sufficient number of poles to represent the speech formants with an extra two to four poles to simulate the effect of possible zeros and for general spectral shaping. Typically p is 8–16, and so for a sampling frequency of 8 kHz, 1–2 ms of the past speech history is used. Thus, the analysis is referred to as STP.

From Rabiner and Schafer [6] the prediction error of Figure 11.15(a) is expressed as

$$e(n) = s(n) - \bar{s}(n) \tag{11.6}$$

$$e(n) = s(n) - \sum_{k=1}^{p} a_k s(n-k). \tag{11.7}$$

Taking the z transform, it can be seen that

$$E(z) = S(z)A(z) \tag{11.8}$$

where $E(z)$ is the error, $S(z)$ is the speech and $A(z)$ is the predictor filter. Thus, the predictor filter is

$$A(z) = 1 - \sum_{k=1}^{p} a_k z^{-k} \tag{11.9}$$

which is the inverse transform of the vocal tract. Hence, passing the original speech through this inverse transform filter, $A(z)$, produces the residual $E(z)$ which is the ideal excitation source.

The excitation signal is selected through the minimisation of the mean squared prediction error over a quasi-stationary 10–30 ms or 80–240 sample speech segment. The expression to be minimised is given by

$$\sum_{n} e^2(n) = \sum_{n} \left[s(n) - \sum_{k=1}^{p} a_k s(n-k) \right]^2. \tag{11.10}$$

Upon setting the partial derivatives of this expression, with respect to a_k, to zero, we arrive at a set of p equations, delivering the p filter coefficients.

The filter coefficients a_k need to be quantised before transmission to the decoder, while the stability of the LPC STP synthesis filter should be maintained. Owing to the need for stability the filter coefficients must remain within the unit circle. The quantisation of any filter coefficients near the unit circle may result in a quantised value outside the circle and hence will be prone to instability problems. In order to maintain stability the coefficients, a_k, are usually transformed into another parameter before quantisation. A more appropriate parameter is the LAR;

$$\mathrm{LAR}_i = \log \frac{1 - k_i}{1 + k_i} \tag{11.11}$$

where the parameters k_i are the reflection coefficients taken from vocal tract analysis [6]. A sufficient and necessary condition for the stability of $A(z)$ is $|k_i| < 1$, which can be artificially enforced when arriving at values violating this condition. When transforming k_i to LAR_i, using Equation (11.11) a reduced quantisation sensitivity is achieved, facilitating their quantisation using a lower number of bits. However, the most commonly used transformed spectral parameters are the LSP [144] or LSFs [118]. LSFs have well behaved statistical properties and if their ordering property is observed, they will ensure the stability of the filter. The ordering property of the LSFs is expressed as $f_0 < f_1 < f_2 < \cdots < f_N$, where f_n are the LSFs.

11.2.2 Long-term Prediction

The STP process will remove the short-term redundancy of the speech signal, but in certain circumstances will typically result in a high prediction residual peak. For instance, when an increasing sample is predicted on the basis of the previous 8–16 samples but the speech waveform passes its peak and starts to decrease, a high prediction residual peak will occur. This typically occurs at the start of a new pitch period, resulting in a long-term periodicity in the residual. This long-term periodicity corresponds in the spectral domain to a fine needle structure. In order to remove the corresponding long-term residual periodicity and to model this fine spectral structure, LTP can be performed. However, for the vocoder structure of the coders described in this report, the pulse-like voiced excitation sources remove the necessity of the LTP. Thus this report never considers the LTP.

11.2.3 Final Analysis-by-Synthesis Model

The LPC model described thus far determines the best excitation signal by minimising the mean squared difference between the original and synthesised speech. However, the theory of auditory masking can be used to further reduce the perceived signal distortion [498]. The perceived distortion at the output of the decoder will be greatest in areas of low signal strength; therefore, warping or shaping the noise spectrum so most energy occurs in the formant regions will reduce the subjective effect of the noise. The error weighting filter is defined by

$$W'(z) = \frac{A(z)}{A(z/\gamma)} = \frac{1 - \sum_{k=1}^{p} a_k z^- k}{1 - \sum_{k=1}^{p} a_k \gamma^k z^{-k}} \tag{11.12}$$

where γ is a weighting factor between 0 and 1 that represents the degree of weighting of the error spectrum. A good choice for γ is between 0.8 and 0.9. A computationally more efficient method is to weight the original and synthesised speech, before they are subtracted, as seen in Figure 11.16. This is because the filters $A(z)$ and $1/A(z)$ cancel each other in the synthesis loop, where $\bar{s_w}(n)$ is synthesised a large number of times. The synthesised filter becomes

$$W(z) = \frac{1}{A(z/\gamma)} = \frac{1}{1 - \sum_{k=1}^{p} a_k \gamma^k z^{-k}}. \tag{11.13}$$

This concludes an overview of LPC modelling, where STP, LTP and error weighting have been introduced. Next, an introduction into measuring the quality of the reconstructed speech is given.

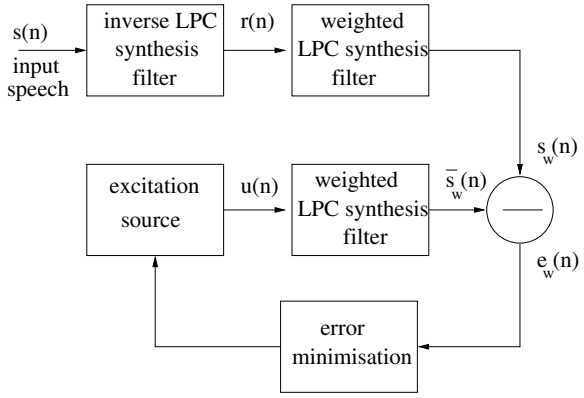

Figure 11.16: AbS with error weighting.

11.3 Speech Quality Measurements

Once the speech coder is implemented it is imperative that speech quality can be appropriately assessed. Hence, the speech quality measure must be chosen carefully. Measuring the quality of the synthesised speech can be performed using both objective and subjective measures [85]. Objective measures compare the original and reconstructed waveform and calculate a measure of the distortion between the two signals. Subjective measures involve listening tests, where judgement is passed on the intelligibility and quality of the reconstructed speech. Objective measures are simpler to repeatedly implement and evaluate, allowing the speech quality to be continually assessed during a coder's development phase. However, subjective measures are always important to assess the human perception of the quality of a speech coder.

11.3.1 Objective Speech Quality Measures

The most frequently used objective speech quality measures are the SEGSNR and the CD measures. They require the reconstructed speech to be a waveform replica of the input speech. Thus, representing unvoiced frames with a random sequence prevents the use of objective measures on unvoiced frames.

The SEGSNR is a waveform distortion measure that is defined as the distortion between the original and synthesised speech. The SEGSNR is calculated over a quasi-stationary interval of a speech frame, thus, the distortion from a high-energy portion of speech will not overwhelm the distortion evaluation from a low-energy portion of speech. The SEGSNR measure is defined by

$$\mathrm{SEGSNR} = 10 \log \frac{\sum_{n=1}^{\mathrm{FL}} s(n)^2}{\sum_{n=1}^{\mathrm{FL}} (\bar{s}(n) - s(n))^2} \tag{11.14}$$

where FL always refers to the frame length.

The CD measure is a frequency spectrum distortion measure, that determines the logarithmic spectral envelope distortion between the original and synthesised speech. The CD is given by

$$\mathrm{CD} = \frac{1}{\ln 10}\sqrt{2\sum_{i=1}^{N_l}(C_{\mathrm{orig}}(i) - C_{\mathrm{synth}}(i))^2} \tag{11.15}$$

where C_{orig} and C_{synth} are the cepstrum coefficients and N_l is the number of the coefficients.

Due to the low bitrates considered in this report, the synthesised waveform is never a close enough match to the original waveform to utilise the described objective measures. Instead, the techniques used at low bitrates concentrate on retaining the perceptual quality of the reconstructed speech, rather than reproducing a waveform match with the original signal.

11.3.2 Subjective Speech Quality Measures

Subjective measures involve listening tests with different quality ratings and test conditions. They include speech quality tests, speech intelligibility tests, pair-wise comparison tests and informal listening tests. They are generally performed on both standardized coders to give a benchmark and on the experimental speech coders.

The two main speech quality tests are the MOS and the Diagnostic Acceptability Measure (DAM) [499]. The DAM is the test traditionally used when selecting speech coding standards. The listeners assess how the speech coder affects various communication quality attributes. The MOS is the test traditionally implemented for commercial purposes, where the speech quality is classified by listeners into the categories excellent, good, fair, poor and bad. The speech is then assigned a score from 5 to 1, respectively.

The Diagnostic Rhyme Test (DRT) [500] examines a speech coder's intelligibility and rates the decoded speech on a scale from 0 to 100, where 100 represents no intelligibility errors. Rhyming words are commonly used as the test data, where the word pairs vary only in the first consonant.

Less formally, the pair-wise comparison test is where the listener hears two examples of a sentence, usually created by two different coders, and is asked to indicate the preference. The preference percentages are then represented as a measure of the speech coder's quality.

Lastly, informal listening tests are often used under loosely specified experimental conditions. For low-bitrate speech coders, at bitrates less than 4 kbps, it is often difficult to apply objective measures and time consuming to perform subjective tests. Thus, informal listening tests can be used as a quick measure of coder improvement. Specifically, an informal listening test might involve commenting on whether a specified distortion has been reduced by a slight change in the coder's operation.

11.3.3 2.4 kbps Selection Process

The selection of the new DoD speech coding standard for 2.4 kbps provides an informative insight into the methods used for determining the quality of a speech coder. The types of environment under which a speech coder must operate efficiently are also examined, along with the compromise between the requirements desired by the multitude of potential applications that may use the current 2.4 kbps standard.

The basic system requirements were that its performance must match the quality produced by the FS-1016 CELP speech coder at 4.8 kbps. It was also important that the speech coder has a low power consumption and can produce high-quality speech in a range of environments. The quality of the speech must be sufficiently high to enable speaker recognition. The model must also have the ability to operate in tandem with other systems working at different rates. The Terms of Reference were described by Tremain *et al.* [501] and consisted of a list of parameters with their respective minimum acceptable values, and the objective measurements which users would wish the coder to achieve. The selected algorithm was the speech coder which provided the best overall performance to meet the Terms of Reference in a variety of noisy environments.

The test structures for the 2.4 kbps selection process [502] measured intelligibility, voice quality, talker recognizability and communicability. The tests performed were the DRT for intelligibility and the DAM, the MOS, and the Degradation Mean Opinion Score (DMOS) for voice quality. For recognisability, a test was developed at the Naval Research Laboratory (NRL), while communicability was measured using a test designed for the U.S. Air Force Rome Laboratory (USAF-RL). The tests were performed in a number of noise environments which included an office, a car and aircraft. The tests were also performed in a quiet environment.

The DRT for intelligibility was briefly described above in Section 11.3.2. For test data the DDVPC have a large lexicon of DRT word pairs in a variety of acoustic environments.

As regards the voice quality measure, the DAM, MOS and DMOS tests were examined [503], and were briefly highlighted in Section 11.3.2. It was found [503] that the MOS tests provided the most reliable set of performance measures, thus the traditional DAM measure was neglected.

As mentioned earlier, a test for speaker recognizability was developed by the NRL [504]. A new test was required since virtually no testing for recognizability has previously been performed. There are two levels of recognizability; the highest is that the phone users are recognizable as themselves; the lower level of recognition is where speakers can be distinguished as different.

The testing approach employed involves a ‘same–different’ decision being performed on the basis of whether pairs of sentences were spoken by either the same or different people. Both male and female speakers were used, with the sentence pairs constructed from processed and unprocessed speech. The term processed implies that the speech has been passed through the test speech coder, while the term unprocessed means the speech is unmodified. The sentence pairs contained ‘processed–processed’ pairs and ‘processed–unprocessed’ pairs.

The employed communicability test was designed on behalf of the NASF-RL by the ARCON corporation [505]. Communicability is a measure of the speech coder’s quality under simulated operational use, including a variety of environments and different numbers of people interacting. A specified task requiring the combined effort of at least two people, linked via the speech coder, is performed. Each person, involved in the test, rates various aspects of the speech coder on a seven-point scale. The aspects are the level of the effort required in communicating using the coder, the quality of the received speech, the effect of the scheme on communication and task performance and the overall acceptability of the model.

The overall selection of the new 2.4 kbps coding standard involved combining the performance scales of the algorithm in each test. The encoder’s speech quality was assigned

30% of the marks, the intelligibility was assigned 35%, the recognizability was given 15%, while the communicability was assigned 20%. The combined test total was assigned 85% of the overall marks with the algorithm's complexity being given the remaining 15%.

The evaluation procedure initially concentrated on finding the speech coder candidates which exceeded the minimum requirements in the Terms of Reference. Subsequently, the remaining candidates were examined in more depth to find the coder that best achieved the objectives described in the Terms of Reference. As mentioned in Section 11.1.2, the winning candidate was the MELP coder developed by Texas Instruments. The other coders to meet the minimum requirements were the AMBE developed by Digital Voice Systems Inc., the WI coder developed by AT&T and the STC scheme developed by the Lincoln Laboratory at MIT.

This overview of speech quality measures has considered both subjective and objective speech measures. It has also given an informative insight into the role of speech quality measures in selecting the winning candidate for speech coding standards. Finally, the speech database implemented throughout the developed speech coders is documented in the following section.

11.4 Speech Database

The speech database used for our experimental purposes is detailed in Table 11.1, and subsequently will be referred to by the speaker code.

Table 11.1: Details of the speech database.

Speaker code	Speaker sex	Dialect of English	Number of 20 ms frames	Utterance
AM1	Male	American	114	Live wires should be kept covered
AF1	Female	American	120	The kitten chased the dog down the street
AM2	Male	American	152	The jacket hung on the back of the wide chair
AF2	Female	American	144	To reach the end he needs much courage
BF1	Female	British	123	Glue the sheet to the dark blue background
BF2	Female	British	148	Rice is often served in round bowls
BM1	Male	British	123	Four hours of steady work faced us
BM2	Male	British	158	The box was thrown beside the parked truck
Training	Mixed	American	2250	Conversation

The database also contains 45 seconds of speech which was used as training data for the quantisers designed within the speech coders. The speech is a mixture of American male and female utterances.

The speech database contains about 20 seconds of speech, uttered by four male and four female speakers with either American or British accents. The speech was recorded with no background noise and initially was stored in a 12-bit linear PCM representation. Figures 11.17 and 11.18 display the pitch period track of each file, which was determined manually for each speech frame. Frames which showed no visual evidence of voicing, in

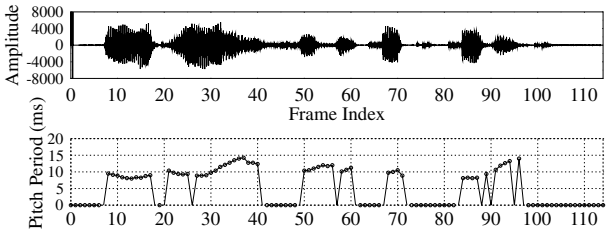

(a) AM1 – Live wires should be kept covered.

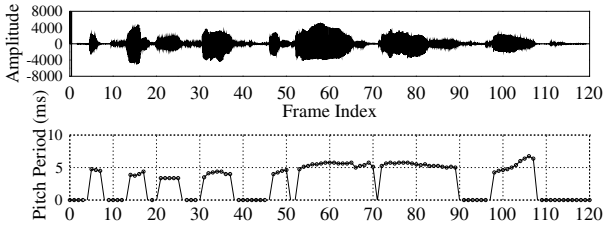

(b) AF1 – The kitten chased the dog down the street.

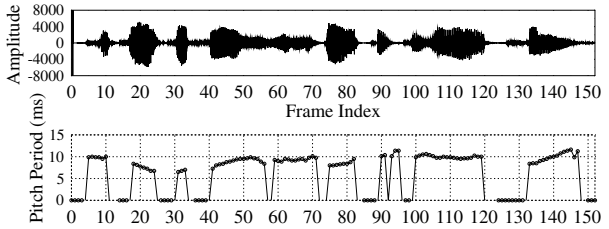

(c) AM2 – The jacket hung on the back of the wide chair.

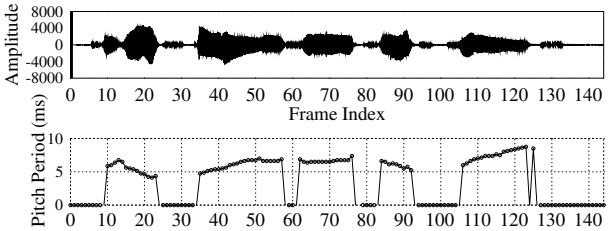

(d) AF2 – To reach the end he needs much courage.

Figure 11.17: Manual pitch period tracks for the American speakers: (a) AM1, (b) AF1, (c) AM2 and (d) AF2 from the speech database.

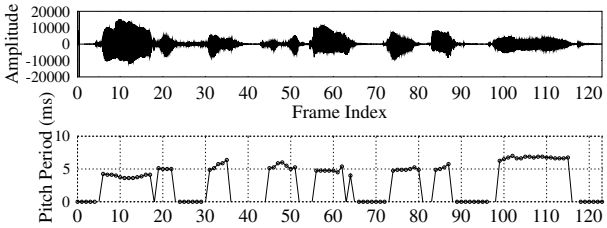

(a) BF1 – Glue the sheet to the dark blue background.

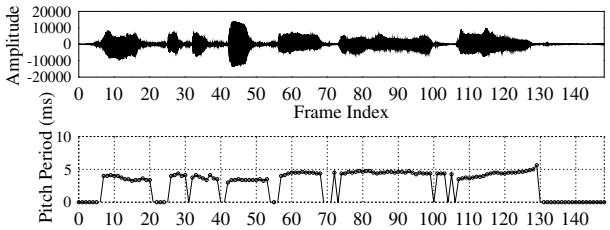

(b) BF2 – Rice is often served in round bowls.

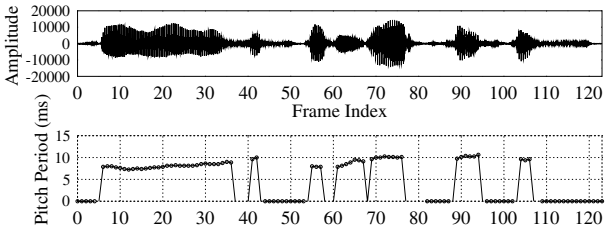

(c) BM1 – Four hours of steady work faced us.

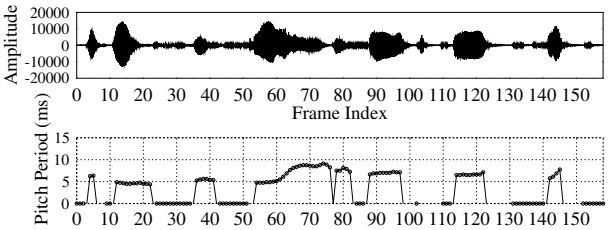

(d) BM2 – The box was thrown against the parked truck.

Figure 11.18: Manual pitch period tracks for the British speakers: (a) BF1, (b) BF2, (c) BM1 and (d) BM2 from the speech database.

periodicity terms, were set to a pitch period of zero. For some speech frames it was difficult to determine the pitch period, or even if the frame was voiced. These frames typically occurred at the end of voiced utterances. Later in this low-rate-coding-oriented part of the book, particularly in Chapters 12 and 13, the manually determined pitch period tracks of Figure 11.1 will be used to assess automated pitch detectors. For the speech frames where our pitch period determination was unreliable, the manually determined tracks were simply ignored in any assessment of the pitch period detectors.

The pitch periods for the speakers were only permitted to be in the range of 18 to 2.5 ms, or 54 to 400 Hz. These limits were introduced due to our bitrate constraints. Allowing pitch periods between 20 and 147 samples at a sampling rate of 8 kHz results in only seven bits being required to transmit the 128 legitimate parameter values, while covering most expected pitch periods. It is acknowledged that some speakers will have pitch periods outside this region, particularly children, however, the pitch period range selected permits us to use an integer pitch period length in samples which covers a wide range of expected pitch periods.

11.5 Chapter Summary

This chapter has given a rudimentary overview of the factors influencing the development of speech coders, paying particular attention to the recent selection of a 2.4 kbps speech coder to replace the DoD FS1015 standard. Speech coding for bitrates less than 2.4 kbps was also reviewed. A brief description of LPC was given in Section 11.2, where AbS was also introduced. A review of assessing the speech quality was given in Section 11.3, where particular attention was given to the speech quality measures adopted for the DoD 2.4 kbps standard. Finally, the speech database used throughout this low-rate-coding-oriented part of the book was introduced. In the next chapter we focus our attention on the most predominant coding techniques used at coding rates below 2.4 kbps, namely on vocoders.

Chapter 12

Linear Predictive Vocoder

In this chapter we introduce a basic LPC vocoder, operating on 20 ms frames, which will provide a benchmarker for the low-bitrate coders that are developed in Chapters 14 and 15. In addition, Section 12.2 introduces the LSF quantiser to be used throughout the developed coders. The notion of pitch detection is introduced in Section 12.3, and the adaptive postfilter that is implemented in the developed decoders is described in Section 12.6.

12.1 Overview of a Linear Predictive Vocoder

The basic LPC vocoder schematic is shown in Figure 12.1 and detailed next. In the encoder, LPC STP analysis is performed initially in order to determine the LPC STP synthesis filter coefficients, which are then quantised into LSFs for transmission to the decoder, as described in Section 12.2. After LPC STP analysis, the short-term correlation has been removed from the speech waveform leaving the STP residual, which contains the prediction errors associated with the LPC STP analysis. This STP residual has its RMS energy determined, quantised and sent to the decoder where it is used to scale the unvoiced excitation. The STP residual is also used in the pitch detection process, described in detail in Section 12.3, where the LPC STP residual displays more conclusive evidence of voicing due to the removal of the short-term correlation. Incorporated in the pitch detector is a voiced–unvoiced decision, which sets a flag to inform the decoder whether voiced or unvoiced excitation should be used in the synthesis process.

At the decoder either random Gaussian noise for unvoiced excitation, detailed in Section 12.4, or a periodic pulse stream for voiced excitation, described in Section 12.5, is passed to the LPC STP synthesis filter. The subsequent output waveform is then passed to an adaptive postfilter, described in Section 12.6, which improves the perceived quality of the synthesised waveform by emphasising the speech spectrum's formants and the spectral pitch harmonics' formants. The resultant waveform is the reconstructed speech signal.

Following this overview of the LPC vocoder, the important implementation issues are discussed. Firstly, the methods for quantising the LSFs are considered.

Voice and Audio Compression for Wireless Communications Second Edition
L. Hanzo, F. C. A. Somerville and J. P. Woodard

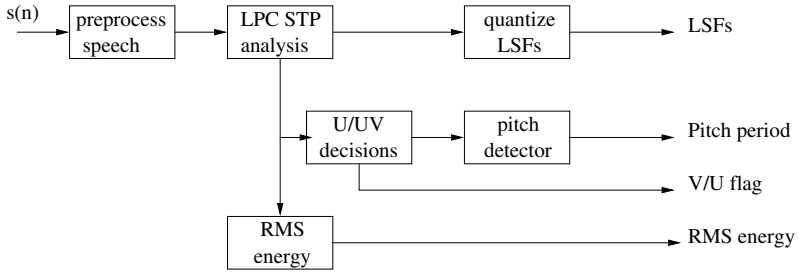

(a) Encoder

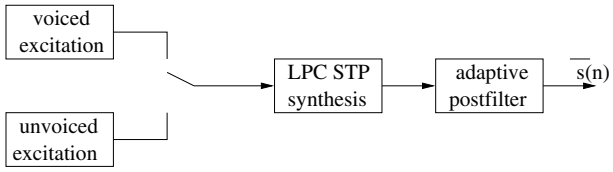

(b) Decoder

Figure 12.1: Schematic of the implemented LPC vocoder.

12.2 Line Spectrum Frequencies Quantisation

For low-bitrate speech coders a significant portion of the available bitrate is consumed by the transmission of the LSF parameters. Thus, next we investigate an economical method of transmitting the LSFs while maintaining good perceptual speech quality. Two quantisation methods are discussed here. The first is the scalar quantiser used in the DoD CELP standardFS-1016 [100], which requires 34 bits/30 ms, the second is the vector quantiser from the ITU standard G.729 [147], which transmits 18 bits/10 ms. The LSF quantiser is incorporated from a speech coding standard due to the extensive training which will have been undertaken in the standardisation process. Importantly, in order to operate the quantiser at its full potential the same preprocessing as in the standard must be employed, in order to ensure that the quantiser is operating on speech similar to its training data. Initially the scalar quantiser from FS1016 is described.

12.2.1 Line Spectrum Frequencies Scalar Quantisation

The SQ from FS-1016 [100] uses 34-bit nonuniform SQ for the LSFs, with the bit assignment for the LSFs given in Table 12.1. The SQ is designed to send the LSFs once every 30 ms speech frame which are smoothly interpolated over the 7.5 ms subframes. Since the SQ operates separately on each speech frame, the quality of the SQ will not be affected by decreasing the speech frame length to 20 ms.

Table 12.1: Bit allocation for LSF coefficients from FS-1016.

	LSF coefficient									
	1	2	3	4	5	6	7	8	9	10
Number of bits allocated	3	4	4	4	4	3	3	3	3	3

The speech coding standard FS-1016 [100] includes preprocessing of the speech signals in the form of a Hamming window and 15 Hz bandwidth expansion of the LPC STP filter coefficients. The Hamming window is given by:

$$w_{\text{ham}}(n) = \begin{cases} 0.54 - 0.46\cos\left(\dfrac{2\pi n}{\text{FL}}\right) & 0 \leq n \leq \text{FL} - 1 \\ 0 & \text{elsewhere} \end{cases}$$

where FL is the speech frame length.

The 15 Hz bandwidth expansion is achieved by modifying the LPC STP filter coefficients according to the following expression:

$$\hat{a}_i = a_i \times 0.994^i, \quad 1 \leq i \leq 10 \tag{12.1}$$

where a_i is the ith LPC STP filter coefficient.

Figure 12.2 demonstrates the performance of the 34-bit SQ for the speech file BF1. It shows that while the SQ is generally good at following the unquantised LSF values, there are occasions where the unquantised LSF values exceed the dynamic range of the SQ.

The performance of an LSF quantiser is typically determined using the SD measure, given by

$$S_d = \sqrt{\frac{1}{I}\sum_{i=1}^{I}[10\log(P_i) - 10\log(\hat{P}_i)]^2} \tag{12.2}$$

where S_d is the SD, P_i is the ith point in the frequency spectrum using unquantised LSF values, $\hat{P}_i$ is the ith point in the frequency spectrum using quantised LSF values and I is the number of points in the frequency spectrum. The frequency spectra are obtained by converting the unquantised and quantised LSF values into unquantised and quantised LPC STP filter coefficients, respectively. The frequency responses created by these filter coefficients are P_i and $\hat{P}_i$.

An LSF quantiser is aiming to achieve three targets in its SD measure [116]: (1) the average SD is approximately 1 dB; (2) the percentage of speech frames with an SD in the 2–4 dB range is less than 2%; and, finally, (3) the percentage of speech frames with an SD of greater than 4 dB is negligible.

Table 12.2 gives details about the performance of the SQ in meeting these performance criteria. It shows that the percentage of outlier frames in the 2–4 dB range and in the range above 4 dB are much higher than desired. However, the average SD is approximately 1 dB.

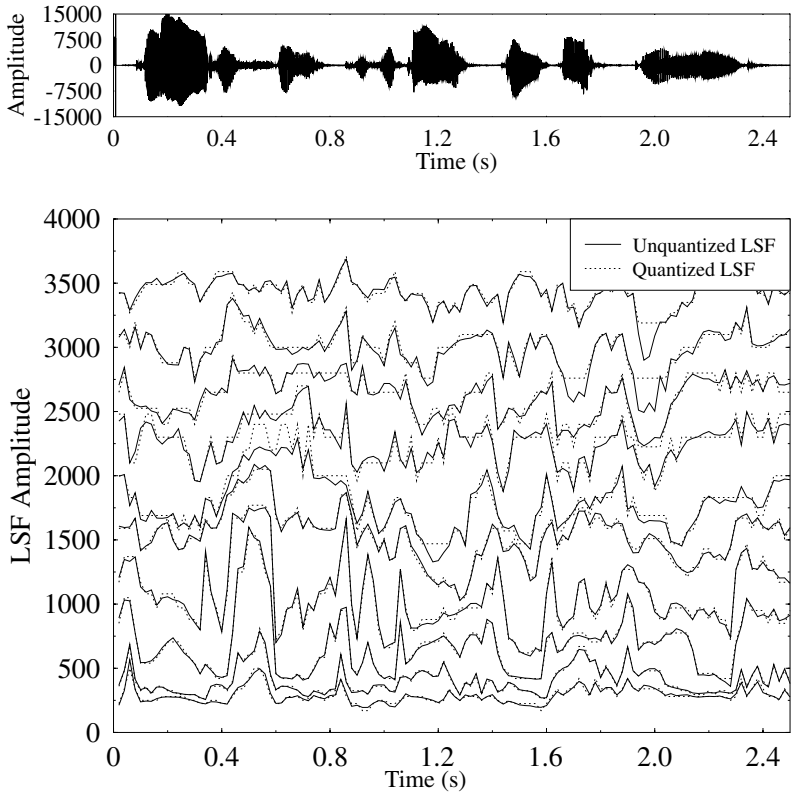

Figure 12.2: The performance of the FS1016 34-bit SQ for speaker BF1. Here LSF1 is the lowest trace with LSF10 being the uppermost trace. Occasionally the unquantised LSF values exceed the limits of the SQ: this occurs in LSF8, LSF9 and LSF10 around the 2 s mark.

Figure 12.3(a) displays the PDF of the LSF SQ SD, showing the existence of a long tail to the right. Next we introduce the LSF VQ from G.729 [147].

Table 12.2: SD performance of the FS1016 SQ and the G.729 VQ.

Quantiser	Mean SD (dB)	SD (%) within 2–4 dB	SD (%) > 4 dB
Scalar	1.16	10.85	1.10
Vector	0.78	1.09	0.00

12.2.2 Line Spectrum Frequencies Vector Quantisation

The VQ from G.729 [147] is a predictive two-stage VQ which sends 18 bits/10 ms. If the LSF coefficients were transmitted every 10 ms, then with our 20 ms frame length 36-bits would be

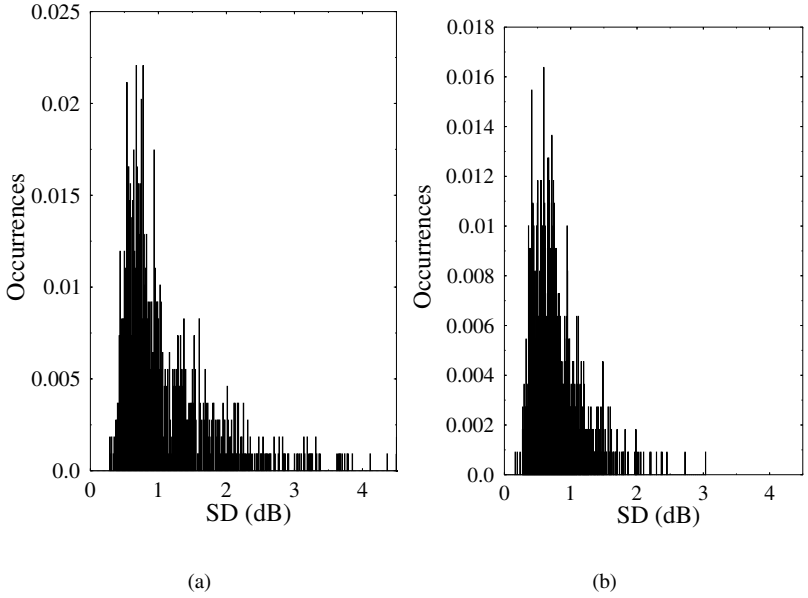

Figure 12.3: The SD PDF for (a) the FS1016 SQ and (b) G.729 VQ. It can be seen that the SD PDF of the VQ in (b) is much more compact.

required to encode the LSFs every speech frame. This higher bitrate requirement compared with the SQ is not acceptable. A suitable alternative is to calculate the LSF coefficients for a 10 ms subframe but only send one set of quantised LSF values for the two subframes, to produce a bitrate of 18 bits/20 ms. The extra computational complexity of performing the required preprocessing on 10 ms subframes must be tolerated so that the quantiser is working on the speech data it was trained for. However, due to the predictive nature of the LSF VQ, the quantisation itself is only performed once every 20 ms.

The preprocessing of the speech performed in G.729 [147] includes a high-pass input filter, windowing and bandwidth expansion. The high-pass input filter has a cutoff frequency of 140 Hz and divides the input signal by two, in order to avoid overflows in the G.729 [147] fixed point implementation. The input filter's transfer function is given by

$$H_{h1}(z) = \frac{0.4636718 - 0.92724705z^{-1} + 0.4636718z^{-2}}{1 + 1.19059465z^{-1} + 0.9114024z^{-2}}. \tag{12.3}$$

Similarly, at the output of the decoder a high-pass output filter with a cutoff frequency of 100 Hz is introduced. The signal must also be multiplied by two, restoring the correct amplitude level. The output filter's transfer function is given by [147]

$$H_{h2} = \frac{0.93980581 - 1.8795834z^{-1} + 0.93980581z^{-2}}{1 - 1.9330735z^{-1} + 0.93589199z^{-2}}. \tag{12.4}$$

The windowing used in G.729 [147] is a hybrid window and spreads over several 10 ms speech frames. It includes 120 samples from previous speech frames, the 80 samples of the current speech frame and 40 samples from the future speech frame. The window is displayed graphically in Figure 12.4, where the peak of the window is over the end of the current speech frame, and the function created using the following expression [147]:

$$w_p(n) = \begin{cases} 0.54 - 0.46\cos\left(\dfrac{2\pi n}{399}\right) & 0 \leq n \leq 199 \\ \cos\left(\dfrac{2\pi(n-200)}{159}\right) & 200 \leq n \leq 239. \end{cases}$$

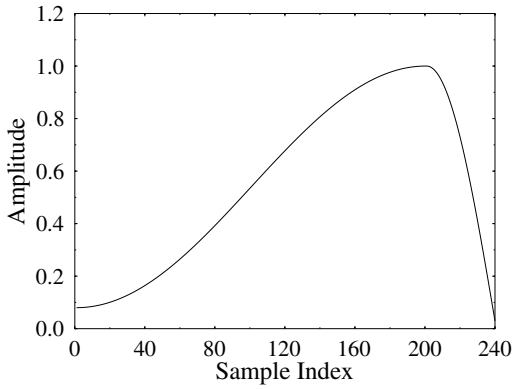

Figure 12.4: The hybrid window employed in G.729 to preprocess the speech.

The final preprocessing performed is a 60 Hz bandwidth expansion of the LPC STP filter coefficients. This is implemented by using another windowing function on the autocorrelation coefficients, $r(k)$, from the LPC STP analysis. The autocorrelation windowing function is given by [147]

$$w_{\text{lag}}(k) = \exp\left[-\frac{1}{2}\left(\frac{2\pi f_o k}{8000}\right)^2\right] \quad k = 1 \ldots 10 \tag{12.5}$$

with a bandwidth expansion of 60 Hz, $f_o = 60$.

Figure 12.5 demonstrates the performance of the 18-bit VQ for the speech file BF1, also used in Figure 12.2. It demonstrates that the predictive nature of the VQ ensures the unquantised values never exceed the limit of the quantiser.

The performance of the VQ was also evaluated using the SD measure. Table 12.2 shows the success of the VQ at meeting the three SD criteria. The average SD measure is less than 1 dB and the number of outlier frames having SDs greater than 2 dB is negligible. The right-hand side of Figure 12.3(b) displays the PDF of the SD measure for the VQ, where it can be seen that the VQ's PDF is much more compact than the SQ, implying a better performance.

Due to the superior SD performance and the reduced bitrate, the LSF VQ was used in all speech coders developed in this low-bitrate oriented part of the book. Next we investigate one

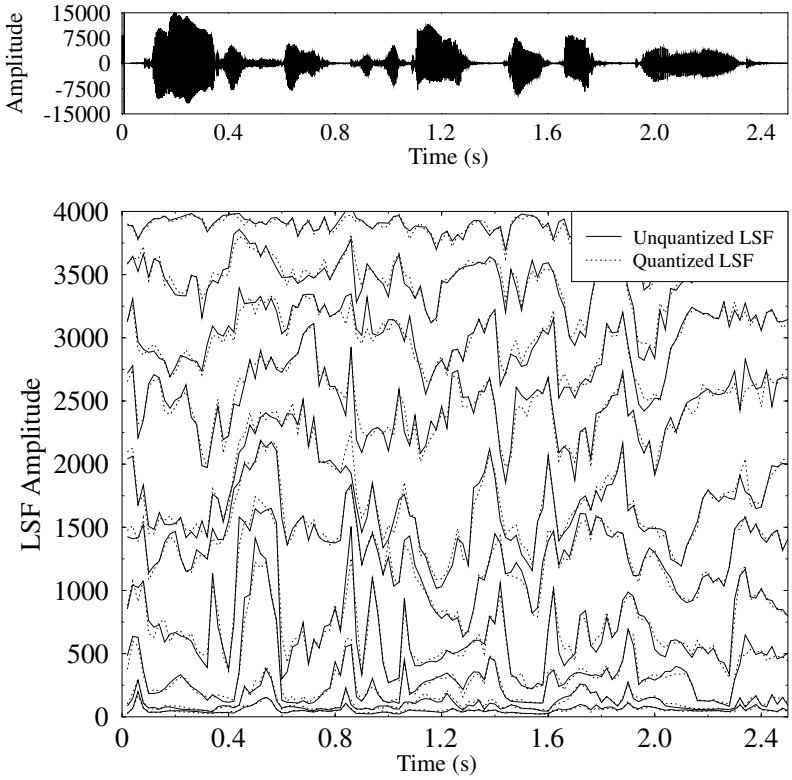

Figure 12.5: The performance of the G.729 18-bit VQ for utterance BF1. Here the lowest trace is LSF1, while LSF10 is the upper trace. The VQ performs well at quantising the LSF values.

of the most critical tasks in low-bitrate speech coders, namely the selection of a reliable and robust pitch detector.

12.3 Pitch Detection

In traditional vocoders, the decision as regards to the extent of voicing in a speech segment is critical. It is important to note that pitch detection is an arduous task due to a number of factors, such as the non-stationary nature of speech, the filtering effect of the vocal tract and the presence of noise. Incorrect voicing decisions cause distortion in the reconstructed speech, and distortion is also apparent if the common phenomenon of pitch doubling occurs. Pitch doubling happens when the energy level of adjacent harmonics is higher than the energy of the fundamental frequency. In addition, smaller pitch errors occur if the analysis window is too short, whereas a non-stationary signal may be encountered if the analysis window is too long.

A detailed explanation of the considerations, together with the various approaches to pitch detection can be found, for example, in the monograph by Hess [14]. Many different

methods exist for pitch detection of speech signals, giving an indication of the difficulty involved in producing a robust pitch detector. Perhaps the most commonly used approaches are the autocorrelation-based methods, where the ACF for a segment of speech is determined. Subsequently, the time-offset where the normalised correlation becomes maximum is deemed to be the pitch period duration. The normalising parameter is the autocorrelation at zero delay, namely, the signal's energy. If the maximum correlation value exceeds a certain threshold the segment of speech is considered voiced, while beneath this threshold an unvoiced segment is indicated.

Another approach to pitch detection is to use a pattern recogniser where a selection of speech properties are assessed to make a voiced–unvoiced classification [506]. Atal and Rabiner [506] claim that voiced–unvoiced classification and pitch determination are two distinct problems that are best treated separately. The speech classification can be determined using measures such as signal energy, zero-crossing rate and the energy of the prediction error, where each selected measure reacts differently to voiced and unvoiced speech. The output quantities of the above classifiers are assessed and an overall decision about voicing is made. Since no decision concerning the pitch is carried out, the voiced–unvoiced decision can be performed on speech segments having a length less than a pitch period. In addition, this method lends itself to implementation with a neural network [507].

Another popular method for pitch determination is to use the cepstrum [508]. Similarly to the autocorrelation method, if the peak cepstral value exceeds a threshold, the speech is considered voiced. If the cepstral peak value did not exceed the threshold a zero-crossing count is performed, where if the number of zero-crossings exceeds a threshold the speech is deemed unvoiced, otherwise the frame is considered voiced. For voiced segments the pitch period is again the location of the peak cepstral value. However, the calculation of the FFT of the speech segment that is required for obtaining the cepstral peak value is computationally intensive.

Recently the wavelet transform has been applied to the task of pitch detection [509]. The wavelet approach to pitch detection is event based, which means that both the pitch period and the glottal closure instant (GCI) are located. The pitch determination methods previously mentioned are all non-event based and assume that the pitch period is stationary within the analysis window.

Kadambe and Boudreaux-Bartels [509] used a dyadic wavelet transform denoted by $\mathrm{D_Y WT}$. For the $\mathrm{D_Y WT}$ the time-domain discontinuities in the speech signal, such as those at the pitch related speech signal peaks, are represented by the corresponding local maxima in the time-domain after the wavelet transform. Explicitly, the action of glottal closure will create a discontinuity in the speech signal, thus, the resultant time-domain representation after the $\mathrm{D_Y WT}$ will contain local maxima at the locations of glottal closure. However, the maxima must exceed a certain threshold for a speech segment to be labelled as voiced. The $\mathrm{D_Y WT}$ is performed at different time-domain resolutions or scales, hence ensuring that it adequately resolves the expected fundamental frequency range (54–400 Hz). For a voiced speech segment, the local maxima at different scales will be aligned. An additional feature of the wavelet transform is that it does not require a full pitch period to operate effectively. The use of the wavelet transform is described in detail in Section 13.5.

A further review of pitch detection methods was given by Rabiner *et al.* [510]. In the documented LPC vocoder the ubiquitous autocorrelation approach was employed. Figure 12.6 shows the ACF for various delays for a segment of voiced speech, demonstrating

that for a voiced speech segment a correlation spike occurs at the appropriate pitch period, with further peaks at the pitch harmonics.

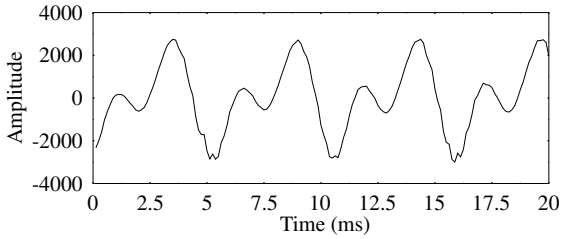

(a) Voiced speech

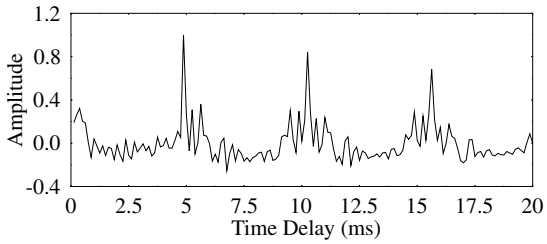

(b) Autocorrelation function

Figure 12.6: Example showing the autocorrelation for a voiced speech frame from speech file AF2.

12.3.1 Voiced–Unvoiced Decision

For the pitch predictor investigations initially a simple scheme was employed, where the speech was low-pass filtered to 900 Hz. Noise tends to contaminate the low-energy, high-frequency speech components, thus by removing the high-frequency noise the prominence of the pitch related signal components increases. The next stage involves centre clipping setting the low-magnitude signal segments to zero, in order to increase the prominence of the signal's periodicity, with autocorrelation subsequently performed. This simple pitch detector failed to detect some voiced frames, particularly those near the start or end of a voiced sequence.

An alternative pitch detection technique can be constructed using the approach of the G.728 recommendation [109]. Here the signal utilised for pitch detection is the residual signal after the LPC STP analysis, since the pitch period becomes more prominent in the residual signal due to the removal of the short-term correlation by the LPC process. The ACF selects the best candidate, A, in the current residual frame for the pitch period and the best candidate, B, around the old pitch period used in the previous frame. Preferential treatment of candidate B attempts to remove the chance of pitch doubling, through the introduction of pitch tracking as follows. If the pitch gain at delay B is more than 40% of the pitch gain for

delay A, then candidate B is selected, otherwise candidate A is selected. If the successful candidate has a pitch period gain higher than 0.7 then the frame is considered voiced, with a pitch period equal to the selected delay. Determination of unvoiced frames depends on whether the previous frame was voiced or unvoiced. If the previous frame was unvoiced a pitch period gain of less than 0.7 indicates an unvoiced frame, hence the pitch period is set to zero. However, if the previous frame was voiced then a pitch gain of greater than 0.5 would indicate a voiced frame.

The voicing strength is defined by the following normalised correlation function:

$$\frac{\sum_{n=0}^{\mathrm{FL}} s(n) \times s(n-P)}{\sum_{n=0}^{\mathrm{FL}} s(n-P) \times s(n-P)} \tag{12.6}$$

where FL is the frame length in samples and P is the selected pitch period length in samples. Thus, the voicing strength is the ratio of the cross-correlation of the speech signal, $s(n)$, and pitch period duration delayed speech signal, $s(n-P)$, to the energy of the pitch period duration delayed speech signal. The evolution of the voicing strength for speech file AM1 is displayed in Figure 12.7. The voicing strength can be seen to frequently fall to low levels while the time-domain plot of the speech clearly shows that it is voiced. A pitch in the range 54–400 Hz is permitted, as this is the typical range of human fundamental frequency. Figure 12.8 demonstrates that the current autocorrelation-based pitch detector produces both gross pitch errors and pitch halving errors with more than half of the utterance BF1 subjected to pitch halving. The performance of this autocorrelation-based pitch detector is compared in Table 12.4, for the entire speech database, against the manual pitch period track of Figures 11.17 and 11.18 from Section 11.4. It was found that 12.7% of frames were incorrectly labelled.

12.3.2 Oversampled Pitch Detector

A method frequently employed to improve the performance of autocorrelation-based pitch detectors is oversampling, where oversampling will increase the time-domain resolution of the search. Both the DoD 4.8 kbps standard FS-1016 [197] and the VSELP coder utilized in the GSM half-rate coder [97] use oversampling to improve the pitch tracker's performance.

For the GSM VSELP coder the signal is up to six times oversampled, thus allowing non-integer delays to be accepted as the pitch period. Table 12.3 shows the integer delays allowed for various pitch period ranges.

Table 12.3: Allocation of non-integer delays for the GSM VSELP half-rate coder.

Delay range	Delay resolution	Number of sample points
21–22, 2/3	1/3	6
23–34, 5/6	1/6	72
35–49, 2/3	1/3	45
50–89, 1/2	1/2	80
90–142	1	52

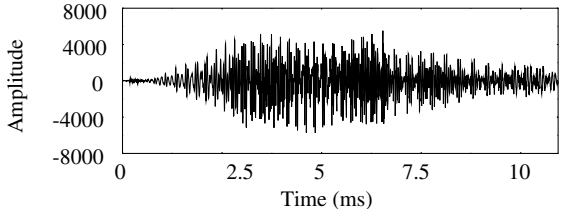

(a) Utterance – wires

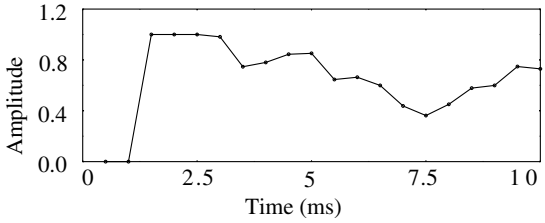

(b) Voicing strength

Figure 12.7: Example showing the evolution of voicing strengths for the speech file AM1.

Observing Table 12.3 it can be seen that the GSM VSELP coder provides child and adult female speakers with the highest resolution, while adult male speakers have a lower resolution. This variable resolution produces a relative pitch error with respect to the pitch itself which is nearly constant, maintaining a similar pitch detection quality for all speakers.

In order to calculate the voicing strength of a non-integer delay l_d/D_s at a sampling frequency f_s and oversampling rate D_s, the up-sampling is performed and the equivalent integer delay l_d at sampling frequency $D_s \cdot f_s$ is found. From Figure 12.9 it can be seen that the up-sampled signal is generated by inserting $D_s - 1$ samples between every original input sample with the inserted samples being zero-valued. The resultant signal is low-pass filtered to obey the Nyquist rate, thus producing an oversampled version of the input signal.

For the DoD 4.8 kbps standard FS-1016 [100] the up-sampling is performed with an eight-point Hamming window sinc re-sampling function. Thus, to oversample by a factor of six

$$w_{f_{id}}(i) = w_{\text{ham}}(12(i + f_{id}))\frac{\sin(\pi(i + f_{id}))}{\pi(i + f_{id})} \tag{12.7}$$

where

$$i = \frac{-N_{ip}}{2}, \frac{-N_{ip}}{2} + 1, \ldots, \frac{N_{ip}}{2} - 1$$

and $N_{ip} = 8$ is the number of interpolation points. The non-integer delays are given by $f_{id} = \frac{1}{6}, \frac{1}{3}, \frac{1}{2}, \frac{2}{3}, \frac{5}{6}$ with the integer delays given by M. The Hamming window is given by

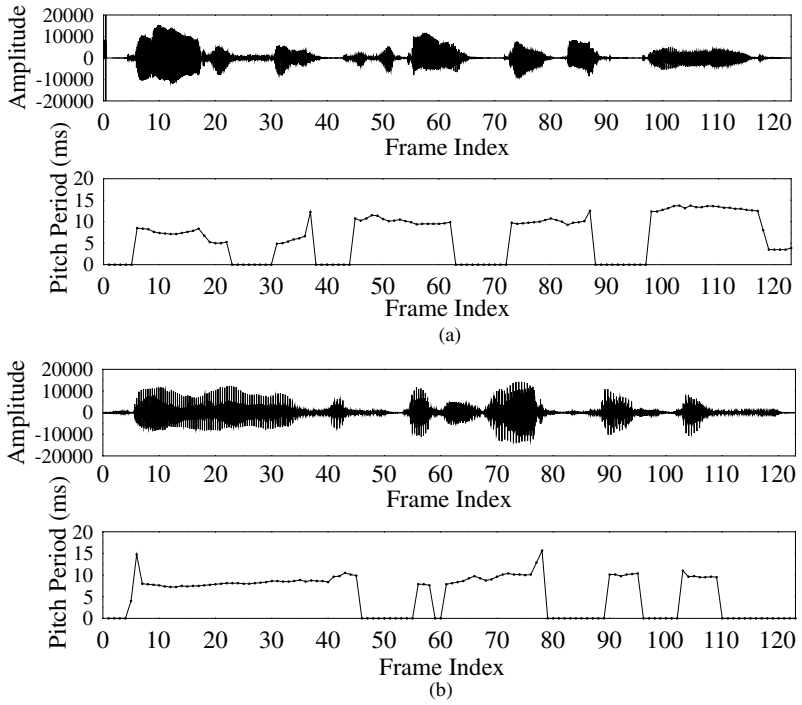

Figure 12.8: Pitch period decisions for (a) BF1 and (b) BM1. For BF1 a gross pitch error is visible at frame 36 in comparison to the manual track of Figure 11.18, with the rest of the speech utterance subjected to pitch halving. For BM1 gross pitch errors are visible at frames 5 and 77.

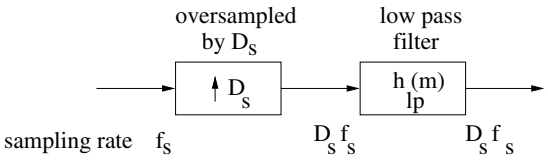

Figure 12.9: Schematic of the process of interpolation, where the inserted $D_s - 1$ values are zero samples.

$w_{\text{ham}}(k) = 0.54 + 0.46\cos(\pi k/6N_{ip})$, where $k = -6N_{ip}, -6N_{ip}+1, \ldots, 6N_{ip} = -48$ to 48.

Then for a non-integer delay $M + f_{id}$ we have

$$r_{M+f_{id}}(i) = \sum_{k=-N_{ip}/2}^{N_{ip}/2} w_{f_{id}}(k) r_{M+f_{id}}(i - M + k) \tag{12.8}$$

where the index, i, is some point in the speech frame from which all delays are calculated and $r_{M+f_{id}}(i)$ represents a sampling point at the new sampling frequency D_s. Figure 12.10

shows a speech signal which has been oversampled by a factor of six, where the peaks and valleys are more extreme and the signal is smoother.

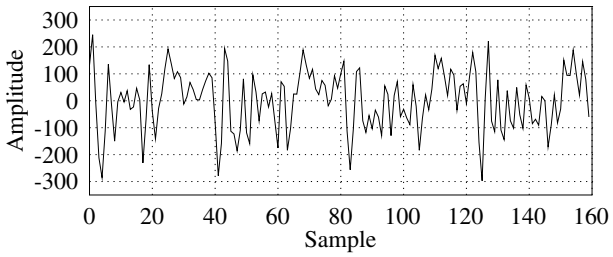

(a) Original signal

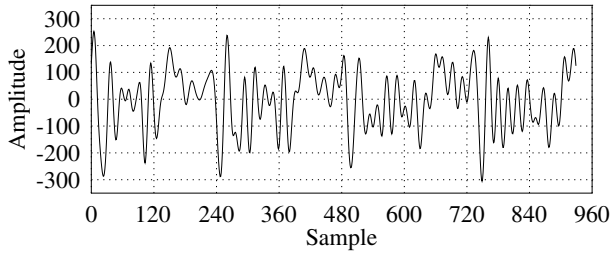

(b) Oversampled by six

Figure 12.10: Oversampling of a speech signal by a factor of six.

Table 12.4: A comparison between the performance of the developed pitch detectors and the manual pitch period track for the speech database. W_U represents the percentage of frames that are labelled voiced when they should have been identified as unvoiced. W_V indicates the number of frames that have been labelled as unvoiced when they are actually voiced. P_G represents the number of frames where a gross pitch error has occurred. The total number of incorrect frames is given by $W_U + W_V + P_G$.

Pitch detector	W_U (%)	W_V (%)	P_G (%)	Total (%)
ACF-based method	1.6	5.3	5.8	12.7
Oversampled ACF method	5.4	3.9	4.7	14.0
Oversampled ACF with tracking	3.1	2.3	1.8	7.2

The oversampled speech signal can be subjected to autocorrelation computation in order to locate the most likely pitch period delay and to determine the voicing strengths. Figure 12.11 shows the updated pitch period decisions for the same utterances as displayed in

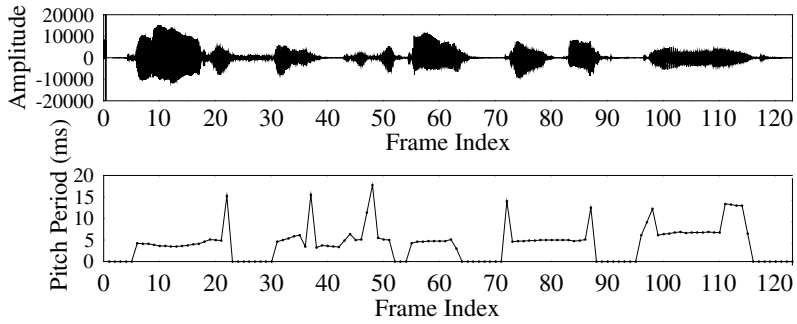

(a)

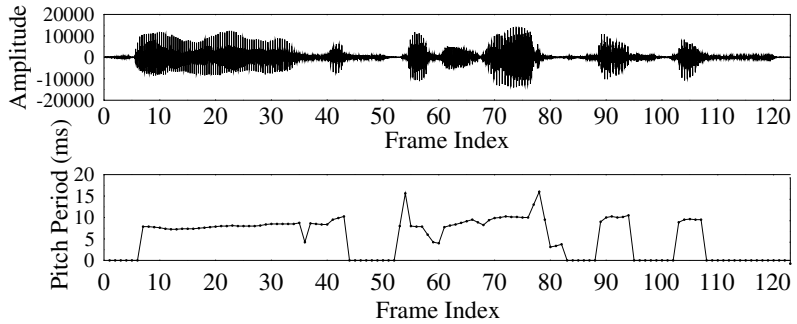

(b)

Figure 12.11: Pitch period decisions based on the technique of Section 12.3.2 for (a) BF1 and (b) BM1. Here the ACF has been oversampled by six. For BF1 the pitch halving has been corrected, however, many gross pitch errors have been introduced. For BM1 the gross pitch errors are now located at frames 52 and 77. For comparison we refer to Figures 11.18 and 12.8.

Figure 11.18 and 12.8, where the voiced–unvoiced threshold levels were updated from 0.7 and 0.5 to 0.8 and 0.5. Figure 12.11 shows that most of the pitch halving was removed from the pitch track; however, many more gross pitch errors were introduced. This oversampled pitch detector was compared against the manual track of Figures 11.17 and 11.18 in Table 12.4, where 14.0% of the frames were incorrectly determined.

12.3.3 Pitch Tracking

Explicit checking for pitch doubling and halving, together with pitch tracking mechanisms, are frequently employed in pitch detectors. The GSM half-rate VSELP coder [97] performs explicit checking for pitch doubling and halving. Figure 12.12 describes its operation with the flow chart followed below.

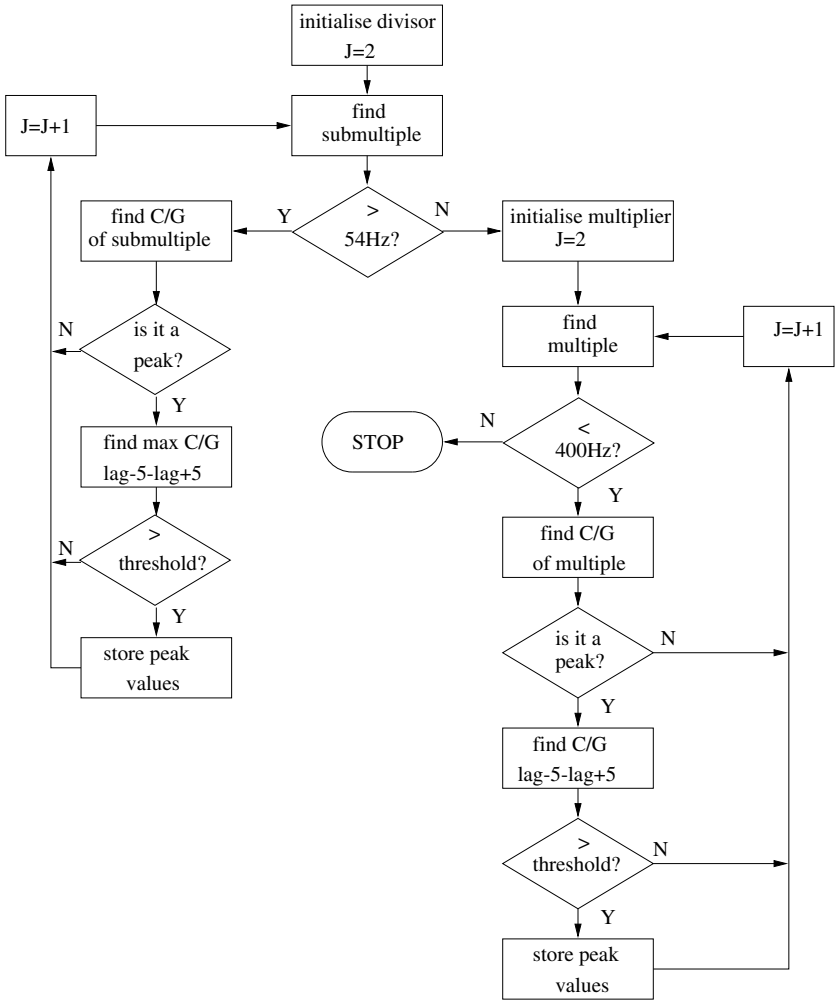

Figure 12.12: Flow chart for checking pitch doubling and halving in the 5.6 kbps half-rate GSM VSELP coder.

As seen in Figure 12.12, initially all of the submultiples, down to 54 Hz, of the best pitch are checked. Once the submultiple has been located the adjacent integer peaks are examined to ensure that the associated prediction gain of the proposed submultiples is the highest possible value. The prediction gain is given by C_1^2/G_1, where

$$C_1 = \sum_{n=0}^{\mathrm{FL}} s(n) \times s(n-P) \tag{12.9}$$

$$G_1 = \sum_{n=0}^{\mathrm{FL}} s^2(n-P) \tag{12.10}$$

with P the proposed pitch delay, and C_1 is the correlation of $s(n)$ in the numerator of Equation (12.6) while G_1 is the energy of $s(n)$ in the denominator of Equation (12.6).

If the prediction gain at the proposed pitch submultiple is still higher than its neighbours then the prediction gains of the surrounding non-integer delays are examined. The delay exhibiting the highest prediction gain is compared against a threshold as seen in Figure 12.12. If the threshold is exceeded, the associated submultiple is selected as the pitch delay. Once all possible submultiples have been checked all multiples of the current proposed pitch delay are examined, up to 400 Hz. A similar procedure is followed for the pitch multiples with the best proposed pitch delay selected as the true pitch delay.

The threshold for selecting a new pitch delay is given by [97]

$$\frac{C_1^2}{G_1} > R(0) - \frac{R(0)}{10^x} \tag{12.11}$$

where $R(0) = \sum_{n=0}^{\mathrm{FL}} s^2(n)$ and

$$x = \alpha_{CG} \log_{10}\left(\frac{R(0)}{R(0) - C_{\mathrm{best}}^2/G_{\mathrm{best}}}\right) \tag{12.12}$$

where C_{best}^2 and G_{best} are the values for the proposed pitch delay and the factor $\alpha_{CG} = 2.75$ was determined experimentally.

A simple pitch tracking mechanism was also introduced into the pitch detector. The Inmarsat standard [511] performs a simple pitch tracking method, whereby

$$0.8P_{\mathrm{past}} \leq P_{\mathrm{current}} \leq 1.2P_{\mathrm{past}} \tag{12.13}$$

thus, the pitch delay of the current speech frame must be close to the determined pitch delay of the previous speech frame. Our final pitch detector procedure is given in Figure 12.13.

From Figure 12.13 it can be seen that the first pitch detector task is to check whether the previous frame was voiced. If it was, then the pitch tracking mechanism described by Equation (12.13) uses the previous frame to constrain the current pitch in the vicinity of the past pitch. However, if the last frame was unvoiced then the pitch tracking mechanism checks whether the last but one frame was voiced, and thus if it can be used in the pitch tracking. If neither frame was voiced then no pitch tracking restrictions are imposed upon the pitch detector. Subsequently, the residual signal is oversampled by six, followed by the ACF calculation. The voicing strength for the delay selected by the ACF computation is compared with a threshold, as described in Section 12.3.1 and seen in Figure 12.12. If this threshold is not exceeded the frame is declared unvoiced. The frames that have exceeded the threshold are voiced and have their submultiples checked, as described by Figure 12.12, and the final pitch period is then assigned to this voiced frame.

The pitch tracks for the utterances in Figure 12.8 are given in Figure 12.14. It can be seen that the improvements to the pitch detector have removed the gross pitch error and the majority of the pitch halving. A performance comparison with the manual pitch track of Figures 11.17 and 11.18 in Section 11.4 is given in Table 12.4, where 7.2% of frames were incorrect.

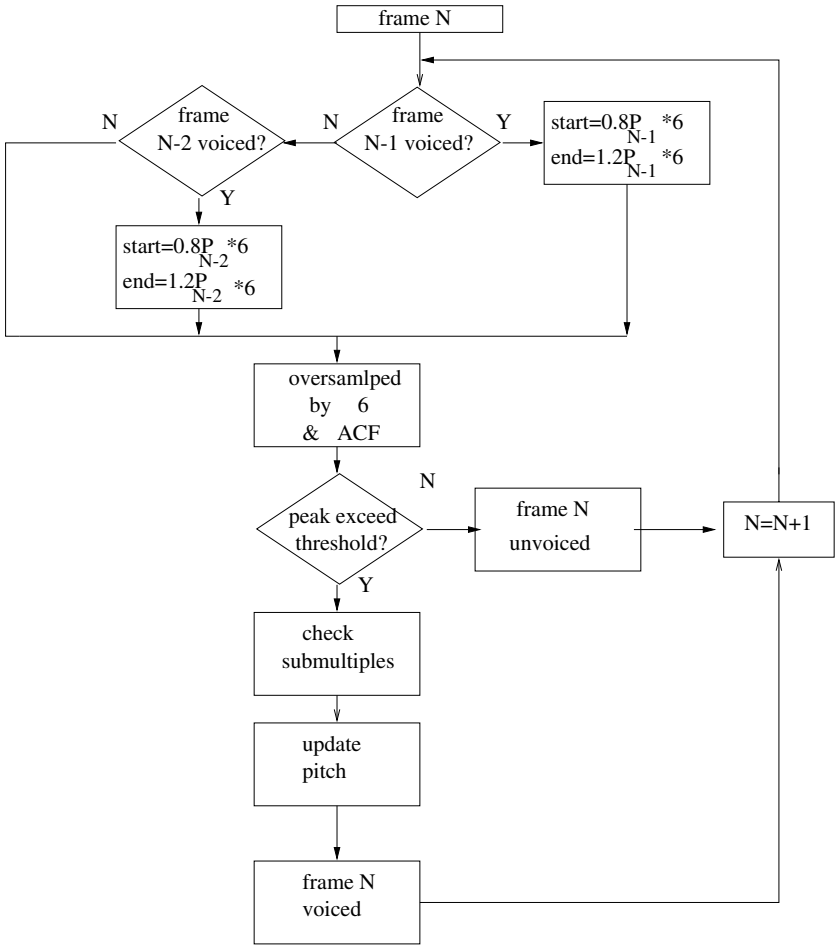

Figure 12.13: Proposed flow chart for pitch detection.

12.3.3.1 Computational Complexity

The computational complexity of an operation is measured in FLOPS, where the number of multiplications or additions performed per second is calculated, with a complexity value larger than 25 MFLOPS deemed to be prohibitive here. The computational complexity for the oversampled pitch detector is given in Table 12.5, demonstrating that the use of oversampled signals in pitch detection proportionally increases the computational complexity of the process. Table 12.5, in the first column, details the computational costs of the oversampled pitch detector in a worst-case scenario of a fundamental frequency of 400 Hz and when there is no past pitch period which allows pitch tracking to be employed. As mentioned above the complexity of 36.3 MFLOPS renders the use of a fully oversampled pitch detector prohibitively complex. It should be noted that the computational complexity values in Table 12.5 used the FFT function to reduce the complexity of the autocorrelation process.

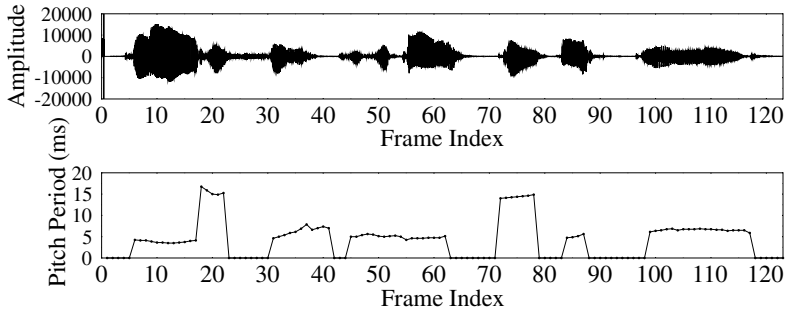

(a)

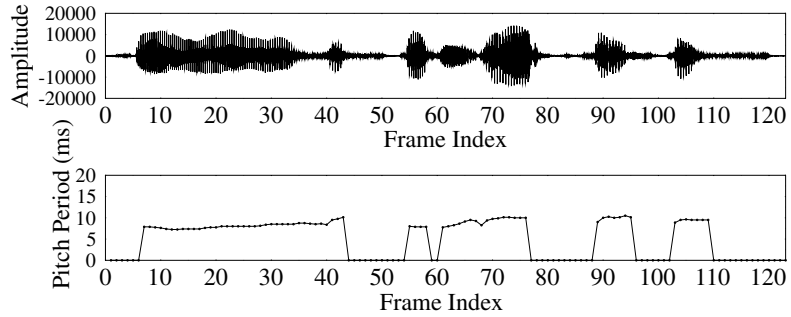

(b)

Figure 12.14: Pitch period decisions based on the flow chart of Figure 12.13 for (a) BF1 and (b) BM1. Here the ACF has been oversampled by six and pitch tracking has been adopted. All gross pitch errors have been removed from BF1, with pitch halving occurring between frames 16 and 20, and between frames 70 and 76. For BM1 no pitch errors occur. For comparison we refer to Figures 11.18, 12.8 and 12.11.

Throughout this low-bitrate oriented part of the book – where possible the computational complexity was decreased using the FFT.

12.3.4 Integer Pitch Detector

In order to reduce the computational complexity of the oversampled pitch detector, oversampling could be restricted to the final search for the nearest non-integer delay. In Figure 12.12 this is the block where the maximum value of C_1^2/G_1 for the pitch values of $\mathrm{lag}-5$ to $\mathrm{lag}+5$ is located. In the second column of Table 12.5 it can be seen that this partial oversampling procedure reduces the complexity to 27.3 MFLOPS, a value that is still prohibitive. It should be noted that, if oversampling is removed from the autocorrelation

Table 12.5: Computational complexity for worst-case scenario for three pitch detectors with differing amounts of oversampling.

Procedure	Fully oversampled by six (MFLOPS)	Partially oversampled by six (MFLOPS)	No oversampling (MFLOPS)
Constructing oversampled array	2.2	2.2	—
Calculating autocorrelation	5.1	1.1	1.1
Checking submultiples	29.0	24.0	2.3
Total	36.3	27.3	3.4

procedure, the voiced–unvoiced thresholds should be returned to the 0.7 and 0.5 levels, used by the G.728 pitch detector [109] as described in Section 12.3.1.

In the final column of Table 12.5 the computational complexity for a pitch detector with no oversampling is given, but both pitch tracking and checking of submultiples is included. A computational complexity of 3.4 MFLOPS is more acceptable, thus the performance of this pitch detector is considered. This pitch detector is identical to the pitch detector described in Section 12.3.2, but all of the oversampling has been removed. The new pitch detector results were surprisingly good, with results comparable to the oversampling by six pitch detector, where from Table 12.4 it can be seen that 7.2% of frames had a pitch detection error. For the integer pitch detector the parameter α_{CG} from Equation (12.12) was adjusted so $\alpha_{CG} = 3$. The quality of the integer sampling pitch detector suggests that the improvement in pitch detector quality is predominantly due to the pitch tracking and checking of pitch submultiples, rather than the oversampling process. Thus, an integer pitch detector with both pitch tracking and checking of pitch submultiples was used for the implementation of the LPC vocoder.

Following this examination of pitch detection, various aspects of the LPC decoder are investigated. The first stages of the decoder are the generation of voiced and unvoiced excitation sources.

12.4 Unvoiced Frames

For speech frames that are classed as unvoiced, at the decoder a Gaussian random process can be used to represent unvoiced excitation. The Gaussian random process is scaled by the RMS of the LPC residual signal, as defined by:

$$\mathrm{RMS} = \sqrt{\frac{\sum_{n=1}^{\mathrm{FL}} r(n)^2}{\mathrm{FL}}} \tag{12.14}$$

where FL is the frame length of the speech segment and $r(n)$ is the LPC residual signal, described in Section 11.2. The Gaussian random process was generated by applying the Box–Muller algorithm [177].

For transmission the RMS value requires quantisation. In the described LPC coder a Lloyd–Max quantiser [10] was employed for the task, which requires knowledge of the RMS

parameters' PDF. This was supplied in the form of a PDF generated from the unquantised RMS values of 45 s of speech from the training database, and it is portrayed in Figure 12.15. Table 12.6 displays the SNR values found for a 2- to 6-bit SQ. For our coder the 5-bit quantiser was selected, because this produced a similar SNR value to the SQs described later in Section 14.5.2.

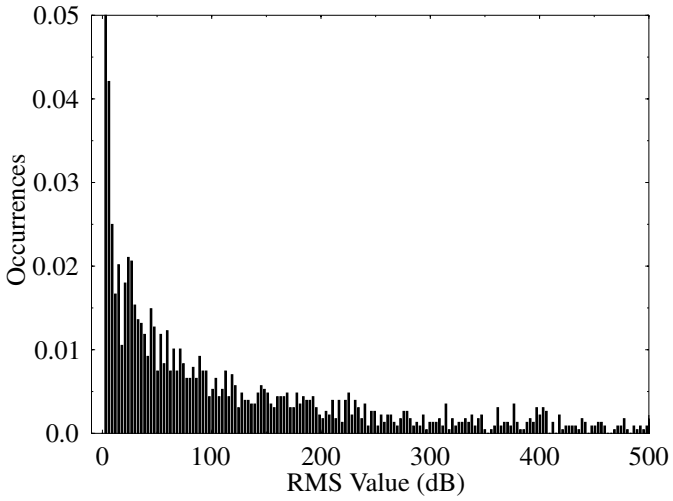

Figure 12.15: Typical PDF of the RMS of the weighted LPC residual.

Table 12.6: SNR values for a range of RMS SQs.

SQ	SNR (dB)
2-bit	2.79
3-bit	8.63
4-bit	19.07
5-bit	25.85
6-bit	32.28

12.5 Voiced Frames

For speech frames that are classified as voiced, the excitation source, which is passed to the LPC STP synthesis filter, is a stream of pulses. These pulses are situated a pitch period distance apart with their energy scaled to reproduce speech of the same energy as the original speech waveform.

12.5.1 Placement of Excitation Pulses

At the beginning of a voiced sequence of frames the first pulse is situated at the start of the frame, while subsequent pulses are placed a pitch period number of samples beyond the previous pulse. Thus, the decoder must remember the position of the last pulse in every voiced speech frame in order to calculate the position of the first pulse in the next voiced speech frame. The positioning of the pulses bears no resemblance to the position of pitch periods in the original speech, thus, it is highly probable that the synthesised and original speech waveform will not be time aligned. This prevents any of the objective measures described in Section 11.3.1 from being utilised to determine the speech coder's performance. Instead, subjective measures will have to be relied on.

12.5.2 Pulse Energy

In order to recreate speech of the same energy as the original, the energy of the periodic pulses must be scaled. Explicitly, the energy of the reconstructed speech must equal the energy of the original speech, formulated as

$$\sum_{n=0}^{\mathrm{FL}}[\rho_a\delta(n) * h(n)]^2 = \sum_{n=0}^{\mathrm{FL}}[s(n) - m(n)]^2 \tag{12.15}$$

where $s(n)$ is the original speech, $m(n)$ is the memory of the LPC STP synthesis filter, $h(n)$ is the impulse response of the LPC STP synthesis filter, ρ_a is the amplitude of each pulse and the Kronecker delta function $\delta(n)$ represents the location of the pulses. The energy of the excitation signals must also be equal, thus

$$\sum_{n=0}^{\mathrm{FL}}[\rho_a \cdot \delta(n)]^2 = \sum_{n=0}^{\mathrm{FL}} r(n)^2 \tag{12.16}$$

where $r(n)$ is the LPC STP residual. Since the RMS energy of the LPC STP residual has already been calculated in Equation (12.14), the combined energy of the pulses, ρ_a^2, can be calculated with the RMS value of the speech. Thus, the same RMS value can be transmitted for both voiced and unvoiced frames.

For I_p pulses per frame, the energy of each pulse will be ρ_a^2/I_p and the amplitude of each pulse becomes $\sqrt{\rho_a^2/I_p}$. Hence, the RMS of the LPC STP residual is sent to the decoder for both voiced and unvoiced frames.

The final stage of the LPC decoder is the adaptive postfilter, which is used to improve the perceived quality of the synthesised speech, and is described next.

12.6 Adaptive Postfilter

For a speech coder that operates at bitrates less than 16 kbps, the coding noise becomes a problem. Namely, a lower coding rate raises the quantisation noise level, thus potentially increasing the complexity of preventing the noise from exceeding the audibility threshold. For AbS speech coding models, the weighting of the LPC STP filter at the encoder can

help to reduce coding noise, while at the output of the decoder an adaptive postfilter can be implemented. For the basic LPC vocoder described here, the adaptive postfilter can also be used to improve the output speech.

An adaptive postfilter [110] is a series of filters whose parameters alter every frame in an attempt to conceal the coding noise. The principle of postfiltering is that, at the output of the decoder, the formant and pitch peaks of the synthetic speech are emphasised and the valleys, which are contaminated by quantisation noise, are attenuated in order to render their effect less audible.

An adaptive postfilter consists of three distinct sections: a STPF, a LTPF and adaptive gain control (AGC), as demonstrated in Figure 12.16.

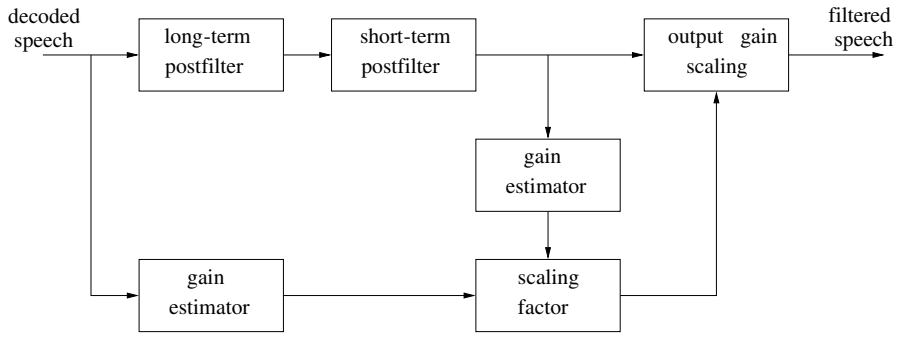

Figure 12.16: An adaptive postfilter.

The STPF follows the peaks and valleys of the spectral envelope, emphasising the formants while attenuating the spectral valleys. The weighted LPC STP synthesis filter creates the shape of the spectral envelope, thus the STPF is based on the weighted synthesis filter. However, the weighted synthesis filter introduces a spectral tilt in the high-frequency regions, hence influencing the energy of the formants. Subsequently, an all-zero filter is introduced in the numerator of Equation (12.17) to remove the spectral tilt, together with an additional first-order filter to further reduce the tilt, namely the bracketed term of Equation (12.17), as seen in the following:

$$H_{\mathrm{spf}}(z) = \frac{1 - \sum_{k=1}^{10} \beta_{\mathrm{pf}}^{k} a_k z^{-k}}{1 - \sum_{k=1}^{10} \alpha_{\mathrm{pf}}^{k} a_k z^{-k}} [1 - \mu_{\mathrm{pf}} z^{-1}] \tag{12.17}$$

where $\mu_{\mathrm{pf}} = 0.5k_1$ and k_1 is the first reflection coefficient from the LPC STP analysis, detailed in Section 11.2. With α_{pf}^{k} and β_{pf}^{k} controlling the amount of STPF.

This reduces the spectral tilt most dramatically for voiced speech, since voiced speech has previously been exposed to low-pass filtering due to the spectral tilt present in the weighted synthesis filter.

The LTPF follows the peaks and valleys of the pitch harmonics, again emphasising the peaks and attenuating the valleys. It is based on the one-tap pitch predictor, $(1 - g_{\mathrm{pf}} z^{-p})$, used in LTP analysis, which was described in Section 11.2. However, an all-zero filter is cascaded with it to allow more flexibility and greater control over the frequency response. The LTPF is switched off during unvoiced speech since there are no pitch harmonics. Thus, the LTPF must have unity power gain to ensure that voiced speech is not amplified over

unvoiced speech. Hence, the LTPFs transfer function is given by

$$H_{\mathrm{lpf}}(z) = G_{\mathrm{lpf}} \frac{1 + \gamma_{\mathrm{pf}} z^{-P}}{1 - g_{\mathrm{pf}} z^{-P}} \tag{12.18}$$

where $0 < \gamma_{\mathrm{pf}}, g_{\mathrm{pf}} < 1$, G_{lpf} is the adaptive gain of the filter, P is the pitch period of the speech frame, and γ_{pf} and g_{pf} control the extent of the long-term postfiltering. The amount of long-term postfiltering is proportional to the voicing strength in a speech frame, thus

$$\gamma_{\mathrm{pf}} = \gamma_{1\mathrm{pf}} f(x) \tag{12.19}$$

$$g_{\mathrm{pf}} = g_{1\mathrm{pf}} f(x) \tag{12.20}$$

where

$$f(x) = \begin{cases} 0 & \text{if } v_{\mathrm{s}} < U_{\mathrm{th}} \\ v_{\mathrm{s}} & \text{if } U_{\mathrm{th}} < v_{\mathrm{s}} \leq 1 \\ 1 & \text{if } v_{\mathrm{s}} > 1 \end{cases} \tag{12.21}$$

with U_{th} being the threshold for enabling the LTPF and v_{s} is the voicing strength indicator, generally based on the tap weight of the single tap long-term predictor. Thus,

$$v_{\mathrm{s}} = \frac{\sum_{n=0}^{\mathrm{FL}} \bar{s}(n) \times \bar{s}(n-P)}{\sum_{n=0}^{\mathrm{FL}} \bar{s}(n-P)^2}$$

where P is the pitch period, FL is the frame length and $\bar{s}(n)$ is the decoded speech. This is equivalent to the pitch detector voicing strength of Equation (12.6). Chen and Gersho have shown [110] that the gain of the LTPF can be controlled by

$$G_{\mathrm{lpf}} = \frac{1 - g_{\mathrm{pf}}/v_{\mathrm{s}}}{1 + \gamma_{\mathrm{pf}}/v_{\mathrm{s}}}. \tag{12.22}$$

When selecting the parameters of the LTPF in Equation (12.18), typically g_{pf} in Equation (12.22) is set to a low value, thus decreasing the interframe memory effects in the LTPF.

The final section of the adaptive postfilter is the AGC, which attempts to prevent the time-variant amplification of the speech signal. The AGC operates by estimating the magnitude of the input and output signals of the postfilter, where subsequently the output signal is adjusted on a sample-by-sample basis. The action of the AGC is described by a scaling factor of

$$G_{\mathrm{pf}} = \frac{\sigma_{1\mathrm{pf}}(n)}{\sigma_{2\mathrm{pf}}(n)} \tag{12.23}$$

where

$$\sigma_{1\mathrm{pf}}(n) = \xi_{\mathrm{pf}} \cdot \sigma_{1\mathrm{pf}}(n-1) + (1 - \xi_{\mathrm{pf}}) \cdot |\bar{s}(n)| \tag{12.24}$$

$$\sigma_{2\mathrm{pf}}(n) = \xi_{\mathrm{pf}} \cdot \sigma_{2\mathrm{pf}}(n-1) + (1 - \xi_{\mathrm{pf}}) \cdot |\hat{s}(n)| \tag{12.25}$$

and $\bar{s}(n)$ is the input to the postfilter, $\hat{s}(n)$ is the output from the postfilter, while ξ_{pf} determines the rate of change for the AGC. Equations (12.24) and (12.25) constitute a

weighted sum of the current signal magnitudes $|\bar{s}(n)|$ and $|\hat{s}(n)|$ together with the previous values $\sigma_{1\mathrm{pf}}(n-1)$ and $\sigma_{2\mathrm{pf}}(n-1)$.

Typical adaptive postfilter responses are shown in Figure 12.17. The STPF frequency response shows how the introduction of the first-order filter and the spectral tilt filter, both shown in Equation (12.17), remove the spectral tilt introduced by the all-pole filter. The postfilter frequency response demonstrates how the postfilter attenuates both the spectral envelope valleys and the pitch harmonic valleys. Following the subjective optimisation of various postfilter parameters the optimised selected parameters are given in Table 12.7.

Table 12.7: Appropriate adaptive postfilter values for the LPC vocoder, described in Equations (12.17)–(12.24).

Parameter	Value
α_{pf}	0.70
β_{pf}	0.45
μ_{pf}	0.50
γ_{pf}	0.50
g_{pf}	0.00
ξ_{pf}	0.99

12.7 Pulse Dispersion Filter

In the MELP coder [486] described in Section 11.1.2.6, which was selected for the DoD standard at 2.4 kbps, one of the novel features employed was the pulse dispersion filter. In essence it helps to spread some of the excitation pulse energy away from the main excitation impulse by following the principle of glottal pulse shaping [494, 512, 513], as highlighted in this section.

12.7.1 Pulse Dispersion Principles

A typical glottal waveform is given in Figure 12.18 and is used to spread the excitation pulse energy away from the main excitation pulse. Its shape is defined by the glottal opening time, T_P, and the closure time, T_N. Rosenberg [513] investigated the ratio of opening and closure time with respect to the pitch period P. An opening time of $T_P/P = 0.40$, and closing time of $T_N/P = 0.16$ was found to produce the most natural sounding speech. Rosenberg also investigated which specific glottal pulse shape produced the most natural synthesised speech, with the polynomial expression

$$f(t) = \begin{cases} \alpha\left[3\left(\dfrac{t}{T_P}\right)^2 - 2\left(\dfrac{t}{T_P}\right)^3\right] & 0 \leq t \leq T_P \\ \alpha\left[1 - \left(\dfrac{t-T_P}{T_N}\right)^2\right] & T_P \leq t \leq T_P + T_N \end{cases} \tag{12.26}$$

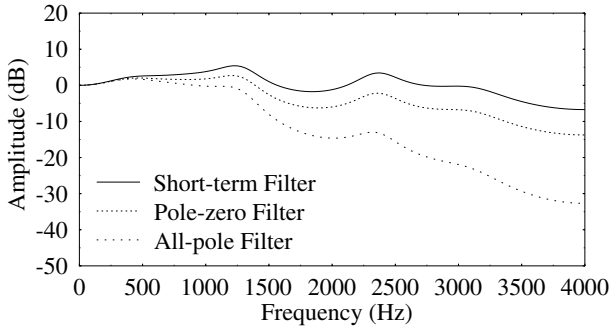

(a)

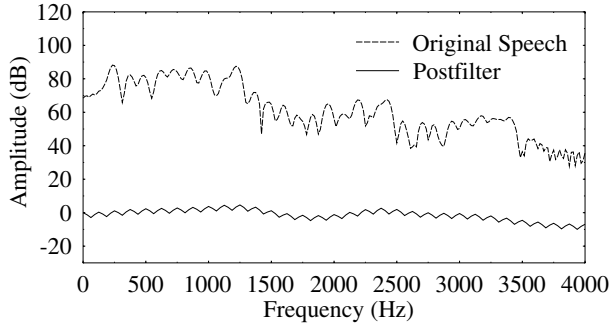

(b)

Figure 12.17: Postfilter frequency responses from AM1 for the diphthong /ɑɪ/ in 'l*i*ve', showing (a) the STPF and (b) the LTPF and combined postfilter. The speech frame had a fundamental frequency of 125 Hz. The selected postfilter parameters were $\alpha_{\rm pf} = 0.70$, $\beta_{\rm pf} = 0.45$, $\mu_{\rm pf} = 0.50$, $\xi_{\rm pf} = 0.99$, $\gamma_{\rm pf} = 0.l5$ and $g_{\rm pf} = 0$.

found to be best, where α controlled the amplitude of the glottal pulse. This polynomial expression was used to create the glottal pulse shape of Figure 12.18, where we had $P = 65$ samples, $T_P = 26$ samples and $T_N = 10$ samples.

The principle of glottal pulse shaping was exploited by Holmes [494] to shape the excitation of a formant vocoder and by Sambur *et al.* [512] to form the excitation for a LPC vocoder. They both found that the introduction of the glottal pulse shaping improved the naturalness of the synthesised speech.

12.7.2 Pitch Independent Glottal Pulse Shaping Filter

The pulse dispersion filter adopted by McCree and Barnwell [486] was a triangular-shaped pulse [513] which was spectrally flattened, as shown in Figure 12.19. The process of

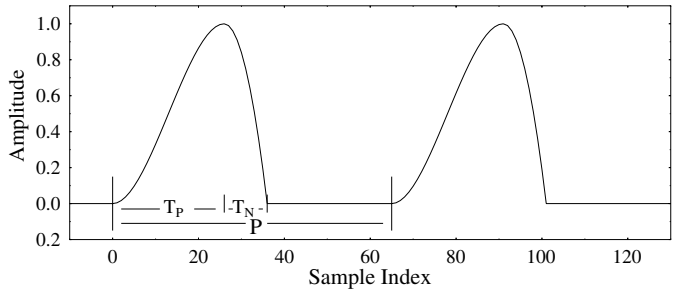

Figure 12.18: The typical shape of a glottal wave for human speech according to Equation (12.26), with $T = 65$ samples, $T_P = 26$ samples and $T_N = 10$ samples, which is used to spread the excitation pulse energy away from the main excitation pulse. The action of the filter is demonstrated in Figure 12.20.

spectrally flattening the glottal pulse, of which the start and end states are shown in Figure 12.19, involves manipulating the frequency domain representation of the triangular glottal pulse. The principle of spectral glottal pulse flattening is invoked [486] because the synthesised speech excitation waveform should be spectrally flat, hence this condition should also be imposed on the glottal pulse shape. The time-domain representation of this spectrally flattened pulse is shown in Figure 12.19(b). The spectral flattening was performed using linear prediction, where the triangular glottal pulse shape was passed through an linear prediction filter to produce the pulse dispersion filter.

This triangular glottal pulse shape was also investigated by Rosenberg [513], where it was found to produce inferior quality speech to the polynomial shape of Equation (12.26). However, it is notable that, for the same glottal opening and closure ratio T_P/T_N, the triangular shape spreads the waveform energy further from the impulse source than does the polynomial glottal pulse. Figure 12.20(c) demonstrates the time-domain energy spread achieved by the MELP coder, employing a triangular pulse shape when compared with the synthesised speech of the second trace. The delay is caused by the FIR implementation of the pulse dispersion filter.

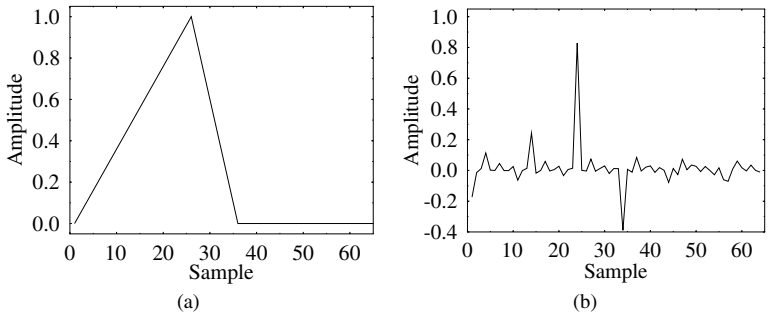

Figure 12.19: (a) A triangular glottal pulse shape together with (b) its spectrally flattened pulse dispersion filter [486].

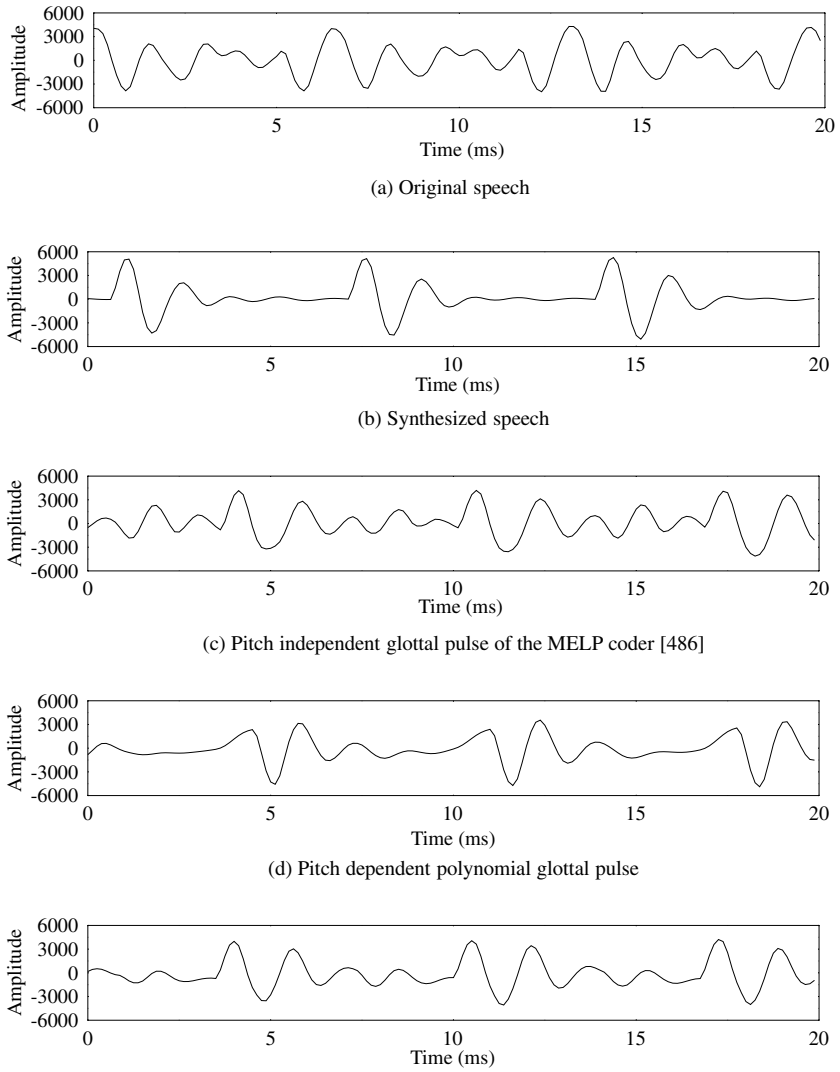

(a) Original speech

(b) Synthesized speech

(c) Pitch independent glottal pulse of the MELP coder [486]

(d) Pitch dependent polynomial glottal pulse

(e) Pitch dependent triangular glottal pulse

Figure 12.20: The energy spread produced by differently shaped pulse dispersion filters compared with the original synthesised speech, where the FIR implementation of the different pulse dispersion filters introduces a delay. The utterance is taken from BM2 for the back vowel /ɑ/ in 'p*ar*ked'.

McCree and Barnwell [486] placed their triangular pulse dispersion filter after the LPC synthesis filter, whereas previously the glottal pulse filtering was performed on the excitation [512]. Implementing the pulse dispersion filter after the LPC synthesis filter has the disadvantage that in order to avoid imperfections, due to different filter delays, a fixed FIR filter must be employed. As seen in Figure 12.19, McCree and Barnwell used a typical

male pitch period of 65 samples, at a sampling rate of 8 kHz, for the pulse dispersion filter. Their scheme was designed to benefit the male speaker most from the energy spread, since it is the longer pitch period that permits the greatest time-domain resonance decay between the pitch pulses. Thus, while the pulse dispersion filter improves the speech quality for male speakers, it does slightly reduce the speech quality of female speakers.

12.7.3 Pitch-dependent Glottal Pulse Shaping Filter

The pitch-independent glottal pulse shape of Section 12.7.2 reduced the quality of synthesised speech for female speakers. However, a pitch-dependent glottal pulse shaping filter should avoid this effect. Following the recommendation of Rosenberg [513] the polynomial of Equation (12.26) was spectrally flattened, using linear prediction, and then it was adopted to spread the excitation waveform energy before the LPC synthesis filter. Imposing the pulse dispersion filter on the excitation followed the method of Holmes [494] and Sambur *et al.* [512], as opposed to McCree and Barnwell [486] who applied the pulse dispersion filter to the synthesised speech. The performance of this pitch-dependent glottal pulse shaping filter is characterised in Figure 12.20(d), where it can be seen that the resultant synthesised speech contains much less energy spread than the pitch-independent triangular pulse dispersion filter of McCree and Barnwell [486] shown in Figure 12.20(c).

To produce a more effective pitch dependent glottal pulse shaping filter, the polynomial of Equation (12.26) was replaced by a spectrally flattened triangular glottal waveform pulse. The performance of this pitch-dependent triangular pulse is characterised in Figure 12.20(e). This glottal waveform shape produces good energy spread for male speakers, with its pitch-dependent nature ensuring that the speech quality of female speakers is not degraded.

However, by employing a glottal waveform shaping filter before the LPC synthesis filter the excitation source would be constrained to be an impulse, since this is the form of excitation the glottal waveform shaping was originally designed for. Within this treatise, notably in Chapter 14, different forms of excitation are employed which would be unable to incorporate this glottal pulse shaping filter. The pulse dispersion filter, introduced by McCree and Barnwell [486], operates on the synthesised speech thus permitting its successful operation in conjunction with the other excitations detailed later. In summary, it was found most perceptually beneficial to invoke the pitch-independent triangular pulse dispersion filter of McCree and Barnwell seen in Figure 12.19.

12.8 Results for Linear Predictive Vocoder

The basic LPC vocoder described in this chapter was implemented, with the utterances from the speech database in Section 11.4 processed to test the LPC vocoder's performance. The time- and frequency-domain performance of the vocoder for individual 20 ms frames of speech are shown in Figures 12.21, 12.22 and 12.23, where the waveforms at different stages of the speech coder are shown. In the figures, trace (a) displays the original waveform, trace (b) shows the impulse and frequency response of the LPC STP synthesis filter, with trace (c) showing the LPC STP residual waveform. The reconstructed waveforms at different stages are also displayed, where trace (d) shows the excitation waveform, trace (e) displays the speech waveform after the LPC synthesis filter, trace (f) contains the impulse and frequency

response of the adaptive postfilter, trace (g) shows the speech waveform after the postfilter and, finally, trace (h) displays the output speech following the pulse dispersion filter. The input and output speech waveforms are shown inside the pre- and post-processing filters, described in Section 12.2.2, thus, the output speech will still be high-pass filtered to 100 Hz. The performance of the LPC vocoder for these speech frames is described next.

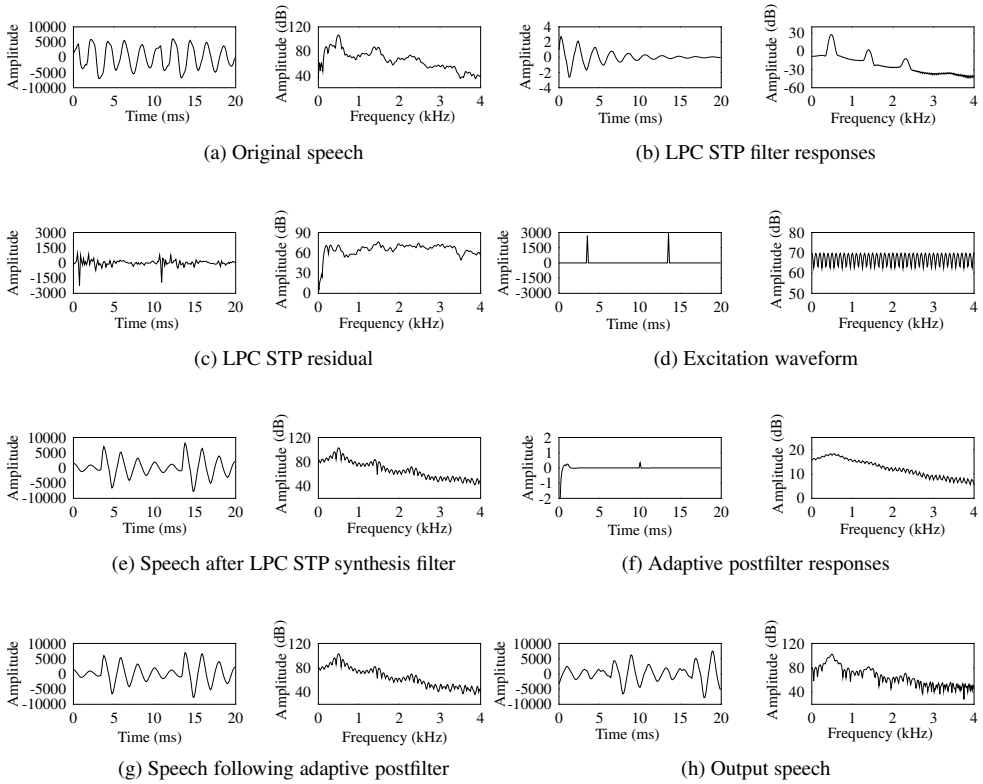

Figure 12.21: Comparison of the time and frequency domains of: (a) the original speech; (b) the LPC STP filter impulse and frequency response; (c) the LPC STP residual; (d) the LPC excitation waveform; (e) the speech waveform after the LPC STP filter; (f) the adaptive postfilter impulse and frequency domain response; (g) the speech waveform after the adaptive postfilter; (h) the output speech after the pulse dispersion filter. The 20 ms speech frame is the mid vowel /ɜ˞/ in the utterance 'w*or*k' for the testfile BM1. For comparison with the other coders developed in this study using the same speech segment, please refer to Table 17.2.

Figure 12.21 displays a waveform from the testfile BM1, for the mid vowel /ɜ˞/ in the utterance 'w*or*k'. From the time-domain representation of Figure 12.21(a) we can infer that the waveform's periodicity is approximately 80 samples, corresponding to 10 ms or to a pitch of 100 Hz. This manifests itself in the frequency domain in terms of 100 Hz-spaced spectral needles. From the frequency domain representation of Figure 12.21(b) we can infer that there are spectral envelope peaks around 500, 1400, 2200 and 3500 Hz corresponding to

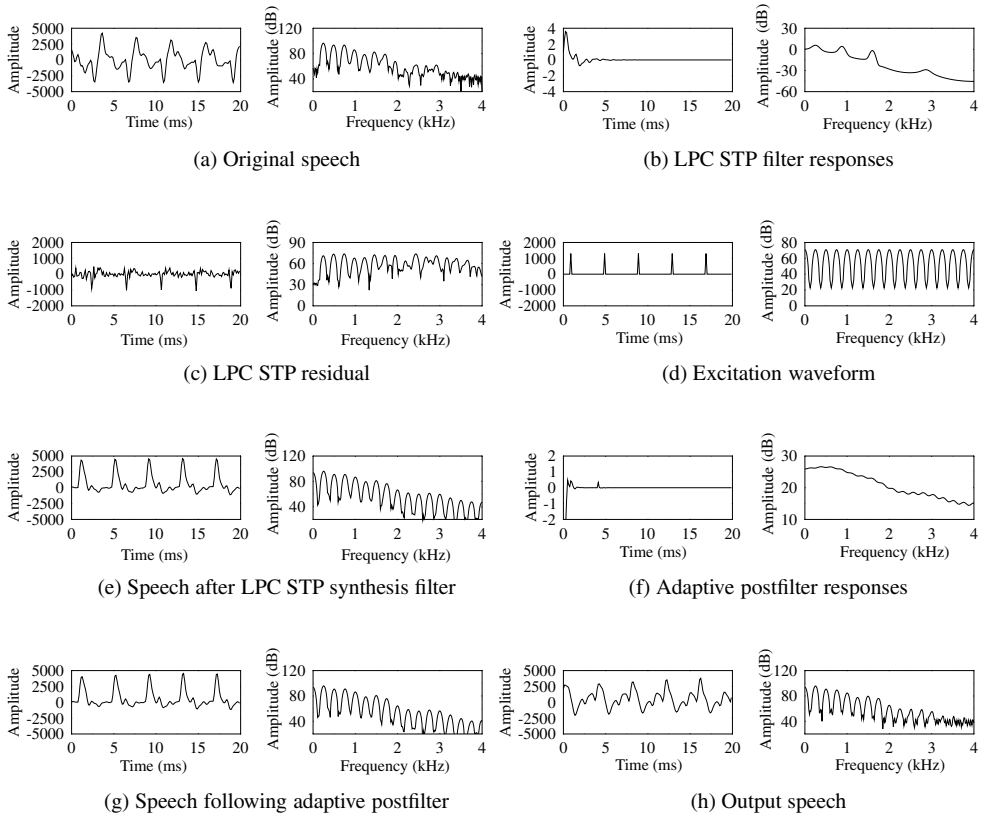

(a) Original speech

(b) LPC STP filter responses

(c) LPC STP residual

(d) Excitation waveform

(e) Speech after LPC STP synthesis filter

(f) Adaptive postfilter responses

(g) Speech following adaptive postfilter

(h) Output speech

Figure 12.22: Time and frequency domain comparison of (a) the original speech, (b) the LPC STP filter impulse and frequency response, (c) the LPC STP residual, (d) the LPC excitation waveform, (e) the speech waveform after the LPC STP filter, (f) the adaptive postfilter impulse and frequency domain response, (g) the speech waveform after the adaptive postfilter, (h) the output speech after the pulse dispersion filter. The 20 ms speech frame is the liquid /r/ in the utterance '*r*ice' for the testfile BF2. For comparison with the other coders developed in this study using the same speech segment please refer to Table 17.2.

the formants. The LPC decoder has assigned two excitation pulses to this frame, as shown in Figure 12.21(d), which attempt to model the two pitch-related pulses in Figure 12.21(c). The reconstructed speech of Figure 12.21(e) contains the same type of waveform as the original, however, the synthesised speech cannot maintain the amplitude of the original throughout the pitch period. In the frequency domain the formants are well represented. For this particular speech frame the introduction of the adaptive postfilter in Figure 12.21(g) has little effect, with only the first formant being emphasised and a small amount of long-term postfiltering occurring. The pulse dispersion filter introduces a delay into the speech waveform and reduces the amount of periodic voicing evident in the frequency spectrum, as shown in Figure 12.21(h).

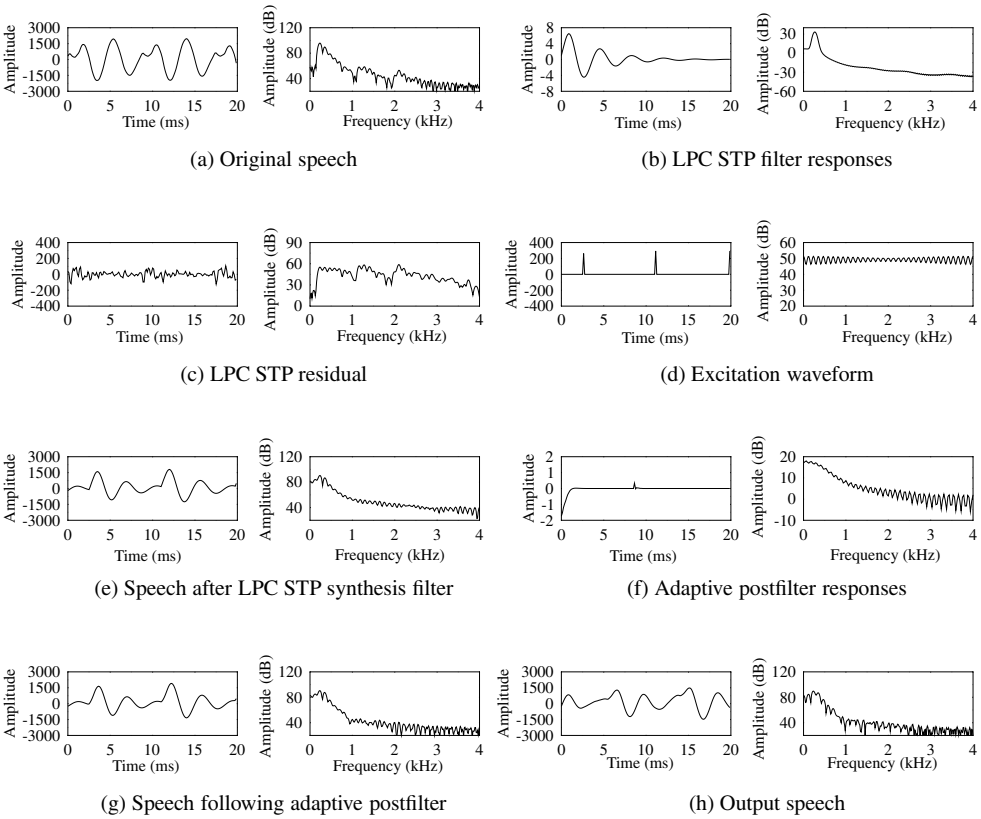

(a) Original speech

(b) LPC STP filter responses

(c) LPC STP residual

(d) Excitation waveform

(e) Speech after LPC STP synthesis filter

(f) Adaptive postfilter responses

(g) Speech following adaptive postfilter

(h) Output speech

Figure 12.23: Comparison of the time and frequency domains of: (a) the original speech; (b) the LPC STP filter impulse and frequency response; (c) the LPC STP residual; (d) the LPC excitation waveform; (e) the speech waveform after the LPC STP filter; (f) the adaptive postfilter impulse and frequency domain response; (g) the speech waveform after the adaptive postfilter; (h) the output speech after the pulse dispersion filter. The 20 ms speech frame is the nasal /n/ in the utterance 'thrown' for the testfile BM2. For comparison with the other coders developed in this study using the same speech segment please refer to Table 17.2.

The utterance shown in Figure 12.22 is from the testfile BF2, for the liquid /r/ from the utterance '*r*ice'. As typical, the female speaker has a much shorter pitch period than the male speaker of Figure 12.21. From the frequency domain representation in Figures 12.22(a) and (b) it can be seen that the waveform has formants at 200, 800, 1500 and 2800 Hz. In addition, the speech spectrum appears voiced beneath 1800 Hz and unvoiced above. Figure 12.22(d) shows that the LPC decoder has assigned five pitch pulses to this frame, which correspond to the five pitch periods seen in the original waveform. The pitch period is about 35 samples, corresponding to approximately 4.4 ms and a pitch frequency of about 220 Hz. In the time-domain the synthesised speech signal of Figure 12.22(e) contains a dominant peak in each pitch period, but very little energy elsewhere. In the frequency

domain the synthesised speech spectrum is visibly voiced throughout the 4 kHz. For this speech frame the introduction of an adaptive postfilter decreases the amplitude of the pitch period harmonics at higher frequencies. The introduction of the pulse dispersion filter in Figure 12.22(h) reduces the amount of periodic voicing evident in the higher frequencies of the speech spectrum, while in the time-domain it spreads the energy of the waveform throughout the pitch period. It could be suggested that the pulse dispersion filter spreads too much of the energy away from the dominant peak. This highlights a disadvantage of the pitch-independent pulse dispersion filter which was based on a typical male pitch period, and can exaggerate the dispersion of energy for a shorter pitch period.

A frame of the BM2 testfile is displayed in Figure 12.23, where characteristics of the nasal /n/ from the utterance 'throw*n*' are shown. From Figure 12.23(a) it can be seen that the speech waveform has a pitch period of about 70 samples, corresponding to 8.75 ms or a pitch of 115 Hz. Observing the frequency spectrum there appear to be formants at 250, 1200 and 2200 Hz, although the LPC STP filter of Figure 12.23(b) only captures the first formant. The failure of the LPC STP filter is further evident in Figure 12.23(c) where the peaks at 1200 and 2000 Hz are replaced by flat frequency spectrum. The frequency spectrum of Figure 12.23(a) shows that above 2300 Hz the spectrum is unvoiced, while in Figure 12.23(e) the spectrum is voiced up to 4 kHz. In addition, from Figure 12.23(e) it can be seen that the upper two formants are not represented. For this speech frame the addition of the postfilter decreases the amplitude of the pitch period harmonics above 1 kHz, as shown in Figure 12.23(g). Observing Figure 12.23(h) the pulse dispersion filter further reduces voicing, especially in the high-frequency region.

The perceptual quality of the synthesised speech was informally assessed, where the reproduced speech sounded slightly synthetic, with particular 'buzziness' in the case of high-pitched female speakers.

The bit allocation for each 20 ms voiced or unvoiced speech frame is given by Table 12.8. For both voiced and unvoiced frames the LPC STP synthesis filter coefficients were vector quantised as LSFs for transmission, using 18-bits per frame. A voiced–unvoiced flag was also sent with both voiced and unvoiced frames. For all speech frames a 5-bit SQ, described in Section 12.4, was used to transmit the RMS of the LPC STP residual signal, indicating the energy of the synthesised excitation. For voiced frames the pitch period ranged from 20 to 147 samples, thus seven bits were required to represent its value. The total bitrate for voiced frames was 1.55 kbps, while for unvoiced frames it was 1.2 kbps.

Table 12.8: Bit allocation table for the investigated LPC vocoder.

Parameter	Unvoiced	Voiced
LSFs	18	18
V/U flag	1	1
RMS value	5	5
Pitch	—	7
Total/20 ms	24	31
Bitrate	1.2 kbps	1.55 kbps

The computational complexity for this basic LPC vocoder was dominated by the pitch detector, where in Section 12.3.2 its complexity was found to be 3.4 MFLOPS. The delay of the LPC vocoder was 60 ms, with 40 ms required at the encoder for the pitch detection and 20 ms required at the decoder.

12.9 Chapter Summary

This chapter has introduced a benchmark LPC vocoder, using the random Gaussian noise of Section 12.4 for unvoiced frames, and the pulses of Section 12.5 for voiced frames. The chapter has detailed important aspects of low-bitrate speech coders which will be harnessed with the speech coders developed in later chapters. The investigated aspects were LSF quantisation, pitch detection, adaptive postfiltering and pulse dispersion filtering. It was found that for a 1.55 kbps speech coder the reproduced speech was intelligible, but sounded distinctly synthetic. Figures 12.21, 12.22 and 12.23 illustrated that the speech can sound intelligible without faithfully reproducing the time-domain waveforms. In the next chapter we invoke various wavelet-based pitch detection techniques.

Chapter 13

Wavelets and Pitch Detection

13.1 Conceptual Introduction to Wavelets

In this section we provide a simple conceptual introduction to wavelets, while a more rigorous mathematical exposure is offered in the next section.

In recent years wavelets have stimulated substantial research interest in a variety of applications. Their theory and practice have been documented in a number of books [514–516] and tutorial treatises [517–519]. Historically, the theory of wavelets was recognised as a distinct discipline in the early 1980s. Daubechies [520] and Mallat [521] generated significant interest in the field by invoking the mathematical technique of wavelets in signal processing applications. Wavelets have many applications where previously the classical tool of Fourier theory may have been applied. Hence, here wavelet theory is initially introduced through comparison with Fourier theory. Section 13.2 contains some of the mathematics underlying wavelet theory, while Sections 13.3, 13.4 and 13.5 describe how wavelets may be applied to the pitch detection of speech signals. Thus, for a focussed discussion on the application of wavelets to pitch detection, the reader may proceed to Section 13.3.

13.1.1 Fourier Theory

Fourier theory states that any signal $f(x)$, which is 2π-periodic, can be represented by an infinite series of sine and cosine functions defined by [522]

$$f(x) = a_0 + \sum_{k=1}^{\infty} [a_k \cos(x) + b_k \sin(x)] \tag{13.1}$$

where a_k and b_k are real coefficients. Thus, we can consider the signal $f(x)$ to be constructed from a set of basis functions.

The Fourier transform is used to convert a signal between the time and frequency domain, giving a tool through which we can analyse the signal $f(x)$ in both domains, although often one domain will be more convenient than the other. The conversion between domains can

occur since the coefficients of the sine and cosine functions, used to represent the time-domain signal, indicate the contribution of different frequencies to the signal $f(x)$.

While the Fourier transform produces localised values in the frequency domain, in the time domain the sine and cosine functions have an infinite support, hence, in order to localise the time-domain signal, windowing must be used, leading to the short-term Fourier transform (STFT). Figure 13.1 displays the localisation achieved by the STFT in both the time and frequency domain, yielding a uniform partitioning of the time–frequency plane since the same window is used for all frequencies. Due to localisation in the frequency domain the STFT can also be viewed as a filterbank [517], which is shown in Figure 13.2. Specifically, a filter centered at f_0 is created with a bandwidth f_b. Subsequently, this filter can be transformed to create a filter at $2 \cdot f_0$ with a bandwidth of f_b to analyse the contribution constituted by these frequencies. This process can be continued indefinitely, but the filters always have a bandwidth f_b.

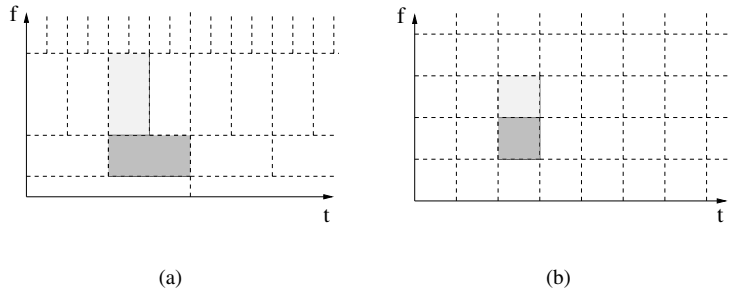

Figure 13.1: The (a) STFT and (b) wavelet transform time–frequency domain spaces.

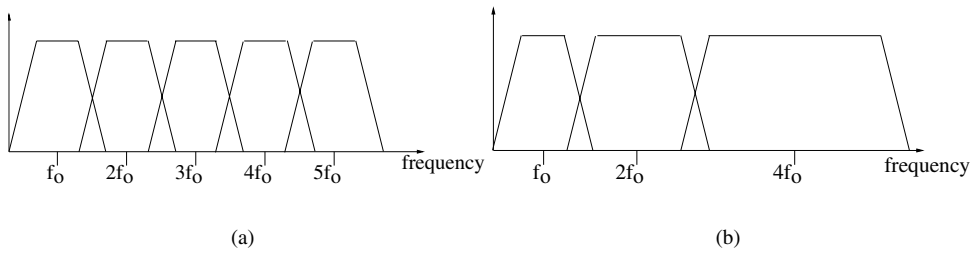

Figure 13.2: The (a) STFT and (b) wavelet transform filterbank models.

Having the same localisation, or resolution, in all regions of the time–frequency plane is often not ideal. The wavelet transform, which is described next, supports a variable width localisation in the time–frequency space.

13.1.2 Wavelet Theory

A wavelet is defined as a function which obeys certain conditions [520] allowing it to represent a signal $f(x)$ by a series of basis functions, in a fashion similar to the Fourier series. The wavelet decomposition of $f(x)$ can be formulated as

$$f(x) = \sum_{ik} d_{ik}\psi_{ik}(x) \tag{13.2}$$

where d_{ik} are the coefficients of the decomposition and ψ_{ik} are the basis functions.

The wavelet transform can be used to analyse a signal $f(x)$, but unlike the STFT its localisation resolution varies over the time–frequency space. This flexibility in resolution makes it particularly useful for analysing signal discontinuities, where during a short time period an extensive range of frequencies is present. It can be noted that the instance of glottal closure is represented by a discontinuity in the speech waveform. As demonstrated by Figure 13.1, the wavelet transform can either analyse a large range of frequencies over a short period of time, or analyse a narrow band of frequencies over a long time period.

Hence, it can be argued that the wavelet transform permits the analysis of a signal $f(x)$ to be viewed at different time and frequency domain scales. For a lengthy time window the global features of the signal $f(x)$ become prominent, while for a short time period the localised features of the signal $f(x)$ are observed. It is possible to study the frequency features in a similar manner.

The localisation of the wavelet transform can also be viewed as a filterbank [517], which is shown in Figure 13.2 along with the STFT. As suggested by Figure 13.1(b) a filter is created at f_0 with a bandwidth of f_b, analysing these frequencies for the signal $f(x)$ within the time duration of $[-t_{fb}, t_{fb}]$. This filter can be transformed to a filter centered at $2 \cdot f_0$ with bandwidth $2 \cdot f_b$, where the energy of these frequencies in $f(x)$ over the time duration $[-t_{fb}/2, t_{fb}/2]$ is considered. This procedure can be continued indefinitely.

Thus, our brief conceptual comparison between the Fourier and wavelet transform has been completed, highlighting the similarities and differences between the two methodologies. A study of wavelets and discontinuities is now performed.

13.1.3 Detecting Discontinuities with Wavelets

Previously, it has only been briefly mentioned that wavelets can be used to detect discontinuities due to the instants of glottal closure [509]. The duration between two consecutive instants of glottal closures is the pitch period of the speech signal. There have been several applications of wavelets for detecting discontinuities, with a few of them highlighted below.

Firstly, two methods applying wavelet analysis to speech signals are reviewed. Stegmann *et al.* [523] used a $\mathrm{D_Y WT}$, to distinguish between voiced, unvoiced and transient periods of speech, where the term dyadic will be elaborated on below. According to this method the different behaviour exhibited by the wavelet coefficients, at each scale, allowed the individual speech frames to be categorised into one of the above three speech classes. The different wavelet scales observe different sections of the speech spectrum, thus, the variation in the distribution of the spectral energy in voiced and unvoiced speech segments permits discrimination between the classes. This voiced–unvoiced detector follows a philosophy similar to previous methods analysing the statistics of voiced and unvoiced speech [506,507].

Kadambe and Boudreaux-Bartels [509] investigated the use of $D_Y WT$ for the pitch detection of speech signals. They used Mallat and Zhong's [524] class of spline wavelets on dyadic scales. Thresholding of located discontinuities together with their evolution across the wavelet scales were used to identify the glottal pulses, where the speech waveform's pitch period was determined by the duration between consecutive glottal pulses. Kadambe and Boudreaux-Bartels found their method to be robust to noise and superior in accuracy to the autocorrelation-based methods of Section 12.3.

Another area where the detection of discontinuities is desirable is in biomedical signal processing [525], where their use in the analysis of electrocardiography (ECG) signals is highlighted in [526]. An ECG signal has a characteristic shape termed the QRS complex, which is displayed in Figure 13.3, where it can be seen that a large positive spike is surrounded by two small negative spikes. Cardiac problems can be identified from unusual shapes of the QRS complex, thus automatic localisation of the QRS complexes would be desirable. Li *et al*. [526] detected the sharp discontinuities in the QRS complex with the aid of the spline wavelets suggested by Mallat and Zhong [524] and found the automatic localisation of QRS complexes to be reliable.

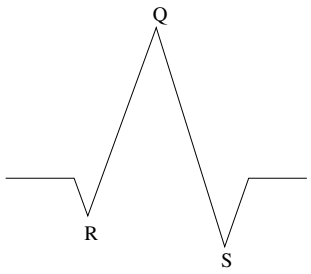

Figure 13.3: A typical QRS complex of an ECG signal.

The applications described use predominantly the class of polynomial spline wavelets introduced by Mallat and Zhong [524]. Mallat *et al*. [521, 524, 527] have undertaken seminal research into the task of edge detection in images, where an edge is a discontinuity in the image. Edge detection has much in common with the previously mentioned one-dimensional discontinuities, such as glottal pulses, but occurs in two dimensions. Mallat *et al*. were interested in reconstructing images entirely from edge information, hence, assisting in image compression.

Following this rudimentary overview of detecting discontinuities using wavelets, the mathematics of wavelet theory is now introduced, although for a complete description the book by Koornwinder [514] is recommended. The mathematics of wavelet theory can also be found in the books by Vetterli and Kovačević [528] and Chui [515, 516].

13.2 Introduction to Wavelet Mathematics

We commence our brief introduction to the mathematics defining wavelet functions with the description of the mother wavelet, from which a class of wavelets can be derived. Hence, the

mother wavelet function, ψ, is described by [514]

$$\psi_{a,b}(t) = \frac{1}{\sqrt{a}}\psi\left(\frac{t-b}{a}\right) \tag{13.3}$$

where a is the frequency, or dilation variable, and b is the position, or time-domain translation. Thus, wavelets exist for every combination of a and b. The Fourier transform, $\hat{\psi}(\omega)$, of the mother wavelet, $\psi(t)$, is defined by

$$\hat{\psi}(\omega) = \int_{-\infty}^{\infty} \psi(t) e^{-jt\omega}\, \mathrm{d}t. \tag{13.4}$$

Any function that obeys certain constraints can be considered a mother wavelet. The reader is referred to the books by Koornwinder [514] and Chui [515] for further clarification. The continuous wavelet transform (CWT) of a function $f(t)$ is then defined by

$$F(a,b) = \int_{-\infty}^{\infty} f(t)\psi_{a,b}(t)\, \mathrm{d}t \tag{13.5}$$

which is analogous to the Fourier transform when the $e^{j\omega t}$ kernel is replaced by $\psi_{a,b}t$.

However, it is generally more useful to perform the discrete wavelet transform (DWT), or the $\mathrm{D_Y WT}$ derived from the CWT by imposing the following discretisation [514]:

$$F(a,b) = F(2^{-i}, 2^{-i}k), \quad \text{where } i, k \in Z \tag{13.6}$$

implying that the dilation and translation indices are both elements of the discrete dyadic space Z. Within a dyadic space each time- and frequency-domain wavelet scale is downsampled by two compared with the previous scale. Hence, from Equation (13.3) we find that the mother wavelet function takes the form of

$$\psi(t) = 2^{i/2} \cdot \psi(2^i t - k) \tag{13.7}$$

producing a set of orthogonal basis functions exhibiting different resolutions as a function of i and k. The basic mathematics of multiresolution analysis are now introduced.

13.2.1 Multiresolution Analysis

As described in Section 13.1.2, wavelets are particularly useful when observing signals at different time or frequency scales. This technique is termed multiresolution analysis and divides the frequency space Z into a sequence of subspaces, V_m, where

$$\cdots \subset V_2 \subset V_1 \subset V_0 \subset V_{-1} \subset V_{-2} \subset \cdots \tag{13.8}$$

implying that V_m will become the space Z as $m \to -\infty$. The subspaces V_m, excluding $m = 0$, are generated through the dilation of the subspace V_0. Thus, the space V_{-1} contains both the functions of V_0 and the functions that oscillate twice as fast, while only half of the functions

of V_0 oscillate slowly enough to be in V_1, which is described for a function $f(x)$ as follows:

$$f(x)\epsilon V_0 \Leftrightarrow f(2x)\epsilon V_{-1} \tag{13.9}$$

$$f(x)\epsilon V_0 \Leftrightarrow f(2^{-1}x)\epsilon V_1. \tag{13.10}$$

The subspace V_0 is generated through the father wavelet, ϕ, which is a wavelet family constructed before the mother wavelet and from which the mother wavelet is derived. The subspace V_0 contains the integer translations of the father wavelet $\phi_{0,n}$ defined by

$$\phi_{0,n} = \phi(x - n). \tag{13.11}$$

Hence, any function $f(x)\epsilon V_0$ can be described by

$$f(x) = \sum_{n=-\infty}^{\infty} a_n \phi(x - n) \tag{13.12}$$

where a_n are the coefficients of the decomposition and $f(x)$ is constructed from a weighted combination of integer translated father wavelets. From Equation (13.12) several statements may be inferred. Firstly, assuming that $\phi(x)\epsilon V_0$, and since $V_0 \subset V_{-1}$ it can be said that $\phi(x)\epsilon V_{-1}$. However, Equation (13.10) states that if $\phi(x)\epsilon V_{-1}$, then $\phi(2^{-1}x)\epsilon V_0$. Hence, the two-scale difference equation can be constructed, by rewriting Equation (13.12) using Equation (13.7) to arrive at

$$\phi(x) = \sqrt{2} \sum_{n=-\infty}^{\infty} h_n \phi(2x - n) \tag{13.13}$$

where $\sqrt{2}h_n$ are a set of coefficients different from a_n, which allow h_n to be termed the filter coefficients of $\phi(x)$. Physically this implies reconstructing the father wavelet by a weighted sum of its second 'harmonic' components positioned at locations $-\infty \leq h_n \leq \infty$. The terminology 'two-scale difference equation' arises from the relation of two different scales of the same function. The mother wavelet $\psi(x)$ is generated from the father wavelet, since $\psi(x)\epsilon V_0$, by the following relationship:

$$\psi(x) = \sqrt{2} \sum_{n=-\infty}^{\infty} g_n \phi(2x - n) \tag{13.14}$$

where $\sqrt{2}g_n$ are a set of coefficients constrained by $g_n = (-1)^n h_{1-n}$.

This concludes our basic introduction to wavelet mathematics, leading us to a description of the wavelets used in this chapter, namely, the polynomial spline wavelets introduced by Mallat and Zhong [524].

13.2.2 Polynomial Spline Wavelets

The family of polynomial splines are useful for practical applications since they have a compact time-domain support, thus, they are efficient to implement in the time domain with only a few non-zero coefficients. The wavelets introduced by Mallat and Zhong [524] are

constructed in detail in Appendix A, leading to the polynomial spline wavelets defined in the frequency domain by

$$\hat{\phi}(\omega) = \left(\frac{\sin(\omega/2)}{\omega/2}\right)^3 \tag{13.15}$$

$$\hat{\psi}(\omega) = j\omega\left(\frac{\sin(\omega/4)}{\omega/4}\right)^4. \tag{13.16}$$

These wavelets are designed such that $\hat{\phi}(\omega)$ is symmetrical with respect to 0, while $\hat{\psi}(\omega)$ is anti-symmetrical with respect to 0. The filter coefficients of $\hat{\phi}(\omega)$ and $\hat{\psi}(\omega)$, namely h_n and g_n in Equations (13.13) and (13.14), are given, respectively, by the 2π-periodic functions defined in Appendix A:

$$H(\omega) = e^{j\omega/2}\left(\cos\left(\frac{\omega}{2}\right)\right)^3 \tag{13.17}$$

$$G(\omega) = 4je^{j\omega/2}\sin\left(\frac{\omega}{2}\right). \tag{13.18}$$

Appendix A also defines the filter coefficients values given in Table 13.1. Figure 13.4 displays the impulse and frequency responses for the filter coefficients $h(n)$ of the father wavelet and the filter coefficients $g(n)$ of the mother wavelet $\hat{\psi}(\omega)$. These filter values are used in a pyramidal structure to produce a wavelet transform. This pyramidal structure is described next.

Table 13.1: Filter coefficients $h(n)$ and $g(n)$ defined in Equations (13.13) and (13.14) for the quadratic spline wavelet of Equations (13.17) and (13.18).

n	$h(n)$	$g(n)$
-1	0.125	0
0	0.375	-2.0
1	0.375	2.0
2	0.125	0

13.2.3 Pyramidal Algorithm

Mallat introduced a pyramid structure for the efficient implementation of orthogonal wavelets [521] based on techniques known from sub-band filtering. The pyramidal algorithm is illustrated in Figure 13.5.

If the input signal to the pyramidal algorithm is $A_i(\omega)$, where i represents the scale of the signal, then passing through the low-pass filter $H(\omega)$ of Figure 13.4(a) and downsampling by a factor of two, the output is a low-pass filtered signal $A_{i+1}(\omega)$ of the input. This low-pass signal is termed the smoothed signal, since it is a smoothed version of the input signal.

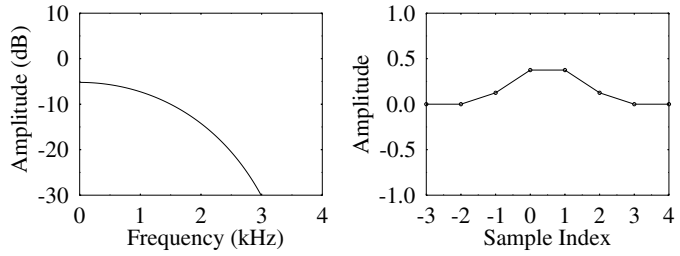

(a)

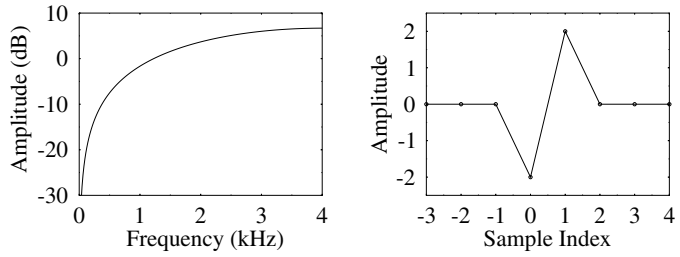

(b)

Figure 13.4: The impulse responses and frequency responses for the (a) $h(n)$ and (b) $g(n)$ filters described by Table 13.1 using the quadratic spline wavelets of Equations (13.17) and (13.18).

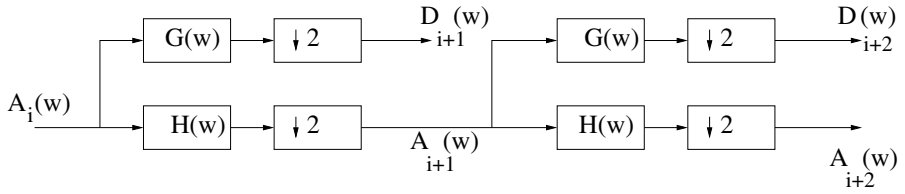

Figure 13.5: Pyramidal algorithm for multiresolution analysis.

If the input signal $A_i(\omega)$ is passed through the high-pass filter $G(\omega)$ of Figure 13.4(b) and downsampled by a factor of two, then the output signal $D_{i+1}(\omega)$ is a high-pass filtered version of the input signal. This high-pass output signal is termed the detail signal, as it contains the difference between the input signal $A_i(\omega)$ and the low-pass output signal $A_{i+1}(\omega)$. At the next stage of Figure 13.5 passing the smoothed signal $A_{i+1}(\omega)$ through the filters $H(\omega)$ and $G(\omega)$ and downsampling by two results in the smoothed and detailed signals $A_{i+2}(\omega)$ and $D_{i+2}(\omega)$, respectively. This process can be continued until the signal has been analysed to the desired resolution.

The fundamental frequency of speech signals is assumed to vary from 54 to 400 Hz and the sampling rate for the speech waveforms is 8 kHz. Hence, the first mother wavelet ranges from 2 to 4 kHz. This frequency band will contain higher-order harmonics of the fundamental frequency together with noise. Frequently, at the input to the speech encoder there is also present a high-pass input filter with a cutoff frequency of 100 Hz, as seen in Section 12.2.2. Thus, increasing the $\mathrm{D_Y WT}$ scale from a mother wavelet of 2000–4000 Hz until the mother wavelet covers 125–250 Hz, namely from scale $i+1$ to scale $i+5$, ensures that all frequencies passed to the speech encoder and $\mathrm{D_Y WT}$ process are considered. Following the selection of appropriate $\mathrm{D_Y WT}$ scales the practical implementation of the $\mathrm{D_Y WT}$ is discussed.

13.2.4 Boundary Effects

An important issue associated with the $\mathrm{D_Y WT}$ is to consider the effect of time-domain boundary discontinuities due to the speech waveform's frame structure. For the computer vision problem of Mallat and Zhong [524] the discontinuities occur at the edge of the image, while in speech coding the boundaries occur at the frame edges. The method used by Mallat and Zhong to overcome the boundary discontinuity is to make the signal periodic with respect to $2T$, where T is the number of samples in the original signal and extend it symmetrically from T to $2T$.

Kadambe and Boudreaux-Bartels [509] introduced a subframe inside each speech frame to ensure that the frame boundaries did not affect the subframe under analysis, thus effectively removing any discontinuities. The approach by Stegmann *et al.* [523] was similar, but with a lookahead to the following speech frame that introduced a delay of 8 ms.

The approach adopted was to use a lookback history into frame $N-1$ for the frame boundary at the start of frame N, while to avoid any delay, at the end of frame boundary periodicity was implemented to extend the speech signal.

13.3 Preprocessing the Wavelet Transform Signal

The $\mathrm{D_Y WT}$ of a 20 ms segment of speech is shown in Figure 13.6. For the first scale the high-pass $\mathrm{D_Y WT}$ of Figure 13.4(b) amplifies the higher frequency, predominately noisy signals and hence no periodicity is apparent. However, as the scales increase from D_{i+1} to D_{i+5}, the periodicity of the speech signal becomes more evident for both the time and frequency domain plots shown in Figure 13.6 for the $D_i(\omega)$ signals. We note here that although the time-domain waveforms of Figure 13.6 are plotted on the finest scale, i.e. $i=1$, they are waveforms subsampled by a factor of 2^i. The procedure for extracting the relevant information from Figure 13.6 is now considered.

Observing Figure 13.6 it can be seen that some form of preprocessing must be performed in order to determine the instants of glottal closure, and hence the fundamental frequency of the speech waveform. From Figure 13.6 the maxima and minima during each scale of the $\mathrm{D_Y WT}$ provides most information about the speech waveform's pitch period. Hence, Figure 13.7(a) illustrates the initial preprocessing, whereby positive impulses are placed at the maxima and negative impulses at the minima. Each of these impulses are assumed to represent possible instants of glottal closure.

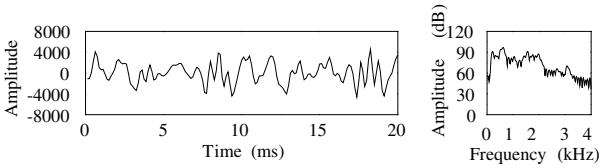

(a) Speech, A_i

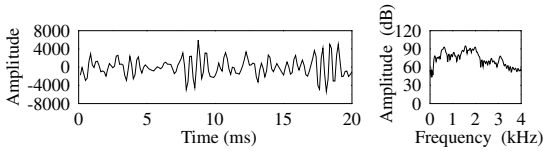

(b) $\mathrm{D_Y WT}$ at scale D_{i+1}

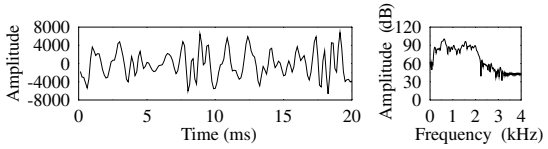

(c) $\mathrm{D_Y WT}$ at scale D_{i+2}

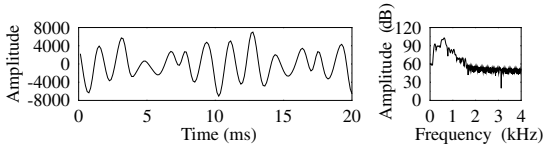

(d) $\mathrm{D_Y WT}$ at scale D_{i+3}

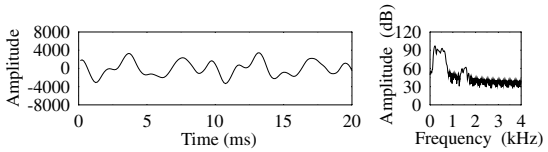

(e) $\mathrm{D_Y WT}$ at scale D_{i+4}

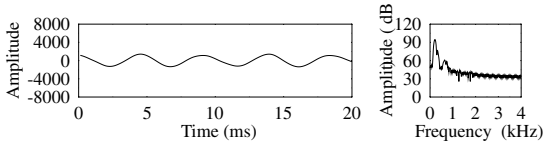

(f) $\mathrm{D_Y WT}$ at scale D_{i+5}

Figure 13.6: The $\mathrm{D_Y WT}$ of 20 ms of speech for the testfile AM1 uttering the diphthong /ɑɪ/ as in 'w*i*res'. For each scale of the $\mathrm{D_Y WT}$ the time and frequency domain response are portrayed, enabling the process of the $\mathrm{D_Y WT}$ to be clearly interpreted. The (a) speech is followed by the $\mathrm{D_Y WT}$ scales (b) 2000–4000 Hz, (c) 1000–2000 Hz, (d) 500–1000 Hz, (e) 250–500 Hz and (f) 125–250 Hz, using the quadratic spline wavelet of Figure 13.4 and Table 13.1.

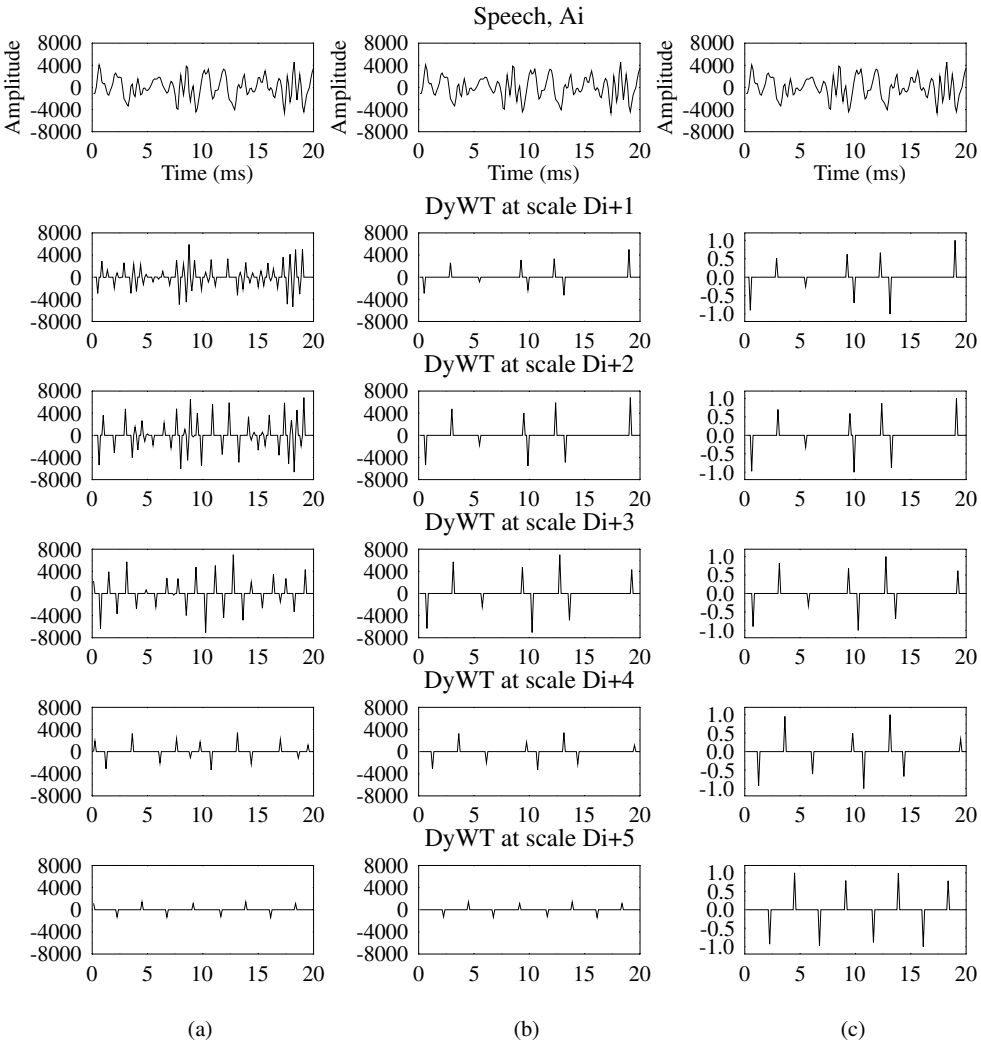

Figure 13.7: The $\mathrm{D_Y WT}$ of 20 ms of speech for the testfile AM1 uttering the diphthong /ɑɪ/ as in 'w*i*res'. In (a) impulses have been placed at the locations of the maxima and minima of the detail signals, $D_{i+1} \ldots D_{i+5}$. In (b) all spurious pulses have been removed. In (c) the impulses have been normalised with respect to the largest impulse at each scale.

The following sections describe the processes used to identify and eliminate the false glottal closure locations.

13.3.1 Spurious Pulses

Due to the presence of upper harmonics true instants of glottal closure will manifest themselves in every $\mathrm{D_Y WT}$ scale, hence all impulses that do not obey this criterion are

eliminated. The remaining impulses are given in Figure 13.7(b) and the elimination process is described below.

If an impulse is located in scale $i + 5$, then scale $i + 4$ is examined to look for an impulse in the vicinity of the pulse in scale $i + 5$. If a corresponding pulse exists, then scale $i + 3$ is examined. This is repeated for all scales. If any of the scales fail to contain an impulse in the correct neighbourhood, the search is abandoned and the impulses are declared void. The terms 'vicinity' and 'neighbourhood' are used since the addition of 2^i zeros between the coefficients of the multiresolution filters $h(n)$ and $g(n)$ cause the pulses to spread out, as the scale increases.

Following the removal of superfluous impulses, the remaining impulses, which have been confirmed at all resolutions, are amalgamated to one scale with impulses placed indicating the remaining possible instants of glottal closure, which are termed candidate glottal pulses. These candidate glottal pulse locations represent the amplitudes and positions of the impulses they are combined from.

13.3.2 Normalisation

Observing Figure 13.7(b), we see that the amplitudes of the $\mathrm{D_Y WT}$ decrease with scale increase, due to the attenuation of the filter $H(\omega)$ shown in Figure 13.4. Hence, normalisation of the impulses to the maximum peak at that resolution is performed, ensuring that the candidate glottal pulses are not dominated by the high-magnitude lower-scale impulses. The impulses after normalisation are displayed in Figure 13.7(c). Subsequent to this initial normalisation process, the final simplification procedure is detailed below.

13.3.3 Candidate Glottal Pulses

The candidate glottal pulses sum the amplitude of the normalised pulses from each scale, but are situated at the impulse location from scale $i = 1$, the scale with the finest time resolution. The candidate glottal pulses are renormalised to the highest pulse magnitude, as demonstrated in Figure 13.8.

The final information known about the candidate glottal pulses is that they must be at least 20 samples, or 2.5 ms apart, due to the highest expected fundamental frequency of 400 Hz. Thus, for any candidate glottal pulses within 20 samples of each other the smallest is discarded. The results from the $\mathrm{D_Y WT}$ are now suitable for use in voiced–unvoiced classification and pitch detection.

13.4 Voiced–unvoiced Decision

The ability of the $\mathrm{D_Y WT}$ to categorise speech as voiced or unvoiced has been shown previously by Stegmann *et al.* [523] and Kadambe and Boudreaux-Bartels [509]. The process of the $\mathrm{D_Y WT}$ across the scales gradually removes the higher frequency components present in the speech waveform. For unvoiced speech most energy is present in the higher frequencies, as demonstrated in Figure 11.2, while for voiced speech the energy is more evenly distributed. Thus, the voiced speech is expected to maintain its energy across the dyadic scales better than the unvoiced speech, allowing a voiced–unvoiced decision to be made. A suitable value for

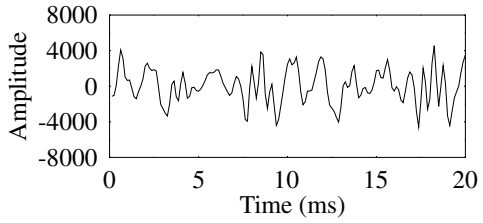

(a) Original speech

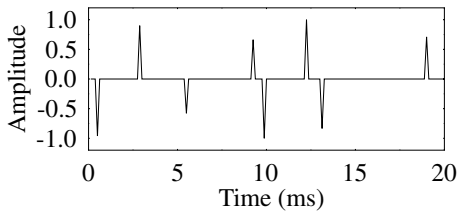

(b) Amalgamated pulses

Figure 13.8: Example of wavelet based preprocessing for the testfile AM1 uttering the diphthong /ɑɪ/ as in 'w*i*res', with a combined impulse at the location of the impulse in scale $i = 1$, and then normalised to the highest pulse magnitude.

controlling these decisions was found to be the ratio of the RMS energy in the frequency range 2–4 kHz, to the RMS energy in the frequency band 0–2 kHz. This is equivalent to the ratio of the RMS energy of A_{i+1}, to the RMS energy of D_{i+1}, given by

$$r_{\text{th}} = \sqrt{\frac{\sum_{n=0}^{\text{FL}} D_{i+1}(n)^2}{\sum_{n=0}^{\text{FL}} A_{i+1}(n)^2}} \tag{13.19}$$

where FL is the speech frame length.

A suitable threshold for the voiced–unvoiced test was found to be $r_{\text{th}} = 2$, where frames with a ratio higher than $r_{\text{th}} = 2$ are found to be unvoiced, otherwise the frame is voiced. Thus, for a frame of speech to be classified unvoiced it must contain twice as much energy in the 2–4 kHz band as in the 0–2 kHz frequency band.

This threshold measure performs well at distinguishing between voiced and unvoiced speech. However, it tends to classify any frames of silence as voiced speech, due to the even spread of energy across the frequency range for silent speech. A simple voiced-silence detector was implemented by considering the RMS energy of the input speech, A_i. A frame with an RMS energy value of less than 100 dB is classified as silent, otherwise the RMS energy level indicates a voiced speech frame. The process of pitch detection is now investigated.

13.5 Wavelet-based Pitch Detector

Following the above preprocessing procedures, described in Section 13.3, the frames classified as voiced in Section 13.4 contain a group of candidate glottal pulse locations from which the pitch period of the speech frame can be deduced.

Assuming that the largest positive and negative pulses are true glottal pulse locations, a range of possible pitch periods can be calculated. Namely, the candidate pitch periods are classified on the basis of the time durations between the largest positive pulse and all other positive pulses, or the largest negative pulse and all negative pulses. Figure 13.9 displays the potential pitch periods for each speech frame in two speech files. These speech files correspond to the speech files used in Chapter 12 for the autocorrelation-based pitch detectors in Figure 12.8, 12.11 and 12.14. The resultant graphs are fairly complex, however, it can be observed that the candidate pitch periods are commonly placed at the true pitch period and its harmonics. Typically the true pitch period and two or three harmonics are present.

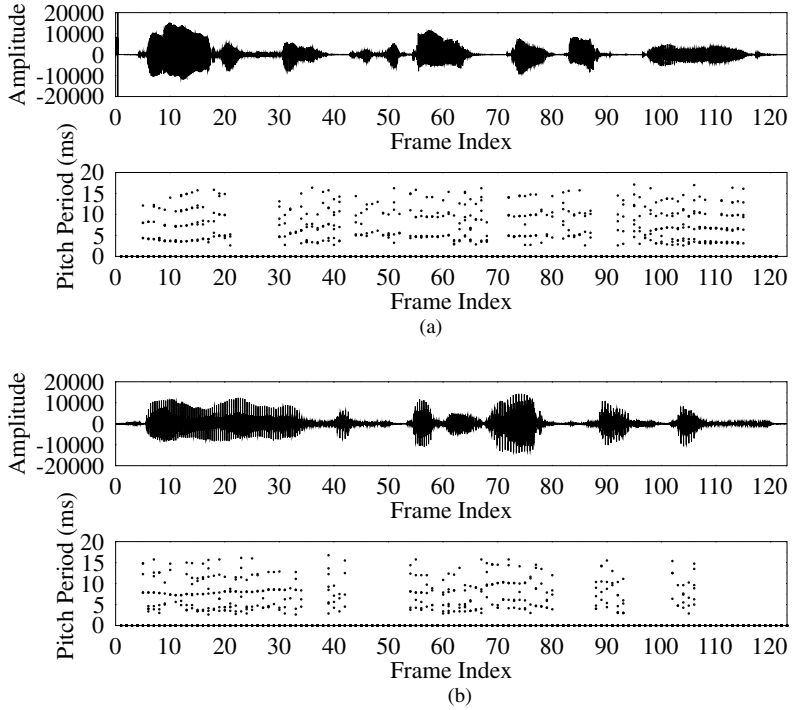

Figure 13.9: Candidate pitch periods for (a) testfile BF1 and (b) testfile BM1. The potential pitch periods tend to consist of the true pitch and its harmonics.

Interpretation of Figure 13.9 in our scheme was performed with the aid of dynamic programming, however, firstly some previously implemented methods are described. Specifically, Kadambe and Boudreaux-Bartels [509] used thresholding to identify the true pitch period related pulses, however, it was found that the pulse amplitudes associated with the voiced speech waveforms varied so much that it was impossible to find a suitable threshold.

Sukkar *et al*. [529] considered the relative amplitudes of consecutive candidate glottal pulses to determine the true instants of glottal closure, with a threshold employed for controlling which pulses to accept. However, once again it was found that the excessive variation in speech waveform shapes and candidate pulse amplitude prevented the identification of a suitable threshold. A novel pitch detection method involving dynamic programming is now investigated.

13.5.1 Dynamic Programming

The implementation of a dynamic programming algorithm for determining a voiced speech frame's pitch period will introduce additional delay into a speech coder. An additional delay of 60 ms, or three speech frames, was introduced allowing the current frame N and the future two frames $N+1$ and $N+2$ to be examined by the dynamic program. The history of the pitch track is also examined by considering the pitch period of the previous frame. Since the minimum pitch period is 20 samples, or 2.5 ms, there can be at most seven candidate pitch periods from the positive pulses and seven candidate pitch periods, within an interval of the 20 ms frame length, from the negative pulses. Thus, the dynamic program will examine a maximum of 14 candidate pitch periods over three speech frames, namely seven positive and seven negative pulses from each frame. Every candidate pitch period P_{N_i} in frame N is assigned a minimum cost, C_{dp_i}, defined by:

$$C_{dp_i} = |f_{N_i} - f_{N+1_j}| + |f_{N+1_j} - f_{N+2_k}| + a_{dp}|f_{N-1} - f_{N_i}| \tag{13.20}$$

where f_{N_i}, f_{N+1_j} and f_{N+2_k} refer to the candidate fundamental frequencies of speech frames N, $N+1$ and $N+2$, respectively. The fundamental frequency of frame $N-1$ is given by f_{N-1} and a_{dp} is a scaling function that defines the amount of pitch tracking, or the correlation between consecutive pitch values. Thus, according to Equation (13.20) the difference between the candidate fundamental frequencies, of consecutive speech frames, determines the cost of each pitch period candidate in frame N. It is not necessarily assumed that the pitch period candidate with the smallest cost function, C_{dp_i} is the true pitch period, instead the procedure given in Figure 13.10 is followed and described next.

The pitch detector design philosophy was influenced by the observations that the pitch detector performed best when strict pitch tracking was employed after a couple of consecutive pitch periods closely followed the predicted pitch period evolution. However, the extent of pitch tracking was greatly reduced at the beginning of a voiced sequence and was removed completely after a long period, namely 240 ms, of unvoiced speech. This is demonstrated by the sections of Figure 13.10 that consider the time elapsed from the last voiced frame, the TIME ELAPSE parameter, where if TIME ELAPSE is exceeded no pitch tracking is employed. If TIME ELAPSE is not exceeded, then provided that the consecutive pitch values are similar, i.e. $P_{N-1} \sim P_{N-2}$, extensive pitch tracking is performed, associated with a high a_{dp} in Equation (13.20) and Figure 13.10; otherwise, weak pitch tracking is introduced.

Figure 13.10 also contains a section that reintroduces the previous pitch period, P_{N-1}, in a set number of consecutive frames. This was implemented since it was found that occasionally the true pitch period would not be among the candidate pitch periods, thus, reintroducing the previous pitch period allowed the correct pitch track to be maintained. However, it was assumed that the true pitch period would only be missing from a certain number of

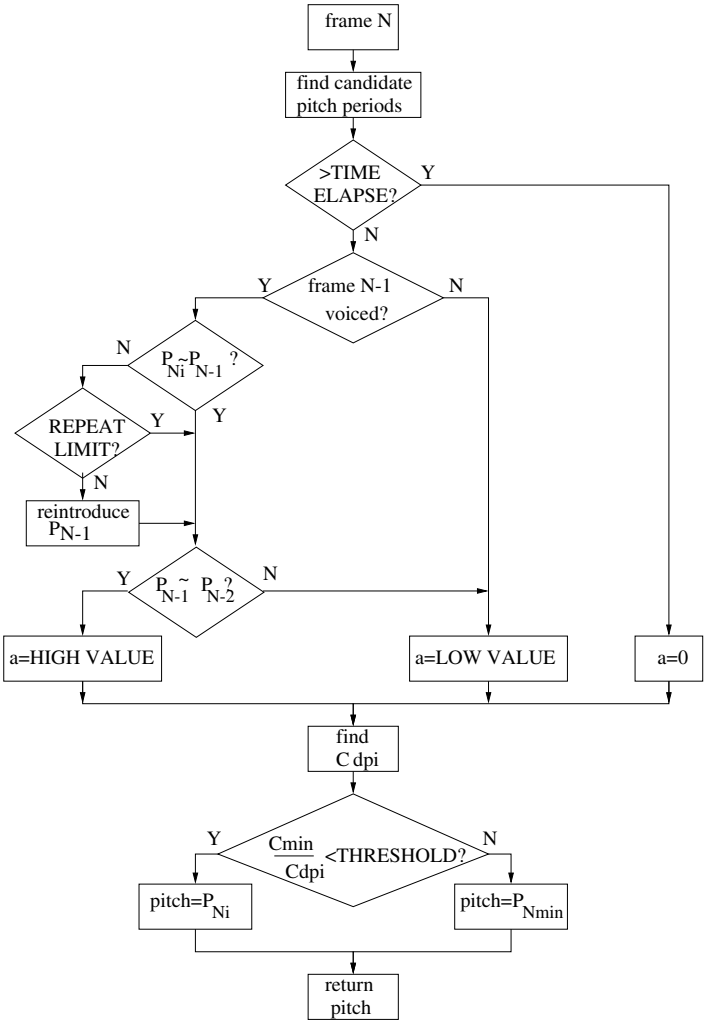

Figure 13.10: Procedure for determining the pitch period of a voiced speech frame using dynamic programming and the cost function of Equation (13.20).

consecutive voiced frames, within a voiced sequence, controlled by the REPEAT LIMIT parameter.

The final processes, at the bottom of Figure 13.10, consider whether the minimum cost function of Equation (13.20) provides the true pitch period. The higher fundamental frequencies have less resolution than the lower fundamental frequencies, thus, the dynamic programming algorithm tends to favour the longer pitch periods where higher cost functions are scored. Hence, the ratio of the minimum cost $C_{\min}$ to all other costs is considered, where values higher than the THRESHOLD parameter result in the minimum cost being kept. However, a value less than the threshold results in a different pitch period being accepted.

The selected pitch periods for the two speech files shown in Figure 13.9 are portrayed in Figure 13.11. It can be seen that the wavelet-based dynamic programming pitch detector performs better than the oversampled autocorrelation-based pitch detector of Figure 12.14, because in Figure 12.14 pitch halving is observed. A comparison between the dynamic programming pitch detector and the manual track of Figure 11.18 in Section 11.4 is given in Table 13.3, where 6.8% of frames are shown as incorrectly labelled. The computational complexity for the wavelet-based dynamic programming pitch detector is shown in Table 13.2 as 2.70 MFLOPS, a reduction from the 3.4 MFLOPS required by the autocorrelation-based pitch detector.

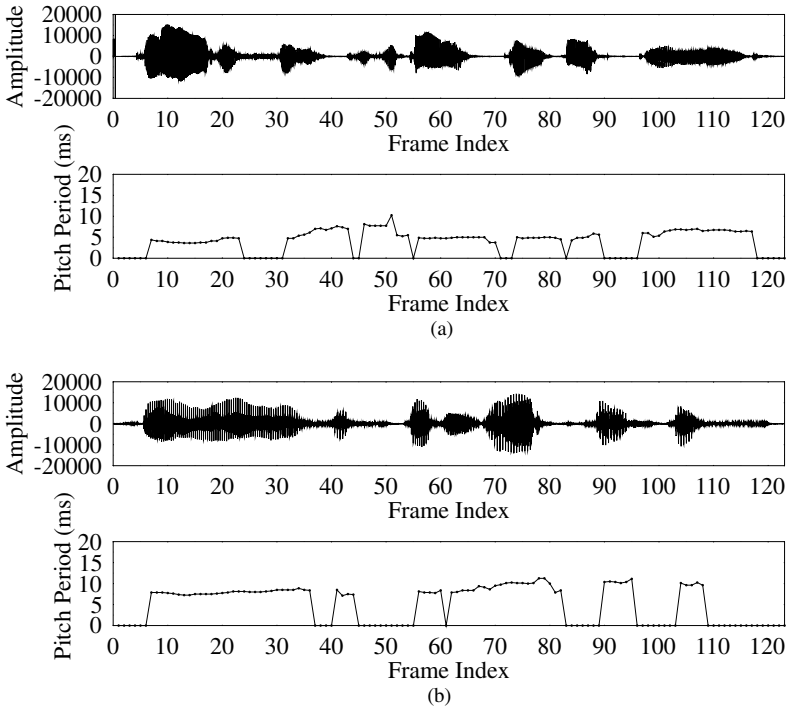

Figure 13.11: The pitch period decisions for (a) testfile BF1 and (b) testfile BM1. The trace from BF1 has some pitch halving between frames 45 and 50, while BM1 has a good pitch track. For comparison we refer to Figure 12.14.

The main disadvantage with this method of pitch period prediction is the 60 ms delay that is incorporated in the coder. An additional problem is that while the dynamic algorithm performs well for the displayed speech frames when a pitch estimation error does occur the strong pitch tracking element propagates the error. This type of error is very audible and disconcerting, thus, the use of the ACF from Section 12.3 is investigated further in the next Section.

Table 13.2: Computational complexity for the wavelet-based dynamic programming pitch detector.

Operation	Complexity /MFLOPS
$D_Y WT$	1.23
Preprocessing	1.00
Dynamic programming	0.47
Total	2.70

13.5.2 Autocorrelation Simplification

An attractive alternative to using dynamic programming in the selection of the correct candidate pitch period is to employ the wavelet analysis for simplifying the autocorrelation approach to pitch detection. This autocorrelation approach was investigated in Section 12.3, where the ACF was performed on the 20–147 sample range to select the correct pitch period. Harnessing the wavelet transform would permit the ACF to be computed for only 15 possible pitch periods, namely the 14 candidate pitch periods and the reintroduced previous pitch period. This would simplify the autocorrelation procedure by more than 80%.

The process of selecting the pitch period is shown in Figure 13.12, and described next. The 14 candidate pitch periods together with the reintroduced previous pitch period are passed to the ACF evaluation block in Figure 13.12. The candidate pitch period which produces the highest autocorrelation value is selected for the pitch period. Finally, some simple pitch tracking is performed, where isolated voiced or unvoiced frames are removed and where pitch periods not related to either neighbour are corrected.

This simplified pitch tracking procedure introduces a delay of 40 ms into the pitch detector, an improvement on the 60 ms required by dynamic programming. The selected pitch periods for the two speech files shown in Figure 13.9 are given in Figure 13.13. Figure 13.13 can be compared with the oversampled autocorrelation based pitch detector of Figure 12.14 and the dynamic programming algorithm of Figure 13.11. For the testfile BF1, the oversampled autocorrelation pitch detector of Figure 12.14 produced two regions of pitch halving lasting for the complete utterances. The wavelet-based dynamic programming pitch detector of Figure 13.11 produced a small pitch error around frame 50. The most recently developed wavelet-based autocorrelation pitch detector of Figure 13.13 also contains pitch errors, which always occur at the start and end of voiced utterances, while maintaining the correct pitch track for the remainder of the utterance. The majority of these pitch errors occur at instants of low signal energy and are inaudible in the reconstructed speech signal.

For the testfile BM1 the oversampled autocorrelation pitch detector of Figure 12.14 and the wavelet-based dynamic programming pitch detector of Figure 13.11 produced no errors. In Figure 13.13 pitch doubling occurs around frame 40 and frame 80 at the low-energy termination of voiced utterances. Again these two errors were inaudible in the reconstructed speech. The performance of this wavelet-based pitch detector is compared in Table 13.3 against the manual track of Section 11.4, where a total of 3.9% of the speech frames were incorrectly classified.

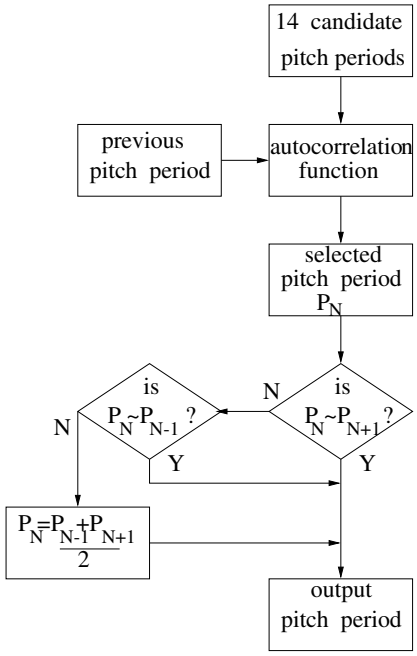

Figure 13.12: The control structure for a wavelet-assisted autocorrelation-based pitch detector. Here the wavelet transform is used to reduce the possible pitch periods searched by the ACF evaluation process.

Table 13.3: A comparison between the performance of the developed wavelet-based pitch detectors and a manual pitch track for the speech database. W_U represents the percentage of frames that are labelled voiced when they should have been identified as unvoiced. W_V indicates the number of frames that have been labelled as unvoiced when they are actually voiced. P_G represents the number of frames where a gross pitch error has occurred. The total number of incorrect frames is given as $W_U + W_V + P_G$.

Pitch detector	W_U (%)	W_V (%)	P_G (%)	Total %
Wavelets and dynamic programming	1.5	1.1	4.1	6.8
Wavelets and ACF	1.3	0.3	2.3	3.9

The computational complexity of this wavelet-assisted autocorrelation-based pitch detector is given in Table 13.4. It can be seen that at 2.67 MFLOPS the computational complexity is slightly lower than that of the wavelet-based dynamic programming approach of Table 13.2. Due to its low complexity and low delay, this wavelet-based autocorrelation pitch detector was selected for use in our speech coders.

This wavelet-assisted autocorrelation-based pitch detector is the fourth one that was investigated, all of which have been informally assessed. Their parameters are detailed in

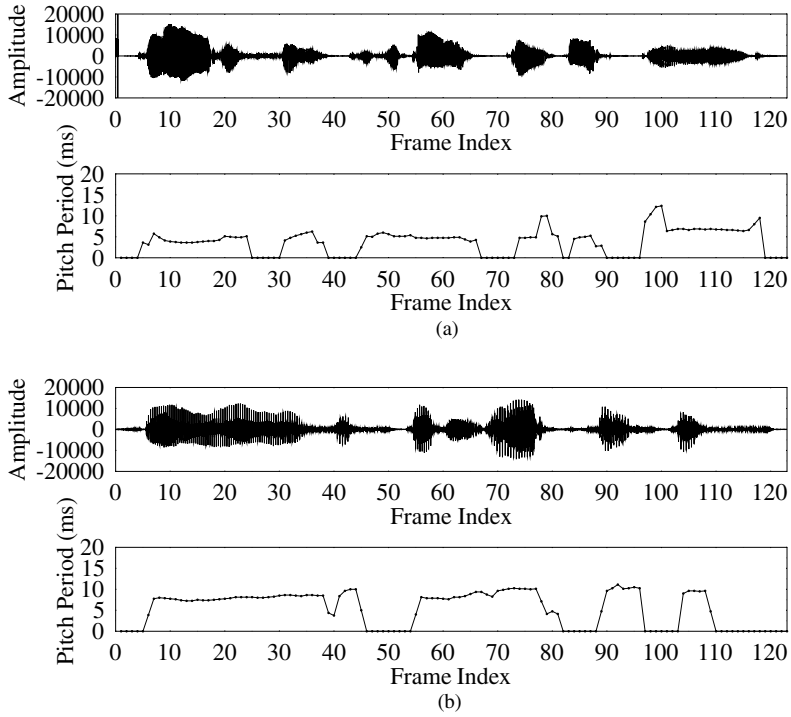

Figure 13.13: The pitch period decisions for (a) the testfile BF1 and (b) the testfile BM1. The BF1 trace has some pitch halving at the low-energy start and end of voiced utterances. The BM1 trace has some pitch doubling around frame 40 and 80. For a comparison we refer to Figures 12.14 and 13.11.

Table 13.4: Computational complexity for the wavelet-assisted autocorrelation-based pitch detector.

Operation	Complexity (MFLOPS)
$D_Y WT$	1.23
Preprocessing	1.00
Autocorrelation	0.24
Total	2.67

Table 13.5 along with their computational complexity, delay and error performance details. These pitch detectors are briefly reviewed next.

The first pitch detector, described in Section 12.3.1, was used in the G.728 recommendation [109]. It performed ACF computations with very simple pitch tracking. The results, shown in Figure 12.8, displayed excessive regions of pitch halving. The performance of this pitch detector was improved through the addition of oversampling [100] and extensive pitch tracking [97], detailed in Section 12.3.2. The pitch detector produced a substantially improved

Table 13.5: Review of considered pitch detectors.

Pitch detector	Complexity (MFLOPS)	Delay (ms)	Percentage of error frames (%)
ACF	1.1	40	12.7
ACF with pitch tracking	3.4	20	7.2
Wavelet and dynamic programming	2.7	60	6.8
Wavelet and ACF	2.7	40	3.9

performance, as seen in Figure 12.14; however, it was excessively complex. Section 12.3.4 described a pitch detector with the oversampling removed, but with the extensive pitch tracking remaining. This pitch detector had a more acceptable complexity and similar performance to Figure 12.14.

The introduction of wavelets decreased the complexity of the pitch detection procedure. With the incorporation of dynamic programming, in Section 13.5.1, a high-quality pitch detector was created, as shown in Figure 13.11; however, this method required a 60 ms delay. Finally, in Section 13.5.2 the ACF was incorporated into the wavelet-based scheme in order to produce a pitch detector. This pitch detector had reduced delay, low complexity and few errors. These errors were inaudible and occurred during low-energy speech segments at utterance terminations. Hence, in our coders, the wavelet-assisted autocorrelation-based pitch detector was favoured.

13.6 Chapter Summary

This chapter has introduced the concept of the $\mathrm{D_Y WT}$ in Sections 13.1 and 13.2. The resultant transformed speech signal was analysed in Section 13.3 facilitating its employment in voiced–unvoiced decisions, as detailed in Section 13.4, as well as in the context of pitch detection in Section 13.5.

It was demonstrated that a wavelet-based pitch detector relying on autocorrelation techniques performs better than the less-sophisticated autocorrelation-assisted pitch detectors of Chapter 12, since the associated pitch detection error probability was 3.9% in the former scheme, as opposed to 7.2% in the latter autocorrelation-based pitch detector selected from Chapter 12. The wavelet-based autocorrelation-assisted pitch detector had the additional benefit of imposing a reduced computational complexity of 2.7 MFLOPS instead of the 3.4 MFLOPS complexity of the less-sophisticated detector of Chapter 12.

Having created a benchmark LPC vocoder, we investigated the appropriate choice of LSF quantisation techniques and selected an appropriate pitch period detection method. Let us now embark on investigating a prototype waveform interpolation codec in the next chapter.

Chapter 14

Zinc Function Excitation

14.1 Introduction

This chapter introduces a PWI speech coder that uses ZFE [497]. A PWI scheme operates by encoding one pitch period-sized segment, a prototype segment, of speech for each frame. The slowly evolving nature of speech permits PWI to reduce the transmitted bitrates, while smooth waveform interpolation at the decoder between the prototype segments maintains good synthesised speech quality. Figure 14.1(a) shows two 20 ms frames of voiced speech, with a pitch period in both frames highlighted in each to demonstrate the slow waveform evolution of speech. The same pitch periods are again highlighted for the LPC STP residual waveform, in Figure 14.1(b), demonstrating that PWI can also be used on the residual signal. Finally, Figure 14.1(c) displays the frequency spectrum for both frames, showing the evolution of the speech waveform in the frequency domain. The excitation waveforms employed in this chapter are the zinc basis functions [497], which efficiently model the LPC STP residual while reducing the speech's 'buzziness' when compared with the classical vocoders of Chapter 12 [497]. The previously introduced schematic in Figure 11.13 portrays the encoder structure for the IZFPE, which has the form of a closed loop LPC-based coding method with optimised ZFE prototype segments for the speech. A similar structure is used in the PWI-ZFE coder described in this chapter.

This chapter follows the basic outline of the IZFPE coder introduced by Hiotakakos and Xydeas [496], but some sections of the scheme have been developed further. The chapter begins with an overview of the PWI-ZFE scheme, detailing the operational scenarios of the arrangement. This is followed by the introduction of the zinc basis functions together with the optimisation process at the encoder, where the wavelets of Chapter 13 are harnessed to reduce the complexity of the process. For voiced speech frames, the pitch detector employed and the prototype segment selection process are described, with a detailed discussion of the interpolation process, where the parameters required for transmission are also given. In addition, the unvoiced excitation and adaptive postfilter are briefly described. Finally, the performance of both a single ZFE and multiple ZFE arrangements are detailed.

Voice and Audio Compression for Wireless Communications Second Edition
L. Hanzo, F. C. A. Somerville and J. P. Woodard

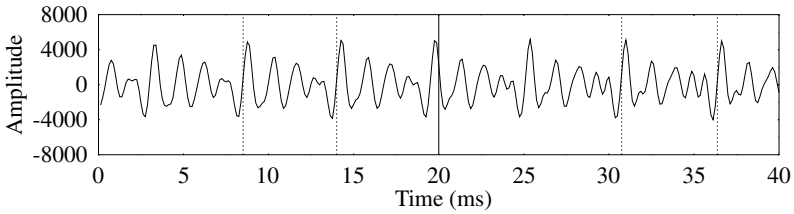

(a) Original speech

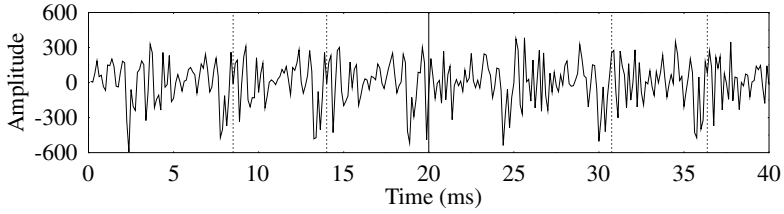

(b) LPC STP residual

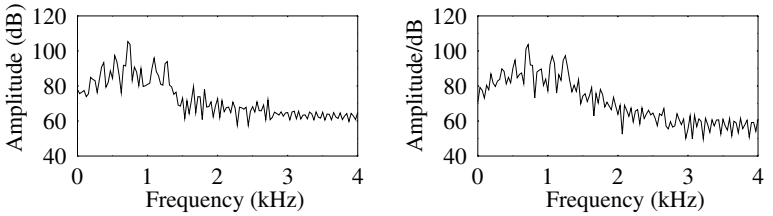

(c) Frequency domain speech

Figure 14.1: Two speech frames demonstrating the smoothly evolving nature of the speech waveform and that of the LPC STP residual in the time and frequency domain. The speech frames are from AF1, uttering the back vowel /ɔ/ in 'dɒg'.

14.2 Overview of Prototype Waveform Interpolation Zinc Function Excitation

This section gives an in-depth description of the PWI-ZFE scheme, considering all possible operational scenarios at both the encoder and decoder. The number of coding scenarios is increased by the separate treatment of voiced and unvoiced frames, and also by the need to accurately represent the voiced excitation.

14.2.1 Coding Scenarios

For the PWI-ZFE encoder the current, the next and the previous two 20 ms speech frames are evaluated, as shown in Figure 14.2, which is now described in depth. The knowledge of the four 20 ms frames, namely frames $N+1$, N, $N-1$ and $N-2$, is required in order to adequately treat voiced–unvoiced boundaries. It is these transition regions which are usually

the most poorly represented speech segments in classical vocoders. The parameters encoded and transmitted during voiced and unvoiced periods are summarised towards the end of the chapter in Table 14.10, while the various coding scenarios are summarised in Tables 14.1 and 14.2.

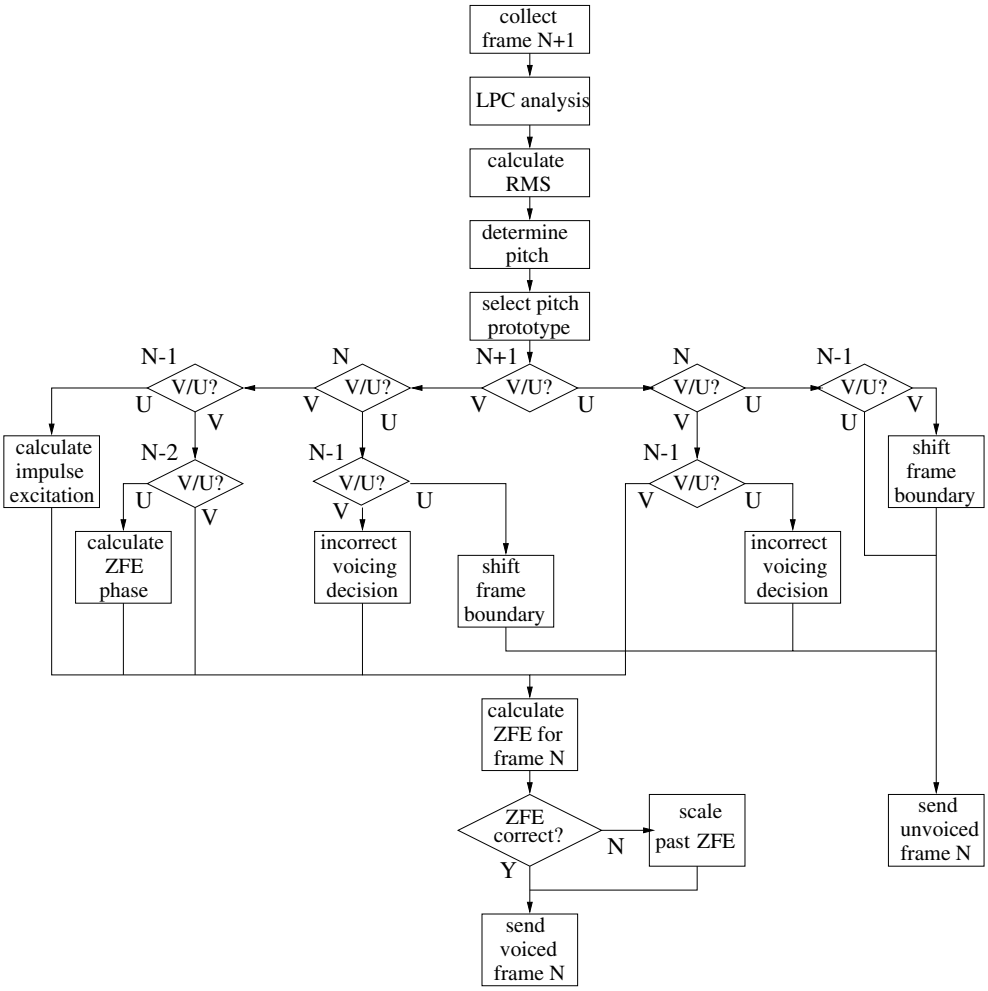

Figure 14.2: The encoder control structure for the PWI-ZFE arrangement.

LPC STP analysis is performed for all speech frames and the RMS value is determined from the residual waveform. The pitch period of the speech frame is also determined. However, if the speech frame lacks any periodicity, then the pitch period is assigned as zero and the speech frame is labelled as unvoiced. The various possible combinations of consecutive voiced (V) and unvoiced (U) frames are now considered.

Table 14.1: Summary of encoder scenarios (see the text for more detail).

$N+1$	N	$N-1$	Summary
U	U	U	Frame N is located in an unvoiced sequence. Quantise and transmit the RMS value of the LPC STP residual to the decoder.
U	U	V	A voiced–unvoiced transition boundary has been encountered. Calculate the section of frame N that is voiced and include this boundary shift parameter, b_s, in the transmission of frame N to the decoder.
V	U	U	An unvoiced–voiced transition boundary has been encountered. Calculate the section of frame N that is voiced and include this boundary shift parameter, b_s, in the transmission of frame N to the decoder.
U	V	U	Assume that frame N should have been classified as unvoiced, hence, treat this scenario as an U–U–U sequence.
V	V	V	Frame N is situated in a voiced sequence. Calculate the ZFE parameters, A_1, B_1 and λ_1. Quantize the amplitude parameters A_1 and B_1, and transmit parameters to the decoder.
V	U	V	Assume frame N should have been labelled as voiced, hence, treat this case as a V–V–V sequence.
U	V	V	Treat this situation as a V–V–V sequence.
V	V	U	The start of a sequence of voiced frames has been encountered. Represent the excitation in the prototype segment with an impulse.

14.2.1.1 U–U–U Encoder Scenario

If all of the speech frames $N+1$, N and $N-1$ are classified as unvoiced, U–U–U, then the unvoiced parameters for frame N are sent to the decoder. The unvoiced parameters are the LPC coefficients, sent as LSFs, a voicing flag which is set to *off* and the quantised RMS value of the LPC STP residual, as described in Table 14.1.

14.2.1.2 U–U–V Encoder Scenario

With a voicing sequence of U–U–V, where frame $N-1$ is voiced, together with the unvoiced parameters an extra parameter b_s, the boundary shift parameter, must be conveyed to the decoder to be used for the voicing transition regions. In order to determine the voiced to unvoiced transition point, b_s, frame N is examined, searching for evidence of voicing, in segments sized by the pitch period. The boundary shift parameter b_s represents the number of pitch periods in the frame that contain voicing. At the decoder this voiced section of the predominantly unvoiced frame N is represented by the ZFE reserved for the voiced segments.

Table 14.2: Summary of decoder scenarios (see the text for more detail).

$N+1$	N	Summary
U	V	A voiced–unvoiced transition has been encountered. Label the portion of frame $N+1$ that is voiced, and subsequently interpolate from the pitch prototype segment in frame N to the voiced sections in frame $N+1$.
U	U	Frame N is calculated using a Gaussian noise excitation scaled by the RMS value for frame N.
V	U	An unvoiced–voiced transition has been encountered. Label the portion of frame N that is voiced and represent the relevant section of frame N by voiced excitation.
V	V	Interpolation is performed between the pitch prototype segments of frame N and frame $N+1$.

14.2.1.3 V–U–U Encoder Scenario

The boundary shift parameter is also sent for the voicing sequence V–U–U. However, for this sequence the predominantly unvoiced frame N is examined, in order to identify how many pitch period durations can be classified as voiced. The parameter b_s in frame N then represents the number of pitch periods in the unvoiced frame N that contain voicing. At the decoder this section of frame N is synthesised using voiced excitation.

14.2.1.4 U–V–U Encoder Scenario

A voicing sequence U–V–U is assumed to have an incorrect voicing decision in frame N. Hence, the voicing flag in frame N is set to zero and the procedure for a U–U–U sequence is followed.

14.2.1.5 V–V–V Encoder Scenario

For a voiced sequence of frames V–V–V the ZFE parameters for frame N are calculated. The ZFE is described by the position parameter λ_1 and the amplitude parameters A_1 and B_1, as shown earlier in Figure 11.14. Further ZFE waveforms are shown in Figure 14.5, which also illustrates the definition of the ZFE phase referred to below. If frame $N-2$ was also voiced, then the chosen ZFE is restricted by certain phase constraints, which will be detailed in Section 14.3, otherwise frame N is used to determine the phase restrictions. The selected ZFE represents a pitch-duration segment of the speech frame, which is referred to as the pitch prototype segment. If a ZFE that complies with the required phase restrictions is not found, then the ZFE parameters from frame $N-1$ are scaled, in terms of the RMS energy of the respective frames, and then they are used in frame N. This is performed since it is assumed that the previous frame parameters will be an adequate substitute for frame N, due to the speech parameters slow time-domain evolution. The parameters sent to the decoder include the LSFs and a voicing flag set to *on*. The ZFE parameters A_1, B_1 and λ_1 are required by

the decoder to synthesise voiced speech, and the pitch prototype segment is defined by its starting point and the pitch period duration of the speech segment.

14.2.1.6 V–U–V Encoder Scenario

A voiced sequence of frames is also assumed for the voicing decisions V–U–V, with the frame N being assigned a pitch period half way between the pitch period for frame $N-1$ and frame $N+1$.

14.2.1.7 U–V–V Encoder Scenario

The voicing sequence U–V–V also follows the procedure of a V–V–V string, since the unvoiced decision of frame $N+1$ is not considered until the V–U–V or U–U–V scenarios.

14.2.1.8 V–V–U Encoder Scenario

The voicing decision V–V–U indicates that frame N will be the start of a voicing sequence. Frame $N+1$, the second frame in the voicing sequence, typically constitutes a better reflection of the dynamics of the voiced sequence than the first frame [496], hence the phase restrictions are determined from this frame. The first voiced frame, namely N, is represented by an excitation pulse similar to that used by the LPC vocoder of Chapter 12 (see [105]).

The speech encoder introduces a delay of 40 ms into the system, where the delay is caused by the necessity for frame $N+1$ to verify voicing decisions. In the decoder control structure, shown in Figure 14.3, only the frames $N+1$ and N are considered when synthesising frame N, thus an additional 20 ms delay is introduced.

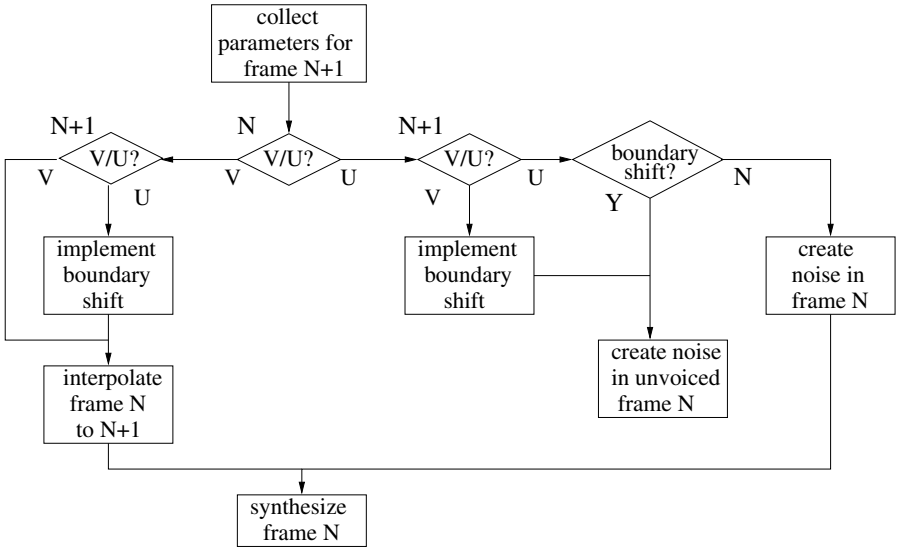

Figure 14.3: The decoder control structure for PWI-ZFE arrangement.

14.2.1.9 U–V Decoder Scenario

If the sequence U–V occurs for the frames $N+1$ and N respectively, then a voiced–unvoiced transition is encountered. Here the boundary shift parameter b_s, transmitted in frame $N+1$, is multiplied by the pitch period in frame N, indicating the portion of frame $N+1$ which was deemed voiced. The ZFE for frame N is interpolated to the end of the voiced portion of frame $N+1$. Subsequently, the interpolation frame N is synthesised.

14.2.1.10 U–U Decoder Scenario

When the sequence U–U occurs for frame indices $N+1$ and N, if frame $N-1$ is unvoiced then frame N will be represented by a Gaussian noise excitation. However, if frame $N-1$ was voiced, some of frame N will already be represented by a ZFE pulse. This will be indicated by the value of the boundary shift parameter b_s, thus only the unvoiced section of frame N is represented by Gaussian noise.

14.2.1.11 V–U Decoder Scenario

The sequence V–U indicates an unvoiced–voiced transition, hence, the value of the boundary shift parameter b_s conveyed by frame N is observed. Only the unvoiced section of frame N is represented by Gaussian noise, with the voiced portion represented by a ZFE interpolated from frame $N+1$.

14.2.1.12 V–V Decoder Scenario

The sequence V–V directs the decoder to interpolate the ZFE parameters between frame N and frame $N+1$. This interpolation process is described in Section 14.6, where it occurs for the region between pitch prototype segments. Thus, each speech frame has its first half interpolated, while classified as frame $N+1$, with its second half interpolated during the next iteration, while classified as frame N.

Following this in-depth description of the control structure of a PWI-ZFE scheme, as given by Figures 14.2 and 14.3, a deeper insight into the description of the ZFE is now given.

14.3 Zinc Function Modelling

The continuous zinc function used in the PWI-ZFE scheme to represent the LPC STP residual is defined by [497]

$$z_k(t) = A_k \cdot \mathrm{sinc}(t - \lambda_k) + B_k \cdot \mathrm{cosc}(t - \lambda_k) \tag{14.1}$$

where

$$\mathrm{sinc}(t) = \frac{\sin(2\pi f_c t)}{2\pi f_c t}, \quad \mathrm{cosc}(t) = \frac{1 - \cos(2\pi f_c t)}{2\pi f_c t},$$

k is the kth zinc function, A_k, B_k determine the amplitude of the zinc function and λ_k determines its location. For the discrete time case with a speech bandwidth of $f_c = 4\,\mathrm{kHz}$

and a sampling frequency of $f_s = 8\,\text{kHz}$ we have [496]:

$$z_k(n) = A_k \cdot \text{sinc}(n - \lambda_k) + B_k \cdot \text{cosc}(n - \lambda_k) = \begin{cases} A_k & n - \lambda_k = 0 \\ \dfrac{2B_k}{n\pi} & n - \lambda_k = \text{odd} \\ 0 & n - \lambda_k = \text{even.} \end{cases} \tag{14.2}$$

14.3.1 Error Minimisation

From Figure 11.16, which describes the AbS process, the weighted error signal $e_w(n)$ can be described by

$$e_w(n) = s_w(n) - \bar{s}_w(n) \tag{14.3}$$

$$= s_w(n) - m(n) - \left(\sum_{k=1}^{K} z_k(n) * h(n) \right) \tag{14.4}$$

$$= y(n) - \left(\sum_{k=1}^{K} z_k(n) * h(n) \right) \tag{14.5}$$

where $y(n) = s_w(n) - m(n)$, $m(n)$ is the memory of the LPC synthesis filter due to previous excitation segments, while $h(n)$ is the impulse response of the weighted synthesis filter, $W(z)$, and K is the number of ZFE pulses employed. Thus, the error, $e_w(n)$, is the difference between the weighted original and weighted synthesised speech, with the synthesised speech being the ZFE passed through the synthesis filter, $W(z)$. This formulation of the error signal, where the filter's contribution is divided into filter memory $m(n)$ and impulse response $h(n)$, reduces the computational complexity required in the error minimisation procedure. It is the IIR nature of the filter, which requires the memory to be considered in the error equation. For further details of the mathematics, Steele and Hanzo [530, Chapter 3] is recommended. The sum of the squared weighted error signal is given by

$$E_w^{k+1} = \sum_{n=1}^{excint} (e_w^{k+1}(n))^2 \tag{14.6}$$

where $e_w^{k+1}(n)$ is the kth-order weighted error, achieved after k zinc basis functions have been modelled, and *excint* is the length over which the error signal has to be minimised, here the pitch prototype segment length.

Appendix B describes the process of minimising the squared error signal using Figure 11.16 and Equations (14.1) to (14.6). It is shown that the MSE signal is minimised if the expression

$$\zeta_{\text{MSE}} = \frac{R_{es}^2}{R_{ss}} + \frac{R_{ec}^2}{R_{cc}} \tag{14.7}$$

is maximised as a function of the ZFE position parameter λ_{k+1}, and

$$R_{es} = \sum_{n=1}^{excint} (\mathrm{sinc}(n - \lambda_{k+1}) * h(n)) \times e_w^k(n) \tag{14.8}$$

$$R_{ec} = \sum_{n=1}^{excint} (\mathrm{cosc}(n - \lambda_{k+1}) * h(n)) \times e_w^k(n) \tag{14.9}$$

$$R_{ss} = \sum_{n=1}^{excint} (\mathrm{sinc}(n - \lambda_{k+1}) * h(n))^2 \tag{14.10}$$

$$R_{cc} = \sum_{n=1}^{excint} (\mathrm{cosc}(n - \lambda_{k+1}) * h(n))^2 \tag{14.11}$$

where $*$ indicates convolution.

Due to bitrate limitations it is now assumed that a single ZFE is used, i.e. $k = 1$, and furthermore that the value *excint* becomes equivalent to the pitch period duration, with λ_k controlling the placement of the ZFE in the range [1, *excint*].

The ZFE amplitude coefficients are given by Equations (B.14) and (B.15) of Appendix B, repeated here for convenience:

$$A_k = \frac{R_{es}}{R_{ss}} \tag{14.12}$$

$$B_k = \frac{R_{ec}}{R_{cc}}. \tag{14.13}$$

The optimisation involves computing ζ_{MSE} in Equation (14.7) for all legitimate values of λ_1 in the range [1, *excint*], subsequently finding the corresponding values for A_1 and B_1 from Equations (14.12) and (14.13). The computational complexity for this optimisation procedure is now assessed.

14.3.2 Computational Complexity

The associated complexity is evaluated as follows and tabulated in Table 14.3. The calculation of the minimisation criterion ζ_{MSE} requires the highest computational complexity, where the convolution of both the sinc and cosc functions with the impulse response $h(n)$ is performed. From Equation (14.2) it can be seen that the sinc function is only evaluated when $n - \lambda_k = 0$, while the cosc function must be evaluated whenever $n - \lambda_k$ is odd. The convolved signals, involving the sinc and cosc signals, are then multiplied by the weighted error signal $e_w(n)$ to calculate R_{es} and R_{ec}, in Equations (14.8) and (14.9), respectively. Observing Equations (14.6) to (14.13), the computational complexity's dependence on the *excint* parameter can be seen. Thus, in Table 14.3 all values are calculated with the extreme values of *excint*, which are 20 and 147, the possible pitch period duration range in samples. The complexity increase is exponential, as shown in Figure 14.4 by the dashed curve, where it can be seen that any pitch period longer than 90 samples in duration will exceed a complexity of 20 MFLOPS.

Table 14.3: Computational complexity for error minimisation in the PWI-ZFE encoder for the extremities of the *excint* variable.

Procedure	*excint* = 20 (MFLOPS)	*excint* = 147 (MFLOPS)
Convolve sinc and $h(n)$	0.02	1.06
Convolve cosc and $h(n)$	0.20	78.0
Calculate A_1	0.04	2.16
Calculate B_1	0.04	2.16
Total	0.3	83.38

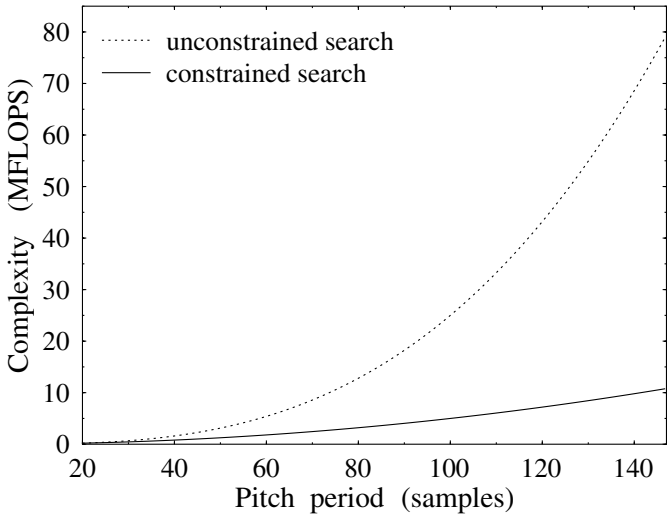

Figure 14.4: Computational complexity for the permitted pitch period range of 20 to 147 sample duration, for both an unrestricted and constrained search.

14.3.3 Reducing the Complexity of Zinc Function Excitation Optimisation

The complexity of the ZFE minimisation procedure can be reduced by considering the GCIs introduced in Chapter 13. In Chapter 13 wavelet analysis was harnessed to produce a pitch detector, where the pitch period was determined as the distance between two GCIs. These GCIs indicate the snapping shut, or closure, of the vocal folds, which provides the impetus for the following pitch period. The energy peak caused by the GCI will typically be in close proximity to the position of the ZFE placed by the ZFE optimisation process. This permits the possibility of reducing the complexity of the AbS process. Figure 14.4 shows that as the number of possible ZFE positions increases linearly, the computational complexity increases exponentially. Hence, constraining the number of ZFE positions will ensure that the

computational complexity remains at a realistic level. The constraining process is described next.

The first frame in a voiced sequence has no minimisation procedure; simply, a single pulse is situated at the glottal pulse location within the prototype segment. For the other voiced frames, in order to maintain a moderate computational complexity, the number of possible ZFE positions is restricted as if the pitch period is always 20 samples. A suitable constraint is to have the ZFE located within 10 samples of the GCI situated in the pitch prototype segment. Table 14.4 repeats the calculations of Table 14.3, for complexities related to 20 and 147 sample pitch periods, for a restricted search. In Figure 14.4 the solid curve represents the computational complexity of a restricted search procedure in locating the ZFE. The maximum complexity for a 147 sample pitch period is 11 MFLOPS. The degradation to the speech coder's performance, caused by restricting the number of ZFE locations, is quantified in Section 14.4.2.

Table 14.4: Computational complexity for error minimisation in the PWI-ZFE encoder with a restricted search procedure.

Procedure	*excint* $= 20$ (MFLOPS)	*excint* $= 147$ (MFLOPS)
Convolve sinc and $h(n)$	0.02	0.15
Convolve cosc and $h(n)$	0.20	10.73
Calculate A_1	0.04	0.29
Calculate B_1	0.04	0.29
Total	0.30	11.46

14.3.4 Phases of the Zinc Functions

There are four possible phases of the ZFE produced by four combinations of positive or negative valued A_1 and B_1 parameters, which is demonstrated in Figure 14.5 for parameter values of $A_1 = \pm 1$ and $B_1 = \pm 1$. Explicitly, if $|A_1| = 1$ and $|B_1| = 1$, then the possible phases of the ZFE are the following: $A_1 = 1$ $B_1 = 1$, $A_1 = 1$ $B_1 = -1$, $A_1 = -1$ $B_1 = 1$, and $A_1 = -1$ $B_1 = -1$. The phase of the ZFE is determined during the error minimisation process, where the calculated A_1, B_1 values of Equations (14.12) and (14.13) will determine the ZFE phase. It should be noted that for successful interpolation at the decoder the phase of the ZFE should remain constant throughout each voiced sequence.

Following this insight into zinc function modelling, the practical formulation of an PWI-ZFE coder is now discussed. Initially, the procedures requiring pitch period knowledge are discussed, which are followed by details of voiced and unvoiced excitation considerations.

14.4 Pitch Detection

The PWI-ZFE coder located the voiced frame's pitch period using the autocorrelation-based wavelet pitch detector described in Section 13.5.2, which has a computational complexity of

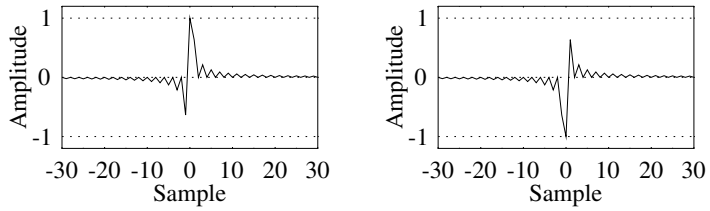

(a) $A = +1$, $B = +1$

(b) $A = -1$, $B = +1$

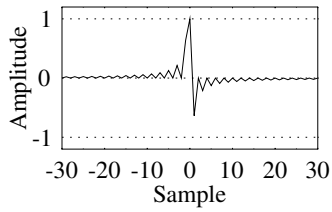

(c) $A = +1$, $B = -1$

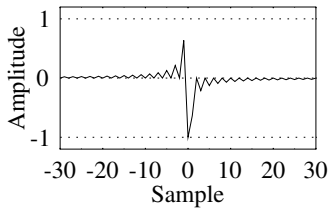

(d) $A = -1$, $B = -1$

Figure 14.5: The four different phases possible for the ZFE waveform of Equation (14.1).

2.67 MFLOPS. This section investigates methods of making voiced–unvoiced decisions for pitch-sized segments, and methods for identifying a pitch period segment.

14.4.1 Voiced–unvoiced Boundaries

Classifying a segment of speech as voiced or unvoiced is particularly difficult at the transition regions, hence a segment of voiced speech can easily become classified as unvoiced. Thus, in the transition frame, pitch-duration sized segments are examined for evidence of voicing. In this case the autocorrelation approach cannot be used, as several pitch periods are not available for the correlation procedure. Instead, a side result of the wavelet-based pitch detector is utilised, namely that for every speech frame candidate glottal pulse locations exist.

Therefore, if the first voiced frame in a voiced sequence is frame N, then frame $N - 1$ is examined for boundary shift. If a periodicity close to the pitch period of frame N exists over an end portion of frame $N - 1$, this end portion of frame $N - 1$ is designated as voiced. Similarly, if the final voiced frame in a voiced sequence is frame N, then frame $N + 1$ is examined for boundary shift. Any starting portion of frame $N + 1$ that has periodicity close to the pitch period of frame N is declared voiced.

In the speech decoder it is important for the ZFE parameters to be interpolated over an integer number of pitch periods. Thus, the precise duration of voiced speech in the transition frame is not completely defined until the λ_1 interpolation process, to be described in Section 14.6, is concluded.

14.4.2 Pitch Prototype Selection

For each speech frame classed as voiced, a prototype pitch segment is located, parameterised, encoded and transmitted. Subsequently, at the decoder interpolation between adjacent prototypes is performed. For smooth waveform interpolation the prototype must be a pitch period in duration, since this speech segment captures all elements of the pitch period cycle, thus enabling a good reconstruction of the original speech.

The prototype selection for the first voiced frame is demonstrated in Figure 14.6. If P is the pitch period of the voiced frame, then P samples in the centre of the frame are selected as the initial prototype selection, as shown in the second trace of Figure 14.6. Following Hiotakakos and Xydeas [496], the maximum amplitude is found in the frame, as shown in the middle trace of Figure 14.6. Finally, the zero-crossing immediately to the left of this maximum is selected as the start of the pitch prototype segment, as indicated at the bottom of the figure. The end of the pitch prototype segment is a pitch period duration away. Locating the start of the pitch prototype segment near a zero crossing helps to reduce discontinuities in the speech encoding process.

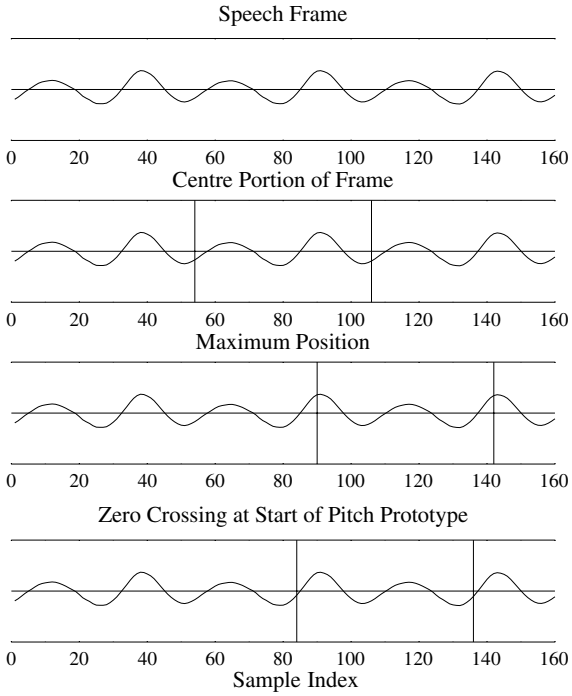

Figure 14.6: Pitch prototype selection for AM2 uttering the nasal consonant /n/ from 'e*n*d'.

It is also beneficial in the interpolation procedure of the decoder if consecutive ZFE locations are smoothly evolving. Therefore, close similarity between consecutive prototype segments within a voiced sequence of frames is desirable. Thus, after the first frame, the procedure of Hiotakakos and Xydeas [496] is no longer followed. Instead the cross-correlation between consecutive pitch prototype segments [488] of the other speech frames

is performed. These subsequent pitch prototype segments are calculated from the maximum cross-correlation between the current speech frame and previous pitch prototype segment. Figure 14.7 shows how, at the encoder, the speech waveform prototype segments can be concatenated to produce a smoothly evolving waveform.

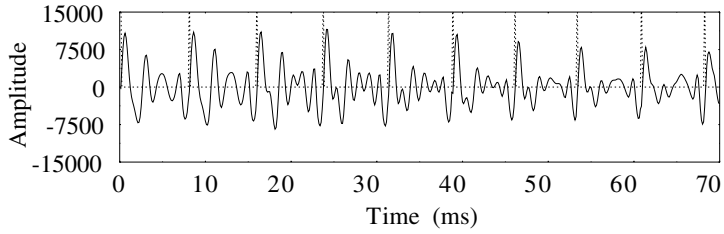

Figure 14.7: Concatenated speech signal prototype segments producing a smoothly evolving waveform. The dotted lines represent the prototype boundaries.

In order to further improve the probability that consecutive ZFEs have similar locations within their prototype segments, any GCIs that are not close to the previous segment's ZFE location are discarded, with the previous ZFE location used to search for the new ZFE in the current prototype segment.

At the encoder, the introduction of constraints on the location of the ZFE pulse, to within ± 10 positions, reduces the SEGSNR value, as shown in Table 14.5. The major drawback of the constrained search is the possibility that the optimisation process is degraded through the limited range of ZFE locations searched. In addition, it is possible to observe the degradation to the MSE optimisation, caused by the phase restrictions imposed on the ZFEs and detailed in Section 14.3.4. Table 14.5 displays the SEGSNR values of the concatenated voiced prototype speech segments. The unvoiced segments are ignored, since these speech spurts are represented by noise, thus a SEGSNR value would be meaningless.

Table 14.5: SEGSNR results for the optimisation process with and without phase restrictions, or a constrained search.

	Unconstrained search (dB)	Constrained search (dB)
No phase restrictions	3.36	2.68
Phase restrictions	2.49	1.36

Observing Table 14.5 for a totally unconstrained search, the SEGSNR achieved by the ZFE optimisation loop is 3.36 dB. The process of either implementing the above-mentioned ZFE phase restriction or constraining the permitted ZFE locations to the vicinity of the GCIs reduces the voiced segments' SEGSNR after ZFE optimisation by 0.87 dB and 0.68 dB, respectively. Restricting both the phase and the ZFE locations reduces the SEGSNR by 2 dB. However, in perceptual terms the ZFE interpolation procedure, described in Section 14.6, actually improves the subjective quality of the decoded speech due to the smooth speech waveform evolution facilitated, despite the SEGSNR degradation of about 0.87 dB caused by imposing phase restrictions. Similarly, the extra degradation of about 1.13 dB caused by

constraining the location of the ZFEs also improves the perceived decoded speech quality due to smoother waveform interpolation.

14.5 Voiced Speech

For frames designated as voiced the excitation signal is a single ZFE. For a single ZFE the equations defined in Section 14.3 and Appendix B are simplified, since the kth stage error Equation (14.5) becomes

$$e_w^0(n) = y(n). \tag{14.14}$$

Therefore, Equation (14.6) for the weighted error of a single ZFE is given by

$$E_w^1(n) = \left(\sum_{n=1}^{excint} e_w^1(n) \right)^2 \tag{14.15}$$

where $e_w^1(n) = y(n) - [z(n) * h(n)]$. Equations (14.8) and (14.9) are simplified to

$$R_{es} = \sum_{n=1}^{excint} (\mathrm{sinc}(n - \lambda_1) * h(n)) \times y(n) \tag{14.16}$$

$$R_{ec} = \sum_{n=1}^{excint} (\mathrm{cosc}(n - \lambda_1) * h(n)) \times y(n). \tag{14.17}$$

Calculating the ZFE, which best represents the pitch prototype, involves locating the value of λ_1 between zero and the pitch period that maximises the expression for ζ_{MSE} given in Equation (14.7). While calculating ζ_{MSE}, $h(n)$ is the impulse response of the weighted synthesis filter $W(z)$, and the weighted error signal e_w is the LPC residual signal minus the LPC STP filter's memory, as shown by Equation (14.14). The use of prototype segments produces a ZFE determination process that is a discontinuous task, thus the actual filter memory is not explicitly available for the ZFE optimisation process. Subsequently the filter's memory is assumed to be due to the previous ZFE. Figure 14.8 shows two consecutive speech frames, where the previous pitch prototype segment has its final p samples highlighted as LPC synthesis filter memory values, while for the current pitch prototype segment these p samples constitute virtual filter memory. Thus, for the error minimisation procedure the speech between the prototype segments has been effectively removed.

Once the value of λ_1 that produces the maximum ζ_{MSE} value has been determined, the appropriate values of A_1 and B_1 are calculated using Equations (14.12) and (14.13). Figure 14.7 displayed the smooth evolution of the concatenated pitch prototype segments. If the ZFEs selected for these prototype segments are passed through the weighted LPC STP synthesis filter, the resulting waveform should be a good match for the weighted speech waveform used in the minimisation process. This is shown in Figure 14.9, characterising the AbS approach used in the PWI-ZFE encoder.

The above procedure is only followed for the phase constraining frame, for subsequent frames in a voiced sequence the ZFE selected must have the phase dictated by the phase constraining frame. If phase restrictions are not followed, then during the interpolation

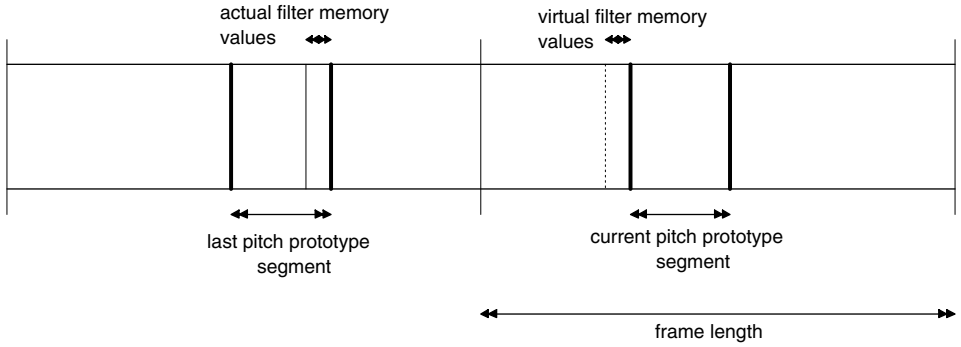

Figure 14.8: Determining the LPC filter memory.

process a change in the sign of A_1 or B_1 will result in some small-valued interpolated ZFEs as the values pass through zero. For each legitimate zinc pulse position, λ_1, the signs of A_1 and B_1 are initially checked, where the value of ζ_{MSE} is calculated only if the phase restriction is satisfied. Therefore, the maximum value of ζ_{MSE} associated with a suitably phased ZFE is selected as the excitation signal. It is feasible that a suitably phased ZFE will not be found, indeed with the test database 13% of the frames did not have a suitable ZFE. If this occurs, then the previous ZFE is scaled, as explained below, and used for the current speech frame. The scaling is based on the RMS value of the LPC residual after STP analysis which is defined by

$$A_1(N) = \delta_s A_1(N-1) \tag{14.18}$$

$$B_1(N) = \delta_s B_1(N-1) \tag{14.19}$$

where

$$\delta_s = \frac{\text{RMS of LPC residual } N}{\text{RMS of LPC residual } N-1}. \tag{14.20}$$

The value of $\lambda_1(N)$ is assigned to be the ZFE position in frame $N-1$, becoming $\lambda_1(N-1)$.

14.5.1 Energy Scaling

The values of A_1 and B_1 determined in the voiced speech encoding process produce an attenuation in the signal level from the original prototype signal. The cause of this attenuation is due to the nature of the minimisation process described in Section 14.3, where the best waveform match between the synthesised and original speech is found. However, the minimisation process does not consider the relative energies of the original weighted waveform and the synthesised weighted waveform. Thus, the values of the A_1 and B_1 parameters are scaled to ensure that the energies of the original and reconstructed prototype signals are equal, requiring that

$$\sum_{n=1}^{excint} (z(n) * h(n))^2 = \sum_{n=1}^{excint} (\bar{s}_w(n) - m(n))^2 \tag{14.21}$$

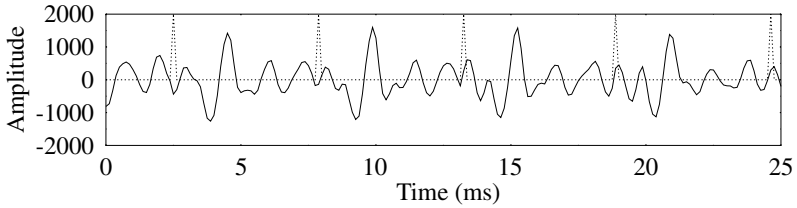

(a) Prototype segments of the weighted speech

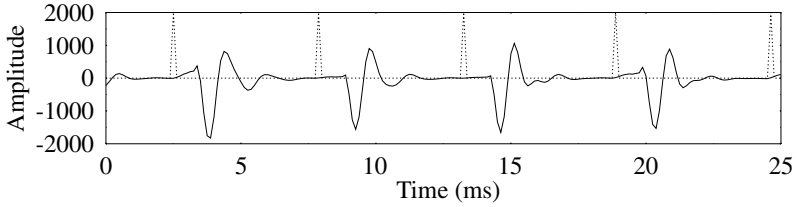

(b) Synthesized prototypes for the weighted speech

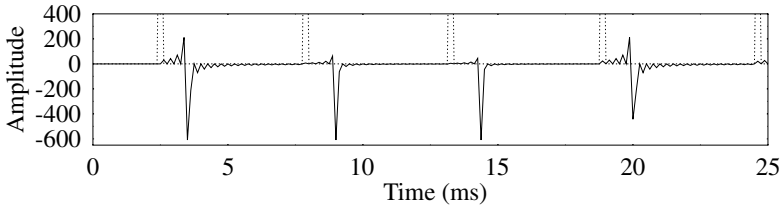

(c) Zinc function excitation

Figure 14.9: Demonstrating the process of AbS encoding for prototype segments that have been concatenated to produce a smoothly evolving waveform. The dotted spikes indicate the boundaries between prototype segments.

where $h(n)$ is the impulse response of the weighted LPC STP synthesis filter, $\bar{s}_w(n)$ is the weighted speech signal and $m(n)$ is the memory of the weighted LPC STP synthesis filter. Ideally, the energy of the excitation signals will also be equal, thus

$$\sum_{n=1}^{excint} z(n)^2 = \sum_{n=1}^{excint} r(n)^2 \tag{14.22}$$

where $r(n)$ is the LPC STP residual.

The above equation shows that it is desirable to ensure that the energy of the synthesised excitation is equal to the energy of the LPC STP residual for the prototype segment. Upon expanding the left-hand side of Equation (14.22) to include A_1 and B_1 and also introducing

the scale factor S_{AB} that will ensure that Equation (14.22) is obeyed, we have

$$\sum_{n=1}^{excint} [\sqrt{S_{AB}} A_1 \sin c(n-\lambda_1) + \sqrt{S_{AB}} B_1 \cos c(n-\lambda_1)]^2 = \sum_{n=1}^{excint} r(n)^2 \qquad (14.23)$$

where

$$S_{AB} = \frac{\sum_{n=1}^{excint} r(n)^2}{\sum_{n=1}^{excint} [A_1 \sin c(n-\lambda_1) + B_1 \cos c(n-\lambda_1)]^2}. \qquad (14.24)$$

Here the factor S_{AB} represents the difference in energy between the original and synthesised excitation. Thus, by multiplying both the A_1 and B_1 parameters by $\sqrt{S_{AB}}$ the energies of the synthesised and original excitation prototype segments will match.

14.5.2 Quantisation

Once the A_1 and B_1 parameters have been determined they must be quantised. The Lloyd–Max quantiser, described in Section 12.4, requires knowledge of the A_1 and B_1 parameters' PDFs, which are shown in Figure 14.10, where the PDF is generated from the unquantised A_1 and B_1 parameters of the training speech database, described in Section 11.4.

The Lloyd–Max quantiser was used to create 4-, 5- and 6-bit SQs for both the A_1 and B_1 parameters. Table 14.6 shows the SNR values for the A_1 and B_1 parameters for the various quantisation schemes.

Table 14.6: SNR values for SQ of the A_1 and B_1 parameters.

Quantiser scheme	SNR for A_1 (dB)	SNR for B_1 (dB)
4-bit	10.45	10.67
5-bit	18.02	19.77
6-bit	26.47	27.07

In order to gain further insight into the performance of the various quantisers, the SEGSNR and SD measures were calculated for the synthesised and original speech prototype segments. Together with the quantised A_1 and B_1 values the SEGSNR and SD measures were calculated for the unquantised A_1 and B_1 values. Table 14.7 shows the SEGSNR values achieved. While low, the SEGSNR values demonstrate that the 6-bit quantisation produces a SEGSNR performance similar to the unquantised parameters.

Table 14.8 shows the SD values achieved, which demonstrate again that the 6-bit quantisers produce little degradation. The 6-bit A_1 and B_1 SQs were selected due to their transparency in the SEGSNR and SD tests. They have SNR values of 26.47 and 27.07 dB, respectively, as seen in Table 14.6.

The interpolation of the voiced excitation performed at the decoder is described next, where pitch synchronous interpolation of the ZFE and LSFs are implemented.

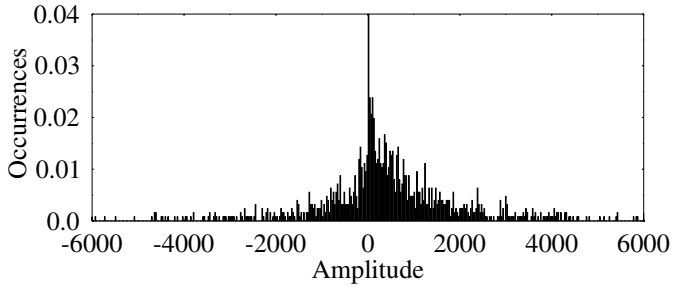

(a) PDF for the ZFE A parameter

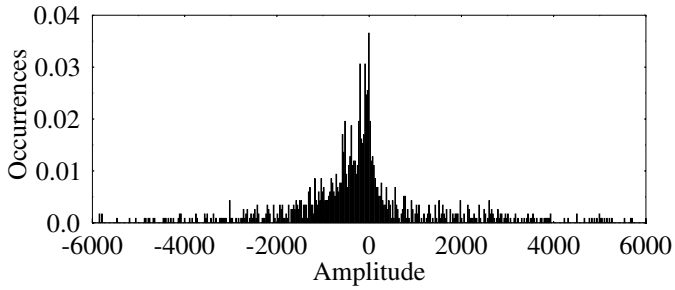

(b) PDF for the ZFE B parameter

Figure 14.10: Graphs for the PDFs of (a) A_1 and (b) B_1 ZFE parameters, created from the combination of A_1 and B_1 parameters from 45 seconds of speech.

Table 14.7: SEGSNR values between the original and synthesised prototype segments for a selection of SQs for the A_1 and B_1 parameters.

Quantiser scheme	SEGSNR (dB)
Unquantised	1.36
4-bit	0.21
5-bit	1.00
6-bit	1.29

14.6 Excitation Interpolation Between Prototype Segments

Having determined the prototype segments for the adjacent speech frames, interpolation is necessary in order to provide a continuous excitation signal between them. The interpolation process is investigated in this section.

Table 14.8: SD values for the synthesised prototype segments for a selection of SQs for the A_1 and B_1 parameters.

Quantiser scheme	SD (dB)
Unquantised	4.53
4-bit	4.90
5-bit	4.60
6-bit	4.53

14.6.1 ZFE Interpolation Regions

The associated interpolation operations will first be stated in general terms, subsequently, using the equations derived and the parameter values of Table 14.9, they will be augmented using a numerical example. We also refer to traces three and four of Figures 14.11 and 14.12, which portray the associated interpolation operations.

Table 14.9: Transmitted parameters for voiced speech.

Speech frame	Pitch period	Zero crossing	A_1	B_1	λ_1
$N-1$	52	64	-431	186	16
N	52	56	-573	673	20

Initially we follow the method of Hiotakakos and Xydeas [496] with interpolation performed over an interpolation region $d_{\rm pit}$, where $d_{\rm pit}$ contains an integer number of pitch periods. The provisional interpolation region, $d'_{\rm pit}$, which may not contain an integer number of pitch periods, begins at the start of the prototype segment in frame $N-1$ and finishes at the end of the prototype segment in frame N. The number of pitch synchronous intervals, $N_{\rm pit}$, between the two prototype regions is given by the ratio of the provisional interpolation region to the average pitch period during this region [496]:

$$N_{\rm pit} = nint\left\{\frac{2d'_{\rm pit}}{P(N)+P(N-1)}\right\} \tag{14.25}$$

where $P(N)$ and $P(N-1)$ represent the pitch period in frames N and $N-1$, respectively, and $nint$ signifies the nearest integer. If $P(N)$ and $P(N-1)$ are different, then the smooth interpolation of the pitch period over the interpolation region is required. This is achieved by calculating the average pitch period alteration necessary to convert $P(N-1)$ to $P(N)$ over $N_{\rm pit}$ pitch synchronous intervals, where the associated pitch interpolation factor $\epsilon_{\rm pit}$ is defined as [496]

$$\epsilon_{\rm pit} = \frac{P(N)-P(N-1)}{N_{\rm pit}-1}. \tag{14.26}$$

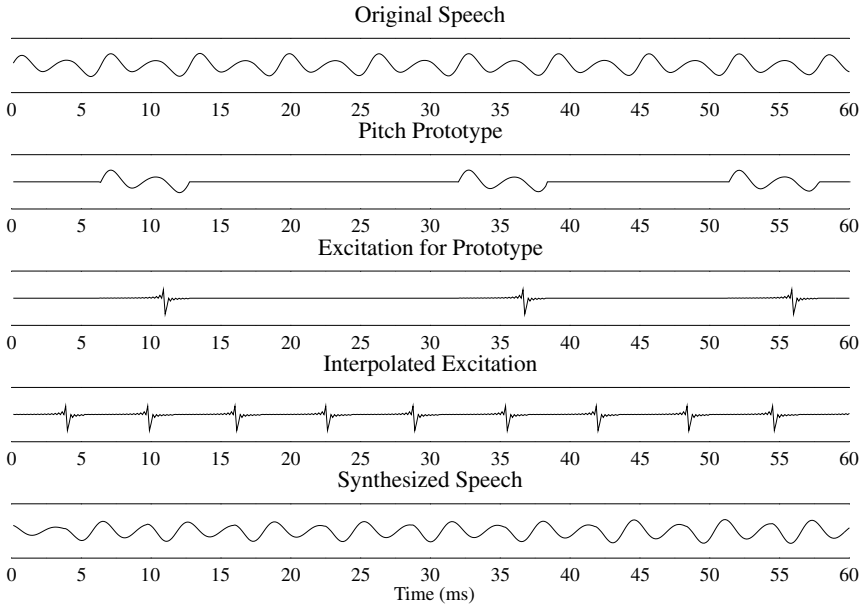

Figure 14.11: An example of the original and synthesised speech for a 60 ms speech waveform from AF2 uttering the front vowel /i/ from 'h*e*', where the frame length is 20 ms. The prototype segment selection and ZFE interpolation are also shown.

The final interpolation region, d_{pit}, is given by the sum of the pitch periods over the interpolation region constituted by N_{pit} number of pitch period intervals [496]:

$$d_{\text{pit}} = \sum_{n_p=1}^{N_{\text{pit}}} p(n_p) \tag{14.27}$$

where $p(n_p)$ are the pitch period values between $P(N-1)$ and $P(N)$, with $p(n_p) = P(N-1) + (n_p - 1) \cdot \epsilon_{\text{pit}}$ and $n_p = 1 \ldots N_{\text{pit}}$. In general the start and finish of the prototype region in frame N will be altered by the interpolation process, since the provisional interpolation region d'_{pit} is generally extended or shortened, to become the interpolation region d_{pit}. To ensure correct operation between frame N and frame $N-1$, the change in the prototype position must be noted:

$$\textit{change} = d'_{\text{pit}} - d_{\text{pit}} \tag{14.28}$$

and then we assign $\textit{start}(N) = \textit{start}(N) - \textit{change}$, where $\textit{start}(N)$ is the beginning of the prototype segment in frame N. Thus, the start of the prototype segment in frame N together with the position of the ZFE parameter λ_1 within the frame are altered, in order to compensate for the changes to the interpolation region. Maintaining the position parameter λ_1 at the same location of the prototype segment sustains the shape within the prototype excitation, but introduces a time misalignment with the original speech, where this time misalignment has no perceptual effect.

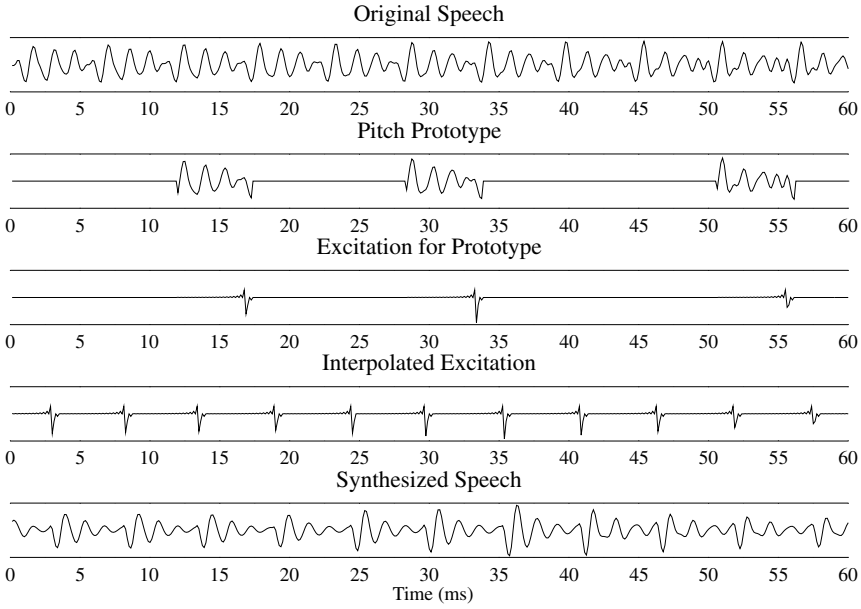

Figure 14.12: An example of three 20 ms segments of the original and synthesised speech for predominantly voiced speech from AF1 uttering the back vowel /ɔ/ 'd*o*g'. The prototype segment selection and ZFE interpolation are also shown.

14.6.2 ZFE Amplitude Parameter Interpolation

The interpolated positions for the ZFE amplitude parameters are given by [496]

$$A_{1,n_p} = A_1(N-1) + (n_p - 1)\frac{A_1(N) - A_1(N-1)}{N_{\text{pit}} - 1} \tag{14.29}$$

$$B_{1,n_p} = B_1(N-1) + (n_p - 1)\frac{B_1(N) - B_1(N-1)}{N_{\text{pit}} - 1} \tag{14.30}$$

where the formulae reflect a linear sampling of the A_1 and B_1 parameters between the adjacent prototype functions. Explicitly, given the starting value $A_1(N-1)$ and the difference $\Delta_{\text{pit}} = A_1(N) - A_1(N-1)$ the corresponding gradient is $[\Delta_{\text{pit}}/N_{\text{pit}} - 1]$, where N_{pit} is the number of pitch synchronous intervals between $A_1(N)$ and $A_1(N-1)$ allowing us to calculate the appropriate values A_{1,n_p}.

14.6.3 ZFE Position Parameter Interpolation

Interpolating the position of the ZFEs in a similar manner to their amplitudes does not produce a smoothly evolving excitation signal. Instead, the pulse position within each prototype segment is kept stationary throughout a voiced sequence. This introduces time misalignment between the original and synthesised waveforms, but maintains a smooth excitation signal. In order to compensate for changes in the length of prototype segments

the normalised location of the initial ZFE position is calculated according to

$$\lambda_r = \frac{\lambda_1(N)}{P(N)} \tag{14.31}$$

where $P(N)$ is the pitch period of the first frame in the voiced frame sequence. For all subsequent frames in the voiced sequence the position of the ZFE is calculated by

$$\lambda_1(N) = nint\{\lambda_r * P(N)\} \tag{14.32}$$

where $nint\{\cdot\}$ represents rounding to the nearest integer.

For the sake of illustration the interpolation process is given below for the two speech frames whose parameters are described in Table 14.9. The initial provisional interpolation region commences at the beginning of the prototype segment in frame $N-1$ and finishes at the end of the prototype segment in frame N. Since the zero crossing in frame $N-1$ is at sample index 64 the provisional interpolation region in frame $N-1$ is of duration $(160-64)$, while in frame N it finishes one pitch period duration, namely 52 samples, after the zero crossing at position 56, yielding

$$d'_{\rm pit} = (160-64) + (56+52) = 204.$$

Using Equation (14.25), the number of pitch synchronous intervals, between the two consecutive prototype segments in frames N and $N-1$, is given by $d'_{\rm pit}$ divided by the average pitch period duration of $[P(N)+P(N-1)]/2$, yielding

$$N_{\rm pit} = nint\left\{\frac{2\times 204}{52+52}\right\} = 4.$$

As $P(N)$ and $P(N-1)$ are identical, the pitch interpolation factor $\epsilon_{\rm pit}$ of Equation (14.26) will be zero, while the interpolation region containing $N=4$ consecutive pitch periods and defined by Equation (14.27) becomes

$$d_{\rm pit} = \sum_{n_p=1}^{4} 52 = 208.$$

The interpolated ZFE magnitudes and positions can then be calculated using the parameters in Table 14.9 and Equations (14.29) to 14.32 for frame $N-1$, the first voiced frame in the sequence, yielding

$$\begin{aligned}
A_{1,n_p} &= -431 + n_p \times \frac{-573+431}{3} = -478; -526; -573;\\
B_{1,n_p} &= 186 + n_p \times \frac{673-186}{3} = 348; 511; 673;\\
\lambda_r &= \frac{16}{52} = 0.308\\
\lambda_1(N) &= 0.308 * 52 = 16.
\end{aligned}$$

Again, the associated operations are illustrated in traces three and four of Figures 14.11 and 14.12.

14.6.4 Implicit Signalling of Prototype Zero Crossing

In order to perform the interpolation procedure described above, the zero-crossing parameter of the prototype segments must be transmitted to the decoder. However, it can be observed that the zero-crossing values of the prototype segments are approximately a frame length apart, thus following the principle of interpolating between prototype segments in each frame. Hence, instead of explicitly transmitting the zero-crossing parameter, it can be assumed that the start of the prototype segments are a frame length apart. An arbitrary starting point for the prototype segments could be $\mathrm{FL}/2$, where FL is the speech frame length.

Using this scenario, the interpolation procedure example of Section 14.6.3 is repeated with both zero crossings set to 80. The initial provisional interpolation region is calculated as

$$d'_{\mathrm{pit}} = (160 - 80) + (80 + 52) = 212.$$

The number of pitch synchronous intervals is given by

$$N_{\mathrm{pit}} = nint\{\frac{2 \times 212}{52 + 52}\} = 4.$$

Thus, the interpolation region defined by Equation (14.27) will become

$$d_{\mathrm{pit}} = \sum_{n_p=1}^{4} 52 = 208$$

yielding the same distance as in the example of Section 14.6.3, where the zero-crossing value was explicitly transmitted. Hence, it is feasible not to transmit the zero-crossing location to the decoder. Indeed, the assumption of a zero-crossing value of 80 had no perceptual effect on speech quality at the decoder.

14.6.5 Removal of ZFE Pulse Position Signalling and Interpolation

In the λ_1 transmission procedure, although λ_1 is transmitted every frame, only the first λ_1 in every voiced sequence is used in the interpolation process, thus λ_1 is predictable and hence it contains much redundancy. Furthermore, when constructing the excitation waveform at the decoder, every ZFE is permitted to extend over three interpolation regions, namely, its allotted region together with the previous and the next region. This allows ZFEs near the interpolation region boundaries to be fully represented in the excitation waveform, while ensuring that every ZFE will have a tapered low-energy value when it is curtailed. It is suggested that the true position of the ZFE pulse, λ_1, is arbitrary and need not be transmitted. Following this hypothesis, our experience shows that we can set $\lambda_1 = 0$ at the decoder, which has no audible degrading effect on the speech quality.

14.6.6 Pitch Synchronous Interpolation of Line Spectrum Frequencies

The LSF values can also be interpolated on a pitch synchronous basis, following the approach of Equations (14.29) and (14.30), giving

$$\mathrm{LSF}_{i,n} = \mathrm{LSF}_i(N-1) + (n_p - 1)\frac{\mathrm{LSF}_i(N) - \mathrm{LSF}_i(N-1)}{N_{\mathrm{pit}} - 1} \tag{14.33}$$

where $\mathrm{LSF}_i(N-1)$ is the previous ith LSF and $\mathrm{LSF}_i(N)$ is the current ith LSF.

14.6.7 ZFE Interpolation Example

An example of the ZFE reconstructing the original speech is given in Figure 14.11, which is a speech waveform from the testfile AF2. Following the steps of the encoding and decoding process in the figure, initially a pitch prototype segment is selected at the centre of the frame. Then a ZFE is selected at the encoder to represent this prototype segment. At the decoding stage the ZFE segments are interpolated, according to Sections 14.6.1–14.6.5, in order to produce a smooth excitation waveform, which is subsequently passed through the LPC STP synthesis filter to reconstruct the original speech. The time misalignment introduced by the interpolation process described earlier can be clearly seen, where the prototype shifting is caused by the need to have an integer number of pitch prototype segments during the interpolation region. The synthesised waveform does not constitute a strict waveform replica of the original speech, which is the reason for the coder's low SEGSNR. However, it produces perceptually good speech quality.

Figure 14.12 portrays a voiced speech section, where the same process as in Figure 14.11 is followed. The synthesised waveform portrays a similar smooth waveform evolution to the input speech, but the synthesised waveform has problems maintaining the waveform's amplitude throughout all of the prototype segment's resonances. McCree and Barnwell [486] suggest that this type of waveform would benefit from the postfilter described in Section 12.6. Thus far, only voiced speech frames have been discussed, hence next we provide a brief description of the unvoiced frame encoding procedure.

14.7 Unvoiced Speech

For frames that are classified as unvoiced, a random Gaussian sequence is used as the excitation source at the decoder. The same noise generator was used for the PWI-ZFE coder and the basic LPC vocoder of Chapter 12, namely the Box–Muller algorithm, which is used to produce a Gaussian random sequence scaled by the RMS energy of the LPC STP residual, where the noise generation process was described in Section 12.4.

Finally, the operation of an adaptive postfilter within the PWI-ZFE coder is examined.

14.8 Adaptive Postfilter

The adaptive postfilter from Section 12.6 was also used for the PWI-ZFE speech coder, however, the adaptive postfilter parameters were reoptimised to become $\alpha_{\mathrm{pf}} = 0.75$, $\beta_{\mathrm{pf}} = 0.45$,

$\mu_{\rm pf} = 0.60$, $\gamma_{\rm pf} = 0.50$, $g_{\rm pf} = 0.00$ and $\xi_{\rm pf} = 0.99$. Finally, following the adaptive postfilter, the synthesised speech was passed through the pulse dispersion filter of Section 12.7.

Following this overview of the PWI-ZFE coder, the quality of the reconstructed speech is now assessed.

14.9 Results for Single Zinc Function Excitation

In this section the performance of the PWI-ZFE speech coder described in this chapter is assessed. Figures 14.13, 14.14 and 14.15 show examples of the original and synthesised speech in the time and frequency domains for sections of voiced speech, with these graphs described in detail next. These detailed speech frames were also used to examine the LPC vocoder of Section 12.1; hence, Figure 14.13 can be compared with Figure 12.21, Figure 14.14 with Figure 12.22 and Figure 14.15 can be gauged against Figure 12.23.

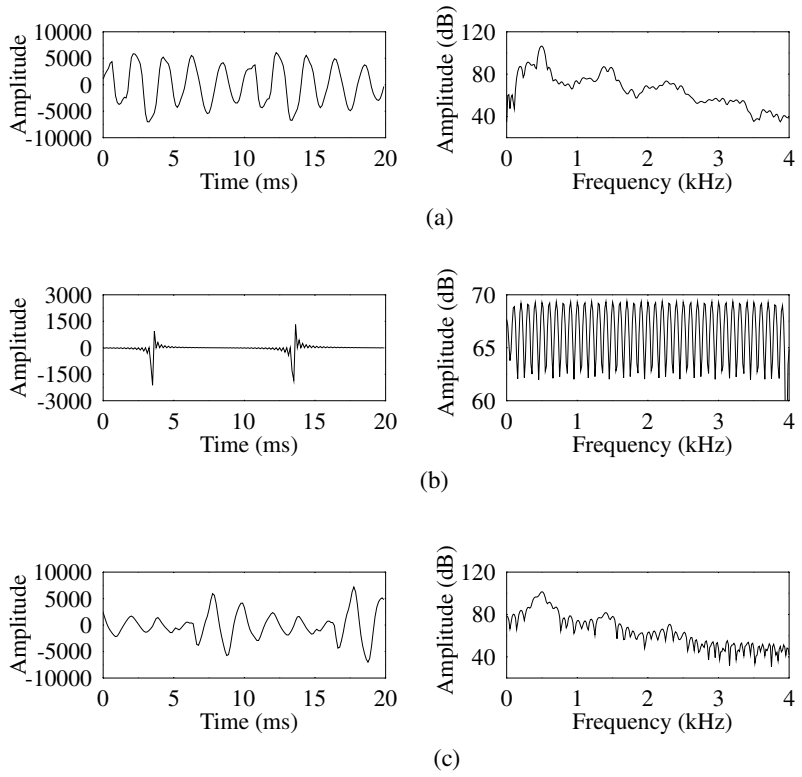

Figure 14.13: Comparison of the time and frequency domains of (a) the original speech; (b) the ZFE waveform and (c) the output speech after the pulse dispersion filter. The 20 ms speech frame is the mid vowel /ɜ/ in the utterance 'w*or*k' for the testfile BM1. For comparison with the other coders developed in this study using the same speech segment, please refer to Table 17.2.

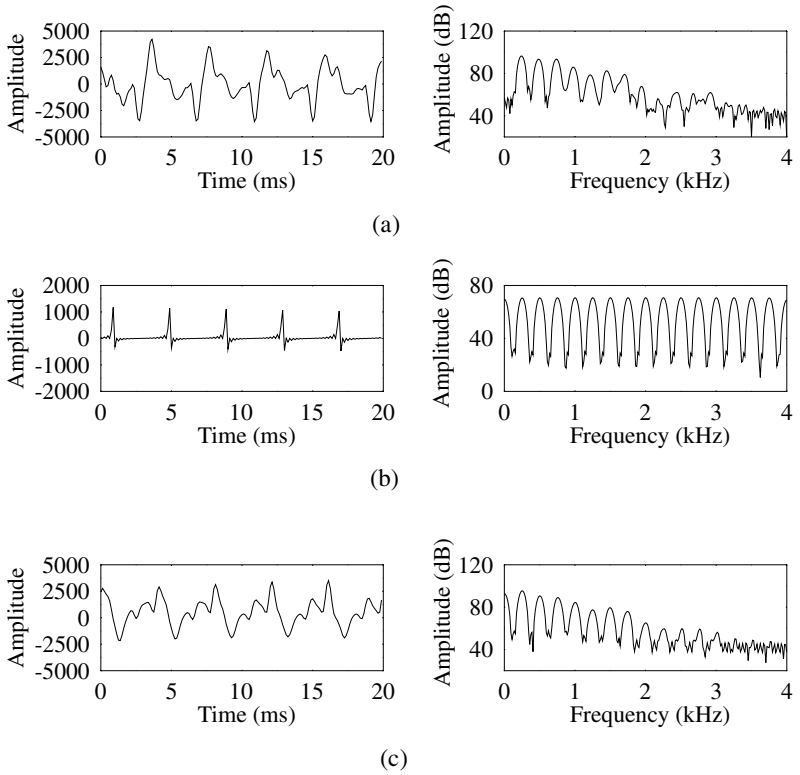

Figure 14.14: Comparison of the time and frequency domains of (a) the original speech, (b) the ZFE waveform and (c) the output speech after the pulse dispersion filter. The 20 ms speech frame is the liquid /r/ in the utterance '*r*ice' for the testfile BF2. For comparison with the other coders developed in this study using the same speech segment please refer to Table 17.2.

The speech segment displayed in Figure 14.13 is a 20 ms frame from testfile BM1. The reproduced speech is of similar evolution to the original speech, but cannot maintain the amplitude for the decaying resonances within each pitch period, which is due to the concentrated pulse-like nature of the ZFE. From Figures 14.13(a) and 14.13(c), a time misalignment between the original and synthesised waveform is present, where the cause of the misalignment was described in Section 14.6; specifically, the interpolation region must contain an integer number of pitch prototype segments, hence, often requiring the interpolation region to be extended or shortened. Consequently, the later pitch prototype segments are shifted slightly, introducing the time misalignment seen in Figure 14.13(c). In the frequency domain, the overall spectral envelope match between the original and synthesised speech is good, but, as expected, the associated SEGSNR is low due to the waveform misalignment experienced.

The speech segment displayed in Figure 14.14 shows the performance of the PWI-ZFE coder for the testfile BF2. Comparing Figure 14.14(c) with Figure 12.22(h), it can be seen that

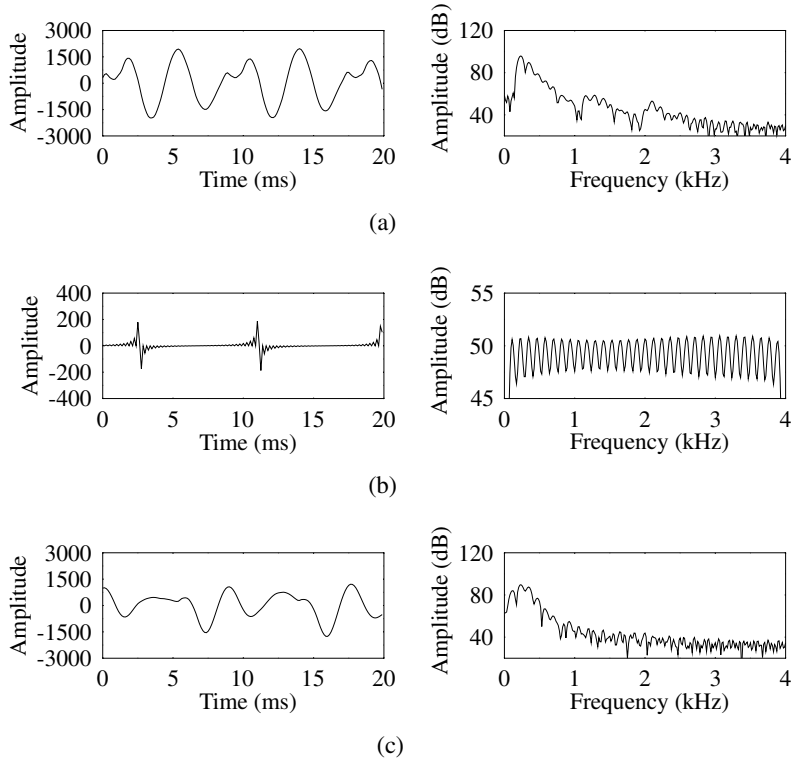

Figure 14.15: Comparison of the time and frequency domains of (a) the original speech, (b) the ZFE waveform and (c) the output speech after the pulse dispersion filter. The 20 ms speech frame is the nasal /n/ in the utterance 'throw*n*' for the testfile BM2. These signals can be compared with the basic vocoder's corresponding signals in Figure 12.23.

the synthesised waveforms in both the time and frequency domains are similar. Observing the frequency domain graphs, it is noticeable that the inclusion of unvoiced speech above 1800 Hz is not modelled well by the distinct voiced–unvoiced nature of the PWI-ZFE scheme. The introduction of mixed-multiband excitation in Chapter 15 is expected to improve the representation of this signal.

The speech segment displayed in Figure 14.15 is for the testfile BM2. The synthesised speech waveform displayed in Figure 14.15(c) is noticeably better than the output speech in Figure 12.23(h). For Figure 14.15(c) the first formant is modelled well, however, the upper two formants are missing from the frequency spectrum, which is a failure in the LPC STP process and will persist in all of our developed speech coders.

Informal listening tests showed that the reproduced speech for the PWI-ZFE speech coder contained less 'buzziness' than the LPC vocoder of Chapter 12.

The bit allocation of the ZFE coder is summarised in Table 14.10. For unvoiced speech the RMS parameter requires the five bits described in Section 12.4, with the boundary shift

Table 14.10: Bit allocation table for the investigated 1.9 kbps PWI-ZFE coder.

Parameter	Unvoiced	Voiced
LSFs	18	18
Voiced–unvoiced flag	1	1
RMS value	5	—
b_s offset	3	—
pitch	—	7
A_1	—	6
B_1	—	6
Total (20 ms)	27	38
Bitrate (kbps)	1.35	1.90

parameter b_s offset requiring a maximum of

$$\frac{\text{frame length}}{\text{minimum pitch}} = \frac{160}{20} = 8$$

values or three bits to encode.

For voiced speech the pitch period can vary from 20 to 147 samples, thus requiring seven bits for transmission. Section 14.5.2 justified the use of six bits to SQ the A_1 and B_1 ZFE amplitude parameters.

The computational complexity of the speech coder is dominated by the ZFE minimisation loop, even when using a constrained search. Table 14.11 displays the computational complexity of the coder for a pitch period of 20 or 147 samples.

Table 14.11: Total maximum and minimum computational complexity for a PWI-ZFE coder.

	Pitch period	
Operation (MFLOPs)	20	147
Pitch detector	2.67	2.67
ZFE minimisation	0.30	11.46
Total	2.97	14.13

14.10 Error Sensitivity of the 1.9 kbps PWI-ZFE Coder

In this chapter we have investigated the design of a 1.9 kbps speech coder employing PWI-ZFE techniques. However, we have not examined the speech coder's performance within a communications system, specifically its robustness to transmission errors. In this section

we study how the degradation caused by a typical mobile environment affects the PWI-ZFE output speech quality.

The degradation in the PWI-ZFE speech coder's performance is caused by the hostile nature of a mobile communications environment. A mobile environment typically contains both fast and slow fading, which affects the signal level at the receiver. In addition, many different versions of the signal arrive at the receiver, each having taken different paths with different fading characteristics and different delays, thus introducing inter-symbol interference. It is these mobile environment characteristics which introduce errors into the parameters received by the speech decoder.

In this section we commence by examining how possible errors at the decoder would affect the output speech quality and introduce some error correction techniques. These errors are then examined in terms of objective speech measures and informal listening tests. We then consider dividing the transmission bits into protection classes, which is a common technique that is adopted to afford the most error-sensitive bits the greatest protection. Finally, we demonstrate the speech coder's performance for different transmission environments.

14.10.1 Parameter Sensitivity of the 1.9 kbps PWI-ZFE Coder

In this section we consider the importance of the different PWI-ZFE parameters of Table 14.10 in maintaining synthesised speech quality. In addition, we highlight checks that can be made at the decoder, which may indicate errors and suggest error correction techniques. Considering the voiced and unvoiced speech frames separately, the speech coder has 10 different parameters that can be corrupted, where the vector-quantised LSFs, described in Section 12.2.2, can be considered to be four different groups of parameters. These parameters have between seven bits, for the pitch period, and a single bit, for the voiced–unvoiced flag, which can be corrupted. In total there are 46 different bits, namely the 38 voiced bits of Table 14.10 and the RMS and b_s unvoiced parameters.

Finally, we note that due to the interpolative nature of the PWI-ZFE speech coder, any errors that occur in the decoded bits will affect more than just the frame where the error occurred.

14.10.1.1 Line Spectrum Frequencies

The LSF vector quantiser, described in Section 12.2.2 and taken from G.729 [147], represents the LSF values using four different parameters. The LSF VQ consists of a fourth-order MA predictor, which can be switched on or off with the flag L0. The vector quantisation is then performed in two stages. A 7-bit VQ index, L1, is used for the first stage. The second stage VQ is a split vector quantiser, using the indices L2 and L3, with each codebook containing five bits.

14.10.1.2 Voiced–unvoiced Flag

It is anticipated that the voiced–unvoiced flag will be the most critical bit for the successful operation of the PWI-ZFE speech coder. The very different excitation models employed for voiced and unvoiced speech mean that if the wrong type of excitation is adopted, this is expected to have a serious degrading effect.

At the decoder it is possible to detect isolated errors in the voiced–unvoiced flag, namely V–U–V and U–V–U sequences in the $N+1$, N, $N-1$ frames. These sequences will indicate an error, since at the encoder they were prohibited frame combinations, as described in Section 14.2.1. However, the PWI-ZFE decoder does not operate on a frame-by-frame basis, instead it performs interpolation between the prototype segments of frame N and $N+1$, as described in Section 14.2.1. Thus, without introducing an extra 20 ms delay, by performing the interpolation between frames $N-1$ and N, it is impossible to completely correct an isolated error in the voiced–unvoiced flag.

14.10.1.3 Pitch Period

The pitch period parameter of Table 14.10 is only sent for voiced frames, where having the correct pitch period is imperative for producing high-quality synthesised speech. In Section 13.5.2 some simple pitch period correction was already performed, where checks were made to ensure a smooth pitch track is followed. By repeating this pitch period correction at the decoder the effect of an isolated pitch period error can be reduced. However, similarly to the voiced–unvoiced flag, the use of frames N and $N+1$ in the interpolation process permits an isolated pitch period to have a degrading effect.

14.10.1.4 Excitation Amplitude Parameters

The ZFE amplitude parameters, A and B, control the shape of the voiced excitation. The A and B parameters of Table 14.10 can have both positive and negative values, however, as described in Section 14.3.4, the phase of the amplitude parameters must be maintained throughout the voiced sequence. At the decoder it is possible to maintain phase continuity for the amplitude parameter in the presence of an isolated error, with the correction that if the phase of the A or B parameter has been found to change during a voiced sequence, then the previous A or B parameter can be repeated.

14.10.1.5 Root Mean Square Energy Parameter

For unvoiced speech frames the excitation is formed from random Gaussian noise scaled by the received RMS energy value, seen in Table 14.10 and as described in Section 14.7. Thus, if corruption of the RMS energy parameter occurs, then the energy level of the unvoiced speech will be incorrect. However, since the speech sound is a low-pass-filtered slowly varying process, abrupt RMS changes due to channel errors can be detected and mitigated.

14.10.1.6 Boundary Shift Parameter

The boundary shift parameter, b_s, of Table 14.10 is only sent for unvoiced frames and defines the location where unvoiced speech becomes voiced speech, or *vice versa*. The corruption of the boundary shift parameter will move this transition point, an event which is not amenable to straightforward error concealment.

14.10.2 Degradation from Bit Corruption

Following this discussion on the importance of the various PWI-ZFE parameters and the possible error corrections which could be performed at the speech decoder, we now investigate the extent of the degradation which errors cause to the reproduced speech quality. The error sensitivity is examined by separately corrupting each of the 46 different voiced and unvoiced bits of Table 14.10, where 18 LSF plus the V/U bits are sent for all frames, additionally 19 bits are only sent for voiced frames and eight bits are only sent for unvoiced frames. For each selected bit, the corruption was inflicted 10% of the time. Corrupting a bit for 10% of the time is a compromise between consistently or constantly corrupting the bit in all frames and corrupting the bit in only a single isolated frame. If the bit is constantly corrupted then any error propagation effect is masked, while corrupting the bit in only a single frame requires that for completeness every possible frame is taken to be that single frame, resulting in an arduous process.

Figure 14.16 displays the averaged results for the speech files AM1, AM2, AF1, AF2, BM1, BM2, BF1 and BF2, described in Section 11.4. The SEGSNR and CD objective speech measures, described in Section 11.3.1, were used to evaluate the degradation effect. In addition, the synthesised corrupted speech due to the different bit errors was compared through informal listening tests.

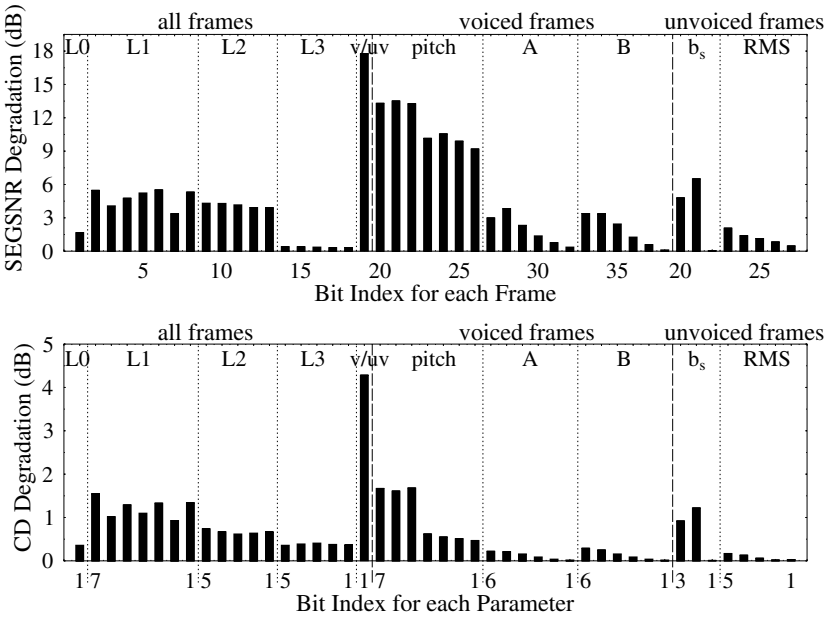

Figure 14.16: The error sensitivity of the different transmission bits for the 1.9 kbps PWI-ZFE speech coder. The graph is divided into bits sent for all speech frames, bits sent only for voiced frames and bits sent only for unvoiced frames. For the CD degradation graph containing the bit index for each parameter, bit 1 is the least significant bit.

Observing Figure 14.16 it can be seen that both the SEGSNR and CD objective measures rate the error sensitivity of the different bits similarly, both indicating that the voiced–

unvoiced flag being correct is the most critical for successful synthesis of the output speech. This was confirmed by listening to the synthesised speech, which was frequently unintelligible when there was 10% error in the voiced–unvoiced flag bit. In addition, from Figure 14.16 it can be seen that both the pitch period and boundary shift parameters produce a significant degradation due to bit errors. However, informal listening tests do not indicate such significant quality degradation, although an incorrect pitch period does produce audible distortion. It is suggested that the time misalignment introduced by the pitch period and boundary shift parameter errors is artificially increasing the SEGSNR and CD degradation values.

Thus, while the SEGSNR and CD objective measures indicate the relative sensitivities of the bits within each parameter, more accurate interpretation of the sensitivity of each parameter has to rely more on informal listening tests.

14.10.2.1 Error Sensitivity Classes

The SEGSNR and CD objective measures together with the informal listening tests allow the bits to be grouped into three classes for transmission to the decoder. These classes are detailed in Table 14.12, where class 1 requires the greatest protection and class 3 requires the least protection.

Table 14.12: The transmission classes for the bits of the 1.9 kbps PWI-ZFE speech coder, with class 1 containing the most error-sensitive bits and class 3 bits requiring little error protection.

Class	Coding bits						
1	Voiced–unvoiced flag						
2	L1[7] pitch[7] A[6]	L1[5] pitch[6] A[5]	L1[3] pitch[5] B[6]	L1[1] pitch[4] B[5]	pitch[3]	pitch[2]	pitch[1]
3	L0 L2[5] L3[5] A[4] B[4]	L1[6] L2[4] L3[4] A[3] B[3]	L1[4] L2[3] L3[3] A[2] B[2]	L1[2] L2[2] L3[2] A[1] B[1]	L2[1] L3[1]		

In Table 14.12 the error sensitivity classes are based on the bits sent every speech frame and bits sent only for voiced frames, giving 38 bits. For unvoiced frames the boundary parameter shift, b_s, is given the same protection as the most significant three pitch period bits, while the RMS value is given the same protection as the least significant four pitch period bits and A[6].

Class 1 contains only the voiced–unvoiced flag, which has been identified as being very error sensitive. Class 2 contains 15 bits, while class 3 contains 22 bits.

The relative bit error sensitivities have been used to improve channel coding within a GSM-like speech transceiver [531] and a FRAMES-like speech CDMA transceiver [532].

Following this analysis of the performance of a PWI-ZFE speech coder, using a single ZFE to represent the excitation, the potential for speech quality improvement with extra ZFE pulses is now examined.

14.11 Multiple Zinc Function Excitation

So far in this chapter a single ZFE pulse has been employed to represent the voiced excitation. However, a better speech quality may be achieved by introducing more ZFE pulses [497]. The introduction of extra ZFEs will be at the expense of a higher bitrate, thus a dual-mode PWI-ZFE speech coder could be introduced to exploit an improved speech quality when traffic density of the system permits.

Revisiting the ZFE error minimisation process of Section 14.3.1, where due to the orthogonality of the zinc basis functions the weighted error signal upon using k ZFE pulses is given by

$$E_w^{k+1} = \sum_{n=1}^{P} (e_w^{k+1}(n))^2$$

where P is the length of the prototype segment, over which minimisation is carried out, with the synthesised weighted speech represented by

$$\bar{s_w}(n) = \sum_{k=1}^{K} z_k(n) * h(n) \tag{14.34}$$

where $z_k(n)$ is the kth ZFE pulse, K is the number of pulses being employed and $h(n)$ is the impulse response of the weighted LPC synthesis filter.

14.11.1 Encoding Algorithm

The encoding process for a single ZFE was previously described in Table 14.1 and Figure 14.2. For a multiple ZFE arrangement the same process is followed, but the number of ZFE pulses is extended to K, as shown in Figure 14.17 and described next. Thus, for the phase constrained frame, which we also refer to as the phase restriction frame, a phase is determined independently for each of the K excitation pulses. Similarly, for other voiced frames the phase of the kth pulse is based on the phase restriction for the kth pulses. Furthermore, if a suitable ZFE is not found for the kth ZFE pulse in frame N, then the kth ZFE in frame $N-1$ is scaled and reused.

For scenarios with a different number ZFE pulse per prototype segment Table 14.13 displays the percentage of voiced frames, where some scaling from the previous frame's ZFE pulses must be performed. It can be seen that with three ZFE pulses employed, one-third of the voiced frames contain scaled ZFE pulses from the previous frame. In addition, some frames have several scaled ZFE pulses from the previous frame.

The implementation of the single ZFE, in Section 14.3.3, showed that for smooth interpolation it is beneficial to constrain the locations of the ZFE pulses. Constraining the K ZFE locations follows the same principles as those used in determining the single ZFE location, but it was extended to find K constrained positions. For the first voiced frame the

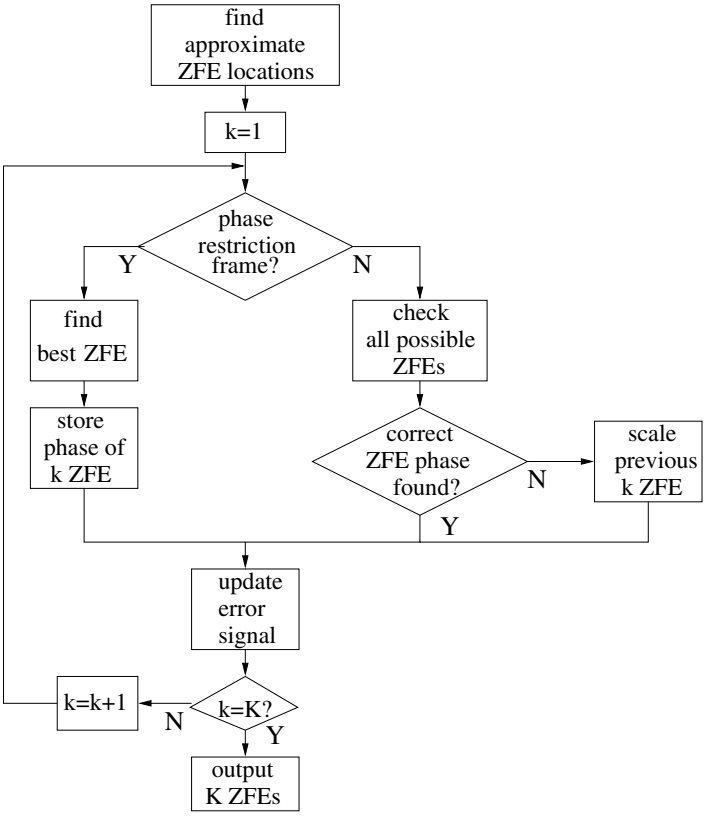

Figure 14.17: The control structure for selecting multiple ZFEs in PWI-ZFE coders.

largest K impulses, determined by wavelet analysis according to Chapter 13 and located within the prototype segment, are selected for the positions that the ZFE pulses must be in proximity to. For further voiced frames the impulses from the wavelet analysis are examined, with the largest impulses near the K ZFE pulses in frame $N-1$ selected as excitation. If no impulse is found near the kth ZFE location in frame $N-1$, this position is repeated as the kth ZFE in frame N. It is feasible that there will be less than K wavelet analysis impulses within the prototype segment, thus in this situation the extra ZFEs are set to zero. They are subsequently introduced when impulses occur within the prototype segment that are unrelated to any ZFE pulses in frame $N-1$.

The SEGSNR values achieved for the minimisation process at the encoder with different numbers of ZFE pulses per prototype segment indicate the excitation representation improvement. Figure 14.18 displays the results, showing that the improvement achieved by adding extra pulses saturates as the number of ZFE pulses increases, so when eight ZFE pulses are employed no further SEGSNR gain is achieved. The limit in SEGSNR improvement is due to the constraint that ZFE pulses are expected to be near the GCIs found by the wavelet analysis. There will be a limited number of impulses within the prototype segment, thus a limited number of ZFE pulses can be employed for each prototype segment. The performance

Table 14.13: The percentage of speech frames requiring previous ZFEs to be scaled and repeated, for K ZFE pulses in PWI-ZFE coders.

Total K	Rescaled ZFE needed (%)	>1 ZFE rescaled (%)	>2 ZFE rescaled (%)	>3 ZFE rescaled (%)	>4 ZFE rescaled (%)
1	12.9	—	—	—	—
2	20.3	5.1	—	—	—
3	33.0	7.1	1.0	—	—
4	42.3	16.5	5.1	0.6	—
5	57.9	28.4	10.7	2.5	0.1

of a three pulse ZFE scheme at the encoder is given in Figure 14.19, which can be compared with the performance achieved by a single ZFE, shown in Figure 14.9. It can be seen that the addition of two extra ZFE pulses improves the excitation representation, particularly away from the main resonance.

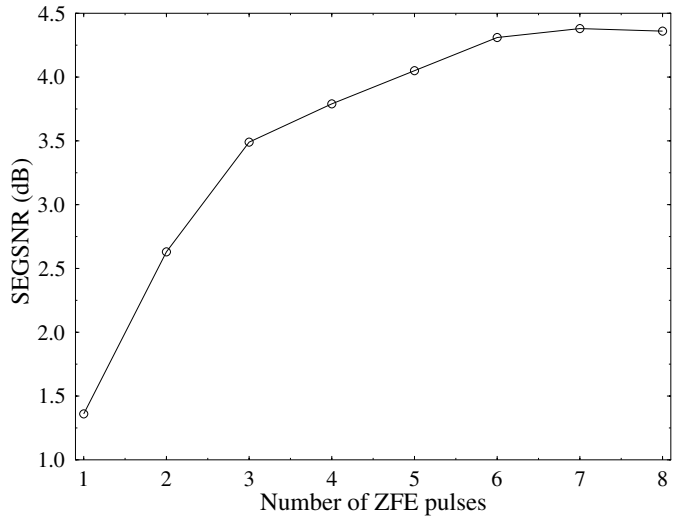

Figure 14.18: The SEGSNR achieved at the encoder minimisation process for different number of ZFE pulses used in the representation. The inclusion of each new ZFE pulse requires 19 extra bits/20 ms, or 0.95 kbps extra bitrate, for the encoding of the A_k and B_k parameters and the additional ZFE pulse positions λ_k, as seen in Table 14.14.

At the decoder the same interpolation process implemented for the single ZFE is employed, as described in Section 14.6, again extended to K ZFE pulses. For all ZFE pulses the amplitude parameters are linearly interpolated, with the ZFE pulse position parameter and prototype segment location assumed at the decoder, as in the single pulse coder of earlier sections. Explicitly, the kth ZFE pulse position parameter is kept at the same location within each prototype segment. For the three-pulse PWI-ZFE scheme, the adaptive postfilter

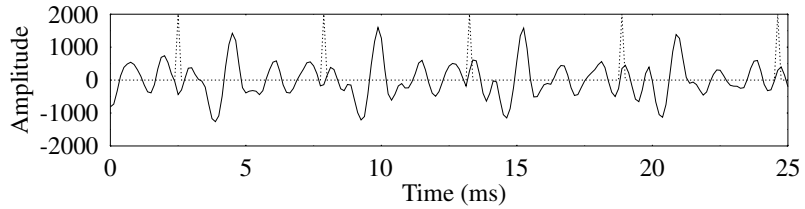

(a) Prototype segments of the weighted speech

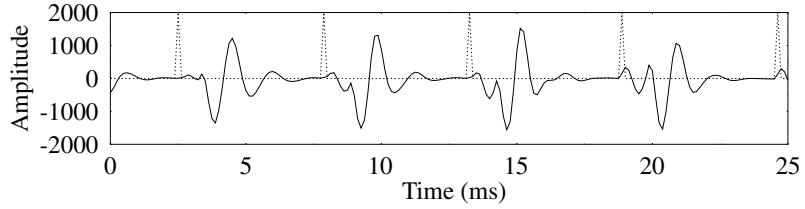

(b) Synthesised prototypes for the weighted speech

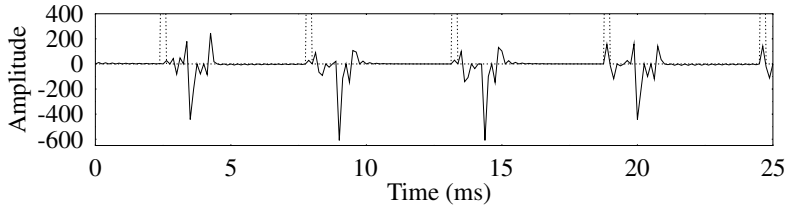

(c) Zinc function excitation

Figure 14.19: Demonstration of the process of AbS encoding for prototype segments that have been concatenated to produce a smoothly evolving waveform, with the excitation represented by three ZFE pulses. The dotted lines in the figure indicate the boundaries between prototype segments.

parameters were reoptimised becoming $\alpha_{\rm pf} = 0.75$, $\beta_{\rm pf} = 0.45$, $\mu_{\rm pf} = 0.40$, $\gamma_{\rm pf} = 0.50$, $g_{\rm pf} = 0.00$ and $\xi_{\rm pf} = 0.99$.

14.11.2 Performance of Multiple Zinc Function Excitation

A three-pulse ZFE scheme was implemented to investigate the potential for improved speech quality using extra ZFE pulses. Three excitation pulses were adopted to study the feasibility of a speech coder at 3.8 kbps, where the bit allocation scheme was given in Table 14.14.

Figure 14.20 displays the performance of a three-pulse ZFE scheme for the mid vowel /ɜ/ in the utterance 'w*or*k' for the testfile BM1. The identical portion of speech synthesised using a single ZFE was given in Figure 14.13. From Figure 14.20(b) it can be seen that the second largest ZFE pulse is approximately half-way between the largest ZFE pulses. In the frequency spectrum the pitch appears to be 200 Hz, which is double the pitch from Figure 14.13(b). The pitch doubling is clearly visible in the time and frequency domains of Figure 14.20(c). For

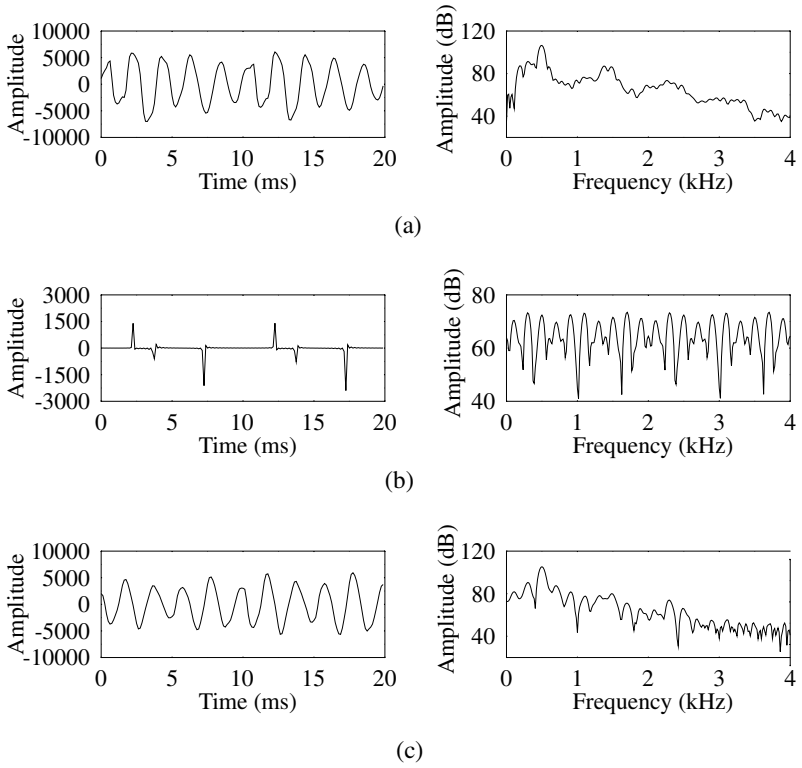

Figure 14.20: Comparison of the time and frequency domains of (a) the original speech, (b) the three-pulse ZFE waveform and (c) the output speech after the pulse dispersion filter. The 20 ms speech frame is the mid vowel /ɜ/ in the utterance 'w*or*k' for the testfile BM1. For comparison with the other coders developed in this study using the same speech segment, please refer to Table 17.2.

this speech frame the addition of extra ZFE pulses fails to improve the speech quality, where this is due to the secondary excitation pulse producing a pitch-doubling effect in the output speech.

Figure 14.21 displays the results from applying a three-pulse ZFE scheme to a 20 ms frame of speech from the testfile BF2. The same speech frame was investigated in Figures 14.14 and 12.22. Observing Figure 14.21(b) it can be seen that, similarly to Figure 14.20(b), a ZFE pulse is placed midway between the other ZFE pulses; however, since this pulse has much less energy, it does not have a pitch-doubling effect. When compared with the single ZFE of Figure 14.15(c) the multiple ZFEs combine to produce a speech waveform, shown in Figure 14.21(c), much closer in both the time and frequency domains to the original, although at the cost of a higher bitrate and complexity.

Figure 14.22 portrays a three-pulse ZFE scheme applied to a speech frame from the testfile BM2, which can be compared with Figure 14.15. From Figure 14.22(b) it can be seen that no pitch doubling occurs. For this speech frame the limiting factor in reproducing the original speech are the missing formants. However, observing Figure 14.22(c)

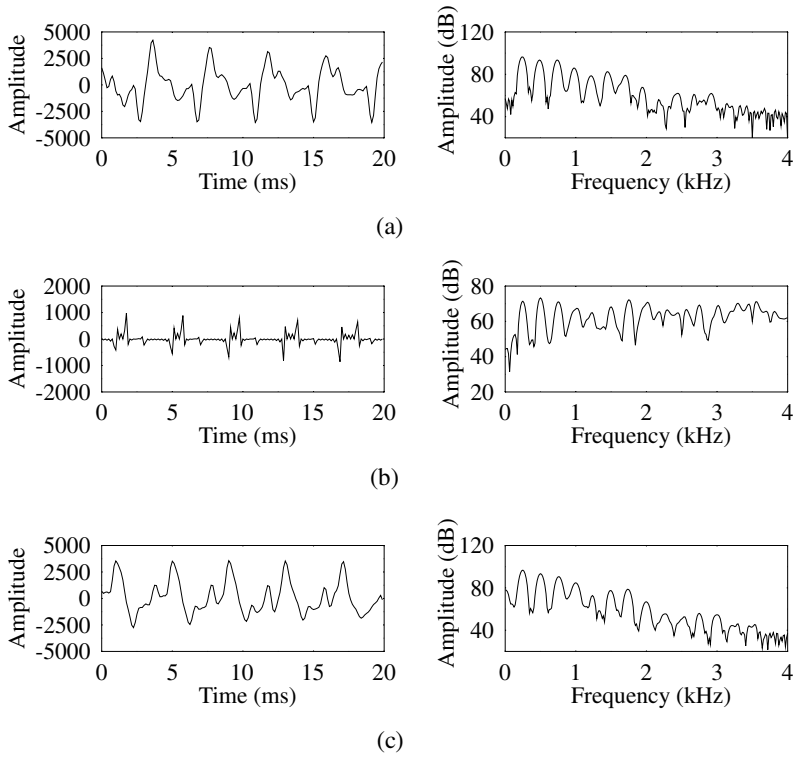

Figure 14.21: Comparison of the time and frequency domains of (a) the original speech, (b) the three-pulse ZFE waveform and (c) the output speech after the pulse dispersion filter. The 20 ms speech frame is the liquid /r/ in the utterance '*r*ice' for the testfile BF2. For comparison with the other coders developed in this study using the same speech segment, please refer to Table 17.2.

demonstrates that three ZFE pulses results in an improved performance compared with a single ZFE.

Informal listening tests were conducted using the PWI-ZFE speech coder with three ZFE pulses, where it was found that sudden and disconcerting changes could occur in the quality of the reproduced speech. It is suggested that this effect was created by the varying success of the excitation to represent the speech. In addition, for many speech files there was a background roughness to the synthesised speech. The problems with implementing a multiple ZFE pulse scheme are caused by the interpolative nature of the speech coder. The benefits, which are gained in improved representation of the excitation signal, are counteracted by increased problems in both obeying phase restrictions and in creating a smoothly interpolated synthesised speech waveform.

For the 3.8 kbps multiple ZFE speech coder the extra bits are consumed by the two extra ZFE pulses, with the bit allocation detailed in Table 14.14. The location of the two extra ZFE pulses, λ_2 and λ_3, with respect to the first ZFE pulse, must be transmitted to the decoder,

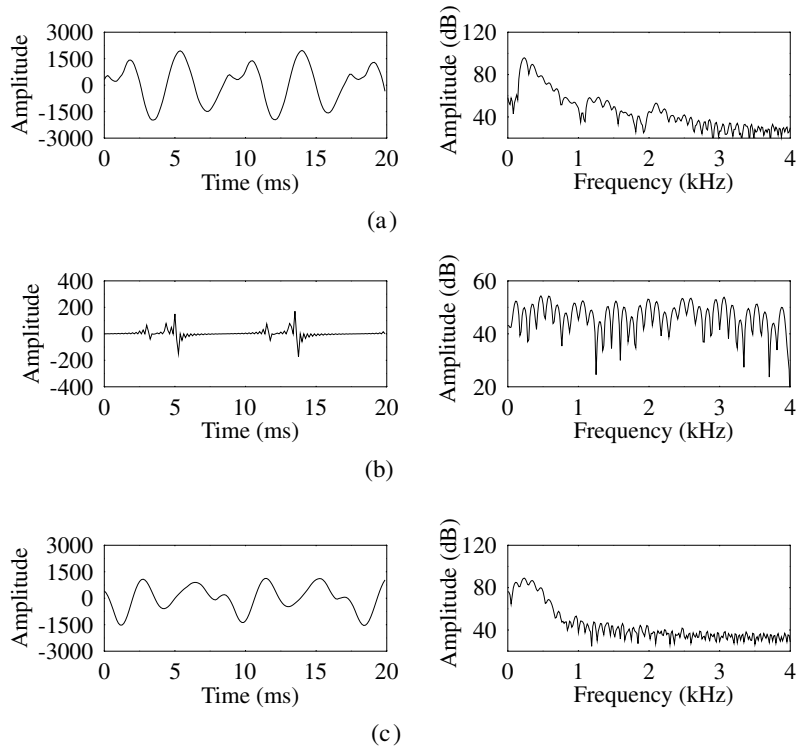

Figure 14.22: Comparison of the time and frequency domains of (a) the original speech, (b) the three-pulse ZFE waveform and (c) the output speech after the pulse dispersion filter. The 20 ms speech frame is the nasal /n/ in the utterance 'throw*n*' for the testfile BM2. For comparison with the other coders developed in this study using the same speech segment, please refer to Table 17.2.

while, similarly to the single ZFE coder, the first pulse location can be assumed at the decoder. With a permissible pitch period range of 20–147 samples, seven bits are required to encode each position parameter, λ. This parameter only requires transmission for the first frame of a voiced sequence, since for further frames the pulses are kept in the same location within the prototype region, as argued in Section 14.6.3. The A and B amplitude parameters for the extra ZFE pulses are scalar quantised to six bits.

In order to produce a dual-rate speech coder it must be possible to change the coder's transmission rate during operation. In this multiple ZFE scheme, if a ZFE pulse were omitted from the frame, reducing the bitrate, at the decoder the ZFE pulse would be interpolated across the interpolation region to zero. Similarly, if an extra ZFE pulse was harnessed, then at the decoder the ZFE would be interpolated from zero. This interpolation from zero degrades the assumption that the previous prototype segment at the encoder is similar to the previous interpolation region at the decoder. Thus, it is prudent to only permit coding rate changes between voiced frame sequences.

Table 14.14: Bit allocation table for voiced speech frames in the 3.8 kbps investigated PWI-ZFE coder employing three ZFEs.

Parameter	Voiced
LSFs	18
Voiced–unvoiced flag	1
Pitch	7
1st pulse	
A_1	6
B_1	6
2nd pulse	
λ_2	7
A_2	6
B_2	6
3rd pulse	
λ_3	7
A_3	6
B_3	6
Total/20 ms	76
Bitrate (kbps)	3.80

14.12 A Sixth-rate, 3.8 kbps GSM-like Speech Transceiver[1]

14.12.1 Motivation

Although the standardisation of the third-generation wireless systems has been completed, it is worthwhile considering potential evolutionary paths for the mature GSM system. This tendency was hallmarked by the various GSM Phase2 proposals, endeavouring to improve the services supported or by the development of the half-rate and enhanced full-rate speech codecs. In this section, two potential improvements and their interactions in a source-sensitivity matched transceiver are considered, namely employing an approximately sixth-rate, 1.9 kbps speech codec and turbo coding [216,217] in conjunction with the GSM system's GMSK partial response modem.

The bit allocation of the 1.9 kbps PWI-ZFE speech codec was summarised in Table 14.10, while its error sensitivity was quantified in Section 14.10. The SEGSNR and CD objective measures together with the informal listening tests allow the bits to be ordered in terms of their error sensitivities. The MSB is the voiced–unvoiced flag. For voiced frames the three MSBs in the LTP delay are the next MSBs, followed by the four least significant LTP delay bits. For unvoiced frames the boundary parameter shift, j, is given the same protection as the most significant three pitch period bits, while the RMS value is given the same protection

[1]This section is based on F. C. A. Brooks, B. L. Yeap, J. P. Woodard and L. Hanzo, "A Sixth-rate, 3.8 kbps GSM-like speech transceiver". *Proceedings of ACTS'98* (Rhodes, Greece), 1998.

as the group of four least significant pitch period bits and bit $A[6]$, the LSB of the ZFE amplitude A.

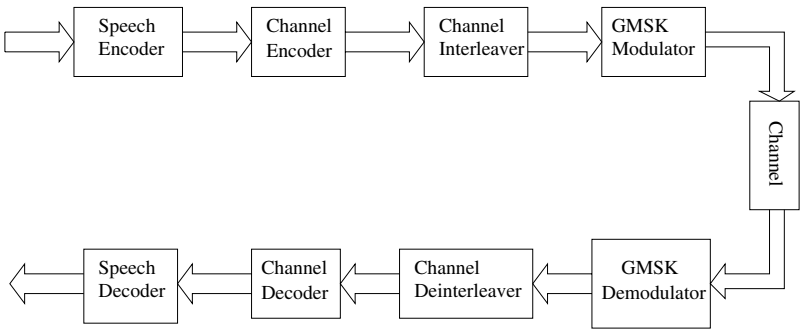

Figure 14.23: GSM-like system block diagram.

14.12.2 The Turbo-coded Sixth-rate 3.8 kbps GSM-like System

The amalgamated GSM-like system [158] is illustrated in Figure 14.23. In this system, the 1.9 kbps speech coded bits are channel encoded with a half rate convolutional or turbo encoder [216, 217] with an interleaving frame length of 81 bits, including termination bits. Therefore, assuming negligible processing delay, 162 bits will be released every 40 ms, or two 20 ms speech frames, since the 9×9 turbo-interleaver matrix employed requires two 20 ms, 38-bit speech frames before channel encoding commences. Hence, we set the data burst length to be 162 bits. The channel encoded speech bits are then passed to a channel interleaver. Subsequently, the interleaved bits are modulated using GMSK [158] with a normalised bandwidth, $B_n = 0.3$, and transmitted at 271 kbps across the COST 207 [331] Typical Urban channel model. Figure 14.24 is the Typical Urban channel model used and each path is fading independently with Rayleigh statistics, for a vehicular speed of 50 km h^{-1} or 13.89 m s^{-1} and transmission frequency of 900 MHz.

The GMSK demodulator equalises the received signal, which has been degraded by the wideband fading channel, using perfect channel estimation [158]. Subsequently, soft outputs from the demodulator are deinterleaved and passed to the channel decoder. Finally, the decoded bits are directed towards the speech decoder in order to extract the original speech information. In the following sections, the channel coder and interleaver/deinterleaver, and GMSK transceiver are described.

14.12.3 Turbo Channel Coding

We compare two channel coding schemes, constraint length $K = 5$ convolutional coding as used in the GSM [158] system and a turbo channel codec [216,217]. The turbo codec uses two $K = 3$ so-called RSC component codes employing octally represented generator polynomials of 7 and 5, as well as eight iterations of the Log-MAP [533] decoding algorithm. This makes it approximately 10 times more complex than the convolutional codec.

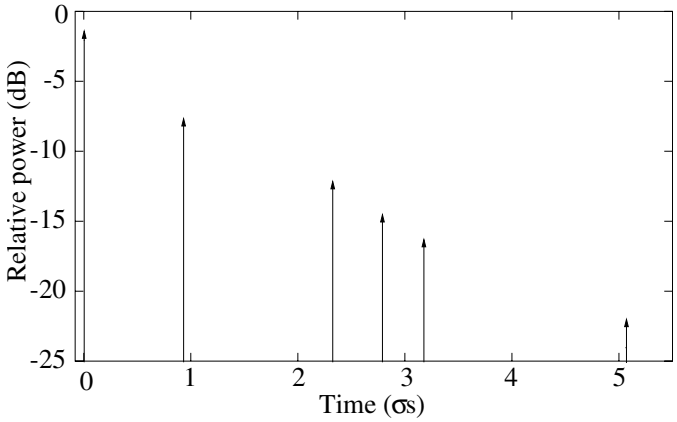

Figure 14.24: The impulse response of the COST207 Typical Urban channel used [331].

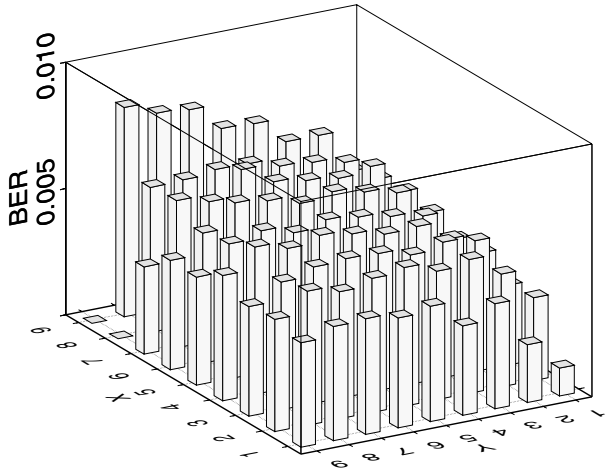

Figure 14.25: The error sensitivity of the different information bits within the 9×9 block interleaver used in the turbo codec.

It is well known that turbo codes perform best for long interleavers. However, due to the low bitrate of the speech codec we are constrained to using a low frame length in the channel codecs. A frame length of 81 bits is used, with a 9×9 block interleaver within the turbo codec. This allows two sets of 38 coded bits from the speech codec and two termination bits to be used. The BERs of the 79 transmitted bits with the 9×9 block interleaver used for the turbo codec, for a simple AWGN channel at a SNR of 2 dB, is shown in Figure 14.25. It can be seen that bits near the bottom right-hand corner of the interleaver are better protected than bits in other positions in the interleaver. By placing the more sensitive speech bits here we are able to give significantly more protection to the voiced–unvoiced flag and to some of the other sensitive speech bits, than to the low-sensitivity bits of Figure 14.16. Our current work investigates providing more significant unequal error protection using turbo codes with

irregular parity bit puncturing. Finally, an interburst channel interleaver is used, in order to disperse the bursty channel errors and to assist the channel decoders, as proposed for GSM [158].

14.12.4 The Turbo-coded GMSK Transceiver

As mentioned in Section 14.12.2, a GMSK modulator with $B_n = 0.3$, which is employed in the current GSM [158] mobile radio standard, is used in our system. GMSK belongs to a class of continuous phase modulation (CPM) [158], and possesses high spectral efficiency and constant signal envelope, hence allowing the use of nonlinear power efficient class-C amplifiers. However, the spectral compactness is achieved at the expense of controlled intersymbol interference (CISI), and therefore an equaliser, typically a Viterbi equaliser (VE), is needed. The conventional VE [158] performs maximum likelihood sequence estimation by observing the development of the accumulated metrics, which are evaluated recursively, over several bit intervals. The length of the observation interval depends on the complexity afforded. Hard decisions are then released at the end of the equalisation process. However, because log likelihood ratios (LLRs) [534] are required by the turbo decoders, we could use a variety of soft output algorithms instead of the VE, such as the maximum *a posteriori* (MAP) [221] algorithm, the Log-MAP [533], the Max-Log-MAP [535, 536] and the soft output Viterbi algorithm (SOVA) [27,537,538]. We chose to use the Log-MAP algorithm as it gave the optimal performance, like the MAP algorithm, but at a much lower complexity. Other schemes such as Max-Log-MAP and SOVA are computationally less intensive, but provide sub-optimal performance. Therefore, for our work, we have opted for the Log-MAP algorithm in order to obtain the optimal performance, hence giving the upper bound performance of the system.

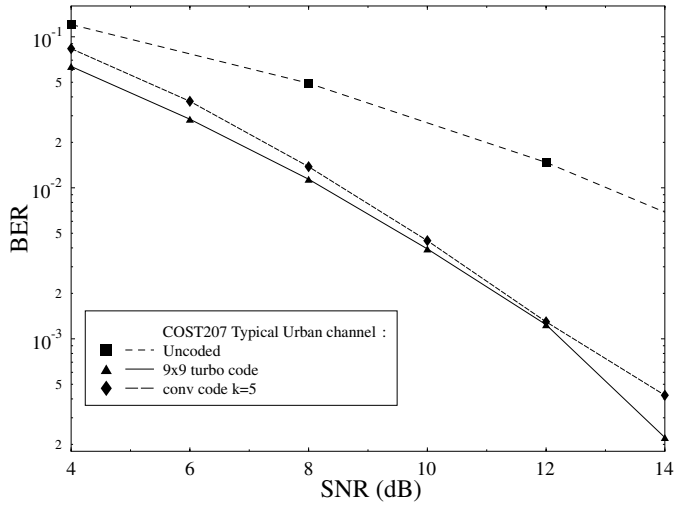

Figure 14.26: The BER performance for the turbo and convolutional coded systems over the COST 207 Typical Urban channel [331].

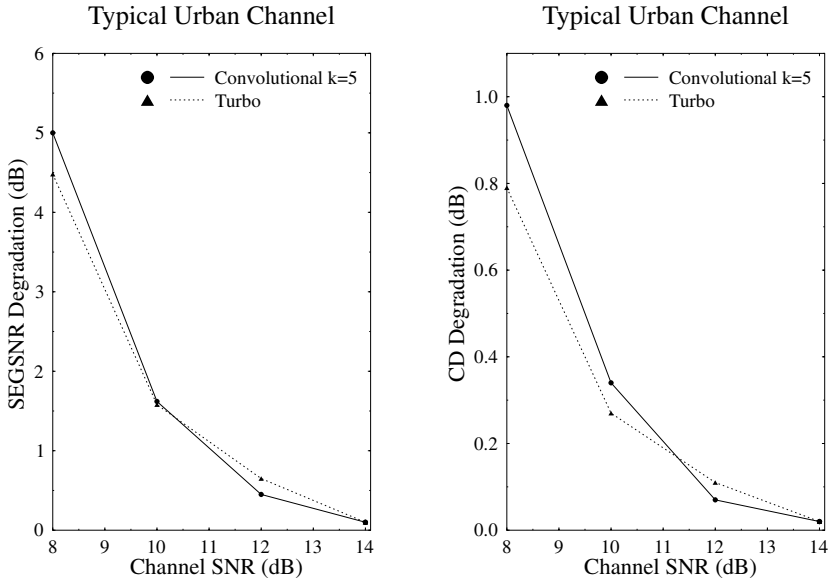

Figure 14.27: The speech degradation performance for the turbo and convolutionally coded systems over the COST 207 Typical Urban channel [331].

14.12.5 System Performance Results

The performance of our sixth-rate GSM-like system was compared with an equivalent conventional GSM system using convolutional codes instead of turbo codes. The $\frac{1}{2}$ rate convolutional code [158] has the same code specifications as in the standard GSM system [158]. Figure 14.26 illustrates the BER performance over a Rayleigh fading COST207 Typical Urban channel [331] and Figure 14.27 shows the speech degradation, in terms of both the CD and the SEGSNR, for the same channel. Due to the short interleaver frame length of the turbo code the turbo- and convolutionally coded performances are fairly similar in terms of both BER and speech degradation, hence the investment of the higher complexity turbo codec is not justifiable, demonstrating an important limitation of short-latency interactive turbo-coded systems. However, we expect to see higher gains for higher bitrate speech codecs, such as, for example, the 260-bit/20 ms full-rate and the enhanced full-rate GSM speech codecs, which would allow us to use larger frame lengths for the turbo code, an issue currently investigated.

14.13 Chapter Summary

This chapter has described a PWI-ZFE coder previously suggested by Hiotakakos and Xydeas [496]. However, their work was further developed in this chapter to reduce the bitrate and complexity, while improving speech quality. Sections 14.2–14.4 gave an overview of the speech coder, with Figure 14.4 demonstrating the prohibitive complexity of the original ZFE optimisation process proposed by Hiotakakos and Xydeas [496]. This prohibitive complexity was significantly reduced by introducing wavelets into the optimisation process.

Section 14.5 described the voiced speech encoding procedure, involving ZFE optimisation and ZFE amplitude coefficient quantisation. Energy scaling was also proposed to ensure that the original speech amplitude was maintained in the synthesised speech. The interpolation performed at the decoder was detailed in Section 14.6, where the justifications for not sending either the starting location of the prototype segment or the ZFE position parameter were given. The PWI-ZFE description was completed in Sections 14.7 and 14.8, which briefly described the unvoiced speech and adaptive postfilter requirements, respectively.

The PWI-ZFE speech coder at 1.9 kbps was found to produce speech with a more natural quality than the basic LPC vocoder of Chapter 12. It has also been shown in this chapter that numerous benefits were attainable in reducing the computational complexity through the use of the wavelet transform of Chapter 13 with no discernible reduction in speech quality. Particularly useful was the ability of the wavelet transform to suggest GCIs. The chapter also outlined an interpolation method at the decoder which permitted the ZFE amplitude parameters to be transmitted without the position parameter, reducing the bitrate. Finally, in Section 14.11 multiple ZFE was considered; however, the quality of the synthesised speech was often found to be variable. In the next chapter, MBE will be invoked in an effort to improve the associated speech quality.

Chapter 15

Mixed-multiband Excitation

15.1 Introduction

This chapter investigates the speech coding technique of mixed-multiband excitation (MMBE) [103] which is frequently adopted in very-low-bitrate voice compression. The principle behind MMBE is that low-bitrate speech coders, which follow the classical vocoder principle of Atal and Hanauer [481] invoking distinct separation into voiced–unvoiced segments, usually result in speech of a synthetic quality due to a distortion generally termed 'buzziness'. This 'buzzy' quality is particularly apparent in portions of speech which contain only voiced excitation in some frequency regions, but dominant noise in other frequency bands of the speech spectrum. A classic example is the fricative class of phonemes, which contain both periodic and noise excitation sources. In low-bitrate speech coders this type of speech waveform can be modelled successfully by combining voiced and unvoiced speech sources. Figure 15.1 shows the case of the voiced fricative /z/ as in '*z*oo', which consists of voiced speech up to 1 kHz and predominantly noisy speech above this frequency. Improved voiced excitation sources, such as the ZFE described in Chapter 14, can remove some of the synthetic quality of the reconstructed speech. However, the ZFE does nothing to combat the inherent problem of 'buzziness', which is associated with a mixed voiced–unvoiced spectrum that often occurs in human speech production.

MMBE addresses the problem of 'buzziness' directly through splitting the speech into several frequency bands, similarly to sub-band coding [284] on a frame-by-frame adapted basis. These frequency bands have their voicing assessed individually with an excitation source of pulses, noise or a mixture of both being selected for each frequency band. Figure 15.2 shows the PDF of the voicing strength for the training speech database of Table 11.1, where the voicing strength is defined later in Equation (15.9). It demonstrates that although the voicing strengths have significant peaks near the values of 0.3 and 1, representing unvoiced and voiced frames, respectively, there are a number of frames with intermediate voicing strength. It is these frames, constituting about 35% having voicing strengths between 0.4 and 0.85, which will benefit from being represented by a mixture of voiced and unvoiced excitation sources.

Voice and Audio Compression for Wireless Communications Second Edition
L. Hanzo, F. C. A. Somerville and J. P. Woodard

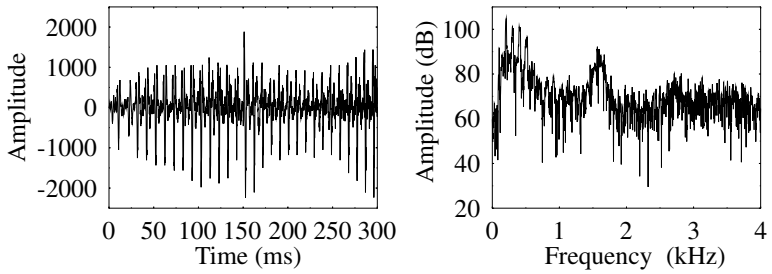

Figure 15.1: Example of a sustained voiced fricative /z/ present in '*z*oo'. Observing the frequency domain, the phoneme is clearly voiced beneath 1 kHz and much more noisy above 1 kHz.

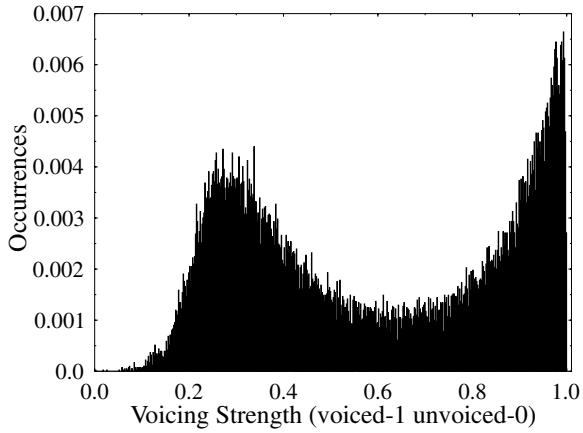

Figure 15.2: The distribution of voicing strengths for the training speech database of Table 11.1.

This chapter commences with Section 15.2 giving an overview of a MMBE coder. Section 15.3 details the filters which construct the multiband structure, and discusses the additional complexity they introduce. An augmented exposure of a MMBE encoder is given in Section 15.4, with a closer view of a MMBE decoder detailed in Section 15.5. Finally, Section 15.6 presents and examines the addition of the MMBE to the LPC vocoder of Chapter 12 and the PWI-ZFE scheme described in Chapter 14.

15.2 Overview of Mixed-multiband Excitation

The control structure of a MMBE model is shown in Figures 15.3 and 15.4, which are considered next. The corresponding steps can also be followed with reference to the encoder and decoder schematics shown in Figure 15.5. After LPC analysis has been performed on the 20 ms speech frame, pitch detection occurs in order to locate any evidence of voicing. A frame deemed unvoiced has the RMS of its LPC residual quantised and sent to the decoder.

Speech frames labelled as voiced are split into M frequency bands, with M constrained to be a constant value. These frequency bands generally have a bandwidth which contains an

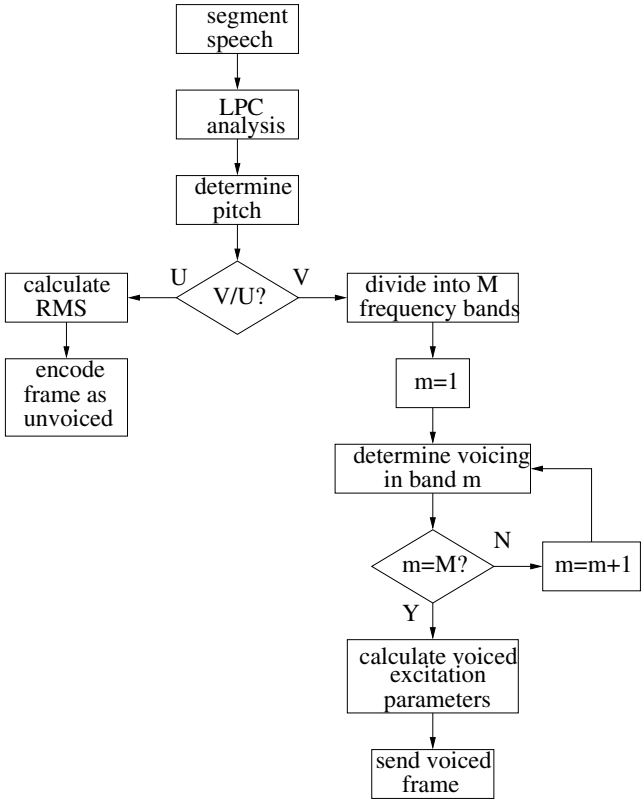

Figure 15.3: Control structure for a MMBE encoder.

integer number of pitch-related spectral needles, where in the ideal situation each frequency band would have a width of one pitch-related spectral needle. However, in practical terms, due to coding efficiency constraints, each frequency band contains several pitch-related needles. The lower the fundamental frequency, the higher the number of pitch-related needles per frequency band. A consequence of the time-variant pitch period is the need for the time-variant adaptive filterbank, which generates the frequency bands, to be reconstructed every frame in both the encoder and decoder, as shown in Figure 15.5, thus increasing the computational costs. Every frequency band is examined for voicing before being assigned a voicing strength which is quantised and sent to the decoder. Reproduction of the speech at the decoder requires knowledge of the pitch period, in order to reconstruct the filterbanks of Figure 15.5(b), together with the voicing strength in each band. The voiced excitation must also be determined and its parameters have to be sent to the decoder.

At the decoder, following Figure 15.5(b), both unvoiced and voiced speech frames have a pair of filterbanks created. However, for unvoiced frames the filterbank is declared fully unvoiced with no pulses employed. For the voiced speech frames, both voiced and unvoiced excitation sources are created.

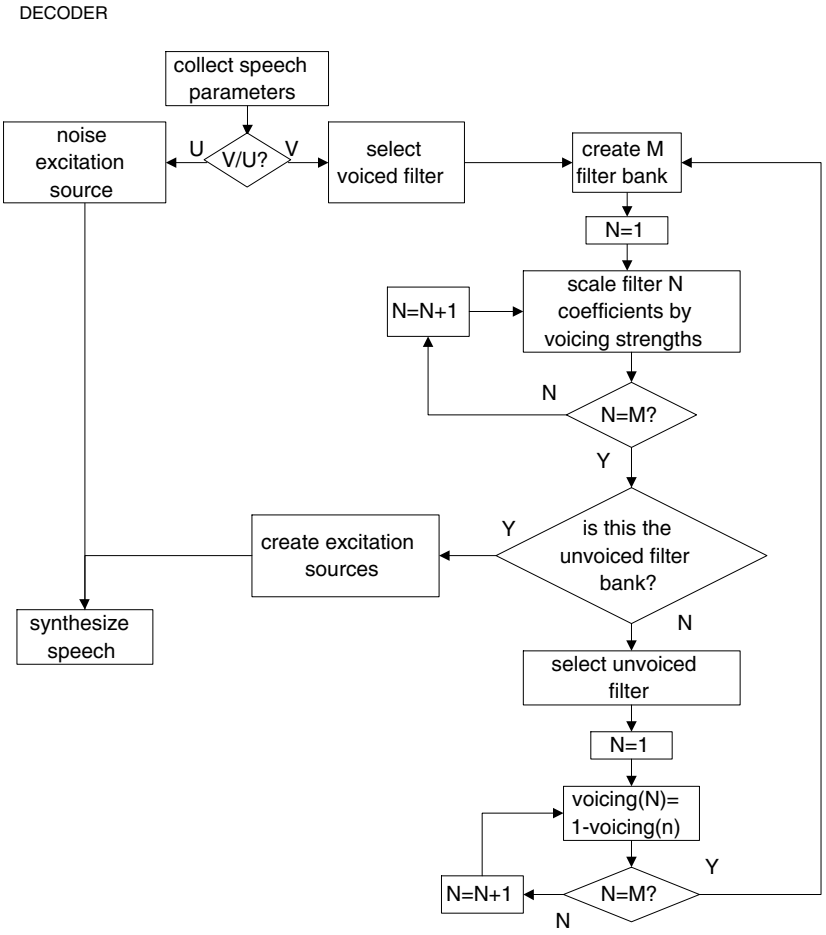

Figure 15.4: Control structure for a MMBE decoder.

Following Figure 15.4, both the voiced and unvoiced filterbanks are created using the knowledge of the pitch period and the number of frequency bands, M. For the voiced filterbanks, the filter coefficients are scaled by the quantised voicing strengths determined at the encoder. A value of 1 represents full voicing, while a value of 0 signifies a frequency band of noise, with values between these extremes representing a mixed excitation source. The voicing strengths are adjusted for the unvoiced filterbank ensuring that the voicing strengths of each voiced and unvoiced frequency band combine to unity. This constraint maintains a combined resultant from the filterbanks that is spectrally flat over the entire frequency range. The mixed excitation speech is then synthesised, as shown in Figure 15.5(b), where the LPC filter determines the spectral envelope of the speech signal. The construction of the filterbanks is described in detail in Section 15.3.

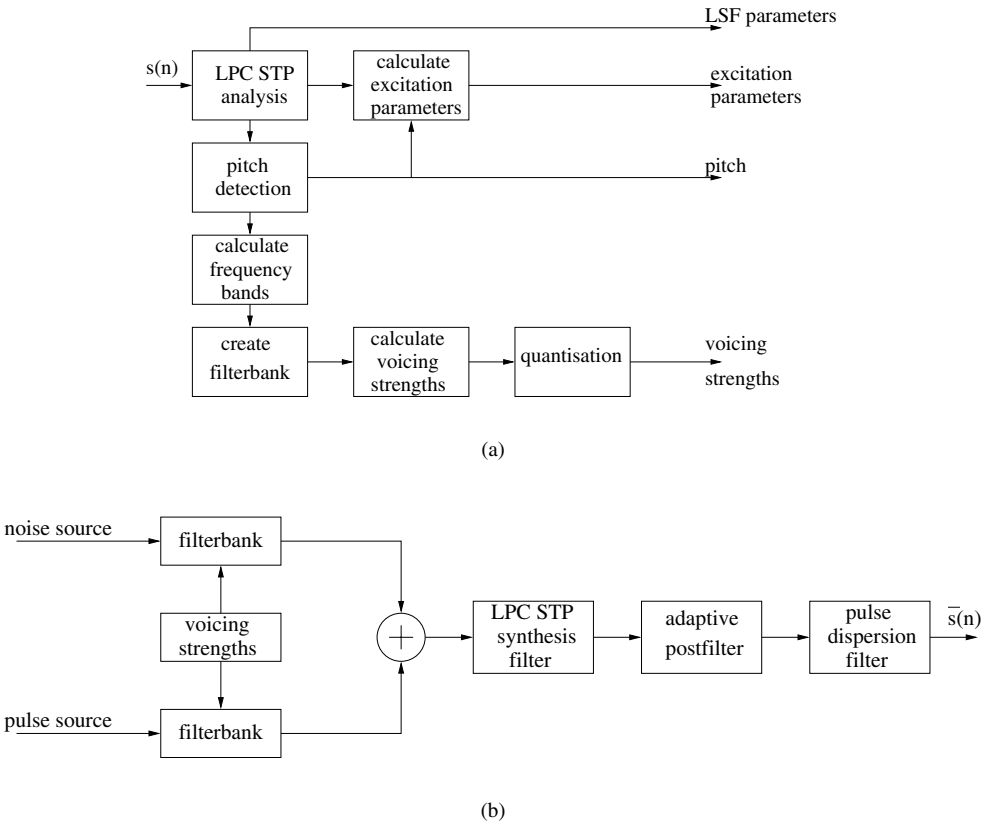

Figure 15.5: Schematic of (a) the encoder and (b) the decoder for a MMBE scheme.

15.3 Finite Impulse Response Filter

The success of MMBE is dependent on creating a suitable bank of filters. The filterbank should be capable of producing either fully voiced or unvoiced speech together with mixed speech. Two well-established techniques for producing filterbanks are FIR filters and QMFs, a type of FIR filter.

QMFs [286] are designed to divide a frequency spectrum in half, thus a cascade of QMFs can be implemented until the spectrum is divided into appropriate frequency bands. If a signal has a sampling frequency f_s, then a pair of QMFs will divide the signal into a band from 0 to $f_s/4$ and a band from $f_s/4$ to $f_s/2$. Both filters will have their 3 dB point at $f_s/4$. The filterbank of our MMBE coder was not constructed from QMFs, because the uniform division of the frequency spectrum imposes restrictions on the shape of the filterbank.

FIR filters contain only a finite number of non-zero impulse response taps, thus, for a FIR filter of length K, the impulse response is given by

$$h_T(n) = \begin{cases} b_n & 0 \leq n \leq K-1 \\ 0 & \text{otherwise} \end{cases}$$

where $h_T(n)$ is the impulse response of the filter and b_n are the filter coefficients. Using discrete convolution, the filter's output signal is given by

$$y_T(n) = \sum_{m=0}^{K-1} h_T(m) \cdot x_T(n-m) \tag{15.1}$$

where y_T is the filter output and x_T is the filter input. Computing the Z-transform of Equation (15.1), we arrive at the following filter transfer function:

$$H(z) = \sum_{m=0}^{K-1} h_T(m) z^{-m}. \tag{15.2}$$

The impulse response of an ideal low-pass filter transfer function $H(z)$ is the well-known infinite duration sinc function given below:

$$h_T(n) = \frac{1}{\pi n r_c} \sin(2\pi n r_c) \tag{15.3}$$

where r_c is the cutoff frequency which has been normalised to $f_s/2$. In order to create a windowed ideal FIR low-pass filter, we invoke a windowing function $w(n)$, which is harnessed as follows:

$$h_T(n) = \frac{1}{\pi n r_c} w_{\text{ham}}(n) \sin(2\pi n r_c) \tag{15.4}$$

where $w_{\text{ham}}(n)$ was chosen in our implementation to be the Hamming window given by

$$w_{\text{ham}}(n) = 0.54 - 0.46 \cos\left(\frac{2\pi n}{K}\right) \tag{15.5}$$

with K being the filter length. In order to transform the low-pass filter to a band-pass filter, h_T^{BP}, the ideal windowed low-pass filter, h_T^{LP} is scaled by the expression [539]

$$h_T^{\text{BP}}(n) = h_T^{\text{LP}}(n) \cos\left(2\pi n \left(\frac{r_l + r_u}{2}\right)\right) \tag{15.6}$$

where r_l is the lower normalised band-pass frequency and r_u is the upper normalised band-pass frequency.

A filterbank consists of the low-pass filter together with the band-pass filters such that the entire frequency range is covered. Thus, as demonstrated in Figure 15.6, the filterbank contains both a low-pass filter and band-pass filters in its constitution.

Following this overview of MMBE, the extra processes required by MMBE within a speech encoder are discussed in the next section.

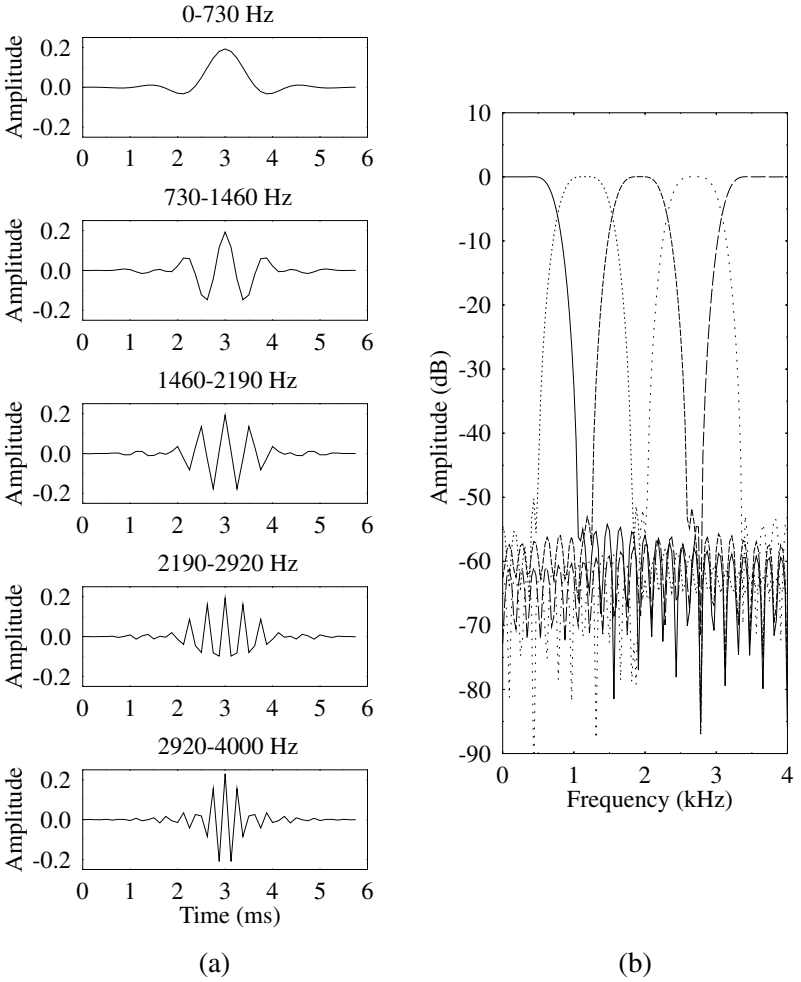

Figure 15.6: (a) The impulse responses and (b) the frequency responses for a filterbank constructed from a low-pass and four band-pass filters. They have frequency ranges 0–730 Hz, 730–1460 Hz, 1460–2190 Hz, 2190–2920 Hz and 2920–4000 Hz. A filter order or 47 was used.

15.4 Mixed-multiband Excitation Encoder

At the encoder the task of the filterbank is to split the frequency band and facilitate the determination of the voicing strengths in each frequency band. In order to accommodate an integer number of the spectral domain pitch-related needles, each frequency band's bandwidth is a multiple of the fundamental frequency. The total speech bandwidth, $f_s/2$, is occupied by a number of pitch-related needles, $N_n \cdot F0 \cdot M$, where f_s is the sampling frequency, $F0$ is the fundamental frequency and M is the number of bands in the filterbank,

while N_n is the number of needles for each sub-band, which can be expressed as [540]

$$N_n = \frac{f_s/2}{M \cdot F0}. \tag{15.7}$$

The resultant N_n value is rounded down to the nearest integer. Any remaining frequency band between $f_s/2$ and the final filter cutoff frequency is assumed unvoiced.

For example, with a sampling frequency of 8 kHz and a filterbank design having five bands the number of harmonics in each band can be determined. For a fundamental frequency of 100 Hz it follows that

$$N_n = \frac{4000}{100 \times 5} = 8$$

implying that there will be eight pitch needles for each sub-band. Similarly, for a fundamental frequency of 150 Hz, we have

$$N_n = \frac{4000}{150 \times 5} = 5.33. \tag{15.8}$$

Thus, each band will contain five pitch needles, with the frequencies 3750 to 4000 Hz being incorporated in the upper frequency band.

The method of dividing the frequency spectrum as suggested by Equation (15.7) is not a unique solution. It would be equally possible to increase the bandwidth of the higher filters due to the human ear's placing less perceptual emphasis on these regions. However, the above pitch-dependent, but even spread of the frequency bands allows a simple division of the frequency spectrum. Since the decoder reconstructs the filter from $F0$, no extra side information requires transmission.

15.4.1 Voicing Strengths

For every voiced speech frame, the input speech is passed through each filter in the filterbank, in order to locate any evidence of voicing in each band. Figure 15.7 shows the transfer function of the filterbank created and the filtered speech in both the time and frequency domains. Observing the top of Figure 15.7(a), below 3 kHz the original spectrum appears predominantly voiced, whereas above 3 kHz it appears more unvoiced, as shown by the periodic and aperiodic spectral fine structure present. The corresponding time-domain signal waveforms of Figure 15.7(b) seem to contain substantially attenuated harmonics of the fundamental frequency $F0$, although the highest two frequency bands appear more noise-like.

The voicing strength is found in our coder using several methods [486], because if the voicing is inaccurately calculated the reconstructed speech will contain an excessive 'buzz' or 'hiss', that is, too much periodicity or excessive noise, respectively. Initially the voicing strength, $v_{\rm s}$, is found using the normalised pitch-spaced filtered waveform correlation [486]:

$$v_{\rm s} = \frac{\sum_{n=0}^{\rm FL-1} f(n) * f(n-P)}{\sqrt{\sum_{n=0}^{\rm FL-1} f(n)^2 \sum_{n=0}^{\rm FL-1} f(n-P)^2}} \tag{15.9}$$

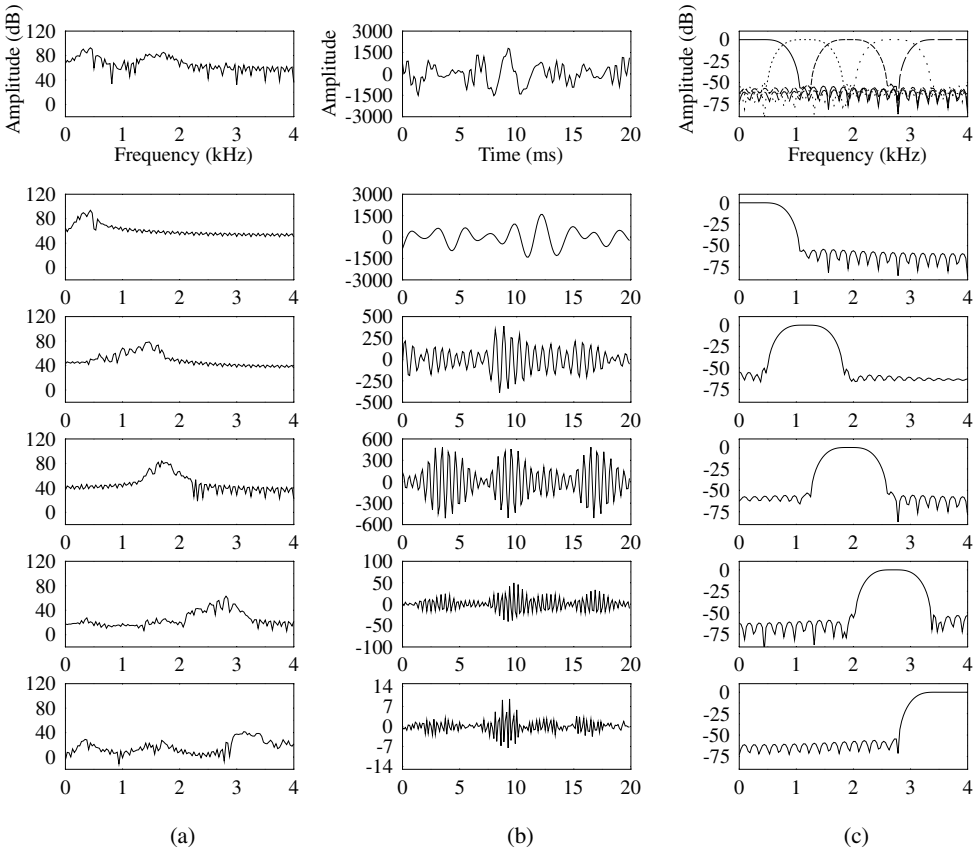

Figure 15.7: (a) The frequency-domain and (b) the time-domain representation of the original waveform AM1 when uttering diphthong /aɪ/ in 'wi*re*s' together with the filtered waveform. (c) The frequency responses of the filterbank are also shown. A filter order of 47 was used.

where $f(n)$ is the filtered speech of a certain bandwidth, FL is the frame length and P is the pitch period for the speech frame. However, at the higher frequencies the correlation can be very low even for voiced speech. The time-domain envelope of the filtered speech will be a better indication of voicing [486], as demonstrated by Figure 15.8.

The envelope of the band-pass-filtered speech is found through low-pass filtering the full-wave rectified filtered speech signal. The one-pole low-pass filtered rectified band-pass signal is given by

$$f(n) = \frac{1}{1 + 2\pi f_c/f_s} \cdot \left[2\pi \frac{f_c}{f_s} s(n) + f(n-1) \right] \tag{15.10}$$

where f_c is the cutoff frequency, $s(n)$ is the input signal of the filter, $f(n)$ is the output signal of the filter and f_s is the sampling frequency. The cutoff frequency was taken to be 500 Hz, since this is just above the highest expected fundamental frequency. The voicing strength, v_{s}, is then calculated using Equation (15.9) for the low-pass filtered, rectified band-pass signal.

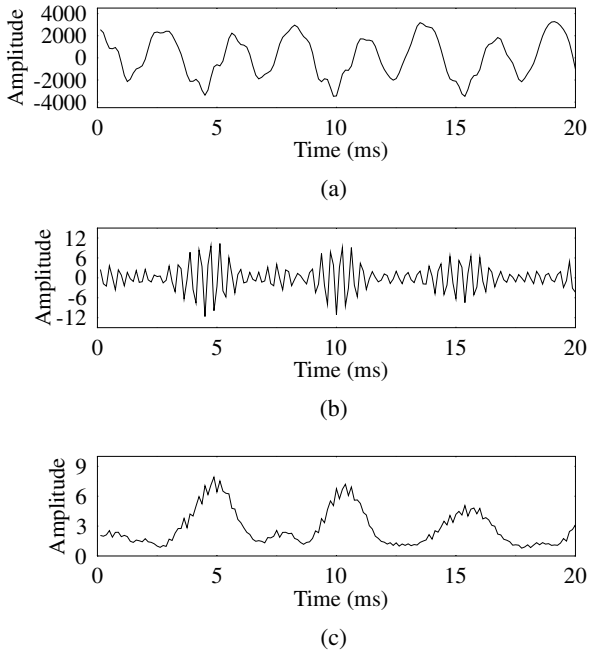

Figure 15.8: Time domain waveforms of (a) the original speech, (b) the band-pass-filtered speech and (c) the envelope of the band-pass-filtered speech.

Subsequently, each frequency band is assigned the largest calculated voicing strength achieved from the original band-pass signal or the low-pass filtered rectified band-pass signal. The PDF of the selected voicing strengths for a 20-band filterbank is given in Figure 15.9 for the training database. The graph represents all of the voicing strengths recorded in every frequency band, providing sufficient fine resolution training data for the Lloyd–Max quantiser to be used.

The PDF for the voicing strength values was passed to the Lloyd–Max quantiser described in Section 12.4. The Lloyd–Max quantiser allocates eight levels for the voicing strengths using a total of three bits, with level 0 constrained to be 0.2 and level 8 constrained to 1. If level 0 was assigned to be 0, the quantiser would be too biased towards the lower-valued voicing strengths. The same quantiser is used to encode every frequency band, producing the SNR values for a 1- to 15-band MMBE scheme given in Figure 15.10, where the speech files AM1, AM2, AF1, AF2, BM1, BM2, BF1 and BF2 were used to test the quality of the MMBE quantiser.

This section has detailed a range of processes invoked in a speech encoder due to MMBE, while procedures required by the MMBE decoder are revealed in the next section.

15.5 Mixed-multiband Excitation Decoder

In the MMBE scheme at the decoder of Figures 15.4 and 15.5(b), two versions of the filterbank are constructed for voiced speech, which will be justified below. Subsequently

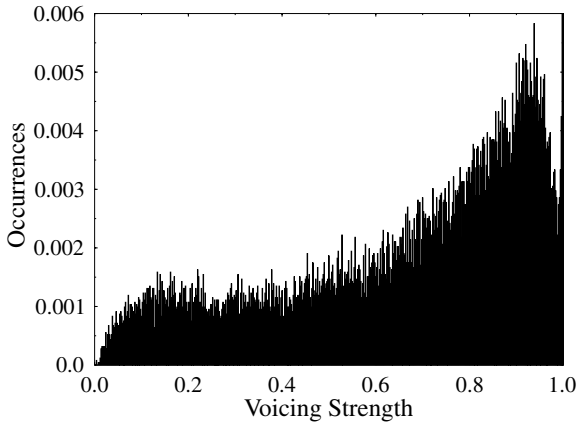

Figure 15.9: The PDF of the voicing strengths for an 20-band filterbank using the database of Table 11.1.

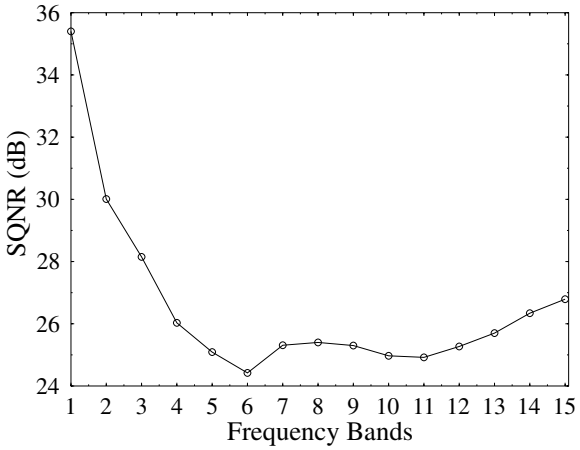

Figure 15.10: SNR values, related to the quantised and unquantised voicing strengths, achieved after the voicing levels in the respective frequency bands are 3-bit quantised for the MMBE coder.

both voiced and unvoiced excitation are passed through these filterbanks and onto the LPC synthesis filter, in order to reproduce the speech waveform.

Explicitly, the power of the filterbank generating the voiced excitation is scaled by the quantised voicing strength, while the filterbank producing the unvoiced excitation is scaled by the difference between unity and the voicing strength. This is performed for each of the frequency bands of the filterbank. Once combined the resultant filterbanks produce an all-pass filter over the 0 to 4000 Hz frequency range, as demonstrated in Figure 15.11. The filterbanks are designed to allow complete voicing, pure noise or any mixture of the voiced and unvoiced excitation. As specified in Section 15.4 any frequency in the immediate vicinity of 4 kHz which was not designated a voicing strength is included in the upper most frequency band.

From the knowledge of the fundamental frequency $F0$ and the number of bands M the decoder computes N_n, the number of pitch-related needles in each frequency band. Thus, with the normalised cutoff frequencies known the corresponding impulse response can be inferred from Equations (15.4) and (15.6).

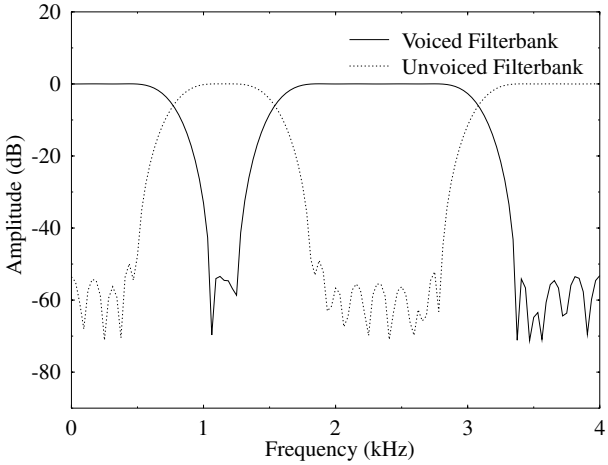

Figure 15.11: Constructed voiced and unvoiced filterbanks for the MMBE decoder. Displayed for a five-band model, with three voiced and two unvoiced bands, using a filter of order 47.

For both voiced and unvoiced speech frames the $(1 - v_s)$ scaled noise excitation is passed to the unvoiced filterbank. The voiced excitation is implemented with either pulses from the LPC vocoder, as detailed in Section 12.5, or using the PWI-ZFE function detailed in Section 14.5. Then, after scaling by v_s, the excitation is passed to the voiced filterbank. The filtered signals are combined and passed to the LPC STP filter for synthesis.

In Figure 15.12 the process of selecting the portion of the frequency spectrum that is voiced and unvoiced is shown. Figure 15.12(a) shows the original speech spectrum with its LPC STP residual signal portrayed in Figure 15.12(b). Figure 15.12(c) and Figure 15.12(d) represent the voiced and unvoiced excitation spectra, respectively. From Figure 15.12(f) it can be seen that beneath 2 kHz the classification is voiced, while above 2 kHz it has been classified as unvoiced. Finally, Figure 15.12(e) demonstrates the synthesised frequency spectrum.

15.5.1 Adaptive Postfilter

The adaptive postfilter from Section 12.6 was used for the MMBE speech coders, with Table 15.1 detailing the optimised parameters for each MMBE speech coder detailed in the next section. Following adaptive postfiltering, the speech is passed through the pulse dispersion filter of Figure 12.19. In the next section we now consider the issues of algorithmic complexity.

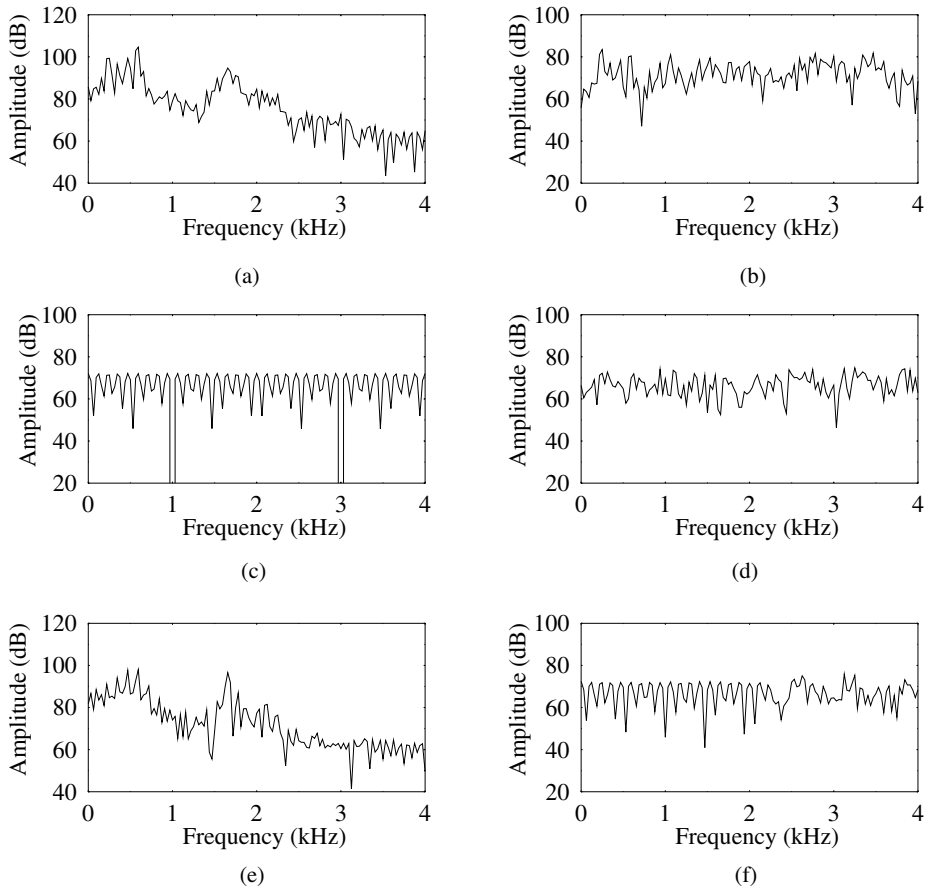

Figure 15.12: An example of the MMBE process for a 20 ms speech frame from the testfile AM1 when uttering the back vowel / ʊ/ in 'sh*ou*ld'. (a) The original and (e) the synthesised frequency spectrum are demonstrated, along with (b) the original and (f) the synthesised excitation spectra and (c) the voiced and (d) the unvoiced excitation spectra.

15.5.2 Computational Complexity

The additional computational complexity introduced by a MMBE scheme in both the encoder and decoder is given in Table 15.2 and Figure 15.13. From Table 15.2 it can be seen that at the encoder the complexity is dominated by the process of filtering the speech into different bands, while at the decoder the MMBE filtering process is dominant. In Figure 15.13 frequency band schemes between one and 15 bands are considered.

Following this description of the MMBE process, the reconstructed speech is examined when MMBE is added to both the benchmark LPC vocoder of Chapter 12 and the PWI-ZFE coder of Chapter 14.

Table 15.1: Appropriate adaptive postfilter values for the MMBE speech coders examined in Section 15.6.

	Values			
Parameter	Two-band MMBE	Five-band MMBE	Three-band MMBE PWI-ZFE	13-band MMBE PWI-ZFE
α_{pf}	0.75	0.80	0.85	0.85
β_{pf}	0.45	0.55	0.55	0.50
μ_{pf}	0.60	0.50	0.60	0.60
γ_{pf}	0.50	0.50	0.50	0.50
g_{pf}	0.00	0.00	0.00	0.00
ξ_{pf}	0.99	0.99	0.99	0.99

Table 15.2: Additional computational complexity introduced at the encoder and decoder by the MMBE scheme, for two- and five-band arrangements.

	Procedure	Two-band (MFLOPS)	Five-band (MFLOPS)
Encoder	Create filterbank	0.02	0.05
	Filter speech into bands	1.54	3.07
	Find voicing strengths	0.35	0.88
Decoder	Create filterbank	0.02	0.05
	Filter excitation sources	3.11	7.77

15.6 Performance of the Mixed-multiband Excitation Coder

This section discusses the performance of the benchmark LPC vocoder of Chapter 12 and the PWI-ZFE coder of Chapter 14, with the addition of MMBE. Both a two-band and a five-band MMBE were added to the LPC vocoder, as detailed in Section 15.6.1, creating speech coders operating at 1.85 and 2.3 kbps, respectively. For the PWI-ZFE coder only a three-band MMBE was added, as detailed in Section 15.6.2, producing a 2.35 kbps speech coder.

15.6.1 Performance of a Mixed-multiband Excitation Linear Predictive Coder

The MMBE scheme, as detailed in this chapter, was added to the basic LPC vocoder described in Chapter 12, with the speech database described in Table 11.1 used to assess the coder's performance. The time- and frequency-domain plots for individual 20 ms frames of speech are given in Figures 15.14, 15.15 and 15.16 for a two-band MMBE model, while Figures 15.17, 15.18 and 15.19 display the corresponding results for a five-band MMBE model. Figures 15.14 and 15.17 represent the same speech segment as Figures 12.21 and Figures 14.13, while Figures 15.15 and 15.18 represent the same speech segment as Figure 12.22 and Figure 14.14, and Figures 15.16 and 15.19 represent the same speech

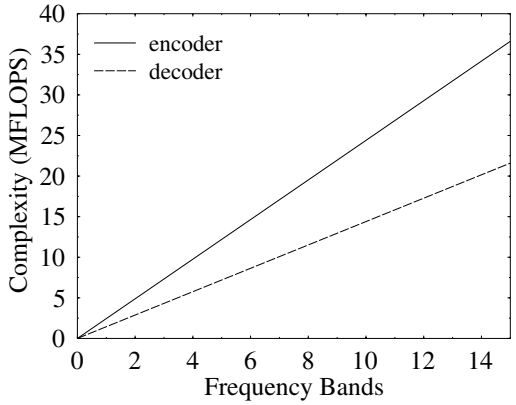

Figure 15.13: The computational complexity in the MMBE encoder and decoder for different numbers of frequency bands.

segment as Figure 12.23 and Figure 14.15. Initially, the performance of a two-band MMBE scheme is studied.

Figure 15.14 displays the performance of a 20 ms speech frame from the testfile BM1. For this speech frame Figure 15.14(b) shows that the entire frequency spectrum is considered voiced, thus the reproduced speech waveform is identical to Figure 12.21.

Figure 15.15 is an utterance from the testfile BF2, where observing Figure 15.15(b) above 2 kHz a mixture of voiced and unvoiced excitation is harnessed. From Figure 15.15(c) it can be seen that the presence of noise above 2 kHz produces a better representation of the frequency spectrum than Figure 12.22(c).

Figure 15.16 is a 20 ms speech frame from the testfile BM2 for the nasal /n/ in the utterance 'throw*n*'. Similarly to Figure 15.15, the frequency spectrum above 2 kHz is modelled by purely unvoiced excitation. Figures 15.15 and 15.16 demonstrate that many speech waveforms contain both voiced and unvoiced components, thus, they emphasise the need for a speech coder which can incorporate mixed excitation.

Through informal listening, a comparison of the synthesised speech from an LPC vocoder with and without MMBE can be made. The introduction of the MMBE removes a significant amount of the 'buzz' inherent in LPC vocoder models, producing more natural sounding speech. Occasionally a background 'hiss' is introduced into the synthesised speech, which is due to the coarse resolution of the frequency bands in a two-band MMBE scheme. In addition, pairwise-comparison tests, detailed in Section 17.2, were conducted to compare the speech quality from the 1.9 kbps PWI-ZFE speech coder of Chapter 14 with the two-band MMBE LPC scheme. These pairwise-comparison tests showed that 30.77% of listeners preferred the PWI-ZFE speech coder, with 23.07% of listeners preferring the two-band MMBE LPC scheme and 46.16% having no preference.

A five-band MMBE scheme was also implemented in the context of the LPC vocoder, which with an increased number of voicing decisions should produce better quality synthesised speech than the two-band MMBE model.

For Figure 15.14, the addition of the extra three extra frequency bands is shown in Figure 15.17 for a speech frame in the testfile BM1. From Figure 15.17(b) it can be seen that

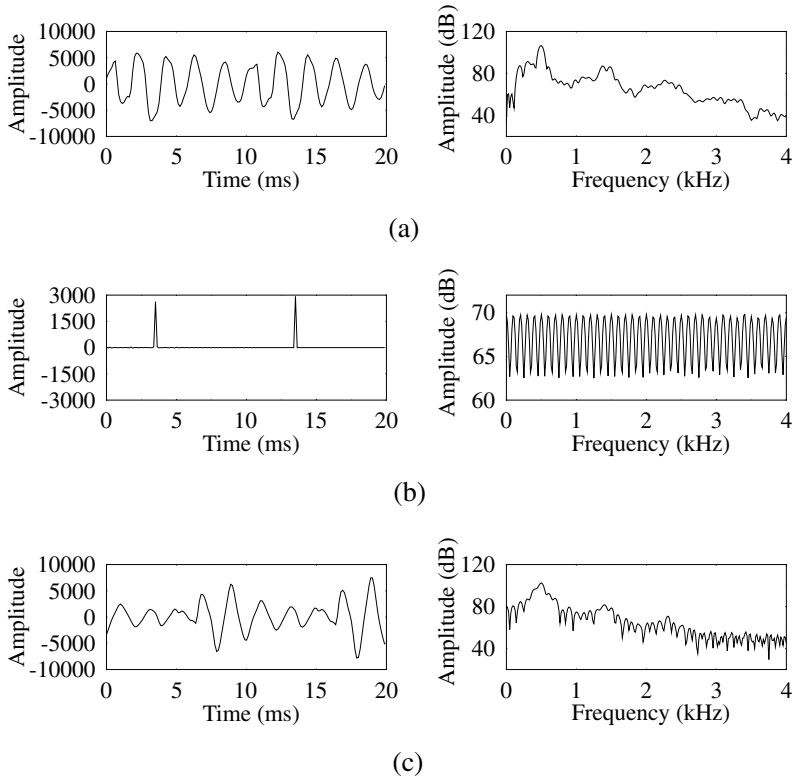

Figure 15.14: Comparison of the time and frequency domains of (a) the original speech, (b) the two-band MMBE waveform and (c) the output speech after the pulse dispersion filter. The 20 ms speech frame is the mid vowel /ɜ/ in the utterance 'w*or*k' for the testfile BM1. For comparison with the other coders developed in this study using the same speech segment, please refer to Table 17.2.

the extra frequency bands produce a mixture of voiced and unvoiced speech above 3 kHz, where for the two-band MMBE model the entire frequency spectrum was fully voiced.

Figure 15.18 portrays the speech frame shown in Figure 15.15 from the BF2 testfile, but with an extra three frequency bands. For this speech frame the additional three frequency bands have no visible effect.

Figure 15.19 displays a speech frame from the testfile BM2 with a five-band MMBE and can be compared with Figure 15.16. For this speech frame the addition of three frequency bands produces fully unvoiced speech above 800 Hz, as shown in Figure 15.19(b), with the effect on the synthesised speech visible in the frequency domain of Figure 15.19(c).

With informal listening tests it was found that the addition of an extra three decision bands to the MMBE scheme has little perceptual effect. It is possible that inherent distortions caused by the LPC vocoder model are masking the improvements. The bit allocation for an LPC vocoder with either a two- or five-band MMBE scheme is given in Table 15.3. The voicing strength of each decision band is quantised with a 3-bit quantiser as described in Section 15.4,

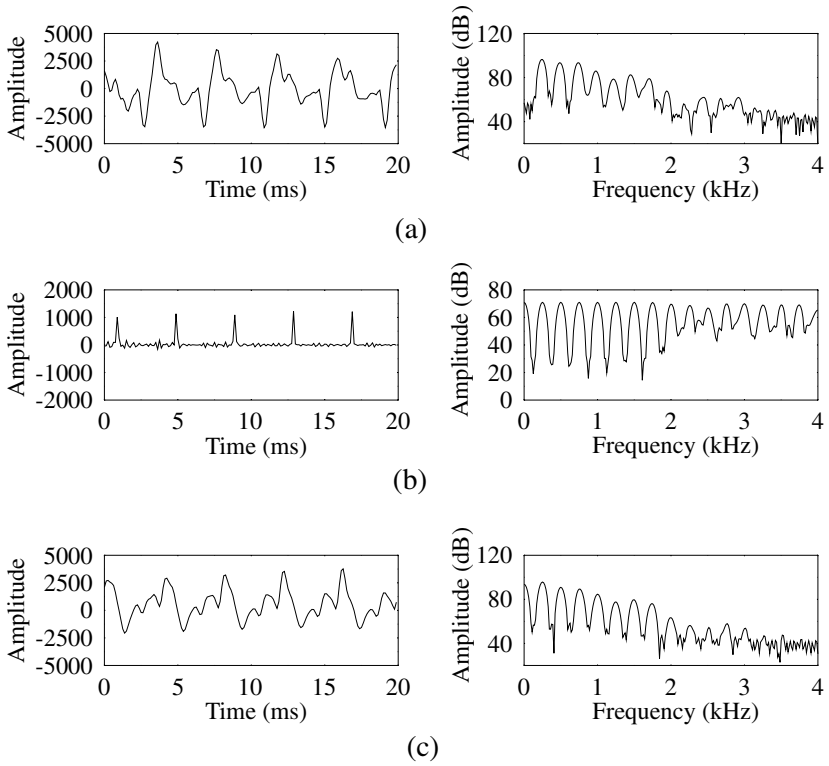

Figure 15.15: Comparison of the time and frequency domains of (a) the original speech, (b) the two-band MMBE waveform and (c) the output speech after the pulse dispersion filter. The 20 ms speech frame is the liquid /r/ in the utterance '*r*ice' for the testfile BF2. For comparison with the other coders developed in this study using the same speech segment, please refer to Table 17.2.

thus, adding 0.15 kbps to the overall bitrate of the coder. The computational complexity of the LPC speech vocoder with a two- and five-band MMBE is given in Table 15.4, where the complexity is dominated by the MMBE function.

In the next section a three-band MMBE scheme is incorporated into the PWI-ZFE coder of Chapter 14.

15.6.2 Performance of a Mixed-multiband Excitation and Zinc Function Prototype Excitation Coder

The MMBE scheme, detailed in this chapter was also added to the PWI-ZFE coder described in Chapter 14. Again, the speech database described in Table 11.1 was used to assess the coder's performance. The time- and frequency-domain plots for individual 20 ms frames of speech are given in Figures 15.20, 15.21 and 15.22 for a three-band MMBE excitation model. These are the speech frames consistently used to consider the performance of the coders,

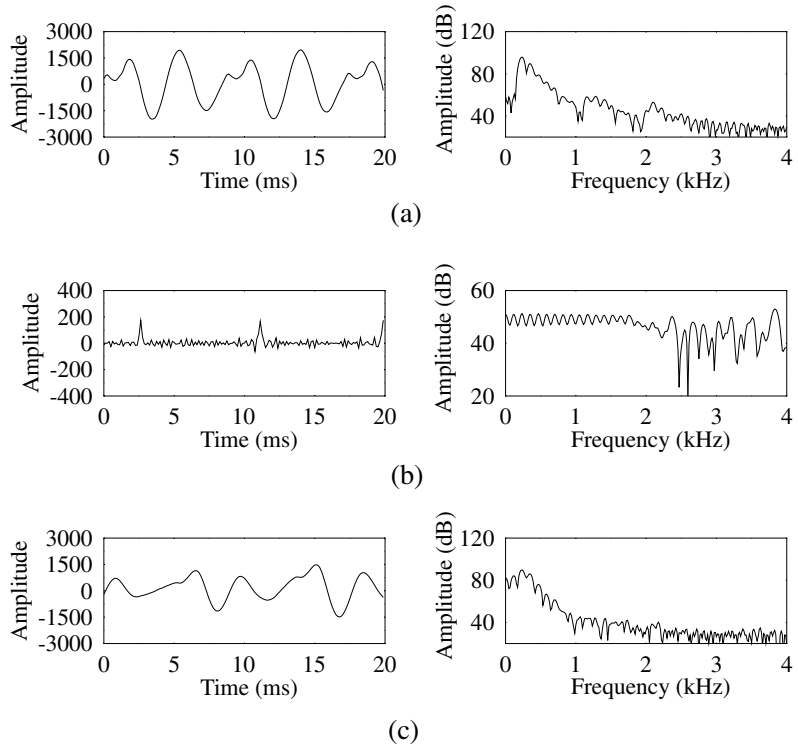

Figure 15.16: Comparison of the time and frequency domains of (a) the original speech, (b) the two-band MMBE waveform and (c) the output speech after the pulse dispersion filter. The 20 ms speech frame is the nasal /n/ in the utterance 'throw*n*' for the testfile BM2. For comparison with the other coders developed in this study using the same speech segment, please refer to Table 17.2.

thus, can be compared with Figures 14.13, 14.14 and 14.15, respectively, together with those detailed in Table 17.2.

Figure 15.20 displays the performance of a three-band MMBE scheme incorporated in the PWI-ZFE speech coder for a speech frame from the testfile BM1. Observing the frequency domain of Figure 15.20(b), a small amount of unvoiced speech is present above 2.5k Hz. The changes made by this noise to the synthesised speech is visible in the frequency domain of Figure 15.20(c).

Similarly to Figure 15.20, for the speaker BF2 Figure 15.21 displays evidence of noise above 2.5 kHz. This noise is again visible in the frequency domain of Figure 15.21(c).

The introduction of a three-band MMBE scheme to the PWI-ZFE speech coder has a more pronounced effect in the context of the testfile BM2, as shown in Figure 15.22. From Figure 15.22(b) it can be seen that above 1.3 kHz the frequency spectrum is entirely noise. In the time domain, much more noise is evident in the excitation waveform than for either Figure 15.20(b) or 15.21(b).

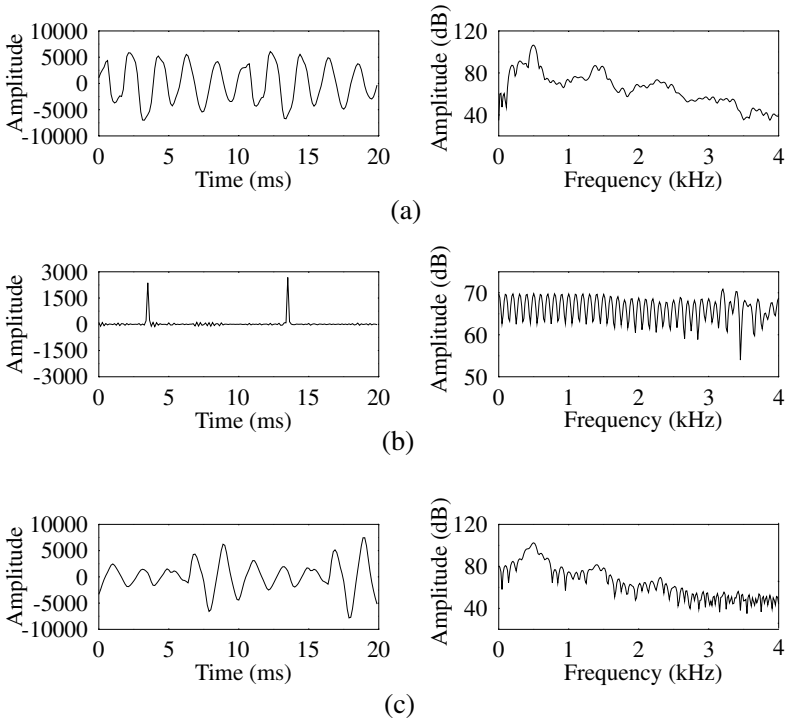

Figure 15.17: Comparison of the time and frequency domains of (a) the original speech, (b) the five-band MMBE waveform and (c) the output speech after the pulse dispersion filter. The 20 ms speech frame is the mid vowel /ɜ/ in the utterance 'w*or*k' for the testfile BM1. For comparison with the other coders developed in this study using the same speech segment, please refer to Table 17.2.

Through informal listening to the PWI-ZFE coder, any audible improvements achieved by the addition of a three-band MMBE can be assessed. The MMBE removes much of the 'buzziness' from the synthesised speech, which particularly improves the speech quality of the female speakers. Occasionally, the MMBE introduces 'hoarseness', indicative of too much noise, particularly to the synthesised speech of male speakers, but overall the MMBE improves speech quality at a slightly increased bitrate and complexity. Pairwise-comparison tests, detailed in Section 17.2, were conducted between the 2.35 kbps three-band MMBE PWI-ZFE speech coder and the 2.3 kbps five-band MMBE LPC scheme. These pairwise-comparison tests showed that 64.10% of listeners preferred the three-band MMBE PWI-ZFE speech coder, with 5.13% of listeners preferring the five-band MMBE LPC scheme and 30.77% having no preference.

As stated previously, each decision band contributes an additional 0.15 kbps to the overall bitrate of a speech coder. Hence, Table 15.5 shows that the addition of the MMBE scheme to the PWI-ZFE coder produced an overall bitrate of 2.35 kbps.

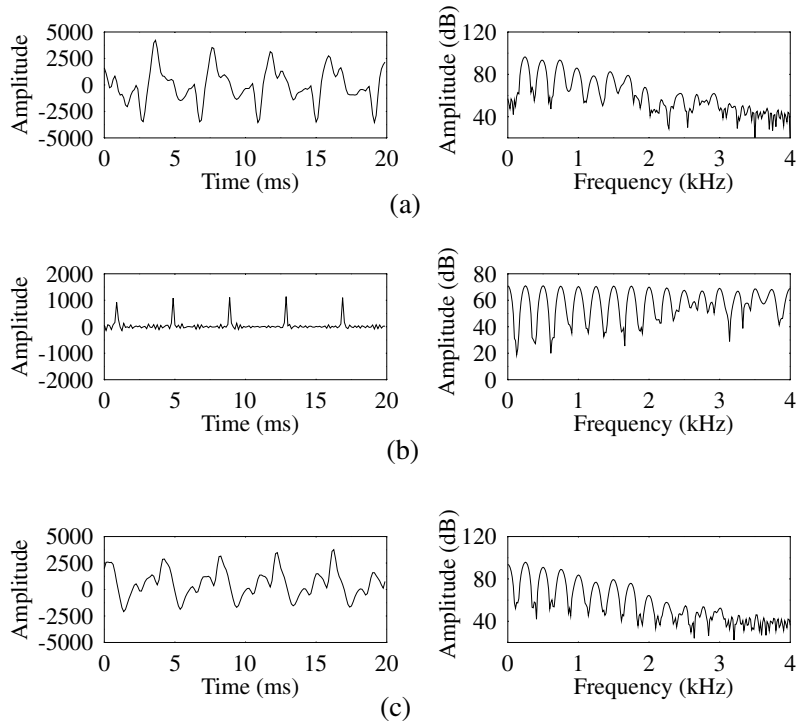

Figure 15.18: Comparison of the time and frequency domains of (a) the original speech, (b) the five-band MMBE waveform and (c) the output speech after the pulse dispersion filter. The 20 ms speech frame is the liquid /r/ in the utterance '*r*ice' for the testfile BF2. For comparison with the other coders developed in this study using the same speech segment, please refer to Table 17.2.

The computational complexity of the PWI-ZFE speech vocoder with a three-band MMBE is given in Table 15.6, which is dominated by the filtering procedures involved in the MMBE process and the ZFE optimisation process.

In this section two schemes have been described which operate at similar bitrates, namely the LPC vocoder with a five-band MMBE operating at 2.3 kbps and the PWI-ZFE coder incorporating a three-band MMBE transmitting at 2.35 kbps. With informal listening tests it was found that the PWI-ZFE coder with a three-band MMBE produced synthesised speech with slightly preferred perceptual qualities, although the quality of the reproduced speech was not dissimilar.

15.7 A Higher Rate 3.85 kbps Mixed-multiband Excitation Scheme

In Sections 15.6.1 and 15.6.2, MMBE schemes operating at different bitrates have been investigated. The varying bits rates were achieved by either altering the excitation or by

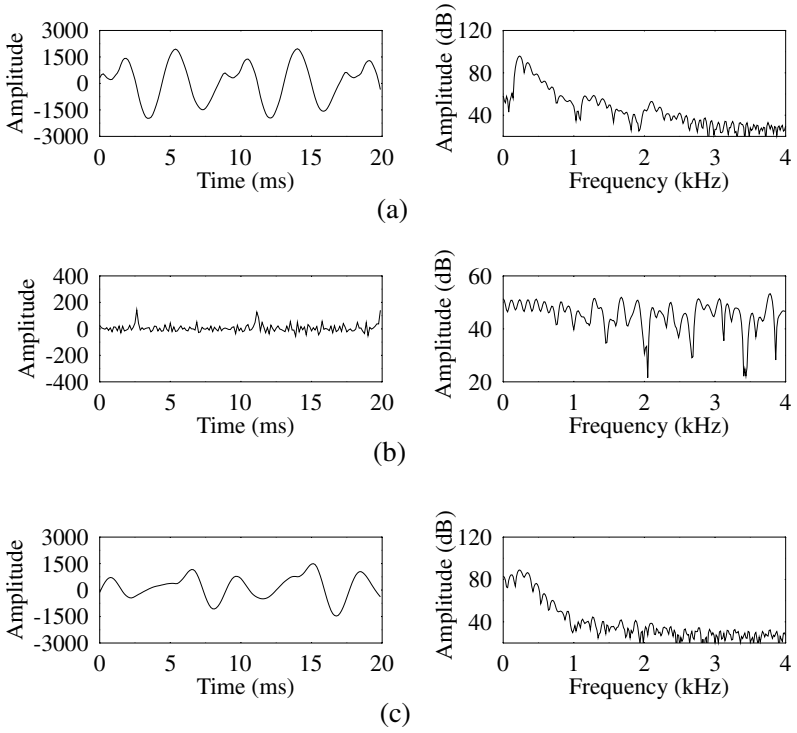

Figure 15.19: Comparison of the time and frequency domains of (a) the original speech, (b) the five-band MMBE waveform and (c) the output speech after the pulse dispersion filter. The 20 ms speech frame is the nasal /n/ in the utterance 'throw*n*' for the testfile BM2. For comparison with the other coders developed in this study using the same speech segment, please refer to Table 17.2.

varying the number of frequency bands employed in the model. The nature of the pitch-dependent filterbank, with the filterbank being reconstructed every frame, permits simple conversion between the number of frequency bands. Following the multiple ZFE investigation of Section 14.11 an MMBE scheme operating at 3.85 kbps, incorporating a single ZFE, was implemented. The bitrate of 3.85 kbps is close to the bitrate of the PWI-ZFE speech coder with three ZFEs of Chapter 14, allowing comparisons between the two techniques at a higher bitrate. The bitrate of 3.85 kbps was achieved with the speech spectrum split into 13 bands, each scalar quantised with three bits as described in Section 15.4.

The performance for an MMBE-ZFE scheme at 3.85 kbps is shown in Figures 15.23, 15.24 and 15.25, which can be compared with Figures 14.20, 14.21 and 14.22 showing the three-pulse ZFE speech coder. Additional pertinent comparisons can be made with the figures detailed in Table 17.2.

For a speech frame from the testfile BM1 displayed in Figure 15.23 the frequency spectrum is still predominantly voiced, with noise being added only above 2.7 kHz. For this speech frame the MMBE extension to the PWI-ZFE model performs better than adding extra

Table 15.3: Bit allocation table for the LPC vocoder voiced frames with two- and five-band MMBE.

Parameter	Two-band	Five-band
LSFs	18	18
Voiced–unvoiced flag	1	1
RMS value	5	5
Pitch	7	7
Voicing strengths	2×3	5×3
Total (20 ms)	37	46
Bitrate (kbps)	1.85	2.30

Table 15.4: Total computational complexity for a basic LPC vocoder encoder with either a two- or five-band MMBE model.

Operation	Two-band complexity (MFLOPS)	Five-band complexity (MFLOPS)
Pitch detector	2.67	2.67
MMBE filtering	1.91	4.00
Total	4.58	6.67

Table 15.5: Bit allocation table for voiced frames in a three-band and 13-bands MMBE PWI-ZFE speech coder.

Parameter	Three-band	Thirteen-band
LSFs	18	18
Voiced–unvoiced flag	1	1
Pitch	7	7
A_1	6	6
B_1	6	6
Voicing strengths	3×3	13×3
Total (20 ms)	47	77
Bitrate (kbps)	2.35	3.85

ZFE pulses, because, as shown in Figure 14.20, these extra ZFE pulses introduced pitch doubling.

Figure 15.24 shows a frame of speech from the testfile BF2. For this speech frame Figure 15.24(b) shows that: up to 1 kHz, the speech is voiced; between 1 and 2 kHz, a mixture of voiced and unvoiced speech is present in the spectrum; between 2 and 3 kHz, the speech is predominantly voiced; while above 3 kHz, only noise is present in the frequency spectrum.

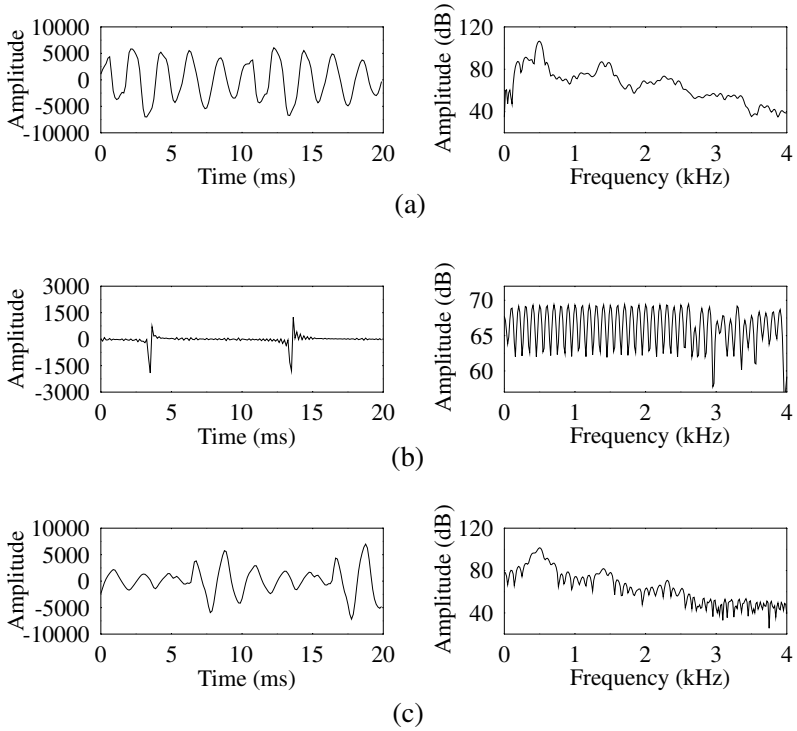

Figure 15.20: Comparison of the time and frequency domains of (a) the original speech, (b) the three-band MMBE ZFE waveform and (c) the output speech after the pulse dispersion filter. The 20 ms speech frame is the mid vowel /ɜ/ in the utterance 'w*or*k' for the testfile BM1. For comparison with the other coders developed in this study using the same speech segment, please refer to Table 17.2.

Table 15.6: Total computational complexity for a PWI-ZFE coder with a three-band MMBE arrangement.

Operation	Three-band complexity (MFLOPS)
Pitch detector	2.67
MMBE filtering	2.05
ZFE minimisation	11.46
Total	16.18

However, when compared with Figure 14.21, it appears that the extra two ZFE pulses improve the reproduced speech more.

For a 20 ms frame from the testfile BM2, the performance is highlighted in Figure 15.25. Observing Figure 15.25(b), it can be seen that the frequency spectrum changes from voiced to

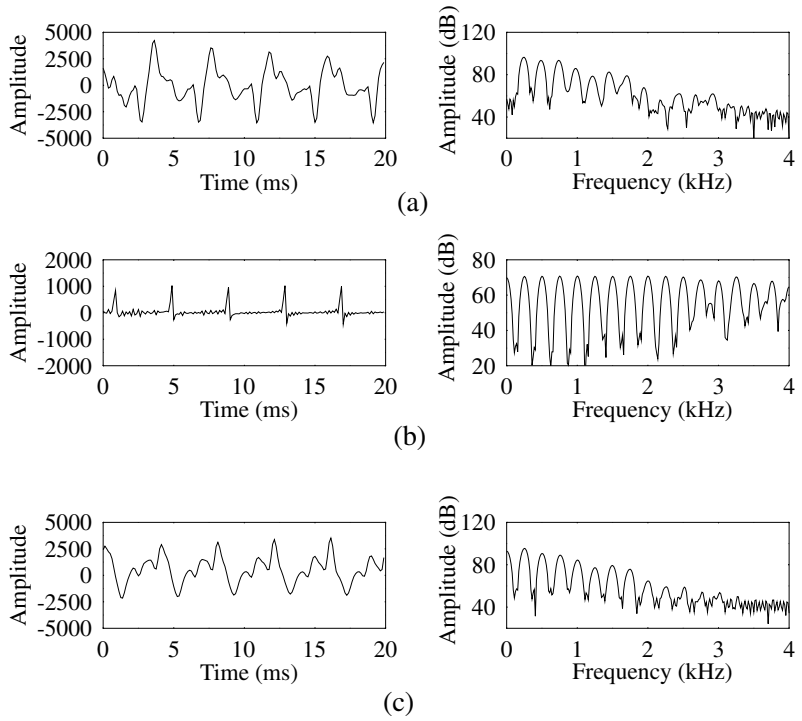

Figure 15.21: Comparison of the time and frequency domains of (a) the original speech, (b) the three-band MMBE ZFE waveform and (c) the output speech after the pulse dispersion filter. The 20 ms speech frame is the liquid /r/ in the utterance '*r*ice' for the testfile BF2. For comparison with the other coders developed in this study using the same speech segment, please refer to Table 17.2.

unvoiced at 900Hz. Furthermore, in the time domain it is difficult to determine the locations of the ZFE pulse.

The relative performances of the PWI-ZFE with a three- and 13-band MMBE has been assessed through informal listening tests. Audibly the introduction of the extra frequency bands improves the natural quality of the speech signal. However, it is debatable whether the improvement justifies the extra 1.5 kbps bitrate contribution consumed by the extra bands. Through pairwise-comparison listening tests, detailed in Section 17.2, the 13-band MMBE extension to the PWI-ZFE speech coder performed better than the addition of two extra ZFE pulses. Given the problems with interpolation detailed in Section 14.11, this was to be expected. The conducted pairwise-comparison tests showed that 30.77% of listeners preferred the 13-band MMBE PWI-ZFE speech coder, with 5.13% of listeners preferring the three-pulse PWI-ZFE scheme and 64.10% having no preference. Before offering our conclusions concerning this chapter, let us in the next section consider an interesting system design example, which is based on our previously designed 2.35 kbps speech codec.

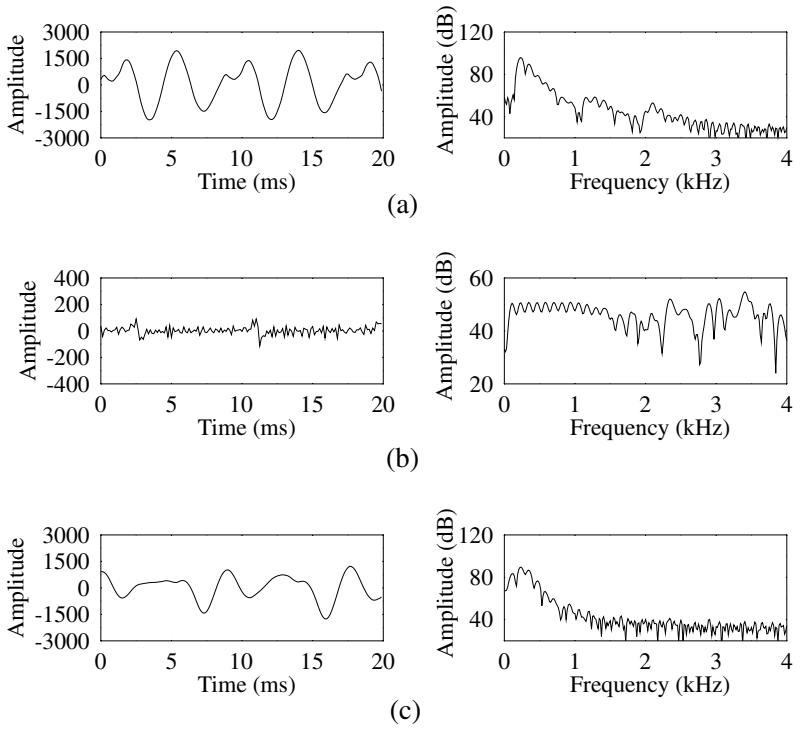

Figure 15.22: Comparison of the time and frequency domains of (a) the original speech, (b) the three-band MMBE ZFE waveform and (c) the output speech after the pulse dispersion filter. The 20 ms speech frame is the nasal /n/ in the utterance 'throw*n*' for the testfile BM2. For comparison with the other coders developed in this study using the same speech segment, please refer to Table 17.2.

15.8 A 2.35 kbps Joint-detection-based CDMA Speech Transceiver[1]

15.8.1 Background

The standardisation of the third-generation wireless systems has reached a mature state in Europe, the USA and Japan, and the corresponding system developments are well under way right across the globe. All three standard proposals are based on W-CDMA, optionally supporting also joint multi-user detection in the up-link. In the field of speech and video source compression, similarly impressive advances have been achieved and hence in this section a complete speech transceiver is proposed and its performance is quantified.

[1]This section is based on F. C. A. Brooks, E. L. Kuan and L. Hanzo, "A 2.35 kbps joint-detection based CDMA speech transceiver", *Proceedings of VTC'99*, Houston, TX, 1999.

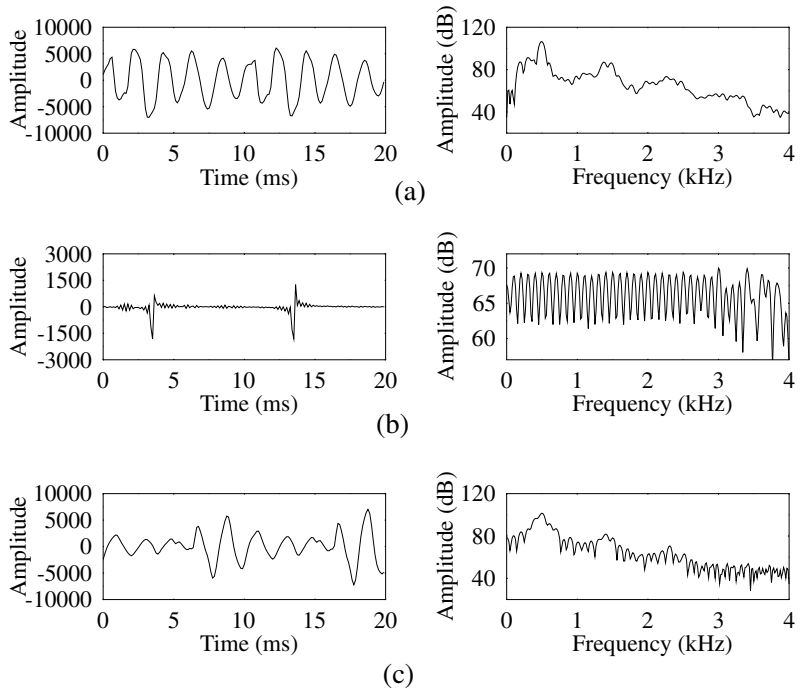

Figure 15.23: Comparison of the time and frequency domains of (a) the original speech, (b) the 13-band MMBE ZFE waveform and (c) the output speech after the pulse dispersion filter. The 20 ms speech frame is the mid vowel /ɜ/ in the utterance 'w*or*k' for the testfile BM1. For comparison with the other coders developed in this study using the same speech segment, please refer to Table 17.2.

15.8.2 The Speech Codec's Bit Allocation

The codec's bit allocation was summarised in Table 15.5, where, again, 18 bits were reserved for LSF vector-quantisation covering the groups of LSF parameters L0, L1, L2 and L3, where we used the nomenclature of the G.729 codec [147] for the groups of LSF parameters, because the G.729 codec's LSF quantiser was used. A one-bit flag was used for the voiced–unvoiced classifier, while for unvoiced speech the RMS parameter was scalar quantised with five bits. For voiced speech the pitch-delay was restricted to 20–147 samples, thus requiring seven bits for transmission. The ZFE amplitude parameters A and B were scalar quantised using six bits, because on the basis of our subjective and objective investigations we concluded that the six-bit quantisation constituted the best compromise in terms of bitrate and speech quality. The voicing strength for each frequency band was scalar quantised and because there were three frequency bands, a total of nine bits per 20 ms were allocated to voicing-strength quantisation. Thus, the total number of bits for a 20 ms frame became 26 or 47, yielding a transmission rate of 2.35 kbps for the voice speech segments.

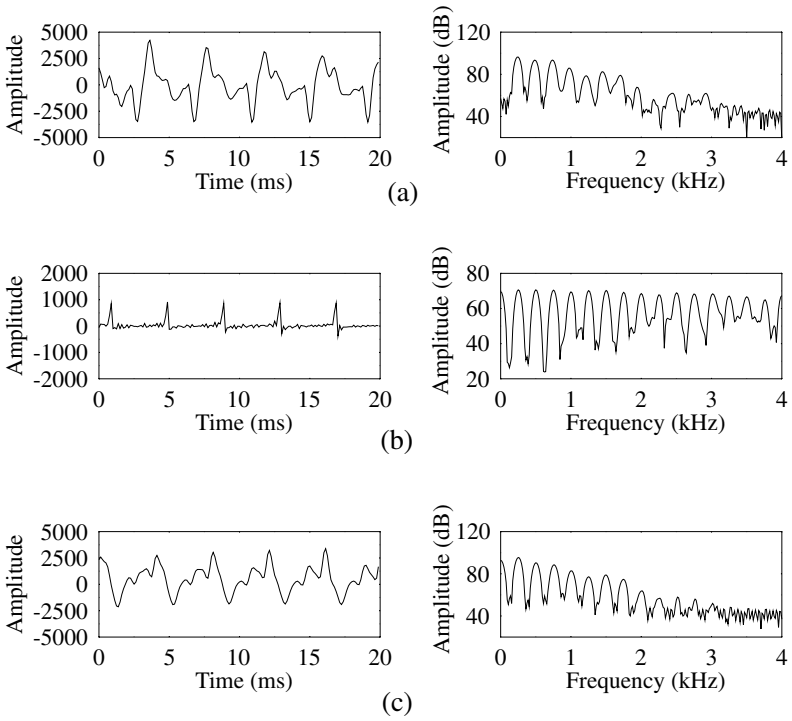

Figure 15.24: Comparison of the time and frequency domains of (a) the original speech, (b) the 13-band MMBE ZFE waveform and (c) the output speech after the pulse dispersion filter. The 20 ms speech frame is the liquid /r/ in the utterance '*r*ice' for the testfile BF2. For comparison with the other coders developed in this study using the same speech segment, please refer to Table 17.2.

15.8.3 The Speech Codec's Error Sensitivity

Following the above description of the 2.35 kbps speech codec we now investigate the extent of the reconstructed speech degradation inflicted by transmission errors. The error sensitivity is examined by individually corrupting each of the 47 bits detailed in Table 15.5 with a corruption probability of 10%. Employing a less than unity corruption probability is common practice, in order to allow the speech degradation caused by the previous corruption of a bit to decay, before the same bit is corrupted again, which emulates a practical transmission scenario realistically.

At the decoder for some of the transmitted parameters it is possible to invoke simple error checks and corrections. At the encoder isolated voiced, or unvoiced, frames are assumed to indicate a failure in the voiced–unvoiced decision and are corrected; an identical process can be implemented at the decoder. For the pitch period parameter, a smoothly evolving pitch track is created at the encoder by correcting any spurious pitch period values and, again, an identical process can be implemented at the decoder. In addition, for voiced frame sequences phase continuity of the ZFE A and B amplitude parameters is maintained at the encoder,

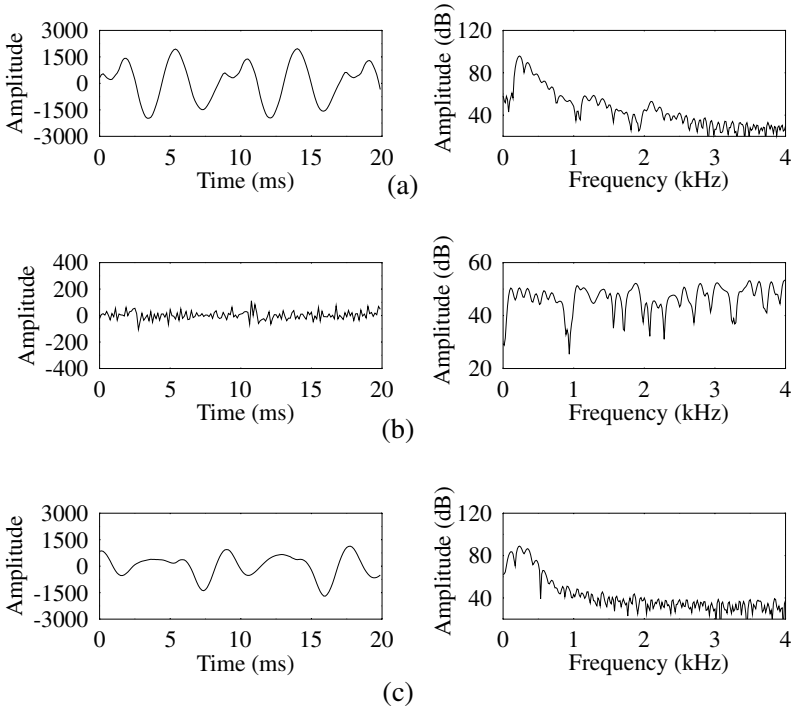

Figure 15.25: Comparison of the time and frequency domains of (a) the original speech, (b) the 13-band MMBE ZFE waveform and (c) the output speech after the pulse dispersion filter. The 20 ms speech frame is the nasal /n/ in the utterance 'throw*n*' for the testfile BM2. For comparison with the other coders developed in this study using the same speech segment, please refer to Table 17.2.

thus, if a phase change is perceived at the decoder, an error occurrence is assumed and the previous frame's parameters can be repeated.

Figure 15.26 displays the so-called SEGSNR and CD objective speech measures for a mixture of male and female speakers, having British and American accents. Observing Figure 15.26 it can be seen that both the SEGSNR and CD objectives measures rate the error sensitivity of the different bits similarly. The most sensitive parameter is the voiced–unvoiced flag, followed closely by the pitch bits, while the least sensitive parameters are the three voicing strengths bits of the bands $B1$–$B3$, as seen in Figure 15.26.

15.8.4 Channel Coding

In order to improve the performance of the system, channel coding was employed. Two types of error correction codes were used, namely, turbo codes and convolutional codes. Turbo coding is a powerful method of channel coding, which has been reported to produce excellent results [216, 217]. Convolutional codes were used as the component codes for the turbo coding and the coding rate was set to $r = 1/2$. We used a 7×7 block interleaver as the turbo interleaver. The FMA1 spread speech/data burst 1 [541] was altered slightly to

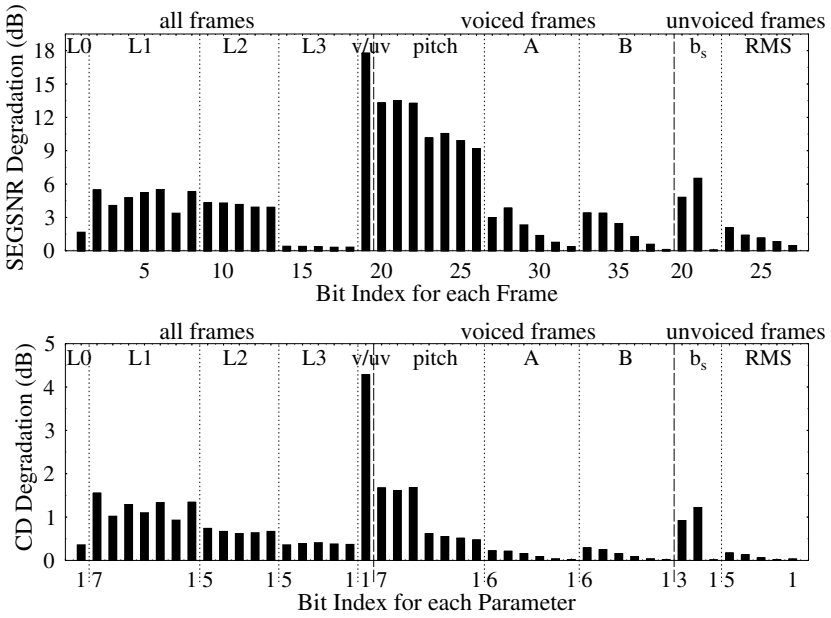

Figure 15.26: The error sensitivity of the different transmission bits for the 2.35 kbps speech codec. For the CD degradation graph, containing the bit index for each parameter, bit 1 is the LSB.

fit the turbo interleaver. Specifically, the two data blocks were modified to transmit 25 data symbols in the first block and 24 symbols in the second. In order to obtain the soft-decision inputs required by the turbo decoder, the Euclidean distance between the CDMA receiver's data estimates and each legitimate constellation point in the data modulation scheme was calculated. The set of distance values were then fed into the turbo decoder as soft inputs. The decoding algorithm used was the SOVA [537, 538] with eight iterations for turbo decoding. As a comparison, a half-rate, constraint-length three convolutional codec was used to produce a set of benchmark results. Note, however, that while the turbo codec used so-called RSC codecs, the convolutional codec was non-recursive, which has better distance properties.

15.8.5 The JD-CDMA Speech System

The JD-CDMA speech system used in our investigations is illustrated in Figure 15.27 for a two-user scenario. The encoded speech bits generated by the 2.35 kbps PWI speech codec were channel encoded using a half-rate turbo encoder having a frame length of 98 bits, including the convolutional codec's termination bits, where a 7×7 turbo interleaver was used. The encoded bits were then passed to a channel interleaver and modulated using four-level QAM (4-QAM). Subsequently, the modulated symbols were spread by the spreading sequence assigned to the user, where a random spreading sequence was used. The uplink conditions were investigated, where each user transmitted over a seven-path COST 207 Bad Urban channel [331], which is portrayed in Figure 15.28. Each path was faded independently using Rayleigh fading with a Doppler frequency of $f_{\rm D} = 80\,{\rm Hz}$ and a Baud rate of

$R_{\rm b} = 2.167\,$MBaud. Variations due to path loss and shadowing were assumed to be eliminated by power control. The additive noise was assumed to be Gaussian with zero mean and a covariance matrix of $\sigma^2\mathbf{I}$, where σ^2 is the variance of the noise. The burst structure used in our experiments mirrored the spread/speech burst structures of the FMA1 mode of the FRAMES proposal [541]. The MMSE-BDFE was used as the multiuser receiver [309], where perfect channel estimation and perfect decision feedback were assumed. The soft outputs for each user were obtained from the MMSE-BDFE and passed to the respective channel decoders. Finally, the decoded bits were directed towards the speech decoder, where the original speech information was reconstructed.

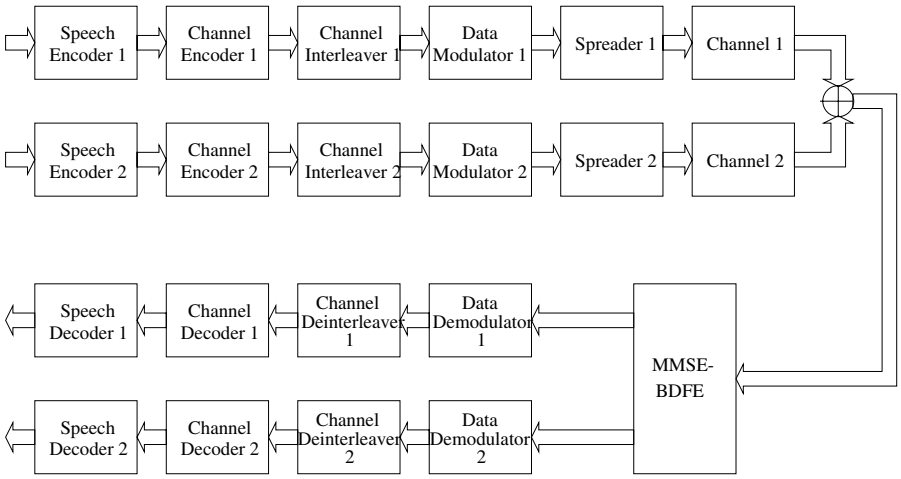

Figure 15.27: FRAMES-like two-user uplink CDMA system.

15.8.6 System Performance

The BER performance of the proposed system is presented in Figures 15.29 and 15.30. Specifically, Figure 15.29 portrays the BER performance of a two-user JD-CDMA speech transceiver. Three different sets of results were obtained for the uncoded, turbo-coded and non-systematic convolutional-coded systems, respectively. As it can be seen from the Figure, channel coding substantially improved the BER performance of the system. However, in comparing the BER performances of the turbo-coded system and the convolutional-coded system, convolutional coding appears to offer a slight performance improvement over turbo coding. This can be attributed to the fact that a short turbo interleaver was used, in order to maintain a low speech delay, while the non-systematic convolutional codec exhibited better distance properties. It is well-understood that turbo codecs achieve an improved performance in conjunction with long turbo interleavers. However, due to the low bitrate of the speech codec 47 bits per 20 ms were generated and hence we were constrained to using a low interleaving depth for the channel codecs, resulting in a slightly superior convolutional coding performance.

In Figure 15.30, the results were obtained by varying the number of users in the system between $K = 2$ and 6. The BER performance of the system degrades only slightly when the

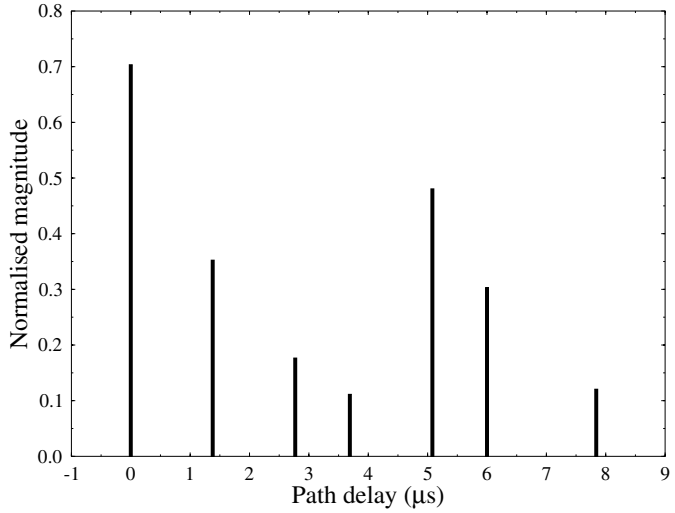

Figure 15.28: Normalised channel impulse response for a seven-path Bad Urban channel [331].

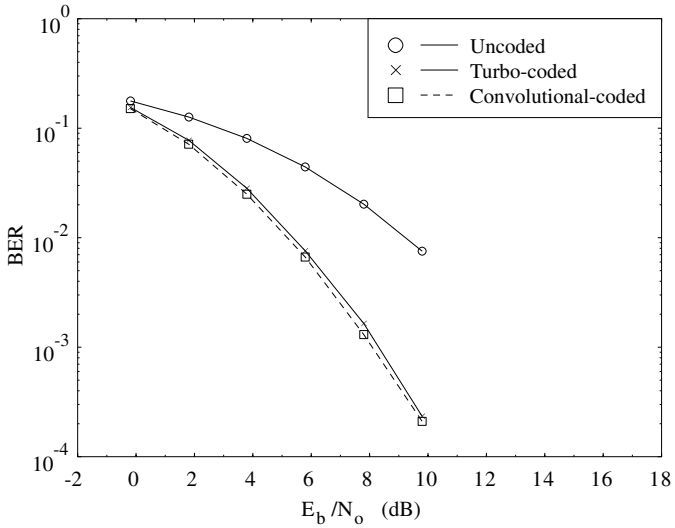

Figure 15.29: Comparison of the BER performance of an uncoded, convolutional-coded and turbo-coded two-user CDMA system, employing half-rate, constraint-length three constituent codes.

number of users is increased. This is due to the employment of the joint detection receiver, which mitigates the effects of multiple access interference. It should also be noted that the performance of the system for $K = 1$ is also shown and the BER performances for $K = 2$–6 degrade only slightly from this single-user bound.

The SEGSNR and CD objective speech measures for the decoded speech bits are depicted in Figure 15.31, where the turbo-coded and convolutional-coded systems were compared for

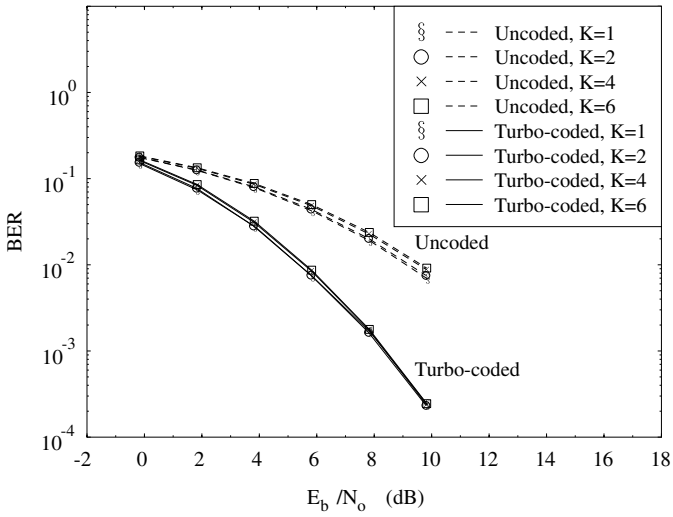

Figure 15.30: Comparison of the BER performance of an uncoded, convolutional-coded and turbo-coded CDMA system for K = 2, 4 and 6 users.

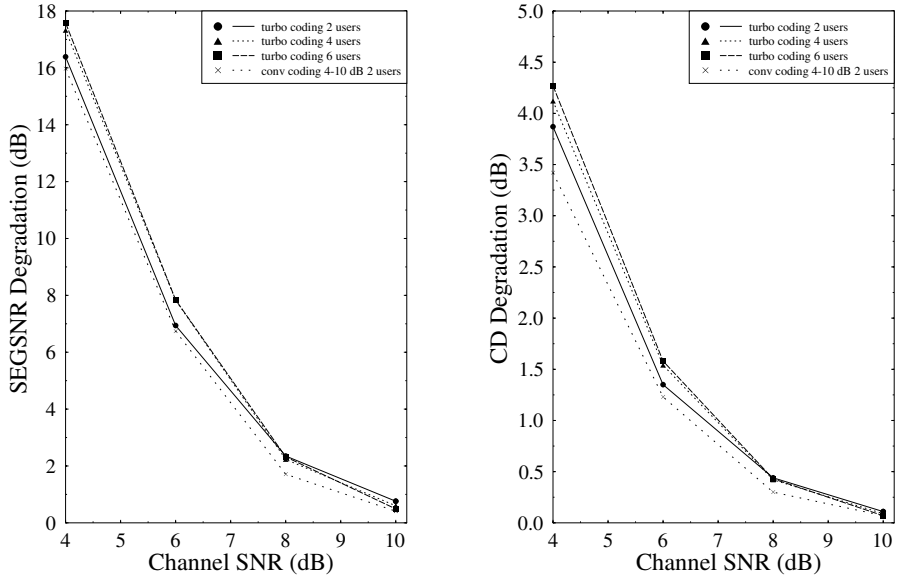

Figure 15.31: SEGSNR and CD objective speech measures for the decoded speech bits for $K = 2$, 4 and 6 users.

$K = 2$ users. As expected on the basis of our BER curves, the convolutional codecs result in a lower speech quality degradation compared to the turbo codes, which were constrained to employ a low interleaver depth. Similar findings were observed in these Figures also for $K = 4$ and 6 users. Again, the speech performance of the system for different number of users is similar, demonstrating the efficiency of the JD-CDMA receiver.

15.8.7 Conclusions on the JD-CDMA Speech Transceiver

The encoded speech bits generated by the 2.35 kbps PWI speech codec were half-rate channel-coded and transmitted using a DS-CDMA scheme. At the receiver the MMSE-BDFE multiuser joint detector was used, in order to detect the information bits, which were then channel-decoded and passed on to the speech decoder. In our work, we compared the performance of turbo codes and convolutional codes. It was shown that the convolutional codes outperformed the more complex turbo codes in terms of their BER performance and also in speech SEGSNR and CD degradation terms. This was due to the short interleaver constraint imposed by the low speech delay requirement, because turbo codes require a high interleaver length in order to perform effectively. It was also shown that the system performance was only slightly degraded, as the number of users was increased from $K = 2$ to 6, demonstrating the efficiency of the JD-CDMA scheme.

15.9 Chapter Summary

In this chapter we have investigated the performance of MMBE when added to the LPC vocoder of Chapter 12 and the PWI-ZFE coder of Chapter 14. Initially, an overview of MBE was given, followed by detailed descriptions of the MMBE in both the encoder and decoder, given in Sections 15.4 and 15.5, respectively.

Section 15.6.1 gave a detailed analysis of two- and five-band MMBEs added to the LPC vocoder, with Section 15.6.2 containing the analysis of a three-band MMBE added to the PWI-ZFE coder. The five-band MMBE LPC vocoder and the three-band MMBE PWI-ZFE coder operated at similar bitrates, hence, they were compared through informal listening. It was found that the three-band MMBE PWI-ZFE coder offered the best natural speech quality. The corresponding time- and frequency-domain waveforms of our coders investigated so far were summarised consistently using the same 20 ms speech frames. The associated figure numbers are detailed in Table 17.2.

Chapter 16

Sinusoidal Transform Coding Below 4 kbps

16.1 Introduction

In Chapters 14 and 15 the low-bitrate coding techniques of PWI and MMBE were described in detail. In this chapter we investigate a third speech coding technique, namely STC, which similarly to PWI and MMBE is frequently employed at bitrates less than 4 kbps.

For STC it is assumed that both voiced and unvoiced speech can be represented by component frequencies having appropriate amplitudes and phases, where these frequencies, amplitudes and phases are determined by taking the STFT of a speech frame. Employing the STFT of the speech waveform was proposed originally for the phase vocoder of Flanagan and Golden [542]. This phase vocoder synthesised speech by summing nominal frequencies, each with an associated amplitude and phase, where the frequencies are taken at set intervals determined by the fixed number of channels employed in the phase vocoder. In its current most popular format STC was first proposed by McAulay and Quatieri [543], who suggested that 'peak-picking' be performed on the STFT magnitude spectra, in order to determine the speech waveform's component frequencies. These frequencies have associated amplitudes and phases which can be combined to reproduce the speech waveform, with the number of frequencies determined by the number of peaks in the STFT.

Initially STC was seen as a method for producing medium-rate speech coders [544]. However, STC speech coders typically separate the speech into voiced and unvoiced components, which, owing to the complexities of determining the pitch and due to carrying voiced–unvoiced decisions, can degrade the quality of the synthesised speech. With the success of the CELP coders at medium bitrates [97, 100, 147], which employ their identical synthesis scheme for both voiced and unvoiced speech, STC has never excelled in terms of quality at medium bitrates. As emphasis in speech coding is shifted to bitrates less than 4 kbps, where CELP coders do not perform well, STC coders have been adapted to operate at these lower bitrates. Low-bitrate speech coders typically divide the speech into voiced and

Voice and Audio Compression for Wireless Communications Second Edition
L. Hanzo, F. C. A. Somerville and J. P. Woodard

unvoiced components, which is similar to the method that STC employs. A further review of low- bitrate STC will be given later in Section 16.4.

Together with the ability to perform speech compression, sinusoidal analysis and synthesis have also been employed successfully for speech modification, such as frequency modification [545, 546]. Instead of peak-picking, George and Smith [545, 546] used AbS to determine the component frequencies, amplitudes and phases, a method they found to be more accurate than peak-picking. In addition, a sinusoidal model has been implemented successfully for pitch determination [547].

This chapter commences by detailing in Sections 16.2 and 16.3 the methods harnessed for sinusoidal analysis and synthesis of speech waveforms, respectively. In Section 16.4 techniques required to perform STC at low bitrates are investigated. Sections 16.6, 16.7 and 16.8 describe the methods required to encode the component sine-wave frequencies, amplitudes and phases. In Section 16.9, the PSI performed at the decoder is detailed. Finally, in Section 16.10 the performance of the PWI-STC coder is assessed.

16.2 Sinusoidal Analysis of Speech Signals

Sinusoidal coders represent the speech using sinusoidal basis functions given by [543]

$$s(n) = \sum_{k=1}^{K} A_k \cos(\omega_k n + \phi_k) \tag{16.1}$$

where A_k represents the amplitude of the kth sine wave, ϕ_k represents the phase of the kth sine wave, with ω_k representing the frequency of the kth sine wave and, finally, K is the number of component sine waves.

16.2.1 Sinusoidal Analysis with Peak-picking

The STFT of the speech wave is found using [548]

$$S(\omega) = \sum_{n=-N/2}^{N/2} w(n)s(n)e^{-jn\omega} \tag{16.2}$$

where $w(n)$ is a Hamming window. In the frequency domain the magnitude spectrum will contain peaks at ω_m, with $A_m = |S(\omega_m)|$ and $\phi_m = \arg S(\omega_m)$.

STC operates on frames of speech, where during these frames the speech is assumed stationary, thus the frame length must be sufficiently short to obey this assumption. The first sinusoidal speech coders [543] used speech frames of 10 ms, or 80 samples at a sampling rate of 8 kHz. The analysis window for the 512 sample length STFT was set to 20 ms in order to incorporate the effect of a Hamming window, employed to reduce the Gibb's phenomenon. McAulay and Quatieri found that ideally the analysis window should be $2.5\times$ pitch period (see [548]), however, for simplicity a fixed window of 20 ms was adopted.

Figure 16.1 demonstrates the STFT for a voiced and unvoiced segment of speech. The peaks in the amplitude spectrum are highlighted by the crosses, with the corresponding phase also identified, where the phases are modulo 2π from $-\pi$ to π. The sine waves, which

constitute the speech signal can be determined by locating the peaks in the frequency domain magnitude spectrum [543], where in Figure 16.1 these frequencies were located using the peak-picking method.

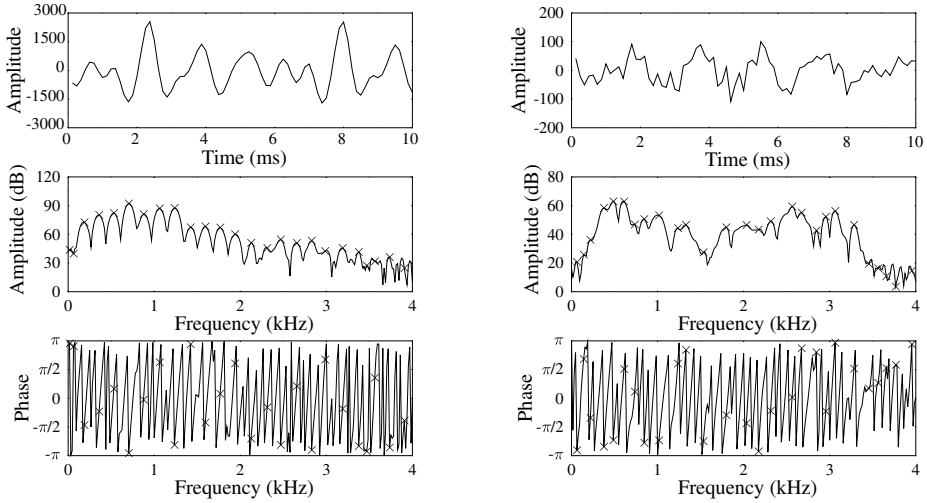

Figure 16.1: Example of sinusoidal analysis performed on (a) voiced and (b) unvoiced speech. The voiced speech segment is back vowel /ɔ/ in 'd*o*g' for AF1, while the unvoiced speech segment is the stop /k/ in '*k*itten' also for AF1. Together with the time-domain waveform, the amplitude and phase of the frequency spectrum are shown.

16.2.2 Sinusoidal Analysis using Analysis-by-synthesis

An alternative method to peak-picking was proposed by George and Smith [545, 546], where the frequencies, amplitudes and phases are determined using AbS. As mentioned above, the peak-picking method assumes stationarity over the analysis period,where if this stationarity constraint is not obeyed, then the STFT peaks will not be the optimum values to represent the speech waveform. In addition, spectral interference in the STFT, caused by the windowing of the input speech data, can also affect the STFT peak values. Thus, the AbS method improves the accuracy of the frequencies, amplitudes and phases used to represent the speech waveform.

If the speech waveform is represented by Equation (16.1), the error signal from the modelling process is given by

$$e(n) = s(n) - \sum_{k=1}^{K} A_k \cos(\omega_k n + \phi_k). \tag{16.3}$$

If the error signal is found iteratively, then

$$e^{k+1} = e^k(n) - A_{k+1} \cos(\omega_{k+1} n + \phi_{k+1}) \tag{16.4}$$

where $e^0(n) = s(n)$. In order to minimise the error signal after sinusoidal modelling we take the MMSE signal given by

$$E^{k+1} = \sum_{n=0}^{\mathrm{FL}} [e^{k+1}(n)]^2 = \sum_{n=0}^{\mathrm{FL}} [e^k(n) - A_{k+1}\cos(\omega_{k+1}n + \phi_{k+1})]^2. \tag{16.5}$$

A variation of this equation will be minimised later in Section 16.7.2. Due to the enhanced accuracy of the AbS procedure, as demonstrated later, it will be harnessed for determining the component frequencies, amplitude and phases. In addition, the AbS process should enable a weighted LPC synthesis filter to be included, when representing the LPC residual waveform by sinusoidal modelling.

Following this review of sinusoidal analysis for speech waveforms, where the component frequencies, amplitudes and phases have been located, the process of re-synthesising the speech is now examined.

16.3 Sinusoidal Synthesis of Speech Signals

Sinusoidal functions, as described in Equation (16.1), can also be employed to synthesise a speech waveform where the required constituent frequencies, amplitudes and phases have been determined through analysis. However, if the synthesised speech frames are concatenated, with no smoothing at the frame boundaries, the resultant discontinuities will be audible in the synthesised speech.

16.3.1 Frequency, Amplitude and Phase Interpolation

Initially, in order to overcome the discontinuity it was proposed that every frequency, amplitude and phase in a frame should be matched to a frequency, amplitude and phase in the adjacent frame [543], thus performing smoothing at the frame boundaries. If an equal number of corresponding frequencies occur in all frames, the matching process is reasonably simple. However, when the number of frequencies in the sinusoidal synthesis differs between frames, then the matching process between these adjacent frames becomes more complex. In this 'differing number of frequencies' scenario the matching process involves the 'birth' and 'death' of sinusoids. The 'birth' process occurs when an extra frequency appears in the sinusoidal representation of the speech waveform, where consequently the additional frequency must be incorporated into the matching process. The 'death' process is initiated when a frequency in the current frame has no counterpart in the subsequent frame. The complexity in this interpolation process arises from the decision whether a frequency undergoes a 'birth' or 'death' process, or it is matched to a frequency in the adjacent frame. Following frequency interpolation, the corresponding amplitudes can be linearly interpolated; however, due to the modulo 2π nature of the phase values they must be 'unwrapped' before interpolation can occur.

16.3.2 Overlap-add Interpolation

In order to circumvent the elaborate frequency matching process, sinusoidal coders typically employ an overlap-add interpolator for removing the frame boundary discontinuities [545]. For the kth frame the speech is synthesised according to

$$\hat{s}^m(n) = \sum_{k=1}^{K} A_k^m \cos(n\omega_k^m + \phi_k^m). \tag{16.6}$$

The synthesised speech $\hat{s}^m(n)$ is determined for the range $0 \leq n \leq 2 \cdot N$, where N is the frame length. The overlap-add interpolator is employed to find the reconstructed speech, given by [545]

$$\hat{s}(n) = w_s(n)\hat{s}^{m-1}(n+N) + (1 - w_s)\hat{s}^m(n) \tag{16.7}$$

where $w_s(n)$ is typically a triangular window [548] of the form

$$w_s(n) = 1 - \frac{n}{N}, \quad 0 \leq n \leq N. \tag{16.8}$$

Thus, the synthesised speech is constructed from the windowed sinusoidal representation of the previous frame interpolated into the current frame, together with the windowed sinusoidal representation of the current frame. Figure 16.2 demonstrates the overlap-add interpolator harnessed in the sinusoidal coder to provide smoothing at the frame boundaries.

Observing Figure 16.2, the synthesised speech is a high-quality reproduction of the original speech. In addition, the previous frame's sinusoids contribute most to the synthesised speech shape at the beginning of the frame, while the current sinusoids predominantly contribute to the end of the current frame. It should be noted that each set of sinusoids contributes to both the current and next speech frame, thus we are assuming stationarity of the speech signal over an interval of $2 \cdot N$.

For sinusoidal coders the major assumption used is that the speech remains stationary over the analysis window, with the validity of this assumption particularly questionable for periods of voicing onset. Figure 16.3 displays a rapidly evolving voicing onset waveform, which together with the displayed synthesised speech characterises the performance of sinusoidal analysis and synthesis at voicing onset. It can be seen that the quality of the reconstructed speech waveform is significantly degraded when compared to Figure 16.2. The reconstructed speech contains too much voicing and produces a smoother evolution from unvoiced to voiced speech than the original waveform.

Having discussed the processes of a sinusoidal coder, we now investigate methods of implementation which will allow a low-bitrate sinusoidal coder to be constructed.

16.4 Low-bitrate Sinusoidal Coders

Sinusoidal coders have previously been adapted to operate at low bitrates [489, 549–551], notably for the DoD 2.4 kbps speech coder competition [484,485] described in Section 11.1.2, although the winning coder did not operate on the basis of sinusoidal principles. Low-bitrate sinusoidal coders frequently employ MBE techniques [552–554], indeed these two forms

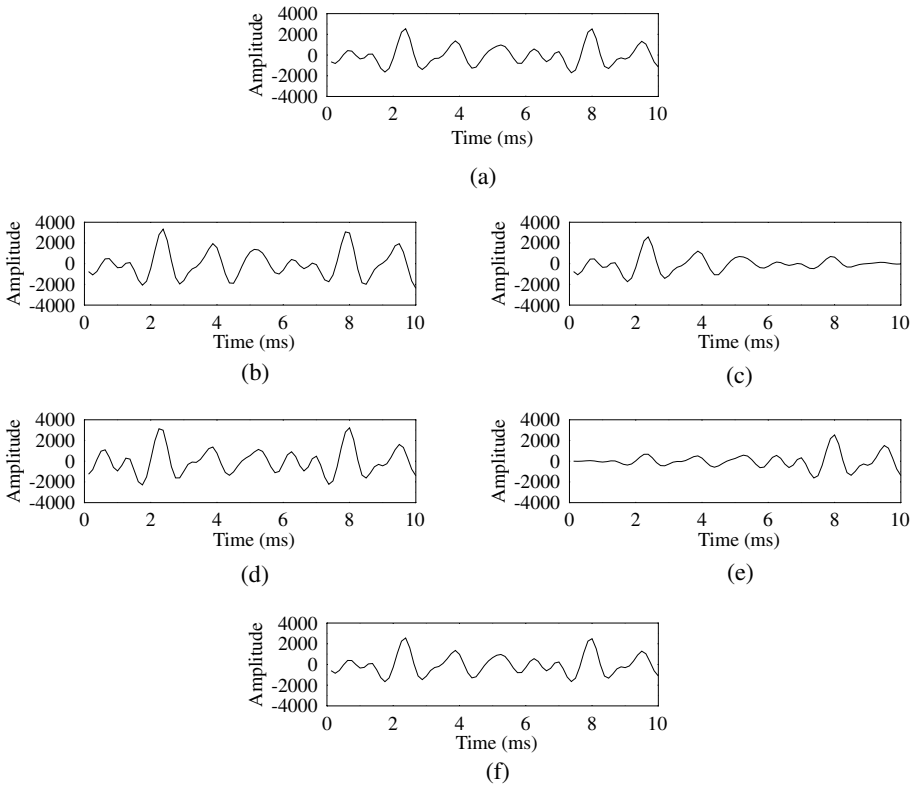

Figure 16.2: The overlap-add process demonstrated for a voiced frame from the testfile AF1 when uttering back vowel/ɔ/ in 'd*o*g': (a) the original speech waveform, with (b) and (d) synthesising the speech based on the previous and current sinusoids, respectively; (c) and (e) the windowed synthesised speech, with (f) the resultant overlap-add synthesised speech waveform.

of harmonic coding become conceptually rather similar at low bitrates. In addition, PWI techniques have also been combined with STC [555].

In low-bitrate sinusoidal coders the bitrate is often reduced to 2.4 kbps by assuming a zero-phase sinusoidal model [489]. Explicitly, at the decoder the location of the pitch pulses is determined using the pitch period and the previous pitch pulse location, but small perturbations are not encoded for transmission. The removal of phase encoding reduces the naturalness of the synthesised speech, particularly introducing 'buzziness' for unvoiced regions, however, some sinusoidal coders overcome this effect by introducing phase dispersion when required [485, 551].

In addition, for voiced speech, in order to reduce the required transmitted bitrate, the sinusoidal model used in the synthesis is assumed to be harmonic, which is given by [489]

$$\hat{s}^m(n) = \sum_{k=1}^{K} A_k^m \cos(nk\omega_0^m + \phi_k^m) \tag{16.9}$$

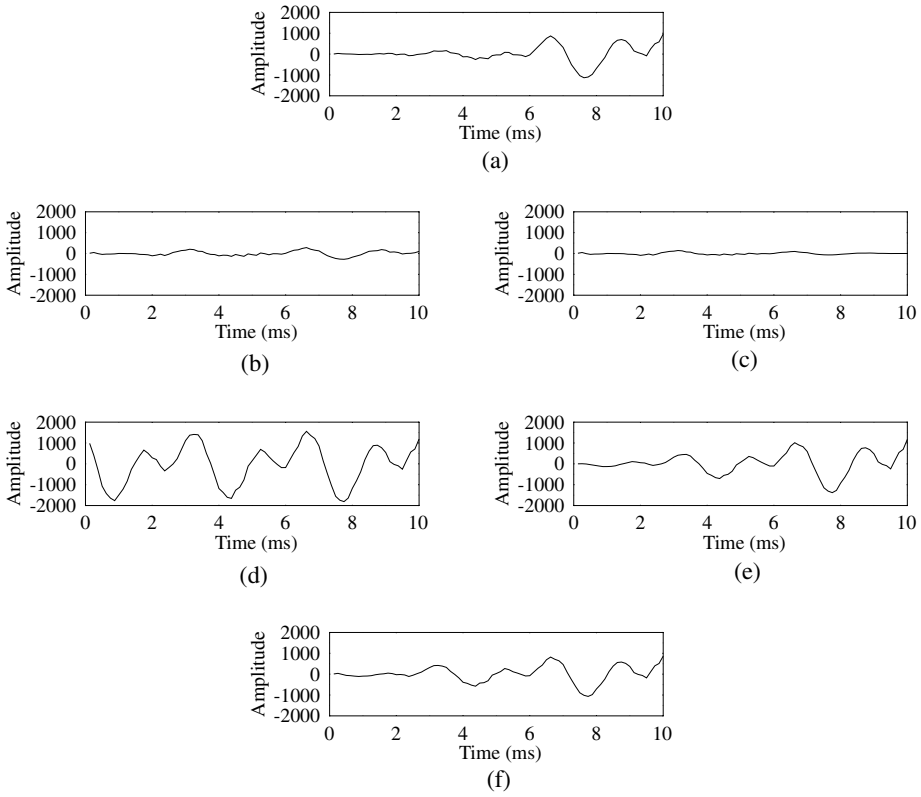

Figure 16.3: Example of sinusoidal analysis and synthesis for a voicing onset frame from the testfile AF1 when uttering the front vowel /e/ in 'ch*a*sed': (a) the original rapidly evolving voicing onset speech waveform; (b) and (c) the speech and windowed speech created from the previous frame's sinusoids, which are predominantly voiced; (d) and (e) the speech and windowed speech from the current sinusoids, producing a voiced waveform; finally, (e) shows the overlap-add synthesised speech waveform.

where ω_0^m is the fundamental frequency associated with the mth frame and K represents the number of harmonics to be modelled.

In order to represent the unvoiced component of the speech a MMBE scheme, similar to Chapter 15, can be invoked, allowing voicing information to be transmitted, subsequently permitting the decoder to mix voiced and unvoiced sounds [549].

For low-bitrate speech coders, the amplitudes associated with each frequency are typically encoded by one of two methods, namely, as LPC coefficients or with VQ. The number of amplitude values required depends on the pitch period. Thus, if the amplitudes are directly quantised methods which allow different lengths to be used, amplitude vectors must be employed.

From the above description of the amplitude and phase information encoding it is clear that, similarly to the PWI and MBE low-bitrate coders of Chapters 14 and 15, the determination of the pitch period is vital for the successful operation of the speech

coder. Following this review of low-bitrate sinusoidal speech coders the sinusoidal coding philosophy described in Sections 16.2 and 16.3 is adapted to become a practical low-bitrate speech coder.

16.4.1 Increased Frame Length

The sinusoidal coder of Sections 16.2 and 16.3 operated on 10 ms frames in order to ensure stationarity over the analysis speech. However, for a low-bitrate scheme this fast parameter update rate is not feasible. The low-bitrate coders explored in Chapters 14 and 15 operated on 20 ms frames, hence the frame length of the sinusoidal coder was extended to 20 ms. Correspondingly, the analysis window was also increased, to 30 ms, for invoking the Hamming window before the STFT. As expected, audibly the increased frame length increases the background noise and reduces the naturalness of the synthesised speech.

As stated above the Hamming window before the STFT was extended to 30 ms, and similarly, the overlap-add window must also be extended. However, a significant problem with the increased frame length is the assumption that, due to the triangular overlap-add window, the speech is stationary for twice the frame length, namely 40 ms. Thus, an alternative overlap-add window was investigated, and the trapezoidal window as shown in Figure 16.4 was adopted for our coder, which is seen to impose less stringent stationarity requirements.

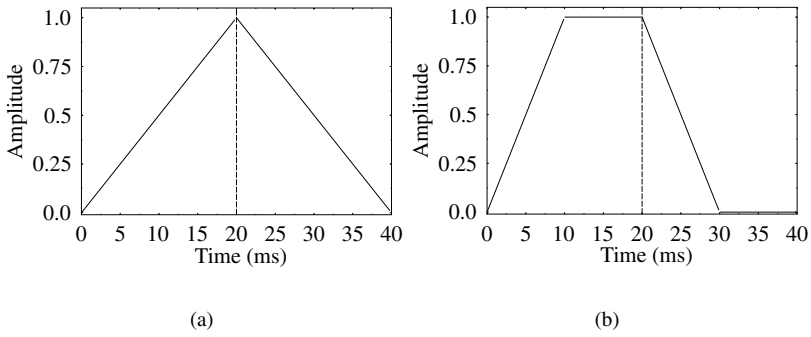

Figure 16.4: The two overlap-add windows investigated for the STC, namely, (a) triangular window and (b) trapezoidal window.

16.4.2 Incorporating Linear Prediction Analysis

For low-bitrate sinusoidal coders, typically one of two methods are employed for encoding the sinusoidal amplitudes. The first is to directly vector quantize the sinusoidal amplitudes, however, the number of amplitudes depends on the pitch period of the speech waveform, thus, initially the amplitude vector would have to be transformed to a predefined length. The second method involves performing LP on the speech waveform with the LP coefficients describing the sinusoidal amplitudes, or the associated spectral envelope, thus ideally the residual signal will have a constant magnitude spectrum. Since LP analysis has already

been implemented for the PWI and MMBE coders of Chapters 14 and 15, respectively, this method was also adopted for encoding the sinusoidal amplitudes. The encoder and decoder schematics for an STC incorporating LP analysis are displayed in Figure 16.5 and they are described next.

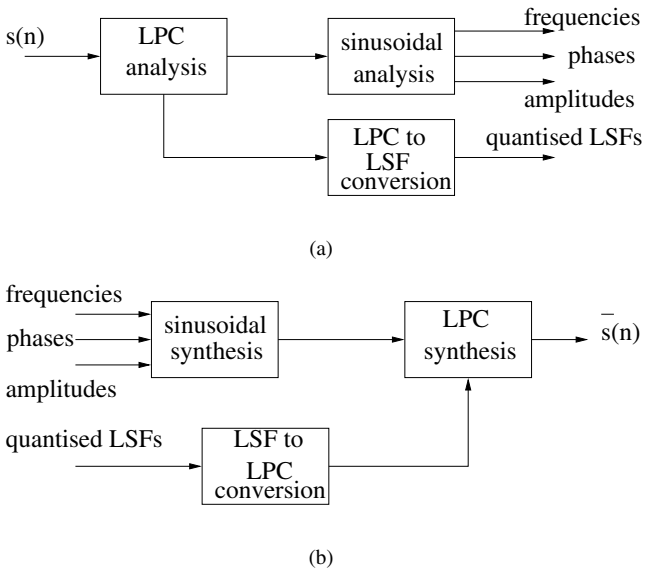

Figure 16.5: Schematic of the (a) encoder and (b) the decoder for a STC employing LP analysis to encode the sinusoidal amplitudes.

At the encoder the LP analysis is performed on the speech waveform, thus, removing short-term redundancies and encoding the amplitudes, or the associated spectral envelope, of the sinusoids. The LPC coefficients are transformed to LSFs, as described in Section 12.2.2, which are vector quantised with 18 bits per frame. The remaining STP LPC residual waveform undergoes sinusoidal analysis for determining the underlying frequencies, amplitudes and phases. At the decoder the LSFs are converted to LP coefficients, while the frequencies, amplitudes and phases reconstruct the LPC excitation using Equation (16.6). Finally, the excitation is passed through the LPC synthesis filter in order to synthesise the speech waveform.

Figure 16.6 demonstrates the associated waveforms together with the corresponding STFT magnitude and phase spectra. The upper trace displays the speech waveform, while the second trace demonstrates the LPC STP residual, which highlights the failure in the assumption that LP analysis produces a constant amplitude residual signal across the frequency domain.

16.5 Incorporating Prototype Waveform Interpolation

The longer frame length of 20 ms, introduced to create a low-bitrate STC coder, will have the effect of reducing the accuracy of the sinusoidal amplitude and phase values, due to

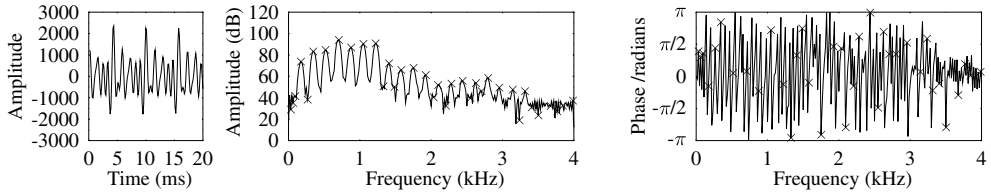

(a)

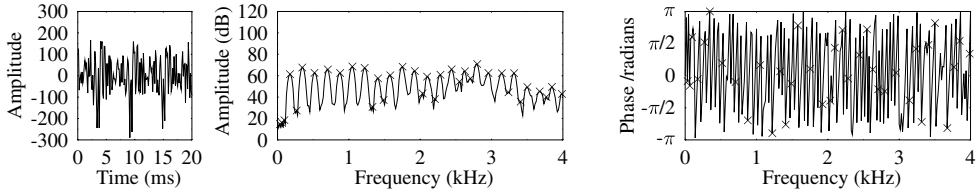

(b)

Figure 16.6: An example of STC-LPC analysis for the (a) voiced speech utterance constituted by the back vowel /ɔ/ in 'dɔg' for the testfile AF1, with (b) LPC analysis incorporated to find the LPC STP residual. The amplitude peaks and corresponding phases are highlighted by crosses.

the increased length over which stationarity is assumed. This effect can be removed by introducing PWI, so that each set of sinusoidal excitation parameters represents a pitch period, thus, the speech is assumed to be stationary over a length of two pitch periods. The schematic for the PWI-STC is given in Figure 16.7. Initially, the LPC coefficients are determined for the speech frame with the LPC STP residual waveform generated. The LPC coefficients are transformed to LSFs and then vector quantised with 18 bits/20 ms [147]. The FFT of this residual waveform is used for pitch detection, where its preference to the wavelet-assisted autocorrelation-based pitch detector of Section 13.5.2 will be described later in Section 16.6. The LPC STP residual is also passed through a weighted LPC synthesis filter and a weighted speech prototype segment is determined following the principles of Section 14.4.2 and Figure 14.6. This prototype segment is then used in the AbS loop, where the best sinusoidal excitation is selected by comparing the synthetic speech $\bar{s_w}(n)$ to the weighted prototype $s_w(n)$.

16.6 Encoding the Sinusoidal Frequency Component

The sinusoidal frequencies are important to the successful operation of STC, since they indicate the component frequencies of the speech waveform. The most efficient way of encoding the frequencies is to constrain them to be multiples of the pitch period determined for the frame.

The pitch period detector harnessed [489] creates the STFT magnitude spectra of the synthetic excitation for every permissible pitch period, which are the integer pitch periods from 20–147 samples. For each of these synthetic excitation magnitude spectra the spectral

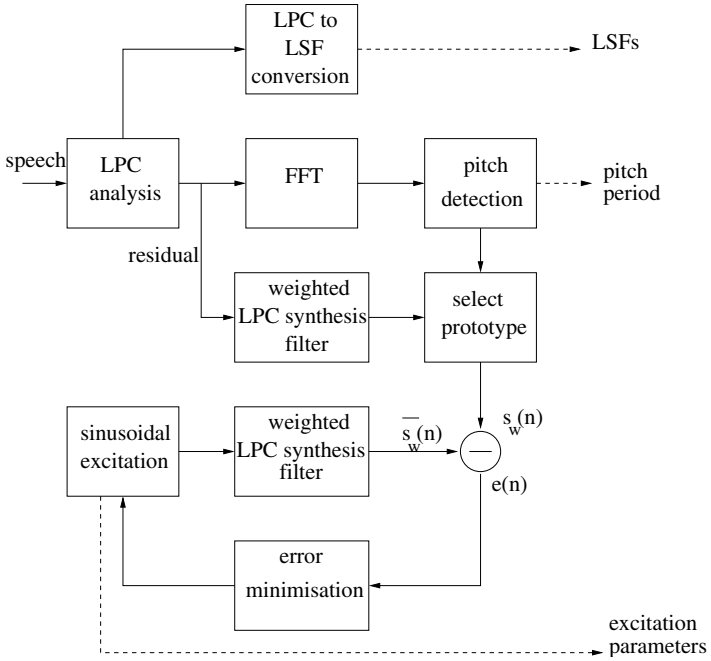

Figure 16.7: Schematic for the STC encoder.

distance from the original LPC STP residual waveform magnitude spectra is calculated, with the closest match selected as the pitch period. For voiced speech segments it is the true pitch period which will, typically, produce the closest spectral match to the original LPC STP residual spectrum. However, unvoiced speech segments have no pitch period, thus, typically, a long pitch period is selected, associated with a low pitch and hence densely spaced pitch harmonics, because this best represents the noise-like unvoiced spectrum. Hence, this process follows the principles of LTP, which was described in Section 11.2, and is used in CELP coders to remove the pitch-related residual pulses, but unlike LTP it is performed in the frequency domain, as highlighted below.

The previous investigated pitch period detectors, of Chapters 12 and 13, operated in the time domain, where the most successful the wavelet-based autocorrelation pitch detector was described in Section 13.5.2, producing an overall pitch determination error rate of 3.9%. The frequency-domain method mentioned above produced an overall error rate of 4.6%, with the percentage of missed unvoiced frames $w_u = 1.2\%$, the percentage of missed voiced frames $w_v = 0.6\%$ and the percentage of gross pitch error $P_g = 2.8\%$. The frequency-domain pitch detector operates by determining which set of harmonic frequencies best represents the STFT of the LPC STP residual, hence, allowing the best harmonic sinusoidal excitation to be determined for the frame. Thus, despite its higher error rate this frequency domain method was adopted for pitch determination within this chapter.

Described in more depth, the frequency-domain pitch detector selects the candidate pitch period which minimises the error between the LPC STP residual STFT magnitude spectra and its harmonic-related pitch-based replica. However, because most noise occurs in the upper

frequency regions only the harmonics beneath 1 kHz are used in the minimisation, formulated as

$$|E(\omega)| = \sum_{\omega=0}^{\pi/4} [|R(\omega)| - G|P(\omega)|]^2 \tag{16.10}$$

where $|E(\omega)|$ is the MMSE between the original and pitch-related harmonic residual magnitude spectrum, $|R(\omega)|$ is the LPC STP residual magnitude spectrum, $|P(\omega)|$ is the magnitude spectrum of the candidate pitch-related excitation whose Fourier transform pair is $p(t) = \sum_{m=0}^{M} \cos(nm\omega_0 - \phi_m)$, G is the gain associated with the pitch period, ω is the normalised frequency and $\pi/4$ represents the frequencies up to 1 kHz, because 2π corresponds to 8 kHz. In order to determine the gain we differentiate $|E(\omega)|$ with respect to G, yielding

$$\frac{\delta|E(\omega)|}{\delta G} = -2 \sum_{\omega=0}^{\pi/4} |P(\omega)|[|S(\omega)| - G|P(\omega)|] = 0 \tag{16.11}$$

which produces a gain value of

$$G = \frac{\sum_{\omega=0}^{\pi/4} |P(\omega)||S(\omega)|}{\sum_{\omega=0}^{\pi/4} |P(\omega)|^2}. \tag{16.12}$$

The corresponding best pitch period is found by substituting G into Equation (16.10), thus when

$$G = \frac{[\sum_{\omega=0}^{\pi/4} |P(\omega)||S(\omega)|]^2}{\sum_{\omega=0}^{\pi/4} |P(\omega)|^2} \tag{16.13}$$

is maximised, $|E(\omega)|$ in Equation (16.10) is minimised.

Figure 16.8 demonstrates the pitch detector's operation for a voiced speech frame, where Figure 16.8(a) contains the LPC STP residual together with its STFT magnitude spectra, while Figure 16.8(b) displays the selected pitch period, from which it can be seen that a good match has been found.

For unvoiced frames, typically a long pitch period is selected, creating many densely spaced frequency harmonics which produces perceptually acceptable unvoiced speech.

16.7 Determining the Excitation Components

Every harmonic frequency found in Section 16.6 will have a corresponding amplitude and phase component. Based on a permissible pitch period of 20 to 147 samples, or 54 to 400 Hz, there can be between 10 and 80 corresponding amplitude and phase values in the 4kHz range. In Section 16.2 peak-picking and AbS were suggested for this task and here they are investigated in more depth.

16.7.1 Peak-picking of the Residual Spectra

The peak-picking process described in Section 16.2.1 was implemented in order to determine the amplitudes and phases related to the selected harmonic frequencies. The performance of the peak-picking process was assessed by comparing the original prototype segment with

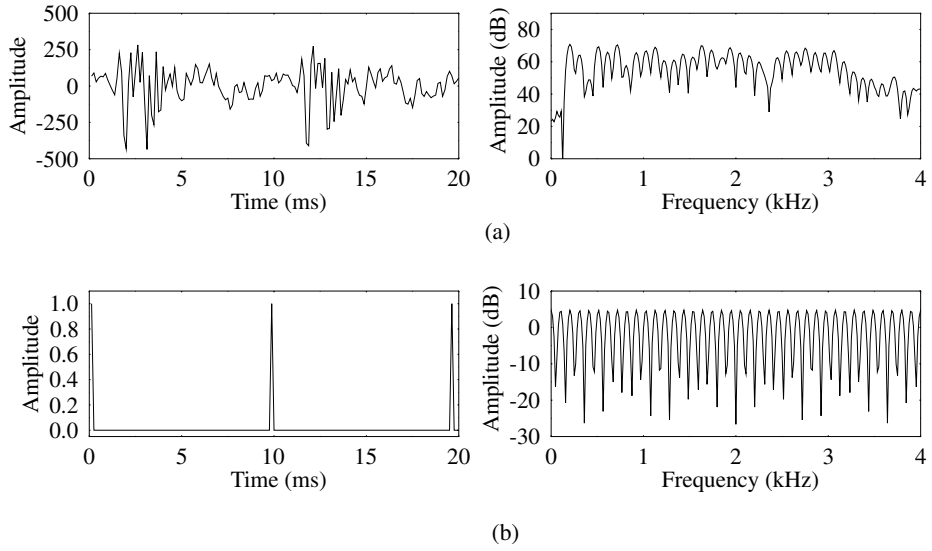

Figure 16.8: The representation of (a) the residual magnitude spectrum by (b) a harmonic pitch period spectrum. The voiced speech segment is the glide /w/ in '*w*ide' for the testfile AM2.

the synthesised prototype segment, where the sinusoidal excitation components remained unquantised. For the peak-picking process a SEGSNR of 4.8 dB was found from the above comparison.

16.7.2 Analysis-by-synthesis of the Residual Spectrum

In Section 16.2.2 the amplitudes and phases were located by minimising Equation (16.5), while in Section 16.4.2 LPC analysis was introduced to represent the amplitudes so that the sinusoids reconstructed the LPC STP residual waveform. Before the sinusoidal parameters are determined the equation for representing the speech waveform is rewritten, in order to include the fundamental frequency already determined. Thus, the speech waveform is synthesised by

$$\tilde{r}(n) = \sum_{k=1}^{K} A_k \cos(nk\omega_0 + \phi_k) \tag{16.14}$$

where ω_0 is the fundamental frequency and $\tilde{r}(n)$ is the reconstructed residual waveform. Following a similar format to the ZFE minimisation process in Section 14.3.1, the original speech waveform can be represented by

$$\tilde{s}(n) = \sum_{k=1}^{K} A_k \cos(nk\omega_0 + \phi_k) * h(n) \tag{16.15}$$

where $h(n)$ is the impulse response of the LPC STP synthesis filter.

With this new representation of the speech waveform the MMSE becomes

$$E_{k+1} = \sum_{n=0}^{P-1} [e_{k+1}(n)]^2 = \sum_{n=0}^{P-1} [e_k(n) - A_{k+1} \cos(n(k+1)\omega_0 + \phi_{k+1}) * h(n)]^2 \quad (16.16)$$

where $e_0(n) = s(n) - m(n)$, with $m(n)$ being the synthesis filter memory, which similarly to Figure 14.8 in Section 14.5 is taken from the previous prototype segment and P the analysis length, namely the length of the prototype segment which is the pitch period. This equation can be further simplified to give

$$E_{k+1} = \sum_{n=0}^{P-1} [e_k(n) - (a_{k+1} \cos(\omega_{k+1}(n)) * h(n) + b_{k+1} \sin(\omega_{k+1}(n)) * h(n))]^2 \quad (16.17)$$

where $\omega_{k+1}(n) = n(k+1)\omega_0$, $a_{k+1} = A_{k+1} \cos \phi_{k+1}$ and $b_{k+1} = -A_{k+1} \sin \phi_{k+1}$ (see [545]). Differentiating Equation (16.17) with respect to a_{k+1} and setting the expression equal to zero we find that

$$\begin{aligned} \frac{\delta E_{k+1}}{\delta a_{k+1}} &= 2 \cdot \sum_{n=0}^{P-1} [\cos(\omega_{k+1}(n)) * h(n)] \\ &\quad \times [e_k(n) - (a_{k+1} \cos(\omega_{k+1}(n)) * h(n) + b_{k+1} \sin(\omega_{k+1}(n)) * h(n))] \\ &= 0. \end{aligned} \quad (16.18)$$

Similarly to George and Smith [545], we define

$$\gamma_{11} = \sum_{n=0}^{P-1} [\cos(\omega_{k+1}(n)) * h(n)]^2 \quad (16.19)$$

$$\gamma_{22} = \sum_{n=0}^{P-1} [\sin(\omega_{k+1}(n)) * h(n)]^2 \quad (16.20)$$

$$\gamma_{12} = \sum_{n=0}^{P-1} [\cos(\omega_{k+1}(n)) * h(n)] \times [\sin(\omega_{k+1}(n)) * h(n)] \quad (16.21)$$

$$\psi_1 = \sum_{n=0}^{P-1} e_k(n) \times [\cos(\omega_{k+1}(n)) * h(n)] \quad (16.22)$$

$$\psi_2 = \sum_{n=0}^{P-1} e_k(n) \times [\sin(\omega_{k+1}(n)) * h(n)]. \quad (16.23)$$

By substituting Equations (16.19), (16.21) and (16.22) into Equation (16.18), we arrive at

$$a_{k+1} \cdot \gamma_{11} + b_{k+1} \cdot \gamma_{12} = \psi_1. \quad (16.24)$$

Similarly, if we differentiate Equation (16.17) with respect to b_{k+1} and set it to zero, then

$$\begin{aligned}\frac{\delta E_{k+1}}{\delta b_{k+1}} &= 2 \cdot \sum_{n=0}^{P-1} [\sin(\omega_{k+1}(n)) * h(n)] \\ &\quad \times [e_k(n) - (a_{k+1} \cos(\omega_{k+1}(n)) * h(n) + b_{k+1} \sin(\omega_{k+1}(n)) * h(n))] \\ &= 0. \end{aligned} \tag{16.25}$$

Then, by substituting Equations (16.20), (16.21) and (16.23) into Equation (16.25), we achieve

$$a_{k+1} \cdot \gamma_{12} + b_{k+1} \cdot \gamma_{22} = \psi_2. \tag{16.26}$$

Solving these the two simultaneous equations produces values for a_{k+1} and b_{k+1} which are given by

$$a_{k+1} = \frac{\gamma_{22} \cdot \psi_1 - \gamma_{12} \cdot \psi_2}{\gamma_{11} \cdot \gamma_{22} - \gamma_{12}^2} \tag{16.27}$$

$$b_{k+1} = \frac{\gamma_{11} \cdot \psi_2 - \gamma_{12} \cdot \psi_1}{\gamma_{11} \cdot \gamma_{22} - \gamma_{12}^2}. \tag{16.28}$$

From these a_{k+1} and b_{k+1} values the amplitudes and phases can be found using $A_{k+1} = \sqrt{{a_{k+1}}^2 + {b_{k+1}}^2}$ and $\phi_{k+1} = -\arctan(b_{k+1}/a_{k+1})$. Since the pitch value of ω_0 has already been found, then once Equations (16.19)–(16.23) have been constructed, the a_{k+1} and b_{k+1} values can be found and A_{k+1} and ϕ_{k+1} can be determined.

Adopting the AbS approach in the PWI-STC coder, when the original and synthesised prototype segments were compared, a SEGSNR of 10.9 dB was achieved.

16.7.3 Computational Complexity

The computational complexity of the PWI-STC encoder will be dominated by the AbS process. In turn, the complexity of the AbS process is dependent on the pitch period and the convolution processes, as suggested by Equations (16.19)–(16.23). The complexity of the AbS is given in Table 16.1, where it can be seen that for a pitch period of 147 samples, corresponding to 80 harmonics, the required complexity of 140 MFLOPS is prohibitive.

16.7.4 Reducing the Computational Complexity

Previously, when George and Smith [545, 546] have adopted AbS for improving the STC parameter representation, they have reduced the complexity of the process by incorporating the DFT. Here the DFT can also be employed for complexity reduction, however, the process is different from that of George and Smith due to the addition of the LPC synthesis filter $h(n)$, together with the lack of the slowly varying amplitude function $g(n)$ from [545].

The M-point DFT for the sequence $x(n)$ is defined by

$$X(m) \equiv \sum_{n=0}^{N-1} x(n) W_M^{mn}, \quad 0 \leq m < M \tag{16.29}$$

Table 16.1: Computational complexity for error minimisation in the PWI-STC encoder.

Procedure	Pitch period $= 20$ number of harmonics $= 10$ (MFLOPS)	Pitch period $= 147$ number of harmonics $= 80$ (MFLOPS)
Convolve sin and $h(n)$	0.01	0.55
Convolve cos and $h(n)$	0.01	0.55
Calculate γ_{11}, γ_{22}, γ_{12}, ψ_1, ψ_2	0.01	0.10
Updating $e^{k+1}(n)$	0.02	0.59
Total for each harmonic	0.05	1.79
Overall total	0.50	140.0

where $W_M^{mn} = e^{-j(2\pi/M)mn}$ and, for completeness, the inverse DFT is given by

$$x(n) = \frac{1}{M} \sum_{n=0}^{N-1} X(m) W_m^{-mn}. \tag{16.30}$$

The DFT is incorporated in order to reduce the complexity with the statements that [545]

$$\sum_{n=0}^{N-1} x(n) \cos\left[\left(\frac{2\pi}{M}\right)mn\right] = \mathrm{Re}[X(m)] \tag{16.31}$$

$$\sum_{n=0}^{N-1} x(n) \sin\left[\left(\frac{2\pi}{M}\right)mn\right] = -\mathrm{Im}[X(m)]. \tag{16.32}$$

Then it can be noted that the DFT of the error signal $e_k(n)$ and that of the LPC synthesis filter impulse response $h(n)$ are given by

$$E_k(m) = \sum_{n=0}^{N-1} e_k(n) W_M^{mn} \tag{16.33}$$

$$H(m) = \sum_{n=0}^{N-1} h(n) W_M^{mn}. \tag{16.34}$$

With the examination of ψ_1 from Equation (16.22) a reduction in its complexity can be achieved, if initially the convolution is rewritten as a summation:

$$\psi_1 = \sum_{n=0}^{N-1} e_k(n) \times \sum_{m=0}^{M-1} h(m) \cdot \cos(\omega_{k+1}(n-m)). \tag{16.35}$$

In order to allow the summations to become separable, the trigonometric identity $\cos(x+y) = \cos(x)\cos(y) - \sin(x)\sin(y)$ is harnessed, simplifying the equation to

$$\psi_1 = \sum_{n=0}^{N-1} e_k(n) \cdot \cos(\omega_{k+1}(n)) \times \sum_{m=0}^{M-1} h(m) \cdot \cos(\omega_{k+1}(m))$$

$$+ \sum_{n=0}^{N-1} e_k(n) \cdot \sin(\omega_{k+1}(n)) \times \sum_{m=0}^{M-1} h(m) \cdot \sin(\omega_{k+1}(m)). \tag{16.36}$$

Utilizing from Section 16.7.2 that $\omega_{k+1}(n) = n(k+1)\omega_0$ together with the relationship $\omega_0 = 2\pi/P$, where P is the prototype segment length that is equal to N and M, allows $w_{k+1} = 2n\pi i/M$ to be defined. Equations (16.33) and (16.34) can then be employed to define

$$\psi_1 = \mathrm{Re}(E_k(i)) \cdot \mathrm{Re}(H(i)) + \mathrm{Im}(E_k(i)) \cdot \mathrm{Im}(H(i)). \tag{16.37}$$

Similarly, ψ_2 defined in Equation (16.23) can be rewritten using the trigonometric identity $\sin(x+y) = \sin(x)\cos(y) + \cos(x)\sin(y)$, giving

$$\psi_2 = \sum_{n=0}^{N-1} e_k(n) \cdot \sin(\omega_{k+1}(n)) \times \sum_{m=0}^{M-1} h(m) \cdot \cos(\omega_{k+1}(m))$$

$$- \sum_{n=0}^{N-1} e_k(n) \cdot \cos(\omega_{k+1}(n)) \times \sum_{m=0}^{M-1} h(m) \cdot \sin(\omega_{k+1}(m)) \tag{16.38}$$

which when described in terms of the DFTs of $E_k(m)$ and $H(m)$ becomes

$$\psi_2 = \mathrm{Re}(E_k(i)) \cdot \mathrm{Im}(H(i)) - \mathrm{Im}(E_k(i)) \cdot \mathrm{Re}(H(i)). \tag{16.39}$$

The term γ_{11} from Equation (16.19) can also be simplified by replacing the convolution term by a summation, becoming

$$\gamma_{11} = \sum_{n=0}^{N-1} \left[\sum_{m=0}^{M-1} h(m) \cdot \cos(\omega_{k+1}(n-m)) \right]^2. \tag{16.40}$$

Separating the n and m components the expression becomes

$$\gamma_{11} = \sum_{n=0}^{N-1} \cos^2(\omega_{k+1}(n)) \times \left[\sum_{m=0}^{M-1} h(m) \cdot \cos(\omega_{k+1}(m)) \right]^2$$

$$+ \sum_{n=0}^{N-1} \sin^2(\omega_{k+1}(n)) \times \left[\sum_{m=0}^{M-1} h(m) \cdot \sin(\omega_{k+1}(m)) \right]^2$$

$$+ \sum_{n=0}^{N-1} \cos(\omega_{k+1}(n)) \cdot \sin(\omega_{k+1}(n))$$
$$\times \left[\sum_{m=0}^{M-1} h(m) \cdot \cos(\omega_{k+1}(m))\right] \cdot \left[\sum_{m=0}^{M-1} h(m) \cdot \sin(\omega_{k+1}(m))\right]. \quad (16.41)$$

This can be expressed in terms of $E_k(m)$ and $H(m)$ by

$$\gamma_{11} = \sum_{n=0}^{N-1} \cos^2(\omega_{k+1}(n)) \cdot \mathrm{Re}(H(i))^2 + \sum_{n=0}^{N-1} \sin^2(\omega_{k+1}(n)) \cdot \mathrm{Im}(H(i))^2$$
$$- \sum_{n=0}^{N-1} \cos(\omega_{k+1}(n)) \cdot \sin(\omega_{k+1}(n)) \cdot \mathrm{Re}(H(i)) \cdot \mathrm{Im}(H(i)). \quad (16.42)$$

Similarly, the expression for γ_{22} from Equation (16.20) can be simplified:

$$\gamma_{22} = \sum_{n=0}^{N-1} \sin^2(\omega_{k+1}(n)) \times \left[\sum_{m=0}^{M-1} h(m) \cdot \cos(\omega_{k+1}(m))\right]^2$$
$$+ \sum_{n=0}^{N-1} \cos^2(\omega_{k+1}(n)) \times \left[\sum_{m=0}^{M-1} h(m) \cdot \sin(\omega_{k+1}(m))\right]^2$$
$$- \sum_{n=0}^{N-1} \cos(\omega_{k+1}(n)) \cdot \sin(\omega_{k+1}(n))$$
$$\times \left[\sum_{m=0}^{M-1} h(m) \cdot \cos(\omega_{k+1}(m))\right] \cdot \left[\sum_{m=0}^{M-1} h(m) \cdot \sin(\omega_{k+1}(m))\right] \quad (16.43)$$

which can be rewritten as

$$\gamma_{22} = \sum_{n=0}^{N-1} \sin^2(\omega_{k+1}(n)) \cdot \mathrm{Re}(H(i))^2 + \sum_{n=0}^{N-1} \cos^2(\omega_{k+1}(n)) \cdot \mathrm{Im}(H(i))^2$$
$$+ \sum_{n=0}^{N-1} \cos(\omega_{k+1}(n)) \cdot \sin(\omega_{k+1}(n)) \cdot \mathrm{Re}(H(i)) \cdot \mathrm{Im}(H(i)). \quad (16.44)$$

Finally, the expression γ_{12} from Equation (16.21) can be written as

$$\gamma_{12} = \sum_{n=0}^{N-1} \cos^2(\omega_{k+1}(n)) \cdot \mathrm{Re}(H(i)) \cdot \mathrm{Im}(H(i))$$
$$- \sum_{n=0}^{N-1} \sin^2(\omega_{k+1}(n)) \cdot \mathrm{Re}(H(i)) \cdot \mathrm{Im}(H(i))$$

$$+\sum_{n=0}^{N-1}\cos(\omega_{k+1}(n))\cdot\sin(\omega_{k+1}(n))\cdot\mathrm{Re}(H(i))^2$$
$$-\sum_{n=0}^{N-1}\cos(\omega_{k+1}(n))\cdot\sin(\omega_{k+1}(n))\cdot\mathrm{Im}(H(i))^2. \quad (16.45)$$

Equations (16.42), (16.44) and (16.45) contain summations involving only sin and cos functions. These functions can be rewritten using the following identities:

$$\sum_{n=0}^{N-1}\cos^2(\omega_{k+1}(n)) = \frac{1}{2}\sum_{n=0}^{N-1}\cos(2\omega_{k+1}(n)) + \frac{N}{2} \quad (16.46)$$

$$\sum_{n=0}^{N-1}\sin^2(\omega_{k+1}(n)) = \frac{N}{2} - \frac{1}{2}\sum_{n=0}^{N-1}\cos(2\omega_{k+1}(n)) \quad (16.47)$$

$$\sum_{n=0}^{N-1}\cos(\omega_{k+1}(n))\cdot\sin(\omega_{k+1}(n)) = \frac{1}{2}\sum_{n=0}^{N-1}\sin(2\omega_{k+1}(n)). \quad (16.48)$$

However, if it is taken into account that $\sum_{n=0}^{N-1}\sin(2\omega_{k+1}(n)) = 0$ for all ω_{k+1} (and also, that $\sum_{n=0}^{N-1}\cos(\omega_{k+1}(n)) = N$ when $\omega_{k+1} = 0$ and $\sum_{n=0}^{N-1}\cos(\omega_{k+1}(n)) = 0$ when $\omega_{k+1} \neq 0$), then Equations (16.42), (16.44) and (16.45) become

$$\gamma_{11} = \frac{N}{2}\,\mathrm{Re}(H(i))^2 + \frac{N}{2}\,\mathrm{Im}(H(i))^2 \quad (16.49)$$

$$\gamma_{22} = \frac{N}{2}\,\mathrm{Re}(H(i))^2 + \frac{N}{2}\,\mathrm{Im}(H(i))^2 \quad (16.50)$$

$$\gamma_{12} = 0. \quad (16.51)$$

The updated computational complexity of the AbS algorithm is given in Table 16.2, where the maximum complexity is the more realisable value of 24.2 MFLOPS.

Table 16.2: Computational complexity for error minimisation in the PWI-STC encoder.

Procedure	Pitch period = 20 number of harmonics = 10 (MFLOPS)	Pitch period = 147 number of harmonics = 80 (MFLOPS)
Calculate DFT of $h(n)$	0.23	0.23
Calculate DFT of $e(n)$	0.23	0.23
Calculate γ_{11}, γ_{22}, ψ_1,ψ_2	—	—
Updating $e^{k+1}(n)$	0.01	0.07
Total for each harmonic	0.24	0.30
Overall total	2.63	24.23

16.8 Quantising the Excitation Parameters

Following the calculation of the excitation parameters using AbS, an efficient means of encoding them for transmission to the decoder is required.

16.8.1 Encoding the Sinusoidal Amplitudes

In order to encode the sinusoidal amplitudes for transmission both VQ and SQ are considered. Initially VQ is examined by creating a constant length vector. SQ is also examined by dividing the amplitude parameters into frequency bands for quantisation.

16.8.1.1 Vector Quantisation of the Amplitudes

VQ [126] is the most efficient quantisation method, thus it is important to consider VQ for encoding the sinusoidal amplitudes. Ideally, in order to be able to encode the remaining signal efficiently, a constant length vector is required. Thus, for each frame the amplitude vectors have their frequency domain spacing or sampling rate adjusted, in order to produce 80 spectral lines per amplitude vector per frame. This sampling rate adjustment is performed using interpolation and decimation, where the interpolation procedure was described in Section 12.3.2.

16.8.1.2 Interpolation and Decimation

If the vector length conversion is to be performed for every possible vector size, assuming pitch period values between 54 and 400 Hz there can be between 10 and 80 harmonics with associated amplitude values, thus 70 different sampling rate changes must be considered. By zero-padding each amplitude vector to the next multiple of 5, the rational sampling rate conversions can be reduced to those given in Table 16.3. These sampling rate conversions were invoked with one-stage interpolation and one-stage decimation. A sinc resampling function, as described in Section 12.3.2 was employed for interpolation, with a 17th-order FIR low-pass filter used for decimation. Figure 16.9 shows the rational sampling rate conversion process using interpolation and decimation, with factors M and L yielding a sampling rate conversion factor of M/L.

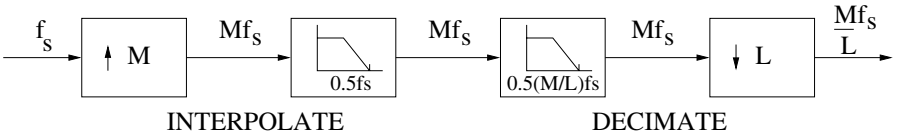

Figure 16.9: Schematic of the interpolation and decimation stages to perform a rational sampling rate conversion, which is illustrated in Figure 16.10.

In order to recover the original amplitude vectors the inverse rational sampling rate conversion was performed. Figure 16.10 displays an example of a rational sampling rate conversion for the amplitude vector. For the voiced speech frame, shown in Figure 16.10, a pitch period of 64 samples was selected, corresponding to a pitch-related amplitude spacing of 125 Hz and to an amplitude vector containing 32 elements. In Figure 16.10(a)

Table 16.3: The rational sampling rate conversion factors required to transform every amplitude vector to a length of 80 samples.

Amplitude vector length	Sampling rate conversion factor M/L
10	8
15	16/3
20	4
25	16/5
30	8/3
35	16/7
40	2
45	16/9
50	8/5
55	16/11
60	4/3
65	16/13
70	8/7
75	16/15

this amplitude vector has been zero-padded to contain 35 elements, thus a rational sampling rate conversion of 16/7 is performed. Figure 16.10(b) shows the interpolation by a factor of 16, with Figure 16.10(c) showing the decimation by a factor of 7, thus the amplitude vector now has 80 samples. The reverse sampling rate change is performed with a conversion ratio of 7/16, shown in Figures 16.10(d) and 16.10(e); finally, the first 32 elements are used for the amplitude vector.

With every speech frame having an amplitude spectrum containing 80 samples it is possible to implement more easily vector quantisation to encode each spectra.

16.8.1.3 Vector Quantisation

With the amplitude spectra at a constant vector length of 80 samples, VQ becomes relatively easy. Before the sinusoidal amplitude spectra are vector quantised they are normalised by the RMS energy, which is then scalar quantised using the Lloyd–Max algorithm described in Section 12.4.

The VQ was performed using a combination of the generalised Lloyd algorithm and a pairwise nearest neighbour (PNN) design, where the reader is referred to the monograph by Gersho and Gray [126] for further details on VQ. Briefly, the generalised Lloyd algorithm starts with an initial codebook, which is used to encode a set of training data. For the STC implementation the employed quantisation distortion measure is

$$d(x, y) = \|x - y\|^2 = \sum_{i=1}^{k} (x_i - y_i)^2 \tag{16.52}$$

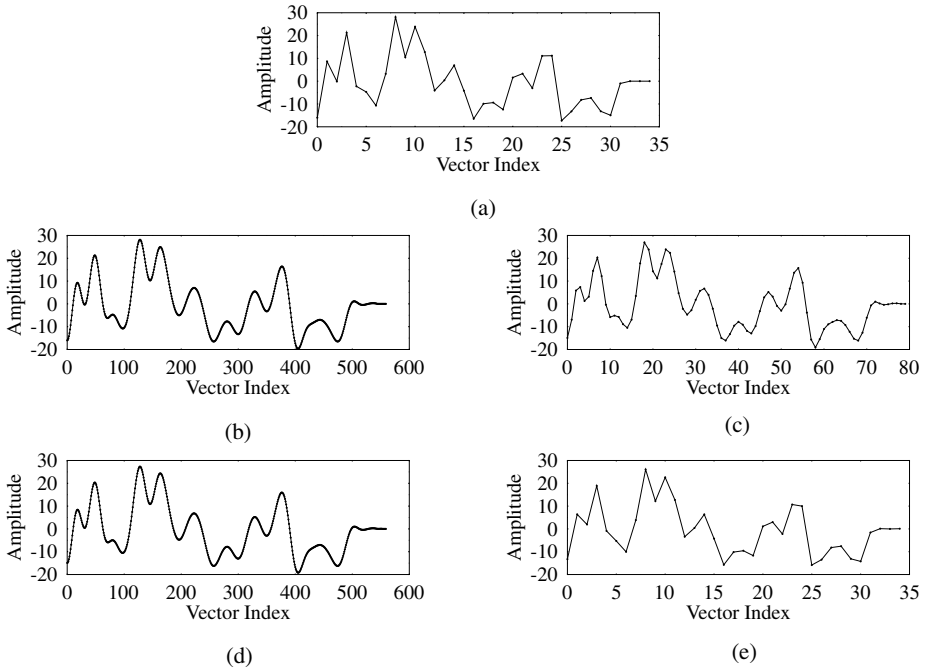

Figure 16.10: An example of a $16/7$ sampling rate conversion for the speaker AM2, from the front vowel utterance /æ/ in 'b*a*ck', where this utterance has a pitch period of 64 samples, corresponding to a pitch-related amplitude spacing of 125 Hz: (a) the amplitude vectors zero padded to 35 samples; (b) and (c) the 16/7 sampling rate conversion to produce vectors of 80 samples; (d) and (e) the 7/16 inverse sampling rate conversion to reproduce the original vector.

where x is the training vector, y is the codebook entry and k is the number of elements, or vector components, in the vector. The codebook entry, constituting the centroid of a cell, which has the lowest distortion when quantising the training vector is selected to host the training vector concerned. Once all of the training vectors have been assigned to a codebook entry every cell has its centroid recalculated on the basis of the entries in its cell, where the centroid of the cell is the codebook entry. The centroid is found using

$$Y_j = \frac{M^{-1} \sum_{i=1}^{M} x_i S_j(x_i)}{M^{-1} \sum_{i=1}^{M} S_j(x_i)}, \quad \text{for } j = 1, 2, \ldots, N \tag{16.53}$$

where M is the training set size, N is the codebook size, x_i is the training vector and $S_j(x_i)$ is a selector which indicates whether $x_i \in S_j$.

The training data set is subsequently passed through the new codebook assigning all entries to the newly computed cells, after which the new codebook centroids are again recalculated. This iterative process is continued until the optimum codebook, for the training data set, is found.

In order to create the initial codebook for the generalised Lloyd algorithm, the PNN algorithm was used [126]. The PNN algorithm commences with an M-sized codebook, where every training vector is a codebook entry, subsequently codebook entries are merged, until a codebook of the required size N is obtained. The cell merging is performed by considering the overall distortion increase upon tentatively merging every cell with every other cell, in order to find the pair inflicting the lowest overall distortion. Thus, at each iteration of the PNN algorithm the codebook size decreases by 1.

16.8.1.4 Vector Quantisation Performance

The amplitude vector describing the spectral envelope of the pitch spaced harmonics was divided into four separate vectors for quantisation, with each vector containing 20 samples. The process for the VQ of the amplitude is shown in Figure 16.11, where more efficient quantisation is achieved by normalising the amplitude vector by its RMS energy before being placed in the VQ codebook.

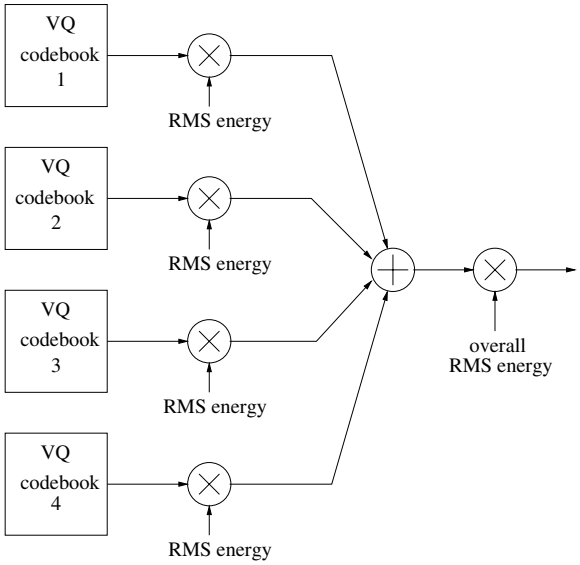

Figure 16.11: Schematic of VQ for the amplitude vector.

To demonstrate the suitability of the amplitude vector for quantisation, Figure 16.12 shows the PDF of the amplitudes. In Figure 16.12 the sharp peak at zero is caused by zero-padding employed in the interpolation process, as described in Section 16.8.1.2. The individual elements of the amplitude vector have their PDFs given in Appendix C which show that the PDFs of the individual elements also support quantisation.

The performance of the VQ was considered using four 8-bit vector quantisers, together with a 5-bit scalar quantiser for the overall RMS energy and 2-bit scalar quantisers for the codebook RMS energies, requiring a bitrate of 45 bits/20 ms or 2.25 kbps. VQ produced a SEGSNR measure of 10.54 dB, however, the interpolation and decimation process required to produce a constant length vector requires a computational complexity of 6.7 MFLOPS.

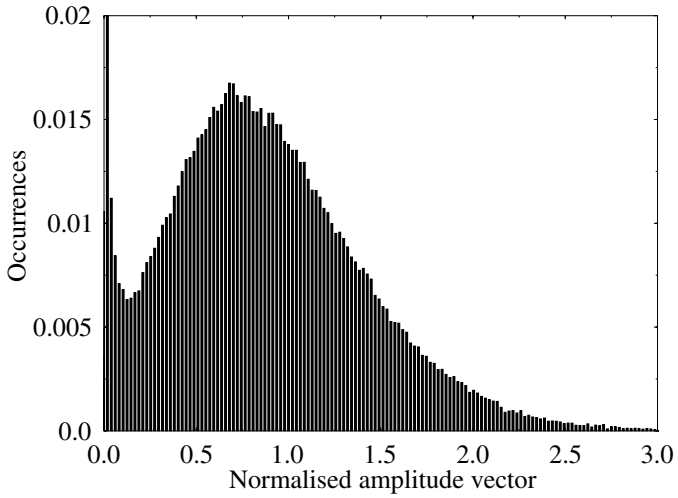

Figure 16.12: The combined PDF for the normalised amplitude vector.

16.8.1.5 Scalar Quantisation of the Amplitudes

An alternative to VQ is to employ SQ in order to encode the sinusoidal amplitudes. For the VQ the amplitude vector was expanded to always contain 80 values, with every element represented in the VQ. However, for SQ the number of transmitted amplitude values is predetermined as M, with the pitch-spaced amplitude elements divided between the M bands. Each of the M bands is assigned to have the RMS energy of its constituent amplitude elements.

Restating Equation (15.7), from the MMBE speech coder of Chapter 15, the number of pitch spaced spectral amplitude elements in each band is given by

$$N_n = \frac{f_s/2}{M \cdot F0} \tag{16.54}$$

where f_s is the sampling frequency, $F0$ is the fundamental frequency, M is the number of spectral amplitude bands in which the transmitted amplitude values are assumed to be identical and N_n is the number of amplitude elements in each of the M bands.

Similarly to the VQ method, the SQ process starts by quantising the overall full-band RMS value with five bits. Subsequently, each of the M transmitted amplitude parameters is assigned a value, determined as the average normalised RMS energy level of its N_n number of constituent amplitude elements. Each of the M transmitted amplitude parameters are quantised with two bits. The performance of the SQ was considered with $M = 20$ transmitted amplitude parameters, thus, with the overall RMS parameter a total of 45 bits/20 ms or 2.25 kbps is required for transmission. The scalar quantiser produced a SEGSNR value of 5.18 dB for this spectral magnitude parameter, with a negligible computational complexity.

Sections 16.8.1.1 and 16.8.1.5 show that VQ performs better than SQ at encoding the amplitude parameters, however, they also show the significant increase in computational complexity required. Table 16.2 demonstrates that the PWI-STC speech coder is already

fairly complex, where the implementation of a vector quantiser would increase the computational complexity to higher than 30 MFLOPS. Hence, due to computational complexity requirements the scalar quantiser was selected to encode the sinusoidal amplitude parameters.

16.8.2 Encoding the Sinusoidal Phases

16.8.2.1 Vector Quantisation of the Phases

It was anticipated that the phase values could be quantised in a similar manner to the amplitude values, as was shown in Figure 16.11. Figure 16.13 displays the PDF of the phase values. From our detailed investigations we concluded that, in contrast to the pitch-related spectral amplitude values, the phase values are not amenable to VQ.

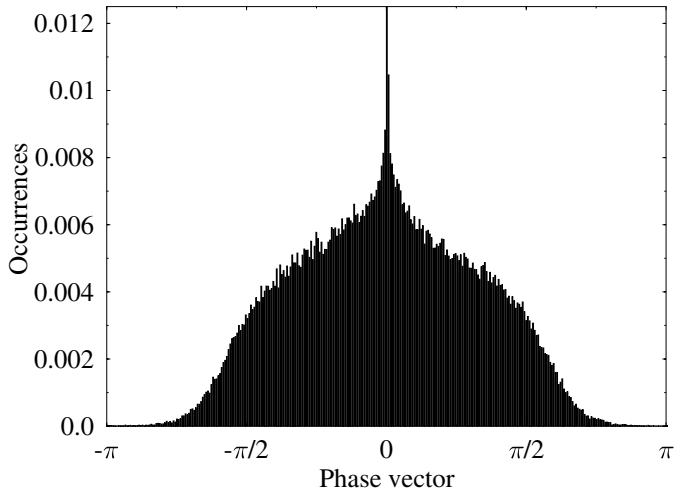

Figure 16.13: The combined PDF for the normalised phase vector.

16.8.2.2 Encoding the Phases with a Voiced–unvoiced Switch

The traditional method for representing sinusoidal phases is to classify them as either voiced or unvoiced [548, 549], while ignoring their exact phase values. This can be justified on the basis of the knowledge that voiced phases can be represented by 0, while unvoiced phases can be represented by a uniformly distribution over the range $-\pi$ to π.

McAulay and Quatieri [548] adopted the approach of Makhoul *et al.* [491] where a voicing transition frequency was determined. Beneath the voicing transition frequency the phases are assumed voiced, while above this frequency the phases are considered unvoiced. The decision whether a harmonic is voiced or unvoiced is typically determined by the closeness of fit between a purely voiced magnitude spectrum and the original magnitude. McAulay *et al.* [548, 549] based this measure on the speech spectrum itself, however, because we determine the component frequencies, amplitude and phases of the LPC residual

spectrum, rather than those of the speech signal, this is the most appropriate signal to employ when assessing voicing characteristics.

The extent of voicing present in each harmonic was determined using the LPC residual spectrum and the SNR applied to quantify the match between the residual and synthetic, fully voiced LPC STP residual, as suggested by McAulay *et al.* [548, 549], which is given by

$$\mathrm{SNR} = 10 \log \frac{A_{\mathrm{orig}}(k\omega_0)^2}{[A_{\mathrm{synth}}(k\omega_0) - A_{\mathrm{orig}}(k\omega_0)]^2} \tag{16.55}$$

where A_{orig} refers to the original LPC residual magnitude spectrum, A_{synth} refers to a fully voiced magnitude spectrum and $k\omega_0$ is the kth harmonic of the determined normalised fundamental frequency ω_0.

We concluded experimentally that 30 dB represented a good voiced/unvoiced threshold for each harmonic, with values above the threshold declared voiced. Following the categorisation of the harmonics, the voicing transition frequency must be determined. This process examined the voiced–unvoiced state of each harmonic, where if more than two consecutive low SNR harmonics were located, which were deemed unvoiced, the rest of the harmonics were also assumed unvoiced, otherwise all harmonics were assumed voiced. Hence, a voicing transition harmonic parameter was transmitted to the decoder, which when combined with the transmitted pitch period indicates the voicing transition frequency above which the LPC STP residual was deemed unvoiced. With a 54 Hz fundamental frequency a permissible maximum of 80 harmonics exist in the 4 kHz, thus, seven bits will be required to transmit the voicing transition harmonic parameter.

16.8.3 Encoding the Sinusoidal Fourier Coefficients

In this section an alternative set of parameters to the amplitude and phase values are considered for transmission. The AbS approach of Section 16.7.2 operates by determining the values a_{k+1} and b_{k+1}, from Equations (16.27) and (16.28), from which the amplitude and phase values are found using $A_{k+1} = \sqrt{a_{k+1}^2 + b_{k+1}^2}$ and $\phi_{k+1} = -\arctan(b_{k+1}/a_{k+1})$. Thus, the a_{k+1} and b_{k+1} parameters are the real and imaginary Fourier coefficients, which can be encoded for transmission to the decoder as an alternative to the amplitude and phase values. The a_{k+1} and b_{k+1} values can be scalar quantised in the same manner as the amplitude value, as described in Section 16.8.1.5. The a_{k+1} and b_{k+1} parameters have their overall RMS values scalar quantised with five bits and then the normalised values are divided into 10 frequency bands, each encoded with two bits producing an overall bitrate of 50 bits/20 ms or 2.5 kbps.

16.8.3.1 Equivalent Rectangular Bandwidth Scale

The SQ of the amplitude parameter divided the amplitude values into frequency bands, with Equation (16.54) employed for this purpose. However, this equation ignores the information that, for human hearing, lower frequencies are perceptually more important. The Equivalent Rectangular Bandwidth (ERB) scale [556] weights the frequency spectrum in order to place more emphasis on the perceptually more important lower frequencies. Thus, it can

be employed in the PWI-STC coder to produce a better SQ of the Fourier coefficients a_{k+1} and b_{k+1} of Equations (16.27) and (16.28).

The conversion between the frequency spectrum and the transformed ERB scale is given by [556]:

$$f_{\mathrm{ERB}} = 11.17 \times \ln\left(\frac{f + 312}{f + 14675}\right) + 43.0 \tag{16.56}$$

where f_{ERB} represents the ERB frequency scale and f is the conventional frequency spectrum.

Figure 16.14 displays the relationship between the ERB scale and frequency over 0–4 kHz. In order to divide the Fourier coefficients into M bands, the harmonic frequencies and the corresponding Fourier coefficients are converted to the ERB scale. In the ERB scale domain the transformed frequencies are divided into M bands using Equation (15.7). Each of these M bands is then assigned a value determined as the average normalised RMS energy of its N_n constituent Fourier coefficients. In the frequency domain the M bands will be perceptually weighted.

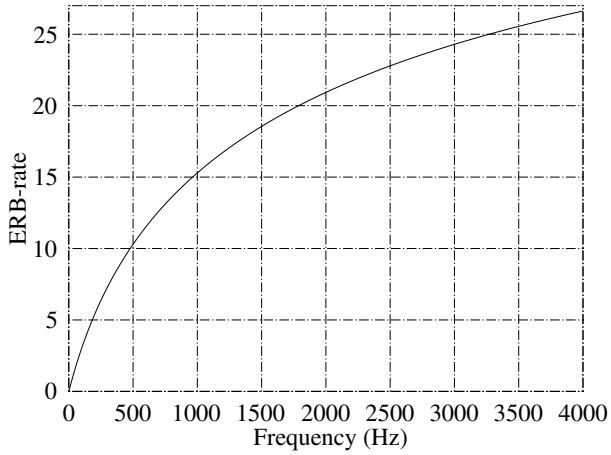

Figure 16.14: Conversion between the ERB scale and frequency bandwidth according to Equation (16.56).

In our final coder the Fourier coefficients of Equations (16.27) and (16.28) were selected for transmission to the decoder instead of the magnitude and phase parameters. This choice was primarily due to problems in determining the correct frequency point, detailed in Section 16.8.2.2, for switching from voiced to unvoiced speech in the process of coding the phases of the harmonics.

16.8.4 Voiced–unvoiced Flag

It was found that both the Fourier coefficients of Equations (16.27) and (16.28) and the amplitude and phase parameters produced too dominant voiced excitation during the unvoiced portions of speech. For the Fourier coefficients this extra periodicity was caused

by the grouping of parameters into frequency bands, removing too much of the phase signal's randomness.

In order to overcome this problem the voiced–unvoiced decision of Section 13.4 was employed to set a voiced–unvoiced flag. At the decoder, if this flag was set to indicate a voiced frame the Fourier coefficients of Equations (16.27) and (16.28) were used to determine the sinusoidal phases with $-\arctan(b_{k+1}/a_{k+1})$. However, if an unvoiced frame was indicated the sinusoidal phases were uniformly distributed over $-\pi$ to π.

16.9 Sinusoidal Transform Decoder

The schematic of the STC decoder is shown in Figure 16.15, where the frequencies, amplitudes and phases are determined from the transmitted parameters in order to reconstruct the residual waveform. The synthesised excitation is passed through a LPC synthesis filter together with the adaptive postfilter and pulse dispersion filter for reproducing the speech waveform.

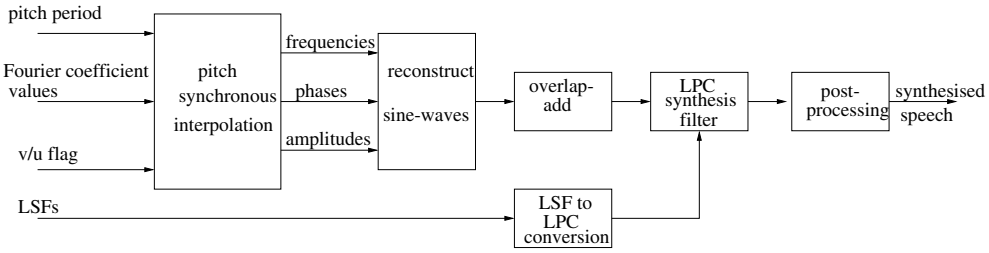

Figure 16.15: Schematic for the STC-PWI decoder.

The amplitudes are reconstructed using the transmitted quantised RMS values for the Fourier coefficients and the relationship $A_{k+1} = \sqrt{a_{k+1}^2 + b_{k+1}^2}$. For frames labelled voiced the phases are reconstructed using $-\arctan(b_{k+1}/a_{k+1})$, while for unvoiced frames the phases are set to random values uniformly distributed over $-\pi$ to π. The sinusoidal frequencies are reconstructed using the transmitted pitch period in order to determine the pitch spaced excitation harmonics. These component frequencies, amplitudes and phases are employed to reconstruct the residual waveform.

To compensate for the long analysis window of 20 ms, interpolation can be performed on a pitch synchronous basis, similarly to Chapter 14, for producing a smoothly evolving waveform. Similarly to the PWI-ZFE speech coder and MMBE speech coders, the interpolated excitation waveform can be passed through the LPC synthesis filter, adaptive postfilter, and pulse dispersion filter to reproduce the speech waveform.

Following this overview of the STC decoder, below we concentrate on the pitch synchronous interpolation which is performed in the schematic of Figure 16.15.

16.9.1 Pitch Synchronous Interpolation

Performing pitch synchronous interpolation at the decoder allows the developed STC coder to be viewed as a PWI-STC coder, because a PWI scheme has been adopted where the excitation is implemented using STC.

With a link to PWI coders established, the interpolation process can closely follow Section 14.6. The LSFs and pitch period parameter can be interpolated as described in Sections 14.6.6 and 14.6.1, respectively. The prototype segment's zero crossing parameter is set to zero, because the Fourier coefficient parameters contain the phase information for the prototype segment. The interpolation of the sinusoidal excitation parameters is described in detail next.

16.9.1.1 Fourier Coefficient Interpolation

The overall RMS value for the Fourier coefficient parameters can be linearly interpolated across consecutive pitch duration segments using:

$$O_{\mathrm{RMS},n_p} = O_{\mathrm{RMS}}(N-1) + (n_p - 1) \cdot \frac{O_{\mathrm{RMS}}(N) - O_{\mathrm{RMS}}(N-1)}{N_{\mathrm{pit}} - 1} \tag{16.57}$$

where $O_{\mathrm{RMS}}(N)$ is the overall RMS value of the current frame, $O_{\mathrm{RMS}}(N-1)$ is the overall RMS value of the previous frame, O_{RMS,n_p} is the overall RMS value of the n_pth interpolation segment and N_{pit} is the number of pitch synchronous intervals between $O_{\mathrm{RMS}}(N)$ and $O_{\mathrm{RMS}}(N-1)$.

In addition, the RMS value for each of the M number of frequency sub-bands must also be linearly interpolated, using:

$$\mathrm{RMS}_{m,n_p} = \mathrm{RMS}_m(N-1) + (n_p - 1) \cdot \frac{\mathrm{RMS}_m(N) - \mathrm{RMS}_m(N-1)}{N_{\mathrm{pit}} - 1} \tag{16.58}$$

where $\mathrm{RMS}_m(N-1)$ is the previous RMS value of the mth sub-band, while $\mathrm{RMS}_m(N)$ is the current mth RMS value.

16.9.2 Frequency Interpolation

The frequencies of the component sine waves are the harmonics of the fundamental frequency determined at the encoder, which is transmitted as the pitch period. Thus, interpolated frequencies are generated for each interpolation region by using the harmonics of the interpolated fundamental frequency.

16.9.3 Computational Complexity

The computational complexity of the PWI-STC decoder is dominated by the sinusoidal synthesis process described by Equation (16.6), where the transmitted Fourier coefficients have been converted into amplitude and phase parameters. Previously, in Section 16.3, it was detailed that both the present and past sinusoidal parameters were used to reconstruct the speech waveform, with a trapezoidal window used to weight the contribution of the

sinusoidal parameters from each frame. The computational complexity of the sinusoidal synthesis process is dependent on the number of harmonics to be summed, where the number of harmonics can vary from 10 to 80. For a sinusoidal synthesis process that is constructed over two frame lengths or 40 ms, and which contains 10 harmonics, the complexity is 1.8 MFLOPS. For a sinusoidal synthesis process that includes 80 harmonics the computational complexity is 14.1 MFLOPS.

The pitch synchronous procedure implemented in the decoder, following the philosophy of Section 16.3.2, further increases this complexity, because the sinusoidal process must be performed for every interpolation region. For a sinusoidal process having a pitch period of 20 samples, or 400 Hz, with 10 harmonics in the 4 kHz band up to eight 20 sample interpolation regions could be present within a 160 sample speech frame of 20 ms, producing a computational complexity of 14.4 MFLOPS. If 80 harmonics are employed in the sinusoidal synthesis process only one interpolation region will occur within the speech frame.

The computational complexity of the PWI-STC decoder can be decreased by replacing the sinusoidal synthesis of Equation (16.6) by the inverse FFT. The inverse FFT process has a computational complexity of $N \log_2 N$, where N is the FFT length, in this case 512 samples. Thus, the associated computational complexity, using the FFT-based interpolation, for any number of harmonics will be 0.23 MFLOPS. If eight interpolation regions are present within the 20 ms speech frame then the computational complexity will be 1.84 MFLOPS.

16.10 Speech Coder Performance

Initially, the performance of a PWI-STC speech coder at 3.8 kbps was assessed, where the Fourier coefficients were divided into 10 bands for SQ and transmission to the decoder. In Chapters 14 and 15, initially a lower rate speech coder was developed, before increasing the bitrate of the speech coder to 3.8 kbps. In both of these chapters the increased bitrate did not correspond to a sufficient increase in speech quality in order to justify the added complexity and increased bitrate. By contrast here, initially a higher bitrate speech coder is developed and then its bitrate is decreased to 2.4 kbps. For the 10-band PWI-STC speech coder the adaptive postfilter parameters, described in Section 12.6, were optimised to $\alpha_{\rm pf} = 0.85$, $\beta_{\rm pf} = 0.50$, $\mu_{\rm pf} = 0.50$, $\gamma_{\rm pf} = 0.50$, $g_{\rm pf} = 0.00$ and $\xi_{\rm pf} = 0.99$.

For examining the PWI-STC speech coder's performance the speech frames used to assess the previously developed speech coders were adopted. Thus, Figures 16.16, 16.17 and 16.18 can be compared with the other 3.8 kbps speech coders demonstrated in Figures 14.20, 14.21 and 14.22 for the PWI-ZFE scheme of Section 14.11.2 together with Figures 15.23, Figure 15.24 and Figure 15.25 for the MMBE-ZFE scheme of Section 15.7.

Figure 16.16 displays the results for the 10-band PWI-STC speech coder for an utterance from the testfile BM1, which can be compared with the similar bitrate speech coders of Figures 14.20 and 15.23. From Figure 16.16(b) it can be seen that, unlike in Figure 14.20(b), the reconstructed excitation has the correct pitch period. In the frequency domain the excitation spectrum follows the shape of the formants and slightly emphasises the higher frequencies. For the time-domain synthesised speech of Figure 16.16(c) it can be seen that the decay between pitch periods is more pronounced than for Figure 15.23(c), however, in the frequency domain the PWI-STC speech coder better represents the formants than the MMBE-ZFE scheme of Figure 15.23(c).

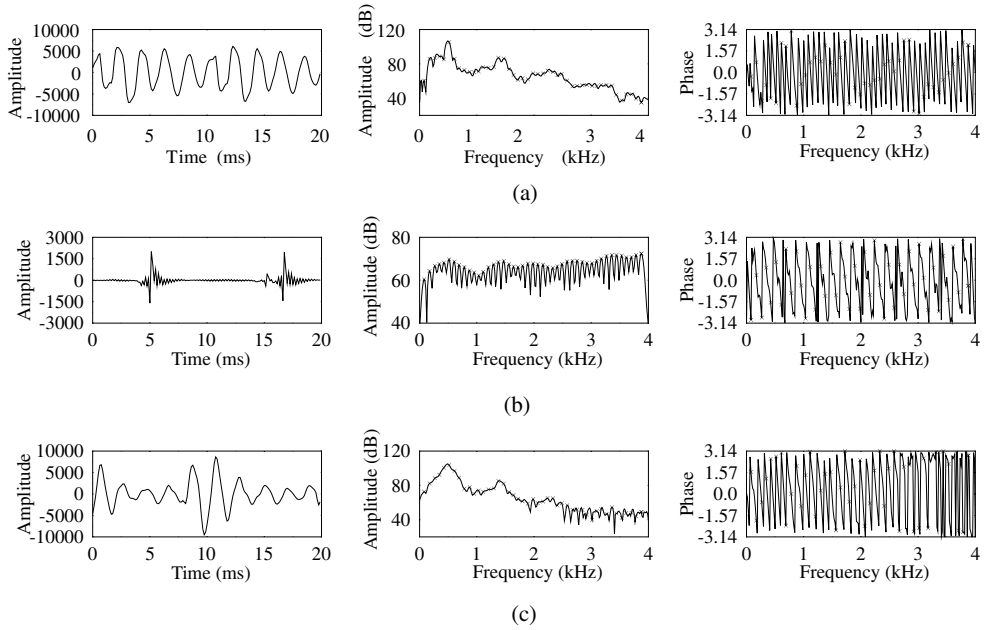

Figure 16.16: Comparison of the time and frequency domains of (a) the original speech, (b) the 10-band PWI-STC waveform and (c) the output speech after the pulse dispersion filter. The 20 ms speech frame is the mid vowel /ɜ/ in the utterance 'w*or*k' for the testfile BM1. For comparison with the other coders developed in this study using the same speech segment, please refer to Table 17.2.

Figure 16.17 portrays a 10-band PWI-STC speech coder from the testfile BF2, which can be compared with Figures 14.21 and 15.24 for the PWI-ZFE and MMBE speech coders, respectively. From Figure 16.17(b) it can be seen that the time-domain excitation is dominated by pulses, while in the frequency domain the magnitude spectrum is flat. Figure 16.17(c) shows that the PWI-STC speech coder manages to reproduce both the time- and frequency-domain waveforms more accurately than either Figure 14.21(c) or 15.24(c).

Figure 16.18 displays the results for a speech frame from the testfile BM2 using the 10-band PWI-STC speech coder, here comparisons can be drawn with Figures 14.22 and 15.25. It should be noted that for this speech frame the LPC coefficients fail to represent the second and third formants. Figure 16.18(b) shows that the reconstructed excitation attempts to compensate for this by shaping the magnitude spectrum to follow the speech formants. Although this effect is insufficient to reproduce the missing formants in the synthesised speech spectrum of Figure 16.18(c), the shape of the first formant is better represented than in Figures 14.22(c) and 15.25(c).

The bit allocation for the 3.8 kbps PWI-STC speech coder is summarised in Table 16.4. The LPC coefficients are transformed to LSFs and quantised using 18 bits [147]. The frequencies of the component sine waves are set to be the harmonics of the fundamental frequency, which are determined from the pitch period that is transmitted to the decoder employing seven bits. The sinusoidal parameters are represented by the 10 Fourier coefficients

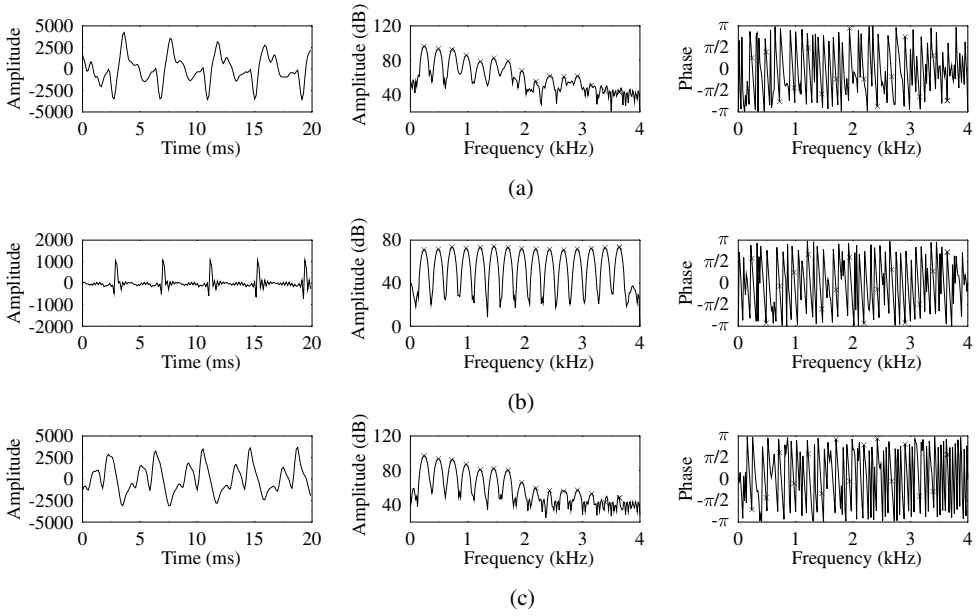

Figure 16.17: Comparison of the time and frequency domains of (a) the original speech, (b) the 10-band PWI-STC waveform and (c) the output speech after the pulse dispersion filter. The 20 ms speech frame is the liquid /r/ in the utterance '*r*ice' for the testfile BF2. For comparison with the other coders developed in this study using the same speech segment, please refer to Table 17.2.

Table 16.4: Bit allocation table for the investigated PWI-STC coders at 3.8 and 2.4 kbps.

Parameter	Required bits	
LPC coefficients	18	18
Pitch period	7	7
Voiced–unvoiced switch	1	1
Overall RMS for a_k	5	5
Overall RMS for b_k	5	5
a_k bands	10×2	3×2
b_k bands	10×2	3×2
Total (20 ms)	76	48
Bitrate (kbps)	3.8	2.4

a_k and b_k, with the overall RMS of both the a_k and b_k Fourier coefficients scalar quantised using five bits. The a_k and b_k parameters are converted into the ERB scale before being split into 10 evenly spaced bands each. The average RMS value for each of these 10 bands is scalar quantised with two bits. A voiced–unvoiced flag is also sent to allow random phases to be applied for unvoiced frames.

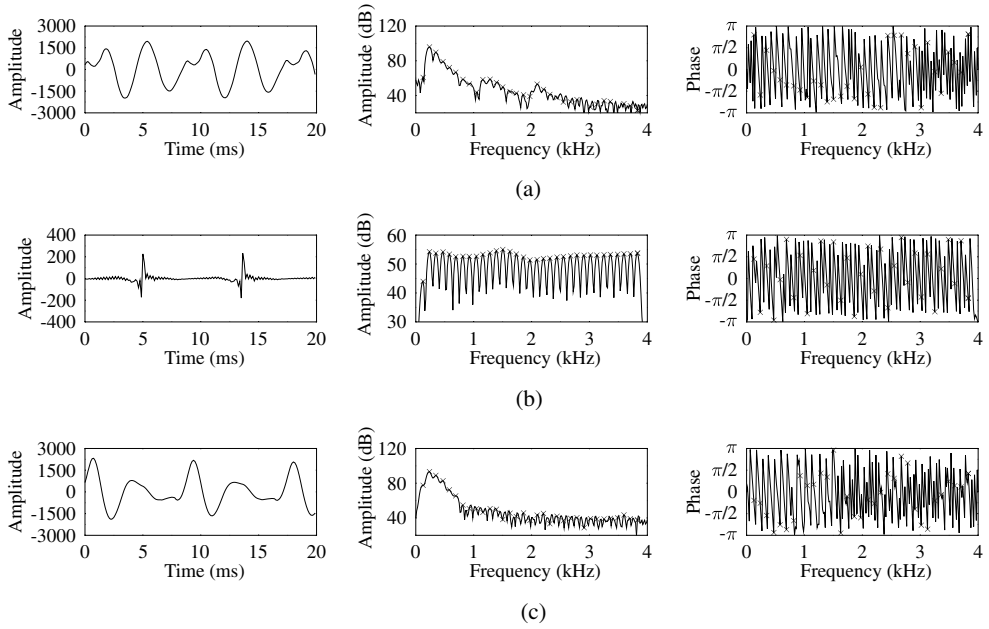

Figure 16.18: Comparison of the time and frequency domains of (a) the original speech, (b) the 10-band PWI-STC waveform and (c) the output speech after the pulse dispersion filter. The 20 ms speech frame is the nasal /n/ in the utterance 'throw*n*' for the testfile BM2. For comparison with the other coders developed in this study using the same speech segment, please refer to Table 17.2.

Pairwise-comparison tests, detailed in Section 17.2, were conducted between the 3.8 kbps 10-band PWI-STC speech coder and the 3.85 kbps 13-band MMBE PWI-ZFE speech coder together with the 3.8 kbps three-pulse PWI-ZFE scheme, where the comparison speech coders were developed in Chapters 15 and 14, respectively. For the 3.8 kbps 10-band PWI-STC speech coder and the 3.85 kbps 13-band MMBE PWI-ZFE speech coder, these pairwise-comparison tests showed that 7.69% of listeners preferred the 10-band PWI-STC speech coder, with 30.77% of listeners preferring the 13-band MMBE PWI-ZFE scheme and 61.54% having no preference. For the 3.8 kbps 10-band PWI-STC speech coder and the 3.8 kbps three-pulse PWI-ZFE speech coder, these pairwise-comparison tests showed that 17.95% of listeners preferred the 10-band PWI-STC speech coder, with 53.85% of listeners preferring the three-pulse PWI-ZFE scheme and 28.20% having no preference. Thus, the 3.8 kbps 10-band PWI-STC speech coder does not perform as well as the speech coders previously developed.

The 10-band PWI-STC speech coder was also adjusted in order to produce a lower rate speech coder at 2.4 kbps, expecting that the corresponding reduction in speech quality will not be dramatic. The 2.4 kbps PWI-STC speech coder contained three frequency bands. The parameters from the adaptive postfilter of Section 12.6 were re-optimised to $\alpha_{\rm pf} = 0.80$, $\beta_{\rm pf} = 0.45$, $\mu_{\rm pf} = 0.50$, $\gamma_{\rm pf} = 0.50$, $g_{\rm pf} = 0.00$ and $\xi_{\rm pf} = 0.99$. The results for the same speech frames as in Figures 16.16, 16.17 and 16.18 are given in Figures 16.19, 16.20 and

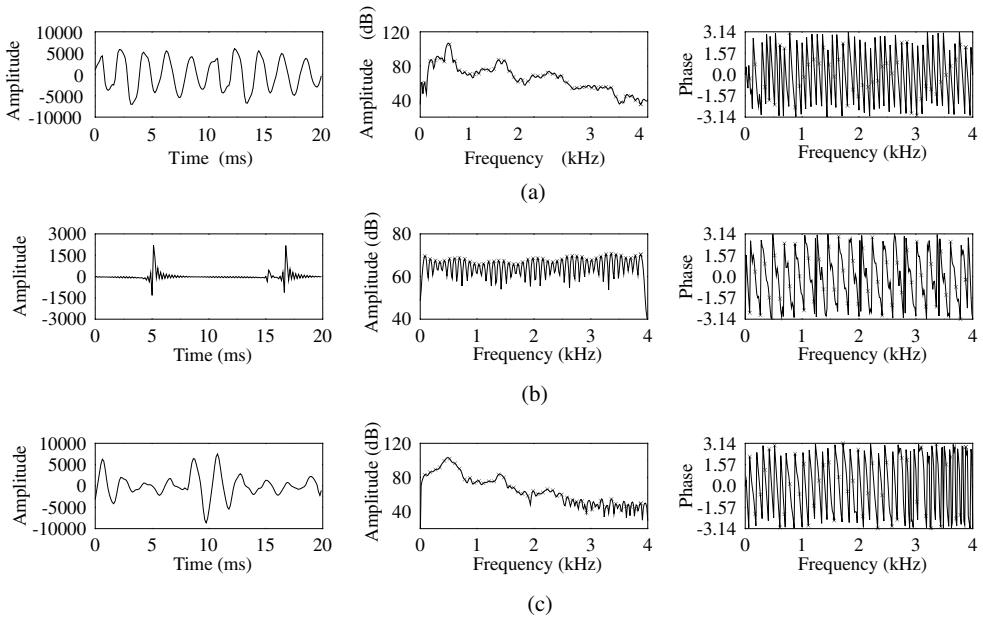

Figure 16.19: Comparison of the time and frequency domains of (a) the original speech, (b) the three-band PWI-STC waveform and (c) the output speech after the pulse dispersion filter. The 20 ms speech frame is the mid vowel /ɜ:/ in the utterance 'w*or*k' for the testfile BM1. For comparison with the other coders developed in this study using the same speech segment, please refer to Table 17.2.

16.21. These figures can also be compared with the two previously developed speech coders at 2.35 kbps, namely the five-band MMBE speech coders employing simple pulse excitation and the three-band MMBE speech coder incorporating ZFE to represent the voiced speech. The results for these speech coders were given in Figures 15.17, 15.18 and 15.19 together with Figures 15.20, 15.21 and 15.22, respectively.

Figure 16.19 displays the results for the three-band PWI-STC speech coder for an utterance from the testfile BM1, which can be compared with Figures 15.17 and 15.20 generated at similar rates. In addition, Figure 16.19 can be contrasted with the 10-band PWI-STC speech coder of Figure 16.16. The reduction to three frequency bands produces a flatter excitation spectrum and decreases the depth of the null between the first and second formants. When Figure 16.19(c) is compared with Figures 15.17(c) and 15.20(c), it can be seen that the three-band PWI-STC speech coder has a synthesised frequency spectrum which better represents the original spectrum.

Figure 16.20 portrays the results for a segment of speech from the testfile BF2, where the speech frame was also examined in Figures 15.18 and 15.21. Figure 16.20 related to the three-band PWI-STC speech coder can also be compared with Figure 16.17, where the reduction in the number of frequency bands decreases the amplitude of the first resonance in each pitch period. When compared with Figures 15.18 and 15.21, the performance of the three-band PWI-STC speech coder is deemed similar.

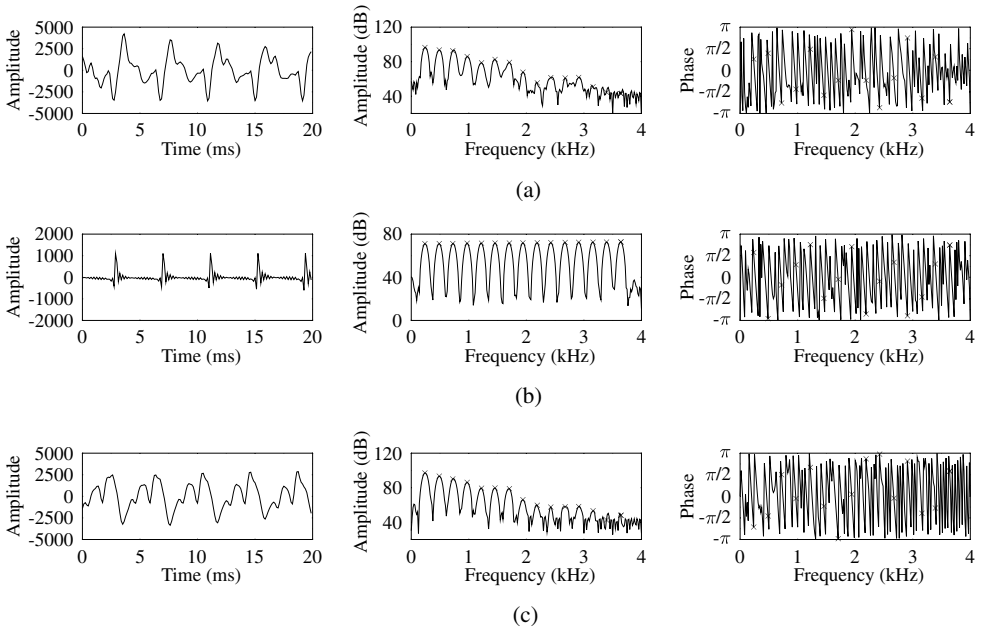

Figure 16.20: Comparison of the time and frequency domains of (a) the original speech, (b) the three-band PWI-STC waveform and (c) the output speech after the pulse dispersion filter. The 20 ms speech frame is the liquid /r/ in the utterance '*r*ice' for the testfile BF2. For comparison with the other coders developed in this study using the same speech segment, please refer to Table 17.2.

Figure 16.21 displays the performance of the three-band PWI-STC speech coder for the testfile BM2 and can be compared with the 10-band PWI-STC speech coder of Figure 16.18. It can be seen from Figure 16.21(b) that the reduction in the number of frequency bands produces an excitation spectrum which places more emphasis on the lower frequencies. This results in a larger amplitude for the dominant time-domain resonance within the pitch period. The three-band PWI-STC speech coder can also be contrasted with the five-band MMBE speech coder and the three-band MMBE-ZFE speech coder of Figures 15.19 and 15.22, respectively. It can be seen from Figure 16.21(c) that the PWI-STC speech coder produces a more dominant first formant and a larger time-domain resonance.

The 2.4 kbps PWI-STC speech coder contained only three different frequency bands, otherwise it was identical to the 10-band PWI-STC speech coder. The bit allocation can be seen in Table 16.4.

Pairwise-comparison tests, detailed in Section 17.2, were conducted between the 2.4 kbps three-band PWI-STC speech coder and the 2.35 kbps three-band MMBE PWI-ZFE speech coder together with the 2.3 kbps five-band MMBE LPC scheme, where both speech coders were developed in Chapter 15. For the 2.4 kbps three-band PWI-STC speech coder and the 2.35 kbps three-band MMBE PWI-ZFE speech coder, these pairwise-comparison tests showed that 20.51% of listeners preferred the three-band PWI-STC speech coder, with 12.82% of listeners preferring the three-band MMBE PWI-ZFE scheme and 66.67% having no preference. For the 2.4 kbps three-band PWI-STC speech coder and the 2.3 kbps

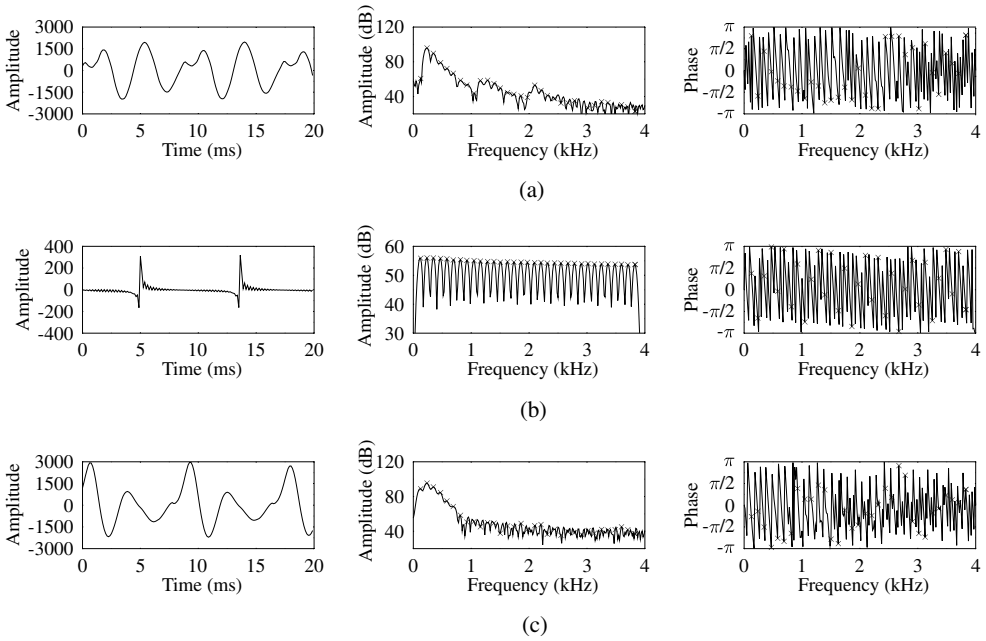

Figure 16.21: Comparison of the time and frequency domains of (a) the original speech, (b) the three-band PWI-STC waveform and (c) the output speech after the pulse dispersion filter. The 20 ms speech frame is the nasal /n/ in the utterance 'thrown' for the testfile BM2. For comparison with the other coders developed in this study using the same speech segment, please refer to Table 17.2.

five-band MMBE LPC speech coder, these pairwise-comparison tests showed that 10.26% of listeners preferred the three-band PWI-STC speech coder, with 30.77% of listeners preferring the three-band MMBE PWI-ZFE scheme and 58.97% having no preference. These listening tests show that it was difficult to determine a preference for the speech coders developed at approximately 2.4 kbps.

16.11 Chapter Summary

In this chapter we have described STC which has recently been advocated for low-bitrate speech coding for example, by McAulay and Quatieri [543]. The chapter began with a description of the STC coding algorithm developed by McAulay and Quatieri [548]. This chapter further develops STC by incorporating the PWI philosophy in order to reduce the required bitrate. Instead of the determination of the sinusoidal parameters by peak-picking the AbS technique introduced by George and Smith was employed [545, 546]. The error minimisation process was modified in order to reduce the computational complexity of the AbS procedure. The located sinusoidal parameters were transmitted to the decoder as Fourier coefficients. At the decoder pitch synchronous interpolation was performed in order to improve the synthesised speech quality with the inverse FFT harnessed for decreasing the computational complexity of the sinusoidal synthesis process.

Chapter 17

Conclusions on Low-rate Coding

17.1 Summary

This chapter commences with an overview of the different speech codecs developed throughout the low-bitrate coding-oriented part of the book, namely in Part IV. For each speech codec the bitrate, delay and complexity are given. Following the speech codec summary, the details of the conducted informal listening tests are given, thus, assessing the quality of each speech coder. The robustness of the speech codec was only investigated for the 1.9 kbps PWI-ZFE speech coder, where the details are given in Section 14.10.

Table 17.1: Summary of the bitrate, delay and computational complexity for the developed speech codecs.

Speech codec	Bitrate (kbps)	Delay (ms)	Complexity (MFLOPS)
LPC vocoder, C1	1.55	60	3.4
PWI-ZFE, C2	1.90	70–80	14.13
PWI-ZFE, C3	3.80	70–80	37.05
Two-band MMBE LPC, C4	1.85	60	4.58
Five-band MMBE LPC, C5	2.30	60	6.67
Three-band MMBE PWI-ZFE, C6	2.35	70–80	16.18
13-band MMBE PWI-ZFE, C7	3.85	70–80	21.30
Three-band PWI-STC, C8	2.40	60	26.07
10-band PWI-STC, C9	3.80	60	26.07

From Table 17.1 it can be seen that for all speech codecs the requirement for a delay of less than 80 ms is met. However, for the higher-bitrate PWI-ZFE speech codec at 3.8 kbps, the maximum targeted computational complexity of 25 MFLOPS is exceeded. We did not attempt to reduce this computational complexity, because the speech codec did not constitute a sufficiently promising design at its bitrate, in order to justify the associated

research effort. In addition, the PWI-STC speech codecs narrowly exceeded the complexity limit of 25 MFLOPS.

In addition to the review of the bitrate, delay and complexity given in Table 17.1, we also detail the location of pertinent figures and tables for each of our speech codecs, with this information summarised in Table 17.2.

Table 17.2: Summary of the relevant figures and tables for each of our developed speech codecs.

Speech codec	Characteristic waveform figure	Bit allocation table	Schematic figures	Complexity
1.55 kbps LPC vocoder, C1	12.21, 12.22, 12.23	12.8	12.1	Section 12.3.4
1.9 kbps PWI-ZFE, C2	14.13, 14.14, 14.15	14.10	11.13	Figure 14.4, Table 14.4
3.8 kbps PWI-ZFE, C3	14.20, 14.21, 14.22	14.14	11.13	Figure 14.4
1.85 kbps two-band MMBE LPC, C4	15.14, 15.15, 15.16	15.3	15.5	Table 15.2
2.3 kbps five-band MMBE LPC, C5	15.17, 15.18, 15.19	15.3	15.5	Table 15.2
2.35 kbps three-band MMBE PWI-ZFE, C6	15.20, 15.21, 15.22	15.5	15.5	Figure 15.13
3.85 kbps 13-band MMBE PWI-ZFE, C7	15.23, 15.24, 15.25	15.5	15.5	Figure 15.13
2.4 kbps three-band PWI-STC, C8	16.19, 16.20, 16.21	16.4	16.7, 16.15	Table 16.2, Section 16.9.3
3.8 kbps 10-band PWI-STC, C9	16.16, 16.17, 16.18	16.4	16.7, 16.15	Table 16.2, Section 16.9.3

17.2 Listening Tests

The speech quality of the designed speech codecs, detailed in Tables 17.1 and 17.2, was assessed using pairwise-comparison tests. For the pairwise-comparison test a speech utterance was passed through two speech codecs, namely speech codec A and speech codec B, with the listener requested to express a preference for speech codec A, speech codec B or neither speech coder. The utterance was passed through each speech codec twice, in order to give the listener more scope when selecting the best speech codec.

Thirteen listeners were used in the pairwise-comparison tests, with three different utterances passed through each speech codec A–B pair. The listening tests were conducted through headphones. Eight different utterances were employed during the listening tests, where none of these utterances had been used in the design of the speech codecs.

The utterances were a mixture of male and female speakers with British and American accents and had differing lengths. Table 17.3 details the results of the pairwise-comparison tests.

Table 17.3: Details of the listening tests conducted using the speech codecs detailed in Table 17.1. For the pairwise-comparison tests the listeners were given a choice of preferring speech codec A, speech codec B or neither.

		Preference		
Speech codec A	Speech codec B	A (%)	B (%)	Neither (%)
1.85 kbps two-band MMBE LPC, C4	1.9 kbps PWI-ZFE, C2	23.07	30.77	46.16
2.3 kbps five-band MMBE LPC, C5	2.35 kbps three-band MMBE PWI-ZFE, C6	5.13	64.10	30.77
2.3 kbps five-band MMBE LPC, C5	2.4 kbps three-band PWI-STC, C8	30.77	10.26	58.97
2.35 kbps three-band MMBE PWI-ZFE, C6	2.4 kbps three-band PWI-STC, C8	12.82	20.51	66.67
3.8 kbps PWI-ZFE, C3	3.85 kbps 13-band MMBE PWI-ZFE, C7	5.13	30.77	64.10
3.8 kbps PWI-ZFE, C3	3.8 kbps 10-band PWI-STC, C9	53.85	17.95	28.20
3.85 kbps 13-band MMBE PWI-ZFE, C7	3.8 kbps 10-band PWI-STC, C9	30.77	7.69	61.54

From Table 17.3 we can see that for the top two comparison tests, where periodic pulse excitation from the LPC vocoder was compared with PWI-ZFE excitation, in both cases the PWI-ZFE excitation was preferred. The performance of the three-band PWI-STC 2.4 kbps speech codec is variable, with it being preferred to the 2.35 kbps three-band MMBE PWI-ZFE speech codecs, but being judged to be inferior to the 3.8 kbps five-band MMBE LPC speech codec. Observing Table 17.3 it can be inferred that for the speech codecs operating around 2.4 kbps there was no conclusive best performer in terms of speech quality.

For the speech codecs operating at approximately 3.8 kbps the 13-band MMBE PWI-ZFE speech codec performed best, followed by the 3.85 kbps three-pulse PWI-ZFE speech coder, with the 10-band PWI-STC speech coder performing least impressively.

The overall conclusion based on the listening tests was that the single pulse PWI-ZFE was the best voiced excitation source, where in order to achieve a higher bitrate the addition of MMBE was most successful.

17.3 Summary of Very-low-rate Coding

The low-bitrate-oriented part of the book has primarily investigated three speech coding techniques frequently used at bitrate below 4 kbps, namely PWI, MBE and STC. The voiced excitation technique of ZFE and the use of wavelets in speech coding have also been investigated.

The low-bitrate-oriented part of the book commenced by creating a basic LPC vocoder, which allowed decisions to be made about LSF quantisation, pitch detection and post-processing. It was determined that the vector quantiser from G.729 [147] performed the LSF quantisation best. Several different autocorrelation-based pitch detectors were investigated, reiterating the importance and difficulty of pitch detection, with an algorithm incorporating pitch tracking eventually selected. An adaptive postfilter and pitch-independent pulse dispersion filter were also selected.

In Chapter 13 an investigation into wavelets and pitch detection was performed. Polynomial spline wavelets introduced by Mallat and Zhong [524] were selected in order to produce the $\mathrm{D_Y WT}$ for processing the speech. Subsequent to the $\mathrm{D_Y WT}$ a selection of possible candidate pitch periods remained, where both dynamic programming and autocorrelation were performed for the sake of determining the true pitch period. We concluded that the combination of $\mathrm{D_Y WT}$ and subsequent autocorrelation computation produced the best pitch detector design.

Chapter 14 introduced ZFE in order to represent the voiced speech in a PWI scheme, creating a PWI-ZFE speech coder. The ZFE pulses were initially introduced at higher bitrates by Sukkar *et al.* [497] and have previously been used by Hiotakakos and Xydeas at low bitrates [496]. This chapter introduced the principle of using GCIs determined by the $\mathrm{D_Y WT}$ in order to reduce the complexity of the ZFE optimisation loop, where the GCIs were also used in order to ensure a smoothly evolving waveform within the synthesised prototype segments of the speech encoder. The chapter also adopted the pitch prototype selection process proposed by Kleijn [105]. At the decoder, the chapter further developed the interpolation process of Hiotakakos and Xydeas [496] such that no information was required about either the pitch prototype location or the ZFE location, decreasing the number of bits requiring transmission by six per 20 ms frame.

The error sensitivity of the PWI-ZFE speech codec was also examined, where the importance of the voiced–unvoiced flag was emphasised. Finally, Chapter 14 investigated a higher bitrate speech codec with three ZFEs pulses employed in order to represent the voiced excitation. It was found that the extra ZFE pulses improved the representation of the voiced speech, however, this was counteracted by the phase restrictions imposed for the interpolation process together with the difficulty in producing smooth interpolation at the decoder.

A MMBE scheme was detailed in Chapter 15, where the frequency bands were based on the pitch period [540], thus required recalculation for every speech frame. The MMBE scheme was harnessed in both the LPC vocoder and the PWI-ZFE speech codec, in order to produce a selection of different speech codecs between 1.9 and 3.85 kbps. It was found that at the same bitrate the MMBE scheme based on the PWI-ZFE performed best.

In Chapter 16, STC at low bitrates was investigated, where a PWI scheme was again implemented for creating PWI-STC speech codecs at 2.4 and 3.8 kbps. In this chapter the AbS technique, used to determine the sinusoidal parameters and introduced by George and Smith [545, 546], was further developed in order to incorporate the weighted LPC synthesis filter. It was then modified for the sake of reducing the associated computational complexity. The sinusoidal parameters were transmitted to the decoder as scalar quantised Fourier coefficients a_k and b_k, where these Fourier coefficients were associated with harmonics of the determined pitch.

17.4 Further Research

This low-bitrate-coding-oriented part of the book demonstrated that for speech codecs operating at bitrates below 4 kbps the principle of PWI is particularly useful. The predominant advantage of the PWI is that it allows the available bits to concentrate on encoding a single pitch period, rather than three or four pitch periods as would be typical without PWI. Thus, it is suggested that further work on very-low-bitrate speech codecs should employ PWI as its foundation.

For the three voiced excitation methods employed in the low-bitrate-coding-oriented part of the book, namely for ZFE, MMBE and STC-based compression, it was found that the associated performances were similar. When considering the most appropriate excitation for a speech coder it is interesting to examine the winner of the US DoD competition for the new 2.4 kbps speech coder. This was the speech coder [486] which employed the most basic model for the excitation, but incorporated additional aspects, such as a pulse dispersion filter, in order to model the human speech production system more closely. In the history of speech coding understanding human speech production has produced many important developments, such as the LPC model and MBE, and should continue to provide inspiration in the future.

An area of research which is currently receiving much interest is the creation of multirate speech codecs, which will be present in third-generation communication systems. In Chapters 14 and 15 we attempted to convert a speech codec to a higher-bitrate scheme, while in Chapter 16 conversion to a lower-bitrate arrangement was investigated. The bitrate changes that were performed approximately doubled or halved the original bitrate, but the resultant codecs did not constitute the most attractive design tradeoff at these modified bitrates. Thus, an interesting area of further work would be to investigate how to increase or decrease a speech coder's bitrate, while maintaining an appropriate speech quality at a variable bitrate.

Chapter 18

Comparison of Speech Codecs and Transceivers

18.1 Background to Speech Quality Evaluation

Throughout the previous chapters of the book we have typically used the SEGSNR or CD objective quality speech measures. These measures are ubiquitous in speech compression research, because they are convenient to use in comparing slightly modified versions of the same codec family during the development process. Their evaluation imposes no computational difficulties either. However, when comparing different coding principles or the effects of transmission errors, they are often less reliable, especially in the context of speech codecs, which aim for optimising the subjective or perceptual speech quality, rather than the waveform representation quality of a particular codec. Hence, the objective of this chapter is to provide a slightly deeper exposure of various speech quality assessment methods.

The major difficulty associated with the assessment of speech quality is the consequence of a philosophical dilemma. Namely, should speech quality evaluation be based on unreliable, subjective human judgements or on reproducible objective evaluations, which may be highly uncorrelated with personal subjective quality assessments? Even high-fidelity (HIFI) entertainment systems exhibit different subjective music reproduction qualities, let alone low-bitrate speech codecs. It is practically impossible to select a generic set of objective measures in order to characterise speech quality, because all codecs result in different speech impairments. Some objective measures, which are appropriate for quantifying one type of distortion might be irrelevant to estimate another, just as one listener might prefer some imperfections to others. Using a statistically relevant, high number of trained listeners and various standardised tests mitigates the problems encountered, but incurs cost and time penalties. During codec development quick and cost-efficient objective preference tests are usually used, followed by informal listening tests, before a full-scale formal subjective test is embarked upon.

The literature of speech quality assessment was documented in a range of excellent treatises by Kryter [557], Jayant and Noll [10], Kitawaki *et al*. [85, 87]. In [18], Papamichalis

Voice and Audio Compression for Wireless Communications Second Edition
L. Hanzo, F. C. A. Somerville and J. P. Woodard

gives a comprehensive overview of the subject with references to Jayant's and Noll's work [10]. Further important contributions are due to Halka and Heute [558] as well as Wang *et al*. [559].

18.2 Objective Speech Quality Measures

18.2.1 Introduction

Whether we evaluate the speech quality of a waveform codec, vocoder or hybrid codec, objective distance measures are needed to quantify the deviation of the codec's output signal from the input speech. In this respect any formal metric or distance measure of the mathematics, such as the Euclidean distance, could be employed to quantify the dissimilarity of the original and the processed speech signal, as long as symmetry, positive definitiveness and the triangle inequality apply. These requirements were explicitly formulated as follows [86].

- Symmetry: $d(x, y) = d(y, x)$.
- Positive definiteness: $d(x, x) = 0$ and $d(x, y) > 0$, if $x \neq y$.
- Triangular inequality: $d(x, y) \leq d(x, z) + d(y, z)$.

In practice the triangle inequality is not needed, but our distance measure should be easy to evaluate and preferably it ought to have some meaningful physical interpretation. The symmetry requires that there is no distinction between the reference signal and the speech to be evaluated in terms of distance. The positive definiteness implies that the distance is zero if the reference and tested signals are identical.

A number of objective distance measures fulfill all criteria, some of which have waveform-related time-domain interpretations, while others have frequency-domain related physical meaning. Often time-domain waveform codecs such as PCM are best characterised by the former criteria, while frequency domain codecs, such as transform and sub-band codecs, are best characterised by the latter. AbS hybrid codecs using perceptual error-weighting are the most difficult to characterise and usually only a combination of measures gives satisfactory results. Objective speech quality measures have been studied in depth by Quackenbush *et al*. [21], hence here only a rudimentary overview is provided.

The simplest and most widely used metrics or objective speech quality measures are the SNRs, such as the conventional SNR, the SEGSNR and the frequency-weighted SNR [560, 561]. As they are essentially quantifying the waveform similarity of the original and the decoded signal, they are most useful in terms of evaluating waveform-coder distortions. Nonetheless, they are often invoked in medium-rate codecs, in order to compare different versions of the same codec, for example during the codec development process.

Frequency-domain codecs are often best characterised in terms of the spectral distortion between the original and processed speech signal, evaluating it either on the basis of the spectral fine structure, or (for example, when judging the quality of a spectral envelope quantiser) in terms of the spectral envelope distortion. Some of the often used measures are the so-called spectral distance, log spectral distance, CD, LLR, noise-masking ratios and composite measures, most of which were proposed (for example, by Barnwell *et al*. [560–562]) during the late 1970s and early 1980s. However, most of the above measures are

inadequate for quantifying the subjective quality of a wide range of speech-coder distortions. They are particularly bad at fault predicting these quality degradations across different types of speech codecs. A particular deficiency of these measures is that when a range of different distortions are present simultaneously, these measure are incapable of evaluating the grade of the individual imperfections, although this would be desirable for codec developers.

Following the above introductory elaborations, let us now consider some of the widely used objective measures in a little more depth.

18.2.2 Signal-to-noise Ratios

For discrete-time, zero-mean speech signals, the error and signal energies of a block of N speech samples are given by

$$E_e = \frac{1}{N} \sum_{u=1}^{N} (s(u) - \hat{s}(u))^2 \tag{18.1}$$

$$E_s = \frac{1}{N} \sum_{u=1}^{N} s^2(u). \tag{18.2}$$

Then the conventional SNR is computed as:

$$\text{SNR (dB)} = 10 \log_{10}(E_s/E_e). \tag{18.3}$$

When computing the arithmetic means in Equations (18.1), the gross averaging over long sequences conceals the codecs' low SNR performance in low-energy speech segments and attributes unreasonably high objective scores to the speech codec. Computation of the geometric mean of the SNR guarantees higher correlation with perceptual judgements, because it gives proper weighting to the lower SNR performance in low-energy sections. This is achieved by computing the so-called SEGSNR. Firstly, the speech signal is divided into segments of 10–20 ms and SNR(u) (dB) is computed for $u = 1 \ldots N$, i.e. for each segment in terms of decibels. Then the segmental SNR(u) values are averaged in terms of decibels, as follows:

$$\text{SEGSNR (dB)} = \frac{1}{N} \sum_{n=1}^{N} \text{SNR}(u) \text{ (dB)} \tag{18.4}$$

Equation (18.4) effectively averages the logarithms of the SNR(u) values, which corresponds effectively to the computation of the geometric mean. This gives proper weighting to low-energy speech segments and therefore gives values more closely related to the subjective quality of the speech codec. A further refinement is to limit the segmental SNR(u) terms to be in the range of $0 < \text{SNR}(u) < 40$ (dB), because outside this interval it becomes uncorrelated with subjective quality judgements.

18.2.3 Articulation Index

A useful frequency-domain related objective measure is the so-called articulation index (AI) proposed by Kryter in [557]. The speech signal is split into 20 sub-bands of increasing

bandwidths and the sub-band SNRs are computed. Their range is limited to $\mathrm{SNR} = 30\,\mathrm{dB}$, and then the average SNR over the 20 bands is computed as follows:

$$\mathrm{AI} = \frac{1}{20} \sum_{i=1}^{20} \mathrm{SNR}_i \; . \tag{18.5}$$

The subjective importance of the sub-bands is weighted by appropriately choosing the bandwidth of all sub-bands, which then contribute 1/20th of the total SNR. An important observation is that Kryter's original bandsplitting table stretches to 6100 Hz and when using a bandwidth of 4 kHz, the two top bands falling beyond 4 kHz are therefore neglected, limiting AI inherently to 90%. When using $B = 3\,\mathrm{kHz}$, $\mathrm{AI} \leq 80\%$. The evaluation of the AI is rather complex due to the bandsplitting operation.

18.2.4 Cepstral Distance

The CD is the most highly correlated objective measure, when compared to subjective measures. It maintains its high correlation over a wide range of codecs, speakers and distortions, while reasonably simple to evaluate. It is defined in terms of the cepstral coefficients of the reference and tested speech, as follows:

$$\mathrm{CD} = \left[(c_0^{\mathrm{in}} - c_0^{\mathrm{out}})^2 + 2 \sum_{f=1}^{\infty} (c_j^{\mathrm{in}} - c_j^{\mathrm{out}})^2 \right]^{\frac{1}{2}}. \tag{18.6}$$

The input and output cepstral coefficients are evaluated by the help of the LPC filter coefficients a_j of the all-pole filter [86], which is elaborated on below.

Explicitly, the cepstral coefficients can be determined from the filter coefficients a_i $(i = 1 \ldots p)$ with the help of a recursive relationship, derived as follows. Let us denote the stable all-pole speech model by the polynomial $A(z)$ of order M in terms of z^{-1}, assuming that all of its roots are inside the unit circle. It has been shown in [563] that the following relationship holds for the Taylor series expansion of $\ln\,[A(z)]$:

$$\ln[A(z)] = -\sum_{k=1}^{\infty} c_k \cdot z^{-k}; \quad c_0 = \ln(E_p/R_0) \tag{18.7}$$

where the coefficients c_k are the cepstral coefficients and c_0 is the logarithmic ratio of the prediction error and the signal energy. By substituting

$$A(z) = 1 + \sum_{k=1}^{\infty} a_k \cdot z^{-k} \tag{18.8}$$

or by exploiting that $a_0 = 1$

$$A(z) = 1 + \sum_{k=0}^{M} a_k \cdot z^{-k}. \tag{18.9}$$

Upon differentiating the left-hand side of Equation (18.7) with respect to z^{-1} we arrive at

$$\frac{\delta[\ln A(z)]}{\delta z^{-1}} = \frac{1}{A(z)} \frac{\delta A(z)}{\delta z^{-1}} \tag{18.10}$$

$$\frac{\delta[\ln A(z)]}{\delta z^{-1}} = \frac{1}{\sum_{k=0}^{M} a_k \cdot z^{-k}} \sum_{k=1}^{M} k \cdot a_k \cdot z^{-(k-1)}. \tag{18.11}$$

Differentiating the right-hand side of Equation (18.7) as well as equating it to the differentiated left-hand side according to Equation (18.9) yields

$$\left(\sum_{k=0}^{M} a_k \cdot z^{-k} \right)^{-1} \sum_{k=1}^{M} k \cdot a_k \cdot z^{-(k-1)} = - \sum_{k=1}^{\infty} k \cdot c_k \cdot z^{-(k-1)}. \tag{18.12}$$

Rearranging Equation (18.12) and multiplying both sides by z^{-1} results in Equation (18.13):

$$\sum_{k=1}^{M} k \cdot a_k \cdot z^{-k} = - \left(\sum_{k=0}^{M} a_k \cdot z^{-k} \right) \cdot \sum_{k=1}^{\infty} k \cdot c_k \cdot z^{-k}. \tag{18.13}$$

By expanding the indicated sums and performing the necessary multiplications the following recursive equations result, which is demonstrated by an example in the next section:

$$c_1 = -a_1 \tag{18.14}$$

$$c_j = -\frac{1}{j} \left(j \cdot a_j + \sum_{i=1}^{j-1} i \cdot c_i \cdot a_{j-i} \right); \quad j = 2 \ldots p \tag{18.15}$$

and by truncating the second sum in Equation (18.13) on the right-hand side at $2p$, because the higher-order terms are of diminishing importance, we arrive at

$$c_j = -\frac{1}{j} \sum_{k=1}^{p} (j-i) \cdot c_{j-i} \cdot a_i; \quad j = (p+1) \ldots 2p. \tag{18.16}$$

Now, in possession of the filter coefficients the cepstral coefficients can be derived.

Having computed the cepstral coefficients $c_0 \ldots c_{2p}$ we can determine the CD as repeated below for convenience:

$$\text{CD} = \left[(c_0^{\text{in}} - c_0^{\text{out}})^2 + 2 \cdot \sum_{j=1}^{2p} (c_j^{\text{in}} - c_j^{\text{out}})^2 \right]^{\frac{1}{2}} \tag{18.17}$$

$$c_1 = a_1$$

$$c_j = a_j - \sum_{r=1}^{j-1} \frac{r}{j} \cdot c_r \cdot a_{j-r}, \quad \text{for } j = 2 - -p \tag{18.18}$$

$$c_j = - \sum_{r=1}^{p} \frac{j-r}{j} c_{j-r} \cdot a_r, \quad \text{for } j = p+1, p+2, -3p$$

where p is the order of the all-pole filter $A(z)$. The optimum predictor coefficients a_r are computed to minimise the energy of the prediction error residual:

$$e(u) = s(u) - \hat{s}(u). \tag{18.19}$$

This requires the solution of the following set of p equations:

$$\sum_{E=1}^{p} a_r \cdot R(|i-r|) = R(i), \quad \text{for } i = 1 \ldots p \tag{18.20}$$

where the autocorrelation coefficients are computed from the segmented and Hamming-windowed speech as follows. First, the speech $s(u)$ is segmented into 20 ms or $N = 160$ samples long sequences. Then $s(u)$ is multiplied by the Hamming window function.

$$w_{(n)} = 0.54 - 0.45 \cos \frac{2\pi u}{N}. \tag{18.21}$$

In order to smooth the frequency domain oscillations introduced by the rectangular windowing of $s(u)$. Now the autocorrelation coefficients $R(i) i = 1 \ldots p$ are computed from the windowed speech $s_w(n)$ as

$$R(i) = \sum_{n=0}^{N-1-i} s_w(u) - s_w(u+i), \quad i = 1 \ldots p. \tag{18.22}$$

Finally, Equation (18.20) is solved for the predictor coefficients $a(i)$ by the Levinson–Durbin algorithm [77]:

$$\begin{aligned} E(0) &= R(0) \\ \epsilon_i &= \left[\sum_{j=1}^{i-1} a_j^{i-1} \cdot R(i-j) \right] \Big/ E^{(i-1)}, \quad i = 1 \ldots p \\ a_{(i)}^{(i)} i &= r_i \\ a_j &= a_j^{(i-1)} - k_i \cdot a_{i-j}^{(i-1)}, \quad j = 1 \ldots (i-1) \\ E^{(i)} &= (1 - \epsilon_i^2) \end{aligned} \tag{18.23}$$

where r_i, $i = 1 \ldots p$, are the reflection coefficients. After p iterations $(i = 1 \ldots p)$ the set of LPC coefficients is given by

$$a_j = a_j^{(p)}, \quad j = 1 \ldots p \tag{18.24}$$

and the prediction gain is given by $G = E(i)/E^{10}$. The computation of the CD is summarised in the flow chart of Figure 18.1.

It is plausible that the CD measure is a spectral domain parameter, because it is related to the LPC filter coefficients of the speech spectral envelope. In harmony with our expectations, it is shown in [86] that the CD is identical to the logarithmic root mean square spectral distance (LRMS-SD) between the input and output spectral envelopes often used in speech

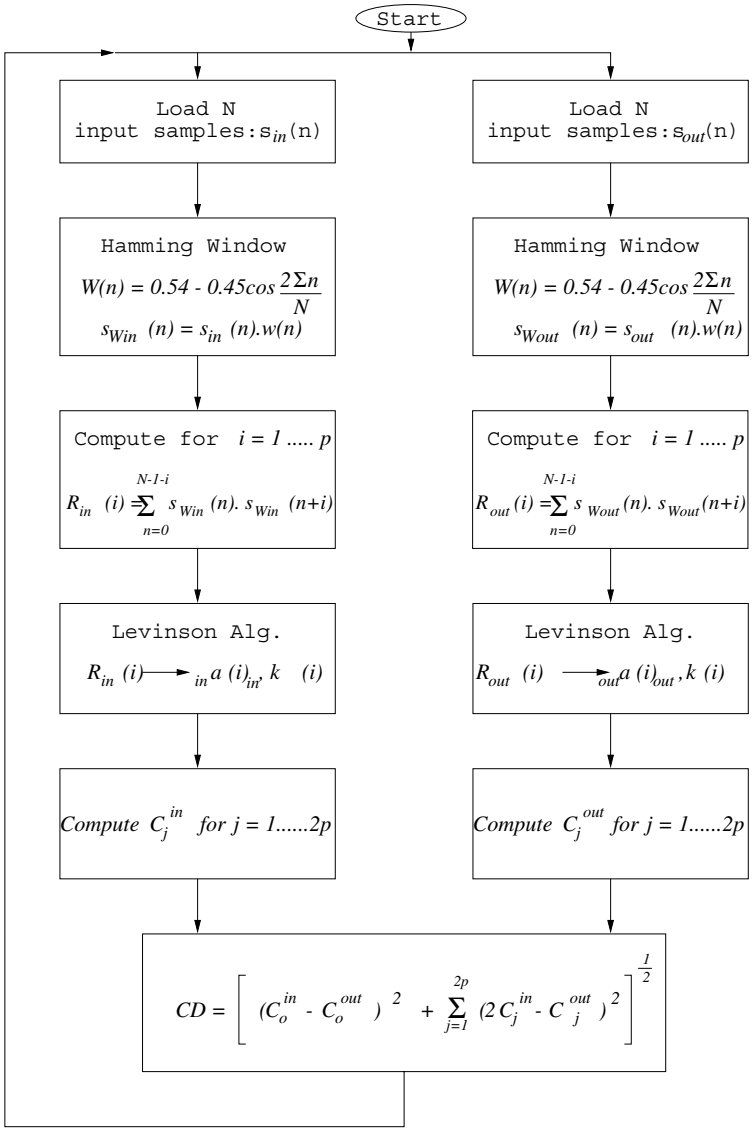

Figure 18.1: CD computation flowchart.

quality evaluations:

$$\text{LRMS-SD} = \left[\int_{-\pi}^{\pi} |\ln |b_{\text{in}}/A_{\text{in}}(f)|^2 - ln|G_{\text{out}}/A_{\text{out}}(f)|^2 \, \mathrm{d}f \right]^{\frac{1}{2}}. \tag{18.25}$$

In the next section we consider a simple example.

18.2.5 Example: Computation of Cepstral Coefficients

Let us make the derivation of Equations (18.14)–(18.16) plausible by expanding the sums in Equation (18.13) and by computing the multiplications indicated. In this way, let us assume $p = 4$ and compute $c_1 \ldots c_{2p}$:

$$\begin{aligned} a_1 z^{-1} + 2a_2 z^{-2} + 3a_3 z^{-3} + 4a_4 z^{-4} \\ = -(c_1 z^{-1} + 2c_2 z^{-2} + 3c_3 z^{-3} + 4c_4 z^{-4} + 5c_5 z^{-5} + 6c_6 z^{-6} \\ + 7c_7 z^{-7} + 8c_8 z^{-8}) \cdot (1 + a_1 z^{-1} + a_2 z^{-2} + a_3 z^{-3} + a_4 z^{-4}). \end{aligned} \quad (18.26)$$

By computing the product at the right-hand side, we arrive at

$$\begin{aligned} a_1 z^{-1} + 2a_2 z^{-2} + 3a_3 z^{-3} + 4a_4 z^{-4} \\ = c_1 z^{-1} + 2c_2 z^{-2} + 3c_3 z^{-3} + 4c_4 z^{-4} + 5c_5 z^{-5} + 6c_6 z^{-6} \\ + 7c_7 z^{-7} + 8c_8 z^{-8} + c_1 a_1 z^{-2} + 2c_2 a_1 z^{-3} + 3c_3 a_1 z^{-4} \\ + 4c_4 a_1 z^{-5} + 5c_5 a_1 z^{-6} 6c_6 a_1 z^{-7} + 7c_7 a_1 z^{-8} + 8c_8 a_1 z^{-9} \\ + c_1 a_2 z^{-3} + 2c_2 a_2 z^{-4} + 3c_3 a_2 z^{-5} + 4c_4 a_2 z^{-6} + 5c_5 a_2 z^{-7} \\ + 6c_6 a_2 z^{-8} + 7c_7 a_2 z^{-9} + 8c_8 a_2 z^{-10} + c_1 a_3 z^{-4} + 2c_2 a_3 z^{-5} \\ + 3c_3 a_3 z^{-6} + 4c_4 a_3 z^{-7} + 5c_5 a_3 z^{-8} + 6c_6 a_3 z^{-9} \\ + 7c_7 a_3 z^{-10} + 8c_3 a_3 z^{-11}. \end{aligned} \quad (18.27)$$

Now by matching the terms of equal order in z^{-1} on both sides

z^{-1}:

$$c_1 = -a_1 \quad (18.28)$$

z^{-2}:

$$\begin{aligned} 2a_2 &= 2c_2 + a_1 c_1 \\ 2c_2 &= -a_1 c_1 - 2a_2 \end{aligned} \quad (18.29)$$

z^{-3}:

$$3c_3 = -3a_3 - 2a_1 c_2 - a_2 c_1 \quad (18.30)$$

z^{-4}:

$$4c_4 = -4a_4 - 3a_1 c_3 - 2a_2 c_2. \quad (18.31)$$

In general,

$$jc_j = -ja_j - \sum_{i=1}^{j-1} ic_i a_{j-i}, \quad j = 1 \ldots p. \quad (18.32)$$

However, there also exists a number of terms with an order of higher than p that must cancel each other on the right-hand side of Equation 18.27:

z^{-5}:

$$5c_5 + 4c_4 a_1 + 3c_3 a_2 + 2c_2 a_3 + c_1 a_4 = 0 \quad (18.33)$$

$$5c_5 = -4c_4a_1 - 3c_3a_2 - 2c_2a_3 - c_1a_4 \tag{18.34}$$

z^{-6}:

$$6c_6 = -5c_5a_1 - 4c_4a_2 - 3c_3a_3 - 2c_2a_4 \tag{18.35}$$

z^{-7}:

$$7c_7 = -6c_6a_1 - 5c_5a_2 - 4c_4a_3 - 3c_3a_4 \tag{18.36}$$

z^{-8}:

$$8c_8 = -7c_7a_1 - 6c_6a_2 - 5c_5a_3 - 4c_4a_4. \tag{18.37}$$

In general,

$$jc_j = -\sum_{i=1}^{p}(j-i)c_{j-i}a_i, \quad j = p+1\ldots. \tag{18.38}$$

Let us now continue our review of various objective speech quality measures in the spirit of Papamichalis' discussions [18] in the next section.

18.2.6 Logarithmic Likelihood Ratio

The likelihood ratio (LR) distance measure introduced by Itakura also uses the LPC coefficients of the input and output spectral envelope to quantify the spectral deviation introduced by the speech codec. The LR is defined as the ratio of the LPC residual energy before and after speech coding. As the LPC coefficients $\underline{a}_{r\mathrm{in}} = [a_0, a_1, \ldots, a_p]$ are computed by Durbin's algorithm to minimise the LPC residual's energy, replacing $\underline{a}_{r\mathrm{in}}$ by another LPC coefficient vector $\underline{a}_{r1}$ out computed from the decoded speech certainly increases the LPC residual energy, therefore $\mathrm{LR} \geq 1$.

The formal definition of the LR is given by

$$\mathrm{LR} = \frac{\underline{a}_{\mathrm{out}}^{\mathrm{T}}\underline{R}^{\mathrm{out}}\underline{a}_{\mathrm{out}}}{\underline{a}_{\mathrm{in}}^{\mathrm{T}}\underline{R}^{\mathrm{in}}\underline{a}_{\mathrm{in}}} \tag{18.39}$$

where $\underline{a}_{\mathrm{in}}$, $\underline{R}^{\mathrm{in}}$ and $\underline{a}_{\mathrm{out}}$, $\underline{R}^{\mathrm{out}}$ represent the LPC filter coefficient vectors and autocorrelation matrices of the input as well as output speech, respectively. The LR defined in (18.39) is non-symmetric, which contradicts to our initial requirements. Fortunately, this can be rectified by the symmetric transformation:

$$\mathrm{LRS} = \frac{\mathrm{LR} + 1/\,\mathrm{LR}}{2} - 1. \tag{18.40}$$

Finally, the symmetric LLR (SLLR) is computed from

$$\mathrm{SLLR} = 10\log_{10}(\mathrm{LRS}). \tag{18.41}$$

The computational complexity incurred is significantly reduced if LR is evaluated instead of the matrix multiplications required by (18.39) exploiting the following relationship:

$$\underline{a}^{\mathrm{T}} \cdot \underline{Ra} = R_a(0)R(0) + 2\sum_{i=1}^{P} R_a(i) \cdot R(i), \tag{18.42}$$

where $R(i)$ and $R_a(i)$ represent the autocorrelation coefficients of the signal and that of the LPC filter coefficients $\underline{a}$, as computed in (18.23).

18.2.7 Euclidean Distance

If any comprehensive set of spectral parameters closely related to the spectral deviation between input and output speech is available, the Euclidean instance between the sets of input and output speech parameters gives useful insights into the distortions inflicted. Potentially suitable sets are the LPC coefficients, the reflection coefficients defined in the context of (18.23), the autocorrelation coefficients given in (18.28), the so-called LSFs most often used recently or the highly robust LARs. LARs are defined as

$$\mathrm{LAR}_i = \ln \frac{1 + r_i}{1 - r_i}, \quad i = 1 \ldots p \tag{18.43}$$

and are very robust against channel errors and have a fairly limited dynamic range, which alleviates their quantisation. With this definition of LARs, the Euclidean distance is formulated as

$$D_{\mathrm{LAR}} = \left[\sum_{i=1}^{p} (\mathrm{LAR}_i^{\mathrm{in}} - \mathrm{LAR}_i^{\mathrm{out}})^2 \right]^{\frac{1}{2}}. \tag{18.44}$$

18.3 Subjective Measures [18]

Once the development of a speech codec is finalised, objective and informal subjective tests are followed by formal subjective tests [18]. Depending on the type, bitrate and quality of the specific codec, different subjective tests are required to test quality and intelligibility. Quality is usually tested by the so-called DAM, paired preference tests or the most wide-spread MOS. Intelligibility is tested by consonant–vowel–consonant (CVC) logatours or by DRTs. Formal subjective speech assessment is generally a lengthy investigation carried out by specially trained unbiased crew using semi-standardised test material, equipment and conditions.

18.3.1 Quality Tests

In DAM tests the trained listener is asked to rate the speech codec tested using phonetically balanced sentences from the so-called Harvard list in terms of both speech quality and background quality. Some terms used at Dynastat (USA) to describe speech impairments are listed in Table 18.1 [18] following Papamichalis. As regards to background qualities, some examples of terms used at Dynastat are summarised in Table 18.2 [18] following Papamichalis. The speech and background qualities are rates in the listed categories on a 100-point scale by each listener and then their average scores are evaluated for each category, giving also the standard deviations and standard errors. Before averaging the results of various categories appropriate weighting factors can be used to emphasise features particularly important for a specific application of the codec.

In *pairwise preference tests* the listeners always compare the same sentence processed by two different codecs, even if a large number of codecs have to be tested. To ensure consistency in the preferences, unprocessed and identically processed sentences can also be included.

Table 18.1: Typical terms used to characterise speech impairments in DAM tests. Copyright © Papamichalis [18], 1987.

Speech impairment	Typical of
Fluttering	Amplitude modulated speech
Thin	Highpass filtered speech
Rasping	Peak clipped speech
Muffled	Lowpass filtered speech
Interrupted	Packetised speech
Nasal	Low-bitrate vocoders

Table 18.2: Typical terms used for background qualities in DAM tests. Copyright © Papamichalis [18], 1987.

Background	Typical of
Hissing	Noisy speech
Buzzing	Tandemed dig systems
Babbling	Low-bitrate codecs with bit errors
Rumbling	Low-frequency-noise marked speech

The results are summarised in the preference matrix. If the comparisons show a clean preference order for differently processed speech and an approximately random preference (50%) for identical codecs in the preference matrix's main diagonal, the results are accepted. However, if no clear preference order is established, different tests have to be deployed.

18.4 Comparison of Subjective and Objective Measures

18.4.1 Background

An interesting comparison of the objective AI described in Section 18.2.3 and of various subjective tests was given by Kryter [564], as shown in Figure 18.3. Observe that the lower the size of the test vocabulary used, the higher the intelligibility scores for a fixed AI value, which is due to the less subtle differences inherent in a smaller test vocabulary.

The *modulated noise reference unit (MNRU)* proposed by Law and Seymour [171] to relate subjective quality to objective measures is widely used by the CCITT as well. The MNRU block diagram is shown in Figure 18.2.

The MNRU is used to add noise, amplitude modulated by the speech test material, to the reference speech signal, rendering the noise speech-correlated. The SNR of the reference signal is gradually lowered by the listener using the attenuators in Figure 18.2 to perceive identical loudness and subjective qualities, when comparing the noisy reference signal and the tested codec's output speech. During this adjustment and comparison phase the switches 52 and 53 are closed and 51 is being switched between the reference and tested speech signals.

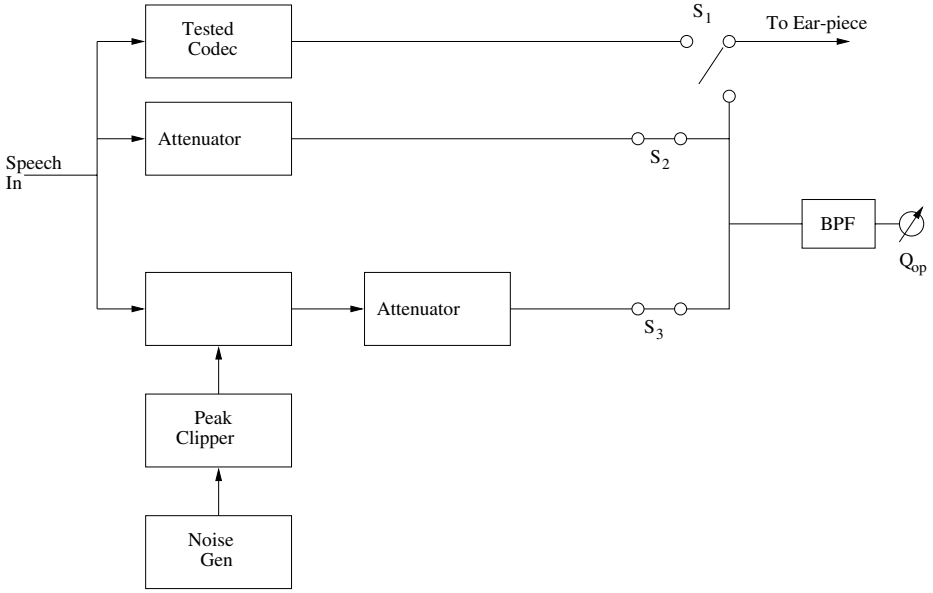

Figure 18.2: MNRU block diagram.

Once both speech signals make identical subjective impressions, switches 52 and 53 are used to measure the reference signal's and noise signal's power and, hence, the so-called opinion equivalent Q (dB) (Qop in decibels) expressed in terms of the SNR computed. Although the Qop value appears to be an objective measured value, it depends on various listeners subjective judgements and is therefore classified as a subjective measure. The Qop value is easily translated into the more easily interpreted MOS measure using the reference speech's MOS versus Qop characteristic depicted in Figure 18.3.

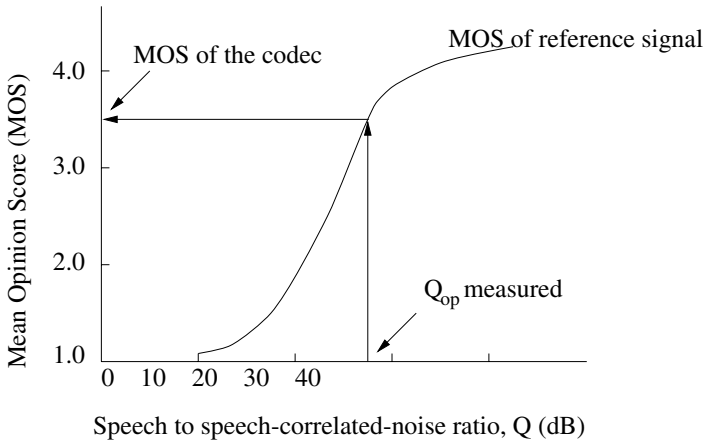

Figure 18.3: Translating Qop into MOS.

18.4.2 Intelligibility Tests

In intelligibility tests the listeners are asked to recognise which one of a pair of words is uttered, where the two words only differ in one phoneme, which is a consonant [565]. Alternatively, CVC logatours can also be used. According to Papamichalis in the DRT developed by Dynastat [18] a set of 96 rhyming pairs of words are utilised, some of which are: meat–beat, pear–tear, saw–thaw, bond–pond, etc. The pairs are specially selected to test the following phonetic attributes: voicing, nasality, sustention, sibilation, graveness and compactness. If, for example, the codec under test consistently fails to distinguish between vast–fast, zoo–sue, goat–coat, i.e., to deliver clear voiced sounds such as v, z, g, etc., it points out for the designer that the codec's LTP responsible for the spectral fine-structure or voicing information in the spectrum does not work properly. Vital information can be gained about the codecs shortcomings by consistently grouping and evaluating the recognition failures. Typical DRT values are between 75 and 95 and, for high intelligibility, DRT > 90 is required.

In a similar fashion, most objective and subjective measures can be statistically related to each other, but the goodness of match predicted for new codecs varies over a wide range. For low-bitrate codecs, one of the most pertinent relationships devised is [87]

$$\mathrm{MOS} = 0.04\,\mathrm{CD}_2 - 0.80\,\mathrm{CD} + 3.565. \tag{18.45}$$

This formula is the best second-order fit to a high number of MOS-CD measurements carried out over a variety of codecs and imperfections.

In summary, speech quality evaluation is usually based on quick objective assessments during codec development, followed by extensive formal subjective tests, when the development is finalised. A range of objective and subjective measures was described, where the most popular objective measures are the simple time-domain SEGSNR and the somewhat more complex, frequency-domain CD measure. The CD objective measure is deemed to have the highest correlation with the most widely applicable subjective measure, the MOS, and their relationship is expressed in Equation (18.45). Having reviewed a variety of objective and subjective speech quality measures, let us now compare a range of previously considered speech codecs in the next section.

18.5 Subjective Speech Quality of Various Codecs

In previous chapters we have characterised many different speech codecs. Here we attempt a rudimentary comparison of some of the previously described codec schemes in terms of their subjective and objective speech quality as well as error sensitivity. We will conclude this chapter by incorporating some of the codecs concerned in various wireless transceivers and portray their SEGSNR versus channel SNR performance. Here we refer back to Figure 1.6 and with reference to Cox and Kroon's work [1, 2] we populate this figure with actual formally evaluated MOS values, which are shown in Figure 18.4. Observe that over the years a range of speech codecs have emerged, which attained the quality of the 64 kbps G.711 PCM speech codec, although at the cost of significantly increased coding delay and implementational complexity. The 8 kbps G.729 codec is the most recent addition to this range of ITU standard schemes, which significantly outperforms all previous standard ITU codecs in robustness terms. The performance target of the 4 kbps ITU codec (ITU4) is also

to maintain this impressive set of specifications. The family of codecs that were designed for various mobile radio systems, such as the 13 kbps RPE GSM scheme, the 7.95 kbps IS-54, the IS-96, the 6.7 kbps JDC and 3.45 kbps half-rate JDC arrangement (JDC/2), exhibits slightly lower MOS values than the ITU codecs. Let us now consider the subjective quality of these schemes in a little more depth.

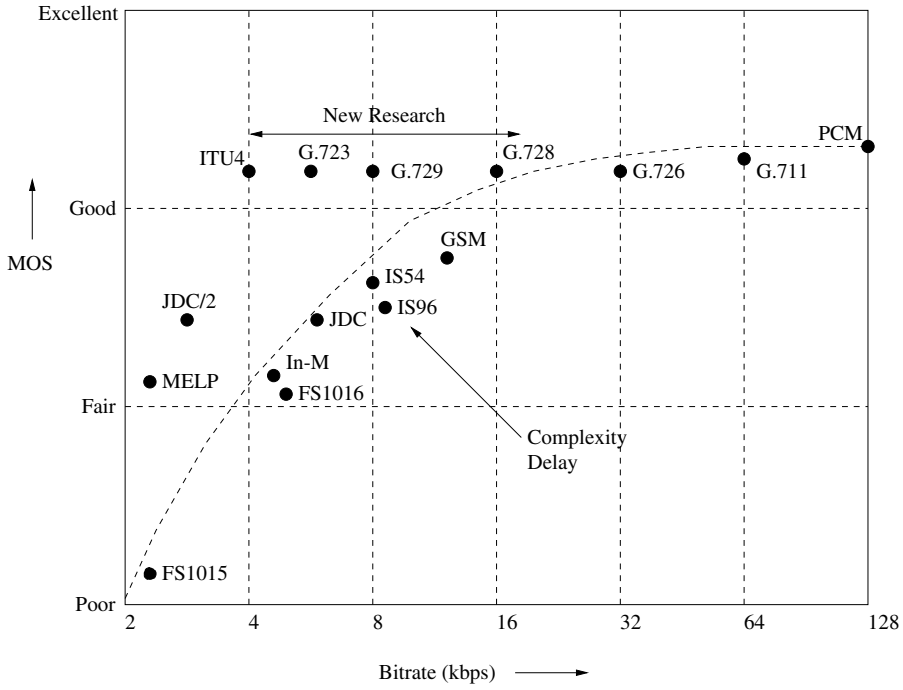

Figure 18.4: Subjective speech quality of various codecs [1]. Copyright © IEEE, 1996.

The subjective speech quality of a range of speech codecs is characterised in Figure 18.4. While during our introductory discussions we portrayed the waveform coding, vocoding and hybrid coding families in a similar, but more inaccurate, stylised illustration, this figure is based on large-scale formal comparative studies.

The 2.4 kbps Federal Standard codec FS-1015 is the only vocoder in this group and it has a rather synthetic speech quality, associated with the lowest subjective assessment in the figure. The 64 kbps G.711 PCM codec and the G.726/G.727 ADPCM schemes are waveform codecs. They exhibit a low implementational complexity associated with a modest bitrate economy. The remaining codecs belong to the hybrid coding family and achieve significant bitrate economies at the cost of increased complexity and delay.

Specifically, the 16 kbps G.728 backward-adaptive scheme maintains a similar speech quality to the 32 and 64 kbps waveform codecs, while also maintaining an impressively low 2 ms delay. This scheme was standardised during the early 1990s. The similar-quality, but significantly more robust 8 kbps G.729 codec was approved in March 1996 by the ITU. This activity overlapped with the G.723.1 developments. The 6.4 kbps mode maintains a speech quality similar to the G.711, G.726, G.727, G.728 and G.728 codecs, while the 5.3 mode

exhibits a speech quality similar to the cellular speech codecs of the late 1980s. Work is under way at the time of writing towards the standardisation of ITU4.

In parallel to the ITU's standardisation activities a range of speech coding standards have been proposed for regional cellular mobile systems. The standardisation of the 13 kbps RPE-LTP GSM-FR codec dates back to the second half of the 1980s, representing the first standard hybrid codec. Its complexity is significantly lower than that of the more recent CELP-based codecs. Observe in the figure that there is also an identical-rate GSM-EFR, which matches the speech quality of the G.729 and G.728 schemes. The original GSM-FR codec's development was followed a little later by the release of the 8 kbps VSELP IS-54 American cellular standard. Due to advances in the field the 7.95 kbps IS-54 codec achieved a similar subjective speech quality to the 13 kbps GSM-FR scheme. The definition of the 6.7 kbps Japanese JDC VSELP codec was almost coincident with that of the IS-54 arrangement. This codec development was also followed by a half-rate standardisation process, leading to the 3.2 kbps PSI-CELP scheme. The IS-96 American CDMA system also has its own standardised CELP-based speech codec, which is a variable-rate scheme, allowing bitrates between 1.2 and 14.4 kbps, depending on the prevalent voice activity. The perceived speech quality of these cellular speech codecs contrived mainly during the late 1980s was found subjectively similar to each other under the perfect channel conditions of Figure 18.4. Lastly, the 5.6 kbps GSM-HR also met its specification in terms of achieving a similar speech quality to the 13 kbps original GSM-FR arrangements, although at the cost of quadruple complexity and higher latency.

Following the above elaborations as regards to the perceived speech quality of a range of speech codecs, let us now consider their objective speech quality and robustness aspects in the next section.

18.6 Error Sensitivity Comparison of Various Codecs

As a rudimentary objective speech quality measure-based bit-sensitivity comparison, in Figure 18.5 we portrayed the SEGSNR degradations of a number of speech codecs for a range of BERs, when applying random errors. The SEGSNR degradation is not, in general, a reliable measure of speech quality; nonetheless, it indicates, adequately, how rapidly this objective speech quality measure decays for the various codecs when exposed to a given fixed BER. As expected, the backwards-adaptive G.728 and the forward-adaptive G.723.1 schemes, which have been designed mainly for benign wireline connections, have the fastest SEGSNR degradation upon increasing the BER. By far the best performance is exhibited by the G.729 scheme, followed by the 13 kbps GSM codec. In the next section we highlight how these codecs perform over Gaussian and Rayleigh-fading channels using three different transceivers.

18.7 Objective Speech Performance of Various Transceivers

In this section we embark upon the comparison of the previously analysed speech codecs under identical experimental circumstances, when used in identical transceivers over both

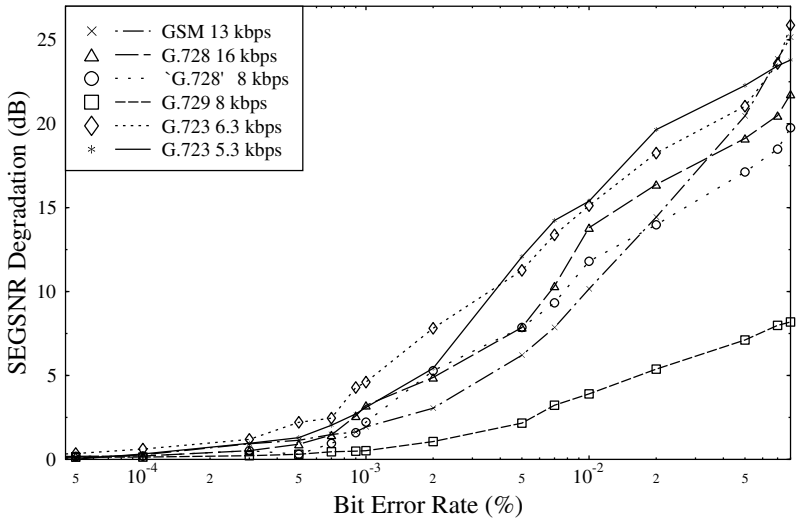

Figure 18.5: SEGSNR degradation versus BER for the investigated speech codecs.

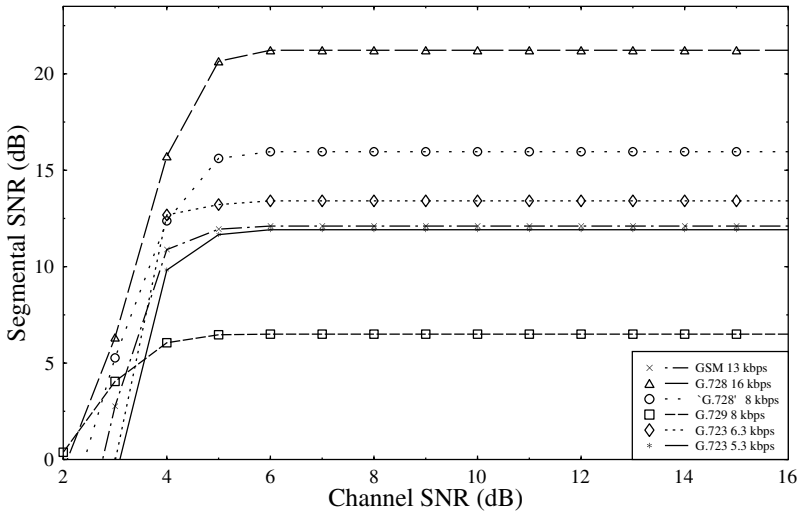

Figure 18.6: SEGSNR versus channel SNR performance of various speech codecs using the BCH(254,130,18) code and BPSK over Gaussian channels.

Gaussian and Rayleigh channels. These results are portrayed in Figures 18.6–18.11, which are detailed during our further discourse. Three different modems, namely one, two and four bits per symbol BPSK, 4QAM and 16QAM were employed in conjunction with the six different modes of operations of the four speech codecs that were protected by the BCH(254,130,18) channel codec. Note that no specific source-sensitivity matched multi-class channel coding was invoked here, in order to ensure identical experimental conditions

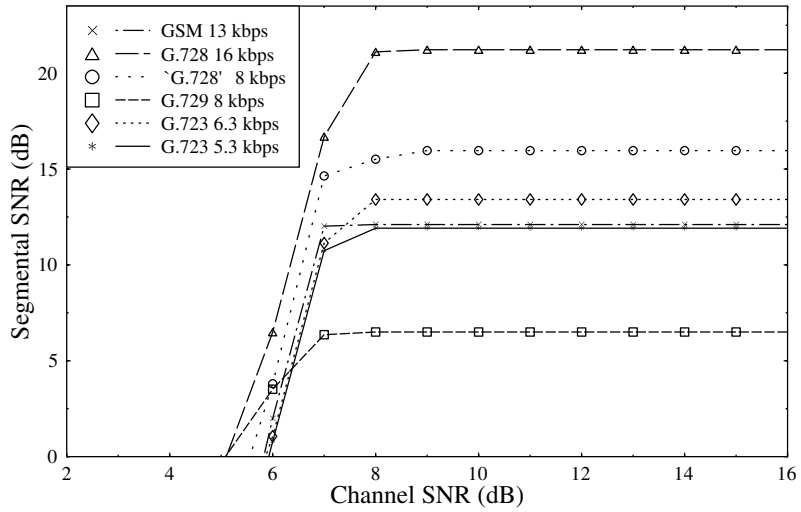

Figure 18.7: SEGSNR versus channel SNR performance of various speech codecs using the BCH(254,130,18) code and 4QAM over Gaussian channels.

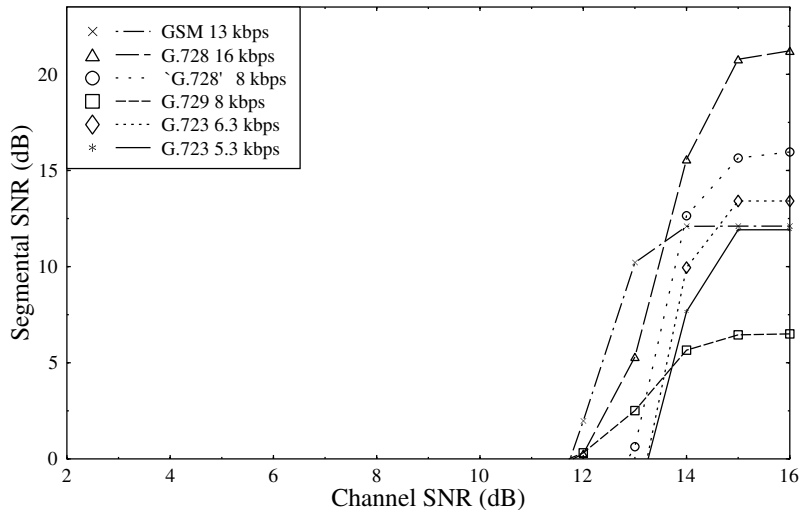

Figure 18.8: SEGSNR versus channel SNR performance of various speech codecs using the BCH(254,130,18) code and 16QAM over Gaussian channels.

for all speech codecs. Although, in general the SEGSNR is not a good absolute measure, when comparing speech codecs operating on the basis of different coding algorithms, it can be used as a robustness indicator, exhibiting a decaying characteristic for degrading channel conditions and hence allowing us to identify the minimum required channel SNRs for the various speech codecs and transceiver modes. Hence, here we opted for using the SEGSNR in these comparisons, providing us with an opportunity to point out its weaknesses on the

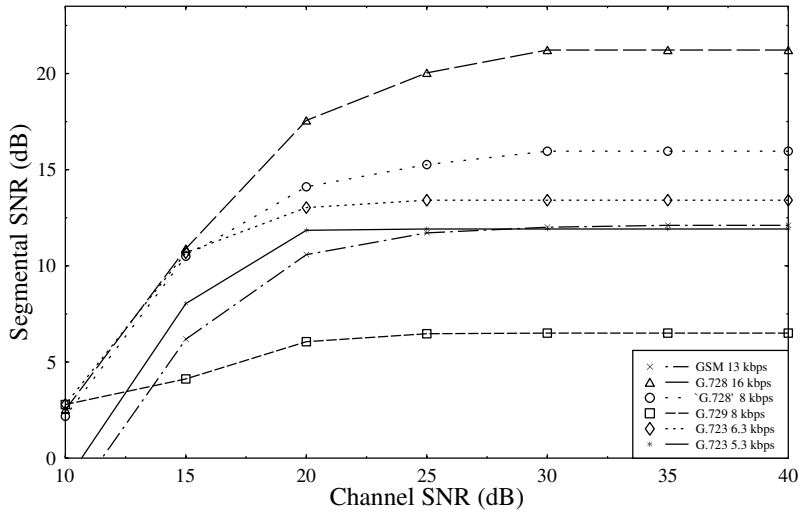

Figure 18.9: SEGSNR versus channel SNR performance of various speech codecs using the BCH(254,130,18) code and BPSK over Rayleigh channels.

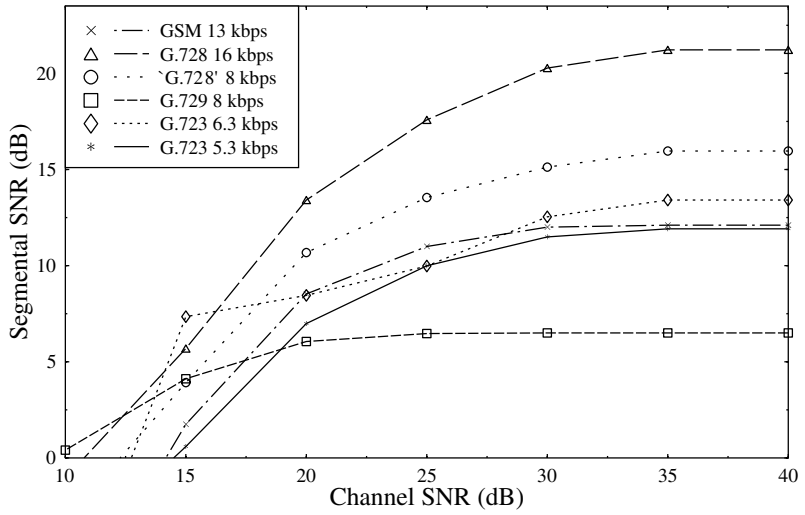

Figure 18.10: SEGSNR versus channel SNR performance of various speech codecs using the BCH(254,130,18) code and 4QAM over Rayleigh channels.

basis of our *a priori* knowledge as regards to the codecs' formally established subjective quality.

Under error-free transmission and no-background-noise conditions the subjective speech quality of the 16 kbps G.728 scheme, the 8 kbps G.729 codec and the 6.4 kbps G.723.1 arrangement is characterised by a MOS of approximately four. In other words, their perceived speech quality is quite similar, despite their different bitrates. Their similar speech quality

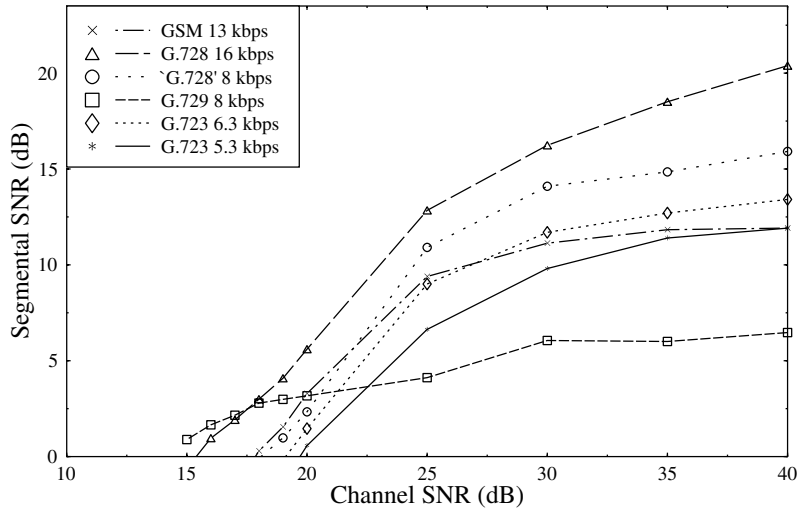

Figure 18.11: SEGSNR versus channel SNR performance of various speech codecs using the BCH(254,130,18) code and 16QAM over Rayleigh channels.

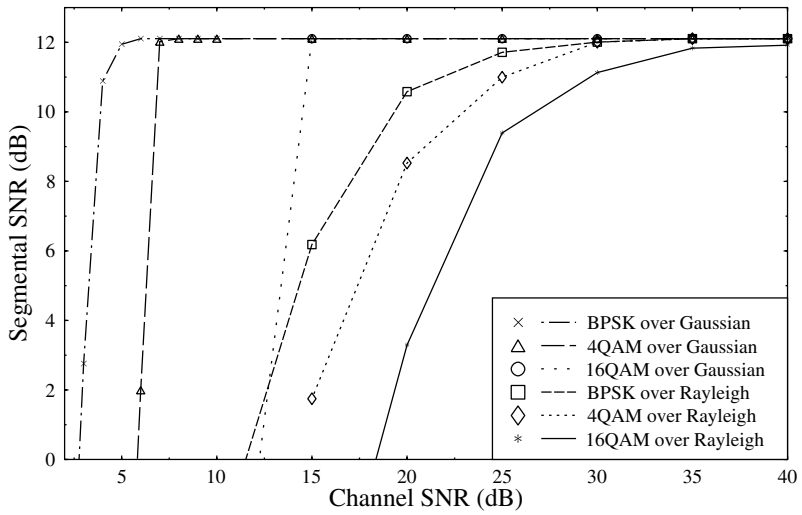

Figure 18.12: SEGSNR degradation versus channel SNR performance of the 13 kbps RPE-LTP GSM speech codec using the BCH(254,130,18) code and BPSK, 4QAM as well as 16QAM over both Gaussian and Rayleigh channels.

at such different bitrates is a ramification of the fact that they represent different milestones during the evolution of speech codecs, because they were contrived in the above chronological order. They also exhibit different implementational complexities. The 13 kbps GSM codec and the 5.3 kbps G.723 arrangements are slightly inferior in terms of their subjective quality, both of which are characterised by a MOS of about 3.5. We note here, however, that there

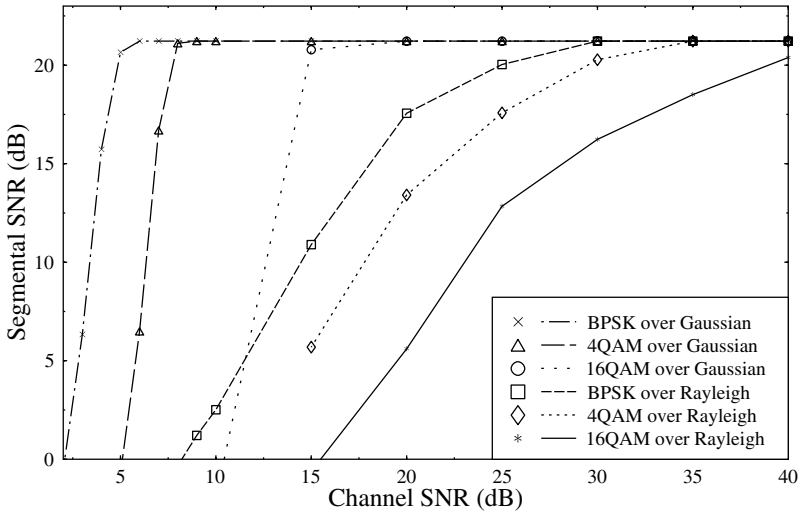

Figure 18.13: SEGSNR degradation versus channel SNR performance of the 16 kbps backward-adaptive G.728 speech codec using the BCH(254,130,18) code and BPSK, 4QAM as well as 16-QAM over both Gaussian and Rayleigh channels.

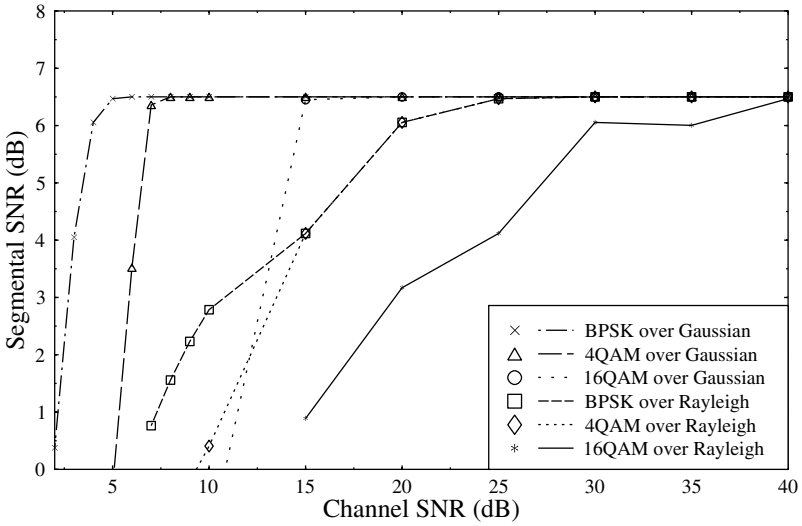

Figure 18.14: SEGSNR degradation versus channel SNR performance of the 8 kbps forward-adaptive G.729 speech codec using the BCH(254,130,18) code and BPSK, 4QAM as well as 16QAM over both Gaussian and Rayleigh channels.

exists a recently standardised so-called enhanced full-rate, 13 kbps GSM speech codec, which also has an MOS of about 4 under perfect channel conditions.

The above subjective speech qualities are not reflected by the corresponding SEGSNR curves portrayed in Figures 18.6–18.11. For example, the 8 kbps G.729 codec has the lowest SEGSNR, although it has a MOS similar to G.728 and the 6.4 kbps G.723.1 schemes in terms

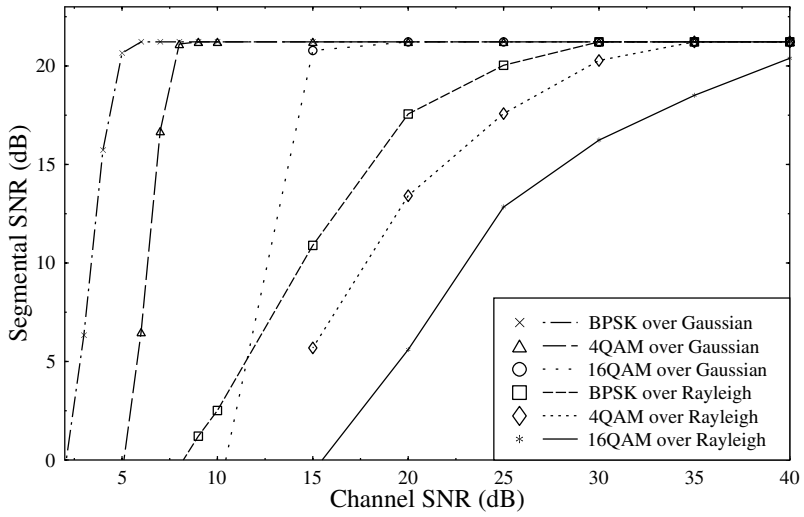

Figure 18.15: SEGSNR degradation versus channel SNR performance of the 5.3 kbps G.723.1 speech codec using the BCH(254,130,18) code and BPSK, 4QAM as well as 16QAM over both Gaussian and Rayleigh channels.

Table 18.3: Minimum required channel SNR for maintaining less than 1 dB SEGSNR degradation for the investigated speech transceivers using the BCH(254,130,18) code and BPSK, 4QAM as well as 16QAM over both Gaussian and Rayleigh channels.

		BPSK		4QAM		16QAM	
Codec	Rate (kbps)	AWGN	Rayleigh	AWGN	Rayleigh	AWGN	Rayleigh
GSM	13	4	20	7	27	13	34
G.728	16	5	26	8	30	15	40
'G.728'	8	5	25	7	31	15	35
G.729	8	4	19	7	20	14	28
G.723.1	6.4	4	18	8	31	15	35
G.723.1	5.3	4	19	7	29	15	35

of subjective speech quality. As expected, this is due to the high-pass filtering operation at its input, as well as a ramification of the more pronounced perceptually motivated speech quality optimisation, as opposed to advocating high-quality waveform reproduction. A further interesting comparison is offered by the 8 kbps 'G.728-like' non-standard codec, which exhibits a higher SEGSNR than the identical bitrate G.729 scheme, but sounds significantly inferior to the G.729 arrangement. These differences become even more conspicuous, when they are exposed to channel errors in the low-SNR region of the curves. In terms of error resilience the G.729 scheme is by far the best in the group of codecs tested. The minimum required channel SNR values for the various transceivers over the Gaussian and Rayleigh channels are summarised in Table 18.3. Observe in the Rayleigh-channel curves of

Figures 18.9–18.11 that the backwards-adaptive codecs have a rapidly decaying performance curve, whereas for example the G.729 forward-adaptive ACELP scheme exhibits a more robust behaviour. Finally, in Figures 18.12–18.15 we organised our previous results in a different way, plotting all of the different SEGSNR versus channel SNR curves related to a specific speech codec in the same figure, allowing a direct comparison of the expected speech performance of the various transceivers over various channel conditions.

18.8 Chapter Summary

In this closing chapter we commenced our discourse by a rudimentary overview of speech quality measures, which can be used for assessing the achievable speech quality of various codecs. Initially, the family of objective measures was considered and various SNR-based objective speech quality metrics were introduced, followed by the definition of the AI, the CD, the LLR and the Euclidean distance metrics. We also alluded to the various issues involved in subjective testing and reflected on the employment of both subjective as well as objective speech quality measures. The chapter was concluded with a rudimentary comparison of various speech transceivers in terms of their achievable speech quality and robustness against transmission errors.

Chapter 19

The Voice over Internet Protocol

19.1 Introduction

VoIP facilitates voice communications over packet-switched networks, which by now pervades our daily lives in the form of an increasing number of low-cost, best-effort voice services. The concept of packet-switched networks spread from fixed wireline-based local area networks (LAN) and fixed wide area networks (WAN) to wireless links, because a section of the connection is often wireless. This chapter concentrates on introducing the reader to the general principles of VoIP, which apply equally to fixed and wireless connections. However, the specific techniques of VoIP that are particularly useful for wireless connections are highlighted.

Establishing a reliable and high-quality voice call on a packet-switched network involves overcoming several challenges. The first challenge is to locate the participants who could be anywhere, connected by either a fixed or a wireless link. Once they have been located, a reliable signalling mechanism is required in order to establish a connection between the call participants. Furthermore, the choice of the voice codec that will be used must also be negotiated between the parties, both of which may be able to activate a number of different voice codecs. Finally, the encoded voice signal must be transmitted across the network, where the voice packets are subjected to reordering, delay or even loss/erasure. Popular VoIP implementations include standardised solutions, such as the International Engineering Task Force (IETF) Session Initiation Protocol (SIP) [566] and the International Telecommunications Union (ITU) H.323 [567] system. In addition to the above-mentioned standard solution, a number of proprietary schemes, such as Skype, have also been successfully launched. Any speech codec can be used in VoIP solutions, provided that both participants of the call are capable of using the selected codec, but naturally, certain standardised voice codecs are more popular. More specifically, speech codecs that are typically used in VoIP calls are often chosen from the ITU family of codecs, including G.711 [568], G723.1 [569] and G729 [570], as well as from the family of popular speech codecs typically used in wireless mobile networks such as GSM [571, 572] and UMTS [573]. Furthermore, wideband speech codecs, such as

Voice and Audio Compression for Wireless Communications Second Edition
L. Hanzo, F. C. A. Somerville and J. P. Woodard

G729.1 [574] are also becoming more popular and allow VoIP schemes to provide superior quality in comparison to standard telephone calls.

This chapter concentrates on the two most popular methods of implementating a VoIP scheme, namely, the IETF's SIP [566, 575] and the ITU's H.323 standard [567, 576, 577]. Both the SIP and H.323 schemes use the Real-time Transport Protocol (RTP) [578] as their data transfer mechanism, hence this will also be described in this chapter.

19.2 Session Initiation Protocol

19.2.1 Introduction

The SIP is rapidly becoming the most popular protocol for VoIP, which is a text-based protocol, has a simple implementation and has many syntax-related similarities to the Hyper-Text Transfer Protocol (HTTP) traditionally used in the Internet. In addition to supporting VoIP, the SIP, as the terminology implies, was designed to create and manage a session between two clients. Once established, the session can be used for exchanging signals representing arbitrary types of media, such as for instance, voice, video or multimedia messaging.

A SIP call will include several different network elements, clients, servers, proxies and registrars, as detailed below. A client is the end point of a SIP call and is defined as a network element, which sends SIP requests and receives SIP responses, where a human user will interact with a client in order to set up and receive VoIP calls. A SIP server is a network element, that processes SIP requests and returns responses, while a SIP proxy is a network element, that contains both a server and a client, and will route messages between two SIP clients. Finally, the registrar accepts registration requests from a SIP client and hence it is instrumental in locating SIP clients by providing a location service to SIP servers.

Part of the establishment of a VoIP session using SIP is to describe the particular media format that the two clients will exchange during the call. This media is described using the Session Description Protocol (SDP) [579], which will be detailed in Section 19.2.3. In addition to the SIP, the SDP may also provide security features to support the authentication of SIP messages and the encryption of multimedia signals, however, this is considered to be beyond the scope of a speech coding book and hence will not be described in further detail.

19.2.2 SIP Signalling

19.2.2.1 Registration

Before a client can set up a voice call, or participate in any type of SIP session, it must first register with a server, which provides a registration facility and the specific type of server, that offers this service is referred to as a registrar. The registrar keeps a record of any clients that have registered and hence it is capable of providing location information for other SIP servers. The registrar plays a critical role in allowing the SIP user to move location, for instance, within a mobile network.

SIP addresses have a similar structure to email addresses, but must include the keyword 'sip'. The registrar remembers the mapping from SIP addresses to IP address and this allows the client to move between different registrars, while still being located. The registration message sequence is shown in Figure 19.1, where the SIP client issues a register to the

local registrar. Then, provided that the registration is successful, the registrar will return the successful (OK) SIP response message.

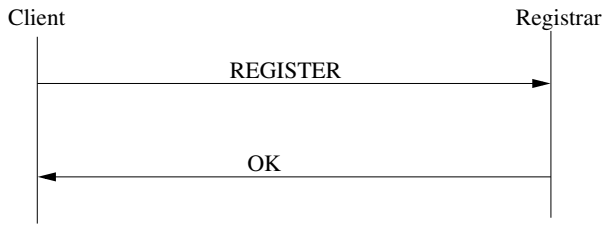

Figure 19.1: SIP registration procedure.

A typical REGISTER message is given below, where john@soton.ac.uk registers with the local registrar, registrar@soton.ac.uk:

- REGISTER sip:registrar@soton.ac.uk SIP/2.0
- Via: SIP/2.0/UDP 192.168.0.1; branch=z9hG4bKab6th79
- From: John Doe <sip:john@soton.ac.uk>
- To: John Doe <sip:john@soton.ac.uk>
- Call-ID: mcowifj998@soton.ac.uk
- CSeq: 4710 REGISTER
- Content-Length: 0

As seen in the above list, the *REGISTER* message begins by indicating the specific client that the request should be sent to, namely registrar@soton.ac.uk and that the SIP version used is version 2.0. The *Via* field indicates the transport mechanism that should be used for the response, which is in this case the User Data Protocol (UDP), and the IP address the response should be returned to, which is 192.168.0.1. Next the caller and called party are identified by their respective SIP addresses, which implies that the SIP client inserts its own address (john@soton.ac.uk) in both the *From* and *To* fields. The REGISTER request contains several fields used for assisting in matching the returned response to the request. A sequence number *CSeq* is used for matching the request and response primitives, the *Call-ID* uniquely identifies the call, while the *branch* field of *Via* is used by both the client and server to identify the transaction. Finally, the *Content-Length* field is set to zero. in order to indicate that this SIP message does not contain a body.

All SIP request messages are acknowledged by sending the *SIP response message*, which contains a status code. For example, the *status code* 200 represents an *OK* response. A typical *OK* response to the above-mentioned *REGISTER* message is given below:

- SIP/2.0 200 OK
- Via: SIP/2.0/UDP 192.168.0.1; branch=z9hG4bKab6th78;
  received=192.168.0.4

- From: John Doe <sip:john@soton.ac.uk>
- To: John Doe <sip:john@soton.ac.uk>
- Call-ID: mcowifj998@soton.ac.uk
- CSeq: 4710 REGISTER
- Content-Length: 0

The client attempts to match the *branch, Call-ID* and *CSeq* codes and finds that this is the response to its REGISTER message, but the response to the REGISTER message does not contain a message body.

The above-mentioned SIP response message is returned in reply to all other SIP messages. Again, a *status code* is used to indicate the success, failure or ongoing status of the procedure. Similar status codes are grouped together in a code family. For example, the set of codes 2xx, such as the above-mentioned status code 200, indicates that the message was successful. By contrast, the family of 3xx format codes relates to redirection information, the codes 4xx indicate some form of client error, the 5xx codes indicate a server error, while 6xx indicates some form of global failure. A few examples of specific status/error codes are as follows: 200 (OK), 100 (trying), 180 (ringing), 181 (call is being forwarded), 182 (queued), 404 (not found) and 486 (busy). The SIP response message contains both the error code and a textual description which may be displayed to the client user. Even if a SIP client is unable to explicitly interpret a specific error code, it may still be able interpret at least the type of response received and display the received textual information to the user for more explicit interpretation.

19.2.2.2 Call Setup

Following the above-mentioned registration procedure, the client is allowed to initiate a SIP session in order to create a voice call. The SIP primitives are rarely exchanged directly between clients, instead they are typically routed via SIP proxies. The basic signalling exchange required for establishing a SIP call is portrayed in Figure 19.2, where all messages are routed via two proxies. The caller initiates a SIP session with the Callee by sending an *INVITE* message to the SIP server he/she has registered with (Proxy A). Proxy A is unaware of the location of the Callee, hence it forwards the *INVITE* request to Proxy B. As the Callee is registered with Proxy B, he/she receives the *INVITE* message. Provided that the Callee is willing to receive the call, a response message with code 200 (OK) is returned. Finally, the *ACK* primitive is used to complete handshaking and the session is established. There can be multiple SIP proxies between the two clients that have to be involved in establishing a SIP call. If a proxy receives an *INVITE* primitive destined for an unknown client, then it will forward this message to other SIP proxies it is aware of. The SIP proxy will receive a response from each of the proxies contacted, indicating whether the Callee has been located. The corresponding status codes are 200 (OK) or 404 (not found). The specific route followed by the message through SIP servers is recorded inside the message bodies, which allows future SIP messages transmitted during the same session to follow the same route without requiring the servers to store any routing information.

The *INVITE* primitive is used to initiate all of the sessions between two clients and a typical *INVITE* message is given below:

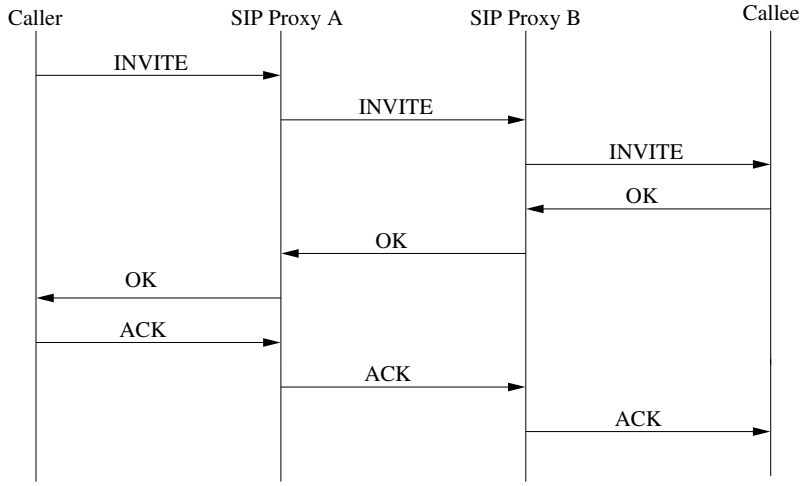

Figure 19.2: SIP call setup procedure.

- INVITE sip:jane@company.com SIP/2.0
- Via: SIP/2.0/UDP 192.168.0.1; branch=z9hG4bKab6th78
- Max-forwards: 40
- From: John Doe <sip:john@soton.ac.uk>
- To: Jane Smith <sip:jane@company.com>
- Call-ID: mcowifj998@soton.ac.uk
- CSeq: 4711 INVITE
- Content-Type: application/sdp
- Content-Length: 142
- <SDP contents>

The *INVITE* message is forwarded to the SIP address of the callee, in this exampleplejane@company.com. The message also contains the SDP information described in Section 19.2.3, which will define the specific voice codecs that the caller (john@soton.ac.uk) is capable of using. The *INVITE* message is then sent to the local server at 192.168.0.1, the server receives the *INVITE* message and checks with the local registrar, whether the callee is present in its SIP network. If the callee is indeed present, the INVITE message is forwarded to him/her. By contrast, if the callee has not registered with the local registrar, the SIP server can either forward the *INVITE* message to other servers, or return a response message containing the code 404 (not found).

When the *INVITE* message reaches the callee, this will be acknowledged by returning the standard SIP response message, including the status code. A typical response message to the

INVITE primitive containing the OK status code of 200 is given below, where the response message includes the SDP description indicating the specific types of speech codecs that can be used by the callee.

- SIP/2.0 200 OK
- Via: SIP/2.0/UDP 192.168.0.1; branch=z9hG4bKab6th78; received=192.168.0.4
- From: John Doe <sip:john@soton.ac.uk>
- To: Jane Smith <sip:jane@company.com>
- Call-ID: mcowifj998@soton.ac.uk
- CSeq: 4711 INVITE
- Content-Type: application/sdp
- Content-Length: 100
- <SDP contents>

The final message required for setting up a voice call is the *ACK* primitive and is used for completing the handshaking between the two clients. A typical *ACK* message is given below:

- ACK sip:jane@company.com SIP/2.0
- Via: SIP/2.0/UDP 192.168.0.1; branch=z9hG4bKab6th79
- Max-forwards: 40
- From: John Doe <sip:john@soton.ac.uk>
- To: Jane Smith <sip:jane@company.com>
- Call-ID: mcowifj998@soton.ac.uk
- CSeq: 4711 ACK
- Content-Length: 0

19.2.2.3 Terminate a Call

An active SIP session can be terminated by either the caller or callee using the *BYE* message, as shown in Figure 19.3, where the caller hangs up on the callee. The callee should complete the call termination by returning the status response message of 200, signalling the OK code.

A typical *BYE* message is given below, where Jane has terminated her call with John:

- BYE sip:john@soton.ac.uk SIP/2.0
- Via: SIP/2.0/UDP 192.168.0.1; branch=z9hG4bKab6th80
- Max-forwards: 40

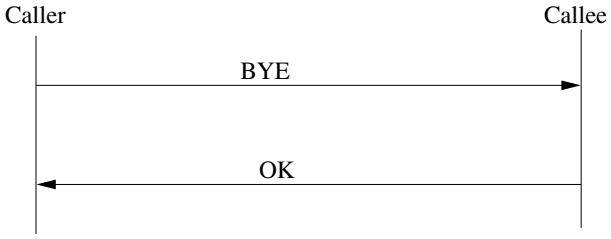

Figure 19.3: SIP call termination procedure.

- From: Jane Smith <sip:jane@company.com>
- To: John Doe <sip:john@soton.ac.uk>
- Call-ID: mcowifj998@soton.ac.uk
- CSeq: 1000 BYE
- Content-Length: 0

19.2.2.4 Cancel a Call

At any time during the call-setup process, the caller may decide to abort the call. If this decision is made before a positive response has been received by the caller, then the caller can issue the CANCEL message, in order to terminate the call setup, as shown in Figure 19.4. However, if the caller has received any type of response message, his/her client should follow the call termination procedure *CANCEL* outlined below:

- CANCEL sip:john@soton.ac.uk SIP/2.0
- Via: SIP/2.0/UDP 192.168.0.1; branch=z9hG4bKab6th78
- Max-forwards: 40
- From: Jane Smith <sip:jane@company.com>
- To: John Doe <sip:john@soton.ac.uk>
- Call-ID: mcowifj998@soton.ac.uk
- CSeq: 4711 CANCEL
- Content-Length: 0

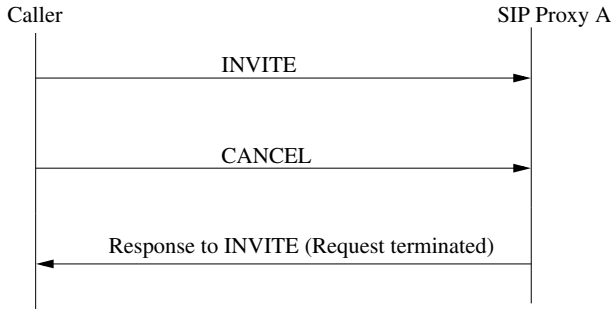

Figure 19.4: SIP cancellation procedure.

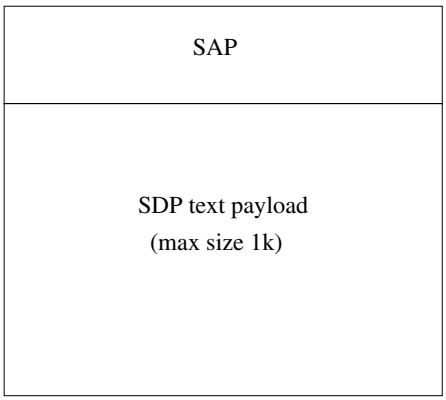

Figure 19.5: SDP packet.

19.2.3 Session Description Protocol

The SDP [579] was originally designed for advertising the transmission media used in a multicast session. Later, the SDP was also adopted by the SIP as the *defacto* method of advertising the media, which will be used in a VoIP call. The format of a SDP message is given in Figure 19.5, where the Session Announcement Protocol (SAP) may be chosen to be SIP.

The SDP payload includes a message, which allows the two ends of the voice call to establish, whether they have any speech codecs, which can be used by both of them. Typically, each SIP client should be able to use the ITU's G.711 [568] codec, in order to ensure that at least one speech codec is available for setting up the call. The SDP description includes a session name, a media type and a media format together with the requested transport mechanism. In addition, features such as the channel bandwidth and the recommended packet periodicity can be included. An example of the SDP description used for the G729 [570] codec's media session is provided below:

- $v = 0$
- $o =$ jane 123456789 987654321 IN IP4 192.168.0.1

- $s =$ -
- $t =$ 1983397522 1983404722
- $m =$ audio 53146 RTP/AVP 18
- $a =$ rtpmap:18 G729/8000
- $a =$ ptime:40

In this example $v = 0$ indicates the specific SDP version used, in this case version zero. The next field, o, defines the owner and identifier of the session and is constructed from multiple fields, as follows:

$$o = <\textit{username}><\textit{session id}><\textit{version}><\textit{network type}><\textit{address type}><\textit{address}>$$

The username is the login name of the session initiator, while the session id and version should be combined with the username to create a unique, user-specific identifier. The network type and address type indicate the type of network connection being used, where IN indicates the Internet, while IP4 indicating that IPv4 is used. Finally, the address identifies the host machine, where the session originates from.

The session name, namely the s field, must be included and it contains the name of the session, although it can also be left blank. The time, namely the t field, must be included and specifies the start and stop time of the session in seconds. The media attribute field m is constructed from the following multiple fields:

$$m = <\textit{media}><\textit{port}><\textit{transport}><\textit{fmt list}>$$

For a VoIP call the first attribute should be set to audio, the second field indicates the specific port number the media should be sent to, the third field indicates the transport mechanism used for the media for VoIP, which is usually RTP/AVP, which stands for the RTP using the audio/video profile over UDP [578, 580]. The final attribute indicates the media payload format and is defined in [580], where the identifier 18 was reserved for a G.729 payload type. The remaining attribute field, namely field a, further extends the description of the selected speech coder, where the *rtpmap* attribute has the following format:

$$a = rtpmap : <\textit{payload type}><\textit{encoding name}/\textit{clock rate}>[<\textit{encoding parameters}>]$$

The payload type is 18, which matches the previous media payload format, the encoder's acronym of G729 represents the ITU G.729 narrowband speech codec, which uses a sampling rate of 8000. The *ptime* attribute has the following format: $a = \textit{ptime} : <\textit{packet time}>$ and it recommends the specific number of speech packets to be mapped to each RTP/UDP packet by suggesting the length of the speech segment in each packet, which is expressed in milliseconds.

If a SIP client supports the employment multiple audio formats, then multiple speech codecs can be suggested in the media attribute field. The following example shows a client that supports the employment of the G.711 [568], GSM [571] and G.729 [570] speech coders, which have the payload types of 0, 3 and 18, respectively:

- $v = 0$
- $o =$ jane 123456789 987654321 IN IP4 192.168.0.1
- $s =$ -
- $t =$ 1983397522 1983404722
- $m =$ audio 53146 RTP/AVP 0 3 18
- $a =$ rtpmap:0 PCMU/8000
- $a =$ rtpmap:3 GSM/8000
- $a =$ rtpmap:18 G729/8000

When the callee receives a SDP content in an *INVITE* message containing multiple speech codecs, the response message will contain a list of the common elements between the suggested codecs and the codecs it also supports.

Having considered the basics of VoIP-aided speech communications in the context of the SIP, let us now consider the employment of the ITU's H.323 standards, as a design alternative.

19.3 H.323 Standards

19.3.1 Introduction

The H.323 recommendation was developed as an ITU standard [567] to ensure the interoperability of the different multimedia communication systems developed and it constitutes the standard of choice for carrying voice traffic over packet networks that are controlled by an operator, such as a packet network between two public-switched telephone networks (PSTNs). H.323 is not a complete VoIP standard, instead it specifies the different standards which can be used for the various procedures in a VoIP call and provides an overview of how the different standards can be used together. To set up and maintain a VoIP call, the ITU standards H.225 [577] and H.245 [576] are recommended. Similarly to the SIP, H.323 also specifies that RTP [578] should be used as the voice transport mechanism. Only a system which entirely obeys the specified standards can be considered a H.323 network.

An H.323 network is constituted by several different components, including terminals, gateways, gatekeepers and multi-point control units (MCUs). The terminal is the endpoint of an H.323 call and can be a personal computer (PC) running an H.323 stack, or may be a standalone device such as H.323-enabled telephone. The gateway provides a connection between an H.323 network and other types of networks, such as a PSTN. The gateway must be capable of translating signalling messages and converting media formats between the two networks. Terminals within the same H.323 network do not communicate via the gateway. The gatekeeper is an optional element within an H.323 network and, if it is present, it provides the following services: registration, bandwidth management, accounting and, additionally, it may also provide call-routing. Finally, the MCU is used to support conference calls between multiple terminals.

19.3.2 H.323 Signalling

This section describes the procedures that must be followed in order to create and maintain a VoIP call in an H.323 network. Initially H.225 signalling is used to set up the connection between two terminals and subsequently H.245 signalling is used for establishing the capabilities of the terminals and to create the communication link for the media packets. H.245 signalling is also used by the terminal in order to register with a gatekeeper.

19.3.2.1 Registration

In order for a terminal to commence H.323 services, allowing it to initiate and receive voice calls, it must first locate a gatekeeper and carry out the registration procedure shown in Figure 19.6.

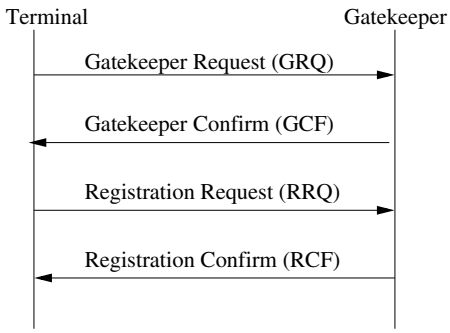

Figure 19.6: H.323 registration.

In order to discover and register with the local gatekeeper, the terminal will send a Gatekeeper Request (GRQ) message to the well-known discovery multicast address for gatekeepers. If a gatekeeper is present in the network, it will either return the Gatekeeper Confirm (GCF) message, indicating that it is willing to act as a gatekeeper for the terminal, or send the Gatekeeper Reject (GRJ) message.

Once a suitable gatekeeper is located, the terminal sends the Registration Request (RRQ) message. This message includes information such as the type of terminal, its address information, which allows the gatekeeper to route calls destined for it, and any credentials required for demonstrating that the terminal is entitled to H.323 services. The gatekeeper will either accept the terminal and return the Registration Confirm (RCF) message, or reject the terminal using the Registration Reject (RRJ) message.

19.3.2.2 Call Establishment

Following the registration procedure, the terminal can initiate or receive VoIP calls. If the terminal wishes to initiate a voice call, then it will use the H.225 signalling procedure, outlined in Figure 19.7, in order to contact the called party and to set up a call.

When a terminal initiates a VoIP call, it must first request access to the network from the local gatekeeper using the Admission Request (ARQ) message, which is part of the *Registration, Admission* and *Status* (RAS) signalling procedure specified by H.225. The ARQ

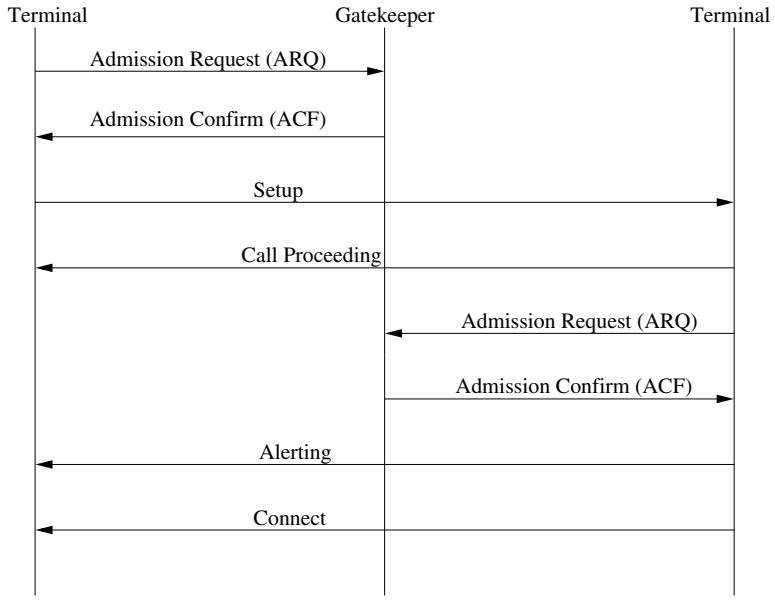

Figure 19.7: H.323 call establishment.

message includes the type of call the terminal intends to initiate, which allows the gatekeeper to monitor the available bandwidth within the network. It also specifies whether the terminal wishes to establish a direct call to another terminal, or to be routed via the gatekeeper to the end destination for the call. The gatekeeper will return either an *Admission Confirm* (ACF) or an *Admission Reject* (ARJ) message to the terminal. The maximum bandwidth available for the call is also included in the ACF message, which is decided by the gatekeeper by monitoring the available bandwidth in the H.323 network. Naturally, this bandwidth may be lower than that requested by the terminal.

Following an ACF message received from the gatekeeper, the H.225 call signalling message referred to as *Setup* is sent to the called terminal. If the H.323 network does not contain a gatekeeper, then the RAS messages are skipped and the call-setup procedure starts with the Setup message. The Setup message contains both the number of the calling and called party, together with information about the type of call being initiated. The called party will return the *Call Proceeding* message, in order to indicate that it has started the process of accepting a call. If a gatekeeper is present in the H.323 network, the called terminal must receive permission to access the network using the same admission procedure. Once the called terminal has been admitted to the network, it will send an *Alerting* message to the calling terminal, which indicates that the 'phone is ringing'. Finally, once the called user has answered the alert, the *Connect* message is returned to the calling terminal and the call establishment is complete.

19.3.2.3 Capability Exchange

As part of the call setup, the participating terminals must set up a H.245 control channel and exchange information concerning their respective capabilities, as shown by the H.245 signaling procedure outlined in Figure 19.8.

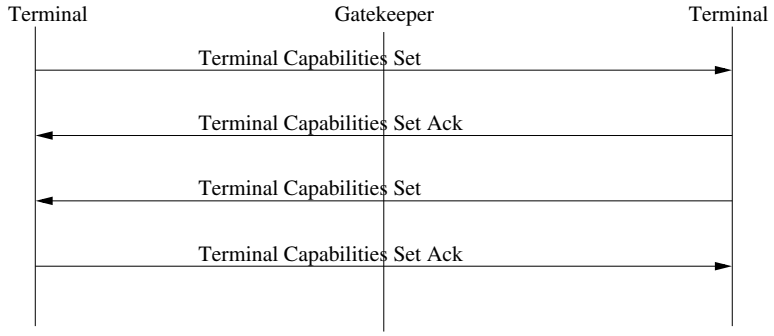

Figure 19.8: H.323 capability exchange.

The *Terminal Capability Set* message contains a list of different audio, video and data codecs that the terminal is capable of using. This description is sufficiently detailed, so that it also specifies, which codecs can be supported simultaneously. The *Terminal Capability Set Acknowledgement* message is used to confirm the receipt of the Terminal Capability Set message. Both terminals send the Terminal Capability Set message, which informs both terminals of the set of speech codecs, which are mutually supported.

19.3.2.4 Establishment of Media Communication

In order to transfer voice, video or data between the two terminals, appropriate logical channels must be setup, which are shown in Figure 19.9. Each terminal is responsible for setting up the logical channel it will use to send the media data to the other terminal. In H.323 the media data is carried by an RTP connection, hence the endpoint address for the RTP and the format of the RTP media is described in the *Open Logical Channel* messages. The *Open Logical Channel Acknowledgement* message is used to confirm the information received in the Open Logical Channel message. The call is now set up and voice communication between the two terminals may commence.

19.3.2.5 Call Termination

For a terminal to terminate a voice call the termination procedure shown in Figure 19.10 has to be followed, where the call can be terminated by either party. The call is terminated in the reverse order of the call setup. Firstly, the H.245 control channel's operation is terminated, where the terminal curtailing the call sends the *End Session Command*. When a terminal receives the End Session Command, it stops receiving on the logical channel, issues an End Session Command message for the logical channel it created and stops transmitting data on this channel. The H.225 call signalling channel is closed by the terminating party issuing the *Release Complete* message. Finally, if a gatekeeper is present in the network, both terminals

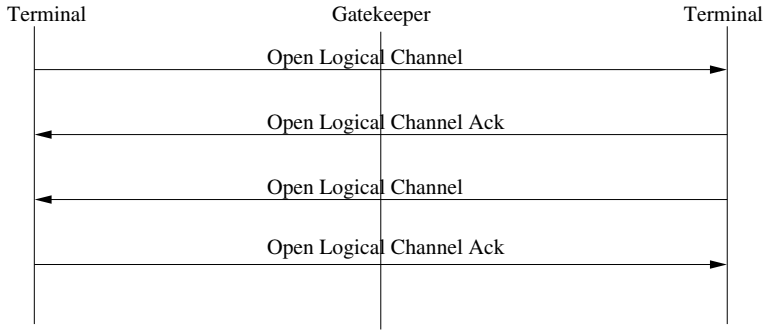

Figure 19.9: H.323 media establishment.

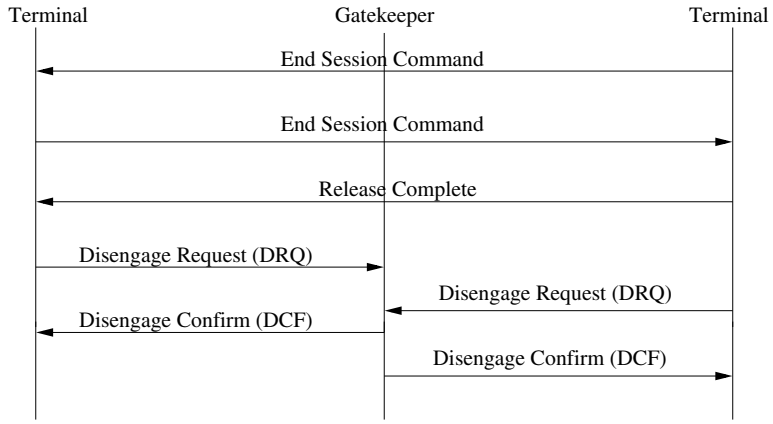

Figure 19.10: H.323 call termination.

use the *Disengage Request* (DRQ) message to inform the gatekeeper that they have dropped the call and hence they no longer require any bandwidth in the network.

19.4 Real-time Transport Protocol

The RTP [578] is used by both the SIP and the H.323 standard in order to transport the encoded speech packets and, hence, this section describes the structure of RTP packets in more depth. RTP packets are designed to carry different data payload formats, depending on the specific speech codec used in the VoIP call, where the RTP header indicates the payload format used. In addition to the payload type indicator, the RTP headers include both time and sequence information, in order to compensate for the potential network-congestion-induced packet reordering, delay and packet loss, which may occur in both fixed and wireless networks.

19.4.1 RTP Header Format

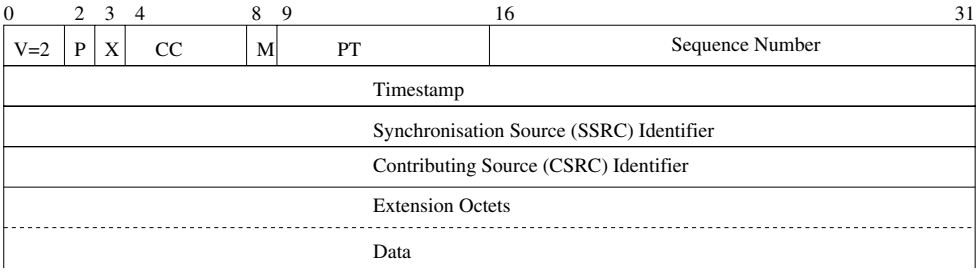

Figure 19.11: RTP payload format.

The general RTP packet structure is seen in Figure 19.11, where v is the RTP version number, while P indicates the padding bits. When P is set, it indicates that padding octets are attached after the payload. Furthermore, X indicates the extension bit, which should be set, if the header includes so-called extension octets, while CC is the number of contributing source (CCRC) identifiers that are present in the header. The field M indicates the marker bit, which has a meaning dependent on the payload type, for instance, for speech codecs using silence suppression it indicates the transition from a silence to a voice segment. The PT bits indicate the payload type of the RTP packet. The sequence number or packet index is used for detecting packets that arrive out of sequence and also to detect packet loss events. The *timestamp* reflects the time instant of the first octet in the payload and is used to detect delayed packets. Finally, the synchronisation and contributing source identifiers (SSRC and CRSC) are listed, which are unique identifiers used for distinguishing both the source and routing path of the RTP packet in the network.

19.4.2 RTP Profiles and Payloads

Common media codecs, including the well-known speech codecs, have their RTP profile described in [580]. This section briefly outlines the payload format for the G.711 and G.729 speech coders.

19.4.2.1 RTP Payload for G.711

The ITU's classic 64 kbps G.711 PCM codec is the voice codec, which every SIP and H.323 VoIP terminal should support. Again, the G.711 standard describes the basic logarithmically companded PCM voice codec, which simply encodes audio/speech samples as 8-bit samples. Each G.711 octet is mapped to a RTP octet, giving the RTP payload format seen in Figure 19.12.

19.4.2.2 RTP Payload for G.729

The G.729 scheme is another commonly supported speech codec in VoIP systems, which may include a VAD and comfort noise generation, hence it is particularly applicable to wireless

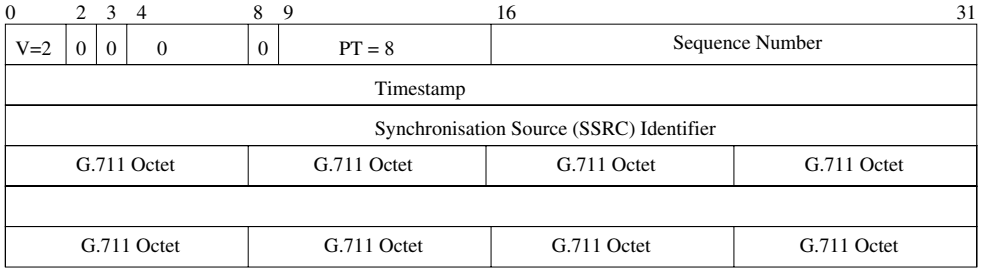

Figure 19.12: RTP payload format for G.711.

systems. The RTP payloads are specified for both voice, as seen in Figure 19.13, and for comfort noise, as portrayed in Figure 19.14. The respective length of the RTP packets is used to distinguish between the voice and comfort noise. In addition, the first voice frame following a comfort noise frame should have the above-mentioned marker bit set to 1. This marker bit combined with the timestamp information should allow the G.729 decoder to accurately determine the length of the silence period. The G.729 voice codec extracts the speech parameters from 10 ms duration speech frames and transfers this information to the decoder. The RTP payload format simply describes how these parameters are mapped to a RTP packet.

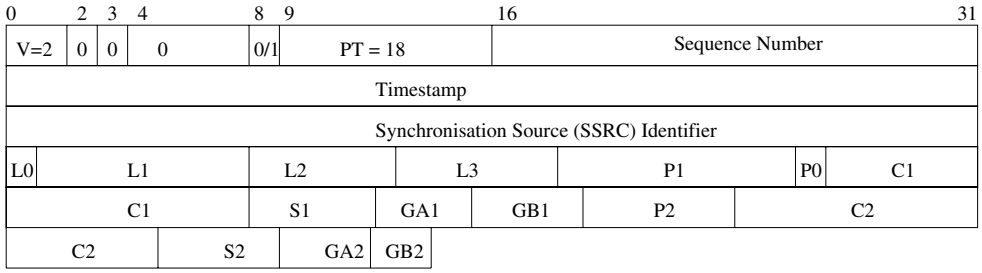

Figure 19.13: RTP payload format for voice frames with a G.729 speech coder.

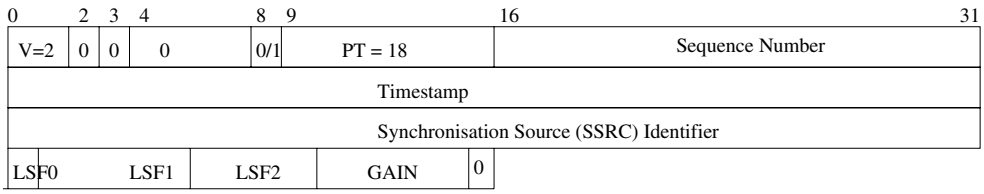

Figure 19.14: RTP payload format for comfort noise frames with a G.729 speech coder.

19.5 Conclusion

This chapter has provided a rudimentary introduction to the two most popular techniques of creating VoIP calls, namely the SIP and H.323. By describing both schemes it is apparent that they use similar principles. A VoIP client must register first in order to receive VoIP services. The registration procedure is critical in allowing the admission of a user to the network. A reliable signalling system is used to set up the voice call and to negotiate the encoding of the voice signals to be exchanged. Finally, the voice data is packetised and transmitted between two VoIP terminals using the RTP, which has been designed to cope with both latency and packet loss events.

Appendix A

Constructing the Quadratic Spline Wavelets

Previously, in Equation (13.4), the Fourier transform of a wavelet was determined, hence the Fourier transform of a father wavelet $\phi(x)$ is given by

$$\hat{\phi}(\omega) = \int_{-\infty}^{\infty} \phi(x) e^{-jx\omega} \, \mathrm{d}x. \tag{A.1}$$

Using the two-scale difference Equation (13.13) we can rewrite the above equation to achieve

$$\hat{\phi}(\omega) = \sqrt{2} \sum_{n=-\infty}^{\infty} h_n \int_{-\infty}^{\infty} \phi(2x - n) e^{-jx\omega} \, \mathrm{d}x. \tag{A.2}$$

Here we introduce the beneficial substitution $y = 2x - n$ allowing Equation (A.2) to be rewritten as

$$\hat{\phi}(\omega) = \frac{1}{\sqrt{2}} \sum_{n=-\infty}^{\infty} h_n e^{-jn\omega/2} \int_{-\infty}^{\infty} \phi(y) e^{-jy\omega/2} \, \mathrm{d}y. \tag{A.3}$$

Employing the identity

$$H(\omega) = \frac{1}{\sqrt{2}} \sum_{n=-\infty}^{\infty} h_n e^{-jn\omega}. \tag{A.4}$$

Equation (A.3) becomes

$$\hat{\phi}(\omega) = H\left(\frac{\omega}{2}\right) \phi\left(\frac{\omega}{2}\right). \tag{A.5}$$

Iterating this result we achieve

$$\hat{\phi}(\omega) = \left[\prod_{i=1}^{I} H(2^{-i}\omega)\right] \phi(2^{-I}\omega) \quad \text{for } I = 1, 2, \ldots. \tag{A.6}$$

Observing that as $I \Rightarrow \infty$ $\hat{\phi}(0) = \int \phi(x)\,\mathrm{d}x = 1$, leaving

$$\hat{\phi}(\omega) = \prod_{i=1}^{\infty} H(2^{-i}\omega). \tag{A.7}$$

Similarly, for the mother wavelet, if we use the identity

$$G(\omega) = \frac{1}{\sqrt{2}} \sum_{n=-\infty}^{\infty} g_n e^{-jn\omega} \tag{A.8}$$

we find that

$$\hat{\psi}(\omega) = \prod_{i=1}^{\infty} G(2^{-i}\omega). \tag{A.9}$$

Mallat and Zhong [524] defined the coefficients of the father wavelet $\hat{\phi}(\omega)$ as a spline function given by

$$H(\omega) = \left[\cos\left(\frac{\omega}{2}\right)\right]^{2n+1} \tag{A.10}$$

where $2n+1$ is the order of the spline function. Thus, the father wavelet of Equation (A.7) is given by

$$\hat{\phi}(\omega) = \prod_{i=1}^{\infty}\left[\cos\left(2^{-i}\frac{\omega}{2}\right)\right]^{2n+1}. \tag{A.11}$$

Expanding this equation becomes

$$\hat{\phi}(\omega) = \left[\frac{e^{j\omega/2}+1}{2e^{j\omega/4}} \times \frac{e^{j\omega/4}+1}{2e^{j\omega/8}} \times \cdots\right]^{2n+1}. \tag{A.12}$$

Considering the denominator as a series we find that

$$e^{j\omega/4} \times e^{j\omega/8} \times \cdots \Rightarrow e^{j\omega/2} \quad \text{as } i \Rightarrow \infty. \tag{A.13}$$

Considering the numerator as a series we find that

$$\frac{e^{j\omega/2}+1}{2} \times \frac{e^{j\omega/4}+1}{2} \times \cdots \Rightarrow \frac{1-e^{j\omega}}{2^I(1-e^{-j\omega/2^I})} \quad \text{as } i \Rightarrow I. \tag{A.14}$$

Using L'Hôpital's rule we see that

$$\frac{2^I(1-e^{j\omega})}{1-e^{-j\omega/2^I}} \Rightarrow \frac{e^{j\omega}-1}{j\omega} \quad \text{as } I \Rightarrow \infty. \tag{A.15}$$

Hence, the father wavelet is given by

$$\hat{\phi}(\omega) = \left[\frac{\sin(\omega/2)}{\omega/2}\right]^{2n+1}. \tag{A.16}$$

Mallat and Zhong [524] defined the coefficients of the mother wavelet $\hat{\psi}(\omega)$ by

$$G(\omega) = 4j \sin\left(\frac{\omega}{4}\right). \tag{A.17}$$

The mother wavelet $\hat{\psi}(\omega)$ can now be calculated using the Fourier domain version of Equation (13.14), namely

$$\hat{\psi}(\omega) = G\left(\frac{\omega}{2}\right)\hat{\phi}\left(\frac{\omega}{2}\right). \tag{A.18}$$

Substituting in $G(\omega)$ and $\hat{\phi}(\omega)$, we achieve

$$\hat{\psi}(\omega) = 4j \sin\left(\frac{\omega}{4}\right) \cdot \left(\frac{\sin(\omega/4)}{\omega/4}\right)^{2n+1}. \tag{A.19}$$

Producing the following mother wavelet:

$$\hat{\psi}(\omega) = j\omega\left(\frac{\sin(\omega/4)}{\omega/4}\right)^{2n+2}. \tag{A.20}$$

Mallat and Zhong [524] implemented a polynomial where $2n + 1 = 3$, and subsequently introduced a shifting constant w_{sc} that ensures $\psi(x)$ is anti-symmetrical with regards to 0 and $\phi(x)$ is symmetrical about 0. This shifting constant w_{sc} is set to $\frac{1}{2}$ and added to the filter coefficients producing the following filter coefficients:

$$H(\omega) = e^{j\omega/2}\left[\cos\left(\frac{\omega}{2}\right)\right]^3 \tag{A.21}$$

$$G(\omega) = 4je^{j\omega/2} \sin\left(\frac{\omega}{2}\right) \tag{A.22}$$

and the following father and mother wavelets, respectively,

$$\hat{\phi}(\omega) = \left[\frac{\sin(\omega/2)}{\omega/2}\right]^3 \tag{A.23}$$

$$\hat{\psi}(\omega) = j\omega\left[\frac{\sin(\omega/4)}{\omega/4}\right]^4. \tag{A.24}$$

Using the identities of Equations (A.4) and (A.8), the time-domain filter coefficients for $h(n)$ and $g(n)$ can be determined, thus:

$$H(\omega) = e^{j\omega/2}\left[\frac{1 + e^{j\omega}}{2e^{j\omega/2}}\right]^3. \tag{A.25}$$

Simplifying, to become

$$H(\omega) = \tfrac{1}{8}(e^{-j\omega} + 3 + 3e^{j\omega} + e^{2j\omega}). \tag{A.26}$$

Producing the coefficients

$$h_{-1} = \frac{\sqrt{2}}{8}, \quad h_0 = \frac{3\sqrt{2}}{8}, \quad h_1 = \frac{3\sqrt{2}}{8} \quad \text{and} \quad h_2 = \frac{\sqrt{2}}{8}.$$

Similarly, for $g(n)$,

$$G(\omega) = 4je^{j\omega/2}\left[\frac{e^{j\omega/2} - e^{-j\omega/2}}{2j}\right]. \tag{A.27}$$

Simplifying, to become

$$G(\omega) = 2e^{j\omega} - 2. \tag{A.28}$$

Producing the coefficients $g_0 = -2\sqrt{2}$ and $g_1 = 2\sqrt{2}$.

Appendix B

Zinc Function Excitation

This appendix details the approach required to minimise the weighted error signal using ZFE, from Section 14.3.1. Following the approach of Hiotakakos and Xydeas [496] and Sukkar *et al*. [497], the noise weighted error signal is given by

$$E_w^{k+1}(n) = \sum_{n=1}^{excint} [e_w^{k+1}(n)]^2 \tag{B.1}$$

and using Equations (14.1)–(14.6)

$$E_w^{k+1}(n) = \sum_{n=1}^{excint} [e_w^k(n) - [A_{k+1}\,\mathrm{sinc}(n-\lambda_{k+1}) + B_{k+1}\,\mathrm{cosc}(n-\lambda_{k+1})] * h(n)]^2 \tag{B.2}$$

where A_{k+1} and B_{k+1} are the amplitude parameters for the $(k+1)$ ZFE, and λ_{k+1} is the position parameter for the $(k+1)$ ZFE.

In order to minimise the above expression as a function of A_{k+1}, we differentiate it with respect to A_{k+1}, giving:

$$\begin{aligned}\frac{\delta E_w^{k+1}(n)}{\delta A_{k+1}} = & -2 \sum_{n=1}^{excint} [sinc(n-\lambda_{k+1}) * h(n)] \\ & \times [e_w^k(n) - [A_{k+1}\,\mathrm{sinc}(n-\lambda_{k+1}) + B_{k+1}\,\mathrm{cosc}(n-\lambda_{k+1})] * h(n)] \\ & = 0.\end{aligned} \tag{B.3}$$

Expanding the above expression yields

$$A_{k+1} \cdot \sum_{n=1}^{excint} [\mathrm{sinc}(n - \lambda_{k+1}) * h(n)]^2$$

$$= \sum_{n=1}^{excint} e_w^k(n)[\mathrm{sinc}(n - \lambda_{k+1}) * h(n)]$$

$$- B_{k+1} \cdot \sum_{n=1}^{excint} \mathrm{cosc}(n - \lambda_{k+1}) * h(n) \times \sum_{n=1}^{excint} sinc(n - \lambda_{k+1}) * h(n) \qquad \text{(B.4)}$$

and, upon introducing the shorthand

$$R_{ss} = \sum_{n=1}^{excint} [\mathrm{sinc}(n - \lambda_{k+1}) * h(n)]^2 \qquad \text{(B.5)}$$

$$R_{es} = \sum_{n=1}^{excint} [\mathrm{sinc}(n - \lambda_{k+1}) * h(n)] \times e_w^k(n) \qquad \text{(B.6)}$$

$$R_{cs} = \sum_{n=1}^{excint} [\mathrm{sinc}(n - \lambda_{k+1}) * h(n)] \times [\mathrm{cosc}(n - \lambda_{k+1}) * h(n)] \qquad \text{(B.7)}$$

$$R_{cc} = \sum_{n=1}^{excint} [\mathrm{cosc}(n - \lambda_{k+1}) * h(n)]^2 \qquad \text{(B.8)}$$

$$R_{ec} = \sum_{n=1}^{excint} [\mathrm{cosc}(n - \lambda_{k+1}) * h(n)] \times e_w^k(n) \qquad \text{(B.9)}$$

we have

$$A_{k+1} = \frac{R_{es} - B_{k+1} \times R_{cs}}{R_{ss}}. \qquad \text{(B.10)}$$

Similarly, if we differentiate Equation (B.2) with respect to B_{k+1}, we arrive at

$$\frac{\delta E_w^{k+1}(n)}{\delta B_{k+1}} = -2 \sum_{n=1}^{excint} [\mathrm{cosc}(n - \lambda_{k+1}) * h(n)]$$
$$\times [e_w^k(n) - [A_{k+1}\,\mathrm{sinc}(n - \lambda_{k+1}) + B_{k+1}\,\mathrm{cosc}(n - \lambda_{k+1})] * h(n)]$$
$$= 0. \qquad \text{(B.11)}$$

Expanding, this yields

$$\begin{aligned} B_{k+1} \cdot \sum_{n=1}^{excint} & [\mathrm{cosc}(n - \lambda_{k+1} * h(n)]^2 \\ = & \sum_{n=1}^{excint} e_w^k(n) \cdot [\mathrm{cosc}(n - \lambda_{k+1}) * h(n)] \\ & - A_{k+1} \cdot \sum_{n=1}^{excint} \mathrm{cosc}(n - \lambda_{k+1}) * h(n) \times \sum_{n=1}^{excint} \mathrm{sinc}(n - \lambda_{k+1}) * h(n) \end{aligned} \quad \text{(B.12)}$$

and, upon introducing the shorthand of Equations (B.7)–(B.8), we arrive at

$$B_{k+1} = \frac{R_{ec} - A_{k+1} \times R_{cs}}{R_{cc}}. \quad \text{(B.13)}$$

As the terms $\mathrm{cosc}(n - \lambda_{k+1})$ and $\mathrm{sinc}(n - \lambda_{k+1})$ are orthogonal, their cross-correlation term R_{cs} will be zero. Hence, from Equations (B.10) and (B.13) we have

$$A_{k+1} = \frac{R_{es}}{R_{ss}} \quad \text{(B.14)}$$

$$B_{k+1} = \frac{R_{ec}}{R_{cc}}. \quad \text{(B.15)}$$

If we now substitute Equations (B.14) and (B.15) and Equations (B.5)–(B.9) back into the original error expression of Equation (B.2), then we arrive at

$$E_w^{k+1} = \sum_{n=1}^{excint} [e_w^k(n) - [A_{k+1}\,\mathrm{sinc}(n - \lambda_{k+1}) + B_{k+1}\,\mathrm{cosc}(n - \lambda_{k+1})] * h(n)]^2. \quad \text{(B.16)}$$

Expanding with the squared term yields

$$\begin{aligned} E_w^{k+1} = & \sum_{n=1}^{excint} e_w^k(n) \\ & - \sum_{n=1}^{excint} 2e_w^k(n)[A_{k+1}\,\mathrm{sinc}(n - \lambda_{k+1}) + B_{k+1}\,\mathrm{cosc}(n - \lambda_{k+1})] * h(n) \\ & + \sum_{n=1}^{excint} [[A_{k+1}\,\mathrm{sinc}(n - \lambda_{k+1}) + B_{k+1}\,\mathrm{cosc}(n - \lambda_{k+1})] * h(n)]^2 \end{aligned} \quad \text{(B.17)}$$

which is constituted by three distinct expressions. The first expression is given by

$$X = \sum_{n=1}^{excint} e_w^k(n)^2 \quad \text{(B.18)}$$

with the second by

$$Y = \sum_{N=1}^{excint} 2e_w^k(n)[(A_{k+1}\,\mathrm{sinc}(n-\lambda_{k+1}) + B_{k+1}\,\mathrm{cosc}(n-\lambda_{k+1})) * h(n)] \tag{B.19}$$

which can be further simplified using Equations (B.5)–(B.9) yielding

$$\begin{aligned} Y = & \sum_{n=1}^{excint} 2A_{k+1} \cdot e_w^k(n) \cdot [\mathrm{sinc}(n-\lambda_{k+1}) * h(n)] \\ & + \sum_{n=1}^{excint} 2B_{k+1} \cdot e_w^k(n) \cdot [\mathrm{cosc}(n-\lambda_{k+1}) * h(n)] \\ & = 2A_{k+1} \cdot R_{es} + 2B_{k+1} \cdot R_{ec}. \end{aligned} \tag{B.20}$$

The third term from Equation (B.17) is given by

$$Z = \sum_{n=1}^{excint} [[A_{k+1}\,\mathrm{sinc}(n-\lambda_{k+1}) + B_{k+1}\,\mathrm{cosc}(n-\lambda_{k+1})] * h(n)]^2 \tag{B.21}$$

which can be expanded to

$$\begin{aligned} Z = & \sum_{n=1}^{excint} A_{k+1}^2 \cdot [\mathrm{sinc}(n-\lambda_{k+1}) * h(n)]^2 \\ & + \sum_{n=1}^{excint} 2A_{k+1} \cdot B_{k+1} \cdot [\mathrm{sinc}(n-\lambda_{k+1}) * h(n)] \cdot [\mathrm{cosc}(n-\lambda_{k+1}) * h(n)] \\ & + \sum_{n=1}^{excint} B_{k+1}^2 \cdot [\mathrm{cosc}(n-\lambda_{k+1}) * h(n)]^2. \end{aligned} \tag{B.22}$$

If this expression is simplified using Equations (B.5)–(B.9) and remembering that R_{cs} was equal to zero, we obtain

$$Z = A_{k+1}^2 \cdot R_{ss} + B_{k+1}^2 \cdot R_{cc}. \tag{B.23}$$

Upon using Equations (B.14) and (B.15), we arrive at

$$Z = A_{k+1} \cdot R_{es} + B_{k+1} \cdot R_{ec}. \tag{B.24}$$

If we reconstruct Equation (B.17), then

$$E_w^{k+1} = X - Y + Z$$

which upon using Equations (B.18), (B.20) and (B.24) leads to

$$E_w^{k+1} = \sum_{n=1}^{excint} e_w^k(n)^2 - A_{k+1}R_{es} - B_{k+1}R_{ec}. \tag{B.25}$$

The expression $E_w^k(n)^2 = \sum_{n=1}^{excint} e_w^k(n)^2$ will always be positive, and it is independent of A_{k+1} and B_{k+1}, thus the error E_w^{k+1} will be minimised when $[A_{k+1}R_{es} + B_{k+1}R_{ec}]$ is maximised. So,

$$\zeta_{\mathrm{MSE}} = \frac{R_{es}^2}{R_{ss}} + \frac{R_{ec}^2}{R_{cc}} \tag{B.26}$$

where ζ_{MSE} must be maximised over the range $n = 1$ to *excint*.

Appendix C

Probability Density Function for Amplitudes

This appendix presents the PDFs for the normalised amplitude residual vector from the STC speech coder of Chapter 16. Section 16.8.1.4 describes the VQ process for the normalised amplitude residual vector and this appendix indicates the suitability of the amplitude residual vector for quantisation.

Voice and Audio Compression for Wireless Communications Second Edition
L. Hanzo, F. C. A. Somerville and J. P. Woodard

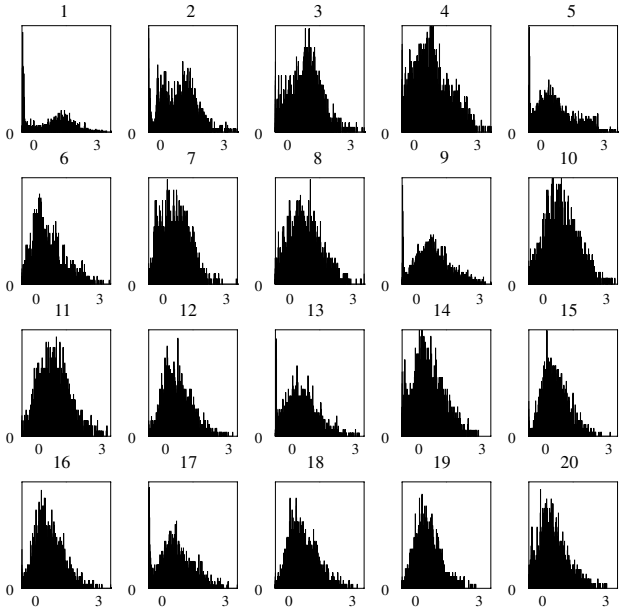

Figure C.1: The PDF for the normalised amplitude residual vector, elements 1 to 20. The abscissa represents the value of the amplitude residual element, with the ordinate representing the value's occurrence.

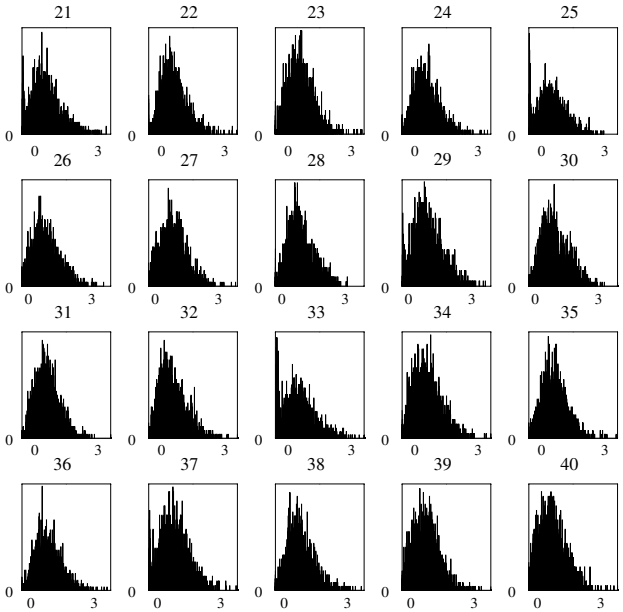

Figure C.2: The PDF for the normalised amplitude residual vector, elements 21 to 40. The abscissa represents the value of the amplitude residual element, with the ordinate representing the value's occurrence.

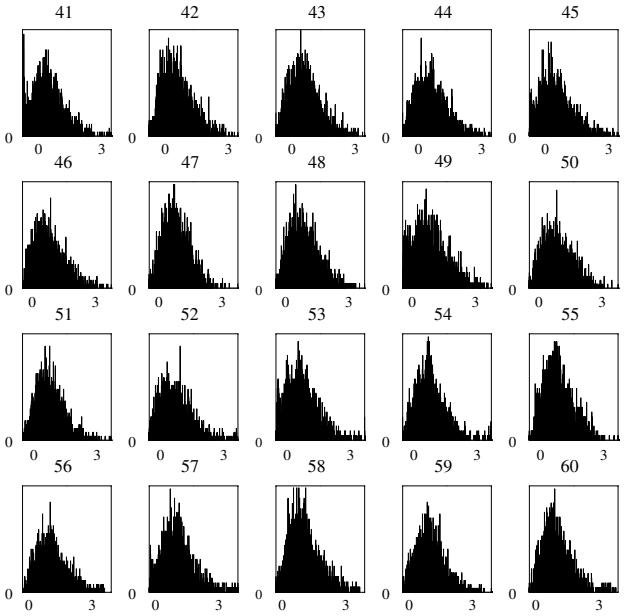

Figure C.3: The PDF for the normalised amplitude residual vector, elements 41 to 60. The abscissa represents the value of the amplitude residual element, with the ordinate representing the value's occurrence.

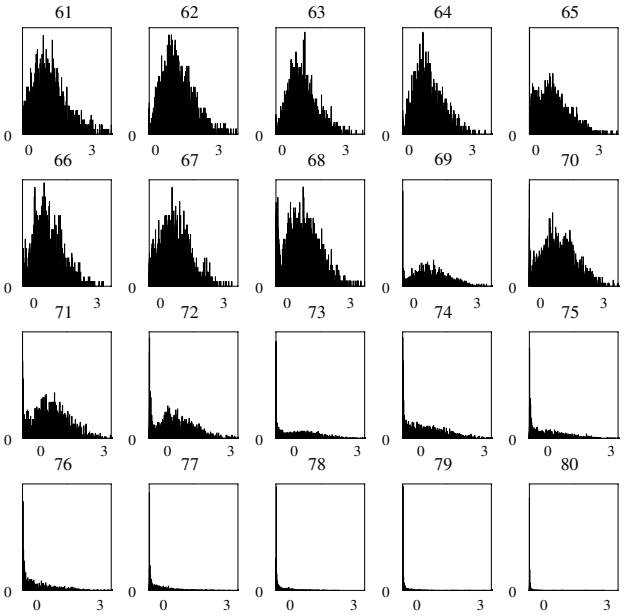

Figure C.4: The PDF for the normalised amplitude residual vector, elements 61 to 80. The abscissa represents the value of the amplitude residual element, with the ordinate representing the value's occurrence.

Bibliography

[1] R. Cox and P. Kroon, "Low bit-rate speech coders for multimedia communications", *IEEE Communications Magazine*, pp. 34–41, December 1996.

[2] R. Cox, "Speech coding and synthesis", in *Speech Coding Standards* (W. Kleijn and K. Paliwal, eds.), ch. 2, pp. 49–78, Amsterdam: Elsevier, 1995.

[3] R. Steele, *Delta Modulation Systems*. London: Pentech Press, 1975.

[4] K. Cattermole, *Principles of Pulse Code Modulation*. London: Hiffe Books, 1969.

[5] J. Markel and A. Gray Jr., *Linear Prediction of Speech*. New York: Springer, 1976.

[6] L. Rabiner and R. Schafer, *Digital Processing of Speech Signals*. Englewood Cliffs, NJ: Prentice-Hall, 1978.

[7] B. Lindblom and S. Ohman, *Frontiers of Speech Communication Research*. New York: Academic Press, 1979.

[8] J. Tobias, ed., *Foundations of Modern Auditory Theory*. New York: Academic Press, 1970. ISBN: 0126919011.

[9] B. Atal and J. Remde, "A new model of LPC excitation for producing natural-sounding speech at low bit rates", in *Proceedings of International Conference on Acoustics, Speech, and Signal Processing, ICASSP'82* (Paris, France), pp. 614–617, April 1982.

[10] N. Jayant and P. Noll, *Digital Coding of Waveforms, Principles and Applications to Speech and Video*. Englewood Cliffs, NJ: Prentice-Hall, 1984.

[11] P. Kroon, E. Deprettere and R. Sluyter, "Regular pulse excitation – a novel approach to effective efficient multipulse coding of speech", *IEEE Transactions on Acoustics, Speech and Signal Processing*, vol. 34, pp. 1054–1063, October 1986.

[12] P. Vary and R. Sluyter, "MATS-D speech codec: Regular-pulse excitation LPC", in *Proceedings of the Nordic Seminar on Digital Land Mobile Radio Communications (DMRII)* (Stockholm, Sweden), pp. 257–261, October 1986.

[13] P. Vary and R. Hoffmann, "Sprachcodec für das europäische Funkfernsprechnetz", *Frequenz 42 (1988) 2/3*, pp. 85–93, 1988.

[14] W. Hess, *Pitch Determination of Speech Signals: Algorithms and Devices*. Berlin: Springer, 1983.

[15] G. Gordos and G. Takacs, *Digital Speech Processing (Digitalis Beszed Feldolgozas)*. Budapest: Technical Publishers (Muszaki Kiado), 1983 (in Hungarian).

[16] M. Schroeder and B. Atal, "Code excited linear prediction (CELP): High-quality speech at very low bit rates", in *Proceedings of International Conference on Acoustics, Speech, and Signal Processing, ICASSP'85* (Tampa, Florida, USA), pp. 937–940, IEEE, 26–29 March 1985.

[17] D. O'Shaughnessy, *Speech Communication: Human and Machine*. Reading, MA: Addison-Wesley, 1987. ISBN: 0780334493.

[18] P. Papamichalis, *Practical Approaches to Speech Coding*. Englewood Cliffs, NJ: Prentice-Hall, 1987.

[19] J. Deller, J. Proakis and J. Hansen, *Discrete-time Processing of Speech Signals*. Englewood Cliffs, NJ: Prentice-Hall, 1987.

[20] P. Lieberman and S. Blumstein, *Speech Physiology, Speech Perception, and Acoustic Phonetics*. Cambridge: Cambridge University Press, 1988.

[21] S. Quackenbush, T. Barnwell III and M. Clements, *Objective Measures of Speech Quality*. Englewood Cliffs, NJ: Prentice-Hall, 1988.

[22] S. Furui, *Digital Speech Processing, Synthesis and Recognition*. New York: Marcel Dekker, 1989.

[23] R. Steele, C.-E. Sundberg and W. Wong, "Transmission of log-PCM via QAM over Gaussian and Rayleigh fading channels", *IEE Proceedings*, vol. 134, Part F, pp. 539–556, October 1987.

[24] R. Steele, C.-E. Sundberg and W. Wong, "Transmission errors in companded PCM over Gaussian and Rayleigh fading channels", *AT&T Bell Laboratories Technical Journal*, vol. 63, pp. 955–990, July–August 1984.

[25] C.-E. Sundberg, W. Wong and R. Steele, "Weighting strategies for companded PCM transmitted over Rayleigh fading and Gaussian channels", *AT&T Bell Laboratories Technical Journal*, vol. 63, pp. 587–626, April 1984.

[26] W. Wong, R. Steele and C.-E. Sundberg, "Soft decision demodulation to reduce the effect of transmission errors in logarithmic PCM transmitted over Rayleigh fading channels", *AT&T Bell Laboratories Technical Journal*, vol. 63, pp. 2193–2213, December 1984.

[27] J. Hagenauer, "Source-controlled channel decoding", *IEEE Transactions on Communications*, vol. 43, pp. 2449–2457, September 1995.

[28] "GSM 06.90: Digital cellular telecommunications system (Phase 2+)". Adaptive Multi-Rate (AMR) speech transcoding, version 7.0.0, Release 1998. European Telecommunications Standardisation Institute (ETSI).

[29] S. Bruhn, E. Ekudden and K. Hellwig, "Adaptive Multi-Rate: A new speech service for GSM and beyond", in *Proceedings of 3rd ITG Conference on Source and Channel Coding* (Technical University Munich, Germany), pp. 319–324, 17th–19th January 2000.

[30] L. Chiariglione, "MPEG: a technological basis for multimedia application", *IEEE Multimedia*, vol. 2, pp. 85–89, Spring 1995.

[31] L. Chiariglione, "The development of an integrated audiovisual coding standard: MPEG", *Proceedings of the IEEE*, vol. 83, pp. 151–157, February 1995.

[32] L. Chiariglione, "MPEG and multimedia communications", *IEEE Transactions on Circuits and Systems for Video Technology*, vol. 1, pp. 5–18, February 1997.

[33] "Information technology – Coding of moving pictures and associated audio for digital storage media up to about 1.5 Mbit/s – Part 3: Audio, IS11172-3". ISO/IEC JTC1/SC29/WG11/ MPEG-1, MPEG-ITU, 1992.

[34] D. Pan, "A tutorial on MPEG/Audio compression", *IEEE Multimedia*, vol. 2, no. 2, pp. 60–74, Summer 1995.

[35] K. Brandenburg and G. Stoll, "ISO-MPEG1 audio: A generic standard for coding of high-quality digital audio", *Journal of Audio Engineering Society*, vol. 42, pp. 780–792, October 1994.

[36] S. Shlien, "Guide to MPEG1 audio standard", *IEEE Transactions on Braodcasting*, vol. 40, pp. 206–218, December 1994.

[37] P. Noll, "MPEG digital audio coding", *IEEE Signal Processing Magazine*, vol. 14, pp. 59–81, September 1997.

[38] K. Brandenburg and M. Bosi, "Overview of MPEG audio: Current and future standards for low-bit-rate audio coding", *Journal of Audio Engineering Society*, vol. 45, pp. 4–21, January/February 1997.

[39] "Information technology – Generic coding of moving pictures and associated audio – Part 3: Audio, IS13818-3 ". ISO/IEC JTC1/SC29/WG11/MPEG-2, MPEG-ITU, 1994.

[40] M. Bosi, K. Brandenburg, S. Quackenbush, L. Fielder, K. Akagiri, H. Fuchs, M. Dietz, J. Herre, G. Davidson and Y. Oikawa, "ISO/IEC MPEG-2 advanced audio coding", *Journal of Audio Engineering Society*, vol. 45, pp. 789–814, October 1997.

[41] ISO/IEC JTC1/SC29/WG11/N2203, MPEG-4 Audio Version 1 Final Committee Draft 14496-3, http://www.tnt.uni-hannover.de/project/mpeg/audio/documents/, March 1998.

[42] R. Koenen, "MPEG-4 overview". http://www.cselt.it/mpeg/standards/mpeg-4/mpeg-4.htm.

[43] S. R. Quackenbush, "Coding of natural audio in MPEG-4", in *Proceedings of ICASSP*, vol. 6 (Seattle, WA), pp. 3797–3800, May 1998.

[44] K. Brandenburg, O. Kunz and A. Sugiyama, "MPEG-4 natural audio coding", *Signal Processing: Image Communication*, vol. 15, no. 4, pp. 423–444, 2000.

[45] L. Contin, B. Edler, D. Meares and P. Schreiner, "Tests on MPEG-4 audio codec proposals", *Signal Processing: Image Communication*, vol. 9, pp. 327–342, May 1997.

[46] ISO/IEC JTC1/SC29/WG11/N2203, MPEG-4 Audio Version 2 Final Committee Draft 14496-3 AMD1, http://www.tnt.uni-hannover.de/project/mpeg/audio/documents/w2803.html, July 1999.

[47] E. D. Scheirer, "The MPEG-4 structured audio standard", in *Proceedings of ICASSP*, vol. 6 (Seattle, WA), pp. 3801–3804, May 1998.

[48] B. Vercoe, W. Gardner and E. Scheirer, "Structured audio: Creation, transmission and rendering of parametric sound representation", *Proceedings of the IEEE*, vol. 86, pp. 922–940, May 1998.

[49] B. Edler, "Speech Coding in MPEG-4", *International Journal of Speech Technology*, vol. 2, pp. 289–303, May 1999.

[50] S. Alamouti, "A simple transmit diversity technique for wireless communications", *IEEE Journal on Selected Areas in Communications*, vol. 16, pp. 1451–1458, October 1998.

[51] L. Hanzo, W. T. Webb and T. Keller, *Single and Multicarrier Quadrature Amplitude Modulation : Principles and Applications for Personal Communications, WLANs and Broadcasting* (2nd Edn). New York: John Wiley & Sons, Inc.–IEEE Press, April 2000.

[52] B. Atal, V. Cuperman and A. Gersho, eds., *Advances in Speech Coding*. Dordrecht: Kluwer, January 1991. ISBN: 0792390911.

[53] A. Ince, ed., *Digital Speech Processing: Speech Coding, Synthesis and Recognition*. Dordrecht: Kluwer, 1992.

[54] J. Anderson and S. Mohan, *Source and Channel Coding – An Algorithmic Approach*. Dordrecht: Kluwer, 1993.

[55] A. Kondoz, *Digital Speech: Coding for Low Bit Rate Communications Systems*. New York: John Wiley & Sons Inc., 1994.

[56] W. Kleijn and K. Paliwal, eds., *Speech Coding and Synthesis*. Amsterdam: Elsevier, 1995.

[57] C. Shannon, *Mathematical Theory of Communication*. University of Illinois Press, 1963.

[58] J. Hagenauer, "Quellengesteuerte kanalcodierung fuer sprach-und tonuebertragung im mobilfunk", *Aachener Kolloquium Signaltheorie*, pp. 67–76, March 1994.

[59] A. Viterbi, "Wireless digital communications: A view based on three lessons learned", *IEEE Communications Magazine*, pp. 33–36, September 1991.

[60] S. Lloyd, "Least squares quantisation in PCM", *Institute of Mathematical Statistics Meeting* (Atlantic City, NJ), September 1957.

[61] S. Lloyd, "Least squares quantisation in PCM", *IEEE Transactions on Information Theory*, vol. 28, no. 2, pp. 129–136, 1982.

[62] J. Max, "Quantising for minimum distortion", *IRE Transactions on Information Theory*, vol. 6, pp. 7–12, 1960.

[63] W. Bennett, "Spectra of quantised signals", *Bell Systems Technical Journal*, vol. 25, no. 3, pp. 446–472, July 1946.

[64] H. Holtzwarth, "Pulse code modulation und ihre verzerrung bei logarithmischer quanteilung", *Archiv der Elektrischen Uebertragung*, pp. 227–285, January 1949.

[65] P. Panter and W. Dite, "Quantisation distortion in pulse-count modulation with non-uniform spacing of levels", *Proceedings of the IRE*, vol. 39, pp. 44–48, January 1951.

[66] B. Smith, "Instantaneous companding of quantised signals", *Bell System Technical Journal*, vol. 36, pp. 653–709, 1957.

[67] P. Noll and R. Zelinski, "A contribution to the quantisation of memoryless model sources", *Technical Report*, Heinrich Heinz Institute, Berlin, 1974 (in German).

[68] M. Paez and T. Glisson, "Minimum mean-squared-error quantisation in speech PCM and DPCM systems", *IEEE Transactions on Communications*, vol. 20, no. 2, pp. 225–230, April 1972.

[69] A. Jain, *Fundamentals of Digital Image Processing*. Englewood Cliffs, NJ: Prentice-Hall, 1989.

[70] R. Salami, "Robust low bit rate analysis-by-synthesis predictive speech coding". *PhD thesis*, University of Southampton, UK, 1990.

[71] R. Salami, L. Hanzo, R. Steele, K. Wong and I. Wassell, "Speech coding", *Mobile Radio Communications* (R. Steele and L. Hanzo, eds.), Piscataway, NJ: IEEE Press, 1999, ch. 3, pp. 186–346.

[72] S. Haykin, *Adaptive Filter Theory*. Englewood Cliffs, NJ: Prentice-Hall, 1996.

[73] W. Webb, "Sizing up the microcell for mobile radio communications", *IEE Electronics and Communications Journal*, vol. 5, pp. 133–140, June 1993.

[74] K. Wong and L. Hanzo, "Channel coding", *Mobile Radio Communications* (R. Steele and L. Hanzo, eds.), Piscataway, NJ: IEEE Press, 1999, ch. 4, pp. 347–488.

[75] A. Jennings, *Matrix Computation for Engineers and Scientists*. New York: John Wiley & Sons, Inc., 1977.

[76] J. Makhoul, "Stable and efficient lattice methods for linear prediction", *IEEE Transactions on Acoustic Speech Signal Processing*, vol. 25, pp. 423–428, October 1977.

[77] J. Makhoul, "Linear prediction: A tutorial review", *Proceedings of the IEEE*, vol. 63, pp. 561–580, April 1975.

[78] N. Jayant, "Adaptive quantization with a one-word memory", *Bell Systems Technical Journal*, vol. 52, pp. 1119–1144, September 1973.

[79] R. Steedman, "The common air interface MPT 1375", *Cordless Telecommunications in Europe: The Evolution of Personal Communications*, ed. W. Tuttlebee, London: Springer, 1990. ISBN 3540196331.

[80] L. Hanzo, "The British cordless telephone system: CT2", *The Mobile Communications Handbook*, ed. J. Gibson, Boca Raton, FL: CRC Press/IEEE Press, 1996, ch. 29, pp. 462–477.

[81] H. Ochsner, "The Digital European CORDLESS Telecommunications Specification, DECT", *Cordless Telecommunications in Europe: The Evolution of Personal Communications*, ed. W. Tuttlebee, London: Springer, 1990, pp. 273–285, ISBN 3540196331.

[82] S. Asghar, "Digital European Cordless Telephone", *The Mobile Communications Handbook*, ed. J. Gibson, Boca Raton, FL: CRC Press/IEEE Press, 1996, ch. 30, pp. 478–499.

[83] "Personal Handy Phone (PHP) system". RCR Standard, STD-28, Japan.

[84] "CCITT recommendation G.721".

[85] N. Kitawaki, M. Honda and K. Itoh, "Speech-quality assessment methods for speech coding systems", *IEEE Communications Magazine*, vol. 22, pp. 26–33, October 1984.

[86] A. Gray and J. Markel, "Distance measures for speech processing", *IEEE Transactions on Acoustic Speech Signal Processing*, vol. 24, no. 5, pp. 380–391, 1976.

[87] N. Kitawaki, H. Nagabucki and K. Itoh, "Objective quality evaluation for low-bit-rate speech coding systems", *IEEE Journal on Selected Areas in Communications*, vol. 6, pp. 242–249, February 1988.

[88] P. Noll and R. Zelinski, "Bounds on quantizer performance in the low bit-rate region", *IEEE Transactions on Communications*, pp. 300–304, February 1978.

[89] T. Thorpe, "The mean squared error criterion: Its effect on the performance of speech coders", in *Proceedings of International Conference on Acoustics, Speech, and Signal Processing (ICASSP'89) (Glasgow, UK)*, IEEE, May 1989, pp. 77–80.

[90] J. O'Neal, "Bounds on subjective performance measures for source encoding systems", *IEEE Transactions on Information Theory*, vol. 17, no. 3, pp. 224–231, May 1971.

[91] J. Makhoul, S. Roucos and H. Gish, "Vector quantization in speech coding", *Proceedings of the IEEE*, vol. 73, no. 11, pp. 1551–1588, November 1985.

[92] B. Atal and M. Schroeder, "Predictive coding of speech signals and subjective error criteria", *IEEE Transactions on Acoustics, Speech and Signal Processing*, vol. 27, no. 3, pp. 247–254, June 1979.

[93] R. Steele, "Deploying personal communications networks", *IEEE Communications Magazine*, pp. 12–15, September 1990.

[94] J.-H. Chen, R. Cox, Y. Lin, N. Jayant and M. Melchner, "A low-delay CELP codec for the CCITT 16 kb/s speech coding standard", *IEEE Journal on Selected Areas in Communications*, vol. 10, pp. 830–849, June 1992.

[95] D. Sen and W. Holmes, "PERCELP-perceptually enhanced random codebook excited linear prediction", in *Proceedings of IEEE Workshop on Speech Coding for Telecommunications*, pp. 101–102, IEEE 1993.

[96] S. Singhal and B. Atal, "Improving performance of multi-pulse LPC coders at low bit rates", in *Proceedings of International Conference on Acoustics, Speech, and Signal Processing (ICASSP'84)* (San Diego, CA), IEEE, March 1984, pp. 1.3.1–1.3.4.

[97] "Group speciale mobile (GSM) recommendation", ETSI, April 1988.

[98] L. Hanzo and J. Stefanov, "The Pan-European Digital Cellular Mobile Radio System – known as GSM", *Mobile Radio Communications* (R. Steele and L. Hanzo, eds.), Piscataway, NJ: IEEE Press, 1999, ch. 8, pp. 677–765.

[99] S. Singhal and B. Atal, "Amplitude optimization and pitch prediction in multipulse coders", *IEEE Transactions on Acoustics, Speech and Signal Processing*, pp. 317–327, March 1989.

[100] "Federal standard 1016 – telecommunications: Analog to digital conversion of radio voice by 4,800 bits/second code excited linear prediction (CELP)", February 1991.

[101] S. Wang and A. Gersho, "Phonetic segmentation for low rate speech coding", B. Atal, V. Cuperman and A. Gersho, eds., *Advances in Speech Coding*. Dordrecht: Kluwer, January 1991, pp. 257–266. ISBN: 0792390911.

[102] P. Lupini, H. Hassanein and V. Cuperman, "A 2.4 kbit/s CELP speech codec with class-dependent structure", in *Proceedings of the IEEE International Conference on Acoustics, Speech and Signal Processing (ICASSP'93)* (Minneapolis, MN), IEEE, April 1993, pp. 143–146.

[103] D. Griffin and J. Lim, "Multiband excitation vocoder", *IEEE Transactions on Acoustics, Speech and Signal Processing*, vol. 36, no. 8, pp. 1223–1235, August 1988.

[104] M. Nishiguchi, J. Matsumoto, R. Wakatsuki and S. Ono, "Vector quantized MBE with simplified v/uv division at 3.0Kbps", in *Proceedings of the IEEE International Conference on Acoustics, Speech and Signal Processing (ICASSP'93)* (Minneapolis, MN), IEEE, April 1993, pp. 151–154.

[105] W. Kleijn, "Encoding speech using prototype waveforms", *IEEE Transactions on Speech and Audio Processing*, vol. 1, pp. 386–399, October 1993.

[106] V. Ramamoorthy and N. Jayant, "Enhancement of ADPCM speech by adaptive postfiltering", *Bell Systems Technical Journal*, vol. 63, pp. 1465–1475, October 1984.

[107] N. Jayant and V. Ramamoorthy, "Adaptive postfiltering of 16 kb/s-ADPCM speech", in *Proceedings of International Conference on Acoustics, Speech, and Signal Processing, ICASSP'86* (Tokyo, Japan), pp. 829–832, IEEE, 7–11 April 1986.

[108] J.-H. Chen and A. Gersho, "Real-time vector APC speech coding at 4800 bps with adaptive postfiltering", in *Proceedings of International Conference on Acoustics, Speech, and Signal Processing (ICASSP'87)* (Dallas, TX), IEEE, April 1987, pp. 2185–2188.

[109] ITU-T, *CCITT Recommendation G.728: Coding of Speech at 16 kbit/s Using Low-Delay Code Excited Linear Prediction*, 1992.

[110] J.-H. Chen and A. Gersho, "Adaptive postfiltering for quality enhancement of coded speech", *IEEE Transactions on Speech and Audio Processing*, vol. 3, pp. 59–71, January 1995.

[111] F. Itakura and S. Saito, "Analysis-synthesis telephony based upon the maximum likelihood method", in *IEEE Proceedings of the 6th International Congress on Acoustics* (Tokyo, Japan), pp. C17–20, 1968.

[112] F. Itakura and S. Saito, "A statistical method for estimation of speech spectral density and formant frequencies", *Electronics and Communications in Japan*, vol. 53-A, pp. 36–43, 1970.

[113] N. Kitawaki, K. Itoh and F. Itakura, "PARCOR speech analysis synthesis system", *Review of the Electronic Communication Lab., Nippon TTPC*, vol. 26, pp. 1439–1455, November–December 1978.

[114] R. Viswanathan and J. Makhoul, "Quantization properties of transmission parameters in linear predictive systems", *IEEE Transactions on Acoustic Speech Signal Processing*, vol. 23, no. 3, pp. 309–321, June 1975.

[115] N. Sugamura and N. Farvardin, "Quantizer design in LSP analysis-by-synthesis", *IEEE Journal on Selected Areas in Communications*, vol. 6, pp. 432–440, February 1988.

[116] K. Paliwal and B. Atal, "Efficient vector quantization of LPC parameters at 24 bits/frame", *IEEE Transactions on Speech and Audio Processing*, vol. 1, pp. 3–14, January 1993.

[117] F. Soong and B.-H. Juang, "Line spectrum pair (LSP) and speech data compression", in *Proceedings of International Conference on Acoustics, Speech, and Signal Processing (ICASSP'84)* (San Diego, CA), IEEE, March 1984, pp. 1.10.1–1.10.4.

[118] G. Kang and L. Fransen, "Low-bit rate speech encoders based on line-spectrum frequencies (LSFs)", *Technical Report 8857*, NRL, November 1984.

[119] P. Kabal and R. Ramachandran, "The computation of line spectral frequencies using Chebyshev polynomials", *IEEE Transactions Acoustic Speech Signal Processing*, vol. 34, pp. 1419–1426, December 1986.

[120] M. Omologo, "The computation and some spectral considerations on line spectrum pairs (LSP)", in *Proceedings of EUROSPEECH* (Paris, France), pp. 352–355, 27–29 September 1989.

[121] B. Cheetham, "Adaptive LSP filter", *Electronics Letters*, vol. 23, pp. 89–90, January 1987.

[122] K. Geher, *Linear Circuits*. Budapest: Technical Publishers, 1972 (in Hungarian).

[123] N. Sugamura and F. Itakura, "Speech analysis and synthesis methods developed at ECL in NTT– from LPC to LSP", *Speech Communications*, vol. 5, pp. 199–215, June 1986.

[124] A. Lepschy, G. Mian and U. Viaro, "A note on line spectral frequencies", *IEEE Transactions on Acoustic Speech Signal Processing*, vol. 36, pp. 1355–1357, August 1988.

[125] B. Cheetham and P. Huges, "Formant estimation from LSP coefficients", in *Proceedings IERE 5th International Conference on Digital Processing of Signals in Communications*, pp. 183–189, 20–23 September 1988.

[126] A. Gersho and R. Gray, *Vector Quantization and Signal Compression*. Dordrecht: Kluwer, 1992.

[127] Y. Shoham, "Vector predictive quantization of the spectral parameters for low rate speech coding", in *Proceedings of International Conference on Acoustics, Speech, and Signal Processing (ICASSP'87)* (Dallas, TX), IEEE, April 1987, pp. 2181–2184.

[128] K. Lee, A. Kondoz and B. Evans, "Speaker adaptive vector quantisation of LPC parameters of speech", *Electronic Letters*, vol. 24, pp. 1392–1393, October 1988.

[129] R. Ramachandran, M. Sondhi, N. Seshadri and B. Atal, "A two codebook format for robust quantisation of line spectral frequencies", *IEEE Transactions on Speech and Audio Processing*, vol. 3, pp. 157–168, May 1995.

[130] C. Xydeas and K. So, "Improving the performance of the long history scalar and vector quantisers", in *Proceedings of the IEEE International Conference on Acoustics, Speech and Signal Processing (ICASSP'93)* (Minneapolis, MN), IEEE, April 1993, pp. 1–4.

[131] B. Atal, "Stochastic Gaussian model for low-bit rate coding of LPC area parameters", in *Proceedings of International Conference on Acoustics, Speech, and Signal Processing (ICASSP'87)* (Dallas, TX), IEEE, April 1987, pp. 2404–2407.

[132] R. Salami, L. Hanzo and D. Appleby, "A fully vector quantised self-excited vocoder", in *Proceedings of International Conference on Acoustics, Speech, and Signal Processing (ICASSP'89) (Glasgow, UK)*, IEEE, May 1989, pp. 124–128.

[133] M. Yong, G. Davidson and A. Gersho, "Encoding of LPC spectral parameters using switched-adaptive interframe vector prediction", in *Proceedings of International Conference on Acoustics, Speech, and Signal Processing (ICASSP'88)* (New York, NY), IEEE, April 1988, pp. 402–405.

[134] J. Huang and P. Schultheis, "Block quantization of correlated Gaussian random variables", *IEEE Transactions Communication Systems*, vol. 11, pp. 289–296, September 1963.

[135] R. Salami, L. Hanzo and D. Appleby, "A computationally efficient CELP codec with stochastic vector quantization of LPC parameters", in *URSI International Symposium on Signals, Systems and Electronics* (Erlangen, West Germany), pp. 140–143, 18–20 September 1989.

[136] B. Atal, R. Cox and P. Kroon, "Spectral quantization and interpolation for CELP coders", in *Proceedings of International Conference on Acoustics, Speech, and Signal Processing (ICASSP'89) (Glasgow, UK)*, IEEE, May 1989, pp. 69–72.

[137] R. Laroia, N. Phamdo and N. Farvardin, "Robust and efficient quantisation of speech LSP parameters using structured vector quantisers", in *Proceedings of International Conference on Acoustics, Speech, and Signal Processing (ICASSP'91)* (Toronto, ON), IEEE, May 1991, pp. 641–644.

[138] H. Harborg, J. Knudson, A. Fudseth and F. Johansen, "A real time wideband CELP coder for a videophone application", in *Proceedings of the IEEE International Conference on Acoustics, Speech and Signal Processing (ICASSP'94)* (Adelaide, Australia), IEEE, April 1994, pp. II121–II124.

[139] R. Lefebvre, R. Salami, C. Laflamme and J. Adoul, "High quality coding of wideband audio signals using transform coded excitation (TCX)", in *Proceedings of the IEEE International Conference on Acoustics, Speech and Signal Processing (ICASSP'94)* (Adelaide, Australia), IEEE, April 1994, pp. I193–I196.

[140] J. Paulus and J. Schnitzler, "16kbit/s wideband speech coding based on unequal subbands", in *Proceedings of the IEEE International Conference on Acoustics, Speech and Signal Processing (ICASSP'96)* (Atlanta, GA), IEEE, May 1996, pp. 255–258.

[141] J. Chen and D. Wang, "Transform predictive coding of wideband speech signals", in *Proceedings of the IEEE International Conference on Acoustics, Speech and Signal Processing (ICASSP'96)* (Atlanta, GA), IEEE, May 1996, pp. 275–278.

[142] A. Ubale and A. Gersho, "A multi-band CELP wideband speech coder", in *Proceedings of the IEEE International Conference on Acoustics, Speech and Signal Processing (ICASSP'97)* (Munich, Germany), IEEE, April 1997, pp. 1367–1370.

[143] P. Combescure, J. Schnitzler, K. Fischer, R. Kirchherr, C. Lamblin, A. L. Guyader, D. Massaloux, C. Quinquis, J. Stegmann and P. Vary, "A 16, 24, 32 Kbit/s wideband speech codec based on ATCELP", in *Proceedings of International Conference on Acoustics, Speech, and Signal Processing, ICASSP'99*, IEEE, 1999.

[144] F. Itakura, "Line spectrum representation of linear predictive coefficients of speech signals", *Journal of the Acoustic Society of America*, vol. 57, p. S35, 1975.

[145] L. Rabiner, M. Sondhi and S. Levinson, "Note on the properties of a vector quantizer for LPC coefficients", *The Bell Systems Technical Journal*, vol. 62, pp. 2603–2616, October 1983.

[146] "7 khz audio coding within 64 kbit/s". CCITT Recommendation G.722, 1988.

[147] "Recommendation G.729: Coding of speech at 8 kbit/s using conjugate-structure algebraic-code-excited linear-prediction (CS-ACELP)". Version 6.31, CCITT Study Group XVIII, 30 June 1995.

[148] T. Eriksson, J. Linden and J. Skoglung, "A safety-net approach for improved exploitation of speech correlation", in *Proceedings of the IEEE International Conference on Acoustics, Speech and Signal Processing (ICASSP'95)* (Detroit, MI), IEEE, May 1995, pp. 96–101.

[149] T. Eriksson, J. Linden and J. Skoglung, "Exploiting interframe correlation in spectral quantization — a study of different memory VQ schemes", in *Proceedings of the IEEE International Conference on Acoustics, Speech and Signal Processing (ICASSP'96)* (Atlanta, GA), IEEE, May 1996, pp. 765–768.

[150] H. Zarrinkoub and P. Mermelstein, "Switched prediction and quantization of LSP frequencies", in *Proceedings of the IEEE International Conference on Acoustics, Speech and Signal Processing (ICASSP'96)* (Atlanta, GA), IEEE, May 1996, pp. 757–764.

[151] J. Natvig, "Evaluation of six medium bit-rate coders for the Pan-European digital mobile radio system", *IEEE Journal on Selected Areas in Communications*, vol. 6, no. 2, pp. 324–331, February 1988.

[152] J. Schur, "Über potenzreihen, die im innern des einheitskreises beschränkt sind", *Journal für die reine und angewandte Mathematik*, vol. 14, pp. 205–232, 1917.

[153] W. Webb, L. Hanzo, R. Salami and R. Steele, "Does 16-QAM provide an alternative to a half-rate GSM speech codec ?", in *Proceedings of IEEE Vehicular Technology Conference (VTC'91)* (St. Louis, MO), pp. 511–516, IEEE, 19–22 May 1991.

[154] L. Hanzo, W. Webb, R. Salami and R. Steele, "On QAM speech transmission schemes for microcellular mobile PCNs", *European Transactions on Communications*, vol. 4, no. 5, pp. 495–510, September/October 1993.

[155] J. Williams, L. Hanzo, R. Steele and J. Cheung, "A comparative study of microcellular speech transmission schemes", *IEEE Transactions on Vehicular Technology*, vol. 43, pp. 909–925, November 1994.

[156] "Cellular system dual-mode mobile station-base station compatibility standard IS-54B". *EIA/TIA Interim Standard*, Telecommunications Industry Association Washington DC, 1992.

[157] *Public Digital Cellular (PDC) Standard, RCR STD-27*, Research and Development Centre for Radio Systems, Japan.

[158] R. Steele and L. Hanzo, eds., *Mobile Radio Communications*. New York: IEEE Press – John Wiley & Sons, Inc., 1999.

[159] L. Hanzo, W. Webb and T. Keller, *Single- and Multi-carrier Quadrature Amplitude Modulation*. New York: IEEE Press – John Wiley & Sons, Inc., April 2000.

[160] R. Salami, C. Laflamme, J.-P. Adoul and D. Massaloux, "A toll quality 8 kb/s speech codec for the personal communications system (PCS)", *IEEE Transactions on Vehicular Technology*, vol. 43, no. 3, pp. 808–816, August 1994.

[161] A. Black, A. Kondoz and B. Evans, "High quality low delay wideband speech coding at 16 kbit/sec", in *Proceedings of 2nd International Workshop on Mobile Multimedia Communications* (Bristol University, UK) 11–14 April 1995.

[162] C. Laflamme, J.-P. Adoul, R. Salami, S. Morissette and P. Mabilleau, "16 Kbps wideband speech coding technique based on algebraic CELP", in *Proceedings of International Conference on Acoustics, Speech, and Signal Processing (ICASSP'91)* (Toronto, ON), IEEE, May 1991, pp. 13–16.

[163] R. Salami, C. Laflamme and J.-P. Adoul, "Real-time implementation of a 9.6 kbit/s ACELP wideband speech coder", in *Proceedings of GLOBECOM'92* (Orlando, Florida), 6–9 December 1992.

[164] I. Gerson and M. Jasiuk, "Vector sum excited linear prediction (VSELP)", in B. Atal, V. Cuperman and A. Gersho, eds., *Advances in Speech Coding*. Dordrecht: Kluwer, January 1991, pp. 69–80. ISBN: 0792390911.

[165] M. Ireton and C. Xydeas, "On improving vector excitation coders through the use of spherical lattice codebooks (SLC's)", in *Proceedings of International Conference on Acoustics, Speech, and Signal Processing (ICASSP'89) (Glasgow, UK)*, IEEE, May 1989, pp. 57–60.

[166] C. Lamblin, J. Adoul, D. Massaloux and S. Morissette, "Fast CELP coding based on the barnes-wall lattice in 16 dimensions", in *Proceedings of International Conference on Acoustics, Speech, and Signal Processing (ICASSP'89) (Glasgow, UK)*, IEEE, May 1989, pp. 61–64.

[167] C. Xydeas, M. Ireton and D. Baghbadrani, "Theory and real time implementation of a CELP coder at 4.8 and 6.0 kbit/s using ternary code excitation", in *Proceedings of IERE 5th International Conference on Digital Processing of Signals in Communications*, pp. 167–174, September 1988.

[168] J. Adoul, P. Mabilleau, M. Delprat and S. Morissette, "Fast CELP coding based on algebraic codes", in *Proceedings of International Conference on Acoustics, Speech, and Signal Processing (ICASSP'87)* (Dallas, TX), IEEE, April 1987, pp. 1957–1960.

[169] L. Hanzo and J. Woodard, "An intelligent multimode voice communications system for indoor communications", *IEEE Transactions on Vehicular Technology*, vol. 44, pp. 735–748, November 1995. ISSN 0018-9545.

[170] A. Kataoka, J.-P. Adoul, P. Combescure and P. Kroon, "ITU-T 8-kbits/s standard speech codec for personal communication services", in *Proceedings of IEEE International Conference on Universal Personal Communications 1985* (Tokyo, Japan), pp. 818–822, 6–10 November 1995.

[171] H. Law and R. Seymour, "A reference distortion system using modulated noise", *IEE Paper*, pp. 484–485, November 1962.

[172] P. Kabal, J. Moncet and C. Chu, "Synthesis filter optimization and coding: Applications to CELP", in *Proceedings of International Conference on Acoustics, Speech, and Signal Processing (ICASSP'88)* (New York, NY), IEEE, April 1988, pp. 147–150.

[173] Y. Tohkura, F. Itakura and S. Hashimoto, "Spectral smoothing technique in PARCOR speech analysis-synthesis", *IEEE Transactions on Acoustics, Speech and Signal Processing*, vol. 26, no. 6, pp. 587–596, 1978.

[174] J.-H. Chen and R. Cox, "Convergence and numerical stability of backward-adaptive LPC predictor", in *Proceedings of IEEE Workshop on Speech Coding for Telecommunications* (Hôtel le Chantecler, Saite-Adèle, Quebec, Canada), pp. 83–84, 13–15 October 1993.

[175] S. Singhal and B. Atal, "Optimizing LPC filter parameters for multi-pulse excitation", in *Proceedings of International Conference on Acoustics, Speech, and Signal Processing (ICASSP'83)* (Boston, MA), IEEE, April 1983, pp. 781–784.

[176] M. Fratti, G. Miani and G. Riccardi, "On the effectiveness of parameter reoptimization in multipulse based coders", in *Proceedings of International Conference on Acoustics, Speech, and Signal Processing (ICASSP'92)*, IEEE, March 1992, pp. 73–76.

[177] W. Press, S. Teukolsky, W. Vetterling and B. Flannery, *Numerical Recipes in C*. Cambridge: Cambridge University Press, 1992.

[178] G. Golub and C. V. Loan, "An analysis of the total least squares problem", *SIAM Journal of Numerical Analysis*, vol. 17, no. 6, pp. 883–890, 1980.

[179] M. A. Rahman and K.-B. Yu, "Total least squares approach for frequency estimation using linear prediction", *IEEE Transactions on Acoustics, Speech and Signal Processing*, vol. 35, no. 10, pp. 1440–1454, October 1987.

[180] R. Degroat and E. Dowling, "The data least squares problem and channel equalization", *IEEE Transactions on Signal Processing*, vol. 41, no. 1, pp. 407–411, January 1993.

[181] F. Tzeng, "Near-optimum linear predictive speech coding", in *Proceedings of the IEEE Global Telecommunications Conference*, pp. 508.1.1–508.1.5, IEEE, 1990.

[182] M. Niranjan, "CELP coding with adaptive output-error model identification", in *Proceedings of International Conference on Acoustics, Speech, and Signal Processing (ICASSP'90)* (Albuquerque, New Mexico), IEEE, April 1990, pp. 225–228.

[183] J. Woodard and L. Hanzo, "Improvements to the analysis-by-synthesis loop in CELP codecs", in *Proceedings of IEE Conference on Radio Receivers and Associated Systems (RRAS'95)* (Bath, UK), IEE, September 1995, pp. 114–118.

[184] L. Hanzo, R. Salami, R. Steele and P. Fortune, "Transmission of digitally encoded speech at 1.2 Kbaud for PCN", *IEE Proceedings, Part I*, vol. 139, pp. 437–447, August 1992.

[185] R. Cox, W. Kleijn and P. Kroon, "Robust CELP coders for noisy backgrounds and noisy channels", in *Proceedings of International Conference on Acoustics, Speech, and Signal Processing (ICASSP'89) (Glasgow, UK)*, IEEE, May 1989, pp. 739–742.

[186] J. Campbell, V. Welch and T. Tremain, "An expandable error-protected 4800 bps CELP coder (U.S. federal standard 4800 bps voice coder)", in *Proceedings of International Conference on Acoustics, Speech, and Signal Processing (ICASSP'89) (Glasgow, UK)*, IEEE, May 1989, pp. 735–738.

[187] S. Atungsiri, A. Kondoz and B. Evans, "Error control for low-bit-rate speech communication systems", *IEE Proceedings-I*, vol. 140, pp. 97–104, April 1993.

[188] L. Ong, A. Kondoz and B. Evans, "Enhanced channel coding using source criteria in speech coders", *IEE Proceedings-I*, vol. 141, pp. 191–196, June 1994.

[189] W. Kleijn, "Source-dependent channel coding and its application to CELP", in B. Atal, V. Cuperman and A. Gersho, eds., *Advances in Speech Coding*. Dordrecht: Kluwer, January 1991, pp. 257–266. ISBN: 0792390911.

[190] J. Woodard and L. Hanzo, "A dual-rate algebraic CELP-based speech transceiver", in *Proceedings of IEEE Vehicular Technology Conference (VTC'94)* (Stockholm, Sweden), IEEE, June 1994, pp. 1690–1694.

[191] C. Laflamme, J.-P. Adoul, H. Su and S. Morissette, "On reducing the complexity of codebook search in CELP through the use of algebraic codes", in *Proceedings of International Conference on Acoustics, Speech, and Signal Processing (ICASSP'90)* (Albuquerque, New Mexico), IEEE, April 1990, pp. 177–180.

[192] S. Nanda, D. Goodman and U. Timor, "Performance of PRMA: A packet voice protocol for cellular systems", *IEEE Transactions on Vehicular Technology*, vol. 40, pp. 584–598, August 1991.

[193] M. Frullone, G. Riva, P. Grazioso and C. Carciofy, "Investigation on dynamic channel allocation strategies suitable for PRMA schemes", *Proceedings of the IEEE International Symposium on Circuits and Systems*, pp. 2216–2219, IEEE, May 1993.

[194] J. Williams, L. Hanzo and R. Steele, "Channel-adaptive voice communications", in *Proceedings of IEE Conference on Radio Receivers and Associated Systems (RRAS'95)* (Bath, UK), IEE, September 1995, pp. 144–147.

[195] W. Lee, "Estimate of channel capacity in Rayleigh fading environment", *IEEE Transactions on Vehicular Technology*, vol. 39, pp. 187–189, August 1990.

[196] T. Tremain, "The government standard linear predictive coding algorithm: LPC-10", *Speech Technology*, vol. 1, pp. 40–49, April 1982.

[197] J. Campbell, T. Tremain and V. Welch, "The DoD 4.8 kbps standard (proprosed federal standard 1016)", in B. Atal, V. Cuperman and A. Gersho, eds., *Advances in Speech Coding*. Dordrecht: Kluwer, January 1991, pp. 121–133. ISBN: 0792390911.

[198] J. Marques, I. Trancoso, J. Tribolet and L. Almeida, "Improved pitch prediction with fractional delays in CELP coding", in *Proceedings of International Conference on Acoustics, Speech, and Signal Processing (ICASSP'90)* (Albuquerque, New Mexico), IEEE, April 1990, pp. 665–668.

[199] W. Kleijn, D. Kraisinsky and R. Ketchum, "An efficient stochastically excited linear predictive coding algorithm for high quality low bit rate transmission of speech", *Speech Communication*, vol. 7, no. 3, pp. 305–316, October 1988.

[200] Y. Shoham, "Constrained-stochastic excitation coding of speech at 4.8 kb/s", in B. Atal, V. Cuperman and A. Gersho, eds., *Advances in Speech Coding*. Dordrecht: Kluwer, January 1991, pp. 339–348. ISBN: 0792390911.

[201] A. Suen, J. Wand and T. Yao, "Dynamic partial search scheme for stochastic codebook of FS1016 CELP coder", *IEE Proceedings*, vol. 142, no. 1, pp. 52–58, 1995.

[202] I. Gerson and M. Jasiuk, "Vector sum excited linear prediction (VSELP) speech coding at 8 kbps", in *Proceedings of International Conference on Acoustics, Speech, and Signal Processing (ICASSP'90)* (Albuquerque, New Mexico), IEEE, April 1990, pp. 461–464.

[203] I. Gerson and M. Jasiuk, "Techniques for improving the performance of CELP-type speech codecs", *IEEE Journal on Selected Areas in Communications*, vol. 10, pp. 858–865, June 1992.

[204] I. Gerson, "Method and means of determining coefficients for linear predictive coding". US Patent No 544,919, October 1985.

[205] A. Cumain, "On a covariance-lattice algorithm for linear prediction", in *Proceedings of International Conference on Acoustics, Speech, and Signal Processing (ICASSP'82)*, IEEE, May 1982, pp. 651–654.

[206] W. Gardner, P. Jacobs and C. Lee, "QCELP: a variable rate speech coder for CDMA digital cellular", in *Speech and Audio Coding for Wireless and Network Applications*, B. Atal, V. Cuperman and A. Gersho, eds., pp. 85–92, Dordrecht: Kluwer, 1993.

[207] Telcomm. Industry Association (TIA), Washington, DC, Mobile station – Base station compatibility standard for dual-mode wideband spread spectrum cellular system, *EIA/TIA Interim Standard IS-95*, 1993.

[208] T. Ohya, H. Suda and T. Miki, "5.6 kbits/s PSI-CELP of the half-rate PDC speech coding standard", in *Proceedings of Vehicular Technology Conference*, vol. 3 (Stockholm), pp. 1680–1684, IEEE, May 1994.

[209] T. Ohya, T. Miki and H. Suda, "Jdc half-rate speech coding standard and a real time operating prototype", *NTT Review*, vol. 6, pp. 61–67, November 1994.

[210] K. Mano, T. Moriya, S. Miki, H. Ohmuro, K. Ikeda and J. Ikedo, "Design of a pitch synchronous innovation CELP coder for mobile communications", *IEEE Journal on Selected Areas in Communications*, vol. 13, no. 1, pp. 31–41, 1995.

[211] I. Gerson, M. Jasiuk, J.-M. Muller, J. Nowack and E. Winter, "Speech and channel coding for the half-rate GSM channel", *Proceedings Informations Theoretische Gessellschaft-Fachbericht*, vol. 130, pp. 225–233, November 1994.

[212] A. Kataoka, T. Moriya and S. Hayashi, "Implementation and performance of an 8-kbits/s conjugate structured CELP speech codec", in *Proceedings of the IEEE International Conference on Acoustics, Speech and Signal Processing (ICASSP'94)* (Adelaide, Australia), IEEE, April 1994, pp. 93–96.

[213] R. Salami, C. Laflamme and J.-P. Adoul, "8 kbits/s ACELP coding of speech with 10 ms speech frame: A candidate for CCITT standardization", in *Proceedings of the IEEE International Conference on Acoustics, Speech and Signal Processing (ICASSP'94)* (Adelaide, Australia), IEEE, April 1994, pp. 97–100.

[214] J. Woodard, T. Keller and L. Hanzo, "Turbo-coded orthogonal frequency division multiplex transmission of 8 kbps encoded speech", in *Proceedings of ACTS Mobile Communication Summit'97* (Aalborg, Denmark), ACTS, October 1997, pp. 894–899.

[215] T. Ojanpare et al., "FRAMES multiple access technology", in *Proceedings of IEEE ISSSTA'96*, vol. 1 (Mainz, Germany), pp. 334–338, IEEE, September 1996.

[216] C. Berrou, A. Glavieux and P. Thitimajshima, "Near shannon limit error-correcting coding and decoding: Turbo codes", in *Proceedings of the International Conference on Communications* (Geneva, Switzerland), pp. 1064–1070, May 1993.

[217] C. Berrou and A. Glavieux, "Near optimum error correcting coding and decoding: Turbo codes", *IEEE Transactions on Communications*, vol. 44, pp. 1261–1271, October 1996.

[218] J. Hagenauer, E. Offer and L. Papke, "Iterative decoding of binary block and convolutional codes", *IEEE Transactions on Information Theory*, vol. 42, pp. 429–445, March 1996.

[219] P. Jung and M. Naßhan, "Performance evaluation of turbo codes for short frame transmission systems", *IEE Electronic Letters*, vol. 30, no. 2, pp. 111–112, January 1994.

[220] A. Barbulescu and S. Pietrobon, "Interleaver design for turbo codes", *IEE Electronic Letters*, vol. 30, no. 25, pp. 2107–2108, December 1994.

[221] L. Bahl, J. Cocke, F. Jelinek and J. Raviv, "Optimal decoding of linear codes for minimising symbol error rate", *IEEE Transactions on Information Theory*, vol. 20, pp. 284–287, March 1974.

[222] "COST 207: Digital land mobile radio communications, final report". Office for Official Publications of the European Communities, Luxembourg, 1989.

[223] R. Salami, C. Laflamme, B. Bessette and J.-P. Adoul, "Description of ITU-T recommendation G.729 annex A: Reduced complexity 8 kbits/s CS-ACELP codec", in *Proceedings of the IEEE International Conference on Acoustics, Speech and Signal Processing (ICASSP'97)* (Munich, Germany), IEEE, April 1997, pp. 775–778.

[224] R. Salami, C. Laflamme, B. Bessette and J.-P. Adoul, "ITU-T recommendation G.729 annex A: Reduced complexity 8 kbits/s CS-ACELP codec for digital simultaneous voice and data (DVSD)", *IEEE Communications Magazine*, vol. 35, pp. 56–63, September 1997.

[225] R. Salami, C. Laflamme, B. Besette, J.-P. Adoul, K. Jarvinen, J. Vainio, P. Kapanen, T. Hankanen and P. Haavisto, "Description of the GSM enhanced full rate speech codec", in *Proceedings of ICC'97* (Montreal, Quebec, Canada), vol. 2, pp. 725–729, 8–12 June 1997.

[226] "PCS1900 enhanced full rate codec US1". SP-3612.

[227] "TIA/EIA/IS641, interim standard, TDMA cellular/PCS radio intergface – enhanced full-rate speech codec", May 1996.

[228] "IS-136.1A TDMA cellular/PCS – radio interface – mobile station – base station compatibility digital control channel", August 1996. Revision A.

[229] T. Honkanen, J. Vainio, K. Jarvinen, P. Haavisto, R. Salami, C. Laflamme and J. Adoul, "Enhanced full rate speech codec for IS-136 digital cellular system", in *Proceedings of the IEEE International Conference on Acoustics, Speech and Signal Processing (ICASSP'97)* (Munich, Germany), IEEE, 21–24 April 1997, pp. 731–734.

[230] "Dual rate speech coder for multimedia communications transmitting at 5.3 and 6.3 kbit/s". CCITT Recommendation G.723.1, March 1996.

[231] S. Bruhn, E. Ekudden and K. Hellwig, "Adaptive Multi-Rate: A new speech service for GSM and beyond", in *Proceedings of 3rd ITG Conference on Source and Channel Coding* (Technical University Munich, Germany), pp. 319–324, January 2000.

[232] A. Das, E. Paksoy and A. Gersho, "Multimode and Variable Rate Coding of Speech", in *Speech Coding and Synthesis* W. Kleijn and K. Paliwal, eds., ch. 7, pp. 257–288, Amsterdam: Elsevier, 1995.

[233] T. Taniguchi, S. Unagami and R. Gray, "Multimode coding: a novel approach to narrow- and medium-band coding", *Journal of the Acoustic Society of America*, vol. 84, p. S12, 1988.

[234] P. Kroon and B. Atal, "Strategies for improving CELP coders", in *Proceedings of ICASSP* (New York, USA), vol. 1, pp. 151–154, 11–14 April 1988.

[235] A. D. Jaco, W. Gardner, P. Jacobs and C. Lee, "QCELP: the North American CDMA digital cellular variable rate speech coding standard", in *Proceedings of IEEE Workshop on Speech Coding for Telecommunications*, pp. 5–6, IEEE, 1993.

[236] E. Paksoy, K. Srinivasan and A. Gersho, "Variable bit rate CELP coding of speech with phonetic classification", *European Transactions on Telecommunications*, vol. 5, pp. 591–602, October 1994.

[237] L. Cellario and D. Sereno, "CELP coding at variable rate", *European Transactions on Telecommunications*, vol. 5, pp. 603–613, October 1994.

[238] E. Yuen, P. Ho and V. Cuperman, "Variable Rate Speech and Channel Coding for Mobile Communications", in *Proceedings of Vehicular Technology Conference (VTC)* (Stockholm, Sweden), pp. 1709–1712, 8–10 June 1994.

[239] T. Kawashima, V. Sharma and A. Gersho, "Capacity enhancement of cellular CDMA by traffic-based control of speech bit rate", *IEEE Transactions on Vehicular Technology*, vol. 45, pp. 543–550, August 1996.

[240] W. P. LeBlanc and S. A. Mahmoud, "Low complexity, low delay speech coding for indoor wireless communications", in *Proceedings of Vehicular Technology Conference (VTC)* (Stockholm, Sweden), pp. 1695–1698, IEEE, 8–10 June 1994.

[241] J. E. Kleider and W. M. Campbell, "An adaptive rate digital communication system for speech", in *Proceedings of ICASSP, Munich, Germany*, vol. 3, pp. 1695–1698, IEEE, 21–24th April 1997.

[242] R. J. McAulay and T. F. Quatieri, "Low-rate Speech Coding Based on the Sinusoidal Model", in *Advances in Speech Signal Processing*, S. Furui and M. Sondhi, eds., ch. 6, New York: Marcel Dekker, 1992.

[243] J. E. Kleider and R. J. Pattison, "Multi-rate speech coding for wireless and Internet applications", in *Proceedings of ICASSP* (Phoenix, AZ), IEEE, 15–19 March 1999, pp. 2379–2382.

[244] A. Das, A. D. Jaco, S. Manjunath, A. Ananthapadmanabhan, J. Juang and E. Choy, "Multimode variable bit rate speech coding: an efficient paradigm for high-quality low-rate representation of speech signal", in *Proceedings of ICASSP*, (Phoenix, AZ), 15–19 March 1999, pp. 2307–2310.

[245] "TIA/EIA/IS-127". Enhanced Variable Rate Codec, Speech Service Option 3 for Wideband Spread Spectrum Digital Systems.

[246] F. Beritelli, A. Lombardo, S. Palazzo and G. Schembra, "Performance analysis of an ATM multiplexer loaded with VBR traffic generated by multimode speech coders", *IEEE Journal On Selected Areas In Communications*, vol. 17, pp. 63–81, January 1999.

[247] "Description of a 12 kbps G.729 higher rate extension". ITU-T, Q19/16, September. 1997.

[248] L. Hanzo, W. Webb and T. Keller, *Single- and Multi-carrier Quadrature Amplitude Modulation*. New York: John Wiley & Sons, Inc. – IEEE Press, April 2000.

[249] S. Sampei, S. Komaki and N. Morinaga, "Adaptive modulation/TDMA scheme for large capacity personal multi-media communication systems", *IEICE Transactions on Communications (Japan)*, vol. E77-B, pp. 1096–1103, September 1994.

[250] C. Wong and L. Hanzo, "Upper-bound performance of a wideband burst-by-burst adaptive modem", *IEEE Transactions on Communications*, vol. 48, pp. 367–369, March 2000.

[251] M. Yee, T. Liew and L. Hanzo, "Radial basis function decision feedback equalisation assisted block turbo burst-by-burst adaptive modems", in *Proceedings of Vehicular Technology Conference (VTC'99) (Fall)* (Amsterdam, Netherlands), IEEE, September 1999, pp. 1600–1604.

[252] E. Kuan and L. Hanzo, "Comparative study of adaptive-rate CDMA transmission employing joint-detection and interference cancellation receivers", in *Proceedings of the IEEE Vehicular Technology Conference* (Tokyo, Japan), IEEE, 2000.

[253] E. L. Kuan, C. H. Wong and L. Hanzo, "Burst-by-burst adaptive joint-detection CDMA", in *Proceedings of Vehicular Technology Conference (VTC'99) (Spring)* (Houston, TX), IEEE, May 1999, pp. 1628–1632.

[254] T. Keller and L. Hanzo, "Sub–band adaptive pre–equalised OFDM transmission", in *Proceedings of Vehicular Technology Conference (VTC'99) (Fall)* (Amsterdam, Netherlands), IEEE, September 1999, pp. 334–338.

[255] M. Münster, T. Keller and L. Hanzo, "Co–channel interference suppression assisted adaptive OFDM in interference limited environments", in *Proceedings of Vehicular Technology Conference (VTC'99) (Fall)* (Amsterdam, Netherlands), IEEE, September 1999, pp. 284–288.

[256] T. H. Liew, L. L. Yang and L. Hanzo, "Soft-decision redundant residue number system based error correction coding", in *Proceedings of the IEEE Vehicular Technology Conference (VTC'99)* (Amsterdam, The Netherlands), pp. 2546–2550, September 1999.

[257] S. Bruhn, P. Blocher, K. Hellwig and J. Sjoberg, "Concepts and solutions for link adaptation and inband signalling for the GSM AMR speech coding standard", in *Proceedings of Vehicular Technology Conference (VTC'99) (Spring)* (Houston, TX), IEEE, May 1999, vol. 3, pp. 2451–2455.

[258] "GSM 05.09: Digital cellular telecommunications system (Phase 2+)". Link Adaptation, version 7.0.0, Release 1998.

[259] N. Szabo and R. Tanaka, *Residue Arithmetic and Its Applications to Computer Technology*. New York: McGraw-Hill, 1967.

[260] F. Taylor, "Residue arithmetic: A tutorial with examples", *IEEE Computer Magazine*, vol. 17, pp. 50–62, May 1984.

[261] H. Krishna, K.-Y. Lin and J.-D. Sun, "A coding theory approach to error control in redundant residue number systems - part I: Theory and single error correction", *IEEE Transactions on Circuits and Systems-II: Analog and Digital Signal Processing*, vol. 39, pp. 8–17, January 1992.

[262] J.-D. Sun and H. Krishna, "A coding theory approach to error control in redundant residue number systems - part II: Multiple error detection and correction", *IEEE Transactions on Circuits and Systems-II: Analog and Digital Signal Processing*, vol. 39, pp. 18–34, January 1992.

[263] L.-L. Yang and L. Hanzo, "Performance of residue number system based DS-CDMA over multipath fading channels using orthogonal sequences", *European Transactions on Telecommunications*, vol. 9, pp. 525–536, November–December 1998.

[264] A. Klein, G. Kaleh and P. Baier, "Zero forcing and minimum mean square error equalization for multiuser detection in code division multiple access channels", *IEEE Transactions on Vehicular Technology*, vol. 45, pp. 276–287, May 1996.

[265] W. Webb and R. Steele, "Variable rate QAM for mobile radio", *IEEE Transactions on Communications*, vol. 43, pp. 2223–2230, July 1995.

[266] A. Goldsmith and S. Chua, "Variable-rate variable-power MQAM for fading channels", *IEEE Transactions on Communications*, vol. 45, pp. 1218–1230, October 1997.

[267] J. Torrance and L. Hanzo, "Upper bound performance of adaptive modulation in a slow Rayleigh fading channel", *Electronics Letters*, vol. 32, pp. 718–719, 11 April 1996.

[268] C. Wong and L. Hanzo, "Upper-bound of a wideband burst-by-burst adaptive modem", in *Proceedings of Vehicular Technology Conference (VTC'99) (Spring)* (Houston, TX), IEEE, May 1999, pp. 1851–1855.

[269] M. Failli, "Digital land mobile radio communications COST 207", *Technical Report*, European Commission, 1989.

[270] C. Hong, "Low delay switched hybrid vector excited linear predictive coding of speech". *PhD thesis*, National University of Singapore, 1994.

[271] J. Zhang and H.-S. Wang, "A low delay speech coding system at 4.8 kb/s", in *Proceedings of the IEEE International Conference on Communications Systems*, vol. 3, pp. 880–883, IEEE, November 1994.

[272] J.-H. Chen, N. Jayant and R. Cox, "Improving the performance of the 16 kb/s LD-CELP speech coder", in *Proceedings of International Conference on Acoustics, Speech, and Signal Processing (ICASSP'92)*, IEEE, March 1992.

[273] J.-H. Chen and A. Gersho, "Gain-adaptive vector quantization with application to speech coding", *IEEE Transactions on Communications*, vol. 35, pp. 918–930, September 1987.

[274] J.-H. Chen and A. Gersho, "Gain-adaptive vector quantization for medium rate speech coding", in *Proceedings of IEEE International Conference on Communications 1985* (Chicago, IL), pp. 1456–1460, IEEE, 23–26 June 1985.

[275] J.-H. Chen, Y.-C. Lin and R. Cox, "A fixed-point 16 kb/s LD-CELP algorithm", in *Proceedings of International Conference on Acoustics, Speech, and Signal Processing (ICASSP'91)* (Toronto, ON), IEEE, May 1991, pp. 21–24.

[276] J.-H. Chen, "High-quality 16 kb/s speech coding with a one-way delay less than 2 ms", in *Proceedings of International Conference on Acoustics, Speech, and Signal Processing (ICASSP'90)* (Albuquerque, New Mexico), IEEE, April 1990, pp. 453–456.

[277] J. De Marca and N. Jayant, "An algorithm for assigning binary indices to the codevectors of a multi-dimensional quantizer", in *Proceedings of IEEE International Conference on Communications 1987* (Seattle, WA), pp. 1128–1132, IEEE, 7–10 June 1987.

[278] K. Zeger and A. Gersho, "Zero-redundancy channel coding in vector quantization", *Electronic Letters*, vol. 23, pp. 654–656, June 1987.

[279] J. Woodard and L. Hanzo, "A low delay multimode speech terminal", in *Proceedings of IEEE Vehicular Technology Conference (VTC'96)* (Atlanta, GA), vol. 1, pp. 213–217, IEEE, 28 April–1 May 1996.

[280] Y. Linde, A. Buzo and R. Gray, "An algorithm for vector quantiser design", *IEEE Transactions on Communications*, vol. 28, no. 1, pp. 84–95, January 1980.

[281] W. Kleijn, D. Krasinski and R. Ketchum, "Fast methods for the CELP speech coding algorithm", *IEEE Transactions on Acoustics, Speech and Signal Processing*, vol. 38, no. 8, pp. 1330–1342, August 1990.

[282] S. D'Agnoli, J. D. Marca and A. Alcaim, "On the use of simulated annealing for error protection of CELP coders employing LSF vector quantizers", in *Proceedings of IEEE Vehicular Technology Conference (VTC'94)* (Stockholm, Sweden), IEEE, June 1994, pp. 1699–1703.

[283] X. Maitre, "7 kHz audio coding within 64 kbit/s", *IEEE Journal on Selected Areas of Communications*, vol. 6, pp. 283–298, February 1988.

[284] R. Crochiere, S. Webber and J. Flanagan, "Digital coding of speech in sub-bands", *Bell Systems Technical Journal*, pp. 1069–1085, October 1976.

[285] R. Crochiere, "An analysis of 16 Kbit/s sub-band coder performance: dynamic range, tandem connections and channel errors", *Bell Systems Technical Journal*, vol. 57, pp. 2927–2952, October 1978.

[286] D. Esteban and C. Galand, "Application of quadrature mirror filters to split band voice coding scheme", in *Proceedings of International Conference on Acoustics, Speech, and Signal Processing (ICASSP'77)* (Hartford, CT), IEEE, May 1977, pp. 191–195.

[287] J. Johnston, "A filter family designed for use in quadrature mirror filter banks", in *Proceedings of International Conference on Acoustics, Speech, and Signal Processing (ICASSP'80)* (Denver, CO), IEEE, April 1980, pp. 291–294.

[288] H. Nussbaumer, "Complex quadrature mirror filters", in *Proceedings of International Conference on Acoustics, Speech, and Signal Processing (ICASSP'83)* (Boston, MA), IEEE, April 1983, pp. 221–223.

[289] C. Galand and H. Nussbaumer, "New quadrature mirror filter structures", *IEEE Transactions on Acoustic Speech Signal Processing*, vol. 32, pp. 522–531, June 1984.

[290] S. Quackenbush, "A 7 kHz bandwidth, 32 kbps speech coder for ISDN", in *Proceedings of International Conference on Acoustics, Speech, and Signal Processing (ICASSP'91)* (Toronto, ON), IEEE, May 1991, pp. 1–4.

[291] J. Johnston, "Transform coding of audio signals using perceptual noise criteria", *IEEE Journal on Selected Areas of Communication*, vol. 6, no. 2, pp. 314–323, 1988.

[292] E. Ordentlich and Y. Shoham, "Low-delay code-excited linear-predictive coding of wideband speech at 32kbps", in *Proceedings of International Conference on Acoustics, Speech, and Signal Processing (ICASSP'91)* (Toronto, ON), IEEE, May 1991, pp. 9–12.

[293] R. Soheili, A. Kondoz and B. Evans, "New innovations in multi-pulse speech coding for bit rates below 8 kb/s", in *Proceedings of Eurospeech* (Paris, France), pp. 298–301, 27–29 September 1989.

[294] V. Sanchez-Calle, C. Laflamme, R. Salami and J.-P. Adoul, "Low-delay algebraic CELP coding of wideband speech", in *Signal Processing VI: Theories and Applications*, J. Vandewalle, R. Boite, M. Moonen and A. Oosterlink, eds., pp. 495–498, Amsterdam: Elsevier Science Publishers, 1992.

[295] G. Roy and P. Kabal, "Wideband CELP speech coding at 16 kbit/sec", in *Proceedings of International Conference on Acoustics, Speech, and Signal Processing (ICASSP'91)* (Toronto, ON), IEEE, May 1991, pp. 17–20.

[296] R. Steele and W. Webb, "Variable rate QAM for data transmission over Rayleigh fading channels", in *Proceeedings of Wireless'91* (Calgary, Alberta), pp. 1–14, IEEE, 1991.

[297] Y. Kamio, S. Sampei, H. Sasaoka and N. Morinaga, "Performance of modulation-level-control adaptive-modulation under limited transmission delay time for land mobile communications", in *Proceedings of IEEE Vehicular Technology Conference (VTC'95)* (Chicago, IL), pp. 221–225, IEEE, 15–28 July 1995.

[298] K. Arimochi, S. Sampei and N. Morinaga, "Adaptive modulation system with discrete power control and predistortion-type non-linear compensation for high spectral efficient and high power efficient wireless communication systems", in *Proceedings of IEEE International Symposium on Personal, Indoor and Mobile Radio Communications (PIMRC'97)* (Marina Congress Centre, Helsinki, Finland), IEEE, September 1997, pp. 472–477.

[299] M. Naijoh, S. Sampei, N. Morinaga and Y. Kamio, "ARQ schemes with adaptive modulation/TDMA/TDD systems for wireless multimedia communication systems", in *Proceedings of IEEE International Symposium on Personal, Indoor and Mobile Radio Communications (PIMRC'97)* (Marina Congress Centre, Helsinki, Finland), IEEE, September 1997, pp. 709–713.

[300] A. Goldsmith, "The capacity of downlink fading channels with variable rate and power", *IEEE Transactions on Vehicular Technolgy*, vol. 46, pp. 569–580, August 1997.

[301] M.-S. Alouini and A. Goldsmith, "Area spectral efficiency of cellular mobile radio systems", *IEEE Transactions on Vehicular Technology*, vol. 48, no. 4, pp. 1047–1066, July 1999. http://www.systems.caltech.edu.

[302] A. Goldsmith and P. Varaiya, "Capacity of fading channels with channel side information", *IEEE Transactions on Information Theory*, vol. 43, pp. 1986–1992, November 1997.

[303] T. Liew, C. Wong and L. Hanzo, "Block turbo coded burst-by-burst adaptive modems", in *Proceedings of Microcoll'99* (Budapest, Hungary), pp. 59–62, March 1999.

[304] C. Wong, T. Liew and L. Hanzo, "Blind-detection assisted, block turbo coded, decision-feedback equalised burst-by-burst adaptive modulation". *IEEE Journal of Selected Areas in Communication*, 1999.

[305] H. Matsuoka, S. Sampei, N. Morinaga and Y. Kamio, "Adaptive modulation system with variable coding rate concatenated code for high quality multi-media communications systems", in *Proceedings of IEEE Vehicular Technology Conference (VTC'96)*, vol. 1 (Atlanta, GA), pp. 487–491, IEEE, April–May 1996.

[306] V. Lau and M. Macleod, "Variable rate adaptive trellis coded QAM for high bandwidth efficiency applications in Rayleigh fading channels", in *Proceedings of IEEE Vehicular Technology Conference (VTC'98)* (Otawa, ON), IEEE, May 1998, pp. 348–352.

[307] A. Goldsmith and S. Chua, "Adaptive coded modulation for fading channels", *IEEE Transactions on Communications*, vol. 46, pp. 595–602, May 1998.

[308] T. Keller and L. Hanzo, "Adaptive orthogonal frequency division multiplexing schemes", in *Proceeding of ACTS Mobile Communication Summit'98* (Rhodes, Greece), ACTS, June 1998, pp. 794–799.

[309] E. Kuan, C. Wong and L. Hanzo, "Burst-by-burst adaptive joint detection CDMA", in *Proceedings of Vehicular Technology Conference (VTC'99) (Spring)* (Houston, TX), IEEE, May 1999.

[310] R. Chang, "Synthesis of band-limited orthogonal signals for multichannel data transmission", *Bell Systems Technical Journal*, vol. 46, pp. 1775–1796, December 1966.

[311] L. Cimini, "Analysis and simulation of a digital mobile channel using orthogonal frequency division multiplexing", *IEEE Transactions on Communications*, vol. 33, pp. 665–675, July 1985.

[312] K. Fazel and G. Fettweis, eds. *Multi-Carrier Spread-Spectrum*. Dordrecht: Kluwer, 1997. ISBN 0-7923-9973-0.

[313] T. May and H. Rohling, "Reduktion von Nachbarkanalstörungen in OFDM–Funkübertragungssystemen", in *2. OFDM–Fachgespräch in Braunschweig*, 1997.

[314] S. Müller and J. Huber, "Vergleich von OFDM–Verfahren mit reduzierter Spitzenleistung", in *2. OFDM–Fachgespräch in Braunschweig*, 1997.

[315] F. Classen and H. Meyr, "Synchronisation algorithms for an OFDM system for mobile communications", in *Codierung für Quelle, Kanal und Übertragung*, no. 130 in ITG Fachbericht (Berlin), pp. 105–113, VDE–Verlag, 1994.

[316] F. Classen and H. Meyr, "Frequency synchronisation algorithms for OFDM systems suitable for communication over frequency selective fading channels", in *Proceedings of IEEE Vehicular Technology Conference (VTC'94)* (Stockholm, Sweden), IEEE, June 1994, pp. 1655–1659.

[317] S. Shepherd, P. van Eetvelt, C. Wyatt-Millington and S. Barton, "Simple coding scheme to reduce peak factor in QPSK multicarrier modulation", *Electronics Letters*, vol. 31, pp. 1131–1132, July 1995.

[318] A. Jones, T. Wilkinson and S. Barton, "Block coding scheme for reduction of peak to mean envelope power ratio of multicarrier transmission schemes", *Electronics Letters*, vol. 30, pp. 2098–2099, 1994.

[319] M. di Benedetto and P. Mandarini, "An application of MMSE predistortion to OFDM systems", *IEEE Transactions on Communications*, vol. 44, pp. 1417–1420, November 1996.

[320] P. Chow, J. Cioffi and J. Bingham, "A practical discrete multitone transceiver loading algorithm for data transmission over spectrally shaped channels", *IEEE Transactions on Communications*, vol. 48, pp. 772–775, 1995.

[321] K. Fazel, S. Kaiser, P. Robertson and M. Ruf, "A concept of digital terrestrial television broadcasting", *Wireless Personal Communications*, vol. 2, pp. 9–27, 1995.

[322] H. Sari, G. Karam and I. Jeanclaude, "Transmission techniques for digital terrestrial TV broadcasting", *IEEE Communications Magazine*, pp. 100–109, February 1995.

[323] J. Borowski, S. Zeisberg, J. Hübner, K. Koora, E. Bogenfeld and B. Kull, "Performance of OFDM and comparable single carrier system in MEDIAN demonstrator 60 GHz channel", in *Proceedings of ACTS Mobile Communication Summit'97* (Aalborg, Denmark), ACTS, October 1997, pp. 653–658.

[324] I. Kalet, "The multitone channel", *IEEE Transactions on Communications*, vol. 37, pp. 119–124, February 1989.

[325] Y. Li and N. Sollenberger, "Interference suppression in OFDM systems using adaptive antenna arrays", in *Proceedings of Globecom'98* (Sydney, Australia), pp. 213–218, IEEE, 8–12 November 1998.

[326] F. Vook and K. Baum, "Adaptive antennas for OFDM", in *Proceedings of IEEE Vehicular Technology Conference (VTC'98)* (Otawa, ON), IEEE, May 1998, pp. 608–610.

[327] T. Keller, J. Woodard and L. Hanzo, "Turbo-coded parallel modem techniques for personal communications", in *Proceedings of IEEE Vehicular Technology Conference (VTC'97)* (Phoenix, AZ), pp. 2158–2162, IEEE, 4–7 May 1997.

[328] T. Keller and L. Hanzo, "Blind-detection assisted sub-band adaptive turbo-coded OFDM schemes", in *Proceedings of Vehicular Technology Conference (VTC'99) (Spring)* (Houston, TX), IEEE, May 1999, pp. 489–493.

[329] "Universal mobile telecommunications system (UMTS); UMTS terrestrial radio access (UTRA); concept evaluation", *Technical Report TR 101 146*, ETSI, 1997.

[330] *Technical Report*, http://standards.pictel.com/ptelcont.htm#Audio or ftp://standard.pictel.com/sg16_q20/1999_09_Geneva/.

[331] M. Failli, "Digital land mobile radio communications COST 207", *Technical Report*, European Commission, 1989.

[332] J. Proakis, *Digital Communications*, 3rd edn. New York: McGraw-Hill, 1995.

[333] H. Malvar, *Signal Processing with Lapped Transforms*. London: Artech House, 1992.

[334] K. Rao and P. Yip, *Discrete Cosine Transform: Algorithms, Advantages and Applications*. New York: Academic Press Ltd., 1990.

[335] W. B. Kleijn and K. K. Paliwal, *Speech Coding and Synthesis*. Amsterdam: Elsevier, 1995.

[336] P. Combescure, J. Schnitzler, K. Fischer, R. Kirchherr, C. Lamblin, A. L. Guyader, D. Massaloux, C. Quinquisd, J. Stegmann and P. Vary, "A 16, 24, 32 kbit/s wideband speech codec based on ATCELP", in *Proceedings of ICASSP* (Phoenix, AZ), vol. 1, pp. 5–8, IEEE, March 1999.

[337] J. Schnitzler, C. Erdmann, P. Vary, K. Fischer, J. Stegmann, C. Quinquis, D. Massaloux and C. Lamblin, "Wideband speech coding for the GSM adaptive multi-rate system", in *Proceedings of 3rd Informations Theoretische Gessellschaft Conference on Source and Channel Coding* (Technical University Munich, Germany), pp. 325–330, January 2000.

[338] A. Murashima, M. Serizawa and K. Ozawa, "A multi-rate wideband speech codec robust to background noise", in *Proceedings of ICASSP, Istanbul, Turkey*, vol. 2, pp. 1165–1168, June 2000.

[339] R. Steele and L. Hanzo, eds. *Mobile Radio Communications*, 2nd edn. New York: IEEE Press – John Wiley & Sons, Inc., 1999.

[340] R. V. Cox, J. Hagenauer, N. Seshadri and C.-E. Sundberg, "Subband speech coding and matched convolutional channel coding for mobile radio channels", *IEEE Transactions on signal processing*, vol. 39, pp. 1717–1731, August 1991.

[341] J. Hagenauer, "Rate-compatible punctured convolutional codes (rcpc codes) and their applications", *IEEE Transactions on Communications*, vol. 36, pp. 389–400, April 1988.

[342] N. S. Othman, S. X. Ng and L. Hanzo, "Turbo-dected unequal protection audio and speech transceivers using serially concatenated convolutional codes, trellis coded modulationa and space-time trellis coding", in *Proceedings of the IEEE Vehicular Technology Conference (UTC'05)* (Dallas, TX), IEEE, September 2005.

[343] S. X. Ng, J. Y. Chung and L. Hanzo, "Turbo-dected unequal protection MPEG-4 telephony using trellis coded modulatioan and space-time trellis coding", in *Proceedings of IEE International Conference on 3G mobile communication Technologies (3G 2004)* (London), pp. 416–420, IEEE, October 2004.

[344] M. Tüchler and J. Hagenauer, "Exit charts of irregular codes", in *Proceedings of Conference on Information Science and Systems* (Princeton University), March 2002 (CD-ROM).

[345] M. Tüchler, "Design of serially concatenated systems depending on the block length", *IEEE Transactions on Communications*, vol. 52, pp. 209–218, February 2004.

[346] S. ten Brink, "Convergence behavior of iteratively decoded parallel concatenated codes", *IEEE Transactions on Communications*, vol. 49, pp. 1727–1737, October 2001.

[347] B. Bessette, R. Salami, R. Lefebvre, M. Jelinek, J. Rotola-Pukkila, J. Vainio, H. Mikkola and K. Jarvinen, "The adaptive multirate wideband speech codec", *IEEE Transactions on Speech and Audio Processing*, vol. 10, pp. 620–636, November 2002.

[348] L. R. Bahl, J. Cocke, F. Jelinek and J. Raviv, "Optimal decoding of linear codes for minimal symbol error rate", *IEEE Transactions on Information Theory*, vol. 20, pp. 284–287, March 1974.

[349] S. Benedetto, D. Divsalar, G. Montorsi and F. Pollara, "Serial concatenation of interleaved codes: performance analysis, design, and iterative decoding", *IEEE Transactions on Information Theory*, vol. 44, pp. 909–926, May 1998.

[350] A. Ashikhmin, G. Kramer and S. ten Brink, "Extrinsic information transfer functions: model and erasure channel properties", *IEEE Transactions on Information Theory*, vol. 50, pp. 2657–2673, November 2004.

[351] I. Land, P. Hoeher and S. Gligorević, "Computation of symbol-wise mutual information in transmission systems with logAPP decoders and application to EXIT charts", in *Proceedings of International ITG Conference on Source and Channel Coding (SCC)* (Erlangen, Germany), pp. 195–202, January 2004.

[352] S. Dolinar and D. Divsalar, "Weight distributions for turbo codes using random and nonrandom permutations", *JPL-TDA Progress Report 42-122*, pp. 56–65, August 1995.

[353] A. Lillie, A. Nix and J. McGeehan, "Performance and design of a reduced complexity iterative equalizer for precoded isi channels", in *Proceedings of IEEE Vehicular Technology Conference (VTC'03) (Fall)* (Orlando, FL), IEEE, October 2003.

[354] International Standard Organisation, "Information technology-coding of audio-visual objects-part3: Audio", *ISO/IEC 14496-3:2001*, 2001.

[355] "Specification for the use of video and audio coding in dvb services delivered directly over ip", *DVB Document A-84 Rev.1*, November 2005.

[356] "IP Datacast over DVB-H: Architecture", *DVB Document A098*, November 2005.

[357] "Extended AMR Wideband codec; Transcoding functions", *3GPP TS 26.290*.

[358] S. Ragot and B. Bessette and R. Lefebvre, "Low-complexity multi-rate lattice vector quantization with application to wideband speech coding at 32 kb/s", *Proceedings of ICASSP'04*, May 2004.

[359] B. Bessette, R. Lefebvre and R. Salami, "Universal speech/audio coding using hybrid acelp/tcx techniques", in *Proceedings of ICASSP'05* (Philadelphia, PA), vol. 3, pp. 301–304, 18–23 March 2005.

[360] J. Sjoberg, "Rtp payload format for the extended adaptive multi-rate wideband (amr-wb+) audio codec", *Request for Comments 4352*, IETF January 2006.

[361] "Method for the subjective assessment fo intermediate quality level of coding systems", *Recommendation ITU-R BS.1534*.

[362] L. Fielder, M. Bosi, G. Davidson, M. Davis, C. Todd and S. Vernon, "AC-2 and AC-3: Low complexity transform-based audio coding", in *Collected Papers on Digital Audio Bit-Rate Reduction*, N. Gilchrist and C. Grewin, eds., pp. 54–72, Audio Engineering Society, 1996.

[363] K. Tsutsui, H. Suzuki, O. Shimoyoshi, M. Sonohara, K. Akagiri and R. Heddle, "ATRAC: adaptive transform acoustic coding for MiniDisc", in *Collected Papers on Digital Audio Bit-Rate Reduction*, N. Gilchrist and C. Grewin, eds., pp. 95–101, Audio Engineering Society, 1996.

[364] J. Johnston, D. Sinha, S. Doward and S. Quackenbush, "AT&T perceptual audio coding (PAC)", in *Collected Papers on Digital Audio Bit-Rate Reduction*, N. Gilchrist and C. Grewin, eds., pp. 73–81, Audio Engineering Society, 1996.

[365] G. C. P. Lokhoff, "Precision Adaptive Subband Coding (PASC) for the Digital Compact Cassette (DCC)", *IEEE Transactions on Consumer Electronic*, vol. 38, pp. 784–789, November 1992.

[366] N. S. Jayant, J. Johnston and R. Sofranek, "Signal compression based on models of human perception", *Proceedings of IEEE*, vol. 81, pp. 1385–1422, October 1993.

[367] E. Zwicker, "Subdivision of the audible frequency range into critical bands (frequenzgruppen)", *The Journal of the Acoustical Society of America*, vol. 33, p. 248, February 1961.

[368] K. Brandenburg, "Introduction to perceptual coding", in *Collected Papers on Digital Audio Bit-Rate Reduction*, N. Gilchrist and C. Grewin, eds., pp. 23–30, Audio Engineering Society, 1996.

[369] T. Painter and A. Spanias, "Perceptual coding of digital audio", *Proceedings of the IEEE*, vol. 88, pp. 451–513, Apr 2000.

[370] H. Fletcher, "Auditory patterns", *Reviews of Modern Physics*, pp. 47–65, January 1940.

[371] D. D. Greenwood, "Critical bandwidth and the frequency coordinates of the Basilar membrane", *The Journal of the Acoustical Society of America*, vol. 33, no. 10, pp. 1344–1356, October 1961.

[372] B. Scharf, "Critical bands", in *Foundations of Modern Auditory Theory*, ed. Jerry Tobias, New York: Academic, 1970.

[373] E. Zwicker and H. Fastl, *Psychoacoustics - Facts and Models*. Berlin: Springer, 1990.

[374] R. Hellman, "Asymmetry of masking between noise and tone", *Perception and Psychophysics*, vol. 11, pp. 241–246, 1972.

[375] P. Noll, "Digital audio coding for visual communications", *Proceedings of the IEEE*, vol. 83, pp. 925–943, June 1995.

[376] K. Brandenburg, "OCF - A new coding algorithm for high quality sound signals", in *Proceedings of ICASSP* (Dallas, TX), IEEE, April 1987, pp. 141–144.

[377] J. Johnston, "Transform coding of audio signals using perceptual noise criteria", *IEEE Journal on Selected Areas in Communications*, vol. 6, pp. 314–323, February 1988.

[378] D. Esteban and C. Galand, "Application of quadrature mirror filters to split band voice coding scheme", in *Proceedings of ICASSP*, IEEE, May 1977, pp. 191–195.

[379] R. E. Crochiere, S. A. Webber and J. L. Flanagan, "Digital coding of speech in subbands", *The Bell Systems Technical Journal*, vol. 55, pp. 1069–1085, October 1976.

[380] J. M. Tribolet and R. E. Crochiere, "Frequency domain coding of speech", *IEEE Transactions on Acoustics, Speech, and Signal Processing*, vol. 27, pp. 512–530, October 1979.

[381] N. S. Jayant and P. Noll, *Digital Coding of Waveforms: Principles and Applications to Speech and Video Coding*. Englewood Cliffs, NJ: Prentice-Hall, 1984.

[382] R. Zelinski and P. Noll, "Adaptive transform coding of speech signals", *IEEE Transactions on Acoustics, Speech, and Signal Processing*, vol. 25, pp. 299–309, August 1977.

[383] J. Herre and J. Johnston, "Continuously signal-adaptive filterbank for high-quality perceptual audio coding", in *Proceedings of IEEE ASSP Workshop on Applications of Signal Processing to Audio and Acoustics (WASPAA)*, IEEE, October 1997.

[384] P. P. Vaidyanathan, "Multirate digital filters, filter banks, polyphase networks and applications: a tutorial", *Proceedings of the IEEE*, vol. 78, pp. 56–93, January 1990.

[385] P. P. Vaidyanathan, *Multirate Systems and Filter Banks*. Englewood Cliffs, NJ: Prentice-Hall, 1993.

[386] A. Akansu and M. T. J. S. (Eds), *Subband and Wavelet Transforms, Designs and Applications*. Norwell, MA: Kluwer, 1996.

[387] H. S. Malvar, *Signal Processing with Lapped Transforms*. Boston, MA: Artech House, 1992.

[388] H. S. Malvar, "Modulated QMF filter banks with perfect reconstruction", *Electronics Letters*, vol. 26, pp. 906–907, June 1990.

[389] J. H. Rothweiler, "Polyphase quadrature filters: a new subband coding technique", in *Proceedings of ICASSP* (Boston, MA), pp. 1280–1283, April 1983.

[390] M. Temerinac and B. Edler, "LINC: a common theory of transform and subband coding", *IEEE Transactions on Communications*, vol. 41, no. 2, pp. 266–274, 1993.

[391] H. J. Nussbaumer, "Pseudo QMF filter bank", *IBM Technical Disclosure Bulletin*, vol. 24, pp. 3081–3087, November 1981.

[392] J. P. Princen and A. B. Bradley, "Analysis/synthesis filter bank design based on time domain aliasing cancellation", *IEEE Transactions on Acoustics, Speech and Signal Processing*, vol. 34, pp. 1153–1161, October 1986.

[393] S. Shlien, "The modulated lapped transfrom, its time-varying forms, and its applications to audio coding standards", *IEEE Transactions on Speeech and Audio Processing*, vol. 5, pp. 359–366, July 1997.

[394] B. Edler, "Coding of audio signals with overlapping block transform and adaptive window functions", *Frequenz*, vol. 43, pp. 252–256, September 1989 (in German).

[395] K. Brandenburg and G. Stoll, "ISO-MPEG-1 audio: a generic standard for coding of high-quality digital audio", in *Collected Papers on Digital Audio Bit-Rate Reduction*, N. Gilchrist and C. Grewin, eds., pp. 31–42, Audio Engineering Society, 1996.

[396] H. S. Malvar, "Lapped transform for efficient transform/subband coding", *IEEE Transactions on Acoustics, Speech and Signal Processing*, vol. 38, pp. 969–978, June 1990.

[397] Y. Mahieux, J. Petit and A. Charbonnier, "Transform coding of audio signals using correlation between succesive transform blocks", in *Proceedings of ICASSP* (Glasgow, UK), IEEE, 23–26 May 1989, pp. 2021–2024.

[398] J. Johnston and A. Ferreira, "Sum-difference stereo transform coding", in *Proceedings of ICASSP* (San Fransisco, CA), IEEE, 23–26 March 1992, pp. II–569–II–572.

[399] S. Park, Y. Kim and Y. Seo, "Multi-layer bit-sliced bit-rate scalable audio coding", in *Proceedings of the 103rd Convention of the Audio Engineering Society*, *Preprint 4520*, September 1997.

[400] N. Iwakami, T. Moriya and S. Miki, "High-quality audio coding at less than 64 kbps by using transform-domain weighted interleave vector quantization (TwinVQ)", in *Proceedings of ICASSP* (Detroit, MI), pp. 3095–3098, 9–12 May 1995.

[401] J. Herre and J. Johnston, "Enhancing the performance of perceptual audio coders by using temporal noise shaping (TNS)", in *Proceedings of the 101st Convention of the Audio Engineering Society*, *Preprint 4384*, December 1996.

[402] R. A. Salami and L. Hanzo, "Speech coding", in *Mobile Radio Communications*, R. Steele and L. Hanzo, eds., ch. 3, pp. 187–335, New York: IEEE Press – John Wiley & Sons, Inc., 1999.

[403] J. Herre, K. Brandenburg and D. Lederer, "Intensity stereo coding", in *Proceedings of the 96th Convention of the Audio Engineering Society*, *Preprint 3799*, May 1994.

[404] J. Johnston, "Perceptual transform coding of wideband stereo signals", in *Proceedings of ICASSP* (Glasgow, UK), pp. 1993–1996, 23–26 May 1989.

[405] R. G. van der Waal and R. N. J. Veldhuis, "Subband coding of stereophonic digital audio signals", in *Proceedings of ICASSP* (Toronto, ON), vol. 5, pp. 3601–3604, 14–17 April 1991.

[406] T. V. Sreenivas and M. Dietz, "Vector quantization of scale factors in advanced audio coder (AAC)", in *Proceedings of ICASSP* (Seattle, WA), vol. 6, pp. 3641–3644, 12–15 May 1998.

[407] D. A. Huffman, "A method for the construction of minimum-redundancy codes", *Proceedings of IRE*, vol. 40, pp. 1098–1101, September 1952.

[408] International Standard Organisation, ISO/IEC JTC1/SC29/WG11/N2203TF, MPEG-4 Audio Version 1 Final Committee Draft 14496-3 Subpart 4:TF, http://www.tnt.uni-hannover.de/project/mpeg/audio/documents/, May 1998.

[409] K. Ikeda, T. Moriya, N. Iwakami, A. Jin and S. Miki, "A design of TwinVQ audio codec for personal communication systems", in *Proceedings of the 4th IEEE International Conference on Universal Personal Communications*, pp. 803–807, IEEE, 1995.

[410] K. Ikeda, T. Moriya and N. Iwakami, "Error protected TwinVQ audio coding at less than 64 kbit/s", in *Proceedings of IEEE Speech Coding Workshop*, pp. 33–34, IEEE, 1995.

[411] T. Moriya, N. Iwakami, K. Ikeda and S. Miki, "Extension and complexity reduction of TwinVQ audio coder", in *Proceedings of ICASSP* (Atlanta, GA), pp. 1029–1032, 7–10 May 1996.

[412] ITU, "Coding of speech at 8 kbit/s using conjugate-structure algebraic code-excited linear prediction (CS-ACELP)". *ITU Recommendation G.729*, 1995.

[413] T. Moriya, "Two-channel conjugate vector quantizer for noisy channel speech coding", *IEEE Journal on Selected Areas in Communications*, vol. 10, pp. 866–874, 1992.

[414] N. Kitawaki, T. Moriya, T. Kaneko and N. Iwakami, "Comparison of two speech and audio coders at 8 kbit/s from the viewpoints of coding scheme and quality", *IEICE Transactions on Communications*, vol. E81-B, pp. 2007–2012, November 1998.

[415] T. Moriya, N. Iwakami, A. Jin, K. Ikeda and S. Miki, "A design of transform coder for both speech and audio signals at 1 bit/sample", in *Proceedings of ICASSP* (Munich, Germany), pp. 1371–1374, 21–24 April 1997.

[416] T. Moriya and M. Honda, "Transform coding of speech using a weighted vector quantizer", *IEEE Journal on Selected Areas in Communications*, vol. 6, pp. 425–431, February 1988.

[417] H. Purnhagen, "An overview of MPEG-4 Audio version 2", in *Proceedings of AES 17th International Conference on High-Quality Audio Coding*, MPEG-ITU, September 1999.

[418] H. Purnhagen, "Advances in parametric audio coding", in *Proceedings of IEEE Workshop on Applications of Signal Processing to Audio and Acoustics* (New York), pp. W99–1–W99–4, IEEE, October 1999.

[419] H. Purnhagen and N. Meine, "HILN - The MPEG-4 parametric audio coding tools", in *Proceedings IEEE International Symposium on Circuits and Systems* (Geneva, Switzerland), pp. III–201–III–204, IEEE, May 2000.

[420] B. Edler and H. Purnhagen, "Concepts for hybrid audio coding schemes based on parametric techniques", *Proceedings of the AES 105th Convention*, Preprint 4808, September 1998.

[421] S. Levine, T. Verma and J. O. Smith, "Multiresolution sinusoidal modelling for wideband audio with modifications", in *Proceedings of ICASSP* (Seattle, WA), vol. 6, pp. 3585–3588, 12–15 May 1998.

[422] T. S. Verma and T. H. Y. Meng, "Analysis/synthesis tool for transient signals that allows a flexible sines+transients+noise model for audio", in *Proceedings of ICASSP* (Seattle, WA), vol. 6, pp. 3573–3576, 12–15 May 1998.

[423] S. Levine and J. O. Smith III, "A switched parametric and transform audio coder", in *Proceedings of ICASSP* (Phoenix, AZ), pp. 985–988, 15–19 March 1999.

[424] M. R. Schroeder and B. S. Atal, "Code Excited Linear Prediction (CELP): high quality speech at very low bit rates", in *Proceedings of ICASSP* (Tampa, FL), pp. 937–940, April 1985.

[425] M. Nishiguchi and J. Matsumoto, "Harmonic and noise coding of lpc residuals with classified vector quantization", in *Proceedings of ICASSP* (Detroit, MI), vol. 1, pp. 484–487, 9–12 May 1995.

[426] M. Nishiguchi, K. Iijima and J. Matsumoto, "Harmonic vector excitation coding of speech at 2 kbit/s", in *Proceedings of IEEE Workshop on Speech Coding for Telecommunications*, pp. 39–40, IEEE, 1997.

[427] International Standard Organisation, ISO/IEC JTC1/SC29/WG11/N2203PAR, MPEG-4 Audio Version 1 Final Committee Draft 14496-3 Subpart 2: Parametric Coding, http://www.tnt.uni-hannover.de/project/mpeg/audio/documents/, March 1998.

[428] International Standard Organisation, ISO/IEC JTC1/SC29/WG11/N2203CELP, MPEG-4 Audio Version 1 Final Committee Draft 14496-3 Subpart 3: CELP, http://www.tnt.uni-hannover.de/project/mpeg/audio/documents/, May 1998.

[429] R. Taori, R. J. Sluijter and A. J. Gerrits, "On scalability in CELP coding systems", in *Proceedings of IEEE Workshop on Speech Coding for Telecommunications* (Pennsylvania, PA), pp. 67–68, IEEE, 7–10 September 1997.

[430] K. Ozawa, M. Serizawa and T. Nomura, "High quality MP-CELP speech coding at 12 kb/s and 6.4 kb/s", in *Proceedings of IEEE Workshop on Speech Coding for Telecommunications*, pp. 71–72, IEEE, September 1997.

[431] E. F. Deprettere and P. Kroon, "Regular excitation reduction for effective and efficient LP-coding of speech", in *Proceedings of ICASSP* (Tampa, FL), pp. 965–968, April 1985.

[432] C. Laflamme, J. P. Adoul, R. A. Salami, S. Morissette and P. Mabilleau, "16kbit/s wideband speech coding technique based on algebraic CELP", in *Proceedings of ICASSP* (Toronto, ON), vol. 1, pp. 13–16, May 1991.

[433] P. Kroon, R. J. Sluyter and E. F. Deprettere, "Regular-pulse excitation – a novel approach to effective and efficient multipulse coding of speech", *IEEE Transactions on Acoustics, Speech, and Signal Processing*, vol. 34, pp. 1054–1063, October 1986.

[434] P. Chaudhury, "The 3GPP proposal for IMT-2000", *IEEE Communications Magazine*, vol. 37, pp. 72–81, December 1999.

[435] G. Foschini Jr. and M. Gans, "On limits of wireless communication in a fading environment when using multiple antennas", *Wireless Personal Communications*, vol. 6, pp. 311–335, March 1998.

[436] V. Tarokh, N. Seshadri and A. Calderbank, "Space–time codes for high data rate wireless communication: performance criterion and code construction", *IEEE Transactions on Information Theory*, vol. 44, pp. 744–765, March 1998.

[437] V. Tarokh, H. Jafarkhani and A. Calderbank, "Space–time block codes from orthogonal designs", *IEEE Transactions on Information Theory*, vol. 45, pp. 1456–1467, July 1999.

[438] V. Tarokh, H. Jafarkhani and A. Calderbank, "Space–time block coding for wireless communications: performance results", *IEEE Journal on Selected Areas in Communications*, vol. 17, pp. 451–460, March 1999.

[439] G. Bauch, "Concatenation of space–time block codes and Turbo-TCM", in *Proceedings of IEEE International Conference on Communications, Vancouver, Canada*, pp. 1202–1206, IEEE, June 1999.

[440] D. Agrawal, V. Tarokh, A. Naguib and N. Seshadri, "Space–time coded OFDM for high data-rate wireless communication over wideband channels", in *Proceedings of IEEE Vehicular Technology Conference* (Ottawa, ON), pp. 2232–2236, IEEE, May 1998.

[441] Y. Li, J. Chuang and N. Sollenberger, "Transmitter diversity for OFDM systems and its impact on high-rate data wireless networks", *IEEE Journal on Selected Areas in Communications*, vol. 17, pp. 1233–1243, July 1999.

[442] A. Naguib, N. Seshadri and A. Calderbank, "Increasing data rate over wireless channels", *IEEE Signal Processing Magazine*, vol. 17, pp. 76–92, May 2000.

[443] A. Naguib, V. Tarokh, N. Seshadri and A. Calderbank, "A space–time coding modem for high-data-rate wireless communications", *IEEE Journal on Selected Areas in Communications*, vol. 16, pp. 1459–1478, October 1998.

[444] H. Holma and A. Toskala, *WCDMA for UMTS*. New York: John Wiley & Sons, Inc. – IEEE Press, April 2000.

[445] R. W. Chang, "Synthesis of band-limited orthogonal signals for multichannel data transmission", *Body, Space and Technology Journal*, vol. 46, pp. 1775–1796, December 1966.

[446] J. Cimini, "Analysis and simulation of a digital mobile channel using orthogonal frequency division multiplexing", *IEEE Transactions on Communications*, vol. 33, pp. 665–675, July 1985.

[447] K. Fazel and G. Fettweis, *Multi-carrier Spread Spectrum*. Dordrecht: Kluwer, 1997.

[448] P. R. K. Fazel, S. Kaiser and M. Ruf, "A concept of digital terrestial television broadcasting", *Wireless Personal Communications*, vol. 2, pp. 9–27, 1995.

[449] I. J. H. Sari and G. Karam, "Transmission techniques for digital terrestial tv broadcasting", *IEEE Communications Magazine*, vol. 33, pp. 100–109, February 1995.

[450] J. Borowski, S. Zeiberg, J. Hbner, K. Koora, E. Bogenfeld and B. Kull, "Performance of OFDM and comparable single carrier system in median demonstration 60 GHz channel", in *Proceedings of ACTS Summit* (Aalborg, Denmark), ACTS, pp. 653–658, October 1997.

[451] J. C. I. Chuang, Y. G. Li and N. R. Sollenberger, "OFDM based high-speed wireless access for Internet applications", in *Proceedings of PIMRC Fall* (London, UK), 18–21 September 2000, pp. 797–803.

[452] L. Hanzo and J. P. Woodard, "An intelligent multimode voice communications system for indoor communications", *IEEE Transactions on Vehicular Technology*, vol. 44, pp. 735–749, November 1995.

[453] T. Keller, M. Muenster and L. Hanzo, "A turbo-coded burst-by-burst adaptive wideband speech transceiver", *Journal on Selected Areas in Communications*, vol. 18, pp. 2363–2372, November 2000.

[454] L. Hanzo, C. H. Wong and P. Cherriman, "Channel-adaptive wideband wireless video telephony", *IEEE Signal Processing Magazine*, vol. 17, pp. 10–30, July 2000.

[455] MPEG Audio Web Page, http:// www.tnt.uni-hannover.de/project/mpeg/audio/.

[456] C. Berrou, A. Glavieux and P. Thitimajshima, "Near shannon limit error-correcting coding and decoding: Turbo codes", in *Proceedings of IEEE International Conference on Communications*, pp. 1064–1070, IEEE, May 1993.

[457] L. Bahl, J. Cocke, F. Jelinek and J. Raviv, "Optimal decoding of linear codes for minimizing symbol error rate", *IEEE Transactions on Information Theory*, vol. 20, pp. 284–287, March 1974.

[458] M. Faili, "Digital land mobile radio communications COST 207", *Technical Report*, European Commission, Luxembourg, 1989.

[459] R. Koenen, "MPEG-4 Overview", in *ISO/IEC JTC1/SC29/WG11 N4668, version 21-Jeju Version*, ISO/IEC, http://www.chiariglione.org/mpeg/standards/mpeg-4/mpeg-4.htm, March 2002.

[460] R. Koenen, "MPEG-4 multimedia for our time", *IEEE Spectrum*, vol. 36, no. 2, pp. 26–33, February 1999.

[461] International Standard Organisation ISO/IEC JTC1/SC29/WG11 N2503, "Information technology – very low bitrate audio–visual coding", in *ISO/IEC 14496-3. Final Draft International Standard. Part 3: Audio*, 1998.

[462] J. Herre, and B. Grill, "Overview of MPEG-4 audio and its applications in mobile communications", in *Proceedings of WCCC-ICSP* (Beijing, China), vol. 1, pp. 11–20, 21–25 August 2000.

[463] F. Pereira and T. Ebrahimi, *The MPEG-4 Book*. Englewood Cliffs, NJ: Prentice-Hall PTR/IMSC Press, 2002.

[464] S. Lin and D. J. Costello, Jr., *Error Control Coding: Fundamentals and Applications*. Englewood Cliffs, NJ: Prentice-Hall, 1983.

[465] G. Ungerböck, "Channel Coding with Multilevel/Phase Signals", *IEEE Transactions on Information Theory*, vol. 28, pp. 55–67, January 1982.

[466] L. Hanzo, T. H. Liew and B. L. Yeap, *Turbo Coding, Turbo Equalisation and Space Time Coding for Transmission over Wireless channels*. New York: John Wiley & Sons, Inc. IEEE Press, 2002.

[467] L. Hanzo, S. X. Ng, W. T. Webb and T. Keller, *Quadrature Amplitude Modulation: From Basics to Adaptive Trellis-Coded, Turbo-Equalised and Space–Time Coded OFDM, CDMA and MC-CDMA Systems*. New York: John Wiley & Sons, Inc. IEEE Press, 2004.

[468] V. Tarokh, N. Seshadri and A. R. Calderbank, "Space–time codes for high rate wireless communication: performance analysis and code construction", *IEEE Transactions on Information Theory*, vol. 44, pp. 744–765, March 1998.

[469] L. Hanzo, P.J. Cherriman and J. Street, *Wireless Video Communications: Second to Third Generation Systems and Beyond*. Piscataway, NJ: IEEE Press, 2001.

[470] L. Hanzo, F.C.A. Somerville, and J.P. Woodard, *Voice Compression and Communications: Principles and Applications for Fixed and Wireless Channels*. Chichester, UK: John Wiley & Sons, Ltd IEEE Press, 2001.

[471] S. X. Ng, J. Y. Chung and L. Hanzo, "Turbo-detected unequal protection MPEG-4 wireless video telephony using trellis coded modulation and space–time trellis coding", in *IEE International Conference on 3G Mobile Communication Technologies (3G 2004)* (London, UK), IEEE, October 2004.

[472] E. Zehavi, "8-PSK trellis codes for a Rayleigh fading channel", *IEEE Transactions on Communications*, vol. 40, pp. 873–883, May 1992.

[473] S. X. Ng, J. Y. Chung and L. Hanzo, "Integrated wireless multimedia turbo-transceiver design – Interpreting Shannon's lessons in the turbo-era", in *IEE Sparse-Graph Codes Seminar* (London: IEE), October 2004.

[474] R.V. Cox, J. Hagenauer, N. Seshadri, and C-E. W. Sundberg, "Subband speech coding and matched convolutional coding for mobile radio channels", *IEEE Transactions on Signal Processing*, vol. 39, pp. 1717–1731, August 1991.

[475] B. Bessette, R. Salami, R. Lefebvre, M. Jelinek, J. Rotola-Pukkila, J. Vainio, H. Mikkola and K. Jarvinen, "The Adaptive Multirate Wideband speech codec (AMR-WB)", *IEEE Transactions on Speech and Audio Processing*, vol. 10, pp. 620–636, November 2002.

[476] 3GPP TS 26.173, "Adaptive multi-rate wideband speech ANSI-C code", in *3GPP Technical Specification*, 2003.

[477] S. X. Ng and L. Hanzo, "On the MIMO channel capacity of multi-dimensional signal sets", in *IEEE Vehicular Technology Conference (VTC'04)* (Los Angeles, CA), IEEE, September 2004.

[478] T. Fingscheidt and P. Vary, "Softbit speech decoding: A new approach to error concealment", *IEEE Transactions on Speech and Audio Processing*, vol. 9, pp. 240–251, March 2001.

[479] B. Atal and M. Schroeder, "Predictive coding of speech signals", *Bell Systems Technical Journal*, pp. 1973–1986, October 1970.

[480] I. Wassel, D. Goodman and R. Steele, "Embedded delta modulation", *IEEE Transactions on Acoustics, Speech and Signal Processing*, vol. 36, pp. 1236–1243, August 1988.

[481] B. Atal and S. Hanauer, "Speech analysis and synthesis by linear prediction of the speech wave", *The Journal of the Acoustical Society of America*, vol. 50, no. 2, pp. 637–655, 1971.

[482] M. Kohler, L. Supplee and T. Tremain, "Progress towards a new government standard 2400bps voice coder", in *Proceedings of the IEEE International Conference on Acoustics, Speech and Signal Processing (ICASSP'95)* (Detroit, MI), IEEE, May 1995, pp. 488–491.

[483] K. Teague, B. Leach and W. Andrews, "Development of a high-quality MBE based vocoder for implementation at 2400bps", in *Proceedings of the IEEE Wichita Conference on Communications, Networking and Signal Processing*, pp. 129–133, IEEE, April 1994.

[484] H. Hassanein, A. Brind'Amour, S. Déry and K. Bryden, "Frequency selective harmonic coding at 2400bps", in *Proceedings of the 37th Midwest Symposium on Circuits and Systems*, vol. 2, pp. 1436–1439, 1995.

[485] R. McAulay and T. Quatieri, "The application of subband coding to improve quality and robustness of the sinusoidal transform coder", in *Proceedings of the IEEE International Conference on Acoustics, Speech and Signal Processing (ICASSP'93)* (Minneapolis, MN), IEEE, April 1993, pp. 439–442.

[486] A. McCree and T. Barnwell III, "A mixed excitation LPC vocoder model for low bit rate speech coding", *IEEE Transactions on Speech and Audio Processing*, vol. 3, no. 4, pp. 242–250, 1995.

[487] P. Laurent and P. L. de La Noue, "A robust 2400bps subband LPC vocoder", in *Proceedings of the IEEE International Conference on Acoustics, Speech and Signal Processing (ICASSP'95)* (Detroit, MI), IEEE, May 1995, pp. 500–503.

[488] W. Kleijn and J. Haagen, "A speech coder based on decomposition of characteristic waveforms", in *Proceedings of the IEEE International Conference on Acoustics, Speech and Signal Processing (ICASSP'95)* (Detroit, MI), IEEE, May 1995, pp. 508–511.

[489] R. McAulay and T. Champion, "Improved interoperable 2.4 kb/s LPC using sinusoidal transform coder techniques", in *Proceedings of International Conference on Acoustics, Speech, and Signal Processing (ICASSP'90)* (Albuquerque, New Mexico), IEEE, April 1990, pp. 641–643.

[490] K. Teague, W. Andrews and B. Walls, "Harmonic speech coding at 2400 bps", in *Proceedings of the 10th Annual Mid-America Symposium on Emerging Computer Technology* (Norman, OK), 1996.

[491] J. Makhoul, R. Viswanathan, R. Schwartz and A. Huggins, "A mixed-source model for speech compression and synthesis", *The Journal of the Acoustical Society of America*, vol. 64, no. 4, pp. 1577–1581, 1978.

[492] A. McCree, K. Truong, E. George, T. Barnwell and V. Viswanathan, "A 2.4kbit/s coder candidate for the new U.S. federal standard", in *Proceedings of the IEEE International Conference on Acoustics, Speech and Signal Processing (ICASSP'96)* (Atlanta, GA), IEEE, May 1996, pp. 200–203.

[493] A. McCree and T. Barnwell III, "Improving the performance of a mixed excitation LPC vocoder in acoustic noise", in *Proceedings of International Conference on Acoustics, Speech, and Signal Processing (ICASSP'92)*, IEEE, March 1992, pp. 137–140.

[494] J. Holmes, "The influence of glottal waveform on the naturalness of speech from a parallel formant synthesizer", *IEEE Transactions on Audio and Electroacoustics*, vol. 21, pp. 298–305, June 1973.

[495] W. Kleijn, Y. Shoham, D. Sen and R. Hagen, "A low-complexity waveform interpolation coder", in *Proceedings of the IEEE International Conference on Acoustics, Speech and Signal Processing (ICASSP'96)* (Atlanta, GA), IEEE, May 1996, pp. 212–215.

[496] D. Hiotakakos and C. Xydeas, "Low bit rate coding using an interpolated zinc excitation model", in *Proceedings of the ICCS'94* (The Westin Stamford, Singapore), pp. 865–869, 14–18 November 1994.

[497] R. Sukkar, J. LoCicero and J. Picone, "Decomposition of the LPC excitation using the zinc basis functions", *IEEE Transactions on Acoustics, Speech and Signal Processing*, vol. 37, no. 9, pp. 1329–1341, 1989.

[498] M. Schroeder, B. Atal and J. Hall, "Optimizing digital speech coders by exploiting masking properties of the human ear", *Journal of the Acoustical Society of America*, vol. 66, pp. 1647–1652, December 1979.

[499] W. Voiers, "Diagnostic acceptability measure for speech communication systems", in *Proceedings of International Conference on Acoustics, Speech, and Signal Processing (ICASSP'77)* (Hartford, CT), IEEE, May 1977, pp. 204–207.

[500] W. Voiers, "Evaluating processed speech using the diagnostic rhyme test", *Speech Technology*, January/February 1983.

[501] T. Tremain, M. Kohler and T. Champion, "Philosophy and goals of the D.O.D 2400bps vocoder selection process", in *Proceedings of the IEEE International Conference on Acoustics, Speech and Signal Processing (ICASSP'96)* (Atlanta, GA), IEEE, May 1996, pp. 1137–1140.

[502] M. Bielefeld and L. Supplee, "Developing a test program for the DoD 2400bps vocoder selection process", in *Proceedings of the IEEE International Conference on Acoustics, Speech and Signal Processing (ICASSP'96)* (Atlanta, GA), IEEE, May 1996, pp. 1141–1144.

[503] J. Tardelli and E. Kreamer, "Vocoder intelligibility and quality test methods", in *Proceedings of the IEEE International Conference on Acoustics, Speech and Signal Processing (ICASSP'96)* (Atlanta, GA), IEEE, May 1996, pp. 1145–1148.

[504] A. Schmidt-Nielsen and D. Brock, "Speaker recognizability testing for voice coders", in *Proceedings of the IEEE International Conference on Acoustics, Speech and Signal Processing (ICASSP'96)* (Atlanta, GA), IEEE, May 1996, pp. 1149–1152.

[505] E. Kreamer and J. Tardelli, "Communicability testing for voice coders", in *Proceedings of the IEEE International Conference on Acoustics, Speech and Signal Processing (ICASSP'96)* (Atlanta, GA), IEEE, May 1996, pp. 1153–1156.

[506] B. Atal and L. Rabiner, "A pattern recognition approach to voiced–unvoiced–silence classification with applications to speech recognition", *IEEE Transactions an Acoustics, Speech and Signal Processing*, vol. 24, pp. 201–212, June 1976.

[507] T. Ghiselli-Crippa and A. El-Jaroudi, "A fast neural net training algorithm and its application to speech classification", *Engineering Applications of Artificial Intelligence*, vol. 6, no. 6, pp. 549–557, 1993.

[508] A. Noll, "Cepstrum pitch determination", *Journal of the Acoustical Society of America*, vol. 41, pp. 293–309, February 1967.

[509] S. Kadambe and G. Boudreaux-Bartels, "Application of the wavelet transform for pitch detection of speech signals", *IEEE Transactions on Information Theory*, vol. 38, pp. 917–924, March 1992.

[510] L. Rabiner, M. Cheng, A. Rosenberg and C. MGonegal, "A comparative performance study of several pitch detection algorithms", *IEEE Transactions on Acoustics, Speech, and Signal Processing*, vol. 24, no. 5, pp. 399–418, 1976.

[511] DVSI, *Inmarsat-M Voice Codec*, Issue 3.0, August 1991.

[512] M. Sambur, A. Rosenberg, L. Rabiner and C. McGonegal, "On reducing the buzz in LPC synthesis", *Journal of the Acoustical Society of America*, vol. 63, pp. 918–924, March 1978.

[513] A. Rosenberg, "Effect of glottal pulse shape on the quality of natural vowels", *Journal of the Acoustical Society of America*, vol. 49, no. 2, pt. 2, pp. 583–590, 1971.

[514] T. Koornwinder, *Wavelets: An Elementary Treatment of Theory and Applications*. Singapore: World Scientific, 1993.

[515] C. Chui, *Wavelet Analysis and its Applications*, *vol. I: An Introduction to Wavelets*. New York: Academic Press, 1992.

[516] C. Chui, *Wavelet Analysis and its Applications*, *vol. II: Wavelets: A Tutorial in Theory and Applications*. New York: Academic Press, 1992.

[517] O. Rioul and M. Vetterli, "Wavelets and signal processing", *IEEE Signal Processing Magazine*, vol. 8, no. 4, pp. 14–38, October 1991.

[518] A. Graps, "An introduction to wavelets", *IEEE Computational Science & Engineering*, vol. 2, no. 2, pp. 50–61, Summer 1995.

[519] A. Cohen and J. Kovačević, "Wavelets: The mathematical background", *Proceedings of the IEEE*, vol. 84, pp. 514–522, April 1996.

[520] I. Daubechies, "The wavelet transform, time-frequency localization and signal analysis", *IEEE Transactions on Information Theory*, vol. 36, pp. 961–1005, September 1990.

[521] S. Mallat, "A theory for multiresolution signal decomposition: the wavelet representation", *IEEE Transactions on Pattern Analysis and Machine Intelligence*, vol. 11, pp. 674–693, July 1989.

[522] H. Baher, *Analog & Digital Signal Processing*. New York: John Wiley & Sons, Inc., 1990.

[523] J. Stegmann, G. Schröder and K. Fischer, "Robust classification of speech based on the dyadic wavelet transform with application to CELP coding", in *Proceedings of the IEEE International Conference on Acoustics, Speech and Signal Processing (ICASSP'96)* (Atlanta, GA), IEEE, May 1996, pp. 546–549.

[524] S. Mallat and S. Zhong, "Characterization of signals from multiscale edges", *IEEE Transactions on Pattern Analysis and Machine Intelligence*, vol. 14, pp. 710–732, July 1992.

[525] M. Unser and A. Aldroubi, "A review of wavelets in biomedical applications", *Proceedings of the IEEE*, vol. 84, pp. 626–638, April 1996.

[526] C. Li, C. Zheng and C. Tai, "Detection of ECG characteristic points using wavelet transforms", *IEEE Transactions in Biomedical Engineering*, vol. 42, pp. 21–28, January 1995.

[527] S. Mallat and W. Hwang, "Singularity detection and processing with wavelets", *IEEE Transactions on Information Theory*, vol. 38, pp. 617–643, March 1992.

[528] M. Vetterli and J. Kovačević, *Wavelets and Subband Coding*. Englewood Cliffs, NJ: Prentice-Hall, 1995.

[529] R. Sukkar, J. LoCicero and J. Picone, "Design and implementation of a robust pitch detector based on a parallel processing technique", *IEEE Journal on Selected Areas in Communications*, vol. 6, pp. 441–451, February 1988.

[530] R. Steele and L. Hanzo, eds. *Mobile Radio Communications*. Piscataway, NJ: IEEE Press, 1999.

[531] F. Brooks, B. Yeap, J. Woodard and L. Hanzo, "A sixth-rate, 3.8kbps GSM-like speech transceiver", in *Proceeding of ACTS Mobile Communication Summit'98* (Rhodes, Greece), ACTS, June 1998, pp. 647–652.

[532] F. Brooks, E. Kuan and L. Hanzo, "A 2.35kbps joint-detection CDMA speech transceiver", in *Proceedings of Vehicular Technology Conference (VTC'99) (Spring)* (Houston, TX), IEEE, May 1999, pp. 2403–2407.

[533] P. Robertson, E. Villebrun and P. Hoeher, "A comparison of optimal and sub-optimal MAP decoding algorithms operating in the log domain", in *Proceedings of the International Conference on Communications* (Seattle, WA), pp. 1009–1013, 18–22 June 1995.

[534] P. Robertson, "Illuminating the structure of code and decoder of parallel concatenated recursive systematic (turbo) codes", *IEEE Globecom* (San Francisco, CA), pp. 1298–1303, IEEE, 28 November–2 December 1994.

[535] W. Koch and A. Baier, "Optimum and sub-optimum detection of coded data disturbed by time-varying inter-symbol interference", *IEEE Globecom*, pp. 1679–1684, IEEE, 2–5 December 1990.

[536] J. Erfanian, S. Pasupathy and G. Gulak, "Reduced complexity symbol dectectors with parallel structures for ISI channels", *IEEE Transactions on Communications*, vol. 42, pp. 1661–1671, 1994.

[537] J. Hagenauer and P. Hoeher, "A Viterbi algorithm with soft-decision outputs and its applications", in *IEEE Globecom*, pp. 1680–1686, IEEE, 1989.

[538] C. Berrou, P. Adde, E. Angui and S. Faudeil, "A low complexity soft-output Viterbi decoder architecture", in *Proceedings of the International Conference on Communications* (Geneva, Switzerland), pp. 737–740, 23–26 May 1993.

[539] L. Rabiner, C. McGonegal and D. Paul, *FIR Windowed Filter Design Program – WINDOW*, ch. 5.2. Piscataway, NJ: IEEE Press, 1979.

[540] S. Yeldner, A. Kondoz and B. Evans, "Multiband linear predictive speech coding at very low bit rates", *IEE Proceedings in Vision, Image and Signal Processing*, vol. 141, pp. 284–296, October 1994.

[541] A. Klein, R. Pirhonen, J. Skoeld and R. Suoranta, "FRAMES multiple access mode 1 — wideband TDMA with and without spreading", in *Proceedings of IEEE International Symposium on Personal, Indoor and Mobile Radio Communications (PIMRC'97)* (Marina Congress Centre, Helsinki, Finland), IEEE, September 1997, pp. 37–41.

[542] J. Flanagan and R. Golden, "Phase vocoder", *The Bell Systems Technical Journal*, pp. 1493–1509, November 1966.

[543] R. McAulay and T. Quatieri, "Speech analysis/synthesis based on sinusoidal representation", *IEEE Transactions on Acustics, Speech and Signal Processing*, vol. 34, pp. 744–754, August 1986.

[544] L. Almeida and J. Tribolet, "Nonstationary spectral modelling of voiced speech", *IEEE Transactions on Acoustics, Speech and Signal Processing*, vol. 31, pp. 664–677, June 1983.

[545] E. George and M. Smith, "Analysis-by-synthesis/overlap-add sinusoidal modelling applied to the analysis and synthesis of musical tones", *Journal of the Audio Engineering Society*, vol. 40, pp. 497–515, June 1992.

[546] E. George and M. Smith, "Speech analysis/synthesis and modification using an analysis-by-synthesis/overlap-add sinusoidal model", *IEEE Transaction on Speech and Audio Processing*, vol. 5, pp. 389–406, September 1997.

[547] R. McAulay and T. Quatieri, "Pitch estimation and voicing detection based on a sinusoidal speech model", in *Proceedings of ICASSP'90*, pp. 249–252, 1990.

[548] R. McAulay and T. Quatieri, "Sinusoidal coding", in *Speech Coding and Synthesis*, W.B. Keijn and K.K. Paliwal, eds., ch. 4, Amsterdam: Elsevier Science, 1995.

[549] R. McAulay, T. Parks, T. Quatieri and M. Sabin, "Sine-wave amplitude coding at low data rates", in *Advances in Speech Coding*, V.B.S. Atal and A. Gersho, eds., pp. 203–214, Dordrecht: Kluwer, 1991.

[550] M. Nishiguchi and J. Matsumoto, "Harmonic and noise coding of LPC residuals with classified vector quantization", in *Proceedings of the IEEE International Conference on Acoustics, Speech and Signal Processing (ICASSP'95)* (Detroit, MI), IEEE, May 1995, pp. 484–487.

[551] V. Cuperman, P. Lupini and B. Bhattacharya, "Spectral excitation coding of speech at 2.4 kb/s", in *Proceedings of the IEEE International Conference on Acoustics, Speech and Signal Processing (ICASSP'95)* (Detroit, MI), IEEE, May 1995, pp. 496–499.

[552] S. Yeldner, A. Kondoz and B. Evans, "High quality multiband LPC coding of speech at 2.4 kbit/s", *Electronics Letters*, vol. 27, no. 14, pp. 1287–1289, 1991.

[553] H. Yang, S.-N. Koh and P. Sivaprakasapillai, "Pitch synchronous multi-band (PSMB) speech coding", in *Proceedings of the IEEE International Conference on Acoustics, Speech and Signal Processing (ICASSP'95)* (Detroit, MI), IEEE, May 1995, pp. 516–518.

[554] E. Erzin, A. Kumar and A. Gersho, "Natural quality variable-rate spectral speech coding below 3.0kbps", in *Proceedings of the IEEE International Conference on Acoustics, Speech and Signal Processing (ICASSP'97)* (Munich, Germany), IEEE, April 1997, pp. 1579–1582.

[555] C. Papanastasiou and C. Xydeas, "Efficient mixed excitation models in LPC based prototype interpolation speech coders", in *Proceedings of the IEEE International Conference on Acoustics, Speech and Signal Processing (ICASSP'97)* (Munich, Germany), IEEE, April 1997, pp. 1555–1558.

[556] O. Ghitza, "Auditory models and human performance in tasks related to speech coding and speech recognition", *IEEE Transactions on Speech and Audio Processing*, vol. 2, pp. 115–132, January 1994.

[557] K. Kryter, "Methods for the calculation of the articulation index", *Technical Report*, American National Standards Institute, 1965.

[558] U. Halka and U. Heute, "A new approach to objective quality-measures based on attribute matching", *Speech Communications*, vol. 11, pp. 15–30, 1992.

[559] S. Wang, A. Sekey and A. Gersho, "An objective measure for predicting subjective quality of speech coders", *Journal on Selected Areas in Communications*, vol. 10, pp. 819–829, June 1992.

[560] T. Barnwell III and A. Bush, "Statistical correlation between objective and subjective measures for speech quality", in *Proceedings of International Conference on Acoustics, Speech, and Signal Processing, ICASSP'78* (Tulsa, OK), pp. 595–598, IEEE, April 1978.

[561] T. Barnwell III, "Correlation analysis of subjective and objective measures for speech quality", in *Proceedings of International Conference on Acoustics, Speech, and Signal Processing (ICASSP'80)* (Denver, CO), IEEE, April 1980, pp. 706–709.

[562] P. Breitkopf and T. Barnwell III, "Segmental preclassification for improved objective speech quality measures", in *IEEE Proceedings of International Conference on Acoustic Speech Signal Processing*, pp. 1101–1104, 1981.

[563] L. Hanzo and L. Hinsenkamp, "On the subjective and objective evaluation of speech codecs", *Budavox Telecommunications Review*, no. 2, pp. 6–9, 1987.

[564] K. Kryter, "Masking and speech communications in noise", in *The Effects of Noise on Man*, ch. 2, New York: Academic Press, 1970. ISBN: 9994669966.

[565] A. House, C. Williams, M. Hecker and K. Kryter, "Articulation testing methods: consonated differentiation with a closed-response set", *Journal of the Acoustic Society of America*, vol. 37, no. 1, pp. 158–166, January 1965.

[566] "RFC 3261: SIP Session Initiation Protocol". Internet Engineering Task Force (IETF), June 2002.

[567] "H.323: Packet-Based Multimedia Communications Systems". International Telecommunications Union (ITU), June 2006.

[568] "G711: Pulse Code Modulation (PCM) of Voice Frequencies". International Telecommunications Union (ITU), November 1988.

[569] "G723.1: Dual Rate Speech Coder for Multimedia Communications Transmitting at 5.3 and 6.3 kbits/s". International Telecommunications Union (ITU), May 2006.

[570] "G729: Coding of Speech at 8kbits/s using Conjugate-Structure Algebraic-Code-Excited Linear Predication (CS-ACELP)". International Telecommunications Union (ITU), March 1996.

[571] "06.10: Full Rate Speech Transcoding". European Telecommunications Standardisation Institute (ETSI), June 2001.

[572] "06.51: GSM Enhanced Full Rate (EFR) Speech Processing Functions: General Description". International Telecommunications Union (ITU), December 2000.

[573] "26.071: Advanced Multi-Rate (AMR) Speech Codec: General Description". Third Generation Partnership Project (3GPP), January 2005.

[574] "G729.1: G.729 based Embedded Variable Bit-Rate Coder: An 8-32 kbit/s Scalable Wideband Coder Bitstream Interoperable with G.729". International Telecommunications Union (ITU), May 2006.

[575] "RFC 3665: Session Initiation Protocol (SIP) Basic Call Flow Examples". Internet Engineering Task Force (IETF), December 2003.

[576] "H.245: Control Protocol for Multimedia Communication". International Telecommunications Union (ITU), May 2006.

[577] "H.225.0: Call Signalling Protocols and Media Stream Packetization for Packet-based Multimedia Communication Systems". International Telecommunications Union (ITU), May 2006.

[578] "RFC 3550: RTP A Transport Protocol for Real-Time Applications". Internet Engineering Task Force (IETF), July 2003.

[579] "RFC 2327: SDP Session Description Protocol". Internet Engineering Task Force (IETF), April 1998.

[580] "RFC 3551: RTP Profile for Audio and Video Conferences with Minimal Control". Internet Engineering Task Force (IETF), July 2003.

Index

Author Index

C

D

E

F

G

H

I

J

K

L

M

N

O

P

Q

R

S

T

U

V

W

X

Y

Z